

Medical Radiology · Diagnostic Imaging

Series Editors: M.F. Reiser · H.-U. Kauczor · H. Hricak · M. Knauth

Christoph Stippich *Editor*

Clinical Functional MRI

Presurgical Functional Neuroimaging

Second Edition

Medical Radiology

Diagnostic Imaging

Series editors

Maximilian F. Reiser
Hans-Ulrich Kauczor
Hedvig Hricak
Michael Knauth

Editorial Board

Andy Adam, London
Fred Avni, Brussels
Richard L. Baron, Chicago
Carlo Bartolozzi, Pisa
George S. Bisset, Durham
A. Mark Davies, Birmingham
William P. Dillon, San Francisco
D. David Dershaw, New York
Sam Sanjiv Gambhir, Stanford
Nicolas Grenier, Bordeaux
Gertraud Heinz-Peer, Vienna
Robert Hermans, Leuven
Hans-Ulrich Kauczor, Heidelberg
Theresa McLoud, Boston
Konstantin Nikolaou, Munich
Caroline Reinhold, Montreal
Donald Resnick, San Diego
Rüdiger Schulz-Wendtland, Erlangen
Stephen Solomon, New York
Richard D. White, Columbus

For further volumes:
<http://www.springer.com/series/4354>

Christoph Stippich
Editor

Clinical Functional MRI

Presurgical Functional Neuroimaging

Second Edition



Editor

Christoph Stippich, MD
Professor and Division Head
Division of Diagnostic and Interventional Neuroradiology
University Hospitals Basel
Basel
Switzerland

ISSN 0942-5373

Medical Radiology

ISBN 978-3-662-45122-9

DOI 10.1007/978-3-662-45123-6

ISSN 2197-4187 (electronic)

ISBN 978-3-662-45123-6 (eBook)

Library of Congress Control Number: 2015933163

Springer Berlin Heidelberg New York Dordrecht London

© Springer-Verlag Berlin Heidelberg 2015

This work is subject to copyright. All rights are reserved by the Publisher, whether the whole or part of the material is concerned, specifically the rights of translation, reprinting, reuse of illustrations, recitation, broadcasting, reproduction on microfilms or in any other physical way, and transmission or information storage and retrieval, electronic adaptation, computer software, or by similar or dissimilar methodology now known or hereafter developed. Exempted from this legal reservation are brief excerpts in connection with reviews or scholarly analysis or material supplied specifically for the purpose of being entered and executed on a computer system, for exclusive use by the purchaser of the work. Duplication of this publication or parts thereof is permitted only under the provisions of the Copyright Law of the Publisher's location, in its current version, and permission for use must always be obtained from Springer. Permissions for use may be obtained through RightsLink at the Copyright Clearance Center. Violations are liable to prosecution under the respective Copyright Law.

The use of general descriptive names, registered names, trademarks, service marks, etc. in this publication does not imply, even in the absence of a specific statement, that such names are exempt from the relevant protective laws and regulations and therefore free for general use.

While the advice and information in this book are believed to be true and accurate at the date of publication, neither the authors nor the editors nor the publisher can accept any legal responsibility for any errors or omissions that may be made. The publisher makes no warranty, express or implied, with respect to the material contained herein.

Printed on acid-free paper

Springer-Verlag GmbH Berlin Heidelberg is part of Springer Science+Business Media (www.springer.com)

To my beloved family Alexandra, Tim, Jan and Nils

Foreword

In the economic world, a inscription suggests that the book was considered by its publishers, after a close look at sales, to appeal to a large enough, possibly growing readership. In the scientific world, a inscription of a monograph suggests that the authors succeeded in finding readers for their special topic *and* keeping them. In the case of “Clinical Functional MRI”, I’m sure, it is more than just *keeping* readers: it is making the entire clinical neuro-community aware of the increasing importance of this field. At the same time the new edition provides a state-of-the-art summary, as it were, helpful to all those colleagues who are unable to closely follow the pertinent literature. As 7 years have passed since its first publication, “Clinical Functional MRI” was completely revised, and new chapters on emerging subtopics – e.g., on resting-state presurgical fMRI, presurgical fMRI in epilepsy, DTI-tractography, and brain plasticity as seen in fMRI and DTI – were added. Christoph Stippich, now heading neuroradiology at University of Basel/Switzerland, proved his excellence as editor by refining the book’s concept, unifying the text, and strengthening his team of experts. My prediction? A third edition in less than 7 years.

Klaus Sartor, MD
Emeritus Professor of Neuroradiology
University of Heidelberg Medical Center
Heidelberg
Germany

Preface to the Second Edition

Since the publication of this textbook's first edition, presurgical functional magnetic resonance imaging (fMRI) has undergone relevant development and is increasingly used in many neurocenters worldwide. fMRI has progressed towards a more standardized and user friendly neuroimaging modality, but is still not a simple clinical routine application and requires special expertise. Meanwhile, first official recommendations on stimulation paradigms have been published online by the American Society for Functional Neuroradiology, and larger multi-center trials have been rolled out using consensus imaging protocols. Despite considerable technical and methodological variabilities, a very substantial body of evidence has been generated that further supports presurgical fMRI's role as a feasible, robust and valid clinical imaging tool. In addition, diffusion-tensor-imaging (DTI) and diffusion-tensor-tractography (DTT) have proven their value to visualize functionally important white matter structures as well as pathological alterations, which can be meaningfully combined with presurgical fMRI also for functional neuronavigation. More recently, resting-state fMRI (RS-fMRI) has entered this clinical arena providing noninvasive measures of functional brain networks and connectivity studies even without active cooperation of the patients. EEG-correlated fMRI in imaging epilepsies has seen further development, as well as multimodality functional neuroimaging with MEG, PET or SPECT. A rapidly increasing number of functional imaging studies have contributed to a better understanding of neuroplastic changes that can occur in various brain pathologies. Such phenomena should be considered with caution, when presurgical fMRI data need to be interpreted.

With the second edition of this textbook, we account for these developments and have implemented new chapters on DTI, RS-fMRI, EEG-fMRI and brain plasticity – all written by renowned experts in their respective fields. All other chapters have been updated and fully revised. This increase in information is unavoidably reflected by a slightly larger volume of this textbook, which is still very comprehensive and practically oriented. Again, it has been a great pleasure writing this book together, and we hope that it will be of value for all working, or intending to work, in the field of clinical functional neuroimaging, and in particular with presurgical fMRI and DTI.

Last, but not least, I would like to thank Drs. Maria Blatow and Meritxell Garcia for their support and assistance.

Basel, Switzerland

Christoph Stippich, MD

Preface to the First Edition

Over the past decade, functional magnetic resonance imaging (fMRI) has undergone a continuing process of technical and methodological maturation and refinement, facilitating its application in a clinical environment. One of the earliest and best validated clinical applications of fMRI was, and remains, presurgical assessment of brain function in patients with brain tumors and epilepsies. There is a substantial body of evidence that fMRI is suited to localizing different body representations in the primary motor and somatosensory cortex, as well as to localizing and lateralizing language function prior to surgery. This diagnostic information permits function-preserving and safe treatment. However, fMRI cannot be considered an established diagnostic neuroimaging modality as yet. To this end, a consensus on standardization of imaging procedures, data processing, data evaluation, and medical interpretation of imaging findings is mandatory. Various dedicated hard- and software components require medical certification and, last but not least, recommendations or guidelines need to be issued by the relevant medical associations. Until then, it is each investigator's responsibility to establish his/her own routines and standards. This requires a profound knowledge of all topics relevant to the presurgical application of fMRI.

There are several textbooks available relating to (clinical) fMRI covering neurophysiology, neuroanatomy, neurosurgery, neurology, neuropsychology, (neuro)radiology, etc., as well as various aspects of functional neuroimaging, most of the latter being dedicated to neuroscientific research. In addition, the abundant original literature published on presurgical fMRI is somewhat heterogeneous, yielding partly conflicting results, which in turn makes it difficult and time-consuming for the reader to extract the clinically relevant information. Furthermore, fMRI is not the sole method in the field of functional neuroimaging. There are other powerful tools such as EEG/MEG, PET, or SPECT that complement each other when combined in a meaningful way. The same holds true for MR spectroscopy and diffusion tensor imaging (DTI). Consequently, dealing with fMRI is intrinsically complex, multimodal, and multidisciplinary.

The motivation for writing this book was the idea of creating a comprehensive text covering the whole field of presurgical fMRI from physiological, anatomical, and methodological basics up to neuroplasticity. Besides compiling the current knowledge on presurgical fMRI, the core of this book has a clear focus on practical issues, providing guidance for those less familiar with the field. Experienced investigators may profit from the various strategies, tips, and tricks given, as well as from a deeper insight into different areas directly linked to presurgical fMRI. For easier reading, this book has been designed as an assembly of successive chapters, each dealing with a specific topic and providing a particular point of view on presurgical fMRI. Therefore, it is not necessary to go through the whole book – areas of specific interest can be selected easily from the “keypoints” sections and from extensive illustrations.

Each chapter has been written by experienced clinicians and researchers, some world renowned in their respective fields. It has been a great pleasure writing this book together, and we hope that it will be of value for all working, or intending to work, in the field of clinical functional neuroimaging, and in particular with presurgical fMRI.

Last, but not least, I would like to thank Professor Klaus Sartor for encouraging me to edit this book and Dr. Maria Blatow for her support and assistance.

Heidelberg, Germany

Christoph Stippich, MD

Contents

| | |
|---|-----|
| Presurgical Functional MRI and Diffusion Tensor Imaging | 1 |
| Christoph Stippich | |
| Revealing Brain Activity and White Matter Structure Using Functional and Diffusion-Weighted Magnetic Resonance Imaging | 13 |
| Rainer Goebel | |
| Functional Neuroanatomy | 61 |
| Thomas P. Naidich and Tarek A. Yousry | |
| Task-Based Presurgical Functional MRI in Patients with Brain Tumors | 89 |
| Christoph Stippich, Maria Blatow, and Meritxell Garcia | |
| Presurgical Resting-State fMRI. | 143 |
| Monica G. Allen, Abraham Z. Snyder, Carl D. Hacker, Timothy J. Mitchell, Eric C. Leuthardt, and Joshua S. Shimony | |
| Simultaneous EEG-fMRI in Epilepsy..... | 159 |
| R. Wiest, E. Abela, and C. Rummel | |
| Diffusion Imaging with MR Tractography for Brain Tumor Surgery..... | 179 |
| Alberto Bizzi | |
| Functional Neuronavigation..... | 229 |
| Volker M. Tronnier | |
| Presurgical Functional Localization Possibilities, Limitations, and Validity | 247 |
| Stéphane Lehéricy, Delphine Leclercq, Hugues Duffau, Pierre-François Van de Moortele, and Christine Delmaire | |
| Multimodality in Functional Neuroimaging..... | 269 |
| Jan Kassubek, Hans-Peter Müller, and Freimut D. Juengling | |
| Brain Plasticity in fMRI and DTI | 289 |
| R. Beisteiner and E. Matt | |
| Clinical BOLD fMRI and DTI: Artifacts, Tips, and Tricks | 313 |
| Ronald Peeters and Stefan Sunaert | |
| Index..... | 337 |

Contributors

- E. Abela, MD**, Support Center for Advanced Neuroimaging (SCAN), Institute for Diagnostic and Interventional Neuroradiology, University Hospital Bern, Bern, Switzerland
Department of Neurology, University Hospital Bern, Bern, Switzerland
- Monica G. Allen**, Mallinckrodt Institute of Radiology, Washington University School of Medicine, Saint Louis, MO, USA
- R. Beisteiner**, Department of Neurology, Highfield MR Center, Medical University of Vienna, Vienna, Austria
- Alberto Buzzi, MD**, Department of Neuroradiology, Humanitas Clinical and Research Hospital IRCCS, Rozzano (Milano), Italy
- Maria Blatow, MD**, Division of Diagnostic and Interventional Neuroradiology, Clinic for Radiology and Nuclear Medicine, University Hospitals Basel, Basel, Switzerland
- Christine Delmaire, MD**, Department of Neuroradiology, CHRU Lille, Hopital Roger Salengro, boulevard du Pr Leclerc, Lille cedex, France
- Hugues Duffau, MD, PhD**, Department of Neurosurgery, Hôpital Gui de Chauliac and INSERM U1051, Montpellier University Medical Center, Montpellier, France
- Meritxell Garcia, MD**, Division of Diagnostic and Interventional Neuroradiology, Clinic for Radiology and Nuclear Medicine, University Hospitals Basel, Basel, Switzerland
- Rainer Goebel**, Department of Cognitive Neuroscience, Maastricht University, Maastricht, The Netherlands
- Carl D. Hacker**, Department of Biomedical Engineering, Washington University School of Medicine, Saint Louis, MO, USA
- Freimut D. Juengling, MD**, PET/CT Center NW-Switzerland, Claraspital Basel, Basel, Switzerland
- Jan Kassubek, MD**, Department of Neurology, University of Ulm, Ulm, Germany
- Delphine Leclercq, MD**, Department of Neuroradiology, Groupe Hospitalier Pitié-Salpêtrière, Université Pierre et Marie Curie – Paris 6, Paris, France
- Stéphane Lehéricy, MD, PhD**, Centre de NeuroImagerie de Recherche – CENIR, Institut du Cerveau et de la Moelle – ICM, Sorbonne Universités, UPMC Univ Paris 06, UMR S 1127, CNRS UMR 7225, Paris, France
Department of Neuroradiology, Groupe Hospitalier Pitié-Salpêtrière, Université Pierre et Marie Curie – Paris 6, Paris, France
- Eric C. Leuthardt**, Department of Neurosurgery, Washington University School of Medicine, Saint Louis, MO, USA

E. Matt, Department of Neurology, Highfield MR Center, Medical University of Vienna, Vienna, Austria

Timothy J. Mitchell, Washington University School of Medicine, Saint Louis, MO, USA

Hans-Peter Müller, PhD, Department of Neurology, University of Ulm, Ulm, Germany

Thomas P. Naidich, Mount Sinai School of Medicine, One Gustave Levy Place, New York, NY, USA

Department of Neuroradiology and Neurosurgery, Irving and Dorothy Regenstreif Research, New York, NY, USA

Ronald Peeters, PhD, Department of Radiology, University Hospitals of the Catholic University of Leuven, Leuven, Belgium

C. Rummel, PhD, Support Center for Advanced Neuroimaging (SCAN), Institute for Diagnostic and Interventional Neuroradiology, University Hospital Bern, Bern, Switzerland

Joshua S. Shimony, Washington University School of Medicine, Saint Louis, MO, USA

Abraham Z. Snyder, Washington University School of Medicine, Saint Louis, MO, USA

Stefan Sunaert, MD, PhD, Department of Radiology, University Hospitals of the Catholic University of Leuven, Leuven, Belgium

Christoph Stippich, MD, Professor and Division Head, Division of Diagnostic and Interventional Neuroradiology, University Hospitals Basel, Basel, Switzerland

Volker M. Tronnier, MD, PhD, Department of Neurosurgery, Universitätsklinikum Schleswig-Holstein, Campus Lübeck, Lübeck, Germany

Pierre-François Van de Moortele, MD, PhD, Center for Magnetic Resonance Research, University of Minnesota, Minneapolis, MN, USA

R. Wiest, MD, Support Center for Advanced Neuroimaging (SCAN), Institute for Diagnostic and Interventional Neuroradiology, University Hospital Bern, Bern, Switzerland

Tarek A. Yousry, Lysholm Department of Neuroradiology, The National Hospital for Neurology and Neurosurgery, Institute of Neurology, London, UK

Presurgical Functional MRI and Diffusion Tensor Imaging

Christoph Stippich

Contents

| | |
|---|---|
| 1 | Introduction..... |
| 2 | Blood-Oxygenation-Level-Dependent Functional MRI (BOLD fMRI)..... |
| 3 | Diffusion Tensor Imaging (DTI) and DTI Tractography (DTT) |
| 4 | Presurgical fMRI and DTI..... |
| 5 | Content Overview |
| | References..... |

Abstract

Functional magnetic resonance imaging (fMRI) provides noninvasive localisation and lateralisation of specific brain functions by measuring local hemodynamic changes coupled to neuronal activation. Different magnetic properties of oxygenated (diamagnetic) and deoxygenated (paramagnetic) hemoglobin are exploited to generate the blood oxygen level dependent (BOLD) contrast. Diffusion tensor magnetic resonance imaging (DTI) measures anisotropic (directional) diffusion of protons along myelinated fibers and thereby provides detailed information on the white matter architecture. Specific white matter tracts can be reconstructed using diffusion tensor tractography (DTT). During the last two decades both novel MR-modalities have revolutionised the imaging research on human brain function and structural connectivity under physiological and pathological conditions.

Task-based presurgical fMRI in patients with brain tumors or epilepsies represents the best established and validated clinical application. Essential cortical motor and language areas can be localised and the language dominant hemisphere can be determined prior to treatment. DTI and DTT provide complimentary data on important white matter connections, e.g., the pyramidal tract and arcuate fascicle. This imaging information is indispensable to establish the best possible treatment for each individual patient, and to achieve the ultimate goal of surgery: function preserving complete or most radical removal of the pathology. To this end fMRI and DTI are integrated meaningfully into functional neuronavigation. While promising, resting-state fMRI is currently still under initial clinical investigation.

The responsible clinical application requires standardised imaging and data processing as well as a profound knowledge of the imaging techniques employed, the underlying functional neuroanatomy, physiology and pathology, neuroplastic alterations, influencing factors, artifacts, pitfalls, validity and limitations. Finally, information on other functional neuroimaging modalities and multimodal integration is essential.

C. Stippich, MD
Professor and Division Head, Division of Diagnostic and Interventional Neuroradiology, University Hospitals Basel, Petersgraben 4, Basel CH 4031, Switzerland
e-mail: christoph.stippich@usb.ch

1 Introduction

Functional magnetic resonance imaging (fMRI) is a modern, noninvasive imaging technique to measure and localize specific functions of the human brain without the application of radiation (Bandettini et al. 1992; Kwong et al. 1992). Brain function is indirectly assessed with high spatial resolution via detection of local hemodynamic changes in capillaries (Menon et al. 1995) and draining veins (Frahm et al. 1994) of the so-called functional areas, e.g., regions of the human brain that govern motor, sensory, language, or memory functions. In *task-based fMRI (fMRI)*, specific stimulation of the respective neurofunctional system is required (Belliveau et al. 1991). The stimuli are presented in a predefined manner during the fMRI measurement, which is called a stimulation paradigm. The measurement of spontaneous brain activation is also possible, by using *resting-state fMRI (RS-fMRI)* techniques (Purdon and Weisskoff 1998). Here, low-frequency fluctuations in the hemodynamics of the brain are analyzed for synchrony to detect interconnected areas that constitute different functional systems. RS-fMRI is typically employed to study *functional brain connectivity* in neuroimaging research. Clinical applications are currently under initial investigation (Lee et al. 2013).

The *blood-oxygen-level-dependent (BOLD)* fMRI technique makes use of blood as an intrinsic contrast (Ogawa et al. 1990, 1992, 1993), superseding the intravenous application of paramagnetic contrast agents (Belliveau et al. 1991) or radioactive substances (Mazziotta et al. 1982; Raichle 1983; Fox et al. 1986; Holman and Devous 1992). The different magnetic properties of oxygenated and deoxygenated hemoglobin are exploited to generate the BOLD contrast. Although the underlying physiological mechanisms of neurovascular coupling are not ultimately understood, there seems to be a very good correspondence of BOLD signals with actual neuronal activity (Logothetis et al. 2001; Logothetis 2002, 2003; Logothetis and Pfeuffer 2004; Logothetis and Wandell 2004).

New powerful gradient systems and the development of ultrafast MR sequences enable examination of the entire brain in clinically feasible time frames. Furthermore, fMRI profits from high main magnetic field strength and multichannel head coils in terms of improved signal-to-noise ratio (SNR), higher spatial resolution, and/or shorter examination times. Better functionality of data processing and immediate data analysis, as obtained with *real-time fMRI*, facilitate the usability of fMRI in the clinical context (Fernandez et al. 2001; Weiskopf et al. 2003; Steger and Jackson 2004; Moller et al. 2005). Today, most vendors offer some functionality with their MR imagers to analyze fMRI data at the scanners' console directly.

Thus, functional MRI not only offers a variety of novel options for clinical diagnostics and research but also opens up a new diagnostic field of radiology and neuroradiology, by shifting paradigms from strictly morphological imaging

to measurement and visualization of brain function (Stippich et al. 2002a; Thulborn 2006).

The combination of fMRI with *diffusion tensor imaging (DTI)* has proven scientific and clinical relevance (Bick et al. 2012). By measuring the directed diffusion of protons along myelinated fibers, DTI provides complementary information on white matter architecture, i.e., on the course and integrity of functionally important white matter tracts. In neuroimaging research, DTI is mainly applied to study the human brain's *structural connectivity*, whereas *diffusion tensor tractography (DDT)* is often also employed for clinical applications (Leclercq et al. 2011). DTI measurements can be obtained together with fMRI in the same scanning session, which gives an even more complete picture of each patient's individual brain pathology.

With this textbook, we aim to provide the reader with thorough and comprehensive information on the abovementioned advanced MRI techniques, namely, task-based fMRI, resting-state fMRI, diffusion tensor imaging, and tractography in the presurgical context, which constitute their best established and validated clinical applications. A meaningful combination of these advanced MRI techniques with standard MR sequences (T2-FLAIR, T1-weighted sequences pre- and post-contrast administration) as well as with diffusion- and perfusion-weighted MRI is recommended to complete the state-of-the-art preoperative structural and functional neuroimaging in patients with brain tumors and drug-resistant epilepsy (Svolos et al. 2013) (Fig. 1). On current MR imagers with main magnetic field strength of 1.0 T or above, equipped with powerful gradients and multichannel head coils, such protocols should not require more than 45 min of scanning time. Regarding functional studies, 20 min should be approximated for a multiparadigm language mapping and 5–10 min for a somatotopic motor or somatosensory mapping. It is recommended to acquire the T1-weighted 3D post-contrast data set – which will be used for the overlay of functional on structural images and for neuronavigation – within the same scanning session in order to minimize coregistration inaccuracies. Typically, another meaningfully selected MR sequence is added to the protocol within that time frame, e.g., susceptibility-weighted imaging (SWI). MR spectroscopy (MRS) and chemical shift imaging (CSI) are other MR modalities for advanced neuroimaging in oncology which may be added selectively and provide important complementary information on brain and tumor metabolism (Tsougos et al. 2012).

2 Blood-Oxygenation-Level-Dependent Functional MRI (BOLD fMRI)

Enhanced synaptic activity resulting from stimulation of neurons leads to a local increase in energy and oxygen consumption in functional areas. The following local hemodynamic

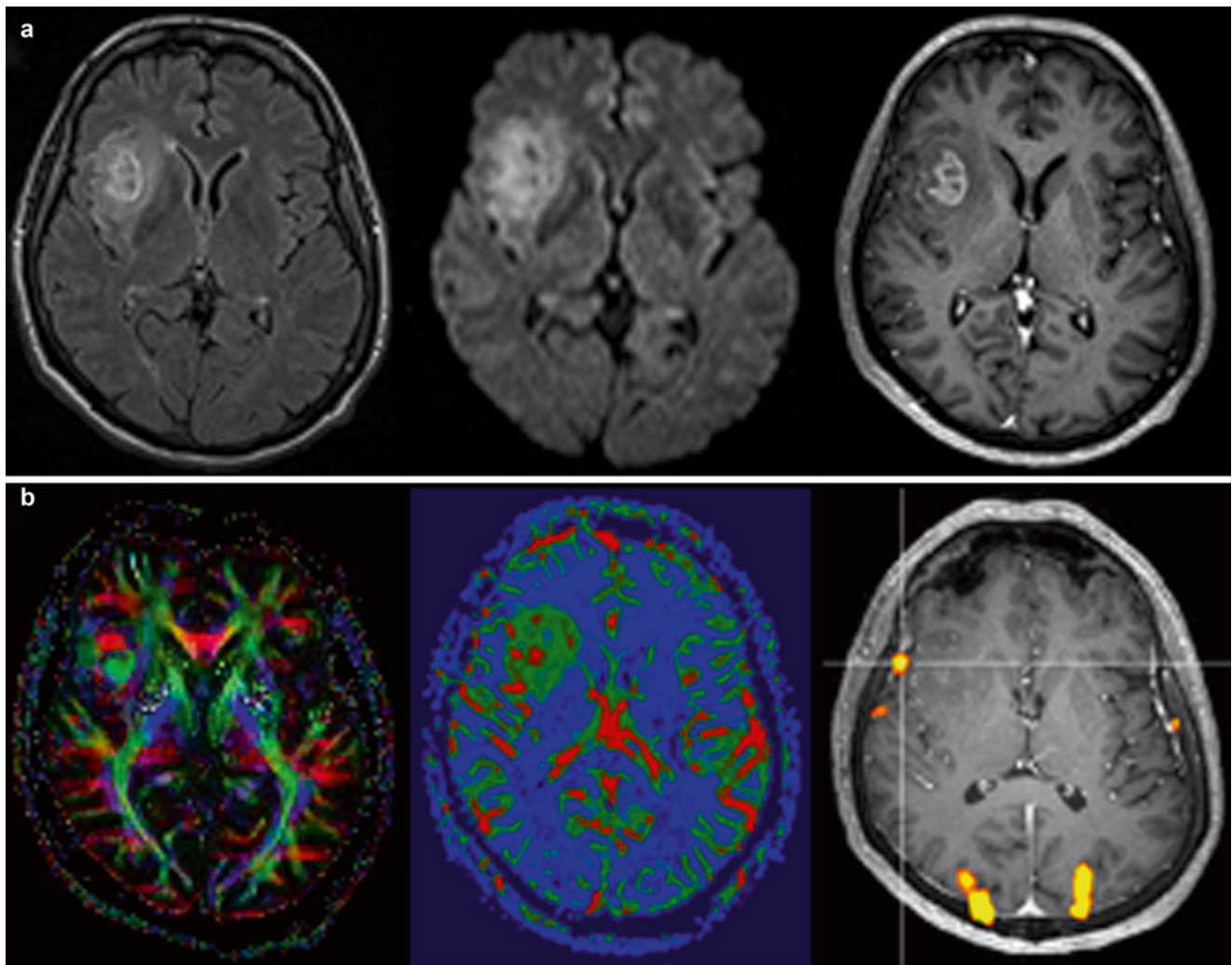


Fig. 1 The state-of-the-art preoperative multimodality MR imaging in a right glioblastoma affecting the basal ganglia, insula, and inferior frontal lobe as visualized on standard MR sequences (**a**, upper row). Advanced MR imaging (**b**, lower row) revealed disintegration of white matter architecture/alterations in fractional

anisotropy on color-coded DTI maps (left), increased relative blood volume on dynamic susceptibility contrast-enhanced (DSCE) perfusion imaging (middle), and right language dominance on BOLD fMRI (right) in this left-handed male patient (Color figure online)

changes transmitted via neurovascular coupling are measured by fMRI with high spatial accuracy:

- Increase of regional cerebral blood volume (rCBV)
- Increase of regional cerebral blood flow (rCBF)
- Relative increase of oxyhemoglobin in capillaries and venous blood

In principle, fMRI measurements can be accomplished with different techniques; BOLD fMRI being the most frequently used in human brain is therefore often referred to as the *standard* technique (Thulborn et al. 1996; Thulborn 1998, 2006). Bolus tracking measures rCBV making use of external contrast agents (Belliveau et al. 1991), and spin tagging assesses rCBF using arterial blood for intrinsic contrast (Detre et al. 1992). In contrast, BOLD technique (Ogawa et al. 1990, 1992, 1993) takes advantage of the different magnetic properties of oxygenated (oxy-Hb) and deoxygenated (deoxy-Hb)

hemoglobin to generate an image contrast. Paramagnetic deoxy-Hb produces local field inhomogeneities in a measurable range for MRI resulting in a signal decrease in susceptibility-weighted MR sequences (T2*), whereas diamagnetic oxy-Hb does not interfere with the external magnetic field. Specific neuronal stimulation augments local cerebral oxygen consumption, which initially results in a decrease of oxy-Hb and an increase in deoxy-Hb in the functional area. To provide the active neurons with oxygenated blood, perfusion (rCBF, rCBV) in capillaries and draining veins is increased within several seconds. This mechanism not only equalizes the initial decrease of local oxy-Hb concentration but even overcompensates it (Fox and Raichle 1986). Deoxy-Hb is progressively washed out which is reflected by a reduction of local field inhomogeneity and a raise of BOLD signal in T2*-weighted MR images (Turner et al. 1991).

BOLD measurements are currently exerted with ultrafast single-shot echo-planar-imaging (EPI) sequences as gradient echo (GRE) or spin echo (SE) (Stippich et al. 2002a, b). GRE sequences usually obtain higher BOLD signal predominantly from venous origin, whereas SE sequences also measure lower BOLD signals arising from the capillary bed in brain parenchyma (Hulvershorn et al. 2005a, b). Temporal resolution in paradigms with a blocked or parametric design corresponds to the chosen block duration but could be substantially improved (<100 ms) by the introduction of event-related measurements (Buckner et al. 1996). fMRI, however, cannot attain the temporal resolution of electroencephalography (EEG) (Berger 1929; Gevins 1995; Gevins et al. 1995) or magnetoencephalography (MEG) (Hari and Ilmoniemi 1986; Hämäläinen et al. 1993) but lacks the need for a complicated model-based calculation for source localization and offers higher spatial precision due to a direct correlation with the surface anatomy. Signal intensity and realizable spatial resolution vary with the magnetic field strength. MR scanners with magnetic field strengths below 1.0 Tesla (T) are not suitable for clinical functional BOLD imaging. The broadly available 1.5 T scanners allow reliable measurements of cortical activation provided that powerful gradient systems (possibly >30 mT/m) are on hand, while high-magnetic-field scanners with 3 T or above even permit functional imaging of subcortical structures and the brain stem (Thulborn 1999; Zambreanu et al. 2005). Despite excellent SNR and spatial resolution, the application of fMRI at field strengths 7.0 T or above has to be considered experimental (Goa et al. 2014; Hua et al. 2013; Huber et al. 2014). This is mainly due to technical and logistical difficulties as well as to the very limited availability of ultrahigh-field MR imagers in a clinical setting. Advantages of fMRI over positron emission tomography (PET) (Mazziotta et al. 1982; Raichle 1983; Fox et al. 1986) or single photon emission computer tomography (SPECT) (Holman and Devous 1992) – other methods measuring brain activity indirectly with lower spatial/temporal resolution (glucose or oxygen metabolism, blood flow/perfusion changes) – are its noninvasiveness, lack of radiation, reproducibility, and broad availability of clinical scanners.

Task-based presurgical BOLD fMRI represents the best established and validated clinical application of fMRI, whereas resting-state fMRI should still be considered under initial clinical investigation. Due to the intrinsically low SNR, it is mandatory to perform multiple repeated stimulations during each task-based fMRI measurement in order to obtain robust BOLD signals. Statistical correlation of BOLD signal time courses with the chosen stimulation protocol (paradigm) enables the identification of those brain areas that show hemodynamic changes in synchrony with the task. A prerequisite for this is a further processing of fMRI data, which is normally done after the measurements with freely available or commercial software (Cox 1996; Friston 1996; Gold et al. 1998; Roberts 2003). However, not all of these programs have

been certified for medical use. Nowadays, most manufacturers of clinical high-magnetic-field scanners offer options for an *online* processing of fMRI data (*real-time fMRI*) (Fernandez et al. 2001; Moller et al. 2005; Posse et al. 2013). Since the functionality and the statistical calculations used vary considerably between the different softwares, the appropriate choice largely depends on individual criteria and preferences. Basically, any data processing software for fMRI should at least offer image alignment, motion correction, temporal and spatial data smoothing, multiple statistical tests to assess functional activation, and options for spatial normalization (Stippich et al. 2002a, b). Furthermore, each fMRI software used for neurosurgery or radiation treatment should provide precise and reliable tools for superimposing functional on morphological images, for the integration of fMRI with DTI data, and for data export (e.g., into neuronavigation systems).

This textbook has its traditional focus on presurgical functional neuroimaging. Today, presurgical task-based fMRI is the most widely used modality and is commonly combined with DTI and DTT to visualize both functionally important cortical areas and white matter tracts. Hence, we have now added essential information on this complementary MR modality but keep the focus strictly on pre- and intraoperative applications in patients with brain tumors and epilepsy. A detailed description of diffusion MRI is beyond the scope of this book – for this purpose, we refer the reader to the extensive literature available.

3 Diffusion Tensor Imaging (DTI) and DTI Tractography (DTT)

Diffusion MR signal mainly originates from protons that move in the extracellular space of biological tissues (Brownian motion) (LeBihan 2006, 2013; LeBihan and Johansen-Berg 2012). Within a given voxel, the diffusion may be fully free and undirected (isotropic) or directed (anisotropic) due to barriers preventing proton movement (e.g., myelinated axons). DTI is capable to detect such anisotropic diffusion (Basser et al. 1994; LeBihan et al. 2001), but for this end diffusion must at least be measured in six different directions. Anisotropic diffusion can then be modeled mathematically using a 3D Gaussian probability function from which a 3×3 matrix is calculated, named *diffusion tensor*. The diffusion tensor is characterized by *eigenvalues* and *eigenvectors* and indicates the main orientation of diffusion within a voxel. The *fractional anisotropy* (FA) quantifies such directed diffusion. Isotropic (undirected) diffusion corresponds to an FA value of 0 which translates graphically to a sphere. In contrast, an FA value of 1 reflects the opposite extreme, i.e., a totally directed (anisotropic) diffusion which would graphically translate to a line but does not occur in biological tissues – thus, the typical shape of the FA is an ellipsoid.

Myelinated axons are lipophilic and represent diffusion barriers for hydrophilic protons that travel perpendicularly. In turn, this results in a preferred orientation and higher velocity of diffusion along such barriers. Thus, DTI reflects the white matter architecture and the course of functionally important fiber bundles rather indirectly by measuring the anisotropic diffusion of protons between and along axons. Basically, DTI fiber tracts are reconstructed by following and connecting the predominant directed diffusion across adjacent voxels. Standard DTI measurements and most mathematical algorithms employed for analyzing DTI data have limitations when different orientations of diffusion need to be differentiated within a voxel, when crossing fibers need to be reconstructed, or when diffusion anisotropy is affected by the brain's pathology, e.g., by tumor invasion or edema (Cortez-Conradis et al. 2013; Kallenberg et al. 2013; Kleiser et al. 2010; Stadlbauer et al. 2010). At the expense of scanning/processing time, more advanced MR techniques enable the assessment of the contribution of the differential intravoxel anisotropy (diffusion spectrum imaging, q-ball imaging, HARDI, etc.) or the employment of a more sophisticated (e.g., probabilistic or advanced deterministic) modeling for tractography (Bauer et al. 2013; Kuhnt et al. 2013a, b; O'Donell et al. 2012). In general, the *quality* of DTI images depends on the number of directions measured, the number of averages used, and the spatial resolution chosen, which are all inversely related to scanning time.

4 Presurgical fMRI and DTI

Presurgical fMRI and DTI measurements are carried out to facilitate function-preserving and safe treatment in patients with brain tumors and epilepsy by localizing and lateralizing specific brain functions, functionally important axonal connections, or epileptic activity, noninvasively (Bick et al. 2012; Dimou et al. 2013; Centeno and Carmichael 2014). This diagnostic information cannot be obtained from morphological brain imaging alone or from invasive measures prior to treatment.

Consequently, presurgical fMRI and DTI are always performed in individual patients to achieve a functional diagnosis. This differs fundamentally from applications in basic neuroscience research where normal or altered brain function is usually investigated in group studies to better understand physiological or pathological conditions in general. A direct contribution to the patient management is not required. In contrast, for clinical diagnostic applications, the experimental setup as well as the processing and evaluation of the data need to be adapted to the clinical environment so that patients – who may present with neurological or cognitive deficits – can be examined successfully in a standardized way. Still, in clinical fMRI and DTI, this is typically achieved via local experts, individual routines, and own validation (Pillai 2010). The novel applications of resting-state fMRI (RS-MRI) may have

practical advantages, as an active cooperation of the patient is not required (Lang et al. 2014). Uncooperative, sedated, or anesthetized patients or children who are not able to perform task-based fMRI properly may profit from RS-MRI. Potentially, RS-fMRI could also be applied intraoperatively (Nimsky 2011). The available data on presurgical RS-fMRI are very limited, however, and therefore do not justify to draw any firm conclusion on its clinical feasibility and validity, yet.

During the last years, more and more devices and software solutions have become commercially available that facilitate the clinical application of fMRI. These products are mainly dedicated to stimulation and data processing. Moreover, first attempts have been made to define robust clinical applications for task-based fMRI. To this end, paradigms have been proposed and published online by the American Society of Functional Neuroradiology (for details, please visit www.asfnr.org/paradigms.html). At least in the USA, CPT codes have been established for reimbursement of clinical fMRI examinations. It is important to note, however, that fMRI and DTI cannot be considered as fully standardized methods routinely used in clinical diagnostic neuroimaging. Hence, depending on the local situations, it may still be required to perform presurgical fMRI and DTI examinations in the framework of scientific studies until all hard- and software components used for medical application have been certified and official recommendations or guidelines have been issued by the relevant national medical association. Until then, individual routines and standards still need to be established for data acquisition, processing, and evaluation, as well as for the medical interpretation and documentation of clinical fMRI and DTI findings. For a meaningful clinical application, a profound knowledge of the specifications of the different software packages used, of possible sources of errors and imaging artifacts, and of relevant limitations of the techniques employed is indispensable. As a basic principle, presurgical fMRI and DTI examinations should be performed, evaluated, and interpreted by trained and experienced physicians with particular expertise in this area, since careless use of this very promising technique could endanger patients.

There are numerous studies available suggesting a high reliability of fMRI to localize the different cortical representations of the human body within the primary motor and somatosensory cortices (Fig. 2) as well as the motor and sensory language areas (Fig. 3) prior to brain surgery, if indications and limits of the method are considered. The same holds true for the noninvasive determination of the dominant brain hemisphere for language function.

Additional attention needs to be paid to technique-related inaccuracies due to the superposition of functional and morphological images, the referencing of fMRI data in neuro-navigation systems, or the surgery-induced localization errors following removal of brain tissue or loss of cerebro-spinal fluid (brain shift) (Reinges et al. 2004; Wittek et al.

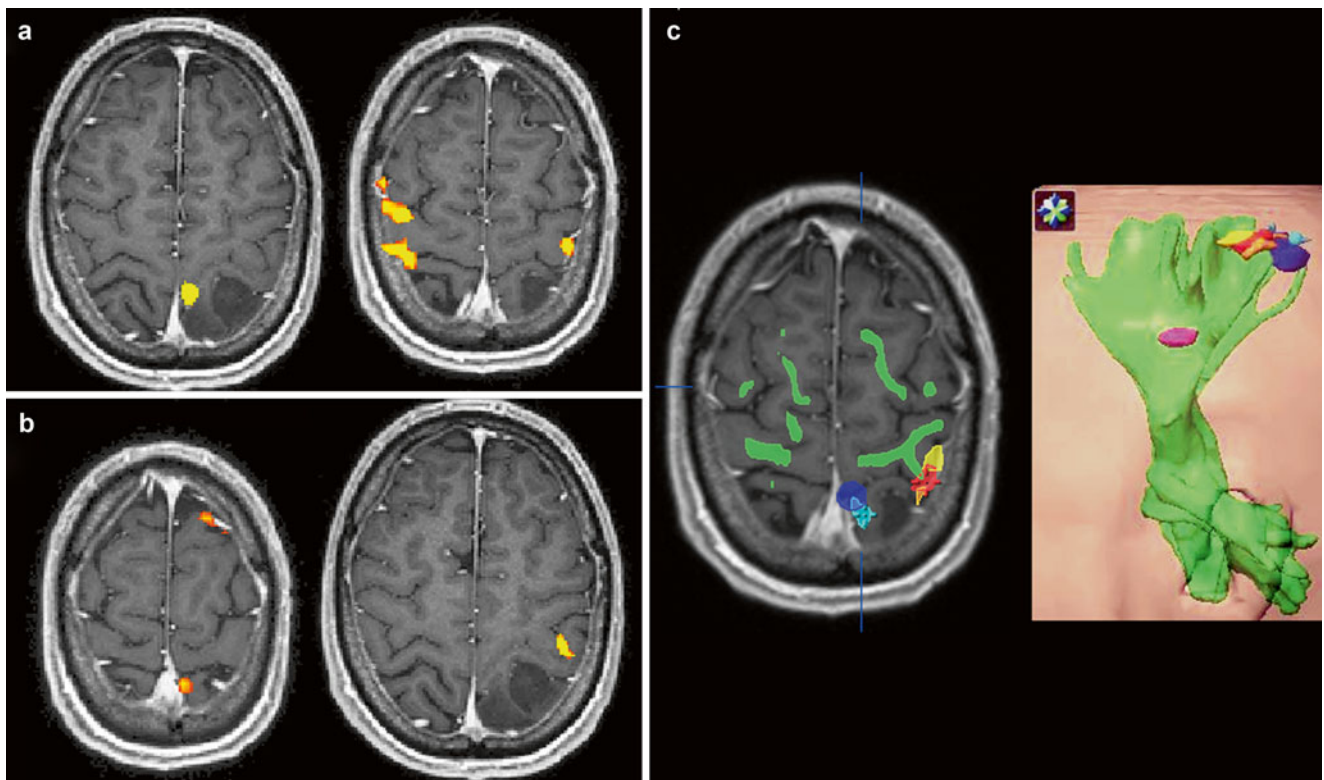


Fig. 2 Preoperative fMRI somatotopic mapping of the motor (a) and somatosensory (b) homunculus and DTI tractography of the cortico-spinal (pyramidal) tract in a symptomatic patient with a left parietal astrocytoma. Voluntary movements of the toes and fingers on the right side were used for motor mapping, and fully automated pneumatically driven tactile stimulation of digits 1 and 2 to the right foot and hand, respectively, was employed for somatosensory stimulation. Of note is the enhanced co-activation of the premotor and primary hand

representations in the right hemisphere during voluntary right hand movements as an fMRI indicator for tumor-associated neuroplastic reorganization. Integration of the abovementioned different functional body representations (foot motor (dark blue), foot somatosensory (light blue), hand motor (yellow), hand somatosensory (orange), tongue motor (purple)) and of the pyramidal tract (green) into a 3D data set for functional neuronavigation (c, left), 3D surface view (c, right) (Color figure online)

2005). Safety of surgical procedures in functional areas or their proximity can be improved by concomitant visualization of functional landmarks and important fiber tracts (e.g., pyramidal tract, arcuate fascicle) using diffusion tensor imaging (DTI) (Coenen et al. 2001; Holodny et al. 2001; Krings et al. 2001; Stippich et al. 2003a; Ulmer et al. 2004b; Holodny et al. 2005; Shinoura et al. 2005). The same holds true for the combined use of fMRI and EEG (Towle et al. 2003), MEG (Kober et al. 2001; Grummich et al. 2006) or PET (Baumann et al. 1995; Bittar et al. 1999). Tumor-induced hemodynamic changes can lead to erroneous fMRI localization and missing or artificial BOLD signals (Holodny et al. 1999, 2000; Schreiber et al. 2000; Krings et al. 2002; Ulmer et al. 2004a, b). Electrophysiological techniques are unsusceptible to these problems, since they directly measure electromagnetic fields resulting from synaptic activity (Berger 1929; Hari and Ilmoniemi 1986; Hämäläinen et al. 1993). However, localization of electromagnetic sources requires complicated modeling and calculations and is therefore limited in precision and accuracy. Furthermore, it should be borne in mind that fMRI and DTI results are gen-

erated by using mathematical correlations and therefore vary with the chosen statistical parameters or thresholds. Consequently, the size and extent of fMRI cortical activations or of reconstructed DTI fiber tracts do not reflect the *truth* and may confront the operator with an unfounded safety margin. Thus, resection borders cannot be determined reliably on the basis of fMRI or DTI data without standardization and validation.

When applied in a standardized way, fMRI has the diagnostic potential to substantially contribute to the planning and implementation of function-preserving therapies in patients with brain tumors and epilepsy (Lee et al. 1999; Gaillard et al. 2000; Grabowski 2000; Hirsch et al. 2000; Sunaert and Yousry 2001; Baxendale 2002; Binder et al. 2002; Rutten et al. 2002; Stippich et al. 2003a, b; Van Westen et al. 2005; Stippich et al. 2007; Thulborn 2006). Prior to and during neurosurgical interventions, fMRI can help to reduce the need for invasive diagnostic procedures, as intra-arterial WADA test (Wada and Rasmussen 1960; Rausch et al. 1993; Benbadis et al. 1998; Abou-khalil and Schlaggar 2002) or intraoperative electrocorticography (Penfield 1937; Cedzich et al. 1996;

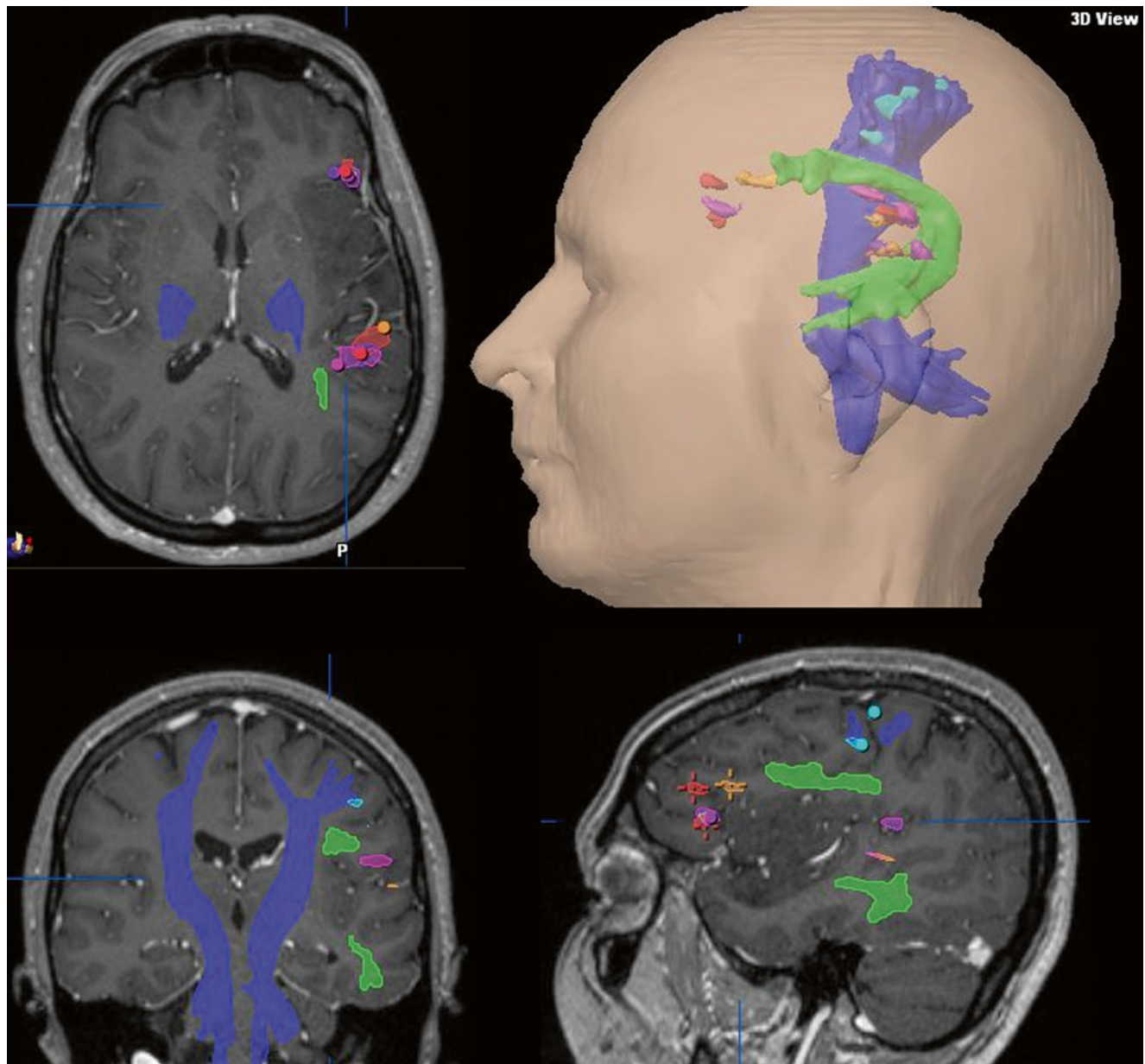


Fig. 3 Preoperative fMRI language mapping of the motor (Broca) and sensory (Wernicke) language areas and DTI tractographies of the arcuate fascicle (green) and pyramidal tract (purple) integrated into the T1-weighted post-contrast 3D MRI used for functional neuronavigation in a female patient with a symptomatic left astrocytoma involving the

inferior frontal and superior temporal lobes and the insula; transverse, coronal, and sagittal views, 3D surface view. fMRI revealed a left language dominance and a good spatial agreement between the functional localizations obtained with four different language paradigms for both essential language areas (Color figure online)

Duffau et al. 2002, 2003). Whether the embedding of fMRI and DTI in presurgical diagnostics can indeed reduce surgery-related morbidity and mortality should be investigated in prospective clinical trials (Zacharaki et al. 2012). Prerequisites are a consensus on measuring techniques, analysis procedures, and medical evaluation of clinical fMRI as well as the establishment of official recommendations and guidelines by the assigned medical association. As stated earlier, first attempts in that direction are underway.

5 Content Overview

Chapter 2 provides an easy, but in-depth, access to the techniques and underlying physiology of the abovementioned different *fMRI* and *DTI techniques* (Bandettini et al. 1992; Kwong et al. 1992; Ogawa et al. 1993; Basser et al. 1994; Purdon and Weisskoff 1998). The principles and basics of MRI, fMRI, and DTI, as well as the different established experimental designs for task-based fMRI, are presented

along with the options for specific data analysis. The resting-state fMRI technique is explained in detail and what methods can be implemented to study functional connectivity in different resting-state networks. Finally, diffusion tensor imaging and tractography are addressed (LeBihan and Johansen-Berg 2012). On a solid methodological basis, the capabilities to study structural connectivity and to employ presurgical tractography are demonstrated.

Chapter 3 extensively deals with the relevant morphological and functional *neuroanatomy* to facilitate the reader's access to presurgical fMRI and DTI. In addition to a detailed systematic description of the surface anatomy and cytoarchitecture of the human brain, important morphological criteria for a straightforward identification of different anatomical structures are discussed. Comprehensive information on the functional neuroanatomy of the motor and language systems is provided. Here, it cannot be sufficiently stressed that a profound knowledge of the relevant neuroanatomy is indispensable for a correct medical interpretation of clinical fMRI and DTI data. In any case, the *precentral knob* is the only reliable anatomical landmark for a functional area, namely, the motor hand representation (Yousry et al. 1997; Fesl et al. 2003). There are no morphological landmarks for areas related to cognitive brain functions such as language or memory (Ojemann et al. 1989; Ojemann 1991). Due to the vast physiological interindividual anatomical variability (Amunts et al. 1999, 2000) and the dependence on various individual factors, functional areas are traditionally mapped intraoperatively by means of electrophysiological methods (Penfield 1937, 1950; Woolsey et al. 1979; Ojemann et al. 1989; Ojemann 1991; Uematsu et al. 1992; Cedzich et al. 1996; Duffau et al. 1999). However, this information is preoperatively inaccessible, and the time needed for surgery is therefore significantly prolonged. fMRI and DTI, on the other hand, yield relevant diagnostic information on anatomy, pathology, and function prior to surgery in one single examination. Thus, the indication for presurgical fMRI and DTI results from:

- Clinical signs and symptoms
- The limitations of morphological imaging
- The necessity to measure and visualize normal, modified neuroplastic, and pathological (e.g., epileptic) brain activity

Chapter 4 covers *presurgical task-based BOLD fMRI*, which represents fMRI's best established, validated, and most widely used clinical application. Particular notice is given to practical and methodological-technical aspects (Sect. 3) as well as to specific requirements of fMRI diagnostics in patients with rolandic brain tumors (Sect. 4) or lesions with critical spatial relationship to language areas (Sect. 5). Diagnostic aims and selection criteria for patients are discussed, clinically tested examination protocols are proposed (Stippich et al. 1999, 2000, 2002b, 2003b, 2004, 2005, 2007; Stippich 2010), and their applications are illustrated with

example cases. Further, potentials and limits of presurgical task-based fMRI are depicted (Sect. 6).

Chapter 5 highlights the initial experience with *resting-state fMRI (RS-fMRI)* as a novel functional neuroimaging modality in the presurgical work-up of patients with brain tumors (Mitchell et al. 2013). Here, no stimulation or active cooperation of the patients is required to assess important functional systems, which is potentially of great value to further facilitate the clinical application of fMRI (Posse et al 2013). RS-fMRI provides additional information on the *connectivity* between different functionally important brain areas, which may be exploited in the future to study the effects of lesions, treatment, and medication on brain function (Niu et al 2014; Smucny et al. 2014; Otten et al. 2012; Martino et al. 2011). Such neuroplastic alterations in brain function may be compensatory or pathological in nature.

Chapter 6 refers to the highly specific application of presurgical fMRI in patients with *epilepsy* which requires fundamentally different data acquisition and processing techniques as compared to both task-based and resting-state fMRI, such as EEG-correlated fMRI for the localization of epileptogenic foci (Centeno and Carmichael 2014; Chiang et al. 2014). To this end, major technical and methodological problems had to be solved, which now enables us to use electrical devices (EEG) inside MR scanners to correct for interferences and related artifacts and thereby precisely detect and localize the sources of epileptic activity in the human brain. EEG-correlated fMRI is by no means a standard application (Pittau et al. 2014). It should be considered as a valuable additional investigation tool in the field of epilepsy imaging which is available in some leading medical centers worldwide.

Chapter 7 accounts for *DTI* and *DTT* with their proven value for functional brain tumor surgery with respect to both preoperative neuroimaging and intraoperative navigation (Potgieser et al. 2014; Shahar et al. 2014; Sternberg et al. 2014; Kuhnt et al. 2013a, b). In this setting, DTI is fully complementary to fMRI, by providing additional relevant information on the course and integrity of important white matter tracts in relation to a surgical target. Hence, these techniques should be applied in combination whenever possible. Specific attention is given to the corticospinal tract and sensorimotor system; the arcuate, uncinate, inferior fronto-occipital fascicles and language systems; as well as the superior longitudinal fascicle, optic radiation, and the visuospatial attention network.

Chapter 8 addresses the specific aspects of functional neuronavigation (Orringer et al. 2012; Risholm et al. 2011). With the help of the functional landmarks provided by fMRI and DTI, the spatial relationship between the brain tumor or epileptogenic zone, functional brain areas, and essential white matter tracts can be evaluated preoperatively, which facilitates the selection of the most cautious therapy.

Functional neuronavigation permits planning and implementation of radical and, at the same time, function-preserving operations. This goal is rarely achieved with morphological information alone, especially in the presence of brain malformations, anatomical variants, or a disturbed or destroyed anatomy due to tumor growth or pathology-related neuroplastic changes of brain function. Technical inaccuracies and corrections for brain shift due to intraoperative loss of cerebrospinal fluid and tissue removal have to be taken into account (Kuhnt et al. 2012a).

Chapter 9 is dedicated to the *validation* of presurgical fMRI and DTI with established reference procedures such as intraoperative electrocorticography (ECoG) or intra-arterial administration of barbiturates (Wada test) (Leclercq et al. 2011). For a thorough understanding of the topic, these reference procedures are presented in detail together with a repetition of the relevant methodological aspects and limitations of fMRI. Today, it can be assumed that presurgical task-based fMRI is a robust and valid tool to localize different representations of the human body in the primary motor and somatosensory cortices, to localize essential language centers—namely, Broca's and Wernicke's areas—and to lateralize the brain's dominant hemisphere for language function. There is also substantial evidence that DTT is reliable to visualize the pyramidal tract, the arcuate fascicle, the optic radiation, and other large white matter bundles both pre- and intraoperatively (Shahar et al. 2014). fMRI and DTI have the potential to help to reduce the number of invasive measures needed, to better select those patients who require such interventions, and to facilitate the planning and targeted intraoperative positioning of electrodes. If and to what extent a substitution of invasive measures may be appropriate is not fully clear, yet.

This topic is inherently related to Chap. 10 which provides the reader with an overview on *multimodal investigations* comparing fMRI to other methods of functional neuroimaging (Wehner 2013). These methods include multiparametric functional and structural MRI and MR spectroscopy (MRS), positron emission tomography (PET), and single positron emission computed tomography (SPECT)—the latter two techniques are from the domain of nuclear medicine that utilize radioactive substances/tracers and can be employed together with CT or MR scanners for hybrid imaging (Nensa et al. 2014)—just as the electrophysiological methods electroencephalography (EEG) and magnetoencephalography (MEG) that noninvasively measure electromagnetic fields as a direct correlate of neuronal (synaptic) activity with a very high temporal resolution (Grummich et al. 2006). These techniques are therefore not susceptible to hemodynamic or metabolic influencing factors.

Chapter 11 covers neuroplasticity from its definition to its implications for diagnosis, treatment, and prognosis in the clinical context from a neuroimaging's perspective (Niu et al. 2014; Tozakidou et al. 2013; Partovi et al. 2012). The measurable

neuroplastic changes are also discussed on the basis of the underlying pathophysiology down to the cellular and molecular levels. The current understanding of neuroplasticity imaging is condensed from an extensive literature research on patients with stroke, epilepsy, brain tumors, multiple sclerosis, and peripheral nervous system disorders used to interpret neuroplastic imaging findings. Clinical examples are provided with a focus on neuroplasticity of the motor system, which in turn is helpful to better understand phenomena that may be observed in preoperative functional neuroimaging. Clear and valuable considerations are provided for a practical imaging of neuroplasticity.

Chapter 12 accounts for pitfalls, drawbacks, and diagnostic errors in clinical BOLD fMRI and DTI. Important imaging artifacts, influencing factors of brain lesions and pharmaceutical effects on the measurable BOLD response and DTI data, are presented and discussed in detail. Practical suggestions to overcome these problems are provided for a successful application of presurgical diagnostic fMRI and DTI.

References

- Abou-Khalil B, Schlaggar BL (2002) Is it time to replace the Wada test? *Neurology* 59(2):160–161
- Amunts K, Schleicher A et al (1999) Broca's region revisited: cytoarchitecture and intersubject variability. *J Comp Neurol* 412(2):319–341
- Amunts K, Malikovic A et al (2000) Brodmann's areas 17 and 18 brought into stereotaxic space—where and how variable? *Neuroimage* 11(1):66–84
- Bandettini PA, Wong EC et al (1992) Time course EPI of human brain function during task activation. *Magn Reson Med* 25(2):390–397
- Basser PJ, Mattiello J, LeBihan D (1994) Estimation of the effective self-diffusion tensor from the NMR spin echo. *J Magn Reson B* 103(3):247–254
- Bauer MH, Kuhnt D et al (2013) Reconstruction of white matter tracts via repeated deterministic streamline tracking – initial experience. *PLoS One* 8(5):e63082. doi:[10.1371/journal.pone.0063082](https://doi.org/10.1371/journal.pone.0063082), Print 2013
- Baumann SB, Noll DC et al (1995) Comparison of functional magnetic resonance imaging with positron emission tomography and magnetoencephalography to identify the motor cortex in a patient with an arteriovenous malformation. *J Image Guid Surg* 1(4):191–197
- Baxendale S (2002) The role of functional MRI in the presurgical investigation of temporal lobe epilepsy patients: a clinical perspective and review. *J Clin Exp Neuropsychol* 24(5):664–676
- Belliveau JW, Kennedy DN Jr et al (1991) Functional mapping of the human visual cortex by magnetic resonance imaging. *Science* 254(5032):716–719
- Benbadis SR, Binder JR et al (1998) Is speech arrest during wada testing a valid method for determining hemispheric representation of language? *Brain Lang* 65(3):441–446
- Berger H (1929) Über das Elektroenzephalogramm des Menschen. *Arch Psychiatr Nerven* 87:527–570
- Bick AS, Mayer A, Levin N (2012) From research to clinical practice: implementation of functional magnetic imaging and white matter tractography in the clinical environment. *J Neurol Sci* 312(1–2):158–165. doi:[10.1016/j.jns.2011.07.040](https://doi.org/10.1016/j.jns.2011.07.040), Epub 2011 Aug 23
- Binder JR, Achten E et al (2002) Functional MRI in epilepsy. *Epilepsia* 43(Suppl 1):51–63
- Bittar RG, Olivier A et al (1999) Presurgical motor and somatosensory cortex mapping with functional magnetic resonance imaging and positron emission tomography. *J Neurosurg* 91(6):915–921

- Buckner RL, Bandettini PA et al (1996) Detection of cortical activation during averaged single trials of a cognitive task using functional magnetic resonance imaging. *Proc Natl Acad Sci U S A* 93(25): 14878–14883
- Cedzich C, Taniguchi M et al (1996) Somatosensory evoked potential phase reversal and direct motor cortex stimulation during surgery in and around the central region. *Neurosurgery* 38(5):962–970
- Centeno M, Carmichael DW (2014) Network connectivity in epilepsy: resting state fMRI and EEG-fMRI contributions. *Front Neurol* 5:93. doi:[10.3389/fneur.2014.00093](https://doi.org/10.3389/fneur.2014.00093), eCollection 2014
- Chiang S, Levin HS, Haneef Z (2014) Computer-automated focus lateralization of temporal lobe epilepsy using fMRI. *J Magn Reson Imaging*. doi:[10.1002/jmri.24696](https://doi.org/10.1002/jmri.24696)
- Dimou S, Battisti RA et al (2013) A systematic review of functional magnetic resonance imaging and diffusion tensor imaging modalities used in presurgical planning of brain tumour resection. *Neurosurg Rev* 36(2):205–214; discussion 214. doi:10.1007/s10143-012-0436-8, Epub 2012 Nov 29
- Cortez-Conradis D, Favila R et al (2013) Diagnostic performance of regional DTI-derived tensor metrics in glioblastoma multiforme: simultaneous evaluation of p, q, L, Cl, Cp, Cs, RA, RD, AD, mean diffusivity and fractional anisotropy. *Eur Radiol* 23(4):1112–1121. doi:[10.1007/s00330-012-2688-7](https://doi.org/10.1007/s00330-012-2688-7), Epub 2012 Oct 21
- Cox RW (1996) AFNI: software for analysis and visualization of functional magnetic resonance neuroimages. *Comput Biomed Res* 29(3):162–173
- Detre JA, Leigh JS et al (1992) Perfusion imaging. *Magn Reson Med* 23(1):37–45
- Dimou S, Battisti RA et al (2013b) A systematic review of functional magnetic resonance imaging and diffusion tensor imaging modalities used in presurgical planning of brain tumour resection. *Neurosurg Rev* 36(2):205–214. doi:[10.1007/s10143-012-0436-8](https://doi.org/10.1007/s10143-012-0436-8); discussion 214, Epub 2012 Nov 29
- Duffau H, Capelle L et al (1999) Intra-operative direct electrical stimulations of the central nervous system: the Salpetriere experience with 60 patients. *Acta Neurochir (Wien)* 141(11):1157–1167
- Duffau H, Capelle L et al (2002) Intraoperative mapping of the subcortical language pathways using direct stimulations. An anatomico-functional study. *Brain* 125(Pt 1):199–214
- Duffau H, Capelle L et al (2003) Usefulness of intraoperative electrical subcortical mapping during surgery for low-grade gliomas located within eloquent brain regions: functional results in a consecutive series of 103 patients. *J Neurosurg* 98(4):764–778
- Fernandez G, de Greiff A et al (2001) Language mapping in less than 15 minutes: real-time functional MRI during routine clinical investigation. *Neuroimage* 14(3):585–594
- Fesl G, Moriggl B et al (2003) Inferior central sulcus: variations of anatomy and function on the example of the motor tongue area. *Neuroimage* 20(1):601–610
- Fox PT, Raichle ME (1986) Focal physiological uncoupling of cerebral blood flow and oxidative metabolism during somatosensory stimulation in human subjects. *Proc Natl Acad Sci U S A* 83(4):1140–1144
- Fox PT, Mintun MA et al (1986) Mapping human visual cortex with positron emission tomography. *Nature* 323(6091):806–809
- Frahm J, Merboldt KD et al (1994) Brain or vein – oxygenation or flow? On signal physiology in functional MRI of human brain activation. *NMR Biomed* 7(1–2):45–53
- Friston K (1996) Statistical parametric mapping and other analyses of functional imaging data. In: John M, Toga AW (eds) *Brain mapping: the methods*. Academic Press, New York, pp 363–386
- Gaillard WD, Bookheimer SY, Cohen M (2000) The use of fMRI in neocortical epilepsy. *Adv Neurol* 84:391–404
- Gevins A (1995) High-resolution electroencephalographic studies of cognition. *Adv Neurol* 66:181–195; discussion 195–198
- Gevins A, Leong H et al (1995) Mapping cognitive brain function with modern high-resolution electroencephalography. *Trends Neurosci* 18(10):429–436
- Goa PE, Koopmans PJ et al (2014) BOLD fMRI signal characteristics of S1 and S2-SSFP at 7 Tesla. *Front Neurosci* 8:49. doi:[10.3389/fnins.2014.00049](https://doi.org/10.3389/fnins.2014.00049)
- Gold S, Christian B et al (1998) Functional MRI statistical software packages: a comparative analysis. *Hum Brain Mapp* 6(2):73–84
- Grabowski TJ (2000) Investigating language with functional neuroimaging. In: John M, Toga AW (eds) *Brain mapping: the systems*. Academic Press, San Diego, pp 425–461
- Grummich P, Nimsky C et al (2006) Combining fMRI and MEG increases the reliability of presurgical language localization: a clinical study on the difference between and congruence of both modalities. *Neuroimage* 32(4):1793–1803
- Hämäläinen M, Ilmoniemi RJ et al (1993) Magnetoencephalography -theory, instrumentation and applications to noninvasive studies of the working human brain. *Rev Mod Phys* 65:413–487
- Hari R, Ilmoniemi RJ (1986) Cerebral magnetic fields. *Crit Rev Biomed Eng* 14(2):93–126
- Hirsch J, Ruge MI et al (2000) An integrated functional magnetic resonance imaging procedure for preoperative mapping of cortical areas associated with tactile, motor, language, and visual functions. *Neurosurgery* 47(3):711–721; discussion 721–722
- Holman BL, Devous MD Sr (1992) Functional brain SPECT: the emergence of a powerful clinical method. *J Nucl Med* 33(10):1888–1904
- Holodny AI, Schulder M et al (1999) Decreased BOLD functional MR activation of the motor and sensory cortices adjacent to a glioblastoma multiforme: implications for image-guided neurosurgery. *AJNR Am J Neuroradiol* 20(4):609–612
- Holodny AI, Schulder M et al (2000) The effect of brain tumors on BOLD functional MR imaging activation in the adjacent motor cortex: implications for image-guided neurosurgery. *AJNR Am J Neuroradiol* 21(8):1415–1422
- Holodny AI, Schwartz TH et al (2001) Tumor involvement of the corticospinal tract: diffusion magnetic resonance tractography with intraoperative correlation. *J Neurosurg* 95(6):1082
- Holodny AI, Gor DM et al (2005) Diffusion-tensor MR tractography of somatotopic organization of corticospinal tracts in the internal capsule: initial anatomic results in contradistinction to prior reports. *Radiology* 234(3):649–653
- Hua J, Qin Q et al (2013) Whole-brain three-dimensional T2-weighted BOLD functional magnetic resonance imaging at 7 Tesla. *Magn Reson Med*. doi:[10.1002/mrm.25055](https://doi.org/10.1002/mrm.25055)
- Huber L, Goense J et al (2014) Investigation of the neurovascular coupling in positive and negative BOLD responses in human brain at 7T. *Neuroimage* 97:349–362
- Hulvershorn J, Bloy L et al (2005a) Spatial sensitivity and temporal response of spin echo and gradient echo bold contrast at 3 T using peak hemodynamic activation time. *Neuroimage* 24(1):216–223
- Hulvershorn J, Bloy L et al (2005b) Temporal resolving power of spin echo and gradient echo fMRI at 3T with apparent diffusion coefficient compartmentalization. *Hum Brain Mapp* 25(2):247–258
- Kallenber K, Goldmann T et al (2013) Glioma infiltration of the corpus callosum: early signs detected by DTI. *J Neurooncol* 112(2):217–222. doi:[10.1007/s11060-013-1049-y](https://doi.org/10.1007/s11060-013-1049-y), Epub 2013 Jan 24
- Kleiser R, Staempfli P et al (2010) Impact of fMRI-guided advanced DTI fiber tracking techniques on their clinical applications in patients with brain tumors. *Neuroradiology* 52(1):37–46. doi:[10.1007/s00234-009-0539-2](https://doi.org/10.1007/s00234-009-0539-2), Epub 2009 May 29
- Kober H, Nimsky C et al (2001) Correlation of sensorimotor activation with functional magnetic resonance imaging and magnetoencephalography in presurgical functional imaging: a spatial analysis. *Neuroimage* 14(5):1214–1228
- Krings T, Reinges MH et al (2001) Functional and diffusion-weighted magnetic resonance images of space-occupying lesions affecting the motor system: imaging the motor cortex and pyramidal tracts. *J Neurosurg* 95(5):816–824
- Krings T, Reinges MH et al (2002) Factors related to the magnitude of T2* MR signal changes during functional imaging. *Neuroradiology* 44(6):459–466

- Kuhnt D, Bauer MH, Nimsky C (2012a) Brain shift compensation and neurosurgical image fusion using intraoperative MRI: current status and future challenges. *Crit Rev Biomed Eng* 40(3):175–185
- Kuhnt D, Bauer MH et al (2012b) Intraoperative visualization of fiber tracking based reconstruction of language pathways in glioma surgery. *Neurosurgery* 70(4):911–919. doi:[10.1227/NEU.0b013e318237a807](https://doi.org/10.1227/NEU.0b013e318237a807); discussion 919–920
- Kuhnt D, Bauer MH et al (2013a) Optic radiation fiber tractography in glioma patients based on high angular resolution diffusion imaging with compressed sensing compared with diffusion tensor imaging – initial experience. *PLoS One* 8(7):e70973. doi:[10.1371/journal.pone.0070973](https://doi.org/10.1371/journal.pone.0070973), Print 2013
- Kuhnt D, Bauer MH et al (2013b) Functional imaging: where do we go from here? *J Neurosurg Sci* 57(1):1–11
- Kwong KK, Belliveau JW et al (1992) Dynamic magnetic resonance imaging of human brain activity during primary sensory stimulation. *Proc Natl Acad Sci U S A* 89(12):675–679
- Lang S, Duncan N, Northoff G (2014) Resting-state functional magnetic resonance imaging: review of neurosurgical applications. *Neurosurgery* 74(5):453–464. doi:[10.1227/NEU.0000000000000307](https://doi.org/10.1227/NEU.0000000000000307); discussion 464–465
- LeBihan D (2006) From Brownian motion to mind imaging: diffusion MRI. *Bull Acad Natl Med* 190(8):1605–1627; discussion 1627
- LeBihan D (2013) Apparent diffusion coefficient and beyond: what diffusion MR imaging can tell us about tissue structure. *Radiology* 268(2):318–322. doi:[10.1148/radiol.13130420](https://doi.org/10.1148/radiol.13130420)
- LeBihan D, Johansen-Berg H (2012) Diffusion MRI at 25: exploring brain tissue structure and function. *Neuroimage* 61(2):324–341. doi:[10.1016/j.neuroimage.2011.11.006](https://doi.org/10.1016/j.neuroimage.2011.11.006), Epub 2011 Nov 20
- LeBihan D, Mangin JF et al (2001) Diffusion tensor imaging: concepts and applications. *J Magn Reson Imaging* 13(4):534–546
- Leclercq D, Delmaire C et al (2011) Diffusion tractography: methods, validation and applications in patients with neurosurgical lesions. *Neurosurg Clin N Am* 22(2):253–268. doi:[10.1016/j.nec.2010.11.004](https://doi.org/10.1016/j.nec.2010.11.004), ix
- Lee CC, Ward HA et al (1999) Assessment of functional MR imaging in neurosurgical planning. *AJNR Am J Neuroradiol* 20(8):1511–1519
- Lee MH, Smyser CD, Shimony JS (2013) Resting-state fMRI: a review of methods and clinical applications. *AJNR Am J Neuroradiol* 34(10):1866–1872. doi:[10.3174/ajnr.A3263](https://doi.org/10.3174/ajnr.A3263), Epub 2012 Aug 30
- Logothetis NK (2002) The neural basis of the blood-oxygen-level-dependent functional magnetic resonance imaging signal. *Philos Trans R Soc Lond B Biol Sci* 357(1424):1003–1037
- Logothetis NK (2003) The underpinnings of the BOLD functional magnetic resonance imaging signal. *J Neurosci* 23(10):3963–3971
- Logothetis NK, Pfeuffer J (2004) On the nature of the BOLD fMRI contrast mechanism. *Magn Reson Imaging* 22(10):1517–1531
- Logothetis NK, Wandell BA (2004) Interpreting the BOLD signal. *Annu Rev Physiol* 66:735–769
- Logothetis NK, Pauls J et al (2001) Neurophysiological investigation of the basis of the fMRI signal. *Nature* 412(6843):150–157
- Martino J, Honma SM et al (2011) Resting functional connectivity in patients with brain tumors in eloquent areas. *Ann Neurol* 69(3):521–532. doi:[10.1002/ana.22167](https://doi.org/10.1002/ana.22167), Epub 2011 Mar 11
- Mazziotta JC, Phelps ME et al (1982) Tomographic mapping of human cerebral metabolism: auditory stimulation. *Neurology* 32(9):921–937
- Menon RS, Ogawa S et al (1995) BOLD based functional MRI at 4 Tesla includes a capillary bed contribution: echoplanar imaging correlates with previous optical imaging using intrinsic signals. *Magn Reson Med* 33(3):453–459
- Mitchell TJ, Hacker CD et al (2013) A novel data-driven approach to preoperative mapping of functional cortex using resting-state functional magnetic resonance imaging. *Neurosurgery* 73(6):969–982. doi:[10.1227/NEU.0000000000000141](https://doi.org/10.1227/NEU.0000000000000141); discussion 982–983
- Moller M, Freund M et al (2005) Real time fMRI: a tool for the routine presurgical localisation of the motor cortex. *Eur Radiol* 15(2):292–295
- Nensa F, Beiderwellen K et al (2014) Clinical applications of PET/MR: current status and future perspectives. *Diagn Interv Radiol*. doi:[10.5152/dir.14008](https://doi.org/10.5152/dir.14008) [Epub ahead of print]
- Nimsky C (2011) Intraoperative acquisition of fMRI and DTI. *Neurosurg Clin N Am* 22(2):269–277. doi:[10.1016/j.nec.2010.11.005](https://doi.org/10.1016/j.nec.2010.11.005), ix
- Niu C, Zhang M et al (2014) Motor network plasticity and low-frequency oscillations abnormalities in patients with brain gliomas: a functional MRI study. *PLoS One* 9(5):e96850. doi:[10.1371/journal.pone.0096850](https://doi.org/10.1371/journal.pone.0096850), eCollection 2014
- O'Donnell LJ, Rigolo L et al (2012) fMRI-DTI modeling via landmark distance atlases for prediction and detection of fiber tracts. *Neuroimage* 60(1):456–470. doi:[10.1016/j.neuroimage.2011.11.014](https://doi.org/10.1016/j.neuroimage.2011.11.014), Epub 2011 Dec 2
- Ogawa S, Lee TM et al (1990) Brain magnetic resonance imaging with contrast dependent on blood oxygenation. *Proc Natl Acad Sci U S A* 87(24):9868–9872
- Ogawa S, Tank DW et al (1992) Intrinsic signal changes accompanying sensory stimulation: functional brain mapping with magnetic resonance imaging. *Proc Natl Acad Sci U S A* 89(13):5951–5955
- Ogawa S, Menon RS et al (1993) Functional brain mapping by blood oxygenation level-dependent contrast magnetic resonance imaging. A comparison of signal characteristics with a biophysical model. *Biophys J* 64(3):803–812
- Ojemann GA (1991) Cortical organization of language. *J Neurosci* 11(8):2281–2287
- Ojemann G, Ojemann J et al (1989) Cortical language localization in left, dominant hemisphere. An electrical stimulation mapping investigation in 117 patients. *J Neurosurg* 71(3):316–326
- Orringer DA, Golby A, Jolesz F (2012) Neuronavigation in the surgical management of brain tumors: current and future trends. *Expert Rev Med Devices* 9(5):491–500. doi:[10.1586/erd.12.42](https://doi.org/10.1586/erd.12.42)
- Otten ML, Mikell CB et al (2012) Motor deficits correlate with resting state motor network connectivity in patients with brain tumours. *Brain* 135(Pt 4):1017–1026. doi:[10.1093/brain/aws041](https://doi.org/10.1093/brain/aws041), Epub 2012 Mar 8
- Partovi S, Jacobi B et al (2012) Clinical standardized fMRI reveals altered language lateralization in patients with brain tumor. *AJNR Am J Neuroradiol* 33(11):2151–2157. doi:[10.3174/ajnr.A3137](https://doi.org/10.3174/ajnr.A3137), Epub 2012 May 17
- Penfield W (1937) Somatic motor and sensory representation in the cerebral cortex of man as studied by electrical stimulation. *Brain* 60:389–443
- Penfield W (1950) The cerebral cortex of man. MacMillan, New York: 57 ff
- Pillai JJ (2010) The evolution of clinical functional imaging during the past 2 decades and its current impact on neurosurgical planning. *AJNR Am J Neuroradiol* 31(2):219–225. doi:[10.3174/ajnr.A1845](https://doi.org/10.3174/ajnr.A1845)
- Pittau F, Groullier F et al (2014) The role of functional neuroimaging in pre-surgical epilepsy evaluation. *Front Neurol* 5:31. doi:[10.3389/fneur.2014.00031](https://doi.org/10.3389/fneur.2014.00031), eCollection 2014
- Posse S, Ackley E et al (2013) High-speed real-time resting-state fMRI using multi-slab echo-volumar imaging. *Front Hum Neurosci* 7:479. doi:[10.3389/fnhum.2013.00479](https://doi.org/10.3389/fnhum.2013.00479), eCollection 2013
- Potgieser AR, Wagelmakers M et al (2014) The role of diffusion tensor imaging in brain tumor surgery: a review of the literature. *Clin Neurol Neurosurg* 124C:51–58. doi:[10.1016/j.clineuro.2014.06.009](https://doi.org/10.1016/j.clineuro.2014.06.009) [Epub ahead of print]
- Purdon PL, Weisskoff RM (1998) Effect of temporal autocorrelation due to physiological noise and stimulus paradigm on voxel-level false-positive rates in fMRI. *Hum Brain Mapp* 6:239–249
- Raichle ME (1983) Positron emission tomography. *Annu Rev Neurosci* 6:249–267
- Rausch R, Silfvenius H et al (1993) Intra-arterial amobarbital procedures. In: Engel JJ (ed) *Surgical treatment of the epilepsies*. Raven Press, New York, pp 341–357
- Reinges MH, Nguyen HH et al (2004) Course of brain shift during microsurgical resection of supratentorial cerebral lesions: limits of conventional neuronavigation. *Acta Neurochir (Wien)* 146(4):369–377; discussion 377

- Risholm P, Golby AJ, Wells W 3rd (2011) Multimodal image registration for preoperative planning and image-guided neurosurgical procedures. *Neurosurg Clin N Am* 22(2):197–206, viii. doi:[10.1016/j.nec.2010.12.001](https://doi.org/10.1016/j.nec.2010.12.001)
- Roberts TP (2003) Functional magnetic resonance imaging (fMRI) processing and analysis. ASNR Electronic Learning Center Syllabus 1–23
- Rutten GJ, Ramsey NF et al (2002) Development of a functional magnetic resonance imaging protocol for intraoperative localization of critical temporoparietal language areas. *Ann Neurol* 51(3):350–360
- Schreiber A, Hubbe U et al (2000) The influence of gliomas and non-gliial space-occupying lesions on blood-oxygen-level-dependent contrast enhancement. *AJNR Am J Neuroradiol* 21(6):1055–1063
- Shahar T, Rozovski U et al (2014) Preoperative imaging to predict intraoperative changes in tumor-to-corticospinal tract distance: an analysis of 45 cases using high-field intraoperative magnetic resonance imaging. *Neurosurgery* 75(1):23–30
- Shinoura N, Yamada R et al (2005) Preoperative fMRI, tractography and continuous task during awake surgery for maintenance of motor function following surgical resection of metastatic tumor spread to the primary motor area. *Minim Invasive Neurosurg* 48(2):85–90
- Smucny J, Wylie KP, Tregellas JR (2014) Functional magnetic resonance imaging of intrinsic brain networks for translational drug discovery. *Trends Pharmacol Sci.* doi:[10.1016/j.tips.2014.05.001](https://doi.org/10.1016/j.tips.2014.05.001) [Epub ahead of print]
- Stadlbauer A, Buchfelder M et al (2010) Fiber density mapping of gliomas: histopathologic evaluation of a diffusion-tensor imaging data processing method. *Radiology* 257(3):846–853. doi:[10.1148/radiol.10100343](https://doi.org/10.1148/radiol.10100343), Epub 2010 Sep 30
- Steger TR, Jackson EF (2004) Real-time motion detection of functional MRI data. *J Appl Clin Med Phys* 5(2):64–70
- Sternberg EJ, Lipton ML, Burns J (2014) Utility of diffusion tensor imaging in evaluation of the peritumoral region in patients with primary and metastatic brain tumors. *AJNR Am J Neuroradiol* 35(3):439–444. doi:[10.3174/ajnr.A3702](https://doi.org/10.3174/ajnr.A3702), Epub 2013 Sep 19
- Stippich C (2010) Presurgical functional magnetic resonance imaging. *Radiologe* 50(2):110–122
- Stippich C, Hofmann R et al (1999) Somatotopic mapping of the human primary somatosensory cortex by fully automated tactile stimulation using functional magnetic resonance imaging. *Neurosci Lett* 277(1):25–28
- Stippich C, Kapfer D et al (2000) Robust localization of the contralateral precentral gyrus in hemiparetic patients using the unimpaired ipsilateral hand: a clinical functional magnetic resonance imaging protocol. *Neurosci Lett* 285(2):155–159
- Stippich C, Heiland S et al (2002a) Functional magnetic resonance imaging: physiological background, technical aspects and prerequisites for clinical use. *Röfo* 174(1):43–49
- Stippich C, Ochmann H, Sartor K (2002b) Somatotopic mapping of the human primary sensorimotor cortex during motor imagery and motor execution by functional magnetic resonance imaging. *Neurosci Lett* 331(1):50–54
- Stippich C, Kress B et al (2003a) Preoperative functional magnetic resonance tomography (fMRI) in patients with rolandic brain tumors: indication, investigation strategy, possibilities and limitations of clinical application. *Röfo* 175(8):1042–1050
- Stippich C, Mohammed J et al (2003b) Robust localization and lateralization of human language function: an optimized clinical functional magnetic resonance imaging protocol. *Neurosci Lett* 346(1–2): 109–113
- Stippich C, Romanowski A et al (2004) Fully automated localization of the human primary somatosensory cortex in one minute by functional magnetic resonance imaging. *Neurosci Lett* 364(2): 90–93
- Stippich C, Romanowski A et al (2005) Time-efficient localization of the human secondary somatosensory cortex by functional magnetic resonance imaging. *Neurosci Lett* 381(3):264–268
- Stippich C, Rapps N et al (2007) Localizing and lateralizing language in patients with brain tumors: feasibility of routine preoperative functional MR imaging in 81 consecutive patients. *Radiology* 243(3):828–36.
- Sunaert S, Yousry TA (2001) Clinical applications of functional magnetic resonance imaging. *Neuroimaging Clin N Am* 11(2):221–236, viii
- Svolos P, Tsolaki E et al (2013) Investigating brain tumor differentiation with diffusion and perfusion metrics at 3T MRI using pattern recognition techniques. *Magn Reson Imaging* 31(9):1567–1577
- Thulborn KR (1998) A BOLD move for fMRI. *Nat Med* 4(2):155–156
- Thulborn KR (1999) Clinical rationale for very-high-field (3.0 Tesla) functional magnetic resonance imaging. *Top Magn Reson Imaging* 10(1):37–50
- Thulborn K (2006) Clinical functional magnetic resonance imaging. In: Haacke EM (ed) *Current protocols in magnetic resonance imaging*. Wiley, New York
- Thulborn KR, Davis D et al (1996) Clinical fMRI: implementation and experience. *Neuroimage* 4(3 Pt 3):S101–S107
- Towle VL, Khorasani L et al (2003) Noninvasive identification of human central sulcus: a comparison of gyral morphology, functional MRI, dipole localization, and direct cortical mapping. *Neuroimage* 19(3):684–697
- Tozakidou M, Wenz H et al (2013) Primary motor cortex activation and lateralization in patients with tumors of the central region. *Neuroimage Clin* 2:221–228. doi:[10.1016/j.nicl.2013.01.002](https://doi.org/10.1016/j.nicl.2013.01.002), eCollection 2013
- Tsougos I, Svolos P et al (2012) Differentiation of glioblastoma multiforme from metastatic brain tumor using proton magnetic resonance spectroscopy, diffusion and perfusion metrics at 3 T. *Cancer Imaging* 12:423–436. doi:[10.1102/1470-7330.2012.0038](https://doi.org/10.1102/1470-7330.2012.0038)
- Turner R, Le Bihan D et al (1991) Echo-planar time course MRI of cat brain oxygenation changes. *Magn Reson Med* 22(1):159–166
- Uematsu S, Lesser R et al (1992) Motor and sensory cortex in humans: topography studied with chronic subdural stimulation. *Neurosurgery* 31(1):59–71; discussion 71–72
- Ulmer JL, Hacein-Bey L et al (2004a) Lesion-induced pseudodominance at functional magnetic resonance imaging: implications for preoperative assessments. *Neurosurgery* 55(3):569–579; discussion 580–581
- Ulmer JL, Salvan CV et al (2004b) The role of diffusion tensor imaging in establishing the proximity of tumor borders to functional brain systems: implications for preoperative risk assessments and postoperative outcomes. *Technol Cancer Res Treat* 3(6):567–576
- Van Westen D, Skagerberg G et al (2005) Functional magnetic resonance imaging at 3T as a clinical tool in patients with intracranial tumors. *Acta Radiol* 46(6):599–609
- Wada J, Rasmussen T (1960) Intracarotid injection of sodium amytal for the lateralization of cerebral speech dominance. Experimental and clinical observations. *J Neurosurg* 17:266–282
- Wehner T (2013) The role of functional imaging in the tumor patient. *Epilepsia* 54(Suppl 9):44–49. doi:[10.1111/epi.12443](https://doi.org/10.1111/epi.12443)
- Weiskopf N, Veit R et al (2003) Physiological self-regulation of regional brain activity using real-time functional magnetic resonance imaging (fMRI): methodology and exemplary data. *Neuroimage* 19(3):577–586
- Wittek A, Kikinis R et al (2005) Brain shift computation using a fully nonlinear biomechanical model. *Med Image Comput Comput Assist Interv* 8(Pt 2):583–590
- Woolsey CN, Erickson TC, Gilson WE (1979) Localization in somatic sensory and motor areas of human cerebral cortex as determined by direct recording of evoked potentials and electrical stimulation. *J Neurosurg* 51(4):476–506
- Yousry TA, Schmid UD et al (1997) Localization of the motor hand area to a knob on the precentral gyrus. A new landmark. *Brain* 120(Pt 1):141–157
- Zacharaki EI, Morita N et al (2012) Survival analysis of patients with high-grade gliomas based on data mining of imaging variables. *AJNR Am J Neuroradiol* 33(6):1065–1071. doi:[10.3174/ajnr.A2939](https://doi.org/10.3174/ajnr.A2939), Epub 2012 Feb 9
- Zambreanu L, Wise RG et al (2005) A role for the brainstem in central sensitisation in humans. Evidence from functional magnetic resonance imaging. *Pain* 114(3):397–407

Revealing Brain Activity and White Matter Structure Using Functional and Diffusion-Weighted Magnetic Resonance Imaging

Rainer Goebel

Contents

| | | |
|-----|--|----|
| 1 | Physical Principles of MRI | 14 |
| 1.1 | Spin Excitation and Signal Reception..... | 15 |
| 1.2 | Image Reconstruction | 18 |
| 2 | Physiological Principles of fMRI | 21 |
| 2.1 | Neurovascular Coupling..... | 21 |
| 2.2 | The BOLD Effect..... | 22 |
| 2.3 | The BOLD Hemodynamic Response..... | 22 |
| 2.4 | Limits of Spatial and Temporal Resolution | 24 |
| 3 | FMRI Data Analysis | 24 |
| 3.1 | Block- and Event-Related Designs | 25 |
| 3.2 | Basic Analysis Steps | 27 |
| 3.3 | Statistical Analysis of Functional Data..... | 31 |
| 3.4 | Integration of Anatomical and Functional Data..... | 44 |
| 3.5 | Group Analysis of Functional Data Sets..... | 45 |
| 3.6 | Selected Advanced Data Analysis Methods | 49 |
| 4 | Functional Connectivity and Resting-State Networks | 51 |
| 4.1 | Functional and Effective Connectivity..... | 51 |
| 4.2 | Resting-State Networks..... | 51 |
| 5 | Diffusion-Weighted MRI and Tractography | 53 |
| 5.1 | Diffusion Tensor Imaging | 53 |
| 5.2 | Validation and Improvements | 55 |
| 5.3 | Applications | 55 |
| | References | 57 |

Abstracts

Magnetic resonance imaging (MRI) is based on the magnetic *excitation* of body tissue and the reception of returned electromagnetic signals from the body. Excitation induces phase-locked *precession* of protons with a frequency proportional to the strength of the surrounding magnetic field as described by the *Larmor equation*. This fact can be exploited for *spatial encoding* by applying magnetic field *gradients* along spatial dimensions on top of the strong static magnetic field of the scanner. The obtained frequency-encoded information for each slice is accumulated in two-dimensional *k space*. The *k* space data can be transformed into *image space* by *Fourier analysis*.

Functional MRI (fMRI) allows *localizing brain function* since increased local neuronal activity leads to a surprisingly strong increase in local blood flow, which itself results in measurable increases in local magnetic field homogeneity. Increased local blood flow delivers chemical energy (glucose and oxygen) to the neurons. The temporary increase and decrease of local blood flow, triggered by increased neuronal activity, is called the *hemodynamic response* starting 2–4 s after stimulus onset. Increased local blood flow results in an *oversupply of oxygenated hemoglobin* in the vicinity of increased neuronal activity. The oversupply flushes *deoxygenated hemoglobin* from the capillaries and the downstream venules. Deoxygenated hemoglobin is paramagnetic reducing the homogeneity of the local magnetic field resulting in a weaker MRI signal than would be measurable without it. Oxygenated hemoglobin is diamagnetic and does not strongly reduce field homogeneity. Since the increased local blood flow replaces deoxygenated hemoglobin with oxygenated hemoglobin, local field homogeneity increases, leading to a stronger MRI signal as compared to a nonactivated state. Measured functional brain images thus reflect neuronal activity changes as blood oxygenation level-dependent (*BOLD*) contrast.

Functional images are acquired using the fast *echo-planar imaging* (EPI) pulse sequence allowing acquisition of a 64×64 image matrix in less than 100 ms. To sample

R. Goebel
Department of Cognitive Neuroscience, Maastricht University,
Oxfordlaan 55, 6229 EV Maastricht, The Netherlands
e-mail: r.goebel@maastrichtuniversity.nl

signal changes over time, a set of slices typically covering the whole brain is *measured repeatedly*. Activation of neurons results in a BOLD signal increase of only about 1–5 % and lie buried within strong physical and physiological noise fluctuations of similar size. Proper *preprocessing* steps, including 3D motion correction and removal of drifts, reduce the effect of artifacts increasing the *signal-to-noise ratio* (SNR). In order to reliably *detect* stimulus-related effects, proper *statistical data analysis* is performed. In order to *estimate* response profiles, condition-related time course episodes may be averaged in various *regions-of-interest* (ROIs). The core statistical tool in fMRI data analysis is the *general linear model* (GLM) that allows the analysis of *blocked* and *event-related experimental designs*. To run a GLM, a *design matrix* (model) has to be constructed containing reference functions (*predictors*, model time courses) for all effects of interest (conditions) as well as confounds. The GLM fits the created model to the data independently for each voxel's data (time course) providing a set of beta values estimating the effects of each condition. These beta values are compared with each other using *contrasts* resulting in a statistical value at each voxel. The statistical values of all voxels form a three-dimensional *statistical map*. To protect against wrongly declaring voxels as significant, statistical maps are *thresholded* properly by taking into account the *multiple comparison problem*. This problem is caused by the large number of independently performed statistical tests (one for each voxel).

In recent years, *parallel imaging techniques* have been developed, which allow acquiring MRI data simultaneously with two or more receiver coils. Parallel imaging can be used to increase temporal or spatial resolution. It also helps to reduce EPI imaging artifacts, such as geometrical distortions and signal dropouts in regions of different neighboring tissue types.

MRI has not only revolutionized functional brain imaging targeting gray matter neuronal activity but also enabled insights into the human white matter structure using diffusion-weighted magnetic resonance imaging. With proper measurement and modeling schemes including diffusion tensor imaging (DTI), major long-range fiber tracts can be reconstructed using computational tractography providing important information to guide neurosurgical procedures potentially reducing the risk of lesioning important fiber tracts.

Since its invention in the early 1990s, functional magnetic resonance imaging (fMRI) has rapidly assumed a leading role among the techniques used to localize brain activity. The spatial and temporal resolution provided by state-of-the-art MR technology and its non-invasive character, which allows multiple studies of the same subject, are some of the main advantages of fMRI over the other functional neuroimaging

techniques that are based on changes in blood flow and cortical metabolism (e.g., positron-emission tomography, PET). fMRI is based on the discovery of Ogawa et al. (1990), that *magnetic resonance imaging* (MRI, also called nuclear magnetic resonance imaging) can be used in a way that allows obtaining signals depending on the level of blood oxygenation. The measured signal is therefore also called “BOLD” signal (BOLD=blood oxygenation level-dependent). Since locally increased neuronal activity leads to increased local blood flow, which again changes local blood oxygenation, fMRI allows indirect measurements of neuronal activity changes. With appropriate data analysis and visualization methods, these BOLD measurements allow drawing conclusions about the localization and dynamics of brain function.

This chapter describes the basic principles and methodology of functional and diffusion-weighted MRI. After a description of the physical principles of MRI at a conceptual level, the physiology of the blood oxygenation level-dependent (BOLD) contrast mechanism is described. The subsequent, major part of the chapter provides an introduction to the current strategies of statistical image analysis techniques with a focus on the analysis of single-subject data because of its relevance for pre-surgical mapping of human brain function. This is followed by a description of functional connectivity focusing on the analysis of resting state fMRI data. Finally, principles of diffusion-weighted MRI measurements are described including diffusion tensor imaging, which is the most common acquisition and modeling approach in clinical MRI.

1 Physical Principles of MRI

Magnetic resonance imaging allows visualizing both anatomical and functional data of the human brain. This section shortly describes the main concepts of the physical principles of MRI. More detailed descriptions of the physical basis of MRI are available in several introductory texts, for example, Huettel et al. (2004), Bandettini et al. (2000), Brown and Semelka (1999), NessAiver (1997), and Schild (1990).

A typical whole-body MR scanner has a hollow bore (tube) about 1 m across. Inside of that bore a cylinder is placed containing the primary magnet producing a very strong *static, homogeneous magnetic field* (B_0). Today, nearly all scanners create the magnetic field with superconducting electromagnets whose wires are cooled by cryogens (e.g., liquid helium). Most standard clinical scanners used to image the human brain possess a magnetic field strength of 1.5 T, which is 30,000 times the strength of the Earth's magnetic field (1 T = 10,000 G). In recent years, installation of tomographs with 3.0 T has become common in major hospitals and research centers. In a few research labs, the human brain is imaged at ultrahigh fields such as 7 and 9.4 T. At higher field strengths it gets increasingly difficult to create a homogenous magnetic field, which is necessary for accurate spatial

decoding of the raw measurement data. Since homogenous fields are easier to create for scanners with small bores, scanners with higher magnetic fields (10–20 T) are currently only available for animal use. Besides the main magnet, additional coils are located inside the cylinder including shimming coils, gradient coils, and a radio frequency (RF) coil. The shimming coils are used to shape the magnetic field increasing its homogeneity. The gradient coils are used to temporarily change the magnetic field linearly along any direction which is essential for spatial localization (see below). The RF coil is used to send radio frequency pulses into the subject.

In a typical brain scanning session, a subject or patient in supine position is slowly moved into the scanner bore using a maneuverable table. Scanning of anatomical and functional images is managed from a terminal in a control room by specifying slice positions and by running appropriate MRI *pulse sequences*. The control room usually has a window behind the computer terminal, which allows looking into the scanner room. Before the subject is moved into the scanner, the head is placed in a small replaceable coil, called the *head coil*. This coil surrounds the head and is used to send radio frequency pulses into the subject as well as to receive electromagnetic echoes. When receive-only head coils are used, the radio frequency pulses are provided by the RF coil in the cylinder of the scanner. The head coil is an example of a *volume coil*, which is designed such that the sensitive volume (e.g., brain) experiences a fairly uniform RF field. Surface coils are receive-only RF coils that are placed directly upon the surface of the anatomy to be imaged. They provide very high signal-to-noise in their immediate vicinity, but recorded images suffer from extreme nonuniformity because the obtained signal intensity drops rapidly with distance and approaches zero about one coil diameter away from the coil. Phased array coils

are an attempt to combine the positive properties of volume and surface coils by combining images from two or more surface coils to produce a single image (see Sect. 1.2.6).

The physical principles of MRI are the same for anatomical and functional imaging. What makes functional imaging special is described in Sect. 2. The operation of MRI can be described in two major themes. The first theme refers to the excitation and recording of electromagnetic signals reflecting the properties of the measured object. The second theme refers to the construction of two- and three-dimensional images reflecting how the measured object properties vary across space.

1.1 Spin Excitation and Signal Reception

Magnetic resonance imaging is based on the magnetic excitation of body tissue and the recording of returned electromagnetic signals from the body. All nuclei with an odd number of protons are magnetically excitable. The atom of choice for MRI is ^1H , the most common isotope of hydrogen having a nucleus with only one proton. Hydrogen protons are ideally suited for MRI because they are abundant in human tissue and possess particularly favorable magnetic properties. Water is the largest source of protons in the body followed by fat. Protons have magnetic properties because they possess a *spin*: they rotate like a spin top around their own axes inducing a small directed magnetic field. In a normal environment, the magnetic fields of the spins in the human body are oriented randomly and, thus, cancel each other out. If, however, the body of a subject is placed in the strong static magnetic field of a MRI tomography (called \mathbf{B}_0), the spins orient themselves in line with that field, either parallel or antiparallel (Fig. 1). Since a slightly larger proportion of spins aligns parallel to the

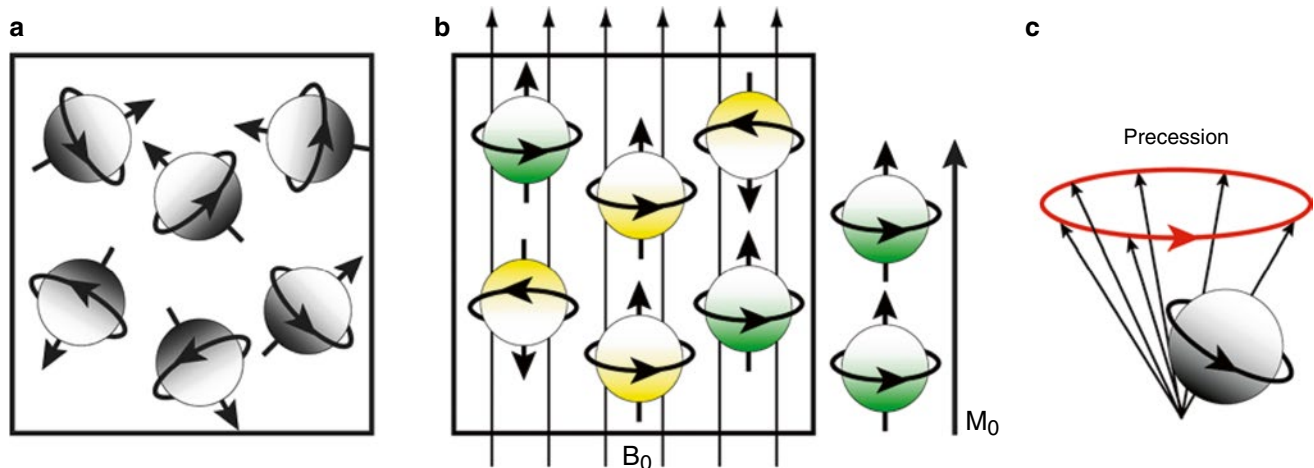


Fig. 1 Spinning protons are little magnets because of the spin property. (a) Without an external magnetic field, the directions of the spins are randomly distributed. (b) When placed within a large magnetic field, the spins align either with the field (parallel) or against the field (antiparallel). A slight excess of spins aligns with the external magnetic

field resulting in a net magnetic field parallel to the external magnetic field. (c) A spin is actually not aligning its axis of rotation with the external magnetic field as shown in (a) and (b) but rotates around the direction of the field. This motion is called precession

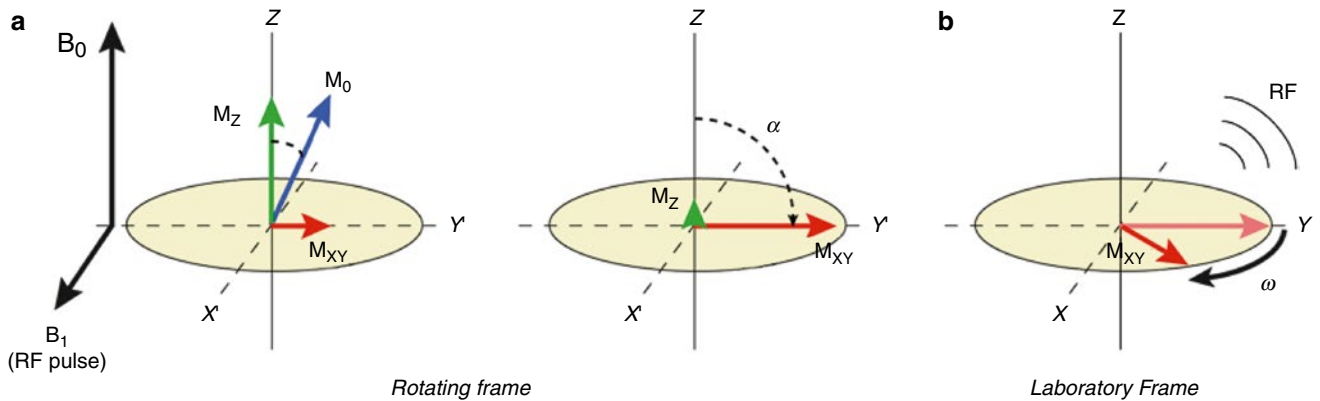


Fig. 2 Spins in the lower energy state can be excited by an electromagnetic pulse at the resonance frequency ω_0 forcing the spins absorbing the transmitted energy to precess in phase. (a) As an effect of excitation, the net magnetic field M_0 (blue vector) smoothly tips down toward the x - y plane. The longitudinal component M_z (green vector) decreases over time while the transverse component M_{xy} (red vector)

scanner magnetic field, the body gets magnetized. The excess number of spins aligned with the external magnetic field is proportional to the strength of the external magnetic field and is in the order of 10^{15} spins at 1.5 T in a $2 \times 2 \times 2$ mm volume of water. The total magnetic field of the excess spins is called M_0 . Just as a spinning top wobbles about its axis, the spinning protons wobble, or *precess*, about the axis of the external B_0 field (Fig. 1c). The precession frequency of the protons depends on the strength of the surrounding magnetic field. More precisely, the precession frequency ω is directly proportional to the strength of the external magnetic field and is defined by the *Larmor equation*:

$$\omega_0 = \gamma B_0$$

The symbol ω_0 is known as the precessional, Larmor, or *resonance* frequency. The symbol γ refers to the *gyromagnetic ratio*, which is a constant unique to every atom. For hydrogen protons, $\gamma=42.56$ MHz per Tesla. At the magnetic field strength of a 3 T scanner, the precession frequency of hydrogen protons is thus 128 MHz.

If an applied electromagnetic pulse has the same frequency as the proton's precession frequency, then the protons get "excited" by absorbing the transmitted energy. This important principle is called *resonance* and gives the method "magnetic resonance imaging" its name. Since the precession frequency is in the range of radio frequency waves, the applied electromagnetic pulse is also called a radio frequency (RF) pulse. As an effect of excitation, spins flip from the parallel (lower-energy) state to the antiparallel (higher-energy) state. The RF pulse furthermore lets the excited protons precess *in phase*. As a result, the magnetization vector M_0 moves down toward the x - y plane (Fig. 2). The x - y plane is perpendicular to the static magnetic field and is also referred to as the *transverse plane*. The angle, α , of rotation

increases. This view assumes that the observer is moving with the precessing protons (rotating frame of reference). (b) Viewed from outside (laboratory frame of reference), the net magnetization vector rotates with angular velocity ω_0 given by the Larmor equation. The rotating magnetic field in the x - y plane emits radiofrequency waves, which can be measured by a receiver coil

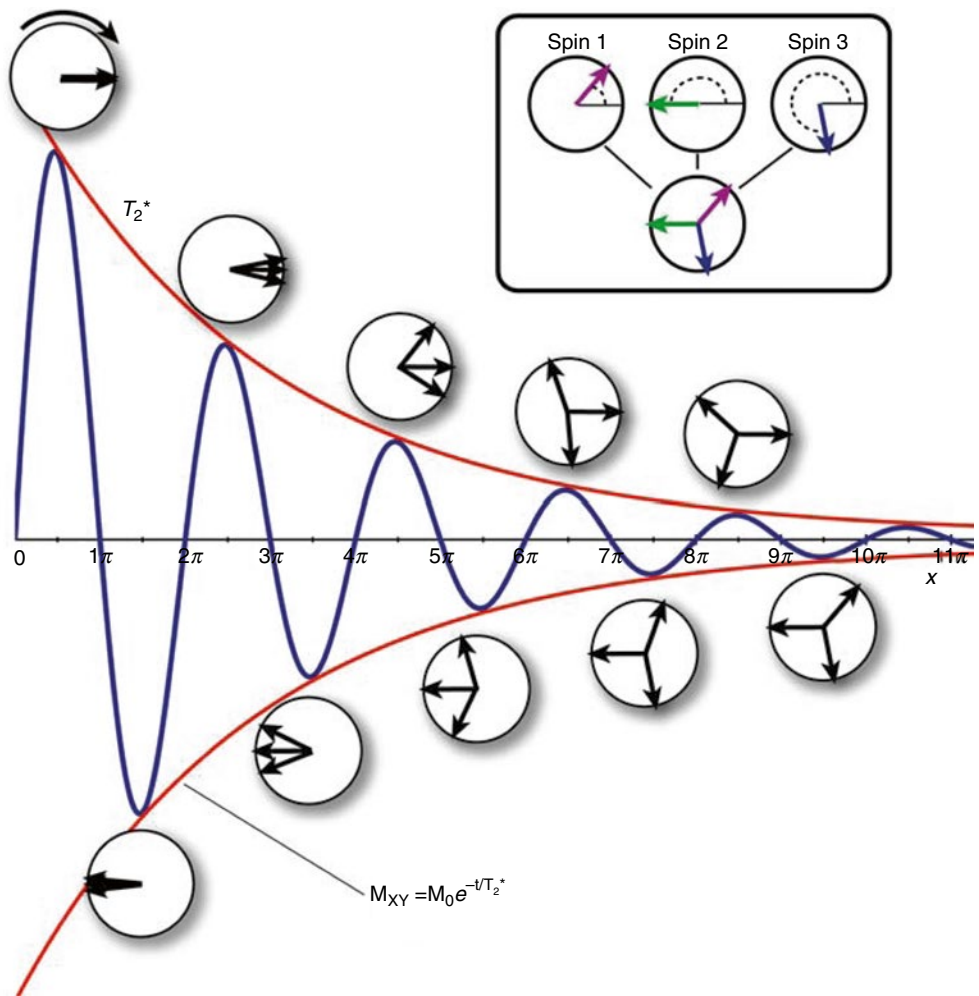
toward the x - y plane is a function of the strength and duration of the RF pulse. If $\alpha=90^\circ$, the magnetization vector is completely moved into the x - y plane with an equal amount of spins aligned parallel and antiparallel (Fig. 2b). Since the protons precess in phase, that is, they point in the same direction within the x - y plane, the magnetic fields of the spins add up to form a net magnetic field M_{xy} in the x - y plane. This *transversal component* of the rotating electromagnetic field can be measured (received) in the receiver coil (antenna) because it induces a detectable current flow.

The established inphase precession is, however, not stable after the RF transmitter is turned off. Because of interactions between the magnetic fields of the protons, the transverse magnetization decays within a few tenth of milliseconds. These spin-spin interactions lead to slightly different local magnetic field strengths and, thus, to slightly different precession frequencies leading to phase shifts between the precessing spins (*dephasing*). The dephasing process is also called *transversal relaxation*. It progresses initially rapidly but slows down over time following an exponential function with time constant T_2 with values in the range of 30–150 ms. Due to magnetic field inhomogeneities in the static magnetic field and in physiological tissue, the spins get out of phase actually faster than T_2 , and therefore the measured raw signal in the receiver coil, the *free induction decay* (FID), decays with a shorter time constant T_2^* (Fig. 3):

$$M_{xy} = M_0 e^{-t/T_2^*}$$

The fact that local field inhomogeneities lead to different precession frequencies increasing the speed of dephasing is an important observation for functional MRI because local field inhomogeneities also depend on the local physiological state, especially the state of local blood oxygenation, which

Fig. 3 The signal amplitude (red curve) of the measured raw MR signal, the free induction decay (*FID*), decays exponentially with time constant T_2^* . The raw signal itself is oscillating at the resonance frequency (blue curve). The signal is lost due to dephasing as indicated by the phase coherency plots (circles) with three representative, superimposed spins (see inset). The amplitude of the signal at any moment in time is determined by the sum of the spin vectors. When the spins are all in phase (left side), the maximum signal is obtained, that is, the vector sum equals \mathbf{M}_0 . When the spins are completely out of phase (right side), the signal is completely lost, that is, the sum of the spin vectors equals zero



itself depends on the state of local neuronal activity. Measurements of changing local magnetic field inhomogeneities (T_2^* parameter), thus, provide indirect measurements of local neuronal activity.

The speed of spin dephasing is determined by random effects as well as by fixed effects due to magnetic field inhomogeneities. The dephasing effect of constant magnetic field inhomogeneities can be reversed by the application of a 180° RF pulse. A time duration of $t = \tau$ is allowed to elapse while the spins go out of phase. Then a 180° RF pulse is applied flipping the dephased spin vectors about the X' or Y' axis in the rotating frame of reference. As an effect of the pulse, the order of the spins is reversed (Fig. 4). At the *echo time* $TE = 2\tau$, the vectors are back in phase producing a large signal, the *spin echo*. This process is similar to a race situation in which participants run with different (but constant) speed. At time τ they get a signal ("180° pulse") to turn around and go back; assuming they continue in the same speed, they will all arrive at the starting line at the same time (2τ).

The amplitude of the obtained spin echo will be smaller than the amplitude during the FID because part of the signal

is inevitably lost due to random spin-spin interactions (T_2 decay). As soon as the spins are all back in phase at the echo time, they immediately start to go out of phase again. An additional 180° RF pulse will generate a second echo (Fig. 4). This process can be continued as long as enough signal is available. By setting the time of the 180° pulse, the amplitude of the T_2 signal can, thus, be assessed at any moment in time.

Besides dephasing, the spins reorient themselves with the direction of the strong static magnetic field of the scanner since the excited spins slowly go back into low-energy state realigning with the external magnetic field. This reorientation process is called *longitudinal relaxation* and progresses slower as the dephasing process. The increase (recovery) of the longitudinal component \mathbf{M}_z follows an exponential function with time constant T_1 with values in the range 300–2,000 ms:

$$\mathbf{M}_z = \mathbf{M}_0 (1 - e^{-t/T_1})$$

Note that the absorbed RF energy is not only released in a way that it can be detected outside the body as RF waves but part of the energy is given to the surrounding tissue, called the *lattice*.

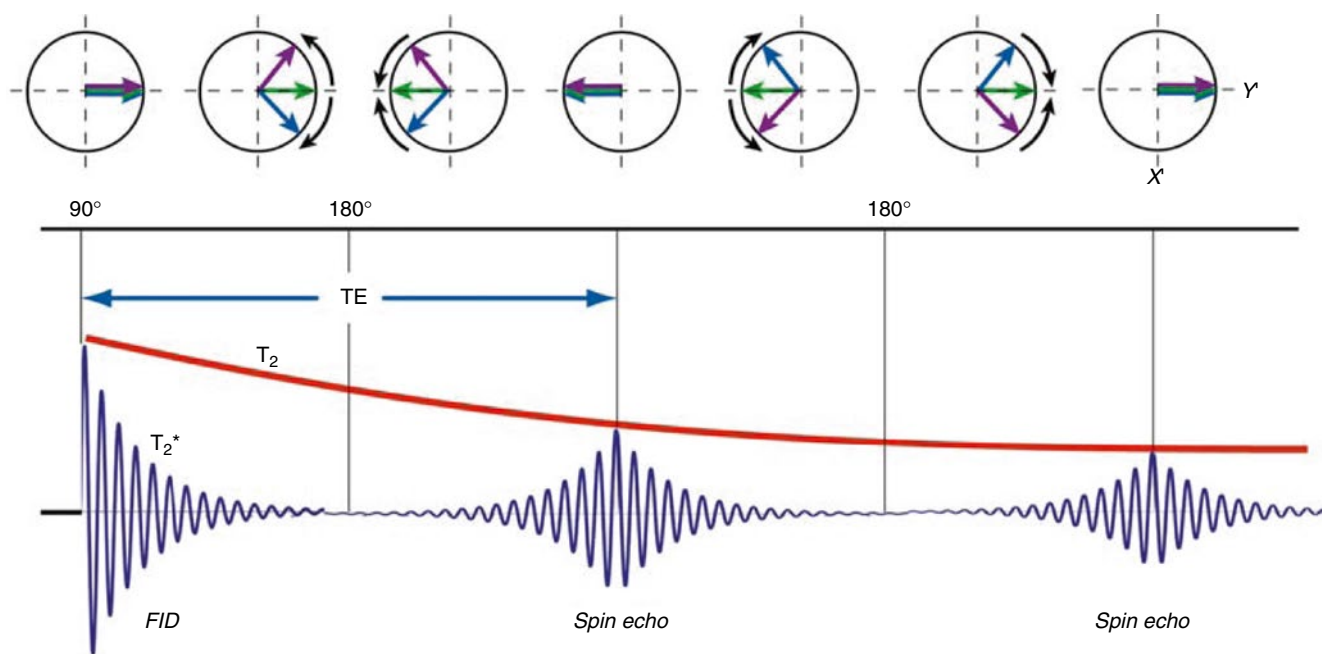


Fig. 4 The effect of constant magnetic field inhomogeneities can be reversed by application of a 180° RF pulse, which flips the dephased vectors about the X' axis. This is indicated in the upper row with three spin vectors, one precessing at the resonance frequency (green vector), one precessing slightly faster (violet vector), and one precessing slightly slower (blue vector) leading to dephasing. The 180° RF pulse reverses the order of the spins but not the direction of rotation. The

faster spin now runs behind catching up over time, while the slower spin runs ahead slowly falling back. At time TE (echo time), the vectors are back in phase producing a large signal, the spin echo. A second 180° RF pulse will generate a second echo (right side). The maximum amplitude of the echoes gets smaller over time because signal is inevitably lost due to random spin-spin interactions (T_2 decay, red curve)

The spin-lattice interactions determine the speed of T_1 recovery, which is unique to every tissue. Tissue-specific T_1 and T_2 values enable MRI to differentiate between different types of tissue when using properly designed MRI pulse sequences.

1.2 Image Reconstruction

The described principles of magnetic resonance do not explain how one can obtain images of the brain. This requires attributing components of the signal to those positions in space from which they originated. Although not identical for all measurement sequences, the principles for localizing signal sources typically contain the combined application of three fundamental techniques: *selective excitation of a slice*, *frequency encoding*, and *phase encoding*. Each of these steps allows localizing the source of the signal with respect to one spatial dimension. Paul C. Lauterbur and Peter Mansfield were awarded the 2003 Nobel Prize in Medicine for their discovery that *magnetic field gradients* can be used for spatial encoding. The gradient coils of the MRI scanner allow adding a magnetic field to the static magnetic field, which causes the field strength to vary linearly with distance from the center of the magnet. According to the Larmor equation, spins on one side are exposed to a higher magnetic field and

precess faster while spins on the other side are exposed to a lower magnetic field and precess slower than spins in the center (Fig. 5b).

1.2.1 Selective Slice Excitation

A magnetic field gradient is used to select a slice of the imaged object (*slice selection gradient*). Since spins precess with different frequencies along a gradient, protons can be excited selectively: An applied electromagnetic pulse of a certain frequency band will excite only those protons along the gradient precessing at the same frequency band. Spins outside that range will precess at different frequencies and will, thus, not absorb the transmitted RF energy. The selectively excited protons are located in a slice oriented perpendicular to the gradient direction. A gradient along the z -axis will result in an axial slice, a gradient along the x -axis in a sagittal slice, and a gradient along the y -axis in a coronal slice. Oblique slices can be obtained by applying two or three gradients simultaneously. The position and thickness of the selected slice depend on the slope of the applied gradient and the frequency band of the applied RF pulse. After selective slice excitation, the measured echo will be restricted to a compound signal from the excited protons within the slice. For subsequent spatial encoding, the slice selection gradient is turned off.

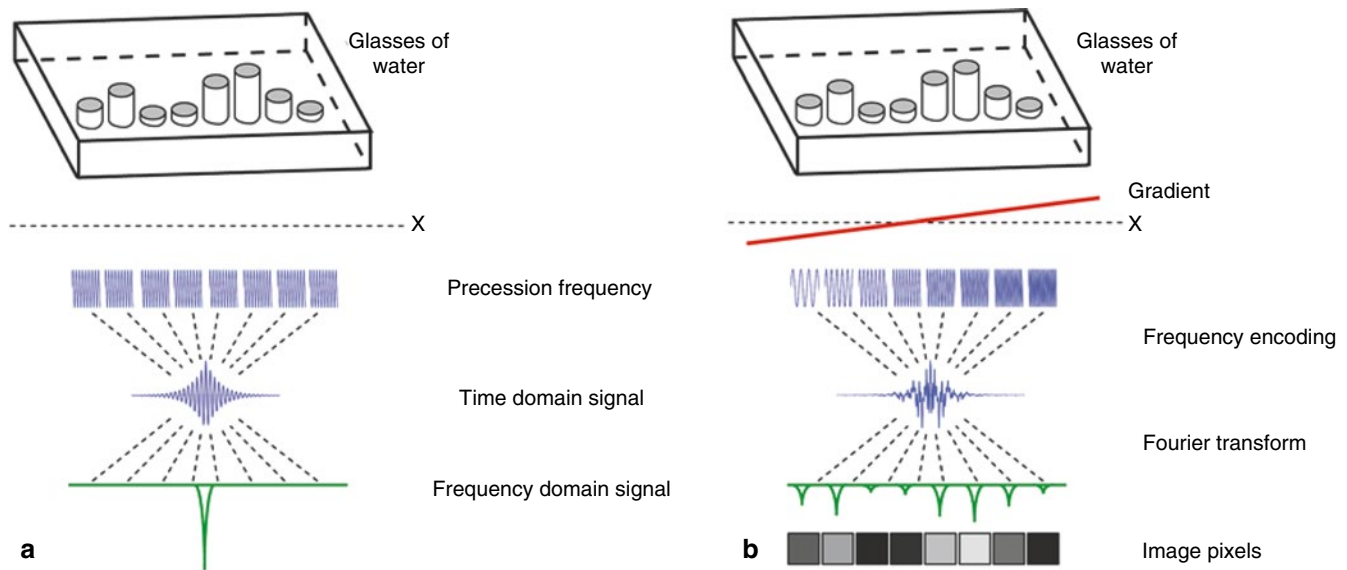


Fig. 5 Assume that eight glasses with different amounts of water are placed in the MRI scanner along the x -axis and that a single, thick slice containing all glasses has been excited. (a) In the absence of any gradients, all of the excited protons from all glasses are spinning at the same frequency. The received signal also oscillates at that frequency and its amplitude reflects the sum of excited water protons of all glasses. Since all protons precess at the same frequency, the Fourier transform cannot be used to identify signals from different spatial positions along the x -axis. (b) If a gradient is applied in the x direction, the spins will

precess at frequencies that depend upon their position along the gradient. Spatial information is now frequency encoded: The strength of the signal at each frequency is directly related to the number of excited protons from the respective glass of water. The obtained composite time-domain signal is the sum of these frequencies. The Fourier transform can now be used to determine the strength of the signal at each frequency. Since frequencies encode different spatial positions, an “image” of eight pixels can be formed. The gray values of these pixels reflect the relative amount of water in the different glasses

1.2.2 Frequency Encoding

While receiving the signal (FID or echo) from the excited slice, a magnetic field gradient can be applied along one of the two remaining spatial dimensions. This second gradient, running along one dimension of the excited slice, is called *frequency-encoding gradient*. Note that this gradient is not used to selectively excite protons but to encode a spatial dimension for those protons already excited in the slice. Due to the applied gradient, the protons within the slice precess with different frequencies along the respective dimension allowing differentiating spatial positions in the received signal (Fig. 5). The frequency-encoding gradient is also called *readout gradient* since it is tuned on during reception of the signal from the protons. The strength of the signal at each frequency is directly related to the strength of the signal at the encoded spatial position. The measured composite time-domain signal consists of the sum of all frequency responses. The Fourier transform (FT) can be used to get from the composite signal the strength of the signal at each frequency (amplitude and phase information). Since space has been frequency encoded, the FT provides the strength of the signal at different spatial positions. The obtained frequency-specific information can thus be used to form a spatial image (Fig. 5b). In such an image, the gray level is used to represent the strength of the signal at each picture element (pixel).

1.2.3 Phase Encoding

A further encoding step is required in order to be able to also separate signal components originating from different positions along the second dimension in the imaging plane. This is achieved by briefly adding another gradient to the static magnetic field oriented along the remaining (third) spatial dimension before receiving an echo. This third magnetic field gradient is called *phase-encoding gradient*. While the frequency-encoding gradient is turned on during reception of the signal, the phase-encoding (PE) gradient is *turned off* just before receiving the echo and is, thus, not (permanently) changing the frequency at different spatial positions. This is necessary since frequency-encoding gradients in two dimensions would result in ambiguous spatial encoding in a similar way as the same number (e.g., 6) can be obtained in many different ways by the sum of two numbers (e.g., $2+4$, $3+3$, $5+1$). Prior to readout, the brief duration of the phase-encoding gradient results in a short moment of different precession frequencies within each row of the slice. After turning off the phase-encoding gradient, the protons within each row precess again with the same frequency but they will now precess with a systematic *phase shift* along the positions within each row. The amount of phase shift depends on the position of a proton along the encoded second image dimension. Through proper combination of frequency encoding in one dimension and phase encoding in the other dimension,

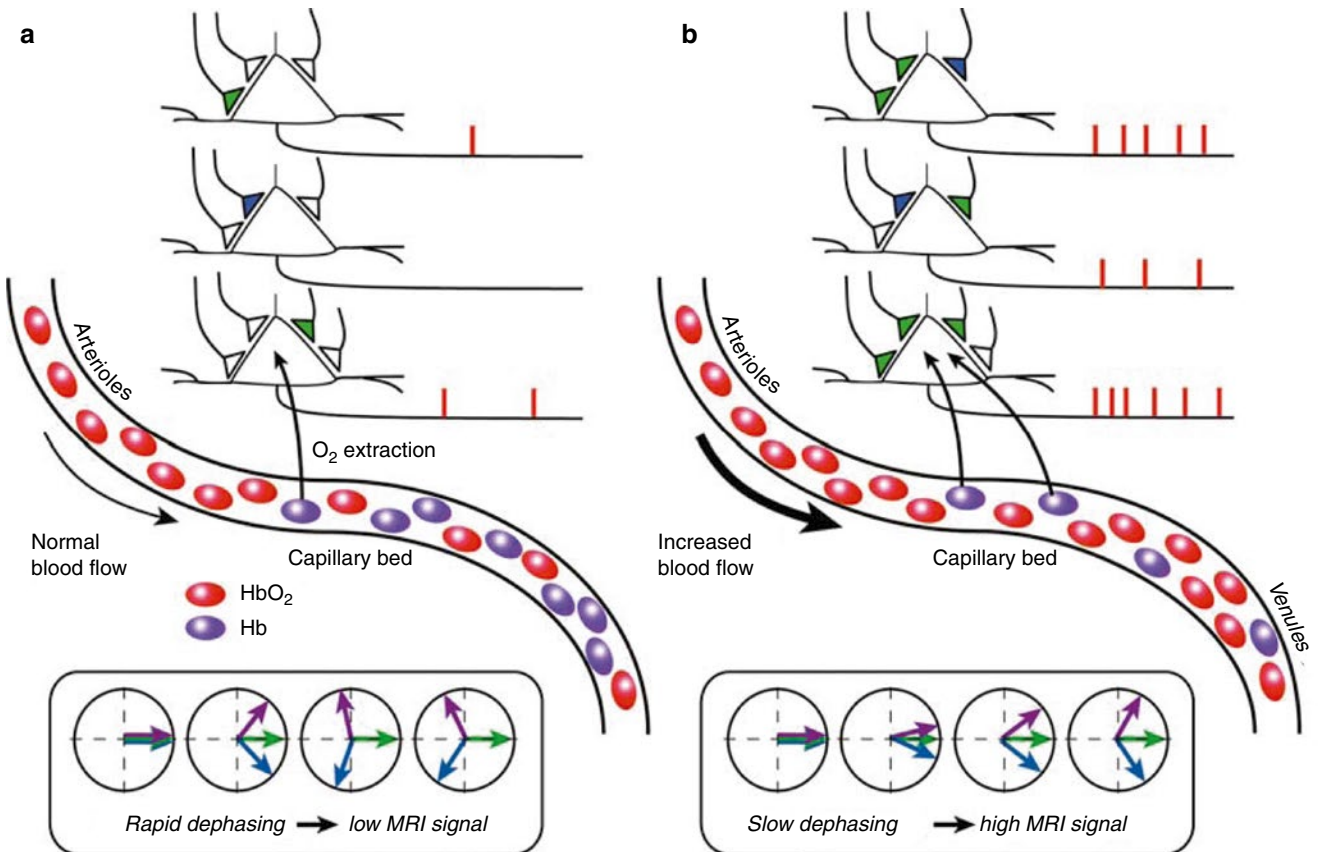


Fig. 6 From neural activity to BOLD MRI responses. (a) If a cortical region is in baseline mode, neural activity – including synaptic signal integration and spike generation – is low (upper part). Cerebral blood flow (CBF) is at a basal level. A constant oxygen extraction rate fueling neural activity leads to a fixed deoxygenated hemoglobin (Hb) to oxygenated hemoglobin (HbO_2) ratio in the capillary bed and venules. Since Hb is paramagnetic, it distorts the magnetic field. The Hb-related magnetic field inhomogeneities lead to rapid dephasing of excited spins

resulting in a low MRI signal level (lower part). (b) If the cortical region is in activated state, synaptic signal integration and spiking activity increases, leading to an increased oxygen extraction rate (upper part). CBF strongly increases delivering oxygen beyond local need, which essentially flushes Hb away from the capillary bed (middle part). Since HbO_2 does not substantially distort the homogeneity of the local magnetic field, excited spins dephase slower than in the baseline state (lower part) resulting in an enhanced MRI signal (BOLD effect)

all positions within a 2D image can be uniquely encoded with a desired resolution. Unfortunately a single application of the phase-encoding gradient is not sufficient to encode the second image dimension. The process of excitation and phase encoding must be repeated many times for a single slice. At each repetition, the strength of the phase-encoding gradient is slightly changed in order to ultimately obtain a complete frequency x phase encoding of the slice.

1.2.4 Two-Dimensional k Space

The data obtained from a series of excitation – recording cycles – can be arranged in a two-dimensional space called k space. Each row of k space corresponds to the data of one excitation – recording cycle with a different phase-encoding step. As described above, the echo signal of one line in k space contains a frequency-encoded representation of one dimension of the selected slice. While the slice selection and frequency-encoding gradients are the same from cycle to cycle, the slope of the phase-encoding gradient is changed by

a constant value across cycles and, thus, from line to line in k space. The imposed phase shift for a specific proton depends on the strength of the phase-encoding gradient and on the proton's position along the second image dimension. A series of phase-encoding steps “fills” k space in such a way that the second slice dimension ultimately also gets frequency encoded. The k space thus contains two-dimensional frequency-encoded information of the slice, which can be transformed into two-dimensional *image space* by application of the two-dimensional Fourier transform (2D FT).

1.2.5 Echo-Planar Imaging

The described procedure is applied for each slice of a scanned volume. A properly specified series of electromagnetic pulses allowing to construct one or more 2D images from electromagnetic echoes is called an *MRI pulse sequence*. The most often-used sequence for functional MRI is *gradient-echo echo-planar imaging* (GE-EPI). This sequence enables very rapid imaging of a slice by performing all phase-encoding

steps after a single 90° excitation pulse. This sequence requires switching the readout gradient rapidly on and off to fill k space line by line resulting in a series of (e.g., 64) small *gradient echoes* within the duration of a single T_2^* decay. A complete image can thus be obtained in about 50–100 ms as opposed to several seconds with standard (functional) imaging sequences. GE-EPI is very sensitive to field inhomogeneities influencing the speed of dephasing (T_2^* contrast). This is essential for functional imaging (see below) but also produces image distortions called susceptibility artifacts, which occur especially at tissue boundaries. Running EPI sequences requires a high-performance (i.e., expensive) gradient system to enable very rapid gradient switching.

1.2.6 Parallel Imaging and Parallel Excitation

In the last 15 years, *parallel imaging* (e.g., Pruessmann et al. 1999) has become a standard technique that has been introduced with different names by scanner manufacturers such as “SENSE,” “IPAT,” or “SMASH.” The basic idea of parallel imaging is the simultaneous acquisition of MRI data with at least two (typically 32 or more) receiver coils, each having a different spatial sensitivity. During image reconstruction, complementary information from the different receiver coils can be combined to fill k space in parallel reducing the number of time-consuming phase-encoding steps. Besides appropriate coils (phased array coils), parallel imaging requires that MRI scanners are equipped with multiple processing channels operating in parallel. Note that parallel imaging may be used either to increase temporal resolution when using a standard matrix size or to increase spatial resolution using a larger matrix with a conventional image acquisition time. Using parallel imaging to reduce scan time without sacrificing image quality is especially relevant for patient scans. Furthermore, parallel imaging may also reduce GE-EPI imaging artifacts because it allows acquiring standard image matrices with shorter echo times; typical EPI artifacts, such as signal dropouts in regions of neighboring tissue types and geometrical distortions, increase with increasing echo times.

In recent years, *parallel excitation* techniques are gaining increasing interest that work by exciting more than one slice in parallel: If, for example, eight slices are excited simultaneously, a whole-brain scan with 64 slices would be completed in the same time as eight nonsimultaneously recorded slices. In order to enable such powerful “multiband” techniques, an advanced excitation hardware (multiple transmit channels) is needed that is not yet standard on most MRI scanners. Furthermore, special MRI pulse sequences are needed (Moeller et al. 2010; Setsompop et al. 2012). Since multiple slices are acquired truly in parallel, imaging time is substantially reduced as compared to standard single-slice excitation techniques. This is especially beneficial for real-time fMRI neurofeedback studies (e.g., Goebel et al. 2010) since more time points (albeit temporally correlated)

can help to calculate more stable feedback values in a given time window. Note, however, that the data received from multiple slices need to be separated which becomes increasingly difficult with an increasing number of simultaneously excited slices. In order to avoid loss in image quality, the multiband factor (number of simultaneously excited slices) used for neuroscience applications is currently rather low, that is, in the range of 2–4.

2 Physiological Principles of fMRI

Neuronal activity consumes energy, which is produced by chemical processes requiring glucose and oxygen. The vascular system supplies these substances by a complex network of large and small vessels. The arterial part of the vascular system transports oxygenated blood through an increasingly fine-grained network of blood vessels until it reaches the capillary bed where the chemically stored energy (oxygen) is transferred to the neurons. If the brain is in resting state, 30–40 % of the oxygen is extracted from the blood in the capillary bed. The venous system transports the less-oxygenated blood away from the capillary bed. Oxygen is transported in the blood via the hemoglobin molecule. If hemoglobin carries oxygen, it is called oxygenated hemoglobin (HbO_2), while it is called deoxygenated hemoglobin (Hb) when it is devoid of oxygen. While the arterial network contains almost only oxygenated hemoglobin, the capillary bed and the venous network contain a mixture of oxygenated and deoxygenated hemoglobin.

2.1 Neurovascular Coupling

A local increase of neuronal activity immediately leads to an increased oxygen extraction rate in the capillary bed and, thus, in an increase in the relative concentration of deoxygenated hemoglobin. This fast response to increased neuronal activity is described as the “initial dip” (Fig. 7). After a short time of about 3 s, the increased local neuronal activity also leads to a strong increase in local blood flow. This response of the vascular system to the increased energy demand is called the *hemodynamic response*. Recent studies indicate that synaptic signal integration (measured by the local field potential, LFP) is a better predictor of the strength of the hemodynamic response than spiking activity (Logothetis et al. 2001; Mathiesen et al. 2000). It thus seems likely that the hemodynamic response primarily reflects the input and local processing of neuronal information rather than the output signals (Logothetis and Wandell 2004). Note that it is not yet completely known how the neurons “inform” the vascular system about their increased energy demand. Important theories about this *neurovascular coupling* are described, among many others, by Fox et al. (1988), Buxton

et al. (1998), and Magistretti et al. (1999). It appears likely that astrocytes play an important role because these special glial cells are massively connected with both neurons and the vascular system. The hemodynamic response consists in increased local cerebral blood flow (CBF) as well as increased cerebral blood volume (CBV), probably as a mechanical consequence of increased blood flow. The hemodynamic response not only compensates quickly for the slightly increased oxygen extraction rate but it is so strong that it results in a substantial local *oversupply* of oxygenated hemoglobin (Figs. 6 and 7). Note that it is not yet clear why the vascular system responds with a much stronger increase in cerebral blood flow than appears to be necessary. The increased CBV may help to explain the poststimulus undershoot (Fig. 7) observed in typical fMRI responses (balloon model, Buxton et al. 1998). While CBF and oxygen extraction rate may quickly return to baseline, the elastic properties of the dilated venules will require many seconds until baseline size is reached. In the expanded space of the dilated vessels, more deoxygenated hemoglo-

bin will accumulate reducing the MRI signal below the pre-stimulus baseline level.

2.2 The BOLD Effect

The most common method of functional MRI is based on the BOLD effect (Ogawa et al. 1990). This exploits the fact that oxygenated hemoglobin has different magnetic properties than deoxygenated hemoglobin. More specifically, while oxygenated hemoglobin is diamagnetic, deoxygenated hemoglobin is paramagnetic altering the local magnetic susceptibility, creating magnetic field distortions within and around the blood vessels in the capillary bed and venules. During the hemodynamic response (oversupply phase), the oxygenated to deoxygenated hemoglobin ratio increases resulting in a more homogeneous local magnetic field. As follows from the description in Sect. 1, excited spins dephase slower in a more homogeneous magnetic field leading to a stronger measured MRI signal in the activated state when compared to a resting state (Fig. 6). The BOLD effect, thus, measures increased neuronal activity indirectly via a change in local magnetic field (in)homogeneity, which is caused by an oversupply of oxygenated blood (Fig. 6). Note that these field inhomogeneities are only detectable with MRI because of the different magnetic properties of oxy- and deoxygenated hemoglobin. The change in the local HbO_2/Hb ratio and its associated change in magnetic field homogeneity, thus, acts as an endogenous marker of neural activity.

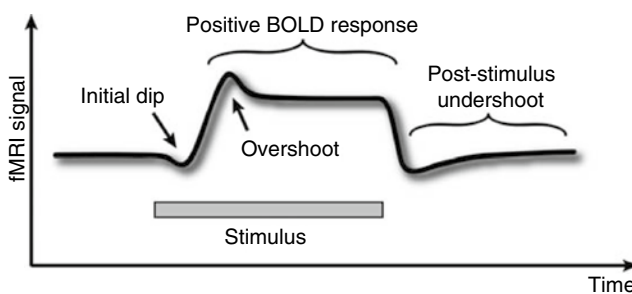


Fig. 7 Idealized time course of the hemodynamic response following a long (about 20 s) stimulation event. The theoretically expected initial dip is not reliably measured in human fMRI studies. For long stimulation events, the signal rises initially to a higher value (overshoot) than the subsequently reached plateau. When the stimulus is turned off, the signal often falls below the baseline signal level (undershoot), which is then approached slowly

2.3 The BOLD Hemodynamic Response

The time course of evoked fMRI signals, reflecting the BOLD hemodynamic response, is well studied for the primary visual cortex (V1). After application of a short visual stimulus of 100 ms, the observed (positive) signal response

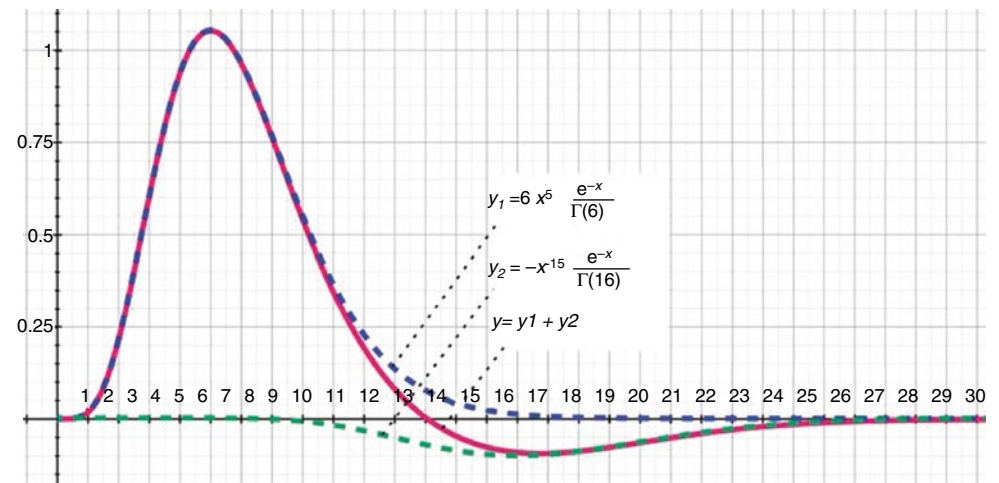


Fig. 8 The two gamma function allows to model typical hemodynamic impulse responses. One gamma function models the peak (τ) and dispersion (σ) of the positive BOLD response, while the second gamma function models the peak and dispersion of the undershoot response. Parameter A scales the amplitudes of the individual gamma functions

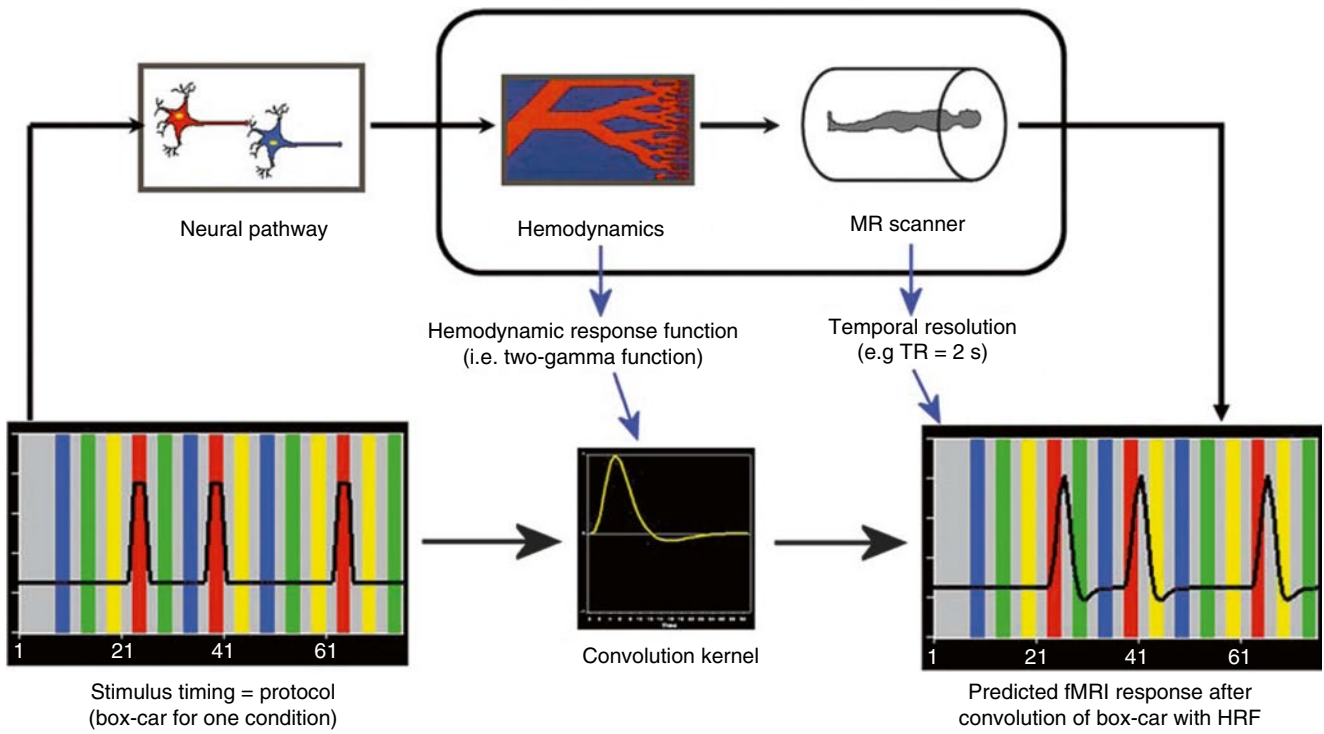


Fig. 9 Calculation of expected fMRI signal response for one condition of a protocol using convolution. The calculated response depends on the chosen model for the BOLD hemodynamic response function (HRF), for example, two gamma function (middle part). The expected

response is obtained by convolution of the box-car time course (left) with the chosen HRF. The convolved time course is downsampled to the temporal resolution (sampling intervals) of the fMRI measurements given by the volume TR value (right)

starts to rise after 2–3 s (oversupply phase) and reaches a maximum level after 5–6 s. About 10 s later, the signal reaches again the baseline level. As compared to the neuronal response of about 100 ms duration, the corresponding fMRI response is characterized by a delayed, gradual response profile extending as long as 20 s. Despite this sluggish response, the latency of response onsets appear to reflect quite precisely neuronal onset times (Menon and Kim 1999): If the left and right visual field are stimulated sequentially with a stimulus onset asynchrony of only 100 ms, response profiles from the right and left primary visual cortex are systematically shifted according to the applied temporal offset. More generally, the fMRI signal may reflect the flow of information processing across different brain areas as a sequence of shifted response profiles. Estimates of the temporal resolution with respect to onset delays are more in the order of hundreds of milliseconds than in the order of seconds (Formisano and Goebel 2003).

Assuming a linear time invariant (LTI) system, one can predict the expected time course of arbitrary long stimulation periods from the known response to a short stimulus. The response to a very short stimulus is called the *impulse response function* or, in the context of fMRI, the *BOLD hemodynamic response function* (HRF). The output (expected fMRI response) of an LTI system is the *convolution* of the input time course (e.g., stimulation “box-car”

time course) with the system’s response to an impulse function (Fig. 9). For primary visual cortex (V1), Boynton et al. (1996) showed that the measured responses to stimuli with varying amplitudes and durations could be indeed predicted well from the response profile obtained from a short visual stimulus. A well-suited function to model the hemodynamic impulse function is the probability density function (pdf) of the gamma distribution scaled by parameter A :

$$y(x; A, \tau, \sigma) = Ax^{\tau/\sigma-1} \frac{e^{-x/\sigma}}{\sigma^{\tau/\sigma} \Gamma(\tau/\sigma)}$$

Parameters τ and σ define the onset and dispersion of the response peak, respectively. While Boynton et al. (1996) used a single gamma function to characterize the impulse response function, the sum of two gamma functions (Friston et al. 1998) allows to also capture the undershoot usually observed in fMRI responses. The first gamma function typically peaks 5 s after stimulus onset ($\tau=6$), while the second gamma function peaks 15 s after stimulus onset ($\tau=16$, see Fig. 8). After convolution of a stimulus time course with the impulse function (Fig. 9), the calculated time course can be directly used as a reference function for statistical data analysis (see Sect. 3.3).

Note that the linear system assumption is reasonably valid only for stimuli of sufficiently long duration. For a series of

short stimuli separated by intervals shorter than 2–4 s, non-linear interaction effects have to be expected (e.g., Robson et al. 1998). Note further that the calculation (convolution) of expected time courses requires as input the valid specification of the time course of assumed neuronal response profiles, which is often not simply a copy of stimulus timing. A simple box-car time course, for example, assumes that neurons in a stimulated cortical area are active with constant amplitude in prolonged “on” periods. It is, however, well known that this assumption is too simplistic for neurons in early sensory areas. For higher cortical areas, for example, frontal areas involved in working memory, the neuronal response profile might differ substantially with respect to stimulus timing. Assuming that neuronal responses are correctly specified, it appears reasonable to use the same hemodynamic response function for all brain regions to predict expected BOLD signal time courses since neurovascular coupling should be similar in different brain areas. In case that it is difficult to specify proper input response profiles, a more general approach should be used (e.g., deconvolution analysis; see Sect. 3.3).

While fMRI responses clearly reflect the oversupply phase of the hemodynamic response, the theoretically expected initial dip (Fig. 7) has not been reliably detected in standard human fMRI measurements (for animal studies, see, e.g., Kim et al. 2000). This component of the idealized hemodynamic response is thus not included in the standard single or two gamma convolution kernels (Fig. 8). Data analysis of almost all fMRI studies is therefore based on the signals coming from the much stronger and sustained positive BOLD response.

2.4 Limits of Spatial and Temporal Resolution

The ultimate spatial and temporal resolution of fMRI is not primarily limited by technical constraints but by properties of the vascular system. The spatial resolution of the vascular system, and hence fMRI, seems to be in the order of 0.5–1 mm since relevant blood vessels run vertically through the cortex in roughly that distance (Duvernoy et al. 1981). An achievable resolution of 0.5–1 mm might be just enough to resolve *cortical columns*. A cortical column contains thousands of neurons possessing similar response specificity. A conventional brain area, such as the fusiform face area, could contain a set of cortical columns, each coding a different basic (e.g., face) feature. Cortical columns could, thus, form the basic building blocks (“alphabet”) of complex representations (Fujita et al. 1992). Since neurons within a column code for roughly the same feature, measuring the brain at the level of cortical columns promises to provide a relevant level for describing brain functioning. In cat visual cortex,

for example, orientation columns could be measured with fMRI at ultrahigh magnetic fields (4 and 9 T, Kim et al. 2000). The observed pattern of active orientation columns systematically changed when showing cats gratings of different orientations. Using ultrahigh magnetic fields (e.g., 7 T), columnar resolution appears to be within reach also for human brain imaging (e.g., Cheng et al. 2001; Yacoub et al. 2008; Zimmermann et al. 2011).

Despite the sluggishness of the fMRI signal, it has been shown that the obtained responses may reflect timing information with very high temporal precision. The signal of the left and right visual cortex, for example, reliably reflects temporal differences between stimulation of the left and right visual field as short as 100 ms (Menon and Kim 1999). When properly taking care of different hemodynamic delays in different brain areas, the analysis of BOLD onset latencies may also be very useful in revealing the sequential order of activity across brain areas within trials of complex cognitive tasks (fMRI mental chronometry, e.g., Formisano and Goebel 2003). In order to measure the brain with a temporal resolution in the order of milliseconds, other methods such as electroencephalography (EEG) and magnetoencephalography (MEG) must be used. If one succeeds in performing a proper combined analysis of EEG/MEG and fMRI data (Scherg et al. 1999; Dale and Halgren 2001; Bledowski et al. 2006), it becomes possible to describe brain function both with respect to its topographic distribution as well as with respect to its precise timing. While EEG/MEG data and fMRI data are conventionally obtained in different sessions, it has become possible to measure EEG data directly during fMRI recording sessions (e.g., Mulert et al. 2004).

3 FMRI Data Analysis

A major goal of functional MRI measurements is the localization of the neural correlates of sensory, motor, and cognitive processes. Another major goal of fMRI studies is the detailed characterization of the response profile for known regions-of-interest (ROIs) across experimental conditions. In this context, the aim of conducted studies is often not to map new functional brain regions (whole-brain analysis) but to characterize further how known specialized brain areas respond to (subtle) differences in experimental conditions (ROI-based analysis). Furthermore, it is often of interest to estimate the shape of the response and how it varies across different conditions and brain areas. Inspection of the shape of (averaged) time courses may also help to separate signal fluctuations due to measurement artifacts from stimulus-related hemodynamic responses. In order to obtain fMRI data with relatively high temporal resolution, functional time series are acquired using fast MR sequences sensitive to BOLD contrast. As described above most fMRI experiments

use the gradient echo EPI sequence, which allows acquisition of a 64×64 matrix in 50–100 ms. A typical functional scan of the whole brain with 20–40 slices lasts only 1–2 s on state-of-the-art MRI scanners. The data obtained from scanning all slices once at different positions (e.g., 30 slices covering the whole brain) is subsequently referred to as a *functional volume* or a *functional 3D image*. The measurement of an uninterrupted series of functional volumes is referred to as a *run*. A run, thus, consists of the repeated measurement of a functional volume and, hence, the repeated measurement of the individual slices. The sampling interval – the time until the same brain region is measured again – is called *volume TR*. The volume TR specifies the temporal resolution of the functional measurements since all slices comprising one functional volume are obtained once during that time. Note, however, that the slices of a functional volume are not recorded simultaneously, which implies that data from different regions of the brain are recorded at different moments in time (see “Slice Scan Time Correction” in Sect. 3.2). During a functional experiment, a subject performs tasks typically involving several experimental conditions. A short experiment can be completed in a single run, which typically consists of 100–1,000 functional volumes. Assuming a run with 500 volumes each consisting of 30 slices of 64×64 pixels and that two bytes are needed to store each pixel, the amount of raw data acquired per run would be $500 \times 30 \times 64 \times 64 \times 2 = 122,880,000$ bytes or roughly 117 MB. In more complex experiments, a subject typically performs multiple runs in one scanning session resulting in about 500 MB of functional data per subject per session. Using fast parallel imaging techniques and/or high-resolution scanning (e.g., slices with 128×128 pixels) several gigabytes (GBs) of raw image space data will be recorded per subject.

Given the small amplitude of task-related BOLD signal changes of typically 1–5 % and the presence of many confounding effects, such as signal drifts and head motion, the localization and characterization of brain regions responding to experimental conditions of the stimulation protocol is a nontrivial task. The major analysis steps of functional and associated anatomical data will be described in the following paragraphs including spatial and temporal *preprocessing*, *statistical data analysis*, *coregistration* of functional and anatomical data sets, and *spatial normalization*. Although these essential data analysis steps are performed in a rather standardized way in all major software packages, including AFNI (<http://afni.nimh.nih.gov/afni/>), BrainVoyager (<http://www.brainvoyager.com/>), FSL (<http://www.fmrib.ox.ac.uk/fsl/>), and SPM (<http://www.fil.ion.ucl.ac.uk/spm/>), there is still room for improvements as will be discussed below. For the visualization of functional data, high-resolution anatomical data sets with a resolution of (or close to) 1 mm in all three dimensions are often collected in a recording session.

In most cases, these anatomical volumes are scanned using slow T1-weighted MR sequences that are optimized to produce high-quality images with very good contrast between the gray and white matter. In some analysis packages, anatomical data sets do not only serve as a structural reference for the visualization of functional information but are often also used to improve the functional analysis itself, for example, by restricting statistical data analysis to gray matter voxels or to analyze topological representations on extracted cortex meshes. The preprocessing of high-resolution anatomical data sets and their role in functional data analysis will be described in Sect. 3.4. Since some data analysis steps depend on the details of the experimental paradigm, the next section shortly describes the two most frequently used experimental designs.

3.1 Block- and Event-Related Designs

In the first years of fMRI measurements, experimental designs were adapted from positron-emission tomography (PET) studies. In the typical PET design, several *trials* (individual stimuli, or more generally, cognitive events) were clustered in *blocks*, each of which contained trials of the same condition (Fig. 10). As an example, one block may consist of a series of different pictures showing happy faces and another block may consist of pictures showing sad faces. The statistical analysis of such *block designs* compares the mean activity obtained in the different experimental blocks. Block designs were necessary in PET studies because of the limited temporal resolution of this imaging technique requiring about a minute to obtain a single whole-brain functional image. Since the temporal resolution of fMRI is much higher than PET, it has been proposed to use *event-related designs* (Blamire et al. 1992; Buckner et al. 1996; Dale and Buckner 1997). The characteristics of these designs (Fig. 10) follow closely those used in event-related potential (ERP) studies. In event-related designs, individual trials of different conditions are not clustered in blocks but are presented in a random sequence with sufficient time between trials to separate successive responses. Responses to trials belonging to the same condition are selectively averaged, and the calculated mean responses are statistically compared with each other. While block designs are well suited for many experiments, event-related designs offer several advantages over block designs, especially for cognitive tasks. An important advantage of event-related designs is the possibility to present stimuli in a randomized order (Fig. 10) avoiding cognitive adaptation or expectation strategies of the subjects. Such cognitive adaptations are likely to occur in block designs since a subject knows what type of stimuli to expect within a block after having experienced the first few trials. Another important advantage of event-related designs is that the *response profile* for different trial types

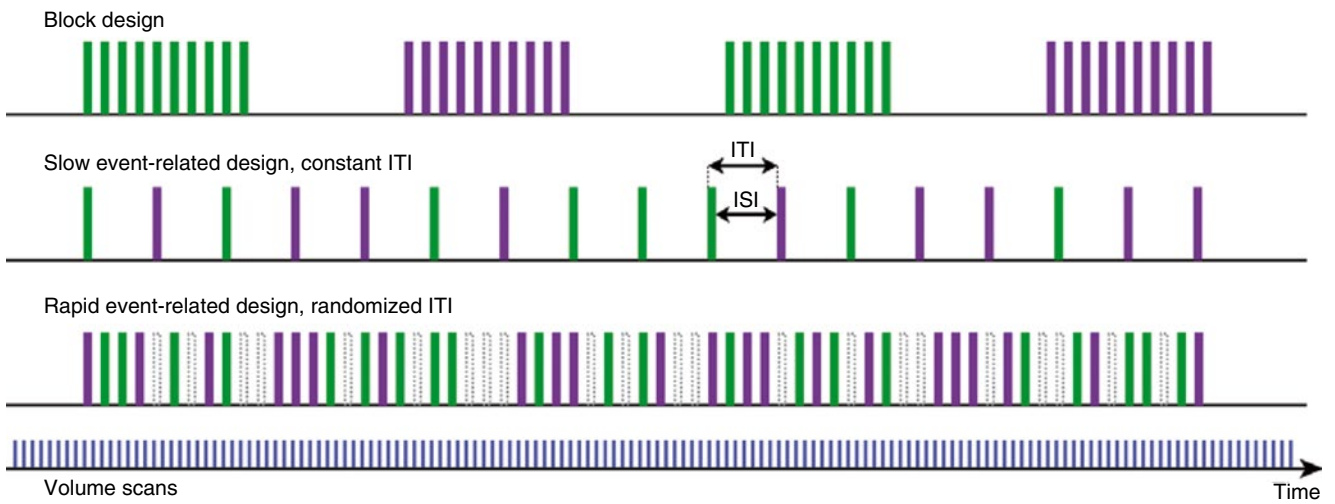


Fig. 10 In a block design (*upper row*), trials (events) belonging to the same condition are grouped together and are separated by a baseline block. In this example, two blocks of two main conditions (*green* – condition 1, *violet* – condition 2) are depicted. In slow event-related

designs, trials of different conditions appear in randomized order and are spaced sufficiently far apart to avoid largely overlapping BOLD responses. Optimal intertrial intervals (ITIs) are about 12 s

(and even single trials) can be *estimated* by event-related averaging. Furthermore, event-related designs allow *post hoc sorting* of individual brain responses. One important example of post hoc sorting is the separation of brain responses for correctly vs. incorrectly performed trials.

The possibilities of event-related fMRI designs are comparable to standard behavioral and ERP analyses. Note, however, that the hemodynamic response extends over about 20–30 s (Fig. 8) after presentation of a short stimulus; if only the positive BOLD response is considered, the signal extends over 10–15 s. The easiest way to conduct event-related fMRI designs is to temporally separate individual trials far enough to avoid overlapping responses of successive trials. Event-related designs with long temporal intervals between individual trials are termed *slow event-related designs* (Fig. 10). For stimuli of duration of 1–2 s, the optimal *intertrial interval* (ITI) for statistical analysis is about 12 s (Bandettini and Cox 2000; Maus et al. 2010a). Since it has been shown that the fMRI signals of closely spaced trials add up approximately linearly (Boynton et al. 1996; Dale and Buckner 1997, see Sect. 2.3), it is also possible to run experiments with inter trial intervals of 2–6 s. Designs with short temporal intervals between trials are called *rapid event-related designs* (Fig. 10). While the measured response of rapid event-related designs will contain a combination of overlapping responses from closely spaced trials, condition-specific event-related time courses can be isolated using deconvolution analysis. Deconvolution analysis works correctly only under the assumption of a linear system (see Sect. 3.2) and requires randomized intertrial intervals (“jitter”), which can be easily obtained by adding “null” (baseline) trials when trial sequences are created for an experiment. Note, however, that single-trial analyses are only possible when using a slow event-related

design. While adding null trials and simple permutations of trial types produce already good event sequences for rapid event-related designs, statistical power can be maximized by using more advanced randomization procedures (Wager and Nichols 2003; Maus et al. 2010b). In general, block- and event-related designs can be statistically analyzed using the same mathematical principles (see Sect. 3.3.3).

It is important to note that conventional fMRI data does not provide an absolute signal of brain activity limiting the quantitative interpretation of results. The major part of the signal amplitude is related to proton density and T_2 tissue contrast varying across brain regions within and between subjects. Small BOLD-related signal fluctuations, thus, neither have a defined origin nor a unit. In light of these considerations, signal strengths in main experimental conditions cannot be interpreted absolutely but have to be assessed relative to the signal strength in other main or control conditions within voxels. As a general control condition, many fMRI experiments contain a baseline (“rest,” “fixation”) condition with “no task” for the subject. Such simple control conditions allow analyzing brain activity that is common in multiple main conditions that would not be detectable when only comparisons between main conditions could be performed. More complex experimental (control) conditions differ from the main condition(s) only in specific cognitive component allowing isolating brain responses specific to that component.

Responses to main conditions are often expressed as percent signal change relative to a baseline condition. Furthermore, it is recommended to vary conditions within subjects – and even within runs – since the lack of an absolute signal level increases variability when comparing effects across runs, sessions, or subjects. Some experiments require a *between subjects* design, including comparisons of

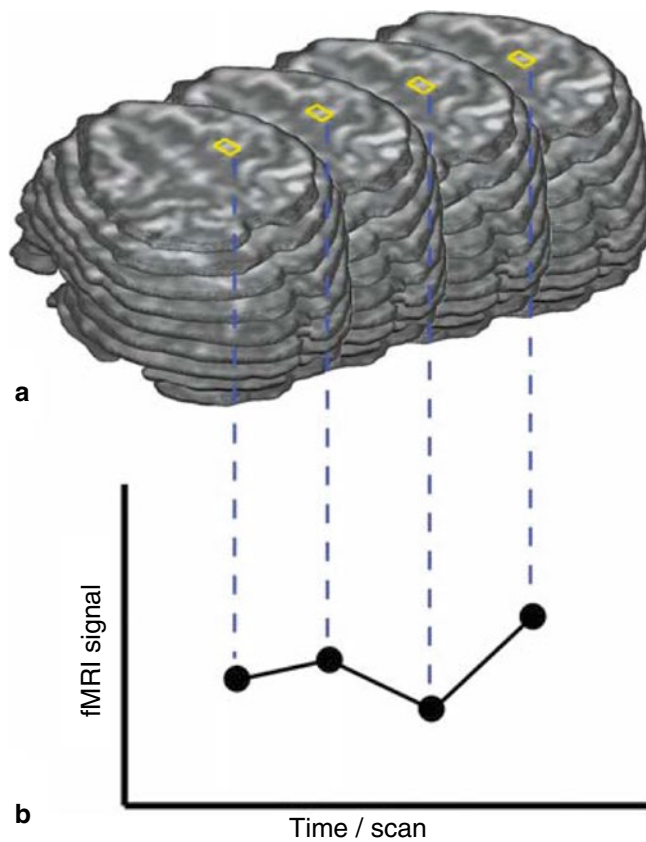


Fig. 11 During functional MRI measurements, a set of slices, often covering the whole brain, is scanned repeatedly over time. Although the repeated slice measurements look almost identical, small task-related signal fluctuations may occur at different brain regions at different moments in time (a). To visualize these subtle fluctuations, the time course of any desired brain region (region-of-interest, ROI) may be depicted (b). The smallest separate brain region one can select to display a time course in a two-dimensional image (slice) is called pixel (picture element) while the smallest region in a three-dimensional “image” is called voxel (volume element)

responses between different subject groups, for example, males vs. females or treatment group vs. control group. Note that the BOLD signal measured with conventional fMRI may be affected by medications that modify the neurovascular coupling, for example, by increasing or decreasing baseline cerebral blood flow (CBF). In order to obtain more quantitative evaluation of activation responses, it is, thus, recommended for patient studies to combine standard BOLD measurements with CBF measurements using arterial spin labeling (ASL) techniques (e.g., Buxton et al. 2004).

3.2 Basic Analysis Steps

3.2.1 Two Views on fMRI Data Sets

In order to better understand different fMRI data analysis steps, two different views on the recorded four-dimensional data sets are helpful. In one view (Fig. 11a), the 4D data is

conceptualized as a *sequence of functional volumes* (3D images). This view is very useful to understand spatial analysis steps. During 3D motion correction, for example, each functional volume of a run is aligned to a selected reference volume by adjusting rotation and translation parameters. The second view focuses on time courses of individual voxels (“voxel” = “volume element” analogous to “pixel” = picture element). This second view (Fig. 11b) helps to understand those preprocessing and statistical procedures, which process *time courses of individual voxels*. Most standard statistical analysis procedures including the general linear model (GLM) operate in this way. In a GLM analysis, for example, the data is processed “voxel-wise” (univariate) by fitting a model to the time course of each voxel independently.

3.2.2 Preprocessing of Functional Data

In order to reduce artifact and noise-related signal components, a series of *preprocessing* operations is typically performed prior to statistical data analysis. The most essential *preprocessing* steps are (1) head motion detection and correction, (2) slice scan timing correction, (3) removal of linear and nonlinear trends in voxel time courses, and (4) spatial and temporal smoothing of the data.

3.2.2.1 Detection and Correction of Head Motion

The quality of fMRI data is strongly hampered in the presence of substantial head movements. Data sets are usually rejected for further analysis if head motion exceeds 5 mm. Although head motion can be corrected in image space, displacements of the head reduce the homogeneity of the magnetic field, which is fine-tuned (“shimmed”) prior to functional scans for the head position at that time. If head movements are small, 3D motion correction is an important step to improve data quality for subsequent statistical data analysis. Motion correction operates by selecting a functional volume of a run (or a volume from another run of the same scanning session) as a reference to which all other functional volumes are aligned. Most head motion algorithms describe head movements by six parameters assessing translation (displacement) and rotation at each time point with respect to the reference volume. These six parameters are appropriate to characterize motion of *rigid bodies*, since any spatial displacement of rigid bodies can be described by translation along the *x*-, *y*-, and *z*-axes and rotation around these axes. The values of these six parameters are estimated iteratively by analyzing how a source volume should be translated and rotated in order to better align with the reference volume; after applying a first estimate of the parameters, the procedure is repeated to improve the “fit” between the transformed (motion-corrected) and target (reference) volume. A *similarity* or *error measure* quantifies how good the transformed volume fits the reference volume. An often-used error measure is the sum of squared intensity differences at corresponding positions in the reference volume and the transformed

volume. The iterative adjustment of the parameter estimates stops if no further improvement can be achieved, that is, when the error measure reaches a minimum. After the final motion parameters have been *detected* by the iterative procedure, they can be applied to the source volume to produce a *motion-corrected* volume replacing the original volume in the output (motion-corrected) data set. For visual inspection, fMRI software packages are usually presenting line plots of the three translation and three rotation parameters across time showing how the estimated values change from volume to volume. The obtained parameter time courses may also be integrated in subsequent statistical data analysis with the aim to remove residual motion artifacts (for details, see Sect. 3.3).

Note that the assumption of a rigid body is not strictly valid for fMRI data since the individual slices of a functional volume are not scanned in parallel. Since abrupt head motions may occur at any moment in time, the assumption of a rigid body is violated. Imagine, for example, that a subject does not move while the first five slices of a functional volume are scanned, then moves 2 mm along the y-axis, and then lies still until scanning of that volume has been completed. The six parameters of a rigid body approach are not sufficient to capture such “within-volume” motion correctly. Fortunately, head movements from volume to volume are typically small and the assumption of a moving rigid body is, thus, largely valid.

3.2.2.2 Slice Scan Time Correction

For statistical analysis, a functional volume is usually considered as measured at the same time point. Individual slices (or a few slices when using state-of-the-art “multiband” sequences) of a functional volume are, however, scanned sequentially in standard 2D functional (EPI) measurements, that is, each slice (or set of slices in multiband sequences) is obtained at a different time point within a functional volume measurement. For a functional volume of 30 slices and a volume TR of 3 s, for example, the data of the last slice is measured almost 3 s later than the data of the first slice. Despite the sluggishness of the hemodynamic response (Fig. 8), an imprecise specification of time in the order of 3 s will lead to suboptimal statistical analysis, especially in event-related designs. It is, thus, desirable to preprocess the data in such a way that the resulting processed data appears as if all slices of a functional volume were measured at the same moment in time. Only then would it be, for example, possible to compare and integrate event-related responses from different brain regions correctly with respect to temporal parameters such as onset latency. In order to correct for different slice scan timings, the time series of individual slices are temporally “shifted” to match a reference time point, for example, the first or middle slice of a functional volume. The appropriate temporal shift of the time courses of the other slices is then performed by resampling the original data accordingly. Since this process involves sampling at time points that fall between measurement time points, the new values need to be estimated by interpolation of values from past and future time points (Fig. 12). The most

often-used interpolation methods are linear, cubic spline, and sinc interpolation. Note that the time points of slice scanning depend also on the *acquisition order* specified at the scanner console. Besides an ascending or descending order, slices are often scanned in an interleaved mode, that is, the odd slice numbers are recorded first followed by the even slice numbers. After appropriate temporal resampling, all slices within a functional volume of the new data set represent the same time point (Fig. 12) and can, thus, be statistically analyzed with the same hemodynamic response function; if slice scan time correction is not performed, hemodynamic response functions should be adjusted (shifted) on a per-slice basis.

3.2.2.3 Removal of Drifts and Temporal Smoothing of Voxel Time Series

Due to physical and physiological noise, voxel time courses are often nonstationary exhibiting signal drifts over time. If the signal rises or falls with a constant slope from beginning to end of a run, the drift is described as a *linear trend*. If the signal level slowly varies over time with a nonconstant slope, the drift is described a nonlinear trend. Since drifts describe slow signal changes, they can be removed by Fourier analysis using a *temporal high-pass filter*. The original signal in the time domain is transformed in frequency space using the Fourier transform (FT). In the frequency-domain drifts can be easily removed because low-frequency components, underlying drifts, are isolated from higher-frequency components reflecting task-related signal changes. After applying a high-pass filter in the frequency domain (removing low frequencies), the data is transformed back into the time domain by the inverse Fourier transform (Fig. 13). As an alternative approach, drifts can be modeled and removed in the time domain using appropriate basis sets in a general linear model analysis. This approach can be performed either as a preprocessing step or as part of statistical data analysis (for details, see Sect. 3.3.3). Removal of drifts is recommended as a preprocessing step since it is not only relevant for statistical data analysis but also for the calculation of event-related time courses.

While less important, another temporal preprocessing step is *temporal smoothing* of voxel time courses removing *high-frequency signal fluctuations*, which are considered as noise. While this step increases the signal-to-noise ratio, temporal smoothing is not recommended when analyzing event-related designs since it may distort estimates of temporally relevant parameters, such as the onset or width of average event-related responses. Temporal smoothing also increases serial correlations between values of successive time points that need to be corrected (see Sect. 3.3.3.6).

3.2.2.4 Spatial Smoothing

To further enhance the signal-to-noise ratio, the data is often spatially smoothed by convolution with a 3D Gaussian kernel. In this process, each voxel is replaced by a weighted

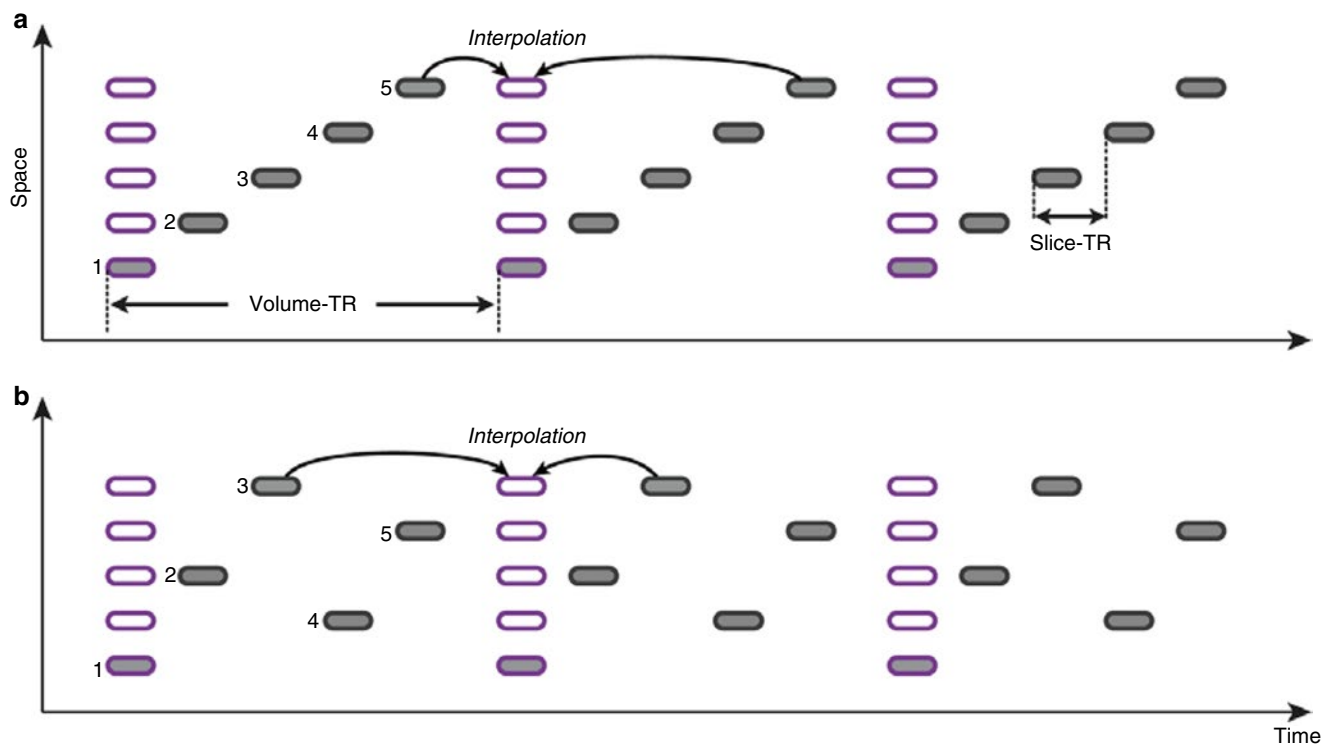


Fig. 12 During slice scan time correction, slices within each functional volume (black rectangles) are “shifted in time” resulting in a new time series (violet rectangles) in which all slices of a functional volume are virtually measured at the same moment in time. To calculate intensity values at time points falling in-between measured time points, past and

future values have to be integrated typically using sinc or linear interpolation. For correct interpolation, the volume TR, slice TR, and slice scanning order must be known. (a) Five slices are scanned in ascending order. (b) Five slices are scanned in interleaved order

average value calculated across neighboring voxels. The shape and width of the Gaussian kernel determines the weights used to multiply the values of voxels in the neighborhood, that is, weights decrease with increasing distance from the considered voxel; voxels further apart from the center will, thus, contribute less to the weighted average than voxels close to the center of the considered voxel. Note that smoothing reduces the spatial resolution of the data and should be therefore applied with care. Many studies, however, aim to detect regions larger than a few voxels, that is, brain areas in the order of 1 cm^3 or larger. Under these conditions, spatial smoothing with an appropriate kernel width of 4–8 mm is useful since it suppresses noise and enhances task-related signals. Spatial smoothing also increases the extent of activated brain regions, which is exploited in the context of group analyses (see Sect. 3.5) facilitating the integration of signals from corresponding but not perfectly aligned brain regions.

From the description and discussion of standard preprocessing steps, it should have become clear that there are no universally correct criteria to choose preprocessing steps and parameters because choices depend to some extent on the goal of data analysis. Some steps depend also on the experimental design of a study. If, for example, a high-pass temporal filter is used with a cutoff point that is too high,

interesting task-related signal fluctuations could easily be removed accidentally from the data.

Besides the described core preprocessing steps, additional procedures may be applied. The next sections will describe three additional preprocessing steps.

3.2.2.5 Mean Intensity Adjustment

Besides drifts in *individual* voxel time courses, the mean intensity level averaged across all voxels might exhibit drifts over time. These global drifts can be corrected by scaling the intensity values of a functional volume in such a way that the new mean value is identical to the mean intensity value of a reference volume. Mean intensity adjustment is not strictly necessary since modern scanners keep a rather constant mean signal level over time. Under this condition, mean intensity adjustment may even produce a negative effect by reducing true activation effects. If, for example, large parts of the brain activate during a main condition as compared to a rest condition, the mean signal level is higher during active periods, and a mean intensity adjustment step will “correct” this. A plot of the mean signal level over time might be, however, helpful to identify problems of the scanner quality, especially when such a plot shows “spikes,” that is, strong signal decreases (or increases) at isolated time points.

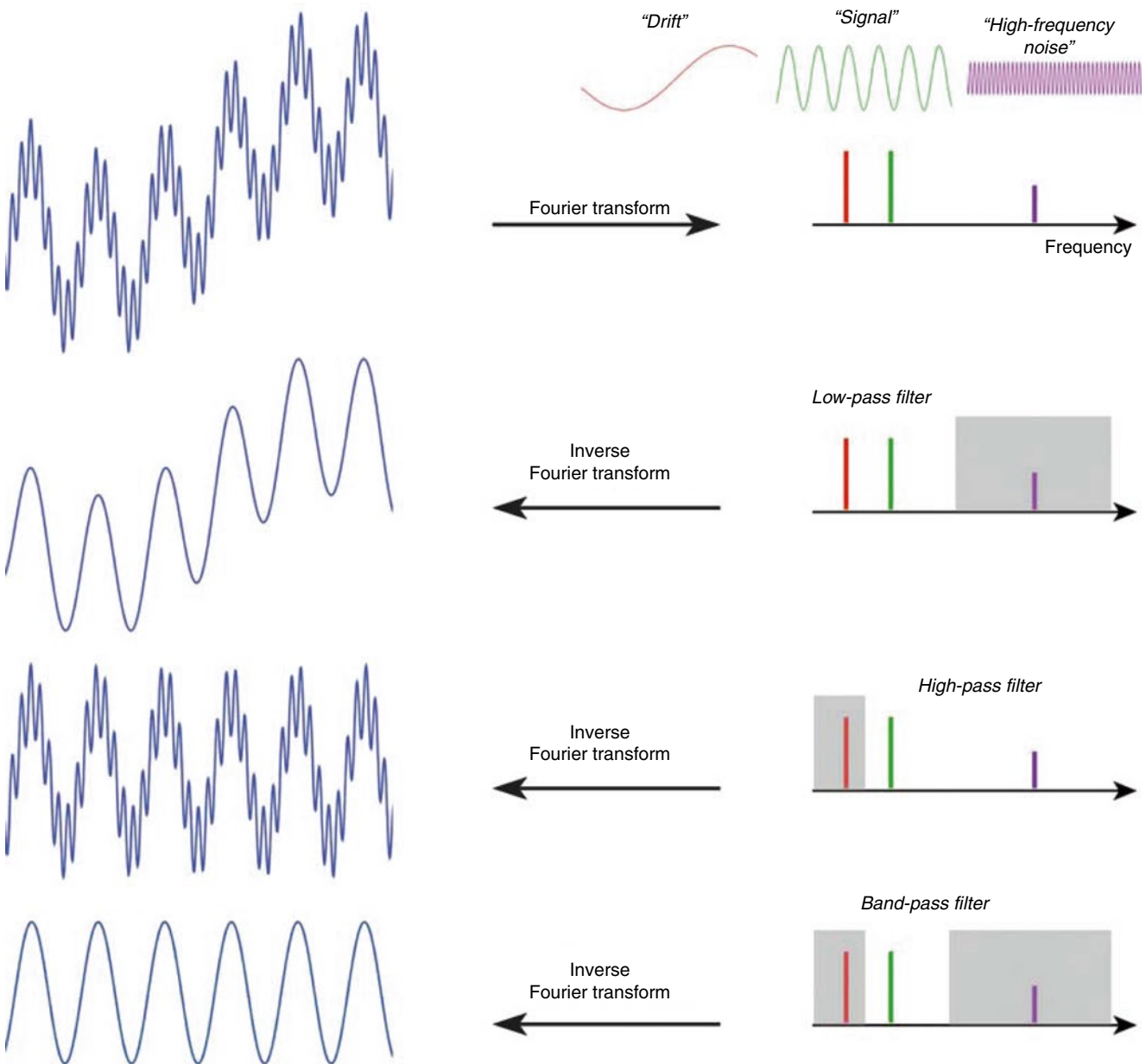


Fig. 13 Principle of temporal filtering using Fourier analysis. The time-domain signal can be converted in an equivalent frequency-domain signal using the Fourier transform (upper row). In this simplified example, the composite signal (upper row, left) consists only of three frequencies representing a drift, signal, and high-frequency noise

component (upper row, right). In the frequency domain, frequencies can be filtered to remove unwanted signal components. The filtered signal can then be converted back into the time domain using the inverse Fourier transform. In the second row, a low-pass filter is applied, in the third row a high-pass filter, and in the fourth row a band-pass filter

3.2.2.6 Motion Correction Within and Across Runs

A scanning session typically consists of a series of runs. In such a situation, head movements may not only occur within runs but also between runs. A simple approach to align all functional volumes of all runs of a scanning session with each other consists in specifying the same reference volume for all runs. If a session consists, for example, of three runs, all functional volumes could be aligned to the middle volume of the

second run. Since functional data is often aligned with a 3D anatomical data set recorded in the same session, it is recommended to choose a functional volume as a reference, which is recorded just before (or after) the anatomical data set. Note, however, that across-run motion correction works only if the slice positions are specified identically in all runs. If across-run motion correction is not possible, each run can also be individually adjusted to a common 3D anatomical data set.

3.2.2.7 Distortion Correction of Functional Images

The BOLD sensitive GE-EPI sequence is used for most fMRI studies because of its speed, but it has the disadvantage that images suffer from signal dropouts and geometric distortions, especially in brain regions close to other tissue types such as air and liquor (susceptibility artifacts). These artifacts can be reduced substantially by using optimized EPI sequence parameters (e.g., Weiskopf et al. 2006) and parallel imaging techniques (see Sect. 1.3). A complete removal of dropouts and geometric distortions is, however, not possible. Further improvements may be obtained by distortion correction routines, which may benefit from special scans measuring magnetic field distortions (e.g., field maps). The distortion-corrected images may improve coregistration results between functional and anatomical data sets enabling a more precise localization of brain function.

3.3 Statistical Analysis of Functional Data

Statistical data analysis aims at identifying those brain regions exhibiting increased or decreased responses in specific experimental conditions as compared to other (e.g., control) conditions. Due to the presence of physiological and physical noise fluctuations, observed differences between conditions might occur simply by chance. Note that measurements provide only a *sample* of data, but we are interested in true effects in the underlying *population*. At the level of individual functional scans, time points are treated as subjects, that is, sample corresponds to the obtained repeated measurements at every TR and “population” refers to the estimated but unobservable true condition effects within the subject. In multi-subject (group) analyses, sample usually refers to estimated effects obtained in each subject and population refers to all people from which the sample of subjects has been drawn. Statistical data analysis protects from wrongly accepting effects in small sample data sets by explicitly assessing the effect of measurement variability (noise fluctuations) on estimated condition effects: If it is very unlikely that an observed effect is solely the result of noise fluctuations, it is assumed that the observed effect reflects a true difference between conditions in the population. In standard single-subject statistical fMRI analyses, this assessment is usually performed independently for the time course of each voxel (univariate analysis). The obtained statistical values, one for each voxel, form a three-dimensional *statistical map*. In more complex analyses, each voxel will contain several statistical values reflecting estimated effects of multiple conditions. Since independent testing at each voxel increases the chance to find some voxels with strong differences between conditions simply due to noise fluctuations, further adjustments for *multiple comparisons* need to be made.

3.3.1 From Image Subtraction to Statistical Comparison

Figure 14 shows two fMRI time courses obtained from two different brain areas of an experiment with two conditions, a control condition (“Rest”) and a main condition (“Stim”). Each condition has been measured several times.¹ How can we assess whether the response values are higher in the main condition than in the control condition? One approach consists in subtracting the mean value of the “Rest” condition, \bar{X}_1 , from the mean value of the “Stim” condition, \bar{X}_2 , that is: $d = \bar{X}_2 - \bar{X}_1$. Note that in this example, one would obtain the same mean values in both conditions and, thus, the same difference in cases (a) and (b). Despite the fact that the means are identical in both cases, the difference in case (b) seems to be more “trustworthy” than the difference in case (a) because the measured values exhibit less fluctuations, that is, they *vary less* in case (b) than in case (a).

Statistical data analysis goes beyond simple subtraction by taking into account the amount of variability of the measured data points. Statistical analysis essentially asks how likely it is to obtain a certain effect (e.g., difference of condition means) in a data sample if there is no effect at the population level, that is, how likely it is that an observed sample effect is solely the result of noise fluctuations. This is formalized by the *null hypothesis* stating that there is no effect, for example, no true difference between conditions in the population. In the case of comparing the two means μ_1 and μ_2 , the null hypothesis can be formulated as $H_0: \mu_1 = \mu_2$. Assuming the null hypothesis, it can be calculated how likely it is that an observed sample effect would have occurred simply by chance. This requires knowledge about the amount of noise fluctuations (and its distribution), which can be estimated from the data. By incorporating the number of data points and the variability of measurements, statistical data analysis allows to *estimate the uncertainty of effects* (e.g., mean differences) in data samples. If an effect is large enough so that it is very unlikely that it has occurred simply by chance (e.g., the probability is less than $p=0.05$), one *rejects* the null hypothesis and *accepts* the *alternative hypothesis* stating that there exists a true effect in the population. Note that the decision to accept or reject the null hypothesis is based on a probability value which has been accepted by the scientific community ($p < 0.05$). Since the decision to accept or reject the null hypothesis is based on a probability value, a statistical analysis does not *prove* the existence of an effect, it only suggests “to believe in an effect” if it is very unlikely that the observed effect has

¹Note that in a real experiment, one would not just present once the control and main condition as in Fig. 14, but several “on-off” cycles; with too few repetitions, task-related response could not be distinguished from potential low-frequency drifts (see Sect. 3.2.2).

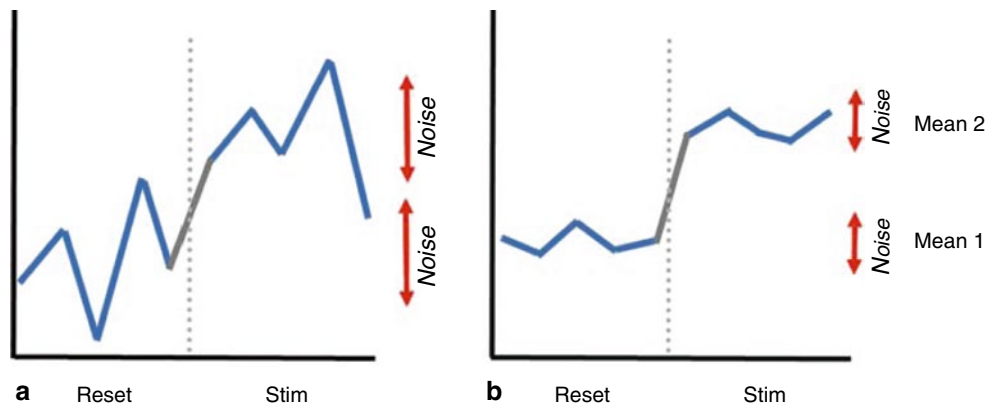


Fig. 14 Principle of statistical data analysis. An experiment with two conditions (“Stim” and “Rest”) has been performed. (a) Time course obtained in area 1. (b) Time course obtained in area 2. Calculation and subtraction of mean 1 (“Rest” condition) from mean 2 (“Stim” condition) leads to the same result in (a) and (b). In a statistical analysis, the

estimated effect (mean difference) is related to its uncertainty, which is estimated by the variability of the measured values within conditions. Since the variance within the two conditions is smaller in (b) than in (a), the estimated effect is more likely to correspond to a true difference in (b) than in (a)

occurred by chance. Note that a probability of $p=0.05$ means that if we would repeat the experiment 100 times, we would accept the alternative hypothesis in about five cases even if there would be no real effect in the population. Since the chosen probability value thus reflects the likelihood of wrongly rejecting the null hypothesis, it is also called *error probability*. The error probability is also referred to as the *significance level* and denoted with the Greek letter α . If one would know that there is no effect in the population but one would incorrectly reject the null hypothesis in a particular data sample, a “false-positive” decision would be made (type 1 error, “false alarm”). Since a false-positive error depends on the chosen error probability, it is also referred to as alpha error. If one would know that there is a true effect in the population but one would fail to reject the null hypothesis in a sample, a “false-negative” decision would be made, that is, one would miss a true effect (type 2 error).

3.3.2 t-Test and Correlation Analysis

The uncertainty of an effect is estimated by calculating the variance of the noise fluctuations from the data. For the case of comparing two mean values, the observed difference of the means is related to the variability of that difference resulting in a t statistic:

$$t = \frac{\bar{X}_2 - \bar{X}_1}{\hat{\sigma}_{\bar{x}_2 - \bar{x}_1}}$$

The numerator contains the calculated mean difference while the denominator contains the estimate of the expected variability, the *standard error* of the mean difference. Estimation of the standard error $\hat{\sigma}_{\bar{x}_2 - \bar{x}_1}$ involves pooling of the variances obtained within both conditions. Since we observe a high

variability in case (a) of the example data (Fig. 14), we will obtain a small t value. Due to the small variability of the data points in (b), we will obtain a larger t value in this case (Fig. 14). The higher the t value, the less likely it is that the observed mean difference is just the result of noise fluctuations. It is obvious that measurement of many data points allows a more robust estimation of this probability than the measurement of only a few data points. The error probability p can be calculated exactly from the obtained t value using the incomplete beta function $I_x(a,b)$ and the number of measured data points N :

$$p = I_{\frac{N-2}{N-2+t^2}} \left(\frac{N-2}{2}, \frac{1}{2} \right)$$

If the computed error probability falls below the standard value ($p < 0.05$), the alternative hypothesis is accepted stating that the observed mean difference exists in the population from which the data points have been drawn (i.e., measured). In that case, one also says that the two means differ *significantly*. Assuming that in our example the obtained p value falls below 0.05 in case (b) but not in case (a), we would only infer for brain area 2 that the “Stim” condition differs significantly from the “Rest” condition.

The described mean comparison method is not the ideal approach to compare responses between different conditions since this approach is unable to capture the gradual rise and fall of fMRI responses, for example, when a voxel exhibits a strong response to a trial of condition B after having not responded strongly to a preceding trial of condition A. As long as the temporal sampling resolution is low (volume TR > 4 s), the mean of different conditions can be calculated easily because transitions of expected responses from different conditions occur within a single time point (Fig. 15). If the

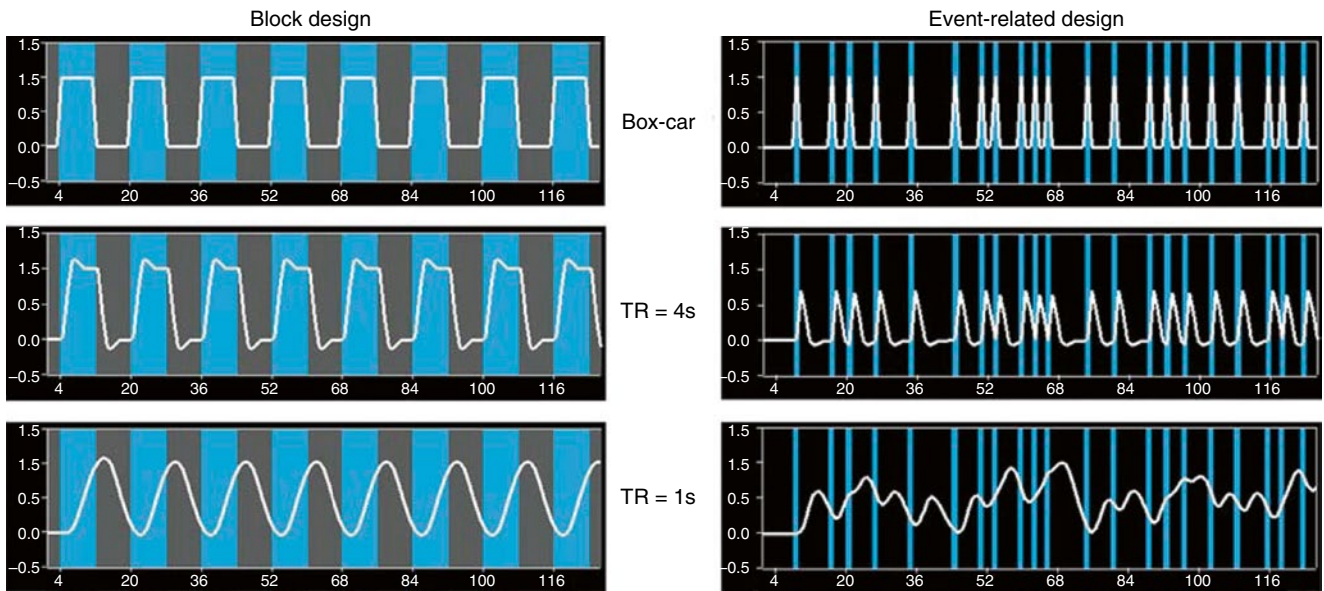


Fig. 15 Calculation of expected fMRI signals for a block- and event-related design. The horizontal axis of each plot represents time (data points). The vertical axis represents the amplitude of the modeled fMRI response. The blue vertical segments correspond to intervals of a single main stimulation condition; the gray segments correspond to a control condition. White curves show predicted BOLD responses. The plots in the upper row depict time courses, which do not take into account the delayed hemodynamic response

profile (“box-car”). The white curves in the other plots represent the expected time courses after application of a standard hemodynamic response function (two gamma function) for a temporal resolution (volume TR) of 4 s (middle row) and 1 s (lower row). Correlation analysis is able to capture the gradual increase and decrease of expected time courses for short TRs while it is impossible to unambiguously categorize time points as belonging to stimulation vs. baseline conditions in the context of a *t* test

temporal resolution is high, the expected fMRI responses change gradually from one condition to the next due to the sluggishness of the hemodynamic response (Fig. 15, TR = 1 s). In this case, time points in the “transitional zone” cannot be assigned easily to different conditions. Without special treatment, the mean response can no longer be easily computed for each condition. As a consequence, the statistical power to detect mean differences may be substantially reduced, especially for short blocks and events.

This problem does not occur when *correlation analysis* is used since this method allows explicitly incorporating the gradual increase and decrease of the expected BOLD signal. The predicted ideal (noise-free) time courses in Fig. 15 can be used as the *reference function* in a correlation analysis. At each voxel, the time course of the reference function is compared with the time course of the measured data from a voxel by calculating the *correlation coefficient r*, indicating the strength of covariation:

$$r = \frac{\sum_{t=1}^N (X_t - \bar{X})(Y_t - \bar{Y})}{\sqrt{\sum_{t=1}^N (X_t - \bar{X})^2 \sum_{t=1}^N (Y_t - \bar{Y})^2}}$$

Index *t* runs over time points (*t* for “time”) identifying pairs of temporally corresponding values from the reference (*X*)

and data (*Y*) time courses. In the numerator the mean of the reference and data time course is subtracted from the respective value of each data pair and the two differences are multiplied. The resulting value is the sum of these cross products, which will be high if the two time courses *covary*, that is, if the values of a pair are both above or below their respective means in most cases. The term in the denominator normalizes the covariation term in the numerator so that the correlation coefficient lies in a range of -1 and +1. A value of +1 indicates that the reference time course and the data time course go up and down in exactly the same way, while a value of -1 indicates that the two time courses run in opposite direction (anticorrelation). A correlation value of 0 indicates that the two time courses do not covary, that is, the value in one time course cannot be used to predict the corresponding value in the other time course.

While the statistical logic is the same in correlation analysis as described for mean comparisons, the null hypothesis now corresponds to the statement that the population correlation coefficient *ρ* equals zero ($H_0: \rho = 0$). By including the number of data points *N*, the error probability can be computed assessing how likely it is that an observed correlation coefficient would occur solely due to noise fluctuations in the signal time course. If this probability falls below 0.05, the alternative hypothesis is accepted stating that there is indeed significant covariation between the reference function

and the data time course. Since the reference function is the result of a model assuming different response strengths in the two conditions (e.g., “Rest” and “Stim”), a significant correlation coefficient indicates that the two conditions lead indeed to different mean activation levels in the respective voxel or brain area. The statistical assessment can be performed also by converting an observed r value into a corresponding t value, $t = r\sqrt{N-2} / \sqrt{1-r^2}$.

3.3.3 The General Linear Model

The described t test for assessing the difference of two mean values is a special case of an analysis of a *qualitative (categorical) independent variable*. A qualitative variable is defined by discrete levels, for example, “stimulus on” vs. “stimulus off” or “male” vs. “female.” If a design contains more than two levels, a more general method such as analysis of variance (ANOVA) need to be used, which can be considered as an extension of the t test to more than two levels and to more than one experimental factor. The described correlation coefficient on the other hand is suited for the analysis of *quantitative independent variables*. A quantitative variable may be defined by any gradual time course. If more than one reference time course has to be considered, *multiple regression analysis* can be used, which can be considered as an extension of the simple linear correlation analysis. The *general linear model*² (GLM) is mathematically identical to a multiple regression analysis but stresses its suitability for both multiple qualitative and multiple quantitative variables. The GLM is suited to implement any parametric statistical test with one dependent variable, including any factorial ANOVA design as well as designs with a mixture of qualitative and quantitative variables (covariance analysis, ANCOVA). Because of its flexibility to incorporate multiple quantitative and qualitative independent variables, the GLM has become the core tool for fMRI data analysis after its introduction into the neuroimaging community by Friston and colleagues (Friston et al. 1994, 1995). The following sections briefly describe the mathematical background of the GLM in the context of fMRI data analysis; a comprehensive treatment of the GLM can be found in the standard statistical literature, for example, Draper and Smith (1998) and Kutner et al. (2005).

From the perspective of multiple regression analysis, the GLM aims to “explain” or “predict” the variation of a dependent variable in terms of a *linear combination* (weighted sum) of several reference functions. The dependent variable corresponds to the observed fMRI time course of a voxel and the reference functions correspond to time courses of expected (noise-free) fMRI responses for different conditions

of the experimental paradigm. The reference functions are also called *predictors*, *regressors*, *explanatory variables*, *covariates*, or *basis functions*. A set of specified predictors forms the *design matrix*, also called the *model*. A predictor time course is typically obtained by convolution of a “box-car” time course with a standard hemodynamic response function (Figs. 8 and 15). A box-car time course is usually defined by setting values to 1 at time points at which the modeled condition is defined (“on”) and 0 at all other time points.

Each predictor time course X_i gets an associated coefficient or *beta weight* b_i that quantifies the contribution of a predictor in explaining variance in the voxel time course y . The voxel time course y is modeled as the sum of the defined predictors, each multiplied with the associated beta weight b . Since this linear combination will not perfectly explain the data due to noise fluctuations, an error value e is added to the GLM system of equations with n data points and p predictors:

$$\begin{aligned} y_1 &= b_0 + b_1 X_{11} + \dots + b_p X_{1p} + e_1 \\ y_2 &= b_0 + b_1 X_{21} + \dots + b_p X_{2p} + e_2 \\ &\vdots && \ddots && \vdots \\ y_n &= b_0 + b_1 X_{n1} + \dots + b_p X_{np} + e_n \end{aligned}$$

The y variable on the left side corresponds to the data, that is, the measured time course of a single voxel. Time runs from top to bottom, that is, y_1 is the measured value at time point 1, y_2 the measured value at time point 2, and so on. The voxel time course (left column) is “explained” by the terms on the right side of the equation. The first column on the right side corresponds to the first beta weight b_0 . The corresponding predictor time course X_0 has a value of 1 for each time point and is, thus, also called “constant.” Since multiplication with 1 does not alter the value of b_0 , this predictor time course (X_0) does not explicitly appear in the equation. After estimation (see below), the value of b_0 typically represents the signal level of the baseline condition and is also called intercept. While its absolute value is not very informative in the context of fMRI data, it is important to include the constant predictor in a design matrix since it allows the other predictors to model small condition-related fluctuations as increases or decreases relative to the baseline signal level. The other predictors on the right-side model the expected time courses of different conditions. For multifactorial designs, predictors may be defined coding combinations of condition levels in order to estimate main and interaction effects. The beta weight of a predictor scales the associated predictor time course and reflects the unique contribution of that predictor in explaining part of the variance in the voxel time course. While the exact interpretation of beta values depends on the details of the design matrix, a large positive (negative) beta weight typically indicates that the voxel exhibits strong activation (deactivation) during the modeled experimental condition relative to baseline. All beta values together characterize a voxel’s “preference” for one or more experimental

²In the fMRI literature, the term “general linear model” refers to its univariate version where “univariate” refers to the number of dependent variables (one). In its general form, the general linear model has been defined for multiple dependent variables, that is, it encompasses tests as general as multivariate covariance analysis (MANCOVA).

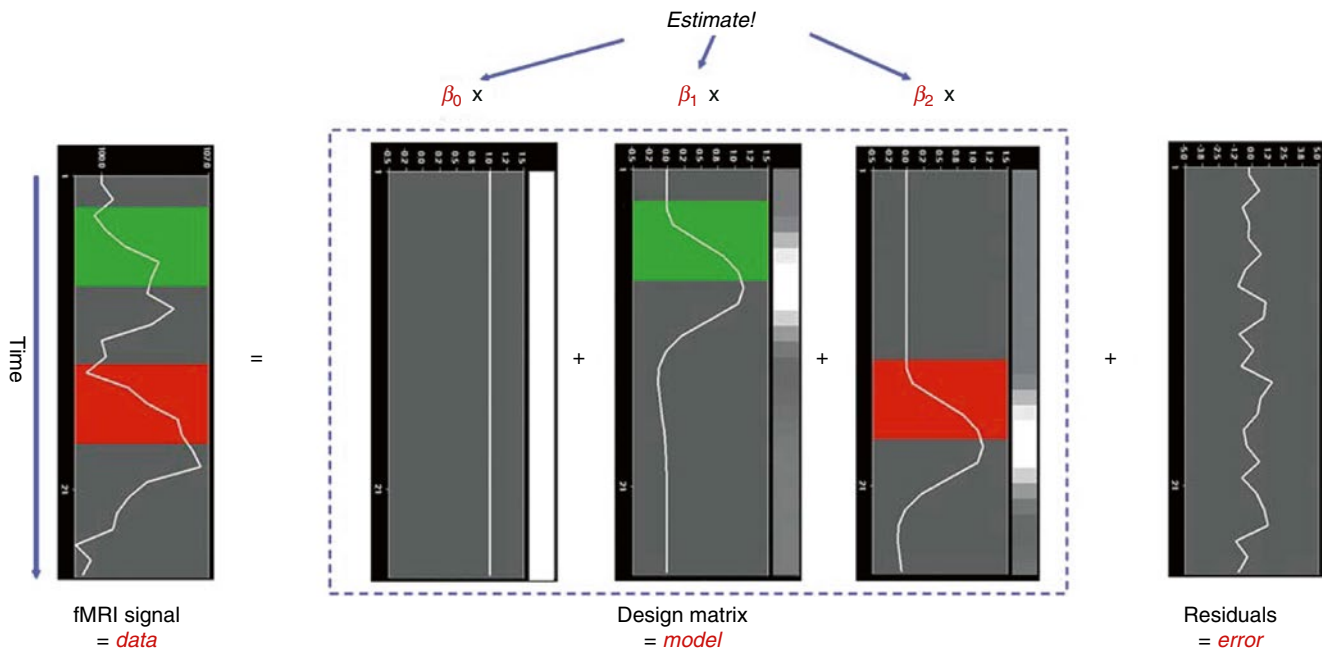


Fig. 16 Graphical display of a general linear model. Time is running from *top to bottom*. Left side shows observed voxel time course (data). The model (design matrix) consists of three predictors, the constant and two main predictors (middle part). Filled green and red rectangles depict stimulation time while the white curves depict expected BOLD responses. Expected responses are also shown in

graphical view using a *black-to-white* color range (*right side* of each predictor plot). Beta values have to be estimated (*top*) to scale the expected responses (predictors) in such a way that their weighted sum predicts the data values as good as possible (in the least squares sense, see text). Unexplained fluctuations (residuals, error) are shown on the *right side*

conditions. The last column in the system of equations contains error values, also called *residuals*, *prediction errors*, or *noise*. These error values quantify the deviation of the measured voxel time course from the predicted time course.

The GLM system of equations may be expressed elegantly using matrix notation. For this purpose, the voxel time course, the beta values, and the residuals are represented as vectors and the set of predictors as a matrix:

$$\begin{bmatrix} y_1 \\ \vdots \\ y_n \end{bmatrix} = \begin{bmatrix} 1 & X_{11} & \cdots & X_{1p} \\ \vdots & \vdots & \vdots & \vdots \\ 1 & X_{n1} & \cdots & X_{np} \end{bmatrix} \begin{bmatrix} b_0 \\ b_1 \\ \vdots \\ b_p \end{bmatrix} + \begin{bmatrix} e_1 \\ e_2 \\ \vdots \\ e_n \end{bmatrix}$$

Representing the indicated vectors and matrix with single letters, we obtain this simple form of the GLM system of equations:

$$\mathbf{y} = \mathbf{X}\mathbf{b} + \mathbf{e}$$

In this notation, the matrix \mathbf{X} represents the design matrix containing the predictor time courses as column vectors. The beta values now appear in a separate vector \mathbf{b} . The term $\mathbf{X}\mathbf{b}$ indicates matrix-vector multiplication. Figure 16 shows a graphical representation of the GLM. Time courses of the signal, predictors, and residuals have been arranged in column form with time running from top to bottom as in the system of equations.

Given the data \mathbf{y} and the design matrix \mathbf{X} , the GLM fitting procedure has to find a set of beta values explaining the data as good as possible. The time course values $\hat{\mathbf{y}}$ predicted by the model are obtained by the linear combination of the predictors:

$$\hat{\mathbf{y}} = \mathbf{X}\mathbf{b}$$

A good fit would be achieved with beta values leading to predicted values $\hat{\mathbf{y}}$ that are as close as possible to the measured values \mathbf{y} . By rearranging the system of equations, it is evident that a good prediction of the data implies small error values:

$$\begin{aligned} \mathbf{e} &= \mathbf{y} - \mathbf{X}\mathbf{b} \\ &= \mathbf{y} - \hat{\mathbf{y}} \end{aligned}$$

An intuitive idea would be to find those beta values minimizing the sum of error values. Since the error values contain both positive and negative values (and because of additional statistical considerations), the GLM procedure does not estimate beta values minimizing the sum of error values but finds those beta values *minimizing the sum of squared error values*:

$$\mathbf{e}'\mathbf{e} = (\mathbf{y} - \mathbf{X}\mathbf{b})'(\mathbf{y} - \mathbf{X}\mathbf{b}) \rightarrow \min$$

The term $\mathbf{e}'\mathbf{e}$ is the vector notation for the sum of squares $\left(\sum_{t=1}^N e_t^2 \right)$. The apostrophe symbol denotes transposition of a

vector (or matrix), that is, a row vector version of \mathbf{e} is multiplied by a column vector version of \mathbf{e} resulting in the sum of squared error values e_r . The optimal beta weights minimizing the squared error values (the “least squares estimates”) are obtained non-iteratively by the following equation:

$$\mathbf{b} = (\mathbf{X}'\mathbf{X})^{-1} \mathbf{X}'\mathbf{y}$$

The term in brackets contains a matrix-matrix multiplication of the transposed design matrix \mathbf{X}' and the non-transposed design matrix \mathbf{X} . This term results in a square matrix with a number of rows and columns corresponding to the number of predictors. Each cell of the $\mathbf{X}\mathbf{X}$ matrix contains the scalar product of two predictor vectors. The scalar product is obtained by summing all products of corresponding entries of two vectors corresponding to the (non-mean normalized) calculation of covariance. This $\mathbf{X}\mathbf{X}$ matrix, thus, corresponds to the (non-mean normalized) predictor variance-covariance matrix.

The resulting square matrix is inverted as denoted by the “ -1 ” symbol. The resulting matrix $(\mathbf{X}'\mathbf{X})^{-1}$ plays an essential role not only for the calculation of beta values but also for testing the significance of contrasts (see below). The remaining term on the right side, $\mathbf{X}'\mathbf{y}$, evaluates to a vector containing as many elements as predictors. Each element of this vector is the scalar product (non-mean normalized covariance term) of a predictor time course with the observed voxel time course.

An important property of the least squares estimation method (following from the independence assumption of the errors, see below) is that the variance of the measured time course can be decomposed into the sum of the variance of the predicted values (model-related variance) and the variance of the residuals:

$$\text{Var}(\mathbf{y}) = \text{Var}(\hat{\mathbf{y}}) + \text{Var}(\mathbf{e})$$

Since the variance of the voxel time course is fixed, minimizing the error variance by least squares corresponds to maximizing the variance of the values explained by the model. The square of the *multiple correlation coefficient R* provides a measure of the proportion of the variance of the data which can be explained by a specified model:

$$R^2 = \frac{\text{Var}(\hat{\mathbf{y}})}{\text{Var}(\mathbf{y})} = \frac{\text{Var}(\hat{\mathbf{y}})}{\text{Var}(\hat{\mathbf{y}}) + \text{Var}(\mathbf{e})}$$

The values of the multiple correlation coefficient vary between 0 (no variance explained) and 1 (all variance explained by the model). A coefficient of $R=0.7$, for example, corresponds to an explained variance of 49 % ($0.7 * 0.7$). An alternative way to calculate the multiple correlation coefficient consists in computing a standard correlation coefficient between the predicted values and the observed values: $R = r_{\hat{\mathbf{y}}\mathbf{y}}$. This equation offers another view on the meaning

of the multiple correlation coefficient quantifying the interrelationship (correlation) of the *combined* set of optimally weighted predictor variables with the observed time course.

3.3.3.1 GLM Diagnostics

Note that if the design matrix (model) does not contain all relevant predictors, condition-related increases or decreases in the voxel time course will be explained by the error values instead of the model. It is, therefore, important that the design matrix is constructed with all expected effects, which may also include reference functions not related to experimental conditions, for example, estimated motion parameters or drift predictors if not removed during preprocessing (see Sect. 3.2.2). In case that all expected effects are properly modeled, the residuals should reflect only “pure” noise fluctuations. If some effects are not (correctly) modeled, a plot of the residuals may show low-frequency fluctuations instead of a stationary noise time course. A visualization of the residuals (for selected voxels or regions-of-interest) is, thus, a good diagnostic to assess whether the design matrix has been defined properly.

3.3.3.2 GLM Significance Tests

The multiple correlation coefficient is an important measure of the “goodness of fit” of a GLM. In order to test whether a specified model significantly explains variance in a voxel time course, a F statistic can be calculated for an R value with $p-1$ degrees of freedom in the numerator and $n-p$ degrees of freedom in the denominator:

$$F_{n-1, n-p} = \frac{R^2(n-p)}{(1-R^2)(p-1)}$$

An error probability value p can then be obtained for the calculated F statistics. A high F value (p value <0.05) indicates that the experimental conditions as a whole have a significant modulatory effect on the data time course (omnibus effect).

While the overall F statistic answers the question whether the specified model significantly explains a voxel’s time course, it does not allow to assess which individual conditions differ significantly from each other. Comparisons between conditions can be formulated as *contrasts*, which are linear combinations of beta values corresponding to null hypotheses. To test, for example, whether activation in a single condition 1 deviates significantly from baseline, the null hypothesis would be that there is no effect in the population, that is, $H_0: b_1=0$. To test whether activation in condition 1 is significantly different from activation in condition 2, the null hypothesis would state that the beta values of the two conditions would not differ: $H_0: b_1=b_2$ or $H_0: (+1)b_1+(-1)b_2=0$. To test whether the mean of condition 1 and condition 2 differs from condition 3, the following contrast could be specified: $H_0: (b_1+b_2)/2=b_3$ or $H_0:$

$(+1)b_1 + (+1)b_2 + (-2)b_3 = 0$. The values used to multiply the respective beta values are often written as a *contrast vector* \mathbf{c} . In the latter example,³ the contrast vector would be written as $\mathbf{c}=[+1 \ 1 -2]$. Using matrix notation, the linear combination defining a contrast can be written as the scalar product of contrast vector \mathbf{c} and beta vector \mathbf{b} . The null hypothesis can then be simply described as $\mathbf{c}'\mathbf{b}=0$. For any number of predictors k , such a contrast can be tested with the following t statistic with $n-p$ degrees of freedom:

$$t = \frac{\mathbf{c}'\mathbf{b}}{\sqrt{\text{Var}(\mathbf{e})\mathbf{c}'(\mathbf{X}'\mathbf{X})^{-1}\mathbf{c}}}$$

The numerator of this equation contains the described scalar product of the contrast and beta vector. The denominator defines the standard error of $\mathbf{c}'\mathbf{b}$, that is, the variability of the estimate due to noise fluctuations. The standard error depends on the variance of the residuals $\text{Var}(\mathbf{e})$ as well as on the design matrix \mathbf{X} . With the known degrees of freedom, a t value for a specific contrast can be converted in an error probability value p using the equation shown earlier. Note that the null hypotheses above were formulated as $\mathbf{c}'\mathbf{b}=0$ implying a *two-sided* alternative hypothesis, that is, $H_a: \mathbf{c}'\mathbf{b} \neq 0$. For one-sided alternative hypotheses, for example, $H_a: b_1 > b_2$, the obtained p value from a two-sided test can be simply divided by 2 to get the p value for the one-sided test. If this p value is smaller than 0.05 and if the t value is positive (since b_1 is assumed to be larger than b_2), the null hypothesis may be rejected.

3.3.3.3 Conjunction Analysis

Experimental research questions often lead to specific hypotheses, which can best be tested by the *conjunction* of two or more contrasts. As an example, it might be interesting to test with contrast \mathbf{c}_1 whether condition 2 leads to significantly higher activity than condition 1 *and* with contrast \mathbf{c}_2 whether condition 3 leads to significantly higher activity than condition 2. This question could be tested with the following conjunction contrast:

$$\mathbf{c}_1 \wedge \mathbf{c}_2 = [-1 \ 1 \ 0] \wedge [0 \ -1 \ 1].$$

Note that a logical “AND” operation is defined for Boolean values (true/false) but that t values associated with individual contrasts can assume any real value. An appropriate way to implement a logical “AND” operation for conjunctions of contrasts with continuous statistical values is to use a mini-

mum operation, that is, the significance level of the conjunction contrast is identical to the significance level of the contrast with the smallest t value: $t_{c1} \wedge t_{c2} = \min(t_{c1}, t_{c2})$. For more details about conjunction testing, see Nichols et al. (2005).

3.3.3.4 Multicollinear Design Matrices

Multicollinearity exists when predictors of the design matrix are highly intercorrelated. To assess multicollinearity, pair-wise correlations between predictors are not sufficient. A better way to detect multicollinearity is to regress each predictor variable on all the other predictor variables and examine the resulting R^2 values. Perfect or total multicollinearity occurs when a predictor of the design matrix is a linear function of one or more other predictors, that is, when predictors are linearly dependent on each other. While in this case solutions for the GLM system of equations still exist, there is no *unique* solution for the beta values. From a mathematical perspective of the GLM, the square matrix $\mathbf{X}'\mathbf{X}$ becomes *singular*, that is, it loses (at least) one dimension, and is no longer invertible in case that \mathbf{X} exhibits perfect multicollinearity. Matrix inversion is required to calculate the essential term $(\mathbf{X}'\mathbf{X})^{-1}$ used for computing beta values and standard error values (see above). Fortunately, special methods, including singular value decomposition (SVD), allow obtaining (pseudo-) inverses for singular (rank-deficient) matrices. Note, however, that in this case the absolute values of beta weights may be difficult to interpret, and statistical hypothesis tests must meet special restrictions.

In fMRI design matrices, multicollinearity occurs if all conditions are modeled as predictors in the design matrix including the baseline (rest, control) condition. Without the baseline condition, multicollinearity is avoided and beta weights are obtained which are easily interpretable. As an example consider the case of two main conditions and a rest condition. If we would not include the rest condition (recommended), the design matrix would not be multicollinear and the two beta weights b_1 and b_2 would be interpretable as increase or decrease of activity relative to the baseline signal level modeled by the constant term (Fig. 17, right). Contrasts could be specified to test single beta weights, for example, the contrast $\mathbf{c}=[1 \ 0]$ would test whether condition 1 leads to significant (de)activation. Furthermore, the two main conditions could be compared with the contrast $\mathbf{c}=[-1 \ 1]$, which would test whether condition 2 leads to significantly more activation than condition 1. If the design matrix would include a predictor for the rest condition, we would obtain perfect multicollinearity and the matrix $\mathbf{X}'\mathbf{X}$ would be singular. Using a pseudo-inverse or SVD approach, we would obtain now three beta values (plus the constant), one for the rest condition, one for main condition 1, and one for main

³Note that the constant term is treated as a confound and it is not included in contrast vectors, i.e., it is implicitly assumed that b_0 is multiplied by 0 in all contrasts. To include the constant explicitly, each contrast vector must be expanded by one entry at the beginning or end.

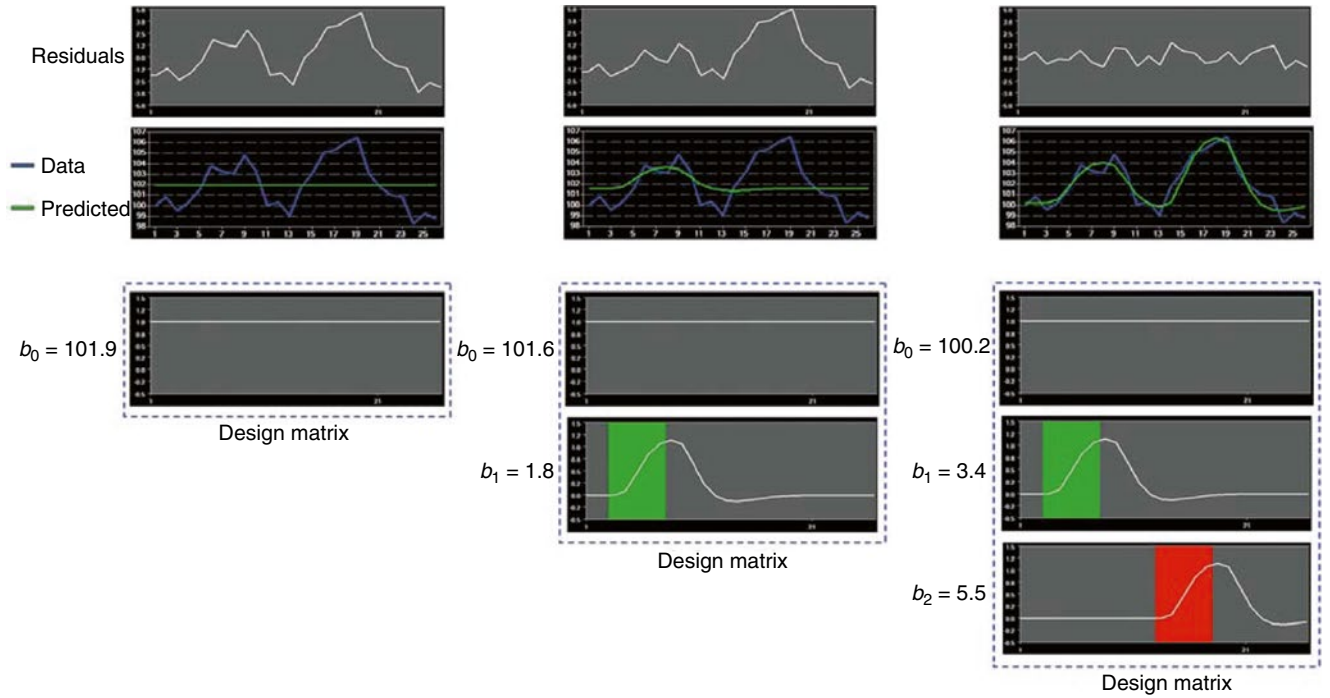


Fig. 17 Three GLMs fitting the same data with different design matrices. *Top row* shows residuals, *second row* predicted (green) and observed (blue) voxel time course. The design matrix on the left contains only one predictor, the constant term. The estimated beta weight (b_0) scales the constant term to the mean signal level. The design matrix in the middle adds a predictor for *green* main condition. The estimated beta weights (b_0, b_1) scale the predictors and the

weighted sum explains more variance than first model, but residual variance is still high. The third model (*right*) adds a predictor for *red* main condition. The estimated beta weights (b_0, b_1, b_2) scale the predictors and weighted sum now explains all task-related signal fluctuations. The residuals reflect now only noise. The example highlights the importance of modeling all known effects in the design matrix

condition 2. While the values of beta weights might not be interpretable, correct inferences of contrasts can be obtained if an additional restriction is met, typically that the sum of the contrast coefficients equals 0. To test whether main condition 1 differs significantly from the rest condition, the contrast $\mathbf{c}=[-1+1 \ 0]$ would now be used. The contrast $\mathbf{c}=[0-1+1]$ would be used to test whether condition 2 leads to more activation than condition 1.

3.3.3.5 GLM Assumptions

Given a correct model (design matrix), the standard estimation procedure of the GLM – ordinary least squares (OLS) – operates correctly only under the following assumptions. The population error values ε must have an expected value of zero and constant variance at each time point i :

$$E[\varepsilon_i] = 0$$

$$\text{Var}[\varepsilon_i] = \sigma^2$$

Furthermore, the error values are assumed to be uncorrelated:

$$\text{cov}(\varepsilon_i, \varepsilon_j) = 0 \text{ for all } i \neq j$$

To justify the use of t and F distributions in hypothesis tests, errors are further assumed to be normally distributed:

$$\varepsilon_i \sim N(0, \sigma^2)$$

In summary, errors are assumed to be normal independent and identically distributed (often abbreviated as “normal i.i.d.”). Under these assumptions, the solution obtained by the least squares method is optimal in the sense that it provides the most efficient unbiased estimation of the beta values. While the OLS approach is robust with respect to small violations, assumptions should be checked. In the context of fMRI measurements, the assumption of uncorrelated error values requires special attention.

3.3.3.6 Correction for Serial Correlations

In fMRI data, one typically observes *serial correlations*, that is, high values are followed more likely by high values than low values and vice versa. The assessment of these serial correlations is not performed on the original voxel time course but on the time course of the residuals since serial correlations in the recorded signal are expected to some

extent from slow task-related fluctuations. Task-unrelated serial correlations most likely occur because data points are measured in rapid succession, that is, they are also observed when scanning phantoms. Likely sources of temporal correlations are physical and physiological noise components such as hardware-related low-frequency drifts, oscillatory fluctuations related to respiration and cardiac pulsation, and residual head motion artifacts. Serial correlations violate the assumption of uncorrelated errors (see section above). Fortunately the beta values estimated by the GLM are correct estimates (unbiased) even in presence of serial correlations. The standard errors of the betas are biased, however, leading to “inflated” test statistics, that is, t or F values are higher than they should be. This can be explained by considering that the presence of serial correlations (serial dependence) reduces the true number of independent observations (effective degrees of freedom) that will, thus, be lower than the nominal number of observations. Without correction, the degrees of freedom are systematically overestimated leading to an underestimation of the error variance resulting in inflated statistical values, that is, t or F values are too high. It is, thus, necessary to correct for serial correlations in order to obtain valid error probabilities. Serial correlations can be corrected using several approaches. In *pre-whitening* approaches, autocorrelation is first estimated and removed from the data; the pre-whitened data can then be analyzed with a standard OLS GLM solution. In *pre-coloring* approaches (e.g., Friston et al. 1995), a strong autocorrelation structure is imposed on the data by temporal smoothing and degrees of freedom are adjusted according to the imposed (known) autocorrelation. The pre-coloring (temporal smoothing) operation acts, however, as a low-pass filter and may weaken experimentally induced signals of interest and is thus not the preferred method. The pre-whitening approach can be expressed in terms of a more powerful estimation procedure than OLS called *generalized least squares* (GLS, Searle et al. 1992). As opposed to the OLS method, GLS works correctly also in case that error values exhibit correlations or when error variances are not homogeneous. Note, however, that this more powerful estimation approach only provides correct results in case that the true (population) variances and covariances of the error values are known. With the known error covariance matrix \mathbf{V} , the betas and their (co-)variances can be calculated with GLS as follows:

$$\mathbf{b} = (\mathbf{X}'\mathbf{V}^{-1}\mathbf{X})^{-1} \mathbf{X}'\mathbf{V}^{-1} \mathbf{y}$$

$$\text{cov}(\mathbf{b}) = (\mathbf{X}'\mathbf{V}^{-1}\mathbf{X})^{-1}$$

With the obtained b values and their covariances, any contrast can then be assessed statistically as described above for the OLS method. When comparing the GLS solution with the OLS solution, it is evident that the inverse of the population error

covariance matrix \mathbf{V}^{-1} is needed to properly treat the effect of covariance of the errors on the parameter estimates (betas and their covariances). Note also that when setting \mathbf{V} as a diagonal matrix (entries outside the main diagonal are zero, i.e., no covariation of errors) with equal variance values (all values of the main diagonal are the same, e.g., 1), the GLS equation reduces to the OLS solution, that is, the \mathbf{V}^{-1} term vanishes.

Since the population covariance matrix of the error values \mathbf{V} is usually not known, it needs to be estimated from the data itself. Since there are too many degrees of freedom (number of time points squared: n^2), \mathbf{V} cannot be estimated for the general case of arbitrary covariance matrices. It is, however, often possible to estimate \mathbf{V} for special cases where only some parameters need to be estimated. The two most important special cases in the context of fMRI data analysis are the treatment of serial correlations (see below) and the treatment of unequal variances when integrating data from different subjects in the context of mixed-effects group analyses.

A simple pre-whitening procedure was developed (Cochrane and Orcutt 1949; Bullmore et al. 1996) independently from the GLS approach but can be shown to be identical to a GLS solution. The procedure assumes that the errors follow a first-order autoregressive, or AR(1), process. After calculation of a GLM using OLS, the amount of serial correlation a_1 is estimated using pairs of successive residual values (e_i, e_{i+1}) , that is, the residual time course is correlated with itself shifted by one time point (lag = 1). In the second step, the estimated serial correlation is removed from the measured voxel time course by calculating the transformed time course $y_i^n = y_{i+1} - a_1 \cdot y_i$. The superscript “ n ” indicates the values of the new, adjusted time course. The same calculation is also applied to each predictor time course resulting in an adjusted design matrix \mathbf{X}^n . In the third step, the GLM is recomputed using the adjusted voxel time course and adjusted design matrix resulting in correct standard errors for beta estimates and, thus, correct significance levels for contrasts (of course under the assumption that the AR(1) model is correct). If autocorrelation is not sufficiently reduced in the new residuals, the procedure can be repeated. If performed using the GLS approach, the first step is identical to the Cochrane-Orcutt method, that is, OLS is used to fit the GLM and the obtained residuals are used to estimate the value of the AR(1) term. The adjustment of the time course y_i and the design matrix described above need, however, not be performed explicitly since these adjustments are handled implicitly in the next step by using a \mathbf{V}^{-1} term in the GLS equations that contains values in the off-diagonal elements derived from the estimated serial correlation term.

While an AR(1) autocorrelation model substantially reduces serial correlations in fMRI data, better results are obtained when using an AR(2) model, that is, both first-order and second-order autocorrelation terms should be estimated and used to construct the error covariance matrix \mathbf{V} for GLS estimation. Since serial correlations differ across voxels,

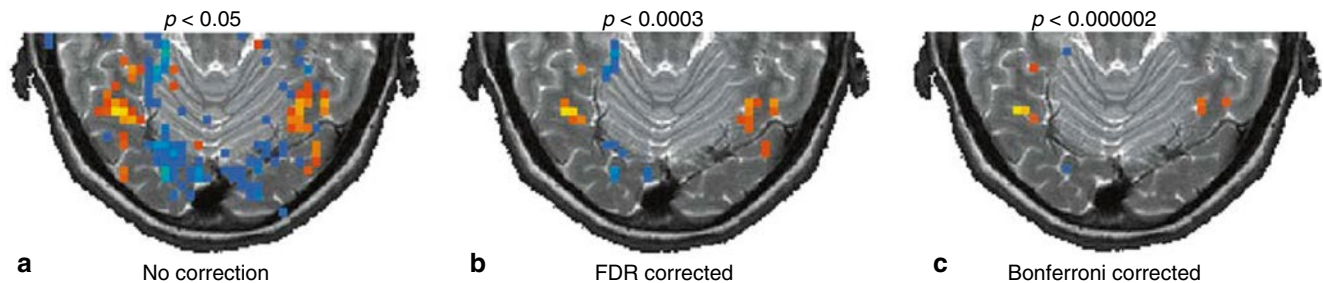


Fig. 18 Comparison of two methods used to solve the multiple comparisons problem. A statistical map has been computed comparing responses to faces and houses. Red/yellow colors depict regions with larger responses to faces than to houses, while blue regions indicate areas with larger responses to houses than to faces. (a) No correction for multiple comparisons has been performed. (b)

Thresholding result when using the false discovery rate approach (FDR). (c) Thresholding result when using the Bonferroni method. The p values shown on top of each panel have been used to threshold the map as provided by the respective method. The FDR method shows more voxels as significant because it is less conservative than the Bonferroni method

serial correlation correction should be performed separately for each voxel time course as opposed to the (also used) estimation of serial correlation values from multiple averaged (neighboring) voxel time courses. An AR(2) serial correlation model applied separately for each voxel time course has been recently shown to be the most accurate approach to treat serial correlations when compared to other models (Lenoski et al. 2008).

3.3.4 Creation of Statistical Maps

The statistical analysis steps were described for a single voxel's time course since standard statistical methods are performed independently for each voxel (univariate “voxel-wise” analysis). Since a typical fMRI data set contains several hundred thousand voxels, a statistical analysis is performed independently hundred thousands of times. Running a GLM, for example, results in a set of estimated beta values attached to each voxel. A specified contrast $\mathbf{c}' \mathbf{b}_v$ will be performed using the same contrast vector \mathbf{c} for each voxel v , but it will use a voxel's vector of beta values \mathbf{b}_v (and the voxel's error term) to obtain voxel-specific t and p values. Statistical test results for individual voxels are integrated in a 3D data set called a *statistical map*. To visualize a statistical map, the obtained values, for example, contrast t values, can be shown at the location of each voxel replacing anatomical intensity values shown as default. As a further useful condition, the statistical values are often only shown for those voxels exceeding a specified *statistical threshold*. This allows visualizing anatomical information in large parts of the brain while statistical information is shown (overlaid) only in those regions exhibiting suprathreshold (usually statistically significant) signal modulations. While anatomical information is normally visualized using a range of gray values, suprathreshold statistical test values are typically visualized using multiple colors, for example, a red-to-yellow range for positive values and a green-to-blue range for negative values. With these colors, a positive (negative) t value just passing a

specified threshold would be colored in red (green), while a very high positive (negative) t value would be colored in yellow (blue) (Fig. 18).

3.3.5 The Multiple Comparison Problem

An important issue in fMRI data analysis is the specification of an appropriate threshold for statistical maps. If there would be only a single voxel's data, a conventional threshold of $p < 0.05$ (or $p < 0.01$) could be used to assess significance of an observed effect quantified by an R , t , or F statistic. Running the statistical analysis separately for each voxel creates, however, a *massive multiple comparison problem*. If a *single test* is performed, the conventional threshold protects from wrongly declaring a voxel as significantly modulated (false positive) with a probability of $p < 0.05$ when there is no effect in the population (α error). Note that in case that the null hypothesis (no effect) holds, an adopted error probability of $p = 0.05$ implies that if the same test would be repeated 100 times, the alternative hypothesis would be accepted wrongly on average in five cases, that is, we would expect 5 % of false positives. If we assume that there is no real effect in any voxel time course, running a statistical test spatially in parallel is statistically identical to repeating the test 100,000 times at a single voxel (each time with new measured data). It is evident that this would lead to about 5,000 false positives, that is, about 5,000 voxels would be labeled “significant” although these voxels would reach the 0.05 threshold purely due to chance.

Several methods have been suggested to control this massive multiple comparison problem. The *Bonferroni correction* method is a simple multiple comparison correction that controls the α error *across all voxels*, and it is therefore called a *family-wise error* (FWE) correction approach. The method calculates single-voxel threshold values in such a way that an error probability of 0.05 is obtained at the global level. With N independent tests, this is achieved by using a statistical

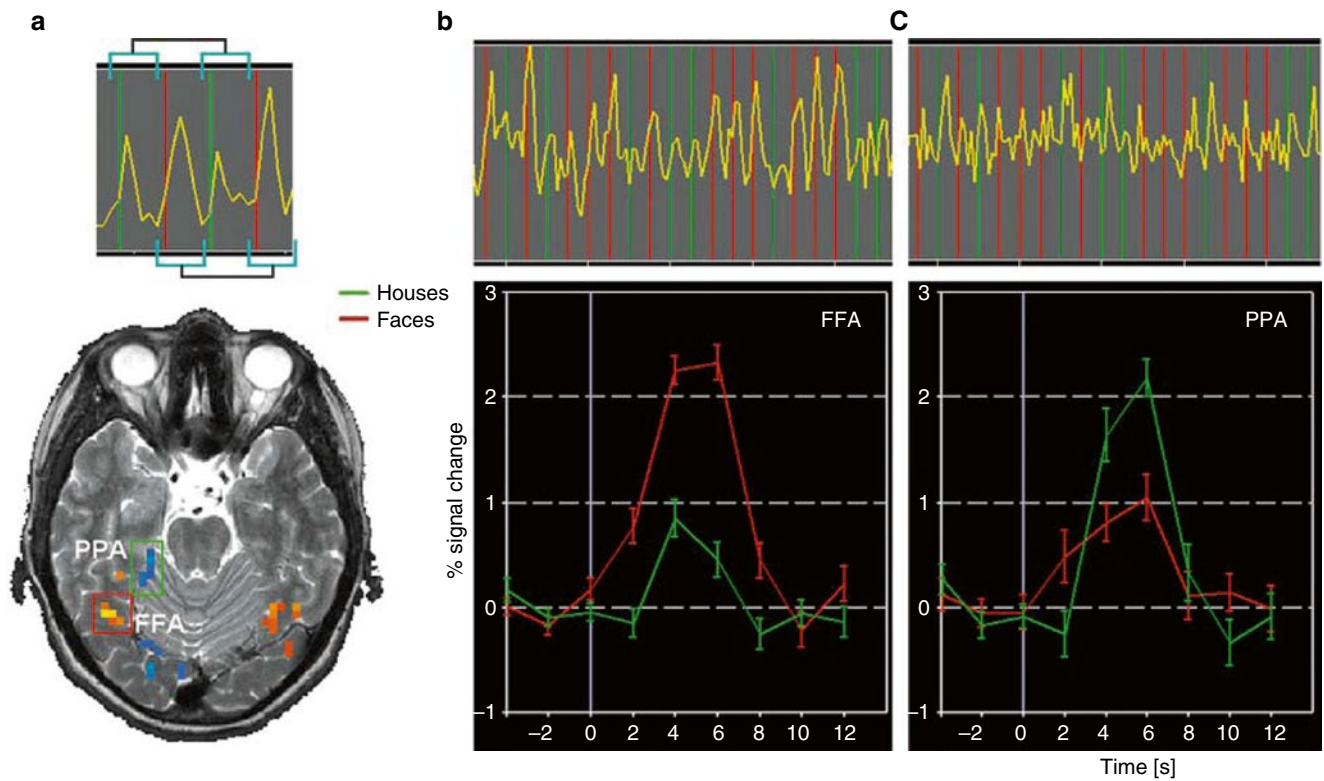


Fig. 19 Principle of event-related averaging and event-related averaging plots from a slow event-related design. (a) The thresholded statistical map shows in red/yellow color brain regions responding more to faces than to houses and in blue color brain regions responding more to houses than to faces. The areas demarcated with red and green rectangles in the lower panel correspond well to fusiform face

area (FFA) and parahippocampal place area (PPA), respectively (O’Craven and Kanwisher 2000). (b) Time course from FFA (*upper panel*) and event-related averaging plot (*lower panel*) obtained by selectively averaging all responses belonging to the same condition. (c) Time course (*upper panel*) and event-related averaging plot (*lower panel*) from PPA

significance level which is N times smaller than usual. The Bonferroni correction can be derived mathematically as follows. Under the assumption of independent tests, the probability that all of N performed tests lead to a sub-threshold result is $(1-p)^N$ and the probability to obtain one or more false-positive results is $1-(1-p)^N$. In order to guarantee a family-wise (global) error probability of $p_{\text{FWE}}=1-(1-p)^N$, the threshold for a single test, p , has to be adjusted as follows: $p=1-(1-p_{\text{FWE}})^{1/N}$. For small p_{FWE} values (e.g., 0.05), this equation can be approximated by $p=p_{\text{FWE}}/N$. This means that to obtain a global error probability of $p_{\text{FWE}}<0.05$, the significance level for a single test is obtained by dividing the family-wise error probability by the number of independent tests. Given 100,000 voxels, we would obtain an adjusted single-voxel threshold of $p_v = p_{\text{FWE}}/N = 0.05/100,000 = 0.0000005$. The Bonferroni correction method ensures that we do not declare even a single voxel wrongly as significantly activated with an error probability of 0.05. For fMRI data, the Bonferroni method would be a valid approach to correct the α error if the data at neighboring voxels would be truly independent from each other. Neighboring voxels, however, show similar response patterns within functionally

defined brain regions, such as the fusiform face area (FFA). In the presence of such spatial correlations, the Bonferroni correction method operates too conservative, that is, it corrects the error probability more strongly than necessary. As a result of a too strict control of the α error, the sensitivity (power) to detect truly active voxels is reduced: Many voxels will be labeled as “not significant” although they likely reflect true effects. As described earlier, wrongly accepting (rejecting) a null (alternative) hypothesis is called type II error or β error.

Worsley et al. (1992) suggested a less conservative approach to correct for multiple comparisons taking explicitly the observation into account that neighboring voxels are not activated independently from each other but are more likely to activate together in clusters. In order to incorporate spatial neighborhood relationships in the calculation of global error probabilities, the method describes a statistical map as a *Gaussian random field* (for details, see Worsley et al. 1992). Unfortunately, application of this correction method requires that the fMRI data are spatially smoothed substantially reducing one of its most attractive properties, namely, the achievable high spatial resolution.

Another correction method incorporating the observation that neighboring voxels often activate in clusters is based on Monte Carlo simulations that generate many random images (maps) using the spatial correlation structure of the original map; the generated maps are used to calculate the likelihood to obtain different sizes of functional clusters by chance for specific (less conservative) single-voxel thresholds (Forman et al. 1995). The calculated cluster extent threshold combined with a less strict single-voxel threshold is finally applied to the statistical map ensuring that a global error probability of $p < 0.05$ is met. This approach does not require spatial smoothing and appears highly appropriate for fMRI data. A disadvantage is that the method is quite compute intensive and that small functional clusters might not be discovered.

While the described multiple comparison correction methods aim to control the family-wise error rate, the *false discovery rate (FDR) approach* (Benjamini and Hochberg 1995) uses a different statistical logic and has been proposed for fMRI analysis by Genovese and colleagues (2002). This approach does not control the overall number of false-positive voxels but the number of false-positive voxels among the subset of voxels labeled as significant. Given a specific threshold, suprathreshold voxels are called “discovered” voxels or “voxels declared as active.” With a specified false discovery rate of $q < 0.05$, one would accept that 5 % of the discovered (suprathreshold) voxels would be false positives. Given a desired false discovery rate, the FDR algorithm calculates a single-voxel threshold, which ensures that the voxels beyond that threshold contain on average not more than the specified proportion of false positives. With a q value of 0.05, this also means that one can “trust” 95 % of the suprathreshold (i.e., color-coded) voxels since the null hypothesis has been rejected correctly. Since the FDR logic relates the number of false positives to the amount of truly active voxels, the FDR method adapts to the amount of activity in the data: The method is very strict if there is not much evoked activity in the data but assumes less conservative thresholds if a larger number of voxels show task-related effects. In the extreme case that not a single voxel is truly active, the calculated single-voxel threshold is identical to the one computed with the Bonferroni method. The FDR method appears ideal for fMRI data because it does not require spatial smoothing and it detects voxels with a high sensitivity (low β error) if there are true effects in the data.

Another simple approach to the multiple comparisons problem is to reduce the number of tests by using anatomical masking. Most correction methods, including Bonferroni and FDR, can be combined with this approach since a smaller number of tests leads to a less strict control of the α error and thus a smaller β error is made as compared to inclusion of all

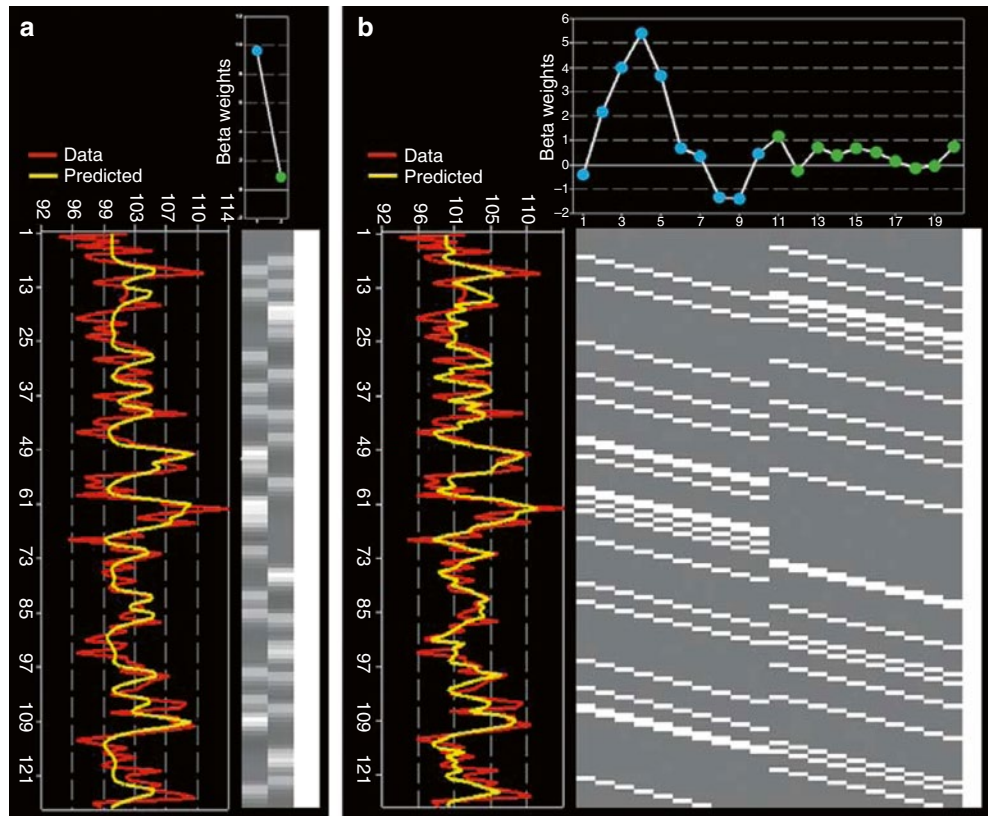
voxels. In a simple version of an anatomical mask, an intensity threshold for the basic signal level can be used to remove voxels outside the head. The number of voxels can be further reduced by masking the brain, for example, after performing a brain extraction step. These simple steps typically reduce the number of voxels from about 100,000 to about 50,000 voxels. In a more advanced version (Goebel and Singer 1999) statistical data analysis may be restricted to gray matter voxels, which may be identified by standard cortex segmentation procedures (e.g., Kriegeskorte and Goebel 2001). This approach not only removes voxels outside the brain but also excludes voxels in the white matter and ventricles. Note that anatomically informed correction methods do not require spatial smoothing of the data and not only reduce the multiple comparisons problem but also reduce computation time since fewer tests (e.g., GLM calculations) have to be performed.

3.3.6 Event-Related Averaging

Event-related designs cannot only be used to *detect* activation effects but also to *estimate* the time course of task-related responses. Visualization of mean response profiles can be achieved by averaging all responses of the same condition across corresponding time points with respect to stimulus onset. Averaged (or even single trial) responses can be used to characterize the temporal dynamics of brain activity within and across brain areas by comparing estimated features such as response latency, duration, and amplitude (e.g., Kruggel and von Cramon 1999; Formisano and Goebel 2003). In more complex, temporally extended tasks, responses to subprocesses may be identified. In working memory paradigms, for example, encoding, delay, and response phases of a trial may be separated. Note that event-related selective averaging works well only for slow event-related designs. In rapid event-related designs, responses from different conditions lead to substantial overlap, and event-related averages are often meaningless. In this case, deconvolution analysis is recommended (see below).

In order to avoid circularity, event-related averages should only be used descriptively if they are selected from significant clusters identified from a whole-brain statistical analysis of the same data. Even a merely descriptive analysis visualizing averaged condition responses is, however, helpful in order to ensure that significant effects are caused by “BOLD-like” response shapes and not by, for example, signal drifts or measurement artifacts. If ROIs are determined using independent (localizer) data, event-related averages extracted from these regions in a subsequent (main) experiment can be statistically analyzed. For a more general discussion of ROI vs. whole-brain analyses, see Friston and Henson (2006), Friston et al. (2006), Saxe et al. (2006), and Frost and Goebel (2013).

Fig. 20 Deconvolution analysis of a rapid event-related design. Time runs from *top to bottom*, design matrix depicted in graphical view. Beta values are plotted horizontally at positions corresponding to the respective predictor. (a) Standard analysis with two main predictors obtained by convolution of stimulus times with standard hemodynamic response model (two gamma function). Beta values can be compared with a standard contrast. (b) Deconvolution analysis fitting the same data. Each condition is modeled with ten “stick” predictors allowing to estimate the time course of condition-related responses as if stimuli were presented in a slow event-related design. Beta values may be compared within and across conditions



3.3.7 Deconvolution Analysis

While standard design matrix construction (convolution of box-car with two gamma function) can be used to estimate condition amplitudes (beta values) in rapid event-related designs, results critically depend on the appropriateness of the assumed standard BOLD response shape: Due to variability in different brain areas within and across subjects, a *static* model of the response shape might lead to non-optimal fits. Furthermore, the isolated responses to different conditions cannot be visualized due to overlap of condition responses over time. To model the shape of the hemodynamic response more flexibly, multiple basis functions (predictors) may be defined for each condition instead of a single predictor. Two often-used additional basis functions are derivatives of the two gamma function with respect to two of its parameters, delay and dispersion. If added to the design matrix for each condition, these basis functions allow capturing of small variations in response latency and width of the response. Other sets of basis functions (i.e., gamma basis set, Fourier basis set) are much more flexible, but obtained results are often more difficult to interpret. *Deconvolution analysis* is a general approach to estimate condition-related response profiles using a flexible and interpretable set of basis functions. It can be easily implemented as a GLM by defining an appropriate design matrix (Fig. 20) that models each bin after

stimulus onset by a separate condition predictor (delta or “stick” functions). This is also called a finite impulse response (FIR) model because it allows estimating any response shape evoked by a short stimulus (impulse). In order to capture the BOLD response for short events, about 20 s is typically modeled after stimulus onset. This would require, for each condition, 20 predictors in case of a TR of 1 s or ten predictors in case of a TR of 2 s (Fig. 20). Despite overlapping responses, fitting such a GLM “recovers” the underlying condition-specific response profiles in a series of beta values, which appear in plots as if event-related averages have been computed in a slow event-related design (Fig. 20). Since each condition is modeled by a series of temporally shifted predictors, hypothesis tests can be performed that compare response amplitudes *at different moments in time* within and between conditions. Note, however, that the deconvolution analysis assumes a linear time invariant system (see Sect. 3.1). In order to uniquely estimate the large number of beta values from overlapping responses, variable ITIs must be used in the experimental design (see Sect. 3.1). The deconvolution model is very flexible allowing to capture any response shape. This implies that also non-BOLD-like time courses will be detected easily since the trial responses are not “filtered” by the ideal BOLD response shape as in conventional analysis.

3.4 Integration of Anatomical and Functional Data

The localization of the neural correlates of sensory, motor, and cognitive functions requires a precise relationship between voxels in calculated statistical maps with voxels in high-resolution anatomical data sets. This is especially important in single-subject analyses and, thus, for presurgical mapping. While it is recommended to also view statistical maps overlaid on a volume of the functional data itself, EPI data sets often do not contain sufficient anatomical detail to specify the precise location of an active cluster in a subject's brain. 3D renderings of high-resolution anatomical data sets may greatly aid in visualizing activated brain regions. Advanced visualization requires that a high-resolution 3D data set is recorded for a subject and that the functional data is *coregistered* to the 3D data set as precisely as possible. Anatomical data sets are also important for most brain normalization methods, which is a prerequisite of the analysis of whole-brain group studies. High-resolution anatomical data sets are typically recorded with T_1 -weighted MRI sequences. A typical structural scan covering the whole brain with a resolution of 1 mm in all three dimensions (e.g., 180 sagittal slices) lasts between 5 and 20 min on current 1.5 and 3.0 scanners.

3.4.1 Visualizing Statistical Maps on Anatomical Images

Having identified a statistically significant region in the functional data set does not easily allow a precise statement about its location in the brain of the subject since the functional data itself does often not contain enough anatomical details.⁴ If anatomical, coplanar images are available, it is already helpful to overlay the functional results (thresholded statistical maps) on these "in-plane" images. Figure 19a shows, for example, a statistical map on a high-resolution, coplanar, T_2 -weighted image. While high-resolution, coplanar images improve localization within the recording plane, the direction along slices is sampled with low resolution due to typical distances between slices of 3–5 mm (slice distance = slice thickness + slice gap). Identification of the anatomical substrate of an activated cluster greatly benefits from visualizing functional data over isotropic high-resolution 3D data sets. Overlaying or fusing images from functional data (MRI, PET, SPECT) with high-resolution anatomical MRI data sets is a common visualization method in functional

⁴While functional sequences are T_2^* weighted, the first functional volume of a run contains the richest anatomical detail because it is T_1 weighted. Unfortunately, this data set is often thrown away either by the scanner directly (during "prep scans") or by transfer of the data to the researcher. We recommend to keep the first functional volume and to use it for visualization and coregistration because of its relative richness in anatomical details.

imaging. In order to correctly fuse functional and anatomical data sets, appropriate coregistration transformations have to be performed.

3.4.2 Coregistration of Functional and Anatomical Data Sets

If functional images are superimposed on coplanar images, spatial transformations (translations and rotations) to align the two data sets are not necessary (except maybe the correction of small head movements and small geometric distortions), since the respective slices are measured at the same 3D positions. Since the coplanar anatomical images are usually recorded with a higher resolution (typically with a 256×256 matrix) than the functional images (typically 64×64 or 128×128 matrices), only a scaling factor has to be applied. To allow high-quality visualization of the functional data in arbitrary resliced anatomical planes, the functional data must be coregistered with high-resolution 3D data sets.

These high-resolution 3D data sets are usually recorded with different slice orientation and position than the functional data, and the coregistration step, thus, requires an affine spatial transformation including translation, rotation, and scaling. These three elementary spatial transformations can be integrated in a single transformation step expressed in a standard 4×4 spatial transformation matrix. If the high-resolution 3D data set has been recorded in the same scanning session as the functional data, the coregistration matrix can be constructed simply by using the scanning parameters (slice positions, pixel resolution, slice thickness) from both recordings. The alignment based on this information would be perfect if there would be no head movement between the anatomical and functional images. To further improve coregistration results, an additional intensity- or gradient-driven alignment step is usually performed after the initial (mathematical) alignment correcting for head displacements (and eventually geometric distortions) between the functional and anatomical recordings. While this step operates similar as described for motion correction, it is likely not possible to align the two data sets perfectly well in all regions of the brain due to signal dropouts and distortions in the functional EPI images. For neurosurgical purposes, it is important to ensure that at least the relevant regions of the brain do not suffer from EPI distortions and that they are perfectly coregistered with the anatomical data. EPI distortions and signal dropouts can be corrected to some extent with special MRI sequence modifications as well as with image processing software. Using appropriate visualization tools, it is also possible to manually align a functional volume with an anatomical 3D data set. The precision of manual alignment depends, however, strongly on acquired expertise.

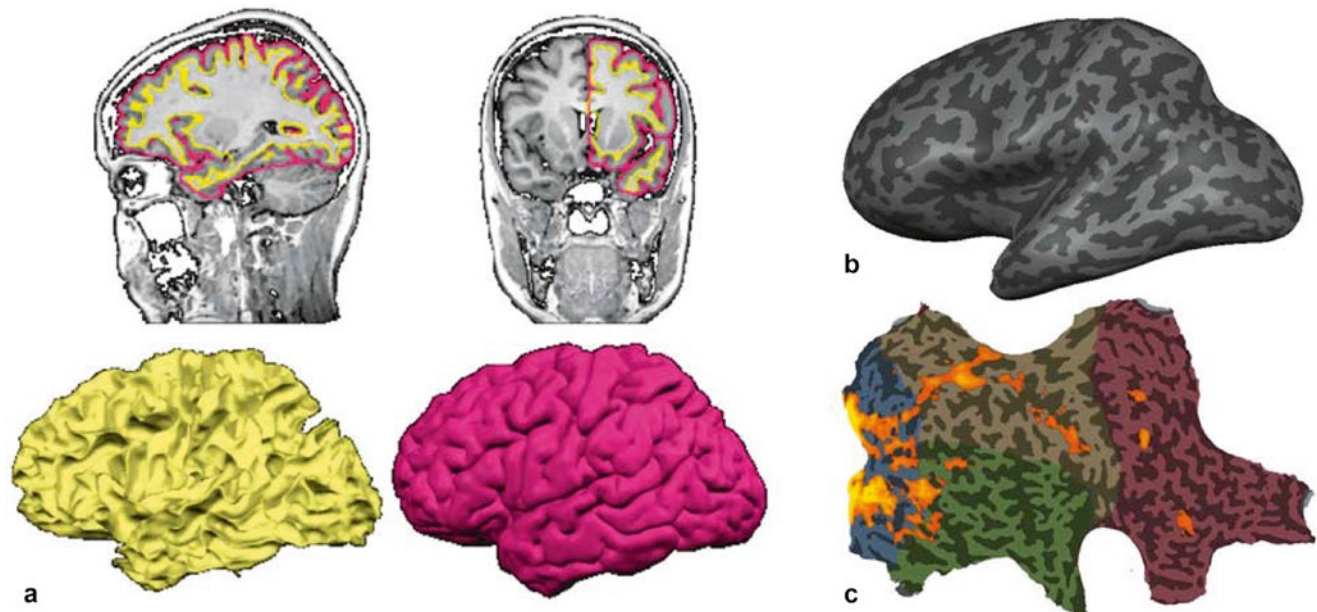


Fig. 21 Cortex representations used for advanced visualization. (a) Segmentation and surface reconstruction of the inner (white/gray matter, yellow) and outer (gray matter/CSF, magenta) boundary of the

gray matter. (b) “Inflated” cortex representation of the left hemisphere obtained by iterative morphing process. (c) “Flat map” of the right cortical hemisphere with superimposed functional data

3.4.3 Visualizing Statistical Maps on Reconstructed Cortex Representations

High-resolution anatomical data sets can be used to create 3D volume or surface renderings of the brain, which allow additional helpful visualizations of functional data on a subject’s brain (Fig. 21c). These visualizations require segmentation of the brain, which can be performed automatically with most available software packages. For more advanced visualizations, segmentation of cortical voxels allows to construct topologically correct mesh representations of the cortical sheet, one for the left and one of the right hemisphere (e.g., Fischl et al. 1999; Kriegeskorte and Goebel 2001). The obtained meshes (Fig. 21a) may be further transformed into inflated (Fig. 21b) and flattened (Fig. 21c) cortex representations. Functional data can then be superimposed on folded, inflated, and flattened representations (Fig. 21c), which is particularly useful for topologically organized functional information, for example, in the context of retinotopic, tonotopic, and somatotopic mapping experiments. To help in orientation, inflated and flattened cortex representations indicate gyral and sulcal regions by color-coding local curvature; concave regions, indicating sulci, may be depicted, for example, with a dark gray color, while convex regions, indicating gyri, may be depicted, for example, with a light gray color (Fig. 21). A general advantage of visualizing functional data on flat maps is that all cortical activation foci from different experiments can be visualized at once at their correct anatomical location in a canonical view. In contrast, visualizing several activated regions using a multi-slice representation

depends on the chosen slice orientation and number of slices. Note that anatomical data is not only important to visualize functional data. Anatomical information may also be used to constrain statistical data analysis as has been described in Sect. 3.3.5. Furthermore, the explicit segmentation of cortical voxels is also the prerequisite for advanced anatomical analyses, including cortical thickness analysis.

3.5 Group Analysis of Functional Data Sets

Presurgical neuroimaging requires detailed single-subject analyses, which can be performed with the methods described in the previous sections. A standardized routine for analyzing (clinical) fMRI data in individuals is given in chapter [Task-based presurgical functional MRI in patients with brain tumors](#). If, however, characterization and statistical assessment of general brain patterns is desired, multiple subjects have to be integrated in groups. Such *group studies* allow generalizing findings from a sample of subjects to the population from which the patients or healthy subjects have been drawn. Group analysis of functional data sets is of clinical relevance when the effects of various brain pathologies or different therapies (e.g., pharmacological effects) on brain function are subject to study.

The integration of fMRI data from multiple subjects is challenging because of the *spatial correspondence problem* between different brains. This problem manifests itself already at a purely anatomical level but presents a funda-

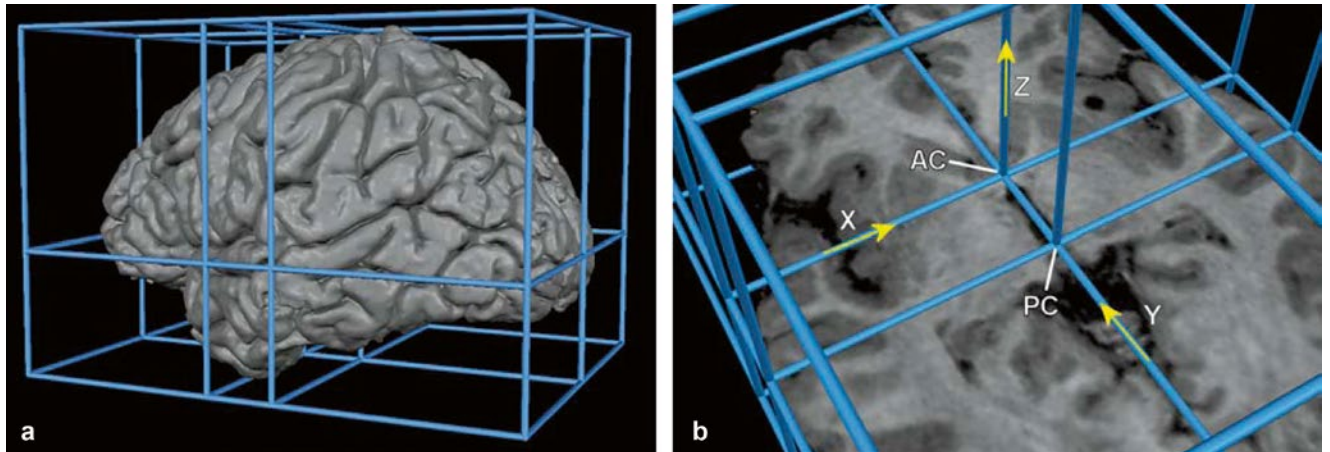


Fig. 22 Definition of Talairach space. (a) View from *left*. (b) View from *top*. Talairach space is defined by three orthogonal axes pointing from left to right (*x*-axis), posterior to anterior (*y*-axis), and inferior to superior (*z*-axis). The origin of the coordinate system is defined by the anterior commissure (AC). Coordinates are in millimeters. The posterior

commissure (PC) is located on the *y*-axis ($y = -23$ mm). The borders of the Talairach grid (a) correspond to the borders of the cerebrum. The most right point of the brain corresponds to $x = 68$ mm, the most left one to $x = -68$ mm, the most anterior one to $y = 70$, the most posterior one to $y = -102$, the most upper one to $z = 74$, and the most lower one to $z = -42$

mental problem of neuroscience when considered as a question of the consistency of structure-function relationships. At the anatomical level, the correspondence problem refers to the differences in brain shape and, more specifically, to differences in the gyral and sulcal pattern varying substantially across subjects. At this macroanatomical level, the correspondence problem would be solved if brains could be matched in such a way that for each macroanatomical structure in one brain, the corresponding region in the other brain would be known. In neuroimaging, the matching of brains is usually performed by a process called *brain normalization*, which involves warping each brain into a common space allowing averaging over (more or less) corresponding regions in different subjects. After brain normalization, a point in the common space identified by its *x*, *y*, and *z* coordinates is assumed to refer to a similar region in any other normalized brain. The most commonly used target space for normalization is the *Talairach space* (see below) and the closely related *MNI template space*. Unfortunately warping brains in a common space does not solve the anatomical correspondence problem very well, that is, macroanatomical structures, such as banks of prominent sulci are often still misaligned with deviations in the order of 0.5–1 cm. In order to increase the chance that corresponding regions overlap, functional data is therefore often smoothed with a Gaussian kernel with a width of about 1 cm. More advanced anatomical matching schemes attempt to directly align macroanatomical structures such as gyri and sulci (see below) and require less (or no) spatial smoothing of functional data.

The deeper version of the correspondence problem addresses the fundamental question of the existence of an identical relationship between certain brain functions and

neuroanatomical structures across subjects. While neuroimaging has successfully demonstrated that there is common structure-function relationship across brains, a high level of variability has also been observed, especially for higher cognitive functions. A more satisfying answer to this fundamental question might only emerge after much more careful investigations, for example, by letting the same subjects perform a large battery of tasks (Frost and Goebel 2012). An interesting approach to the functional correspondence problem has been proposed that aims to only align those brain regions-of-interest (ROIs), which are activated in a given task in all or most subjects.

3.5.1 Talairach Transformation

The most often-used standard space for brain normalization is the *Talairach space* (Talairach and Tournoux 1988) or the closely related *MNI template space*. Talairach transformation is controlled either by the (automatic) specification of a few prominent landmarks or by a data-driven alignment of a subject's brain to a target (average) brain (typically the MNI template brain) that has been previously transformed in (near-) Talairach space. In the explicit landmark-based approach (Talairach and Tournoux 1988), the midpoint of the anterior commissure (AC) is located first, serving as the origin of Talairach space. The brain is then rotated around the new origin (AC) so that the posterior commissure (PC) appears in the same axial plane as the anterior commissure (Fig. 22). The connection of AC and PC in the middle of the brain forms the *y*-axis of the Talairach coordinate system. The *x*-axis runs from the left to the right hemisphere through AC orthogonal to the *y*-axis. The *z*-axis runs from the inferior part of the brain to the superior part through AC orthogonal to both other axes. In order to further constrain the *x*- and

z -axes, a y - z plane is rotated around the y (AC-PC)-axis until it separates the left and right hemisphere (midsagittal plane). The obtained AC-PC space is attractive for individual clinical applications, especially presurgical mapping and neuro-navigation since it keeps the original size of the subject's brain intact while providing a common orientation for each brain anchored at important landmarks. For a full Talairach transformation, a cuboid is defined running parallel to the three axes enclosing precisely the cortex. This cuboid or bounding box requires specification of additional landmarks specifying the borders of the cerebrum. The bounding box is subdivided by several sub-planes. The midsagittal y - z plane separates two sub-cuboids containing the left and right hemisphere, respectively. An axial (x - y) plane through the origin separates two sub-cuboids containing the space below and above the AC-PC plane. Two coronal (x - z) planes, one running through AC and one running through PC, separate three sub-cuboids: the first contains the anterior portion of the brain anterior to the AC, the second contains the space between AC and PC, and the third contains the space posterior to PC. These planes separate 12 sub-cuboids. In a final Talairach transformation step, each of the 12 sub-cuboids is expanded or shrunken linearly to match the size of the corresponding sub-cuboid of the standard Talairach brain. To reference any point in the brain, x , y , and z coordinates are specified in millimeters of Talairach space. Talairach and Tournoux (1988) also defined the "proportional grid" to reference points within the defined cuboids.

In summary, Talairach normalization ensures that the anterior and posterior commissures obtain the same coordinates in each brain and that the sub-cuboids defined by the AC-PC points and the borders of the cortex will have the same size. Note that the specific distances between landmarks in the original postmortem brain are not important for establishing the described spatial relationship between brains. The important aspect of Talairach transformation is that correspondence is established across brains by linearly interpolating the space between important landmarks.

While Talairach transformation provides a recipe to normalize brains, regions at the same coordinates in different individuals do not necessarily point to homologous brain areas. This holds especially true for cortical regions (e.g., Frost and Goebel 2012). For subcortical structures around the AC-PC landmarks, however, the established correspondence is remarkably good even when analyzing high-resolution fMRI data (e.g., De Martino et al. 2013).

As an alternative to specify crucial landmarks, a direct approach of stereotactic normalization has been proposed (e.g., Evans et al. 1993; Ashburner and Friston 1999) that attempts to align each individual brain as good as possible to an average target brain, called *template brain*. The most often-used template brain is provided by the Montréal Neurological Institute (MNI) and has been created by aver-

aging many (>100) single brains after manual Talairach transformation. Although automatic alignment to a template brain has the potential to result in a better correspondence between brain regions, comparisons have shown that the achieved results are not substantially improved as compared to the explicit landmark specification approach, even when using nonlinear spatial transformation techniques. This can be explained by noting that the template brain has lost anatomical details due to extensive averaging. In order to bring functional data of a subject into Talairach space, the obtained spatial transformation for the anatomical data may be applied to the functional data if it has been coregistered with the unnormalized anatomical data set. Using the intensity-driven matching approach, functional data sets may also be directly normalized (without the help of anatomical data sets) because versions of the MNI template brain for functional (EPI) scans are also available. If possible, it is, however, recommended to apply the transformation obtained for the anatomical data also to the functional data because this approach guarantees that the precision of functional-anatomical alignment achieved during coregistration is not changed during the normalization step. More advanced volume-based normalization schemes have been proposed that replace the presented simple intensity-driven approaches (e.g., DARTEL, Ashburner 2007).

3.5.2 Cortex-Based Normalization

In recent years, more advanced brain normalization techniques have been proposed going beyond simple volume space alignment approaches. A particular interesting method attempts to explicitly align the cortical folding pattern (macroanatomy) across subjects (Fischl et al. 1999; Goebel et al. 2004, 2006; Frost and Goebel 2012) starting with topologically correct cortex mesh representations (see Sect. 3.4.3). The folded cortex meshes are first morphed to spherical representations since the restricted space of a sphere allows alignment using only two dimensions (longitude and latitude) instead of three dimensions as needed in volume space. Since the inflation of cortex hemispheres to spheres removes ("flattens") information of the gyral/sulcal folds, the respective information is retained by calculating curvature maps prior to inflation that are projected on the spherical representations. Cortex meshes from different subjects are then aligned on the sphere by *increasing the overlap of curvature information*. Since the curvature of the cortex reflects the gyral/sulcal folding pattern of the brain, this brain matching approach essentially aligns corresponding gyri and sulci across brains. It has been shown that cortex-based alignment substantially increases the statistical power and spatial specificity of group analyses by increasing not only the overlap of macroanatomical regions but also the overlap of corresponding functionally defined specialized brain areas (Frost and Goebel 2012).

3.5.3 Correspondence Based on Functional Localizer Experiments

An interesting approach to establish correspondence between brains is to use functional information directly. Using standardized stimuli, a specific region-of-interest (ROI) may be functionally identified in each subject. The ROIs identified in such *functional localizer experiments* are then used to extract time courses in subsequent main experiments. The extracted time courses of individual subjects are then integrated in group analyses (see below). If the assumption is correct that localizer experiments reveal corresponding brain regions in different subjects, the approach provides an optimal solution to the correspondence problem and will allow detection of subtle differences in fMRI responses at the group level with high statistical power. Statistical sensitivity is further enhanced by avoiding the massive multiple comparison correction problem. Instead of hundreds of thousand voxel-wise tests, only a few tests have to be performed – one for each considered ROI. The approach is statistically sound (no circularity) because the considered regions have been determined *independently* from the main data using special localizer runs. It may also be acceptable to use the same functional data for both localizer and main analysis as long as the contrast to localize ROIs is orthogonal to any contrast used to statistically test more subtle differences. The localizer approach has been applied successfully in many experiments, most notably in studies of the ventral visual cortex (e.g., O’Craven and Kanwisher 2000).

Unfortunately, it is often difficult to define experiments localizing the same pattern of activated brain areas in all subjects, especially in studies of higher cognitive functions, such as attention, mental imagery, working memory, and planning. If at all possible, the selection of corresponding functional brain areas in these experiments is very difficult and depends on the investigator’s choice of thresholding statistical maps and often on additional decisions such as grouping subclusters to obtain the same number of major clusters for each subject. Note that the increased variability of activated regions in more complex experiments could be explained by at least two factors. On the one hand the location of functionally corresponding brain regions may vary substantially across subjects with respect to aligned macro-anatomical structures. On the other hand, subjects may engage in different cognitive strategies to solve the same task leading to a (partially) different set of activated brain areas. Most likely, the observed variability is caused by a mixture of both sources of variability. Another problem of the localizer approach is the tendency to focus only on a few brain areas, namely, those, which can be mapped consistently in different subjects. This tendency bears the danger to overlook other important brain regions. This can be avoided by a recently proposed approach, functionally informed cortex-based alignment (Frost and Goebel 2013), that integrates

ROI-based and whole-cortex analysis using a modified version of cortex-based alignment that uses corresponding pre-mapped ROIs as alignment targets in addition to anatomical curvature information.

3.5.4 Statistical Analysis of Group Data

After brain normalization, the whole-brain data from multiple subjects can be statistically analyzed simply by concatenating time courses at corresponding locations. The corresponding locations can be voxel coordinates in Talairach/MNI space, vertex coordinates in cortex space, or identified ROIs in the localizer approach. Note that the power of statistical analysis depends on the quality of brain normalization. If the achieved alignment of corresponding functional brain areas is poor, suboptimal group results may be obtained since active voxels of some subjects will be averaged with non-active voxels (or active voxels from a non-corresponding brain area) from other subjects. In order to increase the overlap of activated brain areas across subjects in volume space, the functional data of each subject is often smoothed, typically using rather large Gaussian kernels with a full width at half maximum (FWHM) of 8–12 mm. While such an extensive spatial smoothing increases the overlap of active regions, it introduces other problems including potential averaging of non-corresponding functional areas within and across brains; furthermore, functional clusters smaller than the smoothing kernel will be suppressed. While spatial smoothing may be beneficial to reduce noise, it may also reduce detection sensitivity of truly active but small functional clusters. Extensive spatial smoothing may not be necessary when using advanced volumetric normalization schemes (e.g., Ashburner 2007), cortex-based alignment (e.g., Frost and Goebel 2012, 2013), or functional localizers.

After concatenating the data, the statistical analysis described for single-subject data (see Sect. 3.3) can be applied to the integrated time courses. In the context of the GLM, the multi-subject voxel time courses as well as the multi-subject predictors may be obtained by concatenation. After estimating the beta values, contrasts can be tested in the same way as described for single-subject data. While the described concatenation approach leads to a high statistical power due to the large number of blocks or events, the obtained results cannot be generalized to the population level since the data is analyzed as if it stems from a single subject. Significant findings only indicate that the results are replicable for the same “subject” (group of subjects). In order to test whether the obtained results are valid at the population level, the statistical procedure must assess the variability of observed effects across subjects (*random effects analysis*) as opposed to the variability across individual measurement time points as performed in the concatenation approach (*fixed effects analysis*). There are many statistical methods to

assess the variability across subjects for the purpose of proper population inferences. A simple and elegant method is provided by *multilevel summary statistics approach* (e.g., Kirby 1993; Holmes and Friston 1998; Worsley et al. 2002; Beckmann et al. 2003; Friston et al. 2005). In the first analysis stage, parameters (*summary statistics*) are estimated for each subject independently (level 1, fixed effects). Instead of the full time courses, only the resulting first-level parameter estimates (betas) from each subject are carried forward to the second analysis stage where they serve as the *dependent variables*. The second-level analysis assesses the consistency of effects within or between groups based on the variability of the first-level estimates across subjects (level 2, random effects). This hierarchical analysis approach reduces the data for the second stage analysis enormously since the time course data of each subject has been “collapsed” to only one or a few parameter estimates per subject. Since the summarized data at the second level reflects the variability of the estimated parameters across subjects, obtained significant results can be generalized to the population from which the subjects were drawn as a random sample.

To summarize the data at the first level, a standard GLM may be used to estimate effects – beta values – separately for each subject. Instead of one set of beta values in fixed effects analysis, this step will provide a *separate set of beta values for each subject*. The obtained beta values can be analyzed at the second level using again a GLM or a standard ANOVA with one or more within-subjects factors categorizing the beta values. If the data represent multiple groups of subjects, a between factor for group comparisons can be added.

These short explanations indicate that the statistical analysis at the second level does not differ from the usual statistical approach in medical studies. The only major difference to standard statistics is that the analysis is performed separately for each voxel (or vertex) requiring correction for a massive multiple comparison problem as has been described above. Note that in addition to the estimated subject-specific effects of the fMRI design (beta values of first-level analysis), additional external variables (e.g., an IQ value for each subject) may be incorporated as covariates at the second level.

3.6 Selected Advanced Data Analysis Methods

The analysis steps described in previous sections for single subjects and for group comparisons represent essential components of a standard fMRI analysis, which are performed in a similar way for most fMRI studies. Such a standard analysis involves proper preprocessing that includes drift removal and 3D motion correction, coregistration of functional and anatomical data, brain normalization, and a thorough statistical analysis usually based on the general linear model. The

standard procedure produces statistical maps that localize regions showing differential responses with respect to specified experimental hypotheses. Random effects group analyses allow generalization of observed findings from a sample of subjects to the population level. Event-related averages of active brain regions or prespecified ROIs can be used to compare estimated condition time courses within and across brain areas, often revealing additional interesting insights. The following sections shortly describe a selected list of further analysis methods aiming at improving or extending the standard analysis procedure.

3.6.1 Nonparametric Statistical Approaches

As stated in Sect. 3.3.3.5, GLM hypothesis testing requires normally distributed residuals with equal variance. Fortunately, the GLM is robust with respect to minor violations of the normality assumption. To avoid, however, wrong inferences due to non-normal distributions, nonparametric methods may be used, especially when analyzing small data samples.

3.6.2 Bayesian Statistics

It has been proposed to use Bayesian statistics because it provides an elegant framework for multilevel analyses (Friston et al. 2002). In the Bayesian approach, the data of a single experiment (or the data of a single subject) is not considered in isolation, but in light of available a priori knowledge. This a priori knowledge is formalized with prior probabilities $p(H_i)$ for relevant initial hypotheses H_i . Obtained new data D modifies the a priori knowledge resulting in posterior conditional probabilities $p(H_i|D)$, which are updated probabilities of the initial hypotheses given the new data. To calculate these probabilities, the inverse conditional probabilities $p(D|H_i)$ must be known describing the probability to obtain certain observations given that the hypotheses H_i are true. In the context of the *empirical Bayes approach*, these conditional probabilities can be estimated from the data. The empirical Bayes approach is appropriate for the analysis of fMRI data, since it allows an elegant formulation of hierarchical random effects analyses. It is, for example, possible to enter estimated parameters at a lower level as prior probabilities at the next higher level. Furthermore, the approach allows integrating correction for multiple comparisons resulting in thresholding values similar to the ones obtained with the false discovery rate approach.

3.6.3 Brain Normalization

As described earlier, brain normalization methods have an important influence on the quality of group analyses, since optimization of the standard analysis does not lead to substantial improvements if voxel time courses are concatenated from nonmatching brain regions. The described cortex-based normalization technique may substantially improve the alignment of homologous brain regions across

subjects. For more complex tasks, different, nonmatching activity patterns might reflect different cognitive strategies used by subjects. To cope with this situation, it would be desirable to use methods allowing automatic estimation of the similarity of activity patterns across subjects. Such methods could suggest splitting a group in subgroups with different statistical maps corresponding to the neural correlate of different cognitive strategies. Such a clustering approach has been recently implemented in the context of group-level ICA analyses (Esposito et al. 2005).

3.6.4 Data-Driven Analysis Methods

When considering the richness of fMRI data, it may be useful to apply *data-driven analysis methods*, which aim at discovering interesting spatiotemporal relationships in the data, which would be eventually overlooked with a purely hypothesis-driven approach. Data-driven methods, such as *independent component analysis* (ICA, e.g., McKeown et al. 1998a, b; Formisano et al. 2002), do not require a specification of expected, stimulus-related responses since they are able to extract interesting information automatically (“blindly”) from the data. It is, thus, not necessary to specify an explicit statistical model (design matrix). This is particularly interesting with respect to paradigms for which the exact specification of event onsets is difficult or impossible. Spatial ICA of fMRI data has been successfully applied in many tasks including the automatic detection of active networks during perceptual switches of ambiguous stimuli (Castelo-Branco et al. 2002) and the automatic detection of spontaneous hallucinatory episodes in schizophrenic patients (van de Ven et al. 2005). Data-driven methods are exploratory in nature and should not be viewed as replacements but as complementary tools for hypothesis-driven methods: If interesting, unexpected events have been discovered with a data-driven method, one should test these observations in succeeding studies with a hypothesis-driven standard statistical analysis. More generally, ICA has become an important method to reveal functionally connected networks, especially in the context of resting-state fMRI (see below).

3.6.5 Multivariate Analysis of Distributed Activity Patterns

Multi-voxel pattern analysis (MVPA) is gaining increasing interest in the neuroimaging community because it allows to detect differences between conditions with higher sensitivity than conventional univariate analysis by focusing on the analysis and comparison of distributed patterns of activity (Haxby et al. 2001). In such a multivariate approach, data from individual voxels within a region are jointly analyzed. Furthermore, MVPA is often presented in the context of “brain reading” applications reporting that specific mental

states or representational content can be decoded from fMRI activity patterns after performing a “training” or “learning phase.” In this context, MVPA tools are often referred to as classifiers or, more generally, learning machines. The latter names stress that many MVPA tools originate from a field called machine learning, a branch of artificial intelligence. In fMRI research, the support vector machine (SVM, Vapnik 1995) has become a particular popular machine learning classifier, which is used both for analyzing patterns in ROIs and for discriminating patterns that are potentially spread out across the whole brain.

Another popular MVPA approach is the “searchlight” method (Kriegeskorte et al. 2006). In this approach, each voxel is visited, as in a standard univariate analysis, but instead of using data of the visited voxel only for analysis, several voxels in the neighborhood are included forming a set of features for joined multivariate analysis. The neighborhood is usually defined roughly as a sphere, that is, voxels within a certain (Euclidean) distance from the visited voxel are included. The result of the multivariate analysis is then stored at the visited voxel (e.g., a *t* value resulting from a *multivariate* statistical comparison or an accuracy value from a support vector machine classifier). By visiting all voxels and analyzing their respective (partially overlapping) neighborhoods, one obtains a whole-brain map in the same way as when running univariate statistics.

3.6.6 Real-Time Analysis of fMRI Data

The described steps and techniques to analyze functional MRI data are very computation intensive and are, thus, performed in most cases hours or days after data acquisition has been completed. There are many scenarios that would benefit greatly from a *real-time analysis of fMRI data*, especially when studying single subjects as in presurgical mapping. Using appropriately modified analysis tools and state-of-the-art computer hardware, it is nowadays possible to perform real-time fMRI analysis during an ongoing experiment, including 3D motion correction and incremental GLM statistics of whole-brain recordings (Goebel 2012; Weiskopf 2012). It is even possible to run multivariate data-driven tools in real-time, including ICA (Esposito et al. 2003) and multi-voxel pattern analyses (LaConte et al. 2007; Sorger et al. 2010). One obvious benefit of real-time fMRI analysis is *quality assurance*. If, for example, one observes during an ongoing measurement that a patient moves too much or that the (absence of) activity patterns indicates that the task was not correctly understood, the running measurement may be stopped and repeated after giving the subject further instructions. If the ongoing statistical analysis on the other hand indicates that expected effects have reached a desired significance level earlier than expected, one could save scanning time by stopping the

measurement ahead of schedule. Real-time fMRI offers also the possibility to plan optimal slice positioning for subsequent runs based on the results obtained of an initial run. Based on the results of a first run, it would be, for example, possible to position a small slab of slices at an identified functional region for subsequent high-resolution spatial and/or temporal scanning. More advanced applications of real-time fMRI include neurofeedback (Weiskopf et al. 2003) and communication BCIs (Sorger et al. 2012). In fMRI neurofeedback studies, subjects learn to voluntarily control the level of activity in circumscribed brain areas by engaging in mental tasks such as inner speech, visual or auditory imagery, spatial navigation, mental calculation, or recalling (emotional) memories. In recent years, fMRI neurofeedback has been successfully employed as a therapeutic tool for various psychiatric and neurological diseases (e.g., Linden et al. 2012; Subramanian et al. 2011).

4 Functional Connectivity and Resting-State Networks

Generally, three types of brain connectivity are distinguished in brain research (Sporns 2010). *Structural connectivity* (or anatomical connectivity) refers to the physical presence of an axonal projection from one brain area to another. This type of connectivity and how diffusion MRI and computational tractography can be used to identify large axon bundles in the human brain is described in Sect. 5. *Functional connectivity* refers to the correlation structure in the data that can be used to reveal functional coupling between specific brain regions and to reveal functional networks. Finally, *effective connectivity* refers to models that go beyond correlation (or more generally statistical dependency) to more advanced measures of directed influence and causality within networks (Friston et al. 1994).

4.1 Functional and Effective Connectivity

Functional and effective connectivity methods aim to reveal the *functional integration* of brain areas, whereas the classical voxel-wise statistical approach (Sect. 3) is suited to reveal the *functional segregation* (functional specialization) of brain regions. Besides data-driven methods such as independent component analysis (ICA), many approaches have been used to model the interaction between spatially remote brain regions more explicitly. In the simplest case, the time courses from two regions are correlated resulting in a measure (e.g., linear correlation coefficient) of functional connectivity. Functional connectivity can be calculated separately for

different experimental conditions, which allows to assess whether two brain areas change their *functional coupling* in different cognitive contexts (Büchel et al. 1999). In conditions of attention, for example, two remote areas might work more closely with each other than in conditions of no attention.

Models of effective connectivity go beyond simple pairwise correlation analysis and assess the validity of models containing directed interactions between brain areas. These directed effective connections are often symbolized by arrows connecting boxes each representing a different brain area. Structural equation models (SEM, e.g., McIntosh and Gonzalez-Lima 1994) and, more recently, dynamic causal modeling (DCM, e.g., Penny et al. 2004) are used to test effective connectivity models. An interesting *data-driven* approach to effective connectivity modeling is provided by methods based on the concept of *Granger causality*. This approach does not require specification of connectivity models but enables to automatically detect effective connections from the data by mapping Granger causality for any selected reference voxel or region-of-interest (Goebel et al. 2003; Roebroeck et al. 2005, 2011).

4.2 Resting-State Networks

In recent years, functional connectivity studies have gained increased interest where the subject is in a relaxed resting state, that is, in the absence of experimental tasks and behavioral responses. These *resting-state fMRI* (RS-fMRI) studies allow measuring the amount of spontaneous BOLD signal synchronization within and between multiple regions across the entire brain (Biswal et al. 1995). The measured RS-fMRI activity is characterized by low-frequency (0.01–0.1 Hz) BOLD signal fluctuations, which are topologically organized as multiple spatially distributed functional connectivity networks called *resting-state networks* (RSNs) (e.g., van de Ven et al. 2004; De Luca et al. 2006). Spatial ICA (see Sect. 3.6.4) at the individual and group level is commonly applied in resting-state fMRI revealing RSNs that are consistently found in individuals, including the default-mode network (often separated in an anterior and posterior subnetwork), a visual and a auditory network, a sensorimotor network, and two (lateralized) dorsolateral frontoparietal networks (Fig. 23; for further details, see, e.g., Allen et al. 2011). The extracted independent components are usually scaled to spatial z-scores (i.e., the number of standard deviations of their whole-brain spatial distribution). These values express the relative amount a given voxel is modulated by the activation of the component (McKeown et al. 1998b) and hence reflect the amplitude of the correlated fluctuations within the corresponding functional connectivity network.

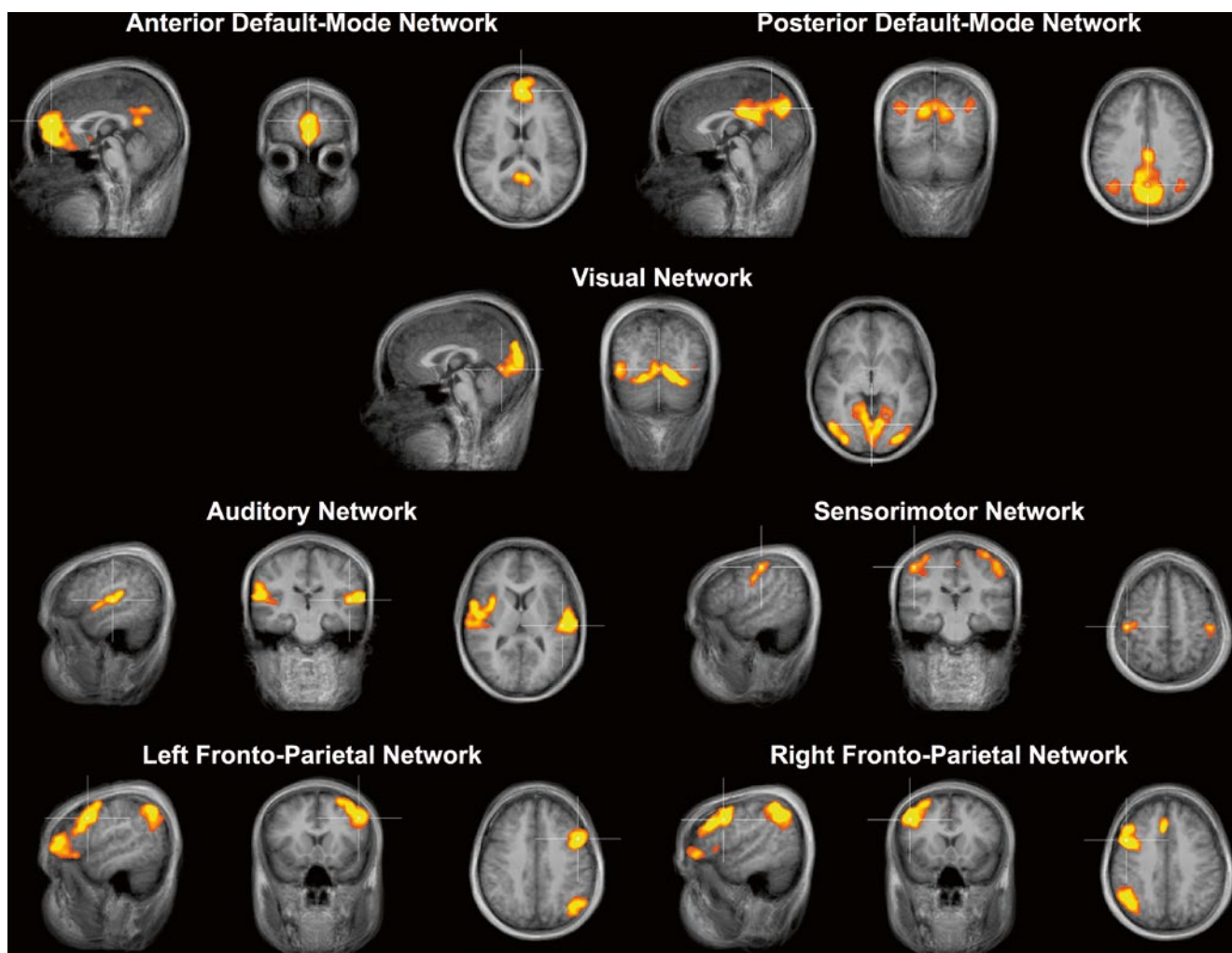


Fig. 23 A subset of major resting-state networks (RSNs) obtained by ICA analysis of the resting-state fMRI data of a group of healthy individuals ($n=8$); the default-mode network (DMN) is split in an anterior and posterior part (upper row)

An alternative (less objective) approach to retrieve RSNs is to calculate whole-brain correlations from seed regions that correspond to core locations of RSNs. In this approach the DMN, for example, can be retrieved by selecting a region in the posterior cingulate cortex as the seed region and then correlating each voxel's time course with the reference time course from the seed region. For both the seed-based correlation and ICA approach, it is recommended to account for possible BOLD effects due to cardiac pulsation and respiratory cycle (Birn et al. 2008) using a physiological noise correction method such as RETROICOR (Glover et al. 2000).

The obtained functional networks during rest conditions demonstrate that the brain is never “at rest” and the description of RSNs is, thus, a useful approach to explore the brain’s functional organization in healthy individuals as well as to examine if it is altered in neurological or psychiatric diseases. Furthermore, it has been possible to relate RSNs to externally modifiable factors, such as different pharmacological treat-

ments or psychological experiences (Khalili-Mahani et al. 2012; Esposito et al. 2014). The default-mode network (DMN) has gained particular attention – the term “default mode” has been introduced by Raichle et al. (2001) to describe resting-state brain function. The DMN is a network of brain regions that include part of the medial temporal lobe (presumed memory functions), part of the medial prefrontal cortex (presumed theory of mind functions), the posterior cingulate cortex along with the adjacent ventral precuneus, and the medial, lateral, and inferior parietal cortex. The DMN is active when the individual is not focused on the outside world and the brain is at wakeful rest corresponding likely to task-independent introspection, mind-wandering, and self-referential thought. During goal-oriented activity, the DMN is deactivated and other regions are active that are sometimes described as the task-positive network (TPN). The DMN has been hypothesized to be relevant to disorders including Alzheimer’s disease, autism, and schizophrenia (Buckner et al. 2008).

5 Diffusion-Weighted MRI and Tractography

In recent years, MRI has not only revolutionized functional brain imaging targeting gray matter neuronal activity but also enabled insights into the human white matter structure using diffusion-weighted magnetic resonance imaging (DW-MRI, dMRI, or DWI). Pulse sequences for dMRI measure the diffusion of water molecules in each voxel providing information about the fibers in that voxel that can be used to assess the “intactness” of the white matter structure and as the basis for computational tractography since the diffusion process is hindered by the boundaries of the fibers forcing the majority of water molecules to diffuse along these fibers.

A diffusion-weighted MR measurement consists of several volumes each measuring the reduction of the signal resulting from diffusion along a specific axis in space that is selected by setting the x , y , and z gradients of the scanner accordingly using a pulsed-gradient spin echo-sequence (PGSE) developed by Stejskal and Tanner (1965).

5.1 Diffusion Tensor Imaging

It has been proposed to model the diffusion measured in a voxel as a 3D Gaussian probability function from which a *diffusion tensor* (3×3 matrix) can be calculated (Basser et al. 1994), which has led to the name *diffusion tensor imaging* (DTI) for the most widely used diffusion-weighted MRI acquisition and modeling approach. In order to construct the diffusion tensor, a minimum of six diffusion-weighted volumes and a non-diffusion-weighted image need to be measured. From the diffusion tensor, the principal diffusion directions (three eigenvectors of the tensor) and associated diffusion coefficients (three eigenvalues λ_1 , λ_2 , λ_3) can be derived. Note that although eigenvectors mathematically represent directions, DTI cannot distinguish opposing directions from each other, that is, the resulting values estimate diffusion along opposing directions, that is, along principle axes of diffusion. The eigenvectors and eigenvalues can be visualized as an ellipsoid. If water molecules diffuse without restrictions in all directions, the resulting “ellipsoid” will have the shape of a sphere, that is, all three axes (eigenvectors) have the same length ($\lambda_1 = \lambda_2 = \lambda_3$) and there is no preferred axis of diffusion. This situation is described as *isotropic diffusion*. In case that water molecules diffuse with low restrictions along one axis but diffusion is hindered in other directions, a strongly elongated (cigar shaped) ellipsoid will be obtained ($\lambda_1 > > \lambda_2 \approx \lambda_3$). This case of restricted diffusion occurs within and around white matter fibers and is described as *anisotropic diffusion*. In this case, the main (longest) axis of the resulting ellipsoid will likely coincide

with the main orientation of fiber bundles running through the measured voxel. This is the principle assumption of DTI. Note, however, that the tensors estimated in each voxel do not provide fibers but only local discrete measurements, that is, putative fibers need to be reconstructed using *computational tractography*, that is, the orientation of estimated tensors need to be “concatenated” across neighboring voxels. Since results of specific tractography procedures are dependent on many factors (see below), visualized fibers need to be interpreted with care.

Several interesting quantities can be derived from the diffusion tensor in each voxel. The *mean diffusivity* quantifies the overall movement of water molecules in a voxel, which depends on tissue type (e.g., CSF vs. the white matter) and the presence of diffusion restrictions (e.g., axons). Figure 2.24b shows that the mean diffusivity is high in the ventricles (yellow color) while it is low in the white and gray matter (orange color). The most common derived scalar quantity is *fractional anisotropy* (FA) that characterizes the overall shape of the diffusion, that is, it quantifies the fraction of the diffusion tensor that can be ascribed to anisotropic diffusion:

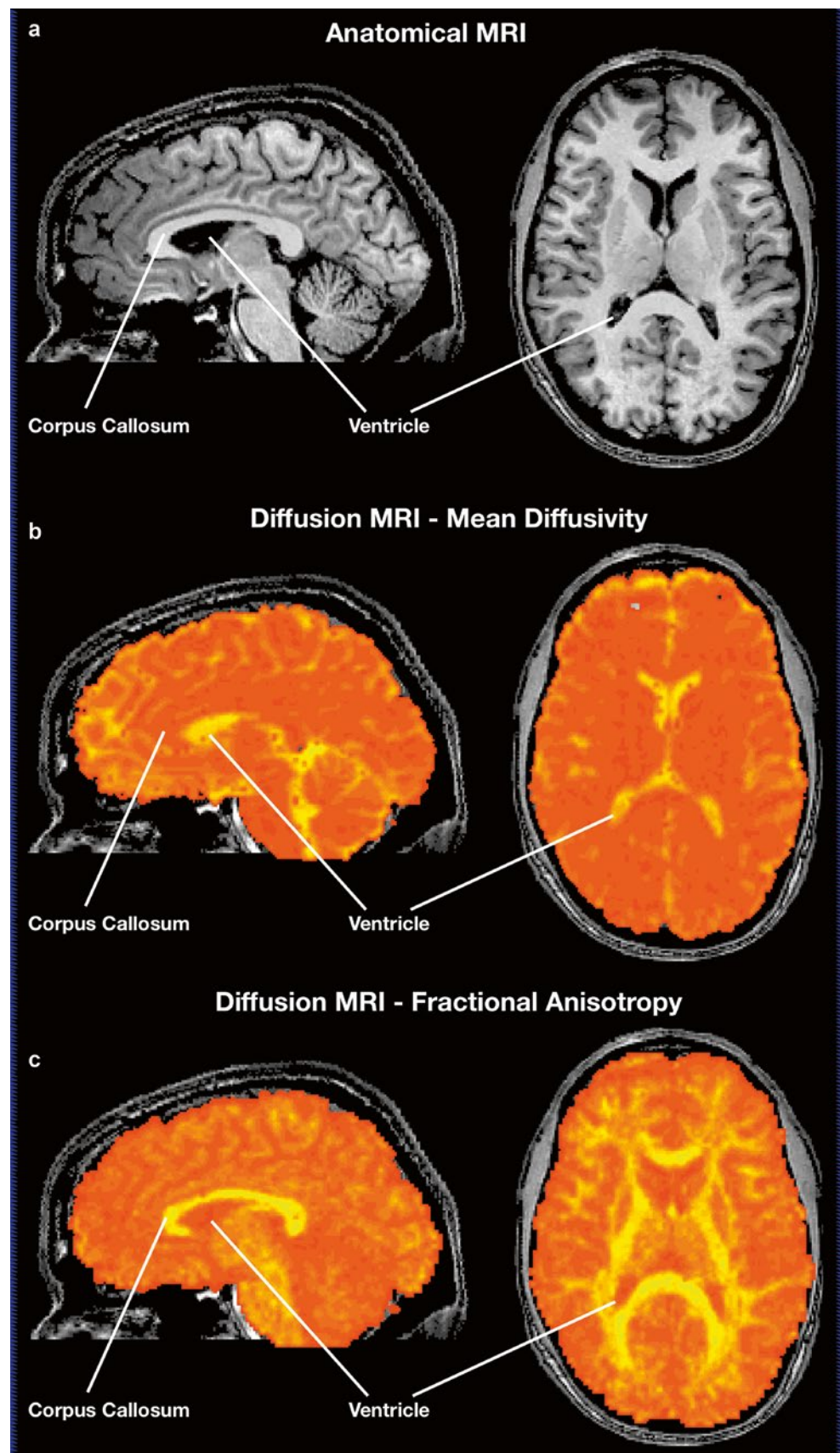
$$FA = \frac{\sqrt{(\lambda_1 - \lambda_2)^2 + (\lambda_2 - \lambda_3)^2 + (\lambda_1 - \lambda_3)^2}}{\sqrt{2(\lambda_1^2 + \lambda_2^2 + \lambda_3^2)}}$$

The FA value varies between 0 (isotropic diffusion, shape of a sphere) and 1 (maximal anisotropy, shape of a line). Figure 2.24c shows that fractional anisotropy is high (yellow color) in the white matter (e.g., in the corpus callosum) but low (orange color) in the gray matter and ventricles. The FA value disregards the specific diffusion axis. A value of 0 indicates no preferred diffusion axis (sphere) while a value of 1 indicates diffusion precisely along a single axis. Since the white matter contains parallel fibers within larger tracts, it contains usually high FA values (>0.3) whereas FA values are low (0.0–0.2) in the gray matter. The FA quantity has gained increasing interest in recent years since it has been shown that FA values in specific tracts can be related to specific diseases and since they correlate with cognitive performance measures such as reading capability (see Sect. 5.3).

5.1.1 Tractography: From Tensors to Fiber Bundles

Based on the preferred orientation of the tensors in neighboring voxels, computational tractography or *fiber tracking* procedures aim to reconstruct the trajectory of fibers in the white matter by “concatenating” neighboring tensors. Fiber tracking is usually launched (seeded) in all voxels (even in sub-voxel coordinate grids) except those with low FA values since they do not reflect strong directness. The tracking process then generates a large amount of short and long reconstructed (“soft-

Fig. 2.24 Important voxel-wise measures that can be extracted from diffusion-weighted MRI scans. (a) Anatomical scan shown as reference. (b) Mean diffusivity map coregistered with anatomy shown in (a); note that diffusivity is high in CSF (ventricles, *yellow color*) but low in gray matter and white matter fiber bundles such as the corpus callosum (*orange color*). (c) Fractional anisotropy (FA) map coregistered with anatomy shown in (a); note that FA is low (*orange color*) in the presence of low diffusion restrictions (ventricles) but high in white matter fiber bundles such as the corpus callosum containing coherently oriented fibers within voxels



ware") fibers. Specific fiber tracts are extracted from the dense fiber field by using regional constraints (e.g., Catani and Thiebaut de Schotten 2008), that is, fibers belonging to a specific tract are included if they pass through one or more specified volumes-of-interest (VOIs). Since the main axis of the tensor indicates an oriented axis and not a direction, fiber tracking is performed in two opposing directions. After both "half-fibers" have been reconstructed, they are finally integrated into a single fiber. In order to reconstruct a (half-) fiber, a small (sub-voxel) step is performed in one of the two directions provided by the main (longest) axis of the ellipsoid at a seed position. At the reached position, the direction for the next small step will be calculated using the tensor orientation and the direction of the previous step. Since the reached position usually does not correspond to integral coordinates (i.e., it falls between voxels), the calculation of the next direction is based on the tensors surrounding the current 3D position; in this interpolation process, tensors influence the calculation with respect to the distance of the corresponding voxels to the current position. After updating the direction, the next step is performed. Again a new direction is calculated at the new position for the next step and so on producing a connected trajectory of short line segments. This process continues until certain stop criteria are reached such as when an FA value is reached that falls below a specified threshold or in case that the reconstructed fiber leaves the white matter. In order to create smooth reconstructed fibers (Fig. 25), the chosen step size needs to be smaller than the distance of the voxels.

5.2 Validation and Improvements

While tractography usually creates interesting results, it is important to realize that visualized fibers are reconstructed from diffusion estimates that are measured at discrete 3D positions (voxels) and, thus, may not necessarily reflect true fiber tracts in the brain. A central concern in current tractography research concerns the question how much one can trust the beautiful pictures generated by fiber tracking procedures. The answer depends on many factors including the quality of the diffusion-weighted measurement which is influenced by scanner parameters (e.g., signal-to-noise ratio) as well as by parameters of the participant such as head motion and physiological noise. The most important limiting factor is related to the voxel size used for *in vivo* studies that is a few orders of magnitudes larger than the small scale at which the diffusion of water molecules happens. With a typical spatial resolution of about 2 mm, only the average diffusion of water molecules in a large cube (voxel) is captured, which does not allow to resolve fine-grained white matter fiber bundles or fiber bundles in the gray matter. The resolution issue relates also to the "kissing or crossing" problem, that is, it can often not be decided in a large voxel whether two (or more) incoming fiber bundles cross in that voxel or whether they merely touch each other and part by changing direction.

Despite its usefulness in many applications, the diffusion tensor model has the drawback of being a unidirectional model. Its orientation estimation works very well in areas characterized by prominent fiber pathways following one direction, giving rise to a unimodal water diffusivity profile. When, however, several different diffusion directions are present in one voxel, the estimated diffusion tensor contains directionality information which has high uncertainty at best (low precision) or is even biased to a wrong average orientation. In order to obtain more valid results from diffusion-weighted measurements, several advanced measurement schemes and analysis methods have been proposed. The most complete approach to estimate the full fiber orientation density function is diffusion spectrum imaging (DSI) that requires, however, very long measurement times (Wedeen et al. 2005). Somewhat less time-consuming advanced approaches are q-ball imaging (Tuch 2004) and spherical deconvolution (Tournier et al. 2004). These modeling approaches go beyond the simple tensor model and fit more complex models to the measured diffusion data that no longer assume a single major diffusion axis but explicitly allow multiple (crossing) fibers in a voxel. In order to provide sufficient constraints for these more complex models, many more diffusion directions (e.g., 100) need to be measured as for conventional DTI scans that require only 6 diffusion directions. Because of the high number of direction measurements, these approaches are also called "HARDI" (high angular resolution diffusion imaging) methods. Since HARDI measurements (Tuch 2002) need much longer scanning time than DTI measurements, they are not common in clinical MRI measurements. Even with more advanced measurement and analysis approaches, reconstructed fiber tracts may vary substantially depending on the used tractography algorithm (Bastiani et al. 2012). To validate fiber tracking algorithms, it is important to have ground-truth data, that is, knowledge about the true trajectory of fiber bundles. One way to perform ground-truth validation is to use "DTI phantoms" that contain known, artificially created fibers, including challenging cases with crossing and kissing fibers (Pullens et al. 2010). Another important validation approach uses postmortem brain tissue that is analyzed both with dMRI as well as with tracers that are released in specific brain areas. Since these tracers traverse backward along axons through other regions, they reveal true region-to-region connectivity that can be used as ground-truth data for DWI-based connectivity analyses of the same tissue (e.g., Seehaus et al. 2013).

5.3 Applications

In recent years, diffusion MRI has led to several interesting applications. Especially the fractional anisotropy measure has become an important biomarker of white matter integrity serving as a local index to diagnose neurological or psychiatric diseases or to predict (lack of) cognitive performance. It

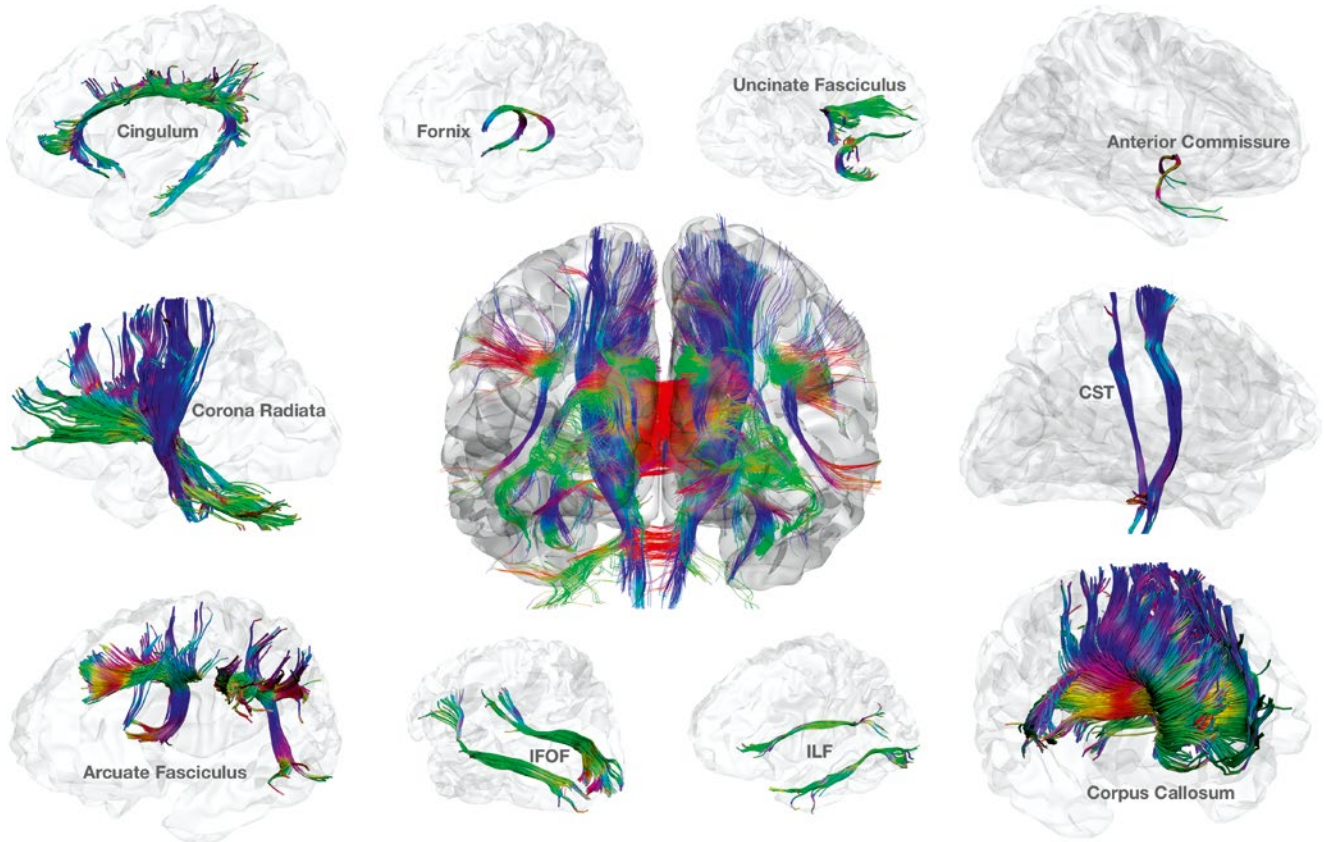


Fig. 25 A subset of major fiber tracts revealed by computational tractography from the diffusion-weighted MRI data of a healthy individual. *CST* corticospinal tract, *IFOF* inferior fronto-occipital fasciculus, *ILF* inferior longitudinal fasciculus

has been, for example, shown that FA values extracted from dMRI measurements from good and poor readers differ, and the size of the difference is largest within a region within the left hemisphere temporoparietal white matter (Klingberg et al. 2000; Deutsch et al. 2005). FA values could also be related to the level of creativity in several brain areas including the prefrontal cortex, basal ganglia, and at the border of the temporal and parietal lobe (Takeuchi et al. 2010). Note, however, that FA values are not fixed (“hard-wired”) properties of the white matter but can change depending on usage of the underlying fibers. It has been, for example, shown that FA values in the white matter in regions of the posterior parietal cortex (containing fibers that presumably mediate visuospatial transformation) significantly increase when subjects train on an intensive visual motor coordination task such as learning to juggle (Scholz et al. 2009). It has also been discovered that FA values reflect the development of cognitive abilities including systematic increases in the corpus callosum and prefrontal cortex during childhood (Barnea-Goraly et al. 2005); the changes observed in prefrontal cortical areas are discussed as related to the development of working memory, attention, and behavioral control. FA measures are also increasingly used for early diagnosis of stroke since reduced diffusion in

affected brain regions is often detected already minutes after the stroke. It is important to note that FA measurements are quantitative values (as opposed to fMRI measurements) that can be compared across people, labs, and scanners.

While computational tractography produces less objective results than FA estimates, reconstructed white matter fiber tracts are especially important to guide neurosurgical procedures potentially reducing the risk of lesioning important fiber tracts, for example, related to language functions. For this and similar purposes, several tools (e.g., Yeatman et al. 2012) are now available that allow extracting major long-range fiber tracts from dMRI data, including *commissural tracts* (e.g., corpus callosum) connecting both cortical hemispheres, *association tracts* (e.g., arcuate fasciculus) connecting regions within the same hemisphere, and *projection tracts* (e.g., corticospinal tract) connecting cortical regions to subcortical areas, the cerebellum, and the spinal cord. Figure 25 shows selected major fiber tracts that have been reconstructed from the dMRI data of a healthy individual; further details about the depicted (as well as other) fiber tracts are described, for example, by Catani and Thiebaut de Schotten (2008) and Yeatman et al. (2012).

5.3.1 The Human Connectome

An important aim of recent brain research is to understand how brain areas communicate with each other. This aim is pursued by investigating anatomical connectivity with dMRI to reconstruct *in vivo* the macroscale human connectome (Sporns et al. 2005), which is the map of all the structural connections in the human brain. This is complemented by functional connectivity studies using fMRI (see Sect. 4.1) and other modalities such as EEG and MEG. In integrative multimodal modeling approaches, the anatomical connectome may serve as an important structural constraint for functional connectivity models since only brain areas that are connected via fiber bundles may communicate directly with each other. Diffusion MRI may even help to estimate the strength of connectivity between brain areas. The currently most prominent attempt along these lines is the *Human Connectome Project* (<http://www.neuroscienceblueprint.nih.gov/connectome/>). This project aims to derive a complete map of all major connections between brain areas by measuring dMRI as well as functional connectivity and genetic data in more than 1,000 individuals (twin pairs and their siblings from 300 families). Besides deriving a connectivity map – the human connectome – the measured data of structural and functional connectivity will be shared to stimulate research in the emerging field of *human connectomics* as well as providing the basis for future studies of abnormal brain circuits in neurological and psychiatric disorders.

References

- Allen EA, Erhardt EB, Damaraju E, Gruner W, Segall JM et al (2011) A baseline for the multivariate comparison of resting-state networks. *Front Syst Neurosci* 5:2
- Ashburner J (2007) A fast diffeomorphic image registration algorithm. *Neuroimage* 38:95–113
- Ashburner J, Friston KJ (1999) Nonlinear spatial normalization using basis functions. *Hum Brain Mapp* 7:254–266
- Bandettini PA, Cox RW (2000) Event-related fMRI contrast when using constant interstimulus interval: theory and experiment. *Magn Reson Med* 43:540–548
- Bandettini PA, Birn RM, Donahue KM (2000) Functional MRI: background, methodology, limits, and implementation. In: Cacioppo JT, Tassinary LG, Berntson GG (eds) *Handbook of psychophysiology*. Cambridge University Press, New York, pp 978–1014
- Barnea-Goraly N, Menon V, Eckert M, Tamm L, Bammer R, Karchemskiy A, Dant CC, Reiss AL (2005) White matter development during childhood and adolescence: a cross-sectional diffusion tensor imaging study. *Cereb Cortex* 15:1848–1854
- Basser PJ, Mattiello J, LeBihan D (1994) Estimation of the effective self-diffusion tensor from the NMR spin echo. *J Magn Reson B* 103:247–254
- Bastiani M, Shah NJ, Goebel R, Roebroeck A (2012) Human cortical connectome reconstruction from diffusion weighted MRI: the effect of tractography algorithm. *Neuroimage* 62:1732–1749
- Beckmann CF, Jenkinson M, Smith SM (2003) General multilevel linear modeling for group analysis in fMRI. *Neuroimage* 20:1052–1063
- Benjamini Y, Hochberg Y (1995) Controlling the false discovery rate: a practical and powerful approach to multiple testing. *J Roy Statist Soc Ser B* 57:289–300
- Birn RM, Murphy K, Bandettini PA (2008) The effect of respiration variations on independent component analysis results of resting state functional connectivity. *Hum Brain Mapp* 29:740–750
- Biswal B, Yetkin FZ, Haughton VM, Hyde JS (1995) Functional connectivity in the motor cortex of resting human brain using echo-planar MRI. *Magn Reson Med* 34:537–541
- Blamire AM, Ogawa S, Ugurbil K et al (1992) Dynamic mapping of the human visual cortex by high-speed magnetic resonance imaging. *Proc Natl Acad Sci U S A* 89:11069–11073
- Bledowski C, Cohen Kadosh K, Wibral M, Rahm B, Bittner RA, Hoechstetter K, Scherg M, Maurer K, Goebel R, Linden DE (2006) Mental chronometry of working memory retrieval: a combined functional magnetic resonance imaging and event-related potentials approach. *J Neurosci* 26:821–829
- Boynton GM, Engel SA, Glover GH, Heeger DJ (1996) Linear systems analysis of functional magnetic resonance imaging in human V1. *J Neurosci* 16:4207–4221
- Brown MA, Semelka RC (1999) *MRI – basic principles and applications*. Wiley-Liss, New York
- Büchel C, Coull JT, Friston KJ (1999) The predictive value of changes in effective connectivity for human learning. *Science* 283:1538–1541
- Buckner RL, Bandettini PA, O’Craven KM, Savoy RL, Petersen SE, Raichle ME, Rosen BR (1996) Detection of cortical activation during averaged single trials of a cognitive task using functional magnetic resonance imaging. *Proc Natl Acad Sci U S A* 93:14878–14883
- Buckner RL, Andrews-Hanna JR, Schacter DL (2008) The brain’s default network: anatomy, function, and relevance to disease. *Ann N Y Acad Sci* 1124:1–38
- Bullmore E, Brammer M, Williams SC et al (1996) Statistical methods of estimation and inference for functional MR image analysis. *Magn Reson Med* 35:261–277
- Buxton RB, Wong EC, Frank LR (1998) Dynamics of blood flow and oxygen metabolism during brain activation: the balloon model. *Magn Reson Med* 39:855–864
- Buxton RB, Uludag K, Dubowitz DJ, Liu TT (2004) Modeling the hemodynamic response to brain activation. *Neuroimage* 23:S220–S233
- Castelo-Branco M, Formisano E, Backes W, Zanella F, Neuenenschwander S, Singer W, Goebel R (2002) Activity patterns in human motion-sensitive areas depend on the interpretation of global motion. *Proc Natl Acad Sci U S A* 99:13914–13919
- Catani M, Thiebaut de Schotten M (2008) A diffusion tensor imaging tractography atlas for virtual *in vivo* dissections. *Cortex* 44: 1105–1132
- Cheng K, Waggoner AK, Tanaka K (2001) Human ocular dominance columns as revealed by high-field functional magnetic resonance imaging. *Neuron* 32:359–374
- Cochrane D, Orcutt GH (1949) Application of least squares regression to relationships containing autocorrelated error terms. *J Am Stat Assoc* 44:32–61
- Dale AM, Buckner RL (1997) Selective averaging of rapidly presented individual trials using fMRI. *Hum Brain Mapp* 5:329–340
- Dale AM, Halgren E (2001) Spatiotemporal mapping of brain activity by integration of multiple imaging modalities. *Curr Opin Neurobiol* 11:202–208
- De Luca M, Beckmann CF, De Stefano N, Matthews PM, Smith SM (2006) fMRI resting state networks define distinct modes of long-distance interactions in the human brain. *Neuroimage* 29:1359–1367
- De Martino F, Moerel M, van de Moortele PF, Ugurbil K, Goebel R, Yacoub E, Formisano E (2013) Spatial organization of frequency preference and selectivity in the human inferior colliculus. *Nat Commun* 4:1386
- Deutsch GK, Dougherty RF, Bammer R, Siok WT, Gabrieli JD, Wandell B (2005) Children’s reading performance is correlated with white matter structure measured by diffusion tensor imaging. *Cortex* 41:354–363
- Draper NR, Smith H (1998) *Applied regression analysis*, 3rd edn. Wiley, New York

- Duvernoy HM, Delon S, Vannson JL (1981) Cortical blood vessels of the human brain. *Brain Res Bull* 7:519–579
- Esposito F, Seifritz E, Formisano E, Morrone R, Scarabino T, Tedeschi G, Cirillo S, Goebel R, Di Salle F (2003) Real-time independent component analysis of fMRI time-series. *Neuroimage* 20: 2209–2224
- Esposito F, Scarabino T, Hyvarinen A, Himberg J, Formisano E, Comani S, Tedeschi G, Goebel R, Seifritz E, Di Salle F (2005) Independent component analysis of fMRI group studies by self-organizing clustering. *Neuroimage* 25:193–205
- Esposito F, Otto T, Zijlstra FRH, Goebel R (2014) Spatially distributed effects of mental exhaustion on resting-state fMRI networks. *PLoS One* 9:e94222
- Evans AC, Collins DL, Mills SR, Brown ED, Kelly RL, Peters TM (1993) 3D statistical neuroanatomical models from 305 MRI volumes. In: Proceedings of IEEE-Nuclear Science Symposium and Medical Imaging Conference. pp 1813–1817
- Fischl B, Sereno MI, Tootell RBH, Dale AM (1999) High-resolution inter-subject averaging and a coordinate system for the cortical surface. *Hum Brain Mapp* 8:272–284
- Forman SD, Cohen JD, Fitzgerald M, Eddy WF, Mintun MA, Noll DC (1995) Improved assessment of significant activation in functional magnetic resonance imaging (fMRI): use of a clustersize threshold. *Magn Reson Med* 3(5):636–647
- Formisano E, Goebel R (2003) Tracking cognitive processes with functional MRI mental chronometry. *Curr Opin Neurobiol* 13:174–181
- Formisano E, Esposito F, Kriegeskorte N, Tedeschi G, Di Salle F, Goebel R (2002) Spatial independent component analysis of functional magnetic resonance imaging time-series: characterization of the cortical components. *Neurocomputing* 49:241–254
- Fox PT, Raichle ME, Mintun MA, Dence C (1988) Nonoxidative glucose consumption during focal physiological neural activity. *Science* 241:462–464
- Friston KJ, Henson RN (2006) Commentary on: divide and conquer; a defense of functional localisers. *Neuroimage* 30:1097–1099
- Friston KJ, Jezzard P, Turner R (1994) The analysis of functional MRI time-series. *Hum Brain Mapp* 1:153–171
- Friston KJ, Holmes AP, Worsley KJ, Poline JP, Frith CD, Frackowiak RSJ (1995) Statistical parametric maps in functional imaging: a general linear approach. *Hum Brain Mapp* 2:189–210
- Friston KJ, Fletcher P, Josephs O, Holmes A, Rugg MD, Turner R (1998) Event-related fMRI: characterizing differential responses. *Neuroimage* 7:30–40
- Friston KJ, Penny W, Phillips C, Kiebel S, Hinton G, Ashburner J (2002) Classical and Bayesian inference in neuroimaging: theory. *Neuroimage* 16:465–483
- Friston KJ, Stephan KE, Lund TE, Morcom A, Kiebel S (2005) Mixed-effects and fMRI studies. *Neuroimage* 24:244–252
- Friston KJ, Rotshtein P, Geng JJ, Sterzer P, Henson RN (2006) A critique of functional localisers. *Neuroimage* 30:1077–1087
- Frost M, Goebel R (2012) Measuring structural-functional correspondence: spatial variability of specialised brain regions after macro-anatomical alignment. *Neuroimage* 59:1369–1381
- Frost M, Goebel R (2013) Functionally informed cortex based alignment: an integrated approach for whole-cortex macro-anatomical and ROI-based functional alignment. *Neuroimage* 83:1002–1010
- Fujita I, Tanaka K, Ito M, Cheng K (1992) Columns for visual features of objects in monkey inferotemporal cortex. *Nature* 360:343–346
- Genovese CR, Lazar NA, Nichols T (2002) Thresholding of statistical maps in functional neuroimaging using the false discovery rate. *Neuroimage* 15:870–878
- Glover GH, Li TQ, Ress D (2000) Image-based method for retrospective correction of physiological motion effects in fMRI: RETROICOR. *Magn Reson Med* 44:162–167
- Goebel R (2012) BrainVoyager – past, present, future. *Neuroimage* 62:748–756
- Goebel R, Singer W (1999) Cortical surface-based statistical analysis of functional magnetic resonance imaging data. *Neuroimage* 9, S64
- Goebel R, Roebroeck A, Kim DS, Formisano E (2003) Investigating directed cortical interactions in time-resolved fMRI data using vector autoregressive modeling and Granger causality mapping. *Magn Reson Imaging* 21:1251–1261
- Goebel R, Hasson U, Lefèvre I, Malach R (2004) Statistical analyses across aligned cortical hemispheres reveal high-resolution population maps of human visual cortex. *Neuroimage* 22(Suppl 2)
- Goebel R, Esposito F, Formisano E (2006) Analysis of functional image analysis contest (FIAC) data with BrainVoyager QX: from single-subject to cortically aligned group general linear model analysis and self-organizing group independent component analysis. *Hum Brain Mapp* 27:392–401
- Goebel R, Zilberman A, Sorger B (2010) Real-time fMRI-based brain-computer interfacing for neurofeedback therapy and compensation of lost motor functions. *Imaging Med* 2:407–414
- Haxby JV, Gobbini MI, Furey ML, Ishai A, Schouten JL, Pietrini P (2001) Distributed and overlapping representations of faces and objects in ventral temporal cortex. *Science* 293:2425–2430
- Holmes AP, Friston KJ (1998) Generalisability, random effects & population inference, in: Fourth International Conference on functional mapping of the human brain. *Neuro Image* 7:S754
- Huetten SA, Song AW, McCarthy G (2004) Functional magnetic resonance imaging. Sinauer Associates, Sunderland
- Khalili-Mahani N, Zoethout RM, Beckmann CF, Baerends E, de Kam ML et al (2012) Effects of morphine and alcohol on functional brain connectivity during “resting state”: a placebo-controlled crossover study in healthy young men. *Hum Brain Mapp* 33:1003–1018
- Kim DS, Duong TQ, Kim SG (2000) High-resolution mapping of iso-orientation columns by fMRI. *Nat Neurosci* 3:164–169
- Kirby KN (1993) Advanced data analysis with SYSTAT. Van Nostrand Reinhold, New York
- Klingberg T, Hedges M, Temple E, Salz T, Gabrieli JD, Moseley ME, Poldrack RA (2000) Microstructure of temporo-parietal white matter as a basis for reading ability: evidence from diffusion tensor magnetic resonance imaging. *Neuron* 25:493–500
- Kriegeskorte N, Goebel R (2001) An efficient algorithm for topologically correct segmentation of the cortical sheet in anatomical MR volumes. *Neuroimage* 14:329–346
- Kriegeskorte N, Goebel R, Bandettini P (2006) Information-based functional brain mapping. *Proc Natl Acad Sci U S A* 103: 3863–3868
- Kruggel F, von Cramon DY (1999) Temporal properties of the hemodynamic response in functional MRI. *Hum Brain Mapp* 8:259–271
- Kutner MH, Nachtsheim CJ, Neter J, Li W (2005) Applied linear statistical models, 5th edn. McGraw-Hill, Boston
- LaConte SM, Peltier SJ, Hu XP (2007) Real-time fMRI using brain-state classification. *Hum Brain Mapp* 28:1033–1044
- Lenoski B, Baxter LC, Karam LJ, Maisog J, Debbins J (2008) On the performance of autocorrelation estimation algorithms for fMRI analysis. *IEEE J Sel Top Signal Process* 2:828–838
- Linden DEJ, Habes I, Johnston SJ, Linden S, Tatineni R, Subramanian L, Sorger B, Healy D, Goebel R (2012) Real-time self-regulation of emotion networks in patients with depression. *PLoS One* 7:e38115
- Logothetis NK, Wandell B (2004) Interpreting the BOLD signal. *Annu Rev Physiol* 66:735–769
- Logothetis NK, Pauls J, Augath M, Trinath T, Oeltermann A (2001) Neurophysiological investigation of the basis of the fMRI signal. *Nature* 412:150–157
- Magistretti PJ, Pellerin L, Rothman DL, Shulman RG (1999) Energy on demand. *Science* 283:496–497
- Mathiesen C, Caesar K, Lauritzen M (2000) Temporal coupling between neuronal activity and blood flow in rat cerebellar cortex as indicated by field potential analysis. *J Physiol* 523:235–246

- Maus B, van Breukelen GJ, Goebel R, Berger MP (2010a) Optimization of blocked designs in fMRI studies. *Psychometrika* 75:373–390
- Maus B, van Breukelen GJ, Goebel R, Berger MP (2010b) Robustness of optimal design of fMRI experiments with application of a genetic algorithm. *Neuroimage* 49:2433–2443
- McIntosh AR, Gonzalez-Lima F (1994) Structural equation modeling and its application to network analysis in functional brain imaging. *Hum Brain Mapp* 2:2–22
- McKeown MJ, Makeig S, Brown GG, Jung TP, Kindermann SS, Bell AJ, Iragui V, Sejnowski TJ (1998a) Blind separation of functional magnetic resonance imaging (fMRI) data. *Hum Brain Mapp* 6: 368–372
- McKeown MJ, Makeig S, Brown GG, Jung TP, Kindermann SS, Bell AJ, Sejnowski TJ (1998b) Analysis of fMRI data by blind separation into independent spatial components. *Hum Brain Mapp* 6: 160–188
- Menon RS, Kim SG (1999) Spatial and temporal limits in cognitive neuroimaging with fMRI. *Trends Cogn Sci* 3:207–216
- Moeller S, Yacoub E, Auerbach E, Strupp JP, Harel N, Ugurbil K (2010) Multi-band multi-slice GE-EPI at 7 Tesla, with 16 fold acceleration using partial parallel imaging with application to high spatial and temporal whole brain fMRI. *Magn Reson Med* 63:1144–1153
- Mulert C, Jager L, Schmitt R, Bussfeld P, Pogarell O, Moller HJ, Juckel G, Hegerl U (2004) Integration of fMRI and simultaneous EEG: towards a comprehensive understanding of localization and time-course of brain activity in target detection. *Neuroimage* 22:83–94
- NessAiver M (1997) All you really need to know about MRI physics. Simply Physics, Baltimore
- Nichols TE, Brett M, Andersson J, Wager T, Poline JB (2005) Valid conjunction inference with the minimum statistic. *Neuroimage* 25:653–660
- O’Craven KM, Kanwisher N (2000) Mental imagery of faces and places activates corresponding stimulus-specific brain regions. *J Cogn Neurosci* 12:1013–1023
- Ogawa S, Lee TM, Kay AR, Tank DW (1990) Brain magnetic resonance imaging with contrast dependent on blood oxygenation. *Proc Natl Acad Sci U S A* 87:9868–9872
- Penny WD, Stephan KE, Mechelli A, Friston KJ (2004) Comparing dynamic causal models. *Neuroimage* 22:1157–1172
- Pruessmann KP, Weiger M, Scheidegger MB, Boesiger P (1999) SENSE: sensitivity encoding for fast MRI. *Magn Reson Med* 42:952–962
- Pullens P, Roebroeck A, Goebel R (2010) Ground truth hardware phantoms for validation of diffusion-weighted MRI applications. *J Magn Reson Imaging* 32:482–488
- Raichle ME, MacLeod AM, Snyder AZ, Powers WJ, Gusnard DA, Shulman GL (2001) A default mode of brain function. *Proc Natl Acad Sci U S A* 98:676–682
- Robson MD, Dorosz JL, Gore JC (1998) Measurements of the temporal fMRI response of the human auditory cortex to trains of tones. *Neuroimage* 7:185–198
- Roebroeck A, Formisano E, Goebel R (2005) Mapping directed influence over the brain using Granger causality and fMRI. *Neuroimage* 25:230–242
- Roebroeck A, Formisano E, Goebel R (2011) The identification of interacting networks in the brain using fMRI: model selection, causality and deconvolution. *Neuroimage* 58:296–302
- Saxe R, Brett M, Kanwisher N (2006) Divide and conquer: a defense of functional localizers. *Neuroimage* 30:1088–1096 (discussion 1097–1089)
- Scherg M, Linden DEJ, Muckli L, Roth R, Drüen K, Ille N, Zanella FE, Singer W, Goebel R (1999) Combining MEG with fMRI in studies of the human visual system. In: Yoshimoto T, Kotani M, Karibe H, Nakasato N (eds) Recent advances in biomagnetism. Tohoku University Press, Sendai
- Schild HH (1990) MRI made easy. Schering AG, Berlin
- Scholz J, Klein MC, Behrens TEJ, Johansen-Berg H (2009) Training induces changes in white-matter architecture. *Nat Neurosci* 12:1370–1371
- Searle SR, Casella G, McCulloch CE (1992) Variance Components. Wiley, New York.
- Seehaus AK, Roebroeck A, Chiry O, Kim DS, Ronen I, Bratzke H, Goebel R, Galuske RAW (2013) Histological validation of DW-MRI tractography in human postmortem tissue. *Cereb Cortex* 23:442–450
- Settimpop K, Gagowski BA, Polimeni JR, Witzel T, Wedeen VJ, Wald LL (2012) Blipped-controlled aliasing in parallel imaging for simultaneous multislice echo planar imaging with reduced g-factor penalty. *Magn Reson Med* 67:1210–1224
- Sorger B, Peters J, van den Boomen C, Zilverstand A, Reithler J, Goebel R (2010) Real-time decoding of the locus of visuospatial attention using multi-voxel pattern classification, 16th edn. Human Brain Mapping, Barcelona
- Sorger B, Reithler J, Dahmen B, Goebel R (2012) A real-time fMRI-based spelling device immediately enabling robust motor-independent communication. *Curr Biol* 22:1333–1338
- Sporns O (2010) Connectome. Scholarpedia 5:5584
- Sporns O, Tononi G, Kotter R (2005) The human connectome: a structural description of the human brain. *PLoS Comput Biol* 1:e42
- Stejskal EO, Tanner JE (1965) Spin diffusion measurements: spin echoes in the presence of a time-dependent field gradient. *J Chem Phys* 42:288–292
- Subramanian L, Hindle JV, Johnston S, Roberts MV, Husain M, Goebel R, Linden D (2011) Real-time functional magnetic resonance imaging neurofeedback for treatment of Parkinson’s disease. *J Neurosci* 31:16309–16317
- Takeuchi H, Taki Y, Sassa Y, Hashizume H, Sekiguchi A, Fukushima A, Kawashima R (2010) White matter structures associated with creativity: evidence from diffusion tensor imaging. *Neuroimage* 51:11–18
- Talairach G, Tournoux P (1988) Co-planar stereotaxic atlas of the human brain. Thieme, New York
- Tournier JD, Calamante F, Gadian DG, Connelly A (2004) Direct estimation of the fiber orientation density function from diffusion-weighted MRI data using spherical deconvolution. *Neuroimage* 23:1176–1185
- Tuch DS (2002) High angular resolution diffusion imaging reveals intravoxel white matter fiber heterogeneity. *Magn Reson Med* 48:577–582
- Tuch DS (2004) Q-ball imaging. *Magn Reson Med* 52:1358–1372
- van de Ven VG, Formisano E, Prvulovic D, Roeder CH, Linden DE (2004) Functional connectivity as revealed by spatial independent component analysis of fMRI measurements during rest. *Hum Brain Mapp* 22:165–178
- van de Ven VG, Formisano E, Roder CH, Prvulovic D, Bittner RA, Dietz MG, Hubl D, Dierks T, Federspiel A, Esposito F, Di Salle F, Jansma B, Goebel R, Linden DE (2005) The spatiotemporal pattern of auditory cortical responses during verbal hallucinations. *Neuroimage* 27:644–655
- Vapnik V (1995) The nature of statistical learning theory. Springer, New York
- Wager TD, Nichols TE (2003) Optimization of experimental design in fMRI: a general framework using a genetic algorithm. *Neuroimage* 18:293–309
- Wedgeen VJ, Hagmann P, Tseng WY, Reese TG, Weisskoff RM (2005) Mapping complex tissue architecture with diffusion spectrum magnetic resonance imaging. *Magn Reson Med* 54:1377–1386
- Weiskopf N (2012) Real-time fMRI and its application to neurofeedback. *Neuroimage* 62:682–692
- Weiskopf N, Veit R, Erb M, Mathiak K, Grodd W, Goebel R, Birbaumer N (2003) Physiological self-regulation of regional brain activity

- using real-time functional magnetic resonance imaging (fMRI): methodology and exemplary data. *Neuroimage* 19:577–586
- Weiskopf N, Hutton C, Josephs O, Deichmann R (2006) Optimal EPI parameters for reduction of susceptibility-induced BOLD sensitivity losses: a whole-brain analysis at 3 T and 1.5 T. *Neuroimage* 33:493–504
- Worsley KJ, Marrett S, Neelin P, Evans AC (1992) A three-dimensional statistical analysis for CBF activation studies in human brain. *J Cereb Blood Flow Metab* 12:900–918
- Worsley KJ, Liao CH, Aston J, Petre V, Duncan GH, Morales F, Evans AC (2002) A general statistical analysis for fMRI data. *Neuroimage* 15:1–15
- Yacoub E, Harel N, Ugurbil K (2008) High-field fMRI unveils orientation columns in humans. *Proc Natl Acad Sci USA* 105: 10607–10612
- Yeatman JD, Dougherty RF, Myall NJ, Wandell BA, Feldman HM (2012) Tract profiles of white matter properties: automating fiber-tract quantification. *PLoS One* 7:e49790
- Zimmermann J, Goebel R, De Martino F, van de Moortele PF, Feinberg D, Adriany G, Chaimov D, Shmuel A, Ügurbil K, Yacoub E (2011) Mapping the organization of axis of motion selective features in human area MT using high-field fMRI. *PLoS One* 6:e28716

Functional Neuroanatomy

Thomas P. Naidich and Tarek A. Yousry

Contents

| | | |
|-----|--|----|
| 1 | Introduction..... | 61 |
| 2 | Surface Anatomy..... | 61 |
| 2.1 | Convexity Surface | 61 |
| 2.2 | Inferior Surface | 65 |
| 2.3 | Superior Surface of the Temporal Lobe | 67 |
| 2.4 | Medial Surface | 68 |
| 3 | Lobar Borders | 68 |
| 4 | Localizing Anatomic Sites Independent of Lobar Anatomy | 71 |
| 4.1 | Talairach-Tournoux Coordinate System and “Talairach Space” | 71 |
| 5 | Identification of Specific Anatomic Structures..... | 72 |
| 5.1 | The Pericentral Cortex | 72 |
| 5.2 | The Superior Temporal Plane | 73 |
| 5.3 | The Occipital Lobe..... | 73 |
| 6 | Cortical Architecture..... | 74 |
| 6.1 | Cytoarchitectonics..... | 74 |
| 6.2 | Somatotopy | 77 |
| 6.3 | Selected Areas Involved in Motor and Speech Function | 78 |
| | Conclusion | 85 |
| | References..... | 86 |

Abstract

We present the surface anatomy of the brain describing in detail the typical configuration of the sulci and gyri and their most frequent variations. After describing the borders of the lobes, we give guidance on the methods of localizing functionally important atomic structures such as the pericentral cortex, Heschl’s gyrus, and the calcarine sulcus.

On the basis of the surface anatomy and the cytoarchitectonic subdivision of the cortex, we describe the function of selected areas related to the motor system and to speech.

1 Introduction

Modern neurophysiology and fMRI have refined our concepts of cerebral organization. This section presents the surface anatomy of the brain and begins to addresses the functional interrelationships among the cortical areas.

2 Surface Anatomy

2.1 Convexity Surface

2.1.1 Sylvian Fissure

The convexity face of the sylvian fissure displays five major arms (rami) that help to define the surface anatomy of the convexity (Fig. 1). The long nearly horizontal portion of the sylvian fissure is the posterior horizontal ramus. At its anterior end, the anterior horizontal ramus and the anterior ascending ramus arise together in a “V” or “Y” configuration. At its posterior end, the prominent posterior ascending ramus and the small posterior descending ramus branch outward in a “T” or “fishtail” configuration. The anterior subcentral sulcus and the posterior subcentral sulcus form two minor arms that extend superiorly into the frontoparietal operculum to delimit the subcentral gyrus. One or multiple

T.P. Naidich
Mount Sinai School of Medicine,
One Gustave Levy Place, New York, NY 10029-6574, USA

Department of Neuroradiology and Neurosurgery,
Irving and Dorothy Regenstrief Research, New York, NY, USA

T.A. Yousry (✉)
Lysholm Department of Neuroradiology,
The National Hospital for Neurology and Neurosurgery,
Institute of Neurology, Queen Square, London WC1N 3BG, UK
e-mail: t.yousry@ucl.ac.uk

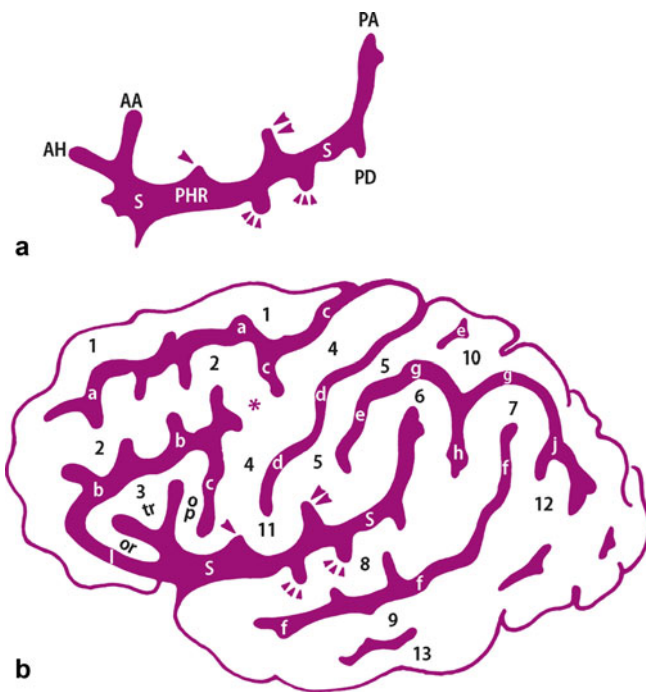


Fig. 1 (a, b) Surface anatomy of the convexity. (a) Sylvian fissure (dark area). The margins of the frontal, parietal, and temporal opercula are defined by the configuration of the sylvian fissure (*S*), its five major rami (the anterior horizontal ramus (*AH*), anterior ascending ramus (*AA*), posterior horizontal ramus (*PHR*), posterior ascending ramus (*PA*), and posterior descending ramus (*PD*), and its minor arms, the anterior subcentral sulcus (*single arrowhead*), posterior subcentral sulcus (*double arrowheads*), and transverse temporal sulci (*triple arrowheads*). (b) Cerebral convexity. The configuration of the sylvian fissure then permits identification of the adjoining gyri and sulci. GYRI: 1 superior frontal gyrus (*SFG*), 2 middle frontal gyrus (*MFG*), 3 inferior frontal gyrus (*or*, pars orbitalis; *tr*, pars triangularis; *op*, pars opercularis), 4 precentral gyrus (*preCG*), 5 postcentral gyrus (*post CG*), 6 supramarginal gyrus (*SMG*), 7 angular gyrus (*AG*), 8 superior temporal gyrus (*STG*), 9 middle temporal gyrus (*MTG*), 10 superior parietal lobule (*SPL*), 11 subcentral gyrus, 12 temporo-occipital arcus, 13 inferior temporal gyrus; * union of the MFG (2) with the preCG (4). SULCI: *a* superior frontal sulcus (*SFS*), *b* inferior frontal sulcus (*IFS*), *c* precentral sulcus (*preCS*), *d* central sulcus (*CS*), *e* postcentral sulcus (*post CS*), *f* superior temporal sulcus (*STS*), *g* intraparietal sulcus (*IPS*), *h* primary intermediate sulcus, *j* secondary intermediate sulcus, *k* accessory intermediate sulcus (not shown in this image), *S* sylvian fissure, *single black arrowhead* anterior subcentral sulcus, *double black arrowheads* posterior subcentral sulcus, *triple black arrowheads* transverse temporal sulci. Note specifically how the anterior horizontal and anterior ascending rami of the sylvian fissure divide the inferior frontal gyrus into the three partes orbitalis (*or*), triangularis (*tr*), and opercularis (*op*). The lateral orbital sulcus (*l*) separates the pars orbitalis from the lateral orbital gyrus (From Naidich et al. (1995); with permission)

transverse temporal sulci extend inferiorly into the temporal lobe in relation to the transverse temporal gyrus of Heschl.

2.1.2 Frontal Lobe

The convexity surface of the frontal lobe is formed by four gyri and three sulci (Fig. 2). The superior frontal gyrus (*SFG*) is a horizontally oriented, roughly rectangular bar of tissue that forms the uppermost margin of the frontal lobe. The middle frontal gyrus (*MFG*) is a horizontally oriented, undulant length of tissue that zigzags posteriorly to merge with the anterior face of the precentral gyrus. The

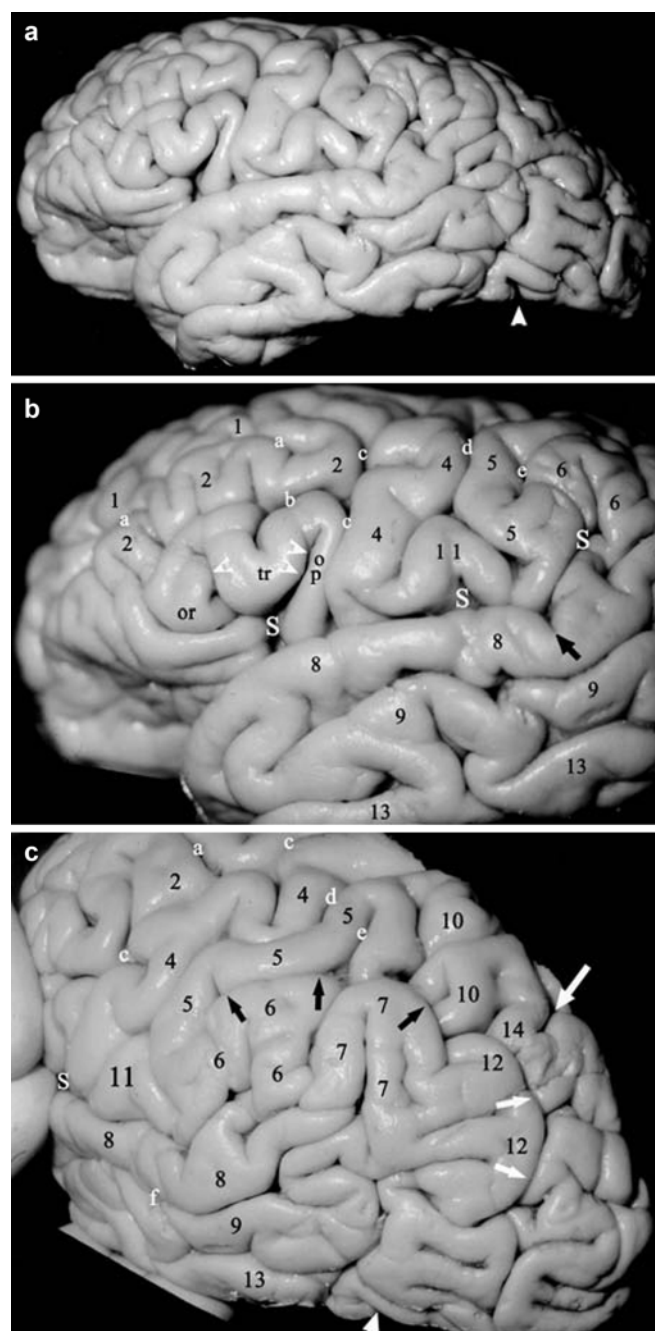


Fig. 2 (a–c) Normal cerebral convexity. (a) Anatomic specimen full surface. (b) Magnified view of the low-middle convexity. (c) Magnified oblique view of the parietal lobe. The surface vessels and the pia-arachnoid have been removed to expose the gyri and sulci more clearly (labels as in Fig. 1.). In (a), the *single large white arrowhead* = preoccipital notch. In (b), the portions of the sylvian fissure (*S*) are indicated: *first white S* = vallecula leading to the anterior horizontal ramus (*single white arrow*) and the anterior ascending ramus (*double white arrow*); *second white S* = posterior horizontal ramus; *third white S* = posterior ascending ramus; *short black arrow* = posterior descending ramus of the sylvian fissure. In (c), the anterior border of the occipital lobe extends from the lateral end of the parieto-occipital sulcus (*large white arrow*) above to the preoccipital notch (*large white arrowhead*) below. The intraparietal sulcus (*multiple large black arrows*) crosses the theoretical lobar border to become the intraoccipital sulcus (*multiple large white arrows*). The inferior parietal lobule is composed of the SMG (6), the AG (7), and the temporo-occipital arcus (second *pli de passage* of Gratiolet) (12). The superior parietal lobule merges into the superior occipital gyrus across the parieto-occipital border through the parieto-occipital arcus (first *pli de passage* of Gratiolet) (14) (a, b from Naidich et al. (1997); (c) From Naidich and Brightbill (1995); with permission)

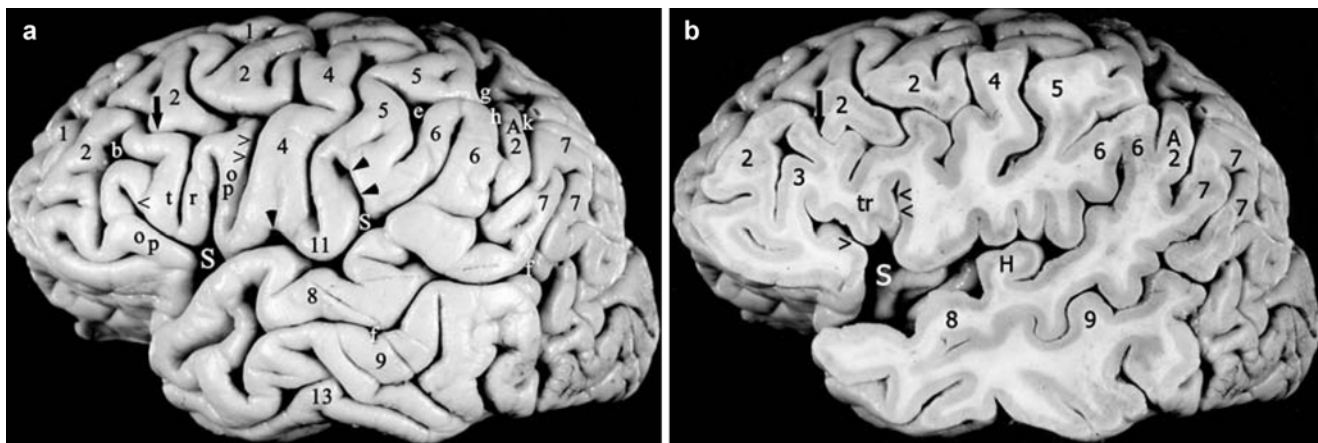


Fig. 3 (a, b) Normal variations in convexity anatomy. (a) Convexity surface of a prepared left hemisphere. (b) Sagittal section of a prepared left hemisphere. A vertically oriented connecting gyrus (*short black arrow*) crosses the inferior frontal sulcus (IFS) (*b*) to unite the pars triangularis (*tr*) with the middle frontal gyrus (MFG) (2). A sulcus triangularis (between the *t* and the *r*) deeply notches the superior surface of the pars triangularis making it appear bifid. The precentral gyrus (4) and the postcentral gyrus (5) unite beneath the central sulcus to form the subcentral gyrus (11), which is delimited by a shallow anterior subcentral sulcus (*single black arrowhead*) and a deep posterior subcentral sulcus (*double black arrowheads*). The inferior portion of the postcentral sulcus (*e*) forms the initial upswing of the arcuate intraparietal sulcus (IPS) (*g*). The posterior ascending ramus of the sylvian fissure (*S*)

indents the inferior parietal lobule (IPL) to form the supramarginal gyrus (SMG) (6). The superior temporal sulcus (STS) (*f*) indents the posterior portion of the IPL to form the angular gyrus (AG) (7). The entire STS parallels the sylvian fissure, hence, its synonym: parallel sulcus. The distal end of the STS within the AG may be designated the angular sulcus. In this specimen, an intercalated accessory preangular gyrus (*A2*) separates the SMG from the AG. Note the relationships of the IPS (*g*), the SMG (6), the AG (7), and the accessory preangular gyrus (*A2*) with the primary intermediate sulcus (*h*), the secondary intermediate sulcus (*j*), and the accessory intermediate sulcus (*k*). In (b), the sagittal section exposes the characteristic appearance of the transverse temporal gyrus of Heschl (*H*) on the superior surface of the temporal lobe (From Naidich et al. (1995); with permission)

inferior frontal gyrus (IFG) is a triangular gyrus that nestles inferiorly against the anteriormost portion of the sylvian fissure. The precentral gyrus (preCG) is a nearly vertical gyrus that forms the posterior border of the frontal lobe, behind the SFG, MFG, and IFG. The superior frontal sulcus (SFS) separates the SFG from the MFG. At its posterior end, the SFS bifurcates to form the superior precentral sulcus. The inferior frontal sulcus (IFS) separates the MFG from the IFG. At its posterior end, the IFS bifurcates to form the inferior precentral sulcus. Together, the superior and inferior portions of the preCS delimit the anterior face of the precentral gyrus, except where the MFG merges with the preCG between the superior and inferior precentral sulci.

The frontal gyri display characteristic configurations (Fig. 1) and variations (Albanese et al. 1989; Naidich et al. 1995, 1997). The IFG has an overall triangular configuration (hence, its synonym: triangular gyrus). The IFS courses above the IFG, bifurcates into the inferior preCS, and thereby separates the triangular IFG from the MFG above and from the preCG behind. The anterior horizontal and anterior ascending rami of the sylvian fissure extend upward into the triangular IFG, partially subdividing it into three portions: the *pars orbitalis*, which abuts the orbital gyri of the frontal lobe; the *pars triangularis* in the center; and the *pars opercularis*, which forms the anteriormost portion of the frontal operculum. Together, the three parts of the IFG resemble an oblique letter "M" (Figs. 1, 2, 3, and 4). Because the anterior ascending ramus of the sylvian fissure cuts through the full thickness of the IFG to reach the insula, the cortex of the

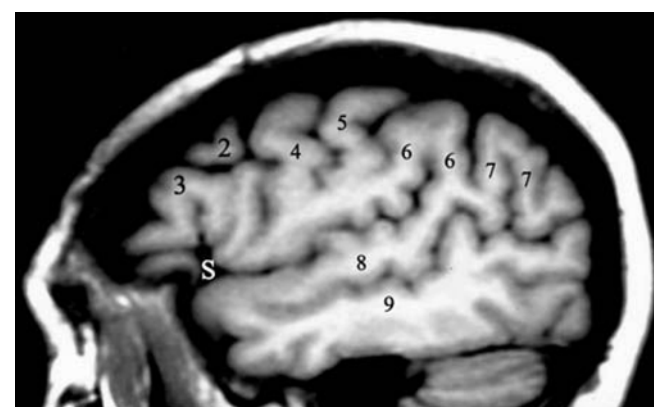


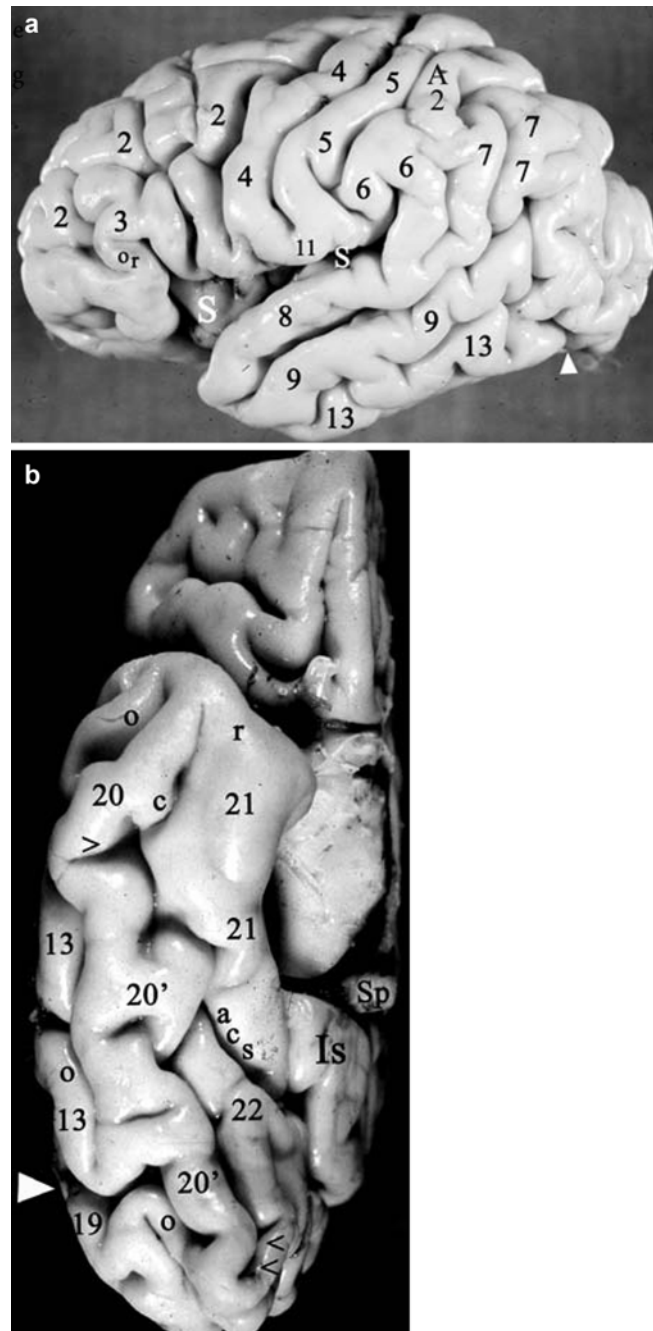
Fig. 4 Sagittal T1-weighted MR imaging of the language-related areas of the normal cerebral convexity. T1-weighted image of a 78-year-old man. Labels as in Figs. 1 and 2 (From Naidich et al. (1997); with permission)

pars opercularis presents both a superficial cortex visible on the surface and a deep cortex within the depths of the fissure (Naidich et al. 2001a).

2.1.3 Temporal Lobe

The convexity surface of the temporal lobe is formed by three horizontal gyri: the superior temporal gyrus (STG), the middle temporal gyrus (MTG), and the inferior temporal gyrus (ITG), separated by the superior temporal sulcus (STS) and the inferior temporal sulcus (ITS) (Fig. 5). The superior and middle temporal gyri extend posteriorly and then swing upward to join with the parietal lobe. The inferior temporal

Fig. 5 (a, b) The temporal lobe. Prepared anatomic specimen of the right hemisphere from a 1-day-old girl. (a) Convexity (reversed to match the other lateral views). The simplified gyral and sulcal pattern reflects the young age. The inferior temporal gyrus (13) extends posteriorly to the preoccipital notch (*large white arrowhead*). An accessory preangular gyrus (A2) is situated superior to the SMG (6) and anterior to the AG (7). Labels as in Figs. 1 and 2. (b) Inferior surface. The brain-stem and the inferior thalamus have been removed to reveal the medial surface more clearly. The inferior temporal gyrus (13) and the inferior occipital gyrus (19) form the inferior margin of the hemisphere, separated by the preoccipital notch (*large white arrowhead*). The lateral occipitotemporal sulcus (*o*) delineates their medial border and separates them from the lateral occipitotemporal gyrus (LOTG) (20) further medially. The medial occipitotemporal sulcus (synonym: collateral sulcus) (*c*) delimits the medial border of the LOTG over its full length. Anteriorly, the collateral sulcus approximates the rhinal sulcus (*r*), and may run into it, or may parallel it. The parahippocampal gyrus (PHG) (21) forms the medial surface of the temporal lobe over its full length and extends posteriorly to become the isthmus (*Is*) of the cingulate gyrus inferior to the splenium (*Sp*). In the anterior half of the temporal lobe, the collateral sulcus (*c*) separates the LOTG (20) from the PHG (21). In the posterior half, the medial occipitotemporal gyrus (MOTG) (lingual gyrus) (22) intercalates itself between the LOTG and the PHG. The collateral sulcus stays with the medial border of the LOTG, so the collateral sulcus (*c*) separates the LOTG (20) from the MOTG (22), while the anterior calcarine sulcus (*acs*) separates the MOTG (22) from the PHG (21). The anterior and posterior transverse collateral sulci (*single and double black arrowheads*) delimit a midportion of the LOTG (20^l) that has been designated by Duvernoy (Duvernoy 1991) as the fusiform gyrus (From Daniels et al. (1987); with permission)



gyrus forms the inferior edge of the convexity surface of temporal lobe and curves onto the inferior surface of the temporal lobe. It is delimited posteriorly by a small notch, the preoccipital notch (synonyms: temporo-occipital notch or incisura), which separates the inferior temporal gyrus anteriorly from the inferior occipital gyrus posteriorly. The STS courses parallel to the posterior horizontal and the posterior ascending rami of the sylvian fissure (hence, its synonym, parallel sulcus). The posterior portion of the STS is directed superiorly and is sometimes designated the angular sulcus. The ITS courses approximately parallel to the inferior margin

of the convexity and may become continuous posteriorly with the inferior occipital sulcus.

2.1.4 Parietal Lobe

The convexity surface of the parietal lobe is formed by three portions: the vertically oriented postcentral gyrus (post CG) anteriorly, and the two superior parietal (SPL) and inferior parietal (IPL) lobules posteriorly (Figs. 1, 2, 3, and 4). The postCG courses vertically just posterior and parallel to the preCG. The postCG is separated from the preCG by the intervening central sulcus (CS) over most of its length.

However, inferiorly, the postCG merges with the preCG inferior to the CS along the subcentral gyrus (subCG) just above the sylvian fissure. Superiorly, the postCG merges with the preCG superior to the CS along the paracentral lobule (paraCL) on the medial surface of the hemisphere. Thus, the precentral and postcentral gyri actually form a continuous band of tissue that circles around the central sulcus from the precentral gyrus through the subcentral gyrus, into the postcentral gyrus and the paracentral lobule, returning into the precentral gyrus.

The posterior border of the post CG is delimited by the superior and inferior postcentral sulci. The superior postCS separates the upper postCG from the superior parietal lobule. The inferior postCS separates the postCG from the inferior parietal lobule. The inferior postCS may be considered the upswing of a long, deep, arcuate intraparietal sulcus (IPS) that ascends behind the lower postCG and then slashes posteriorly across the convexity surface of the parietal lobe, dividing it into the SPL situated superomedial to the IPS and the IPL situated inferolateral to the IPS. The posterior down-swing of the arcuate IPS then crosses the theoretical border between the parietal and occipital lobes and continues into the occipital lobe, where it is designated the intraoccipital sulcus (IOS) (synonym: superior occipital sulcus, SOS) (Figs. 1, 2, 3, and 4). Posteriorly, the SPL becomes continuous with the superior occipital gyrus (SOG) behind it through a narrow band of tissue designated the arcus parietooccipitalis (first *pli de passage* of Gratiolet) (Fig. 2) (Duvernoy 1991).

Within the inferior parietal lobule, the posterior ascending ramus of the sylvian fissure swings upward into the anterior portion of the IPL and is capped by a horseshoe-shaped gyrus designated the supramarginal gyrus (SMG). In parallel fashion, the distal STS swings upward into the posterior portion of the IPL where it is capped by a second horseshoe-shaped gyrus designated the angular gyrus (AG). The AG usually lies just posterior to the SMG, but may be displaced from that position by variant accessory gyri (Figs. 1, 2, 3, and 4) (Naidich et al. 1995, 1997). Together the SMG and the AG constitute most of the IPL. An additional small horseshoe of tissue, designated the second parieto-occipital arcus (second *pli de passage* of Gratiolet), connects the AG with the middle OG posterior to it, completing the IPL (Fig. 2) (Duvernoy 1991). A small primary intermediate sulcus descends from the IPS to separate the SMG from the AG. A small secondary intermediate sulcus descends from the IPS to define the posterior border of the AG, separating the AG from the rest of the IPL posterior to it (Naidich et al. 2001a).

2.1.5 Occipital Lobe

The convexity surface of the occipital lobe has also been divided into three horizontal gyri: the superior occipital gyrus (SOG), the middle occipital gyrus (MOG), and the

inferior occipital gyrus (IOG). These are separated by the superior and inferior occipital sulci (SOS and inferior OS). The SOS (synonym: intraoccipital sulcus) is the direct continuation of the IPS (Figs. 1, 2, 3, and 4). The inferior OS is usually coextensive with the inferior temporal sulcus. Therefore, the MOG lies just posterior to the confluence of the temporal and parietal lobes at the SMG, the AG, the STG, and the MTG. The MOG is the largest portion of the occipital lobe on the convexity. It is usually subdivided into a superior and an inferior portion by a horizontally oriented middle OS (synonym: lateral OS).

2.1.6 Insula

Separating the superior and inferior covers (opercula) of the sylvian fissure discloses the Island of Reil (insula). The insula is delimited circumferentially by the peri-insular sulcus (synonym: circular sulcus), composed of the anterior, superior, and inferior perisylvian sulci (Ture et al. 1999). The central sulcus of the convexity extends over the insula as the central sulcus of the insula, dividing the insula into a larger anterior and a smaller posterior lobule (Fig. 6) (Naidich et al. 2004; Nieuwenhuys et al. 1988; Ture et al. 1999). The anterior lobule typically has three vertically oriented short insular gyri designated the anterior short, middle short, and posterior short insular gyri. These three converge anteroinferolaterally to form the apex of the insula. The posterior lobule of the insula typically displays two oblique gyri: the anterior and posterior long insular gyri. The anterior insula is connected exclusively to the frontal lobe, whereas the posterior insula is connected to both the temporal and the parietal lobes (Naidich et al. 2004; Ture et al. 1999).

2.2 Inferior Surface

2.2.1 The Frontal Lobe

The inferior (orbital) surface of the frontal lobe is formed by the gyrus rectus medially and four orbital gyri laterally, separated by the olfactory and orbital sulci. The gyrus rectus forms the medial margin of the orbital surface of frontal lobe for the full length of the frontal lobe. The lateral border of the gyrus rectus is delimited by the olfactory sulcus (Fig. 7). The orbital gyri are arranged around an “H-shaped” orbital sulcus as the medial orbital, lateral orbital, anterior orbital, and posterior orbital gyri.

2.2.2 The Temporo-occipital Lobes

The inferior surface of the temporo-occipital lobe is formed by the inferior temporal gyrus, the lateral occipitotemporal gyrus (LOTG), the medial occipitotemporal gyrus (MOTG) (synonym: lingual gyrus), and the parahippocampal gyrus (PHG), separated by the lateral occipitotemporal sulcus, the collateral sulcus, and the anterior calcarine sulcus (Fig. 5).

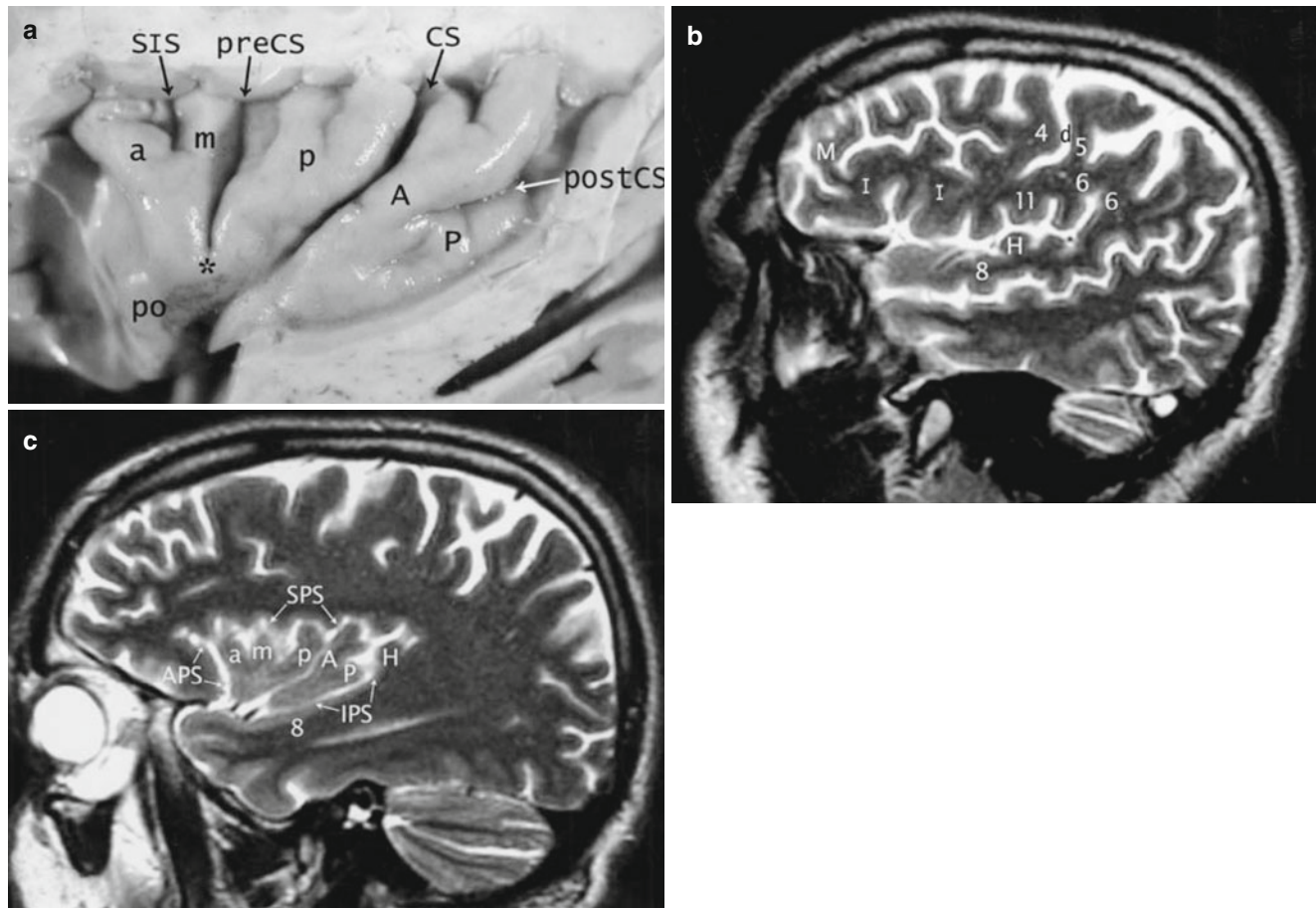


Fig. 6 (a–c) Insula. (a) Prepared anatomic specimen of the convexity surface of the insula, after removal of the overhanging opercula. A 71-year-old man. The central sulcus (*CS*) extends across the triangular insula like a “hockey stick,” dividing it into a larger anterior lobule and a smaller posterior lobule. The anterior lobule typically displays three gyri, the anterior short (*a*), middle short (*m*), and posterior short (*p*) insular gyri, separated by the short insular sulcus (*SIS*) and the precentral sulcus (*preCS*). These three characteristically converge inferiorly to form the apex (*) of the insula. The posterior insular lobule typically displays two gyri, the anterior long (*A*) and the posterior long (*P*) insular gyri, separated by the postcentral sulcus (*postCS*). These too often merge together, anteriorly, just behind the central sulcus. Just inferomedial to the apex (*), the pole of the insula (*po*) forms the most anteroinferomedial portion of the insula. The central sulcus courses under the apex and the pole and then abruptly swings medially toward the supra-

stellar cistern. (b, c) Normal sagittal T2-weighted MRI. A 51-year-old man. Laterally (b), the convexity gyri form two opercula that cover the insula. Superiorly, the inferior frontal gyrus (*I*), the inferior ends of the precentral (4) and postcentral (5) gyri, the subcentral gyrus (11), and the supramarginal gyrus (6) form the frontoparietal operculum. The superior temporal gyrus (8) and Heschl’s gyrus (*H*) form the temporal operculum. *M* middle frontal gyrus. Medially (c), the insula is delimited by the peri-insular sulcus, composed of three segments: the anterior (*APS*), superior (*SPS*), and inferior (*IPS*) peri-insular sulci. The anterior (*a*), middle (*m*), and posterior (*p*) short insular gyri constitute the larger anterior lobule, while the anterior (*A*) and posterior (*P*) long insular gyri form the smaller posterior lobule. The central sulcus courses between the two lobules. Heschl’s gyrus (*H*) snugs up against the posteromedial portion of the posterior long insular gyrus. 8 = superior temporal gyrus (From Naidich et al. (2004) with permission)

Medially, the parahippocampal gyrus forms the medial border of the temporal lobe for the full length of the temporal lobe, from just posterior to the temporal pole to the level of the splenium. Posterior to the splenium, the medial occipitotemporal gyrus forms the medial border of the occipital lobe. Laterally, along the full length of the temporo-occipital lobes, the inferior temporal gyrus and the inferior occipital gyrus curve medially, form the inferior cerebral margin, and pass onto the inferior surface, where they constitute the lateralmost portion of the inferior surface of the temporo-occipital lobes. Only the small preoccipital

notch delimits the inferior temporal gyrus from the inferior occipital gyrus. Centrally, the LOTG runs the full length of the temporo-occipital lobes from the temporal pole to the occipital pole. Throughout its length, the LOTG remains just medial to the ITG and the IOG and is separated from them by the lateral occipitotemporal sulcus. Medially, the medial occipitotemporal sulcus (synonym: collateral sulcus) runs the full length of the LOTG (Fig. 5b). In the anterior half of the temporal lobe, the lateral occipitotemporal sulcus separates the LOTG from the parahippocampal gyrus. In the posterior half of the temporal lobe, the medial occipitotemporal

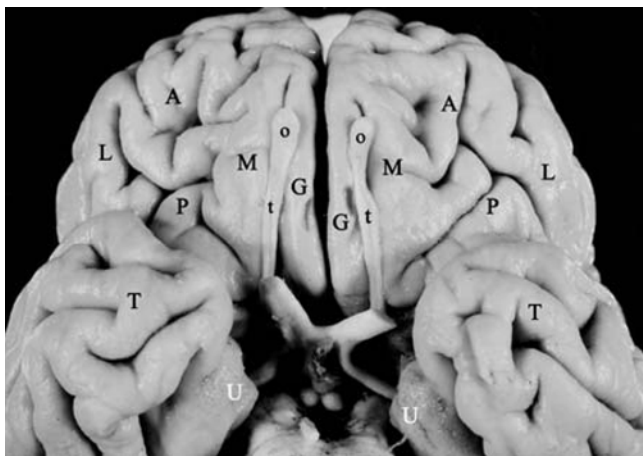


Fig. 7 Inferior surface of frontal lobe. Prepared anatomic specimen of the inferior surfaces of the anterior brain. The inferior surface of the frontal lobes is divided into two portions. The paired paramedian linear gyri recti (*G*) flank the interhemispheric fissure and are delimited laterally by the olfactory sulci, largely obscured here by the olfactory bulbs (*o*) and tracts (*t*). Lateral to the olfactory sulci, the orbital gyri of the frontal lobe are arranged around approximately H-shaped orbital sulci as the paired medial (*M*), lateral (*L*), anterior (*A*), and posterior (*P*) orbital gyri. In true base view, the anterior temporal lobes (*T*) overlap the posterior orbital gyri. Note the paired uncus (*U*)

gyrus intercalates itself between the LOTG and the parahippocampal gyrus. Therefore, in the posterior half of the temporal lobe, the lateral occipitotemporal sulcus separates the LOTG from the MOTG, while the anterior calcarine sulcus separates the MOTG from the PHG.

Two synonyms are commonly used for temporo-occipital gyri. The term *lingual gyrus* usually refers to the MOTG (Duvernoy 1991; Ono et al. 1990). The term *fusiform gyrus* is most often used to designate either the LOTG (Ono et al. 1990) or a large middle portion of the LOTG that crosses the arbitrary border of the temporal and the occipital lobes between the anterior and the posterior transverse collateral sulci (Duvernoy 1991). However, in another usage, Williams et al. (1989) group the MOTG and the LOTG together as the fusiform gyrus. In most brains, the fusiform gyrus is larger on the left (Kopp et al. 1977; Naidich et al. 2001a).

2.3 Superior Surface of the Temporal Lobe

Opening the margins of the sylvian fissure, or resecting the overlying superior operculum, displays the superior surface of the temporal lobe, designated the superior temporal plane. The prominent features of this plane are one or more transverse temporal gyri (of Heschl) (Fig. 8). Heschl's gyrus or gyri (HG) arise just posteromedial to the insula and course obliquely across the superior temporal surface from postero-medial to anterolateral and may be visible at the external surface of the sylvian fissure. The presence of an HG is constant.

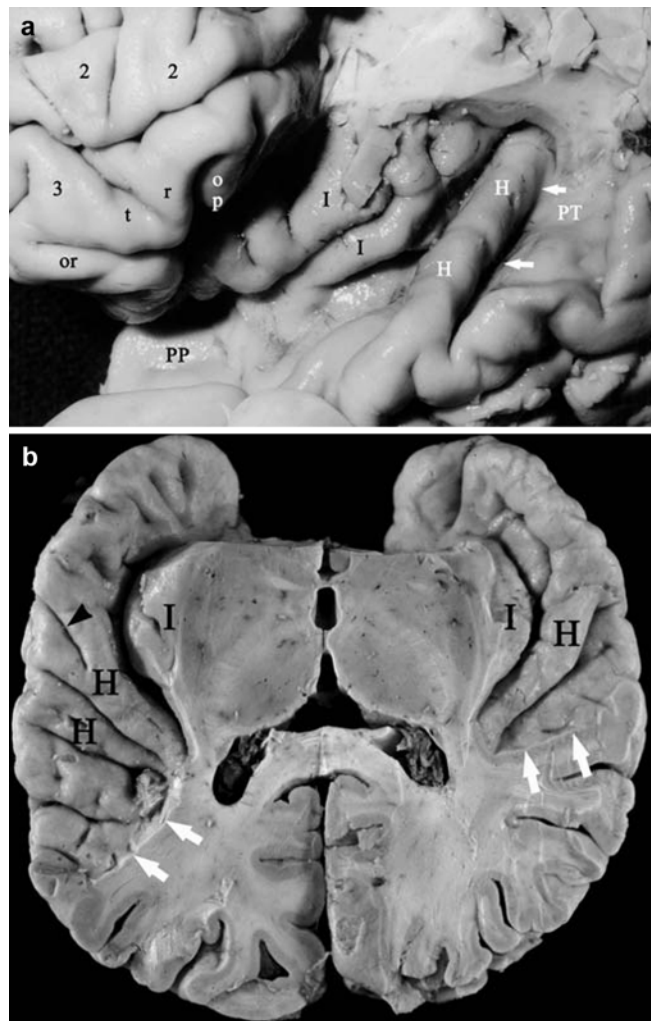


Fig. 8 (a, b). The superior surface of the temporal lobe from prepared anatomic specimens. (a) Anatomy of Heschl's gyrus in relation to the insula. Resection of the frontal and parietal opercula exposes the middle frontal gyrus (2); the pars orbitalis (*or*) triangularis (*tr*) and the residual portion of the opercularis (*op*) of the inferior frontal gyrus (3); the oblique long gyri (black *I*) of the posterior insula; the length of a single Heschl's gyrus (*H*) which courses obliquely across the superior surface of the temporal lobe from just posterior to the insula (posterioromedially) toward the convexity surface of the superior temporal gyrus (anterolaterally); Heschl's sulcus (white arrows) immediately posterior to Heschl's gyrus; the planum polare (*PP*) anterior to the HG; and the planum temporale (*PT*) posterior to HG (From Naidich and Matthews (2000) with permission). (b) Exposure of the superior surfaces of both temporal lobes by resection of the overlying frontal and parietal opercula. Right is to the reader's right. The single right and the dual left Heschl's gyri (*H*) course obliquely across the upper surface of the temporal lobe from just posterior to the insulae (*I*) (posterioromedially) to the convexity surface (anterolaterally). A shallow Beck's sulcus (small black arrowhead) grooves the left HG laterally. Heschl's sulcus delimits the posterior border of HG. The planum polare extends from the temporal pole to the anterior aspect of HG. The planum temporale extends between Heschl's sulcus and the posterior limit of the sylvian fissure (white arrows) and is substantially larger on the left

The number of HG on each side and their symmetry are highly variable. Heschl's gyrus may be single (66–75 %), double (25–33 %), or triple (1 %), both unilaterally and bilaterally

(Yoshiura et al. 2000; Yousry et al. 1997a). Heschl's gyrus is often larger and longer on the left side than the right, but there is no constant relationship between HG and the side of handedness or cerebral dominance (Carpenter and Sutin 1983; Yousry et al. 1997a). A shallow longitudinal sulcus (of Beck) may groove the superior surface of HG, especially laterally, giving it a partially bifid appearance. A deep transverse temporal sulcus (Heschl's sulcus [HS]) typically defines the posterior border of HG.

The oblique Heschl's gyrus divides the superior surface of the temporal lobe into three parts. (1) The flat superior surface of the temporal lobe anterior to HG is designated the planum polare. (2) From HS at the posterior border of HG to the posterior end of the sylvian fissure, the flat superior surface of the temporal lobe is designated the planum temporale. (3) The posterosuperior extension of the planum temporale along the posterior bank of the posterior ascending ramus of the sylvian fissure may be designated the planum parietale. The planum temporale is triangular. It is typically asymmetric on the two sides and most often is larger on the left in humans, chimpanzees and other great apes (Fig. 8) (Gannon et al. 1998). The size of the planum temporale seems to correlate with the side of language dominance (and perhaps with right or left-handedness, gender, or both (Galaburda and Sanides 1980; Galaburda et al. 1998; Geschwind 1965a, b, 1970; Geschwind and Levitsky 1968; Pieniadz and Naeser 1984; Steinmetz and Seitz 1991; Steinmetz et al. 1989b, 1990a, b, 1991). Most of the variation in the sizes of the planum temporale may be ascribed to differing sizes of a cytoarchitectonic zone designated area Tpt (Galaburda and Sanides 1980). Area Tpt has a homologue in nonhuman primates that shows significant asymmetry (left > right) at the cellular level (Gannon et al. 1998).

2.4 Medial Surface

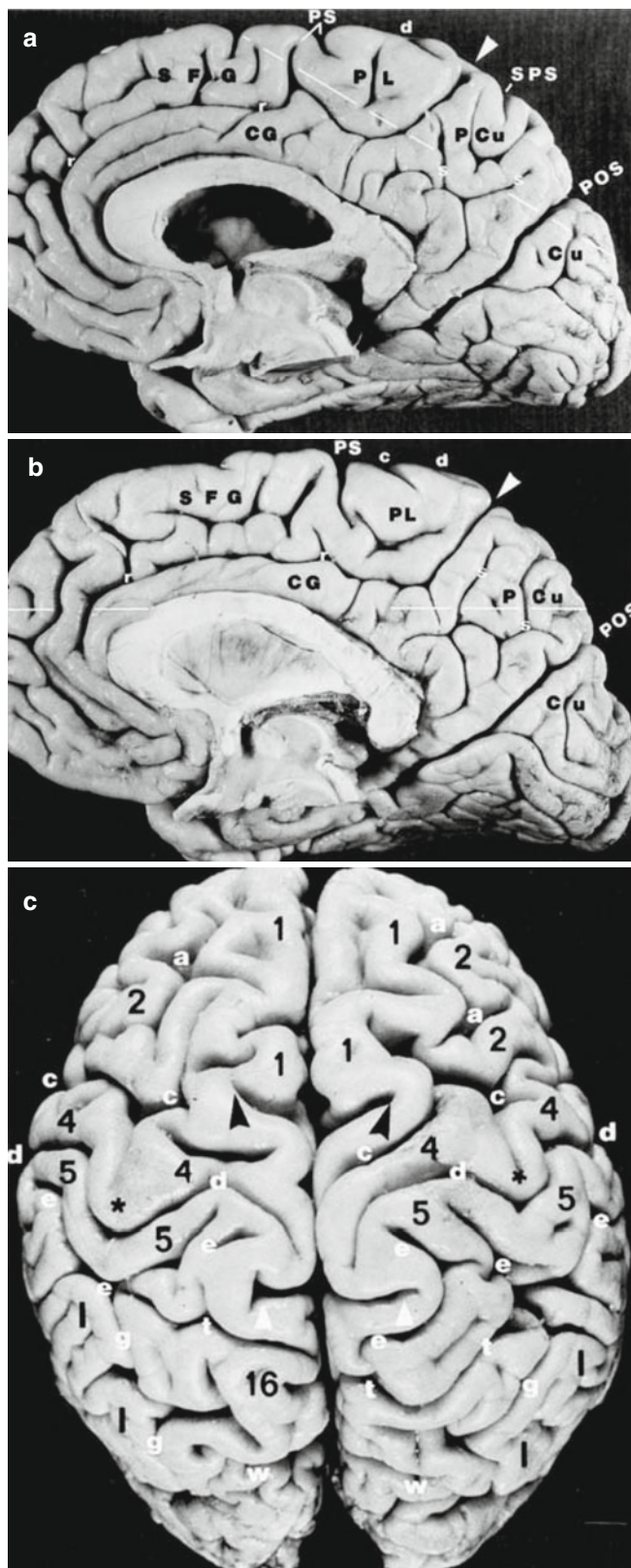
The medial surface of the cerebrum is arranged as a radial array of gyri and sulci that are oriented either co-curvilinear with the corpus callosum or perpendicular to it (Fig. 9). The major gyri of the medial surface are the cingulate gyrus (CingG), the superior frontal gyrus (SFG) (whose medial surface may also be designated the medial frontal gyrus), the paracentral lobule (ParaCL), the precuneus (PreCu), the cuneus (Cu), and the medial occipitotemporal gyrus (MOTG) (synonym: lingual gyrus). The major sulci are the callosal sulcus (CalS), the cingulate sulcus (CingS), the paracentral sulcus (ParaCS), the subparietal sulcus (SubPS), the parieto-occipital sulcus (POS), the calcarine sulcus (CaS), and the anterior calcarine sulcus (AntCaS). The cingulate gyrus encircles the corpus callosum. It is delimited from the corpus callosum centrally by the callosal sulcus and from the superior frontal gyrus and paracentral lobule superficially by the cingulate sulcus.

The gyri that form the medial surface of the brain peripheral to the cingulate gyrus and sulcus are nothing more than the medial aspects of the gyri that constitute the high convexity of the brain. The superior frontal gyrus of the convexity curves over the cerebral margin onto the medial surface to form a broad arc of tissue designated the SFG or medial frontal gyrus. The precentral gyrus and the postcentral gyrus curve over the cerebral margin from the convexity onto the medial surface and join together to form the paracentral lobule. The superior parietal lobule curves over the cerebral margin onto the medial surface to form the precuneus. The superior occipital gyrus curves over the cerebral margin onto the medial surface to form the cuneus. The SFG is separated from the paracentral lobule posterior to it by the paracentral sulcus. The posterior end of the cingulate sulcus sweeps upward to reach the cerebral margin. This radially oriented distal portion of the cingulate sulcus is the pars marginalis (pM). The pars marginalis separates the paracentral lobule anteriorly from the precuneus posteriorly. The upper end of the central sulcus typically curves over the margin onto the medial surface of the hemisphere just anterior to the pars marginalis. This medial portion of the CS courses posteriorly nearly perpendicular to the pars marginalis. The "H"-shaped subparietal sulcus lies posterior to the pars marginalis and separates the inferior end of the precuneus from the cingulate gyrus deep to it. The parieto-occipital sulcus courses parallel to the pars marginalis, joins with the anterior end of the calcarine sulcus, and continues anteriorly as the anterior calcarine sulcus. The POS separates the precuneus anteriorly from the cuneus posteriorly. The calcarine sulcus separates the cuneus superiorly from the MOTG (lingual gyrus) inferiorly. The anterior calcarine sulcus separates the cingulate gyrus anteriorly from the MOTG posteriorly. The calcarine sulcus may remain entirely on the medial surface of the hemisphere, extend posteriorly to reach the occipital pole, or extend beyond medial surface onto either the convexity or inferior surfaces of the occipital lobe.

3 Lobar Borders

The precise borders of the temporal, parietal, and occipital lobes on the convexity are highly arbitrary. Published diagrams from different authors indicate substantially different criteria for partitioning the TPO lobes along the convexity (Yousry 1998). The very definitions of these borders and their lobes have evolved substantially over the years (Yousry 1998). In one common system of nomenclature, one identifies the lobes by first finding the lateral end of the deep parieto-occipital sulcus near the superior margin of the hemisphere. Then one identifies the inconstant preoccipital notch (Gusmão et al. 2002) in the inferior margin of the hemisphere (Fig. 10). The arbitrary anterior border of the occipital lobe

Fig. 9 (a–c) Medial and superior surfaces of both hemispheres. Prepared anatomic specimens. (a, b) Medial surfaces. The major sulci subdivide the medial surface of each cerebral hemisphere into the cingulate gyrus (*CG*), medial surface of the superior frontal gyrus (*SFG*), paracentral lobule (*PL*), precuneus (*PCu*), and cuneus (*Cu*). The posterior end of the cingulate sulcus sweeps sharply upward toward the superior cerebral margin as the marginal portion of the cingulate sulcus (pars marginalis, *white arrowhead*), which separates the paracentral lobule anteriorly from the precuneus posteriorly. Anterior to the pars marginalis, the paracentral sulcus (*PS*) arises from the cingulate sulcus and/or from the cerebral margin to separate the superior frontal gyrus from the paracentral lobule. The vertical and horizontal arms of the “H-shaped” subparietal sulcus (*s*) groove the medial surface of the precuneus and delimit it from the cingulate gyrus inferior to it. The superior ends of the vertical arms of the subparietal sulcus may reach to and notch the superior margin. The superior medial end of the central sulcus (*d*) usually crosses over the cerebral margin onto the medial surface and then recurses sharply posteriorly to course nearly perpendicular to the pars marginalis, just millimeters in front of the pars marginalis. As a consequence, the most superior medial portion of the precentral gyrus (4) merges with the most superior medial portion of the postcentral gyrus (5) around the uppermost end of the central sulcus to form the paracentral lobule anterior to the pars marginalis. A posterior portion of the postcentral gyrus passes posterior to the pars marginalis to merge with the precuneus. The prominent parieto-occipital sulcus (*POS*) courses approximately parallel to the pars marginalis, but posterior to the splenium, and delimits the parietal lobe plus cingulate gyrus antero-superiorly from the occipital plus temporal lobes postero-inferiorly. (c) Superior surface of the two hemispheres. The two cerebral hemispheres border the interhemispheric fissure (*IHF*). Multiple sulci oriented at right angles to the *IHF* form a series of transverse grooves or “cross-bars” across the *IHF*. The paired partes marginales (*white arrowheads*) are often the most prominent of these grooves and extend laterally into the hemispheres for a substantial distance. At the vertex, the lateral edges of the two partes marginales often curve anteriorly to form a bracket, open anteriorly. The paired central sulci (*d*) undulate across the cerebral convexity between the precentral gyri (4) and the postcentral gyri (5). They typically hook sharply posteriorly (*) as they circumscribe the hand motor region of the precentral gyrus (*), and then reverse curvature, become concave posteriorly, and converge toward the *IHF* just anterior to the partes marginales. The two central sulci (*d*) characteristically (but not invariably) pass anterior to and medial to the lateral edges of the partes marginales (“enter the bracket”) and reach to or cross the superior margins of the hemispheres. The postcentral gyri course superiorly, behind the precentral gyri, toward or to the cerebral margins. The medial ends of the postcentral sulci (*e*) usually bifurcate around the partes marginales to form a prominent “parenthesis” configuration (*e, e* in the right hemisphere). The interlocking curves of the precentral gyri (*d*), postcentral gyri (*e*), and the partes marginales (*white arrowheads*) form a characteristic set of interlocking curves that usually identifies these sulci and the adjacent gyri. Other labels: (1) superior frontal gyrus, (2) middle frontal gyrus, (4) precentral gyrus, (5) postcentral gyrus, (16) precuneus, (a) superior frontal sulcus, (c) precentral sulcus, (d) central sulcus, (e) postcentral sulcus, (g) intraparietal sulcus, (r) cingulate sulcus, (s) subparietal sulcus, (t) superior parietal sulcus, and (w) parieto-occipital sulcus (From Naidich et al. (1996); with permission)



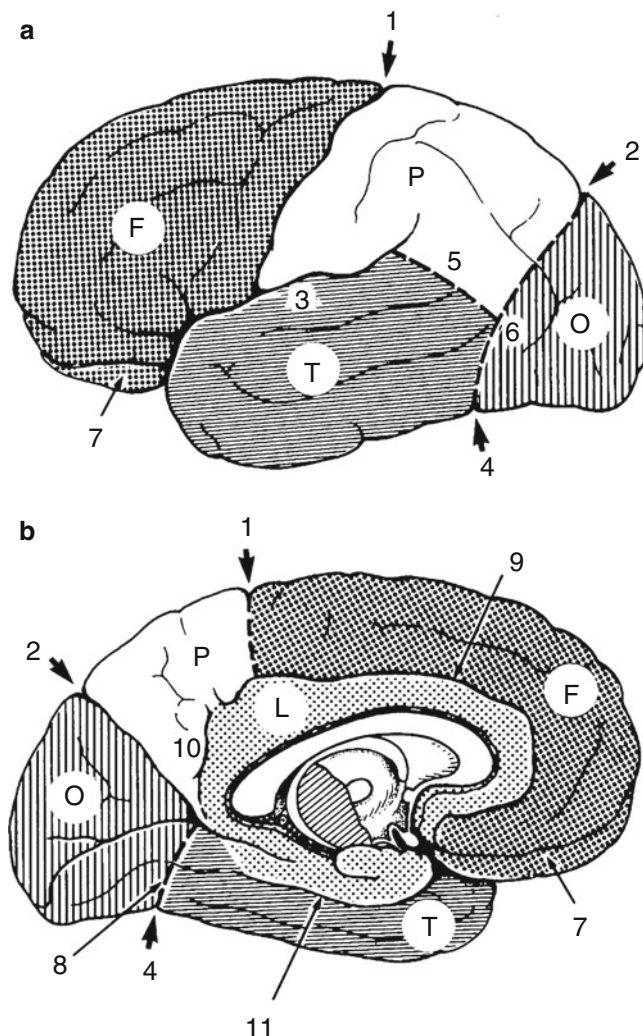


Fig. 10 (a, b) Lobar borders according to Ono, Kubik, and Abernathy. (a) Convexity. (b) Medial surface. The anterior border of the occipital lobe is delimited by the lateral parietotemporal line (6) drawn between the parieto-occipital sulcus and the preoccipital notch. On the convexity, the temporal lobe is separated from the parietal lobe by the temporo-occipital line (5) drawn from the Sylvian fissure to the middle of the anterior border of the occipital lobe. On the basal surface, the temporal lobe is separated from the occipital lobe by the basal parietotemporal line (8) drawn from the preoccipital notch to the union of the parieto-occipital sulcus with the calcarine sulcus (unlabelled). F frontal lobe, O occipital lobe, P parietal lobe, T temporal lobe, 1 central sulcus, 2 parieto-occipital sulcus, 3 Sylvian fissure, 4 preoccipital notch, 5 temporo-occipital line, 6 lateral parietotemporal line, 7 orbital surface, 8 basal parietotemporal line, 9 cingulate sulcus, 10 subparietal sulcus, 11 collateral sulcus (From Ono et al. (1990), p 9; with permission)

is then defined by the drawing the “lateral parietotemporal line” along the convexity from the lateral end of the parieto-occipital sulcus above to the preoccipital notch inferiorly.

Next one demarcates the borders of the temporal and parietal lobes that abut onto the occipital lobe. To do this, one draws the “temporo-occipital line,” defined variably as (1) an

arc from the distal end of the posterior descending ramus of the Sylvian fissure to the midpoint of the anterior border of the occipital lobe (Ono et al. 1990), (2) an arc from the posterior descending ramus of the Sylvian fissure to the anterior border of the occipital lobe, taking care to make sure that the arc is co-curvilinear with the IPS above (Duvernoy 1991; Schwalbe 1881; Yousry 1998), (3) an arc from the posterior descending ramus of the Sylvian fissure to the anterior border of the occipital lobe at the preoccipital notch (Jensen 1871; Yousry 1998), or (4) a straight linear extension from the distal end of the posterior horizontal ramus of the Sylvian fissure to the anterior border of the occipital lobe (Dejerine 1895; Talairach and Tournoux 1988; Yousry 1998).

On the medial surface, the deep parieto-occipital sulcus clearly divides the parietal lobe from the occipital lobe and is the landmark used to define the anterior border of the medial occipital lobe in all systems of nomenclature. On the inferior surface, the demarcation of the lobes again becomes arbitrary. On the inferomedial surface, one may delineate the temporal lobe from the occipital lobe by drawing a basal parietotemporal line from the preoccipital notch to, variably, (1) the inferior end of the parieto-occipital sulcus where it joins the calcarine sulcus (Fig. 10) (Ono et al. 1990), (2) the anterior calcarine sulcus beneath the splenium (Fig. 11) (Duvernoy 1991), or (3) the anterior end of the anterior calcarine sulcus (Jensen 1871; Yousry 1998).

Because the patterns of sulcal branching, the gyral configurations, and the very definitions of the lobes used for anatomic description are so highly variable in this region, it may ultimately prove more accurate to designate the entire region as the TPO confluence. One could then choose to divide the convexity surface of the TPO confluence along the line of the multimodal association cortex from the lateral end of the parieto-occipital sulcus downward to, and then along, the superior temporal sulcus to define three functional compartments, a temporoparietal lobe rostral to the multimodal area (for somatosensory and auditory processing), a temporo-occipital lobe caudal to the multimodal area (for visual processing), and a TPO multimodal association lobe (for integrating the diverse modalities). On the medial surface, one could similarly use the multimodal association cortex that extends along the parieto-occipital sulcus and the anterior calcarine sulcus to divide the medial surface of the hemisphere into a medial parietal region rostral to the multimodal cortex (for somatosensory processing), a caudal temporo-occipital lobe (for visual processing), and the interposed multimodal lobe (for integration) (Naidich et al. 2001a).

The term limbic lobe signifies a broad band of tissue on the medial surfaces of the two hemispheres that, considered together, encircle the brainstem, creating a limbus about the stem. Specifically, the limbic lobe includes the subcallosal area, the cingulate gyrus, the isthmus of the cingulate gyrus, the parahippocampal gyrus, and the piriform lobe, which

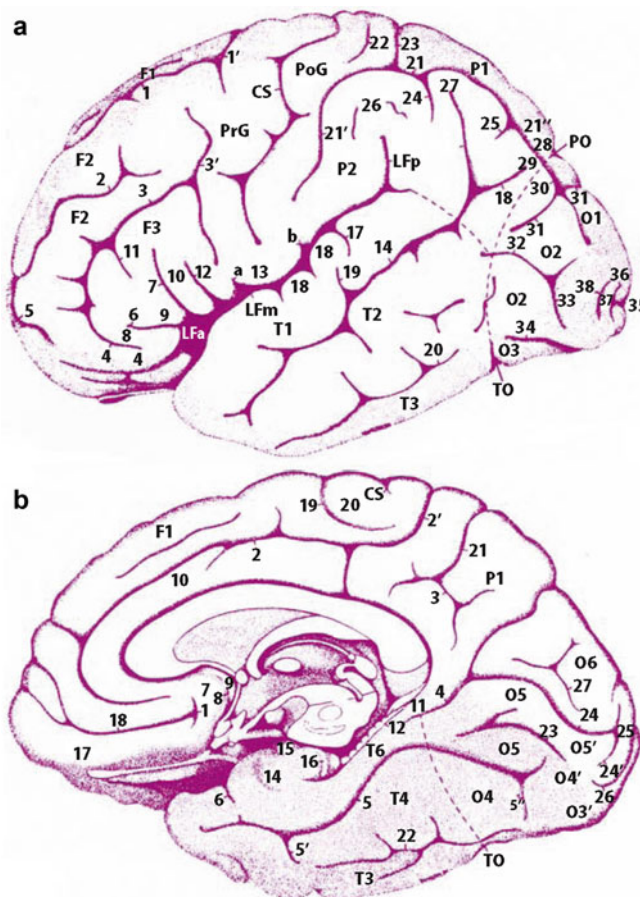


Fig. 11 (a, b) Lobar borders according to Duvernoy. (a) Convexity. (b) Inferomedial surface. The anterior border of the occipital lobe is delimited by the same lateral parietotemporal line drawn between the parieto-occipital sulcus and the preoccipital notch. On the convexity, the temporal lobe is separated from the parietal lobe by a temporo-occipital line drawn co-curvilinear with the intraparietal sulcus from the posterior descending ramus of the sylvian fissure to the anterior border of the occipital lobe. On the basal surface, the temporal lobe is separated from the occipital lobe by a basal parietotemporal line drawn from the preoccipital notch to the anterior calcarine sulcus inferior to the splenium. The posterior end of the superior temporal sulcus bifurcates as it extends into the inferior parietal lobule, making a large angular gyrus (a common variation). The fusiform gyrus is formed from portions of the temporal lobe (*T*4) and the occipital lobe (*O*4) that occupy the midportion of the lateral occipitotemporal gyrus between the anterior (*5'*) and posterior (*5''*) transverse collateral sulci. Convexity surface (a) *LFa*, *LFm*, and *LFp* = lateral fissure (anterior, middle, and posterior segments); *CS* = central sulcus, *PO* = parieto-occipital fissure, *TO* = temporo-occipital incisure, *F1*, *F2*, and *F3* = superior, middle, and inferior frontal gyri; *PrG* = precentral gyrus, *T1*, *T2*, and *T3* = superior, middle, and inferior temporal gyri; *P1* = superior parietal gyrus (lobule); *P2* = inferior parietal gyrus (lobule); *PoG* = postcentral gyrus, *O1*, *O2*, and *O3* = superior, middle (synonym: lateral), and inferior occipital gyri; *21*, *21'*, and *21''* = intraparietal sulcus; *33* = sulcus lunatus. Inferomedial surface (b) *P1* = precuneus, *T3* = inferior temporal gyrus, *T4* = temporal portion of the fusiform gyrus, *T5* = parahippocampal gyrus, *TO* = temporo-occipital incisure, *O3* = inferior occipital gyrus, *O4* = occipital portion of the fusiform gyrus, *O5* = lingual gyrus, *O6* = cuneus, *2* = cingulate sulcus, *2'* = marginal segment of the cingulate sulcus (pars marginalis), *3* = subparietal sulcus, *4* = anterior calcarine sulcus, *22* = lateral occipitotemporal sulcus, *24* = calcarine sulcus. The caudal portions of *O3*, *O4*, and *O5* merge together at the inferior aspect of the occipital lobe (From Duvernoy (1991), pp 5–9; with permission)

according to Duvernoy corresponds to the anterior parahippocampal gyrus (Duvernoy 1991).

Recently, Yasargil emphasized the arbitrary and uncertain borders between the lobes and proposed a new lobar classification in which the continuous circle of tissue formed by the precentral gyrus, subcentral gyrus, postcentral gyrus, and paracentral gyrus was considered to be a separate, distinct *central lobe*. Thus, the Yasargil classification would include seven lobes, the frontal central, parietal, occipital, temporal, insular, and limbic lobes (Yasargil 1994).

4 Localizing Anatomic Sites Independent of Lobar Anatomy

Several attempts have been made to identify functionally relevant anatomic sites, *independent* of the variable lobar and sulcal borders. These systems depend on first establishing reference planes that are based upon a very limited number of deep anatomic structures, then designating all locations in space in terms of coordinates based upon those limited reference planes, and finally identifying all other anatomic features in terms of these coordinates. These attempts may be extended to “correct for” differences in overall head and brain shape by “morphing” the anatomy of any individual brain to superimpose its gross contours on those of a single standard anatomic reference brain. Applied to groups of patients, such systems may detect commonalities otherwise obscured by individual variation, but at the costs of (1) information specific to each individual and (2) understanding of the range of normal variation.

4.1 Talairach-Tournoux Coordinate System and “Talairach Space”

Talairach and Tournoux took a horizontal plane that extended through the brain along a line drawn from the top of the anterior commissure (AC) to the bottom of the posterior commissure (PC). The line is the AC-PC line. The horizontal plane through the anterior and posterior commissures is the Talairach-Tournoux baseline. From this baseline, a vertical plane is raised perpendicular to the baseline at the top of the anterior commissure. This is the VAC (vertical at the anterior commissure). A second similar vertical plane is raised perpendicular to the baseline at the bottom of the posterior commissure. This is the VPC (vertical at the posterior commissure). These planes define the coronal position. The third orthogonal plane is taken as the midline vertical plane through the AC-PC line. All anatomic positions are then defined by their coordinates in the vertical direction (designated from superior to inferior as 1–12), anteroposterior direction (A to I), and transverse direction (designated from

the midline to lateral as a-d). Thus, the central sulcus is found in “a,1–2, F” of the left or right hemisphere. These coordinates are considered to exist in “Talairach space” independent of any sulcal or lobar borders.

5 Identification of Specific Anatomic Structures

5.1 The Pericentral Cortex

The pericentral region consists of two parallel gyri, the precentral and postcentral gyri, separated by the CS. Superiorly, the CS nearly always reaches the cerebral margin and may extend onto the medial interhemispheric surface of the brain. In this location, the precentral and postcentral gyri fuse to each other to form the paracentral lobule around the upper end of the CS. Inferiorly, the CS rarely reaches the sylvian fissure. Instead, the preCG and postCG fuse together to form the subcentral gyrus between the inferior end of the CS and the sylvian fissure. This is partially delimited anteriorly and posteriorly by the anterior and posterior subcentral sulci (Fig. 9). Functional and anatomical MRI have both been used to define significant regions along the preCG (primary motor cortex) and the postCG (primary sensory cortex).

5.1.1 Functional Methods

Functional MRI (fMRI) shows that the motor hand area is located at the middle genu of the CS in a portion of the preCG that displays a characteristic omega or epsilon-shaped “knob” or “knuckle” (Naidich and Brightbill 1996b; Yousry et al. 1997b). Using MEG (magnetoencephalography), it is possible to identify the postCG reliably (Sobel et al. 1993). Using PET (positron emission tomography), it can be shown that the cortical representation of the sensory hand area is located along the anterior bank of the postCG at a characteristic curve of the CS immediately posterior to the motor hand area (Rumeau et al. 1994). On fMRI, detection of an “activated” vein can assist in the identification of the CS, especially in patients with tumors distorting the cortical anatomy (Yousry et al. 1996). Currently fMRI is increasingly used to define the central region preoperatively.

5.1.2 Anatomical Methods

CT has shown that the marked normal variability of the cortical anatomy can limit the use of standard systems for localizing anatomy, such as the Talairach space (Steinmetz et al. 1989a). Therefore, specific signs have been developed to help to identify the individual portions of the pericentral region more directly (Iwasaki et al. 1991; Naidich and Brightbill 1995, 1996a, b; Naidich et al. 1995; Yousry et al.

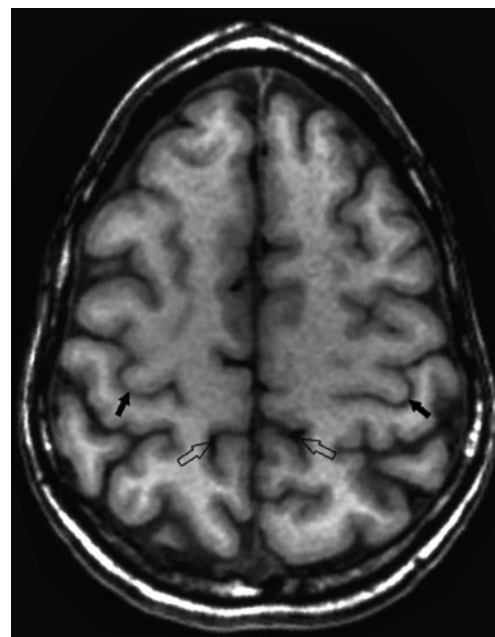


Fig. 12 Pericentral region. Axial landmarks. In the axial plane (T1-weighted MPRAGE sequence), the Ω-shaped knob of the precentral gyrus is easily identified (arrows). The pars marginalis of the cingulate sulcus of both hemispheres appears as a horizontal bracket (open arrows). The medial end of the central sulcus enters the pars bracket immediately anterior to the pars. The full sagittal dimension of the precentral gyrus is thicker than that of the postcentral gyrus. The cortex of the precentral gyrus is thicker than the cortex of the postcentral gyrus

1995, 1997b). The sensitivity and specificity of these signs have been evaluated and the multiple signs combined into a system for localizing the CS and related gyri (Naidich and Brightbill 1996b). Three axial and three sagittal signs are most important. These signs should always be used together, systematically, so that the failure of any one sign is corrected by the concordance of localization given by the other signs (Naidich and Brightbill 1996b).

- Axial Plane Images

The precentral knob: a focal, posteriorly directed protrusion of the posterior surface of the preCG, designated the precentral knob, has been shown by fMRI to be the site of the hand motor area. This focal motor region is seen on axial CT and MRI images as an inverted omega (90 %) or as a horizontal epsilon (10 %) in all cases (Fig. 12). This sign has a high inter-rater reproducibility (Yousry et al. 1997b) as well as high “applicability” (Naidich and Brightbill 1996b).

The pars bracket sign: in axial plane CT and MRI, the pars marginalis of the cingulate sulcus of the left and the right cerebral hemispheres appear together as a horizontal bracket. The medial end of the CS enters the pars bracket immediately anterior to the pars marginalis in 94–96 % of cases (Fig. 12), whereas the postcentral sulcus enters

the pars bracket in only 3 %. Thus, the relationship of a sulcus to the pars bracket permits accurate identification of the CS (the “bracket sign”). This sign is also characterized by a high applicability (Naidich and Brightbill 1996a, b).

Thickness of the pre- and postcentral gyri: the full sagittal dimension of the preCG is thicker than that of the postCG (Fig. 12) (Naidich and Brightbill 1996b; Naidich et al. 1995). Further, the posterior cortex of the preCG is also thicker than the anterior cortex of the postCG at the corresponding site on the other side of the central sulcus (Meyer et al. 1996). Using T1-weighted turbo inversion recovery sequences, the mean cortical thicknesses of the anterior (preCG) and posterior (postCG) banks of the CS were found to be 2.70 and 1.76 mm for both hemispheres with a mean cortical thickness ratio of 1.54 (Fig. 12) (Meyer et al. 1996). The difference in cortical thickness is based on and explained by cytoarchitectonic studies (Brodmann 1909; Naidich and Brightbill 1996b; von Economo and Koskinas 1925). These three signs are the most important and most reliable for attempting to localize the CS in the axial plane (Naidich and Brightbill 1996b).

- Sagittal Plane Images

Lateral sagittal plane. The “M” shape of the inferior frontal gyrus. The anterior horizontal and anterior ascending rami of the sylvian fissure extend upward into the IFG, giving it the shape of a letter “M.” The first vertical line of the “M” represents the pars orbitalis. The middle “v” of the “M” represents the pars triangularis. The posterior vertical line of the “M” represents the pars opercularis of the IFG. Identification of the “M” provides the starting point for subsequent, sequential identification of the preCS, preCG, CS, and postCG (Fig. 13) (Naidich et al. 1995, 1997; Steinmetz et al. 1990a).

Middle sagittal plane: the precentral knob. The posteriorly directed expansion of the preCG at the hand motor area may be identified at the level of the insula as a posteriorly directed hook, which fits neatly into the concavity of the hand sensory region of the postcentral gyrus. This configuration defines the position of the preCG, the CS, and the postCG in 92 % of cases (Fig. 13) (Yousry et al. 1997b).

Medial sagittal plane: the pars marginalis. The posterior portion of the cingulate sulcus, which sweeps upward to reach the cerebral margin, is the pars marginalis. The CS lies millimeters anterior to the pars marginalis. Characteristically the portion of the CS that lies on the medial surface of the brain curves posteriorly to course nearly perpendicular to the pars marginalis (Fig. 13) (Naidich and Brightbill 1996b).

5.2 The Superior Temporal Plane

The transverse temporal gyrus of Heschl courses anterolaterally over the superior surface of the temporal lobe from the posterior border of the insula medially to the convexity surface of the temporal lobe laterally. HG corresponds to Brodmann’s area 41 (Brodmann 1909), the primary auditory cortex (A1). Usually, only a restricted posteromedial portion of HG can be considered the true site of A1 (Liegeois-Chauvel et al. 1991). A second HG may be present posterior and parallel to the first and may occasionally be functionally included in A1 (Liegeois-Chauvel et al. 1995).

Using MRI, HG may be identified accurately in the axial, sagittal, and coronal planes. In the *sagittal plane*, HG has a characteristic shape easily identified on the supratemporal surface just lateral to the insula. Depending on the number of HG present, HG may assume the form of a single “omega,” a “mushroom,” a “heart,” or a double Ω (Fig. 14) (Yousry et al. 1997a). In the *coronal plane* perpendicular to the Talairach-Tournoux baseline, HG is found best in the section that displays the (tentlike) convergence of the two fornices and the eighth cranial nerves (Fig. 14) (Yousry et al. 1997a). In the *axial plane*, HG is found most easily in the section which displays the massa intermedia of the thalamus (Fig. 14) (Yousry et al. 1997a).

5.3 The Occipital Lobe

The occipital lobe is important for the visual areas (V1–V3, Brodmann’s areas 17–19) it contains. The primary visual area (V1, Brodmann’s area 17) is located in the striate cortex. Most of the striate cortex extends along the calcarine sulcus (Korogi et al. 1996). However, the precise site of the striate cortex is variable. The striate cortex may be exposed on the medial surface of the occipital lobe, lie hidden within the depths of the calcarine sulcus, extend into the parieto-occipital or anterior calcarine sulci, and/or lie on the tentorial surface of the occipital lobe (Korogi et al. 1996). The precise configuration of the calcarine sulcus also varies (Fig. 15). Korogi et al. found that the sulcus could be a single continuous sulcus without major branches (50 %), could give off major branches (26 %), and could even show significant disruptions (24 %) (Korogi et al. 1996). In the coronal plane, the calcarine sulci and parieto-occipital sulci were symmetric in only 60 % of cases. One calcarine sulcus was significantly lower than the other in 24 % (by more than 10 mm in 12 % of cases (Korogi et al. 1996). The calcarine and the parieto-occipital sulci formed a “V” in 16 % (Korogi et al. 1996). The exact positions and (a) symmetries of the calcarine and parieto-occipital sulci are also influenced by the magnitude of any occipital petalia. These variations complicate the identification of the calcarine sulcus (Yousry et al. 2001).

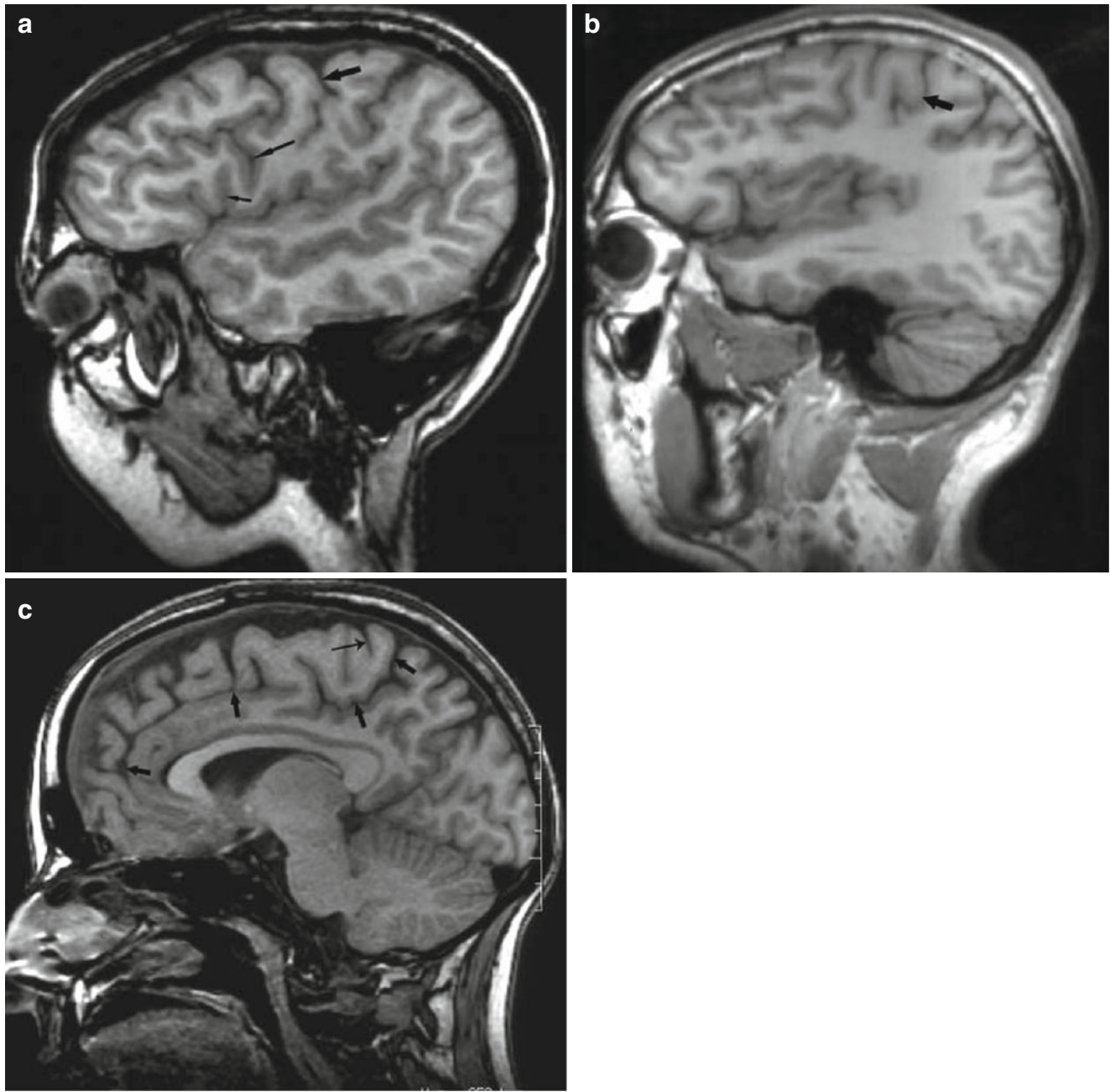


Fig. 13 (a–c) Pericentral region. Sagittal landmarks (T1-weighted MPAGE sequence). (a) In the sagittal plane, the anterior horizontal ramus (unlabeled anteriorly) and anterior ascending ramus (*short thin arrow more posteriorly*) of the sylvian fissure are first identified on the lateral sections and used to identify the M shape of the inferior frontal gyrus. Posterior to this gyrus, in order, lie the precentral gyrus (*long thin arrow*), the subcallosal gyrus, the central sulcus (*short thick arrow*),

and the postcentral gyrus. (b) At the level of the insula, the posteriorly directed hook (*arrow*) of the motor hand area defines the precentral gyrus. (c) The cingulate sulcus and its ramus marginalis (*arrows*) are first identified. The central sulcus (*thin arrow*) lies immediately anterior to the pars marginalis and is oriented such that it curves posteriorly, to course nearly perpendicular to the ramus marginalis

6 Cortical Architecture

6.1 Cytoarchitectonics

The neocortex exhibits six cell layers characterized by differing proportions of cell types, cell densities, and myelination

of fibers. From superficial to deep, the six neocortical layers are designated by Roman numerals: (I) molecular layer, (II) external granule cell layer, (III) external pyramidal cell layer, (IV) internal granule cell layer, (V) internal pyramidal cell layer, and (VI) multiform layer. Further variations within each layer may lead to subdivisions such as layers IVA and

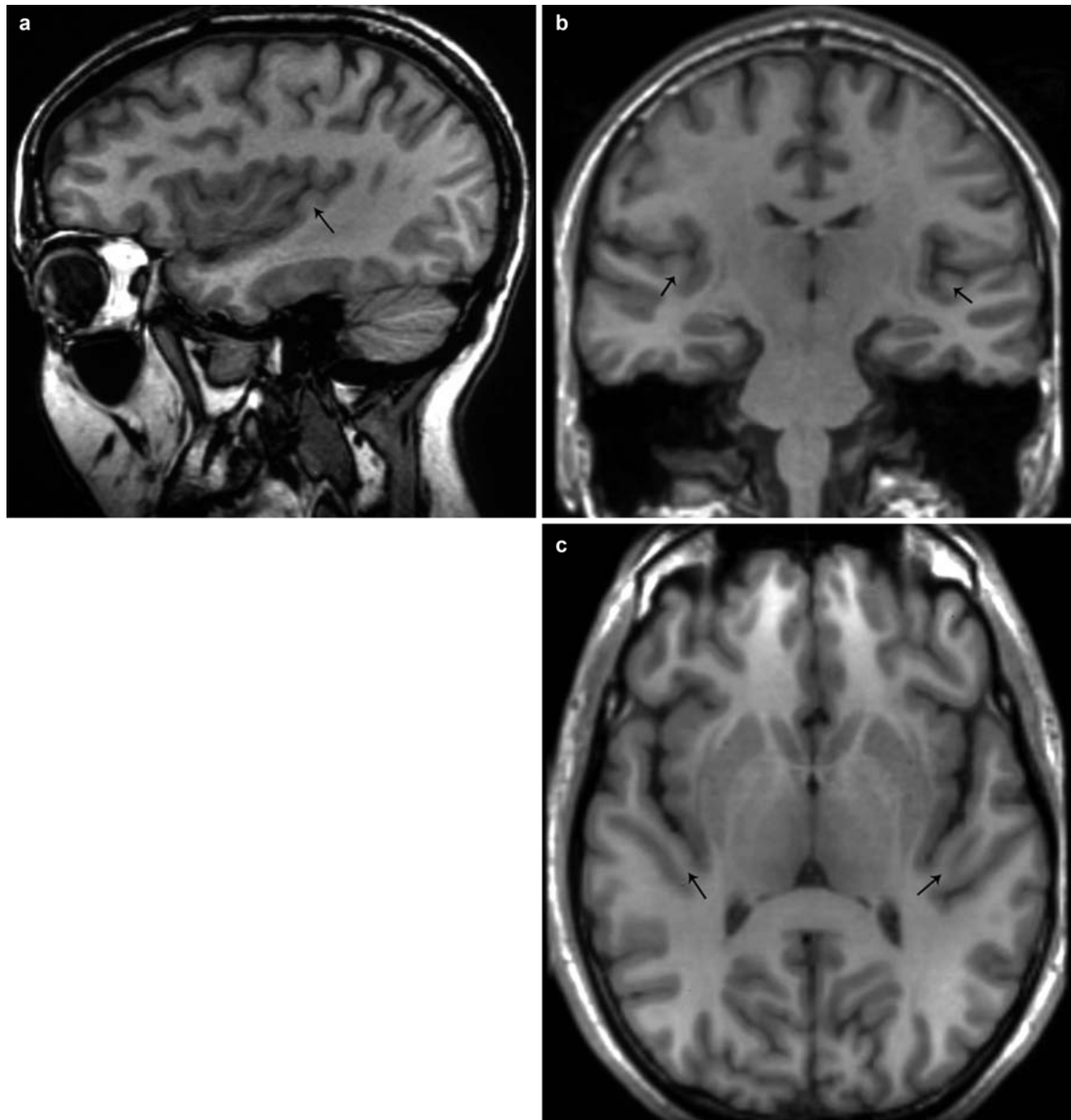


Fig. 14 (a–c) Heschl's gyrus. Landmarks in three planes (T1-weighted MPAGE sequence). (a) In the sagittal plane just lateral to the insula, the shape of HG (arrow) is so characteristic that it can easily be identified directly on the supratemporal surface without the need for additional landmarks. Depending on the presence and extent of any intermediate sulcus, HG may appear Ω-shaped, on medial sections of the temporal lobe and insula. (b) In a coronal plane perpendicular to the

bicommissural plane, the section on which HG (arrows) is identified best is characterized by (1) a tentlike shape formed as the two fornices converge to join with each other and (2) the presence of the eighth cranial nerves. (c) In the axial plane, HG (arrows) is identified by its temporal location and its characteristic anterolateral course on the section in which the adhesion interthalamica (massa intermedia) can be identified

IVB. In general, afferent fibers to the cortex synapse in layers I–IV. Afferents from specific thalamic nuclei end predominantly in layer IV. Efferents from the cortex arise in layers V

and VI. Those efferents directed to the brainstem and spinal cord arise mainly in layer V (Carpenter and Sutin 1983; Gilman and Newman 1996).

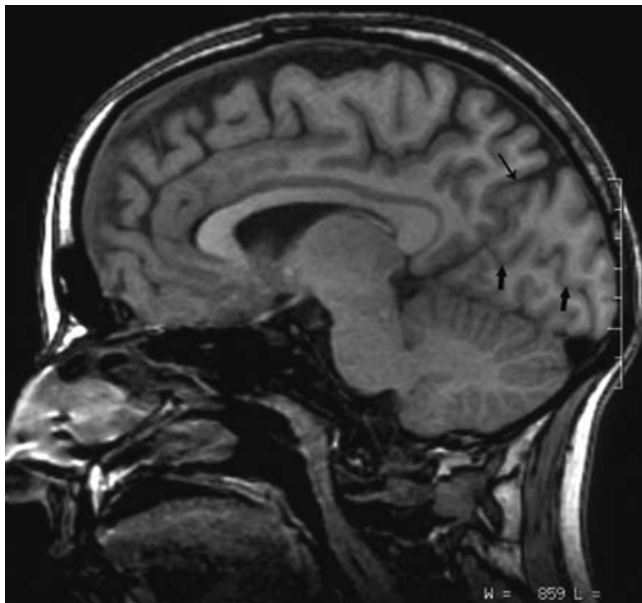


Fig. 15 Occipital lobe (T1-weighted MPRAGE sequence). The calcarine sulcus (arrows) runs obliquely in an anterosuperior direction from the occipital pole to its junction with the parieto-occipital sulcus (thin arrow) to form the anterior calcarine sulcus. The calcarine sulci show a gradual posterior declination

Granule cells are small polymorphic (stellate, tufted, or bipolar) cells that form the major component of the external and internal granule cell layers (II and IV). These are mainly γ -aminobutyric acid-(GABA)-ergic inhibitory neurons. Pyramidal cells are pyramid-shaped cells with their apical dendrites directed superficially to layer I. The basal dendrites span outward laterally. The major axon arises from the base of each pyramidal cell to pass to its target. Small pyramidal cells found in layers II, III, and IV project to intracortical regions (Gilman and Newman 1996). Large pyramidal cells in layer V project to the brainstem and the spinal cord (Gilman and Newman 1996). Giant pyramidal cells with direct corticomotoneuronal connections to the (alpha) motoneurons of the brainstem and the spinal cord are designated Betz cells. In humans, Betz cells are found exclusively in the primary motor cortex (M1).

Throughout the cortex, the cell layers differ in their total thickness, the thickness of each layer, the concentrations of cells within each layer, the conspicuity of each layer, the degree of myelination of the fibers within the layer, and the presence or absence of special cells, like the Betz cells. These variations give each region a specific cytoarchitecture that subserves the function of that region. The cytoarchitectonic variations in the cortex lead to classifications of cortical regions by their cytoarchitecture. If the six-layered neocortical organization is readily discernable, the cortex is designated homotypical. If focal specialization of the cytoarchitecture partly obscures these layers, the cortex is

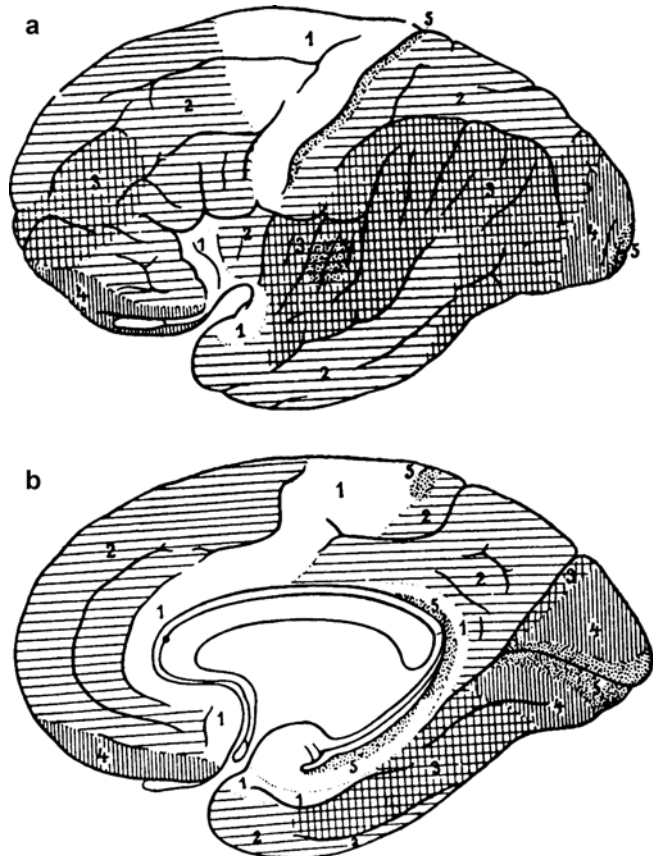


Fig. 16 (a, b) The five types of cerebral isocortex are distributed over the convexity (a) and medial surface (b) of the cerebral hemisphere. Cortex type 1 agranular (motor) heterotypical, 2 frontal homotypical, 3 parietal homotypical, 4 polar homotypical, 5 granulous (sensory) heterotypical (koniocortex). Note that the words frontal and parietal used in this way signify types of isocortex and not anatomic locations or lobes (From von Economo and Koskinas (1925); with permission)

designated heterotypical (von Economo and Koskinas 1925). von Economo and Koskinas (1925) grouped the cortical regions into five types (Fig. 16). Three types were considered homotypical: frontal cortex, parietal cortex, and polar cortex. Two were considered heterotypical cortices: the agranular cortex (specialized for motor function) and the koniocortex (specialized for sensory function). Brodmann (1909) recognized additional variations in cortical architecture, subdivided the cortex into approximately 40 distinct cytoarchitectonic areas, and tried to relate the cortical architecture to function. These regions are now designated the Brodmann's areas (BA) (Fig. 17).

In humans, the motor cortex is formed of three major cortical types:

- The heterotypical agranular isocortex is characterized by increased overall thickness, significantly reduced to absent granule cells in layer IV, and thick well-developed layers of large pyramidal cells in layers III and V (Zilles et al. 1996). In this agranular cortex, even the small cells

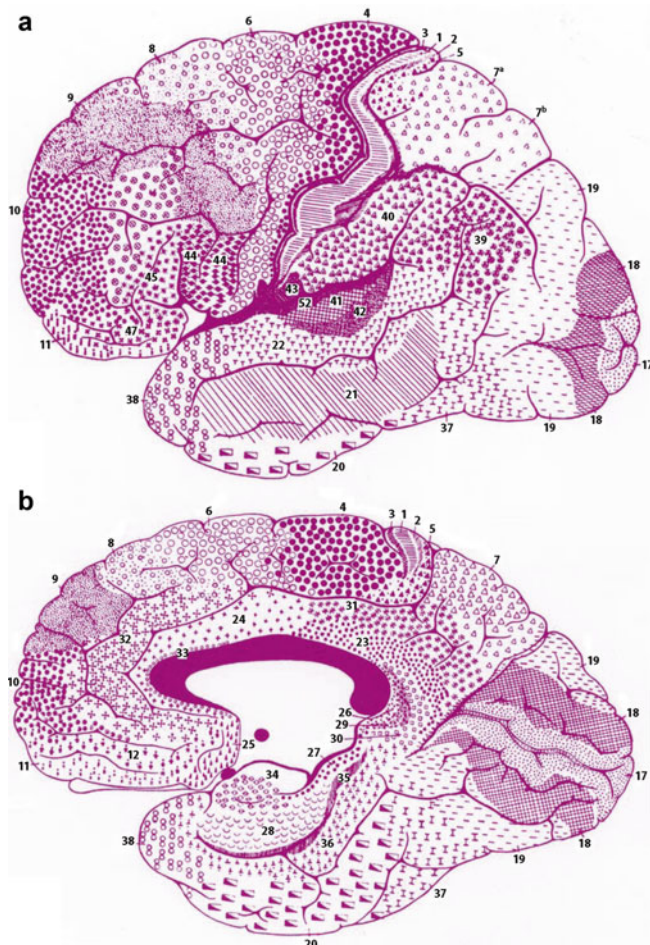


Fig. 17 (a, b) Cytoarchitecture of the human cortex. Convexity (a) and medial (b) surface views of Brodmann's areas. Symbols indicate Brodmann's parcellation of the cortex into the cytoarchitectonic areas that are designated by the Brodmann's area (BA) numbers assigned. Compare with Fig. 1 (Parts a, b from Carpenter and Sutin (1983); with permission)

in layers II (and the region of IV) are predominantly pyramidal in shape. Type (a) corresponds predominantly to BA 4, 6, 8, 24, 44, and 45 and is found in the posterior half of the precentral gyrus, the anterior half of the cingulate gyrus, the anterior portion of the insula, and in a narrow strip which extends from the retrosplenial portion of the cingulate gyrus into the parahippocampal gyrus (Figs. 16 and 17). Within these areas, the primary motor cortex, designated M1 (Brodmann's area 4), is characterized by the presence of giant Betz cells in lower layer V (Zilles et al. 1996). The motor speech areas, BA 44 and BA 45, are found in the inferior frontal gyrus.

- The homotypical frontal cortex is characterized by narrow granule cell layers composed of loosely arrayed small granule cells and by prominent small- and medium-sized pyramidal cells in layers III and V (Carpenter and Sutin 1983). Giant Betz cells are absent. This frontal cortex

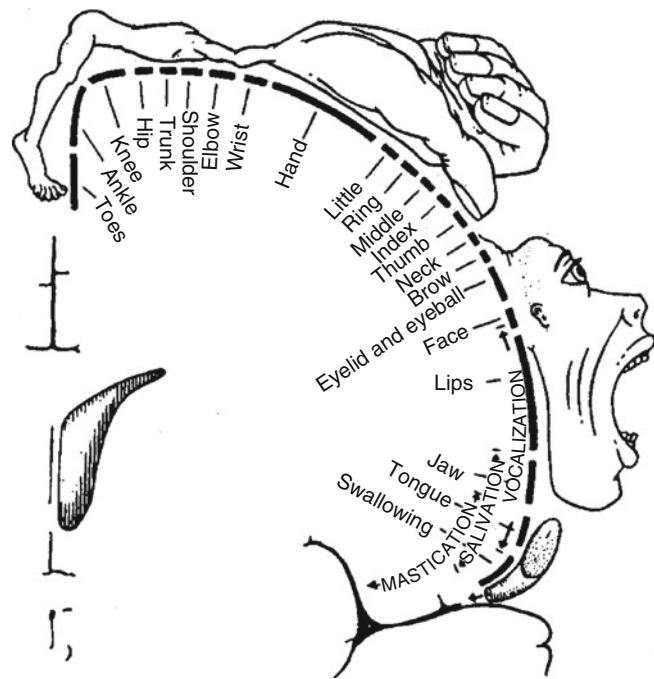


Fig. 18 Somatotopy of the primary motor cortex (M1): the motor homunculus, as described by Penfield and Jasper (From Williams et al. (1989); with permission)

corresponds to BA 9, 10, 11, 46, and 47 and is found along the convexity and the anteriormost medial surfaces of the superior and middle frontal gyri.

- The homotypical polar cortex is characterized by overall cortical thinness, well-developed granule cell layers, and a comparative wealth of cells (Carpenter and Sutin 1983; Naidich et al. 2001b). It corresponds to BA 10.

6.2 Somatotopy

The term somatotopy refers to the topographic organization of function along the cortex. It is a map of the sites at which smaller or larger regions of cortex form functional units that correspond to body parts or to motions across a joint. In specific regions like the primary auditory cortex, the somatotopy may be described by a more specific word such as tonotopy. For white matter, the preferred term is myelotopy. The presence of somatotopy signifies that the functional activity of the cortex is organized topographically along the cortex. Absence of somatotopy signifies that medicine has failed, thus far, to appreciate any topographic organization of that cortex. Somatotopy may be fine, as in the primary motor cortex (BA 4), where relatively restricted zones of cortex correspond to defined manipulation units (Fig. 18). It may be very fine, as in the hand motor area along the precentral gyrus, where there may be representation for the motion of each individual digit. Alternatively, somatotopy may be very

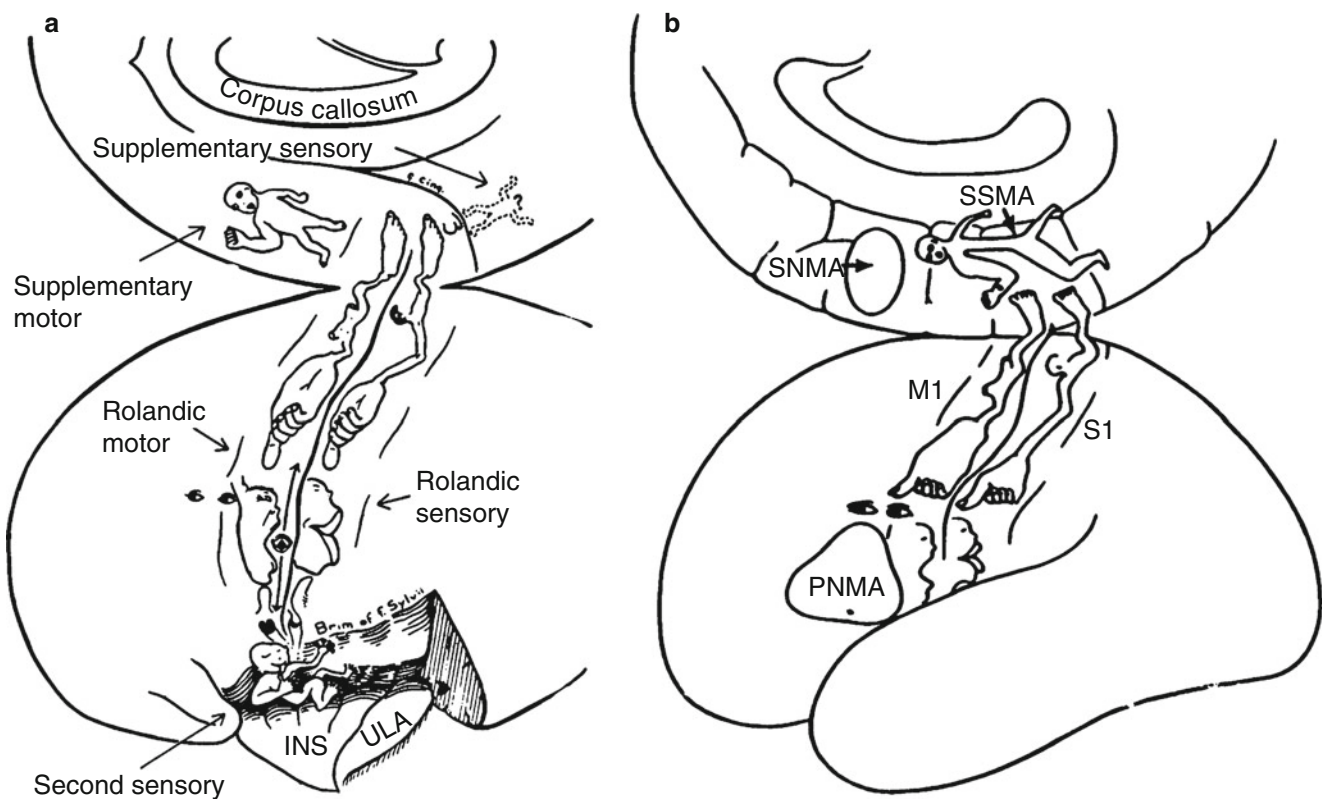


Fig. 19 (a) Somatotopy of the supplementary motor areas (SMA) as represented by Penfield and Jasper. (b) Somatotopy of the pre-SMA (the supplementary negative motor area [SNMA]) and the relation of the pre-SMA to the SMA, simplified from Penfield and Jasper. M1 primary

motor cortex, PNMA primary negative motor cortex, S1 primary sensory cortex, SSMA supplementary somatosensory cortex (a From Luders (1996); (b) From Freund (1996); with permission)

crude, as in the SMA, the pre-SMA, and the cingulate motor cortex (CMC), where cortical zones seem to correspond to broad regions, such as head, trunk, upper and lower extremities, rather than to individual motion units (Fig. 19). Using PET to measure regional cerebral blood flow (rCBF), Grafton et al. (1993) have shown within-arm somatotopy of the primary motor cortex, the SMA, and the CMC. Kleinschmidt et al. (1997) used fMRI to show somatotopy for digits in the human hand motor area and concluded that "... somatotopy within the hand area of the primary motor cortex does not present as qualitative functional segregation but as quantitative predominance of certain movement or digit representation embedded in an overall joint hand area" (Naidich et al. 2001b).

6.3 Selected Areas Involved in Motor and Speech Function

6.3.1 Primary Motor Cortex (M1)

The primary motor cortex is designated M1 and corresponds to BA 4. M1 extends from the anterior part of the paracentral lobule on the medial surface, over the cerebral margin, and

down the convexity along the crown and posterior face of the precentral gyrus (Figs. 3 and 17). Its anteroposterior extent is broader superiorly and on the medial surface. From there, BA 4 tapers progressively downward toward the sylvian fissure. Just above the sylvian fissure and behind the inferior frontal gyrus, BA 4 becomes restricted to a narrow strip along the posterior face of the precentral gyrus, within the central sulcus (Fig. 17).

M1 is heterotypical agranular isocortex characterized by significant overall cortical thickness, reduced to absent granule cells in layer IV, prominent pyramidal cells in layers III and V, and prominent giant Betz cells in lower layer V (Zilles et al. 1996). The individual Betz cells are largest in size superomedially at the paracentral lobule and smallest inferolaterally at the operculum (Carpenter and Sutin 1983). Classically, the somatotopy of M1 is given by the motor homunculus (Fig. 18). Each functional zone was considered to be responsible for directing the action of a group of muscles that effects motion across a joint. Individual neurons within this group innervate different muscles, so that individual muscles are innervated repeatedly in different combinations by multiple different cell clusters to effect action across different joints. In the classic concept, therefore, the

motor map represents motion of the joint, rather than any single body part. More recently, Graziano et al. (2002) have shown that the motor homunculus may better be considered a map of final body postures.

M1 activates anterior horn cells within the spinal cord to generate specific patterns of movement (Marsden et al. 1996). It serves to execute voluntary activity of the limbs, head, face, and larynx, both contralaterally and ipsilaterally. Contralaterally, M1 excites all muscle groups of the extremity. Ipsilaterally, M1 excites the proximal musculature most strongly, especially the shoulder. By direct stimulation of neurons in monkeys, Tanji et al. (1987, 1988) found that 77.2 % of movement-related M1 neurons are contralateral motor neurons, affecting action of the contralateral side, 8.2 % are ipsilateral motor neurons, responsible for action on the ipsilateral side, and 4.5 % are bilateral motor neurons. Stimulation of M1 produces simple motions, such as flexion and extension at one or more joints, and not skilled movements. Regions of M1 exhibit different thresholds for inciting action. These thresholds are lowest for the thumb and highest for the face.

Activation studies confirm activation of the ipsilateral hemisphere by sensorimotor tasks (Li et al. 1996). The ipsilateral activation is greater for motor than for sensory tasks and is greater for the nondominant hand than for the dominant hand (Li et al. 1996). The left and the right primary motor cortices show reciprocal actions. Transcranial magnetic stimulation of the motor cortex may inhibit the contralateral cortex (Allison et al. 2000). Direct focal stimulation of M1 causes excitation of a homologous area in the contralateral M1, surrounded by a zone of inhibition (Allison et al. 2000; Asanuma and Okuda 1962). In fMRI studies, unilateral finger movements activate M1 ipsilaterally. The same movements may also deactivate portions of M1 ipsilaterally (Allison et al. 2000).

6.3.2 Supplementary Motor Area (SMA)

The SMA (Figs. 18 and 19) (Penfield and Welch 1951) is also known by a large number of synonyms, including the SMA proper, caudal SMA, posterior SMA, the supplementary sensorimotor area, M2, and BA 6a α (medial) (Olivier 1996; Rizzolatti et al. 1996; Seitz et al. 1996). In this chapter, the term SMA refers to the SMA proper, distinct from the more anteriorly situated pre-SMA. Anatomically, the SMA proper corresponds to BA 6a α (medial) situated along the medial cerebral cortex in the paracentral lobule and posterior portion of the superior (medial) frontal gyrus. Its specific site varies among individuals, but it is typically found in relation to the medial precentral sulcus (Zilles et al. 1996). Zilles et al. (1996) report that the SMA is located between the VAC and the VPC (Fig. 20).

The SMA is bordered anteriorly by the pre-SMA, posteriorly by the primary motor cortex, laterally by the premotor

cortex on the convexity, and ventrally (inferiorly) by the posterior CMA (Fried 1996; Zilles et al. 1996).

The SMA is a heterotypical agranular isocortex characterized by reduced to absent granule cell layers and by absence of Betz cells in pyramidal cell layer V. The SMA (BA 6a α on the medial surface) can be distinguished from the laterally adjacent premotor area (BA 6a α on the convexity), because the SMA has increased cell density in the lower part of layer III and in layer Va (Zilles et al. 1996). The SMA can be distinguished from the pre-SMA, because the SMA shows poorer delineation of the laminae and poorer distinction of layer III from layer V (Zilles et al. 1996).

The SMA exhibits crude somatotopy. From anterior to posterior, one finds representations of the head, trunk, and upper and lower extremities (Fried et al. 1991). In humans, one stimulation study with subdural electrode grids placed along the mesial cortex elicited a finer somatotopy (Fried et al. 1991). In order from anterior to posterior, these authors found the face, neck, distal upper extremity, proximal upper extremity, proximal lower extremity, and distal lower extremity. The SMA clearly shows greater representation of the contralateral side than the ipsilateral side. The dominant SMA exerts more control than the nondominant SMA, both contralaterally and ipsilaterally. The supplementary eye fields lie in relation to the head portion of the SMA but are distinct from the SMA (Lim et al. 1996; Tanji 1994).

The SMA appears to act in several different ways:

- *Connections to the Cervical Motor Neurons.* The SMA has tight, probably monosynaptic, connections to the cervical motoneurons (94 % contralateral, 6 % ipsilateral). SMA activity in one hemisphere is associated with movement of either arm, especially whole-arm prehension involving the shoulder and trunk muscles. Stimulation of the SMA causes a characteristic posture with raising of the opposite arm (abduction and external rotation at the shoulder with flexion at the elbow) and turning of the head and eyes to gaze at the elevated hand (Carpenter and Sutin 1983; Chauvel et al. 1996; Freund 1996a, b). The trunk and lower extremities show bilateral synergic contractions (Carpenter and Sutin 1983). Distal hand muscles are weakly represented in the SMA. Isolated finger movements, easily elicited by stimulation of M1, are rarely elicited by stimulating SMA. The SMA appears less involved with distal grasping.
- *Posture.* The SMA plays a role in posture, especially in anticipating and correcting posture during motor tasks, so that the final position or task is performed successfully. In normal subjects, when a heavy object is lifted from one hand by the other, there is anticipatory adjustment of the posture of the forearm flexors, so position is maintained despite the unloading (Brust 1996; Viallet et al. 1992).
- *Action.* Stimulation of the SMA leads to an urge to act and an anticipation of action (Fried et al. 1991). In monkeys,

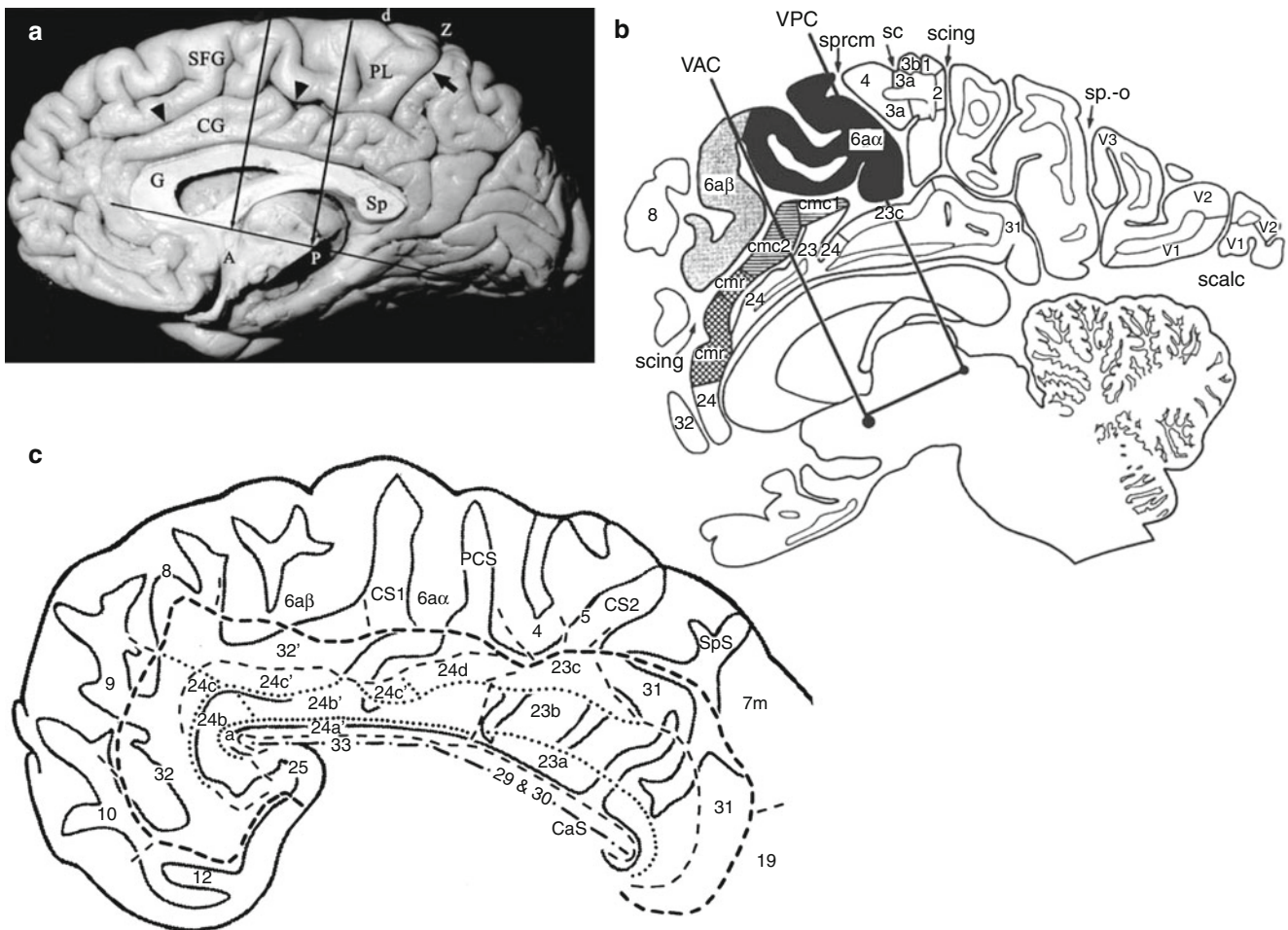


Fig. 20 (a–c) Mesial motor areas: SMA, pre-SMA, and CMA. (a) Gross anatomy of the medial surface of the hemisphere. Prepared specimen, oriented with anterior to the reader's left. This hemisphere displays the co-curvilinearity of the fornix (*F*), the genu (*G*), and splenium (*Sp*) of the corpus callosum; the callosal sulcus (not labeled), the cingulate gyrus (*CG*); the single cingulate sulcus (*arrowheads*); the superior frontal gyrus (*SFG*); and the paracentral lobule (*PL*). The pars marginalis (*arrow, z*) of the cingulate sulcus sweeps upward to the cerebral margin to define the posterior aspect of the paracentral lobule. The central sulcus (*d*) cuts the cerebral margin just anterior to the pars marginalis and then courses a short (and variable) distance down the medial face of the paracentral lobule, almost perpendicular to the pars marginalis. To illustrate the anatomic relationships, the AC-PC line has been drawn from the superior surface of the anterior commissure (AC, here labeled *A*) to the inferior surface of the posterior commissure (PC, here labeled *P*) and the perpendiculars erected to this line at the AC and the PC. The AC-PC line is the baseline for the Talairach-Tournoux coordinate system (Talairach and Tournoux 1988). (b) The medial parasagittal plane, oriented with anterior to the readers' left. *CC* corpus callosum,

AC anterior commissure, *PC* posterior commissure. The *VAC* and *VPC* are the vertical lines erected perpendicular to the *AC-PC* line at *AC* (*VAC*) and *PC* (*VPC*). The cytoarchitectonic areas are numbered after Brodmann and the Vogts. *Black areas* show the position of the *SMA* on the medial surface of the hemisphere. *Solid gray* shows the position of the pre-*SMA*. *Cross hatching* indicates the rostral portion of the cingulate motor area (*cmr*), whereas the *horizontal lines* show the caudal portion of the cingulate motor area (*cmc*), itself divided into parts one and two. *scing* cingulate sulcus, *sc* central sulcus. *V1-V3* are the visual cortical areas. (c) Flat map of the cytoarchitectonic areas of the human cingulate cortex and the locations of adjacent areas. The cingulate sulcus is shown with two separate segments (*CS1*, *CS2*). *Thick lines* outline of the cingulate areas, *thin lines* divide each major cingulate area, *stippling* borders of each sulcus, *dotted lines* the subdivisions of each area, *dot-dash line* the fundus of the callosal sulcus; the fundi of the other sulci are not marked for simplicity. *PCS* paracentral sulcus (a From Naidich et al. (2001); b From Zilles et al. (1996) and Vogt et al. (1997); c Adapted from Vogt et al. (1995); with permission)

Tanji et al. (1987, 1988) used intracellular recording to demonstrate that 38 % of SMA cells fire before any action is performed. At least some SMA neurons fire before M1 neurons.

- *Laterality.* The SMA is involved with selecting the laterality of the task. In monkeys, 27 % of motor-related SMA neurons only fire before deciding on which side to perform an

action (Tanji et al. 1987, 1988). Considering SMA neurons and premotor neurons together as one group of non-M1 neurons, Tanji et al. (1987, 1988) showed that when choosing which upper extremity to use for a job, 16 % of non-M1 cells fire before deciding right, not both; 20 % fire before deciding left, not both; 20 % fire before deciding either, not both; and 40 % fire before deciding both, not either.

- *Coordination and Cooperation.* The SMA serves to assist bimanual coordination and cooperation between the paired upper and the paired lower extremities, especially for self-initiated action. The SMA appears to be required for independent control of the contralateral hand.
- *Sequences of Action.* The SMA is heavily involved in learning and generating sequences of actions and with executing multiple actions involving both sides of the body (Gilman and Newman 1996; Passingham 1996; Shibasaki et al. 1993). It may serve in selecting a specific action from among a group of remembered tasks. In monkeys, Tanji and Shima (1994) found one group of SMA cells that were preferentially activated in relation to a particular order of forthcoming movements, guided by memory. A second group of SMA cells became active after the performance of one particular movement and then remained active during the waiting period before performing a second specific movement. These cells were not active if the preceding or subsequent movement was different. Thus, these cells seem to signal a temporal linkage combining two specific movements (Tanji and Shima 1994). Single unit discharges were also observed in the SMA before the performance of the remembered sequence of movements (preparatory sequencing of neurons) and in the midst of the sequence of movements (tonic sequencing of neurons) (Tanji 1994; Tanji et al. 1987, 1988; Tanji and Shima 1994). Similarly, rCBF in the SMA increases with ideation about sequential motor tasks (e.g., when subjects plan but do not execute fast, isolated finger movements) (Roland 1999). When these tasks are actually executed, increased rCBF can be seen contralaterally in M1 and bilaterally in the SMA. From these data, the SMA seems to be crucial for learned, internally generated (i.e., self-initiated) voluntary motor behavior (Burton et al. 1996; Freund 1996a, b; Freund and Hummelsheim 1985; Rao et al. 1993), especially in the preparation and initiation of such voluntary motor behavior (Freund 1996b; Luders 1996). The SMA seems to be less related to performance of the movements themselves. Simple repetition of fast finger motion does not stimulate SMA (Freund 1996b).

Stimulation studies also show a relation between the complexity of a task and the speed with which the action itself is performed. Simple tasks, like flexion of one joint, are commonly performed rapidly. More complex tasks involving multiple joints, multiple body regions, or both evolve more slowly. In some stimulations, the responses elicited were repeated several times until stimulation stopped (Fried 1996).

- *Attention-Intention Network.* The SMA may form part of an attention-intention network. Fried (1996) found that most ipsilateral and bilateral sequences can be elicited from the right, nondominant SMA. The right hemisphere

has an attention mechanism that spans both hemispheres, whereas the left hemisphere seems to mediate only contralateral attention (Fried et al. 1991). Therefore, the lateralization of attention to the right hemisphere and the lateralization of motor intention to the right SMA may signify a right cerebral dominance for attention and motor intention directed at the external milieu in which the motor action takes place (Fried 1996; Fried et al. 1991; Naidich et al. 2001b).

6.3.3 Pre-supplementary Motor Area (Pre-SMA)

The term pre-SMA signifies a motor area that has also been called rostral SMA, anterior SMA, BA 6a β (medial), and the supplementary negative motor area (Figs. 19 and 20). It corresponds to BA 6a β (medial) (Seitz et al. 1996). The pre-SMA lies along the medial face of the superior (medial) frontal gyrus just anterior to the SMA. It shows individual variability. According to Zilles et al. (1996), the pre-SMA lies predominantly anterior to VAC (Fig. 20). It borders posteriorly on the SMA, laterally on the anterior portion of the premotor cortex on the convexity and ventrally (inferiorly) on the anterior cingulate motor area (Zilles et al. 1996).

The pre-SMA is heterotypical agranular isocortex with no Betz cells. It can be distinguished from the SMA posterior to it because the pre-SMA has more pronounced lamination and clearer demarcation of layer III from layer V (Zilles et al. 1996). The pre-SMA exhibits a somatotopy similar in form to the SMA, but even cruder in detail. From anterior to posterior, there are areas for the head and upper and lower extremities.

The pre-SMA seems to serve in sequencing and preparing complex tasks, especially internally generated, visually guided tasks. Stimulation of the pre-SMA may elicit negative motor activity for diverse tasks. Fried (1996) found that pre-SMA stimulation causes slowing or arrest of the entire spectrum of motor activity tested, including speech. When a patient executes a repetitive task, such as rapid alternating movements of the hand, stimulation of the pre-SMA causes the movements to gradually slow down and come to a halt. Activation studies suggest that the pre-SMA is involved in the decision whether to act, whereas the SMA proper plays a similar role in directing motor action once the decision to act is made (Humberstone et al. 1997; Naidich et al. 2001b).

6.3.4 Cingulate Motor Area (CMA)

The CMA is composed of two portions (Fig. 20), which appear to correspond to the functionally defined anterior cingulate motor area (CMA rostral; cmr) and a posterior cingulate motor area (CMA caudal; cmc). The CMA corresponds to BA 24c and BA 24d (and perhaps the posterior portion of BA 32, BA 32' of Vogt) (Vogt and Vogt 1919, 1926). It lies in the superior (dorsal) and inferior (ventral) banks of the

cingulate sulcus and, in macaques, does not extend onto the medial surface of the cingulate gyrus (Shima et al. 1991). From the callosal sulcus (inferiorly) to the superior frontal gyrus (superiorly), the cerebral cortex undergoes transition from true allocortex (BA 33), through intermediate stages (lower and upper BA 24), to true isocortex (BA 32) (Zilles et al. 1996). Intermediate area BA 24, therefore, is subdivided into three bands coextensive with the cingulate gyrus and sulcus. These three bands are designated BA 24a (ventral band), 24b (intermediate band), and 24c and 24d (dorsal bands). BA 32 lies superior to BA 24c and BA 24d. Dorsal bands BA 24c and 24d are then subdivided further into a rostral zone (cmr), conforming approximately to BA 24c, and a caudal zone (cmc) conforming approximately to BA 24d (Vogt et al. 1995, 1997; Zilles et al. 1996). The cmr lies entirely rostral to VAC. The cmc flanks VAC but lies entirely anterior to the VPC (Fig. 20).

BA 24c and 24d (cmr and cmc) are heterotypical agranular motor cortices (Zilles et al. 1996). In fine detail, both cmr and cmc appear heterogeneous, leading to further subdivisions of their cytoarchitecture and nomenclature (Zilles et al. 1996). Compared with BA 24c, BA 24d shows a thinner overall width of layer V, clearer borders between layers III and V, larger cells in layers III and VI, and, larger cells in layer V.

The CMA exhibits crude somatotopy with multiple representations of the body (Freund 1996b). BA 24c includes representations of the head and the forelimbs (Freund 1996b). Posterior to BA 24c, BA 24d has representations for the forelimbs and the hindlimbs, but with the forelimbs situated caudal to the hindlimbs (Luppino et al. 1991). Thus, the CMA (cmr and cmc) exhibits mixed somatotopy that is partially reversed from that seen in the SMA and in the pre-SMA (Freund 1996b; Luppino et al. 1991; Zilles et al. 1996).

The CMA projects directly to M1 with somatotopic organization (Shima et al. 1991). CMA fibers also project directly to the spinal cord (Shima et al. 1991). Stimulation of the CMA causes contralateral or bilateral movements of the lower and the upper extremities (Freund 1996b). Single-cell studies in macaques show that more than 60 % of CMA motoneurons fire before movement-related activity (Shima et al. 1991). Most are involved in simple movements of the distal forelimb. These cells may show either a short lead time or a long lead time between firing and action. Long lead time cells (500 ms to 2 s) are more common in the anterior than the posterior cingulate area and show this long lead time in response to self-paced tasks, not stimulus-triggered tasks. Few CMA cells respond to visual, auditory, or tactile stimuli. Overall, the anterior CMA appears to be significant for self-paced internally guided tasks. According to Paus et al. (1993), the anterior CMA participates in motor control by facilitating the execution of appropriate responses or by suppressing the execution of inappropriate responses.

The zone designated rostral CMA (cmr) is involved with autonomic function. Cells project to the hypothalamus and periaqueductal gray matter. Stimulation of cmr causes non-volitional vocalization and fear reactions involving the heart, gut, bladder, and genitalia (Jurgens 1983; Nimchinsky et al. 1995, 1997; Naidich et al. 2001b; Vogt et al. 1995, 1997).

6.3.5 Premotor Area

The premotor area (pre-MA) may be designated M2. It extends along the frontal convexity to occupy contiguous portions of the superior frontal gyrus, the middle frontal gyrus, and the precentral gyrus (Figs. 19 and 20). The dorsal pre-MA lies within the posterior portions of the superior and middle frontal gyri. The ventral pre-MA occupies the anterior face and part of the crown of the precentral gyrus anterior to the primary motor area (M1). Like M1, the ventral portion of pre-MA progressively tapers inferiorly. An additional small area, BA 6b, lies further inferiorly, superior to the sylvian fissure and anterior to the motor face area. The pre-MA corresponds to BA 6a α (convexity), BA 6a β (convexity), and BA 6b (Carpenter and Sutin 1983).

The pre-MA is a heterotypical agranular isocortex with large, well-formed pyramidal cells in layers III and V. Betz cells are absent. Large pyramidal cells that resemble Betz cells are present in the border zone abutting onto BA 4 posteriorly, but these cannot be designated Betz cells, by definition. Granule cell layer IV is thin and difficult to discern. The pre-MA exhibits somatotopy that is similar to, but cruder than, the motor homunculus of the primary motor cortex (M1; BA 4).

Stimulation of BA 6a α (convexity) causes responses similar to those elicited by stimulation of the primary motor cortex M1 (BA 4) but requires higher current to elicit the response. Stimulation of BA 6a β (convexity) elicits more general movement patterns, characterized by abduction and elevation of the arm (frequently associated with rotation of the head, eyes, and trunk to the opposite side). Stimulation of the leg region causes synergic patterns of flexion and extension of the contralateral extremity (Carpenter and Sutin 1983; Freund 1996a). These movements resemble the effect of stimulating the SMA (Freund 1996a). Stimulation of BA 6b produces rhythmic, coordinated, complex movements of the face, masticatory, and laryngeal and pharyngeal musculature (Carpenter and Sutin 1983). Like the pre-SMA, the pre-MA contains cells that fire before a motion is initiated and that appear to determine the usage of the extremities: right, left, or both (Tanji et al. 1987, 1988). Intracellular recordings in monkeys indicate that 48 % of motor-related pre-MA neurons fire before all types of motion. Of motor-related pre-MA neurons, 18 % fire exclusively before decisions as to the laterality of subsequent activity, not in relation to the performance of the movement (Tanji et al. 1987, 1988). The pre-MA responds more to visual signals and is active in

visually guided sequential movements. The pre-MA appears active (1) during mental preparation for a motor task directed by verbal instructions; (2) when voluntary movements are performed under somatosensory, auditory, or visual guidance; and (3) when sensory input is necessary to execute the task. The pre-MA appears especially active when a new motor program is established or an old motor program is modified on the basis of new sensory input (Roland et al. 1980a, b). In monkeys, some of the neurons seem to be stimulated both in performing a task and in observing a similar task being performed by the experimenter (especially when the monkey uses manual or oral “observation”). These neurons are designated mirror neurons (Gallese et al. 1996; Naidich et al. 2001b).

6.3.6 Prefrontal Cortex (Pre-FC)

The term prefrontal cortex designates the cortex that is situated anterior to the pre-MA, corresponding to BA 9, BA 10, and BA 46. It lies along the frontal convexity in the superior and middle frontal gyri and extends onto the medial surface of the frontal lobe along the superior (medial) frontal gyrus (Figs. 3, 16, and 17). The pre-FC is a homolateral frontal type of isocortex characterized by a more-or-less clearly recognizable granule cell layer IV and an absence of Betz cells (Zilles et al. 1996). No somatotopy is known.

The pre-FC is involved with executive functions, behavior, and memory. Brodmann's area 46 on the dorsolateral pre-FC appears to be involved with the selection of items, whether selecting different items from an internal memory of possible tasks or selecting freely between movements needed to perform a voluntary action (Rowe et al. 2000). Right dorsolateral pre-FC (BA 9 and BA 46) is involved in decisions of what to do and when to do it (Marsden et al. 1996; Passingham 1996). Neurons of the pre-FC are involved with inhibitory responses to stimuli that require a delay in the motor responses (Gilman and Newman 1996). They are thought to integrate motivational elements with complex sensorimotor stimuli (Gilman and Newman 1996). Hasegawa et al. (2000) have detected pre-FC neurons that appear to track long periods of time (as long as 30 s). Activity of these cells correlates with success of past or future performance of complex tasks, not the immediate activity. These cells may set the tone for general behavior, in a fashion similar to that accomplished by stimulants, enthusiasm, arousal, or fatigue (Hasegawa et al. 2000). Using PET measurement of rCBF during a simple motor task of sequential opposition of the thumb to each finger, Kawashima et al. (1993) showed activation of the contralateral pre-FC for both right- and left-handed tasks. Tasks performed with the nondominant hand, however, additionally activated the ipsilateral primary motor area and ipsilateral pre-FC. Thus, the pre-FC exhibits asymmetric activity with dominant or nondominant simple motor tasks (Naidich et al. 2001b).

6.3.7 Broca's Area

Broca's area is the motor speech area. It conforms to BA 44 and to the posterior portion of BA 45. Broca's area occupies the inferior frontal gyrus (*pars opercularis* and a small posterior portion of *pars triangularis*) in the dominant hemisphere. Some data indicate that many women, but not men, have motor speech areas in the inferior frontal gyri bilaterally (Pugh et al. 1996; Shaywitz et al. 1995). The motor speech area traditionally assigned to the inferior frontal gyrus has recently been suggested to lie instead in the anterior insula (Price 2000). Broca's area is a heterotypical agranular isocortex, characterized by reduced thickness of the granule cell layer IV and by the presence of large pyramidal cells in layers III and V. Betz cells are absent. No somatotopy is known.

Broca's area is believed to generate the signals for the musculature to produce meaningful sound. It may also be involved in the initiation of speech (Alexander et al. 1989; Demonet et al. 1992), the organization of articulatory sequences (Demonet et al. 1992), and in the covert formation of speech (inner speech). Lesions of Broca's area are associated with a form of aphasia termed, variably, motor aphasia, anterior aphasia, non-fluent aphasia, executive aphasia, and Broca's aphasia. Patients who have this form of aphasia exhibit difficulty with the production of speech and, therefore, produce little speech. The speech produced is emitted slowly, with great effort and with poor articulation (Geschwind 1970). There are phonemic deficits. Small grammatical words and word endings are omitted (Geschwind 1970). There is a characteristic, comparable disorder in their written output. Surprisingly, these patients may retain musical ability and, despite severe motor aphasia, may sing melodies correctly and even elegantly (Geschwind 1970). Patients who have Broca's aphasia maintain good comprehension of the spoken and written language. Patients who have lesions restricted to the traditional Broca's area in the inferior frontal gyrus do not exhibit persisting speech apraxia (Dronkers 1996). Recovery after Broca's aphasia appears to involve a transient shift of function to the right hemisphere, followed by a return to normal laterality (Neville and Bavelier 1998). A new capability for speech production has been observed to arise within the right hemisphere of an adult several years after corpus callosotomy (Neville and Bavelier 1998).

Broca's area and its right hemispheric homologue are also involved with auditory hallucinations (Cleghorn et al. 1990; Lennox et al. 2000; McGuire et al. 1993). Schizophrenics experiencing auditory hallucinations show increased metabolism and activation in Broca's area, the left anterior cingulate region, and the left and right superior temporal regions, among other sites (Cleghorn et al. 1990; Lennox et al. 2000; McGuire et al. 1993).

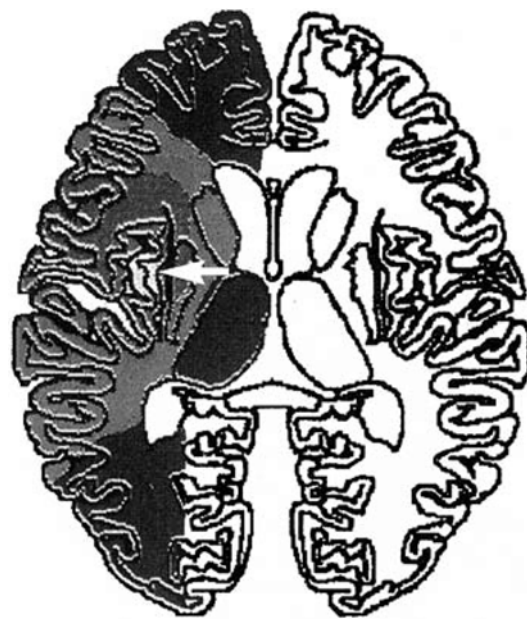


Fig. 21 Speech apraxia. Complete double dissociation in Dronkers' area. Pooled data from 25 patients with speech apraxia show that the only region of involvement common to all cases is the precentral gyrus (white arrow) of the insula. Pooled data from 19 other patients with similar infarctions but no speech apraxia showed no involvement in this same area (From Dronkers (1996); with permission)

6.3.8 Dronkers' Area

Dronkers' area (Dronkers 1996) has no other specific designation. Brodmann did neither parcelate nor number the insular cortex in his final work. Dronkers' area occupies the precentral gyrus of the anterior lobule of the insula. The cortex is a heterotypical agranular isocortex, characterized by a poorly defined layer IV and medium-sized pyramids in layers III and V. No somatotopy has yet been established.

Electrocortical stimulation of the insula during epilepsy surgery has been reported to cause word finding difficulties, but the specific site on the insula was not specified (Ojemann and Whitaker 1978). The anterior insula has been suggested to be the true site of the function that Broca ascribed to the inferior frontal gyrus (Price 2000). Lesions of the precentral gyrus of the insula are associated with speech apraxia (Fig. 21). This is a disorder of the motor planning of speech, i.e., a disorder in programming the speech musculature to produce correct sounds in the correct order with the correct timing (Dronkers 1996). Such patients exhibit inconsistent articulatory errors that approximate the target word. They grope toward the desired word with disruption of prosody and rate (Dronkers 1996). These patients maintain good perception of language and can perceive and recognize speech sounds, including their own articulatory errors.

An alternate conception of speech apraxia is that it represents a disorder in temporal coordination that disrupts the

timing or the integration of movements between two independent articulators. Speech apraxia is distinct from oral apraxia. Oral apraxia is a defect in planning and performing voluntary oral movements with the muscles of the larynx, pharynx, lips, and cheeks, although automatic movements of the same muscles are preserved (Tognola and Vignolo 1980). Oral apraxia often coexists with speech apraxia and has been related to lesions in the left frontal and central opercula, in the anterior insula, and in a small area of the STG (Dronkers 1996; Tognola and Vignolo 1980). The insula has also been reported to be involved in conductive aphasia and Broca's aphasia, where articulatory errors are prominent (Dronkers 1996).

6.3.9 Sensory Appreciation of Speech

The sensory speech area may be designated Wernicke's area (WA). The site(s) of Wernicke's area are very poorly defined (Roland 1999). Most of WA appears to lie along the most caudal part of BA 22 in the STG and the planum temporale (area tpt of Galaburda and Sanides 1980) or TA 1 of Von Economo and Koskinas (1925). Wernicke's area also includes part of the multimodal belt in the STS (Nieuwenhuys 1994; Nieuwenhuys et al. 1988). Thus, one may also include in WA BA 40, BA 39, BA 22, and BA 37. Anatomically, WA is the least well-defined area, largely due to the significant variation in gyral and sulcal anatomy of this region of the brain (von Economo and Koskinas 1925). In most individuals, WA involves parts of the dominant hemisphere around the posterior sylvian fissure, i.e., the SMG, the angular gyrus, the bases of the STG and the MTG, and the planum temporale. Price reports that the role ascribed by Wernicke to WA is actually found along the posterior superior TS (Price 2000). Cytoarchitectonically, Wernicke's area is a homotypically granular cortex.

Wernicke's area serves to recognize speech relayed to it from the left HG. Direct cortical stimulation of WA intraoperatively causes impairment of language (Ojemann 1983; Ojemann and Whitaker 1978; Ojemann et al. 1989). Patients who have lesions in WA exhibit a form of aphasia designated, variably, sensory aphasia, fluent aphasia, posterior aphasia, and Wernicke's aphasia. These patients produce speech fluently, effortlessly, and rapidly, often too rapidly. The output has the rhythm and melody of normal speech but is remarkably empty of content. These patients show poor comprehension of language and poor ability to repeat language. They use poor grammar and exhibit many errors in word usage (termed *paraphrasias*), including well-articulated replacements of simple sounds, such as spoot for spoon (Geschwind 1970). Patients who have Wernicke's aphasia show the same errors in written output. Recovery of function after Wernicke's aphasia appears to involve a long-lasting shift of function to the right hemisphere (Naidich et al. 2001a).

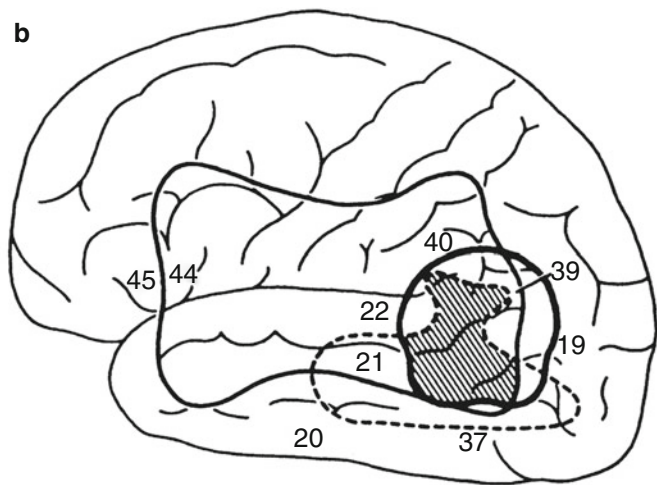


Fig. 22 (a, b) Lesions of the posterior language area. (a) Large depressed area representing an old infarction of the temporoparietal language area in the dominant left hemisphere. (b) Site of pure semantic

deficit for single word comprehension. Area of *broken line* indicates the cortical projection of an extensive subcortical hematoma cavity (From Hart and Gordon (1990); with permission)

6.3.10 Interconnection of Speech Areas: Arcuate Fasciculus

The term *arcuate fasciculus* signifies a broad bundle of fibers that interconnects WA with Broca's area. The arcuate fasciculus may also be designated the anterior limb of the superior longitudinal fasciculus (Nieuwenhuys et al. 1988). It extends between BA 22 and BA 44. The arcuate fasciculus courses from the posterior temporal lobe around the posterior edge of the sylvian fissure to the inferior parietal lobule deep to the SMG and then forward deep to the insula to reach the inferior frontal gyrus. More rostral parts of the STG are also connected with successively more rostral parts of the prefrontal cortex (Nieuwenhuys et al. 1988). The temporal pole is connected with the medial frontal and orbitofrontal cortices through the uncinate fasciculus (Nieuwenhuys et al. 1988). The auditory association areas, particularly the rostral areas, establish connections with the paralimbic cortex of the cingulate gyrus and the PHG (Nieuwenhuys et al. 1988). No myelotomy has yet been determined.

Lesions of the arcuate fasciculus disconnect Wernicke's area from Broca's area, causing a conduction aphasia (Figs. 22 and 23). Patients who have conduction aphasia exhibit good comprehension of the spoken language (WA intact) and fluency of speech (Broca's area intact) but have phonetic errors and poor ability to repeat language. The patient has fluent paraphasic speech and writing with good comprehension of spoken and written language (Geschwind 1970). The inability to repeat speech indicates disruption of the arcuate fasciculus. The disorder in repetition is greatest for the small grammatical words (the, if, is). Repetition of numbers is relatively preserved (Naidich et al. 2001a).



Fig. 23 The arcuate fasciculus interconnects the language areas. Immediately deep to the gyri and sulci of the language areas lie interconnecting fiber tracts, specifically, the arcuate fasciculus (1), extreme capsule (2), inferior longitudinal fasciculus (5), short association fibers (6), superior longitudinal fasciculus (7), and uncinate fasciculus (9); (8) = temporal pole (From England and Wakely (1991), p 95, with permission)

Conclusion

Understanding of the structure and function of the brain depends, in part, on an understanding of the basic anatomic structure of the parts, the cytoarchitecture of the cortex, the functional somatotopy, and the interconnections and dominances among the diverse regions. This chapter has tried to present some of the relevant data and to provide a guide to our current, necessarily limited, understanding of brain function. It is hoped that it may serve as one foundation for advances in understanding the brain.

References

- Albanese E, Merlo A, Albanese A, Gomez E (1989) Anterior speech region. Asymmetry and weight-surface correlation. *Arch Neurol* 46:307–310
- Alexander MP, Hiltbrunner B, Fischer RS (1989) Distributed anatomy of transcortical sensory aphasia. *Arch Neurol* 46:885–892
- Allison JD, Meador KJ, Loring DW, Figueroa RE, Wright JC (2000) Functional MRI cerebral activation and deactivation during finger movement. *Neurology* 54:135–142
- Asanuma H, Okuda O (1962) Effects of transcallosal volleys on pyramidal tract cell activity of cat. *J Neurophysiol* 25:198–208
- Brodmann K (1909) Vergleichende Lokalisationlehre der Grosshirnrinde. Verlag von Johann Ambrosius Barth, Leipzig
- Brust JC (1996) Lesions of the supplementary motor area. *Adv Neurol* 70:237–248
- Burton DB, Chelune GJ, Naugle RI, Bleasel A (1996) Neurocognitive studies in patients with supplementary sensorimotor area lesions. *Adv Neurol* 70:249–261
- Carpenter MB, Sutin J (1983) Human neuroanatomy. In the cerebral cortex. Williams and Wilkins, Baltimore, pp 643–705
- Chauvel PY, Rey M, Buser P, Bancaud J (1996) What stimulation of the supplementary motor area in humans tells about its functional organization. *Adv Neurol* 70:199–209
- Cleghorn JM, Garnett ES, Nahmias C, Brown GM, Kaplan RD, Szechtman H et al (1990) Regional brain metabolism during auditory hallucinations in chronic schizophrenia. *Br J Psychiatry* 157:562–570
- Daniels OL, Haughton VM, Naidich TP (1987) Cranial and spinal magnetic resonance imaging. An atlas and guide. Raven Press, New York
- Dejerine J (1895) Anatomie des centres nerveux. Rueff et Cie, Paris
- Demonet JF, Chollet F, Ramsay S, Cardebat D, Nespolous JL, Wise R et al (1992) The anatomy of phonological and semantic processing in normal subjects. *Brain* 115:1753–1768
- Dronkers NF (1996) A new brain region for coordinating speech articulation. *Nature* 384:159–161
- Duvernoy H (1991) The human brain: surface. Three-dimensional sectional anatomy and MRI. Springer, Berlin
- England MA, Wakely J (1991) Color atlas of the brain and spinal cord. Mosby Year Book, St Louis
- Freund HJ (1996a) Functional organization of the human supplementary motor area and dorsolateral premotor cortex. *Adv Neurol* 70:263–269
- Freund HJ (1996b) Historical overview. *Adv Neurol* 70:17–27
- Freund HJ, Hummelsheim H (1985) Lesions of premotor cortex in man. *Brain* 108:697–733
- Fried I (1996) Electrical stimulation of the supplementary sensorimotor area. *Adv Neurol* 70:177–185
- Fried I, Katz A, McCarthy G, Sass KJ, Williamson P, Spencer SS et al (1991) Functional organization of human supplementary motor cortex studied by electrical stimulation. *J Neurosci* 11:3656–3666
- Galaburda A, Sanides F (1980) Cytoarchitectonic organization of the human auditory cortex. *J Comp Neurol* 190:597–610
- Galaburda AM, LeMay M, Kemper TL (1998) Right-left asymmetries in the brain. Structural differences between the hemispheres may underlie cerebral dominance. *Science* 199:852–856
- Gallese V, Fadiga L, Fogassi L, Rizzolatti G (1996) Action recognition in the premotor cortex. *Brain* 119:593–609
- Gannon PJ, Holloway RL, Broadfield DC, Braun AR (1998) Asymmetry of chimpanzee planum temporale: humanlike pattern of Wernicke's brain language area homolog. *Science* 279:220–222
- Geschwind N (1965a) Disconnection syndromes in animals and man. I. *Brain* 88:237–294
- Geschwind N (1965b) Disconnection syndromes in animals and man. II. *Brain* 88:585–644
- Geschwind N (1970) The organization of language and the brain. Language disorders after brain damage help in elucidating the neural basis of verbal behavior. *Science* 170:940–944
- Geschwind N, Levitsky W (1968) Human brain: left-right asymmetries in temporal speech region. *Science* 161:186–187
- Gilman S, Newman SW (1996) Manter and Gatz's essentials of clinical neuroanatomy and neurophysiology. In the cerebral cortex. FA Davis, Philadelphia
- Grafton ST, Woods RP, Mazziotta JC (1993) Within-arm somatotopy in human motor areas determined by positron emission tomography imaging of cerebral blood flow. *Exp Brain Res* 95:172–176
- Graziano M, Taylor CS, Moore T (2002) Complex movements evoked by microstimulation of precentral cortex. *Neuron* 34:841–851
- Gusmão S, Reis C, Tazinoff U, Mendonça C, Silveira RL (2002) Definition of the anterolateral occipital lobe limit in anatomical specimens and image examination. *Arq Neuropsiquiatr* 60(1):41–46 (in Portuguese)
- Hart J Jr, Gordon B (1990) Delineation of single-word semantic comprehension deficits in aphasia, with anatomical correlation. *Ann Neurol* 27:226–231
- Hasegawa RP, Blitz AM, Geller NL, Goldberg ME (2000) Neurons in monkey prefrontal cortex that track past or predict future performance. *Science* 290:1786–1789
- Humberstone M, Sawle GV, Clare S, Hykin J, Coxon R, Bowtell R et al (1997) Functional magnetic resonance imaging of single motor events reveals human presupplementary motor area. *Ann Neurol* 42:632–637
- Iwasaki S, Nakagawa H, Fukusumi A, Kichikawa K, Kitamura K, Otsuji H et al (1991) Identification of pre- and postcentral gyri on CT and MR images on the basis of the medullary pattern of cerebral white matter. *Radiology* 179:207–213
- Jensen J (1871) Die Furchen und Windungen der menschlichen Großhirnhemisphären. Allgemeine Zeitschrift für Psychiatrie und psychisch-gerichtliche Medizin 27:465–473
- Jurgens U (1983) Afferent fibers to the cingular vocalization region in the squirrel monkey. *Exp Neurol* 80:395–409
- Kawashima R, Yamada K, Kinomura S, Yamaguchi T, Matsui H, Yoshioka S et al (1993) Regional cerebral blood flow changes of cortical motor areas and prefrontal areas in humans related to ipsilateral and contralateral hand movement. *Brain Res* 623:33–40
- Kleinschmidt A, Nitschke MF, Frahm J (1997) Somatotopy in the human motor cortex hand area. A high-resolution functional MRI study. *Eur J Neurosci* 9:2178–2186
- Kopp N, Michel F, Carrier H (1977) Etude de certaines asymétries hémisphériques du cerveau humain. *J Neurol Sci* 34:349–363
- Korogi Y, Takahashi M, Okuda T, Ikeda S, Kitajima M, Yoshizumi K et al (1996) MR topography of the striate cortex: correlation with anatomic sections. *Int J Neuroradiol* 2:534–540
- Lennox BR, Park SB, Medley I, Morris PG, Jones PB (2000) The functional anatomy of auditory hallucinations in schizophrenia. *Psychiatry Res* 100:13–20
- Li A, Yetkin FZ, Cox R, Haughton VM (1996) Ipsilateral hemisphere activation during motor and sensory tasks. *AJNR Am J Neuroradiol* 17:651–655
- Liegeois-Chauvel C, Musolino A, Chauvel P (1991) Localization of the primary auditory area in man. *Brain* 114:139–151
- Liegeois-Chauvel C, Laguitton V, Badier JM, Schwartz D, Chauvel P (1995) Cortical mechanisms of auditory perception in man: contribution of cerebral potentials and evoked magnetic fields by auditory stimulations. *Rev Neurol (Paris)* 151:495–504
- Lim SH, Dinner DS, Luders HO (1996) Cortical stimulation of the supplementary sensorimotor area. *Adv Neurol* 70:187–197
- Luders HO (1996) The supplementary sensorimotor area. An overview. *Adv Neurol* 70:1–16
- Luppino G, Matelli M, Camarda RM, Gallese V, Rizzolatti G (1991) Multiple representations of body movements in mesial area 6 and

- the adjacent cingulate cortex: an intracortical microstimulation study in the macaque monkey. *J Comp Neurol* 311:463–482
- Marsden CD, Deecke L, Freund HJ, Hallett M, Passingham RE, Shibasaki H et al (1996) The functions of the supplementary motor area. Summary of a workshop. *Adv Neurol* 70:477–487
- McGuire PK, Shah GM, Murray RM (1993) Increased blood flow in Broca's area during auditory hallucinations in schizophrenia. *Lancet* 342:703–706
- Meyer JR, Roychowdhury S, Russell EJ, Callahan C, Gitelman D, Mesulam MM (1996) Location of the central sulcus via cortical thickness of the precentral and postcentral gyri on MR. *AJR Am J Neuroradiol* 17:1699–1706
- Naidich TP, Brightbill TC (1995) The intraparietal sulcus. A landmark for localization of pathology on axial CT-scans. *Int J Neuroradiol* 1:3–16
- Naidich TP, Brightbill TC (1996a) The pars marginalis: part 1. A "bracket" sign for the central sulcus in axial plane CT and MRI. *Int J Neuroradiol* 2:3–19
- Naidich TP, Brightbill TC (1996b) Systems for localizing fronto-parietal gyri and sulci on axial CT and MRI. *Int J Neuroradiol* 2:313–338
- Naidich TP, Matthews VP (2000) Integrating neuroanatomy and functional MR imaging: language lateralisation. *ASNR AM Society Neuroradiol* 75–83
- Naidich TP, Valavanis AG, Kubik S (1995) Anatomic relationships along the low-middle convexity: part I – normal specimens and magnetic resonance imaging. *Neurosurgery* 36:517–532
- Naidich TP, Valavanis AG, Kubik S (1997) Anatomic relationships along the low-middle convexity: part II – lesion localization. *Int J Neuroradiol* 3:393–409
- Naidich TP, Hof PR, Gannon PJ, Yousry TA, Yousry I (2001a) Anatomic substrates of language. *Neuroimaging Clin N Am* 11:305–341
- Naidich TP, Hof PR, Yousry TA, Yousry I (2001b) The motor cortex: anatomic substrates of function. *Neuroimaging Clin N Am* 11: 171–193
- Naidich TP, Kang E, Fatterpekar GM, Delman BN, Gultekin SH, Wolfe D et al (2004) The insula: anatomic study and MR imaging display at 1.5 T. *AJR Am J Neuroradiol* 25:222–232
- Neville HJ, Bavelier D (1998) Neural organization and plasticity of language. *Curr Opin Neurobiol* 8:254–258
- Nieuwenhuys R (1994) The human brain: an introductory survey. *Med Mundi* 39:64–79
- Nieuwenhuys R, Voogd J, van Huijzen C (1988) The human central nervous system. A synopsis and atlas. Springer, Berlin, pp 247–292
- Nimchinsky EA, Vogt BA, Morrison JH, Hof PR (1995) Spindle neurons of the human anterior cingulate cortex. *J Comp Neurol* 355:27–37
- Nimchinsky EA, Vogt BA, Morrison JH, Hof PR (1997) Neurofilament and calcium-binding proteins in the human cingulate cortex. *J Comp Neurol* 384:597–620
- Ojemann GA (1983) Brain organization for language from the perspective of electrical stimulation mapping. *Behav Brain Sci* 6:189–230
- Ojemann GA, Whitaker HA (1978) Language localization and variability. *Brain Lang* 6:239–260
- Ojemann G, Ojemann J, Lettich E, Berger M (1989) Cortical language localization in left, dominant hemisphere. An electrical stimulation mapping investigation in 117 patients. *J Neurosurg* 71:316–326
- Olivier A (1996) Surgical strategies for patients with supplementary sensorimotor area epilepsy. The Montreal experience. *Adv Neurol* 70:429–443
- Ono O, Kubik S, Abernathy CD (1990) Atlas of the cerebral sulci. Atlas of the cerebral sulci. Thieme, New York
- Passingham RE (1996) Functional specialization of the supplementary motor area in monkeys and humans. *Adv Neurol* 70:105–116
- Paus T, Petrides M, Evans AC, Meyer E (1993) Role of the human anterior cingulate cortex in the control of oculomotor, manual, and speech responses: a positron emission tomography study. *J Neurophysiol* 70:453–469
- Penfield W, Welch K (1951) The supplementary motor area of the cerebral cortex; a clinical and experimental study. *AMA Arch Neurol Psychiatry* 66:289–317
- Pieniadz JM, Naeser MA (1984) Computed tomographic scan cerebral asymmetries and morphologic brain asymmetries. Correlation in the same cases post mortem. *Arch Neurol* 41:403–409
- Price CJ (2000) The anatomy of language: contributions from functional neuroimaging. *J Anat* 197:335–359
- Pugh KR, Shaywitz BA, Shaywitz SE, Constable RT, Skudlarski P, Fulbright RK et al (1996) Cerebral organization of component processes in reading. *Brain* 119:1221–1238
- Rao SM, Binder JR, Bandettini PA, Hammek TA, Yetkin FZ, Jesmanowicz A et al (1993) Functional magnetic resonance imaging of complex human movements. *Neurology* 43:2311–2318
- Rizzolatti G, Luppino G, Matelli M (1996) The classic supplementary motor area is formed by two independent areas. *Adv Neurol* 70:45–56
- Roland PE (1999) Brain activation. In: Motor functions. Language. Wiley, New York, pp 269–290
- Roland PE, Larsen B, Lassen NA, Skinhøj E (1980a) Supplementary motor area and other cortical areas in organization of voluntary movements in man. *J Neurophysiol* 43:118–136
- Roland PE, Skinhøj E, Lassen NA, Larsen B (1980b) Different cortical areas in man in organization of voluntary movements in extrapersonal space. *J Neurophysiol* 43:137–150
- Rowe JB, Toni I, Josephs O, Frackowiak RS, Passingham RE (2000) The prefrontal cortex: response selection or maintenance within working memory? *Science* 288:1656–1660
- Rumeau C, Tzourio N, Murayama N, Peretti-Viton P, Levrier O, Joliot M et al (1994) Location of hand function in the sensorimotor cortex: MR and functional correlation. *AJR Am J Neuroradiol* 15: 567–572
- Schwalbe G (1881) Lehrbuch der neurologie. Verlag von Eduard Besold, Erlangen
- Seitz RJ, Schlaug G, Knorr U, Steinmetz H, Tellmann L, Herzog H (1996) Neurophysiology of the human supplementary motor area. Positron emission tomography. *Adv Neurol* 70:167–175
- Shaywitz BA, Shaywitz SE, Pugh KR, Constable RT, Skudlarski P, Fulbright RK et al (1995) Sex differences in the functional organization of the brain for language. *Nature* 373:607–609
- Shibasaki H, Sadato N, Lyshkov H, Yonekura Y, Honda M, Nagamine T et al (1993) Both primary motor cortex and supplementary motor area play an important role in complex finger movement. *Brain* 116:1387–1398
- Shima K, Aya K, Mushiake H, Inase M, Aizawa H, Tanji J (1991) Two movement-related foci in the primate cingulate cortex observed in signal-triggered and self-paced forelimb movements. *J Neurophysiol* 65:188–202
- Sobel DF, Gallen CC, Schwartz BJ, Waltz TA, Copeland B, Yamada S et al (1993) Locating the central sulcus: comparison of MR anatomic and magnetoencephalographic functional methods. *AJR Am J Neuroradiol* 14:915–925
- Steinmetz H, Seitz RJ (1991) Functional anatomy of language processing: neuroimaging and the problem of individual variability. *Neuropsychologia* 29:1149–1161
- Steinmetz H, Furst G, Freund HJ (1989a) Cerebral cortical localization: application and validation of the proportional grid system in MR imaging. *J Comput Assist Tomogr* 13:10–19
- Steinmetz H, Rademacher J, Huang YX, Hefter H, Zilles K, Thron A et al (1989b) Cerebral asymmetry: MR planimetry of the human planum temporale. *J Comput Assist Tomogr* 13:996–1005
- Steinmetz H, Ebeling U, Huang YX, Kahn T (1990a) Sulcus topography of the parietal opercular region: an anatomic and MR study. *Brain Lang* 38:515–533

- Steinmetz H, Rademacher J, Jancke L, Huang YX, Thron A, Zilles K (1990b) Total surface of temporo-parietal intrasylvian cortex: diverging left-right asymmetries. *Brain Lang* 39:357–372
- Steinmetz H, Volkmann J, Jancke L, Freund HJ (1991) Anatomical left-right asymmetry of language-related temporal cortex is different in left- and right-handers. *Ann Neurol* 29:315–319
- Talairach J, Tournoux P (1988) Co-planar stereotaxic atlas of the humanbrain. 3-Dimensional proportional system. An approach to cerebral imaging. Thieme, New York
- Tanji J (1994) The supplementary motor area in the cerebral cortex. *Neurosci Res* 19:251–268
- Tanji J, Shima K (1994) Role for supplementary motor area cells in planning several movements ahead. *Nature* 371:413–416
- Tanji J, Okano K, Sato KC (1987) Relation of neurons in the nonprimary motor cortex to bilateral hand movement. *Nature* 327:618–620
- Tanji J, Okano K, Sato KC (1988) Neuronal activity in cortical motor areas related to ipsilateral, contralateral, and bilateral digit movements of the monkey. *J Neurophysiol* 60:325–343
- Tognola G, Vignolo LA (1980) Brain lesions associated with oral apraxia in stroke patients: a clinico-neuroradiological investigation with the CT scan. *Neuropsychologia* 18:257–272
- Ture U, Yasargil DC, Al-Mefty O, Yasargil MG (1999) Topographic anatomy of the insular region. *J Neurosurg* 90:720–733
- Viallet F, Massion J, Massarino R, Khalil R (1992) Coordination between posture and movement in a bimanual load lifting task: putative role of a medial frontal region including the supplementary motor area. *Exp Brain Res* 88:674–684
- Vogt C, Vogt O (1919) Allgemeine ergebnisse unserer hirnforschung. *J Psychol Neurol* 25:279–461
- Vogt O, Vogt C (1926) Die vergleichend-architektonische und vergleichend-reizphysiologische felderung der grobhirnrinde unter besonderer berücksichtigung der menschlichen. *Naturwissenschaften* 14:1190–1194
- Vogt BA, Nimchinsky EA, Vogt LJ, Hof PR (1995) Human cingulate cortex: surface features, flat maps, and cytoarchitecture. *J Comp Neurol* 359:490–506
- Vogt BA, Vogt LJ, Nimchinsky EA (1997) Primate cingulate cortex chemoarchitecture and its disruption in Alzheimer's disease. In: Bloom FE, Bjorklund A, Hokfelt T (eds) *Handbook of chemical neuroanatomy*, vol 13. Elsevier Science, Amsterdam, pp 455–528
- von Economo C, Koskinas GN (1925) *Die Cytoarchitektonik der Hirnrinde des erwachsenen Menschen*. Springer, Berlin
- Williams PL, Warwick R, Dyson M (1989) *Grays anatomy*, 37th edn. Churchill Livingstone, Edinburgh/New York, pp 1047–1063
- Yasargil MG (1994) *Microneurosurgery*. Thieme, Stuttgart
- Yoshiura T, Higano S, Rubio A, Shrier DA, Kwok WE, Iwanaga S et al (2000) Heschl and superior temporal gyri: low signal intensity of the cortex on T2-weighted MR images of the normal brain. *Radiology* 214:217–221
- Yousry TA (1998) Historical perspective: the cerebral lobes and their boundaries. *Int J Neuroradiol* 4:342–348
- Yousry TA, Schmid UD, Jassoy AG, Schmidt D, Eisner WE, Reulen HJ et al (1995) Topography of the cortical motor hand area: prospective study with functional MR imaging and direct motor mapping at surgery. *Radiology* 195:23–29
- Yousry TA, Schmid UD, Schmidt D, Hagen T, Jassoy A, Reiser MF (1996) The central sulcal vein: a landmark for identification of the central sulcus using functional magnetic resonance imaging. *J Neurosurg* 85:608–617
- Yousry TA, Fesl G, Buttner A (1997a) Heschl's Gyrus: anatomic description and methods of identification on magnetic resonance imaging. *Int J Neuroradiol* 3:2–12
- Yousry TA, Schmid UD, Alkadhi H, Schmidt D, Peraud A, Buettner A et al (1997b) Localization of the motor hand area to a knob on the precentral gyrus. A new landmark. *Brain* 120:141–157
- Yousry TA, Yousry I, Naidich TP (2001) Progress in neuroanatomy. In: Demaerel P (ed) *Recent advances in diagnostic neuroradiology*. Springer, Berlin
- Zilles K, Schlaug G, Geyer S, Luppino G, Matelli M, Qu M et al (1996) Anatomy and transmitter receptors of the supplementary motor areas in the human and nonhuman primate brain. *Adv Neurol* 70:29–43

Task-Based Presurgical Functional MRI in Patients with Brain Tumors

Christoph Stippich, Maria Blatow, and Meritxell Garcia

Contents

| | | |
|-----|---|-----|
| 1 | Brain Tumors and Brain Tumor Surgery | 90 |
| 2 | Presurgical Functional Neuroimaging: Rationale and Diagnostic Aims | 90 |
| 3 | Presurgical Task-Based fMRI: Practical, Technical, and Methodological Considerations..... | 94 |
| 3.1 | Practical Issues..... | 94 |
| 3.2 | Legal Aspects..... | 98 |
| 3.3 | Evaluation of Presurgical fMRI Data..... | 98 |
| 3.4 | Analyzing fMRI Data in Individual Patients | 101 |
| 4 | Presurgical fMRI of Motor and Somatosensory Function... | 104 |
| 4.1 | Review of Literature | 104 |
| 4.2 | Selection of Candidates for Presurgical Motor and Somatosensory fMRI | 106 |
| 4.3 | Motor and Somatosensory Paradigms for Presurgical fMRI | 107 |
| 4.4 | Presurgical Somatotopic Mapping of the Primary Motor Cortex..... | 110 |
| 4.5 | Presurgical Somatotopic Mapping of the Primary Somatosensory Cortex | 115 |
| 4.6 | Localization of the Precentral Gyrus in Patients with Preexisting Paresis | 116 |
| 5 | Presurgical fMRI of Language Function | 119 |
| 5.1 | Review of Literature | 119 |
| 5.2 | Special Practical Issues in Presurgical fMRI of Language Function | 123 |
| 5.3 | Selection of Candidates for Presurgical Language fMRI | 124 |
| 5.4 | Language Paradigms for Presurgical fMRI..... | 124 |
| 5.5 | Presurgical fMRI of Language Function | 126 |
| 6 | Diagnostic Capabilities and Limitations of Presurgical Task-Based fMRI..... | 130 |
| | References | 133 |

C. Stippich, MD (✉)

Professor and Division Head, Division of Diagnostic and Interventional Neuroradiology, University Hospitals Basel, Petersgraben 4, Basel CH 4031, Switzerland
e-mail: christoph.stippich@usb.ch

M. Blatow, MD • M. Garcia, MD

Division of Diagnostic and Interventional Neuroradiology, Clinic for Radiology and Nuclear Medicine, University Hospitals Basel, Petersgraben 4, Basel CH 4031, Switzerland

Abstract

Neurosurgery in functionally important brain areas carries a high risk for postoperative neurological deficits. In patients with brain tumors, functional magnetic resonance imaging (fMRI) facilitates presurgical planning and evaluation of surgical outcome for the estimation of an as good as possible balance between maximal tumor resection and minimal loss of function. To this end fMRI is also applied intraoperatively for functional neuronavigation preferably in combination with DTI-tractography. However, fMRI has not reached the status of a standard diagnostic neuroimaging procedure, yet. Preoperative task-based fMRI represents the best established and validated clinical application of fMRI, is increasingly performed in larger medical neurocenters, and in this context can only be performed exclusively in individual patients. Therefore, it differs fundamentally from research application in neuroscience.

This chapter provides a review of the current literature and presents optimized task-based presurgical fMRI protocols for motor, somatosensory, and language function, along with a standardized data evaluation protocol using a dynamic statistical threshold. Examples of physiological brain activation are given, criteria for the selection of candidates for presurgical fMRI are provided, and illustrative cases with typical and atypical presurgical fMRI findings are presented. Complementary applications with diffusion tensor imaging (DTI) and DTI-tractography (DTT) are highlighted. Finally, important diagnostic capabilities and limitations of presurgical fMRI are discussed.

In conclusion, fMRI is feasible for advanced multimodal MR-neuroimaging in the clinical setting and provides important diagnostic information noninvasively, which is otherwise unavailable. Task-based preoperative fMRI is valid, reasonably sensitive, and accurate to localize the different representations of the human body in the primary motor and somatosensory cortex prior to brain tumor surgery, which in general also applies to language localization and lateralization. Although there is a

substantial body of studies on presurgical language fMRI available, the results are still heterogeneous. Here, fMRI has at least the potential to help to reduce the number of invasive diagnostic measures needed and to guide their targeted application. If, and to what extent, intraoperative electrocorticography (ECoG) or the Wada test can be replaced is still not clear, yet. The integration of fMRI with DTI and DTT is complementary and increasingly used, providing important pretherapeutic and intraoperative information on essential cortical and subcortical functional structures in relation to the surgical target.

1 Brain Tumors and Brain Tumor Surgery

The age-adjusted incidence of brain tumors (benign and malignant) has been estimated at approximately 19 per 100,000 persons-years (Parkin and Muir 1992; Ohgaki 2009; Ostrom and Barnholtz-Sloan 2011). Mortality rates from all tumors of the CNS range between 4 and 7 per 100,000 persons/year in men and between 3 and 5 per 100,000 persons/year in women (McKinney 2004; Ohgaki 2009). With the exception of pilocytic astrocytoma, the survival rate of brain neoplasms is poor (Landis et al. 1999) and correlates with the grade of malignancy. Most gliomas are infiltrative and have ill-defined margins making complete surgical removal often impossible. Patients with low-grade gliomas have a median survival of 6–10 years, but these tumors tend to have a malignant transformation. For instance, the mean 5-year survival rate for anaplastic astrocytoma is 11 % and for glioblastoma 1.2 % (Ohgaki 2009), comparable to primary CNS lymphoma or metastatic disease where prolonged survival is rather exceptional.

Histologically, brain tumors can be classified as “primary,” that is, arising from the brain or its linings, or as “secondary” or “metastatic” affecting the CNS predominantly from lung, breast, kidney, gastrointestinal, and skin cancer. In adults, primary and secondary brain tumors can be approximated equiprevalent, whereas in children metastatic disease is rare (Stefanowicz et al. 2011).

Extra-axial tumors are typically noninvasive and affect the brain by displacement or compression. Clinical symptoms may also be related to occlusive hydrocephalus caused by impaired circulation of cerebrospinal fluid (CSF) due to compression of the ventricles or connecting foramina. The primary goal of treatment is complete removal. Intra-axial tumors grow inside the brain parenchyma. The spectrum of appearance is wide – ranging from focal and well-defined masses to diffusely infiltrating processes. Clinical signs and symptoms depend mainly on the location and mass effect. According to protocols of the World Health Organization

(WHO), brain tumors are classified in four grades based on a malignancy scale, that is, on pleomorphism, mitotic activity, endothelial proliferation, and necrosis. Based on cell origin, 12 groups have been defined (Louis et al. 2007).

The treatment of brain tumors and metastases is traditionally based on surgery, radiation, or chemotherapy or a combination of these treatments, tailored to the target location and pathology (Kaye and Laws 2011; DeMonte et al. 2007; Jovčevska et al. 2013). More recently, cellular and molecular biology has opened up new diagnostic and therapeutic options. Advanced neuroimaging – based on morphological, metabolic, and functional assessment – provides very detailed diagnostic information on intracranial pathologies and has helped to guide and refine treatment strategies and estimate procedural risks and prognosis (Jacobs et al. 2005). Reduction of morbidity associated with treatment is of utmost importance, which especially applies to patients in whom complete removal of the lesion is impossible and complete cure cannot be achieved. Here, the goal of neurosurgery is to eliminate as much of the tumor as safely as possible while preserving the eloquent areas of the brain. To achieve this, cutting-edge technology is applied for image-guided neurosurgery and functional neuronavigation (Nimsky et al. 2006; Archip et al. 2007; Kuhnt et al. 2012; Kumar et al. 2014).

2 Presurgical Functional Neuroimaging: Rationale and Diagnostic Aims

Neurosurgical procedures in or next to functionally relevant brain tissue invariably carry the risk of surgery-induced post-operative neurological deficits. Although all brain areas are to a certain extent of functional importance, in clinical practice the term “functionally relevant” or “eloquent” is limited to those brain structures where damage can result in severe neurological compromise and consequently in a significant reduction of the patient’s quality of life. Resection of the so-called “rolandic” or synonymously “central” brain tumors, for example, can lead to injury of the primary motor and somatosensory cortices and therefore cause permanent movement and sensibility impairment. Patients with frontal or temporal lesions of the left hemisphere are particularly prone to suffer from postoperative motor or sensory language deficits, while mesiotemporal interventions can affect memory function. Therefore, the indication for neurosurgery in such patients has to be set rigorously, and other, less invasive, therapeutic options like radiotherapy or neuroradiological interventions – as in the case of vascular malformations – should be considered. This applies especially to patients where curative treatment is not possible. Here, preservation of brain function and the reduction of treatment-associated morbidity

are crucial. Prudent preoperative consideration of the optimal surgical access and resection borders for each patient can be of utmost importance to avoid damage to functionally relevant brain structures (Duffau 2006; Voss et al. 2013; Kundu et al. 2013; Håberg et al. 2004; Kumar et al. 2014; Jia et al. 2013). Similar to brain tumor surgery, epilepsy surgery aims at complete removal of the epileptogenic zone with minimal damage to eloquent brain areas (see chapter “[Presurgical EEG-fMRI in Epilepsy](#)”). Thus, depending on the location of the pathology, the determination of the hemispheric dominance and the precise spatial relationship between the brain tumor or epileptogenic zone and the functionally relevant brain area can be mandatory for the selection of the appropriate therapeutic option and its approach. Ideally, this information should be available before initiation of any therapy in order to minimize postoperative neurosurgical morbidity and duration of postoperative hospitalization. In this view, functional neuroimaging not only offers a variety of novel options for clinical diagnostics and research but also opens up a new diagnostic field of neuroradiology, with a shift from a strictly morphological imaging to the measurement and visualization of brain function (Stippich et al. 2002a).

The standard and most accurate procedure for the mapping of human brain function is intraoperative electrocorticography (ECoG) (Penfield 1937, 1950; Woolsey et al. 1979; Ojemann et al. 1989; Ojemann 1991; Cedzich et al. 1996; Duffau et al. 1999; Cordella and Acerbi 2013), consisting of electrophysiological recordings from the cerebral cortex with surface electrodes, which is a demanding technique offered only by highly specialized medical centers. Application of ECoG considerably increases surgery duration and involves distressing awake craniotomy, since mapping of language and memory-related brain structures requires active collaboration of the patient. A particular disadvantage of ECoG is the fact that it is applied during surgery so that the obtained results cannot be incorporated in the preoperative process of treatment selection and planning. Presurgical determination of hemispheric dominance is traditionally achieved by the invasive Wada test (Wada and Rasmussen 1960; Rausch et al. 1993; Sharan et al. 2011; Cunningham et al. 2008; Wagner et al. 2012), where language and memory functions are assessed neuropsychologically during intra-arterial injection of barbiturates (amobarbital). This method bears all the risks of cerebral angiography with complication rates in up to 11 % of cases (Sharan et al. 2011), is discomforting for the patient, and requires several days of hospitalization. Other frequently applied methods for the identification of functionally important brain structures are positron emission tomography (PET) (Csaba 2003; La Fougère et al. 2009) and single-photon emission computed tomography (SPECT) (La Fougère et al. 2009), which detect changes of cerebral blood flow and glu-

cose metabolism. These techniques, however, are also invasive, utilize ionizing radiation, and thus carry a certain risk of morbidity. In addition, their temporal resolution is low (Müller et al. 1998), and discordance of the results for presurgical diagnostics is recognized. Besides fMRI, other frequently used noninvasive techniques for the assessment of human brain function are electrophysiological methods which measure neuronal activity directly via the detection of electromagnetic fields with an excellent temporal resolution (ms range) – these include electroencephalography (EEG) (Berger 1929; Gevins 1995; Gevins et al. 1995) and magnetoencephalography (MEG) (Hari and Ilmoniemi 1986; Findley et al. 2012; Choudhri et al. 2013). Spatial resolution, however, is lower than that obtained from fMRI, and localization of electromagnetic sources requires complicated mathematical modeling and calculations (based on single- or multidipole models and various spherical head models) and is therefore limited in precision and accuracy (Hämäläinen et al. 1993).

The diagnostic potential of presurgical morphological imaging in the clinical routine with magnetic resonance imaging (MRI) is limited regarding the localization of functionally relevant brain structures. For instance, MRI provides detailed structural information of the brain parenchyma and intracranial pathologies (Osborn et al. 2010; Osborn 2012), but cannot assess brain function. Anatomically identifiable landmarks for specific functions could be described solely for the central region (see chapter “[Functional neuroanatomy](#)”), where reliability reaches a maximum of approximately 95 % in healthy volunteers (Fig. 1). In the presence of anatomical variants, malformations of the brain, or patients with large or vastly infiltrating tumors, these morphological landmarks are not consistently identifiable. Pathological signal changes involving the pre- or postcentral gyrus further challenge presurgical morphological imaging diagnostics. A trustworthy attribution of a functional representation to a defined anatomical landmark is – even with an intact rolandic anatomy – only feasible for the hand motor area, identified as a characteristically dorsally oriented convexity in the precentral gyrus, the so-called hand-knob (Yousry et al. 1997). However, motor activity can also be detected outside of typical landmarks and the pattern of motor cortex activation is modulated by different physiological factors (Yousry et al. 2001). Other representations of the human body in the pre- or postcentral gyrus lack any reliable morphological correlate (Fesl et al. 2003). Their localization can be merely estimated knowing the somatotopic organization of the rolandic cortex in the motor and somatosensory homunculi (Penfield 1937, 1950). Moreover, the localization and extent of activated brain sites can vary under pathological conditions as well as the pattern of brain activation. Besides local mass effects and hemodynamic alterations, brain tumors and

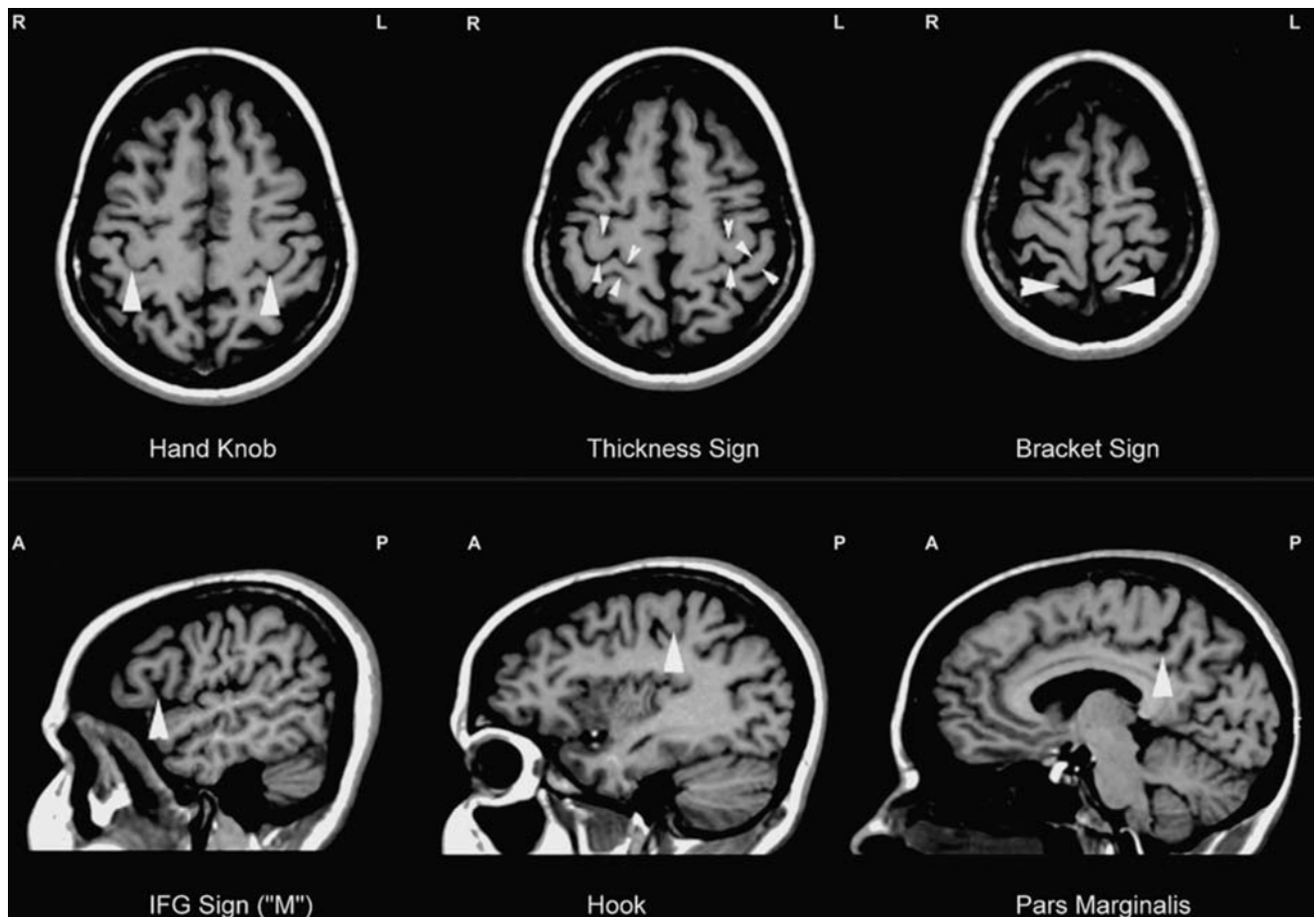


Fig. 1 Anatomical landmarks on morphological MRI according to Naidich and Yousry in transverse (*upper row*) and sagittal (*lower row*) views. *White arrows* indicate the relevant anatomical structures. The “hand-knob” and

“hook” are synonyms for the “precentral knob” (see chapter “[Functional neuroanatomy](#)”) (Modified from Stippich et al. 2003a with permission)

arteriovenous malformations (AVMs) may also induce neuroplastic changes, that is, an altered pattern of activation as compared to the normal brain, known as lesion-induced reorganization or plasticity (Baciu et al. 2003; Bogomolny et al. 2004; Peck and Holodny 2007; Holodny and Shevzov-Zebrun 2011; Holodny and Shevzov-Zebrun et al. 2002; Tuntiyatorn et al. 2011; Briganti et al. 2012; Rösler et al. 2014) which is also observed in patients with epilepsy (Wunderlich et al. 1998; Fandino et al. 1999; Holodny et al. 1999, 2000; Alkadhi et al. 2000; Bittar et al. 2000; Duffau et al. 2000; Lehericy et al. 2002; Roux et al. 2000; Carpenter et al. 2001b; Duffau 2001; Krings et al. 2002a; Rutten et al. 2002b; Baciu et al. 2003; Bogomolny et al. 2004; Peck and Holodny 2007; Kasprjan and Seidel 2010. This also applies to language-associated brain structures (Duffau et al. 2001; Lazar et al. 1997; Springer et al. 1999; Spreer et al. 2001; Duffau et al. 2002a, b; Hertz-Pannier et al. 2002; Lehericy et al. 2002; Petrovich et al. 2004; Stippich et al. 2007a, b;

Partovi et al. 2012a; Briganti et al. 2012; Rösler et al. 2014) which, other than motor cortex representations, display a marked anatomical variability even in healthy subjects (Bogen 1976; Price 2000; Naidich et al. 2001). Additionally, many cognitive brain functions are under the influence of individual factors, such as handedness (Szaflarski et al. 2002), multilingualism (Bello et al. 2006; Hasegawa et al. 2002; Hernandez et al. 2001; Illes et al. 1999; Kim et al. 1997; Klein et al. 1995; Roux and Tremoulet 2002), age (Gaillard et al. 2000a, b, 2001a, b; Schlaggar et al. 2002), or gender (Shaywitz et al. 1995; Frost et al. 1999). This variability suggests the need for the assessment of functional localization in each patient individually.

The use of functional neuroimaging methods is especially valuable prior to neurosurgery in rolandic (Jack et al. 1994; Baumann et al. 1995; Yousry et al. 1995, 1996; Atlas et al. 1996; Mueller et al. 1996; Pujol et al. 1996, 1998; Krings et al. 1997, 1998; Roux et al. 1997, 1999a, b; Schlosser et al.

1997; Stapleton et al. 1997; Yetkin et al. 1997; Dymarkowski et al. 1998; Lee et al. 1998b, 1999; Nitschke et al. 1998; Schulder et al. 1998; Achten et al. 1999; Hirsch et al. 2000; Lehericy et al. 2000b; Kober et al. 2001; Krings et al. 2001; Ozdoba et al. 2002; Liu et al. 2003; Schiffbauer et al. 2003; Stippich et al. 2003a; Towle et al. 2003; Krishnan et al. 2004; Parmar et al. 2004; Reinges et al. 2004; Majos et al. 2005; Roessler et al. 2005; Van Westen et al. 2005; Nimsky et al. 2006), frontal or temporoparietal (Desmond et al. 1995; Binder et al. 1996; Bahn et al. 1997; FitzGerald et al. 1997; Herholz et al. 1997; Hertz-Pannier et al. 1997; Worthington et al. 1997; van der Kallen et al. 1998; Yetkin et al. 1998; Benson et al. 1999; Bittar et al. 1999a, b; Killgore et al. 1999; Ruge et al. 1999; Rutten et al. 1999; Springer et al. 1999; Bazin et al. 2000; Grabowski 2000; Hirsch et al. 2000; Lehericy et al. 2000a; Lurito et al. 2000; Gaillard et al. 2002; Pouratian et al. 2002; Rutten et al. 2002c; Roux et al. 2003; Stippich et al. 2003b, 2006, 2010; Van Westen et al. 2005; Grummich et al. 2006; Voss et al. 2013) and mesiotemporal (Deblaere et al. 2002; Avila et al. 2006; Stippich 2010; Spritzer et al. 2012; Fakhri et al. 2013; Voss et al. 2013) brain areas for the individual functional localization of motor, somatosensory, language-, and memory-related brain activation, as well as for the determination of the hemispheric dominance and epileptogenic zone. At present, functional magnetic resonance imaging (fMRI) is the most widely used method for functional neuroimaging. This modern imaging technique measures brain function indirectly (Kwong et al. 1992) with a higher spatial accuracy, but lower temporal resolution than other noninvasive techniques such as EEG (Gevins et al. 1995) or MEG (Hämäläinen et al. 1993; Tarapore and Matthew 2012). Advantages of fMRI over PET (Fox et al. 1986) (Mazziotta et al. 1982; Raichle 1983), SPECT (Holman and Devous 1992), ECoG, and the Wada test are its noninvasiveness, lack of need for radiation, and broad availability of MR scanners.

fMRI assesses brain activity indirectly via detection of local hemodynamic changes in capillaries (Menon et al. 1995) and draining veins (Frahm et al. 1994) of functional areas. The blood-oxygen-level-dependent (BOLD) technique makes use of blood as an intrinsic contrast agent (Ogawa et al. 1990a, b, 1992). BOLD signals have been shown to reflect actual neuronal activity with high spatial accuracy (Logothetis et al. 2001; Logothetis 2002, 2003; Logothetis and Pfeuffer 2004; Logothetis and Wandell 2004). For details, please refer to chapter “**Revealing brain activity and white matter structure using functional and diffusion-weighted magnetic resonance imaging**” giving information about the physiological basics and methodological-technical aspects of fMRI also in the context of clinical applications. Although fMRI has been quickly established in the research field of basic neuroscience – and

in the past decade, new high-performance gradient systems with higher-field scanners and the development of ultrafast MR-sequences have allowed examination of the entire brain in clinically feasible scanning times – this technique is still rarely used for clinical diagnostics and research mostly due to its higher technical and methodological requirements as compared to clinical morphological MRI. Again, it should be kept in mind that presurgical fMRI has to be performed in individual patients with the goal of a neuroradiological “functional” diagnosis and therefore fundamentally differs from research experiments in basic neuroscience, where the general understanding of brain function in groups of healthy subjects or patients is in the center of interest.

The vast majority of clinical task-based fMRI measurements are performed at 1.5 T systems due to their more widespread distribution. During the last years the clinical availability of higher-field MR-imagers usually with a main magnetic field strength of 3 T is continuously increasing, and a few ultrahigh field MR-machines (up to 9.4 T) have been installed in leading neurocenters around the globe for basic and clinical research. fMRI profits from higher main magnetic fields mainly through higher signal-to-noise ratio (SNR), higher BOLD signal, and better spatial resolution. This is further supported by high-performance gradients and the multichannel head coil technique. An increased sensitivity (determined as the increase in percentage of voxels activated) for motor and somatosensory stimulation and more specific localization in the gray matter has been shown for 3 T fMRI compared to 1.5 T fMRI (Krasnow et al. 2003; García-Eulate et al. 2011). A further study has demonstrated an earlier onset of the hemodynamic response at 7 T in comparison to 1.5 T, hereby reducing the undesired venous contribution to the BOLD response (Van der Zwaag et al. 2009).

Better functionality of data processing and immediate data analysis (so-called real-time fMRI) (Weiskopf et al. 2003, 2004) facilitate the use of fMRI under clinical conditions (Fernandez et al. 2001; Moller et al. 2005; Feigl et al. 2008), (see Sect. 4.1). Most new-generation MR-imagers come along with software packages that have some functionality for processing fMRI data already at the scanners console. These products are designed user friendly and easily to apply. However, the options to monitor the different steps of the underlying data processing are limited as well as the options to analyze and control the fMRI results in detail. This lacking in fundamental functionality may be problematic in cases of unclear, ambiguous, or unexpected fMRI results, determination of artifacts, or when imaging quality is reduced.

Presurgical diagnostic assessment in patients with brain tumors and epilepsy is to date the most commonly established clinical application of fMRI. Historically, due to its good spatial resolution and direct correlation with surface

anatomy, BOLD fMRI was used shortly after its first description (Bandettini et al. 1992; Kwong et al. 1992; Ogawa et al. 1992) for presurgical localization of the primary sensorimotor cortex in patients with rolandic brain tumors (Jack et al. 1994), (see Sect. 4) and shortly after for the determination of the language-dominant hemisphere and localization of the Broca's and Wernicke's language areas (FitzGerald et al. 1997) in patients with left frontal or temporo-parietal tumors (Desmond et al. 1995), (see Sect. 5). There is substantial evidence from validation studies with established reference procedures (see chapter “[Presurgical functional localization possibilities, limitations and validity](#)”) and from multimodal investigations comparing fMRI with other functional neuroimaging methods (see chapter “[Multimodality in functional neuroimaging](#)”), suggesting a good reliability of fMRI data for the (presurgical) localization of functional areas and – not unisono however – for the determination of the language-dominant hemisphere, considering the indications and limitations of this technique.

Basically, the predominant diagnostic aims of presurgical functional neuroimaging are the following:

- Localization of eloquent brain areas with respect to the envisaged site of surgery
- Determination of the dominant hemisphere for specific brain functions
- Localization of the epileptic zone and lateralization of epileptic activity
- Delineation of neuroplastic changes in brain activity

Presurgical fMRI is now commonly used in combination with diffusion tensor imaging (DTI) to additionally delineate functionally important fiber bundles such as the pyramidal tract or the arcuate fascicle (see chapter “[Diffusion Imaging with MR tractography for brain tumor surgery](#)”). The diagnostic information of both modalities is complementary and can be integrated and used for functional neuronavigation (see chapter “[Functional neuronavigation](#)”). Resting state fMRI (rsfMRI) has been extensively used in the last years in the field of neuroscience imaging to study different functional networks of the human brain without direct stimulation. Meanwhile first attempts are underway to employ this new modality for presurgical functional neuroimaging (see chapter “[Presurgical resting state fMRI](#)”).

Standardization of the imaging procedures, data processing, and neuroradiological interpretation of the results is still an issue. Therefore, most clinical fMRI studies still need to be performed in the framework of research trials. General instructions for clinical fMRI have been published in the “[current protocols in magnetic resonance imaging](#)” (Thulborn 2006), and by now, first attempts of the responsible medical associations have been made to release instructions for established clinical applications of fMRI. This is an important step towards a standard diagnostic neuroimaging modality (for details see Sect. 3.1).

3 Presurgical Task-Based fMRI: Practical, Technical, and Methodological Considerations

3.1 Practical Issues

In contrast to experimental applications of fMRI, in research laboratories where permanent test setups can be installed, generally healthy subjects are examined, and the measured results do not necessarily need to be immediately available, the clinical application of fMRI in a hospital setting faces particular challenges. Technically and methodologically custom-tailored developments including hardware, software, imaging protocols, and data evaluation processes (see Sects. 3.3 and 3.4) are required to allow a successful examination of patients with existing deficits, uncooperative or sedated patients, and children (Hajnal et al. 1994; Baudendistel et al. 1996; Buckner et al. 1996; Cox 1996; Friston 1996; Lee et al. 1996, 1998a, b, c; Gold et al. 1998; Stippich et al. 1999, 2000, 2002a; Thulborn and Shen 1999; Bookheimer 2000; Hammeke et al. 2000; Hirsch et al. 2000; Gaillard et al. 2001a, b; Hsu et al. 2001; Roux et al. 2001; Hoeller et al. 2002; Rutten et al. 2002c, d; Roberts 2003; Steger and Jackson 2004; Hulvershorn et al. 2005a, b; Weiskopf et al. 2005; Liu and Ogawa 2006; Priest et al. 2006; Wienbruch et al. 2006). Instructions for dealing with sources of error and solving specific problems arising in clinical fMRI are given in chapter “[Clinical BOLD fMRI & DTI: artifacts, tips and tricks](#)”.

The principal element of any task-based fMRI measurement consists of a “paradigm,” defined by a functional measurement including a stimulation adjusted to the respective brain area to be investigated. Altogether, a complete fMRI protocol comprises one or several different paradigms in addition to at least one morphological 3D data set for image overlay procedures. Clinical fMRI protocols need to be optimized for clinically acceptable examination times, low susceptibility to artifacts, good signal yield, and a reliable localization of functional brain areas. In this context, block-designed paradigms, with cyclically alternating “stimulation” and “baseline” or synonymously “control” conditions, are usually more feasible than the methodologically more demanding event-related paradigms (Fig. 2). Ideally, it should be possible to use clinical fMRI protocols even in patients with existing neurological and cognitive deficits. Thus, particularly when creating complex protocols, such as for language or other cognitive brain functions, a close cooperation with neuropsychological experts is strongly advisable. Prior to any clinical fMRI examination, an accurate documentation of relevant neurological/neuropsychological deficits has to be available in order to avoid erroneous data interpretation. Individual training and stimulation adjustment

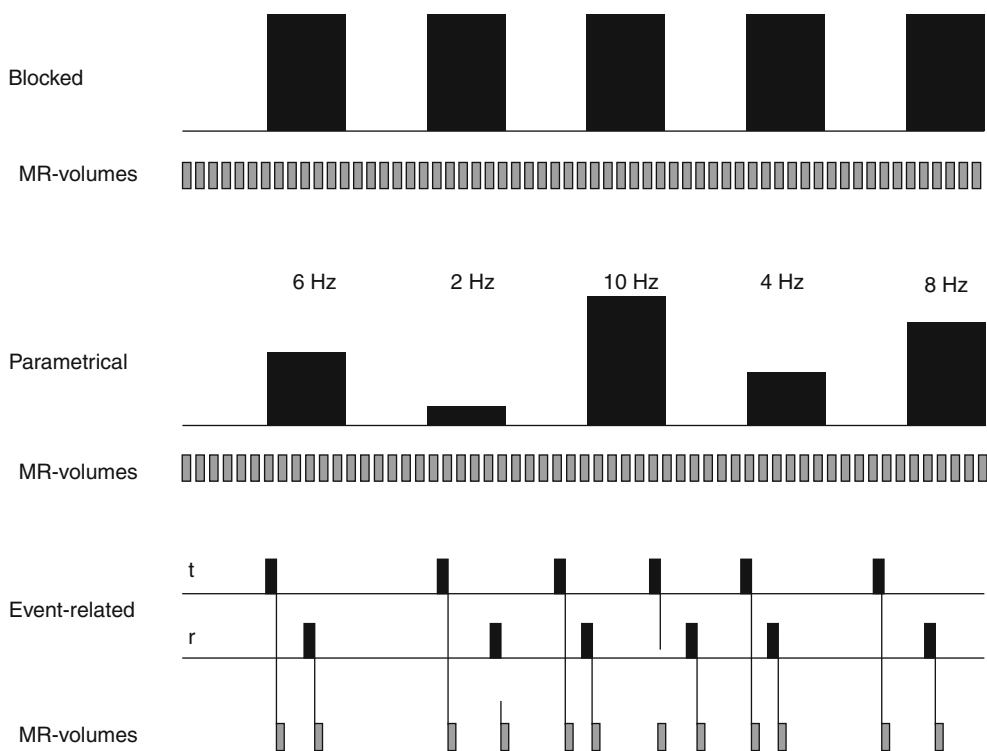


Fig. 2 Schematic illustration of different paradigm designs used for fMRI studies. Conventional “blocked design” consists of different stimulation periods that repeatedly alternate over time, while images are acquired continuously (MR-volumes). Usually a series of identical stimuli (or tasks) is applied during each period. “Parametrical design” is a modification of blocked design with a systematic variation of the applied stimulation between periods (e.g., trigger frequency). “Event-related” design requires triggering and enables to measure BOLD

according to the patient’s abilities are also indispensable. The time required for the pre-measurement training generally exceeds the actual measurement time and can vary in own experience between 20 min and 3 h dependent on the patient’s abilities (Stippich et al. 2002a). By using optimized and standardized protocols, fMRI examinations can be integrated in the clinical MR imaging routine without major problems. To investigate motor function, self-triggered movements are most commonly used (see Sect. 4.3), and non-standardized tactile stimuli (e.g., manual touching of the hand by the examiner) are applied to measure somatosensory function (Hammek et al. 1994). Language functions are examined using various paradigms involving acoustic or visual stimulation (see Sect. 5.3). In the studies on preoperative fMRI published to date, the required measurement times per paradigm show a high variability between 1 min (Stippich et al. 2004) and above 20 min (Rutten et al. 2002c); technical and methodological differences are also considerable. To make “getting started” in preoperative fMRI easier, sample established protocols are presented in Sects. 4.4, 4.5, and 5.4. In our experience, these protocols ensure a robust functional localization at 1.5 T and sufficient BOLD signal

responses to single events (e.g., a single finger movement) with improved temporal resolution. Images can be acquired continuously or discontinuously (shown). To achieve a higher SNR averaging of a larger number of events is required (for details see chapter “[Revealing brain activity and white matter structure using functional and diffusion-weighted magnetic resonance imaging](#)”) (Modified from Stippich et al. 2002a with permission)

(measured parameters: r = correlation of the measured BOLD signals to the applied hemodynamic reference function, $\Delta S\%$ = relative BOLD signal change). It seems possible to use the proposed protocols also on EPI capable MR-imagers with a lower main magnetic field strength up from 1.0 T, but this has not been tested systematically. Scan times per paradigm are 66 or 105 s (fully automatic somatosensory stimulation) (Stippich et al. 2004, 2005), 140 s (motor) (Stippich et al. 2002b), and 234 s (language) (Stippich et al. 2003b). Reproducibility of functional localization and BOLD signal during one MR session as well as on different examination days is high. However, due to the persisting lack of consensus on the performance of clinical fMRI examinations, it is not yet possible to make definitive recommendations on how these should be carried out – thus, we also allude the reader to the large body of data available on this field (see Sects. 4.1 and 5.1).

Examination times in the clinical neuroimaging routine are in general limited and rarely exceed 1 h. Within this time, the entire stimulation equipment needs to be set up at the scanner and subsequently dismantled (Fig. 3). Positioning of the pre-trained patient for MRI is more time consuming than

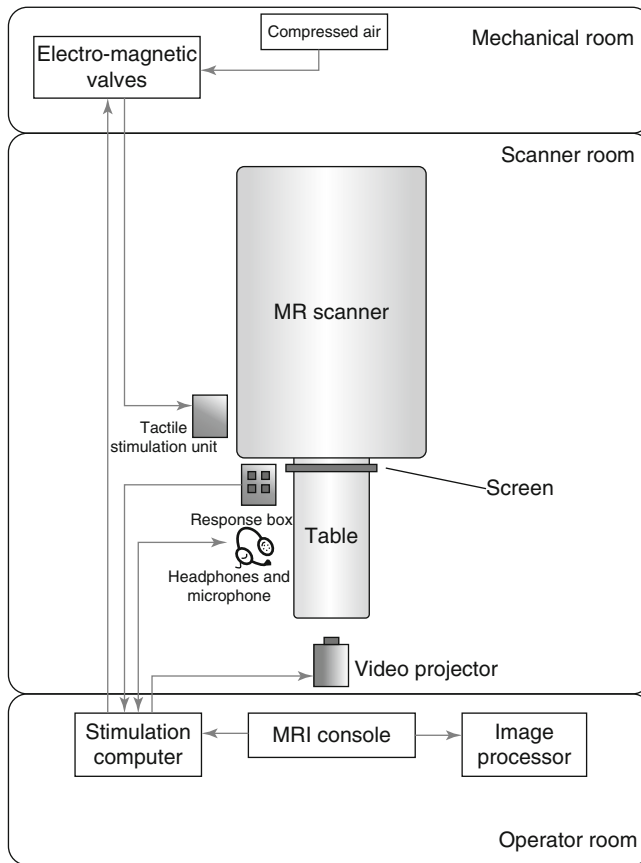


Fig. 3 Scheme of a typical fMRI setup. Electrical equipment placed inside the scanner room requires sufficient shielding. Test measurements should be performed to exclude imaging artifacts. For all electrical stimulation devices and critical metal implants, safety measurements on phantoms are recommended (Georgi et al. 2004; Akbar et al. 2005)

preparation for routine morphological MR imaging. Head fixation should be optimized to reduce motion artifacts and all stimulation devices have to be installed and calibrated (Figs. 4 and 5). Once all is set up, a final performance test prior to the beginning of the fMRI examination is strongly recommended – that is, each patient should shortly repeat the task inside the scanner under supervision of the investigator. In general, all clinical fMRI measurements should be closely monitored by the investigator to document errors arising while the paradigms are carried out. For this reason, our investigators remain in the scan room or observe the patient from outside while the motor paradigms are carried out by the patients. For language fMRI, the patient is asked immediately after each measurement for correct task performance before initiation of the next task. This is also recommended for clinical fMRI of other cognitive functions, such as memory. These brief post-scan interviews are also important to document incorrect task performance accounting for the sometimes unavoidable and time-consuming manual post-processing of erroneous data from patients who are difficult to examine. However, erroneous measurements should be immediately repeated, whenever possible.

The results of clinical fMRI measurements usually need to be already available on the examination day in order to ensure that fMRI data can be considered in the early therapeutic decision-making process. Traditionally, fMRI data are processed right after the fMRI examination (offline) using freely available or commercial software (Cox 1996; Friston 1996; Gold et al. 1998; Roberts 2003). By now, most clinical high-field MR scanners offer optional programs for an immediate “online” processing of the fMRI data (Fernandez et al. 2001; Moller et al. 2005), known as “real-time fMRI” (see Sect. 4.1). The functionality of the different existing “real-time fMRI” software packages is variable and the choice of the appropriate programs is usually made on the basis of individual criteria. However, any data processing software for fMRI should at least include image alignment, motion correction, temporal and spatial data smoothing, and multiple statistical tests to assess functional activation (see chapter “[Revealing brain activity and white matter structure using functional and diffusion-weighted magnetic resonance imaging](#)”). It is also important to note that tools for superimposition of the functional images on morphological images and for data export (e.g., neuronavigation) are essential in presurgical fMRI, whereas the capabilities for spatial normalization can be considered as optional. Of note is that the use of software not certified for medical applications should be avoided for intraoperative applications, for example, for neuronavigation or radiation therapy. On the other hand, research software tools often provide better access to the different underlying data processing steps, which may be relevant for the meaningful interpretation of clinical fMRI data. As a consequence it may be necessary to perform the data analysis in parallel using different software, one dedicated to medical application and one dedicated to research, at least until better solutions become available.

Since no widely accepted guidelines or recommendations for the evaluation and interpretation of clinical fMRI have been released outside the USA, appropriate imaging protocols and criteria for the diagnostic interpretation often need to be defined by the individual institutions. As an important step towards a more standardized diagnostic application of fMRI, the American Society for Functional Neuroradiology (ASFNR) has recently published a set of paradigms that are feasible for clinical application (for details please visit the ASFNR homepage; <http://www.asfnr.org/paradigms.html>). The proposed paradigms cover motor, somatosensory, language, and memory function as well as vision. They are of special value for clinical neurocenters which intend to start with presurgical fMRI, wish to adopt their existing imaging protocols, or aim to participate in currently ongoing multi-center trials.

However, most larger medical centers offering clinical fMRI studies still use their own internal routines today, which are typically the result of a longstanding own “evolutionary” process and thus of specific in-house expertise.



Fig. 4 Typical equipment for visual stimulation. (a) High-resolution video beamer. As for all electronic devices, placement of the device outside the scanner room should be preferred to avoid imaging artifacts.

(b) Semitransparent projection screen mounted to the scanner bore. (c) Commercial mirror system for back projection mounted on the head coil (Reprinted from Stippich 2005, 2010, with permission)



Fig. 5 Fully automated pneumatically driven tactile stimulation. Flexible membranes (4D Neuroimaging, Aachen, Germany) connected to pressure-resistant pneumatic tubes transmit the stimuli to the lips, fingers, or toes (not shown). *Upper left:* the 24-channel high-precision electromagnetic valve system was designed to investigate somatosensory somatotopy (Reprinted from Stippich 2005, 2010, with permission)

An intrinsic advantage of this situation is the thorough understanding of the whole process associated with presurgical fMRI between the different medical partner disciplines involved (neuroradiology, neurosurgery, neurology, radio- and neurooncology, etc.). This highly interdisciplinary process of using presurgical fMRI includes the following:

1. FMRI indication, data acquisition, analysis, and diagnostic interpretation
2. Clinical decision-making also considering fMRI (and DTI) results
3. Planning of an optimal treatment tailored to the specific findings in each individual patient
4. Detailed information of the patients about the desired treatment, its side effects, other possible consequences, and therapeutical alternatives
5. Application of the optimized treatment based on profound knowledge of its methodological and medical limitations
6. Assessment of the posttherapeutic outcome with respect to the pretherapeutic findings

On the other hand, this methodological variability considerably affects the comparability of fMRI studies between different investigators, especially when it is about imaging cognitive brain function (e.g., language or memory). As a consequence the following sections provide recent and in-depth information on legal, methodological, technical, and medical aspects to implement and employ state-of-the-art presurgical task-based fMRI.

3.2 Legal Aspects

Today, there exist a substantial body of evidence that task-based BOLD fMRI is robust, valid, and reasonably precise to localize different cortical representations of the human body within the primary motor and somatosensory cortices, to localize essential motor and receptive language areas, and to determine language dominance prior to brain surgery. More and more stimulation devices and software solutions have become commercially available that facilitate the clinical application of fMRI and that have been certified for medical use. However, fMRI can still not be considered as a standard routine application in clinical diagnostic neuroimaging, since in most countries worldwide (except for the USA), no recommendations or guidelines have been issued by the responsible domestic medical associations. Until then, individual routine procedures and standards need to be established for measuring techniques and examination protocols, data processing, and evaluation, as well as for medical evaluation and documentation of clinical fMRI findings. Validation of preoperative fMRI using established reference procedures (e.g., ECoG, Wada test) (Spritzer et al. 2012; Janecek et al. 2013) by the operator is indispensable, even if the examination protocols suggested in this book are used. As a prerequi-

site clinical fMRI examinations should be performed, evaluated, and interpreted by trained and experienced investigators with particular expertise in this area, since careless use of this very promising technique could endanger patients.

3.3 Evaluation of Presurgical fMRI Data

Presurgical fMRI examinations are always carried out in individual patients with the primary goal of an individual “functional” diagnosis. To achieve this, the surgically relevant brain areas need to be reliably localized and their spatial relationship to the brain tumor or epileptogenic zone accurately identified. Precise localization of the anatomical correlate of the center of gravity of a functional area (focus of activation) and correct naming of the corresponding anatomical structure (gyrus) are of utmost importance, as far as the pathology allows. When determining the language-dominant hemisphere, limitations of the method need to be considered (see Sect. 6).

The use of dynamic statistical thresholds in the data processing helps to reliably localize functional brain areas and to provide defined BOLD signal readings (see Sect. 3.4). Regardless of the software used and of the level of automation achieved, the superposition of the intrinsically distorted echo-planar MR-images (EPI) onto anatomical 3D data sets and the definition of the appropriate display parameters for intraoperative representation of the functional data remain manual procedures. Just like the medical evaluation and documentation of clinical fMRI findings, they require a certain level of experience of the investigator. These investigator-related factors in particular underline the need for the establishment of standardized fMRI protocols, data processing strategies, and evaluation procedures to achieve a consistent quality among the clinical fMRI examinations.

In general, it is important to note that the *spatial extent* of a functional brain area cannot be reliably and accurately determined with BOLD fMRI, since the extent of the local signal display varies according to the statistical threshold chosen for data evaluation (of note, the same applies to DTI-tractography regarding the size and extent of important white matter tracts). Therefore, defining resection margins on the basis of BOLD activations alone is not safe enough and should not be permitted until sufficient data from prospective clinical trials on this topic are available. In addition, the spatial coordinates of the focus of activation change with the statistical threshold as well as with the cluster size and BOLD signal (Fig. 6). When evaluating clinical fMRI data, the use of one or more predetermined (fixed) statistical thresholds – a common approach in research fMRI – does not solve the problem, since BOLD signal intensities and cluster sizes differ significantly between single patients and different paradigms (e.g., foot movement, hand movement), respectively, even if the examinations are carried out in a standardized way. This holds also true for different fMRI measurements per-

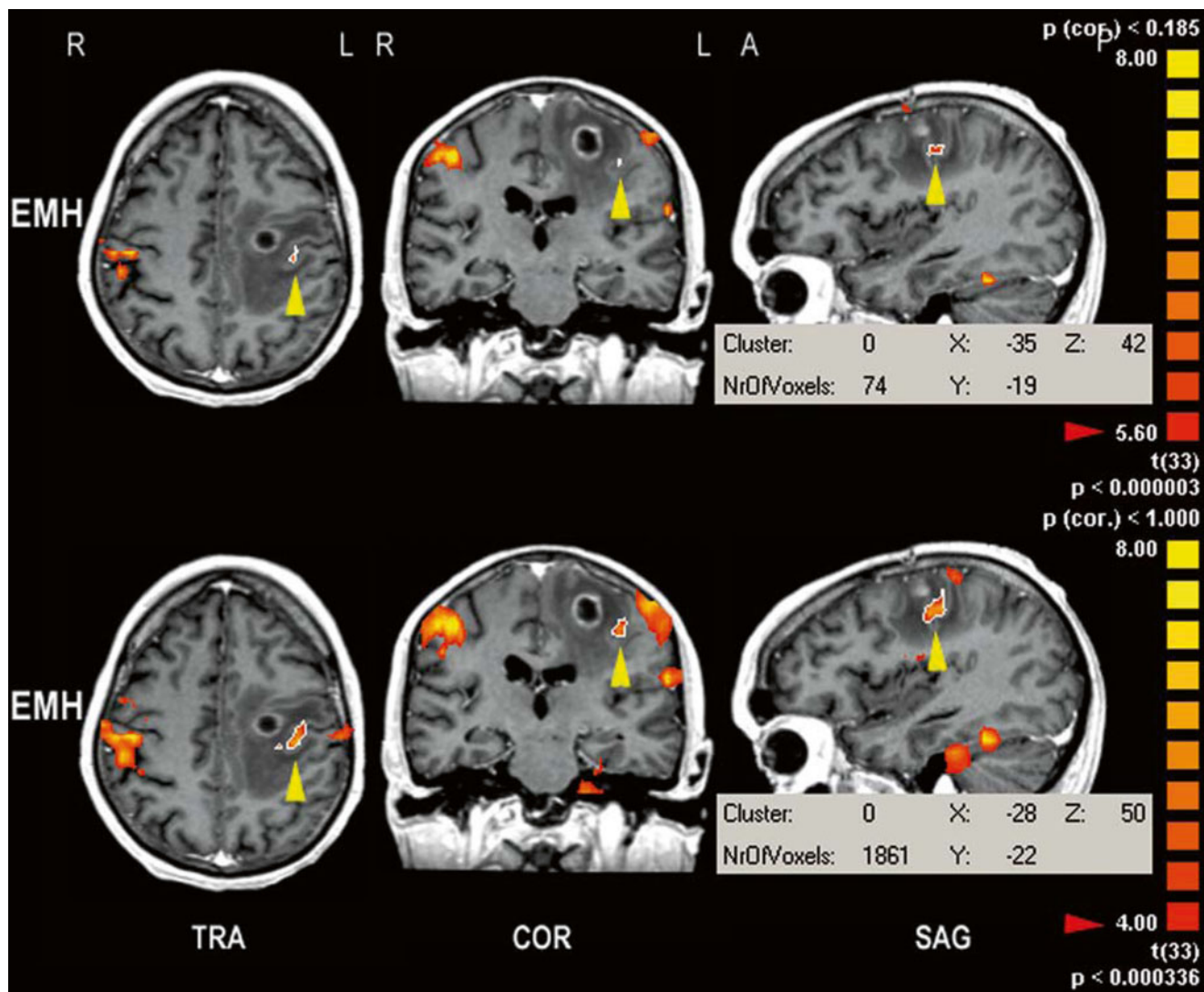


Fig. 6 Influence of the statistical threshold on spatial extent and localization of the center of gravity of BOLD fMRI activation. With decreasing statistical threshold, BOLD clusters increase in size and show a marked shift of spatial coordinates (please compare *upper and lower rows*). The yellow arrowheads indicate primary sensorimotor

activation obtained from contralateral finger opposition in a hemiparetic patient; red arrowheads indicate the statistical threshold used to display functional activation. Gray boxes: spatial coordinates (x , y , z) of the center of gravity of BOLD clusters (cluster size in mm^3 , 1 voxel = 1 mm^3)

formed in the same patient, regardless whether they are acquired on different days or within the same scanning session. More importantly, inaccuracies in localizing functional cortical representations may mislead the neurosurgeon with respect to presurgical assurance, a security which in reality is unfounded and could consequently put the patient at risk. This problem can be overcome by the adaption of the individual fMRI analyses on the basis of clearly defined criteria using dynamic statistical thresholding (Fig. 7), (see Sect. 3.4).

Determination of the dominant hemisphere with fMRI is at least equally challenging. Typically, activated voxels in defined target regions in both hemispheres (e.g., Broca's and Wernicke's areas and their anatomically homologous areas in the contralateral hemisphere) are counted at a particular statistical threshold, upon them lateralization indices (LI) are

calculated from interhemispheric quotients (Stippich et al. 2003b). This procedure has intrinsic problems for several reasons: (1) The BOLD activation measured depends on the paradigm used, but the application of several different paradigms for the identification of language-related brain areas has proven to be more reliable to localize and lateralize language as compared to the application of one single paradigm alone (Ramsey et al. 2001; Rutten et al. 2002c; Zacà et al. 2013). In addition, some linguistically different paradigms do better account for the complexity of language assessment in presurgical fMRI. The single results of the various paradigms are rarely identical, but often congruent. There are, however, no scientific data indicating how conflicting results should be medically interpreted. (2) BOLD activation varies independently between hemispheres if the frequency of

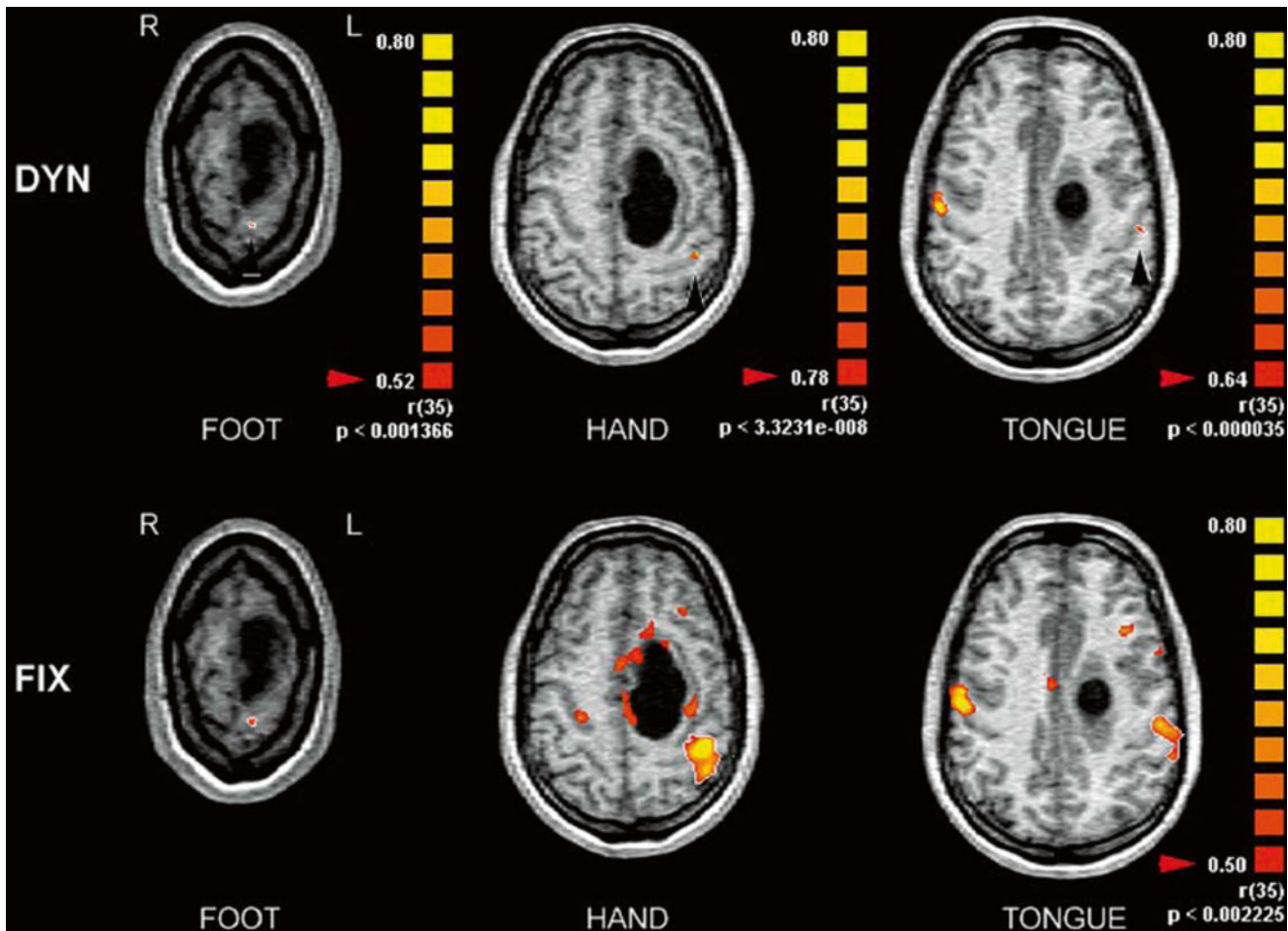


Fig. 7 Comparison of dynamic thresholding (DYN, *upper row*) and fixed thresholding (FIX, *lower row*) in somatotopic mapping of the left primary sensorimotor cortex. Dynamic thresholding enables to adapt the data evaluation to different fMRI measurements in a standardized way. Using the empirically proven cluster size of 36 mm^3 as a standard for data evaluation allows to achieve well-outlined fMRI activations (*black arrowheads*) and enables to precisely assess their anatomical correlates and spatial coordinates as well as to measure BOLD signals under defined conditions (r = correlation of the measured BOLD signals

stimuli is varied, even when the same paradigm is used (Konrad et al. 2005). This means that the lateralization measured depends on both the statistical threshold chosen and the “cerebral workload” associated with the respective task. (3) In contrast to imaging modalities based on ionizing radiation (e.g., CT), MRI yields “relative” rather than “absolute” measurements, so that the results of BOLD fMRI have to be interpreted semiquantitatively. (4) Brain tumors induce neuroplastic changes which may affect motor (Tozakidou et al. 2013) and language lateralization (Partovi et al. 2012a). A right-sided language dominance, for example, as calculated based on preoperative fMRI data in patients with brain tumors affecting the language system, does not mean that the (relatively) reduced language activation in the left hemisphere is no longer essential to maintain language function. The same holds true for the reduced primary motor activa-

tion in rolandic lesions. In contrast, the functional reorganization in these patients reflects the brain’s attempts to functionally cope with the brain tumor. Consequently, tumor-induced altered functional lateralization, which is reproducible in different paradigms, should therefore be considered as an indicator for very “watchful” resections. In such situations, additional intraoperative measures (ECoG) and/or awake craniotomies may even be considered.

In spite of the limitations mentioned, fMRI yields – in the vast majority of patients – important diagnostic information noninvasively which is otherwise unavailable. Functional landmarks facilitate pretherapeutic assessment of the most functional-sparing therapy upon a careful consideration of the benefits and risks, as well as the planning and execution of function-preserving interventions. At the same time, preoperative fMRI has the potential to better prove the indica-

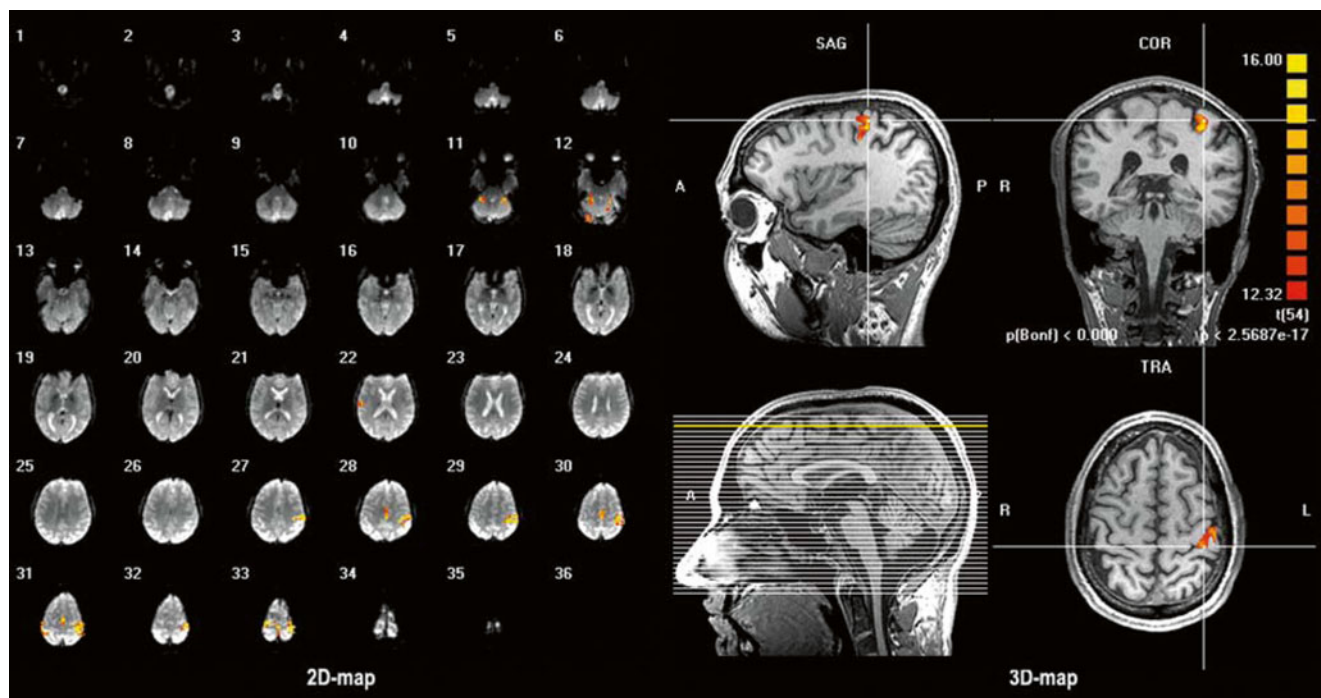


Fig. 8 Overlay of 2D fMRI activation maps (left) on anatomical 3D data sets (right, bottom left) results in 3D fMRI activation maps (right) that are typically used for diagnostic presurgical fMRI. This is usually a manual procedure and requires sufficient experience of the examiner to

tion and reduce the number of invasive diagnostic procedures, such as the Wada test or ECoG, either before or during neurosurgery. However, at this stage fMRI cannot fully replace these invasive measures and should therefore be considered as a supportive diagnostic modality playing a major role in the pretherapeutic tumor assessment.

3.4 Analyzing fMRI Data in Individual Patients

Defining standard analysis processes is a significant prerequisite for the medical interpretation of clinical fMRI data, alongside standardized clinical examination protocols, defined reference values, and automated data processing. These are the minimum requirements if clinically diagnostic information is to be gleaned from fMRI. Diagnostic and pretherapeutic evaluation of non-standardized fMRI examinations in “interesting” patients is highly inadvisable and may put the patients at risk.

A number of freely available and commercial programs are available for fMRI data processing and evaluation (Cox 1996; Friston 1996; Gold et al. 1998; Roberts 2003). Due to the diversity of these programs and the varying requirements and preferences of the individual user, no program can be recommended in particular. The following three-step procedure using dynamic thresholding has been developed for BrainVoyager (BV) but is transferable to other programs.

cope with the distortions of the functional EPI-images and other imaging artifacts (movement artifacts, BOLD signal of venous origin, etc.). The fit should be optimized to the different anatomical structures of interest in patients with rolandic, frontal, or temporoparietal brain tumors

Preprocessing (step 1, for details see chapter “[Revealing brain activity and white matter structure using functional and diffusion-weighted magnetic resonance imaging](#)”): Any interpretation of clinical fMRI data should begin with processing of the raw data, including at minimum image alignment, correction of motion artifacts, and temporal-spatial smoothing. Generally, functional activation maps are then calculated on the basis of a number of successive images (2D fMRI maps), for which various statistical processes can be alternatively used [e.g., t -test, cross correlations, general linear model (GLM), etc.]. As a basic principle, a reference function corrected for the delayed hemodynamic response should be used. A volume map of activations (3D fMRI maps) can be calculated following (manual) superposition of the EPI image layers onto anatomical 3D data sets (Fig. 8). The minimal number of voxels within a cluster to be shown can be freely predetermined, but should be standardized. On the basis of empirical experience, we consider a cluster size of 36 mm^3 appropriate and define this as a standard parameter for all 3D analyses. On the one hand, randomly scattered activations are barely shown at this cluster size; on the other hand, clusters are not so large that small anatomic details are obscured. When defining own standards, it should be borne in mind that the representation of the clusters also depends on spatial smoothing.

Dynamic thresholding (step 2): This evaluation process for individual fMRI data typically begins at the maximal statistical threshold, so that no activation is displayed (empty map). The statistical threshold is then progressively lowered,

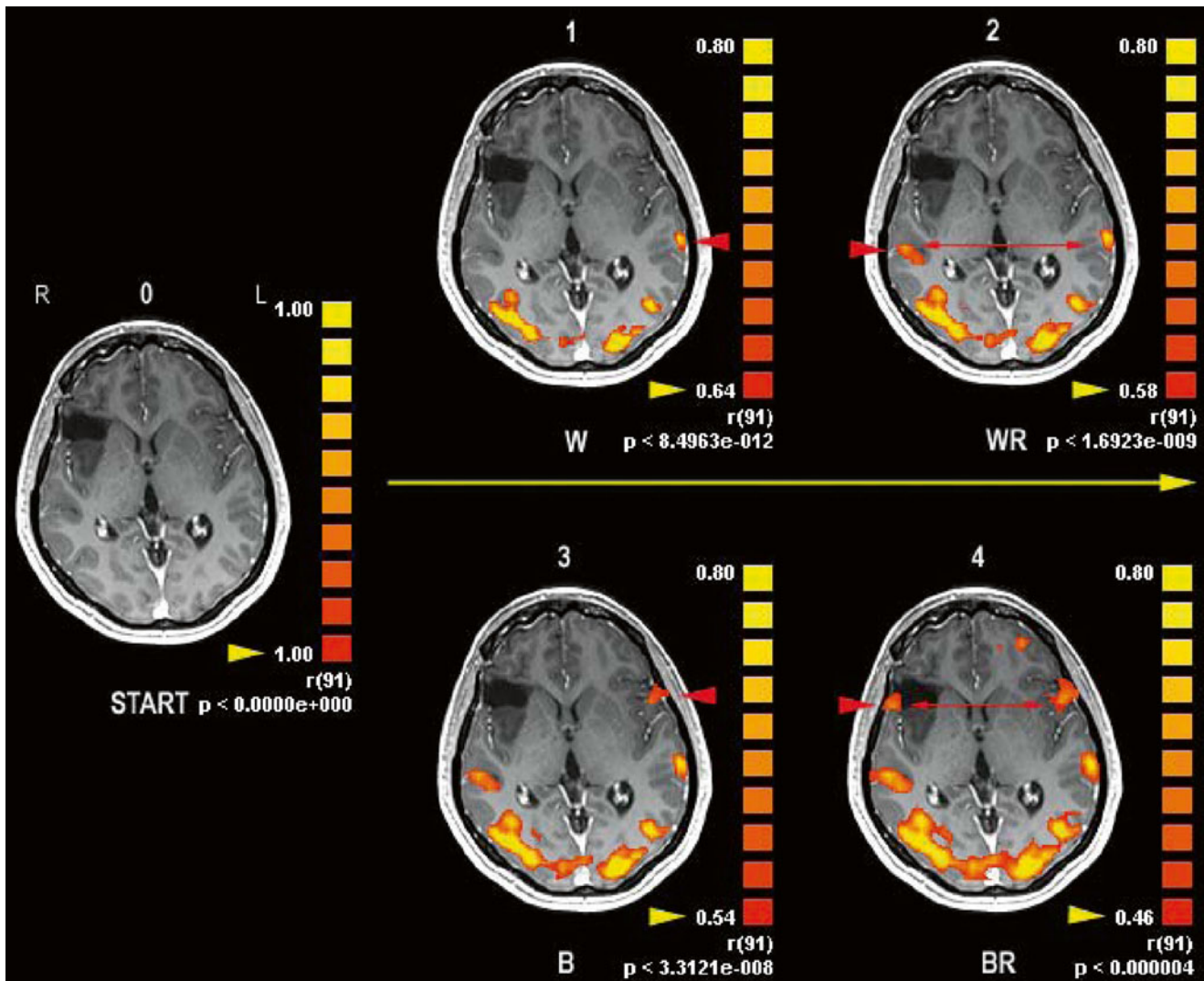


Fig. 9 Dynamic thresholding: evaluation routine for individual clinical fMRI data. Continuous reduction of the statistical threshold (yellow arrowheads) results in a hierarchy of different functional activations (red arrowheads) associated with a given task (e.g., word generation). The starting point (0) is at the maximum statistical threshold ($r=1.00$) where no activation is displayed. Wernicke's activation (W) correlates best with the hrf (1, $r=0.64$) followed by WR (2, $r=0.58$), B (3,

$r=0.54$), and BR (4, $r=0.46$). Regional lateralization indexes (LI) are calculated from BOLD cluster sizes in corresponding functional brain areas in the left and right hemisphere (red double headed arrows). Empirically proven default parameters: clustersize $>35 \text{ mm}^3$, correlation to the hrf: $r>0.4$ with $p<0.05$. Note the strong occipital activation related to the visual trigger presentation

until an activation is detected, which best correlates with the hemodynamic reference function (HRF). Much like the tip of an iceberg, this activation is small and well outlined, in such a way that the anatomic correlate of the activation focus and the spatial coordinates can be accurately determined. The associated correlation of the measured BOLD signal to the HRF (r), the relative BOLD signal changes ($\Delta S\%$), and the cluster size can be measured under defined conditions. By further reducing the statistical threshold, activations in other functional areas appear, to which the measurements mentioned can be applied (Stippich et al. 2000, 2003a, b, 2007a, b; Stippich 2010). Thus, for each fMRI data set there is an individual hierarchy of the various functional activa-

tions associated with the applied paradigm. Simultaneously, the size of clusters already shown on a higher statistical level increases with decreasing threshold. This can be used to determine the dominant hemisphere by calculating the lateralization index according to the established formula $LI = (LH - RH) / (LH + RH)$, where "LH" is the number of voxels in the left and "RH" the number of voxels in the right hemisphere (Stippich et al. 2003b; Partovi et al. 2012a, b). Due to the well-outlined clusters separate LIs can be calculated, for example, for the Broca's and Wernicke's speech areas, enabling a highly detailed analysis of atypical language activation as, for example, influenced by the presence of a brain tumor (Fig. 9). In order to reliably distinguish the measured

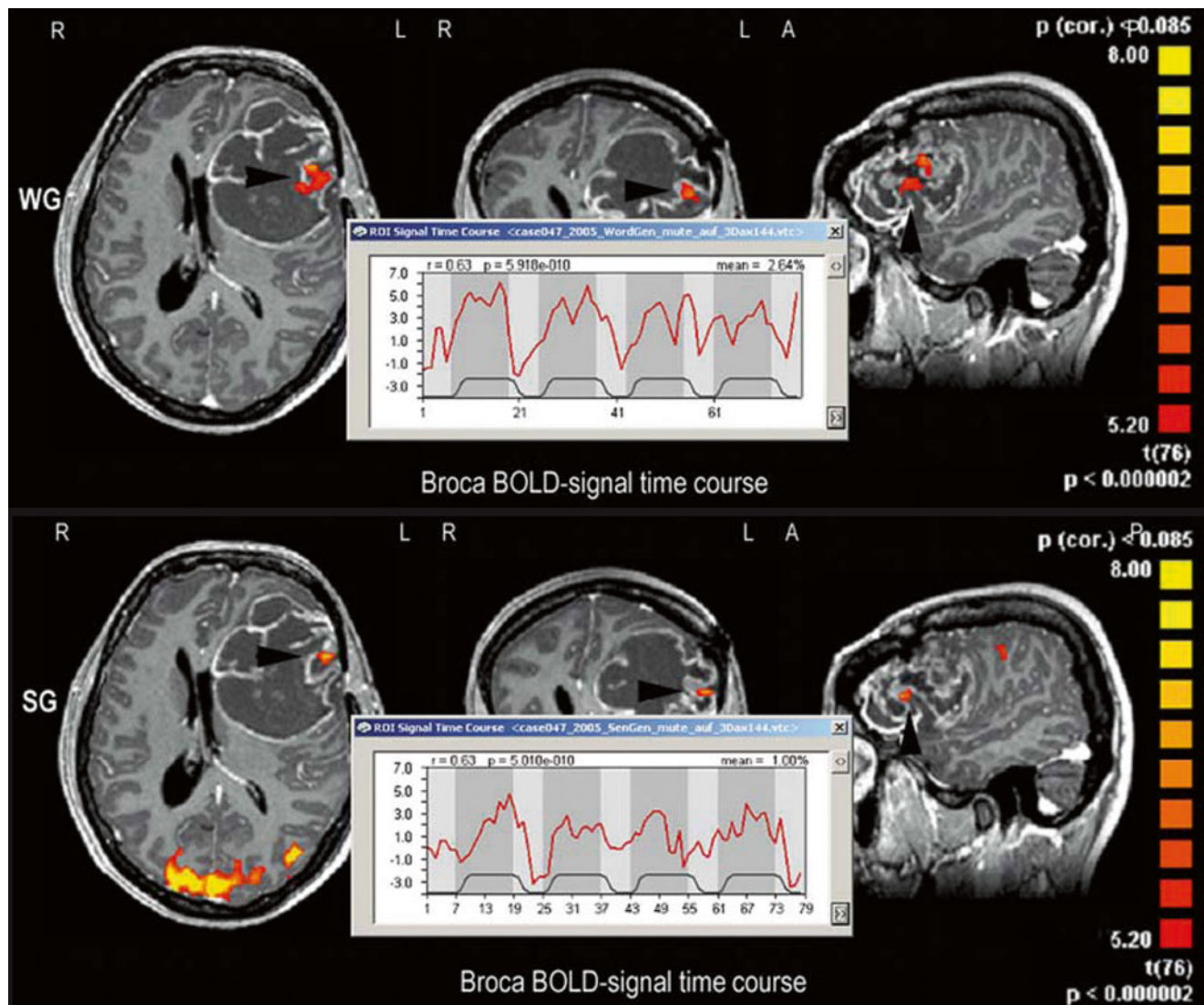


Fig. 10 Measuring BOLD signals under defined conditions helps to distinguish between “true” activation and “artifacts.” In this left-handed patient with a giant left frontal high-grade glioma (WHO grade IV), presurgical fMRI was performed to assess language dominance. fMRI indicated left dominance and functional tissue directly adjacent to the

malignancy. Good reproducibility of the functional localization of Broca’s area using two different paradigms (WG word generation, SG sentence generation) and “physiological” BOLD signal parameters (WG: $r=0.63$, $\Delta S=2.64\%$, SG: $r=0.63$, $\Delta S=1.00\%$) made artifacts unlikely

BOLD signals from noise, $r>0.5$ for motor and language function or $r>0.4$ for somatosensory brain activation have empirically been proven as appropriate lower threshold limits, each with $p<0.05$. Alternatively, or additionally, an error rate can be determined which should not be exceeded in order to evaluate a BOLD activation as “real,” for example, a false discovery rate (FDR) <0.001 (0.1 %).

Checking BOLD signal characteristics (step 3, for details see chapters “[Revealing brain activity and white matter structure using functional and diffusion-weighted magnetic resonance imaging](#)” and “[Clinical BOLD fMRI & DTI: artifacts, tips and tricks](#)”): Measuring BOLD signals under defined conditions can help to separate real activations from

artifacts. Both the correlation with HRF (r) and the signal intensity ($\Delta S\%$) should remain within normal range (Fig. 10). Unphysiologically high signal intensity can arise from activation of “venous” origin – an assumption supported by a sulcal localization of the cluster focus – or by motion artifacts. In the latter case, the strongest usually ring-shaped activations tend to occur in the frontal circumference of the brain opposite the supporting point of the head (occipital). Depending on the dominant motion components, other localizations may also account for erroneous signal. Here, the onset of the measured signal time course corresponds better to the boxcar function of the block design than to the HRF (for details see chapter “[Clinical](#)

BOLD fMRI & DTI: artifacts, tips and tricks”). A reduction or loss of BOLD signal can occur in functional areas compressed or infiltrated by a tumor by limiting the capability of the affected brain tissue to hemodynamically respond to the applied stimulation. Also, the opposite effect has been observed in highly vascularized pathologies, such as arteriovenous malformations that may induce a “steal phenomenon” in the respective functional areas.

4 Presurgical fMRI of Motor and Somatosensory Function

Surgery on rolandic brain tumors entails a high risk of motor and sensory deficits. Task-based fMRI of motor function is the most frequently used presurgical application due to the comparatively low equipment requirements for this examination (no stimulation devices are necessary), the relative ease with which it is performed, and the generally stable functional activation. The diagnostic aim is to localize the primary motor cortex in relation to rolandic tumors. On the basis of morphological MR imaging and clinical findings (motor and/or sensory deficits), the indication for presurgical fMRI should be assessed (see Sect. 4.2) and the appropriate examination protocol individually adjusted (see Sects. 4.4, 4.5 and 4.6). Even patients with tumor-associated pareses can be examined using special paradigms (see Sects. 4.5 and 4.6). According to the site and extent of the tumor, a single fMRI reading can suffice. However, it is often necessary to examine the entire motor and, where appropriate, somatosensory somatotopy. Today, presurgical localization of various body representations in the pre- and postcentral gyrus by fMRI can be considered reliable (see chapter “**Presurgical functional localization possibilities, limitations and validity**”). Even neuroplastic changes (Baciu et al. 2003; Bogomolny et al. 2004; Peck and Holodny 2007; Kasprian and Seidel 2010; Holodny et al. 2011; Tuntiyatorn et al. 2011; Tozakidou et al. 2013) can be examined, although in the presence of brain tumors, shifts in different body representations can be observed as well as changes in functional hemispheric lateralization and in activation of secondary cortical areas (see chapter “**Brain plasticity in fMRI & DTI**”).

4.1 Review of Literature

Shortly after the first reports on BOLD fMRI in healthy subjects (Belliveau et al. 1991; Bandettini et al. 1992; Kwong et al. 1992; Ogawa et al. 1993), the potential usefulness of functional imaging techniques in the clinical context and particularly in the presurgical identification of motor and somatosensory cortices was postulated. The literature concerning functional imaging in patients with

tumoral lesions in and adjacent to the “central” or synonymously “rolandic” region will be reviewed here, while specific literature on patients with epilepsy or lesions near language-related areas will be discussed in Sect. 5.1 and in chapter “**Presurgical EEG-fMRI in epilepsy**”. The first description of presurgical fMRI as a clinically useful application dates from 1994, when Jack et al. provided proof of concept in two patients with brain tumors in the sensorimotor cortex, validating their preliminary results with established electrophysiological techniques (Jack et al. 1994). Soon after, several case studies (Baumann et al. 1995) (Cosgrove et al. 1996) and reports on small patient populations (Puce et al. 1995, 1996; Mueller et al. 1996; Krings et al. 1998) harboring glial tumors or arteriovenous malformations (AVM) confirmed the technical and practical feasibility of fMRI using motor and sensory tasks in the clinical context and stressed the high potential of this new upcoming technique for preoperative risk assessment, therapeutic decision-making, and surgical planning.

During the following years investigations on larger numbers of tumor patients (up to 50) were carried out, whose results had been claimed to represent an important factor for surgical decision-making (Schlosser et al. 1997; Pujol et al. 1998). Comparisons of presurgical fMRI data with the established reference procedure, intracortical stimulation (ICS), are numerous, and only those specifically dealing with brain tumor patients will be mentioned here, since a detailed description of validation studies referring to this is offered in chapter “**Presurgical functional localization possibilities, limitations and validity**”. Virtually all studies report highly concordant results between presurgical fMRI and ICS data in patients with lesions around the central sulcus (Dymarkowski et al. 1998; Achten et al. 1999; Roux et al. 1999a, b) with an accordance ranging from 83 % in 33 patients (Majos et al. 2005) to 92 % in 60 patients (Lehericy et al. 2000b). Task sensitivity for the identification of the sensorimotor region estimated in large groups of tumor patients was 85 % in 103 patients (Krings et al. 2001) and 97 % in 125 patients (Hirsch et al. 2000). Furthermore, it should be briefly noted that various groups focused on the correlation of fMRI results in patients with central lesions with those of other functional imaging procedures, for example, PET (Bittar et al. 1999); for details please refer to chapter “**Multimodality in functional neuroimaging**”.

One of the first attempts to evaluate the impact of fMRI on neurosurgical planning was published by Lee et al. The authors applied preoperative fMRI sensorimotor mapping in 32 tumor patients and report that the results were used to determine the feasibility of surgical resection in 55 %, to aid in the surgical planning in 22 %, and to select patients for invasive intraoperative functional mapping in 78 %. Overall, the fMRI results were useful in one or more of these surgical decision-making categories in 89 % of all examined tumor

patients (Lee et al. 1999). Similar numbers were described by Ternovoi et al. who found that presurgical fMRI results had an influence on therapeutic strategies in 69 % of 16 tumor patients (Ternovoi et al. 2004). Other investigators tried to establish a functional risk prediction (or estimation) for postoperative clinical outcome: Haberg et al. examined 25 patients with primary brain tumors in the near of sensorimotor regions. In 80 % of the patients, successful fMRI measurements were obtained, out of which 75 % were used for preoperative planning. The risk of postoperative loss of function was significantly lower when the distance between the tumor margin and the BOLD activation was 10 mm or more (Håberg et al. 2004). Similar observations have been described by Berntsen et al. (2010). Krishnan et al. who evaluated BOLD activation in 54 patients found that a lesion-to-activation distance of less than 5 mm and incomplete resection were predictors for new postoperative neurological deficits and recommended cortical stimulation within a 10 mm range, given that for a lesion-to-activation distance of >10 mm a complete resection can be safely achieved (Krishnan et al. 2004). In patients with medial frontal lesions, preoperative fMRI was used to establish the area at risk for the resection of specific parts of the supplementary motor area associated with transient postoperative motor deficits and speech disorders (Krainik et al. 2001, 2003, 2004). In a further study, Hall et al. used fMRI-guided resection in 16 patients with low-grade gliomas. Since these tumors are generally not contrast enhancing, resection borders are particularly difficult to define based on morphological imaging alone. Using fMRI for the determination of resection borders, no permanent neurological deficits and no radiological tumor progression within a median follow-up of 25 months were observed (Hall et al. 2005). However, the data available to calculate a safe resection distance between functional activation and lesion borders for prevention of surgically induced neurological deficits are still very limited and do not justify any general conclusion or recommendation (Gil-Robles and Duffau 2010).

Overall, although the abovementioned studies clearly demonstrate the feasibility of presurgical fMRI in the clinical environment and militate for the preoperative contribution of the additional clinical information obtained from fMRI to pretherapeutic decision-making, an effect on the decrease in the posttherapeutic morbidity has not been corroborated yet. In order to achieve this, controlled clinical trials using optimized and standardized protocols would be required. Although most investigators agree on the necessity of a standardized procedure in the clinical routine and several methodological studies presenting optimized protocols for the clinical use have been published (Hirsch et al. 2000; Ramsey et al. 2001; Rutten et al. 2002a, b, c, d; Springer et al. 1999; Stippich et al. 2000, 2002b, 2004, 2005), no large-scale clinical trials addressing the actual benefit for the

patient in terms of decrease in morbidity have been published so far.

Although sensorimotor areas are identified with high success rates using fMRI in patients with central lesions by most investigators, a frequently encountered phenomenon is neuroplasticity (Tuntiyatorn et al. 2011; Tozakidou et al. 2013) which is also found in the language network (Stippich et al. 2007b; Partovi et al. 2012a; Briganti et al. 2012; Rösler et al. 2014). In an early study in seven patients with intracerebral gliomas of the primary sensorimotor cortex, activation was found to be displaced or reduced (Atlas et al. 1996). Roux et al. correlated the type of activation with histologic tumor characteristics in 17 patients. In infiltrating tumors, intratumoral activation was detected, which was displaced and scattered, and correlated with the degree of infiltration, whereas in noninfiltrating tumors activation showed extra-tumoral shift. In tumors at some distance from the motor cortex, no intratumoral activation was measured (Roux et al. 1997). Likewise, a PET study on 51 patients described that central lesions were more frequently associated with altered patterns of activation than lesions in noncentral locations (Bittar et al. 2000). Other studies found significant BOLD signal decrease in areas adjacent to tumor tissue in motor and sensory cortices as compared to the contralateral side. This effect was present in glial tumors, most pronounced in glioblastoma, and presumably related to tumor-induced changes in local cerebral hemodynamics (Holodny et al. 1999, 2000; Schreiber et al. 2000; Krings et al. 2002a; Ludemann et al. 2006; Jiang and Krainik 2010; Tozakidou et al. 2013), while in non-glial tumors (metastasis, cavernoma, abscess, AVM,), no BOLD signal decrease was found (Schreiber et al. 2000). A report on 33 patients with different intra- and extra-axial tumors established the influence of tumor type and distance from the eloquent cortex on activation volumes in fMRI (Liu et al. 2005). In addition to a displacement or a reduction of activation in the primary sensorimotor cortex harboring the tumor, other patterns of lesion-induced reorganization encompass the activation of solely the contralesional cortex (Tozakidou et al. 2013) or an enhanced activation of non-primary sensorimotor areas with increasing degree of paresis (Alkadhi et al. 2000; Carpentier et al. 2001b; Krings et al. 2002b; Reinges et al. 2005). Also in patients with prior surgery (Kim et al. 2005) or newly developed central paresis after tumor resection (Reinges et al. 2005), a significant decrease in BOLD activation was observed. One possible explanation for this tumor-induced BOLD signal loss has been proposed by an fMRI study where tumor blood volume and perfusion were measured. The authors concluded that the BOLD amplitude correlated with total intratumoral blood volume and thus reduced peritumoral perfusion due to a sucking effect by the tumor core (i.e., blood is siphoned off by the tumor similar to the steal phenomenon known from AVMs) was responsible for the reduced BOLD activation (Ludemann et al. 2006; Jiang

and Krainik 2010). Of note is, however, that resection of gliomas whose preoperatively acquired images show perilesional hyperintensity on T2w images, likely reflecting edema, may cause a transient increase in BOLD activation ipsilateral to the tumor, presumably by a decrease of perfusion pressure on the brain tissue adjacent to the resection (Kokkonen et al. 2005). Lesion-induced functional reorganization may reflect the recruitment of plastic neuronal networks to compensate for sensory or motor impairment. On the level of a functional diagnosis in presurgical fMRI, these reorganization phenomena are of major clinical significance for the presurgical planning of resections, since they can potentially cause false-negative results. For further information, please refer to chapter “**Brain plasticity in fMRI & DTI**” on brain plasticity.

In the last decade, the use of combined presurgical fMRI and diffusion tensor imaging (DTI) (see Sect. 6) for tractography has been suggested to provide a better estimation of the proximity of the tumor borders to the eloquent cortex than fMRI measurements alone. In particular for space-occupying lesions affecting the central region, visualization of the origin, direction and functionality of large white matter tracts allowing imaging of functional connectivity were promoted to improve surgical outcome and to aim for a decrease in patient morbidity (Parmar et al. 2004; Ulmer et al. 2004; Shinoura et al. 2005; Stippich et al. 2003a, 2010; Holodny et al. 2001; Wengenroth et al. 2011; Jia et al. 2013; Kumar et al. 2014).

In the last years, the first reports on the application of real-time fMRI (Feigl et al. 2008) in the clinical environment have been published. This rather novel technique enables quick preliminary online analysis of fMRI data, which is particularly useful in presurgical diagnostics, considering that fMRI data acquisition and processing are very time consuming. Möller et al. demonstrated the technical feasibility of presurgical real-time fMRI in ten patients with tumors in the central area immediately prior to surgery Moller et al. (2005). In another study, motor and language tasks were used for real-time fMRI in 11 tumor patients. The authors reported satisfactory activation for hand motor tasks, weaker activation for foot motor tasks, and no useful activation for language tasks at the chosen threshold, concluding that real-time fMRI needed to be optimized, but was generally practicable in the clinical routine (Schwindack et al. 2005). Furthermore, Gasser et al. could obtain the recording of intraoperative fMRI in four anesthetized patients with lesions in the vicinity of the central region. Using a passive stimulation paradigm and analyzing the data during acquisition by online statistical evaluation, they could identify eloquent brain areas taking into account intraoperatively occurring brain shift (Gasser et al. 2005). For further details on intraoperative imaging techniques

and the specific problems caused by intraoperative brain shift (Shahar et al. 2014), see chapter “**Functional neuronavigation**”.

Finally, with the introduction of higher magnetic field scanners for clinical diagnostics, practicability of presurgical fMRI at 3 T has been established in patients with brain tumors (Roessler et al. 2005; Van Westen et al. 2005). For a general review on the role of imaging in disease management and the development of improved image-guided therapies in neurooncology, see also the article by Jacobs et al. (2005).

4.2 Selection of Candidates for Presurgical Motor and Somatosensory fMRI

In patients with rolandic brain tumors, presurgical fMRI is usually performed when neurological symptoms indicate involvement of the sensorimotor cortex and when insufficient information is obtained from morphological imaging. Four different scenarios can be distinguished:

- Due to tumor growth, MR-morphologic rolandic landmarks cannot be identified (see Fig. 15). In these patients, it is neither possible to localize the pre- or postcentral gyrus on the basis of anatomic criteria alone nor to reliably estimate putative surgery-related sensorimotor deficits. Here, fMRI offers somatotopic motor and somatosensory mapping of up to six functional landmarks in the pre- and postcentral cortical representations of the lower and upper extremities, as well as of the facial area. As patients with tumors invading the pre- or postcentral gyrus often present with contralateral motor and/or sensory deficits, the application of appropriate paradigms for the respective deficit may be required.
- Although the rolandic region is morphologically localizable, the “hand-knob” and/or precentral hook is no longer clearly identifiable because of a displacement or compression by the tumor. In this case, the MR-morphologic reference of the motor hand area as an orientation point for the somatotopic mapping of the precentral gyrus is absent: Surgery-related neurological deficits cannot be reliably estimated, and the planning and performance of low-risk interventions are problematic. Any presurgical fMRI should at least image the motor hand area while somatotopic mapping can, with relatively little additional effort, increase the diagnostic value of the examination.
- The tumor lies directly above or below the identifiable motor hand area (see Figs. 16, 17 and 18). In this case, somatotopic mapping is indicated in order to assess the

- local relationship between the tumor and functional areas and hence better estimate surgery-related neurological deficits in the lower extremities or facial area, as well as to provide the operator with additional functional landmarks.
- Presurgical fMRI can also be helpful in cases with a discrepancy between the morphological findings and the clinical status of the patient, for example, when there are little or no neurological deficits despite verifiable tumor growth into the central region. This and similar constellations should prompt a search for atypical brain activation as a result of tumor-associated cerebral plasticity and reorganization. The same applies to patients with recurrent malignancies, where the functional system has already been affected by former treatment (see Fig. 19). One recent study assessing surgical outcome in patients with primary or metastatic brain tumors based on the lesion-to-activation distance (LAD) showed that the LAD to the primary sensorimotor cortex does affect the incidence of motor deficits, while the LAD to the supplementary motor area (SMA) does not (Voss et al. 2013). Nevertheless more studies are needed to draw more robust conclusion on whether damage to secondary areas during surgery in such patients actually leads to additional and permanent neurological deficits.

Despite all these resources helping in the localization of relevant eloquent areas fMRI is still not able to answer the following question: What is the risk of functional deficits after resection of the contrast-enhancing tumor areas in the pre- or postcentral gyrus? The reason is simply that the definition of the resection margins using fMRI have still to be considered non-reliable – as outlined earlier only very limited data are available on that topic (Håberg et al. 2004; Krishnan et al. 2004; Hall et al. 2005; Berntsen et al. 2010; González-Darder and González-López 2010) that do not justify general conclusions on how to determine the “safe” borders for functional-preserving resection based on presurgical fMRI (Gil-Robles and Duffau 2010) (see Sect. 4.1). Such interventions are fundamentally hazardous, not only for jeopardizing the eloquent cortex but also the deep white matter tracts (Rasmussen et al. 2007; Berntsen et al. 2010).

Note

The selection criteria mentioned here are meant as suggestions arising from typical morphological and clinical findings in patients with rolandic brain tumors. It is currently not possible to define a medical indication in the strict sense for fMRI. This is due to the lack of controlled prospective studies demonstrating the clinical benefit of presurgical fMRI in terms of reduced postoperative morbidity or mortality.

4.3 Motor and Somatosensory Paradigms for Presurgical fMRI

A complex neuronal network of functional areas in both hemispheres of the human brain is recruited for the planning and execution of arbitrary movements, whereby somatosensory impulses are processed and consequently motor functions carried out (see chapter “[Functional neuroanatomy](#)”). Knowledge of an identification of the reliable localization of the various body representations in the primary motor and somatosensory cortices is essential in presurgical fMRI diagnostics, since permanent paralysis or sensory deficits can result from surgery-related injury to the respective functional areas. Neurological deficits resulting from damage to the secondary areas can also occur; however, those are typically transient and not as severe as compared to damage to the primary sensorimotor cortices, (Voss et al. 2013). Nevertheless, the functional localization of premotor activations may be of clinical relevance as an additional functional landmark of the precentral gyrus in hemiplegic patients (Stippich et al. 2000) (see Sect. 4.6).

Most investigators use self-triggered movements to assess motor activation and sensorimotor somatotopy, for example, various movements of the tongue or lips, the hand or fingers, and the foot or toes (see Sect. 4.4). Some groups use mechanical devices to better assess movements or to measure various physical parameters (force, acceleration) (Baudendistel et al. 1996). To ensure a successful examination in the clinical setting, it is essential that the paradigms are feasible, motion artifacts are kept to a minimum, and examination time is kept short. Under these conditions, BOLD activations in the primary motor cortex are generally very robust and reliable.

When defining motor paradigms in a block design, it is essential to decide whether only the primary motor cortex or also the secondary areas should be analyzed. In the case where only the primary motor cortex is the target, paradigms may include movements of both sides of the body (e.g., right hand vs. left hand). Since unilateral movements lead to activation of secondary areas in both hemispheres (Stippich et al. 2000, 2007a; Blatow et al. 2007; Tozakidou et al. 2013), secondary areas are active during both, alternating movements of the right and left side of the body (right vs. left contrast) throughout the entire measurement. This results in a continuous activation of the secondary cortical areas that are involved in bilateral movements and is therefore not depicted in the statistical evaluation of fMRI data acquired using conventional block designs due to the lack of “contrast” between the various stimulation blocks. Therefore, if information needs to be obtained regarding secondary motor

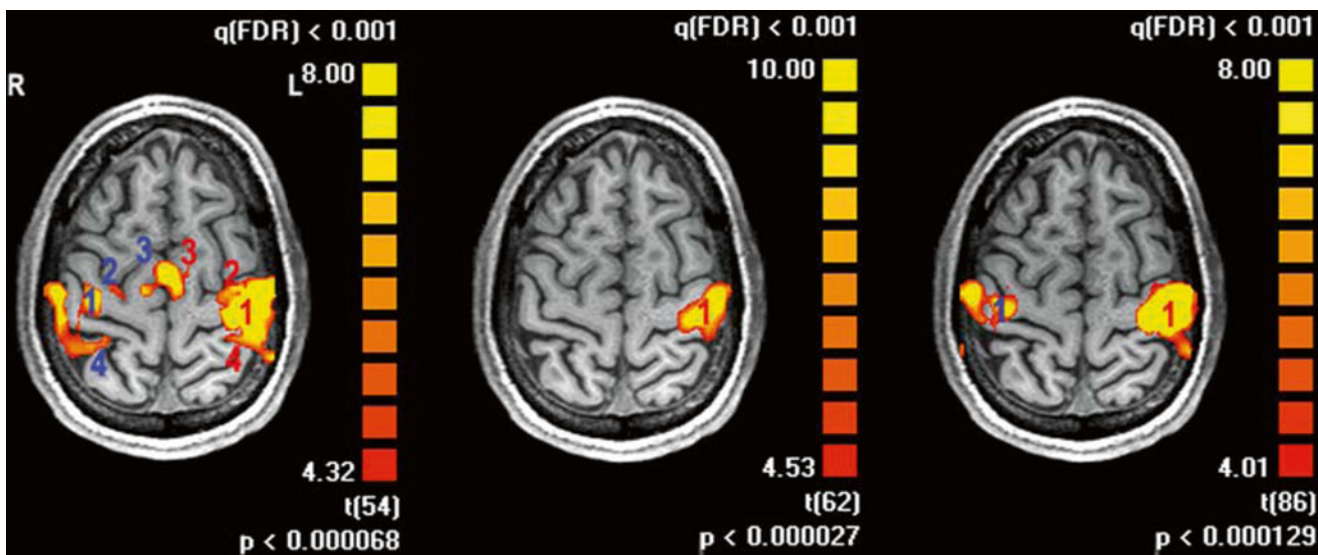


Fig. 11 Variation of paradigms to localize the motor hand area results in different activation patterns. *Left*: complex finger opposition of the right hand vs. rest; strong activation of the cortical motor network in both hemispheres. The large contralateral cluster (*left*) covers the primary sensorimotor cortex (1), premotor cortex (2), and parietal cortex (4). Bilateral supplementary motor activation (3, 3) is displayed in the midline, as well as ipsilateral (*right*) premotor activation (2), primary

sensorimotor coactivation (1), and parietal activation (4). *Middle*: complex finger opposition of the right vs. left hand; strong contralateral (*left*) primary sensorimotor activation (1), but no activation of secondary areas. *Right*: complex finger opposition of the right hand vs. right toe movements and tongue movements; strong contralateral (*left*) primary sensorimotor activation (1) and ipsilateral primary sensorimotor coactivation (1), but no activation of secondary areas

activation, paradigms with strictly unilateral movements of a single part of the body (e.g., right hand only) need to be applied with true “resting” as the control condition. Alternatively, three different stimulation conditions could be integrated in the paradigm, that is, right movement – rest – left movement. However, in this case the number of blocks per paradigm is increased as compared to unilateral movements only and consequently also examination time and susceptibility to motion artifacts. In addition, it should be borne in mind that – *sensu stricto* – information on brain activation in the tumor-unaffected hemisphere is largely insignificant for the resection itself, except for the assessment of tumor-induced neuroplastic changes. More importantly, paradigms enabling the examination of several different cortical body representations within one single fMRI measurement are problematic in brain tumor patients (e.g., foot – hand – face: complete somatotopy). Although with this paradigm the total scan time for the functional mapping of the body’s somatotopy could be reduced compared to three individual measurements, the time needed would substantially exceed the scanning time required for a short paradigm that is focused on a single cortical body representation. Short scanning times are particularly important in the case of agitated patients or patients with paresis, as the probability of motion

artifacts increases with the scan time needed, subsequently affecting accurate identification of functional localizations. In conclusion, short paradigms that provide robust activation and focus on the examination of a single cortical body representation are considered the most clinically feasible (Fig. 11). The investigator needs to decide whether only the primary motor representations should be mapped functionally (in this case the paradigm should consist of alternating blocks with identical movements on both sides of the body, e.g., right vs. left hand) or whether additional information on functional reorganization in secondary cortical areas is of interest (in this case unilateral movements need to be performed vs. “resting”). This decision depends on the individual medical questions to be answered with preoperative fMRI.

Clinical feasibility tests performed on neurosurgical patients with and without tumor-related pareses or sensory disturbances showed that self-triggered movement tasks are better suited to presurgical fMRI than externally controlled paradigms, since only in this way each patient can perform the respective task within his or her range of ability. To keep the likelihood of motion artifacts to a minimum (Hoeller et al. 2002; Krings et al. 2001), the following movement tasks were chosen: Repetitive tongue movements with the mouth closed, opposition of fingers digits

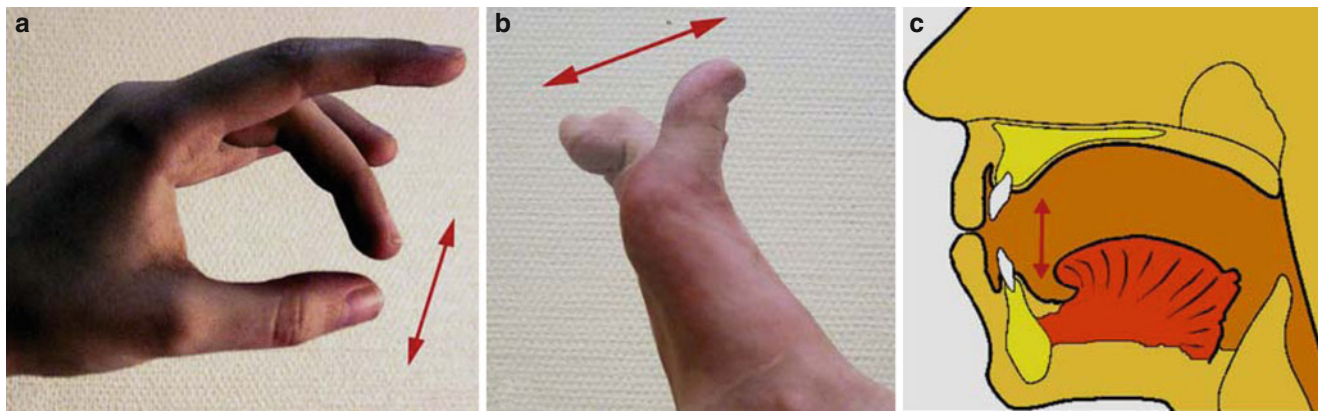


Fig. 12 Recommended self-paced movements to investigate sensorimotor somatotopy in clinical fMRI. (a) Complex finger opposition of digits 2–5 against the thumb in a random order. Movement frequency

~3 Hz. (b) Toe up and down movements, frequency >1 Hz. (c) Tongue up and down movements with the mouth closed. Movement frequency ~3 Hz (Reprinted from Stippich (2005), with permission)

D2–D5 against the thumb (D1) with free choice of the opposition order, and repetitive flexion and extension of all five toes without moving the ankle. Relaxed positioning of the large joints (knees, elbows) using foam cushions is recommended. The prerequisite for this examination is again “resting” as a control condition (Stippich et al. 2002b) (Fig. 12). Alternatively, in the case of a mild paresis of the upper extremity, fist clenching/releasing can be tested. Face, arm, and leg movements, or movement of the feet, can often lead to a poor diagnostic evaluation of the data due to strong motion artifacts and should therefore be avoided. A paradigm with a block duration of 20 s and three repeating cycles resulting to an examination time of 140 s is a suitable compromise between a robust functional localization of the primary motor cortex, high BOLD signal, and an acceptable scan time (Fig. 13).

Determination of motor function with presurgical fMRI is limited in patients with high-grade paresis (Pujol et al. 1998; Krings et al. 2002b). In this case, a reliable preoperative fMRI diagnosis is not guaranteed, if the fMRI protocol is based solely on self-triggered movements contralateral to the tumor. Typically, paresis results from insufficient residual function of the primary motor cortex, which is in turn reflected by a reduced BOLD activation. Nevertheless, many patients with tumor-related paresis can be successfully examined by activating the primary somatosensory lip, finger, and toe representations of the postcentral gyrus (Stippich et al. 1999). The somatosensory stimulation does not require patient cooperation; can also be applied in children and poorly cooperative or sedated patients; and activates both contralateral primary (Stippich et al. 2004) and bilateral secondary (Stippich et al. 2005) somatosensory

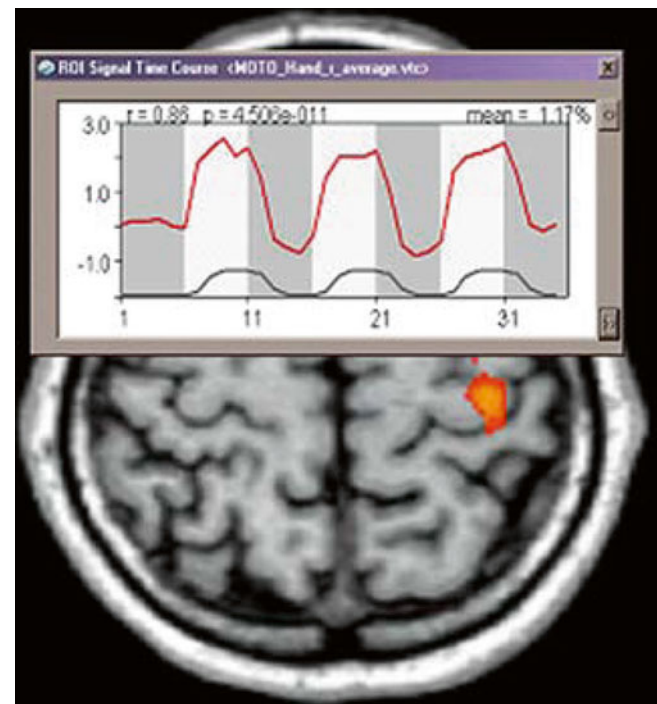


Fig. 13 Clinical standard protocol for motor paradigms. The block-designed paradigm consists of four rest periods (light gray) alternating with three stimulation periods (white), each of 20 s duration. The BOLD signal time course of the motor hand area activation (red line) shows a task-related increase in regional hemodynamics. The black line indicates the hemodynamic reference function (hrf)

areas. Even at 1.5 T fMRI sensitivity is sufficient to localize the cortical somatosensory representations in most patients. It is possible to distinguish various body representations in the postcentral gyrus (Stippich et al. 1999) (see Sect. 5.5)

and even individual finger representations (Kurth et al. 1998). While most published studies used non-standardized stimuli, such as manual hand touching, automatic stimuli guarantee reproducible stimulation conditions. Electric (Kurth et al. 1998; Kampe et al. 2000; Golaszewski et al. 2004), tactile (Stippich et al. 1999; Wienbruch et al. 2006), or vibrotactile (Golaszewski et al. 2002, 2006) stimulators are the most commonly used.

As a further adjunct in preoperative motor fMRI in patients with paresis, complex finger opposition of the non-paretic hand (ipsilateral to the brain tumor) can be used to elicit robust premotor activation as an additional functional landmark for the precentral gyrus on the tumor's side (Stippich et al. 2000). Using this paradigm not only supplementary motor and premotor activation may be achieved but also additional ipsilateral primary motor coactivation that helps to directly localize the primary motor cortex on the tumor's side. If combined with somatosensory stimulation, a total of three functional landmarks for the cortical hand representations on the tumor's side is available for the localization of the precentral sulcus via premotor activation, the precentral gyrus via ipsilateral primary motor coactivation, and the postcentral gyrus using primary somatosensory activation, respectively (see Sect. 4.6, Fig. 22).

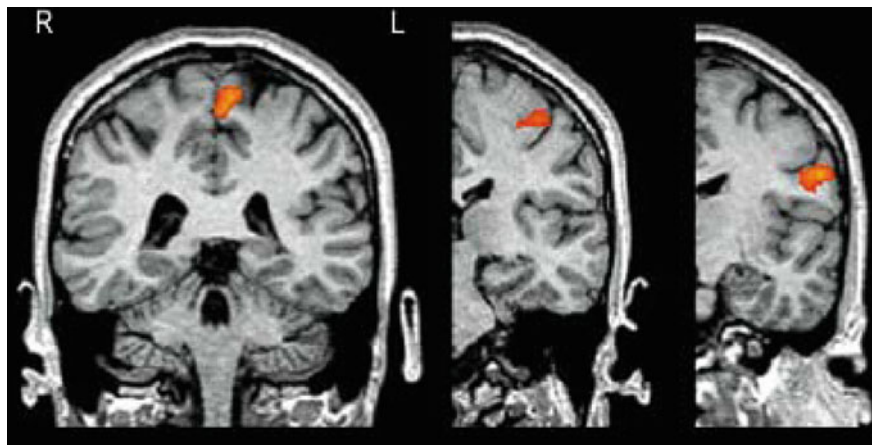
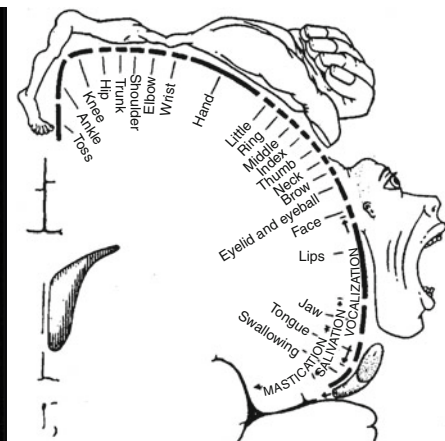


Fig. 14 FMRI motor cortex somatotopy. From *left to right*: foot, hand, and tongue representations, drawing of the motor homunculus

4.4 Presurgical Somatotopic Mapping of the Primary Motor Cortex

Somatotopic motor cortex mapping is the most frequently used presurgical fMRI protocol in patients with rolandic brain tumors (Stippich et al. 2002b). This standard protocol contains three different fMRI measurements. Paradigms should include tongue movements as well as finger and toe movements contralateral to the tumor to localize the primary motor homunculus in relation to the brain tumor (Fig. 14). Even in the case of a completely obscured rolandic anatomy fMRI can provide diagnostic information which may be relevant for the confirmation of the surgical indication as well as for the planning and implementation of function-preserving surgery (Fig. 15). In patients with small tumors that are – by anatomical consideration – not critical for any body representation, it seems appropriate to shorten the protocol by leaving the least relevant body representations unexamined (Figs. 16, 17, and 18). However, the examination of a single body representation alone, for example, the motor hand representation, is often not sufficient to provide the required diagnostic information. Somatotopic mapping also enables assessment of neuroplastic changes of cortical motor activation, for example, in patients with recurrent malignancies prior to repeated surgery (Fig. 19).



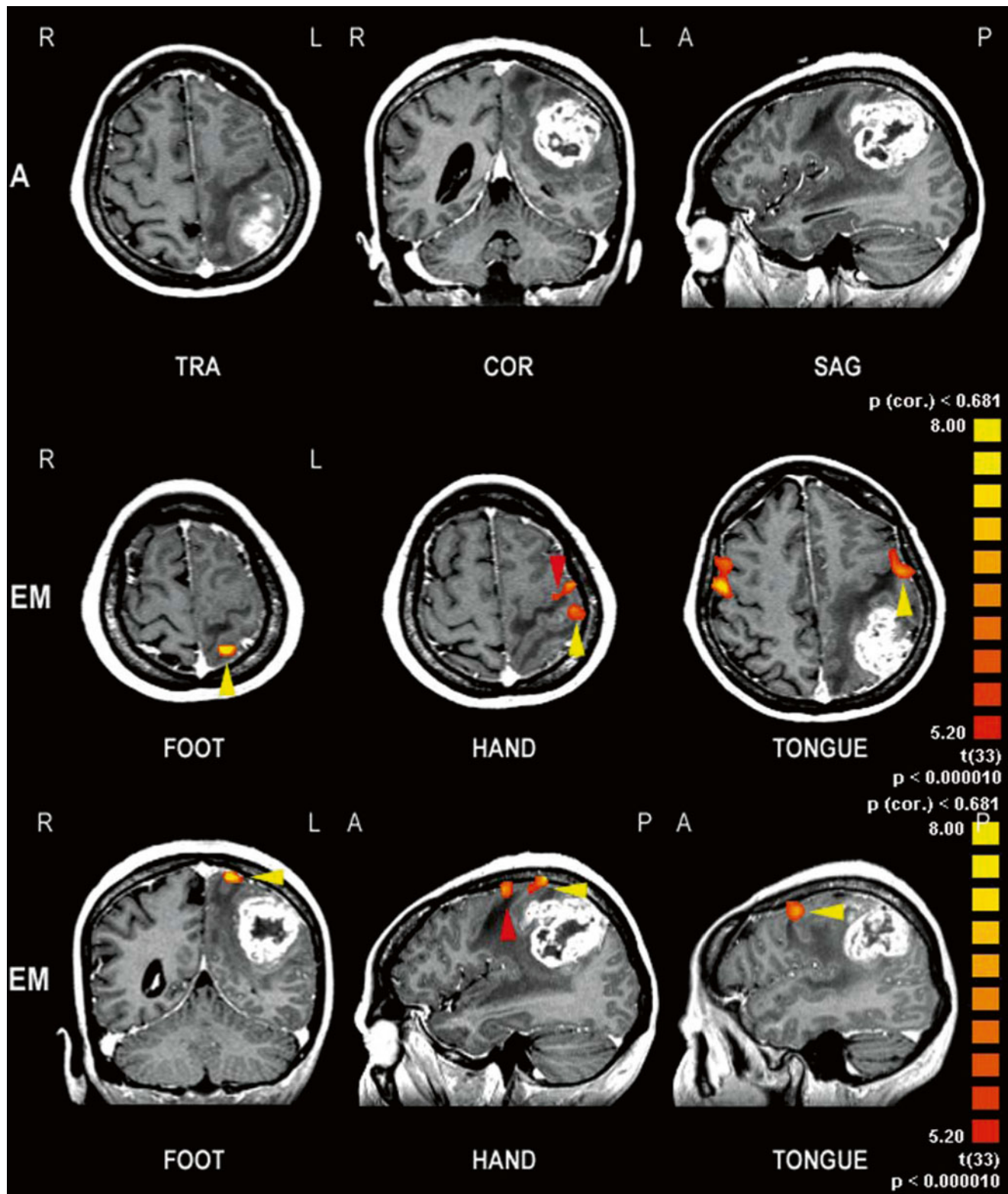


Fig. 15 Presurgical fMRI somatotopic mapping of the motor cortex. On morphological images, no rolandic landmarks can be identified in the left hemisphere due to the mass effect of this large malignant glioma (*upper row, A anatomy*). Foot, hand, and tongue movements (*EM executed movement*) revealed robust fMRI activation of the respective primary motor cortex body representations (*yellow arrowheads*). Using

functional landmarks the rolandic anatomy (precentral gyrus, central sulcus, postcentral gyrus) can be easily identified in relation to the brain tumor. FMRI indicated a parietal localization of the contrast-enhancing glioma. Note the additional premotor activation (*red arrowhead*) localizing the ventral wall of the precentral gyrus/precentral sulcus

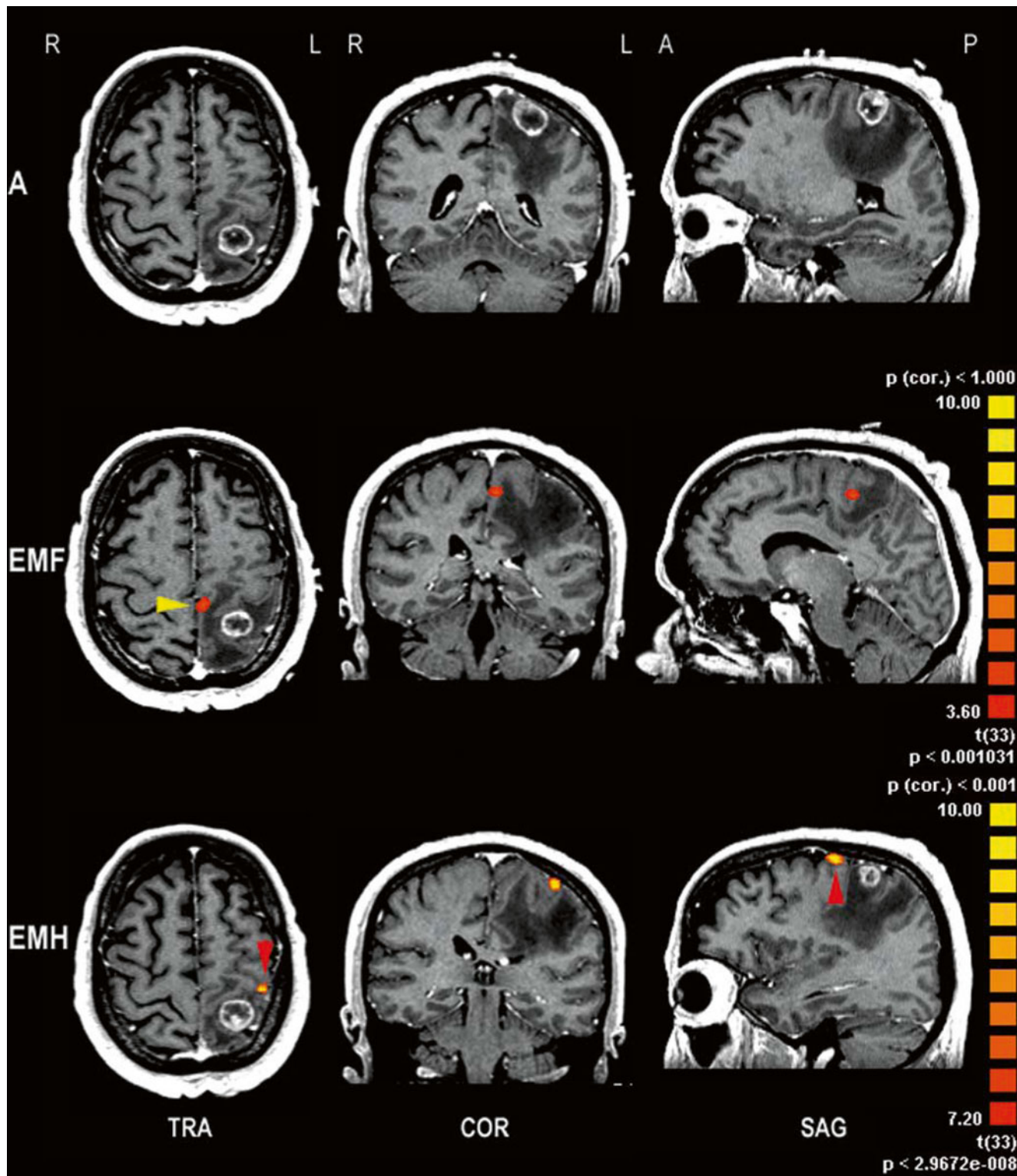


Fig. 16 Presurgical fMRI somatotopic mapping of the upper motor cortex in a left postcentral high-grade glioma. On morphological images, the compressed “precentral knob” can be identified in transverse and

sagittal views. Foot (*EMF*) and hand (*EMH*) movements were associated with activation of the respective primary motor cortex representations, confirming the postcentral localization of the tumor

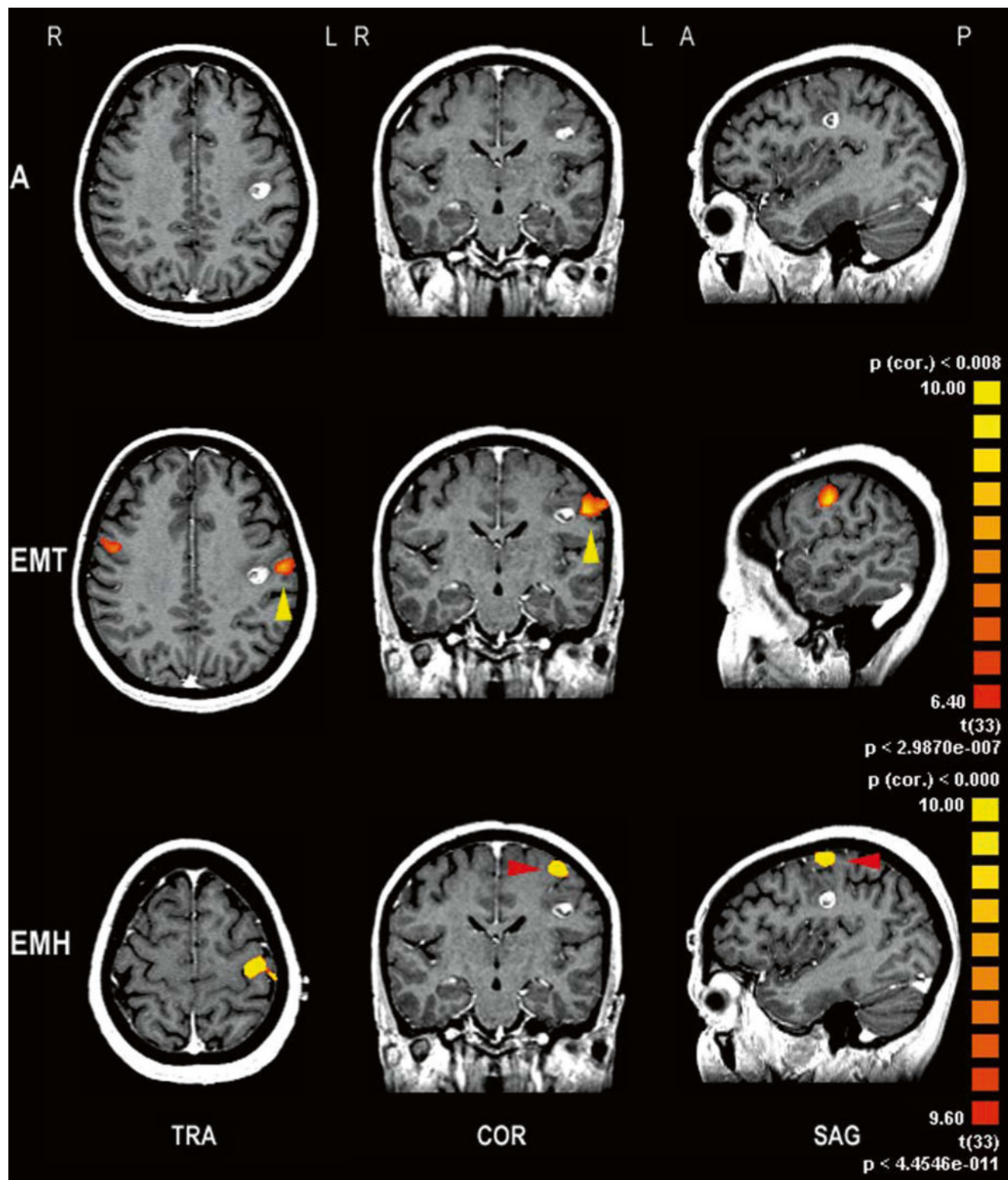


Fig. 17 Presurgical fMRI somatotopic mapping of the lower motor cortex in a left rolandic cavernoma. On morphological images, the rolandic anatomy was intact. Tongue (*MT*) and hand (*MH*) movements

were driven by activation of the respective primary motor cortex representations, confirming the central localization of the tumor and a close spatial relationship to the tongue representation

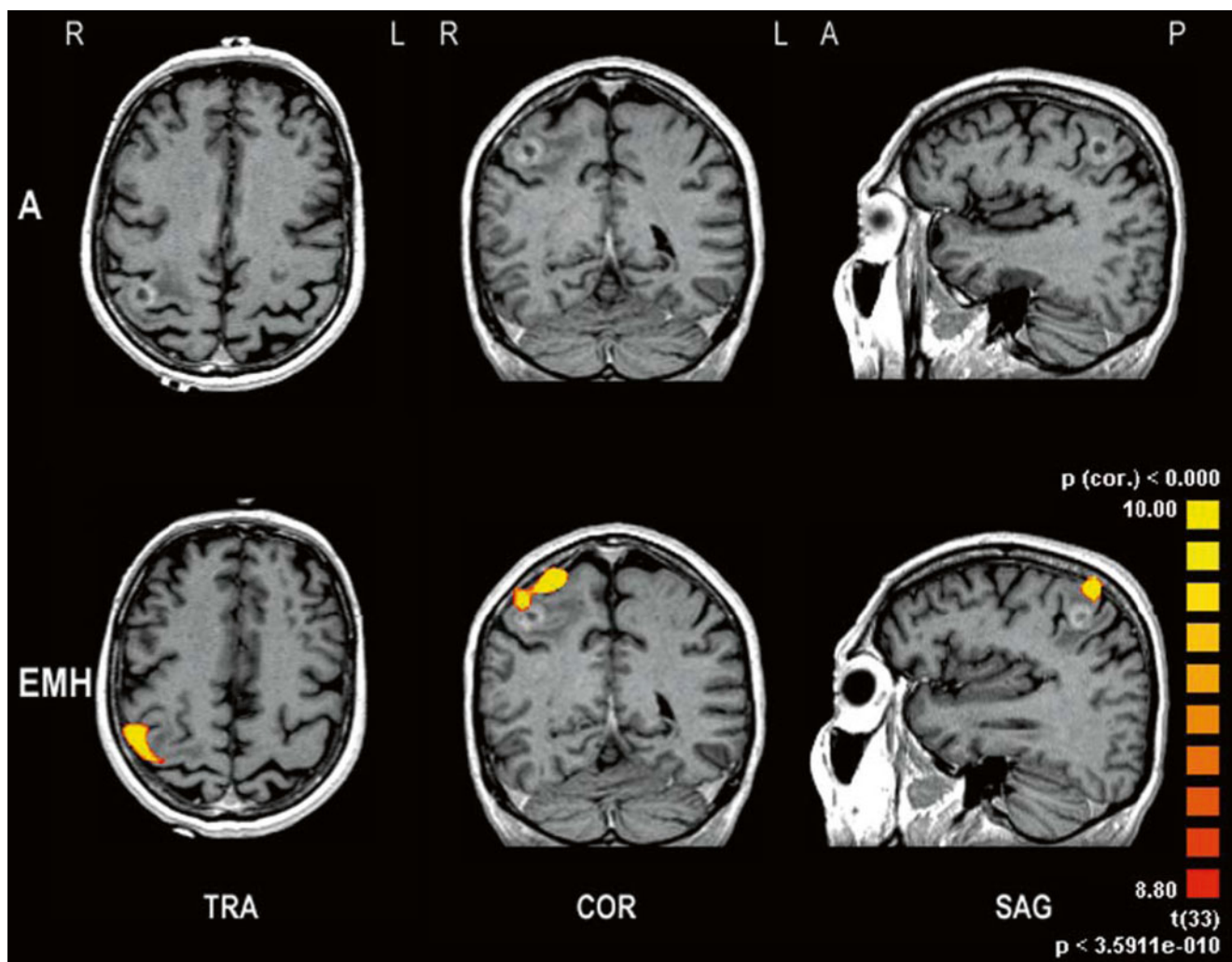
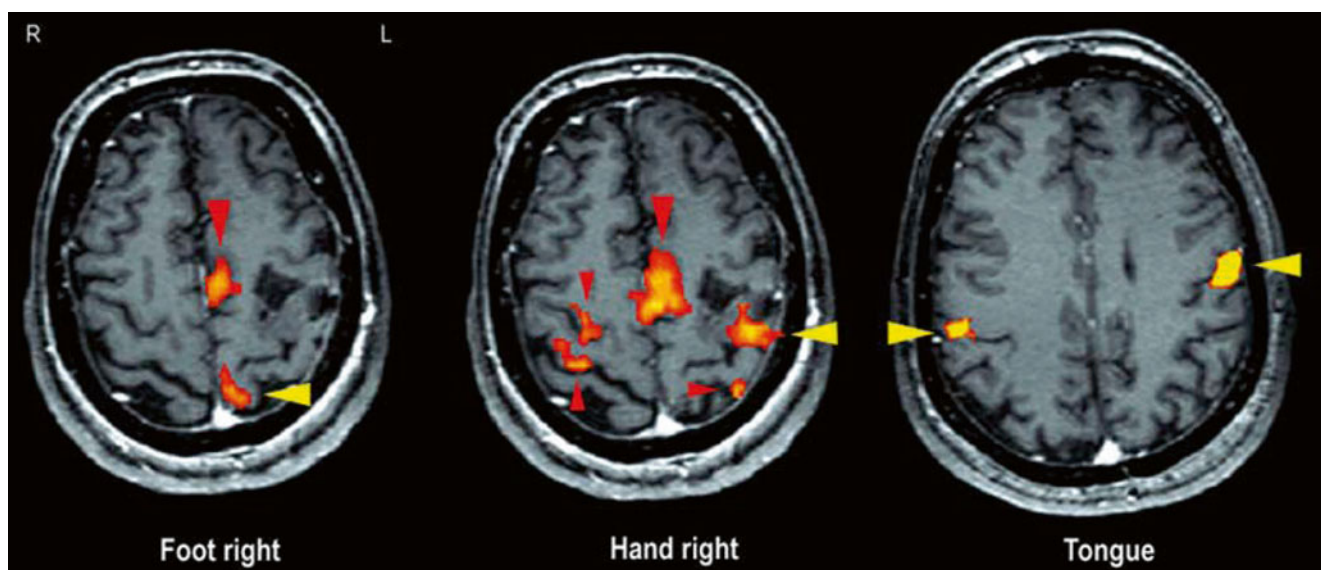


Fig. 18 Presurgical fMRI localization of the motor hand area. On morphological images, a rolandic metastasis is visualized at the motor hand area, bridging the central sulcus towards the postcentral gyrus. fMRI confirmed a close spatial relationship between the

primary motor hand representation and the tumor. Interestingly the center of gravity of the BOLD cluster was shifted upwards from the precentral knob towards the foot representation (see EMH, coronal view)



4.5 Presurgical Somatotopic Mapping of the Primary Somatosensory Cortex

This fMRI protocol was designed to localize the different primary somatosensory body representations of the postcentral gyrus (Stippich et al. 1999) (Fig. 20). In presurgical fMRI, somatotopic somatosensory mapping is mostly used as a diagnostic adjunct, when motor paradigms are difficult to apply – for example, in uncooperative, sedated, or hemiparetic patients or in children, but there is also potential for standardized follow-up measurements on neuroplastic changes of the somatosensory system. The fully automated pneumatically driven 24-channel tactile stimulation used in our institution is artifact-free and produces reproducible stimuli and consistent examination

conditions for comparative and outcome studies. The whole unit can be set up and dismantled within 5 min. Scan time per measurement is 66 s for the localization of the primary somatosensory cortex only (Stippich et al. 2004) or 105 s for a robust primary and secondary somatosensory activation, respectively (Stippich et al. 2005). This presurgical fMRI protocol enables assessment of the spatial relationship between brain tumors and the postcentral gyrus, facilitating the estimation of possible postoperative sensory deficits (Fig. 21).

Diagnostic information about the spatial relationship between the central sulcus or the precentral gyrus and precentral or frontal brain tumors can be indirectly obtained from somatosensory fMRI as both anatomical structures are situated directly anteriorly to the postcentral gyrus.

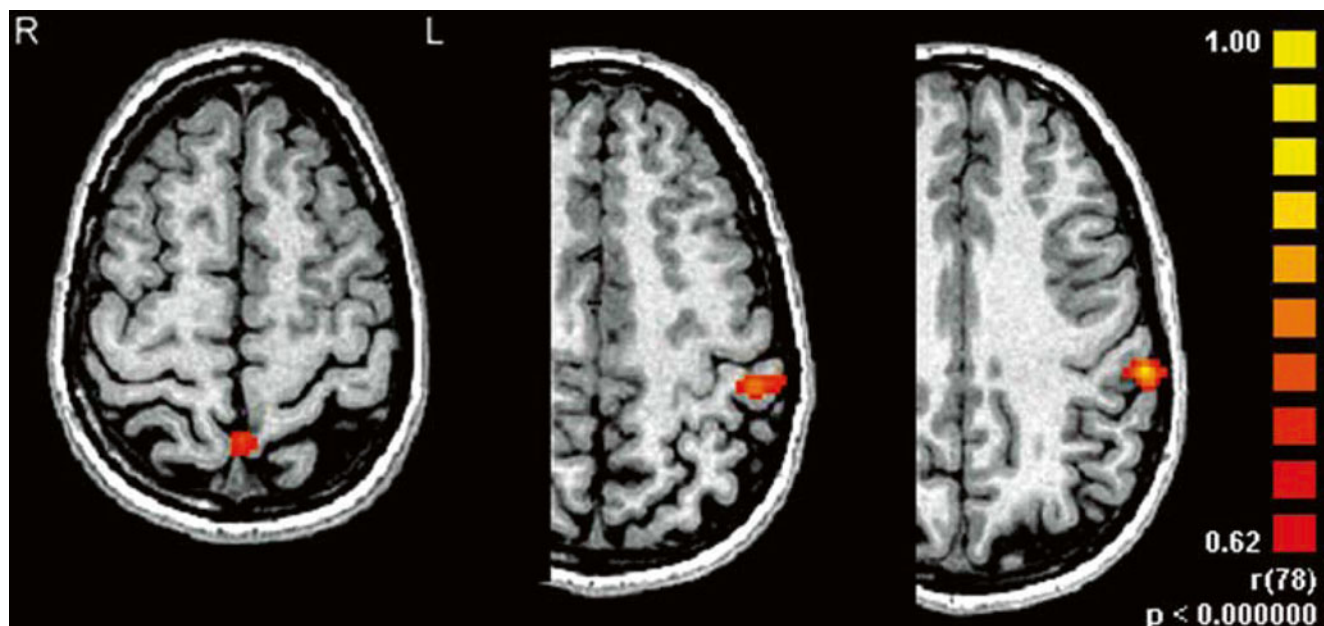


Fig. 20 FMRI primary somatosensory cortex somatotopy. From left to right: toe, finger, and lip representations. Stimulation: D1 and D2 right foot and right hand, upper and lower lips to the right side; stimulus frequency=4 Hz, air pressure=3 bar. Clinical standard fMRI protocols for somatosensory stimulation, conventional block design, stimulation vs.

rest. (a) Primary somatosensory cortex (S1), six periods of rest alternating with five periods of stimulation, each of 6 s duration (Stippich et al. 2004). (b) Secondary somatosensory cortex (S2), four periods of rest alternating with three periods of stimulation, each of 15 s duration (Stippich et al. 2005) (Modified from Stippich et al. 1999 with permission)

Fig. 19 Presurgical fMRI somatotopic mapping of the motor cortex in a hemiparetic patient with a recurrent left rolandic astrocytoma prior to repeated surgery. Foot, hand, and tongue movements revealed robust fMRI activation of the respective primary motor cortex body represen-

tation (yellow arrowheads). Note the increased activation of secondary areas (red arrowheads): in the supplementary motor area during toe and finger movements and in the whole cortical motor network in both hemispheres during finger movements, respectively

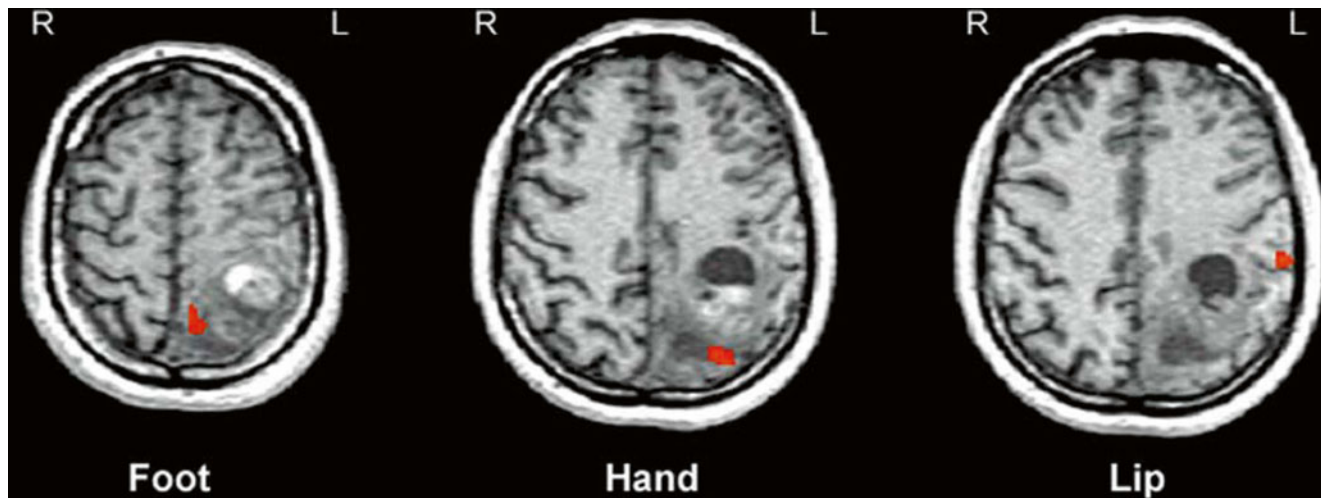


Fig. 21 Presurgical fMRI somatotopic mapping of the primary somatosensory cortex (S1) in a left parietal malignant glioma indicated compression of the upper postcentral gyrus at the level of the foot rep-

resentation and tumor growth into the lower postcentral gyrus with dorsal displacement of the S1 hand representation (Modified from Stippich et al. 1999 with permission)

4.6 Localization of the Precentral Gyrus in Patients with Preexisting Paresis

This special protocol was designed in volunteers to help localizing the precentral gyrus in patients with prominent contralateral paresis (Stippich et al. 2000). Its clinical application is not generally used and thus requires own validation. In these paretic patients, the primary motor cortex is commonly infiltrated by the tumor or severely compressed precluding both a reliable identification of the rolandic anatomy on morphological images and proper performance of contralateral movements for presurgical fMRI. However, as a basic principle, residual contralateral motor function and passive somatosensory stimulation should be first used for the functional localization of the pre- and postcentral gyrus. As a further adjunct complex finger opposition of the non-paretic hand ipsilateral to the brain tumor can be used to activate the whole cortical motor network in both hemispheres, control condition is “resting.” The premotor activation on the tumor’s side may serve as an additional functional

landmark for the precentral gyrus by localizing the anterior wall of the precentral gyrus near the junction of the precentral sulcus with the posterior part of the superior frontal sulcus (Figs. 22 and 23). Please note that the risk for postoperative-related motor deficits cannot be estimated using premotor activation as a functional landmark! However, in healthy volunteers primary motor coactivation can frequently be observed in the motor hand area ipsilateral to the moving hand (Stippich et al. 2007a). Our clinical experience indicates that ipsilateral primary motor coactivation may also be supportive to localize the motor hand area on the tumor side in hemiparetic patients.

In general, the combination of presurgical motor fMRI with anisotropic diffusion-weighted MRI and diffusion tensor imaging (DTI) – tractography – is highly recommended for the assessment of the effects of rolandic brain tumors on the pyramidal tract (Stippich et al. 2003a; Rasmussen et al. 2007; Berntsen et al. 2010; González-Darder and González-López 2010; Dimous et al. 2013; Jia et al. 2013; Kumar et al. 2014) (Figs. 24 and 25).

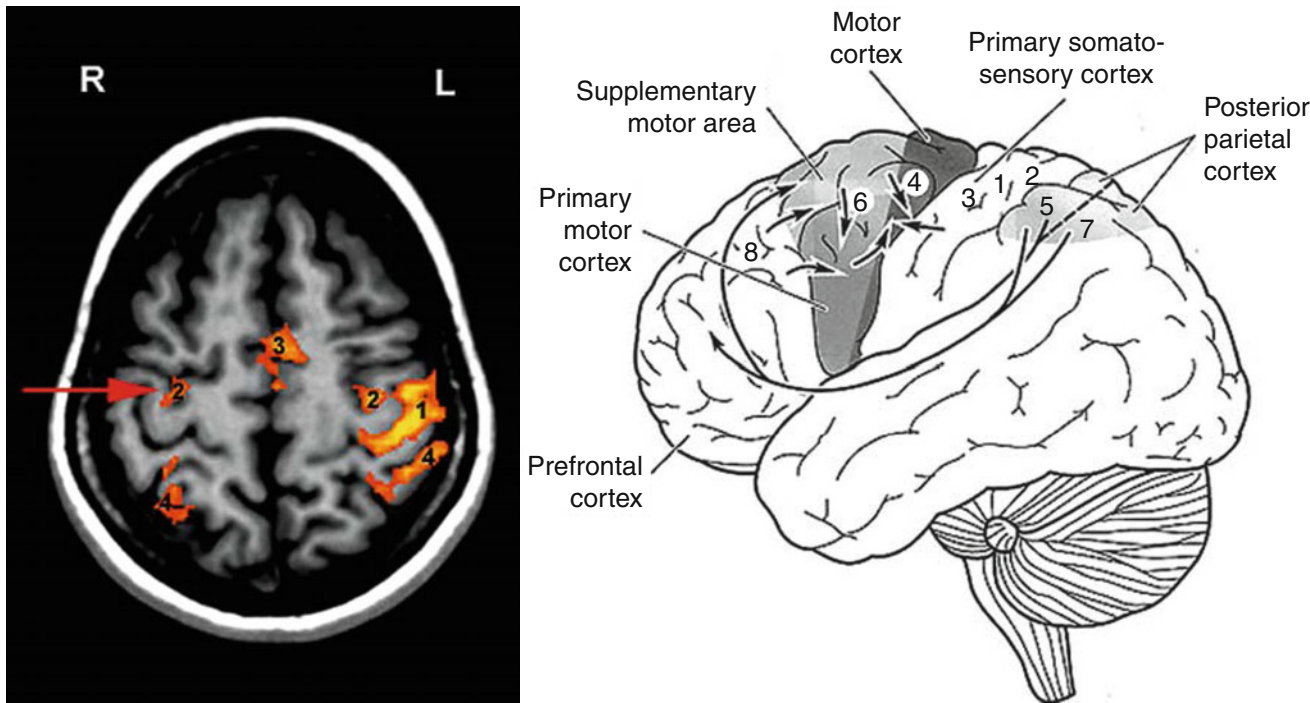
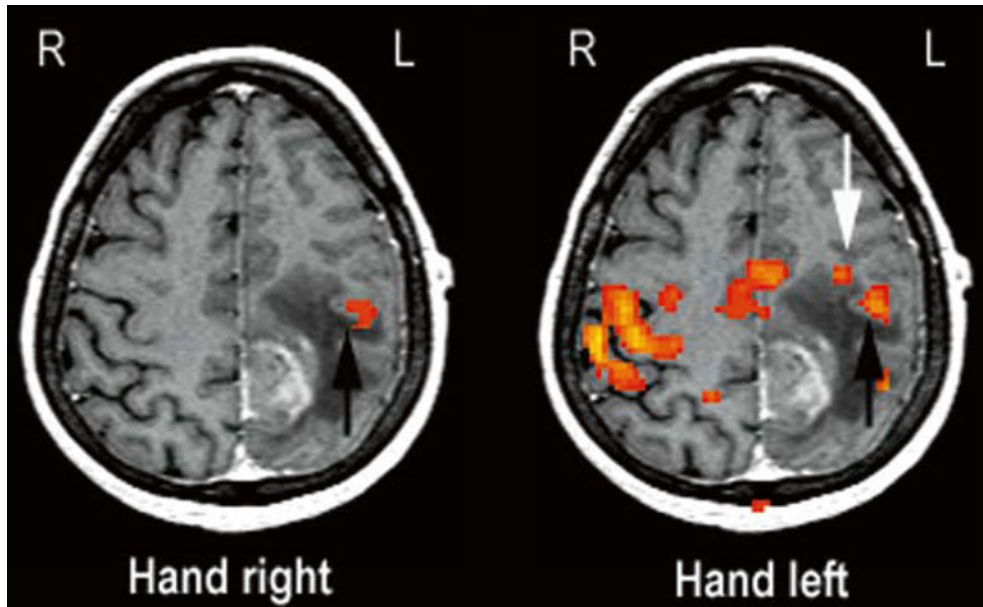


Fig. 22 Typical cortical activation pattern of complex finger opposition (right hand). Premotor activation ipsilateral to the moving hand (red arrow) serves as a functional landmark for the precentral gyrus in hemiparetic patients (a clinical case is presented in Figs. 23 and 24). Premotor activation is typically localized at the anterior wall of the precentral

gyrus directly adjacent to the junction of the precentral sulcus with the superior frontal sulcus. It is important to note that this functional landmark does not localize the motor hand area! In the drawing of the cortical motor and somatosensory network (right), the numbers indicate the Brodmann areas (Reprinted from Stippich (2005), with permission)

Fig. 23 Example of fMRI localization of the motor hand area in a hemiparetic patient with a left malignant glioma using contralateral and ipsilateral movements. Residual motor function of the paretic right hand (grade 3/5) is driven by residual activation of the contralateral motor hand area (black arrow). Complex finger opposition of the non-paretic left hand is associated with activation of the cortical motor network in both hemispheres. Robust ipsilateral primary motor coactivation (black arrow) confirms the localization of the motor hand area. Additional ipsilateral premotor activation (white arrow) indicates the ventral wall of the precentral gyrus



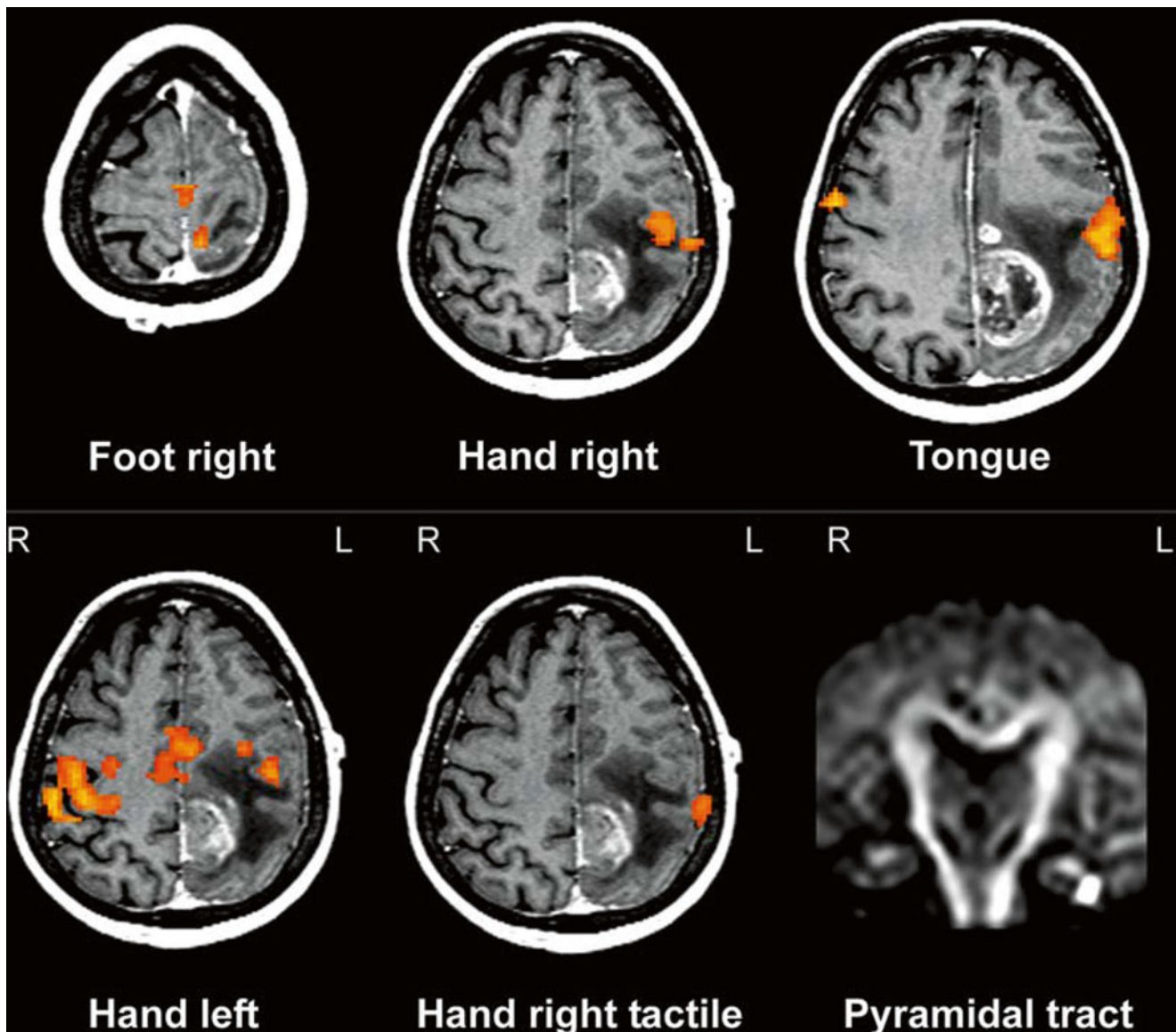


Fig. 24 Presurgical fMRI in rolandic brain tumors – standard and special protocols. *Upper row* (standard protocol): somatotopic mapping of the primary motor cortex indicated a parietal localization of the contrast-enhancing malignant glioma (same patient as Fig. 23). *Lower row* (special protocols): complex finger opposition of the non-paretic left hand (*left*) and fully automated tactile stimulation of the contralesional right hand (*middle*) localized the pre- and postcentral gyrus in relation

to the brain tumor. This diagnostic information is equivalent to that available from contralateral hand movement (please compare *upper row, middle*) and can be obtained also in patients with complete loss of contralateral motor function. Anisotropic diffusion images of the pyramidal tract completed this presurgical MRI protocol. Diffusion tensor tractography could provide more detailed anatomical information (Modified from Stippich et al. 2003a, with permission)

5 Presurgical fMRI of Language Function

The number of groups localizing language brain function pre-operatively is ever growing – a larger collective study included 81 patients (Stippich et al. 2007b). The diagnostic aims of presurgical language fMRI according to the “classical model of language” include the localization of the Broca’s and Wernicke’s speech areas in relation to brain tumors or epileptogenic zones and the identification of the language-dominant hemisphere. In contrast to motor or somatosensory fMRI, the indication for presurgical language fMRI cannot be supported by morphological imaging alone. The latter provides only rough information about whether the potentially function-bearing gyri – namely, the left inferior frontal gyrus (Brodmann areas 44 and 45) or the left superior temporal gyrus (Brodmann area 22) – are affected by the tumor (Fig. 26) or not. However, it has been demonstrated that the classical language model (Lichtheim 1885; Geschwind 1971) is not sufficient to reflect the complexity of cortical language representations (Bookheimer 2002; Gabrieli et al. 1998; Grabowski 2000). Hence, clinical and neuropsychological symptoms are ultimately decisive. Nevertheless, language fMRI can be useful in the presurgical diagnostic situation. Here, presurgical language fMRI protocols should always comprise several different paradigms. There is no such thing as one universal paradigm for fMRI language assessment!

Language fMRI is not used as frequently as motor fMRI in preoperative neuroimaging. This is partly due to the higher equipment load and personnel and logistical requirements, which make implementation of the procedure in the clinical routine more challenging. Moreover, most neurocenters have developed their own methodology, making fMRI results difficult to compare. This variability does not only affect the chosen stimulation paradigm, on which the examination results depend to a great extent, but also the way in which it is presented – visually or acoustically – as well as measurement and evaluation parameters. Even so, and on the basis of results from numerous validation studies using established reference procedures (EcoG, Wada test), it can be assumed that fMRI can reliably and noninvasively localize Broca’s and Wernicke’s language areas prior to brain surgery (Dym et al. 2011; Sharan et al. 2011; Janecek et al. 2013). Determining language dominance with fMRI is possible, and in a meta-analysis a quite good sensitivity (83.5 %) and specificity (88.1 %) has been shown, when compared to the Wada test (Dym et al. 2011). However, the Wada test may still have value in the evaluation of epilepsy surgery candidates with atypical or bilateral language representation or when fMRI data are inconclusive (Sharan et al. 2011; Janecek et al. 2013; Wagner et al. 2012; Bauer et al. 2013) (For a more detailed description on this topic please refer to chapter “[Presurgical functional localization possibilities, limitations and validity](#)”).

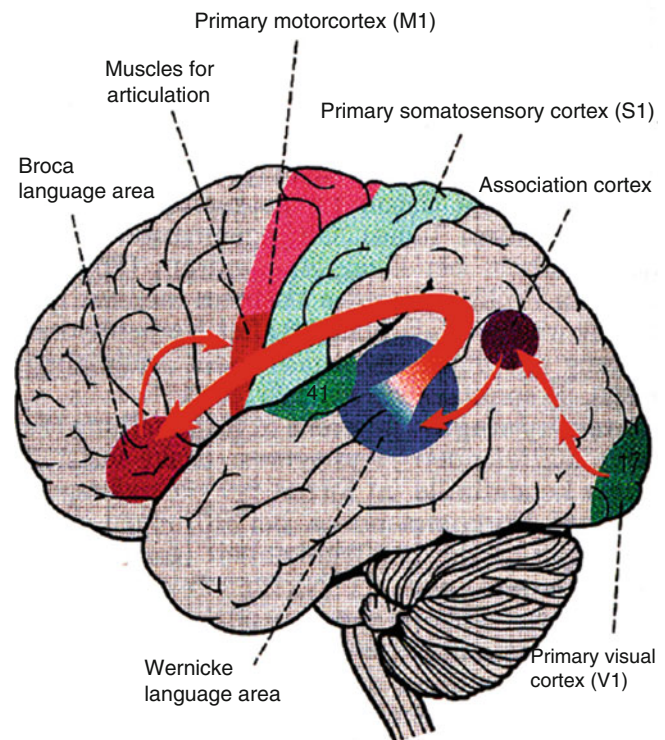


Fig. 25 Schematic drawing of language areas in the left hemisphere according to the classical language model (Wernicke-Lichtheim 1871). Red arrows indicate important anatomo-functional connections (e.g., arcuate fascicle) (Modified from Roche Lexikon Medizin, 4th edn, 1998, Urban and Fischer, Munich, p 1578)

5.1 Review of Literature

In this paragraph, we will try to guide the reader through the complex and to a certain extent inhomogeneous data published on presurgical language fMRI. Since in many studies patients with both brain tumors and epilepsy were included, it seemed not appropriate to distinguish between the two entities. Hence, this chapter covers also information relevant for chapter “[Presurgical EEG-fMRI in epilepsy](#)”.

Already 3 years after the first reports on fMRI, a preliminary study showed that the BOLD signal contrast obtained from simple tests of language and motor function was very similar between patients with epilepsy and normal controls, demonstrating the feasibility of the technique in patients with epilepsy (Morris et al. 1994). Since then, fMRI of language processing has become one of the most clinically relevant applications in the field of epilepsy and also in patients with brain tumors prior to surgery. The main aim of the identification and interpretation of the complex language network is to predict and minimize postoperative language deficits. In patients with epilepsy considered for surgery – who are mainly patients with temporal lobe epilepsy (Hermann et al. 1999) – fMRI is predominantly used for language lateralization (i.e., determination of the hemispheric

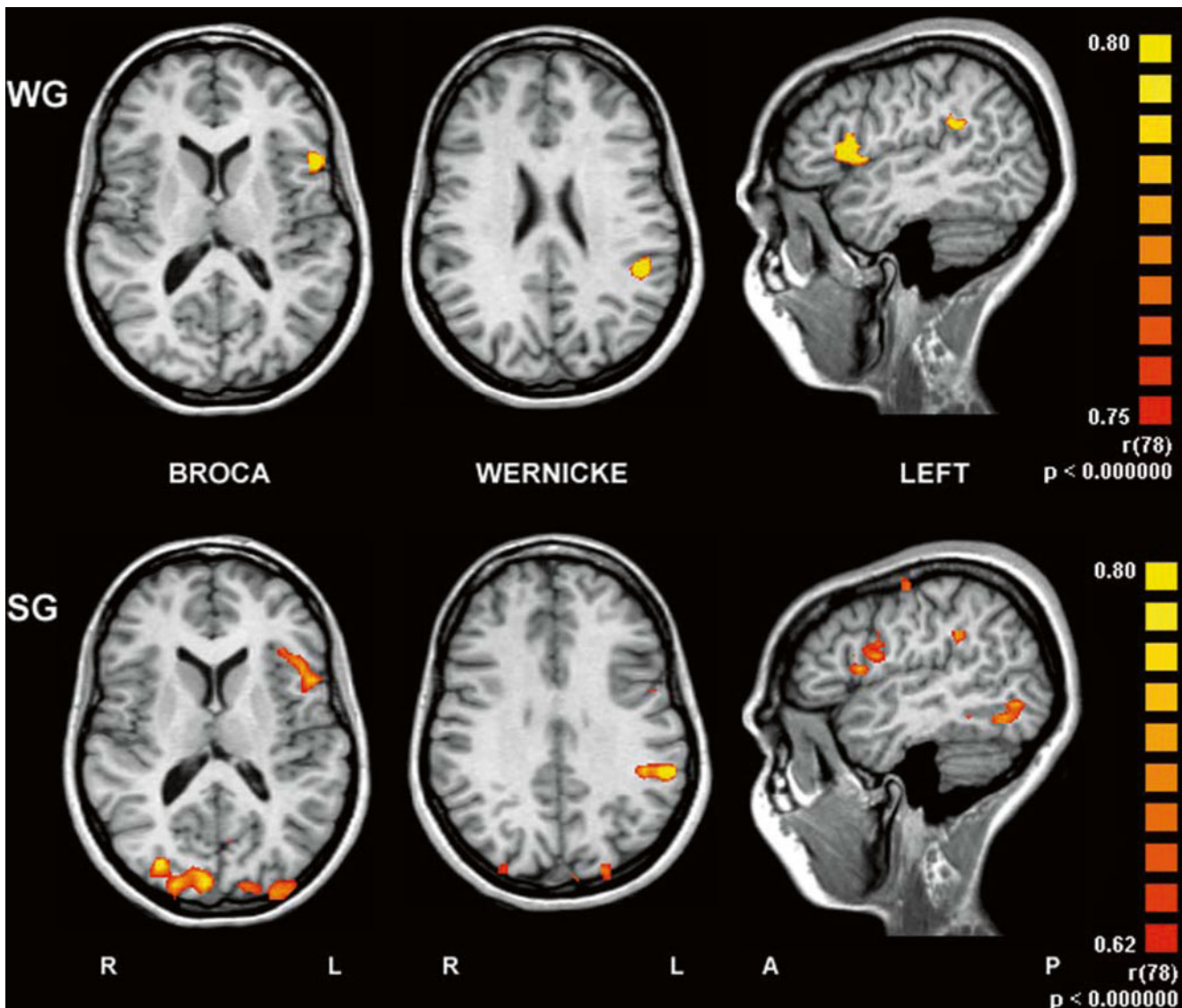


Fig. 26 Functional localization of Broca's and Wernicke's areas using the word-generation (WG) and sentence-generation (SG) paradigms. Note that the functional localizations are congruent, but not perfectly identical (Modified from Stippich et al. 2003b, with permission)

dominance) and only to a lesser extent for the intrahemispheric distribution of the eloquent cortex.

Numerous studies have demonstrated the high reliability of fMRI to identify the language-dominant hemisphere (Binder et al. 1995, 1996, 1997, 2000; Benson et al. 1996; Bahn et al. 1997; FitzGerald et al. 1997; Stapleton et al. 1997; Shaywitz et al. 1995; Cuenod et al. 1995; Hertz-Pannier et al. 1997; van der Kallen et al. 1998; Worthington et al. 1997; Frost et al. 1999; Szaflarski et al. 2002; Dym et al. 2011; Sharan et al. 2011; Janecek et al. 2013). However, the areas identified in different studies of language evaluation vary markedly, likely due to the use of different linguistic activation or control tasks, imaging, and post-processing techniques, among other factors (Dym et al. 2011). Again, there is no single fMRI paradigm that identifies “language

cortex,” as language is a complex process which involves many different components, including specialized sensory systems for speech, text, and object recognition, processing of whole-word information and word meaning, word syntax processing, and multiple mechanisms for written and spoken language production (Binder et al. 2002; Zacà et al. 2013; Barnett et al. 2014). Hence, the activation pattern is crucially dependent on the chosen fMRI task design.

Hearing words – whether the task involves passive listening, repeating, or categorizing – activates the superior temporal gyrus bilaterally compared to a resting state condition (Binder et al. 2000; Price et al. 1996; Wise et al. 1991). The symmetry of this activation can be explained by the task contrast (complex sounds vs. no sounds). The rest condition does not contain any control for prelinguistic auditory pro-

cessing which engages the auditory cortex in both superior temporal gyri. Brain areas associated with semantic word processing might be also activated during the resting state and hence reduce sensitivity for the activation task (Binder et al. 1999). Similar problems occur in designs that oppose reading or naming tasks to a resting or visual-fixation baseline. In a study performed on patients with primarily lateralized lesions, Benson et al. found that such protocols do neither reliably produce lateralized activation nor correlate with language dominance measured with the Wada test (Benson et al. 1999).

The most common types of tasks successfully used for the assessment of language lateralization are the word-generation tasks (also called verbal fluency tasks) and the semantic decision-making tasks, whereby the former tend to show relatively consistent activation of the anterior language areas and the latter a more widely distributed network including the anterior and posterior hemispheric regions (Binder et al. 1997).

In the word-generation tasks, the subjects or patients are confronted with a noun, a semantic category (e.g., animal, food), and are asked to retrieve a phonologically or semantically associated word. In the verb-generation tasks, the subject/patient generates a verb in response to seeing or hearing a noun. These tasks reliably activate the dominant inferior and dorsolateral frontal lobe including the prefrontal and premotor areas (Wise et al. 1991; Warburton et al. 1996; Raichle et al. 1994; Petersen et al. 1988). Many studies have shown that lateralization measures obtained from these frontal activations by fMRI agree well with Wada language lateralization (Bahn et al. 1997; Yetkin et al. 1998; Benson et al. 1999; Lehericy et al. 2000a; Janecek et al. 2013). There is evidence that semantic language tasks such as verb generation in response to nouns, noun categorization, or noun generation within specific categories may be more effective in language lateralization than phonologically based generation tasks such as concealed repetition (Lehericy et al. 2000a). In fMRI studies, word-generation tasks are usually performed silently to avoid movement artifacts. The resulting lack of proof of a proper task performance is usually not a problem when clear activation is observed, but bars the investigator from assessing poor task performance in cases of poor activation.

A semantic decision task was used by Springer and colleagues to address the issue of language dominance in patients with epilepsy (Springer et al. 1999). Fifty right-handed patients with epilepsy were compared with 100 right-handed normal controls. Language activation was accomplished by opposing a semantic decision task to a tone discrimination task. The latter was developed to control for nonlinguistic components of the task (e.g., attention, sound processing, manual response). Using a categorical dominance classification, 94 % of the normal control subjects were considered left-hemispheric dominant, 6 % had a bilateral language representation, and none of the subjects had a right-lateralized

dominance. In the group of patients with epilepsy, there was a greater variability of language dominance, with 78 % showing a left-hemisphere dominance, 16 % showing a roughly symmetric pattern, and 6 % showing a right-hemisphere dominance. Atypical language dominance in patients with epilepsy was associated with an earlier age onset of seizures and with a weaker right-handed dominance. The relatively high prevalence of atypical language representation in patients with epilepsy (Sharan et al. 2011) stresses the importance of the assessment of the hemispheric dominance before interventional procedures in areas potentially relevant for language in either cerebral hemisphere (Spreer et al. 2001).

Further studies with the paradigms described above were performed by Binder and colleagues (1995, 1996, 1997). The activation pattern was in general strongly left lateralized and involved both the prefrontal and posterior association areas. The activation correlated strongly with the language lateralization obtained from the Wada test (Binder et al. 1996). A similar result using a semantic word-decision task was observed by Desmond and colleagues. Seven postoperative patients with temporal lobe epilepsy were examined and the BOLD signal was compared with data from preoperative Wada test. In all cases, using a region-of-interest-based analysis looking only at the inferior frontal regions, the lateralization by fMRI was the same as that observed by the Wada test (Desmond et al. 1995). An attractive feature of semantic word-decision tasks is that of the rating of the behavioral responses through a push-button system on response to stimuli, thereby permitting precise quantification of task performance to be precisely quantified.

As mentioned above, both word-generation and semantic word-decision tasks identify mainly the frontal lobe language areas but are less consistent activators for the temporal language regions. An fMRI paradigm with consistent temporal lobe activation was reported by Gaillard and Balsamo (Gaillard et al. 2002). The paradigm consisted of the silent pronunciation of items in response to a visualized item description. The authors found language lateralization in 27 of 30 patients with temporal lobe epilepsy. The fMRI dominance was consistent with the Wada test in 15 of 20 patients.

Word-generation tasks are also most frequently used in language fMRI studies on brain tumor patients (Latchaw et al. 1995; Herholz et al. 1997; Hirsch et al. 2000; Håberg et al. 2004; Hall et al. 2005; Van Westen et al. 2005). There is the general agreement that a combination of different tasks increases paradigm effectiveness (Zacà et al. 2013). Van Westen et al. used a combination of word generation and rhyming in 20 patients with tumors close to the sensorimotor or language areas in an fMRI study performed at 3 T and reported a paradigm effectiveness varying from 79 to 95 % (Van Westen et al. 2005). In another study on a large group of patients (56 patients with lesions near language-relevant areas), the authors found activation of the Wernicke's area in

91 % and of the Broca's area in 77 % applying a combination of a silent word-generation task (picture naming) upon listening to spoken words. In the same study, language lateralization with fMRI and Wada test was congruent in all 13 patients examined (Hirsch et al. 2000).

Successful fMRI lateralization paradigms have also been reported on children as young as 6 years (Benson et al. 1996; Hertz-Pannier et al. 1997; Stapleton et al. 1997; Logan 1999; Hertz-Pannier et al. 2002), and the hemodynamic response appears to be similar than that observed in adults (Benson et al. 1996; Hertz-Pannier et al. 1997). Word-generation tasks are the most commonly used tasks for the evaluation of pediatric epilepsy surgery candidates and, as in adults, show a general agreement with the Wada test and electrocortical stimulation (Hertz-Pannier et al. 1997; Stapleton et al. 1997; Logan 1999). There is some evidence that young children do activate more widespread than adults, at least in verbal fluency tasks (Gaillard et al. 2000b). FMRI studies on children with paradigms consisting in reading larger passages in the silent naming of a read description of an object (Gaillard et al. 2001b) have also been performed. Important issues such as the adequate choice of the suitable experimental and control conditions in children have been considered in more detail (Bookheimer 2000; Gaillard et al. 2001a).

In a large study assessing language lateralization with fMRI and the Wada test on 229 patients with epilepsy revealed discordant results between the two techniques in 14 % of patients. Even, if the data of this study showed that fMRI may be more sensitive than the Wada test to right-hemisphere language processing, the data also showed a relevant discordance of the results between the two methods. This discordance mainly affected the patients categorized by either test as having a bilateral language representation (Janecek et al. 2013). To date it can be assumed that fMRI is the most appropriate initial examination to localize essential language areas in the preoperative diagnostic workup and is usually sufficient, if a typical language lateralization can be observed. However, in cases with atypical or bilateral language representation or when fMRI is not conclusive for other reasons, further information about language representation needs to be obtained by other, more invasive, methods (Sharan et al. 2011). Further, it should be kept in mind, that the Wada test and fMRI do not provide the same information and are therefore complementary. Only the Wada test can simulate whether a specific function can be performed, if one particular part of the hemisphere is removed.

In contrast to the Wada test, fMRI has the potential to provide detailed maps of the intrahemispheric localization of critical language areas in addition to the information on lateralization (Sharan et al. 2011). There are a number of studies suggesting a close spatial relationship between fMRI activation and intraoperative electrocortical stimulation (FitzGerald et al. 1997; Yetkin et al. 1997; Ruge et al.

1999; Rutten et al. 1999; Schlosser et al. 1999; Lurito et al. 2000; Carpentier et al. 2001a, b; Ojemann et al. 2013). A study by Rutten et al. 2002c compared the results of fMRI quantitatively with intraoperative electrocortical stimulation mapping in thirteen patients. In eight patients critical language areas were detected by electrocortical stimulation, and in seven of the eight patients, sensitivity of fMRI was 100 % (i.e., fMRI correctly detected all critical language areas with a high spatial accuracy). This indicates that such areas could be safely resected without the need for intraoperative electrocortical stimulation. To obtain this high sensitivity, however, a combination of three different fMRI language paradigms (verb generation, picture naming, and sentence processing) was required. On the other hand, on average only 51 % of fMRI activations were confirmed by electrocortical stimulation indicating a low specificity of fMRI. As mentioned before, both fMRI sensitivity and specificity are strongly dependent on the statistical threshold chosen for data evaluation. In this context, this study illustrates again the problems of basing clinical decisions (e.g., surgical strategies) on single fMRI activation maps alone. Different language-related paradigms activate a different set of brain regions, and a combination of different tasks is necessary to achieve a high sensitivity for the identification of the functionally relevant areas (Ramsey et al. 2001).

Still, a generally accepted standard protocol for language fMRI has not been established yet. Further, the extent of activation also substantially depends on the applied statistical threshold (for details see Sect. 3). Finally, the presence of fMRI activation in nonrelevant language areas limits the predictive value of fMRI for the detection of critical language areas. Some regions activated during language tasks obviously play a minor, supportive role for language function, and resection of these areas may not necessarily produce clinically relevant deficits. Because of such difficulties, the clinical role of fMRI in the identification of eloquent cortical areas of cognitive function is still limited. Thus, at this stage, fMRI can be considered as useful for the facilitation of intraoperative electrocortical stimulation, but can still not replace it (Deblaere et al. 2002; Ojemann et al. 2013).

Another question is whether fMRI can replace the Wada test as the reference procedure for the determination of the language and memory dominance in candidates eligible for brain surgery. A recent metaanalysis overseeing more than 400 patients has shown a very high sensitivity and specificity of fMRI to determine language dominance as compared to the Wada-test (Dym et al. 2011). If established as a valid and reliable technique, fMRI would either render the Wada test obsolete or at least reduce its dominant role and only make it indispensable when fMRI is not practical because of either technical issues or patient properties. The idea behind the Wada test is that the parts of one hemisphere supplied by the

anterior circulation are transiently anesthetized using a bolus of short-acting barbiturates (amobarbital), allowing the contralateral hemisphere to be assessed independently (Wada and Rasmussen 1960; Sharan et al. 2011). The Wada test is invasive, carries significant risks, and the validity of its individual results can be compromised by acute drug effects, which may cause behavioral confounds of sedation and agitation. Although the Wada test is commonly designated by the reference procedure in language lateralization tests (Rausch et al. 1993), it is not a standardized procedure. Differences in almost every aspect of methodology and design can be found in the various Wada test protocols described in the literature (Simkins-Bullock 2000) and make between-center comparisons of the results difficult.

In a review of the literature by Baxendale (2002), 70 patients were found in the literature that had undergone both fMRI and Wada test (Desmond et al. 1995; Binder et al. 1996; Bahn et al. 1997; Hertz-Pannier et al. 1997; Worthington et al. 1997; Benbadis et al. 1998; Yetkin et al. 1998; Benson et al. 1999; Bazin et al. 2000; Lehericy et al. 2000a; Carpentier et al. 2001a). With the exception of only one study (Worthington et al. 1997), showing a comparatively low concordance of only 75 % between the two techniques using a verbal fluency task in fMRI, all other studies reported an impressive high concordance between the two techniques despite the use of different language tasks and Wada test protocols. A study by Binder and colleagues correlated the assessment of language lateralization between the two techniques from the respective lateralization indices, whereby for the Wada test a continuous variable was used and for fMRI the asymmetry in the voxels activated in each hemisphere by a semantic word-decision task was considered (Binder et al. 1996). The correlation was extremely strong ($r=0.96$, $p<0.0001$) and all 22 subjects were classified as having the same lateralization by the two modalities. A concordance of almost 100 % was also found in other studies employing categorical analyses for the classification of language representation (Benbadis et al. 1998; Yetkin et al. 1998). While these observations are promising, there are reasons to be cautious about replacing the Wada test by fMRI at this stage (Wagner et al. 2012; Bauer et al. 2013). In all comparative studies between Wada test and fMRI reviewed above, there were less than 35 collective patients with a reversed or atypical cerebral language dominance pattern as defined by the Wada test, an extremely small patient sample on which to base clinical decisions. As mentioned above, there is evidence of a greater variability of language dominance in patients with epilepsy compared to normal controls (Springer et al. 1999; Carpentier et al. 2001a; Janecek et al. 2013). An atypical language representation is perhaps the most important condition to detect, and the limited data currently available from language fMRI studies in patients with epilepsy do not allow to draw any firm conclu-

sions about the sensitivity or specificity of the various fMRI tests (Spritzer et al. 2012). Moreover, the “true” incidence of a significant discrepancy between fMRI and Wada test for language lateralization assessment is not known, and the reasons for the occasional found inconsistencies have not been investigated systematically. For example, Hammeke and colleagues reported a significant discrepancy between fMRI and Wada lateralization indices in approximately one of ten patients (Hammeke et al. 2000). In particular, temporal tumors in the dominant hemisphere have been reported to cause a false-negative activation of the dominant hemisphere (Westerveld et al. 1999; Gaillard et al. 2000a).

Finally, it has to be emphasized that the Wada test is not only applied to determine language dominance (Simkins-Bullock 2000; Sharan et al. 2011), but, and perhaps more importantly, to assess the ability of each hemisphere to sustain verbal memory. Nonetheless, at this stage more studies with a larger patient pool are required to assess whether fMRI can reliably substitute the Wada test, which so far has been repeatedly validated with respect to memory function, language representation, and prediction of both cognitive and seizure outcome (Binder et al. 2002; Simkins-Bullock 2000; Sharan et al. 2011). Moreover, acceptance of fMRI will largely depend on the perceived clinical need for the “lesion test” aspect of the Wada test, which undoubtedly provides more direct information about how well language and memory functions can be supported after functional removal of the contralateral hemisphere (Sharan et al. 2011). Thus, at present, the diagnostic value of fMRI and the Wada test seems to be rather complementary (Sharan et al. 2011). Killgore et al. found that, when combined, fMRI and Wada test provided complementary data that resulted in an improved prediction of postoperative seizure control compared with either procedure alone (Killgore et al. 1999).

5.2 Special Practical Issues in Presurgical fMRI of Language Function

In contrast to the easy-to-perform movement tasks in motor fMRI, assessment of cognitive brain function – and hereby language function – requires an even closer cooperation of the patient. Therefore, all patients have to be well prepared for the fMRI tasks. The individual patient training, that is required prior to any language fMRI study, can – depending on the degree of the preexisting tumor-associated language or other cognitive deficit – take up to several hours. Such training should guarantee the best possible match between the fMRI paradigms used and the patient’s linguistic ability in order to ensure robust functional localizations and BOLD signals. For these reasons, pre-fMRI training is ideally combined with neuropsychological testing, which also includes detailed

documentation of language deficits. The problem of the objective assessment of task performance in cognitive paradigms is very difficult in a clinical MR-setting. Particularly in non-vocalized paradigms, it is challenging to estimate the patient's performance during block-designed fMRI. Devices assessing the patient's response on the task used in nonclinical or research fMRI conditions can only be used in cooperative patients and are thus often unsuited to routine presurgical fMRI. The best guarantee for sufficient patient cooperation during clinical fMRI scanning remains the intensive training prior to the examination mentioned above. In addition, patients are asked to give their subjective appraisal of task success after each single measurement included in the whole examination. Online evaluation of fMRI data ("real-time fMRI") is an important aid offered by most MR-manufacturers today, enabling immediate assessment of the examination success (Fernandez et al. 2001; Feigl et al. 2008). Hence, erroneous measurements can be immediately detected and repeated.

For the examination itself, the visual or acoustic stimulation unit must be installed and later dismantled within a short period of time to avoid unnecessary disruption of the daily workflow in clinical neuroimaging. If one assumes a time frame of 1 h for the entire fMRI examination, including assembly, dismantling, and adjustment of all stimulation devices, the acquisition of a morphological contrast-enhanced T1-weighted 3D data set for neuronavigation, and possibly another two or three diagnostic neuroimaging sequences, approximately 20 min remains for the acquisition of fMRI data. Within this time, several different language paradigms (Hirsch et al. 2000; Ramsey et al. 2001; Rutten et al. 2002c; Van Westen et al. 2005), preferably of varying degrees of difficulty and each with a repeated measurement to confirm functional localization, should be applied, indicating that each clinical language fMRI measurement cannot take much longer than 5 min. In contrast, preoperative motor fMRI is far easier to implement in the clinical workflow as the time needed for somatotopic mapping does usually not exceed 10 min including patient instruction and feedback. Setup of dedicated apparatus is not necessary.

5.3 Selection of Candidates for Presurgical Language fMRI

In contrast to patients with rolandic brain tumors, the selection of suitable candidates for presurgical language fMRI among patients with frontal and temporoparietal tumors is made largely irrespective of detectable morphological changes in potentially functionally important anatomical structures due to the lack of unequivocal morphological landmarks and due to significant anatomic variations in important language areas. Clinical and neuropsychological symptoms are of key importance. In our opinion, presurgical

fMRI for language-associated brain activation makes sense in the following scenarios:

- Patients presenting with tumor-associated language deficits – including tumors in the right hemisphere, since in this case atypical organization of the language-relevant cortical representations has to be assumed (see Fig. 32)
- Patients without language deficits, but with tumors located in the left hemisphere, that are by anatomical consideration in close proximity to the inferior frontal gyrus (Broca's area), the medial frontal insula (Dronkers area), the superior temporal gyrus (Wernicke's area), and the supramarginal or angular gyri (Geschwind area) (see Figs. 27, 28, and 29)
- Left-handed patients, including patients with right-sided brain tumors
- Multilingual patients

Note

The selection criteria mentioned here are meant as suggestions arising from typical MR-morphological and clinical findings in patients with frontal or temporoparietal brain tumors. It is currently not possible to make a medical indication for fMRI in the strict sense. This is due to the lack of controlled prospective studies demonstrating the clinical benefit of presurgical fMRI in terms of reduced postoperative morbidity or mortality.

5.4 Language Paradigms for Presurgical fMRI

Language is conveyed over an extensive network of multiple functional areas to the frontal, temporal, and parietal lobes in both cerebral hemispheres (see chapter "Functional neuroanatomy"). As demonstrated above, language fMRI can be performed using various paradigms. For this reason no general recommendations can be made. The choice of clinically appropriate fMRI protocols should be made on the basis of the abovementioned diagnostic aims and within the framework of the clinical possibilities: To obtain reliable BOLD activations, paradigms need to be standardized and adjustable to the individual abilities of each patient. The language areas essential for intact speech (Broca's, Wernicke's, Geschwind, Dronkers) should be localized, whereas the importance of the identification of other secondary areas in order to preserve them during surgery is not so clear. A number of different word-generation tasks are suitable to this end, whereby language-associated memory, as well as other linguistic and cognitive processes, can also be assessed using task categories for free generation of several words per trigger (Bookheimer 2002). Sentence-generation tasks pose an even greater challenge (Just et al. 1996; Sakai et al. 2001), however, but can be easily standardized when a defined sentence is generated per trigger.

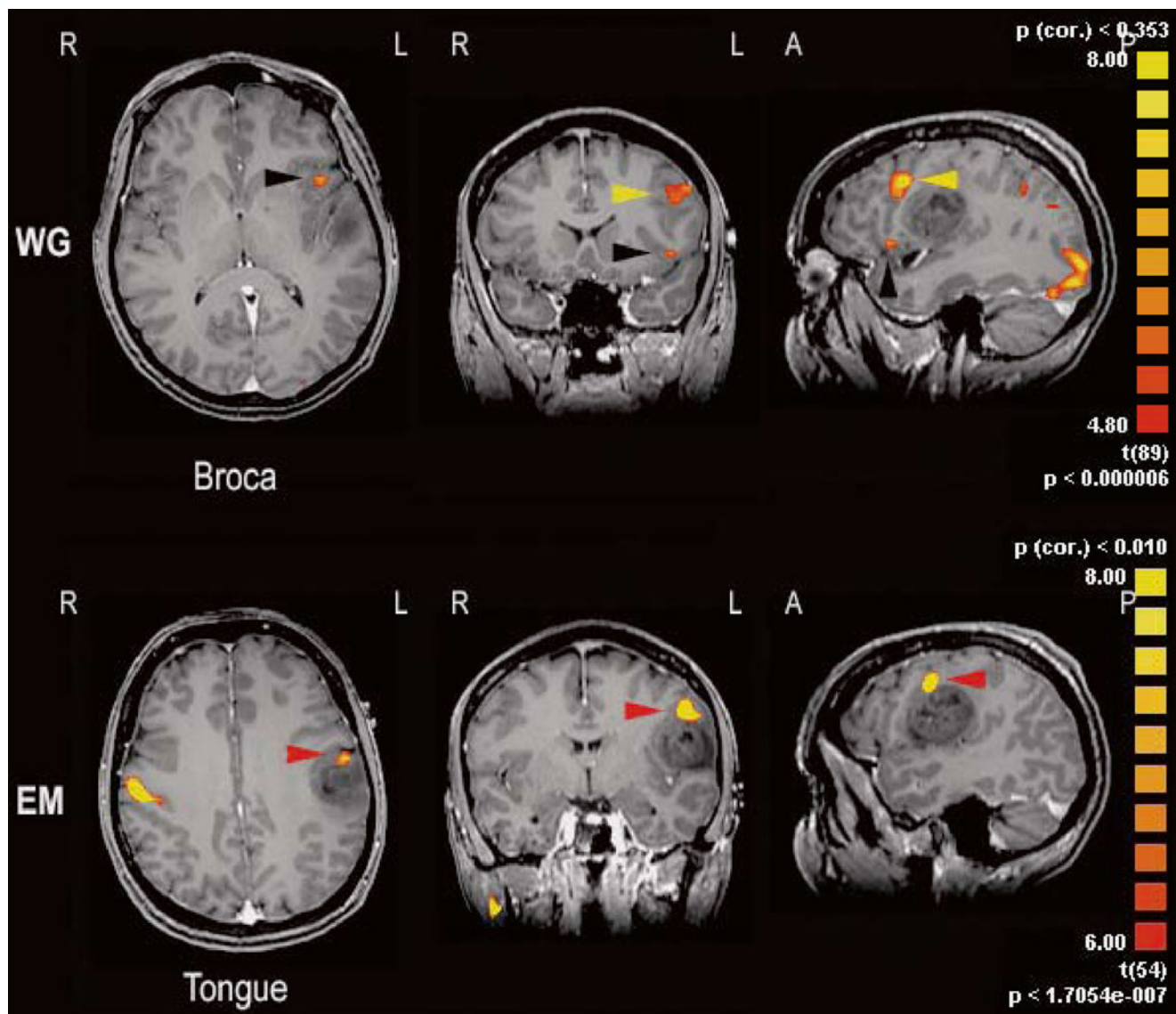


Fig. 27 Presurgical fMRI localization of Broca's area using the word-generation (WG) paradigm in a patient with a left inferior frontal astrocytoma as reflected by the typical activation of the inferior frontal gyrus, pars opercularis (black arrowhead). Note the additional strong

language-associated activation (yellow arrowhead) at the upper edge of the inferior frontal gyrus (pars opercularis). This activation can be distinguished clearly from primary motor tongue activation (EM executed movement) of the inferior precentral gyrus (red arrowhead)

Clinical feasibility tests showed that the individual triggers must be structured as simple and unambiguous as possible in order to detect functional activity robustly. To this end the stimulus presentation frequency should be adjustable to the linguistic abilities of the individual patients, without changing the basic structure of the block design. Task-synchronous motion artifacts can be reduced by using non-vocalized language tasks (overt speech) (Hinke et al. 1993; Rueckert et al. 1994; Palmer et al. 2001), although the resulting brain activation is not identical to that derived from corresponding vocalized paradigms (Partovi et al. 2012b).

The examination protocol suggested here has been specifically designed to fulfill these clinical requirements (Stippich et al. 2003b). Within a measurement time of

approximately 4 min (234 s) per paradigm, reliable functional localization of the Broca's and Wernicke's areas can be achieved, as well as of the anatomically homologous areas in the right hemisphere as a basis on which to calculate regional lateralization indices. Geschwind and Dronkers activation may be observed in addition but is by definition not required according to the classical model of language. At 1.5 T the physiological BOLD signals are quite robust in the abovementioned different functional language areas, with mean correlations between measured BOLD signals and a hemodynamic reference function ranging from $r=0.55$ to $r=0.80$, whereby BOLD signal intensities range typically from 1.5 to 2.5 % (Fig. 27). Both paradigms (sentence and word generation) are visually trig-

gered and can be adjusted to the linguistic ability of the patient by varying the trigger frequency. By using nonmagnetic, optically correctable reflective glasses with a slot for commercial optical lenses, it is possible to correct for ametropia (Stippich et al. 2007b). At the same time, visual stimulation prevents possible undesired superposition of language-associated activations in the Wernicke's speech area (BA21) onto activations in the directly adjacent auditory cortex (BA41, 42), as can occur with acoustic stimulation (Binder et al. 1995).

5.5 Presurgical fMRI of Language Function

In patients with brain tumors, presurgical language fMRI localizes the Broca's and Wernicke's areas in relation to the pathology and enables estimation of hemispheric dominance (Figs. 28 and 29). Besides providing functional landmarks for surgical decision-making and operative planning, different patterns of language activation can be identified, which may be roughly characterized by left dominance, right dominance, equidominance, mixed, or even reversed domi-

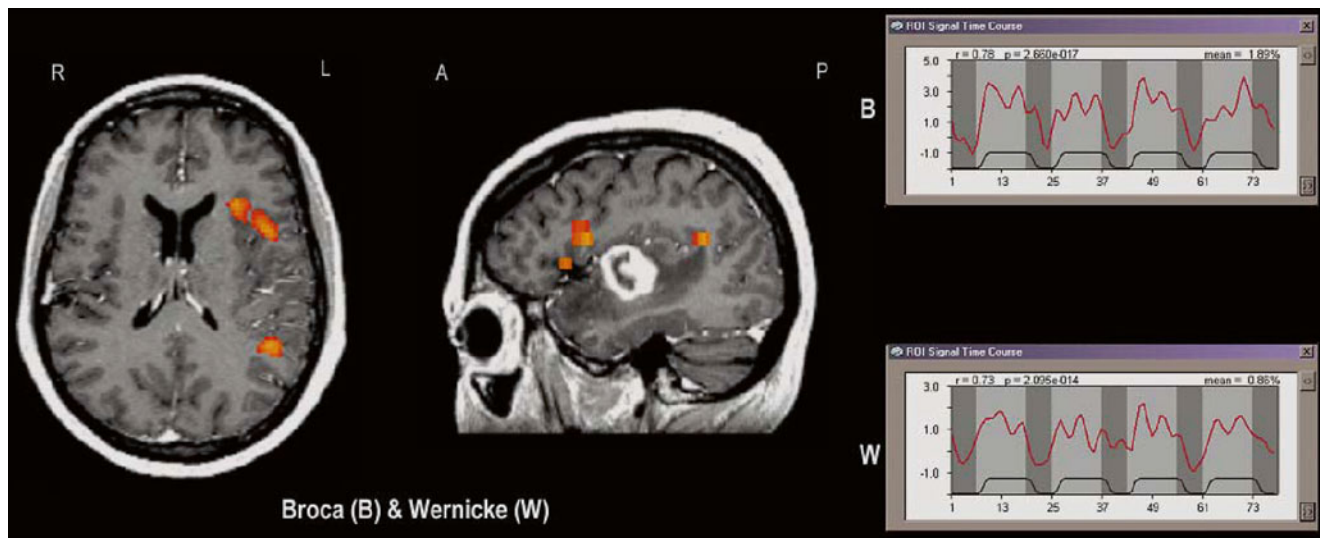


Fig. 28 Presurgical fMRI language localization and lateralization in a right-handed patient with a malignant glioma of the left superior temporal gyrus – critical to Wernicke's area by anatomical consideration. Sentence generation (SG) revealed clear left language dominance and localized Wernicke's area at the dorsal end of the superior temporal

gyrus. BOLD signal time courses for Broca's area (*B*, $r=0.78$, $\Delta S=1.89\%$) and Wernicke's area (*W*, $R=0.73$, $\Delta S=0.86\%$). Note again the two BOLD activations in Broca's area (small cluster at the pars triangularis, larger cluster at the upper pars opercularis)

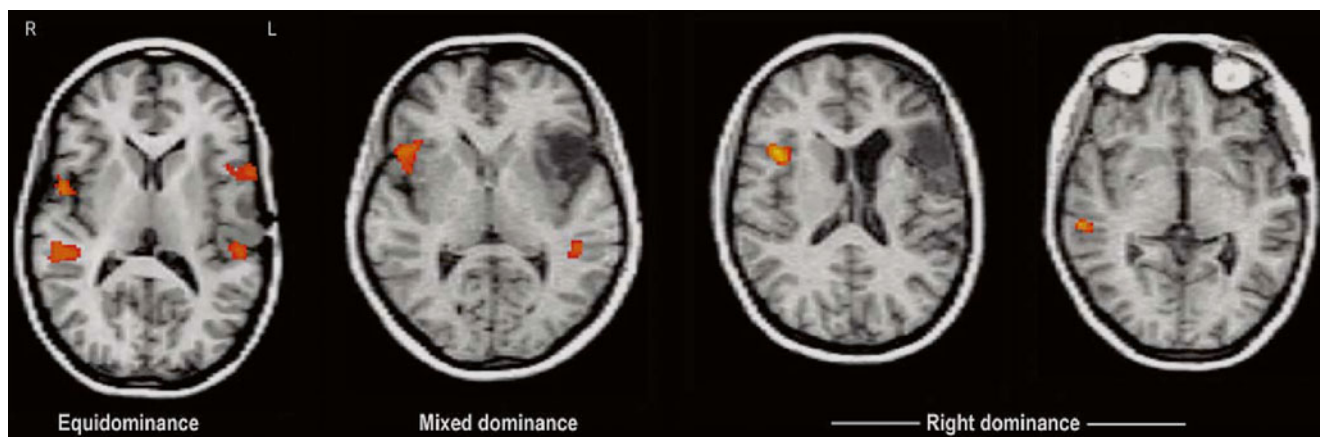


Fig. 29 Patterns of atypical language dominance as revealed by presurgical fMRI: equidominance between both hemispheres, mixed dominance (here with a right dominance for Broca's area and a normal left

dominance for Wernicke's area), and pure right dominance for Broca's and Wernicke's areas

nance. This information is available noninvasively and is more detailed as compared to the information obtained from the Wada test (Fig. 30) (Sharan et al. 2011). However, diagnostic results from different paradigms may differ (Fig. 31). Until now there is no clear rationale for the handling of this problem. Despite a high sensitivity of language fMRI to lateralize language (Dym et al. 2011), the available data to date on the reliability of fMRI for the determination of the language-dominant hemisphere is not fully clear (Janecek et al. 2013; Spritzer et al. 2012). To solve this issue, further validation studies on larger groups of patients in

whom fMRI, reference techniques, and clinical and neuropsychological examinations are carried out in a standardized way are required. With regard to language lateralization, it appears acceptable to dispense with extensive invasive diagnostic examination in cases where, by using several paradigms, a typical left dominance is proven with fMRI (Sharan et al. 2011). On the other hand, additional invasive validation tests should be performed in cases of conflicting results from various different fMRI paradigms and atypical language dominance (Figs. 32 and 33) (Cunningham et al. 2008; Janecek et al. 2013).

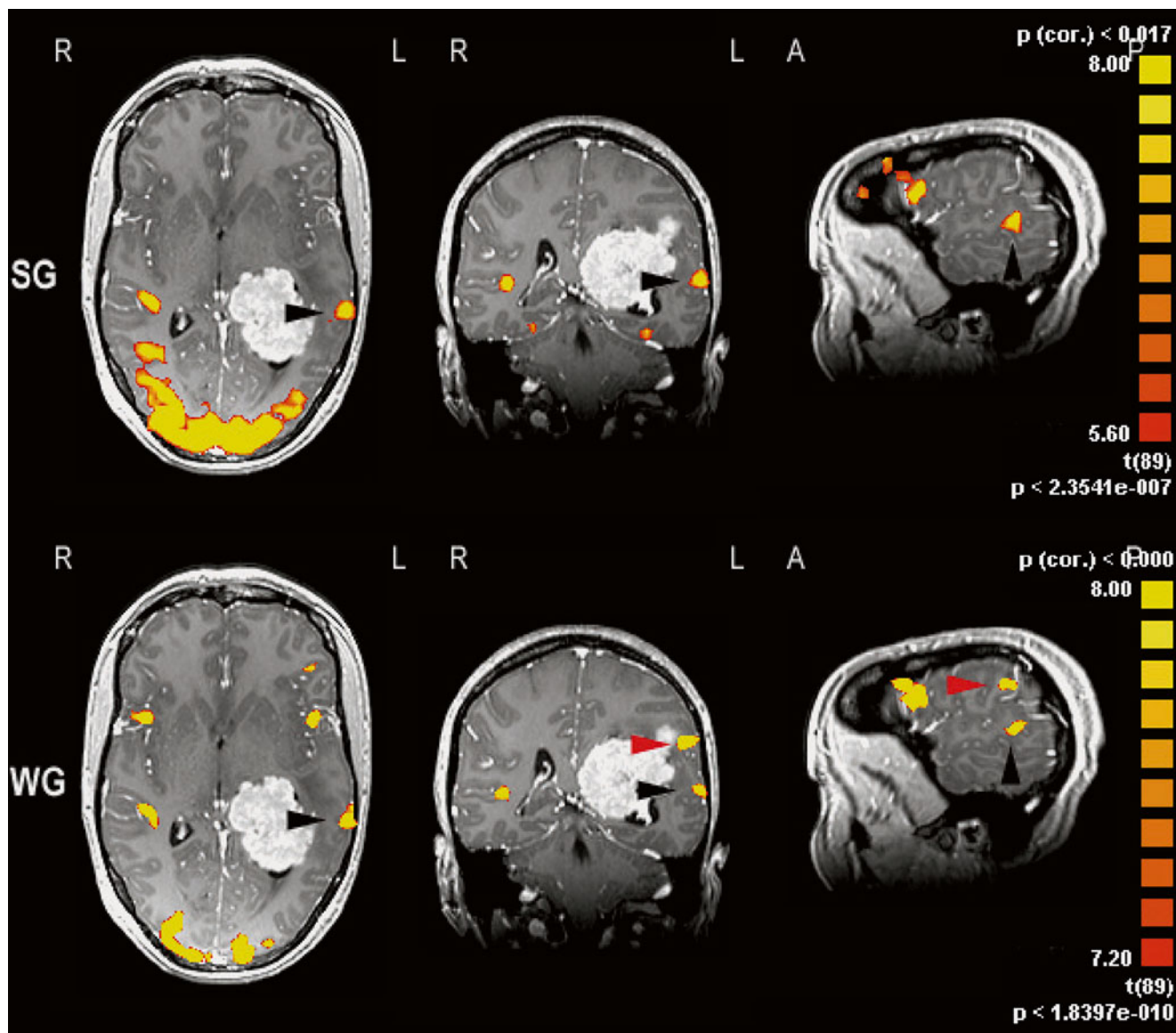


Fig. 30 Presurgical fMRI language localization and lateralization in a patient with a giant intraventricular meningioma using different paradigms. The diagnostic results are not identical, but congruent and support each other. Sentence generation (SG) localized Wernicke's area in its typical localization of the left superior temporal gyrus adjacent to the superior

temporal sulcus (*black arrowhead*) and revealed an equidominance. Word generation (WG) confirmed this finding, but localized a second language center in Wernicke's area in the left supramarginal gyrus (*red arrowhead*) that was also taken into consideration for operation planning and execution. Note the bilateral Broca's activation (also equidominant)

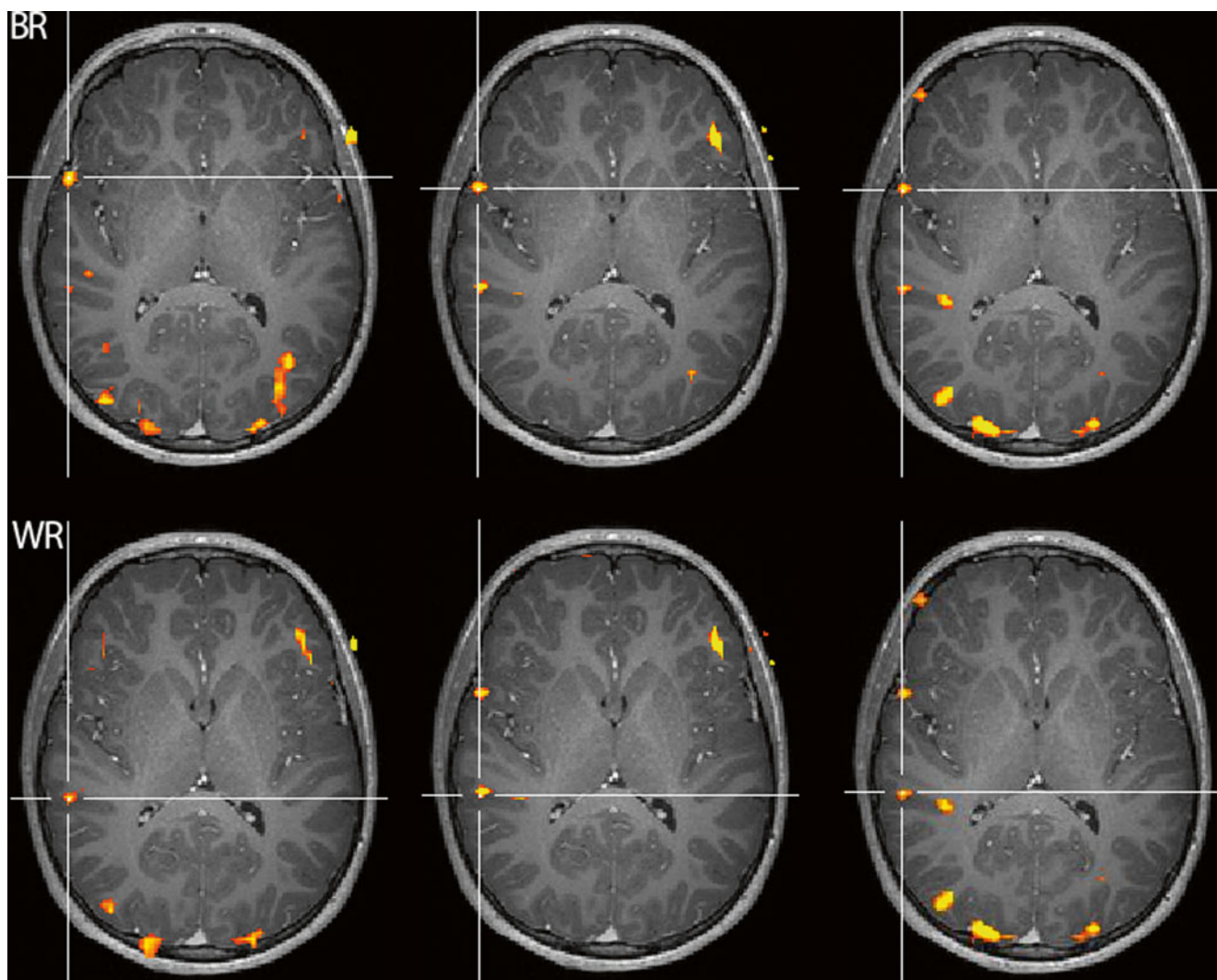


Fig. 31 Presurgical fMRI language lateralization (and localization) in a multilingual left-handed patient. Italian (left), French (middle), and German (right) language paradigms revealed reproducible right hemispheric

language dominance for the anatomical right homologues of Broca's (BR) and Wernicke's (WR) language areas. Awake craniotomy and intraoperative electrocorticography was performed during epilepsy surgery

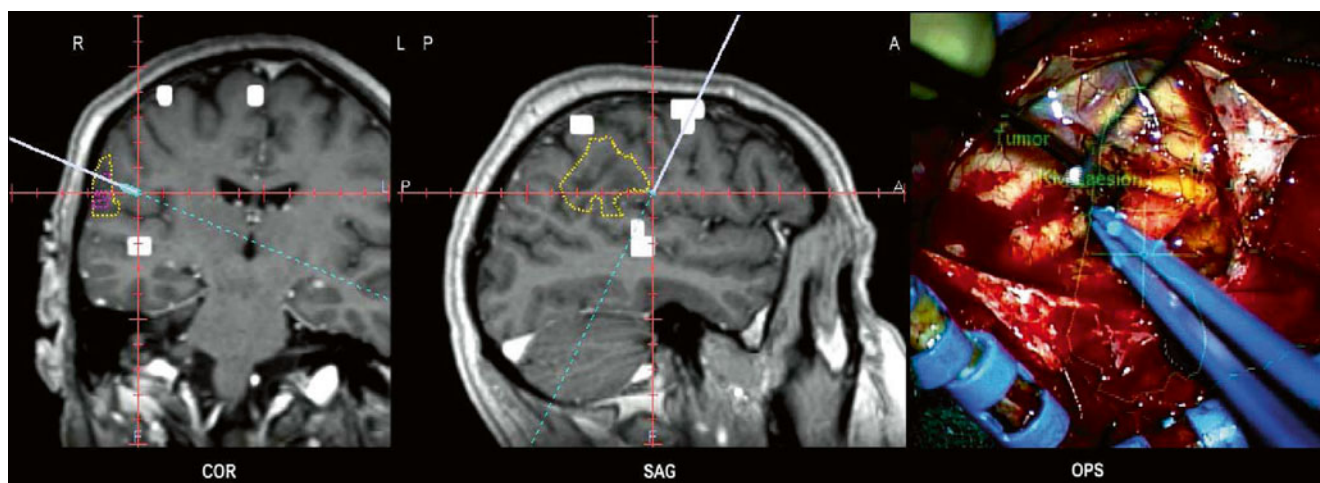
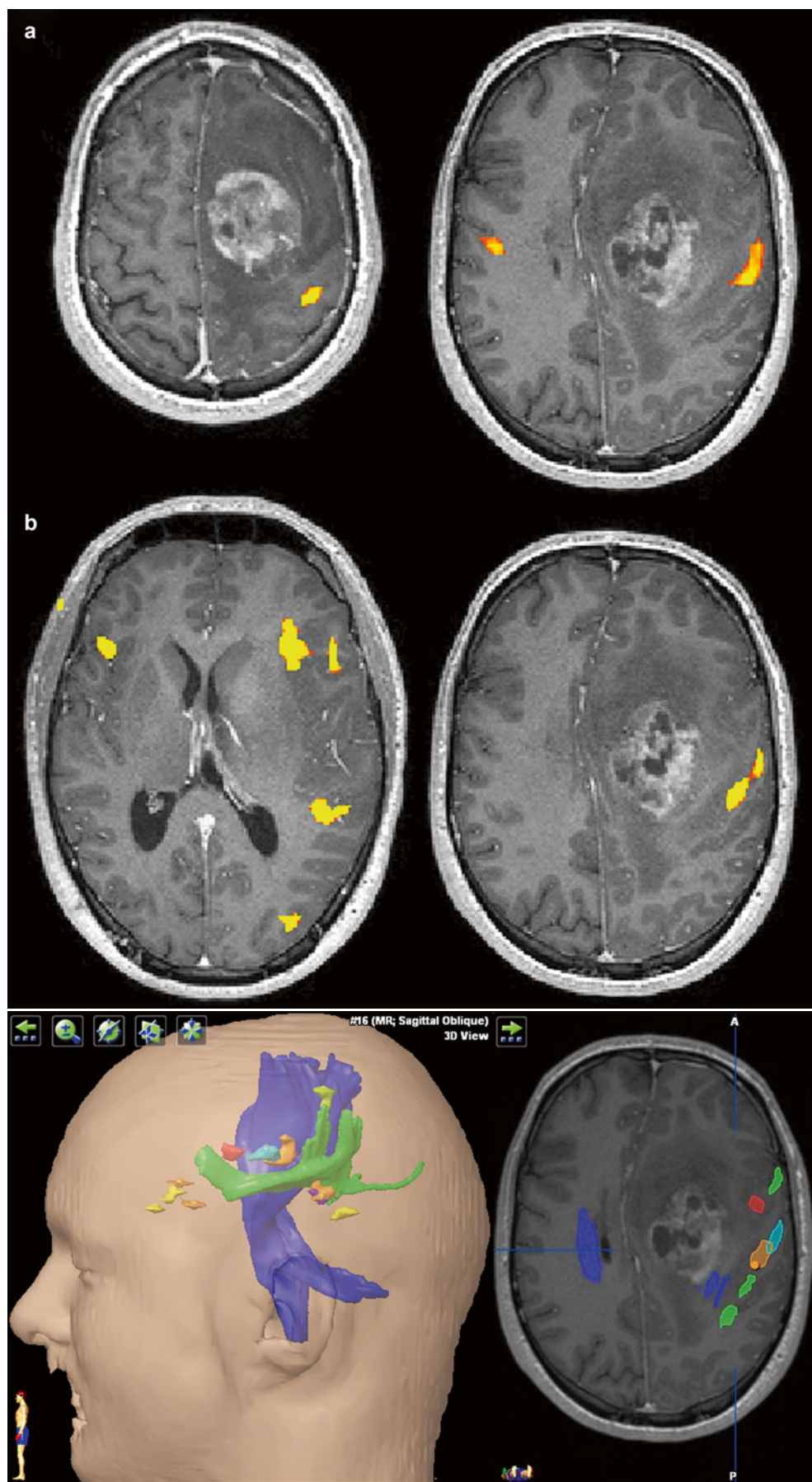


Fig. 32 Intraoperative validation of preoperative fMRI language localization in a right-handed male patient with a right parietal oligoastrocytoma (WHO II) and aphasic symptoms. Atypical right language dominance was diagnosed preoperatively using fMRI and Wada test. Stimulation of the area that showed BOLD activation in the STG (WR)

interrupted language production during awake craniotomy, confirming preoperative fMRI localization. Yellow lines indicate planned resection borders in neuronavigation. Left: coronal (COR) and sagittal (SAG) views; functional activations (white clusters). Right: operative site (OPS)

Fig. 33 (a) Presurgical somatotopic fMRI of motor function (a) provided detailed information on the spatial relationship between the primary motor hand and tongue representations to the left frontal glioblastoma involving the cingulum and corpus callosum. Language fMRI (b) revealed a left language dominance, with a marked activation of the right anatomical homologue of Broca's area, which may indicate tumor-associated neuroplasticity. This overt language paradigm confirmed the primary motor tongue representation on the left when compared to the prior motor study. (b) Integration of the relevant functional activations (landmarks) of the Broca's, Wernicke's, and Geschwind language areas, primary motor and premotor tongue representations, primary motor hand representation, and DTI-tractographies of the pyramidal tract and arcuate fascicle into the T1-weighted contrast-enhanced 3D-MRI used for neuronavigation during extended open biopsy. In these patients, fMRI makes it easier to verify the indication to operate, as well as to plan, functional-sparing surgery, while taking atypical language representations or tumor-induced neuroplastic changes into consideration



6 Diagnostic Capabilities and Limitations of Presurgical Task-Based fMRI

Traditionally, functional areas are electrophysiologically mapped intraoperatively to reliably assess the spatial relationship between the brain tumor and functional cortex (Ojemann et al. 1989; Ojemann 1991; Duffau et al. 1999, 2000, 2001, 2002b, 2003; Duffau 2001, 2005, 2006). Intraoperative ECoG is considered very reliable, but comprises several disadvantages. Duration of surgery can be substantially prolonged and patients often need to be subjected to awake craniotomy. Furthermore, it only provides information from activations of the brain surface, while the by-far larger portion of the cortex deep in the cerebral convolutions remains inaccessible (Cosgrove et al. 1996). Another significant disadvantage of EcoG is that the information is not available preoperatively and can therefore not be implemented in the pretherapeutic assessment of the operative indication and the planning of function-preserving surgery. Likewise, the Wada test as a reference procedure for speech lateralization and memory puts the patient under strain, involves all the risks of arterial catheter angiography, and is not standardized – test results can therefore vary (Wada and Rasmussen 1960; Rausch et al. 1993). After all, morphological imaging with MRI provides very detailed information on intracranial pathologies (Osborn 2012), but not on brain function. fMRI is capable to overcome these disadvantages of the “traditional diagnostic procedures” by visualizing the anatomy, pathology, and function noninvasively within a single examination already prior to surgery. In addition, the course of important WM tracts as the arcuate fascicle can be assessed preoperatively using DTI, and the acquired DTI data can be fused with fMRI in order to enhance pre- and intraoperative planning (Rasmussen et al. 2007; Archip et al. 2007; Berntsen et al. 2010; González-Darder and González-López 2010; Dimous et al. 2013; Jia et al. 2013).

When carried out in a standard way, fMRI is basically capable of providing a clinical “functional diagnosis” for individual patients (Thulborn 2006). Functional landmarks help to estimate possible therapy-related deficits and are thus particularly useful in providing information on the lesion’s location, verifying the indication, and selecting a functional-sparing therapeutic procedure. Once the indication for surgery is made, careful planning and appropriate selection of incision, trepanation, surgical access, and resection margins are essential to function-preserving surgery. Intraoperatively, functional localizations facilitate surgical orientation, although inaccuracies resulting from displaced brain tissue, known

as brain shift, need to be accounted for (Stippich et al. 2002a, 2003a; Rasmussen et al. 2007; Archip et al. 2007; González-Darder and González-López 2010; Kuhnt et al. 2012; Berkels et al. 2014). All these factors increase patient safety and help to minimize the risk of postoperative deficits which would further reduce the quality of life.

According to current knowledge, it can be assumed that presurgical fMRI is able to contribute to a reduction and more targeted selection of invasive diagnostic procedures both before and during neurosurgical interventions in patients with brain tumors or epileptogenic foci. Whether fMRI can have a positive effect on surgery-related morbidity and disease-related mortality remains to be determined in prospective studies. Available results evaluating the use of fMRI data for presurgical planning in relation to functional outcome approve the valuable information obtained by fMRI with respect of the risk of postoperative neurological dysfunction. As mentioned before, it is assumed, in general, that a distance of at least 10 mm between tumor border and functional cortex should be respected for assuring a functionally good postsurgical outcome (Håberg et al. 2004; Krishnan et al. 2004; Berntsen et al. 2010). Assessment of the lesion-to-activation distance (LAD) and the language lateralization index (LI) has in recent work proved to be of value (Kundu et al. 2013; Voss et al. 2013) for evaluation of postoperative outcome. It has been shown that the proximity of the tumor to an activation area might also interact with how the language network is affected (Kundu et al. 2013). Moreover a recent study has demonstrated that the LAD to the primary sensorimotor cortex influences the occurrence of neurological deficits, in contrast to the LAD to the supplementary motor area (SMA) (Voss et al. 2013). Of note is, however, that such attempts should not put the surgeon in an unfounded security as distance measurements can neither solve the problem of ill-defined tumor margins especially in tumors of glial origin or in case of infiltrative tumor growth nor fMRI’s inability to define the exact extent of a functional area, which is arbitrary and given by the chosen statistical threshold during data evaluation. We consider defining “safe resection margins” in presurgical diagnostics on the basis of fMRI data alone as potentially unreliable, since the spatial extent of activated areas depends on the evaluation parameters chosen and can therefore vary. Furthermore, there is not enough data available today that would allow to predict possible post-surgical deficits based on fMRI cerebral reorganization patterns, be it transient or permanent.

Preoperative fMRI has limitations imposed by patient-specific and methodological factors. Despite intensive patient training, optimized examination protocols, and

appropriate head fixation, some patients cannot be examined due to poor cooperation or marked restlessness. When motor paradigms are used, undesirable continuation of movement during resting periods or undesirable and mostly uncontrolled and interspersed accompanying movements in other parts of the body can compromise the quality of the examination, even if individually adjusted evaluation is used to register the respective error precisely. In the end, after this time-consuming process, examination results often need to be discarded. The same applies to strong motion artifacts which cannot be corrected at later data processing stages. Stimulus-related motion artifacts can simulate activations, leading to false high BOLD signals or even to incorrect localization (Hajnal et al. 1994; Krings et al. 2001; Hoeller et al. 2002; Steger and Jackson 2004). With regard to motion artifacts, tongue and toe movements, as well as finger opposition tasks, are less critical than hand, foot, and lip movements. And for language paradigms non-vocalized are less critical than vocalized tasks.

The problems associated with investigating motor function in patients with tumor-related hemipareses have already been addressed (see Sect. 4.6). In most cases, functional localization of the pre- and postcentral gyrus can be achieved by using residual motor function in the affected extremities and applying special paradigms (Stippich et al. 2003a). Compared to motor fMRI, BOLD signals are significantly weaker on tactile stimulation. Particularly in the lower extremities, tactile stimulation does not always achieve sufficient activation. This is accounted for by the lower number of receptors in toe tips, the comparatively small cortical toe representation, and – in our clinical fMRI setup – the ill-defined compressed air pulses when long pneumatic tubes are used.

The success of language fMRI pivotally depends on patient training and optimal adjustment of the paradigm to suit language ability (Stippich et al. 2002a). If patients are over-tested, they perform only a portion of the required tasks leading to lower activation. The same is true of under-testing where too few triggers are given. Additionally, “free thinking” can then lead to uncontrolled activation, for example, when patients get bored. Since, using our paradigms, neither of the sources of error can be controlled directly during fMRI. As a consequence, the paradigm parameters which were proven during pre-fMRI training to be optimal for each individual patient are always used for the preoperative measurement. To increase certainty, the patient is interviewed after each fMRI measurement about whether the task could be successfully accomplished. If this was not the case, the task is repeated. Training always takes place immediately prior to fMRI and lasts at least 20 min in order for the patients to master the paradigms and to avoid interaction of learning effects on examination

results. The training period can last longer in patients with limited linguistic ability.

Of note is that language lateralization – as determined by fMRI – depends on the “cerebral workload” associated with the applied tasks, as the activation in the left hemisphere increases with trigger frequency, whereas activation in the right hemisphere does not fully parallel this effect (Konrad et al. 2005). This implies that the strongest lateralization effect will be measured with paradigms that are optimally adapted to the patient’s individual performance. More importantly brain tumors per se may modulate language lateralization by inducing neuroplastic changes and functional reorganization. In this instance, tumors most likely tend to reduce the activation in the affected hemisphere and may in addition induce an increase of activation in the unaffected hemisphere (Partovi et al. 2012a). This means that brain tumors of the left hemisphere that are critical to essential language areas modulate language lateralization towards the right side, which is in most cases the nondominant one. Consequently, the lateralization indices calculated in patients with brain tumors that affect language function have to be interpreted with special caution: Here, a right language dominance in the presurgical fMRI examination does not necessarily mean that the reduced activation in the left hemisphere is no longer essential to preserve language function, especially when the Broca’s and/or Wernicke’s areas are affected directly by the tumor. In this instance, the assumption that the right hemisphere is fully capable to functionally compensate for the left may be fatal. In contrast, such neuroplastic changes should be interpreted as the brain’s attempts to cope with the pathology, and thus, the residual activation in the classical language areas should be considered as very essential, even, if it is weaker than on the unaffected side.

In the case of uncooperative patients, resting state fMRI has opened up a new field in the investigation of functionally important brain areas (Shimoni et al. 2009; Zhang et al. 2009; Lee et al. 2012; Manglore et al. 2013; Mitchell et al. 2013). Resting state fMRI measures spontaneous, that is, intrinsic, BOLD fluctuations to identify eloquent areas in the brain without the need of task performance by the patients. Therefore, this method is very promising for measuring functional activity in sedated patients, in disabled or uncooperative patients, and in small children. However, until now this technique has been used nearly exclusively for group analysis in research studies. The results on clinical applications in individual patients are very limited and should be considered preliminary. A clear advantage of resting state fMRI is the reduced scanning time in comparison to task-based fMRI, as different neurofunctional systems can be assessed in a single scanning session. Activity correlation in motor regions has been shown to be quite

similar between task-free and task-elicited fMRI (Liu et al. 2009). In one study, more specific analysis and less data variability were found for the motor cortex with resting state fMRI compared with task-based fMRI (Shimoni et al. 2009). These initial reports underline that resting state fMRI may have a clinical potential in pretherapeutic assessment of eloquent areas in patients with brain tumors, vascular lesions, or epilepsy. However, clinical application of resting state fMRI is still limited and further investigation is required to define its role and potency in the clinical and pretherapeutic setting (Lee et al. 2012). A more detailed description on resting state fMRI is given in chapter “[Presurgical resting state fMRI](#)”.

Diffusion tensor imaging (DTI) provides visualization of white matter (WM) tracts and is applied in many centers for the assessment of the relationship between lesions, for example, tumors, and the course of functionally important WM tracts such as the pyramidal tract or the arcuate fascicle. This technique has been reported to be very useful both in the presurgical planning (Morita et al. 2011; Bertani et al. 2012; Hayashi et al. 2012; Abdullah et al. 2013) and for the evaluation of postoperative outcomes (Hayashi et al. 2012). A number of studies are available showing the integration of fMRI with DTI data (Smits et al. 2007) under stereotactic guidance in the intraoperative setting for identification of eloquent areas (Rasmussen et al. 2007; Archip et al. 2007; Berntsen et al. 2010; González-Darder and González-López 2010; Kuhnt et al. 2012; Dimous et al. 2013; Jia et al. 2013; Kumar et al. 2014). Initial results demonstrate the impact of the combination of these two modalities on intraoperative strategies to avoid damaging of the eloquent cortex or WM tracts. Good tumor resection results with preservation of neurological function could be achieved, whereas a safe distance of at least 10 mm between the lesion’s margins and the eloquent area should be maintained in order to avoid transient or permanent neurological deficits (Berntsen et al. 2010). fMRI has proven to be more beneficial for the localization of the functional important areas, whereas DTI data have been shown to be more useful for the resection itself (Rasmussen et al. 2007). Together both techniques show great promise in postsurgical outcomes (Dimous et al. 2013; Jia et al. 2013). Despite such promising results, additional technical inaccuracies must be taken into consideration in neuronavigation and referencing. At this stage further studies are necessary to more accurately define the limits of “safe” resections, especially considering intraoperative brain shift (Gil-Robles and Duffau 2010; González-Darder and González-López 2010).

The position of brain structures can change intraoperatively (“brain shift”), so that preoperatively obtained data do no longer accurately reflect the intraoperative situation

(Wirtz et al. 1997; Wittek et al. 2005; Nimsky et al. 2006). Effluent cerebrospinal fluid alone can lead to shifts of several millimeters after opening of the dura. Moreover, there is often a sharp shift in the position of the brain due to tissue resection. Also for these reasons, preoperative fMRI cannot replace intraoperative mapping of brain function completely. However, preoperatively acquired MRI data are useful as they can be intraoperatively updated with ultrasound hereby to some extent compensating for the brain shift phenomenon (Rasmussen et al. 2007). Intraoperative repetition of fMRI and DTI has also been established with proven value, but on the cost of relevantly longer operation times. Other, investigator-dependent, inaccuracies occur in the manual superposition of the EPI data distorted by the method onto anatomical 3D data sets. As a precaution, a possible localization error of approximately 0.5 cm should always be assumed (Stippich et al. 2003a). Technical improvements include distortion corrections for EPI data sets (Weiskopf et al. 2005; Liu and Ogawa 2006; Priest et al. 2006) enabling for automated superposition procedures, which helps to further reduce inaccuracies in the functional intraoperative localization of eloquent brain structures.

The BOLD signals based on fMRI originate mainly in the capillary bed of the activated brain area and downstream veins (Frahm et al. 1994; Menon et al. 1995). Thus, fMRI measures a hemodynamic secondary phenomenon and not neuronal activity directly. Possible localization errors due to BOLD signals from draining veins can be identified by superimposing functional image data onto contrast-enhanced anatomical T1-weighted image sequences (Krings et al. 1999). Careful analysis of the signal time curves of functional raw data helps to distinguish between parenchymatous and venous activation, since each of both rises at different rates (Krings et al. 2001). A reduced venous contribution to the BOLD signal could be observed at 7 T MR systems; however, for many reasons 7 T scanners cannot be used in clinical routine at this stage (Van der Zwaag et al. 2009). By causing vessel compression and pathological changes in vascular autoregulation, brain tumors can affect the localization and intensity of the BOLD signals measured (Holodny et al. 1999, 2000; Krings et al. 2002a; Ulmer et al. 2003, 2004; Kim et al. 2005; Liu et al. 2005; Hou et al. 2006; Ludemann et al. 2006). Whether artificial activations can occur due to neovascularization remains to be clarified. For this reason, activations within contrast-enhanced portions of brain tumors should be assumed as artifacts until more and reliable study results are available. Such activations should not be used for risk assessment, surgery planning, or functional neuronavigation. The same applies to BOLD signals in strongly vascularized cerebral metastases or arteriovenous malformations (Lazar et al. 1997; Alkadhi et al. 2000; Lehericy et al. 2002; Ozdoba et al. 2002).

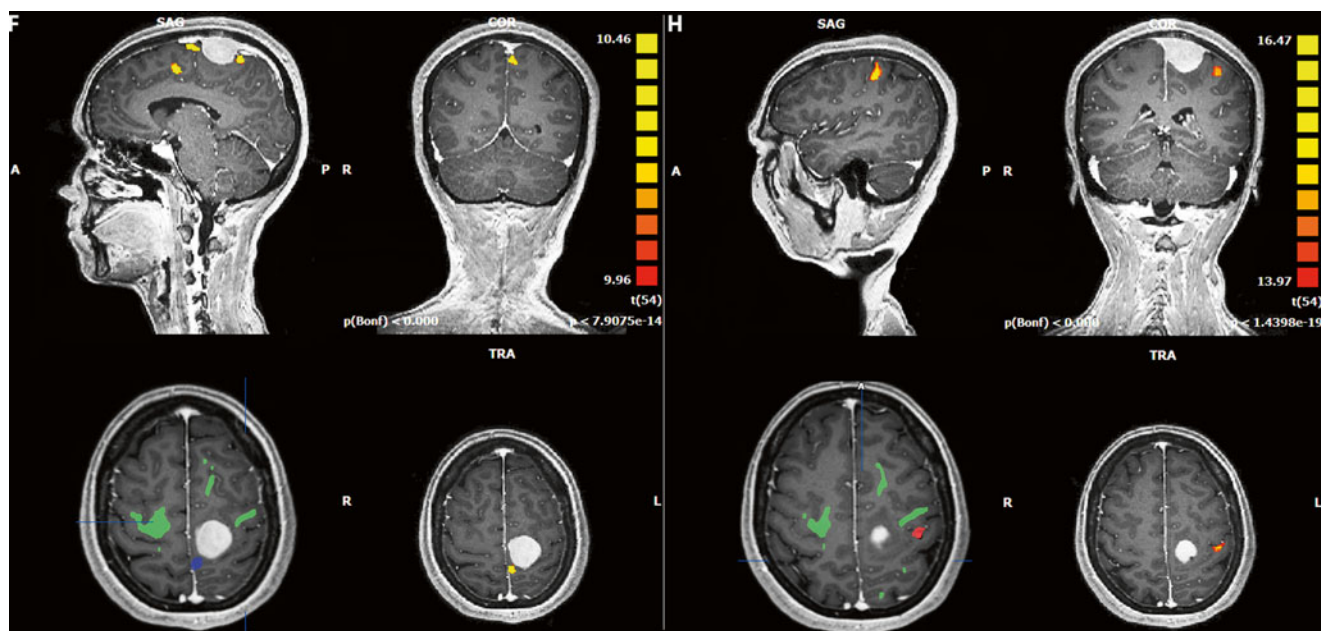


Fig. 34 Presurgical somatotopic motor fMRI and DTI-tractography in a left rolandic meningioma for planning the best surgical access. FMRI localization of the primary motor foot representation (*F*, left image quartet) directly adjacent to the dorsal aspect of the tumor and of the

motor hand representation (*H*, right image quartet). The functional localizations and DTI-tractography were implemented into the T1-weighted 3D data set for functional neuronavigation (*lower row, left* in each quartet)

In summary, task-based fMRI has proven validity and high sensitivity to localize different representations of the human body in the primary motor cortex, to localize essential language areas, and to lateralize language function prior to surgery in patients with brain tumors and epilepsy. Besides providing MR-criteria for selecting, planning, and performing optimized function-preserving treatment tailored to individual patients, fMRI helps to better select patients who require additional pre- and intraoperative invasive diagnostic measures such as the Wada test or electrocorticography and furthermore to reduce the number of such invasive procedures needed through substitution. The method has, however, not reached the status of a fully standardized clinical application in MR-neuroimaging, yet. To this end, further consensus on the performance, analysis, and medical appraisal of presurgical fMRI is warranted, as well as the specification of recommendations and guidelines by the assigned medical societies. Diffusion tensor imaging (DTI) is also of great value in the pre- and intraoperative setting, especially when combined with fMRI, by providing detailed information on functionally important white matter connections such as the pyramidal tract or the arcuate fascicle (Fig. 34). Novel applications employing BOLD-measurements of resting state brain activity (Rs-fMRI) are under initial clinical investigation and may have the potential to further complement pre-operative functional MR by providing additional diagnostic information on important neurofunctional networks and their connectivity.

References

- Abdullah KG, Lubelski D et al (2013) Use of diffusion tensor imaging in glioma resection. *Neurosurg Focus* 34(4):E1
- Achten E, Jackson GD et al (1999) Presurgical evaluation of the motor hand area with functional MR imaging in patients with tumors and dysplastic lesions. *Radiology* 210(2):529–538
- Akbar M, Stippich C, Aschoff A (2005) Magnetic resonance imaging and cerebrospinal fluid shunt valves. *N Engl J Med* 353(13):1413–1414
- Alkadhi H, Kollias SS et al (2000) Plasticity of the human motor cortex in patients with arteriovenous malformations: a functional MR imaging study. *AJNR Am J Neuroradiol* 21(8):1423–1433
- Archip N, Clatz O et al (2007) Non-rigid alignment of pre-operative MRI, fMRI, and DT-MRI with intra-operative MRI for enhanced visualization and navigation in image-guided neurosurgery. *Neuroimage* 35(2):609–624
- Atlas SW, Howard RS 2nd et al (1996) Functional magnetic resonance imaging of regional brain activity in patients with intracerebral gliomas: findings and implications for clinical management. *Neurosurgery* 38(2):329–338
- Avila C, Barros-Loscertales A et al (2006) Memory lateralization with 2 functional MR imaging tasks in patients with lesions in the temporal lobe. *AJNR Am J Neuroradiol* 27(3):498–503
- Baciu M, Le Bas JF et al (2003) Presurgical fMRI evaluation of cerebral reorganization and motor deficit in patients with tumors and vascular malformations. *Eur J Radiol* 46(2):139–146
- Bahn MM, Lin W et al (1997) Localization of language cortices by functional MR imaging compared with intracarotid amobarbital hemispheric sedation. *AJR Am J Roentgenol* 169(2):575–579
- Bandettini PA, Wong EC et al (1992) Time course EPI of human brain function during task activation. *Magn Reson Med* 25(2):390–397
- Barnett A, Marty-Dugas J, McAndrews MP (2014) Advantages of sentence-level fMRI language tasks in presurgical language mapping for temporal lobe epilepsy. *Epilepsy Behav* 32:114–120

- Baudendistel K, Schad LR et al (1996) Monitoring of task performance during functional magnetic resonance imaging of sensorimotor cortex at 1.5 T. *Magn Reson Imaging* 14(1):51–58
- Bauer PR, Reitsma JB et al (2013) Can fMRI safely replace the Wada test for preoperative assessment of language lateralisation? A meta-analysis and systematic review. *J Neurol Neurosurg Psychiatry* 85(5):581–8
- Baumann SB, Noll DC et al (1995) Comparison of functional magnetic resonance imaging with positron emission tomography and magnetoencephalography to identify the motor cortex in a patient with an arteriovenous malformation. *J Image Guid Surg* 1(4):191–197
- Baxendale S (2002) The role of functional MRI in the presurgical investigation of temporal lobe epilepsy patients: a clinical perspective and review. *J Clin Exp Neuropsychol* 24(5):664–676
- Bazin B, Cohen L et al (2000) Study of hemispheric lateralization of language regions by functional MRI. Validation with the Wada test. *Rev Neurol (Paris)* 156(2):145–148
- Belliveau JW, Kennedy DN Jr et al (1991) Functional mapping of the human visual cortex by magnetic resonance imaging. *Science* 254(5032):716–719
- Bello L, Acerbi F et al (2006) Intraoperative language localization in multilingual patients with gliomas. *Neurosurgery* 59(1):115–125; discussion 115–125
- Benbadis SR, Binder JR et al (1998) Is speech arrest during wada testing a valid method for determining hemispheric representation of language? *Brain Lang* 65(3):441–446
- Benson RR, Logan WJ et al (1996) Functional MRI localization of language in a 9-year-old child. *Can J Neurol Sci* 23(3):213–219
- Benson RR, Fitzgerald DB et al (1999) Language dominance determined by whole brain functional MRI in patients with brain lesions. *Neurology* 52(4):798–809
- Berger H (1929) Über das Elektroenzephalogramm des Menschen. *Arch Psychiatr Nerven* 87:527–570
- Berkels B, Cabrilo I et al (2014) Co-registration of intra-operative brain surface photographs and pre-operative MR images. *Int J Comput Assist Radiol Surg* 9(3):387–400
- Berntsen EM, Gulati S et al (2010) Functional magnetic resonance imaging and diffusion tensor tractography incorporate into an intra-operative 3-dimensional ultrasound-based neuronavigation system: impact on therapeutic strategies, extent of resection, and clinical outcome. *Neurosurgery* 67(2):251–264
- Bertani G, Carrabba G et al (2012) Predictive value of inferior fronto-occipital fasciculus (IFO) DTI-fiber tracking for determining the extent of resection for surgery of frontal and temporal gliomas pre-operatively. *J Neurosurg Sci* 56(2):137–143
- Binder JR, Rao SM et al (1995) Lateralized human brain language systems demonstrated by task subtraction functional magnetic resonance imaging. *Arch Neurol* 52(6):593–601
- Binder JR, Swanson SJ et al (1996) Determination of language dominance using functional MRI: a comparison with the Wada test. *Neurology* 46(4):978–984
- Binder JR, Frost JA et al (1997) Human brain language areas identified by functional magnetic resonance imaging. *J Neurosci* 17(1):353–362
- Binder JR, Frost JA et al (1999) Conceptual processing during the conscious resting state. A functional MRI study. *J Cogn Neurosci* 11(1):80–95
- Binder JR, Frost JA et al (2000) Human temporal lobe activation by speech and non-speech sounds. *Cereb Cortex* 10(5):512–528
- Binder JR, Achten E et al (2002) Functional MRI in epilepsy. *Epilepsia* 43(Suppl 1):51–63
- Bittar RG, Olivier A et al (1999a) Localization of somatosensory function by using positron emission tomography scanning: a comparison with intraoperative cortical stimulation. *J Neurosurg* 90(3):478–483
- Bittar RG, Olivier A et al (1999b) Presurgical motor and somatosensory cortex mapping with functional magnetic resonance imaging and positron emission tomography. *J Neurosurg* 91(6):915–921
- Bittar RG, Olivier A et al (2000) Cortical motor and somatosensory representation: effect of cerebral lesions. *J Neurosurg* 92(2):242–248
- Blatow M, Nennig E et al (2007) fMRI reflects functional connectivity of human somatosensory cortex. *Neuroimage* 37(3):927–936
- Bogen JE (1976) Wernicke's region – where is it? *Ann N Y Acad Sci* 290:834–843
- Bogomolny DL, Petrovich NM et al (2004) Functional MRI in the brain tumor patient. *Top Magn Reson Imaging* 15(5):325–335
- Bookheimer SY (2000) Methodological issues in pediatric neuroimaging. *Ment Retard Dev Disabil Res Rev* 6(3):161–165
- Bookheimer S (2002) Functional MRI of language: new approaches to understanding the cortical organization of semantic processing. *Annu Rev Neurosci* 25:151–188
- Briganti C, Sestieri C et al (2012) Reorganization of functional connectivity of the language network in patients with brain gliomas. *AJNR Am J Neuroradiol* 33(10):1983–1990
- Buckner RL, Bandettini PA et al (1996) Detection of cortical activation during averaged single trials of a cognitive task using functional magnetic resonance imaging. *Proc Natl Acad Sci U S A* 93(25):14878–14883
- Carpentier A, Pugh KR et al (2001a) Functional MRI of language processing: dependence on input modality and temporal lobe epilepsy. *Epilepsia* 42(10):1241–1254
- Carpentier AC, Constable RT et al (2001b) Patterns of functional magnetic resonance imaging activation in association with structural lesions in the rolandic region: a classification system. *J Neurosurg* 94(6):946–954
- Cedzich C, Taniguchi M et al (1996) Somatosensory evoked potential phase reversal and direct motor cortex stimulation during surgery in and around the central region. *Neurosurgery* 38(5):962–970
- Choudhri AF, Narayana S et al (2013) Same day tri-modality functional brain mapping prior to resection of a lesion involving eloquent cortex: technical feasibility. *Neuroradiol J* 26(5):548–554
- Cordella R, Acerbi F (2013) Intraoperative neurophysiological monitoring of the cortico-spinal tract in image-guided mini-invasive neurosurgery. *Clin Neurophysiol* 124(6):1244–1254
- Cosgrove GR, Buchbinder BR, Jiang H (1996) Functional magnetic resonance imaging for intracranial navigation. *Neurosurg Clin N Am* 7(2):313–322
- Cox RW (1996) AFNI: software for analysis and visualization of functional magnetic resonance neuroimages. *Comput Biomed Res* 29(3):162–173
- Csaba J (2003) Positron emission tomography in presurgical localization of epileptic foci. *Idegyogy Sz* 56(7–8):249–254
- Cuenod CA, Bookheimer SY et al (1995) Functional MRI during word generation, using conventional equipment: a potential tool for language localization in the clinical environment. *Neurology* 45(10):1821–1827
- Cunningham JM, Morris GL III et al (2008) Unexpected right hemisphere language representation identified by the intracarotid procedure in right-handed epilepsy surgery candidates. *Epilepsy Behav* 13(1):139–143
- Deblaere K, Backes WH et al (2002) Developing a comprehensive presurgical functional MRI protocol for patients with intractable temporal lobe epilepsy: a pilot study. *Neuroradiology* 44(8):667–673
- DeMonte, F., Gilbert, et al (2007) Tumors of the brain and spine, MD Anderson Cancer Care Series. Springer, New York XII, 364 p
- Desmond JE, Sum JM et al (1995) Functional MRI measurement of language lateralization in Wada-tested patients. *Brain* 118(Pt 6):1411–1419
- Dimous S, Battisti RA et al (2013) A systematic review of functional magnetic resonance imaging and diffusion tensor imaging modalities used in presurgical planning of brain tumour resection. *Neurosurg Rev* 36(2):205–214

- Duffau H (2001) Acute functional reorganisation of the human motor cortex during resection of central lesions: a study using intraoperative brain mapping. *J Neurol Neurosurg Psychiatry* 70(4):506–513
- Duffau H (2005) Lessons from brain mapping in surgery for low-grade glioma: insights into associations between tumour and brain plasticity. *Lancet Neurol* 4(8):476–486
- Duffau H (2006) New concepts in surgery of WHO grade II gliomas: functional brain mapping, connectionism and plasticity – a review. *J Neurooncol* 79(1):77–115
- Duffau H, Capelle L et al (1999) Intra-operative direct electrical stimulations of the central nervous system: the Salpetriere experience with 60 patients. *Acta Neurochir (Wien)* 141(11):1157–1167
- Duffau H, Sichez JP, Lehericy S (2000) Intraoperative unmasking of brain redundant motor sites during resection of a precentral angioma: evidence using direct cortical stimulation. *Ann Neurol* 47(1):132–135
- Duffau H, Bauchet L et al (2001) Functional compensation of the left dominant insula for language. *Neuroreport* 12(10):2159–2163
- Duffau H, Capelle L et al (2002a) Intraoperative mapping of the subcortical language pathways using direct stimulations. An anatomic-functional study. *Brain* 125(Pt 1):199–214
- Duffau H, Denvil D, Capelle L (2002b) Long term reshaping of language, sensory, and motor maps after glioma resection: a new parameter to integrate in the surgical strategy. *J Neurol Neurosurg Psychiatry* 72(4):511–516
- Duffau H, Capelle L et al (2003) Usefulness of intraoperative electrical subcortical mapping during surgery for low-grade gliomas located within eloquent brain regions: functional results in a consecutive series of 103 patients. *J Neurosurg* 98(4):764–778
- Dym RJ, Burns J et al (2011) Is functional MR imaging assessment of hemispheric language dominance as good as the WADA test?: a meta-analysis. *Radiology* 261(2):446–455
- Dymarkowski S, Sunaert S et al (1998) Functional MRI of the brain: localisation of eloquent cortex in focal brain lesion therapy. *Eur Radiol* 8(9):1573–1580
- Fakhri M, All Oghablan M et al (2013) Atypical language lateralization: an fMRI study in patients with cerebral lesions. *Funct Neurol* 28(1):55–61
- Fandino J, Kollias SS et al (1999) Intraoperative validation of functional magnetic resonance imaging and cortical reorganization patterns in patients with brain tumors involving the primary motor cortex. *J Neurosurg* 91(2):238–250
- Feigl GC, Safavi-Abbas S et al (2008) Real-time 3 T fMRI data of brain tumor patients for intra-operative localization of primary motor areas. *Eur J Surg Oncol* 34(6):708–715
- Fernandez G, de Greiff A et al (2001) Language mapping in less than 15 minutes: real-time functional MRI during routine clinical investigation. *Neuroimage* 14(3):585–594
- Fesl G, Moriggl B et al (2003) Inferior central sulcus: variations of anatomy and function on the example of the motor tongue area. *Neuroimage* 20(1):601–610
- Findley AM, Ambrose JB et al (2012) Dynamics of hemispheric dominance for language assessed by magnetoencephalographic imaging. *Ann Neurol* 71(5):668–686
- FitzGerald DB, Cosgrove GR et al (1997) Location of language in the cortex: a comparison between functional MR imaging and electrocortical stimulation. *AJNR Am J Neuroradiol* 18(8):1529–1539
- Fox PT, Mintun MA et al (1986) Mapping human visual cortex with positron emission tomography. *Nature* 323(6091):806–809
- Frahm J, Merboldt KD et al (1994) Brain or vein – oxygenation or flow? On signal physiology in functional MRI of human brain activation. *NMR Biomed* 7(1–2):45–53
- Friston K (1996) Statistical parametric mapping and other analyses of functional imaging data. In: Mazziotta J, Toga AW (eds) *Brain mapping: the methods*. Academic, New York, pp 363–386
- Frost JA, Binder JR et al (1999) Language processing is strongly left lateralized in both sexes. Evidence from functional MRI. *Brain* 122(Pt 2):199–208
- Gabrieli JD, Poldrack RA, Desmond JE (1998) The role of left prefrontal cortex in language and memory. *Proc Natl Acad Sci U S A* 95(3):906–913
- Gaillard WD, Bookheimer SY, Cohen M (2000a) The use of fMRI in neocortical epilepsy. *Adv Neurol* 84:391–404
- Gaillard WD, Hertz-Pannier L et al (2000b) Functional anatomy of cognitive development: fMRI of verbal fluency in children and adults. *Neurology* 54(1):180–185
- Gaillard WD, Grandin GB, Xu B (2001a) Developmental aspects of pediatric fMRI: considerations for image acquisition, analysis, and interpretation. *Neuroimage* 13(2):239–249
- Gaillard WD, Pugliese M et al (2001b) Cortical localization of reading in normal children: an fMRI language study. *Neurology* 57(1):47–54
- Gaillard WD, Balsamo L et al (2002) Language dominance in partial epilepsy patients identified with an fMRI reading task. *Neurology* 59(2):256–265
- García-Eulate R, García-García D et al (2011) Functional bold MRI: advantages of the 3 T vs. the 1.5 T. *Clin Imaging* 35(3):236–241
- Gasser T, Ganslandt O et al (2005) Intraoperative functional MRI: implementation and preliminary experience. *Neuroimage* 26(3): 685–693
- Georgi JC, Stippich C et al (2004) Active deep brain stimulation during MRI: a feasibility study. *Magn Reson Med* 51(2):380–388
- Geschwind N (1971) Current concepts: aphasia. *N Engl J Med* 284(12): 654–656
- Gevins A (1995) High-resolution electroencephalographic studies of cognition. *Adv Neurol* 66:181–195; discussion 195–198
- Gevins A, Leong H et al (1995) Mapping cognitive brain function with modern high-resolution electroencephalography. *Trends Neurosci* 18(10):429–436
- Gil-Robles S, Duffau H (2010) Surgical management of World Health Organization Grade II gliomas in eloquent areas: the necessity of preserving a margin around functional structures. *Neurosurg Focus* 28(2):E8
- Golaszewski SM, Zschiegner F et al (2002) A new pneumatic vibrator for functional magnetic resonance imaging of the human sensorimotor cortex. *Neurosci Lett* 324(2):125–128
- Golaszewski SM, Siedentopf CM et al (2004) Modulatory effects on human sensorimotor cortex by whole-hand afferent electrical stimulation. *Neurology* 62(12):2262–2269
- Golaszewski SM, Siedentopf CM et al (2006) Human brain structures related to plantar vibrotactile stimulation: a functional magnetic resonance imaging study. *Neuroimage* 29(3):923–929
- Gold S, Christian B et al (1998) Functional MRI statistical software packages: a comparative analysis. *Hum Brain Mapp* 6(2):73–84
- González-Darder JM, González-López P (2010) Multimodal navigation in the functional microsurgical resection of intrinsic brain tumors located in eloquent motor areas: role of tractography. *Neurosurg Focus* 28(2):E5
- Grabowski TJ (2000) Investigating language with functional neuroimaging. In: Mazziotta J, Toga AW (eds) *Brain mapping: the systems*. Academic, San Diego, pp 425–461
- Grummich P, Nimsky C et al (2006) Combining fMRI and MEG increases the reliability of presurgical language localization: a clinical study on the difference between and congruence of both modalities. *Neuroimage* 32(4):1793–1803
- Håberg A, Kvistad KA et al (2004) Preoperative blood oxygen level-dependent functional magnetic resonance imaging in patients with primary brain tumors: clinical application and outcome. *Neurosurgery* 54(4):902–914; discussion 914–915
- Hajnal JV, Myers R et al (1994) Artifacts due to stimulus correlated motion in functional imaging of the brain. *Magn Reson Med* 31(3):283–291

- Hall WA, Liu H, Truwit CL (2005) Functional magnetic resonance imaging-guided resection of low-grade gliomas. *Surg Neurol* 64(1): 20–27; discussion 27
- Hämäläinen M, Ilmoniemi RJ, Knuutila J, Lounasmaa OV (1993) Magnetoencephalography -theory, instrumentation and applications to noninvasive studies of the working human brain. *Rev Mod Phys* 65:413–487
- Hammeke TA, Yetkin FZ et al (1994) Functional magnetic resonance imaging of somatosensory stimulation. *Neurosurgery* 35(4): 677–681
- Hammeke TA, Bellgowan PS, Binder JR (2000) fMRI: methodology – cognitive function mapping. *Adv Neurol* 83:221–233
- Hari R, Ilmoniemi RJ (1986) Cerebral magnetic fields. *Crit Rev Biomed Eng* 14(2):93–126
- Hasegawa M, Carpenter PA, Just MA (2002) An fMRI study of bilingual sentence comprehension and workload. *Neuroimage* 15(3):647–660
- Hayashi Y, Kinoshita M et al (2012) Correlation between language function and the left arcuate fasciculus detected by diffusion tensor imaging tractography. *J Neurosurg* 117(5):839–843
- Herholz K, Reulen HJ et al (1997) Preoperative activation and intraoperative stimulation of language-related areas in patients with glioma. *Neurosurgery* 41(6):1253–1260; discussion 1260–1262
- Hermann BP, Perrine K et al (1999) Visual confrontation naming following left anterior temporal lobectomy: a comparison of surgical approaches. *Neuropsychology* 13(1):3–9
- Hernandez AE, Dapretto M et al (2001) Language switching and language representation in Spanish-English bilinguals: an fMRI study. *Neuroimage* 14(2):510–520
- Hertz-Pannier L, Gaillard WD et al (1997) Noninvasive assessment of language dominance in children and adolescents with functional MRI: a preliminary study. *Neurology* 48(4):1003–1012
- Hertz-Pannier L, Chiron C et al (2002) Late plasticity for language in a child's non-dominant hemisphere: a pre- and post-surgery fMRI study. *Brain* 125(Pt 2):361–372
- Hinke RM, Hu X et al (1993) Functional magnetic resonance imaging of Broca's area during internal speech. *Neuroreport* 4(6):675–678
- Hirsch J, Ruge MI et al (2000) An integrated functional magnetic resonance imaging procedure for preoperative mapping of cortical areas associated with tactile, motor, language, and visual functions. *Neurosurgery* 47(3):711–721; discussion 721–722
- Hoeller M, Krings T et al (2002) Movement artefacts and MR BOLD signal increase during different paradigms for mapping the sensorimotor cortex. *Acta Neurochir (Wien)* 144(3):279–284; discussion 284
- Holman BL, Devous MD Sr (1992) Functional brain SPECT: the emergence of a powerful clinical method. *J Nucl Med* 33(10):1888–1904
- Holodny AI, Shevzov-Zebrun N (2011) Motor and sensory mapping. *Neurosurg Clin North Am* 22(2):207–218
- Holodny AI, Schulder M et al (1999) Decreased BOLD functional MR activation of the motor and sensory cortices adjacent to a glioblastoma multiforme: implications for image-guided neurosurgery. *AJNR Am J Neuroradiol* 20(4):609–612
- Holodny AI, Schulder M et al (2000) The effect of brain tumors on BOLD functional MR imaging activation in the adjacent motor cortex: implications for image-guided neurosurgery. *AJNR Am J Neuroradiol* 21(8):1415–1422
- Holodny AI, Schwartz TH et al (2001) Tumor involvement of the corticospinal tract: diffusion magnetic resonance tractography with intraoperative correlation. *J Neurosurg* 95(6):1082
- Holodny AI, Schulder M et al (2002) Translocation of Broca's area to the contralateral hemisphere as the result of the growth of a left inferior frontal glioma. *J Comput Assist Tomogr* 26(6):941–943
- Hou BL, Bradbury M et al (2006) Effect of brain tumor neovasculature defined by rCBV on BOLD fMRI activation volume in the primary motor cortex. *Neuroimage* 32(2):489–497
- Hsu CC, Wu MT, Lee C (2001) Robust image registration for functional magnetic resonance imaging of the brain. *Med Biol Eng Comput* 39(5):517–524
- Hulvershorn J, Bloy L et al (2005a) Spatial sensitivity and temporal response of spin echo and gradient echo bold contrast at 3 T using peak hemodynamic activation time. *Neuroimage* 24(1):216–223
- Hulvershorn J, Bloy L et al (2005b) Temporal resolving power of spin echo and gradient echo fMRI at 3 T with apparent diffusion coefficient compartmentalization. *Hum Brain Mapp* 25(2):247–258
- Illes J, Francis WS et al (1999) Convergent cortical representation of semantic processing in bilinguals. *Brain Lang* 70(3):347–363
- Jack CR Jr, Thompson PM et al (1994) Sensory motor cortex: correlation of presurgical mapping with functional MR imaging and invasive cortical mapping. *Radiology* 190(1):85–92
- Jacobs AH, Kracht LW et al (2005) Imaging in neurooncology. *NeuroRx* 2(2):333–347
- Janecek JK, Swanson SJ et al (2013) Language lateralization by fMRI and WADA testing in 229 patients with epilepsy: rates and predictors of discordance. *Epilepsia* 54(2):314–322
- Jia XX, Yu Y et al (2013) FMRI-driven DTT-assessment of corticospinal tracts prior to cortex resection. *Can J Neurol Sci* 40(4):558–563
- Jiang Z, Krainik A (2010) Impaired fMRI activation in patients with primary brain tumors. *Neuroimage* 52(2):538–548
- Jovčevska I, Kočevar N, Komel R (2013) Glioma and glioblastoma – how much do we (not) know? *Mol Clin Oncol* 1(6):935–941
- Just MA, Carpenter PA et al (1996) Brain activation modulated by sentence comprehension. *Science* 274(5284):114–116
- Kampe KK, Jones RA, Auer DP (2000) Frequency dependence of the functional MRI response after electrical median nerve stimulation. *Hum Brain Mapp* 9(2):106–114
- Kasprian G, Seidel S (2010) Modern neuroimaging of brain plasticity. *Radiologe* 50(2):136–143
- Kaye AH, Laws ER (2011) Brain tumors: an encyclopedic approach, expert consult – online and print, 3rd edn. Saunders, St. Louis
- Killgore WD, Glosser G et al (1999) Functional MRI and the Wada test provide complementary information for predicting post-operative seizure control. *Seizure* 8(8):450–455
- Kim KH, Relkin NR et al (1997) Distinct cortical areas associated with native and second languages. *Nature* 388(6638):171–174
- Kim MJ, Holodny AI et al (2005) The effect of prior surgery on blood oxygen level-dependent functional MR imaging in the preoperative assessment of brain tumors. *AJNR Am J Neuroradiol* 26(8):1980–1985
- Klein D, Milner B et al (1995) The neural substrates underlying word generation: a bilingual functional-imaging study. *Proc Natl Acad Sci U S A* 92(7):2899–2903
- Kober H, Nimsky C et al (2001) Correlation of sensorimotor activation with functional magnetic resonance imaging and magnetoencephalography in presurgical functional imaging: a spatial analysis. *Neuroimage* 14(5):1214–1228
- Kokkonen SM, Kiviniemi V et al (2005) Effect of brain surgery on auditory and motor cortex activation: a preliminary functional magnetic resonance imaging study. *Neurosurgery* 57(2):249–256; discussion 249–256
- Konrad F, Nennig E et al (2005) Does the individual adaptation of standardized speech paradigms for clinical functional magnetic resonance imaging (fMRI) effect the localization of the language-dominant hemisphere and of Broca's and Wernicke's areas. *Rofo* 177(3):381–385
- Krainik A, Lehericy S et al (2001) Role of the supplementary motor area in motor deficit following medial frontal lobe surgery. *Neurology* 57(5):871–878
- Krainik A, Lehericy S et al (2003) Postoperative speech disorder after medial frontal surgery: role of the supplementary motor area. *Neurology* 60(4):587–594
- Krainik A, Duffau H et al (2004) Role of the healthy hemisphere in recovery after resection of the supplementary motor area. *Neurology* 62(8):1323–1332

- Krasnow B, Tamm L et al (2003) Comparison of fMRI activation at 3 T and 1.5 T during perceptual, cognitive, and affective processing. *Neuroimage* 18(4):813–826
- Krings T, Buchbinder BR et al (1997) Functional magnetic resonance imaging and transcranial magnetic stimulation: complementary approaches in the evaluation of cortical motor function. *Neurology* 48(5):1406–1416
- Krings T, Reul J et al (1998) Functional magnetic resonance mapping of sensory motor cortex for image-guided neurosurgical intervention. *Acta Neurochir (Wien)* 140(3):215–222
- Krings T, Erberich SG et al (1999) MR blood oxygenation level-dependent signal differences in parenchymal and large draining vessels: implications for functional MR imaging. *AJNR Am J Neuroradiol* 20(10):1907–1914
- Krings T, Reinges MH et al (2001) Functional MRI for presurgical planning: problems, artefacts, and solution strategies. *J Neurol Neurosurg Psychiatry* 70(6):749–760
- Krings T, Reinges MH et al (2002a) Factors related to the magnitude of T2* MR signal changes during functional imaging. *Neuroradiology* 44(6):459–466
- Krings T, Topper R et al (2002b) Activation in primary and secondary motor areas in patients with CNS neoplasms and weakness. *Neurology* 58(3):381–390
- Krishnan R, Raabe A et al (2004) Functional magnetic resonance imaging-integrated neuronavigation: correlation between lesion-to-motor cortex distance and outcome. *Neurosurgery* 55(4):904–914; discussion 914–915
- Kuhnt D, Bauer MH, Nimsky C (2012) Brain shift compensation and neurosurgical image fusion using intraoperative MRI: current status and future challenges. *Crit Rev Biomed Eng* 40(3):175–185
- Kumar A, Chandra PS et al (2014) The role of neuronavigation-guided functional MRI and diffusion tensor tractography along with cortical stimulation in patients with eloquent cortex lesions. *Br J Neurosurg* 28(2):226–233
- Kundu B, Penwarden A et al (2013) Association of functional magnetic resonance imaging indices with postoperative language outcomes in patients with primary brain tumors. *Neurosurg Focus* 34(4):E6
- Kurth R, Villringer K et al (1998) fMRI assessment of somatotopy in human Brodmann area 3b by electrical finger stimulation. *Neuroreport* 9(2):207–212
- Kwong KK, Belliveau JW et al (1992) Dynamic magnetic resonance imaging of human brain activity during primary sensory stimulation. *Proc Natl Acad Sci U S A* 89(12):5675–5679
- la Fougère C, Rominger A et al (2009) PET and SPECT in epilepsy: a critical review. *Epilepsy Behav* 15(1):50–55
- Landis SH, Murray T et al (1999) Cancer statistics, 1999. *CA Cancer J Clin* 49(1):8–31, 1
- Latchaw RE, Ugurbil K, Hu X (1995) Functional MR imaging of perceptual and cognitive functions. *Neuroimaging Clin N Am* 5(2):193–205
- Lazar RM, Marshall RS et al (1997) Anterior translocation of language in patients with left cerebral arteriovenous malformation. *Neurology* 49(3):802–808
- Lee CC, Jack CR Jr et al (1996) Real-time adaptive motion correction in functional MRI. *Magn Reson Med* 36(3):436–444
- Lee CC, Grimm RC et al (1998a) A prospective approach to correct for inter-image head rotation in fMRI. *Magn Reson Med* 39(2):234–243
- Lee CC, Jack CR Jr, Riederer SJ (1998b) Mapping of the central sulcus with functional MR: active versus passive activation tasks. *AJNR Am J Neuroradiol* 19(5):847–852
- Lee CC, Jack CR Jr et al (1998c) Real-time reconstruction and high-speed processing in functional MR imaging. *AJNR Am J Neuroradiol* 19(7):1297–1300
- Lee CC, Ward HA et al (1999) Assessment of functional MR imaging in neurosurgical planning. *AJNR Am J Neuroradiol* 20(8): 1511–1519
- Lee MH, Smyser CD, Shimony JS (2012) Resting-state fMRI: a review of methods and clinical applications. *AJNR Am J Neuroradiol* 34(10):1866–72
- Lehericy S, Cohen L et al (2000a) Functional MR evaluation of temporal and frontal language dominance compared with the Wada test. *Neurology* 54(8):1625–1633
- Lehericy S, Duffau H et al (2000b) Correspondence between functional magnetic resonance imaging somatotopy and individual brain anatomy of the central region: comparison with intraoperative stimulation in patients with brain tumors. *J Neurosurg* 92(4):589–598
- Lehericy S, Biondi A et al (2002) Arteriovenous brain malformations: is functional MR imaging reliable for studying language reorganization in patients? Initial observations. *Radiology* 223(3):672–682
- Lichtheim L (1885) On aphasia. *Brain* 7:433–484
- Liu G, Ogawa S (2006) EPI image reconstruction with correction of distortion and signal losses. *J Magn Reson Imaging* 24(3):683–689
- Liu H, Hall WA, Truwit CL (2003) The roles of functional MRI in MR-guided neurosurgery in a combined 1.5 Tesla MR-operating room. *Acta Neurochir Suppl* 85:127–135
- Liu WC, Feldman SC et al (2005) The effect of tumour type and distance on activation in the motor cortex. *Neuroradiology* 47(11):813–819
- Liu H, Buckner RL et al (2009) Task-free presurgical mapping using functional magnetic resonance imaging intrinsic activity. *J Neurosurg* 111(4):746–754
- Logothetis NK (1999) Functional magnetic resonance imaging in children. *Semin Pediatr Neurol* 6(2):78–86
- Logothetis NK (2002) The neural basis of the blood-oxygen-level-dependent functional magnetic resonance imaging signal. *Philos Trans R Soc Lond B Biol Sci* 357(1424):1003–1037
- Logothetis NK (2003) The underpinnings of the BOLD functional magnetic resonance imaging signal. *J Neurosci* 23(10):3963–3971
- Logothetis NK, Pfeuffer J (2004) On the nature of the BOLD fMRI contrast mechanism. *Magn Reson Imaging* 22(10):1517–1531
- Logothetis NK, Wandell BA (2004) Interpreting the BOLD signal. *Annu Rev Physiol* 66:735–769
- Logothetis NK, Pauls J et al (2001) Neurophysiological investigation of the basis of the fMRI signal. *Nature* 412(6843):150–157
- Louis DN, Ohgaki H et al (2007) The 2007 WHO classification of tumours of the central nervous system. *Acta Neuropathol* 114(2):97–109
- Ludemann L, Forschler A et al (2006) BOLD signal in the motor cortex shows a correlation with the blood volume of brain tumors. *J Magn Reson Imaging* 23(4):435–443
- Lurito JT, Lowe MJ et al (2000) Comparison of fMRI and intraoperative direct cortical stimulation in localization of receptive language areas. *J Comput Assist Tomogr* 24(1):99–105
- Majos A, Tybor K et al (2005) Cortical mapping by functional magnetic resonance imaging in patients with brain tumors. *Eur Radiol* 15(6):1148–1158
- Manglore S, Dawn Bharath RD et al (2013) Utility of resting fMRI and connectivity in patients with brain tumor. *Neurol India* 61(2):144–151
- Mazzuotta JC, Phelps ME et al (1982) Tomographic mapping of human cerebral metabolism: auditory stimulation. *Neurology* 32(9):921–937
- McKinney PA (2004) Brain tumours: incidence, survival, and aetiology. *J Neurol Neurosurg Psychiatry* 75(Suppl II):ii12–ii17
- Menon RS, Ogawa S et al (1995) BOLD based functional MRI at 4 Tesla includes a capillary bed contribution: echoplanar imaging correlates with previous optical imaging using intrinsic signals. *Magn Reson Med* 33(3):453–459
- Mitchell TJ, Hacker CD et al (2013) A novel data-driven approach to preoperative mapping of functional cortex using resting-state functional magnetic resonance imaging. *Neurosurgery* 73(6):969–982
- Moller M, Freund M et al (2005) Real time fMRI: a tool for the routine presurgical localisation of the motor cortex. *Eur Radiol* 15(2):292–295

- Morita N, Wang S et al (2011) Diffusion tensor imaging of the cortico-spinal tract in patients with brain neoplasms. *Magn Reson Med Sci* 10(4):239–243
- Morris GL 3rd, Mueller WM et al (1994) Functional magnetic resonance imaging in partial epilepsy. *Epilepsia* 35(6):1194–1198
- Mueller WM, Yetkin FZ et al (1996) Functional magnetic resonance imaging mapping of the motor cortex in patients with cerebral tumors. *Neurosurgery* 39(3):515–520; discussion 520–521
- Müller RA, Rothermel RD et al (1998) Determination of language dominance by [¹⁵O]-water PET in children and adolescents: a comparison with the Wada test. *J Epilepsy* 11(3):152–161
- Naidich TP, Hof PR et al (2001) Anatomic substrates of language: emphasizing speech. *Neuroimaging Clin N Am* 11(2):305–341, ix
- Nimsky C, Ganslandt O et al (2006) Intraoperative visualization for resection of gliomas: the role of functional neuronavigation and intraoperative 1.5 T MRI. *Neuro Res* 28(5):482–487
- Nitschke MF, Melchert UH et al (1998) Preoperative functional magnetic resonance imaging (fMRI) of the motor system in patients with tumours in the parietal lobe. *Acta Neurochir (Wien)* 140(12):1223–1229
- Ogawa S, Lee TM et al (1990a) Brain magnetic resonance imaging with contrast dependent on blood oxygenation. *Proc Natl Acad Sci U S A* 87(24):9868–9872
- Ogawa S, Lee TM et al (1990b) Oxygenation-sensitive contrast in magnetic resonance image of rodent brain at high magnetic fields. *Magn Reson Med* 14(1):68–78
- Ogawa S, Tank DW et al (1992) Intrinsic signal changes accompanying sensory stimulation: functional brain mapping with magnetic resonance imaging. *Proc Natl Acad Sci U S A* 89(13):5951–5955
- Ogawa S, Menon RS et al (1993) Functional brain mapping by blood oxygenation level-dependent contrast magnetic resonance imaging. A comparison of signal characteristics with a biophysical model. *Biophys J* 64(3):803–812
- Ohgaki H (2009) Epidemiology of brain tumors. In: Methods of molecular biology, cancer biology, vol 472. Humana Press, Totowa, pp 323–341
- Ojemann GA (1991) Cortical organization of language. *J Neurosci* 11(8):2281–2287
- Ojemann G, Ojemann J et al (1989) Cortical language localization in left, dominant hemisphere. An electrical stimulation mapping investigation in 117 patients. *J Neurosurg* 71(3):316–326
- Ojemann GA, Ojemann J, Ramsey NF (2013) Relation between functional magnetic resonance imaging (fMRI) and single neuron, local field potential (LFP) and electrocorticography (ECOG) in human cortex. *Front Hum Neurosci* 7:34
- Osborn AG (2012) Osborn's brain: imaging, pathology, and anatomy, 1st edn. Lippincott Williams & Wilkins
- Osborn AG, Salzman KL, Barkovich AJ (2010) Diagnostic imaging – brain, 2nd edn. Lippincott Williams & Wilkins, Philadelphia
- Ostrom QT, Barnholtz-Sloan JS (2011) Current state of our knowledge on brain tumor epidemiology. *Curr Neurol Neurosci Rep* 11(3):329–335
- Ozdoba C, Nirko AC et al (2002) Whole-brain functional magnetic resonance imaging of cerebral arteriovenous malformations involving the motor pathways. *Neuroradiology* 44(1):1–10
- Palmer ED, Rosen HJ et al (2001) An event-related fMRI study of overt and covert word stem completion. *Neuroimage* 14(1 Pt 1):182–193
- Parkin DM, Muir CS (1992) Cancer incidence in five continents. Comparability and quality of data. *IARC Sci Publ* 120:45–173
- Parmar H, Sitoh YY, Yeo TT (2004) Combined magnetic resonance tractography and functional magnetic resonance imaging in evaluation of brain tumors involving the motor system. *J Comput Assist Tomogr* 28(4):551–556
- Partovi S, Jacobi B, Rapps N, Zipp L, Karimi S, Rengier F, Lyo JK, Stippich C (2012a) Clinical standardized fMRI reveals altered language lateralization in patients with brain tumor. *AJNR Am J Neuroradiol* 33(11):2151–2157
- Partovi S, Konrad F, Karimi S, Rengier F, Lyo JK, Zipp L, Nennig E, Stippich C (2012b) Effects of covert and overt paradigms in clinical language fMRI. *Acad Radiol* 19(5):518–525
- Peck KK, Holodny AI (2007) fMRI clinical applications. In: Reiser MF, Semmler W, Hricak H (eds) Magnetic resonance tomography. Springer, Berlin, pp 1308–1331
- Penfield W (1937) Somatic motor and sensory representation in the cerebral cortex of man as studied by electrical stimulation. *Brain* 60:389–443
- Penfield W (1950) The cerebral cortex of man. MacMillan, New York, 57 ff
- Pesaresi I, Cosottini M et al (2011) Reproducibility of BOLD localization of interictal activity in patients with focal epilepsy: intrasession and intersession comparisons. *MAGMA* 24(5):285–296
- Petersen SE, Fox PT et al (1988) Positron emission tomographic studies of the cortical anatomy of single-word processing. *Nature* 331(6157):585–589
- Petrovich NM, Holodny AI et al (2004) Isolated translocation of Wernicke's area to the right hemisphere in a 62-year-old man with a temporo-parietal glioma. *AJNR Am J Neuroradiol* 25(1):130–133
- Pouratian N, Bookheimer SY et al (2002) Utility of preoperative functional magnetic resonance imaging for identifying language cortices in patients with vascular malformations. *J Neurosurg* 97(1):21–32
- Price CJ (2000) The anatomy of language: contributions from functional neuroimaging. *J Anat* 197(Pt 3):335–359
- Price CJ, Wise RJ et al (1996) Hearing and saying. The functional neuroanatomy of auditory word processing. *Brain* 119(Pt 3):919–931
- Priest AN, De Vita E et al (2006) EPI distortion correction from a simultaneously acquired distortion map using TRAIL. *J Magn Reson Imaging* 23(4):597–603
- Puce A, Constable RT et al (1995) Functional magnetic resonance imaging of sensory and motor cortex: comparison with electrophysiological localization. *J Neurosurg* 83(2):262–270
- Pujol J, Conesa G et al (1996) Presurgical identification of the primary sensorimotor cortex by functional magnetic resonance imaging. *J Neurosurg* 84(1):7–13
- Pujol J, Conesa G et al (1998) Clinical application of functional magnetic resonance imaging in presurgical identification of the central sulcus. *J Neurosurg* 88(5):863–869
- Raichle ME (1983) Positron emission tomography. *Annu Rev Neurosci* 6:249–267
- Raichle ME, Fiez JA et al (1994) Practice-related changes in human brain functional anatomy during nonmotor learning. *Cereb Cortex* 4(1):8–26
- Ramsey NF, Sommer IE et al (2001) Combined analysis of language tasks in fMRI improves assessment of hemispheric dominance for language functions in individual subjects. *Neuroimage* 13(4):719–733
- Rasmussen IA, Lindseth F et al (2007) Functional neuronavigation combined with intra-operative 3D ultrasound: initial experiences during surgical resections close to eloquent brain areas and future direction in automatic brain shift compensation of preoperative data. *Acta Neurochir* 149(4):365–378
- Rausch R, Silivenius H et al (1993) Intra-arterial amobarbital procedures. In: Engel JJ (ed) Surgical treatment of the epilepsies. Raven Press, New York, pp 341–357
- Reinges MH, Krings T et al (2004) Preoperative mapping of cortical motor function: prospective comparison of functional magnetic resonance imaging and [¹⁵O]-H₂O-positron emission tomography in the same co-ordinate system. *Nucl Med Commun* 25(10):987–997
- Reinges MH, Krings T et al (2005) Prospective demonstration of short-term motor plasticity following acquired central pareses. *Neuroimage* 24(4):1248–1255
- Roberts TP (2003) Functional magnetic resonance imaging (fMRI) processing and analysis. ASNR Electronic Learning Center Syllabus: 1–23
- Roessler K, Donat M et al (2005) Evaluation of preoperative high magnetic field motor functional MRI (3 Tesla) in glioma patients by

- navigated electrocortical stimulation and postoperative outcome. *J Neurol Neurosurg Psychiatry* 76(8):1152–1157
- Rösler J, Niraula B et al (2014) Language mapping in healthy volunteers and brain tumor patients with a novel navigated TMS system: evidence of tumor-induced plasticity. *Clin Neurophysiol* 125(3): 526–536
- Roux FE, Tremoulet M (2002) Organization of language areas in bilingual patients: a cortical stimulation study. *J Neurosurg* 97(4): 857–864
- Roux FE, Ranjeva JP et al (1997) Motor functional MRI for presurgical evaluation of cerebral tumors. *Stereotact Funct Neurosurg* 68(1–4 Pt 1):106–111
- Roux FE, Boulanouar K et al (1999a) Cortical intraoperative stimulation in brain tumors as a tool to evaluate spatial data from motor functional MRI. *Invest Radiol* 34(3):225–229
- Roux FE, Boulanouar K et al (1999b) Usefulness of motor functional MRI correlated to cortical mapping in Rolandic low-grade astrocytomas. *Acta Neurochir (Wien)* 141(1):71–79
- Roux FE, Boulanouar K et al (2000) Functional MRI and intraoperative brain mapping to evaluate brain plasticity in patients with brain tumours and hemiparesis. *J Neurol Neurosurg Psychiatry* 69(4):453–463
- Roux FE, Ibarrola D et al (2001) Methodological and technical issues for integrating functional magnetic resonance imaging data in a neuronavigational system. *Neurosurgery* 49(5):1145–1156; discussion 1156–1157
- Roux FE, Boulanouar K et al (2003) Language functional magnetic resonance imaging in preoperative assessment of language areas: correlation with direct cortical stimulation. *Neurosurgery* 52(6):1335–1345; discussion 1345–1347
- Rueckert L, Appollonio I et al (1994) Magnetic resonance imaging functional activation of left frontal cortex during covert word production. *J Neuroimaging* 4(2):67–70
- Ruge MI, Victor J et al (1999) Concordance between functional magnetic resonance imaging and intraoperative language mapping. *Stereotact Funct Neurosurg* 72(2–4):95–102
- Rutten GJ, van Rijen PC et al (1999) Language area localization with three-dimensional functional magnetic resonance imaging matches intrasulcal electrostimulation in Broca's area. *Ann Neurol* 46(3): 405–408
- Rutten GJ, Ramsey NF et al (2002a) FMRI-determined language lateralization in patients with unilateral or mixed language dominance according to the Wada test. *Neuroimage* 17(1):447–460
- Rutten GJ, Ramsey NF et al (2002b) Interhemispheric reorganization of motor hand function to the primary motor cortex predicted with functional magnetic resonance imaging and transcranial magnetic stimulation. *J Child Neurol* 17(4):292–297
- Rutten GJ, Ramsey NF et al (2002c) Development of a functional magnetic resonance imaging protocol for intraoperative localization of critical temporoparietal language areas. *Ann Neurol* 51(3):350–360
- Rutten GJ, Ramsey NF et al (2002d) Reproducibility of fMRI-determined language lateralization in individual subjects. *Brain Lang* 80(3):421–437
- Sakai KL, Hashimoto R, Homae F (2001) Sentence processing in the cerebral cortex. *Neurosci Res* 39(1):1–10
- Schiffbauer H, Berger MS et al (2003) Preoperative magnetic source imaging for brain tumor surgery: a quantitative comparison with intraoperative sensory and motor mapping. *Neurosurg Focus* 15(1):E7
- Schlaggar BL, Brown TT et al (2002) Functional neuroanatomical differences between adults and school-age children in the processing of single words. *Science* 296(5572):1476–1479
- Schlosser MJ, McCarthy G et al (1997) Cerebral vascular malformations adjacent to sensorimotor and visual cortex. Functional magnetic resonance imaging studies before and after therapeutic intervention. *Stroke* 28(6):1130–1137
- Schlosser MJ, Luby M et al (1999) Comparative localization of auditory comprehension by using functional magnetic resonance imaging and cortical stimulation. *J Neurosurg* 91(4):626–635
- Schreiber A, Hubbe U et al (2000) The influence of gliomas and non-gliial space-occupying lesions on blood-oxygen-level-dependent contrast enhancement. *AJNR Am J Neuroradiol* 21(6):1055–1063
- Schulder M, Maldjian JA et al (1998) Functional image-guided surgery of intracranial tumors located in or near the sensorimotor cortex. *J Neurosurg* 89(3):412–418
- Schwindack C, Siminotto E et al (2005) Real-time functional magnetic resonance imaging (rt-fMRI) in patients with brain tumours: preliminary findings using motor and language paradigms. *Br J Neurosurg* 19(1):25–32
- Shahar T, Rozovski U et al (2014) Preoperative imaging to predict intraoperative changes in tumor-to-corticospinal tract distance: an analysis of 45 cases using high-field intraoperative magnetic resonance imaging. *Neurosurgery* 75(1):23–30
- Sharan A, Cher Ooi Y et al (2011) Intracarotid amobarbital procedure for epilepsy surgery. *Epilepsy Behav* 20(2):209–213
- Shaywitz BA, Shaywitz SE et al (1995) Sex differences in the functional organization of the brain for language. *Nature* 373(6515): 607–609
- Shimoni JS, Zhang D et al (2009) Resting state fluctuations in brain activity: a new paradigm for presurgical planning using fMRI. *Acad Radiol* 16(5):578–583
- Shinoura N, Yamada R et al (2005) Preoperative fMRI, tractography and continuous task during awake surgery for maintenance of motor function following surgical resection of metastatic tumor spread to the primary motor area. *Minim Invasive Neurosurg* 48(2):85–90
- Simkins-Bullock J (2000) Beyond speech lateralization: a review of the variability, reliability, and validity of the intracarotid amobarbital procedure and its nonlanguage uses in epilepsy surgery candidates. *Neuropsychol Rev* 10(1):41–74
- Smits M, Vernooij MW et al (2007) Incorporating functional MR imaging into diffusion tensor tractography in the preoperative assessment of the corticospinal tract in patients with brain tumors. *AJNR Am J Neuroradiol* 28(7):1354–1361
- Spreer J, Quiske A et al (2001) Unsuspected atypical hemispheric dominance for language as determined by fMRI. *Epilepsia* 42(7): 957–959
- Springer JA, Binder JR et al (1999) Language dominance in neurologically normal and epilepsy subjects: a functional MRI study. *Brain* 122(Pt 11):2033–2046
- Spritzer SD, Hoerth MT et al (2012) Determination of hemispheric language dominance in the surgical epilepsy patient. *Neurologist* 18(5):329–331
- Stapleton SR, Kiriakopoulos E et al (1997) Combined utility of functional MRI, cortical mapping, and frameless stereotaxy in the resection of lesions in eloquent areas of brain in children. *Pediatr Neurosurg* 26(2):68–82
- Stefanowicz J, Izycka-Świeszewska E et al (2011) Brain metastases in paediatric patients: characteristics of a patient series and review of the literature. *Folia Neuropathol* 49(4):271–281
- Steger TR, Jackson EF (2004) Real-time motion detection of functional MRI data. *J Appl Clin Med Phys* 5(2):64–70
- Stippich C (2005) Clinical functional magnetic resonance imaging: basic principles and clinical applications. *Radiol Up2date* 5:317–336
- Stippich C (2010) Presurgical functional magnetic resonance imaging. *Radiologe* 50(2):110–122
- Stippich C, Hofmann R et al (1999) Somatotopic mapping of the human primary somatosensory cortex by fully automated tactile stimulation using functional magnetic resonance imaging. *Neurosci Lett* 277(1):25–28
- Stippich C, Kapfer D et al (2000) Robust localization of the contralateral precentral gyrus in hemiparetic patients using the unimpaired ipsilateral hand: a clinical functional magnetic resonance imaging protocol. *Neurosci Lett* 285(2):155–159
- Stippich C, Heiland S et al (2002a) Functional magnetic resonance imaging: physiological background, technical aspects and prerequisites for clinical use. *Rofo* 174(1):43–49

- Stippich C, Ochmann H, Sartor K (2002b) Somatotopic mapping of the human primary sensorimotor cortex during motor imagery and motor execution by functional magnetic resonance imaging. *Neurosci Lett* 331(1):50–54
- Stippich C, Kress B et al (2003a) Preoperative functional magnetic resonance tomography (fMRI) in patients with rolandic brain tumors: indication, investigation strategy, possibilities and limitations of clinical application. *Rofo* 175(8):1042–1050
- Stippich C, Mohammed J et al (2003b) Robust localization and lateralization of human language function: an optimized clinical functional magnetic resonance imaging protocol. *Neurosci Lett* 346(1–2): 109–113
- Stippich C, Romanowski A et al (2004) Fully automated localization of the human primary somatosensory cortex in one minute by functional magnetic resonance imaging. *Neurosci Lett* 364(2):90–93
- Stippich C, Romanowski A et al (2005) Time-efficient localization of the human secondary somatosensory cortex by functional magnetic resonance imaging. *Neurosci Lett* 381(3):264–268
- Stippich C, Blatow M et al (2007a) Global activation of primary motor cortex during voluntary movements in man. *Neuroimage* 34: 1227–1237
- Stippich C, Rapps N et al (2007b) Feasibility of routine preoperative functional magnetic resonance imaging for localizing and lateralizing language in 81 consecutive patients with brain tumors. *Radiology* 243:828–836
- Szaflarski JP, Binder JR et al (2002) Language lateralization in left-handed and ambidextrous people: fMRI data. *Neurology* 59(2): 238–244
- Tarapore PE, Matthew CT (2012) Preoperative multimodal motor mapping: a comparison of magnetoencephalography imaging, navigated transcranial magnetic stimulation, and direct cortical stimulation. *J Neurosurg* 117(2):354–362
- Ternovoi SK, Sinitsyn VE et al (2004) Localization of the motor and speech zones of the cerebral cortex by functional magnetic resonance tomography. *Neurosci Behav Physiol* 34(5):431–437
- Thulborn K (2006) Clinical functional magnetic resonance imaging. In: Haacke EM (ed) Current protocols in magnetic resonance imaging. Wiley, New York, Last Update: 20 Aug 2013. ISBN 978-0-471-35345-4
- Thulborn KR, Shen GX (1999) An integrated head immobilization system and high-performance RF coil for fMRI of visual paradigms at 1.5 T. *J Magn Reson* 139(1):26–34
- Towle VL, Khorasani L et al (2003) Noninvasive identification of human central sulcus: a comparison of gyral morphology, functional MRI, dipole localization, and direct cortical mapping. *Neuroimage* 19(3):684–697
- Tozakidou M, Wenz H et al (2013) Primary motor cortex activation and lateralization in patients with tumors of the central region. *NeuroImage Clin* 2:221–228
- Tuntiyatorn L, Wuttiplakorn L, Laohawiriyakamol K (2011) Plasticity of the motor cortex in patients with brain tumors and arteriovenous malformations: a functional MR study. *J Med Assoc Thai* 94(9): 1134–1140
- Ulmer JL, Krouwer HG et al (2003) Pseudo-reorganization of language cortical function at fMRI imaging: a consequence of tumor-induced neurovascular uncoupling. *AJNR Am J Neuroradiol* 24(2): 213–217
- Ulmer JL, Salvan CV et al (2004) The role of diffusion tensor imaging in establishing the proximity of tumor borders to functional brain systems: implications for preoperative risk assessments and postoperative outcomes. *Technol Cancer Res Treat* 3(6):567–576
- van der Kallen BF, Morris GL et al (1998) Hemispheric language dominance studied with functional MR: preliminary study in healthy volunteers and patients with epilepsy. *AJNR Am J Neuroradiol* 19(1):73–77
- van der Zwaag W, Susan F et al (2009) fMRI at 1.5, 3 and 7 T: characterising BOLD signal changes. *Neuroimage* 47(4):1425–1434
- Van Westen D, Skagerberg G et al (2005) Functional magnetic resonance imaging at 3 T as a clinical tool in patients with intracranial tumors. *Acta Radiol* 46(6):599–609
- Voss J, Meier TB et al (2013) The role of secondary motor and language cortices in morbidity and mortality: a retrospective functional MRI study of surgical planning for patients with intracranial tumours. *Neurosurg Focus* 34(4):E7
- Wada J, Rasmussen T (1960) Intracarotid injection of sodium amytal for the lateralization of cerebral speech dominance. Experimental and clinical observations. *J Neurosurg* 17:266–282
- Wagner K, Hader C et al (2012) Who needs a Wada test? Present clinical indications for amobarbital procedures. *J Neurol Neurosurg Psychiatry* 83(5):503–509
- Warburton E, Wise RJ et al (1996) Noun and verb retrieval by normal subjects. Studies with PET. *Brain* 119(Pt 1):159–179
- Weiskopf N, Veit R et al (2003) Physiological self-regulation of regional brain activity using real-time functional magnetic resonance imaging (fMRI): methodology and exemplary data. *Neuroimage* 19(3): 577–586
- Weiskopf N, Scharnowski F et al (2004) Self-regulation of local brain activity using real-time functional magnetic resonance imaging (fMRI). *J Physiol Paris* 98(4–6):357–373
- Weiskopf N, Klose U et al (2005) Single-shot compensation of image distortions and BOLD contrast optimization using multi-echo EPI for real-time fMRI. *Neuroimage* 24(4):1068–1079
- Wengenroth M, Blatow M, Guenther J, Akbar M, Tronnier VM, Stippich C (2011). Diagnostic benefits of presurgical fMRI in patients with brain tumours in the primary sensorimotor cortex. *Eur Radiol* 21(7):1517–25
- Westerveld K, Stoddard K, McCarthy K (1999) Case report of false lateralization using fMRI: comparison of language localization, Wada testing, and cortical stimulation. *Arch Clin Neuropsychol* 14:162–163
- Wienbruch C, Candia V et al (2006) A portable and low-cost fMRI compatible pneumatic system for the investigation of the somatosensory system in clinical and research environments. *Neurosci Lett* 398(3):183–188
- Wirtz CR, Tronnier VM et al (1997) Image-guided neurosurgery with intraoperative MRI: update of frameless stereotaxy and radicality control. *Stereotact Funct Neurosurg* 68(1–4 Pt 1):39–43
- Wise R, Chollet F et al (1991) Distribution of cortical neural networks involved in word comprehension and word retrieval. *Brain* 114(Pt 4):1803–1817
- Wittek A, Kikinis R et al (2005) Brain shift computation using a fully nonlinear biomechanical model. *Med Image Comput Comput Assist Interv* 8(Pt 2):583–590
- Woolsey CN, Erickson TC, Gilson WE (1979) Localization in somatic sensory and motor areas of human cerebral cortex as determined by direct recording of evoked potentials and electrical stimulation. *J Neurosurg* 51(4):476–506
- Worthington C, Vincent DJ et al (1997) Comparison of functional magnetic resonance imaging for language localization and intracarotid speech amyta testing in presurgical evaluation for intractable epilepsy. Preliminary results. *Stereotact Funct Neurosurg* 69(1–4 Pt 2):197–201
- Wunderlich G, Knorr U et al (1998) Precentral glioma location determines the displacement of cortical hand representation. *Neurosurgery* 42(1):18–26; discussion 26–27

- Yetkin FZ, Mueller WM et al (1997) Functional MR activation correlated with intraoperative cortical mapping. *AJNR Am J Neuroradiol* 18(7):1311–1315
- Yetkin FZ, Swanson S et al (1998) Functional MR of frontal lobe activation: comparison with Wada language results. *AJNR Am J Neuroradiol* 19(6):1095–1098
- Yousry TA, Schmid UD et al (1995) Topography of the cortical motor hand area: prospective study with functional MR imaging and direct motor mapping at surgery. *Radiology* 195(1):23–29
- Yousry TA, Schmid UD et al (1996) The central sulcal vein: a landmark for identification of the central sulcus using functional magnetic resonance imaging. *J Neurosurg* 85(4):608–617
- Yousry TA, Schmid UD et al (1997) Localization of the motor hand area to a knob on the precentral gyrus. A new landmark. *Brain* 120(Pt 1):141–157
- Yousry I, Naidich TP, Yousry TA (2001) Functional magnetic resonance imaging: factors modulating the cortical activation pattern of the motor system. *Neuroimaging Clin N Am* 11(2):195–202, viii
- Zacà D, Jarso S, Pillai JJ (2013) Role of semantic paradigms for optimization of language mapping in clinical fMRI studies. *AJNR Am J Neuroradiol* 34(10):1966–1971
- Zhang D, Johnston JM et al (2009) Preoperative sensorimotor mapping in brain tumor patients using spontaneous fluctuations in neuronal activity imaged with fMRI: initial experience. *Neurosurgery* 65(6 Suppl):226–236

Presurgical Resting-State fMRI

Monica G. Allen, Abraham Z. Snyder, Carl D. Hacker,
Timothy J. Mitchell, Eric C. Leuthardt,
and Joshua S. Shimony

Contents

| | | |
|-------------------------|--|-----|
| 1 | Introduction | 143 |
| 1.1 | Background | 143 |
| 1.2 | Resting-State Networks | 144 |
| 2 | Methods | 145 |
| 2.1 | Overview of Processing Methods | 145 |
| 2.2 | General Preprocessing | 146 |
| 2.3 | Preprocessing in Preparation for Seed-Based Correlation Mapping | 146 |
| 2.4 | Global Signal Regression..... | 146 |
| 2.5 | Seed-Based Correlation Mapping | 146 |
| 2.6 | Independent Component Analysis | 147 |
| 2.7 | Clustering Algorithms..... | 148 |
| 2.8 | RSN Mapping Using a Trained Multilayer Perceptron (MLP) | 148 |
| 3 | Application to Presurgical Planning | 149 |
| 3.1 | Introduction..... | 149 |
| 3.2 | Preoperative Sensorimotor Mapping in Brain Tumor Patients Using Seed-Based Approach..... | 150 |
| 3.3 | Preoperative Mapping of Functional Cortex Using MLP..... | 151 |
| Conclusion | 155 | |
| References | 155 | |

Abstract

Purpose: Task-based fMRI has traditionally been used to locate eloquent regions of the brain that are relevant to specific cognitive tasks. These locations have, in turn, been used successfully to inform surgical planning. Resting-state functional MRI (fMRI) uses alternative methods to find networks, but does not require any task performance by a patient.

Materials and Methods: Resting-state fMRI uses correlations in the blood oxygen level-dependent (BOLD) signal to identify connected regions across the brain that form networks. Several methods of analyzing the data have been applied to calculate resting-state networks. In particular, seed-based correlation mapping and independent component analysis (ICA) are two commonly used techniques.

Results: Several studies using these analysis techniques are described in this chapter. Resting-state data has been used successfully as a presurgical planning tool in tumor patients and epilepsy patients.

Conclusions: Resting-state fMRI has been compared favorably to other methods of determining functional connectivity, including task-based fMRI and electrocortical stimulation. These results demonstrate great promise for the future of resting-state fMRI in presurgical planning.

1 Introduction

1.1 Background

Localization of function within the brain using functional magnetic resonance imaging (fMRI) traditionally has been performed by presenting stimuli or imposing tasks (such as finger tapping or object naming) to elicit neuronal responses (Posner and Raichle 1994; Spitzer et al. 1995). This type of experiment has been very effective, as evidenced by over 28,000 publications (listed in PubMed, as of December, 2013) utilizing task-based fMRI. fMRI detects changes in

M.G. Allen (✉) • A.Z. Snyder • T.J. Mitchell • J.S. Shimony
Mallinckrodt Institute of Radiology, Washington University School of Medicine, Saint Louis, MO 63141, USA
e-mail: shimonyj@mir.wustl.edu

C.D. Hacker
Department of Biomedical Engineering, Washington University School of Medicine, Saint Louis, MO 63141, USA

E.C. Leuthardt
Department of Neurosurgery, Washington University School of Medicine, Saint Louis, MO 63141, USA

the blood oxygen level-dependent (BOLD) signal that reflect the neurovascular response to neural activity. Thus, BOLD fMRI is able to identify regions in the brain associated with a given task.

Since the earliest days of fMRI, it has been recognized that the BOLD signal exhibits spontaneous fluctuations (Purdon and Weisskoff 1998). These fluctuations were initially regarded as noise to be averaged out over many trials or task blocks (Triantafyllou et al. 2005). More recent studies have shown that these spontaneous fluctuations reflect the brain's functional organization. The human brain is a disproportionate consumer of metabolic energy relative to its weight: 20 % of the total energy utilization but only 2 % of body weight (Clarke and Sokoloff 1999). This energy appears to be largely used for signaling (Shulman et al. 2004; Attwell and Laughlin 2001; Ames et al. 1992; Lennie 2003; Raichle and Mintun 2006). Task performance only minimally increases energy consumption in the brain (Raichle and Mintun 2006). Therefore, task-based experiments ignore the overwhelming preponderance of the brain's activity. That intrinsic brain activity could be utilized for functional localization was first suggested by Biswal and colleagues who demonstrated that BOLD fluctuations observed in the resting state are correlated within the somatomotor system (Biswal et al. 1995). Correlated intrinsic activity currently is referred to as functional connectivity MRI or resting-state fMRI (rsfMRI). The development of these methods has opened up many exciting possibilities for future neurocognitive research as well as clinical applications, including presurgical planning, which is the subject of this chapter. A historical review is given in (Snyder and Raichle 2012).

1.2 Resting-State Networks

The topographies of functionally connected regions across the brain are known as resting-state networks (RSNs; equivalently intrinsic connectivity networks (Seeley et al. 2007). The resting-state fMRI scans are generally acquired while the subject is in a state of quiet wakefulness (Fox and Raichle 2007). The importance of RSNs lies in the fact that their topography closely corresponds to responses elicited by a wide variety of sensory, motor, and cognitive tasks (Smith et al. 2009). Intrinsic activity persists, albeit in somewhat modified form, during sleep (Samann et al. 2010; Larson-Prior et al. 2009) or even under sedation (Mhuircheartaigh et al. 2010). The persistence of the spontaneous fluctuations during states of reduced awareness suggests that intrinsic neuronal activity plays a role in the maintenance of the brain's functional integrity (Pizoli et al. 2011). Spontaneous BOLD activity has been detected in all mammalian species investigated thus far (Hutchison et al. 2012; Schwarz et al. 2013; Nasrallah et al. 2013), which reinforces the notion that this phenomenon is physiologically

important. However, the precise physiological functions of intrinsic activity remain to be elucidated.

Perhaps the most fundamental RSN is the default mode network (DMN) (Fig. 1a), first identified by a meta-analysis of task-based functional neuroimaging experiments performed with positron emission tomography (PET) (Shulman et al. 1997; Gusnard and Raichle 2001). The defining property of the DMN is that it is more active at rest than during performance of goal-directed tasks. The DMN was first identified using rsfMRI by Greicius et al. (2003). This finding has since been replicated many times, using a variety of analysis methods (Smith et al. 2009; Beckmann et al. 2005; De Luca et al. 2006; Power et al. 2011; Yeo et al. 2011; Damoiseaux et al. 2006; van den Heuvel et al. 2008; Lee et al. 2012a). Some investigators have hypothesized that there are two large anti-correlated systems in the brain (Fox et al. 2005; Golland et al. 2008), one anchored by the DMN and the other comprised of systems controlling executive and attentional mechanisms. This dichotomy has been variously referred to as "task-positive" vs. "task-negative" (Power et al. 2011; Lee et al. 2012a; Fox et al. 2005; Chai et al. 2012; Zhang et al. 2011a) and "intrinsic" vs. "extrinsic" (Golland et al. 2008; Doucet et al. 2011). Although the nomenclature associated with the DMN remains controversial (Jack et al. 2012; Spreng 2012), the topography of the DMN is remarkably consistent across diverse analysis strategies.

Primary sensory and motor RSNs include the somatomotor network (SMN), first identified by Biswal and colleagues (Biswal et al. 1995), which encompasses primary and higher order motor and sensory areas (Fig. 1b). The visual (VIS) network spans much of the occipital cortex (Fig. 1c) (Smith et al. 2009; Beckmann et al. 2005; De Luca et al. 2006; Power et al. 2011; Yeo et al. 2011). The auditory network includes Heschl's gyrus, the superior temporal gyrus, and the posterior insula (Smith et al. 2009). The language network (LAN) includes Broca's and Wernicke's areas but also extends to prefrontal, temporal, parietal, and subcortical regions (Fig. 1d) (Tomasi and Volkow 2012; Lee et al. 2012b; Hacker et al. 2013).

RSNs involved in attentional and cognitive control include the dorsal attention network (DAN) and the ventral attention network (VAN) (Seeley et al. 2007; Power et al. 2011; Yeo et al. 2011; Corbetta and Shulman 2002; Fox et al. 2006a). The DAN (Fig. 1e) includes the intraparietal sulcus and the frontal eye field and is recruited by tasks requiring control of spatial attention. The VAN (Fig. 1f), which includes the temporal-parietal junction and ventral frontal cortex, is involved in the detection of environmentally salient events (Corbetta and Shulman 2002; Fox et al. 2006a; Astafiev et al. 2006). The frontoparietal control network (FPC) (Fig. 1g), which includes the lateral prefrontal cortex and the inferior parietal lobule, is associated with working memory and control of goal-directed behavior

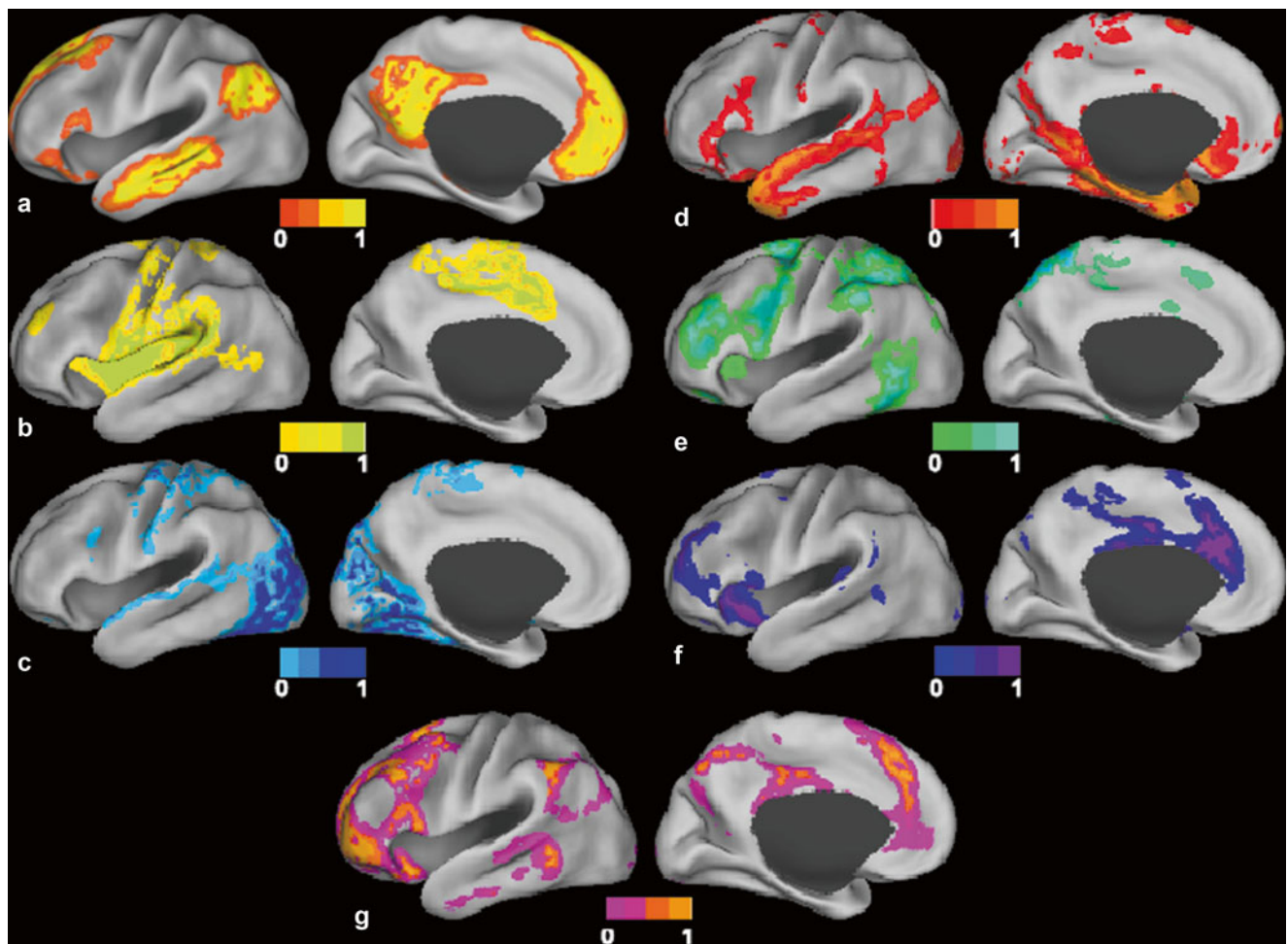


Fig. 1 Surface plots of resting-state networks as derived from fuzzy c-means algorithm (Lee et al. 2012a) (a) Default mode network. (b) Somatomotor network. (c) Visual network. (d) Language network. (e) Dorsal attention network. (f) Ventral attention network. (g) Frontoparietal control network

(Vincent et al. 2008; Power and Petersen 2013). Finally, the cingulo-opercular network (CON), also known as the salience network (Seeley et al. 2007) or the core control network (Dosenbach et al. 2006), includes the medial superior frontal cortex, anterior insula, and anterior prefrontal cortex. The CON is thought to enable the performance of tasks requiring executive control (Power et al. 2011; Power and Petersen 2013; Dosenbach et al. 2006).

2 Methods

2.1 Overview of Processing Methods

Resting-state fMRI methodology is currently dominated by two complementary strategies, spatial independent components analysis (SICA) (Beckmann et al. 2005) and seed-based correlation mapping (Biswal et al. 1995). Both strategies depend on the fact that spontaneous

neural activity is correlated (coherent) within widely distributed regions of the brain. Both strategies yield highly reproducible results at group level (Damoiseaux et al. 2006; Shehzad et al. 2009). SICA decomposes rsfMRI data into a sum of single components, each component corresponding to a spatial topography and a time course. In contrast, seed-based correlation mapping is computed by voxelwise evaluation of the Pearson correlation between the time courses in a targeted region of interest and all other voxels in the brain (Fox et al. 2009). The principal advantage of SICA is that it provides a direct means of separating artifact from BOLD signals of neural origin, although this separation typically requires observer expertise. The results obtained using SICA may vary substantially depending on processing parameters (e.g., number of requested components). Thus, SICA can be difficult to use in the investigation of targeted RSNs, especially in single subjects. In contrast, targeting of selected RSNs is intrinsic to seed-based correlation

mapping. However, the principal difficulty in using seed-based correlation mapping is the exclusion of non-neural artifacts, which is typically accomplished using regression techniques (Fox et al. 2009; Jo et al. 2010; Vincent et al. 2006).

SICA and seed-based correlation mapping both represent strategies for assigning RSN identities to brain voxels. Since SICA makes no a priori assumptions regarding the topography of the obtained components, this method exemplifies unsupervised classification. In contrast, seed-based correlation mapping depends on prior knowledge and so exemplifies supervised classification. For additional discussion of the distinction between supervised vs. unsupervised methodologies, see (Hacker et al. 2013). Below, we present results obtained by two unsupervised methods, SICA and c-means clustering, and two supervised methods, conventional seed-based correlation mapping and RSN mapping using a trained multilayer perception (MLP) classifier.

2.2 General Preprocessing

Preprocessing of fMRI data varies across laboratories. The following describes the procedures used in our laboratory (Shulman et al. 2010). Briefly, these include compensation for slice-dependent time shifts, elimination of systematic odd-even slice intensity differences due to interleaved acquisition, and rigid body correction for head movement within and across runs. The fMRI data are intensity scaled (one multiplicative factor applied to all voxels of all frames within each run) to obtain a mode value of 1,000 (Ojemann et al. 1997). This scaling facilitates assessment of voxelwise variance for purposes of quality assessment but does not affect computed correlations. Atlas transformation is achieved by composition of affine transforms connecting the fMRI volumes with the T1- and T2-weighted structural images. Head movement correction is included in a single resampling to generate a volumetric time series in 3 mm³ atlas space.

2.3 Preprocessing in Preparation for Seed-Based Correlation Mapping

Additional preprocessing in preparation for seed-based correlation mapping includes the following: (1) spatial smoothing (6 mm full-width half-maximum Gaussian blur in each direction), (2) voxelwise removal of linear trends over each run, (3) temporal low-pass filtering to retain frequencies <0.1 Hz, and (4) reduction of spurious variance by regression of nuisance waveforms derived from head motion correction and extraction of the time series from regions of

noninterest in white matter and cerebrospinal fluid. In our lab, this step includes regression of the global signal averaged over the whole brain (Fox et al. 2009; Buckner et al. 2005). A consequence of global signal regression (GSR) is that all subsequently computed correlations are effectively partial correlations of first-order controlling for widely shared variance. As global signal regression currently is a contentious maneuver, this topic is considered further in the next section.

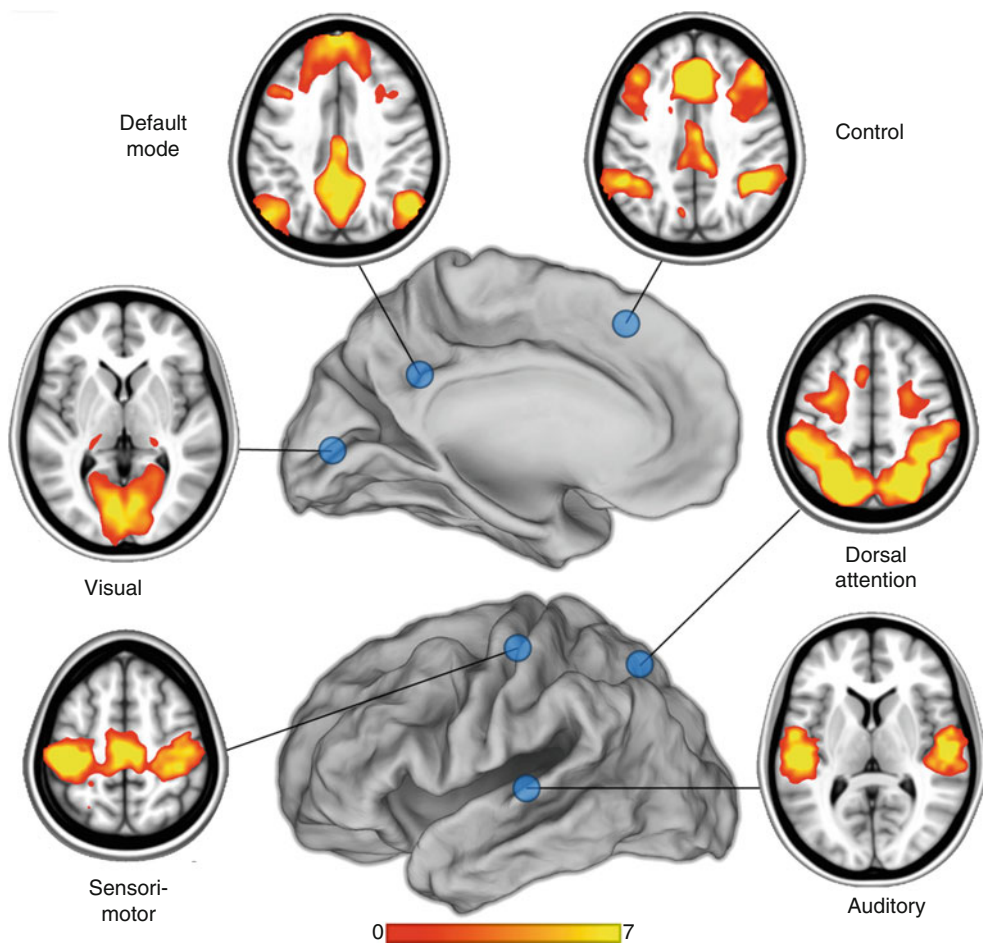
2.4 Global Signal Regression

Global signal regression (GSR) prior to correlation mapping is a highly effective means of reducing widely shared variance and thereby improving the spatial specificity of computed maps (Fox et al. 2009; Aguirre et al. 1998; Macey et al. 2004). Some part of the global signal undoubtedly is of neural origin (Scholvinck et al. 2010). However, much (typically most) of the global signal represents non-neural artifact attributable to physical effects of head motion (Friston et al. 1996; Yan et al. 2013; Power et al. 2012; Satterthwaite et al. 2012) and variations in the partial pressure of arterial carbon dioxide (Wise et al. 2004). In the absence of GSR, all parts of the brain appear to be strongly positively correlated (Chai et al. 2012; Fox et al. 2006a; Lowe et al. 1998; Joel et al. 2011). GSR causes all subsequently computed correlation maps to be approximately zero-centered; in other words, positive and negative values are approximately balanced over the whole brain (Fox et al. 2009). Thus, GSR unambiguously does negatively bias all computed correlations, although iso-correlation contours, i.e., map topographies, remain unchanged. This negative bias has caused some experts in the field research to criticize GSR on the grounds that it induces artifactual anti-correlations (Anderson et al. 2011; Murphy et al. 2009). This objection to GSR has largely been dissipated following the demonstration that some parts of the brain appear to be truly anti-correlated in the resting state, as demonstrated using SICA (Liao et al. 2010; Zuo et al. 2010). More recent objections to GSR focus on the possibility that it can distort quantitative functional connectivity differences across diagnostic groups (Saad et al. 2012). This objection to GSR, however, is irrelevant in the context of using rsfMRI for purposes of RSN mapping in individuals.

2.5 Seed-Based Correlation Mapping

Seed-based correlation mapping is one of the most widely adopted techniques for studying co-fluctuations in intrinsic neuronal activity, or functional connectivity (Shehzad et al. 2009; Cordes et al. 2000). The high

Fig. 2 Examples of multiple resting-state networks generated using a seed-based approach (blue circles in the figure) (Zhang and Raichle 2010). Six of the major networks are illustrated: visual, sensorimotor, auditory, default mode, dorsal attention, and frontoparietal executive control. The scale numbered 0–7 indicates the relative correlation strength



adoption rate of the seed-based approach is partly attributable to the simplicity of its implementation and to the ease with which the results can be interpreted. Biswal et al. used this method to first demonstrate the feasibility of using fMRI to detect spatially distributed networks (Biswal et al. 1995).

Pearson product-moment correlation is the most widely used measure of functional connectivity (Biswal et al. 1995; Greicius et al. 2003; Fox et al. 2005; Lowe et al. 1998; Cordes et al. 2000; Xiong et al. 1999). Seed-based analyses require prior knowledge of the locations of regions of interest, and these can be obtained from previously determined atlas coordinates or from task-based fMRI data. For instance, a simple motor paradigm may be used to generate data involving the motor network. The activation data is then analyzed, and the voxel that is associated with the strongest activation is used as a “seed” region to study the resting-state data. Once the coordinates of the seed region have been identified, the resting-state time courses from the rest of the brain are compared with this region, and a correlation map is generated. An example of multiple RSNs using the seed-based approach is presented in Fig. 2 (Zhang and Raichle 2010).

2.6 Independent Component Analysis

Unsupervised data-driven approaches are of interest to researchers looking to analyze resting-state data without a priori assumptions. SICA is the most widely used data-driven approach to analyze resting-state data (Goldman et al. 2003; Beckmann and Smith 2004; Greicius et al. 2004). SICA decomposes resting-state fMRI data (timexspace) into spatial components that are maximally independent. Each spatial component is associated with a particular time course. The components are useful for differentiating noise data from physiological data as well as identifying statistically independent systems. Comparison studies between seed-based correlation maps and spatial patterns determined by SICA have found similar spatial patterns (Beckmann et al. 2005; Rosazza et al. 2012).

Although the SICA approach eliminates the need for a priori seed identification, the user is required to choose the initial number of components as well as to select which components represent noise and which represent functional networks. Some studies have aimed to automate this process and use SICA as a method for identifying and eliminating noise within the

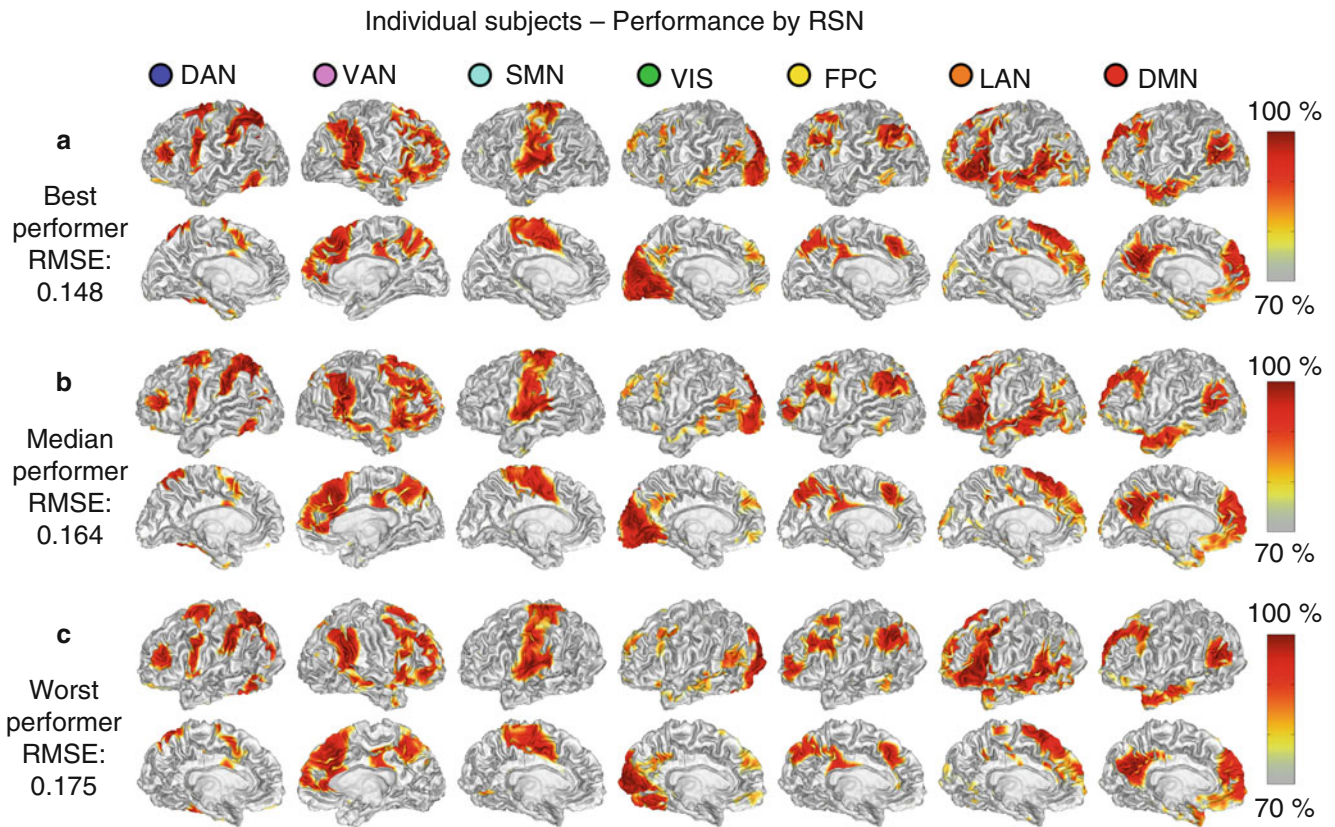


Fig. 3 Single subject, voxel estimation of resting-state networks using trained multilayer perceptron (MLP) in three subjects. The results are from best (a), median (b), and worst (c) performers as determined by

RMS error and demonstrate high quality results in individual subjects even in the worst case. MLP output was converted to a percentile scale and sampled onto each subject's cortical surface (Hacker et al. 2013)

BOLD signal (Starck et al. 2010; Thomas et al. 2002; Tohka et al. 2008).

algorithms include spectral-based clustering (Bellec et al. 2010) and graph-based clustering (van den Heuvel et al. 2008).

2.7 Clustering Algorithms

Another method used to analyze rsfMRI data makes use of clustering algorithms. Clustering algorithms attempt to group items that are alike on the basis of a set of relevant characteristics to the problem of interest. Voxels can be grouped on the basis of similarity of their BOLD time courses by using some distance metric, such as a Pearson correlation. One example of a clustering algorithm is hierarchical clustering (Salvador et al. 2005; Cordes et al. 2002), which builds a dendrogram (a treelike structure) of all members. Other examples of clustering algorithms are the K-means (Golland et al. 2008) and Fuzzy c -means (Lee et al. 2012a) clustering algorithms. In these algorithms, all voxels are assigned membership to one or more of several clusters on the basis of their distances from the cluster centers, which, in turn, are calculated from an average of their members. Clustering algorithms iteratively update memberships and cluster centers until convergence is achieved (Lee et al. 2012a) (Fig. 1). Other variations on clustering

2.8 RSN Mapping Using a Trained Multilayer Perceptron (MLP)

One technique for mapping the topography of known RSNs in individuals uses a Multilayer perceptron (MLP) (Hacker et al. 2013). Perceptrons are machine learning algorithms that can be trained to associate arbitrary input patterns with discrete output labels (Rumelhart et al. 1986). For example, perceptrons can be trained to read handwritten digits, e.g., zip codes on addressed letters (LeCun et al. 1989). Here, an MLP was trained to associate seed-based correlation maps with particular RSNs. Running the trained MLP on correlation maps corresponding to all voxels in the brain generates voxel-wise RSN membership estimates. Thus, RSN mapping using a trained MLP exemplifies supervised classification. An example of the RSN produced by the MLP algorithm in three subjects is presented in Fig. 3. It is critical to note that our MLP assigns RSN membership to rsfMRI correlation maps. This application of machine learning must not be

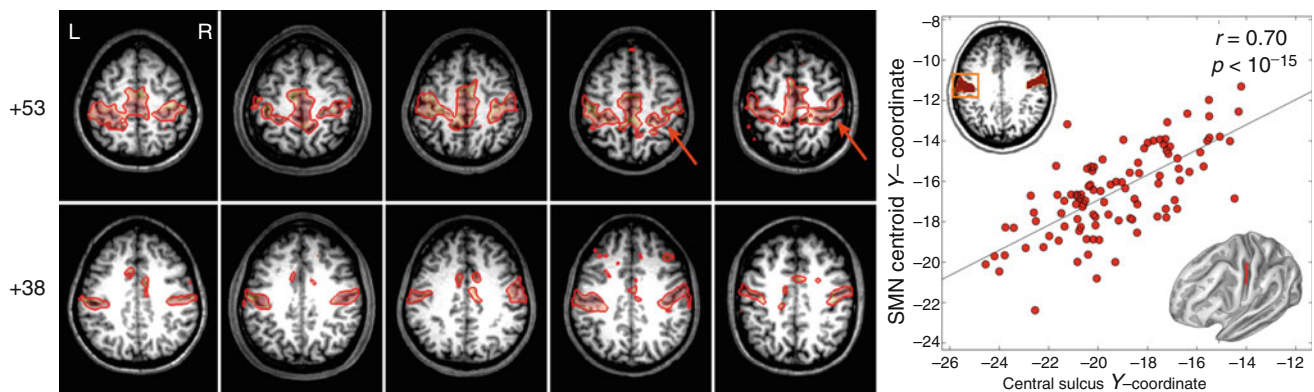


Fig. 4 Multilayer perceptron (MLP) somatomotor network (SMN) validation results derived from five individuals selected to represent the correspondence between SMN variability and anatomical variability in the central sulcus. The plot shows the correlation between the

Talairach y-coordinate of the centroid of the MLP SMN and the y-coordinate centroid of the central sulcus traced over the anatomy (as determined by the FreeSurfer program) in a large validation dataset (Hacker et al. 2013)

confused with other methodologies in which classifiers have been trained to assign diagnostic labels to patients on the basis of their resting-state functional connectivity patterns (Abdulkadir et al. 2011). Our implementation of MLP-based RSN mapping utilizes the same preprocessing steps described above in connection with seed-based correlation mapping and fuzzy c-means clustering (Sects. 2.2, 2.3, and 2.4).

Figure 4 demonstrates the degree to which the MLP captures individual variability, by showing that, in each subject, the location of the central sulcus in the cortical surface segmented using FreeSurfer (Fischl 2012) is highly correlated with the location of the SMN centroid calculated by the MLP. Detailed quantitative evaluation of the MLP performance is given in (Hacker et al. 2013). MLP performance was also compared to alternative RSN estimation schemes such as dual regression and linear discriminant analysis and was found to provide improved “area under the curve estimation” with better orthogonal estimates of RSN membership.

In summary, the MLP accurately generates RSN topography estimates in individuals consistent with previous studies, even in brain regions not represented in the training data, and can be used for generating individual RSN maps. These findings are important to future applications because they demonstrate that this approach can reliably and effectively map multiple RSNs across individual subjects.

3 Application to Presurgical Planning

3.1 Introduction

Multiple studies have demonstrated that maximal resection of a brain tumor while sparing nearby eloquent cortex leads to improved outcomes, with minimal morbidity (Keles et al. 2001, 2006; Lacroix et al. 2001; McGirt et al. 2009; Sanai et al. 2008). Historically, neurosurgeons have been concerned with the localization of the motor and language system on the

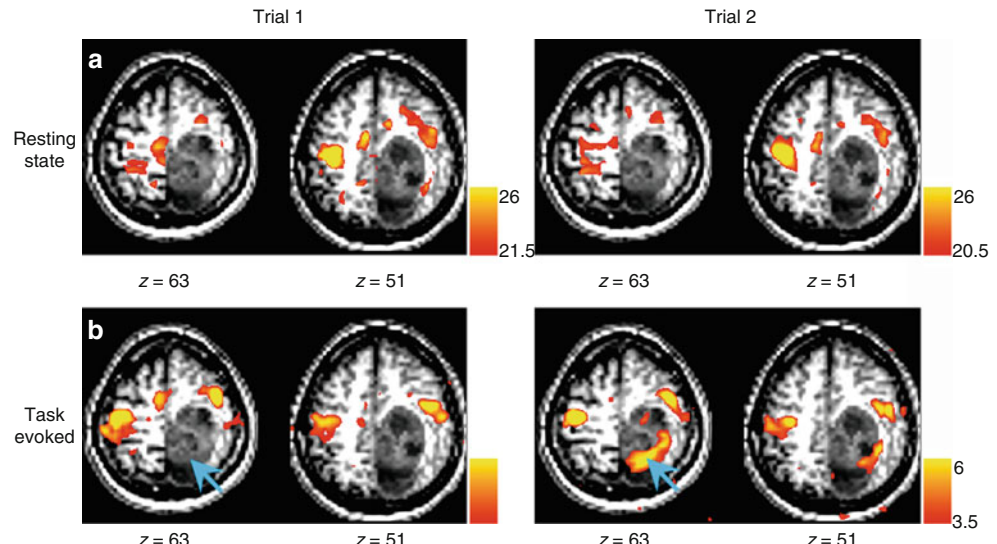
assumption that these parts of the brain (“eloquent” cortex) instantiate critical functionality. However, a broader understanding of brain function suggests that all parts of the brain contribute to important functionality (Yeo et al. 2011; Lee et al. 2012a; Golland et al. 2008; Hacker et al. 2013). Thus, improved functional mapping of multiple RSN beyond motor and language could lead to further improvements in patient outcomes.

Multiple prior publications have explored the use of rsfMRI in presurgical planning. An early case report example of this technique was used to localize the motor cortex in a patient with a brain tumor (Shimony et al. 2009). Kokkonen et al. (2009) similarly compared motor task data to resting-state data and showed that the motor functional network could be localized on the basis of resting-state data in 8 tumor patients, as well as 10 healthy control subjects.

Resting-state fMRI may also be used for presurgical planning in patients with epilepsy. The higher spatial resolution offered by rsfMRI over electroencephalography could provide a distinct advantage in mapping epileptic foci or networks. Seed-based methods were used by Liu et al. (2009) to successfully locate sensorimotor areas by using rsfMRI in patients with tumors or epileptic foci close to sensorimotor areas. They found agreement between rsfMRI, task-based fMRI, and intraoperative cortical stimulation data. In another study from the same laboratory, Stufflebeam and colleagues (Stufflebeam et al. 2011) were able to localize areas of increased functional connectivity in five of six patients that overlapped with epileptogenic areas identified by invasive encephalography. Zhang et al. (2011b) used graph methods and a pattern classifier applied to rsfMRI data to identify subjects as either having medial temporal lobe epilepsy or as normal controls. Using data from 16 patients with intractable medial temporal lobe epilepsy and 52 normal controls, they achieved an average sensitivity of 77.2 % and a specificity of 83.86 % in classification. Bettus et al. (2010) reported that increases in basal functional connectivity were a specific marker of the location of the epileptogenic zone in 22 patients with mesial temporal lobe epilepsy. Weaver et al.

Fig. 5 Comparison of resting state and task-related functional magnetic resonance imaging (fMRI) mapping in a 45-year-old with a diagnosis of glioblastoma multiforme (Case 1).

(a) Resting-state correlation mapping $\times 2$ trials shows correlated activity with a distribution resembling the activation from trial 1 but not trial 2 of the task. (b) Finger-tapping fMRI $\times 2$ trials. Activity within the tumor (blue arrows) was seen in trial 2 but not in trial 1. All colored regions represent activations in the somatomotor network. All images are displayed left-on-left (neurologic convention) (Zhang et al. 2009)



(Weaver et al. 2013) studied four patients with focal epilepsy along with 16 control subjects to determine whether the seizure focus could be found using the functional patterns near the epileptogenic zone. By averaging voxel homogeneity across regions of interest in comparison to other regions, they were able to accurately identify the epileptic focus. Tie et al. (2013) employed ICA data evaluation on a training group of 14 healthy subjects to identify the language network from rsfMRI data. The result of that analysis was then used to identify the language network in a second group of 18 healthy subjects on an individual level. The authors further propose an automated system for determining the language network in individual patients using SICA. A more detailed presentation of our experience using rsfMRI for presurgical mapping with both seed-based and MLP approaches is given in the next sections.

3.2 Preoperative Sensorimotor Mapping in Brain Tumor Patients Using Seed-Based Approach

Zhang and colleagues (2009) described our initial experience with rsfMRI brain mapping for presurgical planning of brain tumor resections in four patients. All tumors were in critical spatial relationship to the primary motor and somatosensory cortices, thus necessitating accurate localization prior to surgery to minimize postoperative deficits. Each of the patients was scanned using rsfMRI and using task-based fMRI while performing a block design finger-tapping task. fMRI in each patient included four 7-min runs (28 min total). The rsfMRI data previously acquired from a group of normal controls ($N=17$) were also used for comparison. Data processing for both resting-state and task-based fMRI was standardized (Zhang et al. 2008).

Preprocessing was done using the above-described methods. Correlation maps were generated using 6 mm radius spherical seed regions of interest (ROIs). The seed regions for

all the normal brains were placed in the left sensorimotor cortex. In the tumor patients, the seed was placed in the hemisphere contralateral to the tumor at coordinates taken from an independent group of subjects that performed a button-press task (Fox et al. 2006b; Zacks et al. 2001). Electrocortical stimulation mapping (ECS) was performed on three of the four tumor patients, and these data, in addition to the task-based fMRI, were used for comparison with the resting-state data.

The 17 control brains were mapped using the seed region in the left sensorimotor cortex. The correlations of resting state activity to the seed region were recorded for each of the other voxels in the brain. The group average was used as a control to show the distribution of the sensorimotor network in a healthy brain. To confirm the reproducibility of this method in individual subjects, the full rsfMRI data set in each subject (28 min) was divided into the four separate scans (7 min) and a separate analysis was performed on each segment. The somatomotor cortex was consistently activated in the same region over the four scans in all control subjects. The four tumor patients were also mapped individually following the placement of the seed regions on the contralateral side of the brain. In the following paragraphs, we discuss two of the four patients from this paper:

Figure 5 shows a glioblastoma multiforme that was diagnosed in the right hemisphere of a 45-year-old man. ECS during surgery revealed that motor cortex was displaced anteriorly. Figure 5a shows the results of resting-state fMRI, which confirmed the anterior displacement of the motor cortex. Figure 5b shows the results of the task-based fMRI that also demonstrated an anterior shift in the motor cortex ipsilateral to the tumor. However, the task-based result was unreliable, as the second trial showed likely artifactual activation in the posterior part of the tumor. Resting-state fMRI was more consistent.

In another case, shown in Fig. 6, a 64-year-old man developed focal motor seizures secondary to a mass in the left

hemisphere (Fig. 6a). Finger-tapping fMRI showed atypical response topography including activation in the right parietal cortex in addition to the expected activation of the somatomotor area (Fig. 6b). Seed-based (Fig. 6c) correlation mapping rsfMRI showed the somatomotor RSN without parietal involvement. Correlation mapping with a seed in the right parietal cortex matched the topography of the DAN (Fig. 6d). Our interpretation of this result is that, during task-based fMRI, the patient had to strongly focus his attention in order to complete the task, which accounts for the prominent activation in the attentional network. This case illustrates the potentially increased specificity of resting-state compared to task-based fMRI. The findings of the rsfMRI were consistent with the intraoperative ECS.

These cases show that the seed-based correlation mapping using resting-state data is consistent with task-based fMRI but, in some cases, more reliable.

3.3 Preoperative Mapping of Functional Cortex Using MLP

Mitchell and colleagues reported the application of MLP-based RSN mapping to presurgical planning in six patients with intractable epilepsy and seven patients with brain tumors (Mitchell and Hacker 2013). Patients with epilepsy underwent electrocorticographic monitoring to localize the epileptogenic zone of seizure onset and to perform functional mapping with ECS. Patients with tumors underwent intraoperative ECS mapping prior to resection of the tumor mass.

For preoperative rsfMRI analysis in the tumor patients, lesions were manually segmented using T1- and T2-weighted images. The MLP was trained and applied de novo in each tumor patient, omitting tumor voxels. To determine the probability that an electrode covers a portion of a RSN, electrode MRI co-registration was used with the results of the MLP analysis, and gray matter voxels located within 30 mm of the electrode were averaged with a factor that was inversely proportional to the square of their distance from the electrode.

For the seizure-monitoring patients, electrodes were segmented on the basis of a CT image co-registered to the patient's MRI using methods similar to those previously described (He et al. 2007; Hermes et al. 2010). Electrodes imaged in the post-grid implantation CT typically are displaced inward relative to the cortical surface imaged on preoperative MRI because of traction from dural over-sewing and postsurgical edema. This inward displacement was corrected by projecting electrode coordinates outwards to the brain surface along a path normal to the plane of the grid.

Electrodes were classified as over eloquent cortex using ECS mapping. Motor regions were defined by the presence of induced involuntary motor movements. Language sites were defined by speech arrest during the stimulation.

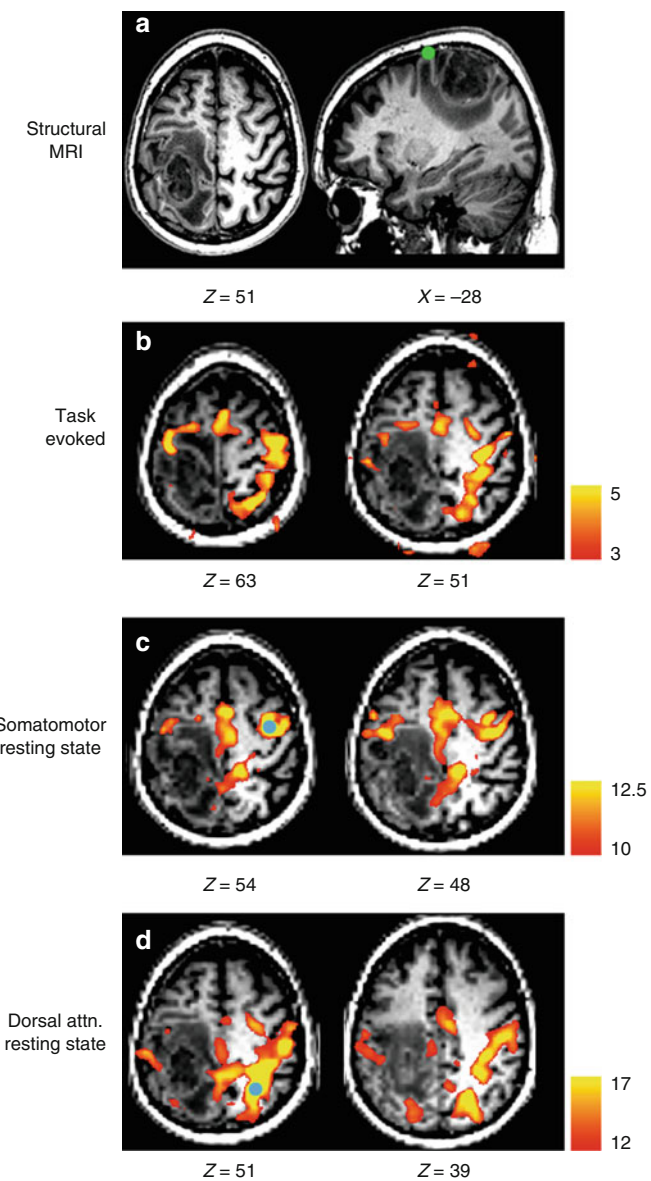
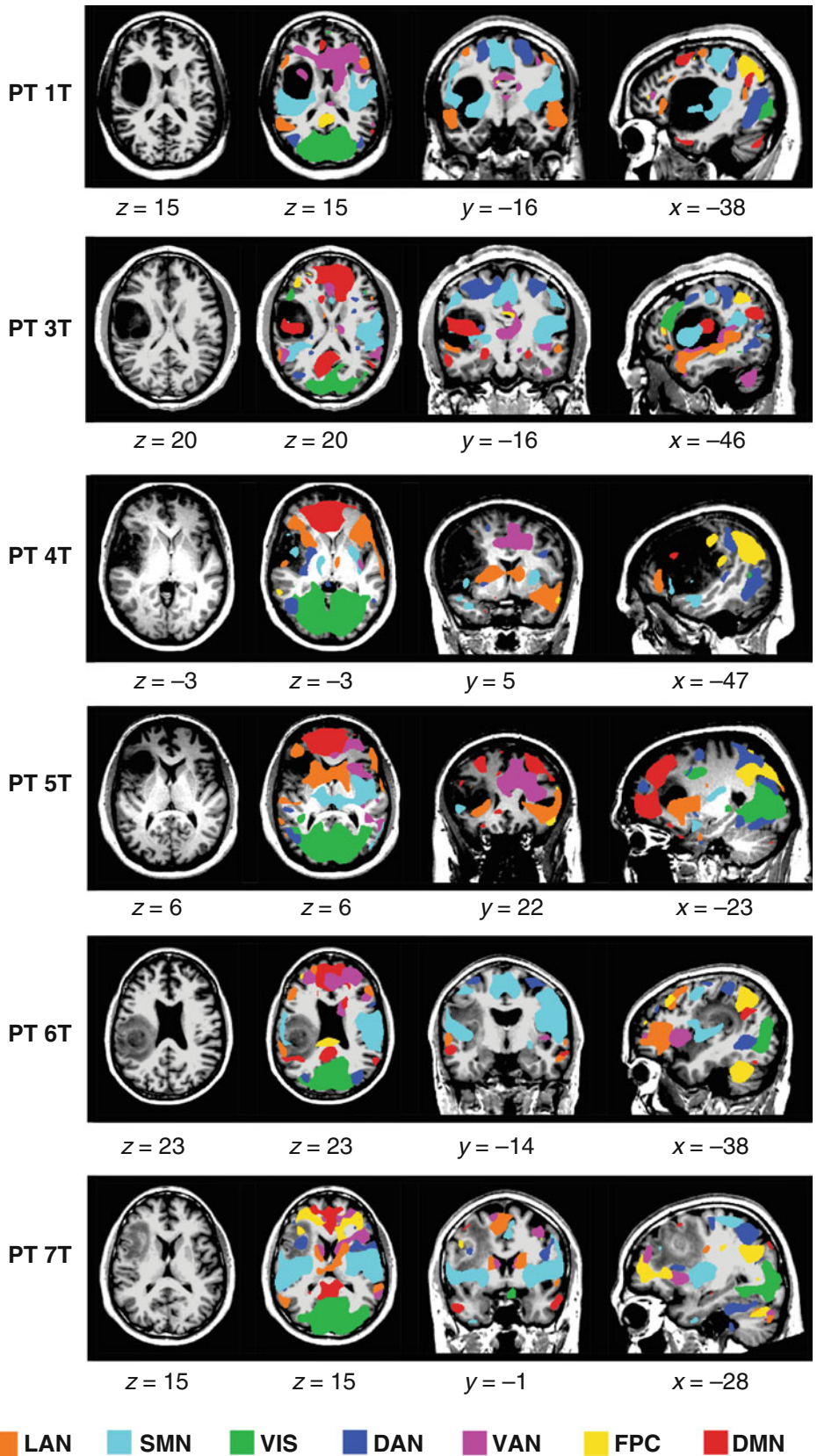


Fig. 6 Magnetic resonance image (MRI) of a 64-year-old man who presented with focal motor seizures (Case 2). (a) Structural MRI revealed a tumor in the left parietal cortex that invades territory near the central sulcus (neurologic convention). The green circle represents the location of the ipsilateral hand response to cortical stimulation. (b) Task-related activity was seen bilaterally in the frontal lobe. In addition, a large band of activity appeared in the right parietal cortex, not consistent with the pattern of activity from the sensorimotor network. (c) Resting-state correlation mapping using a seed in the right (unaffected) hemisphere (blue circle) showed ipsilateral correlations anterior to the tumor as well as a region of activity in the midline of the parietal cortex. Note absence in the correlation mapping results of the parietal activity seen in the task-related map. (d) Parietal activation seen during the task-evoked scan is revealed to represent a separate resting-state network, the dorsal attention network, which is normally dissociated from the sensorimotor network (seed: blue circle). All images are displayed left-on-left (neurologic convention) (Zhang et al. 2009)

For comparison of MLP-based RSN mapping to ECS mapping, an electrode was classified as positive or negative in the MLP results according to the probability of it belonging to the appropriate RSN (motor or language).

Fig. 7 Resting-state network (RSN) maps produced by the multilayer perceptron (MLP) for seven tumor patients. The seven networks, *LAN* language, *SMN* somatomotor network, *VIS* visual, *DAN* dorsal attention network, *VAN* ventral attention network, *FPC* frontoparietal control, and *DMN* default mode network, were mapped in the area of the tumor using the winner-take-all format (Mitchell and Hacker 2013)

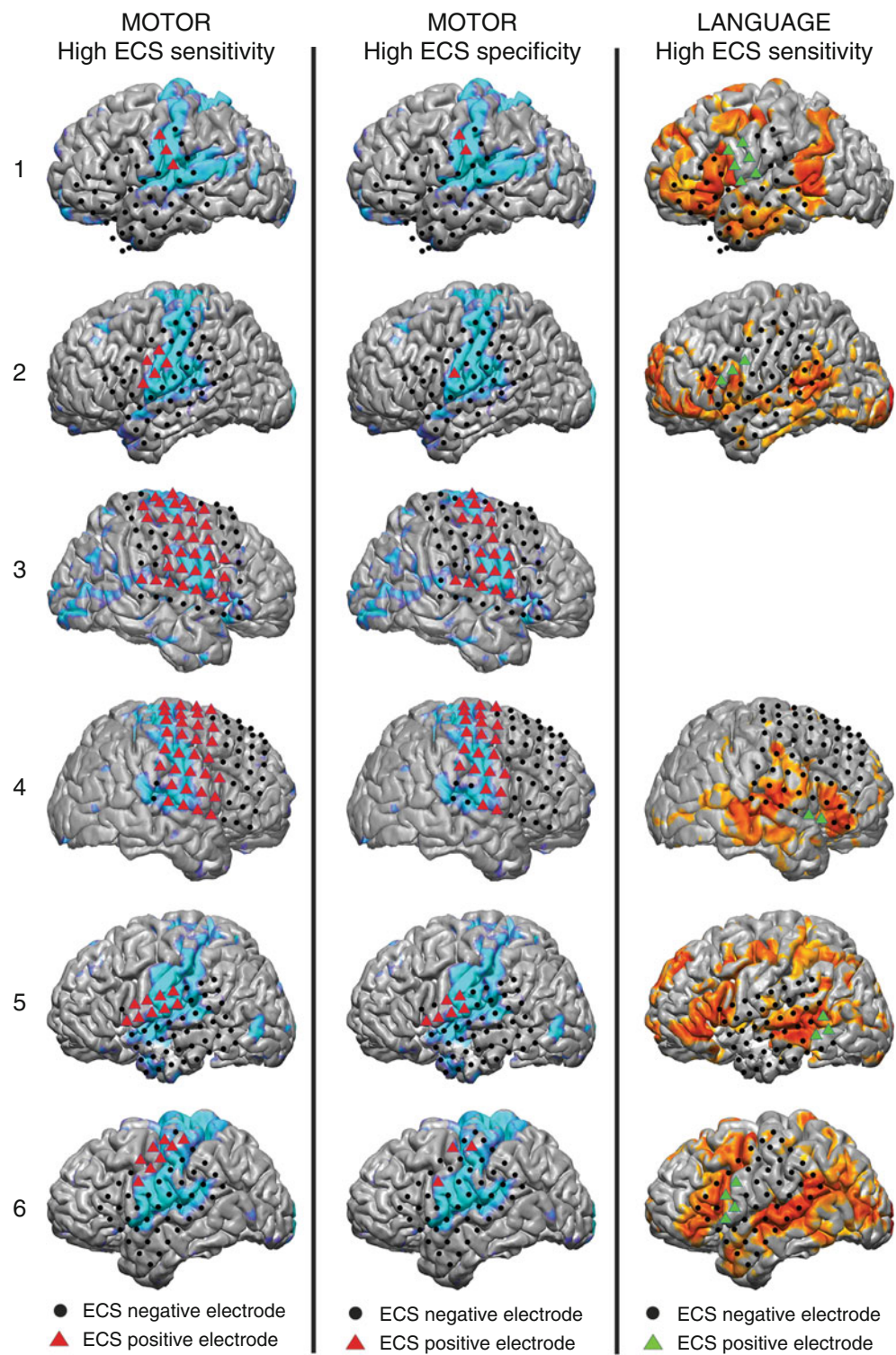


These probabilities were then plotted against the ECS results to generate receiver-operator characteristic (ROC) curves. These ROC curves were averaged, and the area under the averaged curve (AUC) was used as a

measure of the agreement between the MLP and ECS methods.

The resulting RSN maps for the tumor patients are shown in Fig. 7. Structural images in column 1 reveal the extent of the

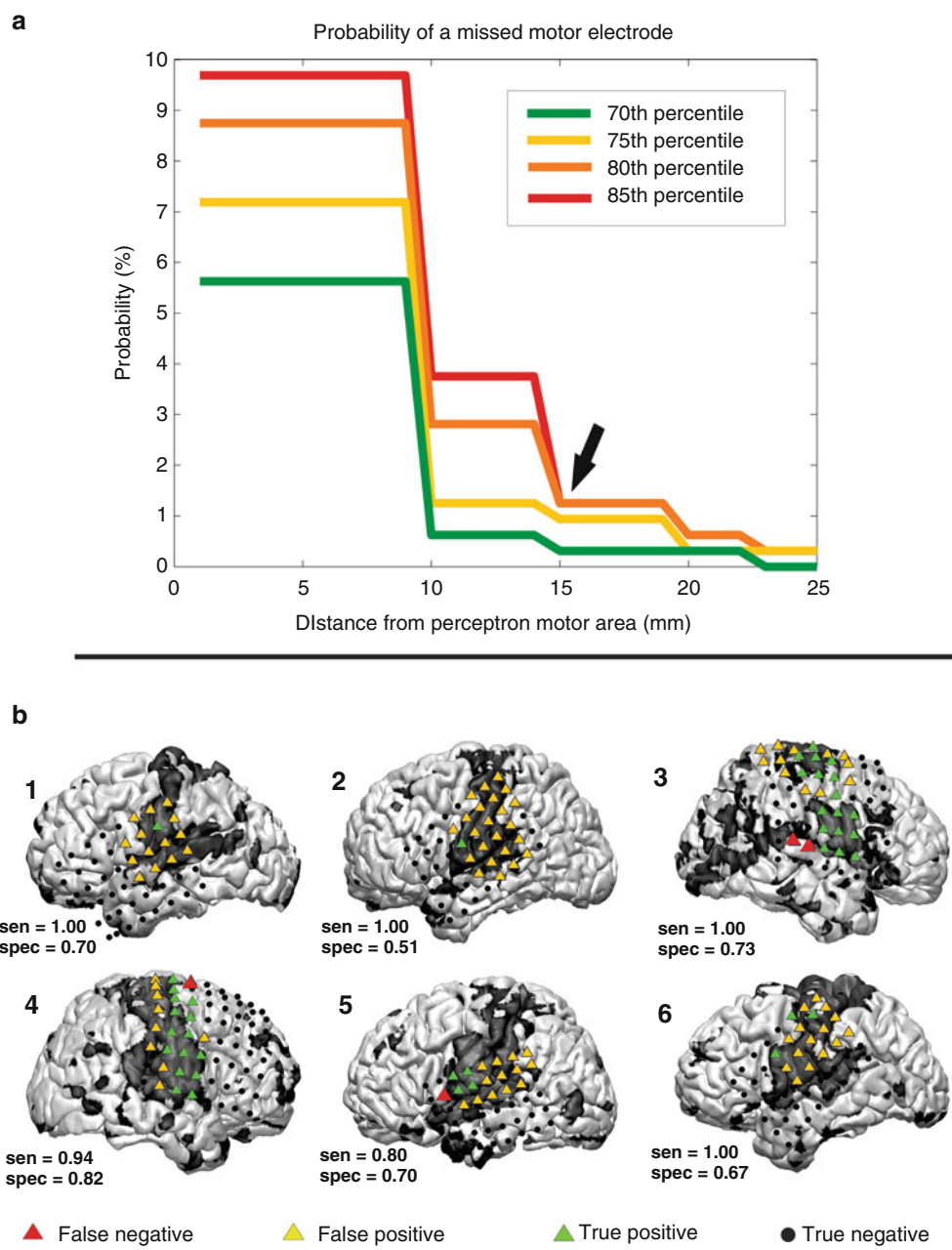
Fig. 8 Comparison of electrocortical stimulation (ECS) and multilayer perceptron (MLP) results for the motor and language cortices in six patients with epilepsy. Colored triangles are ECS positive and black circles are ECS negative. In the *left column*, the high ECS sensitivity method was employed to classify motor electrodes as ECS positive (red triangles) and compared to the MLP results (light blue). In the *middle column*, the high ECS specificity method was employed to classify motor electrodes. In the *right column*, the high ECS sensitive method was used to classify language electrodes as ECS positive (green triangles), with the MLP results displayed in orange (Mitchell and Hacker 2013)



lesion in each patient. Columns 2, 3, and 4 show axial, coronal, and sagittal views of the MLP results displayed in a winner-take-all format. Significant asymmetry across the midline can be seen in networks near the tumor, which is consistent with previous findings (Zhang et al. 2009). Networks were preserved in the presence of a tumor, though they were often shifted with respect to their normal anatomic position. Despite these distortions, there was good agreement between the ECS and MLP results.

Figure 8 demonstrates a high degree of qualitative overlap between the location of the motor and language networks as compared to the ECS results in patients with epilepsy. The positive motor ECS electrodes were centered in the precentral gyrus. The MLP-mapped motor areas encompassed both the pre- and postcentral gyri. The positive language ECS electrodes were centered in the pars opercularis of the inferior frontal gyrus (IFG), approximately in the Brodmann

Fig. 9 The method employed to define a “no-cut” area in patients with epilepsy, in which the probability of damage to motor cortex is substantial. (a) To define the area, several multilayer perceptron (MLP) thresholds (70th, 75th, 80th, 85th percentiles) were used to classify electrodes as covering motor cortex, and the “no-cut” zone was expanded around each of the motor electrodes. The probability of a missed motor electrode, which could result in motor deficits, was plotted against the radius of expansion. (b) Visualization of the method performed at the 85 % and at a radius of expansion of 15 mm. Red triangles mark the motor cortex as determined by ECS that were missed by the MLP method (Mitchell and Hacker 2013)



area (BA) 44. The MLP language-positive regions were in the pars triangularis of the IFG, which corresponds to BA 45. The anteriorly shifted MLP-based localization of the language cortex (BA 45 vs. 44) suggests the possibility that the definition of eloquent cortex should be expanded. Quantitative comparisons were performed with an ROC analysis which yielded an AUC of 0.89 for the motor network and an average AUC of 0.76 for the language network. These findings demonstrate that MLP-based mapping can identify RSNs in the presence of distorted anatomy.

Loci in MLP maps outside the appropriate RSN, but eloquent as determined by ECS, are defined as MLP false negatives. Minimization of MLP false negatives is critical to

reduce surgical morbidity, since resection of a false negative area could lead to a clinical deficit. Figure 9 illustrates the results of an analysis undertaken to minimize MLP motor false negatives. This analysis showed that the probability of a MLP false negative could be reduced to less than 2 % by expanding the “no-cut” zone by 15 mm around the contour corresponding to an 85 % likelihood of belonging to the motor RSN.

In summary, MLP-based RSN mapping robustly identified all networks in all patients, including those with distorted anatomy attributable to mass effect. When the ECS positive sites were analyzed, rsfMRI had AUCs of 0.89 and 0.76 for motor and language, respectively. MLP false

negatives were minimized by including a 15 mm safety margin around the edge of the motor RSN. These findings demonstrate that MLP-defined RSNs are able to identify eloquent cortices.

Conclusion

This chapter presents an introduction to rsfMRI and RSNs. We briefly covered RSN imaging methods and several common analysis techniques. We presented our early experience using this technique for the localization of the motor cortex using seed-based correlation mapping. We then presented MLP-based RSN mapping in detail, as this is our current method of choice for simultaneously mapping multiple RSNs to provide the surgeon with an accurate map of the resting state architecture of the brain prior to surgery. Finally, we reviewed our experience using the MLP-based technique in patients with epilepsy and brain tumors. This experience suggests how MLP-based RSN mapping should be applied to minimize surgical morbidity.

As these results demonstrate, rsfMRI is a promising technique in the context of presurgical planning with the objective of decreasing morbidity while maximizing complete resection of pathological tissue. However, the methodology is still in its early stages of development. Further research is necessary to make these tools more accurate and available in the operating room. Additional research is needed to explore the differences between rsfMRI and ECS mapping and to better understand the consequences of disrupted RSNs other than the motor and language systems. Related engineering development should incorporate the presurgical MRI results into intraoperative neuronavigation systems, including the rsfMRI results in conjunction with white matter fiber bundle anatomy derived from diffusion imaging. An additional possibility is real-time intraoperative rsfMRI during surgery using MRI systems that currently are becoming more common.

Acknowledgments We wish to thank the National Institute of Health for its generous support of this project via NIH R21 CA159470. Dr. Snyder is supported by NIMH Grant P30 NS048056.

References

- Abdulkadir A, Mortamet B, Vemuri P, Jack CR Jr, Krueger G, Kloppel S (2011) Effects of hardware heterogeneity on the performance of SVM Alzheimer's disease classifier. *Neuroimage* 58:785–792
- Aguirre GK, Zarahn E, D'Esposito M (1998) The inferential impact of global signal covariates in functional neuroimaging analyses. *Neuroimage* 8:302–306
- Ames A 3rd, Li YY, Heher EC, Kimble CR (1992) Energy metabolism of rabbit retina as related to function: high cost of Na⁺ transport. *J Neurosci* 12:840–853
- Anderson JS, Druzgal TJ, Lopez-Larson M, Jeong EK, Desai K, Yurgelun-Todd D (2011) Network anticorrelations, global regression, and phase-shifted soft tissue correction. *Hum Brain Mapp* 32:919–934
- Astafiev SV, Shulman GL, Corbetta M (2006) Visuospatial reorienting signals in the human temporo-parietal junction are independent of response selection. *Eur J Neurosci* 23:591–596
- Attwell D, Laughlin SB (2001) An energy budget for signaling in the grey matter of the brain. *J Cereb Blood Flow Metab* 21:1133–1145
- Beckmann CF, Smith SM (2004) Probabilistic independent component analysis for functional magnetic resonance imaging. *IEEE Trans Med Imaging* 23:137–152
- Beckmann CF, DeLuca M, Devlin JT, Smith SM (2005) Investigations into resting-state connectivity using independent component analysis. *Philosophical transactions of the Royal Society of London. B Biol Sci* 360:1001–1013
- Bellec P, Rosa-Neto P, Lyttelton OC, Benali H, Evans AC (2010) Multi-level bootstrap analysis of stable clusters in resting-state fMRI. *Neuroimage* 51:1126–1139
- Bettus G, Bartolomei F, Confort-Gouny S, Guedj E, Chauvel P, Cozzone PJ, Ranjeva JP, Guye M (2010) Role of resting state functional connectivity MRI in presurgical investigation of mesial temporal lobe epilepsy. *J Neurol Neurosurg Psychiatry* 81:1147–1154
- Biswal B, Yetkin FZ, Haughton VM, Hyde JS (1995) Functional connectivity in the motor cortex of resting human brain using echo-planar MRI. *Magn Reson Med* 34:537–541
- Buckner RL, Snyder AZ, Shannon BJ, LaRossa G, Sachs R, Fotenos AF, Sheline YI, Klunk WE, Mathis CA, Morris JC, Mintun MA (2005) Molecular, structural, and functional characterization of Alzheimer's disease: evidence for a relationship between default activity, amyloid, and memory. *J Neurosci* 25:7709–7717
- Chai XJ, Castanon AN, Ongur D, Whittfield-Gabrieli S (2012) Anticorrelations in resting state networks without global signal regression. *Neuroimage* 59:1420–1428
- Clarke DD, Sokoloff L (1999) Circulation and energy metabolism of the brain. In: Siegel GJ, Agranoff BW (eds) *Basic neurochemistry. Molecular, cellular and medical aspects*. Lippincott-Raven, Philadelphia
- Corbetta M, Shulman GL (2002) Control of goal-directed and stimulus-driven attention in the brain. *Nat Rev Neurosci* 3:201–215
- Cordes D, Haughton VM, Arfanakis K, Wendt GJ, Turski PA, Moritz CH, Quigley MA, Meyerand ME (2000) Mapping functionally related regions of brain with functional connectivity MR imaging. *AJNR Am J Neuroradiol* 21:1636–1644
- Cordes D, Haughton V, Carew JD, Arfanakis K, Maravilla K (2002) Hierarchical clustering to measure connectivity in fMRI resting-state data. *Magn Reson Imaging* 20:305–317
- Damoiseaux JS, Rombouts SA, Barkhof F, Scheltens P, Stam CJ, Smith SM, Beckmann CF (2006) Consistent resting-state networks across healthy subjects. *Proc Natl Acad Sci U S A* 103:13848–13853
- De Luca M, Beckmann CF, De Stefano N (2006) fMRI resting state networks define distinct modes of long-distance interactions in the human brain. *Neuroimage* 29:1359–1367
- Dosenbach NU, Visscher KM, Palmer ED, Miezin FM, Wenger KK, Kang HC, Burgund ED, Grimes AL, Schlaggar BL, Petersen SE (2006) A core system for the implementation of task sets. *Neuron* 50:799–812
- Doucet G, Naveau M, Petit L, Delcroix N, Zago L, Crivello F, Jobard G, Tzourio-Mazoyer N, Mazoyer B, Mellet E, Joliot M (2011) Brain activity at rest: a multiscale hierarchical functional organization. *J Neurophysiol* 105:2753–2763
- Fischl B (2012) FreeSurfer. *Neuroimage* 62:774–781
- Fox MD, Raichle ME (2007) Spontaneous fluctuations in brain activity observed with functional magnetic resonance imaging. *Nat Rev Neurosci* 8:700–711
- Fox MD, Snyder AZ, Vincent JL, Corbetta M, Van Essen DC, Raichle ME (2005) The human brain is intrinsically organized into dynamic,

- anticorrelated functional networks. *Proc Natl Acad Sci U S A* 102:9673–9678
- Fox MD, Corbetta M, Snyder AZ, Vincent JL, Raichle ME (2006a) Spontaneous neuronal activity distinguishes human dorsal and ventral attention systems. *Proc Natl Acad Sci U S A* 103:10046–10051
- Fox MD, Snyder AZ, Zacks JM, Raichle ME (2006b) Coherent spontaneous activity accounts for trial-to-trial variability in human evoked brain responses. *Nat Neurosci* 9:23–25
- Fox MD, Zhang D, Snyder AZ, Raichle ME (2009) The global signal and observed anticorrelated resting state brain networks. *J Neurophysiol* 101:3270–3283
- Friston KJ, Williams S, Howard R, Frackowiak RS, Turner R (1996) Movement-related effects in fMRI time-series. *Magn Reson Med* 35:346–355
- Goldman R, Cohen M (2003) Tomographic distribution of resting alpha rhythm sources revealed by independent component analysis. In: Ninth international conference on functional mapping of the human brain, New York, pp 18–22
- Golland Y, Golland P, Bentin S, Malach R (2008) Data-driven clustering reveals a fundamental subdivision of the human cortex into two global systems. *Neuropsychologia* 46:540–553
- Greicius MD, Krasnow B, Reiss AL, Menon V (2003) Functional connectivity in the resting brain: a network analysis of the default mode hypothesis. *Proc Natl Acad Sci U S A* 100:253–258
- Greicius MD, Srivastava G, Reiss AL, Menon V (2004) Default-mode network activity distinguishes Alzheimer's disease from healthy aging: evidence from functional MRI. *Proc Natl Acad Sci U S A* 101:4637–4642
- Gusnard DA, Raichle ME (2001) Searching for a baseline: functional imaging and the resting human brain. *Nat Rev Neurosci* 2:685–694
- Hacker CD, Laumann TO, Szrama NP, Baldassarre A, Snyder AZ, Leuthardt EC, Corbetta M (2013) Resting state network estimation in individual subjects. *Neuroimage* 82:616–633
- He BJ, Snyder AZ, Vincent JL, Epstein A, Shulman GL, Corbetta M (2007) Breakdown of functional connectivity in frontoparietal networks underlies behavioral deficits in spatial neglect. *Neuron* 53:905–918
- Hermes D, Miller KJ, Noordmans HJ, Vansteensel MJ, Ramsey NF (2010) Automated electrocorticographic electrode localization on individually rendered brain surfaces. *J Neurosci Methods* 185: 293–298
- Hutchison RM, Gallivan JP, Culham JC, Gati JS, Menon RS, Everling S (2012) Functional connectivity of the frontal eye fields in humans and macaque monkeys investigated with resting-state fMRI. *J Neurophysiol* 107:2463–2474
- Jack AI, Dawson AJ, Begany KL, Leckie RL, Barry KP, Ciccia AH, Snyder AZ (2012) fMRI reveals reciprocal inhibition between social and physical cognitive domains. *Neuroimage* 66C:385–401
- Jo HJ, Saad ZS, Simmons WK, Milbury LA, Cox RW (2010) Mapping sources of correlation in resting state fMRI, with artifact detection and removal. *Neuroimage* 52:571–582
- Joel SE, Caffo BS, van Zijl PC, Pekar JJ (2011) On the relationship between seed-based and ICA-based measures of functional connectivity. *Magn Reson Med* 66:644–657
- Keles GE, Lamborn KR, Berger MS (2001) Low-grade hemispheric gliomas in adults: a critical review of extent of resection as a factor influencing outcome. *J Neurosurg* 95:735–745
- Keles GE, Chang EF, Lamborn KR, Tihan T, Chang CJ, Chang SM, Berger MS (2006) Volumetric extent of resection and residual contrast enhancement on initial surgery as predictors of outcome in adult patients with hemispheric anaplastic astrocytoma. *J Neurosurg* 105:34–40
- Kokkinen SM, Nikkinen J, Remes J, Kantola J, Starck T, Haapea M, Tuominen J, Tervonen O, Kiviniemi V (2009) Preoperative localization of the sensorimotor area using independent component analysis of resting-state fMRI. *Magn Reson Imaging* 27:733–740
- Lacroix M, Abi-Said D, Fournier DR, Gokaslan ZL, Shi W, DeMonte F, Lang FF, McCutcheon IE, Hassenbusch SJ, Holland E, Hess K, Michael C, Miller D, Sawaya R (2001) A multivariate analysis of 416 patients with glioblastoma multiforme: prognosis, extent of resection, and survival. *J Neurosurg* 95:190–198
- Larson-Prior LJ, Zempel JM, Nolan TS, Prior FW, Snyder AZ, Raichle ME (2009) Cortical network functional connectivity in the descent to sleep. *Proc Natl Acad Sci U S A* 106:4489–4494
- LeCun Y, Boser B, Denker JS, Henderson D, Howard RE, Hubbard W, Jackel LD (1989) Backpropagation applied to handwritten zip code recognition. *Neural Comput* 1:541–551
- Lee MH, Hacker CD, Shimony JS (2012a) Clustering of resting state networks. *PLoS One* 7:e40370
- Lee MH, Smyser CD, Shimony JS (2012b) Resting-State fMRI: a review of methods and clinical applications. *AJR Am J Neuroradiol* 34(10):1866–72
- Lennie P (2003) The cost of cortical computation. *Curr Biol* 13:493–497
- Liao W, Mantini D, Zhang Z, Pan Z, Ding J, Gong Q, Yang Y, Chen H (2010) Evaluating the effective connectivity of resting state networks using conditional Granger causality. *Biol Cybern* 102: 57–69
- Liu H, Buckner RL, Talukdar T, Tanaka N, Madsen JR, Stufflebeam SM (2009) Task-free presurgical mapping using functional magnetic resonance imaging intrinsic activity. *J Neurosurg* 111:746–754
- Lowe MJ, Mock BJ, Sorenson JA (1998) Functional connectivity in single and multislice echoplanar imaging using resting-state fluctuations. *Neuroimage* 7:119–132
- Macey PM, Macey KE, Kumar R, Harper RM (2004) A method for removal of global effects from fMRI time series. *Neuroimage* 22:360–366
- McGirt MJ, Chaichana KL, Gathinji M, Attenello FJ, Than K, Olivi A, Weingart JD, Brem H, Quinones-Hinojosa AR (2009) Independent association of extent of resection with survival in patients with malignant brain astrocytoma. *J Neurosurg* 110:156–162
- Mhuircheartaigh RN, Rosenorn-Lanng D, Wise R, Jbabdi S, Rogers R, Tracey I (2010) Cortical and subcortical connectivity changes during decreasing levels of consciousness in humans: a functional magnetic resonance imaging study using propofol. *J Neurosci* 30: 9095–9102
- Mitchell T, Hacker CD (2013) A novel data driven approach to preoperative mapping of functional cortex using resting state fMRI. *Neurosurgery* 73(6):969
- Murphy K, Birn RM, Handwerker DA, Jones TB, Bandettini PA (2009) The impact of global signal regression on resting state correlations: are anti-correlated networks introduced? *Neuroimage* 44:893–905
- Nasrallah FA, Tay HC, Chuang KH (2013) Detection of functional connectivity in the resting mouse brain. *Neuroimage* 86:417–24
- Ojemann JG, Buckner RL, Corbetta M, Raichle ME (1997) Imaging studies of memory and attention. *Neurosurg Clin N Am* 8:307–319
- Pizoli CE, Shah MN, Snyder AZ, Shimony JS, Limbrick DD, Raichle ME, Schlaggar BL, Smyth MD (2011) Resting-state activity in development and maintenance of normal brain function. *Proc Natl Acad Sci U S A* 108:11638–11643
- Posner MI, Raichle ME (1994) Images of mind. Scientific American Library, New York
- Power JD, Petersen SE (2013) Control-related systems in the human brain. *Curr Opin Neurobiol* 23:223–228
- Power JD, Cohen AL, Nelson SM, Wig GS, Barnes KA, Church JA, Vogel AC, Laumann TO, Miezin FM, Schlaggar BL, Petersen SE (2011) Functional network organization of the human brain. *Neuron* 72:665–678
- Power JD, Barnes KA, Snyder AZ, Schlaggar BL, Petersen SE (2012) Spurious but systematic correlations in functional connectivity MRI networks arise from subject motion. *Neuroimage* 59:2142–2154

- Purdon PL, Weisskoff RM (1998) Effect of temporal autocorrelation due to physiological noise and stimulus paradigm on voxel-level false-positive rates in fMRI. *Hum Brain Mapp* 6:239–249
- Raichle ME, Mintun MA (2006) Brain work and brain imaging. *Annu Rev Neurosci* 29:449–476
- Rosazza C, Minati L, Ghielmetti F, Mandelli ML, Bruzzone MG (2012) Functional connectivity during resting-state functional MR imaging: study of the correspondence between independent component analysis and region-of-interest-based methods. *AJNR Am J Neuroradiol* 33:180–187
- Rumelhart DE, Hinton GE, Williams RJ (1986) Learning representations by back-propagating errors. *Nature* 323:533–536
- Saad ZS, Gotts SJ, Murphy K, Chen G, Jo HJ, Martin A, Cox RW (2012) Trouble at rest: how correlation patterns and group differences become distorted after global signal regression. *Brain Connect* 2:25–32
- Salvador R, Suckling J, Coleman MR, Pickard JD, Menon D, Bullmore E (2005) Neurophysiological architecture of functional magnetic resonance images of human brain. *Cereb Cortex* 15: 1332–1342
- Samann PG, Tully C, Spoormaker VI, Wetter TC, Holsboer F, Wehrle R, Czisch M (2010) Increased sleep pressure reduces resting state functional connectivity. *MAGMA* 23:375–389
- Sanai N, Mirzadeh Z, Berger MS (2008) Functional outcome after language mapping for glioma resection. *N Engl J Med* 358:18–27
- Satterthwaite TD, Wolf DH, Loughead J, Ruparel K, Elliott MA, Hakonarson H, Gur RC, Gur RE (2012) Impact of in-scanner head motion on multiple measures of functional connectivity: relevance for studies of neurodevelopment in youth. *Neuroimage* 60: 623–632
- Scholvinck ML, Maier A, Ye FQ, Duyn JH, Leopold DA (2010) Neural basis of global resting-state fMRI activity. *Proc Natl Acad Sci U S A* 107:10238–10243
- Schwarz AJ, Gass N, Sartorius A, Risterucci C, Spedding M, Schenker E, Meyer-Lindenberg A, Weber-Fahr W (2013) Anti-correlated cortical networks of intrinsic connectivity in the rat brain. *Brain Connect* 3:503–511
- Seeley WW, Menon V, Schatzberg AF, Keller J, Glover GH, Kenna H, Reiss AL, Greicius MD (2007) Dissociable intrinsic connectivity networks for salience processing and executive control. *J Neurosci* 27:2349–2356
- Shehzad Z, Kelly AM, Reiss PT, Gee DG, Gotimer K, Uddin LQ, Lee SH, Margulies DS, Roy AK, Biswal BB, Petkova E, Castellanos FX, Milham MP (2009) The resting brain: unconstrained yet reliable. *Cereb Cortex* 19:2209–2229
- Shimony JS, Zhang D, Johnston JM, Fox MD, Roy A, Leuthardt EC (2009) Resting-state spontaneous fluctuations in brain activity: a new paradigm for presurgical planning using fMRI. *Acad Radiol* 16:578–583
- Shulman GL, Corbetta M, Buckner RL, Fiez JA, Miezin FM, Raichle ME, Petersen SE (1997) Common blood flow changes across visual tasks: I. Increases in subcortical structures and cerebellum but Not in nonvisual cortex. *J Cogn Neurosci* 9:624–647
- Shulman RG, Rothman DL, Behar KL, Hyder F (2004) Energetic basis of brain activity: implications for neuroimaging. *Trends Neurosci* 27:489–495
- Shulman GL, Pope DL, Astafiev SV, McAvoy MP, Snyder AZ, Corbetta M (2010) Right hemisphere dominance during spatial selective attention and target detection occurs outside the dorsal frontoparietal network. *J Neurosci* 30:3640–3651
- Smith SM, Fox PT, Miller KL, Glahn DC, Fox PM, Mackay CE, Filippini N, Watkins KE, Toro R, Laird AR, Beckmann CF (2009) Correspondence of the brain's functional architecture during activation and rest. *Proc Natl Acad Sci U S A* 106:13040–13045
- Snyder AZ, Raichle ME (2012) A brief history of the resting state: the Washington University perspective. *Neuroimage* 62:902–910
- Spitzer M, Kwong KK, Kennedy W, Rosen BR, Belliveau JW (1995) Category-specific brain activation in fMRI during picture naming. *Neuroreport* 6:2109–2112
- Spreng RN (2012) The fallacy of a “task-negative” network. *Front Psychol* 3:145
- Starck T, Remes J, Nikkinen J, Tervonen O, Kiviniemi V (2010) Correction of low-frequency physiological noise from the resting state BOLD fMRI—Effect on ICA default mode analysis at 1.5 T. *J Neurosci Methods* 186:179–185
- Stufflebeam SM, Liu H, Sepulcre J, Tanaka N, Buckner RL, Madsen JR (2011) Localization of focal epileptic discharges using functional connectivity magnetic resonance imaging. *J Neurosurg* 114:1693–1697
- Thomas CG, Harshman RA, Menon RS (2002) Noise reduction in BOLD-based fMRI using component analysis. *Neuroimage* 17:1521–1537
- Tie Y, Rigolo L, Norton IH, Huang RY, Orringer D, Wu W, Mukundan S Jr, Golby AJ (2013) Defining language networks from resting-state fMRI for surgical planning—a feasibility study. *Hum Brain Mapp* 35(3):1018–30
- Tohka J, Foerde K, Aron AR, Tom SM, Toga AW, Poldrack RA (2008) Automatic independent component labeling for artifact removal in fMRI. *Neuroimage* 39:1227–1245
- Tomasi D, Volkow ND (2012) Resting functional connectivity of language networks: characterization and reproducibility. *Mol Psychiatry* 17:841–854
- Triantafyllou C, Hoge RD, Krueger G, Wiggins CJ, Potthast A, Wiggins GC, Wald LL (2005) Comparison of physiological noise at 1.5 T, 3 T and 7 T and optimization of fMRI acquisition parameters. *Neuroimage* 26:243–250
- van den Heuvel M, Mandl R, Hulshoff Pol H (2008) Normalized cut group clustering of resting-state fMRI data. *PLoS One* 3:e2001
- Vincent JL, Snyder AZ, Fox MD, Shannon BJ, Andrews JR, Raichle ME, Buckner RL (2006) Coherent spontaneous activity identifies a hippocampal-parietal memory network. *J Neurophysiol* 96:3517–3531
- Vincent JL, Kahn I, Snyder AZ, Raichle ME, Buckner RL (2008) Evidence for a frontoparietal control system revealed by intrinsic functional connectivity. *J Neurophysiol* 100:3328–3342
- Weaver KE, Chaovallitwongse WA, Novotny EJ, Poliakov A, Grabowski TG, Ojemann JG (2013) Local functional connectivity as a pre-surgical tool for seizure focus identification in non-lesion, focal epilepsy. *Front Neurol* 4:43
- Wise RG, Ide K, Poulin MJ, Tracey I (2004) Resting fluctuations in arterial carbon dioxide induce significant low frequency variations in BOLD signal. *Neuroimage* 21:1652–1664
- Xiong J, Parsons LM, Gao JH, Fox PT (1999) Interregional connectivity to primary motor cortex revealed using MRI resting state images. *Hum Brain Mapp* 8:151–156
- Yan CG, Cheung B, Kelly C, Colcombe S, Craddock RC, Di Martino A, Li Q, Zuo XN, Castellanos FX, Milham MP (2013) A comprehensive assessment of regional variation in the impact of head micro-movements on functional connectomics. *Neuroimage* 76:183–201
- Yeo BT, Krienen FM, Sepulcre J, Sabuncu MR, Lashkari D, Hollinshead M, Roffman JL, Smoller JW, Zollei L, Polimeni JR, Fischl B, Liu H, Buckner RL (2011) The organization of the human cerebral cortex estimated by intrinsic functional connectivity. *J Neurophysiol* 106:1125–1165
- Zacks JM, Braver TS, Sheridan MA, Donaldson DI, Snyder AZ, Ollinger JM, Buckner RL, Raichle ME (2001) Human brain activity time-locked to perceptual event boundaries. *Nat Neurosci* 4:651–655
- Zhang D, Raichle ME (2010) Disease and the brain's dark energy. *Nat Rev Neurol* 6:15–28
- Zhang D, Snyder AZ, Fox MD, Sansbury MW, Shimony JS, Raichle ME (2008) Intrinsic functional relations between human cerebral cortex and thalamus. *J Neurophysiol* 100:1740–1748

- Zhang D, Johnston JM, Fox MD, Leuthardt EC, Grubb RL, Chicoine MR, Smyth MD, Snyder AZ, Raichle ME, Shimony JS (2009) Preoperative sensorimotor mapping in brain tumor patients using spontaneous fluctuations in neuronal activity imaged with functional magnetic resonance imaging: initial experience. *Neurosurgery* 65:226–236
- Zhang Z, Liao W, Zuo XN, Wang Z, Yuan C, Jiao Q, Chen H, Biswal BB, Lu G, Liu Y (2011a) Resting-state brain organization revealed by functional covariance networks. *PLoS One* 6:e28817
- Zhang X, Tokoglu F, Negishi M, Arora J, Winstanley S, Spencer DD, Constable RT (2011b) Social network theory applied to resting-state fMRI connectivity data in the identification of epilepsy networks with iterative feature selection. *J Neurosci Methods* 199: 129–139
- Zuo XN, Kelly C, Adelstein JS, Klein DF, Castellanos FX, Milham MP (2010) Reliable intrinsic connectivity networks: test-retest evaluation using ICA and dual regression approach. *Neuroimage* 49: 2163–2177

Simultaneous EEG-fMRI in Epilepsy

R. Wiest, E. Abela, and C. Rummel

Contents

| | | |
|-----|--|-----|
| 1 | Introduction..... | 159 |
| 2 | Data Acquisition and Analysis..... | 160 |
| 2.1 | The Technology..... | 161 |
| 2.2 | Patient Safety | 161 |
| 2.3 | Technical Equipment..... | 161 |
| 2.4 | Artifacts on EEG Data | 161 |
| 2.5 | Artifacts on fMRI Data | 162 |
| 2.6 | Recording Procedure..... | 163 |
| 2.7 | Modeling the Hemodynamic Response | 163 |
| 2.8 | Spike-Based Evaluation | 164 |
| 2.9 | ICA-Based Evaluation | 164 |
| 3 | Clinical Applications..... | 165 |
| 3.1 | Simultaneous EEG-fMRI in Idiopathic Generalized Epilepsy Syndromes..... | 165 |
| 3.2 | Simultaneous EEG-fMRI in the Presurgical Workup of Pharmacoresistant Focal Epilepsies..... | 169 |
| 4 | Future Directions | 173 |
| | Conclusions..... | 173 |
| | References..... | 173 |

Abstract

Simultaneous recordings of electroencephalogram (EEG) and functional magnetic resonance imaging (fMRI) signals are technically demanding, but offer a unique view onto the spatiotemporal dynamics of large-scale epilepsy-related networks. In this chapter, we present a detailed methodological overview of simultaneous EEG-fMRI, and provide examples of two clinical applications: (i) identification of syndrome-specific functional correlates in idiopathic generalized epilepsies (IGE) and (ii) localization of potentially epileptogenic tissue in patients with pharmacoresistant focal epilepsy syndromes. Studies using EEG-fMRI have shown that there are bilateral areas of deactivation during generalized spike-wave discharges (GSW) in IGE within the thalamus, precuneus, anterior cingulate cortex and inferior parietal cortex. These results underscore the importance of thalamo-cortical interactions in GSW generation, as well as the role of the so-called default mode network in sustaining attention and consciousness. In focal epilepsies, EEG-fMRI provides complementary information during the presurgical work-up of refractory epilepsy, especially in patients with multifocal or non-lesional epilepsies. Overall, simultaneous EEG-fMRI has become an invaluable tool to elucidate the neurophysiology of human epilepsy, and shows promise as a clinical tool for specialized epilepsy centers.

R. Wiest, MD (✉) • C. Rummel, PhD
Support Center for Advanced Neuroimaging (SCAN),
Institute for Diagnostic and Interventional Neuroradiology,
University Hospital Bern, Freiburgstrasse 4,
3010 Bern, Switzerland
e-mail: roland.wiest@insel.ch

E. Abela, MD
Support Center for Advanced Neuroimaging (SCAN),
Institute for Diagnostic and Interventional Neuroradiology,
University Hospital Bern, Freiburgstrasse 4,
3010 Bern, Switzerland

Department of Neurology, University Hospital Bern,
Bern, Switzerland

1 Introduction

The combined, simultaneous acquisition of electroencephalography and functional magnetic resonance imaging (simultaneous EEG-fMRI) bridges the gap between neurophysiology and neuroradiology. It extends the application of clinical fMRI from externally driven task-related protocols to a neurophysiologically driven prediction of hemodynamic responses. This advanced imaging technique arose during the mid-1990s driven by one of the most common and difficult problems in clinical neurology: to localize the source(s)

of epileptic activity in the human brain (Ives et al. 1993; Warach et al. 1996; Seeck et al. 1998; Goldman et al. 2000; Archer et al. 2003b; Laufs 2012). The research agenda has been motivated by the need to combine complementary strengths of both techniques, i.e., the high temporal resolution of EEG and the high spatial resolution of blood-oxygen level-dependent (BOLD) fMRI, and has done important steps forward in mitigating its mutual weaknesses, e.g., the various EEG artifacts induced by the scanner environment or the analytical difficulties that arise due to the often idiosyncratic hemodynamic responses associated with epileptiform activity. Since its inception, over 200 papers have been published on simultaneous EEG-fMRI in adult and pediatric epilepsy patients,¹ and the technique continues to expand into research areas as diverse as motor imagery (Formaggio et al. 2010), cognitive effort (Esposito et al. 2009), reward processing (Plichta et al. 2013), and brain oscillations in wakefulness (Goldman et al. 2002; Jann et al. 2009; Mayhew et al. 2013) and sleep (Picchioni et al. 2011; Caporaso et al. 2012). It has also spurred a number of methodological developments that aim at integrating multimodal data using advanced signal processing methods (Moosmann et al. 2008; Vulliemoz et al. 2009; Caballero-Gaudes et al. 2013) or generative dynamical models of brain function (Daunizeau et al. 2010, 2012), and it is hoped that these efforts might lead to insights from which cognitive neuroimaging and neuroscience in general could benefit substantially (Debener et al. 2006). This research has also helped to develop our current understanding of epilepsy as a network disorder, where specific cortical and subcortical networks constitute fundamental elements that contribute to the generation and spread of focal onset seizures throughout the human brain. These networks are represented either by structural modifications or by functional characteristics of electric activity in the human cortex (Spencer 2002; Blumenfeld et al. 2004; Wiest et al. 2013).

Simultaneous EEG-fMRI thus has its straightforward impact in clinical epileptology, where it serves as an additional diagnostic tool during the presurgical workup of patients considered for epilepsy surgery, and remains under intensive practical and theoretical development (Rosenkranz and Lemieux 2010). The clinical importance of this technique arises from the fact that epilepsy is one of the most common neurological conditions worldwide, with a prevalence of 0.5–1 % of the global population (~35–70 million patients) and an incidence around 50 cases per 100,000/year (Sander 2003). Somatic and psychiatric comorbidity are high and lead to an increased risk of premature death (Gaitatzis et al. 2004, 2012). Indeed, evidence from community-based studies indicates that overall mortality in epilepsy cohorts is two to three times higher than in the general popu-

lation and is directly related to seizures in young patients with suboptimal pharmacological control (Gaitatzis and Sander 2004; Hitiris et al. 2007) but also to preventable causes such as drowning (Bell et al. 2008) or suicide (Pompili et al. 2006). There is evidence from a randomized controlled trial that early surgery for patients with mesial TLE is superior to medical therapy (Wiebe et al. 2001; Engel et al. 2012). For extratemporal epilepsy data on long-term outcomes after surgery are less consistent, reporting seizure-free rates ranging from 27 to 46 % (Tellez-Zenteno et al. 2005).

Theoretical concepts used in clinical practice and research divide the epileptic brain into different zones: the seizure onset zone, the epileptogenic lesion, the epileptogenic zone, the symptomatogenic zone, and the irritative zone (Rosenow and Luders 2001; Luders et al. 2006). The seizure onset zone is the area of the cortex where seizures begin. The epileptogenic lesion is the cortical region of the brain that, when stimulated, produces spontaneous seizures or auras, whereas the epileptogenic zone is defined as the area of cortex that is indispensable for the generation of epileptic seizures. The symptomatogenic zone refers to the region of cortex that produces the initial ictal symptoms or signs. The irritative zone is defined as the area of cortical tissue that generates interictal epileptiform discharges. The irritative zone has thus a functional definition and can be depicted by IEDs in EEG. It thus opens the basis for investigation of simultaneous hemodynamic response of IEDs that approximately resemble the epileptogenic zone. In patients with cortical dysplasia, widely distributed spike-related BOLD responses were associated with widespread seizure onset zones and less favorable outcome (Thornton et al. 2011). For surgical evaluation, EEG-fMRI has demonstrated its potential to improve localization of the irritative zone in complex cases, especially in patients with an unclear focus on EEG (Zijlmans et al. 2007), and EEG-fMRI correlation patterns are spatially accurate at the level of anatomical brain regions, reflecting an underlying network of IEDs (van Houdt et al. 2013).

In this chapter we aim to provide the reader with a brief methodological overview on clinical EEG-fMRI, including typical findings in focal and generalized epilepsies with a special focus on presurgical applications.

2 Data Acquisition and Analysis

When speaking about simultaneous EEG-fMRI recordings, two types of EEG have to be distinguished: scalp EEG and intracranial EEG (iEEG). Using implanted electrodes issues of patient safety are much higher for iEEG-fMRI. Despite this, first reports have been published recently for 1.5 T main magnetic field strength (Vulliemoz et al. 2011; Carmichael et al. 2012). In our review we concentrate on scalp EEG-fMRI. Good reviews on simultaneous EEG-fMRI including

¹Number determined with a PubMed search using “EEG-fMRI OR EEG/fMRI AND epilepsy” from 01.01.1993 to 29.09.2013.

technical issues are given in Lemieux et al. (1997, 1999), Nunez and Silberstein (2000), Gotman et al. (2006), Ritter and Villringer (2006), and Cunningham et al. (2008).

2.1 The Technology

In MR scanners three types of magnetic fields are present:

1. The static and homogeneous magnetic field B_0 aligns the proton spins.
2. The gradient fields G_x , G_y , and G_z are used to fulfill the resonance condition in one voxel at a time and vary their orientation in space with frequencies in the kHz range.
3. The head coil produces the radio-frequency electromagnetic B_1 field (MHz range) necessary for spin rotation (e.g., 90° pulses, 180° pulses).

Due to the structure of the Maxwell equations, dynamically changing magnetic (MRI) and electric fields (EEG) are inseparably interconnected. This fact makes simultaneous EEG-fMRI acquisition more ambitious and cumbersome than fMRI alone. If conductors as, e.g., the EEG electrodes and wires are introduced into MR scanners, the changing magnetic fields may induce currents by three different mechanisms (Lemieux et al. 1997):

1. Wire loops may change the loop area perpendicular to the B_0 field by deformation or change of orientation.
2. The gradient fields G_x , G_y , and G_z constantly change their spatial orientation relative to wire loops.
3. The radio-frequency B_1 field may induce currents in extended wires (electric field component) and loops (magnetic field component).

When strong enough, induced currents may endanger patients by causing burns due to focal heating of EEG electrodes and wires. Also important, the interaction between currents and the magnetic fields may induce artifacts both on the EEG recordings and on functional and structural MR images. To guarantee patient safety and minimize all kinds of artifacts, special equipment and special data-processing algorithms are required. In the following we review the needed instrumentation and the different types of artifacts on EEG and fMRI data. For the latter, each subsection is divided into technical attempts to minimize artifact appearance and data-processing algorithms to eliminate residual influences.

2.2 Patient Safety

In an early publication by Lemieux et al. (1997), the important issue of patient safety during simultaneous EEG-fMRI measurements was addressed. The authors identified the interaction between the radio-frequency electromagnetic fields produced in the head coil and EEG wire loops as the primary safety hazard and concluded that “the recording of

EEG signals during the acquisition of functional and anatomical images can be performed safely if necessary precautions are taken.” It was recommended to avoid loops and crossing wires. In addition serial resistors should be positioned in close proximity to the EEG electrodes in order to limit the currents. The resistor values depend on the instrumentation and must be large enough to limit heating and thus avoid localized burns. Optimal resistor values represent a trade-off between minimization of induced currents and maximization of the EEG signal-to-noise ratio.

2.3 Technical Equipment

The first simultaneous scalp EEG-fMRI recordings have been performed on 1.5 T scanners. Today the use of 3 T scanners is standard. Patient safety issues and most artifacts on EEG and MRI data increase with increasing field strength. This seems to pose a limitation on going to higher and higher field strengths in future developments. While besides the field strength and the ability to acquire high-resolution structural MRI data and BOLD sequences, no special requirements are necessary for the MR scanner; this is different for the EEG equipment. Specialized EEG caps, amplifiers, and transmission wires are required.

Today different MR-compatible EEG caps are commercially available that were optimized to reduce the amount of metal used in the contacts. The rationale behind these developments was to minimize the danger of focal heating at the contact points of stray electrodes and reduce scanner artifacts on the EEG traces due to induction. In addition artifacts on MR images due to local field inhomogeneities are minimized. MR-compatible EEG caps avoid wire loops and bundle wires tightly together in straight lines. The montage time may vary considerably between different types of EEG caps.

Normal EEG amplifiers may contain larger metal parts, which prevent usage in the high magnetic field inside the scanner room. More importantly, to warrant patient safety even during potential device failure, specialized battery-supplied preamplifiers with galvanic separation from the power line have to be used. Metal transmission wires for EEG signals are kept short as they would inductively pick up artifacts from the magnetic fields. To minimize this effect EEG data is transmitted optically to the recording device stationed outside the scanner room via glass fibers.

2.4 Artifacts on EEG Data

EEG recorded inside MR scanners may contain two gross types of artifacts, the gradient artifacts and movement artifacts including the ballistocardiogram as a special case. Gradient artifacts are caused by the rapidly switching gradient fields

G_x , G_y , and G_z and may be 50 times larger in amplitude during scanning than the background EEG (Gotman et al. 2006). They can be avoided in large parts of the recording, if MR images are scanned only in response to visually or computationally identified EEG events (“spike-triggered” or “IED-triggered” EEG-fMRI). When scanning MRI continuously, one can take advantage of the facts that the timing of the gradient artifacts is precisely known (during acquisition of the BOLD volumes) and that they are very stereotypical in shape. This enables a template removal strategy by artifact averaging and subtraction (Allen et al. 1998, 2000). To do so and to avoid aliasing problems (given the high-frequency components of the scanner artifacts), the EEG data has to be sampled with very high frequency for this purpose (i.e., several kHz in contrast to frequencies of a few hundred Hz, which is fully sufficient for ordinary scalp EEG). Very recently, FACET, a flexible Matlab toolbox allowing the combination of different artefact removal algorithms has been made publicly available (Glaser 2013).

Movement artifacts on EEG signals are caused by electrode, wire, and patient motion inside the strong magnetic field. To avoid these it is attempted to stabilize the head and improve patient comfort – especially for long-lasting EEG-fMRI recordings. Foam paddings and vacuum cushions are used to fixate the head; EEG caps should be elastic, and contacts in occipital regions should be stuffed with cushions to avoid pressure marks. As certain movement artifacts (e.g., swallowing, talking, and yawning) may mimic epileptiform EEG activity, it is advisable to use a movement detector in coincidence to veto analysis of movement-associated events. However, for these devices similar precautions apply as for the EEG equipment itself. A general advice is to immobilize EEG wires by bundling them closely together (done in most commercially available EEG caps) and fixing the leads to the scanner in straight lines (e.g., by using suitable sand bags).

A special case of movement artifacts is the ballistocardiogram (BCG, sometimes also called cardioballistogram or pulse artifact). The cardiac cycle induces periodic small-amplitude displacements of head and EEG electrodes due to the pulsation of scalp arteries inside the high magnetic field and thus may induce electric currents. As these displacements are time-locked to the heart rate, simultaneous measurement of high-quality electrocardiogram (ECG) or pulse oximetry enables removal of the BCG by averaging and subtraction techniques similar to the gradient artifacts (Allen et al. 1998). In addition, techniques based on principal (PCA) and independent component analysis (ICA) are available (Srivastava et al. 2005). PCA and ICA assume that the BCG is uncorrelated or statistically independent from brain activation, respectively, and thus corresponding components can be eliminated and cleaned EEG signals can be reconstructed.

Another artifact on the EEG signals is caused by the helium pump used for cooling of the superconducting coils

that generate the static B_0 field. As for gradient artifacts and BCG, the timing (and to lesser amount also the shape) of the artifact is known and could in principle be exploited for artifact reduction. However, a much simpler solution is to switch off the helium pump during short-term EEG-fMRI acquisition. It cannot be stressed strongly enough that a neglect to switch the pump on again after a short period of time might cause serious damage to the MRI scanner. Therefore great care is indispensable when choosing this option.

To remove any residual high-frequency artifacts on the EEG signals that are either due to imperfect artifact removal or electromyogram (EMG) rather than neuronal activity, like any scalp EEG, the EEG recorded inside MR scanners should be passed through a low-pass filter with cut-off frequency at 25 or 30 Hz and can finally be downsampled to a sampling rate of a few hundred Hz before further analysis.

2.5 Artifacts on fMRI Data

In general, EEG artifacts in structural and functional MR images are less an issue in simultaneous EEG-fMRI acquisition than imaging artifacts in EEG. Nevertheless, although minimized in size, current MR-compatible EEG equipment contains metal parts (electrodes and wires). These may distort MR images by two effects. First, conducting material may alter the magnetic field locally due to “susceptibility artifacts” and the possibility of eddy current induction. In the worst case these artifacts can have an electrode centered radius of 7.5 mm and thus can extend into the cortex (Lemieux et al. 1999). As counter measurements special materials with less magnetic susceptibility can be used (Allen et al. 2000).

Second, high-frequency currents in the EEG leads and electromagnetic radiation emitted from the electronics of the EEG preamplifier may reduce the signal-to-noise level of MR images. Proper magnetic shielding of the amplifier largely reduces this effect.

As for the EEG signals, patient movement deteriorates MR image quality. As discussed already above, it can effectively be minimized by improvement of patient comfort. In the preprocessing of fMRI data, the volumes are realigned according to the six estimated rigid-body movement parameters (three translations, three rotations). Despite realignment, the associated parameters (and occasionally also temporal derivatives or time-shifted copies) should be used as nuisance parameters in the data post-processing. When head movement becomes too large (e.g., larger than 1 mm translational displacement or 1° rotational displacement), realignment is no longer reliable, and discarding affected volumes or the whole data set must be considered. After movement correction spatial smoothing using a Gaussian kernel with 6–8 mm Full-width at half maximum (FWHM) is applied to reduce noise.

2.6 Recording Procedure

At our institution we currently use the following instrumentation and setup for simultaneous EEG-fMRI acquisition (Jann et al. 2008). Ninety-two EEG electrodes are placed on the positions of the international 10–10 system on the patients' scalp using the EasyCap (EasyCap GmbH, Inning am Ammersee, Germany). If necessary, electrode cables are fixed to the cap by bandaging material, and routinely sand bags are used to fixate the wires in the scanner and avoid wire movement during the recording. Two additional electrodes are placed below the eyes to record eye movements, and two more electrodes are placed below the left and right clavicles to record the ECG. Electrode impedances are kept below 20 kΩ using electrolyte gel, and the sampling frequency is 5 kHz.

The electrode recording from position Fz is used as recording reference. Electrodes are connected to three MR-compatible amplifiers (BrainAmp; Brain Products, Gilching, Germany), which are battery powered and connected through optical wires to the data acquisition PC. The EEG is amplified, band-pass filtered (0.1–250 Hz), and digitally stored for offline analysis. After offline visual inspection of the measured EEG, channels with increased impedance and corrupt signal are discarded from further analysis.

For the MRI data acquisition, we use a 3 T Siemens Magnetom Trio TIM MR Scanner (Erlangen, Germany) equipped with a standard radio-frequency head coil. During the scans, patients are positioned in the head coil with standard manufacturer-supplied cushions and ear plugs and are asked to stay awake and keep their eyes closed. Functional data is acquired using a multi-slice single-shot T2*-weighted echo planar imaging (EPI) sequence with 35 slices. A total of 460 functional volumes are measured for each patient (duration 16 min). During these functional recordings, the helium pump of the scanner is switched off to reduce artifacts in the EEG.

After acquisition of simultaneous EEG-fMRI recordings, the EEG cap is taken off and structural images are acquired. High-resolution 3-D T1-weighted imaging protocols are used like the magnetization-prepared rapid-acquisition gradient echo sequence (MP-RAGE) or the modified driven equilibrium Fourier transformation sequence (MDEFT).

2.7 Modeling the Hemodynamic Response

The blood oxygen level-dependent (BOLD) signal represents an indirect measurement of neuronal activity. Although its underlying mechanisms are still not fully understood, it is clear that changes of the BOLD signal represent a mixture of the effect of cerebral blood flow (CBV) and the concentration of deoxygenated hemoglobin; see, e.g., Kim et al. (2012) for review. The “balloon model” by Buxton et al. (1998) and its variants give a qualitative explanation of the BOLD changes in

response to neuronal activation (Buxton et al. 1998). In magnetic fields oxygenated hemoglobin (HbO) and deoxygenated hemoglobin (“reduced” hemoglobin, HbR) behave differently. HbO molecules do not have unpaired electrons and therefore are diamagnetic. In contrast, HbR has four unpaired electrons and thus is paramagnetic. In magnetic fields the strong associated dipole moment induces local field inhomogeneities. Locally, this causes faster dephasing of proton spin precession and smaller transversal relaxation time T2. In T2- and T2*-weighted MR images, therefore the state of hemoglobin oxygenation acts as a body's own contrast agent: Immediately after initiation of neuronal activation, the oxygen metabolism and thus the HbR concentration increase locally (“initial dip” for $t < 2$ s). After a short period, the arterioles react and the oxygen demand is overcompensated by increased delivery of oxygenated blood. The concentration of HbR decreases, resulting in locally larger T2 and thus larger signal intensities. A positive peak of +2 to +3 % signal intensity is reached around 6 s after the stimulus. Approximately 10 s after termination of neuronal activation, the signal intensities slightly undershoot due to slower recovery of the cerebral blood volume (CBV) than cerebral blood flow (CBF) and return to baseline with a time scale on the order of 15–20 s. The progression of initial dip, signal peak, undershoot, and return to baseline is called the hemodynamic response function (HRF).

In the neocortex, the BOLD signal reflects peri-synaptic activity in the form of the local field potential rather than the spiking rate of individual neurons, but dissociations between BOLD, spiking, and local field potential may occur under pathological conditions (Logothetis et al. 2001; Logothetis and Wandell 2004; Ekstrom 2010). For example, in epilepsy, a linear relationship between epileptic discharges and hemodynamic responses has been observed, while others obtained contradictory results (Bagshaw et al. 2005; Mirsattari et al. 2006). As in many fMRI studies also in simultaneous EEG-fMRI, the hemodynamic response of the BOLD signal to neuronal activation is modeled by the canonical HRF (Friston et al. 1998) in the whole brain, and linear correlations between a HRF-convolved predictor and each voxel time series are computed within the framework of the general linear model (GLM) (Glover 1999).

Although this procedure is simple and straightforward, it has serious limitations. First, inter- and intraindividual HRF variability is high (Aguirre et al. 1998; Buckner 1998) and derives from multiple sources as, e.g., non-neural (vascular, breathing) signals, idiosyncratic responses of different brain areas to external stimuli, effects of experimental session, task demands, and cognitive set, but also influence of medications acting on the CNS and aging (Kannurpatti et al. 2010, 2011). Second, the assumption of linearity, although a useful approximation, does not hold in all situations (Birn et al. 2001; Birn and Bandettini 2005; Wan et al. 2006). It may be violated when several stimuli occur within less than

a few seconds separation as may be the case in epileptogenic tissue and IEDs. This may require additional analysis to explore the link between IEDs and BOLD signals.

Modifying the HRF it has been shown in epilepsy patients that the BOLD “response” may occur already prior to the spike in scalp EEG (Bagshaw et al. 2004). Similar observations have been made in animal studies. Using simultaneous electrocorticogram (ECoG) and near-infrared spectroscopy (NIRS)² during drug-induced spiking in adult rats, it was observed that hemodynamic changes may precede the electrophysiological changes even when measured with implanted electrodes (Osharina et al. 2010). A possible explanation is that increased neural activity may be present in non-synchronized way already before it becomes observable in ECoG via the synchronized spike, which may terminate the epileptic discharge, rather than being the main signature itself.

Beyond model-based assumptions, exploratory data-driven techniques of fMRI analysis, such as independent component analysis (ICA) or temporal clustering analysis (TCA), have shown their ability to capture BOLD signal changes without imposing constraints on the HRF shape (McKeown et al. 1998; Eichele et al. 2009; Calhoun and Adali 2012). For further methodological and physiological details, see chapter “[Revealing brain activity and white matter structure using functional and diffusion-weighted magnetic resonance imaging](#)”.

2.8 Spike-Based Evaluation

The first simultaneous EEG-fMRI recordings in epilepsy patients have been made by acquisition of manually triggered single BOLD volumes 3 or 4 s after visual recognition of epileptic EEG spikes recorded in the static magnetic B0 field (Warach et al. 1996; Seeck et al. 1998; Krakow et al. 1999). At this delay the hemodynamic response is assumed to be maximal. A direct comparison with non-spike reference BOLD volumes allowed spike localization without the need for removal of gradient artifacts from the raw EEG. A disadvantage of this approach is that it requires continuous EEG reading or automated spike detection and is very inefficient when patients have only a few spikes.

In general, the measurability of synchronized neuronal activity by an EEG electrode at a certain distance depends on the orientation of the cortical source dipole to the electrode

surface. Only the perpendicular part of the dipole contributes to the EEG signal, implying that EEG is (partially) blind to large parts of the folded cortex. In addition, due to the low conductance of the skull, in scalp EEG sources are smeared out tangentially, and high-frequency signals as well as spikes can be attenuated by a factor larger than 50 with respect to direct measurement on the dura (Nunez and Silberstein 2000). This implies that spikes can easily remain undetected in background EEG, especially after application of all the (still imperfect) artifact removal techniques outlined above. As a result, statistics of spike-triggered approaches is overly conservative for two reasons. First, spikes detected on scalp EEG may represent only a fraction of the true epileptic activity. Second, the alleged “spike-free” reference epochs may indeed contain epileptic activity, which only remains unrecognized.

A more modern approach to spike-based evaluation of EEG-fMRI has been developed by the Geneva-London cooperation (Grouiller et al. 2011). In short, their procedure is as follows. Using the same EEG for long-term scalp monitoring of epilepsy patients during presurgical evaluation as for EEG-fMRI, average spike voltage maps can be generated with very good statistics. After preprocessing similar to the procedures outlined above, the correlation coefficient between voltage maps of EEG recorded inside the MR scanner and the average spike voltage map is calculated in a moving window approach. The time course of this correlation coefficient is then used as a predictor for the BOLD responses in a GLM. Grouiller et al. have shown that this approach significantly increases the yield of simultaneous EEG-fMRI in a group of patients with previously inconclusive results, even when interictal spikes were absent on the in-scanner EEG (Grouiller et al. 2011).

2.9 ICA-Based Evaluation

A different approach to analysis of simultaneous EEG-fMRI data has been developed in our institution (Jann et al. 2008; Hauf et al. 2012). After EEG preprocessing as outlined above, an independent component analysis is run on the channels free of permanent artifacts (extended infomax algorithm, Delorme and Makeig 2004). The prime justification for application of ICA (or PCA)-based techniques for EEG decomposition holds for artifact removal (see above), which can indeed be regarded statistically independent from neuronal activity. In practice it has turned out that this technique can also be applied to isolate a single or a small number of components (“factors”) that contain epileptiform activity that coincides with IEDs, while the remainder does not. ICA separation on EEG recorded during MR scanning turned out insufficient but could be improved considerably after inclusion of EEG recorded outside the scanner (Jann et al. 2008).

The ICA based on these two datasets produces a small set of ICA components having only small spectral amplitude

²Like BOLD fMRI also NIRS is sensitive to hemoglobin oxygenation. However, the mechanism is a different one. NIRS exploits different absorption characteristics of oxygenated and deoxygenated hemoglobin. Measuring absorbances at least two wavelengths in $650 \text{ nm} < \lambda < 1,000 \text{ nm}$, separate quantification of the concentration of both chromophores becomes possible. Advantages of NIRS are its comparably small sensitivity to head movements and fast sampling. A major disadvantage is the insensitivity to deeper brain structures.

outside the scanner and markedly increased inside the scanner. This is the expected behavior for factors representing scanner-related and BCG artifacts; see above. The IED-related ICA factors are currently inspected and selected visually, although developments to automatize the factor selection are underway (Rummel et al. 2013). Among all factors those showing signatures of epileptiform activity in coincidence with IEDs are selected. Additionally the load of these factors onto the individual electrodes (e.g., scalp distribution) is considered and compared with the topographic voltage map during IEDs (Hesse and James 2005). In cases where more than one ICA factors represent epileptiform activity, only the one most accurately mirroring the IED observed in the EEG is considered for further analysis, rectified, convolved with a double gamma hemodynamic response function (Glover 1999), and used as predictor for the BOLD signal of the fMRI. Voxelwise correlations between the BOLD signal and the ICA-based predictor are computed using a GLM. The six motion parameters derived from the fMRI preprocessing are used as nuisance parameters in the GLM.

In Hauf et al. (2012) the influence of different thresholding procedures for voxel activation was investigated: peak activation (i.e., the cluster with the maximum correlation), family-wise error correction of the activations for multiple comparisons, and selection of a fixed number of activated voxels (total volume of activated BOLD clusters of $4,000 \pm 200 \text{ mm}^3$). It was found that the effectiveness of simultaneous EEG-fMRI in delineating the seizure onset zone may be best when using a fixed number of activated voxels.

3 Clinical Applications

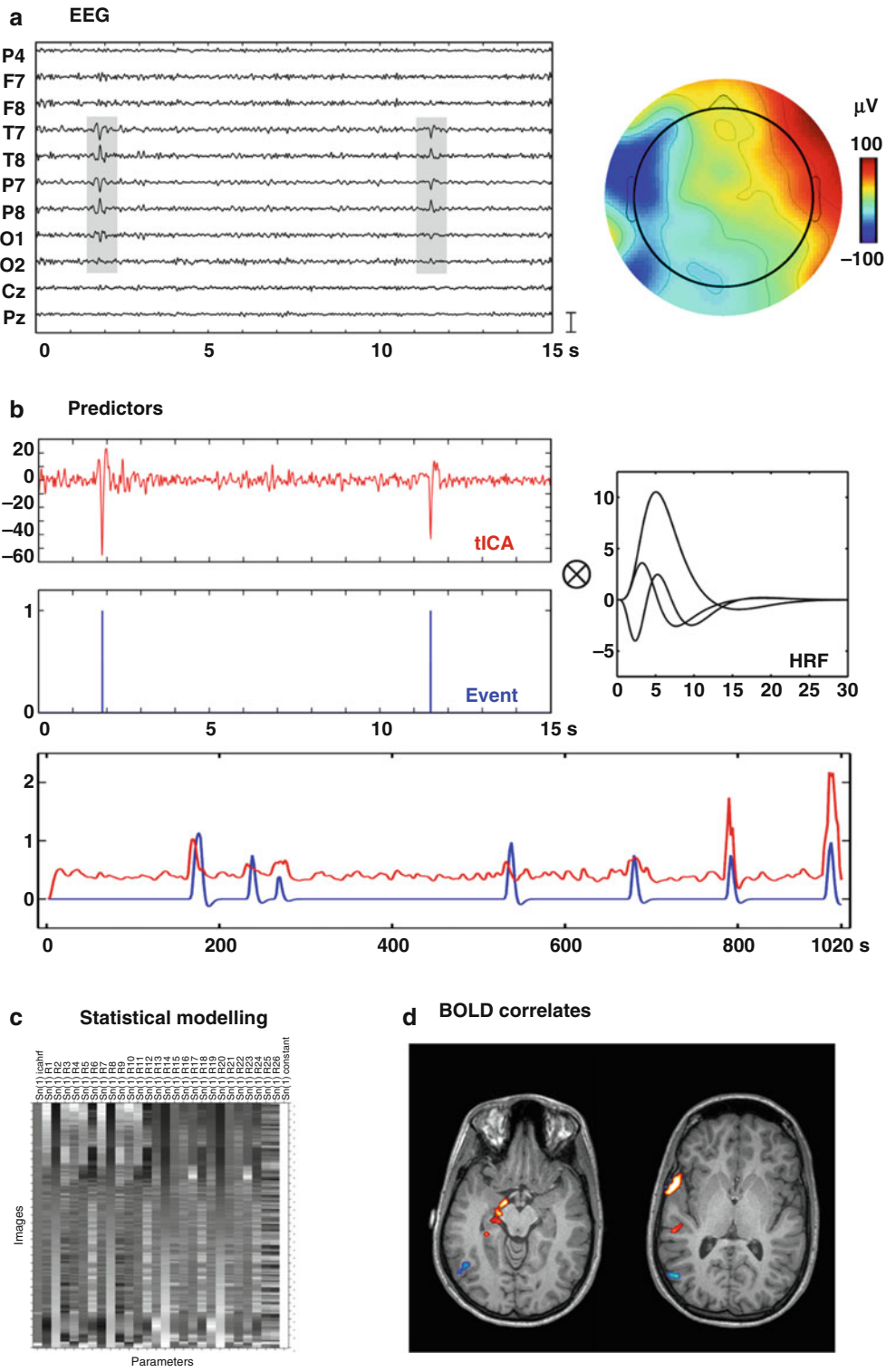
Clinical applications of simultaneous EEG-fMRI in human epilepsy can be broadly summarized in two categories. One concerns the investigation of BOLD correlates of epileptiform EEG signals in clinically well-defined epilepsy syndromes such as absence epilepsy or mesial temporal lobe epilepsy with hippocampal sclerosis. The aim of this line of investigation is not only to achieve a more complete syndromic description but to unravel pathophysiological mechanisms that could lead to a deeper understanding of epileptogenesis and perhaps even to a more refined, evidence-based classification of the epilepsies (Berg et al. 2010). The second application is the localization of epileptogenic foci during the presurgical workup of pediatric and adult patients that suffer from pharmacoresistant epilepsies (Salek-Haddadi et al. 2006; De Tiege et al. 2007). Here, the focus is on localization of the seizure-onset zone, and simultaneous EEG-fMRI has proven especially valuable when no epileptogenic lesion can be detected by conventional MRI protocols (Moeller et al. 2009) or when multifocal seizures are suspected (Zijlmans et al. 2007). In what follows, we review both types of studies.

3.1 Simultaneous EEG-fMRI in Idiopathic Generalized Epilepsy Syndromes

Idiopathic generalized epilepsies (IGE) comprise a group of heterogeneous syndromes in which a strong genetic component is suspected or already identified. These syndromes have been recently reclassified as “genetic epilepsies,” to avoid the ambiguous term “idiopathic” (Berg et al. 2010). We use the denomination IGE for consistency with the current EEG-fMRI literature to date, as mostly use the older terminology. IGE are common and account for ~40 % of epilepsy diagnoses. Their hallmark is generalized spike-wave (GSW) discharges in the EEG, i.e., synchronous, mostly symmetric, bilateral paroxysmal, short (<200 ms) high-amplitude potentials followed by a slow wave. They can occur in isolation but classically appear in short runs with frequencies around 3–4 Hz (Weir 1965). Longer series of GSW discharges impair consciousness for brief periods of time, leading to the clinical picture of absence seizures. The latter are further characterized by sudden behavioral arrest, unresponsiveness, staring, and sometimes mild oral automatisms and/or bilateral eye blinks (Holmes et al. 1987; Panayiotopoulos et al. 1992). The co-occurrence of GSW on EEG and absence seizures define childhood (4–8 years) and juvenile (9–13 years) absence epilepsy (AE). Both syndromes represent ~10 % of all epilepsies in each age group, are readily amenable to pharmacological treatment, and have in general a good prognosis. Other syndromes studied include juvenile myoclonic epilepsy (JME) and benign epilepsy with centrotemporal spikes (BECTS, or “Rolando epilepsy”).

IGE patients have been used in experimental EEG-fMRI studies with three aims: (1) to identify the (syndrome-specific) networks associated with GSW discharges, (2) to map the neural correlates of attention and vigilance (as surrogates for consciousness), and, more recently, to (3) validate complex biophysical models of brain connectivity using fMRI. The first goal has been studied more extensively than the other two and was motivated by the fact that although GSW and absence seizures have been known for long time, their pathophysiological and neuroanatomical basis remains poorly understood, leading to a multiplicity of theories that vary greatly in their interpretation of experimental data (Meeren et al. 2005). However, a consensus has emerged that puts pathological (possibly cyclic) activity within thalamocortical networks at the center of the GSW pathogenesis, with some researchers arguing in favor of a thalamic pacemaker (Buzsaki 1991), others for a cortical generator (Meeren et al. 2005) and yet others for a more integrative view that emphasizes spatially extended interactions between cortex, thalamus, and reticular ascending system as the driving force behind GSW, rather than a single focus (Gloor 1968; Avoli and Gloor 1982; Blumenfeld and McCormick 2000). In general, simultaneous EEG-fMRI studies provide evidence for the latter view, with some recent

Fig. 1 EEG-fMRI analysis stream in epilepsy. Panel (a) shows on the left side the artifact-corrected in-scanner EEG of a 19-year old patient with suspected left mesial temporal lobe epilepsy (MTLE). Shaded areas show occurrences of sharp waves. The right side shows the corresponding scalp topography with a peak negativity on the left fronto-temporal side. Panel (b) shows the construction of statistical predictors, either using temporal independent component analysis (tICA, red) or by generating manual events (blue) that indicate the time-point of sharp waves. After convolution with a hemodynamic response function (HRF), the expected brain responses can be modeled (blue and red traces running from 0 to 1020 seconds in this example). Panel (d) shows the design matrix of a general linear model built using either of the predictors from panel (c). The model also incorporates predictors from movement parameters and their derivatives, and noise signals from white matter and cerebrospinal fluid. Each column of the matrix represents one predictors, each row one time-point (i.e., BOLD image). Panel (e) shows the positive (hot colors) or negative (cool colors) BOLD-correlates of the tICA-predictor projected onto the patients anatomy. Strong signal increases are seen in the left hippocampus and temporal pole, concordant with the patients suspected MTLE

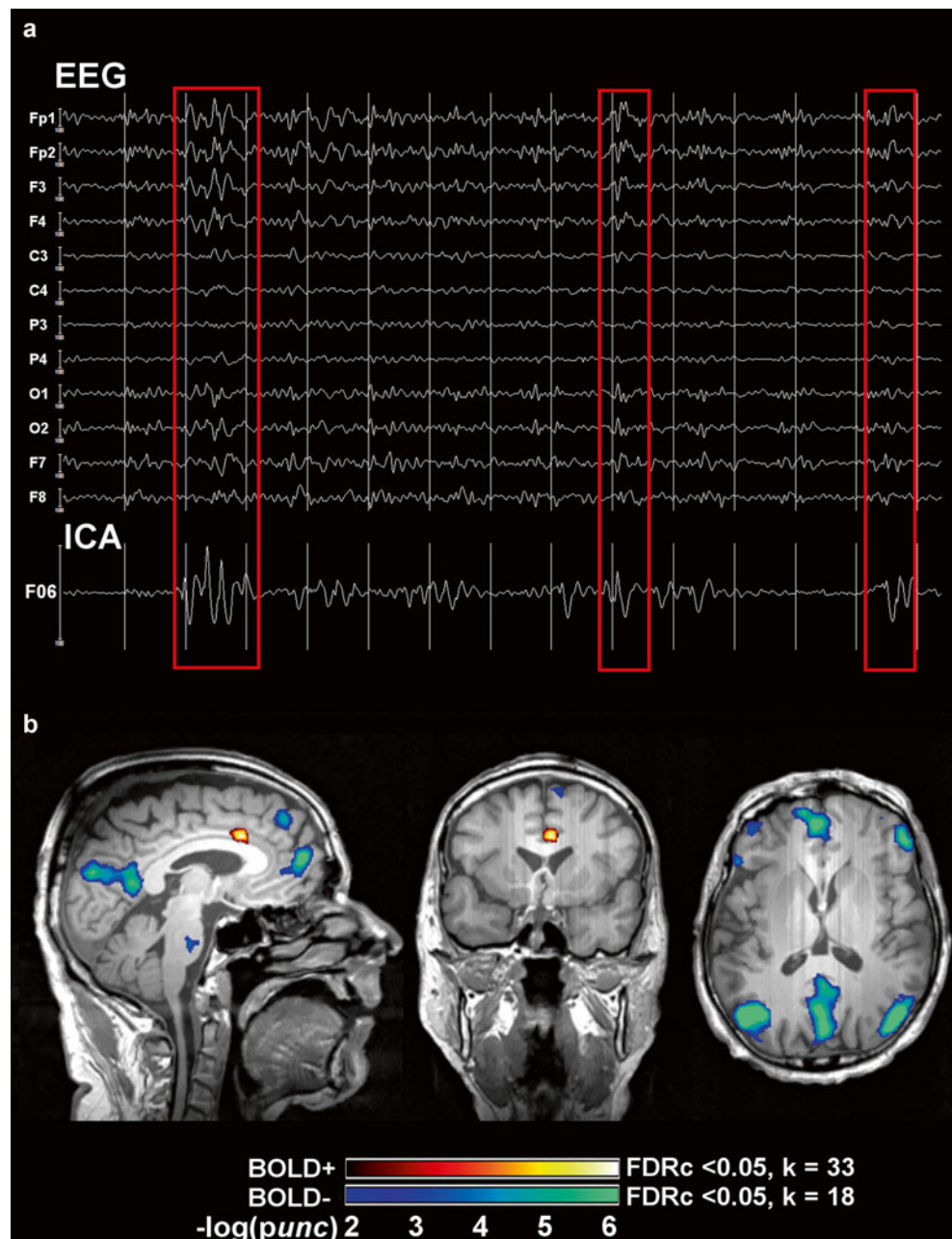


studies indicating that the (structural and functional) networks involved might be even more widespread than initially thought and that there is indeed a strong contribution from cortical areas (Masterton et al. 2013).

One of the earliest simultaneous EEG-fMRI studies by Archer et al. investigated cortical and subcortical patterns of BOLD-signal change at 1.5 T in five patients (four of them suffering from childhood AE) with frequent GSW discharges

during rest (Archer et al. 2003a). Their main finding was a large area of GSW-related BOLD deactivation in the posterior cingulate (retrosplenial cortex) that was highly consistent across patients, and more variable regions of BOLD activation in the angular gyrus and around the precentral sulcus bilaterally (Archer et al. 2003a). Thalamic BOLD activation was only seen in two of five patients. Subsequent studies in adults and children with IGE have reliably

Fig. 2 Example of EEG-fMRI analysis and BOLD correlates of spike-wave discharges in a patient with IGE. Panel (a) shows 14 s of artifact-corrected in-scanner electroencephalogram (EEG) and its associated independent component analysis (ICA) factor that codes for generalized spike wave (GSW) discharges (F06). Red squares mark three time points (seconds 3, 9, and 13) that contain frontally predominant (Fp1, Fp2) GSW discharges. Note the corresponding amplitude oscillations in F06. Panel (b) shows the statistical parametric maps (SPMs) of functional activations (BOLD+) and deactivations (BOLD-) linearly correlated to F06 (and therefore GSW), overlaid on an anatomical scan (neurological convention). Significant signal increases are seen in the anterior cingulate cortex (*hot colors*), and widespread decreases in the precuneus, medial prefrontal cortex, inferior parietal, and dorsolateral prefrontal cortices bilaterally (*cool colors*). SPMs have an uncorrected (*unc*) peak-level threshold at $p < 0.001$ ($= -\log(2)$) and a corrected false-discovery rate cluster-level (FDRc) threshold at $p < 0.05$ (k , critical cluster size)



identified thalamic BOLD signal increases and have also confirmed the high degree of interindividual variability in cortical and subcortical BOLD patterns (Aghakhani et al. 2004; Hamandi et al. 2006; Moeller et al. 2008b, 2010a).

Of note, the set of symmetrical regions that has been found to be commonly deactivated during GSW in IGE, i.e., precuneus, inferior parietal cortex, and ventral medial prefrontal cortex, are core nodes in the now widely known default-mode network (DMN), a network that is highly active and functionally strongly interconnected during conscious rest (Raichle et al. 2001; Greicius et al. 2003) and probably supports attentional and self-referential processes such as autobiographical memory or envisioning the future (Raichle and Snyder 2007; Buckner et al. 2008). Although the role of this GSW-related BOLD signal changes within

the DMN is still poorly understood (but see below for a possible role of the precuneus in GSW generation), it is notable that deviations of DMN activity are commonly seen in neurological disorders, e.g., Alzheimer's disease, multiple sclerosis, or traumatic brain injury (Buckner et al. 2008; Bonnelle et al. 2012; Rocca et al. 2012).

In Figures 1–3 typical examples of GSW-BOLD correlates from our patient database. Figure 1 shows data of a 44-year-old patient with an unclassified IGE since childhood and poor seizure control despite medication. Panel (a) summarizes the general analysis strategy at our lab (see above for details), where the in-scanner EEG is analyzed using a temporal ICA to derive a predictor of the BOLD response that encodes the continuously fluctuating epileptic activity (Jann et al. 2008). Panel (b) shows a typical pattern of BOLD signal change

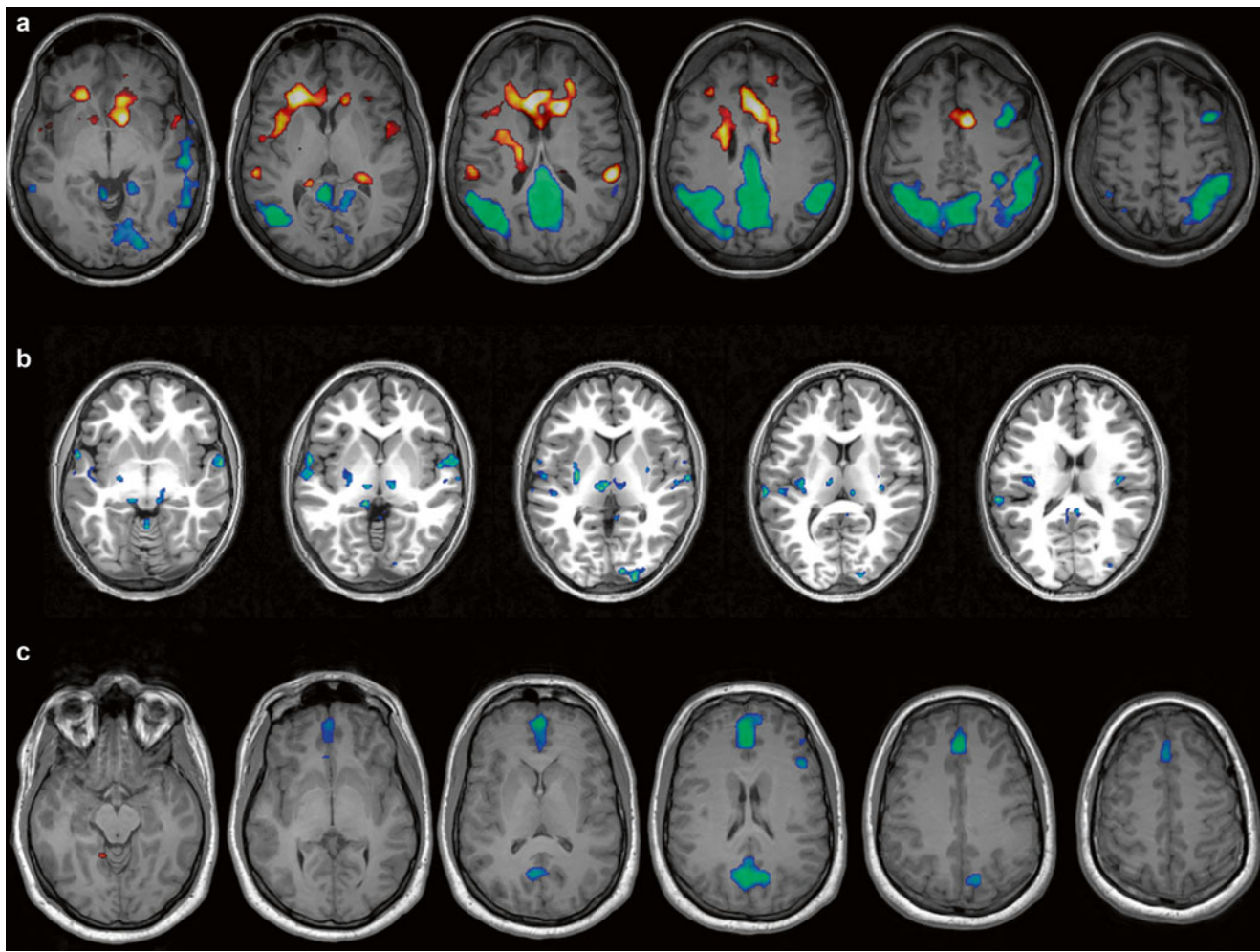


Fig. 3 Examples of the interindividual variability in BOLD correlates of generalized spike-wave discharges in patients with IGE. Hot colors indicate BOLD-signal increase cool colors BOLD-signal decrease. All images are in neurological convention (left hemisphere is on the left side of the image). Panel (a) 29-year old patient with generalized seizures. Strong signal increases are seen in the anterior cingulate cortex,

decreases in the precuneus and parietal lobes bilaterally. Panel (b) 15 year old patient with brief visual symptoms followed by generalized seizures. Bilateral BOLD-signal decreases are seen in the thalamus, and unilateral decrease in the right occipital pole. Panel (c) 23-year old patient with generalized seizures. BOLD-signal decreases localize onto the anterior cingulate cortex and precuneus bilaterally

linearly correlated with epileptic activity; widespread cortical deactivations corresponding to the DMN can be appreciated, as well as a very focal signal increase in the anterior cingulate cortex. As in the Archer et al., no thalamic activations are seen in this case. In Fig. 2 we compile a small case series to illustrate the large interindividual variability of GSW-related (de)activation patterns.

Besides these more observational case series, there have been only a few controlled experimental studies in patients with absence seizures (AS) simultaneously comparing GSW on EEG, fMRI, and behavioral changes. These studies aimed at the second goal mentioned above, i.e., correlating attentional states with GSW discharges and their metabolic correlates. Berman et al. investigated these changes in attention in a group of children suffering from AS using simultaneous EEG-fMRI and to types of tasks, a continuous performance task (CPT) that required sustained attention to deviant letter

stimuli, and a simple repetitive motor task (Berman et al. 2010). CPT performance dropped significantly more than performance on the motor task during AS (as recorded with the in-scanner EEG), and this behavioral impairment was associated with the core corticothalamic BOLD network found in the studies mentioned above and seen in our examples. This study was the first to establish a link between behavior and simultaneous EEG-fMRI, thus indicating that all areas visualized in observational studies with IGE patients (see above) are not a innocuous epiphomenon but might have important effects on cognitive functioning (although this must not always be the case, e.g., Moeller et al. (2010b)).

A concomitant study by the same group analyzed the temporal dynamics of the BOLD response to IGE by shifting the HRF from 16 s before to 24 s after the onset of AS in a large cohort ($n=88$) of AE patients (Bai et al. 2010). They found bilateral BOLD increases in medial and orbital frontal areas

as early as 14 s before AS onset, followed by a late increase in the thalamus (10 s after AS onset) that was paralleled by widespread BOLD decreases in the DMN and bilateral frontoparietal networks that outlasted the AS for more than 20 s. Moreover, they found that HRF in selected regions (e.g., the thalamus or medial and orbital frontal cortex) was highly variable and did not necessarily conform to a “canonical” HRF. As discussed by Bai et al., these results suggest that not all events accompanying AS are captured by scalp EEG and that there might be additional intra- and intersubject variability in the neurovascular coupling between electrical and metabolic activity in IGE that is still poorly understood and cannot be captured with conventional HRF modeling (Bai et al. 2010). Benuzzi et al. analyzed the intersubject variability of BOLD dynamics from 15 before to 9 s after the GSW discharges in a mixed group of 15 adolescents and adults with different IGE syndromes (Benuzzi et al. 2012). At the group level, DMN regions (precuneus, bilateral inferior parietal cortex) as well as the bilateral dorsolateral prefrontal cortex showed transient BOLD increases between 12 and 6 s before GSW discharges, and then an immediate BOLD decrease from GSW starts to ~6 s afterward. The thalamus (together with cerebellum and anterior cingulate cortex) was most active at GSW initiation for a short window of time (roughly 3 s in their analysis). Of note, the individual patterns of the temporal evolution of these changes were highly variable, with some cases showing either very early or very late decreases in the DMN, either short or prolonged increases in the thalamus and different degree of overlap between activated and deactivated areas (Benuzzi et al. 2012). Figure 3 shows an analysis of the temporal evolution of the BOLD response in IGE.

Finally, two recent reports have analyzed the effective connectivity within the thalamocortical BOLD-GSW network, i.e., the dynamic couplings and influences of brain regions on each other (Friston 2011). This is accomplished by using dynamic causal modeling, an advanced biophysical modeling framework that allows to infer (hidden) neural activity based on (observed) BOLD responses (Friston et al. 2003). In one study, Vaudano et al. have found that the

- *High interindividual spatial variability:* multifocal versus symmetric cortical involvement and differential activation of dorsal prefrontal cortices
- *High interindividual temporal variability:* temporally separated versus overlapping DMN activation changes, often “non-canonical” hemodynamic responses
- *Involvement of multiple cortico-subcortical areas:* outside the DMN-thalamus axis: bilateral frontal, sensorimotor, and striato-thalamic networks
- *Clinical significance:* GSW-correlated BOLD changes associated with simultaneous impairment of attention in IGE patients

precuneus has a “permissive” or “gate-keeper” role in GSW generation within the thalamocortical network (Vaudano et al. 2009), which harks back to the idea that a cortical contribution is indeed necessary (see above). Deaunizeau et al took this observation one step further and could show that spontaneous BOLD-signal fluctuations modulate different frequency bands of the EEG, as proposed theoretically by Kilner et al. (2005). This indicates a future area of research, where not only the spatial profiles but also the temporal dynamics of EEG and fMRI events could be used to analyze epileptiform activity.

In sum, simultaneous EEG-fMRI has produced a rich set of novel findings on the functional correlates in IGE. A common theme is the involvement of thalamocortical functional networks in ictal and interictal GSW and a still incompletely understood intersubject variability in the spatial patterns and temporal dynamics of these networks. This variability is not only due to the different and sometimes heterogeneous populations used, since it was also found in more tightly defined subgroups, e.g., children with AS (Bertram 1997; Moeller et al. 2008a; Bai et al. 2010). Therefore, it seems reasonable to assume that it might be biologically meaningful, indicating that GSW, although relatively stereotypical on scalp EEG, might not reflect a unitary phenomenon but a complex set of brain network interactions. Simultaneous EEG-fMRI could thus possibly serve as biomarker for different IGE subtypes (even within syndromes that have been thought to be rather homogeneous on clinical grounds). Much work is needed in this regard.

Box 1

Key Results of Combined EEG-fMRI in Idiopathic Generalized Epilepsies

- *Typical pattern of medio-dorsal thalamic activation and DMN deactivation* (bilateral precuneus, inferior parietal cortices, and medial prefrontal cortices) correlated with ictal and interictal GSW discharges across multiple syndromes.
- *Complex temporal dynamics:* early DMN activation, late persisting DMN deactivation, and mostly short, fast thalamic activation

3.2 Simultaneous EEG-fMRI in the Presurgical Workup of Pharmacoresistant Focal Epilepsies

Simultaneous EEG-fMRI can assist with the presurgical evaluation of patients that suffer from a (potentially) surgically remediable syndrome. This is clinically important, as roughly 30 % of epilepsy patients have or develop pharmacoresistant disease (Kwan and Brodie 2000), i.e., seizures

that cannot be controlled after adequate treatment with two antiseizure medications (as defined by the current consensus definition of the International League Against Epilepsy (Kwan et al. 2010). As mentioned in the introduction, epilepsy surgery can be very effective in this group. The first randomized controlled trial on epilepsy surgery has shown that for a carefully selected cohort of adult mesial temporal lobe epilepsy (MTLE) patients, the number needed to treat (NNT) to render one patient free of seizures that impair awareness at 1 year after surgery is two, and the NNT to render one patient free of *any* seizures is three (Wiebe et al. 2001). To use an illustrative example provided by Wiebe (2004), compare these results to carotid endarterectomy, the widely used standard for symptomatic carotid stenosis, with an NNT of 15 to avoid one disabling ischemic stroke or death in patients with severe stenosis over a follow-up of 2–6 years (Cina et al. 2000). No surgical complications occurred in the randomized controlled trial, whereas others have reported that surgical complications occur in 11 % of patients and that 3 % of patients sustain new, permanent neurological deficits (Engel et al. 2003). This is out-weighted by the fact that successful surgery can reduce the risk of premature death roughly twofold (Bell et al. 2010) and, according to some reports, even lead to low mortality rates that do not differ from the general population (Vickrey et al. 1995; Sperling et al. 1999). A recent study by De Tisi et al. followed 615 adult epilepsy surgery patients over a median follow-up of 8 years and found that a favorable long-term outcome was achieved in about 65 % of cases, where 51 % of patients showed immediate and sustained seizure freedom and an additional 14 % achieved seizure freedom after a complex process of remission and relapse (de Tisi et al. 2011). Some 25 % can be weaned of medication and can be considered as cured, but 40 % of operated epilepsy patients still require antiseizure drugs (ASD) to maintain seizure freedom (Schmidt et al. 2004; Tellez-Zenteno et al. 2005). However, large-scale retrospective studies in MTLE patients ($n=376$, 18 years of follow-up) have shown that even if ASD are continued, roughly 19 % of patients in this category can safely switch from poly- to monotherapy or reduce preoperative monotherapy dosages (Wieser and Hane 2003, 2004). Plausibly owing to seizure freedom and decreased ASD side effects, quality of life improves significantly in operated patients, even if they suffer from postoperative memory decline (Langfitt et al. 2007b). As a consequence, utilization of health-care resources and health-care costs drop in the first 2 years after surgery (Langfitt et al. 2007a), and long-term comparisons of medical and surgical costs between operated and non-operated pharmacoresistant epilepsy patients indicate that epilepsy surgery becomes cost-effective in as little as 7–8 years (King et al. 1997; Langfitt 1997), although this estimate can be as long as 35 years, depending on the precise implementation of the analysis (Platt and

Sperling 2002). Overall, these findings indicate that epilepsy surgery can be highly beneficial in terms of providing relief from individual suffering, prevent further disability, and reduce the health-care costs of society as a whole (Begley et al. 2000). Pharmacoresistant patients should therefore be identified and treated with surgery as early as possible (Kwan and Brodie 2000; Engel et al. 2012). There is still a delay of 18–23 years between development of pharmacoresistance and referral to presurgical evaluation, although recent data also suggest that the trend might be slowly (but modestly) reversing (Haneef et al. 2010).

For epilepsy surgery to be successful, the tissue to be resected and its spatial relationship to functionally relevant (eloquent) cortex have to be identified with precision. This goal requires a synthesis of data from multiple clinical and paraclinical sources of information, i.e., patient history, seizure semiology, neuropsychological examination, ictal and interictal scalp and/or intracranial EEG, and functional and structural neuroimaging (Rosenow and Luders 2001). Whereas standard fMRI with motor, sensory, or cognitive paradigms is used to map eloquent cortex, simultaneous EEG-fMRI is used as an additional tool to assist in mapping the epileptogenic zone (EZ), i.e., “the minimum amount of cortex that must be resected (inactivated or completely disconnected) to produce seizure freedom” (Luders et al. 2006). As mentioned in the introduction to this chapter, the EZ is thought to overlap with the seizure onset zone (SOZ) and the irritative zone (IZ) that generate seizures and IED, respectively. The IZ can thus serve as a proxy of the SOZ and the EZ for clinical purposes, although the different zones must not necessarily be concordant (Luders et al. 2006). Every neuroimaging technique used in epileptology has its strengths and weaknesses when trying to map and disentangle this complex topography. Scalp EEG, for instance, has a very high temporal resolution but is relative insensitive to deep sources of epileptiform activity within the EZ. PET and SPECT require invasive application of radioactive tracers. Structural MRI has a high spatial resolution and can identify even subtle cortical epileptogenic lesions, but these must not overlap with either the IZ or SOZ. Simultaneous EEG-fMRI seems advantageous in this regard, as it can show the metabolic correlates of deep-lying IZs (via IED on scalp EEG) and depict the relationship between IED focus and epileptogenic lesion (via coregistration with high-resolution anatomical images). This might be especially important in those cases where mapping of the different zones is complicated or equivocal, e.g., in patients with the SOZ outside the temporal lobes, in those with multifocal lesions, and in those where no epileptogenic lesion can be identified by standard MRI protocols (Tellez-Zenteno et al. 2005; Jeha et al. 2007; Bien et al. 2009). A few studies have acquired simultaneous EEG-fMRI during the (fortuitous) occurrence of focal seizures (Sierra-Marcos et al. 2013), but safety concerns,

movement artifacts, and the unpredictable nature of seizures limit the clinical applicability of this technique in our view.

There are now a number of clinical observational studies that indicate that local BOLD responses, as mapped with simultaneous EEG-fMRI, co-localize with the SOZ at the lobar level. Krakow et al. investigated 10 patients with focal pharmacoresistant epilepsies (Krakow et al. 1999). BOLD correlates to IED could be found in 6, and in all of them the BOLD correlate was close to the SW maximum in the EEG. The largest study to date includes 63 consecutive patients (59) investigated with frequent IED (Salek-Haddadi et al. 2006). Concordant or approximately concordant BOLD correlates could be found in 23 patients (37 %); 25 had no IED and 11 no BOLD correlates, despite the presence of IED. This low yield might have had technical reasons since the study was performed at 1.5 T with spike triggering, and higher field strengths (Federico et al. 2005) as well as continuous imaging (Al-Asmi et al. 2003) lead to better results. Despite this shortcomings, this study revealed a few interesting results. For instance, there was a pattern of precuneal deactivation in seven patients, reminiscent of the patterns found in IGE (see above). Also, the authors found that BOLD activations showed in general a better concordance with the presumed SW focus than BOLD deactivations (the reason of which is still unknown). Finally, they found that most HRF had physiological waveforms, indicating that “standard” modeling approaches might be sufficient for clinical purposes. Kobayashi et al. investigated 35 patients with temporal lobe epilepsy and found concordant responses in 83 % (Kobayashi et al. 2006). Deactivations were again identified in roughly 50 % of cases. Interestingly, these authors found 16 patients with neocortical BOLD correlates of which 12 had concordant bilateral temporal lobe clusters, indicating that simultaneous EEG-fMRI does not only reveal EZ but can depict parts of the complete epileptogenic network. In a follow-up study, these authors found that this network extended not only to bilateral mesial temporal structures but also to interconnected areas such as the basal ganglia, inferior insula, and lateral temporal gyri (Kobayashi et al. 2009). Of note, contralateral temporal lobe BOLD activity peaked later in comparison to the ipsilateral activity. Thus, these results demonstrate that simultaneous EEG-fMRI, despite the low temporal resolution of the latter, might also show aspects of the temporal dynamics of SW-associated functional networks.

One important question as to the clinical utility of simultaneous EEG-fMRI is how closely it matches with two important gold-standard measures: results from intracranial EEG and postsurgical outcome (Zhang et al. 2012). This question has yet to be addressed prospectively, but there are several reports that provided interesting data on this subject. Seeck et al. provided an early case study of a patient in which simultaneous EEG-fMRI activity was concordant with scalp

EEG source analysis and electrocorticography (ECoG) (Seeck et al. 1998). In the abovementioned case series by Krakow et al. in which six patients showed BOLD correlates of focal SW, 1 localization was also confirmed by ECoG (Krakow et al. 1999). Laufs et al. also found excellent concordance of simultaneous EEG-fMRI in one patient with a right frontocentral SOZ (Laufs et al. 2006). Interestingly, this patient did not show clear IED during the combined recording, and a focal abnormality of the EEG (localized delta activity) was used to derive the fMRI regressor. However, mixed results were reported in two of the largest studies to date by Bagshaw et al. ($n=4$) and Benar et al. ($n=5$) (Bagshaw et al. 2004; Benar et al. 2006). Both validated the findings of simultaneous EEG-fMRI against stereotaxic intracerebral EEG and found concordant BOLD activations to focal SW in 3/4 and 4/5, respectively, but also discordant BOLD correlates in one case per study.

To further clarify these issues, three recent studies have specifically asked whether simultaneous EEG-fMRI can add clinically useful information to the presurgical workup (Zijlmans et al. 2007; Moeller et al. 2009). Zijlmans et al. reviewed 29 patients with simultaneous recordings that had been rejected from surgery due to insufficient certainty in focus localization or multifocality. In their study, new prospects for presurgical reevaluation could be opened in 4, and two underwent intracranial studies that confirmed EEG-fMRI results. Moeller et al. studied another difficult group, patients with non-lesional frontal lobe epilepsy. They found BOLD correlates in 8/9. In two patients that were operated, subtle cortical abnormalities just adjacent to the EEG-fMRI correlates could be identified. A recent study by An et al. in 35 consecutive patients undergoing resective surgery investigated whether the peak of the BOLD response in the preoperative EEG-fMRI study matched the resected volume or not. Postsurgical seizure control was best in those patients where the EEG-related BOLD response was fully concordant with the resected area, whereas in patients with fully discordant BOLD responses, only 1 of 11 reached seizure freedom. This translated into a positive predictive value of the maximal EEG-fMRI response of 70 % and a negative predictive value of 90.9 %. This indicates that EEG-fMRI might be able to better identify those cases where surgery might *not* be successful.

In sum, the studies reviewed above testify to the complexity of results that can be obtained with simultaneous EEG-fMRI. The number of promising results predominates, and the fact that simultaneous recordings might be beneficial especially in difficult cases is encouraging. However, the fact that mapping epileptogenic tissue with simultaneous EEG-fMRI still mainly depends on the detection of IED is an important limitation. Also, adding to the complexity already afforded by the different overlapping zones (or rather networks and network components), the predictive value of IED

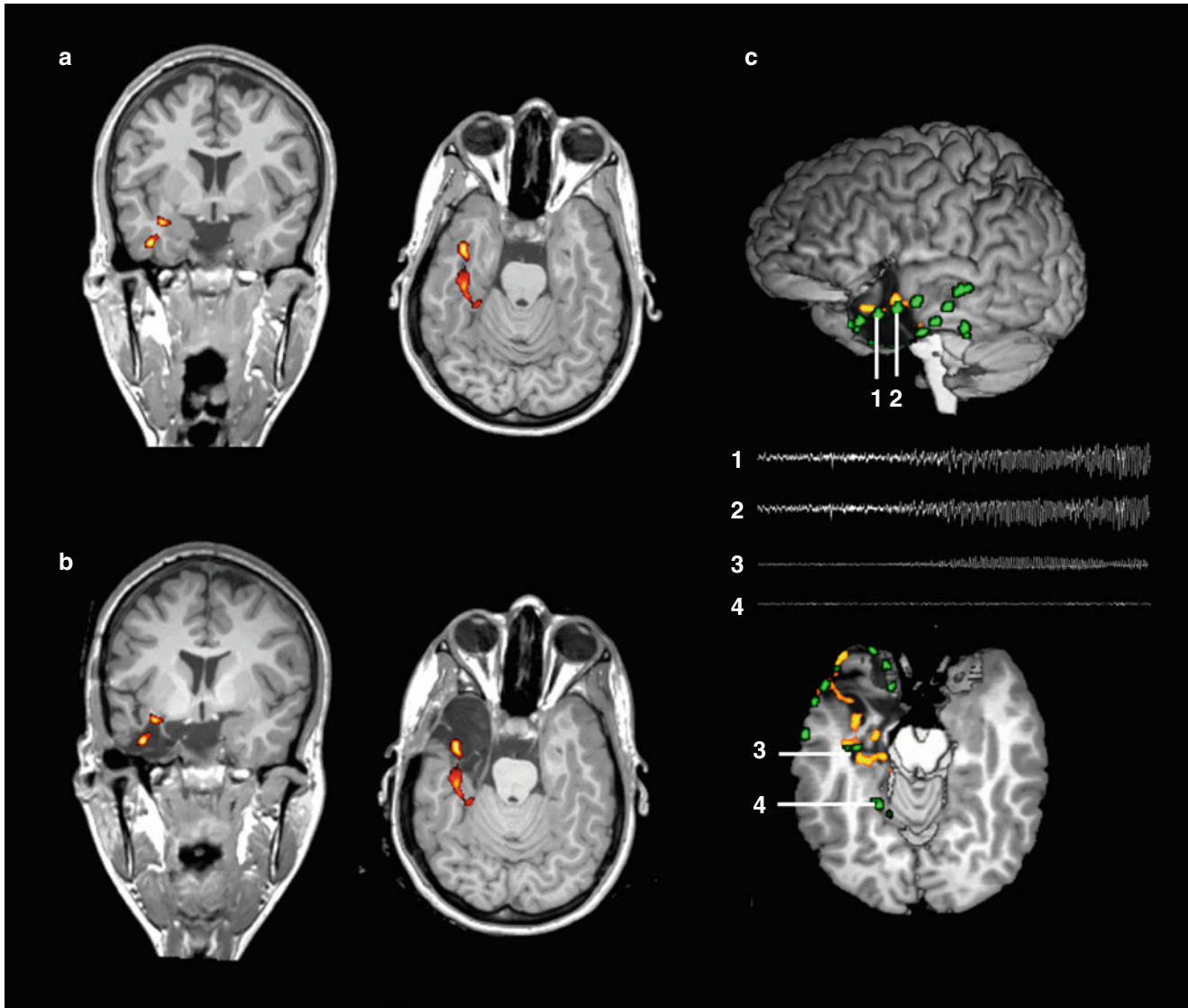


Fig. 4 Presurgical mapping of epileptogenic areas using simultaneous EEG-fMRI. Panel (a) shows a coronal and axial slice of a patient with non-lesional left-sided mesial temporal lobe epilepsy (same patient as in figure 1, neurological convention). Color maps indicate clusters of blood-oxygen level dependent (BOLD) signal increases significantly correlated with interictal epileptiform discharges ($p<0.05$, corrected for multiple comparisons). Panel (b) shows the same clusters projected onto a postoperative anatomical MRI. The peak BOLD cluster is included in the resected area. Panel (c) shows the correspondence

between IED-related BOLD clusters and intracranial EEG signals. The upper image shows a lateral view of the 3D-rendered brain after resection. Green clusters represent intracranial electrode positions, derived from CT-MRI fusion. The lower image shows an axial cut through the upper border of the resection. Traces show the first 10 seconds of seizure evolution in the temporal pole (electrodes 1 and 2) and the hippocampus (3). Note their proximity to the hemodynamic IED-correlates. In contrast, a distant electrode (4) does not show epileptiform activity

to localize the SOZ is not always easy to determine and seems to depend on the neuroanatomical localization of the EZ and the pathophysiology of the underlying disease. For temporal lobe epilepsies, data indicate that IED on scalp EEG indeed predicts the SOZ correctly in ~90 % of cases (Blume et al. 1993, 2001), but for extratemporal sites, e.g., the frontal or parietal lobes, the predictive power of IED is lower, as only ~20 % of patients exhibits unilateral, clearly focal IED (Holmes et al. 2000). Thus, techniques that allow

to map the EZ even without spikes are an important current focus of further research in EEG-fMRI (Rodionov et al. 2007; Grouiller et al. 2011). This could lead to an important new goal for simultaneous EEG-fMRI, i.e., guiding the placement of intracranial electrodes in patients with non-lesional or multifocal epilepsies (Zijlmans et al. 2007). Figure 4 shows one example that combines IED-related hemodynamic responses, post-operative imaging and intracranial EEG signals.

Box 2**Key Points of Combined EEG-fMRI in the Presurgical Workup of Pharmacoresistant Epilepsies****Clinical**

- *Noninvasive, safe, radiation-free method* that can assist decision-making during the workup for epilepsy surgery, a highly effective therapy in carefully selected pharmacoresistant patients.
- *Satisfactory concordance of BOLD activations* with other modalities such as scalp and intracerebral EEG, PET, and SPECT.
- *Added value in complex cases:* localizing value in patients with non-lesional or multifocal epilepsies.

Methodical

- *Artifact reduction is crucial:* optimal recording setup essential, advanced (operator-independent) post-processing techniques can minimize impact noise from various physiological and non-physiological sources.
- *Results are highly dependent on modeling choices:* “non-canonical” hemodynamic models might be advantageous (but cave false positives), motion has to be carefully accounted for.
- *Interpretation is highly dependent on statistical thresholding:* optimal tradeoff between sensitivity and specificity has to be determined and carefully selected on a case-by-case basis.

Challenges

- *The significance of local and distant BOLD deactivations is not fully understood.*
- *Prospective validation studies are lacking.*

4 Future Directions

Epilepsy is a prototypical dynamic disease that includes a large-scale network and not only a circumscribed area of seizure generation. Normal brain function requires complex interactions between different, highly dynamic neural systems that rely on the integrity of structural and functional networks. Thus, a comprehensive evaluation of epilepsy necessitates not only the identification of the epileptogenic zone but the understanding of the functional embedding and interaction of this epileptogenic zone within an epileptic network. There is now emerging evidence that this view of epilepsy as a network disorder is more appropriate on anatomical, neurophysiological, and cognitive levels. Specific cortical and subcortical networks are increasingly recognized as fundamental elements that contribute to the generation and spread of focal onset seizures throughout the human brain. Network theory enables the interpretation of complex neural systems as an assembly of “nodes” and “edges,” rep-

resenting functional and structural elements (brain areas) of a specific network and their structural and functional relationship. Functional network characteristics of the brain can be assessed by EEG and resting state BOLD fMRI either in combination or separately. While functional connectivity is considered as the physiologic process of “communication” between the brain areas within a network, structural network characteristics as measured by diffusion tensor or diffusion spectrum imaging “...can be considered as the “supporting hardware” (van Diessen et al. 2013). Neurophysiologic studies have frequently reported increases in functional connectivity along large-scale networks in the brain and within the affected lobe that harbors the epileptic lesion (Bartolomei et al. 2006; Horstmann et al. 2010). This is in opposite to fMRI-based connectivity studies that reported widespread decreases in functional connectivity (Liao et al. 2010). These differences indicate differences in spatial and temporal resolution between neurophysiologic and fMRI studies. Simultaneous EEG and fMRI studies offer the potential to disentangle the relationship between neurophysiologic and BOLD-associated connectivity (van Dellen et al. 2009; van Wijk et al. 2010). A future goal of MR imaging would be also to measure changes of electromagnetic fields directly without the need of perfusion imaging or BOLD fMRI (Petridou et al. 2006). This technique, called neuronal current imaging, makes use of changes in ionic currents associated with synaptic and suprathreshold activity in the order of nanoamperes. While it has not reached its way into clinical practice, it would certainly lead to further insights into human brain functional organization (Bodurka and Bandettini 2002) and offer a new window for simultaneous recordings of EEG and MRI.

Conclusions

Simultaneous EEG-fMRI is a methodically challenging technique with some important practical pitfalls to consider. However, the capacity of simultaneous EEG-fMRI to provide detailed three-dimensional whole-brain maps of epileptiform activity is unparalleled by other methods, making it an attractive tool for clinical and experimental investigations. Artifact rejection algorithms, statistical analysis techniques, and biophysical models for multimodal data fusion are evolving rapidly, and so is the range of applications. This is an exciting area of imaging neuroscience that could have, given proper validation, a direct impact on our understanding and management of epilepsy patients.

References

- Aghakhani Y, Bagshaw AP, Benar CG, Hawco C, Andermann F, Dubeau F, Gotman J (2004) fMRI activation during spike and wave discharges in idiopathic generalized epilepsy. *Brain* 127:1127–1144

- Aguirre GK, Zarahn E, D'Esposito M (1998) The variability of human, BOLD hemodynamic responses. *Neuroimage* 8:360–369
- Al-Asmi A, Benar CG, Gross DW, Khani YA, Andermann F, Pike B, Dubeau F, Gotman J (2003) fMRI activation in continuous and spike-triggered EEG-fMRI studies of epileptic spikes. *Epilepsia* 44:1328–1339
- Allen PJ, Polizzi G, Krakow K, Fish DR, Lemieux L (1998) Identification of EEG events in the MR scanner: the problem of pulse artifact and a method for its subtraction. *Neuroimage* 8:229–239
- Allen PJ, Josephs O, Turner R (2000) A method for removing imaging artifact from continuous EEG recorded during functional MRI. *Neuroimage* 12:230–239
- Archer JS, Abbott DF, Waites AB, Jackson GD (2003a) fMRI “deactivation” of the posterior cingulate during generalized spike and wave. *Neuroimage* 20:1915–1922
- Archer JS, Briellmann RS, Sygeniotis A, Abbott DF, Jackson GD (2003b) Spike-triggered fMRI in reading epilepsy: involvement of left frontal cortex working memory area. *Neurology* 60:415–421
- Avoli M, Gloor P (1982) Interaction of cortex and thalamus in spike and wave discharges of feline generalized penicillin epilepsy. *Exp Neurol* 76:196–217
- Bagshaw AP, Aghakhani Y, Benar CG, Kobayashi E, Hawco C, Dubeau F, Pike GB, Gotman J (2004) EEG-fMRI of focal epileptic spikes: analysis with multiple haemodynamic functions and comparison with gadolinium-enhanced MR angiograms. *Hum Brain Mapp* 22:179–192
- Bagshaw AP, Hawco C, Benar CG, Kobayashi E, Aghakhani Y, Dubeau F, Pike GB, Gotman J (2005) Analysis of the EEG-fMRI response to prolonged bursts of interictal epileptiform activity. *Neuroimage* 24:1099–1112
- Bai X, Vestal M, Berman R, Negishi M, Spann M, Vega C, Desalvo M, Novotny EJ, Constable RT, Blumenfeld H (2010) Dynamic time course of typical childhood absence seizures: EEG, behavior, and functional magnetic resonance imaging. *J Neurosci* 30:5884–5893
- Bartolomei F, Bosma I, Klein M, Baayen JC, Reijneveld JC, Postma TJ, Heimans JJ, van Dijk BW, de Munck JC, de Jongh A, Cover KS, Stam CJ (2006) Disturbed functional connectivity in brain tumour patients: evaluation by graph analysis of synchronization matrices. *Clin Neurophysiol* 117:2039–2049
- Begley CE, Famulari M, Annegers JF, Lairson DR, Reynolds TF, Coan S, Dubinsky S, Newmark ME, Leibson C, So EL, Rocca WA (2000) The cost of epilepsy in the United States: an estimate from population-based clinical and survey data. *Epilepsia* 41:342–351
- Bell GS, Gaitatzis A, Bell CL, Johnson AL, Sander JW (2008) Drowning in people with epilepsy: how great is the risk? *Neurology* 71:578–582
- Bell GS, Sinha S, Tisi J, Stephani C, Scott CA, Harkness WF, McEvoy AW, Peacock JL, Walker MC, Smith SJ, Duncan JS, Sander JW (2010) Premature mortality in refractory partial epilepsy: does surgical treatment make a difference? *J Neurol Neurosurg Psychiatry* 81:716–718
- Benar CG, Grova C, Kobayashi E, Bagshaw AP, Aghakhani Y, Dubeau F, Gotman J (2006) EEG-fMRI of epileptic spikes: concordance with EEG source localization and intracranial EEG. *Neuroimage* 30:1161–1170
- Benuzzi F, Mirandola L, Pugnagh M, Farinelli V, Tassinari CA, Capovilla G, Cantalupo G, Beccaria F, Nichelli P, Meletti S (2012) Increased cortical BOLD signal anticipates generalized spike and wave discharges in adolescents and adults with idiopathic generalized epilepsies. *Epilepsia* 53:622–630
- Berg AT, Berkovic SF, Brodie MJ, Buchhalter J, Cross JH, van Emde Boas W, Engel J, French J, Glauser TA, Mathern GW, Moshe SL, Nordli D, Plouin P, Scheffer IE (2010) Revised terminology and concepts for organization of seizures and epilepsies: report of the ILAE Commission on Classification and Terminology, 2005–2009. *Epilepsia* 51:676–685
- Berman R, Negishi M, Vestal M, Spann M, Chung MH, Bai X, Purcaro M, Motelow JE, Danielson N, Dix-Cooper L, Enev M, Novotny EJ, Constable RT, Blumenfeld H (2010) Simultaneous EEG, fMRI, and behavior in typical childhood absence seizures. *Epilepsia* 51:2011–2022
- Bertram EH (1997) Functional anatomy of spontaneous seizures in a rat model of limbic epilepsy. *Epilepsia* 38:95–105
- Ben CG, Szinay M, Wagner J, Clusmann H, Becker AJ, Urbach H (2009) Characteristics and surgical outcomes of patients with refractory magnetic resonance imaging-negative epilepsies. *Arch Neurol* 66:1491–1499
- Birn RM, Bandettini PA (2005) The effect of stimulus duty cycle and “off” duration on BOLD response linearity. *Neuroimage* 27:70–82
- Birn RM, Saad ZS, Bandettini PA (2001) Spatial heterogeneity of the nonlinear dynamics in the fMRI BOLD response. *Neuroimage* 14:817–826
- Blume WT, Borghesi JL, Lemieux JF (1993) Interictal indices of temporal seizure origin. *Ann Neurol* 34:703–709
- Blume WT, Holloway GM, Wiebe S (2001) Temporal epileptogenesis: localizing value of scalp and subdural interictal and ictal EEG data. *Epilepsia* 42:508–514
- Blumenfeld H, McCormick DA (2000) Corticothalamic inputs control the pattern of activity generated in thalamocortical networks. *J Neurosci* 20:5153–5162
- Blumenfeld H, McNally KA, Vanderhill SD, Paige AL, Chung R, Davis K, Norden AD, Stokking R, Studholme C, Novotny EJ Jr, Zubal IG, Spencer SS (2004) Positive and negative network correlations in temporal lobe epilepsy. *Cereb Cortex* 14:892–902
- Bodurka J, Bandettini PA (2002) Toward direct mapping of neuronal activity: MRI detection of ultraweak, transient magnetic field changes. *Magn Reson Med* 47:1052–1058
- Bonnelle V, Ham TE, Leech R, Kinnunen KM, Mehta MA, Greenwood RJ, Sharp DJ (2012) Salience network integrity predicts default mode network function after traumatic brain injury. *Proc Natl Acad Sci U S A* 109:4690–4695
- Buckner RL (1998) Event-related fMRI and the hemodynamic response. *Hum Brain Mapp* 6:373–377
- Buckner RL, Andrews-Hanna JR, Schacter DL (2008) The brain's default network: anatomy, function, and relevance to disease. *Ann N Y Acad Sci* 1124:1–38
- Buxton RB, Wong EC, Frank LR (1998) Dynamics of blood flow and oxygenation changes during brain activation: the balloon model. *Magn Reson Med* 39:855–864
- Buzsaki G (1991) The thalamic clock: emergent network properties. *Neuroscience* 41:351–364
- Caballero-Gaudes C, Van de Ville D, Grouiller F, Thornton R, Lemieux L, Seec M, Lazeyras F, Vulliemoz S (2013) Mapping interictal epileptic discharges using mutual information between concurrent EEG and fMRI. *Neuroimage* 68:248–262
- Calhoun VD, Adali T (2012) Multisubject independent component analysis of fMRI: a decade of intrinsic networks, default mode, and neurodiagnostic discovery. *IEEE Rev Biomed Eng* 5:60–73
- Caporaso M, Haneef Z, Yeh HJ, Lenartowicz A, Buttinelli C, Parvizi J, Stern JM (2012) Functional MRI of sleep spindles and K-complexes. *Clin Neurophysiol* 123:303–309
- Carmichael DW, Vulliemoz S, Rodionov R, Thornton JS, McEvoy AW, Lemieux L (2012) Simultaneous intracranial EEG-fMRI in humans: protocol considerations and data quality. *Neuroimage* 63(1):301–309. doi:10.1016/j.neuroimage.2012.05.056, S1053-8119(12)00544-7 [pii]
- Cina CS, Clase CM, Haynes RB (2000) Carotid endarterectomy for symptomatic carotid stenosis. *Cochrane Database Syst Rev*:CD001081
- Cunningham CJ, Zaamout Mel F, Goodyear B, Federico P (2008) Simultaneous EEG-fMRI in human epilepsy. *Can J Neurol Sci* 35(4):420–435

- Daunizeau J, Vaudano AE, Lemieux L (2010) Bayesian multi-modal model comparison: a case study on the generators of the spike and the wave in generalized spike-wave complexes. *Neuroimage* 49:656–667
- Daunizeau J, Lemieux L, Vaudano AE, Friston KJ, Stephan KE (2012) An electrophysiological validation of stochastic DCM for fMRI. *Front Comput Neurosci* 6:103
- Delorme A, Makeig S (2004) EEGLAB: an open source toolbox for analysis of single-trial EEG dynamics including independent component analysis. *J Neurosci Methods* 134(1):9–21. doi:[10.1016/j.jneumeth.2003.10.009](https://doi.org/10.1016/j.jneumeth.2003.10.009), S0165027003003479 [pii]
- De Tiege X, Laufs H, Boyd SG, Harkness W, Allen PJ, Clark CA, Connelly A, Cross JH (2007) EEG-fMRI in children with pharmacoresistant focal epilepsy. *Epilepsia* 48:385–389
- de Tisi J, Bell GS, Peacock JL, McEvoy AW, Harkness WF, Sander JW, Duncan JS (2011) The long-term outcome of adult epilepsy surgery, patterns of seizure remission, and relapse: a cohort study. *Lancet* 378:1388–1395
- Debener S, Ullsperger M, Siegel M, Engel AK (2006) Single-trial EEG-fMRI reveals the dynamics of cognitive function. *Trends Cogn Sci* 10:558–563
- Eichele T, Calhoun VD, Debener S (2009) Mining EEG-fMRI using independent component analysis. *Int J Psychophysiol* 73:53–61
- Ekstrom A (2010) How and when the fMRI BOLD signal relates to underlying neural activity: the danger in dissociation. *Brain Res Rev* 62(2):233–244. doi:[10.1016/j.brainresrev.2009.12.004](https://doi.org/10.1016/j.brainresrev.2009.12.004), S0165-0173(09)00132-5 [pii]
- Engel J Jr, Wiebe S, French J, Sperling M, Williamson P, Spencer D, Gumnit R, Zahn C, Westbrook E, Enos B (2003) Practice parameter: temporal lobe and localized neocortical resections for epilepsy. *Epilepsia* 44:741–751
- Engel J Jr, McDermott MP, Wiebe S, Langfitt JT, Stern JM, Dewar S, Sperling MR, Gardiner I, Erba G, Fried I, Jacobs M, Vinters HV, Mintzer S, Kieburtz K (2012) Early surgical therapy for drug-resistant temporal lobe epilepsy: a randomized trial. *JAMA* 307:922–930
- Esposito F, Mulert C, Goebel R (2009) Combined distributed source and single-trial EEG-fMRI modeling: application to effortful decision making processes. *Neuroimage* 47:112–121
- Federico P, Archer JS, Abbott DF, Jackson GD (2005) Cortical/subcortical BOLD changes associated with epileptic discharges: an EEG-fMRI study at 3 T. *Neurology* 64:1125–1130
- Formaggio E, Storti SF, Cerini R, Fiaschi A, Manganotti P (2010) Brain oscillatory activity during motor imagery in EEG-fMRI coregistration. *Magn Reson Imaging* 28:1403–1412
- Friston KJ (2011) Functional and effective connectivity: a review. *Brain Connect* 1:13–36
- Friston KJ, Fletcher P, Josephs O, Holmes A, Rugg MD, Turner R (1998) Event-related fMRI: characterizing differential responses. *Neuroimage* 7(1):30–40. doi:[10.1006/nimg.1997.0306](https://doi.org/10.1006/nimg.1997.0306), S1053-8119(97)90306-2 [pii]
- Friston KJ, Harrison L, Penny W (2003) Dynamic causal modelling. *Neuroimage* 19:1273–1302
- Gaitatzis A, Sander JW (2004) The mortality of epilepsy revisited. *Epileptic Disord* 6:3–13
- Gaitatzis A, Trimble MR, Sander JW (2004) The psychiatric comorbidity of epilepsy. *Acta Neurol Scand* 110:207–220
- Gaitatzis A, Sisodiya SM, Sander JW (2012) The somatic comorbidity of epilepsy: a weighty but often unrecognized burden. *Epilepsia* 53:1282–1293
- Glaser J (2013) fMRI artifact correction in EEG and EMG data: introducing FACET: a flexible artifact correction and evaluation toolbox for EEG/fMRI data. LAP Lambert Academic Publishing
- Gloor P (1968) Generalized cortico-reticular epilepsies. Some considerations on the pathophysiology of generalized bilaterally synchronous spike and wave discharge. *Epilepsia* 9:249–263
- Glover GH (1999) Deconvolution of impulse response in event-related BOLD fMRI. *Neuroimage* 9:416–429
- Goldman RI, Stern JM, Engel J Jr, Cohen MS (2000) Acquiring simultaneous EEG and functional MRI. *Clin Neurophysiol* 111:1974–1980
- Goldman RI, Stern JM, Engel J Jr, Cohen MS (2002) Simultaneous EEG and fMRI of the alpha rhythm. *Neuroreport* 13:2487–2492
- Gotman J, Kobayashi E, Bagshaw AP, Benar CG, Dubeau F (2006) Combining EEG and fMRI: a multimodal tool for epilepsy research. *J Magn Reson Imaging* 23:906–920
- Greicius MD, Krasnow B, Reiss AL, Menon V (2003) Functional connectivity in the resting brain: a network analysis of the default mode hypothesis. *Proc Natl Acad Sci U S A* 100:253–258
- Grouiller F, Thornton RC, Groening K, Spinelli L, Duncan JS, Schaller K, Simiatchkin M, Lemieux L, Seeck M, Michel CM, Vulliemoz S (2011) With or without spikes: localization of focal epileptic activity by simultaneous electroencephalography and functional magnetic resonance imaging. *Brain* 134:2867–2886
- Hamandi K, Salek-Haddadi A, Laufs H, Liston A, Friston K, Fish DR, Duncan JS, Lemieux L (2006) EEG-fMRI of idiopathic and secondarily generalized epilepsies. *Neuroimage* 31:1700–1710
- Haneef Z, Stern J, Dewar S, Engel J Jr (2010) Referral pattern for epilepsy surgery after evidence-based recommendations: a retrospective study. *Neurology* 75:699–704
- Hauf M, Jann K, Schindler K, Scheidegger O, Meyer K, Rummel C, Mariani L, Koenig T, Wiest R (2012) Localizing seizure-onset zones in presurgical evaluation of drug-resistant epilepsy by electroencephalography/fMRI: effectiveness of alternative thresholding strategies. *AJNR Am J Neuroradiol* 33(9):1818–1824. doi:[10.3174/ajnr.A3052](https://doi.org/10.3174/ajnr.A3052)
- Hesse C, James C (2005) Tracking epileptiform activity in the multi-channel ictal EEG using spatially constrained independent component analysis. *Conf Proc IEEE Eng Med Biol Soc* 2:2067–2070
- Hitiris N, Mohanraj R, Norrie J, Brodie MJ (2007) Mortality in epilepsy. *Epilepsy Behav* 10:363–376
- Holmes GL, McKeever M, Adamson M (1987) Absence seizures in children: clinical and electroencephalographic features. *Ann Neurol* 21:268–273
- Holmes MD, Kutsy RL, Ojemann GA, Wilensky AJ, Ojemann LM (2000) Interictal, unifocal spikes in refractory extratemporal epilepsy predict ictal origin and postsurgical outcome. *Clin Neurophysiol* 111:1802–1808
- Horstmann MT, Bialonski S, Noennig N, Mai H, Prusseit J, Wellmer J, Hinrichs H, Lehnertz K (2010) State dependent properties of epileptic brain networks: comparative graph-theoretical analyses of simultaneously recorded EEG and MEG. *Clin Neurophysiol* 121:172–185
- Ives JR, Warach S, Schmitt F, Edelman RR, Schomer DL (1993) Monitoring the patient's EEG during echo planar MRI. *Electroencephalogr Clin Neurophysiol* 87:417–420
- Jann K, Wiest R, Hauf M, Meyer K, Boesch C, Mathis J, Schroth G, Dierks T, Koenig T (2008) BOLD correlates of continuously fluctuating epileptic activity isolated by independent component analysis. *Neuroimage* 42:635–648
- Jann K, Dierks T, Boesch C, Kottlow M, Strik W, Koenig T (2009) BOLD correlates of EEG alpha phase-locking and the fMRI default mode network. *Neuroimage* 45:903–916
- Jeha LE, Najm I, Bingaman W, Dinner D, Widdess-Walsh P, Luders H (2007) Surgical outcome and prognostic factors of frontal lobe epilepsy surgery. *Brain* 130:574–584
- Kannurpatti SS, Motes MA, Rypma B, Biswal BB (2010) Neural and vascular variability and the fMRI-BOLD response in normal aging. *Magn Reson Imaging* 28:466–476
- Kannurpatti SS, Motes MA, Rypma B, Biswal BB (2011) Non-neural BOLD variability in block and event-related paradigms. *Magn Reson Imaging* 29:140–146
- Kilner JM, Mattout J, Henson R, Friston KJ (2005) Hemodynamic correlates of EEG: a heuristic. *Neuroimage* 28:280–286

- Kim TS, Lee J, Lee JH, Glover GH, Pauly JM (2012) Analysis of the BOLD Characteristics in Pass-Band bSSFP fMRI. *Int J Imaging Syst Technol* 22(1):23–32. doi:[10.1002/ima.21296](https://doi.org/10.1002/ima.21296)
- King JT Jr, Sperling MR, Justice AC, O'Connor MJ (1997) A cost-effectiveness analysis of anterior temporal lobectomy for intractable temporal lobe epilepsy. *J Neurosurg* 87:20–28
- Kobayashi E, Bagshaw AP, Benar CG, Aghakhani Y, Andermann F, Dubeau F, Gotman J (2006) Temporal and extratemporal BOLD responses to temporal lobe interictal spikes. *Epilepsia* 47:343–354
- Kobayashi E, Grova C, Tyvaert L, Dubeau F, Gotman J (2009) Structures involved at the time of temporal lobe spikes revealed by interindividual group analysis of EEG/fMRI data. *Epilepsia* 50:2549–2556
- Krakow K, Woermann FG, Symms MR, Allen PJ, Lemieux L, Barker GJ, Duncan JS, Fish DR (1999) EEG-triggered functional MRI of interictal epileptiform activity in patients with partial seizures. *Brain* 122(Pt 9):1679–1688
- Kwan P, Brodie MJ (2000) Early identification of refractory epilepsy. *N Engl J Med* 342:314–319
- Kwan P, Arzimanoglou A, Berg AT, Brodie MJ, Allen Hauser W, Mathern G, Moshe SL, Perucca E, Wiebe S, French J (2010) Definition of drug resistant epilepsy: consensus proposal by the ad hoc Task Force of the ILAE Commission on Therapeutic Strategies. *Epilepsia* 51:1069–1077
- Langfitt JT (1997) Cost-effectiveness of anterotemporal lobectomy in medically intractable complex partial epilepsy. *Epilepsia* 38:154–163
- Langfitt JT, Holloway RG, McDermott MP, Messing S, Sarosky K, Berg AT, Spencer SS, Vickrey BG, Sperling MR, Bazil CW, Shinnar S (2007a) Health care costs decline after successful epilepsy surgery. *Neurology* 68:1290–1298
- Langfitt JT, Westerveld M, Hamberger MJ, Walczak TS, Cicchetti DV, Berg AT, Vickrey BG, Barr WB, Sperling MR, Masur D, Spencer SS (2007b) Worsening of quality of life after epilepsy surgery: effect of seizures and memory decline. *Neurology* 68:1988–1994
- Laufs H (2012) A personalized history of EEG-fMRI integration. *Neuroimage* 62:1056–1067
- Laufs H, Hamandi K, Walker MC, Scott C, Smith S, Duncan JS, Lemieux L (2006) EEG-fMRI mapping of asymmetrical delta activity in a patient with refractory epilepsy is concordant with the epileptogenic region determined by intracranial EEG. *Magn Reson Imaging* 24:367–371
- Lemieux L, Allen PJ, Franconi F, Symms MR, Fish DR (1997) Recording of EEG during fMRI experiments: patient safety. *Magn Reson Med* 38(6):943–952
- Lemieux L, Hagemann G, Krakow K, Woermann FG (1999) Fast, accurate, and reproducible automatic segmentation of the brain in T1-weighted volume MRI data. *Magn Reson Med* 42(1):127–135
- Liao W, Zhang Z, Pan Z, Mantini D, Ding J, Duan X, Luo C, Lu G, Chen H (2010) Altered functional connectivity and small-world in mesial temporal lobe epilepsy. *PLoS One* 5:e8525
- Logothetis NK, Wandell BA (2004) Interpreting the BOLD signal. *Annu Rev Physiol* 66:735–769
- Logothetis NK, Pauls J, Augath M, Trinath T, Oeltermann A (2001) Neurophysiological investigation of the basis of the fMRI signal. *Nature* 412:150–157
- Luders HO, Najm I, Nair D, Widness-Walsh P, Bingman W (2006) The epileptogenic zone: general principles. *Epileptic Disord* 8(Suppl 2):S1–S9
- Masterton RA, Carney PW, Abbott DF, Jackson GD (2013) Absence epilepsy subnetworks revealed by event-related independent components analysis of functional magnetic resonance imaging. *Epilepsia* 54:801–808
- Mayhew SD, Ostwald D, Porcaro C, Bagshaw AP (2013) Spontaneous EEG alpha oscillation interacts with positive and negative BOLD responses in the visual-auditory cortices and default-mode network. *Neuroimage* 76:362–372
- McKeown MJ, Makeig S, Brown GG, Jung TP, Kindermann SS, Bell AJ, Sejnowski TJ (1998) Analysis of fMRI data by blind separation into independent spatial components. *Hum Brain Mapp* 6:160–188
- Meeren H, van Luijtelaar G, Lopes da Silva F, Coenen A (2005) Evolving concepts on the pathophysiology of absence seizures: the cortical focus theory. *Arch Neurol* 62:371–376
- Mirsattari SM, Wang Z, Ives JR, Bihari F, Leung LS, Bartha R, Menon RS (2006) Linear aspects of transformation from interictal epileptic discharges to BOLD fMRI signals in an animal model of occipital epilepsy. *Neuroimage* 30:1133–1148
- Moeller F, Siebner HR, Wolff S, Muhle H, Boor R, Granert O, Jansen O, Stephani U, Siniatchkin M (2008a) Changes in activity of striato-thalamo-cortical network precede generalized spike wave discharges. *Neuroimage* 39:1839–1849
- Moeller F, Siebner HR, Wolff S, Muhle H, Granert O, Jansen O, Stephani U, Siniatchkin M (2008b) Simultaneous EEG-fMRI in drug-naïve children with newly diagnosed absence epilepsy. *Epilepsia* 49:1510–1519
- Moeller F, Tyvaert L, Nguyen DK, LeVan P, Bouthillier A, Kobayashi E, Tampieri D, Dubeau F, Gotman J (2009) EEG-fMRI: adding to standard evaluations of patients with nonlesional frontal lobe epilepsy. *Neurology* 73:2023–2030
- Moeller F, LeVan P, Muhle H, Stephani U, Dubeau F, Siniatchkin M, Gotman J (2010a) Absence seizures: individual patterns revealed by EEG-fMRI. *Epilepsia* 51:2000–2010
- Moeller F, Muhle H, Wiegand G, Wolff S, Stephani U, Siniatchkin M (2010b) EEG-fMRI study of generalized spike and wave discharges without transitory cognitive impairment. *Epilepsy Behav* 18:313–316
- Moosmann M, Eichele T, Nordby H, Hugdahl K, Calhoun VD (2008) Joint independent component analysis for simultaneous EEG-fMRI: principle and simulation. *Int J Psychophysiol* 67:212–221
- Nunez PL, Silberstein RB (2000) On the relationship of synaptic activity to macroscopic measurements: does co-registration of EEG with fMRI make sense? *Brain Topogr* 13:79–96
- Osharina V, Ponchel E, Aarabi A, Grebe R, Wallois F (2010) Local haemodynamic changes preceding interictal spikes: a simultaneous electrocorticography (ECoG) and near-infrared spectroscopy (NIRS) analysis in rats. *Neuroimage* 50(2):600–607. doi:[10.1016/j.neuroimage.2010.01.009](https://doi.org/10.1016/j.neuroimage.2010.01.009), S1053-8119(10)00014-5 [pii]
- Panayiotopoulos CP, Chroni E, Daskalopoulos C, Baker A, Rowlinson S, Walsh P (1992) Typical absence seizures in adults: clinical, EEG, video-EEG findings and diagnostic/syndromic considerations. *J Neurol Neurosurg Psychiatry* 55:1002–1008
- Petridou N, Plenz D, Silva AC, Loew M, Bodurka J, Bandettini PA (2006) Direct magnetic resonance detection of neuronal electrical activity. *Proc Natl Acad Sci U S A* 103:16015–16020
- Picchioni D, Horovitz SG, Fukunaga M, Carr WS, Meltzer JA, Balkin TJ, Duyn JH, Braun AR (2011) Infraslow EEG oscillations organize large-scale cortical-subcortical interactions during sleep: a combined EEG/fMRI study. *Brain Res* 1374:63–72
- Platt M, Sperling MR (2002) A comparison of surgical and medical costs for refractory epilepsy. *Epilepsia* 43(Suppl 4):25–31
- Plichta MM, Wolf I, Hohmann S, Baumeister S, Boecker R, Schwarz AJ, Zangl M, Mier D, Diener C, Meyer P, Holz N, Ruf M, Gerchen MF, Bernal-Casas D, Kolev V, Yordanova J, Flor H, Laucht M, Banaschewski T, Kirsch P, Meyer-Lindenberg A, Brandeis D (2013) Simultaneous EEG and fMRI Reveals a Causally Connected Subcortical-Cortical Network during Reward Anticipation. *J Neurosci* 33:14526–14533
- Pompili M, Girardi P, Tatarelli R (2006) Death from suicide versus mortality from epilepsy in the epilepsies: a meta-analysis. *Epilepsy Behav* 9:641–648
- Raichle ME, Snyder AZ (2007) A default mode of brain function: a brief history of an evolving idea. *Neuroimage* 37:1083–1090; discussion 1097–1089
- Raichle ME, MacLeod AM, Snyder AZ, Powers WJ, Gusnard DA, Shulman GL (2001) A default mode of brain function. *Proc Natl Acad Sci U S A* 98:676–682

- Ritter P, Villringer A (2006) Simultaneous EEG-fMRI. *Neurosci Biobehav Rev* 30(6):823–838. doi:[10.1016/j.neubiorev.2006.06.008](https://doi.org/10.1016/j.neubiorev.2006.06.008)
- Rocca MA, Valsasina P, Martinelli V, Misci P, Falini A, Comi G, Filippi M (2012) Large-scale neuronal network dysfunction in relapsing-remitting multiple sclerosis. *Neurology* 79:1449–1457
- Rodionov R, De Martino F, Laufs H, Carmichael DW, Formisano E, Walker M, Duncan JS, Lemieux L (2007) Independent component analysis of interictal fMRI in focal epilepsy: comparison with general linear model-based EEG-correlated fMRI. *Neuroimage* 38: 488–500
- Rosenkranz K, Lemieux L (2010) Present and future of simultaneous EEG-fMRI. *MAGMA* 23:309–316
- Rosenow F, Luders H (2001) Presurgical evaluation of epilepsy. *Brain* 124:1683–1700
- Rummel C, Verma RK, Schopf V, Abela E, Hauf M, Berruecos JF, Wiest R (2013) Time course based artifact identification for independent components of resting-state fMRI. *Front Hum Neurosci* 7:214
- Salek-Haddadi A, Diehl B, Hamandi K, Merschhemke M, Liston A, Friston K, Duncan JS, Fish DR, Lemieux L (2006) Hemodynamic correlates of epileptiform discharges: an EEG-fMRI study of 63 patients with focal epilepsy. *Brain Res* 1088:148–166
- Sander JW (2003) The epidemiology of epilepsy revisited. *Curr Opin Neurol* 16:165–170
- Schmidt D, Baumgartner C, Loscher W (2004) Seizure recurrence after planned discontinuation of antiepileptic drugs in seizure-free patients after epilepsy surgery: a review of current clinical experience. *Epilepsia* 45:179–186
- Seeck M, Lazeyras F, Michel CM, Blanke O, Gericke CA, Ives J, Delavelle J, Golay X, Haenggeli CA, de Trbolet N, Landis T (1998) Non-invasive epileptic focus localization using EEG-triggered functional MRI and electromagnetic tomography. *Electroencephalogr Clin Neurophysiol* 106:508–512
- Sierra-Marcos A, Maestro I, Falcon C, Donaire A, Setoain J, Aparicio J, Rumia J, Pintor L, Boget T, Carreno M, Bargallo N (2013) Ictal EEG-fMRI in localization of epileptogenic area in patients with refractory neocortical focal epilepsy. *Epilepsia* 54:1688–1698
- Spencer SS (2002) Neural networks in human epilepsy: evidence of and implications for treatment. *Epilepsia* 43:219–227
- Sperling MR, Feldman H, Kinman J, Liporace JD, O'Connor MJ (1999) Seizure control and mortality in epilepsy. *Ann Neurol* 46:45–50
- Srivastava G, Crottaz-Herbette S, Lau KM, Glover GH, Menon V (2005) ICA-based procedures for removing ballistocardiogram artifacts from EEG data acquired in the MRI scanner. *Neuroimage* 24:50–60
- Tellez-Zenteno JF, Dhar R, Wiebe S (2005) Long-term seizure outcomes following epilepsy surgery: a systematic review and meta-analysis. *Brain* 128:1188–1198
- Thornton R, Vulliemoz S, Rodionov R, Carmichael DW, Chaudhary UJ, Diehl B, Laufs H, Vollmar C, McEvoy AW, Walker MC, Bartolomei F, Guye M, Chauvel P, Duncan JS, Lemieux L (2011) Epileptic networks in focal cortical dysplasia revealed using electroencephalography-functional magnetic resonance imaging. *Ann Neurol* 70:822–837
- van Dellen E, Douw L, Baayen JC, Heimans JJ, Ponten SC, Vandertop WP, Velis DN, Stam CJ, Reijneveld JC (2009) Long-term effects of temporal lobe epilepsy on local neural networks: a graph theoretical analysis of corticography recordings. *PLoS One* 4:e8081
- van Diessen E, Diederich SJ, Braun KP, Jansen FE, Stam CJ (2013) Functional and structural brain networks in epilepsy: what have we learned? *Epilepsia* 54:1855–65
- van Houdt PJ, de Munck JC, Leijten FS, Huiskamp GJ, Colon AJ, Boon PA, Ossenblok PP (2013) EEG-fMRI correlation patterns in the pre-surgical evaluation of focal epilepsy: a comparison with electrocorticographic data and surgical outcome measures. *Neuroimage* 75:238–248
- van Wijk BC, Stam CJ, Daffertshofer A (2010) Comparing brain networks of different size and connectivity density using graph theory. *PLoS One* 5:e13701
- Vaudano AE, Laufs H, Kiebel SJ, Carmichael DW, Hamandi K, Guye M, Thornton R, Rodionov R, Friston KJ, Duncan JS, Lemieux L (2009) Causal hierarchy within the thalamo-cortical network in spike and wave discharges. *PLoS One* 4:e6475
- Vickrey BG, Hays RD, Rausch R, Engel J Jr, Visscher BR, Ary CM, Rogers WH, Brook RH (1995) Outcomes in 248 patients who had diagnostic evaluations for epilepsy surgery. *Lancet* 346:1445–1449
- Vulliemoz S, Thornton R, Rodionov R, Carmichael DW, Guye M, Lhatoo S, McEvoy AW, Spinelli L, Michel CM, Duncan JS, Lemieux L (2009) The spatio-temporal mapping of epileptic networks: combination of EEG-fMRI and EEG source imaging. *Neuroimage* 46:834–843
- Vulliemoz S, Carmichael DW, Rosenkranz K, Diehl B, Rodionov R, Walker MC, McEvoy AW, Lemieux L (2011) Simultaneous intracranial EEG and fMRI of interictal epileptic discharges in humans. *Neuroimage* 54(1):182–190. doi:[10.1016/j.neuroimage.2010.08.004](https://doi.org/10.1016/j.neuroimage.2010.08.004), S1053-8119(10)01071-2 [pii]
- Wan X, Riera J, Iwata K, Takahashi M, Wakabayashi T, Kawashima R (2006) The neural basis of the hemodynamic response nonlinearity in human primary visual cortex: implications for neurovascular coupling mechanism. *Neuroimage* 32:616–625
- Warach S, Ives JR, Schlaug G, Patel MR, Darby DG, Thangaraj V, Edelman RR, Schomer DL (1996) EEG-triggered echo-planar functional MRI in epilepsy. *Neurology* 47:89–93
- Weir B (1965) The morphology of the spike-wave complex. *Electroencephalogr Clin Neurophysiol* 19:284–290
- Wiebe S (2004) Effectiveness and safety of epilepsy surgery: what is the evidence? *CNS Spectr* 9(120–122):126–132
- Wiebe S, Blume WT, Girvin JP, Eliasziw M (2001) A randomized, controlled trial of surgery for temporal-lobe epilepsy. *N Engl J Med* 345:311–318
- Wieser HG, Hane A (2003) Antiepileptic drug treatment before and after selective amygdalohippocampectomy. *Epilepsy Res* 55:211–223
- Wieser HG, Hane A (2004) Antiepileptic drug treatment in seizure-free mesial temporal lobe epilepsy patients with hippocampal sclerosis following selective amygdalohippocampectomy. *Seizure* 13:534–536
- Wiest R, Estermann L, Scheidegger O, Rummel C, Jann K, Seeck M, Schindler K, Hauf M (2013) Widespread grey matter changes and hemodynamic correlates to interictal epileptiform discharges in pharmacoresistant mesial temporal epilepsy. *J Neurol* 260:1601–1610
- Zhang J, Liu W, Chen H, Xia H, Zhou Z, Wang L, Mei S, Liu Q, Li Y (2012) EEG-fMRI validation studies in comparison with iEEG: a review. *Int J Psychophysiol* 84:233–239
- Zijlmans M, Huiskamp G, Hersevoort M, Seppenwoolde JH, van Huffelen AC, Leijten FS (2007) EEG-fMRI in the presurgical work-up for epilepsy surgery. *Brain* 130:2343–2353

Diffusion Imaging with MR Tractography for Brain Tumor Surgery

Alberto Bizzì

Contents

| | | |
|------|--|-----|
| 1 | Introduction | 180 |
| 2 | Neuro-oncology of Gliomas | 181 |
| 2.1 | Histology and Molecular Markers | 181 |
| 2.2 | Pattern of Growth and Velocity of Expansion..... | 182 |
| 2.3 | Aims of Brain Tumor Surgery..... | 182 |
| 3 | Magnetic Resonance Diffusion Imaging Methods..... | 184 |
| 3.1 | Conventional MR Imaging | 184 |
| 3.2 | Diffusion Tensor Imaging | 184 |
| 3.3 | DTI Metrics and Brain Tumor Microstructure..... | 185 |
| 3.4 | MR Tractography | 186 |
| 3.5 | Limitations of DTI and MR Tractography | 187 |
| 3.6 | Crossing Fibers and the Need for Advanced MR Diffusion Imaging Methods | 188 |
| 3.7 | Clinically Feasible Brain Mapping Imaging Protocols and Preprocessing Requirements | 189 |
| 4 | Current Theories About Structural Connectivity of Eloquent Functional Systems..... | 189 |
| 4.1 | Motor System..... | 191 |
| 4.2 | Language System | 192 |
| 4.3 | Visuospatial Attention System | 195 |
| 5 | Mapping WM Tracts for Brain Surgery | 197 |
| 5.1 | Brain Tumor Semeiotic with FA and Directionally Encoded Color Maps..... | 197 |
| 5.2 | Mapping Strategies with MR Tractography | 202 |
| 5.3 | Motor System | 204 |
| 5.4 | Language System | 207 |
| 5.5 | The Dorsal Pathway: Arcuate Fasciculus..... | 207 |
| 5.6 | The Ventral Pathway: IFOF, UF, and ILF | 208 |
| 5.7 | The Temporoparietal Fiber Intersection Area | 210 |
| 5.8 | Frontal Aslant Tract and Subcallosal Fasciculus | 216 |
| 5.9 | Which Fascicles Are Eloquent for Speech? | 216 |
| 5.10 | Visuospatial System | 219 |
| 5.11 | Integration with fMRI | 221 |
| 5.12 | Integration in the Operating Room | 222 |
| 5.13 | Impact in Clinical Practice | 222 |
| | Conclusions | 223 |
| | References | 224 |

A. Bizzì, MD
Department of Neuroradiology,
Humanitas Clinical and Research Hospital IRCCS,
Via Manzoni, 56, Rozzano (Milano) 20089, Italy
e-mail: alberto_bizzi@fastwebnet.it, alberto.bizzi@humanitas.it

Abstract

In the last 15 years, advances in neurosurgery, neuroradiology and neuro-oncology have dramatically changed management of brain tumors, especially of gliomas seated in eloquent areas carrying a higher risk for permanent postoperative neurological deficits.

This chapter provides clinically relevant and practical information and a review of the current literature from glioma biology through MR diffusion basic principles and current theories about connectivity of eloquent brain systems to clinical application of MR tractography, so that the reader can get a thorough interdisciplinary impression of the state of the art.

In contrast to brain metastases and meningiomas, gliomas extensively infiltrate the extracellular space of the gray and white matter, changing the anatomic and functional properties of the brain. MR diffusion imaging has great potentials to contribute to disclose the mechanisms of interaction between gliomas and the host tissue.

Diffusion tensor imaging (DTI) is the most established and validated clinical application of MR tractography, and it is increasingly performed in large medical centers. More advanced diffusion MR acquisition schemes such as high angular resolution diffusion imaging (HARDI) and more sophisticated tractography algorithms such as spherical deconvolution (SD) and Q-ball imaging (QBI) have been developed to overcome DTI limitations. The community is beginning to apply the advanced methods in presurgical mapping.

A detailed understanding of the relationship between eloquent white matter fascicles and infiltrating gliomas is mandatory to correctly plan a resection and interpret the functional neurophysiological responses recorded during intraoperative monitoring (IOM) with electromyography (EMG), motor evoked potential (MEP), and direct intraoperative electrical stimulation (IES). It should be emphasized that MR diffusion tractography provides anatomical, not functional, information.

The neurosurgical community is increasingly recognizing the value of MR diffusion imaging with tractography in evaluating patients with gliomas. MR tractography is a great educational tool for neurosurgeons and neuroradiologists. Presurgical visualization of eloquent fascicles in the proximity of a mass has been associated with a higher probability of total resection in low- and high-grade gliomas. Postoperative MR tractography is increasingly used to correlate postoperative deficits with white matter anatomy and guide rehabilitation strategies.

This chapter presents optimized clinical presurgical HARDI protocols and tractography methods for visualization of the major white matter tracts that are part of the motor, language, and visuospatial attention systems. Practical examples of how to interpret MR tractography findings are given, and illustrative cases with typical and atypical presurgical findings are presented. Complementary applications with functional MR imaging (fMRI) are highlighted. Finally, the clinical value and limitations of pre-surgical MR diffusion imaging are discussed.

Abbreviations

| | | | |
|-------|---|-------|--|
| AC | Anterior commissure | GBM | Glioblastoma multiforme |
| ADC | Apparent diffusion coefficient | HARDI | High angular resolution diffusion imaging |
| AF | Arcuate fasciculus | HGG | High-grade glioma |
| AG | Angular gyrus | IES | Intraoperative electrical stimulation |
| ALA | 5-Aminolevulinic acid | IFG | Inferior frontal gyrus |
| BA | Brodmann area | IFOF | Inferior fronto-occipital fasciculus |
| BOLD | Blood oxygen level dependent | ILF | Inferior longitudinal fasciculus |
| CC | Corpus callosum | IOM | Intraoperative monitoring |
| CL | Linear anisotropy coefficient | IPL | Inferior parietal lobule |
| CP | Planar anisotropy coefficient | ITG | Inferior temporal gyrus |
| CS | Spherical anisotropy coefficient | LGG | Low-grade glioma |
| CST | Corticospinal tract | M1 | Primary motor cortex |
| DEC | Directionally encoded color | MD | Mean diffusivity |
| dIPFC | Dorsolateral prefrontal cortex | MFG | Medial frontal gyrus |
| dODF | Diffusion orientation distribution function | MLF | Medial longitudinal fasciculus |
| DSI | Diffusion spectrum imaging | MRI | Magnetic resonance imaging |
| DTI | Diffusion tensor imaging | MTG | Medial temporal gyrus |
| DWI | Diffusion weighted imaging | ND | Neurite density |
| ECS | Extracellular space | NODDI | Neurite orientation dispersion and density imaging |
| EMC | Extreme capsule | ODI | Orientation dispersion index |
| EOR | Extent of resection | OR | Optic radiations |
| EPI | Echo-planar imaging | PMC | Premotor cortex |
| FA | Fractional anisotropy | PMd | Premotor dorsal |
| FAT | Frontal aslant tract | PMv | Premotor ventral |
| FEF | Frontal eye field | PPC | Posterior parietal cortex |
| FLAIR | Fluid-attenuated inversion recovery | QBI | Q-ball imaging |
| fMRI | Functional magnetic resonance imaging | ROI | Region of interest |
| fODF | Fiber orientation diffusion function | S1 | Primary somatosensory cortex |
| FST | Frontal striatal tract | SCF | Subcallosal fasciculus |
| | | SD | Spherical deconvolution |
| | | SFG | Superior frontal gyrus |
| | | SLF | Superior longitudinal fasciculus |
| | | SMA | Supplementary motor area |
| | | SMG | Supramarginal gyrus |
| | | SPL | Superior parietal lobule |
| | | STG | Superior temporal gyrus |
| | | T2WI | T2-weighted image |
| | | TPFIA | Temporoparietal fiber intersection area |
| | | UF | Uncinate fasciculus |
| | | vIPFC | Ventrolateral prefrontal cortex |
| | | WHO | World Health Organization |
| | | WM | White matter |

1 Introduction

Management of brain tumors has changed dramatically in the last 15 years due to tremendous advancements in neurosurgery, neuroradiology, and neuro-oncology. Advancements in neurosurgery include implementation of microscopic surgery, intraoperative monitoring (IOM), and imaging-guided methods in the operating theater (Keles and Berger 2004). Previously, brain tumors infiltrating the motor, the language,

and the visual systems were considered “inoperable.” Implementation of modern surgical techniques has widened the indications for brain tumor surgery to include lesions located in the so-called eloquent areas. It has been demonstrated that tumor resection according to “functional margins” and when possible beyond MR imaging-defined signal abnormalities (i.e., extended “supratotal resection”) significantly increased overall survival by delaying malignant transformation in diffuse gliomas and recurrence in glioblastoma multiforme (GBM). Refinement of intraoperative functional mapping methods in the last decade has resulted in much more reliable identification of functional margins in the motor and language systems and extension of the intraoperative functional mapping paradigm to include additional high cognitive functions.

Advances in neuroradiology, in particular in the field of functional MR imaging (fMRI) and MR diffusion tensor imaging (DTI), have changed the way surgeons evaluate patients before surgery. Advanced neuroimaging methods can now provide morphological and functional information about changes induced by the tumor on the hosting brain. This new information is quite important and relevant, especially when a diffuse infiltrating glioma is growing within an eloquent brain structure. It has been shown that presurgical mapping with fMRI and DTI may improve surgical targeting, guide surgical strategy and intraoperative assessments, and reduce intraoperative time (Petrella et al. 2006). Clinical use of advanced MR imaging tools is growing in importance, and neurosurgeons worldwide understand more and more the advantages of including these data in the presurgical assessment. Neurosurgeons are increasingly requesting fMRI and DTI as part of their routine presurgical evaluation.

Advances in neuro-oncology have been also quite impressive in the last decade. Substantial progresses have been made in molecular classification of many brain tumors. Large-scale molecular profiling approaches have identified new mutations in gliomas which have allowed subclassification into distinct molecular subgroups with characteristic features of age, localization, and outcome (Sturm et al. 2012). Recent randomized clinical trials have demonstrated that molecular characterization allows identification of subgroups of gliomas that are associated with distinct prognosis and predicted treatment response (Stupp and Hegi 2013). Thus molecular marker analyses should be part of the standard diagnostic work-up in all patients with brain tumors since prognostic and predictive markers have direct implications in routine clinical decision making (Thomas et al. 2013). These results have emphasized the importance of collecting tumor sampling for molecular studies.

All together, the above mentioned advances have changed treatment strategies for this disease, more so when the lesion is located in the proximity of eloquent structures. In the early 1990s, it was quite common to follow a “wait-and-see” attitude

or perform only a stereotactic needle biopsy, while today the aim of achieving radical tumor exeresis has become the standard of care. These advances have paved the way to a *personalized treatment strategy* that is going to influence the outcome of brain tumors in the years to come (Weller et al. 2012).

2 Neuro-oncology of Gliomas

2.1 Histology and Molecular Markers

Primary brain neoplasms are quite heterogeneous tumors with a wide spectrum of biological malignancies that depend on multiple factors such as histopathology, genetics, velocity of tumor expansion, and metabolism. Diffuse infiltrating gliomas are by far the most common type of primary brain neoplasms in adults and are classified by grade on the basis of the histopathological and clinical criteria established in 2007 by the World Health Organization (Louis et al. 2007).

GBMs WHO IV are the most invasive subtype and have a dismal prognosis with a median survival time of 14 months (Stupp et al. 2005). Primary GBMs have the highest proliferative activity, and they may grow very quickly; they usually become symptomatic within a few months. On the contrary, *diffuse astrocytomas WHO II* (fibrillary, protoplasmic, and gemistocytic variants) are tumors of astrocytic origin with relatively low proliferative activity. They are observed across all age groups and are associated with relatively longer survival times in the pediatric population and with shorter survival times in older adults. In the adult population, most astrocytomas will ultimately progress to WHO III *anaplastic astrocytomas* and then to “secondary” GBMs. *Diffuse oligodendrogiomas WHO II* are tumors of oligodendrocytic origin with relatively low proliferative activity. Oligodendrogiomas occur with a peak incidence between the third and fifth decades, and they have 79.5 and 63.6 % survival rates, respectively, at 5 and 10 years. They are the first primary brain tumors that can be stratified routinely and consistently by molecular features into two distinct clinical subgroups. Oligodendrogiomas with deletion of chromosome 1p (with or without deletion of 19q) respond well to chemotherapy and are associated with a relatively longer survival time, whereas those in which 1p is intact (with or without 19q deletion) behave more aggressively, show poor response to therapy, and have shorter overall survival times (Louis et al. 2007). The combined loss of 1p and 19q is the most common chromosomal abnormality occurring in approximately 50 % of oligodendrogiomas. *Mixed gliomas* (oligoastrocytomas) exhibit a mixture of astrocytic and oligodendroglial histological morphology and molecular abnormalities. Mixed gliomas with 1p/19q co-deletions have generally longer survival times compared with those without the co-deletion. Astrocytomas, oligodendrogiomas, and

mixed gliomas will ultimately progress to WHO III and then to “secondary” GBMs. The time of progression-free survival (PFS) will likely depend on the chromosomal, genomic, and epigenomic molecular abnormalities of each tumor. It is important to remark that the survival rate depends not only on cytotype and WHO grade but also on the 1p/19q co-deletion status (Marko and Weil 2012).

Another important glioma molecular marker that seems to have a favorable prognostic value is the presence of mutation in the enzyme isocitrate dehydrogenase (IDH) gene. The IDH mutation is commonly present in WHO II and III gliomas as well as in secondary GBMs (Ichimura et al. 2009). On the contrary, primary GBMs frequently carry the wild-type IDH genotype. More studies are in progress with the aim to confirm that IDH-mutated gliomas have longer overall survival in comparison with gliomas carrying the wild-type IDH genotype. It is currently believed that IDH status is important to segregate secondary from primary GBM.

2.2 Pattern of Growth and Velocity of Expansion

Differently from other brain neoplasms, gliomas infiltrate extensively the extracellular space (ECS) in gray as well as in white matter (WM). Like “guerilla warriors,” glioma cells abuse the host “supply” vessels rather than construct their own for satisfying their oxygen and nutrient requirements (Claes et al. 2007). These properties are found in low-grade gliomas (LGG) as well as in GBM, implying that the invasive phenotype is acquired early in oncogenesis. Glioma cells have the capability to migrate and modulate the ECS. Glioma cells may follow different patterns of growth that depend on preexisting host tissue elements. This growth pattern has significant prognostic implications, and it is a major factor in therapeutic failure. Different glioma subtypes may follow different patterns of infiltration that depend upon the “weapons and tools” used by the invading “guerilla cells” and by the interaction with the environmental factors of the host. Glioma cells of a particular subtype may be extremely successful to infiltrate along myelinated fibers of WM tracts (intrafascicular growth), whereas tumor cells of other subtypes may accumulate in the subpial, perivascular, or perineuronal space (Giese and Westphal 1996). Other subtypes preferentially infiltrate the gray matter’s neuropil in specific anatomic regions such as the insular cortex or the supplementary motor area in the superior frontal gyrus (SFG) (Duffau and Capelle 2004). The most extreme example of diffuse infiltrative glioma growth is represented by gliomatosis cerebri, infiltrating multiple lobes, subcortical nuclei, or other anatomic brain regions (Mawrin 2005). The diffuse infiltrative growth pattern is characteristic for both low- and high-grade gliomas (HGG), regardless of their IDH status.

Measuring the spontaneous velocity of diametric expansion at the time of diagnosis may help to predict the evolution of a glioma and the expected overall patient survival. The velocity of diametric expansion is much higher in GBMs than in LGG; the latter have a spontaneous velocity in the range of 2–8 mm/year with a mean of 5.8 mm/year (Pallud et al. 2013). While LGG may continue to grow and infiltrate brain tissue at a stable velocity, GBMs grow fast and usually dislocate or destroy adjacent native brain structures such as WM fasciculi and gyri (Nimsky et al. 2005). We’ll see later how these differences in velocity of expansion may have important implications for the interpretation of functional and MR diffusion imaging data.

2.3 Aims of Brain Tumor Surgery

Despite the high morbidity risks and the high costs, is surgery the best treatment option for patients with a new diagnosis of brain tumor? The role of surgery in the treatment of gliomas is crucial for controlling seizures and determining histopathological and molecular diagnosis. The infiltrative nature of diffuse gliomas and their common localization in the so-called eloquent areas have historically limited the extent of resection (EOR) because of the greater risk of causing permanent neurological deficits. The controversy about the value of surgery in patients with LGG and HGG has not yet been fully resolved. Stereotactic biopsy is associated with a substantial risk of inaccuracy and sampling error. Currently indications for biopsy are very limited in gliomas. Furthermore, biopsy has no therapeutic impact. Despite the lack of phase III study, most recent data strongly argue in favor of achieving a maximal resection of the tumor as the first therapeutic option. Accordingly, there has been a paradigm shift from a surgical approach that relied mainly on anatomical landmarks to one based on the identification of eloquent brain structures. Observational and retrospective studies provide indication that radical surgical resection may offer a survival advantage over stereotactic biopsy and subtotal resections. Different considerations apply to surgery in LGG and HGG.

In the past in LGG, the “wait-and-see” approach was justified by the absence in the literature of prospective randomized controlled clinical trials providing Level I evidence that extensive surgical resection had an impact on the quality of life and overall patient survival (Laws 2001; Laws et al. 2003). In the majority of clinical studies, EOR was not objectively assessed on postoperative MR imaging. Only more recently, authors have begun to include systematic measurement of residual tumor measured on T2-weighted FLAIR and gadolinium-enhanced T1-weighted postoperative MR imaging. Recent clinical studies have demonstrated that EOR correlate with survival times. LGG patients with resection >90 %

had significantly longer overall survival (Smith et al. 2008). In addition, it was recently shown that supratotal resection beyond MR imaging signal abnormalities significantly increased time of PFS (Yordanova et al. 2011).

In patients with GBM, it is an even more open question whether simple debulking is effective or neurosurgeons should strive to achieve maximal cytoreduction. A randomized study demonstrated that elderly GBM patients treated with open craniotomy rather than stereotactic biopsy have longer overall survival times (171 vs. 85 days), but overall benefit of open surgery to patients seemed to be modest, since time of deterioration did not differ between the two treatment groups (Vuorinen et al. 2003). In the past more emphasis has been placed on the role of radiotherapy and chemotherapy than on surgery. More recently, the issue of complete resection as a causal, not only prognostic, factor for overall survival in patients with GBM has been readressed in a randomized phase III 5-aminolevulinic acid (ALA) study. This study investigated 5-ALA-induced fluorescence as a tool for improving EOR and provided a very high fraction of patients with postoperative MR imaging data acquired within 72 h. Residual tumor in postoperative MR imaging was defined as tissue with a volume of contrast enhancement greater than 0.175 cm^3 . Of the 243 GBM patients included in the ALA study, 121 (49 %) had incomplete resection and 122 (50.2 %) had complete resection: the median overall survival was 11.8 months in the former and 16.9 months in the latter group (Stummer et al. 2008). Long-term survivors (>24 months) were almost exclusively among patients of the complete resection group. It is known that neurosurgeons may be less aggressive during resections in the elderly and when the tumor is near critical areas. It was shown that the difference in survival remained stable and significant when patients were restratified according to age (>60 years) in two groups, corroborating a causal effect of EOR on survival independent of age. The difference in survival among the two groups remained stable also when patients were restratified in two groups of patients with or without tumors in eloquent locations. The EOR not only influences survival but also the efficacy of adjuvant therapies. The ALA cohort study provided for the first time Level 2b evidence that in GBM as a single factor survival depends on complete resection of the enhancing tumor. This level of evidence is inferior to randomized studies (Level 1) yet superior to case-control studies (Level 3), case series (Level 4), or expert opinions (Level 5).

In a more recent study (Stummer et al. 2011), it was reported that extended resections performed using 5-ALA carry a greater risk of temporary impairment of neurological function; patients with a greater risk of developing permanent postoperative deficits were those with preoperative symptoms such as aphasia unresponsive to steroids. The reason for preoperative neurological deficits in those patients

was more likely infiltration and destruction of eloquent brain, rather than vasogenic, edema. Thus, permanent neurological deficits in patients may have resulted from resection of fluorescence-marked tumor intermingled with functional eloquent brain tissue. This emphasizes again the importance of identifying the anatomic boundaries of the lesion with presurgical MR tractography and ultimately the functional limits with subcortical IES. EOR has been shown to be an important predictor of overall survival also in a series of 107 patients with recurrent GBM: if gross total (>95 % by volume) resection is achieved at recurrence, the overall survival is maximized regardless of the initial EOR, suggesting that patients with initial subtotal resection may benefit from additional surgery (Bloch et al. 2012).

Detection of functional boundaries during surgery should be achieved with the aid of intraoperative neurophysiology and supported by presurgical fMRI and MR diffusion tractography (Bello et al. 2010). When a temporary deficit is repeatedly elicited with direct subcortical intraoperative electrical stimulation (IES) in the proximity of the wall of the surgical cavity, the functional limits of the resection are reached, and the resection in that part of the tumor should be stopped. Identification of the functional limits is critical especially in gliomas infiltrating the motor system, in particular when the tumor involves the corticospinal tract (CST). There is very low possibility of function compensation in the CST network when fast ($20 \mu\text{m}$ thick) fibers are damaged because the function cannot be transferred to a nearby or distant network (Robles et al. 2008). Other critical networks that if damaged are likely to produce permanent deficits are the inferior fronto-occipital fasciculus (IFOF), the arcuate fasciculus (AF), and the subcallosal fasciculus (SCF) for the language system and the optic radiations (OR) for the visuospatial system. Damage or resection of several other long-range fascicles is likely to induce severe transitory neurological deficits followed by near to complete recovery in a matter of few weeks or months.

Another important parameter to determine is preoperative estimation of the residual tumor volume. Mandonnet et al. computed a probabilistic atlas of glioma residues with preoperative MR imaging data that allowed a preoperative estimation of the expected EOR. The atlas enhances the anatomic regions where the tumor cannot be resected. In their series of 65 patients with LGG, the success rate of the presurgical classification for partial vs. subtotal resection was 82 % (Mandonnet et al. 2007a). The residual volume was underestimated in nine patients with partial resection and overestimated in three patients with subtotal resection. It is remarkable that the regions with the highest probability of residual tumors are essentially located in the WM. Regions with a probability of residual tumor greater than 70 % include the CST, the IFOF, and the AF. Other regions with high percentage of residual tumor were found in the posterior part of

the corpus callosum and the anterior perforated substance. The last two anatomic structures are not considered functionally essential; however, they are either difficult to access or contain lenticulostriate vessels. This study once again outlines the importance of identifying and safeguarding vital vascular and functional structures during tumor resection.

3 Magnetic Resonance Diffusion Imaging Methods

3.1 Conventional MR Imaging

Magnetic resonance imaging (MRI) is currently the method of choice for illustrating the morphology of brain tumors. MRI is very sensitive to the increased water content that is so common in brain tumors. Water accumulation alters the MR signal on T2- and T1-weighted MR images, and it is one of the first macroscopic changes occurring very early in the natural history of the neoplasm. Water accumulation precedes other metabolic and physiologic changes such as elevation of choline, cerebral blood volume (CBV), methionine and glucose uptake, and protein synthesis that are detected, respectively, by proton MR spectroscopy (H-MRS), perfusion MR imaging, and positron emission tomography (PET). MRI accurately defines the size of the mass and its relationship with relevant anatomic landmarks. MRI identifies the presence of blood products and/or abnormal vessels within the mass that may be important for estimating tumor grade. MRI after intravenous contrast agent injection detects breakdown of the blood-brain barrier, a consistent sign of more aggressive behavior related to the presence of angiogenesis and immature vessels.

However, MRI has several limitations. Like in a guerilla war, visualization of the elusive invasive front may be problematic. MR imaging may significantly underestimate the extent of diffuse infiltrative glioma growth. Infiltrating glioma cells can be found at biopsy beyond the hyperintense area on T2/FLAIR images (Ganslandt et al. 2005). Discrimination of infiltrating tumor from vasogenic edema is often difficult. Evaluation of response to therapy may be problematic due to ambiguous and overlapping MR signal changes in pseudoprogression and recurrent tumor, pseudo-response and true response. It has been acknowledged that radiotherapy- and chemotherapy-induced changes may mimic tumor progression.

Finally, one important limitation of conventional MRI is that it is blind to orientation of WM pathways at magnetic field strength of 1.5 T and below. At ultrahigh field strength, the main tracts can be recognized on T2-weighted MR images; susceptibility imaging is a very sensitive method able to detect the orientation of myelinated WM bundles (Duyn 2013; Sati et al. 2013).

3.2 Diffusion Tensor Imaging

Diffusion MR measures the effects of tissue microstructure on the random walks of water molecules (Brownian motion) in the brain. When molecules can diffuse equally in all directions, diffusion is *isotropic*; when they can diffuse preferentially along a specific direction, it is called *anisotropic*. Isotropic diffusion occurs if there are no barriers like in the cerebrospinal fluid or when the barriers are randomly oriented like in the gray matter. Anisotropic diffusion occurs when there are oriented barriers that favor movement of water along rather than across them. In tissues with an orderly oriented microstructure, such as the WM, diffusivity of water varies with orientation since water molecules are likely to encounter different obstacles and barriers according to the direction in which they move (Chenevert et al. 1990; Doran et al. 1990). In WM water diffuses fastest along the principal orientation of the bundles (parallel diffusivity) and slowest along the cross-sectional plane (radial diffusivity). In the WM, the degree of anisotropy depends primarily on membrane density, mainly in the form of intact axonal membranes.

In 1994, Basser et al. showed that the classic ellipsoid tensor formalism could be deployed to measure anisotropy in the human body (Basser et al. 1994). The tensor not only describes the magnitude of the water diffusion but also the degree and the principal directions of anisotropic diffusion. Mathematically the tensor describes the shape of the ellipsoid with three eigenvalues that represent the diffusivities along the three orthogonal axes and three eigenvectors that provide orientation. The three eigenvalues are numbered in decreasing order by magnitude ($\lambda_1 > \lambda_2 > \lambda_3$). DTI is currently the most robust and efficient method to analyze diffusion MR data. DTI has become so popular because it provides several unique insights into tissue microstructure. It quantifies mean diffusivity (MD) and diffusion anisotropy, which are useful indices of WM integrity, with the eigenvector (e_1) providing the orientation information that enables for tractography.

Multiple imaging parameters informative about tissue microstructure can be calculated from a single DTI acquisition. Fractional anisotropy (FA) measures the eccentricity of water molecules' displacement. Anisotropy is found in other body tissues: peripheral nerves, kidneys, and skeletal and cardiac muscles. However neural bundles show the greatest degree of anisotropy, with parallel diffusion on the order of 2–10 times greater than perpendicular diffusion. In the healthy human brain, the intravoxel orientation coherence of WM bundles is probably the most relevant factor affecting FA (Pierpaoli et al. 1996). FA is a scalar value that describes the degree of anisotropy of a diffusion process. FA ranges between zero and one and its values are displayed in gray-scale maps. A value of zero means that diffusion is free or equally hindered in all directions ($\lambda_1 = \lambda_2 = \lambda_3$): the ellipsoid reduces to a sphere. A value of one means that diffusion

occurs only along one direction and it is hindered or restricted along other directions ($\lambda_1 > 0$; $\lambda_2 = \lambda_3 = 0$); the ellipsoid reduces to a line. This means that the diffusion is confined to that direction alone.

FA is a scalar metric that measures the degree of anisotropy, but does not indicate the shape of the diffusion ellipsoid. Voxels with similar FA value may have different shapes (Alexander et al. 2000). When linear diffusivity prevails ($\lambda_1 \gg \lambda_2 = \lambda_3$), anisotropy has the shape of a cigar; when planar diffusivity prevails ($\lambda_1 = \lambda_2 \gg \lambda_3$), it has the shape of a frisbee. While both linear and planar anisotropy coefficients (CL and CP) are responsible for increased FA, their relative values indicate the shape of the ellipsoid. CL specifically highlights the region of tubular tensors, whereas CP indicates regions of planar tensors. We'll see later how anisotropy shape coefficients at the periphery of a mass may provide relevant information about the modality of growth of the lesion and how they may affect DTI tractography.

MD, parallel diffusivity (λ_1), and radial diffusivity ($(\lambda_2 + \lambda_3)/2$) provide information about the integrity of WM bundles. These indices have become quite popular, and they have been particularly used in the evaluation of neurological diseases such as multiple sclerosis, Alzheimer disease, other dementias, and psychiatric disorders.

The orientation of the largest eigenvalue can be color-coded to provide directionally encoded color (DEC) maps. By convention, bundles oriented along the z-axis (craniocaudal) of the MR scanner are displayed in blue, those coursing in the x-direction (right to left) in red, and those coursing in the y-direction (anterior to posterior) in green. DEC maps provide a simple and effective way to visualize orientation information contained in DTI, and they clearly show the main projection (blue), commissural (red), and association (green) WM pathways (Pajevic and Pierpaoli 1999). On DEC maps, it is possible to identify unambiguously the major projection, commissural, and association pathways in the brain of all mammals.

3.3 DTI Metrics and Brain Tumor Microstructure

How do the above parameters relate to changes in tissue microstructure? In imaging protocols for clinical research, the spatial resolution of DTI is usually in the range of $2.0 \times 2.0 \times 2.0$ mm. Despite the relatively low spatial resolution (2–3 mm), DTI is used as a probe to investigate tissue microstructure, and it is sensitive to molecular water displacements on the order of 5–10 μm . There are three main longitudinally oriented structures that could hinder water diffusion perpendicular to neural bundles: (i) microtubules and neurofilaments of the axonal cytoskeleton, (ii) the axonal membrane, and (iii) the myelin sheath surrounding the axons.

Additional confounders are fast axonal transport and streaming and B_0 susceptibility. Multiple studies have shown that there are no major differences in diffusion measurements between myelinated and unmyelinated bundles; thus the axonal membranes are the primary determinant of anisotropic diffusion of water. Therefore, anisotropy should not be considered myelin specific. Notwithstanding, myelin can modulate the degree of anisotropy.

It is more intuitive to correlate changes in parallel and perpendicular diffusivities rather than changes in FA to WM pathological lesions. Injuries with collapse of the axonal membranes are likely to determine a decrease in parallel diffusivity. Myelin loss and axonal increased permeability to water will likely determine an increase in radial diffusivity, despite integrity of the axonal membranes (Beaulieu et al. 1996).

More complex microstructural changes occur in the brain tissue with glioma cell migration and growth. Glioma cells remodel the extracellular matrix by destroying the surrounding tissue through secretion of matrix-degrading enzymes, such as the plasminogen activator and the family of matrix metalloproteinases. In the majority of tumor types, widening of the ECS, changes in cellular size, destruction of axonal membranes, and a general disruption of the normal brain architecture are associated with accumulation of water in large amounts. Studies have shown a dramatic increase in the ECS volume of gliomas even during the early infiltration stage (Zamecnik 2005). These microstructural changes lead to higher water diffusivity (i.e., increased MD) and reduction in diffusion anisotropy (i.e., decreased FA), especially in the early avascular stage of growth that is typical of LGG. The above histopathology changes will likely be associated with minimal decrease in axial diffusivity and variable increase in radial diffusivity due to enlargement of the ECS and glioma cell infiltration. Overall the increased amount of water in the ECS appears to be the dominant factor leading to increased MD and decreased FA. However, the enlarged ECS is not filled with water alone. In LGG a dense network of glioma cell processes may hinder diffusion even of small molecules. In GBM the expansion of ECS is associated with the over-production of aberrant glycoproteins (i.e., tenascin) in the extracellular matrix that not only stabilize the ECS volume but also serve as a substrate for adhesion and subsequent migration of the tumor cells through the enlarged ECS. Tumor invasion in WM will likely interrupt thousands of axons, thus decreasing tissue anisotropy.

Gliomas have a propensity for microscopic infiltration of WM bundles well beyond their macroscopic borders. Microscopic glioma cell infiltration extends outside of the area of T2-signal hyperintensity, and it is typically undetectable by conventional MR imaging. In areas with T2-signal hyperintensity, tumor infiltration may be indistinguishable from peritumoral vasogenic edema that has a similar propensity to diffuse along WM bundles. DTI has been the focus of extensive studies

that have attempted to answer this relevant clinical question that has important therapy implications. Unfortunately, so far DTI results have been remarkably inconsistent on this topic. The degree of peritumoral edema may be highly variable among tumor types; the degree of glioma cell infiltration along WM bundles also may vary considerably, potentially influenced by multiple factors that are playing a key role in extracellular matrix alteration and in ECS volume expansion such as tumor location, biology, and genetics. Despite early reports suggesting that the infiltrating component might be discriminated from tumor-free perilesional vasogenic edema on the basis of DEC maps (Field et al. 2004), this has proven not to be reliable. Price et al. advocate using the isotropic (p) and anisotropic (q) components of the diffusion tensor instead of FA to characterize glioma microstructure. The authors demonstrated that it was possible to differentiate gross tumor from tumor infiltration on the basis of the anisotropic component q , but not necessarily the latter from perilesional vasogenic edema (Price et al. 2006).

Perhaps the partial failure of classic DTI parameters (i.e., MD, FA, parallel and radial diffusivities) to reliably characterize the many types of microstructural changes occurring in gliomas should come as no surprise and raise a specificity issue. FA and the other diffusion imaging parameters are sensitive but not specific enough to detect complex microstructural changes; therefore, future research should focus into more advanced multicompartmental models taking into account the many factors involved (Zhang et al. 2012; Papadogiorgaki et al. 2013).

3.4 MR Tractography

DTI fiber tracking or tractography is a natural extension of diffusion ellipsoid imaging (Conturo et al. 1999; Mori et al. 1999; Basser et al. 2000). It is the process of integrating voxel-wise tract orientations into a trajectory that connects remote brain regions. In WM regions where the fascicles are compact and parallel, the diffusion ellipsoid is prolate. The orientation of the principal eigenvector does not change much from one voxel to the next. We can use a mathematical procedure (algorithm) to generate a trajectory connecting consecutive coherently ordered ellipsoids within the brain, a muscle, or another fibrous tissue. Starting from a “seed point,” voxel trajectories are generated in all directions until “termination” criteria are satisfied. We can choose one seed point and form a tractogram with all streamlines going through that seed point or delineate two ROIs and generate a tractogram with all streamlines connecting those two brain regions. The algorithm makes two important assumptions that are known as the FA and the angle thresholds. Trajectories cannot extend to voxels with relatively low FA (i.e., FA threshold >0.15–0.20) close to background

noise, because the degree of uncertainty of the ellipsoid orientation would become too high. Trajectories are interrupted when in consecutive voxels the angle formed by the intersection of their respective principal eigenvectors is smaller than a set angle (i.e., angle threshold <35–45°), because it is assumed that the majority of WM fascicles do not U-turn. The algorithm aims to find trajectories through the data field along which diffusion is least hindered. The trajectory or streamline is the basic stone of deterministic tractography, and it cannot be divided in smaller units. It has no direct relationship with any biological structure (axon, bundle, or fascicle) even though it reproduces its macroscopic trajectory in 3D space.

Strategies for performing diffusion tractography can be broadly classified into local or global, model based or model-free, and deterministic or probabilistic. Deterministic tractography methods are the most intuitive, and they are based upon streamline algorithms where the local tract direction is defined by the major eigenvector of the diffusion tensor as described above (Conturo et al. 1999; Mori et al. 1999). Mathematically a streamline can be represented as a 3D-space curve, as described by Basser et al. (2000). One limitation of the deterministic method is that any errors in calculations of the streamlines will be compounded as the streamline progresses from the seed to the termination point. The accuracy and variance of the tract reconstruction is a function of the algorithm, the signal-to-noise ratio, the diffusion tensor eigenvalues, and the tract length.

Limitations of fiber tracking performed with the streamline approach motivated the development of probabilistic tracking algorithms (Jones 2008). The aim of probabilistic tractography is to develop a full representation of the uncertainty associated with any assumption that might be made. Given a model and the data, probabilistic tractography provides a voxel-based map of high and low confidence (values given in percentage) that the trajectory of least hindrance to diffusion will connect the seed with the target point. From a mathematical point of view, the assumptions and the comparisons that can be made in studies across individual subjects and groups are more complete and flexible with probabilistic than with streamline tractography. Notwithstanding, streamline tractography is easier to implement in clinical practice, and its more intuitive approach has contributed to its popularity among neuroanatomists and neuroradiologists.

A DTI tractography atlas for virtual in vivo dissection of the principal human WM tracts using a deterministic approach has been recently published (Catani and Thiebaut de Schotten 2008). The greatest success of fiber tracking is its use for in vivo dissection of major WM fascicles in individual healthy and pathological human brains. Tractography is also of value for segmenting WM pathways and providing quantitative measurements for comparison across subjects or groups.

3.5 Limitations of DTI and MR Tractography

The tensor is the most robust diffusion model; however, it has several limitations when it is applied to brain WM. DTI provides two types of new contrasts, diffusion anisotropy and fiber orientation, which carry rich anatomical information about WM complexity. However, when interpreting MR diffusion data, it is very important to understand well the inherent limitations of each method: (a) MR diffusion measurements are very sensitive to noise, motion, and brain pulsatility and therefore to scanning time. (b) Diffusion anisotropy carries information at the microscopic cellular (protein filaments and microtubules, cell membranes, and myelin) and macroscopic (vessels, glial cell networks, and population of bundles with different orientations) level that is averaged over a relatively large voxel volume. Partial volume effects may become a problem in WM regions with more than one bundle such as the paraventricular zones, where FA is low and the degree of uncertainty in the estimation of bundle orientation increases. (c) DTI does not measure any specific parameter for the intra-axonal restricted water pool. (d) The calculation of the tensor assumes that fiber structures are homogeneous within a voxel, but this assumption is not true when there are two fiber populations; therefore one orientation cannot represent accurately the orientations of two fiber populations. There are two strategies to reduce this problem: increase spatial image resolution by reducing the voxel size or extract information with higher angular resolution from each voxel and abandon the simple tensor model. (e) DTI-based tractography algorithms cannot determine if bundles are crossing or kissing. (f) MR diffusion cannot differentiate the directionality of axons within bundles. (g) At the spatial resolution currently used in clinical MRI, diffusion cannot track streamlines through the gray matter; thus, it cannot track the trajectories of WM bundles to their cortical terminations.

One of the major limitations of the classic tensor model is that for each voxel it provides only a single fiber orientation: this is a major obstacle for tractography and connectivity studies. Using spherical deconvolution methods with a spatial resolution of $2 \times 2 \times 2 \text{ mm}^3$, it has been estimated that the proportion of WM voxels containing more than one bundle (crossing fibers) is about 90 % (Jeurissen et al. 2013). These findings suggest that the DTI model may be inadequate to measure the complexity of fiber trajectories in the WM.

In voxels with more than one fiber population, the orientation measured with classic DTI is the average of the orientations of all bundles present in that voxel. As a result in voxels with crossing fibers, the shape of the diffusion ellipsoid may appear either prolate or oblate. A prolate (stretch out, linear) object has the shape of a spheroid generated by an ellipse rotating about its longer axis with the polar radius

much greater than the equatorial radius ($\lambda_1 > \lambda_2 = \lambda_3$), while an oblate (flatten, planar) object has the shape of a spheroid generated by rotating an ellipse about its shorter axis with the equatorial radius much greater than the distance between the poles ($\lambda_1 = \lambda_2 >> \lambda_3$). A geometric analysis of DTI measurements in the human brain using a three-phase tensor shape diagram demonstrated that there is a tensor shape hierarchy between different WM tracts in the order of commissural, deep projection, and association WM tracts (Alexander et al. 2000). The CC and the CST show the greatest linear shape, while the AF and the subcortical WM tracts show a significant planar component of their tensor measurements. The causes of planar diffusion in the brain are not perfectly understood. Bundles arranged in sheets could explain planar diffusion (Wedgeen et al. 2012); however, a more likely origin is the presence of crossing WM tracts within the large voxels typical of the DTI experiment. The linear shape of CC and CST may outline the compacted nature of the bundles in the central segment of those tracts, whereas the planar shape of the AF at the level of the centrum semiovale may reflect that most voxels contain AF and CC crossing fibers.

The shape of the diffusion ellipsoid of the voxels in the proximity of a focal lesion can be affected by mass effect. Especially in voxels near the borders of fast-growing gliomas, the ellipsoid can become oblate with undefined principal orientation. It is important to evaluate the shape of the ellipsoid when interpreting tractography results in the proximity of a mass, because it might provide a warning sign about false-positive results. Oblate voxels are confusing for tractography because the difference between λ_1 and λ_2 is minimal and noise will cause the principal eigenvector to have random orientation in the plane: tracking might go either way in oblate voxels.

Detection of WM bundles within a tumor and surrounding areas of vasogenic edema may be also problematic. IES has detected the presence of functioning WM tracts within areas of T2-signal hyperintensity at least in LGG. It is assumed that a significant number of electrically competent and signal conducting axons are preserved despite infiltration by glioma cells. Tumor infiltration alters MR diffusivity along WM bundles, and it may distort their geometry. The increased free water content may artificially decrease FA, thus leading to false-negative results if FA decreases below the FA threshold that is commonly used for tractography and to false-positive results due to increasing degree of uncertainty in estimating the orientation of the principal eigenvector. DTI studies have shown interruption of streamlines inside the tumor or areas of vasogenic edema, especially when FA threshold was set at >0.15 (Bastin et al. 2002; Bizzi et al. 2012). This issue raises a sensitivity issue for MR tractography with a relative high rate of false-negative results in areas of decreased FA, high diffusivity, and T2 hyperintensity that are especially common in LGG. Other authors have validated

with IES the tractography findings obtained with FA threshold (>0.10) through regions of tumor infiltration (Bello et al. 2008). An alternative approach is to use advanced diffusion multicompartmental models such as neurite orientation dispersion and density imaging (NODDI) method (Zhang et al. 2012) that will be discussed in detail in the next section. NODDI is a practical high angular resolution diffusion imaging (HARDI) method with two shells for estimating the microstructural complexity of dendrites and axons *in vivo* on clinical MRI scanners. NODDI allows separation of the restricted intra-axonal from the isotropic and hindered compartments and provides estimates of two parameters that are more specific than FA: neurite density and orientation index.

3.6 Crossing Fibers and the Need for Advanced MR Diffusion Imaging Methods

It is important to understand well the limitations of MR tractography, especially when the method is applied in the interest of neurosurgical patients. Tractography can determine the trajectories of major WM fascicles, but it cannot infer in which direction the signal is transmitted along each pathway. It cannot track streamlines to their cortical termination, and it may fail at fiber crossing because the DTI model can recover only a single fiber orientation in each voxel. It is a user-dependent method based on *a priori* anatomic knowledge. It is also important to be aware that tractography does not provide functional information. IES is the only method able to test WM function and generate a subcortical functional map that has proven to maximize tumor resection and minimize hazards.

The ambiguity in determining fiber orientation in a voxel containing more than one fascicle is related to the model applied with DTI, but it is not a limitation of diffusion MRI in general. DTI models the dispersion of water molecules using a Gaussian distribution; thus, the assumption is that the scatter pattern during the diffusion time has an ellipsoid shape. Voxels contain hundreds of thousands of axons that are organized in bundles and fascicles that can have a wide range of complex configurations. The fibers within each voxel may be parallel, fanning, bending, and crossing at an acute or perpendicular angle. DTI is accurate to represent parallel fibers, but it cannot distinguish them from fanning and bending fibers, except for a lower FA value. In voxels with crossing fibers at an acute angle, the principal orientation measured with DTI is misleading, as the mean fiber orientation that has a prolate shape does not correspond to the direction of any fiber. In voxels with orthogonal crossing fibers, DTI fails to identify the two fascicles, and its best approximation is an oblate ellipsoid that contains none of the useful directional information.

In the past decade, there has been a lot of effort to move beyond DTI and solve the crossing fiber problem.

Development of new models and algorithms that exploit more sophisticated imaging acquisition schemes such as HARDI has been addressed (Seunarine and Alexander 2009). The field is very complex, and a detailed description of the many advanced methods goes beyond the purpose of this chapter.

Model-based approaches, such as the multi-tensor model, resolve fiber crossing by modeling distinct fiber populations separately. The model-based approaches assume that the voxel contains distinct populations of fibers and that diffusing molecules do not exchange between fiber populations. The multi-tensor model is a generalization of DTI that replaces the Gaussian model with a mixture of Gaussian densities. The “ball-and-stick” model assumes that water molecules belong to one of two populations: an isotropic component that does not interact with fibers and diffuses freely in the voxel and a restricted component that diffuses inside and immediately around axons (Behrens et al. 2003). The composite hindered and restricted model of diffusion (CHARMED) proposed by Assaf describes the restricted fiber population with a cylinder and the hindered population in extracellular space with an anisotropic Gaussian model (Assaf et al. 2004). The model-based methods do not naturally distinguish fanning and bending configurations from parallel fiber populations.

The aim of nonparametric methods is to estimate from diffusion MRI measurements the fiber orientation diffusion function (fODF) that provides more insight into the underlying fiber configuration. These methods do not rely solely on parametric models of diffusion, but try instead to reconstruct the fODF without placing modeling constraints on its form. Diffusion spectrum imaging (DSI) and Q-ball imaging reconstruct a function called the diffusion orientation distribution function (dODF). Spherical deconvolution (SD) methods recover a more direct estimate of the fODF.

DSI attempts to measure the scatter of diffusion directly and makes no assumptions about tissue microstructure or its shape (Wedgeen et al. 2008). The acquisition requirements are the major limitations of DSI: standard protocols require long acquisition times with 500–1,000 measurements at the expense of image resolution; stringent hardware with very strong gradients is required in order to apply very short pulses. The acquisition requirements in Q-ball imaging are more manageable than DSI. In his original work, Tuch showed that Q-ball can resolve fiber crossing consistently using an acquisition scheme with 252 gradient directions at a $b=4,000 \text{ s mm}^{-2}$ (Tuch 2004), although the approximation of the dODF introduces some blurring, which may reduce angular resolution and precision of peak directions.

The SD algorithm has the advantage of relatively short acquisition times, which are close to standard DTI clinical protocols, reduced computational times compared to some of the other methods, and the ability to resolve crossing fibers with a good angular resolution (Dell’acqua et al. 2010). SD is based on the assumption that the acquired diffusion signals

from a single voxel can be modeled as a spherical convolution between the fiber orientation distribution (FOD) and the fiber response function that describes the common signal profile from the WM bundles contained in the voxel (Tournier et al. 2004). A major limitation of SD is its susceptibility to noise, which often results in spurious peaks in the recovered FODF. Acquisition requirements are compatible with clinical protocols: 64 directions with $b=2,000\text{--}3,000\text{ s mm}^{-2}$ with a total scan time of 16 min. DTI and SD reconstructions can be obtained from the same dataset.

NODDI combines a three-compartmental tissue model with a two-shell HARDI protocol optimized for clinical feasibility. NODDI adopts a tissue model that distinguishes three types of microstructural environment: intracellular (restricted), extracellular space (hindered), and cerebrospinal fluid (isotropic) compartments (Zhang et al. 2012). Each environment affects water diffusion in a unique way and gives rise to a separate normalized MR signal. The intracellular compartment refers to the space bounded by the membrane of neurites, and it is modeled as a set of sticks. NODDI provides measurements of several parameters, among which the two most innovative are neurite density and an index of orientation dispersion that defines variation of neurites orientation within each voxel. These parameters have great potential to provide relevant information for brain tumor tissue characterization and may be particularly efficient to track fibers in voxels with an increased amount of water such as those with vasogenic edema and glioma infiltration. From the same HARDI acquisition, tractography can be performed using the SD algorithm, the NODDI, or the DTI model.

3.7 Clinically Feasible Brain Mapping Imaging Protocols and Preprocessing Requirements

In order to achieve a state-of-the-art tractography study, it is mandatory to acquire diffusion data with relatively high spatial and angular resolution. High spatial resolution plays in favor of tractography because it reduces the gap in size between voxels and fascicles. High angular resolution increases the discrimination of crossing fascicles at an acute angle. Unfortunately, improved spatial resolution always comes at the expense of longer acquisition times and lower signal-to-noise ratio. It is important to verify the capability of the MR unit in order to reach a good compromise between spatial resolution, signal-to-noise ratio, and total acquisition scan time. In clinical practice with a 1.5 or even better a 3.0 T MR unit, the isovolumetric voxel size should be in the range of 1.5–2.0 mm. One common strategy to improve the angular resolution and the signal-to-noise ratio of the HARDI acquisition scheme is to acquire a dataset with 32 or 64 gradient directions and a b-value in the range of 1,500–3,000 s mm^{-2} .

MR units with strong gradients (high maximum amplitude and fast slew rate) are beneficial to keep the TE to a minimum value. Especially if fMRI is also acquired, scan time inferior to 20 min is recommended in order to keep the total study session inferior to 45 min.

DEC maps are very useful for preliminary interpretation of clinical studies in patients with disease, especially when used by experienced users. Low angular resolution DEC maps can be acquired with DTI acquisitions that use a minimum of 6 gradient directions and b-value of 800 s mm^{-2} ; however, the examiner should be aware that performing tractography with a low-quality dataset may increase the likelihood of errors.

For NODDI acquisition scheme, the following imaging parameters are recommended: two shells (b value of 700 and 2,000 s mm^{-2}) with similar TR and TE and, respectively, 20 and 64 gradient directions will result in a total scan time of about 20 min.

Clinical MRI diffusion studies are performed by acquiring single-shot echo-planar images (EPI) with diffusion-sensitizing gradients of different strengths and orientations that are applied for a relatively long time in order to achieve the desired b-value. EPI readout is very sensitive to static magnetic field (B_0) inhomogeneity that produces nonlinear geometric distortion primarily along the phase-encoding direction. Susceptibility artifacts are more pronounced at air-tissue interfaces and are most obvious in the orbitofrontal and mesial temporal regions, near the sphenoid sinus and the temporal petrous bone. In addition, patient bulk motion and additional image distortion induced by eddy currents, which do not cancel out when diffusion gradients are applied for a relatively long time, cause additional artifacts on DWI. Analysis of diffusion imaging studies requires correction for patient motion and for susceptibility and eddy current artifacts. The many acquired DWIs have to be spatially aligned to avoid systematic errors in the parametric maps computed from misaligned DWI (Rohde et al. 2004). Several software are available for correcting DWI artifacts and confounds (Jenkinson et al. 2012; Leemans et al. 2009; Pierpaoli et al. 2010). Their use for preprocessing of DWI is strongly recommended in order to obtain reliable DTI measurements.

In March 2012, the American Society of Functional Neuroradiology (ASFNR) has released a document with guidelines for clinical application of DTI that is available on their website (www.asfnr.org/docs/ASFNR_Guidelines-for-DTI.pdf).

4 Current Theories About Structural Connectivity of Eloquent Functional Systems

The central nervous system consists of several discrete functional systems. There are systems in charge of processing special somatic sensations coming from the outside world:

visual, auditory, tactile, and vestibular systems. Other systems are specialized in processing visceral input: the olfactory, gustatory, and limbic systems. These systems are organized in primary sensory and unimodal cortical areas that will exchange information. These systems converge to the so-called multimodal areas that are located in the associative cortices of the parietal, temporal, and frontal lobes. In addition, there are systems responsible for purposeful movement that will plan for action and coordinate and execute the motor programs.

Virtually all complex systems form networks of interacting components composed of multiple and redundant neural circuits that process and transfer the information either serially or in parallel. A network is made of a group of elementary macro (or micro) components that are closely connected and work as a team. At the macroscale level, nodes and pathways are the basic components. Neurons, dendrites, axons, and synapses are the components at a microscale level. Understanding such complex systems will require knowledge of the ways in which these components interact and the emergent properties of their interactions. Network science does quantitative analysis of different aspects of connectivity that are peculiar of a complex system (Sporns 2014). The motor, language, and visuospatial systems may share similar elementary components; however, their networks display peculiar different and organized patterns.

Each network of a system is dedicated to a specific sensory, motor, or cognitive modality, and it includes several specialized nodes that have different roles in processing information. The cortical regions containing neurons that receive most of their information directly from the thalamus are called primary sensory areas. The distance from the body sensory receptors at the periphery defines secondary and tertiary cortical sensory areas. These are unimodal and multimodal association areas that play an important role in integration and modulation of the input signals reaching the cortex and in planning of motor actions. Secondary motor areas located in the supplementary motor area (SMA) and in the ventral and dorsal premotor (PMv and PMd) cortex compute programs of movement that are conveyed to the primary motor cortex (M1), the area containing cortical neurons that project directly to the spinal cord.

The organization of the main functional systems follows several principles. The information conveyed within each network is processed and transformed at every node level. Information may be amplified, attenuated, and integrated with information conveyed from other nodes of the same system. There are two main groups of neurons at each stage of information processing: projection neurons and local interneurons. In most mammals, the anatomy of the main brain's fascicles is similarly organized. The axons of projection neurons convey the information to the next node stage in the system. Each brain structure may contain nodes of several functional systems. Axons leaving a node of a functional system are bundled together in a fascicle that projects to the

next node. Bundles belonging to different networks and systems can course temporarily within the same fascicle. Along the course of a fascicle, short and long bundles may enter and exit at various locations. The nodes of the sensory and motor systems have a somatotopic organization that is repeated throughout the network. In this way, an orderly neural map of information is retained at each successive level of processing in the brain. Visual, auditory, somatosensory, and motor maps are built at different stages of their respective networks.

Most functional systems are hierarchically organized. In the primary visual cortex, an individual neuron may fire only when it receives the signal input from a very specific outside stimulus. Following the same principle, multiple neurons in the primary visual cortex converge on individual cells in the association cortical areas. At very advanced stages of information processing in the cortex, individual neurons are responsive to highly complex information.

Most WM pathways are bilaterally represented, and they are often symmetrical in volume and length, with only few exceptions (Thiebaut de Schotten et al. 2011b). A statistically significant *leftward* asymmetry was found with DTI for the volume and number of streamlines of the CST and the direct (frontotemporal) segment of the AF, connecting Broca and Wernicke territories (Catani et al. 2005). A statistically significant *rightward* asymmetry was found for the IFOF and the anterior (frontoparietal) segment of the AF. Furthermore, gender differences were found with females having a more bilateral distribution of the AF long segment than males (Catani et al. 2007). Most ascending and descending pathways cross over to the contralateral side of the brain or spinal cord. Pathways of different systems cross at different anatomical levels within the brain.

Compact and large fascicles can be seen at brain gross dissection with the naked eye. Prominent neurologists started to describe the main WM fascicles of the human and monkey brain in the nineteenth century (Dejerine and Dejerine-Klumpke 1895). Fascicles are classified in three main groups according to their orientation and function: projection, commissural, and association. Projection fascicles are coursing in the corona radiata, fornix, and OR: the descending pathways connect the cortex with the thalamic, basal, and brainstem nuclei and spinal cord, while the ascending pathways connect sensory receptors and neurons of the spinal cord with neurons in the brainstem, thalamus, and cortex. The OR connect the lateral geniculate nucleus with the homolateral primary visual cortex. The two most relevant commissural pathways are the corpus callosum and the anterior commissure (AC). The corpus callosum carries fascicles connecting homologous areas of the cerebral cortices of both hemispheres. The AC connects homologous areas of the anterior and ventral temporal lobes, including the amygdala and the olfactory bulbs. Seven major association fascicles have been described in the human brain with postmortem dissecting

methods and in vivo DTI: superior, middle, and inferior longitudinal fascicles, AF, IFOF, uncinate fasciculus (UF), and the cingulum. There are several tractography atlases describing the fiber tracking methods used to identify the main fascicles of the human brain (Catani and Thiebaut de Schotten 2008).

Virtually all systems require the integration of distributed neural activity. Network analysis of human brain systems has consistently identified regions called “hubs” that are critically important for enabling efficient neuronal signaling and communication (van den Heuvel and Sporns 2013). Hub nodes mediate many of the long-range connections between brain modules and are efficiently interconnected to form a “rich club” (van den Heuvel and Sporns 2011). The high level of centrality of brain hubs also renders them points of vulnerability that are susceptible to disconnection and dysfunction in brain disorders. It has been shown that in many neurological diseases, focal lesions are concentrated in the highly connected hubs of the human connectome (Crossley et al. 2014). Lesions may be concentrated in hubs purely because of their greater topological value. Some diseases might affect brain regions with uniform probability but lead to symptoms when the lesion happened to damage a hub. Regarding presurgical mapping for brain tumor surgery, it is important to describe the relationship of the tumor with critical hubs and long-range connections because these are crucial components of eloquent systems. In the following sections, the functional organization of three eloquent systems that are clinically relevant for presurgical mapping is addressed.

4.1 Motor System

The task of the motor system is to maintain performance of basic functions such as balance, posture, locomotion, reaching, and communication through speech and gesture by moving body parts, limbs, and eyes. The motor system produces movement by translating neural signals into contractile force in muscles. The agility and dexterity of an athlete or of a piano player reflect the capabilities of his/her motor system to plan, coordinate, and execute motor programs that have been learned and practiced many times until they can be executed automatically for the most part.

According to modern theories, the motor system acts as a distributed network. The neurons of origin of the network are located in at least five distinct cortical areas of each hemisphere: M1, PMv, PMd, prefrontal, and parietal areas. According to their targets, the descending fibers are divided in four groups: the ventromedial and dorsolateral brainstem pathways, the corticobulbar tract, and the CSTs (Lemon 2008). It is important to emphasize that the CST originates from cortical areas that have different functions: M1, PM, SMA, the cingulate motor area, the primary somatosensory cortex (S1), the posterior parietal cortex, and the parietal

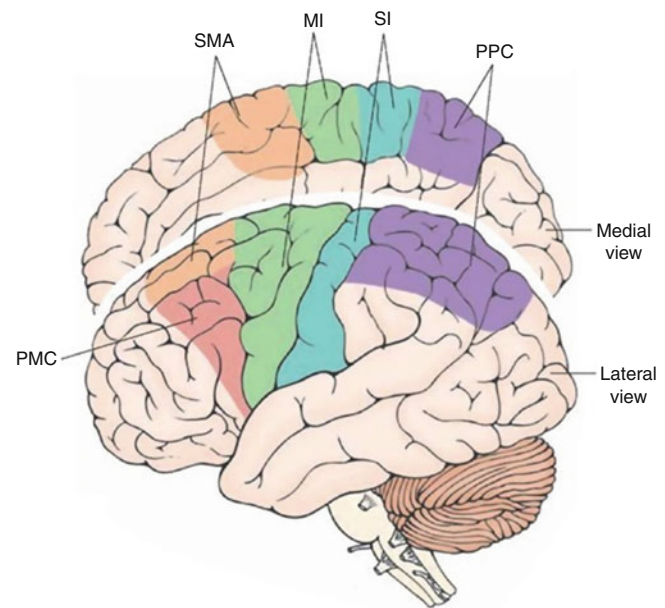


Fig. 1 The corticospinal tract arises from the M1, S1, SMA, PMd, and PMv. Approximately 49 % of the one million axons arise from M1 and 21 % from S1. The remaining 30 % of the fibers originate from the PMc, the region immediately rostral to the precentral gyrus: 19 % arises from the SMA, 7 % from the PMd, and 4 % from the PMv. The descending axonal projections converge in the corona radiata and then enter the internal capsule, maintaining a somatotopic distribution: corticobulbar fibers are located within the genu and corticospinal fiber in the middle third of the posterior limb of the internal capsule with the face-hand-foot represented in the anterior-posterior direction. The PPC does not contribute to the CST but modulates its activity. The axon of the corticospinal tract arise from motoneurons in the cortex of premotor dorsal and ventral (PMc), supplementary motor area (SMA), primary motor (M1) and primary somatosensory (S1) (Modified from <http://what-when-how.com>)

operculum. M1 contains the greatest density of neurons, giving rise to CST and corticobulbar tract. The human CST consists of about one million axons, of which about 49 % originate in the M1, 19 % in the SMA, 21 % in the parietal lobe (S1 and posterior parietal cortex), 7 % in the PMd, and 4 % in the PMv (Fig. 1). The axonal projections of the cortical motor neurons converge in the corona radiata, a fanlike array of descending and ascending fibers connecting the cortex with thalamus, basal nuclei, and spinal cord. More ventrally, the descending tracts enter the internal capsule maintaining a somatotopic distribution: fibers originating from PMv, PMd, and SMA and prefrontal fibers originating from the frontal eye field areas course in the anterior third of the posterior limb, whereas the fibers originating from M1 course in the intermediate third. In the midbrain, the fibers of the corticobulbar tract and CST become even more compact and enter the cerebral peduncles. At this level, the frontal projections are located anteromedially, while tracts originating in the parietal, temporal, and occipital lobes are located more laterally in this order. In the pons, the tracts course between the transverse pontine fibers, before beginning to

cross to the contralateral side in the decussation of the pyramids at the level of the medulla oblongata. This contingent of the CST courses along the lateral columns of the spine. However, about 10 % of the fibers of the CST continue their journey to the spine in the ipsilateral anterior columns and will cross side only when they reach their target. The CST terminates widely within the spinal gray matter, presumably reflecting control of nociceptive, somatosensory, reflex, autonomic, and somatic motor functions. These peculiar features explain why a single neuroanatomical pathway can mediate multiple functions (Lemon and Griffiths 2005).

There are striking differences across species in the organization of the descending pathways and in particular of the CST. Some higher primates have unique direct projections to spinal motor neurons that bypass part of the integrative mechanisms of the spinal cord in order to generate motor output. Tracing studies with retrograde transneuronal transport of rabies virus from single muscles in rhesus monkeys have identified cortico-motoneuronal cells located in the caudal region of M1 that is buried in the central sulcus. This area is the lowest threshold site within M1. These cortico-motoneuronal cells make monosynaptic connections with motor neurons in the spine (Rathelot and Strick 2009). The cortical territories occupied by cortico-motoneuronal cells for different muscles overlap extensively within this region of M1. These findings are against a focal representation of single muscles in M1 and may represent a resource for neuroplasticity. The axons originating in dorsal M1 may have connections with other muscles in addition to the one injected with the rabies virus. Thus, the overlap and intermingling among the different populations of neurons may be the neural substrate to create a wide variety of muscle synergies (Rathelot and Strick 2006). The extent of CST projections from cortico-motoneurons in this newly recognized M1 area correlates with index of dexterity, skilled use of hands and digits across species. Recent studies suggest that the monosynaptic cortico-motoneuronal system is related to voluntary control of relatively independent finger movements. In patients with a brain tumor growing in the proximity or infiltrating the CST, preservation of the axons originating from M1 monosynaptic neurons is mandatory in order to maintain highly skilled movements.

The CST also carries M1 axons that form synapses with interneurons in the spinal cord. This indirect pathway is more rostral, and it is important for coordinating larger groups of muscles in behaviors such as reaching and walking. The motor information provided by the cortico-motoneuronal system via the CST is significantly modulated by information originated in secondary cortical motor areas. It has been shown in the macaque that electrical stimulation of the PMv could produce powerful stimulation of the M1 outputs in the spine, which may represent an important parallel route through which a secondary motor area could exert

its motor effects (Cerri et al. 2003). In addition, the output of M1 is under the influence of motor regions located in the thalamus, basal nuclei, and cerebellum. The activity of these subcortical structures is also very important for smoothly executed movements.

Mapping of the CST in the operating room is not a trivial procedure. Subcortical IES of the CST with the 60 Hz bipolar probe evokes the unnatural and synchronous stimulation of many fascicles together that may well exert mixed excitatory and inhibitory effects on target neurons. On the contrary, IES with the monopolar probe is capable to discriminate the different components of the CST for brain surgery (Bello et al. 2014).

In summary, information in the motor system is processed in a variety of discrete networks that are active simultaneously. In the particular case of the CST, the signal-carrying motor information is conducted along fibers originating in different parts of the network and converging within the CST that carry them to a common target in the brainstem or in the spinal cord.

For the many different functions it carries, the CST is probably the most complex and important pathway of the entire human brain. For sure it is the most important and eloquent structure that must be safeguarded in brain surgery. Lesions along the CST cause a pyramidal disconnection syndrome with neurological signs that vary according to lesion location and the interval from time of onset. Motor deficits can range from hemiparesis to hemiplegia. Lesions cause a breakdown in fine sensorimotor control of the extremities, implying a deterioration not only in motor function but also in the capacity to interrogate correctly the sensory feedback from the limb (Lemon and Griffiths 2005). Implicit in modern concepts of a distributed motor network is that neurological signs resulting from lesions to a descending pathway cannot be interpreted any longer as simply being due to the removal of the lesioned pathway. Soon after an acute focal lesion has damaged the CST, activity-dependent, fast neuroplastic changes occur such as that the clinical outcome is a consequence of compensatory changes of the motor network as a whole, including the response of uninjured fibers.

4.2 Language System

Complex cognitive behaviors such as language are more difficult to localize in the brain than motor and sensory functions. Language is the most accessible part of the mind. Language allows people to communicate using a highly structured stream of sounds. Language emerges spontaneously in all children of the human species, and it has a universal design that is based on two components: *words* and *grammar*. A word is an arbitrary association between a sound and a meaning. Grammar has three subsystems: *morphology*

defines the rules for combining words and affixes in larger words; *syntax* consists of rules for combining words into phrases and sentences; and *phonology* consists of rules combining sounds into a consistent pattern that is characteristic of a specific language.

Interest in the human ability to process speech and language dates back to at least three millennia ago at the time of the Greek philosophers. However, it was only with the invention of the “lesion method” by Paul Broca in 1861 that man began to explore the brain anatomy of language. Knowledge about the neural basis of language processing accelerated 130 years later with the advent of advanced brain imaging methods and neurophysiology (Price 2010; Friederici 2011). In the last decade, the classic theory of language localization proposed by Wernicke and Geschwind has been intensely revised thanks to the large amount of imaging data collected with neurophysiology (event-related potential, magnetoencephalography, and IES) and neuroimaging (fMRI and DTI). In the years to come, neurosurgical patients will provide an important source of new data, especially now that mapping of brain function before and during removal of a focal lesion is recommended according to state-of-the-art medical practice guidelines.

The clinical-anatomical postmortem studies performed in aphasic patients by the neurologists of the nineteenth century paved the way for three important discoveries. First, it was found that language is strongly lateralized to the left cerebral hemisphere. Recently, it was confirmed with fMRI that language is lateralized to the left in about 96 % of right-handed subjects (Pujol et al. 1999). Only 4 % of right-handed individuals show a symmetric blood oxygen level dependent (BOLD) response during a language task. The BOLD response is also lateralized to the left in about 76 % of left-handers; it is symmetric in 14 % of them, whereas it is lateralized to the right side in the remaining 10 %. The asymmetry of the language network has been demonstrated also with deterministic DTI tractography: the direct AF segment connecting Broca with Wernicke territories is found only on the left side in 62 % of right-handed healthy subjects; it is bilateral but left lateralized in 20 % and symmetric only in 17.5 % of subjects (Catani et al. 2007). Second, the early studies showed that three different aphasic syndromes were associated with damage to three specific brain structures: (i) *Broca aphasia* with damage to pars opercularis of the inferior frontal gyrus, (ii) *Wernicke aphasia* with damage to the posterior part of the superior temporal gyrus, and (iii) *conduction aphasia* with damage to the AF that was thought to be a unidirectional pathway carrying information from Wernicke to Broca area. The third important discovery was that both Wernicke and Broca areas were presumed to interact with heteromodal high-order associative areas in the frontal, parietal, and temporal lobes.

In the first anatomic model of language proposed by Wernicke in 1874, there were two cortical centers: one was

dedicated to speech production (Broca area in the posterior half of the IFG) and the other to auditory comprehension (Wernicke area in the posterior STG). Wernicke thought that the two centers were indirectly connected by fibers passing through the external capsule and relaying in the insula. It was Dejerine that proposed that the AF was connecting directly the two centers. The classic model was later modified by Geschwind in 1970 who emphasized the importance of a third cortical center located in the angular gyrus (Geschwind 1970).

Recent studies in patients with stroke, head injury, and neurodegenerative diseases (i.e., Alzheimer and frontotemporal dementia) have uncovered other cortical and subcortical regions that belong to the language network. Patients with damage to the left temporal pole (Brodmann area, BA38) may have difficulty in retrieving names of unique places and persons but can retrieve names of common things. With damage to the midportion of the left MTG (BA20 and BA21), patients have difficulty in recalling both unique and common names, without any associated grammatical and phonemic deficit. Damage to the posterior part of the left inferior temporal gyrus (BA37) instead causes a deficit in recalling words of tools and utensils. The precentral gyrus of the left insula is another language-related area that was not included in the classic models. Patients with stroke lesions in the anterior insula show articulatory planning deficits: a difficulty in pronouncing phonemes in their proper order (Dronkers 1996). Other two areas that are recently considered part of the language network are located in the mesial surface of the frontal lobe. The SMA in the left SFG and the left anterior cingulate cortex (BA24) play an important role in the initiation and maintenance of speech. Damage to these areas, especially after surgery, is often associated with akinesia and mutism, leading patients to fail to communicate by words, gestures, or facial expression. These patients usually recover within a few days (Krainik et al. 2003).

Aphasias are classified in three major syndromes and few subsyndromes. In *Broca aphasia*, the damaged network is involved in both the assembly of phonemes into words and the assembly of words into sentences. The network is thought to be concerned with relational aspects of language, which include the grammatical structure of sentences and the proper use of verbs. The cortical areas damaged in Broca aphasia are frontal BA44, BA45, BA46, and BA47, parietal areas BA39 and BA40, and the insula. In *Wernicke aphasia*, the damaged network is involved in generating speech sounds and in associating the sounds with concepts. Wernicke area is no longer considered the center of auditory comprehension as it was conceived in the Wernicke-Geschwind model (Geschwind 1970). Aphasic patients with lesions in the posterior third of the STG and MTG (BA22) often shift the order of individual sounds and make frequent phonemic paraphasias. These patients also make semantic paraphasias that are errors in selecting words with substitution of one full word with

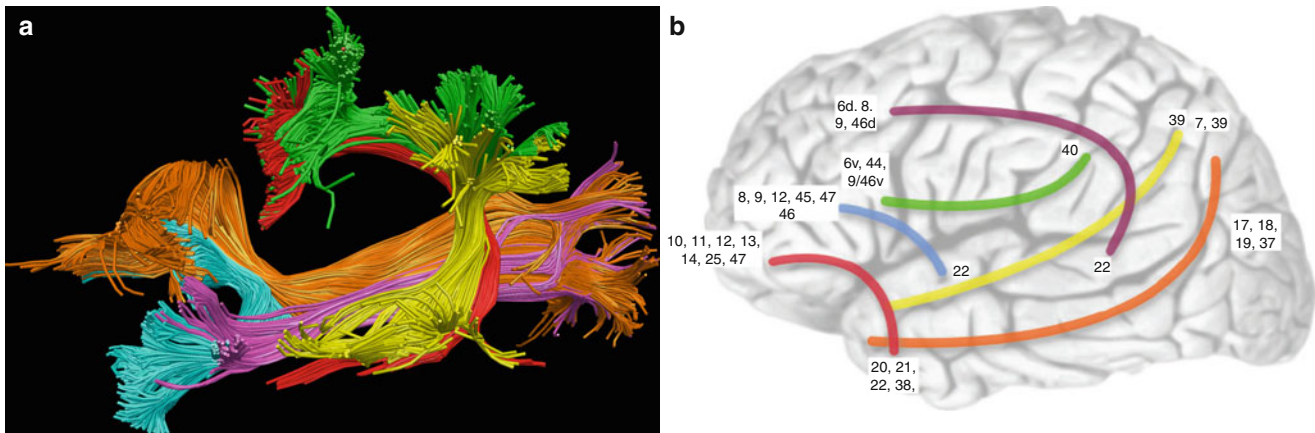


Fig. 2 (a) Modern theories about language have recognized that there is a lot of network redundancy in the system. Several models have been proposed, with some differences in connectivity, but all models acknowledge the importance of a dual-stream system with dorsal and ventral networks. The models that are heavily influenced by humans DTI and postmortem blunt fiber dissection methods suggest as many as five pathways relevant for language: the direct segment of the AF (red), the posterior segment of the AF (yellow), and the third segment of the SLF-III (green) are part of the dorsal pathway; the inferior fronto-occipital fasciculus (IFOF, orange), UF (cyan), and ILF (magenta) are part of the

ventral pathway. The MLF is notably absent in this model. (b) Models that are heavily influenced by autoradiographic tract-tracing studies in the macaque monkey suggest as many as six dissociable fiber tracts. The autoradiography data also suggest the existence of a MLF (yellow) but dispute the existence of an IFOF. The EMC (blue), UF (red), and MLF and ILF (orange) are part of the ventral pathway connecting the inferior part of the frontal lobe with the temporal, parietal, and occipital lobes. The AF (violet) and SLF-III (green) are part of the dorsal pathway. Numbers refer to the corresponding Brodmann areas for putative terminations and connections (Modified from Dick and Tremblay 2012)

another that has a meaning relation. In *conduction aphasia*, the damaged network is required to assemble phonemes into words and coordinate speech articulation. Patients with conduction aphasia cannot repeat sentences word for word and cannot easily name pictures and objects; they make phonemic paraphasias but can produce intelligible speech and comprehend simple sentences. Related lesions involve the STG, SMG, and AG, the insula, and the adjacent WM. There is not much evidence in the literature that a simple disconnection of the AF alone can cause conduction aphasia, as it was originally suggested by Monakow and later by Dejerine (Dejerine and Dejerine-Klumpke 1895). On the contrary, very recently it was shown with DTI tractography that preoperative mild conduction aphasia in glioma patients is strictly associated with involvement of the AF (Bizzì et al. 2012).

The large amount of neuroimaging data becoming available is providing new opportunities for innovative models of the language network (Fig. 2). In 2004 Hickok and Poeppel outlined a dual-stream model of speech processing with a *dorsal stream* mapping acoustic speech signals to the articulatory subnetworks in the IFG and a *ventral stream* processing signals for comprehension. The model assumed a widely distributed network with a strongly left-lateralized dorsal pathway and a largely bilaterally organized ventral pathway (Hickok and Poeppel 2007). The dorsal stream will connect cortical nodes of the articulatory subnetwork located in the left dominant posterior IFG (pars opercularis and triangulär), ventrolateral premotor cortex, and anterior insula with the sensorimotor interface node localized in the posterior STG and AG. The ventral stream will connect a combinatorial

subnetwork located in the anterior MTG and inferior temporal sulcus (ITS) with a lexical interface node located in the posterior MTG and ITS and with the articulatory subnetwork already described.

In 2012 Friederici proposed a functional anatomical model of the language network that was focused on different processing steps from auditory perception to comprehension (Friederici 2012). One novelty of this model was that particular attention was dedicated to the definition of the structural connections between the cortical nodes of the network. In this model of sentence comprehension, several hubs or nodes are connected via the dorsal and ventral pathways. Transformation of sounds in words and phrases occurs within 50–80 ms after acoustic and phonological analysis taking place in the middle portion of the STG. Once the phonological word form is identified, its syntactic information and semantic information are retrieved in the anterior STG/STS. This subnetwork operates in the anterior temporal lobe as comprehension moves from phonemes to words and phrases. Lexical-semantic integration occurs in the MTG. Information transfer within this temporal subnetwork is likely provided by short-range bundles within the IFOF.

A second language subnetwork elaborates syntactic and semantic information and requires nodal processors in the anterior (BA47 and BA45 for semantic processing) and in the posterior (BA44 for syntactic processing) IFG. Information transfer between the anterior temporal and IFG is assumed to be supported by ventral pathways: semantic information is conveyed via the IFOF connecting the pars orbitalis and triangularis (BA47 and BA45) with the temporal and occipital

cortices; syntactic information is conveyed via the UF connecting the pars opercularis (BA44) with the anterior temporal cortex (Anwander et al. 2007). Patients with lesions involving the ventral language stream have been reported to have semantic and syntactic comprehension deficits (Tyler et al. 2011). A third subnetwork of the model proposed by Friederici is in charge of integrating semantic/syntactic processing at a hierarchical level in order to achieve sentence comprehension. Thus elaborated information is bidirectionally exchanged between the IFG, the posterior MTG (BA22 for semantic processing), and the AG (BA39 for syntactic processing). The connection from the IFG to the AG likely occurs via the direct or indirect route of the AF, whereas it is still under debate whether the connection to the MTG occurs via the ventral (IFOF) or the dorsal (AF) pathway.

The contribution of the dorsal and ventral WM pathways connecting the frontal and temporal speech regions is central to understanding how the cortical areas interact to produce a seamless behavioral system. One emerging concept is that the AF is involved primarily in phonology, articulation, and syntax and the IFOF is mainly implicated in semantics. While authors vary in their claims concerning the extent of functional specialization, all authors argue for some degree of functional differentiation. The authors of a recent study performed in 24 patients with chronic stroke in the left hemisphere suggested that segregation of function for the dorsal and ventral pathways is limited to the phonological and semantic tasks (Rolleheiser et al. 2011). On the other hand, morphology and syntax require a synergy between the AF and the IFOF rather than a segregated system. In this DTI study, both dorsal and ventral bundles were associated with syntactic performance in both comprehension and production tasks. Comprehending syntax utilizes equally both the AF and IFOF, while syntactic production is predominantly permitted via the AF. By defining the WM architecture as a synergy, the overall determinant of task performance is not dictated by which WM tract is involved, but by how prefrontal and posterior temporal cortical speech regions use and integrate a constant flow of very complex linguistic information.

4.3 Visuospatial Attention System

What you see is determined by what you attend to. Visuospatial attention is a complex dynamic process that involves filtering relevant information from our spatial environment. We simultaneously attend to and look at objects in a visual scene by means of saccadic eye movements that rapidly bring the fovea onto stimuli of interest. The processing of visual stimuli appearing in the attended spatial location will be enhanced, while stimuli appearing in other parts of the visual field will be suppressed. Visuospatial attention is necessary for selecting and inhibiting visual information over space, because the

environment is overloaded with far more perceptual stimuli that our brain can effectively process. Visuospatial attention allows people to select, modulate, and sustain focus on the information that is most relevant to their own behavioral goals. The selected item may enter visual working memory and/or become the target of a movement.

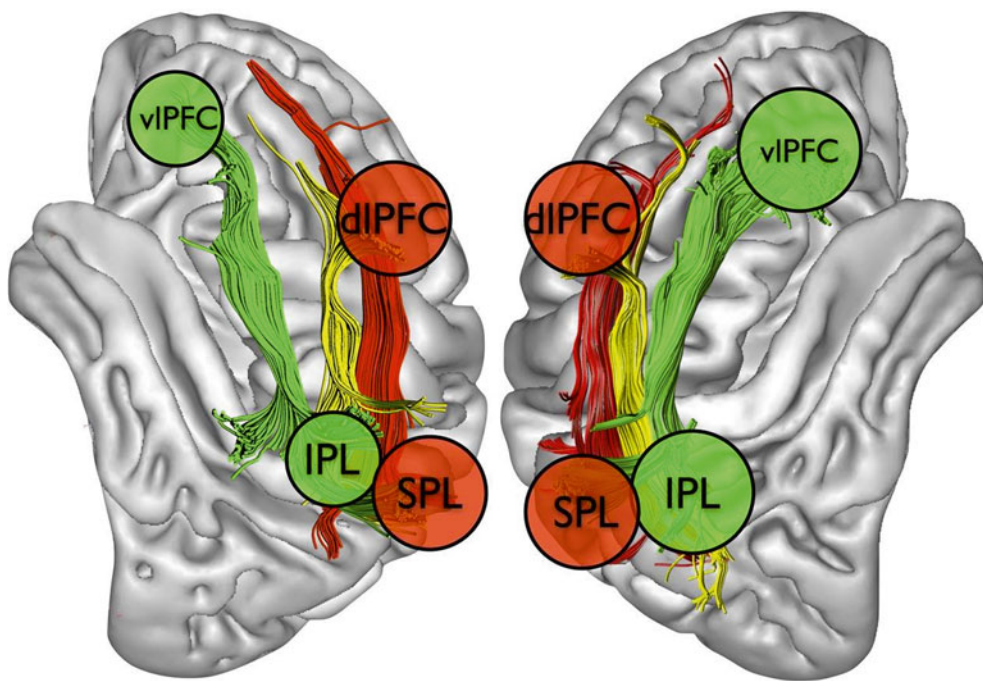
There are multiple forms of attention to external and internal stimuli (Chun et al. 2011). External attention refers to the selection and modulation of sensory information: visual, auditory, olfactory, tactile, and gustatory. Each of these attention systems selects locations in space or modality-specific output. The visual attention system is by far the most developed in humans, while in other animals, the auditory or the olfactory attention systems may be in charge of guiding the behavior of the animals in response to environmental stimuli. Internal attention refers to the selection, modulation, and maintenance of internally generated information, such as task rules, responses, long-term memory, or working memory. Visuospatial attention also interacts with other attention processes.

The concept of spatial selective attention refers operationally to the advantage in speed and accuracy of processing for objects lying in attended regions of space as compared to objects located in non-attended regions (Posner 1980). When several events compete for limited processing and comprehending capacity and control of behavior, attention selection may resolve the competition.

fMRI studies in humans have shown that the anatomical structures which are activated during the performance of attention-related functions are located in the parietal and frontal lobes and form multiple functional parietofrontal networks (Corbetta and Shulman 2002). The posterior parietal cortex (PPC) and the frontal eye field/dorsolateral prefrontal cortex are nodes of a dorsal attention network that is active during the orientation period. The temporoparietal junction and the ventrolateral prefrontal cortex are nodes of a ventral attention network that is active when subjects have to respond to targets presented in unexpected locations. The ventral network is in charge of detecting unexpected but behaviorally relevant events and is responsible for maintaining attention on goals or task demands that is a top-down process. Physiological studies have found that the activity of the frontal and parietal nodes is coordinated during execution of a visual attention task but show distinctive dynamics. In the parietal cortex, bottom-up signals appear first and are characterized by an increase of frontoparietal coherence in the gamma band (25–100 Hz), whereas in the PFC top-down signals emerge first and tend to synchronize in the beta band (12–30 Hz) (Buschman and Miller 2007).

In the monkey brain, the activity of neurons dedicated to visuospatial attention has been recorded simultaneously in the parietal and frontal cortices. Axonal tracing studies have shown that parietal and prefrontal neurons are directly and extensively interconnected through a system of fascicles

Fig. 3 A schematic representation of the parietofrontal visuospatial attentional networks based on fMRI (Corbetta and Shulman 2002) and MR tractography data (Thiebaut de Schotten et al. 2011a). The major cortical nodes are located in the vIPFC and dIPFC, IPL, and SPL. The three segments SLF-I (red), SLF-II (yellow), and SLF-III (green) are believed to connect the parietal and frontal nodes of the dorsal with the ventral attention networks (Figure as originally published in Bartolomeo et al. 2012)



running longitudinally in the centrum semiovale, dorsally to the AF, and laterally to the CST. Three distinct parietofrontal long-range segments of the SLF that had been previously described in the rhesus monkey (Petrides and Pandya 1984) have been recently demonstrated also in the human brain using MR tractography with the SD algorithm (Thiebaut de Schotten et al. 2011a).

The dorsal first segment of the SLF (SLF-I) connects BA5 and BA7 in the PPC including the dorsal bank of the intraparietal sulcus with BA8 and BA9 in the SFG; the SLF-II connects BA39 and BA40 in the inferior parietal lobule (IPL) including the ventral bank of the intraparietal sulcus with BA8 and BA9 in the MFG; the ventral SLF-III connects the AG (BA40) with the BA44, BA45 and BA47 in the IFG. The SLF-I connects the cortical nodes of the dorsal attention network activated during the voluntary orienting of spatial attention toward visual targets, while the SLF-III overlaps with the ventral network that is activated during the automatic capture of spatial attention by visual targets and damaged in people with visuospatial neglect (Fig. 3). The middle SLF-II connects the parietal nodes of the ventral network with the pre-frontal nodes of the dorsal network, and it may represent a direct communication between the two networks. The SLF-II may act as a modulator for the dorsal network, redirecting goal-directed attention mediated by the SLF-I to events identified as salient by the SLF-III as suggested by Corbetta in the fMRI study cited above (Corbetta and Shulman 2002).

The parietofrontal network is bilaterally represented with some degree of asymmetry variable among the three segments. By measuring the volumes of the tracts reconstructed with tractography in 20 healthy subjects, Thiebaut de Schotten et al. found that the SLF-I is symmetrically represented in the two hemispheres, the SLF-III is right lateralized,

and the SLF-II shows a trend of right lateralization but with substantial interindividual differences that are correlated to behavioral signs of right hemisphere specialization (Thiebaut de Schotten et al. 2011a).

An acute stroke occurring in the frontoparietal network will affect the ability to process visuospatial information that usually manifests with neglect. In most of the patients, the deficits are transitory and become apparent only with clinical tests that elicit hemispatial neglect. Patients with visual neglect fail to pay attention to objects presented on the side of space contralateral to a brain lesion. While it is undisputed that right lesions provoke more severe and durable signs of neglect than lesions in the left hemisphere, identification of eloquent anatomic structures that, if injured, will cause visual neglect has fostered an intense debate in recent years.

Visual neglect has been associated with right hemisphere lesions in gray matter structures: in the parietal, frontal, or temporal cortices, in the basal nuclei, or in the thalamus. More recently, visual neglect has been associated with isolated WM injury that was possible to assign to specific frontoparietal WM tracts with the aid of tractography. In a 55-year-old man with transient visual neglect, tractography was essential to determine that a small acute ischemic WM infarct involved the SLF-III (Fig. 4) (Ciaraffa et al. 2012).

Signs of transient neglect were evoked also in two neurosurgical patients during resection of right hemisphere LGG while they were asked to bisect 20 cm horizontal lines. Patients deviated rightward upon IES of the SMG and of the posterior STG, but made no mistakes when the FEF and the anterior part of the STG were stimulated. However, in one patient it was the stimulation of the SLF-II underneath the IPL that evoked the strongest deviation rightward (Thiebaut de Schotten et al. 2005). The importance of SLF-II damage

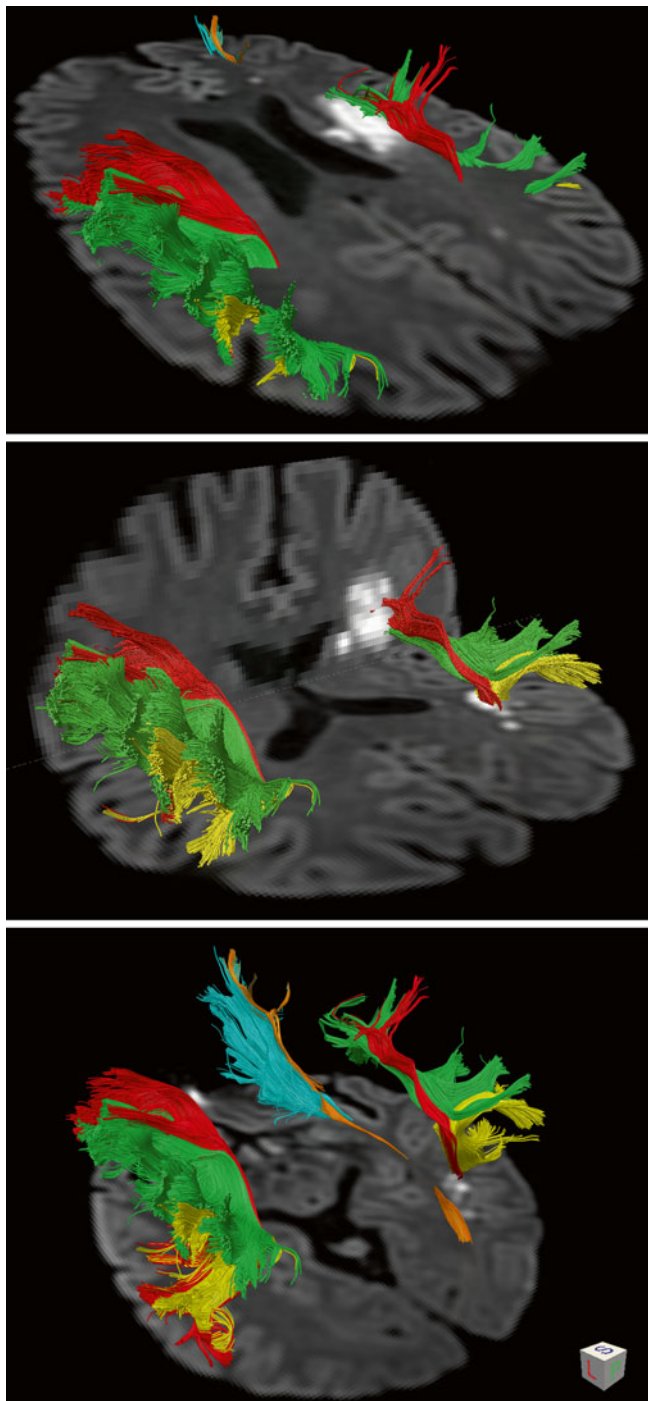


Fig. 4 A 55-year-old right-handed male presenting with acute onset of severe left visual neglect and left hemiparesis. MR DWI showed small multiple acute ischemic infarcts in the right cerebral WM and no evidence of infarcts in GM. DTI tractography was instrumental to accurately localize one infarct to the SLF-III (green) that is a component of the large-scale networks controlling visuospatial attention. Another infarct was localized in the stem of the AF (AF direct in red, AF posterior segment in yellow); the IFOF (orange) and UF (cyan) were not involved. This case report supports the hypothesis that neglect may result from disruption of a distributed attention network (Ciaraffa et al. 2012)

was recently replicated with IES in other 6 neurosurgical patients with right hemisphere gliomas (Vallar et al. 2014), and it is further supported by studies in right hemisphere

stroke patients with chronic unilateral neglect, where maximum lesion overlap was along the trajectory of the SLF (Doricchi and Tomaiuolo 2003; Thiebaut de Schotten et al. 2008). In another study in 38 patients with chronic neglect, the use of a DTI-based atlas of the human brain allowed a detailed analysis of lesion involvement of WM pathways and revealed that damage to the SLF-II (and to the SLF-III with lesser significance) was the best predictor of chronic persistence of left visuospatial neglect (Thiebaut de Schotten et al. 2014). Overall these studies support the role of parietofrontal disconnection in the pathogenesis of neglect and outline the important contribution of tractography studies in assigning lesion location to specific WM tracts.

5 Mapping WM Tracts for Brain Surgery

5.1 Brain Tumor Semeiotic with FA and Directionally Encoded Color Maps

Diffusion imaging with DEC maps and MR tractography is increasingly requested by neurosurgeons because its clinical relevance has been shown. In the motor system, DTI has become more popular than functional MRI because it is capable of identifying CST trajectories. MR tractography nicely illustrates the dorsal and ventral language pathways. When a mass dislocates, the OR tractography provides necessary information in order to plan the surgical approach to the lesion. DEC maps are immediately available at the console, and they can be very practical and useful to determine the relationship of a mass with adjacent tracts. Expert users can identify the course of the main fascicles already on DEC maps. Notwithstanding it is fiber tracking that best illustrates the trajectory of a tract in 3D and its relationship with the tumor.

On DEC maps and with tractography, it is possible to determine whether the main WM tracts are *normal*, *dislocated*, *abnormal*, or *interrupted* (Jellison et al. 2004). In the first section, we have already seen how biologically different diffuse infiltrating slow-growing gliomas and fast-expanding GBMs are. LGG rarely dislocate WM tracts. LGG often infiltrate bundles that are still functioning as it has been demonstrated by IES. Thus, it would be important to detect the trajectory of eloquent WM tracts within the tumor preoperatively. On the contrary, HGG, metastases, and meningiomas have the tendency to displace or destroy bundles.

It is quite common to observe that a tract *dislocated* by a mass becomes more visible on FA and DEC maps because it appears more compact. For instance, the CST dislocated by a mass can show paradoxical increased FA value and maintain a blue hue regardless of whether it is shifted (Fig. 5). Gliomas growing in the temporal and occipital lobes are likely to displace the OR in the opposite direction from their point of origin. Presurgical MR tractography will show the trajectory of the OR with exquisite detail, and it will be useful to neurosurgeons in planning the point of entry for the corticotomy

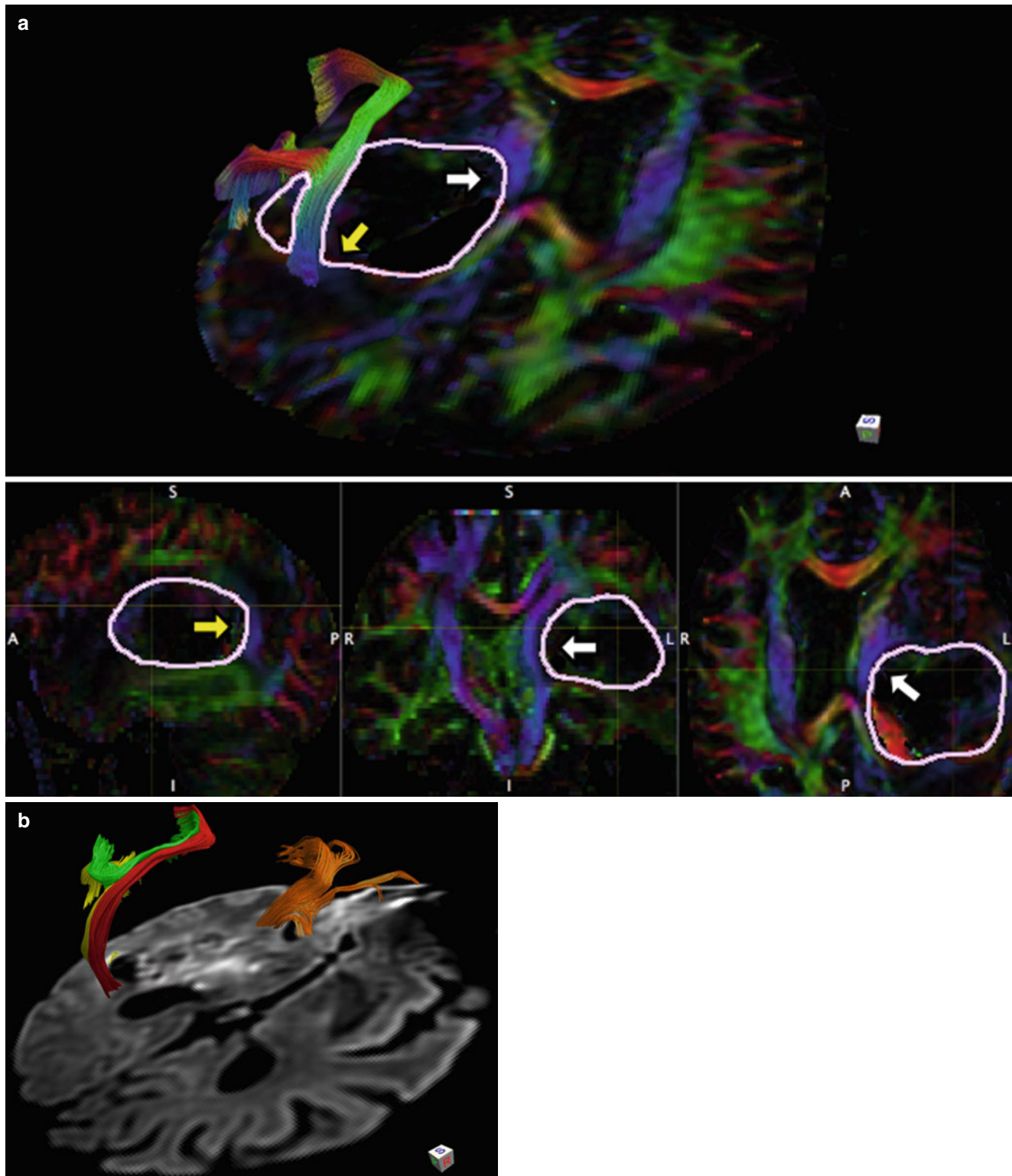


Fig. 5 (a) A 65-year-old right-handed female with recent onset of severe comprehensive aphasia. MRI showed a large enhancing mass deep seated in the left posterior temporal lobe. DEC maps with tractography showed that the mass dislocated anteriorly and medially the left CST (white arrows) and posteriorly the left AF (yellow arrow). In the upper box is MR tractography of the direct segment of the AF with

DEC streamlines. In the lower boxes from the left side are sagittal, coronal, and axial DEC maps with the margins of the mass outlined. A GBM WHO IV was removed at surgery. (b) DTI tractography of the three segments of the AF (direct in red, anterior in green, posterior in yellow) and IFOF (in orange) displayed in 3D over DWI in the axial plane is confirming that the GBM dislocated the AF posteriorly

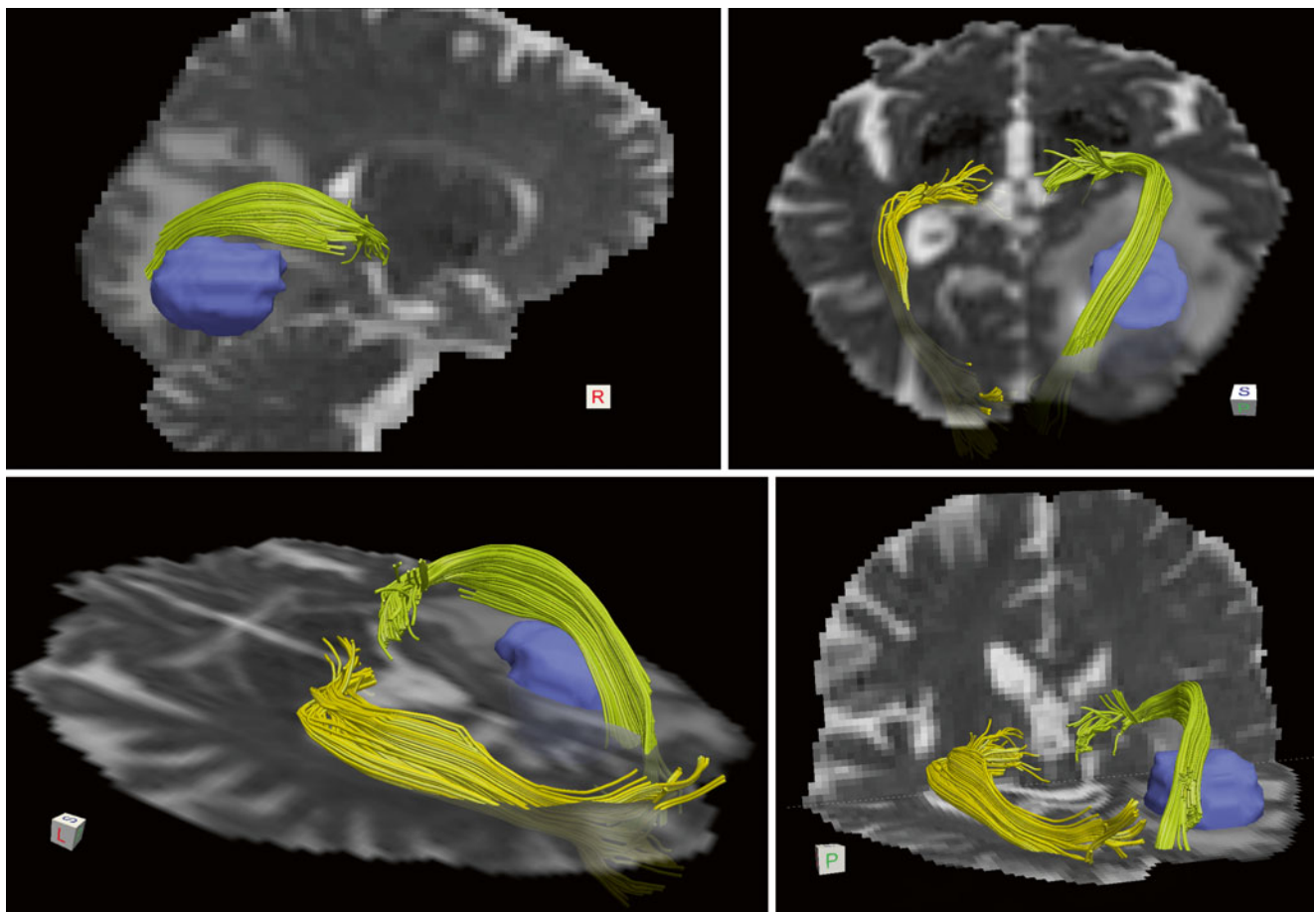


Fig. 6 A 76-year-old male with GBM WHO IV surrounded by abundant perilesional vasogenic edema in the right occipital lobe displacing the OR dorsally. Note the asymmetry with the right OR (light green)

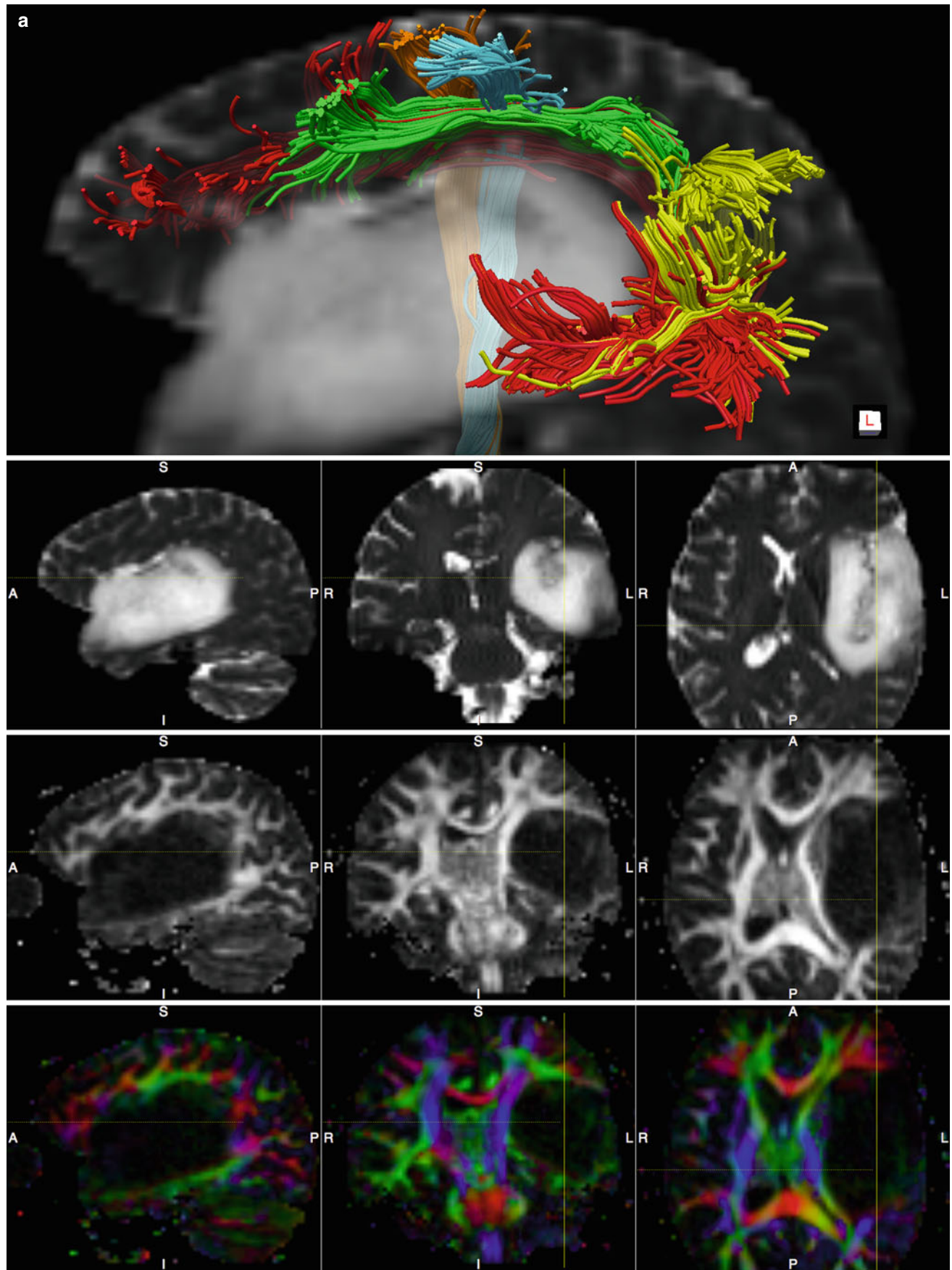
displaced dorsally relative to the left OR (yellow) on multiple T2-weighted MR images with overlaid streamline tractography performed with spherical deconvolution. The mass is colored in blue

(Fig. 6). Gliomas infiltrating the perisylvian cortex are likely to displace dorsally the direct segment of the AF. The position of the AF stem or isthmus in the deep temporal occipital WM is easy to recognize, and it is a practical landmark on axial DEC maps. The AF stem is color-coded in blue, and it is frequently dislocated posteriorly by aggressive tumors. Gliomas often dislocate the AF stem posteriorly and the frontal arm of the AF dorsally. A slow-growing tumor growing in the IFG nearby Broca area is likely to dislocate the frontal arm of the direct AF posteriorly without interrupting its major trajectories. Patients with LGG infiltrating Broca area are unlikely to have speech deficits (Plaza et al. 2009). A mass originating in the ventral precentral gyrus may dislocate the AF medially. More aggressive gliomas originating in ventrolateral precentral cortex (BA6) may initially dislocate the AF medially, and then as they expand, they may interrupt its trajectories causing conduction aphasia (Bizzi et al. 2012).

Intraoperative DTI has been used to show shifting of the CST tract during tumor resection. In a series of 27 patients with glioma, the authors used DEC maps to find that dislocation

of the CST may occur inward and outward. The authors underscored that intraoperative updating of the DTI results is important (Nimsky et al. 2005). A WM tract that is compressed by a mass may turn out to be easier to track especially when FA is increased. This phenomenon is likely due to decreased radial diffusivity with insignificant changes in axial diffusivity. Tracts that are usually more difficult to visualize such as the OR and the contingent of CST fibers projecting to M1 of the face/mouth area may be enhanced when they are compressed by a large mass (Fig. 7).

A WM tract is considered *abnormal* on DEC maps when it is coursing throughout an area of T2-signal hyperintensity, with altered FA and MD, but it shows native orientation (color hue). Despite early reports suggesting that DEC maps might separate diffuse infiltrating gliomas from tumor-free vasogenic edema (Jellison et al. 2004), this differentiation is not reliable. Both expansion of the ECS deployed by infiltrating glioma cells and increased water accumulation secondary to vasogenic edema will likely result in similar and overlapping DTI abnormalities. LGG have a predilection



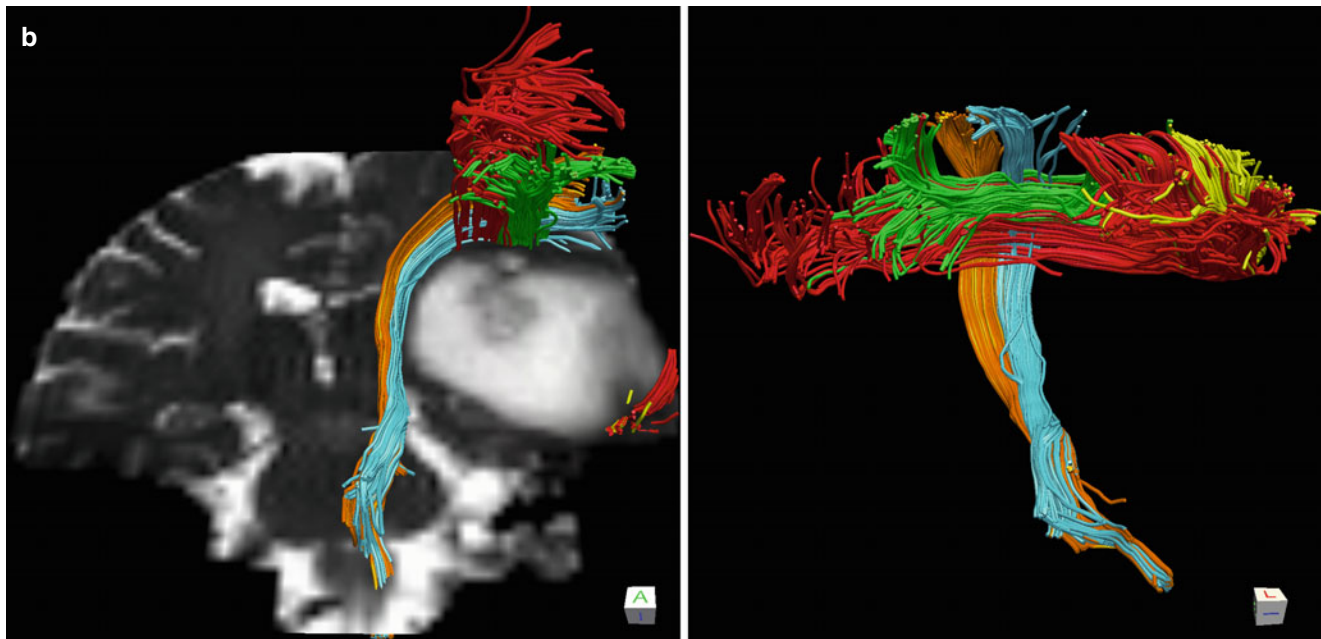


Fig. 7 (continued)

to infiltrate associative unimodal and multimodal cortices in the insula, temporal pole, orbitofrontal cortex, and SFG (Duffau and Capelle 2004). Insular gliomas easily infiltrate adjacent IFOF fibers coursing in the ventral floor of the extreme capsule and the UF in the temporal pole. Cancer cells may follow these fascicles and infiltrate adjacent frontal and temporal lobes: a swollen temporal stem is a hint that the “guerilla glioma cells” are using the tracts as infrastructures to conquer additional territory. On axial DEC maps, the trajectories of the IFOF in the temporal stem and the extreme capsule are coded in green. It is unlikely that LGG will dislocate the IFOF and the UF. On the contrary, GBM originating in adjacent areas are more likely to dislocate or interrupt rather than infiltrate the IFOF. MR tractography identifies the trajectories of the IFOF and UF when they are dislocated. Unfortunately heavy tumor infiltration or vaso-genic edema may result in significant MD increase with FA

drop. In this scenario, MR tractography fails to detect residual bundles because FA decreases below the threshold and the eigenvector may become undetermined. The possibility of false-negative findings should be raised in the radiology report to the neurosurgeon. It is important to keep in mind that MR tractography does not provide functional information and that IES is the only method able to test WM function and to detect presence of functional bundles inside a tumor.

A WM tract is considered *interrupted* when its FA values decreased below the FA threshold used for tractography and its trajectories are lost in the area of the tumor. From a biophysical perspective, this scenario occurs when diffusion becomes isotropic inside the tumor or the main orientation of anisotropy is not coherent anymore with the native orientation of the tract of interest. A threshold of FA >0.2 is usually recommended for tractography in healthy tissue; however, it has been shown that decreasing the threshold to FA >0.1 can help to identify residual

Fig. 7 (a) A 36-year-old male with astrocytoma WHO II. The three segments of the left AF (direct segment in red, posterior segment in yellow, and SLF-III in green) and two components of the CST projecting, respectively, to M1 (yellow) and S1 (cyan) in the area of the face/mouth are displayed over a sagittal T2-weighted MRI (*upper row*). Note in sagittal, coronal, and axial T2-weighted MRI (*2nd row*), FA maps (*3rd row*), and DEC maps (*bottom row*) that the large mass is infiltrating the left insula and the whole temporal lobe and it is displacing the CST medially and the AF dorsally. Presurgical tractography was useful to show that eloquent fascicles (AF and CST) were outside of the mass; thus, a complete resection could be

attempted after detection of the functional limits with IES mapping. Diffusion data were acquired with HARDI (64 gradient directions, $b=2,000$, $2 \times 2 \times 2 \text{ mm}^3$), and tractography was performed with spherical deconvolution algorithm. (b) Tractograms of the CST and AF are displayed over a coronal T2-weighted MRI (*left panel*). The severe mass effect paradoxically enhanced detection of the CST fibers projecting to the face/mouth area. This contingent of fibers is usually poorly visualized with normal anatomy due to crossing fibers, even with spherical deconvolution algorithm. Lateral view of the tractograms from below showing CST streamlines crossing the AF (*right panel*)

trajectories inside a tumor (Bello et al. 2008) with the trade-off of increasing false-positive results. From a neuro-oncological perspective, interruption of a tract may be due to three conditions: tissue destruction, heavy glioma cell infiltration, or vasogenic edema. In the first condition, tractography would provide a true-negative result and in the second a result that requires validation with IES or histopathological examination of the surgical specimen, while in the case of vasogenic edema, it would provide a false-negative result. It has been shown that vasogenic edema may be associated with false-negative results that should not be confused with bundle destruction (Buzzi et al. 2012; Ducreux et al. 2006). We have already mentioned that the use of advanced diffusion imaging methods that use multicompartmental models such as NODDI (Zhang et al. 2012) has potential to better address this critical issue.

The appearance of a ring of increased anisotropy at the periphery of the mass is another controversial condition that has been described in brain tumors. The cause for high FA values at the interface between the mass and surrounding brain tissue is not well understood. Few studies have investigated tensor shape indices in the periphery of focal lesions. Significantly higher CL values have been reported near the enhancing ring of GBM rather than of metastasis (Wang et al. 2009). The authors of another study suggested that CL and CP can distinguish true from pseudo WM trajectories inside an abscess cavity (Kumar et al. 2008). CL and CP mean values measured within the abscess cavity were significantly different compared with those of WM tracts; however, FA, MD, and CS values overlapped. High CP with low CL inside an abscess cavity indicates that the shape of the diffusion tensor is predominantly planar, whereas it is linear in WM tracts. These geometrical DTI indices may be used for differentiating true from pseudo WM tracts inside the abscess cavity and in general at the periphery of a tumor. The finding of high FA and CP inside a tumor should be considered nonspecific, while high FA and CL may indicate the possibility of residual WM tracts within a glioma. Elevated FA and CL at the periphery of a mass should suggest the proximity of a compacted WM tract that can be identified with the aid of DEC maps (Fig. 8a). Finding of elevated CP around the periphery of a mass, especially if associated with elevated MD, should raise suspicion for pseudo WM tracts. In this last scenario, elevated planar diffusivity might be an epiphenomenon of mass effect at the interface between the tumor and brain tissue, especially

when there is accumulation of water in the ECS (i.e., vasogenic edema). NODDI measures innovative parameters such as neurite density and orientation dispersion index that may also help to characterize tumor infiltration and vasogenic edema within and around a mass (Fig. 8b).

5.2 Mapping Strategies with MR Tractography

The main aims of mapping WM structures in neuro-oncology are (i) presurgical planning, (ii) intraoperative guidance during IES and tumor resection, and (iii) postoperative evaluation after tumor resection.

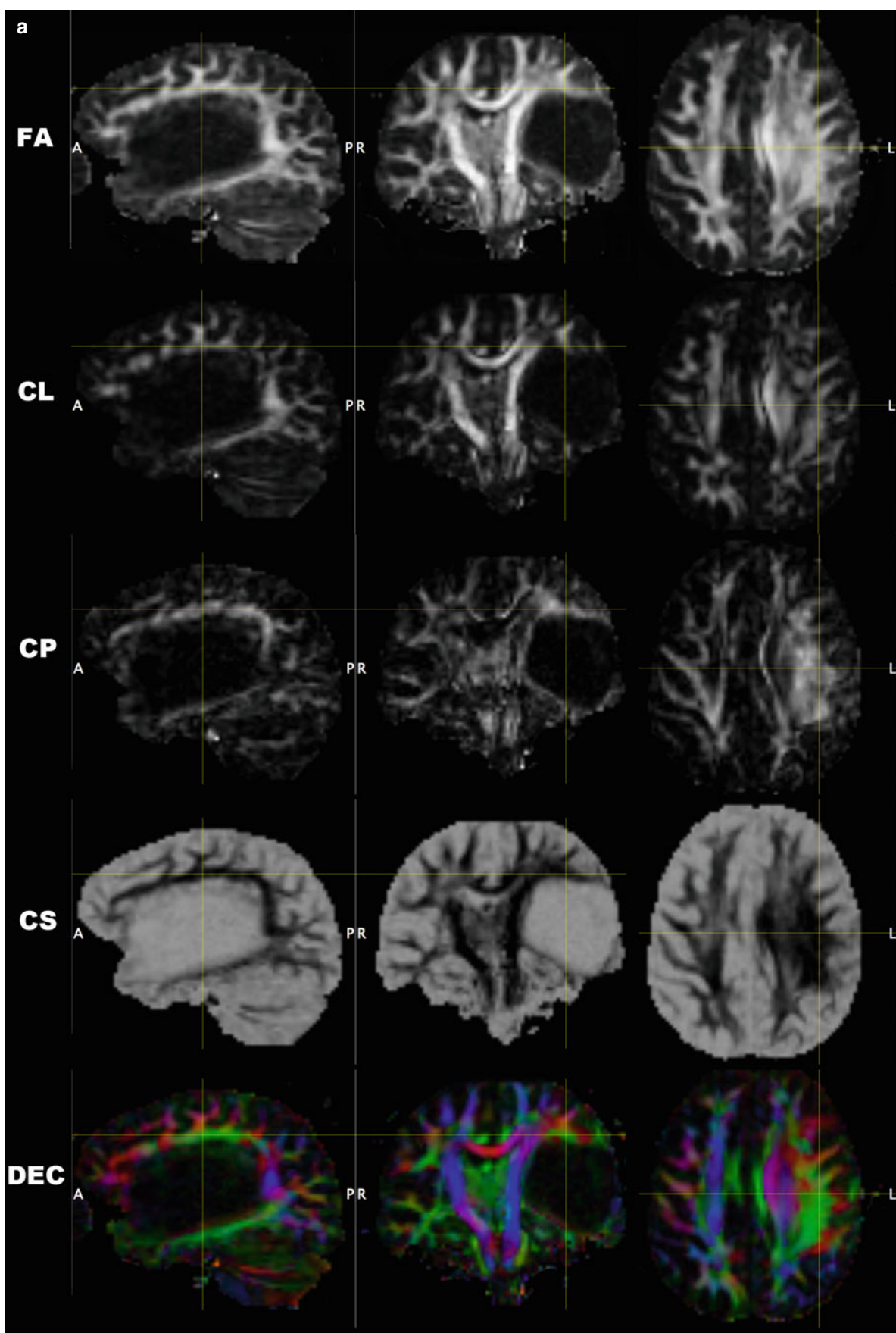
The aim of using tractography for presurgical mapping is to show in 3D space the relationship of the trajectory of the fascicle of interest with the lesion and other anatomical landmarks. Thus, the neurosurgeon can select the best route to reach the lesion without damaging eloquent tracts and can define which tract to test with IES. There is consensus among neurosurgeons that the CST, AF, IFOF, UF, and OR are the most clinically relevant fascicles for presurgical mapping.

The general principle of tractography is to use the orientation information provided by the tensor, the fODF, or the dODF. The most commonly used directional assignment corresponds to the major eigenvector of the diffusion tensor. Starting from one or more “seed” ROI and propagating the trajectories according to the tractography algorithm until the tracts are terminated generate a streamlined tractogram. Specific geometrical and anatomical constraints are used to extract the trajectories that meet specific connection criteria. Geometrical constraints are used to terminate tracking in voxels with very low FA and undetermined fiber orientation (FA threshold) or to avoid unrealistic trajectories with very sharp turns (angle threshold). Rules based on Boolean logic (i.e., true or false) can be applied to select (“IN”) or exclude (“OUT”) specific streamlines or pathways.

It is tradition since the early days of deterministic tractography to filter out spurious streamlines that are known to represent artifacts from a priori knowledge. Spurious tracts represent false-positive streamlines that are mainly due to errors to estimate tract orientation with diffusion imaging in the presence of crossing, bending, and fanning fibers. The

Fig. 8 (a) Parametric maps available from DTI dataset of the same case illustrated in Fig. 7: fractional anisotropy (FA); linear, planar, and spherical anisotropy shape coefficients (CL, CP, CS); and direction-encoded color (DEC) maps. A large mass such as this astrocytoma may disrupt the architecture of the WM around it. When CL is high (bright), there is usually one dominant tract such as the CST in the medial boundary of the lesion in this case. When CP is high there may be two

crossing fibers such as the AF and the CST in the dorsal boundary. CL and CP maps are often more informative than FA alone. (b) Parametric maps available from NODDI dataset of the same case illustrated in Fig. 7: neurite density (ND) and orientation dispersion index (odi). The very low ND value within the mass is suggesting that unlikely there should be residual fibers within the tumor; odi is elevated within the mass, showing a paucity of oriented sticks (fascicles)



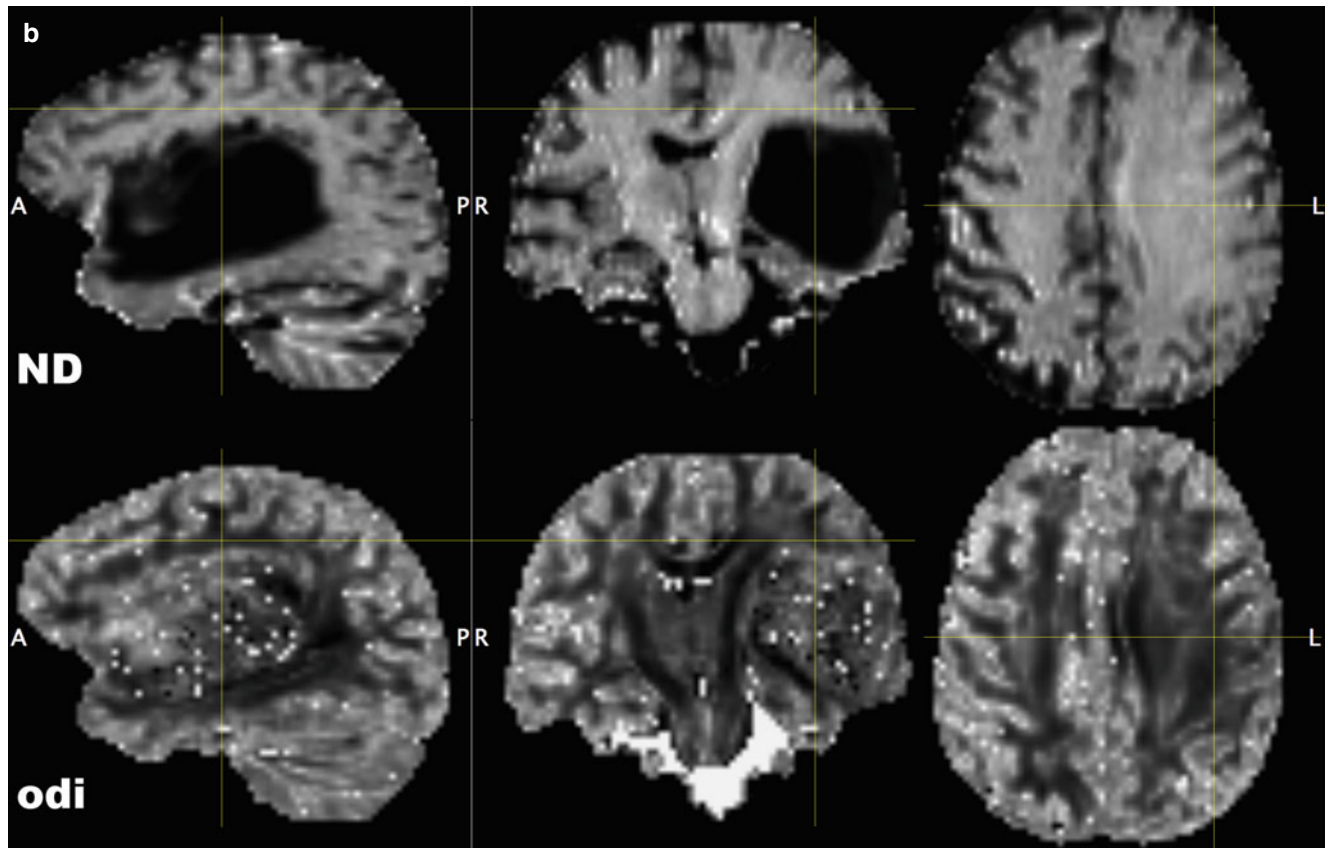


Fig. 8 (continued)

number of spurious tracts is variable, it changes with WM fascicles, and it depends on the quality and spatial resolution of the HARDI dataset. The number of spurious tracts is usually small in the proximity of a LGG, whereas it may increase significantly in the hemisphere ipsilateral to a HGG, especially when the mass is aggressively growing and disarranges WM architecture.

It is important to use a precise and correct terminology when describing imaging findings in a radiology report. Diffusion MR tractography provides anatomical (structural) information that has no functional content. *Fasciculus* and *bundle* are anatomic terms: many axons or fibers form bundles of different diameters; several bundles form a fasciculus. *Streamlines* and *trajectories* should be used when describing results in MR tractography studies. *Pathway* or *stream* is used mainly in functional imaging studies depicting information flow.

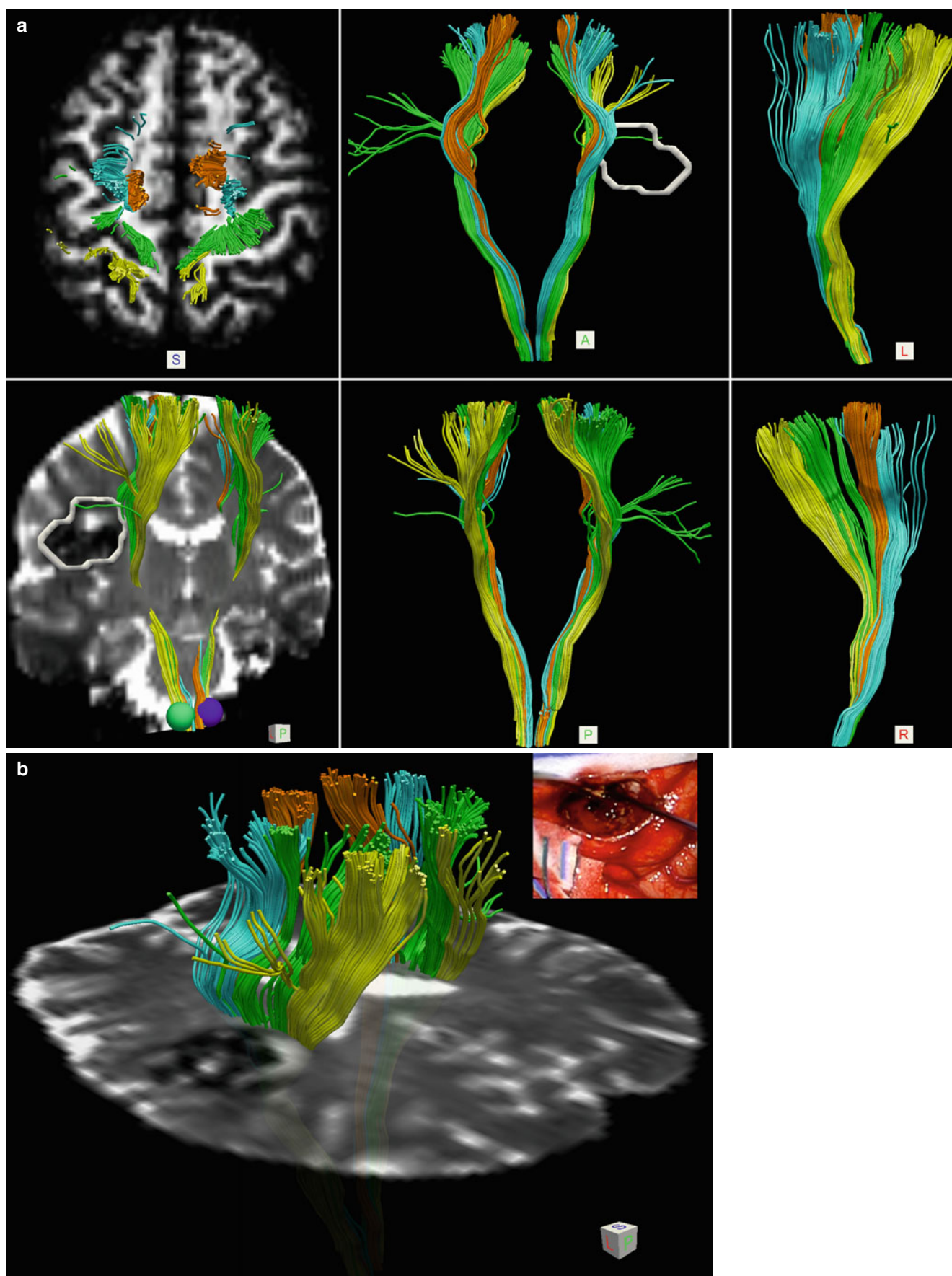
5.3 Motor System

5.3.1 CST

The CST is the most eloquent of the WM structures, and damage to the CST leads to permanent motor and speech deficits. Mapping of the CST is requested when a lesion is located in the paracentral region, SMA, PMd, and PMv and in the proximity of its course at the level of the thalamus, basal nuclei, or brainstem. The CST carries axons organized in bundles projecting from the M1 (49 %), postcentral and PPC (21 %), SMA proper (19 %), PMd (7 %), and PMv (4 %). IES of the CST is best performed with the high-frequency monopolar probe rather than with the low-frequency 60 Hz bipolar probe (Bello et al. 2014). It is mandatory to identify all components of the CST in order to avoid postoperative motor deficits (Fig. 9). The typical course of the CST and the somatotopic organization of its

Fig. 9 (a) A 31-year-old male with cavernous angioma (white circle) seated in the deep WM below the left SMG. The medial margin of the focal lesion is abutting the left CST. Diffusion data were acquired with HARDI (64 gradient directions, $b=2,000, 2 \times 2 \times 2 \text{ mm}^3$), and tractography was performed with spherical deconvolution algorithm. Tractography of the CST components originating from M1 (green), SMA (orange), PM dorsal (cyan), and S1 (yellow). The components of both corticospinal tracts (CST) are displayed over axial FA map at the level of the central sulcus (upper row, left panel) and coronal T2-weighted MRI (lower row, left panel); anterior and posterior views

of both CST in the *middle panels*; lateral and medial view of the left CST on the *right panels*. (b) Tractography showing that the components of the left CST originating from M1 (green) and S1 (yellow) are coursing adjacent to the medial margin of the cavernous angioma. Streamline of the CST originating from SMA (orange) and PMd (cyan) are also shown. Intraoperative view (*left upper corner*) showing direct subcortical electrostimulation of the floor of the surgical cavity with the monopolar probe: a current of 8 mA evoked MEP responses of the right hand and leg, confirming that the CST was very close to the angioma



fascicles are important to know in order to predict potential deficits during removal of a lesion. In M1 the tongue and face areas are located ventrally and laterally to the hand area, and the leg and foot are located dorsally and medially in the paracentral lobule. After leaving the cortex, the CST curves slightly backwards, and then it bends forward before entering the posterior limb of the internal capsule. Along this way, the somatotopic fibers twist about 90° counter-clockwise so that the tongue and face bundles descend anteriorly and the foot and leg bundles posteriorly. At the level of the internal capsule, the hand bundles occupy the midportion of the CST.

Tracking of the CST should be performed with a two-ROI approach using streamline or probabilistic tractography. Delineation of the seed ROI is usually performed on b0 (i.e., T2WI) or FA maps in multiple axial slices in the precentral and postcentral gyri, posterior third of the SFG (i.e., SMA), and MFG (i.e., PMd and PMv). The ROI should include the subcortical WM since fiber tracking does not reach the cortical layers. The ROI in M1 should extend from the mouth to the foot area. Delineation of the target ROI should be done at the level of the pons in the ipsilateral tractus pyramidalis (blue on DEC maps) that is anterior to the pontocerebellar fibers (red on DEC maps) and lemniscus medialis (blue on DEC maps). Some authors prefer to delineate the target ROI in the ipsilateral cerebral peduncle of the midbrain or in the posterior limb of the internal capsule. After connecting the two ROIs, the tractogram should be inspected for a priori anatomic consistency.

Spurious streamlines should be removed with “out-ROI” filters with the aim to show the backbone of a “clean tractogram.” Spurious tracts to the contralateral CST are frequently found along the trajectories of the CC and of the pontocerebellar peduncles. Spurious tracts are due to artifacts of fiber tracking in voxels with crossing fibers. The number of spurious tracts is variable and depends on the quality and spatial resolution of the HARDI dataset; however some spurious tracts should always be expected in the above regions. Out-ROIs are usually needed in the midsagittal plane and in the middle cerebellar peduncles.

Tracking the backbone of the CST from the hand knob area (omega sign) in M1 to the pons is relatively easy. Unfortunately streamline DTI tractography usually fails to reconstruct streamlines originating in the tongue, face, leg, and foot areas due to the presence of crossing fibers with the CC and the SLF at the level of the centrum semiovale (Mandelli et al. 2014). Implementation of HARDI acquisition scheme with more advanced algorithms such as SD (Dell’Acqua et al. 2013), multi-tensor (Yamada et al. 2007), Q-ball, and probabilistic tractography (Bucci et al. 2013) allows depiction of additional trajectories that

are originating from the face, tongue, and foot regions of M1.

5.3.2 SMA Connectivity

The SMA is at the center of a rich network of WM connections with motor, language, and limbic structures. The connectivity of the SMA is of particular interest for brain tumor surgery since it is one of the favorite areas infiltrated by LGG (Duffau and Capelle 2004). The “SMA syndrome” characterized by transient contralateral akinesia and mutism with a usually complete recovery in 6–12 months can follow surgery in this area. Immediate severe postoperative deficits can be quite stressful for the patient. Knowledge of the connections of the SMA can provide new insights on the genesis of the SMA syndrome; assessment of the extension of infiltrating tumors can assist the neurosurgeon in predicting the postoperative course of patients.

The SMA is located in the medial posterior third of the SFG, and it is functionally and connectively divided in two parts by a virtual line arising from the AC and perpendicular to the AC-PC line. The SMA proper and pre-SMA play a different role with regard to motor function. The SMA proper is more directly related to the execution of movement, while the pre-SMA is involved in planning and preparation of higher motor control. Differences in connectivity of the two regions provide an anatomical basis for explaining these functional aspects. The SMA proper is a component of the CST network, and it sends fibers through the corona radiata and the internal capsule to the spinal cord, while the pre-SMA has no direct connection with the cord. The SMA proper is thought to play a role in the direct execution of movement due to this corticospinal projection. Particular attention should be given to track also fibers projecting from the SMA proper when mapping the CST.

In a postmortem dissection and tractography study, Vergani et al. identified five main types of connections: (1) short U-fibers in the depth of the precentral sulcus, directly connecting the SMA proper with M1, especially at the level of the hand region; (2) U-fibers connecting SMA with the cingulate gyrus; (3) an intralobar frontal tract connecting the SMA with pars opercularis BA44 and BA6 (this fascicle has been called by Catani the “frontal aslant tract” (Catani et al. 2012)); (4) fibers connecting the SMA with the striatum; and (5) SMA callosal fibers connecting homologous areas (Vergani et al. 2014). Both the SMA proper and the pre-SMA have direct connections with the head and body of the caudate nucleus. The presence of striatal connections has been demonstrated in a DTI study by Lehericy et al. (2004). This corticostriatal connection is part of a wider network that reverberates back to the cortex through the thala-

mus. It is believed that this corticobasal nuclei-thalamocortical network may be implicated in different aspects of motor control, including initiation, sequencing, and modulation of voluntary movements. A predominance of striatal fibers on the left side in right-handed individuals provides evidence for this pathway to play an important role in language.

5.4 Language System

Mapping of the language system is requested when a lesion is located in the perisylvian region of the dominant hemisphere—insula and frontal, temporal, and parietal lobes—and in the adjacent WM pathways. It has been shown with fMRI using a silent word-generation task that in 96 % of right-handed healthy subjects the dominant hemisphere is on the left side, whereas the BOLD response is bilateral in 4 % of them. In contrast, the BOLD response lateralizes to the right hemisphere only in about 10 % of left-handers, whereas in 76 % it lateralizes to the left and it is bilateral in the remaining 14 % (Pujol et al. 1999). Modern theories about language have recognized that there is a lot of network redundancy in the system. The implications of a dual-stream system with dorsal and ventral networks cannot be overemphasized. The AF is the main component of the dorsal network that is considered critical in syntactic analysis and modulation of acoustic speech signal to the articulatory loop located in the ventrolateral part of the frontal lobe. The IFOF, UF, and inferior longitudinal fasciculus (ILF) are the main fascicles of a ventral perisylvian network that is considered critical for lexical and semantic processing occurring in the anterior temporal lobe. The ventral network is involved in processing sound into meaning and comprehension. However, there are other aspects of language that may rely on a more extended language network with additional fascicles projecting to the IPL (middle longitudinal fasciculus, MLF) and to the SMA (FAT and subcallosal fascicle).

5.5 The Dorsal Pathway: Arcuate Fasciculus

The AF is an essential component of the language system connecting regions devoted to formal aspects of language in temporoparietal areas with regions involved in intentional and social communication in prefrontal areas (Catani and Bambini 2014). According to Catani, the AF has three main cortical projections in the ventrolateral prefrontal (Broca), IPL (Geschwind), and posterior third of the temporal (Wernicke) lobe (Catani et al. 2005): (i) a direct (long seg-

ment) pathway connecting Broca with Wernicke territories, (ii) an anterior segment connecting Broca with the IPL, and (iii) a posterior segment connecting Geschwind territory with the posterior third of the MTG. The three nodes are used in tractography as seed points to track the trajectories of the three segments that form the AF. Macroscopically, the long segment has two arms that converge in a stem (isthmus). The frontoparietal arm courses lateral to the corona radiata in the centrum semiovale, and then it bends ventrally; the temporal arm of the AF courses along a craniocaudal axis lateral to other long-range fascicles that are intersecting in the deep WM underneath the AG and STG: they are the MLF, IFOF, and OR. The frontoparietal and temporal arms of the AF direct converge to form a stem (blue on DEC maps) that is an important landmark for tractography. The anterior and posterior AF segments are lateral to the direct segment; on DEC maps, the streamlines of the anterior segment are green, and those of the posterior segment are predominantly blue.

Tracking of the three segments of the AF should be performed with a two-ROI approach using streamline or probabilistic tractography with delineation of three seed ROIs on multiple axial slices in the posterior IFG including BA6 and PMd (Broca territory), posterior third of MTG (Wernicke territory), and IPL (BA39/BA40, Geschwind territory). DEC and FA maps are quite useful in delineating seed and target ROIs. The ROI in the IPL and in the posterior IFG should include only a small layer of subcortical WM, while ROI delineation in the MTG should include the deep WM and in particular the AF stem.

After connecting each pair of ROIs, the tractogram should be inspected for a priori anatomical consistency. Spurious streamlines should be removed with “out-ROI” filters with the aim to illustrate the backbone of a “clean tractogram.” Spurious tracts are often found overlapping with the trajectories of the CC and IFOF, due to fiber tracking artifacts in voxels with crossing fibers. A statistical significant leftward asymmetry has been reported for the volume and number of streamlines of the direct segment of the AF. Furthermore, males showed a left lateralization, while females had a more bilateral distribution. Individuals with more symmetric distribution performed better at remembering words using semantic association. These findings suggest that the degree of lateralization of the long segment of the AF is heterogeneous in the normal population and paradoxically bilateral representation, not extreme lateralization, might ultimately be advantageous for specific cognitive functions (Catani et al. 2007). In addition, it was shown in a longitudinal DTI study that the volume of the direct segment of the AF in the right hemisphere is an important predictive factor for recovery of language after stroke in the left dominant hemisphere (Forkel et al. 2014a)

In the past, the terms AF and SLF have been used as synonyms, but we agree with Catani that the equivalence of terms is anatomically incorrect despite some overlap between the fascicles. The term SLF should refer to a group of three longitudinal tracts connecting the dorsolateral cortex of the frontal and parietal lobes. The third segment of the SLF (SLF-III) overlaps with the anterior segment of the AF, while SLF-I and SLF-II are not components of the language network. The posterior segment of the AF runs along the craniocaudal axis, and it connects the AG with the posterior third of the MTG. It should not be confused with the MLF that runs longitudinally along the anteroposterior axis of the SFG.

5.6 The Ventral Pathway: IFOF, UF, and ILF

The *IFOF* is a long association fascicle connecting the frontal with the temporal, parietal, and occipital lobes (Catani et al. 2002). The IFOF carries visual information from occipital areas to the temporal lobe, and it is likely to play an important role in visual object recognition and in linking object representation to their lexical labels (Catani and Mesulam 2008). Macroscopically, the IFOF has two arms that converge in the temporal stem: the frontal arm projects to the IFG, MFG, dorsolateral prefrontal cortex, orbitofrontal cortex, and frontal pole; the temporo-parieto-occipital arm provides short-range bundles to the anterior temporal and insular cortex and long-range bundles to the posterior STG and MTG and to the parietal and occipital cortex. Anatomically the IFOF can be subdivided in three segments: frontal, intermediate temporal, and parieto-occipital. Anatomic dissection of 14 postmortem human cerebral hemispheres using the Klingler method has identified two components of the IFOF: a dorsal component connecting the frontal areas with the superior parietal lobule and posterior portion of the superior and middle occipital gyri and a ventral component connecting the frontal areas with the ventral part of the temporal lobe (fusiform gyrus, temporo-occipital sulcus, and inferior temporal gyrus) and with the inferior occipital gyrus (Martino et al. 2011). IFOF terminations have been demonstrated with postmortem dissections within the SPL and superior, middle, and inferior occipital gyri (Martino et al. 2010). The ventral fibers of the IFOF partially overlap with the OR projecting into the superior and inferior banks of the calcarine sulcus. Caversazi et al. used Q-ball residual bootstrap to reconstruct the IFOF using one single ROI delineated in the extreme capsule and thresholds of FA >0.15 and <60° angle (Caversazi et al. 2014). The authors were able to duplicate the above

reported postmortem findings. In comparison with classic DTI-based tractograms, more extended projections of the anterior arm of the IFOF were found in the lateral and medial orbitofrontal gyri, pars orbitalis and triangularis, and rostral portion of the MFG and even in the SFG with Q-ball imaging. More extended projections of the posterior arm of the IFOF were found to project to the lingula, pericalcarine and lateral occipital cortices, cuneus, and caudal portion of the fusiform gyrus. Trajectories of the dorsal component were found to project to the AG and SPL. The anatomy of the IFOF projections to the occipital lobe was consistent among the 20 healthy subjects with greater than 75 % overlap along its entire course.

At the level of the temporal stem, the IFOF occupies the posterior and dorsal two-thirds of the stem, and the streamlines can easily be distinguished from those of the UF coursing in the anteroventral and lateral part of the stem. As the IFOF exits the temporal stem, it runs in the ventral part of both the external and extreme capsules, encasing the inferior part of the claustrum (Ebeling and von Cramon 1992). The extreme capsule should not be considered a tract but a gross anatomy-defined WM structure. The intermediate segment the IFOF runs in the roof of the temporal horn, superior and lateral to the OR. Within the posterior temporal region, the IFOF trajectories run lateral to the tapetum and medial to the MLF, AF direct, and posterior segment of the AF.

In the macaque monkey, the IFOF is less developed than in humans, as monkeys lack the MTG and their IFOF connects primarily to posterior occipital areas (Forkel et al. 2014b; Schmahmann et al. 2007; Thiebaut de Schotten et al. 2012). In the monkeys, the IFOF overlaps to some extent with the extreme capsule, and this explains why it has been reported with that name in the literature (Petrides and Pandya 1988; Schmahmann and Pandya 2006). Other authors have adopted the monkey anatomic terminology also for the human studies and refer to the extreme capsule as the direct connection between the prefrontal areas and the MTG (Saur et al. 2008, 2010).

Tracking of the IFOF is performed with a two-ROI approach using streamline or probabilistic tractography with delineation of the seed ROI in the temporal stem (green on DEC maps) and the target ROI in the deep WM of the occipital lobe at the level of the calcarine fissure. The seed ROI is delineated in multiple axial slices whereas the target ROI in one coronal slice perpendicular to the IFOF trajectories. After connecting the two ROIs, the tractogram should be inspected for a priori anatomical consistency. In the human brain, the IFOF is an easy tract to reconstruct with tractography because it runs longitudinally in the anterior-posterior direction and it is the domi-

nant tract along most of its course. Spurious streamlines should be removed with “out-ROI” filters. Brain tumors expanding in the temporal or parietal lobe are likely to dislocate its trajectories or even to disrupt its course by increasing the number of spurious streamlines. A statistical significant rightward asymmetry has been reported for the volume and number of streamlines of the IFOF (Thiebaut de Schotten et al. 2011b).

The role of the IFOF in semantic processing is supported by IES mapping studies showing with high reproducibility that stimulation of the fascicle throughout its course from the frontal to the occipital lobe evokes semantic paraphasias (Duffau et al. 2008a). The anterior (frontal) arm of the IFOF should be detected with IES and represents the functional boundary in glioma infiltrating the pars opercularis of the IFG, the PMv, or PMd areas of the dominant hemisphere. The intermediate and temporo-occipital segments of the IFOF represent the functional boundary in gliomas infiltrating the insula and the deep temporal lobe.

The *UF* is a hook-shaped bundle connecting the frontal lobe with the anterior temporal lobe. Macroscopically the UF has two arms that converge in the temporal stem: the frontal (dorsal) and the temporal (ventral) arms. At the level of the temporal stem and in the proximity of the anteroventral portion of the extreme and external capsules, the UF and IFOF look like very compacted bundles with the UF located ventral and anterior to the IFOF. From the stem, the UF fans out into the frontal and temporal lobes. In the frontal lobe, the UF bundles project to the lateral and medial orbitofrontal cortex; in the temporal lobe, the bundles project to the pole, amygdala, anterior part of the hippocampus, anterior third of STG, and MTG (Martino et al. 2011).

The UF is part of the limbic system and it is likely involved in emotion and memory. It also plays a role in lexical retrieval, semantic associations, and specific aspects of naming. In a series of 44 patients who underwent awake surgery for removal of a left frontal or temporal glioma, removal of the UF in 18 patients resulted in long-term deficit of famous face naming, but not of picture naming of objects (Papagno et al. 2010, 2014). Patients were able to retrieve biographical information about people they could not name. Proper name impairment is a post-semantic deficit that requires damage of a functional network that has several nodes connected by the UF: the orbitofrontal cortex involved in face encoding, the ventromedial prefrontal cortex involved in the processing of emotions, and the temporal pole involved in naming famous faces (Gorno-Tempini et al. 1998).

Tracking of the UF is performed with a two-ROI approach using streamline or probabilistic tractography with delineation of the seed ROI in the temporal stem and the target ROI in the anterior WM of the temporal lobe at the level of the

anterior commissure. The seed ROI is delineated in multiple axial slices whereas the target ROI in one coronal slice perpendicular to the UF trajectories. After connecting the two ROIs, the tractogram should be inspected for a priori anatomical consistency. The UF is an easy tract to reconstruct with tractography despite its bending and fanning trajectory because it doesn’t cross other compact tracts. Spurious streamlines are scarce and they can be removed with “out-ROI” filters. The UF are symmetrical fascicles without significant differences in tract volume between the two hemispheres.

The *ILF* is a ventral associative bundle with long- and short-range fibers connecting the temporal and occipital lobes. The long bundles course medially to the short fibers and connect visual areas to the temporal pole, amygdala, and hippocampus. The ILF trajectories are coursing ventrally and laterally to the IFOF in the deep WM of the temporal and occipital lobes. The streamlines are green on DEC maps, but without tractography, they are difficult to distinguish from the other fascicles running in the temporoparietal fiber intersection area (TPFIA). Short-range fibers of the ILF connect the fusiform gyrus with the posterior part of the inferior occipital gyrus. From the anterior temporal lobe to the ventrolateral occipital cortex, long-range fibers run medially to short-range fibers; they course horizontally along the ventrolateral wall of the temporal and occipital horns with a posterior and lateral orientation. The ILF runs ventrally and laterally to the IFOF and OR for most of its course, but at the level of the TPFIA, the ILF partially overlaps and crosses the IFOF and OR.

Tracking of the ILF is performed with a two-ROI approach using streamline or probabilistic tractography with delineation of the seed ROI in the occipital WM and the target ROI in the anterior WM of the temporal lobe at the level of the anterior commissure. Both ROIs are delineated in one coronal slice perpendicular to the ILF trajectories. After connecting the two ROIs, the tractogram should be inspected for a priori anatomical consistency. Spurious streamlines can be removed with “out-ROI” filters. The ILF are symmetric fascicles without significant differences in tract volume between the two hemispheres.

The ILF is involved in face and visual object recognition, reading, visual memory, and linking object representations to their lexical labels (Catani and Mesulam 2008). IES of the ILF systematically impaired reading ability at the level of the posterior surgical area. The ILF is involved in both the direct and indirect transfer of information between extrastriatal visual and anterior temporal areas involved in memory and limbic functions (Mandonnet et al. 2009). Moreover, it has been suggested that the ILF together with the UF provides an indirect pathway between the occipital

and frontal language areas supporting semantic and lexical processing. The ILF, MLF, and UF are components of anterior temporal networks involved in selecting verbal labels for objects in a posterior-anterior progression of word comprehension, from generic to specific levels of precision. Overall the anterior temporal network enables mapping sound to meaning (Hickok and Poeppel 2007; Catani and Bambini 2014).

5.7 The Temporoparietal Fiber Intersection Area

The IPL and posterior temporal lobes are considered among the most eloquent areas in the human brain. Lesion studies have reported major language deficits such as aphasia (Fridriksson et al. 2010), alexia, agraphia, hemianopia, and neglect (Müller-Oehring et al. 2003) in patients with a lesion located in the IPL or in the posterior temporal lobe. In the past, clinicians have interpreted neurological deficits of higher cognitive function as a consequence of lesions in associative cortex, neglecting the importance of the WM pathways coursing underneath. Since most focal lesions also affect the subcortical and deep WM, potential damage to adjacent pathways should also be investigated since it may cause a disconnection syndrome (Catani and ffytche 2005). Recently, unexpectedly high postoperative deficit rates were reported in patients with parietal gliomas. In a series of 119 parietal lobe gliomas, Sanai et al. reported a 8.4 % permanent language deficits (Sanai et al. 2012), which is fivefold greater compared with the previously reported experience of the UCSF group with gliomas located within language areas (1.6 %) (Sanai et al. 2008). The 6.7 % rate of permanent visual deficits was also higher than expected in this series. An even higher rate of long-term mild language deficits (42.9 %) was reported in a series of 14 consecutive patients with glioma involving the IPL who were operated with cortical and subcortical IES mapping (Maldonado et al. 2011a). This rate is 21-fold greater compared with the 1.7 % rate of the overall experience of the same Montpellier group with LGG located within eloquent areas (Duffau et al. 2008a). Both studies underscore the importance of the WM pathways coursing underneath the IPL and the posterior temporal lobe that, if damaged, will have consequences far more serious than in other brain cortical and subcortical locations.

In a very recent article, Martino et al. elucidated the complex organization and the surgical importance of the TPFIA that underlies the IPL and posterior temporal lobe, using postmortem cortex-sparing fiber dissection and streamline MR tractography (Martino et al. 2013). The

TPFIA is seated in the WM underneath the AG, posterior MTG, and ITG and may extend underneath the posterior part of the SMG and STG. The authors described seven long-range WM fascicles passing through the TPFIA. In this section, we'll discuss the anatomic relationship among the seven tracts and the MLF in detail since the AF, ILF, IFOF, and OR have been already described in other sections.

Starting the virtual or postmortem dissections from the lateral brain surface at the level of the temporoparietal junction, the posterior segment of the AF is the most superficial bundle. This fascicle runs vertically and connects the AG with the posterior MTG. Medial and slightly anterior to the posterior segment runs the long segment of the AF that connects Broca with Wernicke territories. In the TPFIA, the bundles of the AF direct run vertically. Next there is the MLF that is medial to the stem of the AF direct and lateral to the IFOF.

The MLF is a longitudinal fascicle that is coursing with an anteroposterior orientation in the WM of the SFG, parallel to the other longitudinal fascicles (SLF and ILF). At the posterior end of the STG, the fibers bend dorsally and course in the posterior portion of the corona radiata until they project into the AG. The MLF connects the upper part of the temporal pole and the entire SFG with the AG (Makris and Pandya 2009; Makris et al. 2009). The MLF should not be confused with the posterior segment of the AF because it is deeper located and it has a longitudinal rather than a vertical orientation. It has been suggested that the MLF has a role in language and attention (Makris and Pandya 2009; Menjot de Champfleur et al. 2013). However, Duffau et al. have evaluated eight patients with glioma infiltrating the SFG using IES and have established that damage to the MLF doesn't cause long-term deficits; thus, it is not essential for language. No interference with picture naming was observed by IES of the MLF, and no new permanent language deficits were detected with the Boston Diagnostic Aphasia Examination after extensive resection of gliomas that included large parts of the MLF. In the same IES study, the IFOF was identified in all patients by eliciting semantic paraphasia; thus, it can be easily distinguished from the MLF (De Witt Hamer et al. 2011).

The MLF crosses in the upper half of the TPFIA, and it is more difficult to reconstruct than the AF with DTI streamline tractography; SD helps to some degree to depict the MLF. The seed ROIs should be delineated on coronal FA/DEC maps in the WM of the anterior part of the SFG at the level of the AC; the target ROIs should be delineated in the WM of the AG at the level of the splenium of the CC (Makris et al. 2009).

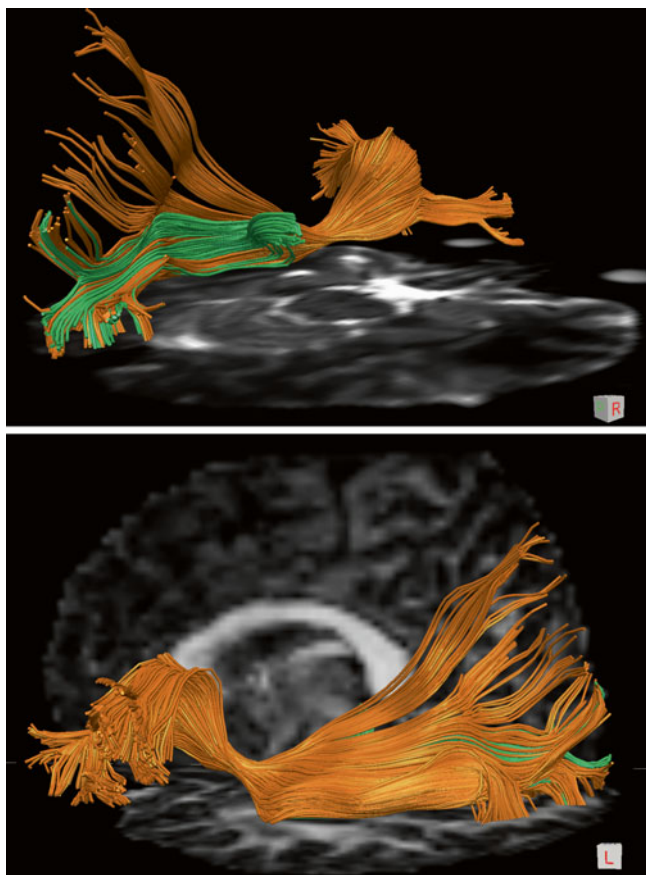


Fig. 10 Medial (upper panel) and lateral (lower panel) views of the left IFOF (orange) and OR (green) displayed over FA map and T2-weighted MRI, respectively. The OR streamlines are intermingled with those of the posterior third of the IFOF and both course along the most medial and ventral part of the temporoparietal fiber intersection area (TPFIA). The IFOF and the OR are the most eloquent fascicles intersecting in the TPFIA. They course along the lateral wall of the occipital horn of the lateral ventricles, and they are difficult to separate with MR tractography. Diffusion data were acquired with HARDI (64 gradient directions, $b=2,000$, $2 \times 2 \times 2 \text{ mm}^3$), and tractography was performed with DTI interpolated streamline algorithm (thresholds FA >0.1 ; angle $<35^\circ$)

In the inferior half of the TPFIA runs the ILF, laterally to the IFOF and ventrally to the MLF. The ILF runs underneath the inferior temporal and occipital gyri and connects the inferior part of the temporal pole with the ITG, the middle and inferior occipital gyri, and the ventral surfaces of the temporal and occipital lobes. The IFOF and the OR are the most critical fascicles intersecting in the TPFIA, and their fibers are difficult to separate with MR tractography. On axial and coronal DEC maps, they appear green along their entire course, and they are seated in between two vertically oriented fascicles (blue on color maps): the AF stem on the lateral side and the tapetum on the medial side. The IFOF

connects the frontal opercular region with the insula and temporobasal, parietal, and occipital cortices and runs medially in the temporal stem, ventral aspect of the extreme and external capsules, and sagittal stratum. The OR fibers are intermingled with those of the IFOF running in the most medial and ventral part of the TPFIA (Fig. 10). The tapetum is the most medial WM structure and consists of interhemispheric fibers that form the roof and lateral wall of the atrium and temporal and occipital horns of the lateral ventricles. The tapetum connects both temporal lobes through the posterior part of the corpus callosum.

In summary, the seven tracts can be identified on axial and coronal DEC maps. Three tracts have a craniocaudal orientation, and their streamlines are directionally colored in blue: they are the posterior and direct segments of the AF laterally and the tapetum medially. In between the vertically oriented tracts, the IFOF and the OR run throughout the entire TPFIA, while the MLF and ILF run longitudinally laterally to the IFOF, respectively, in the upper and lower half of the TPFIA. On DEC maps, it is not possible to distinguish the trajectories of the five anteroposterior oriented tracts; thus, it is necessary to use MR tractography.

In the past, the transcortical approach through the TPFIA was considered the most direct trajectory from the brain surface to reach a tumor in the posterior hippocampus, temporal and occipital horns, or atrium of the lateral ventricle. Recent postoperative data have shown that the TPFIA is one of the most vulnerable parts of the human brain; therefore, knowledge of this important crossroad is now mandatory for surgical planning before a safe resection of deep-seated tumors. When a glioma infiltrating the AG and posterior third of the MTG and ITG extends 2–3 cm into the deep WM, it will likely displace, infiltrate, or interrupt the fascicles coursing in the TPFIA. A detailed MR tractography study of the TPFIA should be performed to better understand the relationship between the mass and the seven fascicles. In our practice, we have seen several patients with gliomas originating within the TPFIA. It is surprising to find that in many occasions, the mass is causing only mild preoperative neurological deficits, despite the presence of eloquent tracts such as the IFOF, AF, and OR. This can be explained by showing with MR tractography that the tracts can be reconstructed in their integrity because the mass is displacing the tracts rather than interrupting them. In this peculiar area, we have seen several rapidly growing gliomas dislocating tracts without interrupting them (Figs. 11 and 12). Visualization of eloquent tracts in the proximity of a glioma may have a positive predictive value for postoperative outcome, because it suggests that the fascicle is partially spared by the tumor and that a relatively radical resection can be attempted.

It has been shown that MR tractography can reliably reproduce and strengthen the knowledge gathered from intraoperative neurophysiologic and postmortem dissection studies, thus having a significant impact on patient management particularly so in cases when the surgical risk should be carefully balanced with the benefits of an extensive resection. Planning a surgical approach anterior or posterior to the

TPFIA may preserve the long and posterior segments of the AF, while in other cases, a longitudinal surgical incision may be indicated to safeguard the IFOF, OR, MLF, and ILF that are running in the anterior-posterior orientation (Martino et al. 2013). Moreover, IES should be strongly considered for safe resection of deep-seated tumors, especially in the dominant hemisphere.

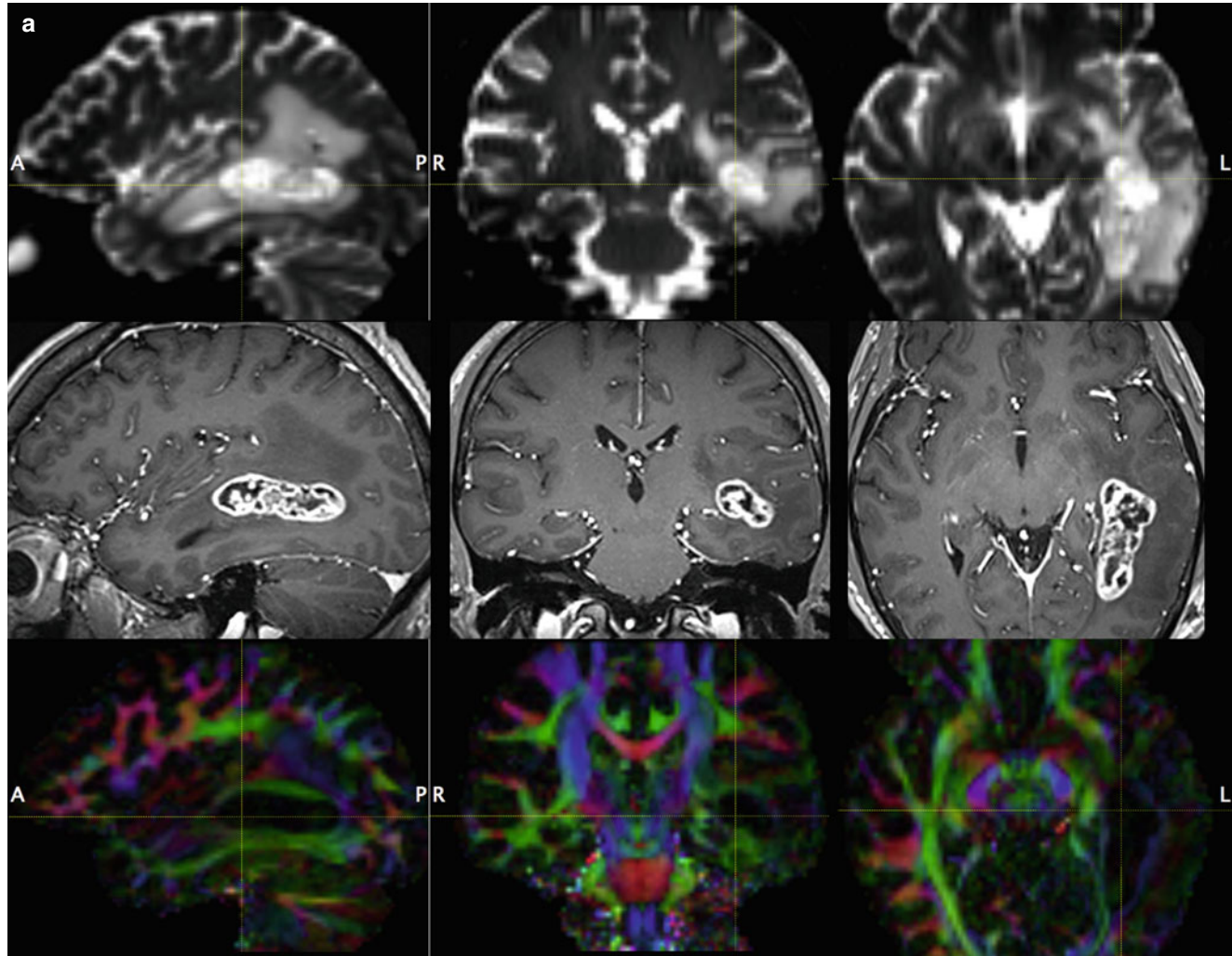


Fig. 11 (a) A 50-year-old male with an enhancing mass seated in the deep left temporo-occipital WM. There is extensive perilesional vasogenic edema that is bright on T2WI, hypointense on T1WI, and low on FA maps. A GBM WHO IV was removed at surgery. DEC maps show decreased hue (FA) and dislocation of several green (associative) tracts in the temporoparietal fiber intersection area (TPFIA). T2WI upper row, T1WI post-gadolinium middle row, DEC maps lower row. (b) Tractography is showing that all fascicles in the TPFIA can be virtually dissected: the mass is dislocating the AF direct (red) and AF posterior (yellow) laterally and the IFOF (orange) medially. The AF direct is the lateral functional boundary, whereas the IFOF is the medial boundary.

The functional limits of the resection were confirmed in the operating room with direct subcortical IES. In this case, the information provided by tractography is by far superior to that provided by DEC maps. Medial view (*left column*) showing the relationship of the AF, SLF-III (*green*), and IFOF with the mass. Anterior view (*bottom row, left column*) showing the mass splaying the AF direct from the IFOF. Left lateral view (*right column*) showing dissection of four of the seven fascicles that form the TPFIA. Diffusion data were acquired with HARDI (64 gradient directions, $b=2,000$, $2 \times 2 \times 2 \text{ mm}^3$), and tractography was performed with DTI interpolated streamline algorithm (thresholds FA >0.1 ; angle $<35^\circ$)

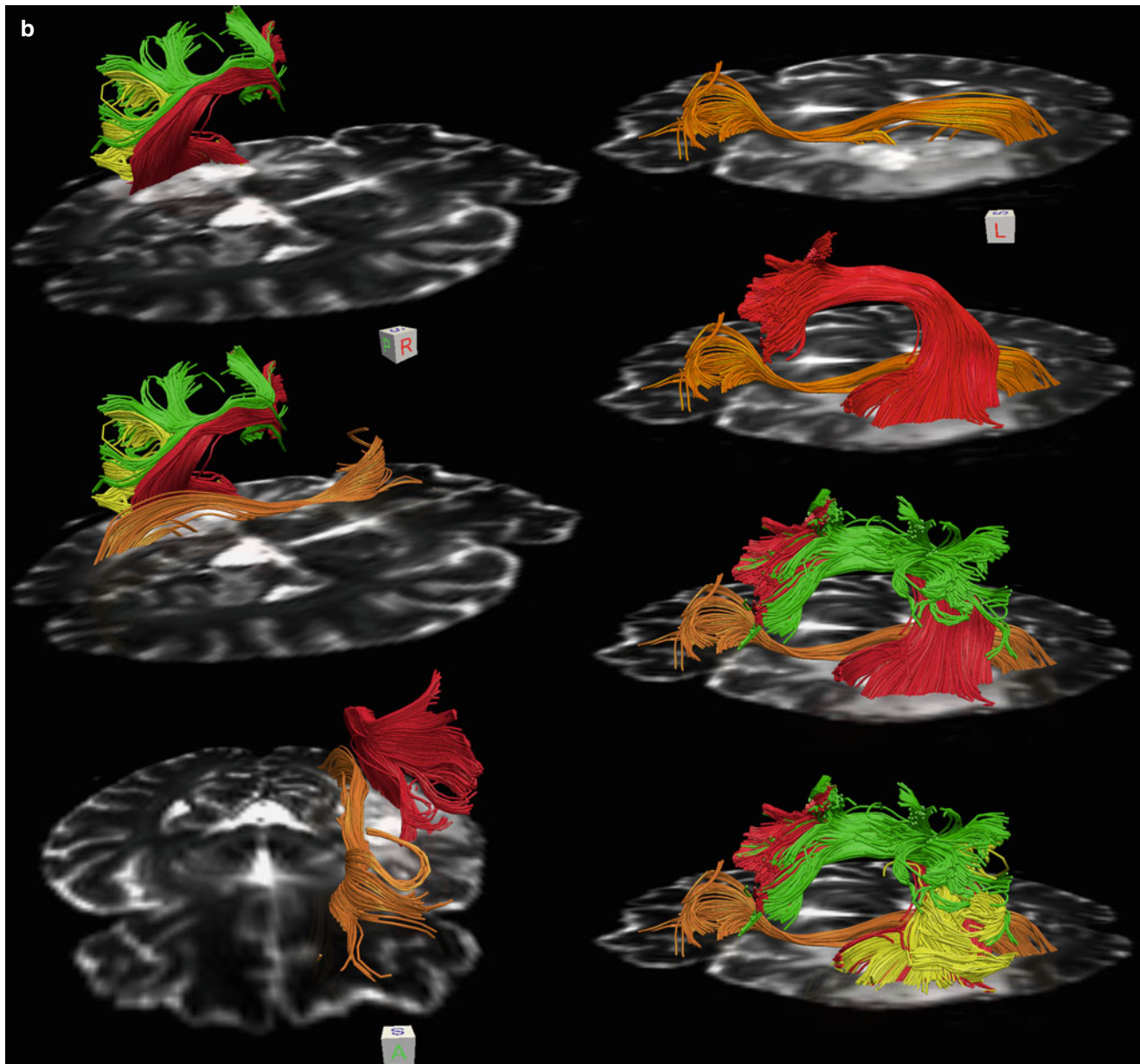
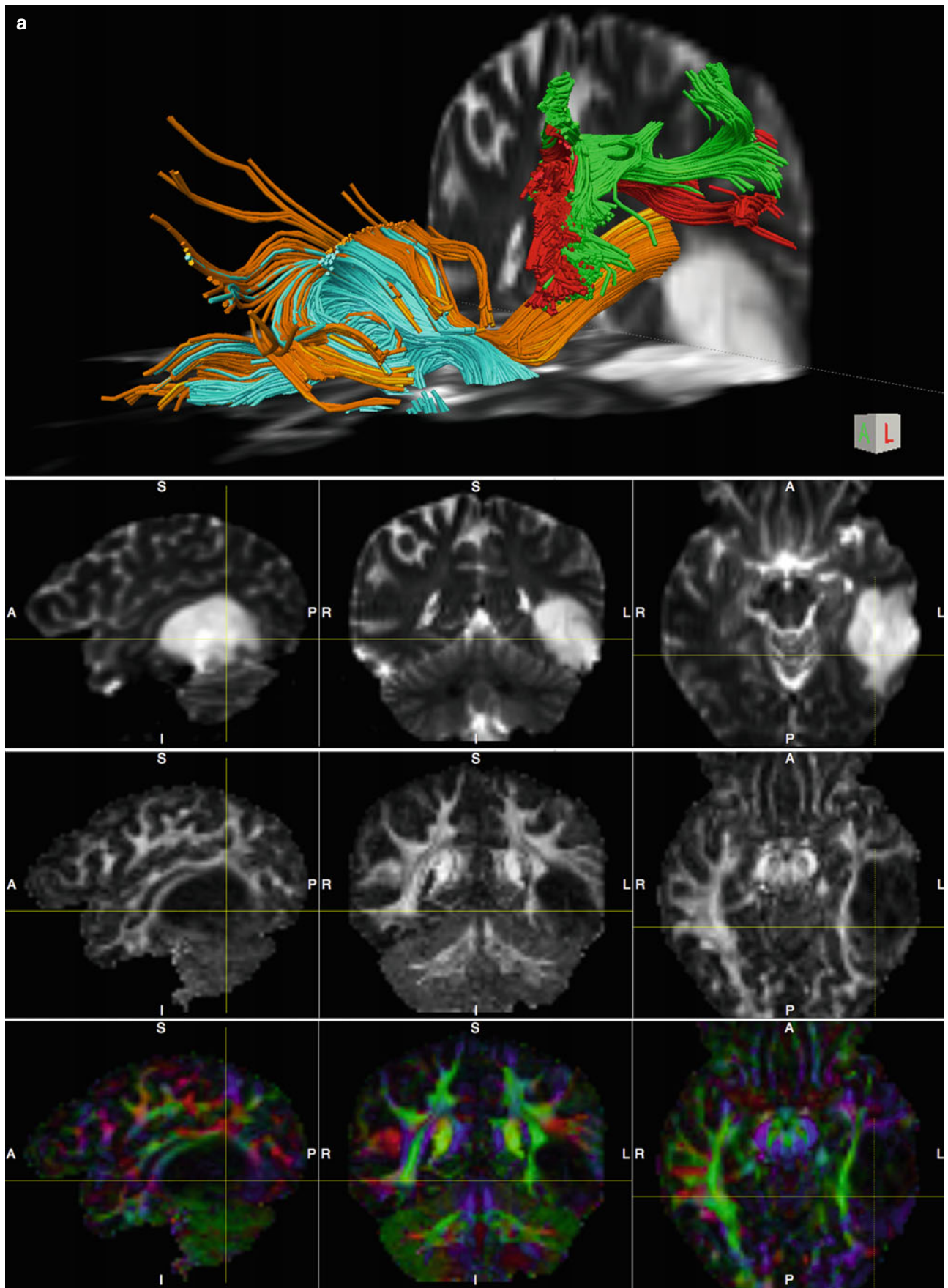


Fig. 11 (continued)



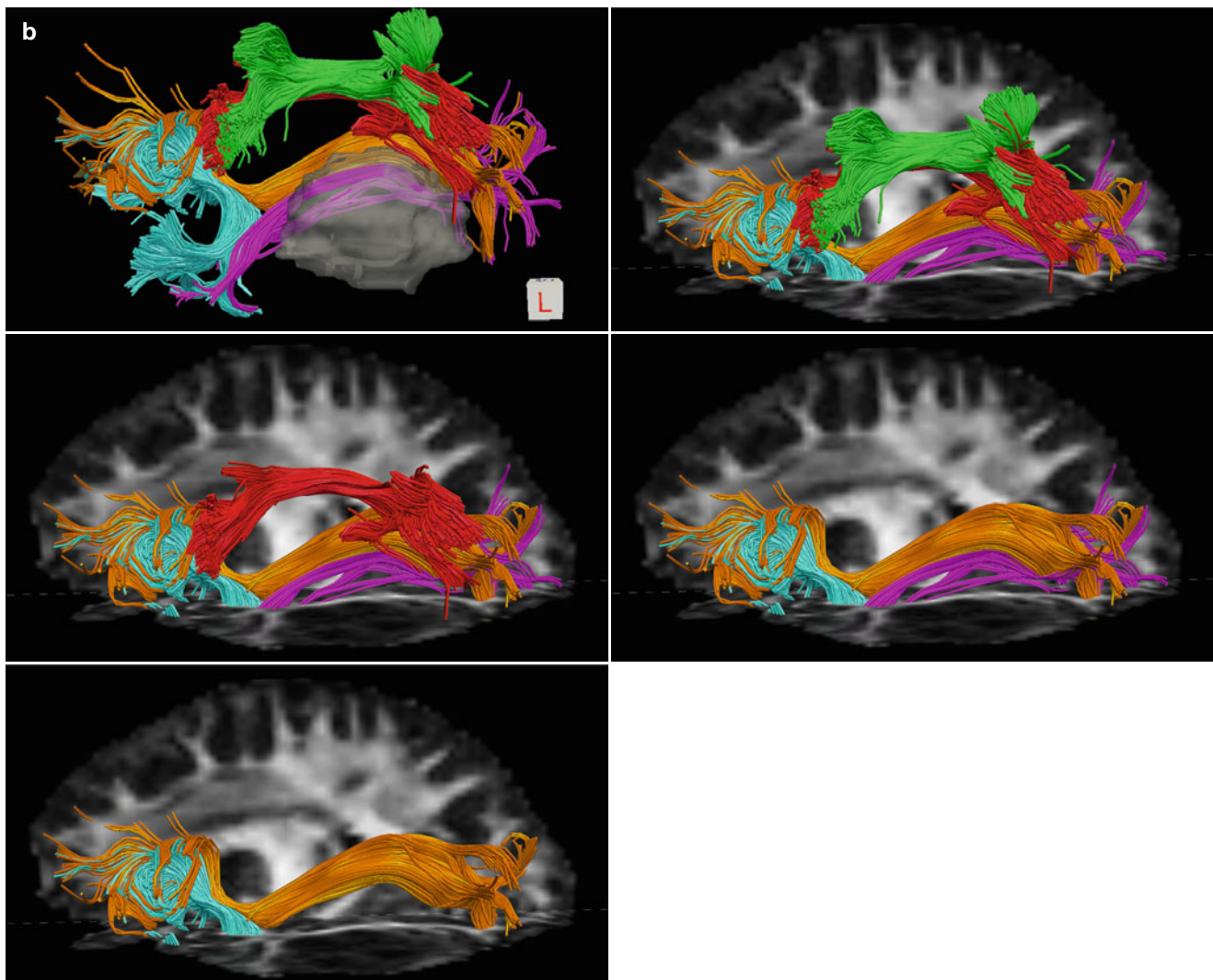


Fig. 12 (continued)

Fig. 12 (a) A 31-year-old female with a mass expanding in the middle, inferior, and fusiform gyri of the left temporal lobe. Tractography (*upper panel*) is showing that the main fascicles in the TPFIA can be virtually dissected: the mass is dislocating dorsally the AF direct (red), medially and superiorly the IFOF (orange) and OR (not shown). The SLF-III (green) and UF (cyan) are also shown. The mass is bright on T2WI (*2nd row*) with very low FA (*3rd row*). DEC maps (*bottom row*) are showing that the mass has displaced medially the association tracts, but only with tractography, it was possible to realize that the IFOF was also displaced dorsally. This information was quite appreciated by the neurosurgeon during presurgical consultation. The functional limits of the resection were confirmed in the operating room with direct subcortical IES. An anaplastic oligodendrogloma WHO III was removed at surgery. (b) Virtual dissection with tractography of the fascicles in the TPFIA. The relationship of five fascicles with the mass (gray) is shown

in the upper panel. After “hiding the mass,” the medial functional margins of the lesion with the ILF (pink) and IFOF (orange) are illustrated over a FA map in the *2nd panel* from above. “Hiding the SLF-III” (green) allows best appreciation of the remarkable dorsal displacement of the temporal arm of the AF direct (red) in the *3rd panel*. “Hiding of the AF direct” allows appreciation of the ILF and IFOF in the *4th panel*. The UF (cyan) is relatively remote from the anterior margin of the lesion. Visualization of eloquent tracts in the proximity of a glioma may have a positive predictive value for postoperative outcome, because it suggests that the fascicle is partially spared by the tumor and that a relatively radical resection can be attempted. Diffusion data were acquired with HARDI (64 gradient directions, $b=2,000$, $2 \times 2 \times 2 \text{ mm}^3$), and tractography was performed with DTI interpolated streamline algorithm (thresholds FA >0.1 ; angle $<35^\circ$)

5.8 Frontal Aslant Tract and Subcallosal Fasciculus

The frontal aslant tract (FAT) is a recently described bilateral frontal intralobar fascicle connecting the anterior part of SMA proper and the pre-SMA with the pars opercularis (BA44) of the IFG. Some fiber projections reach also the adjacent BA6. The FAT is the only intralobar tract connecting two nonadjacent gyri in the frontal lobe, and it has been named “aslant” because of its peculiar oblique orientation in the coronal plane. It has been dissected with streamline tractography using the FACT algorithm (Oishi et al. 2008; Lawes et al. 2008) and with probabilistic tractography (Ford et al. 2010); however, it is best visualized with the SD algorithm (Catani et al. 2012). It is one of the few previously unknown tracts that have been first described with MR tractography (Oishi et al. 2008) and then validated with postmortem dissection studies (Lawes et al. 2008). A significant leftward asymmetry in track volume in right-handed healthy subjects has been reported (Catani et al. 2012), suggesting a role in language connections. In one of our patients with oligoastrocytoma WHO II seated in the lobar WM of the left frontal lobe, tractography showed that the FAT was adjacent to the medial and ventral margin of the mass and the CST was adjacent to the posterior margin, while the AF was relatively remote from it (Fig. 13). At surgery, the mass was resected and the patient experienced severe mutism. Speech initiation deficits lasted longer than expected for a SMA syndrome, and approximately 12 months after surgery, the patient continued to have delayed reaction time to initiate speech. In the postoperative tractography study, it was shown that the deficit was associated with resection of the FAT and preservation of the AF and SMA. In another tractography study performed in 35 patients with primary progressive aphasia, fractional anisotropy values in the FAT correlated with deficits in verbal fluency, confirming that this fascicle is part of the speech network (Catani et al. 2013).

Tracking of the FAT is performed with a two-ROI approach using streamline or probabilistic tractography with delineation of the seed ROIs in pars opercularis (BA44) and of the target ROI in the pre-SMA and anterior SMA proper in multiple axial slices. Placement of spherical ROIs with TrackVis software (<http://trackvis.org/>) is handily used to explore the frontal region for intralobar streamlines before dissecting the frontal tracts.

The SCF has been described in humans and monkeys. The SCF was first described in 1887 by Theodor Meynert who used the term “corona radiata of the caudate nucleus” (Meynert 1887) and later in 1893 by Muratoff (Forkel et al. 2014b). In the monkey, Yakovlev and Locke described the SCF as a projection tract connecting the cingulum to the caudate nucleus (Yakovlev and Locke 1961). Moreover, the fronto-striatal fibers also have strong reciprocal connections with BA24 of the cingulate gyrus and the pre-SMA. For this reason, the SCF is also named the fronto-striatal tract (FST).

In a study of stroke patients using computerized tomography, more severe limitation in spontaneous speech was associated with lesions in the most rostral and medial portion of the FST plus the periventricular WM near the body of the lateral ventricle (Naeser et al. 1989). It is assumed that the FST may play an important role in the development of the intention to act and in the preparation for speech movement, both the initiation and limbic aspects of speech.

The SCF courses within the periventricular zone of the anterior horn of the lateral ventricle, medially to the superior fronto-occipital fasciculus, an association pathway connecting the frontal with the occipital cortex. The two fascicles should be clearly distinguished despite their anatomic proximity in the periventricular zone. To add to the confusion, occasionally the SCF and the superior fronto-occipital fasciculus have been used synonymously in the literature, despite that they have clearly different anatomic and physiologic properties.

In a tractography study in eight healthy subjects, Léhericy et al. dissected fronto-striatal projections and provided the first demonstration that frontal posterior and anterior premotor area projections to the striatum are organized in distinct circuits along the caudal-rostral axis (Léhericy et al. 2004). Fiber tracking of the FST is performed with the two-ROI approach: a seed subcortical ROI is delineated in the caudate head and a target ROI in the pre-SMA. The trajectories of the FST ascend around the lateral walls of the frontal horn of the lateral ventricle and then intermingle with ipsilateral FAT trajectories, originating from the pars opercularis before entering into the pre-SMA. Subcortical IES of the FST evokes delayed speech initiation (Vassal et al. 2013).

5.9 Which Fascicles Are Eloquent for Speech?

The aim of IOM is to map the networks underlying the different but interactive language processes that have to be safeguarded and that will define the functional limits of the resection. Several language tasks are available, and selection of which task to administer to the patient depends on the location of the lesion, presurgical imaging mapping and neuropsychological results, handedness, and job and hobbies of the patient (see Table 1). The PMv (BA6) can be identified asking the patient to count while the neurosurgeon stimulates the surface of the cortex with a low-frequency bipolar probe. When the current depolarizes neurons in the PMv of a patient who is counting or during spontaneous speech, he/she will have a speech arrest (Duffau 2005), even if stimulated in the nondominant hemisphere (Duffau et al. 2008b). Common and important language tasks are picture naming, reading, comprehension, syntax, and language switching from one language to another.

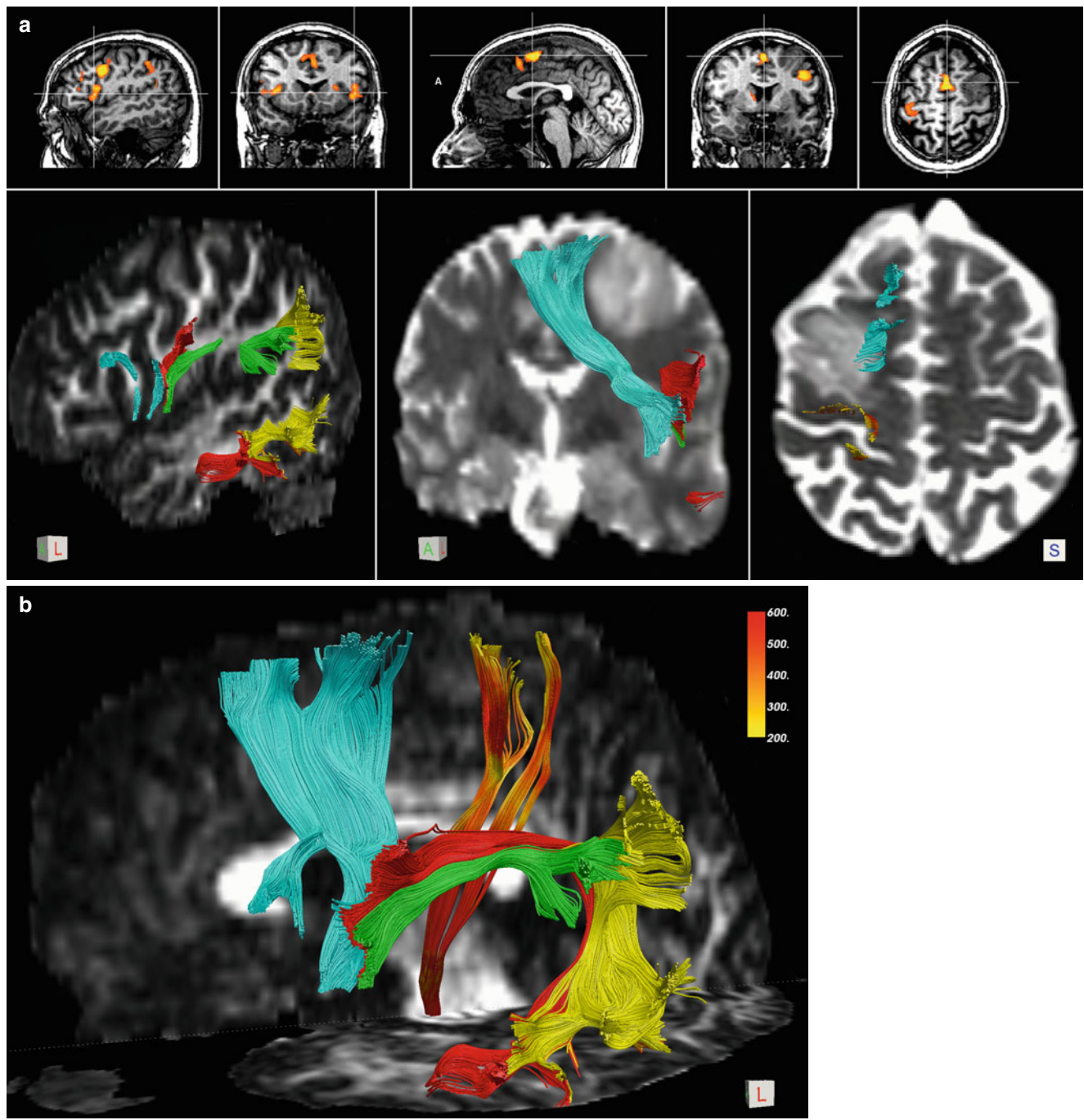


Fig. 13 (a) A 29-year-old male with a mass infiltrating the lobar WM and the left MFG. Functional MRI with the verb generation task (*upper row*, from left to right) is showing BOLD response in left pars opercularis and PMv (sagittal and coronal images), in the pre-SMA and SMA proper (sagittal image), SMA proper and PMd (coronal image), and SMA proper (axial image). Activation areas can be used to assist delineation of ROI for tractography in selected cases. In the *left panel* of the *lower row*, the projections of the FAT (cyan) in pars opercularis and PMv, projections of the AF direct (red) in PMv and posterior MTG, projections of the SLF-III (green) in PMv and SMG, and projections of the posterior segment of the AF (yellow) in AG and MTG are overlaid on a sagittal FA map. The FAT is the medial and ventral limit of resection of the mass as illustrated in the coronal T2WI (*mid panel*). The relationship of the mass with the FAT and CST (red-orange scalar) that are, respectively, the medial and posterior margins of the mass is illustrated in the axial T2WI (*right panel*).

(b) A left lateral oblique view of the same tracts (*colours as in a*) is displayed over sagittal and axial FA maps. Note how big the FAT is in this case, probably enhanced by interruption of the crossing SLF due to the presence of the tumor. Intraoperative monitoring with subcortical IES was not performed in this case, and the patient immediately after surgery presented with severe mutism that lasted for a few weeks. Speech initiation deficits lasted longer than expected for a SMA syndrome, and approximately 12 months after surgery, the patient continued to have delayed reaction time to initiate speech. An oligoastrocytoma WHO II was removed at surgery. The postoperative tractography study (not shown) confirmed that the severe SMA syndrome was associated with resection of the FAT despite preservation of the AF and SMA. Diffusion data were acquired with HARDI (64 gradient directions, $b=1,000$, $2 \times 2 \times 2 \text{ mm}^3$), and tractography was performed with DTI interpolated streamline algorithm (thresholds FA >0.15; angle <45°)

Table 1 The main fascicles and their cortical terminations of the motor, language and visual systems are listed. The MEP electrode position or the task administered to the patient, the recorded incorrect responses and the neurological deficits when the fasciculus of interest is preserved or damaged are indicated for each fasciculus

| System | Fasciculus | Cortical terminations | IES/task | Response | Preserved | Damaged |
|------------------------|------------|--|------------------------------------|---|-------------------------------------|---|
| Motor | CST | M1, PMv, PMd, SMA | Face, arm, tibialis | MEP or movement disorders (dystonic movement or movement arrest) | Transient motor deficits | Permanent motor deficits |
| Language | Lt AF | PMd, PMv, MTG | Picture naming | Phonemic paraphasia, anomia | Transient deficits | Conduction aphasia |
| | Lt IFOF | IFG, OFC, temporal, parietal, occipital | Picture naming | Semantic and verbal paraphasia, anomia | Transient aphasia | Semantic and verbal paraphasia, anomia |
| | Lt UF | OFC, T-pole | Picture naming, famous face naming | Anomia | Transient deficits | Long-term proper name recall |
| | Lt ILF | T-pole-occipital and visual word form area | Categorial reading | Reading disorder | Transient categorial errors | Permanent alexia |
| | Lt FAT | SMA, BA44 | Complex serial articulation | Perseveration, slurring | Speech initiation | Permanent delayed reaction time, deficit of syntax production |
| | Lt SLF-III | PMd, PMv, SMG and posterior STG | Picture naming, numbering | Number errors, articulatory deficits | Transient deficits | Permanent deficits |
| Vision | OR | LGN, V1 | Alternate picture naming | Missed or “positive” responses (as phosphenes or visual illusion) | Quadrantanopsia or even hemianopsia | Quadrantanopsia or even hemianopsia |
| Visuospatial attention | Rt SLF-II | MFG, AG | Bisection line | Bisection error | Hemispatial neglect | Hemispatial neglect |

In gliomas infiltrating the perisylvian region within the dominant hemisphere, mapping of the cortical sites on the brain surface begins with identification of the motor strip, PMv, and posterior IFG (Broca area). After completing corticotomy in order to have access to deep-seated gliomas, resection of the tumor continues only after all functional limits with eloquent subcortical pathways have been identified and disconnected from the tumor. Laterally and medially to gliomas growing in the anterior frontal lobe, there are, respectively, the FAT and the SCF that participate in initiation of speech. In the surroundings of gliomas growing in the suprasylvian region within the frontal or parietal opercula, the SLF-III, AF, and CST from the lateral to medial side are encountered. The AF is the deep limit of the resection also in superficial gliomas infiltrating the MTG and STG. The IFOF and OR are the deep limits in gliomas seating deep to the IPL and posterior temporal region. At the level of the ventral temporo-occipital junction, the posterior part of the ILF should be identified because it is part of the reading network.

Determination of which fascicles are functionally eloquent for language and should be safeguarded during surgery remains an important and debated issue. The AF has been associated with language for a very long time; however, its

role together with that of the UF, MLF, and ILF in maintaining the integrity of the network has been questioned. In a large series of 115 patients with LGG infiltrating language areas, Duffau et al. showed that tumor resection by safeguarding functional boundaries avoids permanent postoperative language deficits (Duffau et al. 2008a, b). The AF is a long-range fascicle and IES of only a focal part of it may evoke phonemic paraphasia. The eloquent part of the AF should be safeguarded, whereas other parts can be removed with the tumor. It is important to emphasize that there is a great variability among patients in location of the eloquent part that can only be identified with subcortical IES. Stimulation of the AF direct segment induces transient phonemic paraphasia and repetition errors that are signs of conduction aphasia. Stimulation of the AF can also disrupt syntax (Vidorreta et al. 2011) or a wide network involved in language switching from native to secondary languages, a skill important to spare in bilingual patients (Bello et al. 2006; Gatignol et al. 2009). Stimulation of the SLF-III induces speech apraxia (Maldonado et al. 2011a), and it may be involved with verbal working memory (Maldonado et al. 2011b), while stimulation of the FAT and SCF induces speech initiation.

We have seen previously how important is the direct subcortical IES of the IFOF in preserving semantic processes of language. The IFOF is the medial functional limit in gliomas located in the frontal operculum, insula, and temporal lobe of the dominant hemisphere. On the contrary to what happens for the left AF, subcortical IES of the left IFOF throughout its course induces semantic paraphasia (Duffau et al. 2005; Bello et al. 2007).

The UF can be removed without permanent deficits if the IFOF is preserved: in Duffau's large series, IES of the left UF did not evoke language deficits (Duffau et al. 2008a, b). However, long-lasting deficits in famous face naming in a series of patients with UF resection after removal of left frontal or temporal gliomas have been reported (Papagno et al. 2010, 2014). Direct IES of the left ILF did not induce language errors in 12 patients with LGG in the temporal lobe (Mandonnet et al. 2007b). However, the posterior part of the ILF should be safeguarded and preserved in gliomas located near the ventral temporo-occipital junction, because the ILF may play a crucial role in reading. In a single glioma patient, direct cortical IES near the visual word form area led to visual paraphasias that were also elicited by subcortical IES of the ILF in the anterior wall of the surgical cavity (Mandonnet et al. 2009). In a series of 8 patients with glioma in the left dominant STG, subcortical IES of the anterior part of the MLF did not elicit language deficits, and the patients did not develop any postoperative permanent language deficit (De Witt Hamer et al. 2011). Thus, the MLF may participate in, but is not essential for, language processing. Taken together, these results suggest that resections of the UF, ILF, and MLF with gliomas seated in the dominant temporal lobe do not cause permanent aphasia. These fascicles are likely part of a network whose function can be compensated by the IFOF.

Cortical IES of the SMA and pre-SMA produces both vocalization and arrest of speech (Penfield and Rasmussen 1950). Patients with lesions of the SMA may present various degrees of speech impairment from a total inability to initiate speech to deficits in phonologic fluency. It has been hypothesized that the SMA through the FAT may facilitate speech initiation. Very recently in a series of 19 patients with WHO II gliomas infiltrating the SMA, pars opercularis and/or the caudate nucleus inhibition of speech has been evoked not only by cortical IES of the BA6, pars opercularis, or SMA but also by direct subcortical IES of the left FAT (Kinoshita et al. 2014). Furthermore, the authors found a significant correlation between the severity of postoperative transitory speech initiation deficits and the distance of the FAT from the wall of the resection cavity. In the same study, IES of the FST generated negative motor responses, suggesting that the FST may be part of the "negative motor network" and may participate in the modulation of motor function including bimanual coordination. Despite the fact that the authors

found a relationship between the speech initiation postoperative deficits and the FAT but not the FST in the left hemisphere, the average distance between tumor resection and left FST showed a positive correlation with verbal phonemic and semantic fluency scores in the immediate postoperative period and pleaded in favor of the involvement of the left FST and caudate in speech control. All together, these studies emphasize how much valuable is the anatomic information provided by pre- and postoperative tractography studies as a way to integrate IES mapping.

In conclusion, the abovementioned language fascicles should be identified with presurgical tractography and IES performed in awake patients every time a mass is seated in the perisylvian region of the dominant hemisphere in order to identify the subcortical functional limits of the resection. At present, the majority of neurosurgeons performing awake surgery would agree that the IFOF is the most essential of all language-related fascicles, followed by the AF and SCF. Damage to the IFOF is very likely to cause permanent language deficits. A resection very close to the AF, SLF-III, FAT, and SCF is likely to induce transitory speech disorders that may recover in a few weeks or months. We predict that the role of diffusion imaging with tractography in the routine evaluation of pre- and postoperative glioma patients will soon become standard of care in neuro-oncology.

5.10 Visuospatial System

5.10.1 OR

The retinogeniculate fibers originate from neurons in the retina and project to the lateral geniculate nucleus. The OR, also called the geniculostriate fibers, are a large bundle of myelinated fibers that originate from relay neurons in the layers of the lateral geniculate nucleus and project to the ipsilateral primary visual area. The OR are part of the ventral part of the posterior thalamic radiations and can be divided into two main components: the dorsal fibers carrying visual information from the lower quadrants of the contralateral visual hemifield and projecting to the cortex of the cuneus into the superior bank of the calcarine fissure and the ventral fibers carrying visual information from the upper quadrant of the contralateral hemifield and projecting to the cortex of the lingual gyrus into the inferior bank of the calcarine fissure. The dorsal fibers originate from the dorsomedial portion of both lateral geniculate nuclei and arch directly caudally to pass through the retro Lenticular limb of the internal capsule before projecting to the cuneus. On the contrary, the ventral fibers originate from the ventrolateral portion of the lateral geniculate nucleus and arch rostral, passing into the WM of the anterior temporal lobes to form a broad U-turn (loop of Meyer) before passing caudally and projecting to the lingula. Damage to the dorsal fibers results in a loss of vision in the

contralateral inferior visual field. Damage to the Meyer loop in the anterior temporal lobe or to any other segment of the ventral contingent results in contralateral superior quadrantanopia. Lesions of the OR may result in quadrantanopia or may involve only a portion of a quadrant of the visual field. The closer a lesion is to the primary visual cortex, the more congruous the visual field loss of one eye can be superimposed to the other eye. The more anterior a lesion is in the OR, the more likely it is that the visual deficit will be incongruous in the two eyes.

Tracking of the OR is performed with a two-ROI approach using streamline or probabilistic tractography with delineation of the seed ROI in the lateral geniculate nucleus and of the target ROI in the ipsilateral WM of the occipital lobe at the level of the calcarine fissure. The seed ROI is delineated in the lateral portion of the thalamus in multiple axial slices or using a sphere; the target ROI is delineated in one coronal slice perpendicular to the OR. The OR course together with the IFOF for most of their course (Fig. 6): the dorsal fibers of the OR overlap with the IFOF as well as the upper two-thirds of the ventral fibers projecting to the inferior bank of the calcarine cortex. Only at the more posterior part of the sagittal stratum, the OR and IFOF diverge to reach their respective cortical terminations. After connecting the two ROIs, the tractogram should be inspected for a priori anatomical consistency. Spurious streamlines can be removed with “out-ROI” filters. The OR are symmetric bundles without significant differences in tract volume between the two hemispheres.

During awake surgery, the OR can be identified with IES administering a picture-naming task that displays simultaneously two objects in opposite quadrants. When the surgeon stimulates the dorsal bundles of the OR, the patient will fail to name the object in the contralateral inferior hemifield; when he stimulates the ventral bundles, the patient will fail to name the object in the contralateral superior hemifield.

5.10.2 Superior Longitudinal Fasciculus

Lesion studies in patients and recent functional imaging studies in healthy human subjects have provided evidence that visuospatial attention relies on a bilateral frontoparietal network, with right hemisphere dominance in most, but not all, individuals. Synchronous activity of neurons in the frontal and parietal cortices during visual search has been demonstrated using multiple electrodes in monkeys and scalp EEG in young and elderly human subjects, suggesting that a bilateral frontoparietal network may play an important role in top-down and bottom-up control mechanisms. Axonal tracing studies in the monkey have demonstrated that frontal and parietal neurons are connected through three separate fascicles coursing longitudinally in the dorsolateral WM of the centrum semiovale (Schmahmann and Pandya 2006). The three segments of the SLF, a major intrahemispheric

association fiber pathway that connects the parietotemporal association areas with the frontal lobe and vice versa, compose the network. In the classical description of Dejerine, the AF was also considered part of the SLF; however, studies in monkeys showed that the SLF and AF are two separate entities. The trajectories of three separate segments of the SLF have been demonstrated also in the human brain with postmortem dissections (Ludwig and Klingler 1956) and more recently with DTI (Makris et al. 2005) and SD (Thiebaut de Schotten et al. 2012) tractography. Overall, the anatomy of the SLF is highly conserved between humans and monkeys.

The *SLF-I* is the most dorsal component and connects the dorsolateral part of the superior parietal lobule and precuneus with the anterior dorsal part of the SFG. The *SLF-II* is the major component of the SLF, and it connects the AG and anterior bank of the intraparietal sulcus with the PMd at the junction of the SFG and MFG. Its trajectories are contiguous with the anterior portion of the AF coursing above the Sylvian fissure and insula. The *SLF-III* is the ventral component of the SLF, and it connects the IPL (Geschwind territory) with the ventral premotor and prefrontal areas (Broca territory).

Tracking of each of the three segments is performed with a two-ROI approach using streamline or probabilistic tractography. The seed ROI is delineated in a coronal slice at the level of the posterior commissure in the subcortical WM of the SPL and IPL. Three target ROIs are delineated on a coronal slice at the level of the anterior commissure in the dorsal subcortical WM of the superior, middle, and inferior/precentral frontal gyri. An additional ROI should be delineated in the temporal WM to filter out the trajectories of the AF direct segment that course for some time intermingled with the SLF-II. After connecting the seed ROI in the parietal WM with each target ROI in the frontal WM, the tractograms should be inspected for a priori anatomic consistency. Spurious streamlines should be removed with “out-ROI” filters. The SLF-III is an easy tract to reconstruct with DTI tractography in the human brain. Reconstruction of the SLF-I and SLF-II with DTI may be inconsistent because these tracts course along the AF and intersect crossing fibers of the CST and CC. Using the SD algorithm often improves the tracking. A statistical significant rightward asymmetry has been reported for the track volume of the SLF-III; no significant differences were found for the SLF-I and SLF-II (Thiebaut de Schotten et al. 2011a).

Brain tumors expanding in the dorsolateral part of the frontal and parietal lobes may dislocate or interrupt the trajectories of the SLF. The branches of the SLF are rarely searched for with IES during surgery; however, preliminary data have shown that direct IES of SLF-III may evoke a motor interference in mapping the motor evoked potential (MEP) of the contralateral hand.

5.11 Integration with fMRI

We have seen how tracking of streamlines in the vicinity or within neoplasm is complicated by tumor infiltration, vasogenic edema, and mass effect leading to tissue deformation and loss of anatomical landmarks. These changes deform the architecture of the WM, and in several cases the use of a priori anatomical approaches for ROI delineation yields unsatisfactory tractography results. Selection of seed and target ROIs based on the results of fMRI has been proposed. Preliminary studies suggested that fMRI-based seed selection may allow for more specific and comprehensive fiber tracking (Schonberg et al. 2006; Smits et al. 2007). The combination and co-registration of clinically feasible fMRI and DTI datasets may help the tractographer to define seed ROIs which are relevant to track the pathway of interest. Schonberg et al. showed that it was feasible and easier to identify the seed and target points, respectively, of the CST and AF with the aid of fMRI finger tapping and speech tasks. According to the author's remarks, tracking of both fascicles was more accurate than with delineation of a priori anatomical seed points.

The initial enthusiasm about performing tractography in a semiautomated fashion by co-registering and combining the two methods has deflated since the early published papers. So far, nothing can beat an experienced neuroradiologist in identifying the key anatomic landmarks especially when the anatomy of a network is distorted, displaced, or partially interrupted by a mass. Streamline tractography results with a priori ROI delineation are quite consistent when using the same acquisition scheme, post-processing, and fiber tracking routine.

In our practice for mapping the speech network, we routinely acquire fMRI and HARDI during the same study session. We are not convinced that combining the two methods in a semiautomatic fashion is worth the effort. fMRI can help identify the seed points of the speech network and to a lesser extent the precentral gyrus when tracking of the CST is requested. We find that fMRI foci of activation are quite helpful to understand the anatomy of sulci and gyri when distorted by an infiltrating tumor. When a mass is dislocating the AF or one of its cortical terminations (seed point), the foci of BOLD response on fMRI are coherently dislocated (Fig. 14). fMRI is particularly useful to identify the exact anatomy of the IFG and adjacent BA6, since a strong cluster

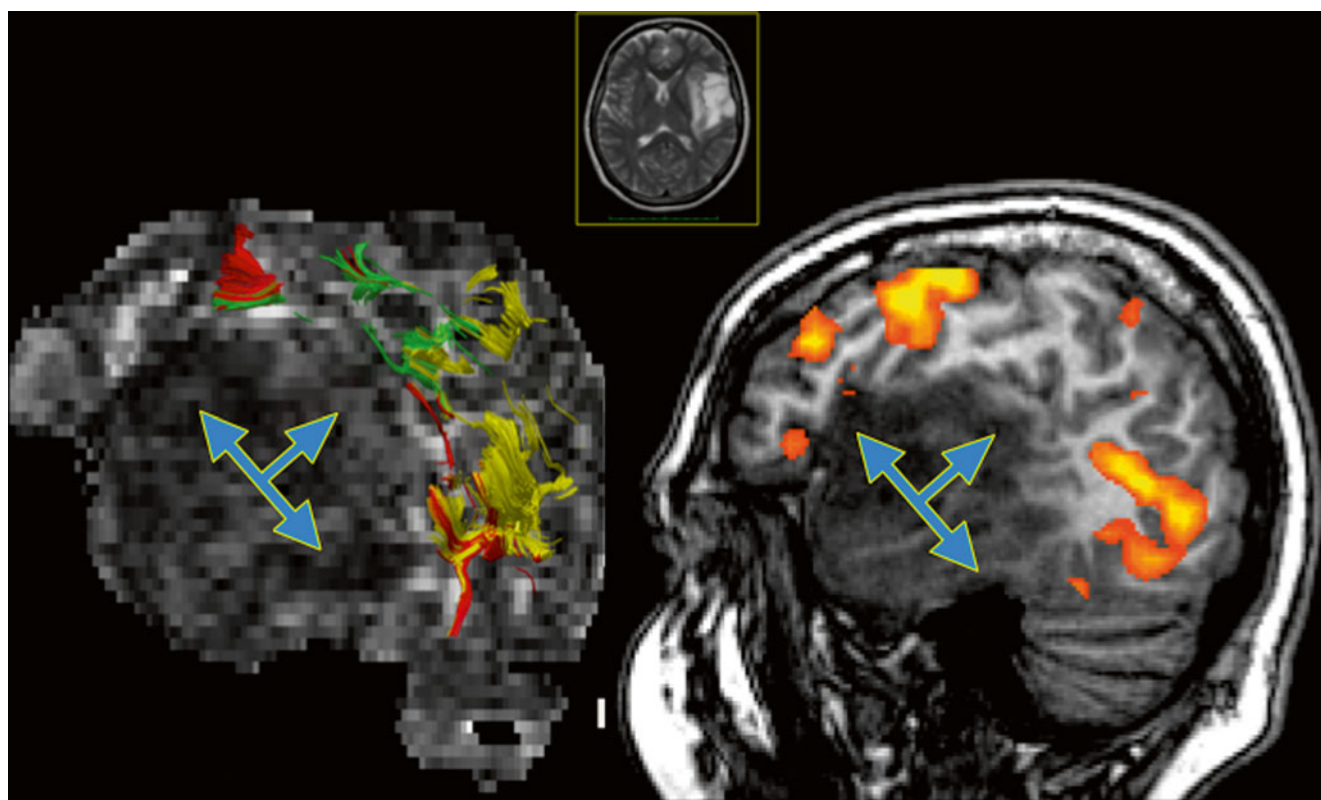


Fig. 14 A 41-year-old female with a large mass in the left temporal lobe that is hyperintense on T2WI without enhancement after gadolinium injection. Sagittal view of tractography of the left AF (left panel) and fMRI with the verb generation task showing BOLD response in PMv and MTG (right panel). Note that the activation foci on fMRI are coherently dislocated by the mass with the cortical terminations of the

three segments of the AF. An oligoastrocytoma WHO II was removed at surgery. The arrows indicate the direction of AF dislocation. Diffusion data were acquired with HARDI (64 gradient directions, $b=1,000$, $2 \times 2 \times 2 \text{ mm}^3$), and tractography was performed with DTI interpolated streamline algorithm (thresholds FA >0.15; angle <45°)

of BOLD response is frequently located in the ventral precentral sulcus (PMv) between these two key anatomy landmarks of the speech network, despite glioma infiltration (Quiñones-Hinojosa et al. 2003; Bizzi et al. 2012).

5.12 Integration in the Operating Room

Three-dimensional objects of selected reconstructed WM fascicles can be reliably integrated into a standard neuronavigation system, allowing for intraoperative visualization and localization of the tracts of interest (Nimsky et al. 2007). Display of MR tractograms in the operating room may be useful to determine the relationship of a mass with adjacent fascicles or when the neurosurgeon desires to refresh his/her anatomical orientation in the operating field, before and after using IES to check the functional limits of a resection on preoperative MRI (Bello et al. 2008). Determination of which tracts, if damaged, may result in permanent neurological deficits remains an open issue. It was demonstrated that intraoperative DTI is technically feasible in 38 patients with tumor in the proximity of the CST. DEC maps immediately available in the operating theater showed marked and highly variable shifting of the CST caused by surgical intervention. In the 27 patients who underwent brain tumor resection, CST dislocation ranged from an inward shift of 8 mm to an outward shift of 15 mm (Nimsky et al. 2005).

The long list of important limitations must be well understood and considered when the tractograms are exported to the operating room. Current DTI methods may provide ambiguous results in reconstruction of crossing, kissing, bending, and fanning bundles. MR tractography cannot track the trajectories to their cortical terminations. It is important to be aware that tractography so far is a user-dependent method based on *a priori* knowledge of the examiner.

The risk of resecting eloquent structures not detected by DTI or HARDI will have to be considered. False-negative results may occur especially in areas of T2-signal hyperintensity within a LGG where the trajectories of the tracts appear interrupted due to abnormally low FA. The presence of an eloquent tract in the vicinity of the surgical cavity should not be the reason for stopping the resection prematurely, because it may decrease the impact of surgery on the natural history of the disease. The dangers of using MR tractography in presurgical evaluation of gliomas and intraoperatively have been recently outlined by Duffau (2014). MR tractography does not provide information about the functional status of a fascicle; thus, IES should always be used in order to avoid long-term postoperative neurological deficits. IES is the only method able to test WM function in order to create a subcortical functional map that has proven to maximize tumor resection and minimize hazards. The main tasks used with

subcortical IES in the operating room with related responses and short- and long-term deficits are reported in the Table 1 for each of the three functional systems discussed in this chapter.

5.13 Impact in Clinical Practice

Presurgical evaluation of patients with glioma has been so far the most successful application of DTI in clinical practice. Other clinical research applications of MR diffusion imaging are in rehabilitation after stroke, multiple sclerosis, mild traumatic brain injury, and degenerative diseases (Alzheimer disease, amyotrophic lateral sclerosis). However, in these diseases DTI is mainly used as a clinical research tool, and it is not yet ready for prime-time patient management.

MR diffusion imaging is the only noninvasive method, allowing *in vivo* detection of the trajectories of main WM fascicles, and it can provide information whether a tract is displaced, infiltrated/edematous, or interrupted by a tumor. The accuracy of MR tractography for detecting motor and speech pathways has been validated with IES, with 82–97 % concordance across studies (Bello et al. 2008; Berman et al. 2004; Leclercq et al. 2010; Ohue et al. 2012). DTI provides unique anatomic information, whereas IES provides functional feedback about eloquent subcortical connections that, if not safeguarded, may result in permanent neurological deficits. In many medical centers worldwide, DTI is frequently requested as an integral part of the presurgical work-up of brain tumor patients, and the FA/DEC maps or the tractograms of the relevant fascicles are frequently uploaded to a neuronavigational device in the operating room together with morphological and functional MR images. Tractograms of the CST, OR, AF, and IFOF are the most requested by neurosurgeons.

In a unique prospective randomized controlled (Class I) trial on 238 consecutive glioma patients, it has been shown that DTI tractography has an impact on outcome after resection of HGG but not of LGG involving the CST (Wu et al. 2007). The authors reported that gross total resection of HGG was more likely with MR tractography guidance rather than without and that new postoperative motor deficits were less frequent. The study showed clear benefits in increasing EOR, median overall survival, and 6-month KPS score, and it is key evidence supporting the use of DTI-aided resection of gliomas, despite a few limitations. In a retrospective study on 190 patients with LGG in eloquent areas, the EOR and the difference between the T2WI and T1WI volume were the strongest independent predictors in improving OS as well as delaying PFS and malignant transformation (Ius et al. 2012). The pre-surgical difference between T2WI and post-contrast T1WI volume may discriminate glioma growing mechanism along the WM: when proliferation is the major mechanism of tumor

expansion, the mass has a regular bulky shape with an equivalent volume on T2WI and post-contrast T1WI; when WM infiltration is predominant, the mass has a more irregular and complex shape with digitations along the WM that is better detected on T2WI than T1WI (Skrap et al. 2012). In addition, in the same study two groups of patients who underwent tumor resection with a different intraoperative protocol including subcortical IES with or without overlap of fMRI and diffusion tractography on a neuronavigational device were compared. Patients with fMRI/DTI had a median EOR of 90 %, while those without had a median EOR of 77 %.

Presurgical estimate of the expected surgical outcome both in terms of EOR and functional outcome is of great interest for patient's counseling and clinical decision making. Information provided by DTI tractography may be extremely useful to identify the candidates that could maximally benefit from surgery. It has been recently shown that DTI could be a useful tool to estimate the chance of performing a total resection in patients with gliomas located near eloquent areas (Castellano et al. 2012). In a retrospective study performed in 27 patients with HGG and 46 with LGG, detection of intact fascicles with tractography was predictive of a higher probability of total resection. On the contrary, detection of infiltrated or displaced fascicles was predictive of a lower probability of total resection, especially for gliomas with a presurgical volume less than 100 cm³. Infiltration and even displacement of the CST reduced the chance of achieving a total resection. Moreover IFOF infiltration in the dominant hemisphere was found predictive of incomplete resection. In particular infiltration of the intermediate segment of the IFOF was associated with a very low probability of performing a total resection. On the contrary, no significant correlation was found between infiltration of the SLF/AF and EOR. These results can be explained by considering that the anatomical distribution of the SLF/AF is usually larger than the functional distribution identified by IES; thus a large part of the SLF can be safely resected. The TPFIA is likely another critical area where infiltration or dislocation of the fascicles will likely decrease the chances of a complete resection. Taken together, these results emphasize that assessment of WM tract involvement is an essential part of presurgical evaluation of patients with gliomas in the proximity or within eloquent fascicles and the importance of including HARDI with MR tractography in presurgical imaging protocols.

The value of DTI in performing clinical-anatomical correlations has been shown in a prospective preoperative study on 19 patients with gliomas infiltrating the ventrolateral frontal language areas. Anatomical data provided by DTI tractography was used with the lesion method to identify key structures of the language system responsible for speech deficits. Patients with glioma growing in the left PMv were more likely to present with presurgical aphasia than those with gli-

oma infiltrating the IFG, including pars opercularis. However, it was tumor extension to infiltrate or interrupt the AF direct segment that was associated with preoperative speech deficits, in particular with conduction aphasia (Bizzi et al. 2012).

Conclusions

Two decades ago, the introduction of DTI changed the way neuroscientists look at WM. Since the first pioneer papers, MR diffusion has developed into a sophisticated and complex MR multidisciplinary field with the contribution of physicists, biomedical engineers, mathematicians, cognitive neurologists, neuroradiologists, and neurosurgeons. With the development of MR tractography, the trajectories of multiple WM fascicles can be identified *in vivo* in the individual subject, and their relationship with a focal lesion can be illustrated and used for presurgical brain mapping. It is now recognized that a detailed understanding of the geometric WM changes induced by a tumor is valuable in order to maximize lesion resection while avoiding permanent postoperative morbidity. This is particularly true in cases of infiltrating gliomas located within eloquent regions of the brain.

Tractography has gained an undisputed educational reputation for teaching WM architecture. Mapping of WM pathways may improve presurgical planning and surgical targeting with neuronavigational devices, and it may reduce intraoperative time. Clinical use of advanced MR imaging tools is growing in importance, and exams in patients are being increasingly requested by neurosurgeons worldwide. The role of MR tractography in assisting neurosurgeons to correctly plan subcortical IES and interpret the electrophysiological responses in the operating theater is increasingly recognized by the neurosurgical community.

Although advanced diffusion imaging methods are currently available in most MRI scanners, well beyond the framework of clinical research protocols and academic institutions, they are not yet considered "standard of care." The processes that lead to establishing clinical practice are also quite complex, especially at a time when emphasis on economic difficulties affects health-care decisions. Functional MRI and DTI are extremely useful methods that can contribute to improve clinical outcome and to reduce complication rates. As all complex methods, they work best when all the members of the team acknowledge their limitations and communicate using a common language.

Acknowledgments The author likes to thank Lorenzo Bello, M.D. (University of Milan), Hugues Duffau, M.D. (Pontpellier University) and Michel Thiebaut de Schotten, Ph.D. (Université Pierre et Marie Curie-Paris) for helpful discussion.

References

- Alexander AL, Hasan K, Kindlmann G, Parker DL, Tsuruda JS (2000) A geometric analysis of diffusion tensor measurements of the human brain. *Magn Reson Med* 44(2):283–291. Retrieved from <http://www.ncbi.nlm.nih.gov/pubmed/10918328>
- Anwander A, Tittgemeyer M, von Cramon DY, Friederici AD, Knosche TR (2007) Connectivity-based parcellation of Broca's area. *Cereb Cortex* 17(4):816–825. doi:[bhk034](https://doi.org/10.1093/cercor/bhk034) [pii] [10.1093/cercor/bhk034](https://doi.org/10.1093/cercor/bhk034)
- Assaf Y, Freidlin RZ, Rohde GK, Bassar PJ (2004) New modeling and experimental framework to characterize hindered and restricted water diffusion in brain white matter. *Magn Reson Med* 52(5): 965–978. doi:[10.1002/mrm.20274](https://doi.org/10.1002/mrm.20274)
- Bartolomeo P, Michel Thiebaut de Schotten M, Chica AB (2012) Brain networks of visuospatial attention and their disruption in visual neglect. *Front Hum Neurosci* 4(6):110. doi: [10.3389/fnhum.2012.00110](https://doi.org/10.3389/fnhum.2012.00110)
- Bassar PJ, Mattiello J, LeBihan D (1994) MR diffusion tensor spectroscopy and imaging. *Biophys J* 66(1):259–267. doi:S0006-3495(94)80775-1 [pii] [10.1016/S0006-3495\(94\)80775-1](https://doi.org/10.1016/S0006-3495(94)80775-1)
- Bassar PJ, Pajevic S, Pierpaoli C, Duda J, Aldroubi A (2000) In vivo fiber tractography using DT-MRI data. *Magn Reson Med* 44(4):625–632. doi: [10.1002/1522-2594\(200010\)44:4<625::AID-MRM17>3.0.CO;2-O](https://doi.org/10.1002/1522-2594(200010)44:4<625::AID-MRM17>3.0.CO;2-O) [pii]
- Bastin ME, Sinha S, Whittle IR, Wardlaw JM (2002) Measurements of water diffusion and T1 values in peritumoural oedematous brain. *Neuroreport* 13(10):1335–1340. Retrieved from <http://www.ncbi.nlm.nih.gov/pubmed/12151798>
- Beaulieu C, Does MD, Snyder RE, Allen PS (1996) Changes in water diffusion due to Wallerian degeneration in peripheral nerve. *Magn Reson Med* 36(4):627–631. Retrieved from <http://www.ncbi.nlm.nih.gov/pubmed/8892217>
- Behrens TEJ, Woolrich MW, Jenkinson M, Johansen-Berg H, Nunes RG, Clare S et al (2003) Characterization and propagation of uncertainty in diffusion-weighted MR imaging. *Magn Reson Med* 50(5):1077–1088. doi:[10.1002/mrm.10609](https://doi.org/10.1002/mrm.10609)
- Bello L, Acerbi F, Giussani C, Baratta P, Taccone P, Songa V et al (2006) Intraoperative language localization in multilingual patients with gliomas. *Neurosurgery* 59(1):115–125. Retrieved from http://www.ncbi.nlm.nih.gov/entrez/query.fcgi?cmd=Retrieve&db=PubMed&dopt=Citation&list_uids=16823307
- Bello L, Gallucci M, Fava M, Carrabba G, Giussani C, Acerbi F et al (2007) Intraoperative subcortical language tract mapping guides surgical removal of gliomas involving speech areas. *Neurosurgery* 60(1):67–80; discussion 80–82. doi:[10.1227/01.NEU.0000249206.58601.DE](https://doi.org/10.1227/01.NEU.0000249206.58601.DE)
- Bello L, Gambini A, Castellano A, Carrabba G, Acerbi F, Fava E, et al (2008) Motor and language DTI Fiber Tracking combined with intraoperative subcortical mapping for surgical removal of gliomas. *Neuroimage* 39(1):369–382. doi:S1053-8119(07)00754-9 [pii] [10.1016/j.neuroimage.2007.08.031](https://doi.org/10.1016/j.neuroimage.2007.08.031)
- Bello L, Fava E, Carrabba G, Papagno C, Gaini SM (2010) Present day's standards in microsurgery of low-grade gliomas. *Adv Tech Stand Neurosurg* 35:113–157. Retrieved from <http://www.ncbi.nlm.nih.gov/pubmed/20102113>
- Bello L, Riva M, Fava E, Ferpozzi V, Castellano A, Ranieri F et al (2014) Tailoring neurophysiological strategies with clinical context enhances resection and safety and expands indications in gliomas involving motor pathways. *Neuro Oncol* 16(8):1110–1128. doi:[10.1093/neuonc/not327](https://doi.org/10.1093/neuonc/not327)
- Berman JI, Berger MS, Mukherjee P, Henry RG (2004) Diffusion-tensor imaging-guided tracking of fibers of the pyramidal tract combined with intraoperative cortical stimulation mapping in patients with gliomas. *J Neurosurg* 101(1):66–72. doi:[10.3171/jns.2004.101.1.0066](https://doi.org/10.3171/jns.2004.101.1.0066)
- Bizzì A, Nava S, Ferrè F, Castelli G, Aquino D, Ciaraffà F et al (2012) Aphasia induced by gliomas growing in the ventrolateral frontal region: assessment with diffusion MR tractography, functional MR imaging and neuropsychology. *Cortex* 48(2):255–272. doi:[10.1016/j.cortex.2011.11.015](https://doi.org/10.1016/j.cortex.2011.11.015)
- Bloch O, Han SJ, Cha S, Sun MZ, Aghi MK, McDermott MW et al (2012) Impact of extent of resection for recurrent glioblastoma on overall survival. *J Neurosurg* 117(6):1032–1038. doi:[10.3171/2012.9.JNS12504](https://doi.org/10.3171/2012.9.JNS12504)
- Bucci M, Mandelli ML, Berman JI, Amirbekian B, Nguyen C, Berger MS, Henry RG (2013) Quantifying diffusion MRI tractography of the corticospinal tract in brain tumors with deterministic and probabilistic methods. *Neuroimage Clin* 3:361–368. doi:[10.1016/j.nicl.2013.08.008](https://doi.org/10.1016/j.nicl.2013.08.008)
- Buschman TJ, Miller EK (2007) Top-down versus bottom-up control of attention in the prefrontal and posterior parietal cortices. *Science* 315(5820):1860–1862. doi:[10.1126/science.1138071](https://doi.org/10.1126/science.1138071)
- Castellano A, Bello L, Michelozzi C, Gallucci M, Fava E, Iadanza A et al (2012) Role of diffusion tensor magnetic resonance tractography in predicting the extent of resection in glioma surgery. *Neuro Oncol* 14(2):192–202. doi:[10.1093/neuonc/nor188](https://doi.org/10.1093/neuonc/nor188)
- Catani M, Bambini V (2014) A model for Social Communication and Language Evolution and Development (SCALED). *Curr Opin Neurobiol* 28C:165–171. doi:[10.1016/j.conb.2014.07.018](https://doi.org/10.1016/j.conb.2014.07.018)
- Catani M, ffytche DH (2005) The rises and falls of disconnection syndromes. *Brain* 128(Pt 10):2224–2239. doi:[10.1093/brain/awh622](https://doi.org/10.1093/brain/awh622)
- Catani M, Mesulam M (2008) The arcuate fasciculus and the disconnection theme in language and aphasia: history and current state. *Cortex* 44(8):953–961. doi:S0010-9452(08)00111-1 [pii] [10.1016/j.cortex.2008.04.002](https://doi.org/10.1016/j.cortex.2008.04.002)
- Catani M, Thiebaut de Schotten M (2008) A diffusion tensor imaging tractography atlas for virtual in vivo dissections. *Cortex* 44(8):1105–1132
- Catani M, Howard RJ, Pajevic S, Jones DK (2002) Virtual in vivo interactive dissection of white matter fasciculi in the human brain. *Neuroimage* 17(1):77–94
- Catani M, Jones DK, ffytche DH (2005) Perisylvian language networks of the human brain. *Ann Neurol* 57(1):8–16
- Catani M, Allin MP, Husain M, Pugliese L, Mesulam MM, Murray RM, Jones DK (2007) Symmetries in human brain language pathways correlate with verbal recall. *Proc Natl Acad Sci U S A* 104(43):17163–17168
- Catani M, Dell'Acqua F, Vergani F, Malik F, Hodge H, Roy P et al (2012) Short frontal lobe connections of the human brain. *Cortex* 48(2)
- Catani M, Mesulam MM, Jakobsen E, Malik F, Martersteck A, Wieneke C et al (2013) A novel frontal pathway underlies verbal fluency in primary progressive aphasia. *Brain* 136(Pt 8):2619–2628. doi:[10.1093/brain/awt163](https://doi.org/10.1093/brain/awt163)
- Caverzasi E, Papinutto N, Amirbekian B, Berger MS, Henry RG (2014) Q-ball of inferior fronto-occipital fasciculus and beyond. *PLoS One* 9(6):e100274. doi:[10.1371/journal.pone.0100274](https://doi.org/10.1371/journal.pone.0100274)
- Cerri G, Shimazu H, Maier MA, Lemon RN (2003) Facilitation from ventral premotor cortex of primary motor cortex outputs to macaque hand muscles. *J Neurophysiol* 90(2):832–842. doi:[10.1152/jn.01026.2002](https://doi.org/10.1152/jn.01026.2002)
- Chenevert TL, Brunberg JA, Pipe JG (1990) Anisotropic diffusion in human white matter: demonstration with MR techniques in vivo. *Radiology* 177(2):401–405. doi:[10.1148/radiology.177.2.2217776](https://doi.org/10.1148/radiology.177.2.2217776)
- Chun MM, Golomb JD, Turk-Browne NB (2011) A taxonomy of external and internal attention. *Annu Rev Psychol* 62:73–101. doi:[10.1146/annurev.psych.093008.100427](https://doi.org/10.1146/annurev.psych.093008.100427)
- Ciaraffà F, Castelli G, Parati EA, Bartolomeo P, Bizzì A (2012) Visual neglect as a disconnection syndrome? A confirmatory case report. *Neurocase*. doi:[10.1080/13554794.2012.667130](https://doi.org/10.1080/13554794.2012.667130)
- Claes A, Idema AJ, Wesseling P (2007) Diffuse glioma growth: a guerilla war. *Acta Neuropathol* 114(5):443–458. doi:[10.1007/s00401-007-0293-7](https://doi.org/10.1007/s00401-007-0293-7)
- Conturo TE, Lori NF, Cull TS, Akbudak E, Snyder AZ, Shimony JS et al (1999) Tracking neuronal fiber pathways in the living human brain. *Proc Natl Acad Sci U S A* 96(18):10422–10427. Retrieved from http://www.ncbi.nlm.nih.gov/entrez/query.fcgi?cmd=Retrieve&db=PubMed&dopt=Citation&list_uids=10468624
- Corbetta M, Shulman GL (2002) Control of goal-directed and stimulus-driven attention in the brain. *Nat Rev Neurosci* 3(3):201–215. doi:[10.1038/nrn755](https://doi.org/10.1038/nrn755)

- Crossley NA, Mechelli A, Scott J, Carletti F, Fox PT, McGuire P, Bullmore ET (2014) The hubs of the human connectome are generally implicated in the anatomy of brain disorders. *Brain* 137(Pt 8):2382–2395. doi:[10.1093/brain/awu132](https://doi.org/10.1093/brain/awu132)
- De Witt Hamer PC, Moritz-Gasser S, Gatignol P, Duffau H (2011) Is the human left middle longitudinal fascicle essential for language? A brain electrostimulation study. *Hum Brain Mapp* 32(6):962–973. doi:[10.1002/hbm.21082](https://doi.org/10.1002/hbm.21082)
- Dejerine J, Dejerine-Klumpke A (1895) Anatomies des centres nerveux. Rueff et Cie, Paris
- Dell'acqua F, Scifo P, Rizzo G, Catani M, Simmons A, Scotti G, Fazio F (2010) A modified damped Richardson-Lucy algorithm to reduce isotropic background effects in spherical deconvolution. *Neuroimage* 49(2):1446–1458. doi:[10.1016/j.neuroimage.2009.09.033](https://doi.org/10.1016/j.neuroimage.2009.09.033)
- Dell'Acqua F, Simmons A, Williams SCR, Catani M (2013) Can spherical deconvolution provide more information than fiber orientations? Hindrance modulated orientational anisotropy, a true-tract specific index to characterize white matter diffusion. *Hum Brain Mapp* 34(10):2464–2483. doi:[10.1002/hbm.22080](https://doi.org/10.1002/hbm.22080)
- Dick AS, Tremblay P (2012) Beyond the arcuate fasciculus: consensus and controversy in the connectional anatomy of language. *Brain* 135(Pt 12):3529–3550. doi:[10.1093/brain/aws222](https://doi.org/10.1093/brain/aws222)
- Doran M, Hajnal JV, Van Bruggen N, King MD, Young IR, Bydder GM (1990) Normal and abnormal white matter tracts shown by MR imaging using directional diffusion weighted sequences. *J Comput Assist Tomogr* 14(6):865–873. Retrieved from <http://www.ncbi.nlm.nih.gov/pubmed/2229559>
- Doricchi F, Tomaiuolo F (2003) The anatomy of neglect without hemianopia: a key role for parietal-frontal disconnection? *Neuroreport* 14(17):2239–2243. doi:[10.1097/01.wnr.0000091132.75061.64](https://doi.org/10.1097/01.wnr.0000091132.75061.64)
- Dronkers NF (1996) A new brain region for coordinating speech articulation. *Nature* 384(6605):159–161. doi:[10.1038/384159a0](https://doi.org/10.1038/384159a0)
- Dureux D, Lepeintre J-F, Fillard P, Loureiro C, Tadié M, Lasjaunias P (2006) MR diffusion tensor imaging and fiber tracking in 5 spinal cord astrocytomas. *AJNR Am J Neuroradiol* 27(1):214–216. Retrieved from <http://www.ncbi.nlm.nih.gov/pubmed/16418387>
- Duffau H (2005) Intraoperative cortico-subcortical stimulations in surgery of low-grade gliomas. *Expert Rev Neurother* 5(4):473–485. doi:[10.1586/14737175.5.4.473](https://doi.org/10.1586/14737175.5.4.473)
- Duffau H (2014) The dangers of magnetic resonance imaging diffusion tensor tractography in brain surgery. *World Neurosurg* 81(1):56–58. doi:[10.1016/j.wneu.2013.01.116](https://doi.org/10.1016/j.wneu.2013.01.116)
- Duffau H, Capelle L (2004) Preferential brain locations of low-grade gliomas. *Cancer* 100(12):2622–2626. doi:[10.1002/cncr.20297](https://doi.org/10.1002/cncr.20297)
- Duffau H, Gatignol P, Mandonnet E, Peruzzi P, Tzourio-Mazoyer N, Capelle L (2005) New insights into the anatomo-functional connectivity of the semantic system: a study using cortico-subcortical electrostimulations. *Brain* 128(Pt 4):797–810
- Duffau H, Gatignol P, Mandonnet E, Capelle L, Taillandier L (2008a) Intraoperative subcortical stimulation mapping of language pathways in a consecutive series of 115 patients with Grade II glioma in the left dominant hemisphere. *J Neurosurg* 109(September):461–471. doi:[10.3171/JNS/2008/109/9/0461](https://doi.org/10.3171/JNS/2008/109/9/0461)
- Duffau H, Leroy M, Gatignol P (2008b) Cortico-subcortical organization of language networks in the right hemisphere: an electrostimulation study in left-handers. *Neuropsychologia* 46(14):3197–3209. doi:[10.1016/j.neuropsychologia.2008.07.017](https://doi.org/10.1016/j.neuropsychologia.2008.07.017)
- Duyn J (2013) MR susceptibility imaging. *J Magn Reson* 229:198–207. doi:[10.1016/j.jmr.2012.11.013](https://doi.org/10.1016/j.jmr.2012.11.013)
- Ebeling U, von Cramon D (1992) Topography of the uncinate fascicle and adjacent temporal fiber tracts. *Acta Neurochir* 115(3–4):143–148. Retrieved from <http://www.ncbi.nlm.nih.gov/pubmed/1605083>
- Field AS, Alexander AL, Wu Y-C, Hasan KM, Witwer B, Badie B (2004) Diffusion tensor eigenvector directional color imaging patterns in the evaluation of cerebral white matter tracts altered by tumor. *J Magn Reson Imaging* 20(4):555–562. doi:[10.1002/jmri.20169](https://doi.org/10.1002/jmri.20169)
- Ford A, McGregor KM, Case K, Crosson B, White KD (2010) Structural connectivity of Broca's area and medial frontal cortex. *Neuroimage* 52(4):1230–1237. doi:[S1053-8119\(10\)00725-1 \[pii\] 10.1016/j.neuroimage.2010.05.018">10.1016/j.neuroimage.2010.05.018](https://doi.org/10.1016/j.neuroimage.2010.05.018)
- Forkel SJ, Thiebaut de Schotten M, Dell'Acqua F, Kalra L, Murphy DGM, Williams SCR, Catani M (2014a) Anatomical predictors of aphasia recovery: a tractography study of bilateral perisylvian language networks. *Brain* 137(Pt 7):2027–2039. doi:[10.1093/brain/awu113](https://doi.org/10.1093/brain/awu113)
- Forkel SJ, Thiebaut de Schotten M, Kawadler JM, Dell'Acqua F, Danek A, Catani M (2014b) The anatomy of fronto-occipital connections from early blunt dissections to contemporary tractography. *Cortex* 56:73–84. doi:[10.1016/j.cortex.2012.09.005](https://doi.org/10.1016/j.cortex.2012.09.005)
- Fridriksson J, Kjartansson O, Morgan PS, Hjaltason H, Magnusdottir S, Bonilha L, Rorden C (2010) Impaired speech repetition and left parietal lobe damage. *J Neurosci* 30(33):11057–11061. doi:[10.1523/JNEUROSCI.1120-10.2010](https://doi.org/10.1523/JNEUROSCI.1120-10.2010)
- Friederici AD (2011) The brain basis of language processing: from structure to function. *Physiol Rev* 91(4):1357–1392. doi:[10.1152/physrev.00006.2011](https://doi.org/10.1152/physrev.00006.2011)
- Friederici AD (2012) The cortical language circuit: from auditory perception to sentence comprehension. *Trends Cogn Sci* 16(5):262–268. doi:[10.1016/j.tics.2012.04.001](https://doi.org/10.1016/j.tics.2012.04.001)
- Ganslandt O, Stadlbauer A, Fahlbusch R, Kamada K, Buslei R, Blumcke I et al (2005) Proton magnetic resonance spectroscopic imaging integrated into image-guided surgery: correlation to standard magnetic resonance imaging and tumor cell density. *Neurosurgery* 56(2 Suppl):291–298; discussion 291–298. Retrieved from <http://www.ncbi.nlm.nih.gov/pubmed/15794826>
- Gatignol P, Duffau H, Capelle L, Plaza M (2009) Naming performance in two bilinguals with frontal vs. temporal glioma. *Neurocase* 15(6):466–477. doi:[912523470 \[pii\] 10.1080/13554790902950434">10.1080/13554790902950434](https://doi.org/10.1080/13554790902950434)
- Geschwind N (1970) The organization of language and the brain. *Science* 170(3961):940–944. Retrieved from <http://www.ncbi.nlm.nih.gov/pubmed/5475022>
- Giese A, Westphal M (1996) Glioma invasion in the central nervous system. *Neurosurgery* 39(2):235–250; discussion 250–252. Retrieved from <http://www.ncbi.nlm.nih.gov/pubmed/8832660>
- Gorno-Tempini ML, Price CJ, Josephs O, Vandenberghe R, Cappa SF, Kapur N et al (1998) The neural systems sustaining face and propername processing. *Brain* 121 (Pt 11):2103–2118. Retrieved from <http://www.ncbi.nlm.nih.gov/pubmed/9827770>
- Hickok G, Poeppel D (2007) The cortical organization of speech processing. *Nat Rev Neurosci* 8(5):393–402. doi:[nm2113 \[pii\] 10.1038/nrn2113](https://doi.org/10.1038/nrn2113)
- Ichimura K, Pearson DM, Kocialkowski S, Bäcklund LM, Chan R, Jones DTW, Collins VP (2009) IDH1 mutations are present in the majority of common adult gliomas but rare in primary glioblastomas. *Neuro Oncol* 11(4):341–347. doi:[10.1215/15228517-2009-025](https://doi.org/10.1215/15228517-2009-025)
- Ius T, Isola M, Budai R, Pauletto G, Tomasino B, Fadiga L, Skrap M (2012) Low-grade glioma surgery in eloquent areas: volumetric analysis of extent of resection and its impact on overall survival. A single-institution experience in 190 patients: clinical article. *J Neurosurg* 117(6):1039–1052. doi:[10.3171/2012.8.JNS12393](https://doi.org/10.3171/2012.8.JNS12393)
- Jellison BJ, Field AS, Medow J, Lazar M, Salamat MS, Alexander AL (2004) Diffusion tensor imaging of cerebral white matter: a pictorial review of physics, fiber tract anatomy, and tumor imaging patterns. *AJNR Am J Neuroradiol* 25(3):356–369. Retrieved from http://www.ncbi.nlm.nih.gov/entrez/query.fcgi?cmd=Retrieve&db=PubMed&dopt=Citation&list_uids=15037456
- Jenkinson M, Beckmann CF, Behrens TEJ, Woolrich MW, Smith SM (2012) FSL. *Neuroimage* 62(2):782–790. doi:[10.1016/j.neuroimage.2011.09.015](https://doi.org/10.1016/j.neuroimage.2011.09.015)
- Jeurissen B, Leemans A, Tournier J-D, Jones DK, Sijbers J (2013) Investigating the prevalence of complex fiber configurations in

- white matter tissue with diffusion magnetic resonance imaging. *Hum Brain Mapp* 34(11):2747–2766. doi:[10.1002/hbm.22099](https://doi.org/10.1002/hbm.22099)
- Jones DK (2008) Studying connections in the living human brain with diffusion MRI. *Cortex* 44(8):936–952. doi:S0010-9452(08)00110-X [pii] [10.1016/j.cortex.2008.05.002](https://doi.org/10.1016/j.cortex.2008.05.002)
- Keles GE, Berger MS (2004) Advances in neurosurgical technique in the current management of brain tumors. *Semin Oncol* 31(5):659–665
- Kinoshita M, de Champfleur NM, Deverdun J, Moritz-Gasser S, Herbet G, Duffau H (2014) Role of fronto-striatal tract and frontal aslant tract in movement and speech: an axonal mapping study. *Brain Struct Funct*. doi:[10.1007/s00429-014-0863-0](https://doi.org/10.1007/s00429-014-0863-0)
- Krainik A, Lehéricy S, Duffau H, Capelle L, Chainay H, Cornu P et al (2003) Postoperative speech disorder after medial frontal surgery: role of the supplementary motor area. *Neurology* 60(4):587–594. Retrieved from <http://www.ncbi.nlm.nih.gov/pubmed/12601097>
- Kumar M, Gupta RK, Nath K, Rathore RKS, Bayu G, Trivedi R et al (2008) Can we differentiate true white matter fibers from pseudofibers inside a brain abscess cavity using geometrical diffusion tensor imaging metrics? *NMR Biomed* 21(6):581–588. doi:[10.1002/nbm.1228](https://doi.org/10.1002/nbm.1228)
- Lawes IN, Barrick TR, Murugam V, Spierings N, Evans DR, Song M, Clark CA (2008) Atlas-based segmentation of white matter tracts of the human brain using diffusion tensor tractography and comparison with classical dissection. *Neuroimage* 39(1):62–79
- Laws ER (2001) Resection of low-grade gliomas. *J Neurosurg* 95(5):731–732. doi:[10.3171/jns.2001.95.5.0731](https://doi.org/10.3171/jns.2001.95.5.0731)
- Laws ER, Parney IF, Huang W, Anderson F, Morris AM, Asher A et al (2003) Survival following surgery and prognostic factors for recently diagnosed malignant glioma: data from the Glioma Outcomes Project. *J Neurosurg* 99(3):467–473. doi:[10.3171/jns.2003.99.3.0467](https://doi.org/10.3171/jns.2003.99.3.0467)
- Leclercq D, Duffau H, Delmaire C, Capelle L, Gatignol P, Ducros M et al (2010) Comparison of diffusion tensor imaging tractography of language tracts and intraoperative subcortical stimulations. *J Neurosurg* 112(3):503–511. doi:[10.3171/2009.8.JNS09558](https://doi.org/10.3171/2009.8.JNS09558)
- Leemans A, Jeurissen B, Sijbers J, Jones DK (2009) ExploreDTI: a graphical toolbox for processing, analyzing and visualizing diffusion MR data. *ISMRM Annu Meet Proc* 17:3537
- Lehéricy S, Ducros M, Krainik A, François C, Van de Moortele P-F, Ugurbil K, Kim D-S (2004) 3-D diffusion tensor axonal tracking shows distinct SMA and pre-SMA projections to the human striatum. *Cereb Cortex* 14(12):1302–1309. doi:[10.1093/cercor/bhh091](https://doi.org/10.1093/cercor/bhh091)
- Lemon RN (2008) Descending pathways in motor control. *Annu Rev Neurosci* 31:195–218. doi:[10.1146/annurev.neuro.31.060407.125547](https://doi.org/10.1146/annurev.neuro.31.060407.125547)
- Lemon RN, Griffiths J (2005) Comparing the function of the corticospinal system in different species: organizational differences for motor specialization? *Muscle Nerve* 32(3):261–279. doi:[10.1002/mus.20333](https://doi.org/10.1002/mus.20333)
- Louis DN, Ohgaki H, Wiestler OD, Cavenee WK (2007) WHO classification of tumors of the central nervous system. IARC Press, Lyon
- Ludwig E, Klingler J (1956) *Atlas cerebri humani*. Little, Brown and Company, Boston
- Makris N, Pandya DN (2009) The extreme capsule in humans and rethinking of the language circuitry. *Brain Struct Funct* 213(3):343–358. doi:[10.1007/s00429-008-0199-8](https://doi.org/10.1007/s00429-008-0199-8)
- Makris N, Kennedy DN, McInerney S, Sorenson AG, Wang R, Caviness VS, Pandya DN (2005) Segmentation of subcomponents within the superior longitudinal fascicle in humans: a quantitative, in vivo, DT-MRI study. *Cereb Cortex* 15(6):854–869. doi:[10.1093/cercor/bhh186](https://doi.org/10.1093/cercor/bhh186)
- Makris N, Papadimitriou GM, Kaiser JR, Sorg S, Kennedy DN, Pandya DN (2009) Delineation of the middle longitudinal fascicle in humans: a quantitative, in vivo, DT-MRI study. *Cereb Cortex* 19(4):777–785. doi:[bhn124](https://doi.org/10.1093/cercor/bhn124) [pii] [10.1093/cercor/bhn124](https://doi.org/10.1093/cercor/bhn124)
- Maldonado IL, Moritz-Gasser S, de Champfleur NM, Bertram L, Moulinié G, Duffau H (2011a) Surgery for gliomas involving the left inferior parietal lobule: new insights into the functional anatomy provided by stimulation mapping in awake patients. *J Neurosurg* 115(4):770–779. doi:[10.3171/2011.5.JNS112](https://doi.org/10.3171/2011.5.JNS112)
- Maldonado IL, Moritz-Gasser S, Duffau H (2011b) Does the left superior longitudinal fascicle subserve language semantics? A brain electrostimulation study. *Brain Struct Funct* 216(3):263–274. doi:[10.1007/s00429-011-0309-x](https://doi.org/10.1007/s00429-011-0309-x)
- Mandelli ML, Berger MS, Bucci M, Berman JI, Amirbekian B, Henry RG (2014) Quantifying accuracy and precision of diffusion MR tractography of the corticospinal tract in brain tumors. *J Neurosurg* 121(2):349–358. doi:[10.3171/2014.4.JNS131160](https://doi.org/10.3171/2014.4.JNS131160)
- Mandonnet E, Jbabdi S, Taitandier L, Galanaud D, Benali H, Capelle L, Duffau H (2007a) Preoperative estimation of residual volume for WHO grade II glioma resected with intraoperative functional mapping. *Neuro Oncol* 9(1):63–69. doi:[10.1215/15228517-2006-015](https://doi.org/10.1215/15228517-2006-015)
- Mandonnet E, Nouet A, Gatignol P, Capelle L, Duffau H (2007b) Does the left inferior longitudinal fasciculus play a role in language? A brain stimulation study. *Brain* 130(Pt 3):623–629
- Mandonnet E, Gatignol P, Duffau H (2009) Evidence for an occipito-temporal tract underlying visual recognition in picture naming. *Clin Neurosurg* 111(7):601–605. doi:[10.1016/j.clineuro.2009.03.007](https://doi.org/10.1016/j.clineuro.2009.03.007)
- Marko NF, Weil RJ (2012) A case for reclassifying infiltrating gliomas in adults. *J Neurooncol* 109(3):587–591. doi:[10.1007/s11060-012-0928-y](https://doi.org/10.1007/s11060-012-0928-y)
- Martino J, Brogna C, Robles SG, Vergani F, Duffau H (2010) Anatomic dissection of the inferior fronto-occipital fasciculus revisited in the lights of brain stimulation data. *Cortex* 46(5):691–699. doi:[10.1016/j.cortex.2009.07.015](https://doi.org/10.1016/j.cortex.2009.07.015)
- Martino J, De Witt Hamer PC, Vergani F, Brogna C, de Lucas EM, Vázquez-Barquero A et al (2011) Cortex-sparing fiber dissection: an improved method for the study of white matter anatomy in the human brain. *J Anat* 219(4):531–541. doi:[10.1111/j.1469-7580.2011.01414.x](https://doi.org/10.1111/j.1469-7580.2011.01414.x)
- Martino J, da Silva-Freitas R, Caballero H, Marco de Lucas E, García-Porrero JA, Vázquez-Barquero A (2013) Fiber dissection and diffusion tensor imaging tractography study of the temporoparietal fiber intersection area. *Neurosurgery* 72(1 Suppl Operative):87–97; discussion 97–98. doi:[10.1227/NEU.0b013e318274294b](https://doi.org/10.1227/NEU.0b013e318274294b)
- Mawrin C (2005) Molecular genetic alterations in gliomatosis cerebri: what can we learn about the origin and course of the disease? *Acta Neuropathol* 110(6):527–536. doi:[10.1007/s00401-005-1083-8](https://doi.org/10.1007/s00401-005-1083-8)
- Menjot de Champfleur N, Lima Maldonado I, Moritz-Gasser S, Machi P, Le Bars E, Bonafé A, Duffau H (2013) Middle longitudinal fasciculus delineation within language pathways: a diffusion tensor imaging study in human. *Eur J Radiol* 82(1):151–157. doi:[10.1016/j.ejrad.2012.05.034](https://doi.org/10.1016/j.ejrad.2012.05.034)
- Meynert TH (1887) In: Sachs BT (ed) *A clinical treatise on diseases of the fore-brain based upon a study of its structure, functions, and nutrition*. G.P. Putman's Sons, New York
- Mori S, Crain BJ, Chacko VP, van Zijl PC (1999) Three-dimensional tracking of axonal projections in the brain by magnetic resonance imaging. *Ann Neurol* 45(2):265–269. Retrieved from http://www.ncbi.nlm.nih.gov/entrez/query.fcgi?cmd=Retrieve&db=PubMed&db=PubMed&list_uids=9989633
- Müller-Oehring EM, Kasten E, Poggel DA, Schulte T, Strasburger H, Sabel BA (2003) Neglect and hemianopia superimposed. *J Clin Exp Neuropsychol* 25(8):1154–1168. doi:[10.1076/jcen.25.8.1154.16727](https://doi.org/10.1076/jcen.25.8.1154.16727)
- Naeser MA, Palumbo CL, Helm-Estabrooks N, Stiassny-Eder D, Albert ML (1989) Severe nonfluency in aphasia. Role of the medial subcallosal fasciculus and other white matter pathways in recovery of spontaneous speech. *Brain* 112 (Pt 1):1–38. Retrieved from <http://www.ncbi.nlm.nih.gov/pubmed/2917272>
- Nimsky C, Ganslandt O, Hastrite P, Wang R, Benner T, Sorensen AG, Fahlbusch R (2005) Intraoperative diffusion-tensor MR imaging: shifting of white matter tracts during neurosurgical procedures—initial experience. *Radiology* 234(1):218–225
- Nimsky C, Ganslandt O, Fahlbusch R (2007) Implementation of fiber tract navigation. *Neurosurgery* 58(1 Suppl):306–318
- Ohue S, Kohno S, Inoue A, Yamashita D, Harada H, Kumon Y et al (2012) Accuracy of diffusion tensor magnetic resonance imaging-

- based tractography for surgery of gliomas near the pyramidal tract: a significant correlation between subcortical electrical stimulation and postoperative tractography. *Neurosurgery* 70(2):283–293; discussion 294. doi:[10.1227/NEU.0b013e31823020e6](https://doi.org/10.1227/NEU.0b013e31823020e6)
- Oishi K, Zilles K, Amunts K, Faria A, Jiang H, Li X et al (2008) Human brain white matter atlas: identification and assignment of common anatomical structures in superficial white matter. *Neuroimage* 43(3):447–457
- Pajevic S, Pierpaoli C (1999) Color schemes to represent the orientation of anisotropic tissues from diffusion tensor data: application to white matter fiber tract mapping in the human brain. *Magn Reson Med* 42(3):526–540. Retrieved from <http://www.ncbi.nlm.nih.gov/pubmed/10467297>
- Pallud J, Blonski M, Mandonnet E, Audureau E, Fontaine D, Sanai N et al (2013) Velocity of tumor spontaneous expansion predicts long-term outcomes for diffuse low-grade gliomas. *Neuro Oncol* 15(5):595–606. doi:[10.1093/neuonc/nos331](https://doi.org/10.1093/neuonc/nos331)
- Papadogiorgaki M, Koliou P, Kotsakis X, Zervakis ME (2013) Mathematical modelling of spatio-temporal glioma evolution. *Theor Biol Med Model* 10:47. doi:[10.1186/1742-4682-10-47](https://doi.org/10.1186/1742-4682-10-47)
- Papagno C, Miracapillo C, Casarotti A, Romero Lauro LJ, Castellano A, Falini A et al (2010) What is the role of the uncinate fasciculus? Surgical removal and proper name retrieval. *Brain*. doi:[awq283](https://doi.org/10.1093/brain/awq283) [pii] [10.1093/brain/awq283](https://doi.org/10.1093/brain/awq283)
- Papagno C, Casarotti A, Comi A, Pisoni A, Lucchelli F, Bizzi A, Riva M, Bello L (2014) Long-term proper name anomia after removal of the uncinate fasciculus. *Brain Struct Funct*. [Epub ahead of print]
- Penfield W, Rasmussen T (1950) The cerebral cortex of man: a clinical study of localization of function. Macmillan, New York
- Petrella JR, Shah LM, Harris KM, Friedman AH, George TM, Sampson JH et al (2006) Preoperative functional MR imaging localization of language and motor areas: effect on therapeutic decision making in patients with potentially resectable brain tumors. *Radiology* 240(3):793–802. doi:[10.1148/radiol.2403051153](https://doi.org/10.1148/radiol.2403051153)
- Petrides M, Pandya DN (1984) Projections to the frontal cortex from the posterior parietal region in the rhesus monkey. *J Comp Neurol* 228(1):105–116. doi:[10.1002/cne.902280110](https://doi.org/10.1002/cne.902280110)
- Petrides M, Pandya DN (1988) Association fiber pathways to the frontal cortex from the superior temporal region in the rhesus monkey. *J Comp Neurol* 273:52–66
- Pierpaoli C, Jezzard P, Basser PJ, Barnett A, Di Chiro G (1996) Diffusion tensor MR imaging of the human brain. *Radiology* 201(3):637–648. Retrieved from http://www.ncbi.nlm.nih.gov/entrez/query.fcgi?cmd=Retrieve&db=PubMed&dopt=Citation&list_uids=8939209
- Pierpaoli C, Walker L, Irfanoglu MO, Barnett A, Basser P, Chang L-C et al (2010) TORTOISE: an integrated software package for processing of diffusion MRI data. *ISMRM Annu Meet Proc* 18:1597
- Plaza M, Gatignol P, Leroy M, Duffau H (2009) Speaking without Broca's area after tumor resection. *Neurocase* 15(4):294–310. doi:[10.1080/13554790902729473](https://doi.org/10.1080/13554790902729473)
- Posner MI (1980) Orienting of attention. *Q J Exp Psychol* 32(1):3–25. Retrieved from <http://www.ncbi.nlm.nih.gov/pubmed/7367577>
- Price CJ (2010) The anatomy of language: a review of 100 fMRI studies published in 2009. *Ann N Y Acad Sci* 1191:62–88. doi:[10.1111/j.1749-6632.2010.05444.x](https://doi.org/10.1111/j.1749-6632.2010.05444.x)
- Price SJ, Jena R, Burnet NG, Hutchinson PJ, Dean AF, Peña A et al (2006) Improved delineation of glioma margins and regions of infiltration with the use of diffusion tensor imaging: an image-guided biopsy study. *AJNR Am J Neuroradiol* 27(9):1969–1974. Retrieved from <http://www.ncbi.nlm.nih.gov/pubmed/17032877>
- Pujol J, Deus J, Losilla JM, Capdevila A (1999) Cerebral lateralization of language in normal left-handed people studied by functional MRI. *Neurology* 52(5):1038–1043. Retrieved from <http://www.ncbi.nlm.nih.gov/pubmed/10102425>
- Quiñones-Hinojosa A, Ojemann SG, Sanai N, Dillon WP, Berger MS (2003) Preoperative correlation of intraoperative cortical mapping with magnetic resonance imaging landmarks to predict localization of the Broca area. *J Neurosurg* 99(2):311–318
- Rathelot J-A, Strick PL (2006) Muscle representation in the macaque motor cortex: an anatomical perspective. *Proc Natl Acad Sci U S A* 103(21):8257–8262. doi:[10.1073/pnas.0602933103](https://doi.org/10.1073/pnas.0602933103)
- Rathelot J-A, Strick PL (2009) Subdivisions of primary motor cortex based on cortico-motoneuronal cells. *Proc Natl Acad Sci U S A* 106(3):918–923. doi:[10.1073/pnas.0808362106](https://doi.org/10.1073/pnas.0808362106)
- Robles SG, Gatignol P, Lehéricy S, Duffau H (2008) Long-term brain plasticity allowing a multistage surgical approach to World Health Organization Grade II gliomas in eloquent areas. *J Neurosurg* 109(4):615–624
- Rohde GK, Barnett AS, Basser PJ, Marenco S, Pierpaoli C (2004) Comprehensive approach for correction of motion and distortion in diffusion-weighted MRI. *Magn Reson Med* 51(1):103–114. doi:[10.1002/mrm.10677](https://doi.org/10.1002/mrm.10677)
- Rolheiser T, Stamatakis EA, Tyler LK (2011) Dynamic processing in the human language system: synergy between the arcuate fascicle and extreme capsule. *J Neurosci* 31(47):16949–16957. doi:[10.1523/JNEUROSCI.2725-11.2011](https://doi.org/10.1523/JNEUROSCI.2725-11.2011)
- Sanai N, Mirzadeh Z, Berger MS (2008) Functional outcome after language mapping for glioma resection. *N Engl J Med* 358:18–27
- Sanai N, Martino J, Berger MS (2012) Morbidity profile following aggressive resection of parietal lobe gliomas. *J Neurosurg* 116(6):1182–1186. doi:[10.3171/2012.2.JNS111228](https://doi.org/10.3171/2012.2.JNS111228)
- Sati P, van Gelderen P, Silva AC, Reich DS, Merkle H, de Zwart JA, Duyn JH (2013) Micro-compartment specific T2* relaxation in the brain. *Neuroimage* 77:268–278. doi:[10.1016/j.neuroimage.2013.03.005](https://doi.org/10.1016/j.neuroimage.2013.03.005)
- Saur D, Kreher BW, Schnell S, Kummerer D, Kellmeyer P, Vry MS et al (2008) Ventral and dorsal pathways for language. *Proc Natl Acad Sci U S A* 105(46):18035–18040. doi:[10.1073/pnas.0805234105](https://doi.org/10.1073/pnas.0805234105)
- Saur D, Schelter B, Schnell S, Kratochvil D, Kupper H, Kellmeyer P et al (2010) Combining functional and anatomical connectivity reveals brain networks for auditory language comprehension. *Neuroimage* 49(4):3187–3197. doi:[S1053-8119\(09\)01193-8](https://doi.org/10.1016/j.neuroimage.2009.11.009) [pii] [10.1016/j.neuroimage.2009.11.009](https://doi.org/10.1016/j.neuroimage.2009.11.009)
- Schmahmann JD, Pandya DN (2006) Fiber pathways of the brain. Oxford University Press, Oxford, UK.
- Schmahmann JD, Pandya DN, Wang R, Dai G, D'Arceuil HE, de Crespiigny AJ, Wedeen VJ (2007) Association fibre pathways of the brain: parallel observations from diffusion spectrum imaging and autoradiography. *Brain* 130(Pt 3):630–653. doi:[10.1093/brain/awl359](https://doi.org/10.1093/brain/awl359)
- Schonberg T, Pianka P, Hendler T, Pasternak O, Assaf Y (2006) Characterization of displaced white matter by brain tumors using combined DTI and fMRI. *Neuroimage* 30(4):1100–1111. doi:[10.1016/j.neuroimage.2005.11.015](https://doi.org/10.1016/j.neuroimage.2005.11.015)
- Seunarine KK, Alexander DC (2009) Multiple fibers: beyond the diffusion tensor. In: Johansen-Berg H, Behrens TE (eds) *Diffusion MRI: from quantitative measurement to in vivo neuroanatomy*. Elsevier, Oxford, pp 55–72
- Skrap M, Mondani M, Tomasino B, Weis L, Budai R, Pauletto G et al (2012) Surgery of insular nonenhancing gliomas: volumetric analysis of tumoral resection, clinical outcome, and survival in a consecutive series of 66 cases. *Neurosurgery* 70(5):1081–1093; discussion 1093–1094. doi:[10.1227/NEU.0b013e31823f5be5](https://doi.org/10.1227/NEU.0b013e31823f5be5)
- Smith JS, Chang EF, Lamborn KR, Chang SM, Prados MD, Cha S et al (2008) Role of extent of resection in the long-term outcome of low-grade hemispheric gliomas. *J Clin Oncol* 26(8):1338–1345. doi:[10.1200/JCO.2007.13.9337](https://doi.org/10.1200/JCO.2007.13.9337)
- Smits M, Vernooij MW, Wielopolski PA, Vincent AJPE, Houston GC, van der Lugt A (2007) Incorporating functional MR imaging into diffusion tensor tractography in the preoperative assessment of the corticospinal tract in patients with brain tumors. *AJNR Am J Neuroradiol* 28(7):1354–1361. doi:[10.3174/ajnr.A0538](https://doi.org/10.3174/ajnr.A0538)

- Sporns O (2014) Contributions and challenges for network models in cognitive neuroscience. *Nat Neurosci* 17(5):652–660. doi:[10.1038/nn.3690](https://doi.org/10.1038/nn.3690)
- Stummer W, Reulen H-J, Meinel T, Pichlmeier U, Schumacher W, Tonn J-C et al (2008) Extent of resection and survival in glioblastoma multiforme: identification of and adjustment for bias. *Neurosurgery* 62(3):564–576; discussion 564–576. doi:[10.1227/01.neu.0000317304.31579.17](https://doi.org/10.1227/01.neu.0000317304.31579.17)
- Stummer W, Tonn J-C, Mehdorn HM, Nestler U, Franz K, Goetz C et al (2011) Counterbalancing risks and gains from extended resections in malignant glioma surgery: a supplemental analysis from the randomized 5-aminolevulinic acid glioma resection study. Clinical article. *J Neurosurg* 114(3):613–623. doi:[10.3171/2010.3.JNS097](https://doi.org/10.3171/2010.3.JNS097)
- Stupp R, Hegi ME (2013) Brain cancer in 2012: molecular characterization leads the way. *Nat Rev Clin Oncol* 10(2):69–70. doi:[10.1038/nrclinonc.2012.240](https://doi.org/10.1038/nrclinonc.2012.240)
- Stupp R, Mason WP, van den Bent MJ, Weller M, Fisher B, Taphoorn MJB et al (2005) Radiotherapy plus concomitant and adjuvant temozolamide for glioblastoma. *N Engl J Med* 352(10):987–996. doi:[10.1056/NEJMoa043330](https://doi.org/10.1056/NEJMoa043330)
- Sturm D, Witt H, Hovestadt V, Khuong-Quang D-A, Jones DTW, Konermann C et al (2012) Hotspot mutations in H3F3A and IDH1 define distinct epigenetic and biological subgroups of glioblastoma. *Cancer Cell* 22(4):425–437. doi:[10.1016/j.ccr.2012.08.024](https://doi.org/10.1016/j.ccr.2012.08.024)
- Thiebaut de Schotten M, Urbanski M, Duffau H, Volle E, Levy R, Dubois B, Bartolomeo P (2005) Direct evidence for a parietal-frontal pathway subserving spatial awareness in humans. *Science* 309:2226
- Thiebaut de Schotten M, Kinkignéhun S, Delmaire C, Lehéricy S, Duffau H, Thivard L et al (2008) Visualization of disconnection syndromes in humans. *Cortex* 44(8):1097–1103. doi:[10.1016/j.cortex.2008.02.003](https://doi.org/10.1016/j.cortex.2008.02.003)
- Thiebaut de Schotten M, Dell'Acqua F, Forkel SJ, Simmons A, Vergani F, Murphy DGM, Catani M (2011a) A lateralized brain network for visuospatial attention. *Nat Neurosci* 14(10):1245–1246. doi:[10.1038/nn.2905](https://doi.org/10.1038/nn.2905)
- Thiebaut de Schotten M, ffytche DH, Bizzì A, Dell'Acqua F, Allin M, Walshe M et al (2011b) Atlasng location, asymmetry and inter-subject variability of white matter tracts in the human brain with MR diffusion tractography. *Neuroimage* 54(1):49–59. doi:[10.1016/j.neuroimage.2010.07.055](https://doi.org/10.1016/j.neuroimage.2010.07.055)
- Thiebaut de Schotten M, Dell'Acqua F, Valabregue R, Catani M (2012) Monkey to human comparative anatomy of the frontal lobe association tracts. *Cortex* 48(1):82–96. doi:[10.1016/j.cortex.2011.10.001](https://doi.org/10.1016/j.cortex.2011.10.001)
- Thiebaut de Schotten M, Tomaiuolo F, Aiello M, Merola S, Silvetti M, Lecce F et al (2014) Damage to white matter pathways in subacute and chronic spatial neglect: a group study and 2 single-case studies with complete virtual “in vivo” tractography dissection. *Cereb Cortex* 24(3):691–706. doi:[10.1093/cercor/bhs351](https://doi.org/10.1093/cercor/bhs351)
- Thomas L, Di Stefano AL, Ducray F (2013) Predictive biomarkers in adult gliomas: the present and the future. *Curr Opin Oncol* 25(6):689–694. doi:[10.1097/CCO.0000000000000002](https://doi.org/10.1097/CCO.0000000000000002)
- Tournier J-D, Calamante F, Gadian DG, Connelly A (2004) Direct estimation of the fiber orientation density function from diffusion-weighted MRI data using spherical deconvolution. *Neuroimage* 23(3):1176–1185. doi:[10.1016/j.neuroimage.2004.07.037](https://doi.org/10.1016/j.neuroimage.2004.07.037)
- Tuch DS (2004) Q-ball imaging. *Magn Reson Med* 52(6):1358–1372. doi:[10.1002/mrm.20279](https://doi.org/10.1002/mrm.20279)
- Tyler LK, Marslen-Wilson WD, Randall B, Wright P, Devereux BJ, Zhuang J et al (2011) Left inferior frontal cortex and syntax: function, structure and behaviour in patients with left hemisphere damage. *Brain* 134(Pt 2):415–431. doi:[10.1093/brain/awq369](https://doi.org/10.1093/brain/awq369)
- Vallar G, Bello L, Bricolo E, Castellano A, Casarotti A, Falini A et al (2014) Cerebral correlates of visuospatial neglect: a direct cerebral stimulation study. *Hum Brain Mapp* 35(4):1334–1350. doi:[10.1002/hbm.22257](https://doi.org/10.1002/hbm.22257)
- Van den Heuvel MP, Sporns O (2011) Rich-club organization of the human connectome. *J Neurosci* 31(44):15775–15786. doi:[10.1523/JNEUROSCI.3539-11.2011](https://doi.org/10.1523/JNEUROSCI.3539-11.2011)
- Van den Heuvel MP, Sporns O (2013) Network hubs in the human brain. *Trends Cogn Sci* 17(12):683–696. doi:[10.1016/j.tics.2013.09.012](https://doi.org/10.1016/j.tics.2013.09.012)
- Vassal F, Schneider F, Sontheimer A, Lemaire J-J, Nuti C (2013) Intraoperative visualisation of language fascicles by diffusion tensor imaging-based tractography in glioma surgery. *Acta Neurochir* 155(3):437–448. doi:[10.1007/s00701-012-1580-1](https://doi.org/10.1007/s00701-012-1580-1)
- Vergani F, Lacerda L, Martino J, Attems J, Morris C, Mitchell P et al (2014) White matter connections of the supplementary motor area in humans. *J Neurol Neurosurg Psychiatry*. doi:[10.1136/jnnp-2013-307492](https://doi.org/10.1136/jnnp-2013-307492)
- Vidorreta JG, Garcia R, Moritz-Gasser S, Duffau H (2011) Double dissociation between syntactic gender and picture naming processing: a brain stimulation mapping study. *Hum Brain Mapp* 32(3):331–340. doi:[10.1002/hbm.21026](https://doi.org/10.1002/hbm.21026)
- Vuorinen V, Hinkka S, Färkkilä M, Jääskeläinen J (2003) Debulking or biopsy of malignant glioma in elderly people – a randomised study. *Acta Neurochir* 145(1):5–10. doi:[10.1007/s00701-002-1030-6](https://doi.org/10.1007/s00701-002-1030-6)
- Wang S, Kim S, Chawla S, Wolf RL, Zhang W-G, O'Rourke DM et al (2009) Differentiation between glioblastomas and solitary brain metastases using diffusion tensor imaging. *Neuroimage* 44(3):653–660. doi:[10.1016/j.neuroimage.2008.09.027](https://doi.org/10.1016/j.neuroimage.2008.09.027)
- Wedeen VJ, Wang RP, Schmahmann JD, Benner T, Tseng WYI, Dai G et al (2008) Diffusion spectrum magnetic resonance imaging (DSI) tractography of crossing fibers. *Neuroimage* 41(4):1267–1277. doi:[10.1016/j.neuroimage.2008.03.036](https://doi.org/10.1016/j.neuroimage.2008.03.036)
- Wedeen VJ, Rosene DL, Wang R, Dai G, Mortazavi F, Hagmann P et al (2012) The geometric structure of the brain fiber pathways. *Science* 335(6076):1628–1634. doi:[10.1126/science.1215280](https://doi.org/10.1126/science.1215280)
- Weller M, Stupp R, Hegi ME, van den Bent M, Tonn JC, Sanson M et al (2012) Personalized care in neuro-oncology coming of age: why we need MGMT and 1p/19q testing for malignant glioma patients in clinical practice. *Neuro Oncol* 14(Suppl 4):iv100–iv108. doi:[10.1093/neuonc/nos206](https://doi.org/10.1093/neuonc/nos206)
- Wu J-S, Zhou L-F, Tang W-J, Mao Y, Hu J, Song Y-Y et al (2007) Clinical evaluation and follow-up outcome of diffusion tensor imaging-based functional neuronavigation: a prospective, controlled study in patients with gliomas involving pyramidal tracts. *Neurosurgery* 61(5):935–948; discussion 948–949. doi:[10.1227/01.neu.0000303189.80049.ab](https://doi.org/10.1227/01.neu.0000303189.80049.ab)
- Yakovlev PI, Locke S (1961) Corticocortical connections of the anterior cingulate gyrus; te cingulum and subcallosal bundle. *Trans Am Neurol Assoc* 86:252–256
- Yamada K, Sakai K, Hoogenraad FGC, Holthuizen R, Akazawa K, Ito H et al (2007) Multitensor tractography enables better depiction of motor pathways: initial clinical experience using diffusion-weighted MR imaging with standard b-value. *AJR Am J Neuroradiol* 28(9):1668–1673. doi:[10.3174/ajnr.A0640](https://doi.org/10.3174/ajnr.A0640)
- Yordanova YN, Moritz-Gasser S, Duffau H (2011) Awake surgery for WHO Grade II gliomas within “noneloquent” areas in the left dominant hemisphere: toward a “supratotal” resection. Clinical article. *J Neurosurg* 115(2):232–239. doi:[10.3171/2011.3.JNS101333](https://doi.org/10.3171/2011.3.JNS101333)
- Zamecnik J (2005) The extracellular space and matrix of gliomas. *Acta Neuropathol* 110(5):435–442. doi:[10.1007/s00401-005-1078-5](https://doi.org/10.1007/s00401-005-1078-5)
- Zhang H, Schneider T, Wheeler-Kingshott CA, Alexander DC (2012) NODDI: practical in vivo neurite orientation dispersion and density imaging of the human brain. *Neuroimage* 61(4):1000–1016. doi:[10.1016/j.neuroimage.2012.03.072](https://doi.org/10.1016/j.neuroimage.2012.03.072)

Functional Neuronavigation

Volker M. Tronnier

Contents

| | | |
|------|---|-----|
| 1 | Introduction | 229 |
| 2 | Principles and Technical Aspects of Neuronavigation and Stereotaxy | 230 |
| 2.1 | Neuronavigation | 230 |
| 2.2 | Stereotaxy | 231 |
| 2.3 | Intraoperative Imaging..... | 231 |
| 3 | Aims and Indications for Functional Neuronavigation | 231 |
| 4 | Applications of Functional Neuronavigation | 233 |
| 4.1 | Motor and Sensory Systems | 233 |
| 4.2 | Language | 234 |
| 4.3 | Visual Cortex | 235 |
| 4.4 | Auditory Cortex..... | 235 |
| 4.5 | Pain | 236 |
| 4.6 | Psychological Function, Memory..... | 236 |
| 4.7 | Resting-State fMRI..... | 237 |
| 4.8 | Diffusion Tensor Imaging (DTI)..... | 238 |
| 4.9 | Implementation of Functional Imaging Data into Intraoperative Imaging | 238 |
| 4.10 | Implementation of Functional Imaging Data into Intraoperative Mapping | 239 |
| 4.11 | Cost-Effectiveness | 239 |
| 5 | Perspectives | 239 |
| 5.1 | Single-Rack Solution..... | 239 |
| 5.2 | Overlay of Functional Imaging Data in the Operation Microscope | 240 |
| 5.3 | Imaging the Basal Ganglia | 240 |
| 5.4 | Neuroplasticity..... | 240 |
| 5.5 | Imaging the Spinal Cord..... | 240 |
| 5.6 | Molecular Imaging | 240 |
| 6 | Summary | 241 |
| | References | 241 |

Abstract

Functional neuronavigation is based on the visualization of functional images within a surgical tracking system. This and other developing techniques help the neurosurgeon to tailor surgical procedures in order to increase diagnostic yield and to preserve brain function while maximizing the necessary extent of resection. The final goal is to improve postoperative survival and quality of life. A major advantage of functional imaging, in comparison with other functional brain mapping techniques, such as direct cortical stimulation (electrical cortical stimulation, ECS) is its noninvasiveness. Furthermore, availability of functional information to the surgeon and patient prior to surgery provides insight not only into a better evaluation of the procedure indication but also into the planning of a function-preserving operation including the most appropriate surgical access to the respective brain areas. In order to implement functional neuronavigation into the daily clinical routine, optimized imaging protocols are indispensable.

1 Introduction

While anatomical MR imaging is widely implemented and has revolutionized surgical decision making and planning, the emergence of functional neuroimaging techniques localizing brain activity has significantly expanded the presurgical role of the different imaging modalities. Noninvasive functional MRI (fMRI) provides the neurosurgeon with images of activated brain regions by detecting indirect effects of neural activity on local blood volume, flow, and oxygen saturation. Electroencephalography (EEG) and magnetoencephalography (MEG) allow direct assessment of the brain's electrophysiology by displaying the temporal and spatial pattern of the neuronal populations generating the underlying neuroelectric and neuromagnetic fields. Positron emission tomography (PET) and single photon emission tomography (SPECT) imaging do not only provide hemodynamic but

V.M. Tronnier, MD, PhD
Department of Neurosurgery, Universitätsklinikum
Schleswig-Holstein, Campus Lübeck,
Ratzeburger Allee 160, Lübeck 23538, Germany
e-mail: volker.tronnier@uksh.de

also metabolic information, which also holds true for magnetic resonance spectroscopy (MRS).

The following chapter will focus on functional neuronavigation for surgery in eloquent brain areas. In addition, the importance of functional imaging in stereotaxy and procedures for pain and movement disorders will be outlined. Since a separate chapter (chapter “[Presurgical EEG-fMRI in epilepsy](#)”) is dedicated to epilepsy surgery, this topic will not be addressed in this chapter.

2 Principles and Technical Aspects of Neuronavigation and Stereotaxy

2.1 Neuronavigation

The development of neuronavigation systems was a major technical advance in neurosurgery, especially for small lesions localized in deep or subcortical regions, where anatomical landmarks are not available. Such systems facilitate the navigation towards lesions tightly focused, avoiding the destruction of eloquent brain areas, in particular when the anatomy is distorted by brain tumors, edema or hemorrhage. All navigational systems consist of similar components: The key instrument is a three-dimensional digitizing device (pointer, forceps, ultrasound probe, or other localization device) which enables the surgeon to localize the targets within the physical space (surgical site). This device is linked to a computer where the same targets are displayed on preoperative three-dimensional images. The interface is a reference system which defines fiducial markers aligning the physical space to the imaging coordinate system. Although morphological information is usually assessed by 3D T1-weighted MR images with gadolinium for contrast-enhancing lesions or T2-weighted and FLAIR images, respectively, for low-grade gliomas, CT can be used for lesions at the skull base or in the case of maxillofacial, ear-nose-throat, and spinal procedures. Different navigational systems are on the market: arm-based systems with grading scales in usually six joints, providing six degrees of freedom. Based on the known position of the joints by electrogoniometers and the length of the phalanges, the position of a particular instrument connected to the arm can be calculated. The main problem of these arm-based devices is that they are not suitable for fixing the arm in a specific position, which therefore has to be done by the surgeon manually.

Optical or acoustic devices based on the principle of satellite navigation are better suitable. These devices work with two or three detecting instruments (IR cameras, video-, or ultrasound systems) with a fixed relationship in space. The distance to active markers (e.g., LEDs) or passive reflectors is calculated via a triangulation method. Obstacles within the line view, as the operating microscope, however can interfere with navigation and the surgical workflow. One solution is the tracking of the microscope itself, where the focus within the ocular is the image-guided “pointer.” Computer systems allow the rapid transformation and correction of new coordinates.

The accuracy of navigational devices depends on the accuracy of the registration, e. g., the localization of the patients’ anatomical landmarks on preoperatively acquired images. Determination of registered points in a volume around the suspected lesion is important in order to achieve the highest accuracy in all three planes. For instance, movement of the galea and the skin by head fixation or different patient positioning compared to the supine position inside the scanner creates inaccuracies. Therefore, laser scanning methods detecting the surface of the face with several hundred points increase registration accuracy.

After completion of the registration, each anatomical point can be displayed on a navigational computer. Due to the high amount of data and the need for a rapid image transformation, powerful workstations are required for high-end navigational devices.

The use of fMRI or other functional imaging modalities provides additional information which is helpful for the planning of a tailored tumor resection while minimizing damage to functional areas. Therefore, the integration of functional data with the anatomical information has strongly been endorsed by neurosurgeons and is now possible via so-called functional neuronavigation. The introduction of these frameless intraoperative neuronavigation systems allows the precise coregistration and transfer of fMRI data into the surgical field. Nowadays techniques for displaying sensorimotor, visual, language, and cognitive functions as well as DTI fiber tracking are available as outlined in more detail below.

Sequence of events of functional neuronavigation is as follows:

fMRI should be carried out according to a standardized paradigm protocol (see chapter “[Task-based presurgical functional MRI in patients with brain tumors](#)”) at least once a day prior to neuronavigation-assisted surgery. This ensures sufficient time for the neuroradiologist to analyze the fMRI data, which is still a very labor-intensive task. It also enables the neurosurgeon to critically evaluate the navigational data and plan the surgical approach accordingly. In the same MRI session, a three-dimensional morphological MRI scan is acquired as a reference of coregistration.

The combined functional-anatomical data set is then sent via net either to the neuronavigation station in the OR or to a separate planning station outside the OR for further processing. The boundaries of elements of interest (tumor, vessels, ventricles, etc.) can be outlined and colored in different slices displayed by MRI or CT. The following three-dimensional reconstruction allows a 3D display of these structures, which facilitates surgical planning.

At the time of surgery, the head is usually fixed in a head holder (Mayfield, Sugita, etc.), to which the registration system (a three point star in most optical devices) is securely connected. The camera system is adjusted to the surgical field or the surgical microscope. If fiducial markers are used (and no laser scanning method), all defined fiducial markers taped to the patients head have to be

identified in the imaging data set for a patient-to-image registration using a rigid body transformation. Alternatively anatomical landmarks can be defined, and these landmarks can be registered with a pointer using a zoomed image to reach higher accuracy. At least four markers or landmarks are required; however, accuracy correlates with the numbers of registered points. Therefore, in clinical use most often six to seven fiducial markers are registered. Most modern systems nowadays offer an automated surface matching method, where numerous recognizable points are marked with a laser pointer and detected by three cameras. The computer calculates the best correspondence between the anatomical and imaging data, expressed in RMS (root mean square error) accuracy. Detecting certain well-defined anatomical landmarks (nose tip, e.g., medial or lateral orbita) facilitates the surgeon to check for a most accurate patient-to-image overlap as possible. The internal root mean square (RMS) of different neuronavigational systems is between 2 and 3.2 mm. The difference between pointer tip and anatomical landmarks is 1.7–2.2 mm. This difference has to be added to the well-known difference of 5–10 mm between functional maps and the site of neural activity as determined by direct electrical stimulation (see chapter “[Presurgical functional localization possibilities, limitations, and validity](#)”). Once the accuracy of the patient to the image registration has been confirmed by the landmark tests, the preplanned contours including the functional voxels are displayed in the surgeons’ field of view within the microscope.

The additional time required for the use of navigation in the OR is between 15 and 30 min (Wirtz et al. 1998).

The description of the basic principles of neuronavigation and computer-assisted (CAS) or image-guided surgery (IGS) is beyond the scope of this chapter, and the reader is kindly referred to other textbooks dealing with this topic (Maciunas 1993; Taylor et al. 1995).

2.2 Stereotaxy

Frame-based stereotaxy was the precursor of neuronavigational systems and is based on the concept of overlaying the images’ coordinate system onto a coordinate system of the physical space referenced to the stereotactic frame. In order to enhance the diagnostic yield, functional or metabolic imaging is often combined with stereotactic targeting. The main indications are the differentiation between low- and high-grade gliomas and between radionecrosis and recurrent tumor growth. Metabolic imaging procedures with thallium SPECT (Hemm et al. 2004), MRS (Son et al. 2001), FDG-PET (Pirotte et al. 2004), or perfusion-weighted MRI (Maia et al. 2004) or even CT enable the identification of target areas of higher metabolic activity, such as more aggressive tumor or higher graded tumors. The recent development of 11-C-methionine, a specific marker for amino acid transport, as a sensitive indicator of tumor recurrence

enables the 11-C-Met PET to differentiate between radionecrosis and recurrent tumor and renders it useful for stereotactic confirmation (Kracht et al. 2004; Pirotte et al. 2004; Tsuyuguchi et al. 2004). Due to its short half-life (20 min) 11-C-Met PET is replaced in many centers by 18-FET-PET, which is equally sensitive, although 18-F-FET is not incorporated in proteins (Neuner et al. 2012; Rapp et al. 2013; Weber et al. 2000).

2.3 Intraoperative Imaging

Although the development of neuronavigation systems has been a major breakthrough in neurosurgical technique, one serious problem is the so-called brain shift, i.e., tissue movement during tumor resection by loss of CSF or insertion of brain spatula (Nabavi et al. 2001), etc. Despite critical pre-surgical planning (Kikinis et al. 1996) and modeling of brain shift effects (Miga et al. 2001), there is still a considerable degree of uncertainty concerning the precise match of the surgical site with the images provided by the neuronavigation system. Intraoperative imaging modalities such as intraoperative CT (Okudera et al. 1993), ultrasound (Koivukangas et al. 1993; Unsgaard et al. 2002), or MRI (Black et al. 1997; Nimsky et al. 2000, 2001; Roberts et al. 1999; Tronnier et al. 1997) are important measures to overcome the problems of brain shift. Since several years also functional data were implemented into intraoperative imaging (Mikuni et al. 2007; Moche et al. 2001; Nimsky et al. 2004; Rasmussen et al. 2007; Risholm et al. 2011; Stadlbaur et al. 2004).

3 Aims and Indications for Functional Neuronavigation

Combining neuronavigation with functional data, usually acquired by fMRI or MEG, helps to minimize postoperative neurological deficits and at the same time allows maximal removal of pathological tissue. Consequently, the application of functional neuronavigation results in a better selection of surgical candidates and a safer resection with reduced morbidity and finally shortens hospital stays and therefore minimizes hospital costs. The advantage of fMRI over other functional imaging techniques is that MRI is already used for navigation itself in most cases due to the high contrast between normal and pathological brain tissue. Therefore, morphological three-dimensional MRI can be easily matched with fMRI data yielding an overlay of functional areas onto anatomical images (Fig. 1). There is no need for additional instrumentation or for the matching of different image formats. Being noninvasive, it can be performed repeatedly, hereby providing information on postoperative reorganization or neuroplasticity (Carpentier et al. 2001; Fandino et al. 1999).

Historically, neurosurgeons have mapped cortical functions invasively by direct cortical stimulation either intraoperatively or preoperatively using implanted subdural grids.

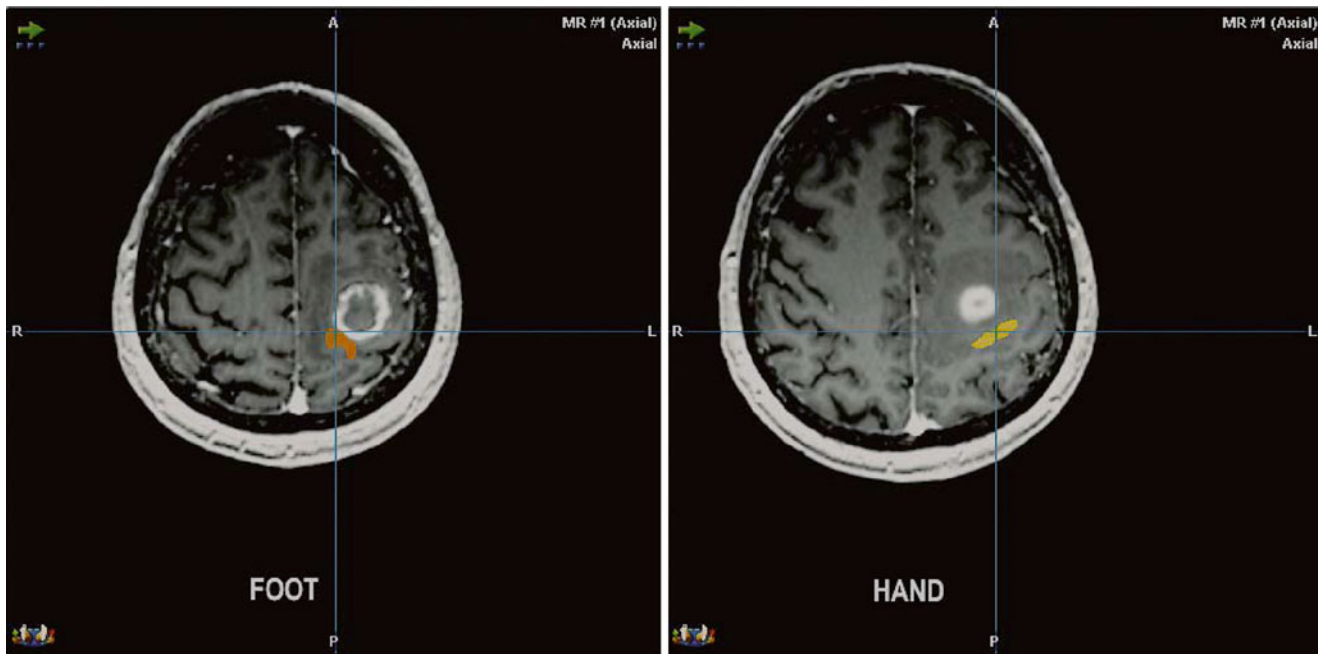


Fig. 1 Overlay of functional activation maps on morphological images (contrast-enhanced T1-weighted 3D data set) visualizing the critical spatial relationship between the left precentral high-grade glioma and

the primary motor foot (*orange cluster*) and hand (*yellow cluster*) representations. Transverse sections (Images: courtesy of C. Stippich, MD) (Color figures online)

However, these methods have severe limitations in terms of presurgical planning and direct intraoperative evaluation of function and are nowadays only used for the confirmation or validation of functional imaging data or intraoperatively when the anatomy has changed due to the procedure. The same applies nowadays for subcortical diffusion tensor imaging of white matter tracts compared to subcortical stimulation (see later).

fMRI imaging studies of motor, somatosensory, and language function as part of the presurgical evaluation process are considered very helpful and used to define the patient's individual risk for a decline in neurological function. This enables most patients to decide between a more aggressive (gross total) and conservative (subtotal or extended biopsy) resection. Finally this information is used to choose the "cortical entry" of lowest risk and to plan the surgical approach avoiding functional "no entry" areas in all cases. fMRI is confirmed intraoperatively with surgical inspection, with intraoperative neuronavigation, and, in selected cases, with cortical stimulation or evoked potentials. Optimized preoperative protocols were developed by Stippich et al. (1999, 2000, 2003) and performed together with a 3D T1-weighted MR sequence used for neuronavigation. Limitations are a reduced patient's compliance, motion artifacts, uncontrolled movements during the resting phase or co-movements of other parts of the body, or a paresis due to tumor growth. Minor inaccuracies can be eliminated by correction algorithms; in rare cases, however, the data acquisition has to be repeated.

Implementation of fMRI information in navigation systems is straightforward to the surgeon, when the functional

information is already integrated and displayed in the data volume normally read into these systems. When the anatomical and functional information is acquired in the same session, no additional registration of fMRI data is necessary, hereby reducing the amount of registration errors.

A major drawback is the fact that fMRI is still very labor-intensive, requiring a group of MRI specialists for patient training, acquisition of MRI and fMRI data, and the post-processing of the data which requires several hours. New real-time fMRI packages of the manufacturers (see later) will help to solve these problems (Moeller et al. 2004).

The importance and usefulness of navigation in neurosurgical cases has been evaluated in 200 neurosurgical cases (Wirtz et al. 1998, 2000) with regard to the planning of the surgical approach, the determination of functional areas, the detection of lesion and its boundaries, and finally the radicality of glioma resection.

For planning the operative approach, in 90 % the use of neuronavigation was considered beneficial by six neurosurgeons, for the definition of anatomy and functional areas in 80 %, for lesion detection in 90 % for definition of tumor boundaries in 75 % and for resection radicality in 65 %.

In a more recent study (Winkler et al. 2005), the additional use of functional MRI has been considered especially helpful for glioma surgery, enabling an extended amount of resection and a reduction of postoperative morbidity as compared to landmark-oriented resection alone. Less impressive were the results for metastases or meningiomas.

A study involving higher magnetic field strengths (3–7 T) has conclusively shown an increase in spatial

resolution and signal-to-noise ratio (Chen and Ugurbil 1999; Thulborn 1999). The future use of nanoparticles as contrast media will possibly demonstrate larger lesions, which can be identified and encircled with the navigation tool. Both developments will have further implications for functionally presurgical evaluation with regard to lesion delineation and preservable neurological function and therapeutic options (Cheng et al. 2014; Wegscheid et al. 2014).

4 Applications of Functional Neuronavigation

4.1 Motor and Sensory Systems

Integration of functional data for sensorimotor function into the neuronavigational system is of substantial benefit for patients with periorolanic tumors, in terms of preoperative risk assessment, surgical access, and trajectory planning (Fig. 2)

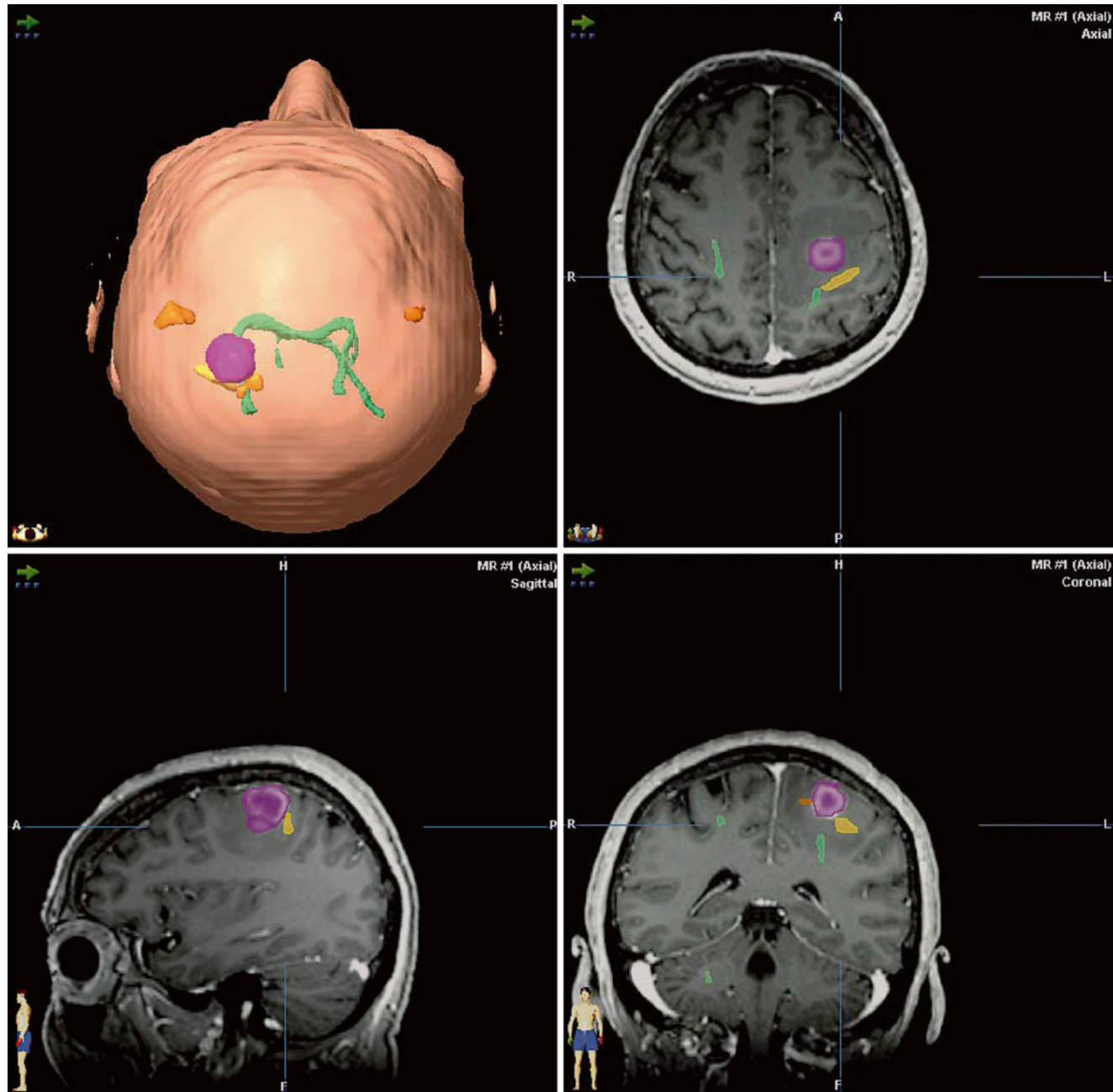


Fig. 2 Integration of BOLD-fMRI somatotopic mapping of the primary motor cortex and of diffusion tensor imaging (DTI) tractography of the pyramidal tract for functional neuronavigation in a patient with a left precentral glioblastoma (same patient in nm). Segmented tumor (pink), foot and tongue representations (orange clusters), hand representation (yellow cluster), pyramidal tract (green lines). The neurosurgeon is provided with

detailed information about the spatial relationship between envisaged site of surgery, functional cortex and fiber tracts, facilitating the planning and the performance of function-preserving resection. Conventional surgical view (top left: *left – left, right – right*). Transverse, sagittal, and coronal views, radiological imaging convention (*right – left, left – right*) (Images: courtesy of C. Stippich, MD) (Color figures online)

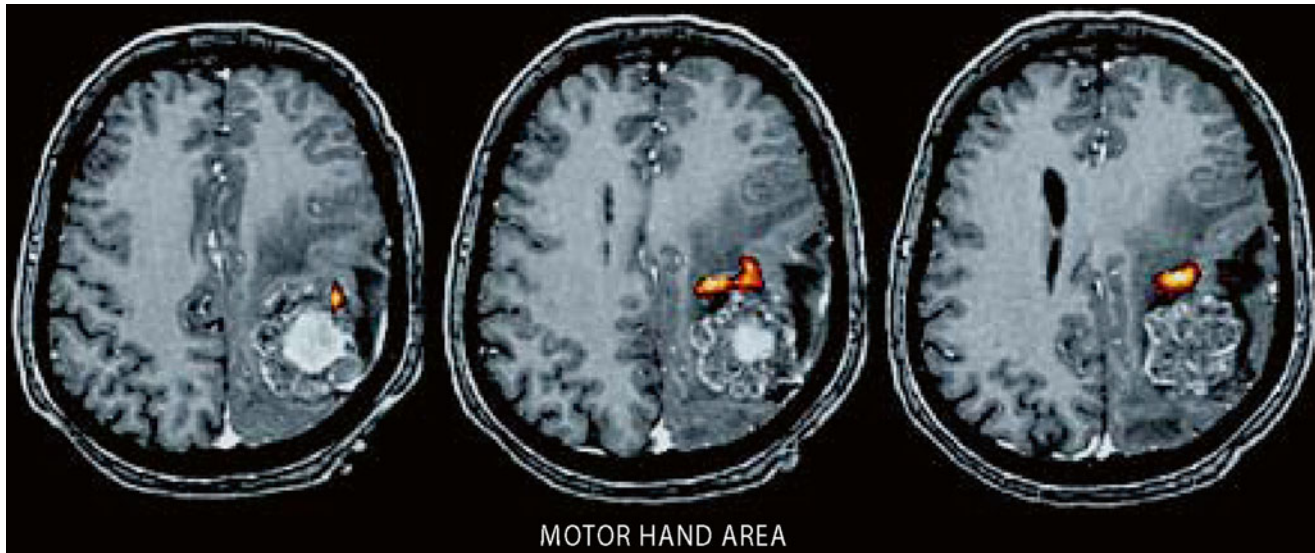


Fig. 3 Hemiparetic patient with a left rolandic metastasis from adenocarcinoma. BOLD-fMRI was performed using hand opening and closure (fist) as motor task. Primary sensorimotor fMRI activation indicated tumor growth into the central region via the postcentral gyrus.

Wengenroth et al. 2011). For example, a patient admitted with a hemiparesis due to a focal central lesion with surrounding edema is first treated with corticosteroid (e.g., 16 mg dexamethasone) in order to evaluate whether the neurological symptoms ameliorate with reduction of mass effect. Persisting paresis strongly indicates tumor involvement in the precentral gyrus or subcortical fiber tracts, which can be confirmed by morphological MRI and diffusion tensor imaging (DTI; see below). In this case, a functional task (e.g., finger tapping) cannot typically be performed contralaterally to the lesion due to the impaired neurological function. However, some information can be obtained from an ipsilateral task eliciting bilateral brain responses (Stippich et al. 2003, 2007; Stoeckel and Binkofski 2010; Tozakidou et al. 2013). Thus, voluntary movements of the unimpaired hand can display the ipsilateral precentral gyrus and premotor area, which—together with postcentral activation induced by contralateral passive somatosensory stimulation—can serve as functional landmarks of the affected motor cortex (see section 4.6 in chapter “[Task-based presurgical functional MRI in patients with brain tumors](#)”). In patients with distinct motor deficiencies, a more robust approach is required with tasks like opening and closing a fist to establish signal changes with fMRI (Fig. 3). Alternatively, resting-state fMRI is performed in several centers, which bypasses specific problems (Mitchell et al. 2013).

Thus, functional imaging allows the display of sensorimotor activation in relation to rolandic brain tumors (Bittar et al. 2000; Fandino et al. 1999; Gallen et al. 1994; Jannin et al. 2002), and its validity can be confirmed by direct electrocortical stimulation during surgery (Leherici et al. 2000; Yousry et al. 1995; Meier et al. 2013). However, effects of plastic changes and reorganization also have to be considered (Carpentier et al. 2001; Fandino et al. 1999), and certain

A parietal approach was chosen to resect the lesion from a posterior direction. Transverse sections with an overlay of functional activation maps on a T1-weighted contrast-enhanced 3D data set readily prepared for DICOM export to neuronavigation

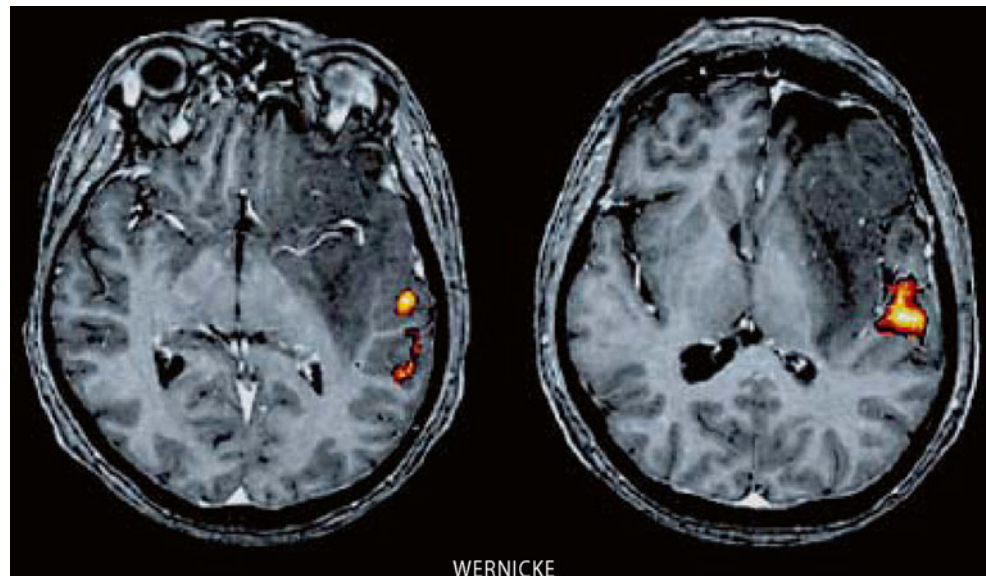
limitations with regard to the variability in the venous drainage and regional hemodynamic responses according to the pathology have to be taken into account.

Finally, promising new imaging techniques such as DTI can track subcortical fibers through the corona radiata, the internal capsule, and the crura cerebri (Coenen et al. 2003; Krings et al. 2001; Le Bihan 2003; Zhu et al. 2012) (see chapters “[Diffusion Imaging with MR tractography for brain tumor surgery](#)”, “[Presurgical functional localization possibilities, limitations, and validity](#)” and “[Multimodality in functional neuroimaging](#)”). Although this technique is limited when these tracts pass through the tumor or of the surrounding edema, and correlations between DTI data and electrophysiological information from subcortical stimulation identifying fiber tracts (Duffau et al. 2002, 2003; Keles and Berger 2004) have to be performed, the integration of DTI and fMRI into one neuronavigation system is a major step towards a safe surgical planning and achievement of cortical and subcortical tumor resection (Kamada et al. 2003; Wu et al. 2007).

4.2 Language

Classical functional neuroanatomy locates the motor output of language to the left inferior frontal gyrus (Broca’s area, BA 44, 45) and the perception of language to the posterior temporal lobe (Wernicke’s area, BA 22). In the past language-related functional mapping for neurosurgical planning relied on two invasive procedures, the Wada test (intracarotid amytal injection) and intraoperative direct cortical stimulation. Language mapping is especially important in patients with lesions in and around the language-dominant hemisphere as well as in epilepsy surgery where it determines the extent of

Fig. 4 Functional localization of the Wernicke's language area in relation to a left frontotemporal low-grade glioma involving the basal ganglia and insula. Word listening (auditory stimulation) was used to elicit BOLD activation. Transverse sections with an overlay of functional activation maps on a T1-weighted contrast-enhanced 3D data set



resection. The distance of resection from language sites, as determined by cortical stimulation, is the most important variable predicting recovery from postoperative speech disturbances. Thus, an accurate localization of all essential language areas is critical for the speed of recovery as well as the avoidance of postoperative neurological deficits.

For neurosurgical purposes, it was first important to demonstrate whether fMRI could replace the Wada test or not (see chapter “[Diffusion Imaging with MR tractography for brain tumor surgery](#)”). In general, there is an excellent correlation between the findings of the Wada test and fMRI for language lateralization (Binder et al. 1996; Rutten et al. 2002), especially in patients with epilepsy (Benson et al. 1999; Woermann et al. 2003). fMRI studies were also correlated with direct electrical cortical stimulation, and a good correlation was found, depending on the language task (Benson et al. 1999; FitzGerald et al. 1997; Signorelli et al. 2003). Based on the preoperative findings in functional imaging, the decision will be made, whether a biopsy, a subtotal resection, or a maximal resection using awake craniotomy will be carried out in brain tumor patients (Fig. 4). Different paradigms have been tried to determine the lateralization for expressive and receptive language areas (Partovi et al. 2012; Zaca et al. 2012), especially in patients with brain tumors or epilepsy. Also in cases with functional deficits, nowadays, resting-state fMRI can be used to demonstrate language neuronal networks (Tie et al. 2014).

4.3 Visual Cortex

The cerebral cortex involved in vision constitutes up to one-third of the cerebral cortex. This reflects the importance of vision in everyday life. Visual information is transferred from the retina to the lateral geniculate nucleus and finally to the

visual cortex following a well-known retinotopic organization. Originally this information was obtained from PET imaging studies (Fox et al. 1986, 1987) and later confirmed by fMRI (Belliveau et al. 1991, 1992). Since it is important to select an optimal stimulation frequency for visual paradigms (Fox and Raichle 1984; Kwong et al. 1992), stimulation was originally performed with LED goggles. Nowadays computer-simulated patterns are commercially available. Tumors afflicting the visual cortex around the calcarine fissure or the optic radiation can produce changes in functional imaging tasks. Particularly in high-grade gliomas involving the occipital lobe or tumors situated in the posterior temporal horn as intraventricular meningiomas or plexus papillomas, critical planning regarding the extent of resection or the surgical access is necessary to avoid disruption of the optic radiation (Fig. 5). Despite the widespread use of functional mapping in surgery, the identification of visual structures is rarely reported with fMRI (Hirsch et al. 2000; Roux et al. 2001a; Schulder et al. 1999; Li et al. 2013), MEG (Nakasato and Yoshimoto 2000) or PET (Fried et al. 1995). More often DTI is nowadays applied to identify the optic radiation in temporal lobe surgery for tumors or epilepsy (Taoka et al. 2008; Winston et al. 2011). Also there are the first reports of electrical subcortical stimulation of the optical pathways (Gras-Combe et al. 2012) published. A combination of fMRI and DTI displaying visual cortical areas as well as the optic radiation would be desirable to minimize the post-operative risk of visual field defects, which can tremendously affect the quality of life.

4.4 Auditory Cortex

Functional activation of the auditory cortex has not been used for neurosurgical procedures or neuronavigation, yet. It is well known that a tonotopic organization of blood flow

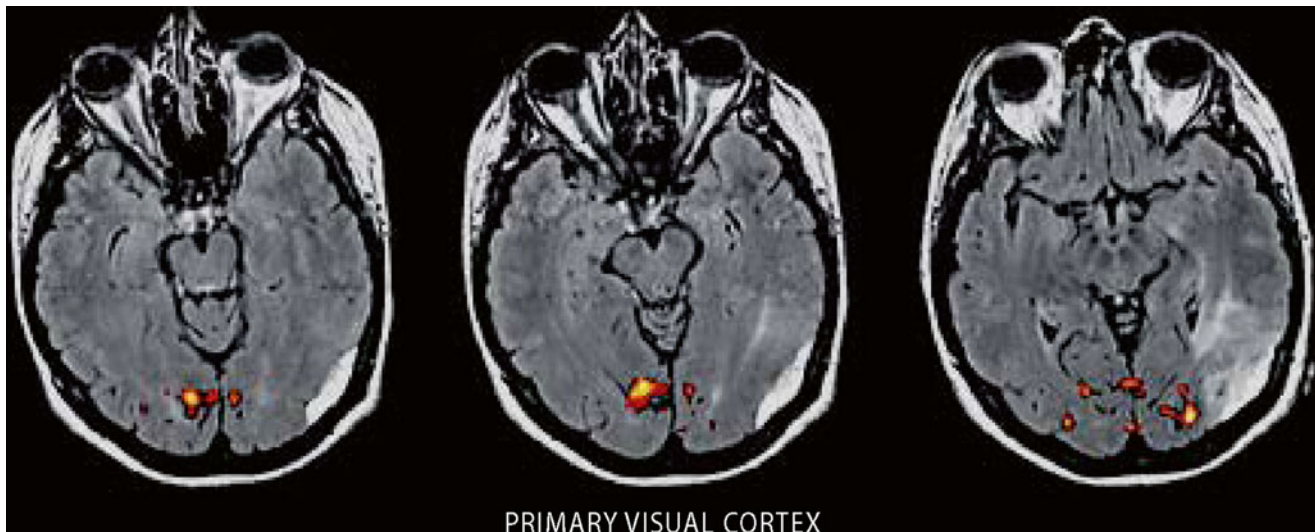


Fig. 5 Functional localization of the primary visual cortex in relation to a left parietooccipital meningioma with signal alterations (perifocal edema) in the left optic radiation. Transverse sections with an overlay

of functional activation maps on a T2-weighted fluid-attenuated inversion recovery MR sequence (FLAIR)

responses to different tonal frequencies exists. Sound stimulation activates the primary auditory cortex in the contralateral hemisphere, whereas speech causes bilateral activation (Binder et al. 1994; Lauter et al. 1985). Based on new hypotheses about the origins or consequences of tinnitus, causing neuroplastic changes in the auditory cortex (Langguth et al. 2003; Mahlke and Wallhäuser-Franke 2004; Mühlnickel et al. 1998), a case report described the effects of chronic auditory cortex stimulation implanted with the help of auditory fMRI neuronavigation (DeRidder et al. 2004). Auditory fMRI was superimposed on morphological 3D MRI and displayed together in a neuronavigation system, which was used to place an epidural paddle electrode. After successful test stimulation, an impulse generator was implanted with an excellent result after 10 months.

4.5 Pain

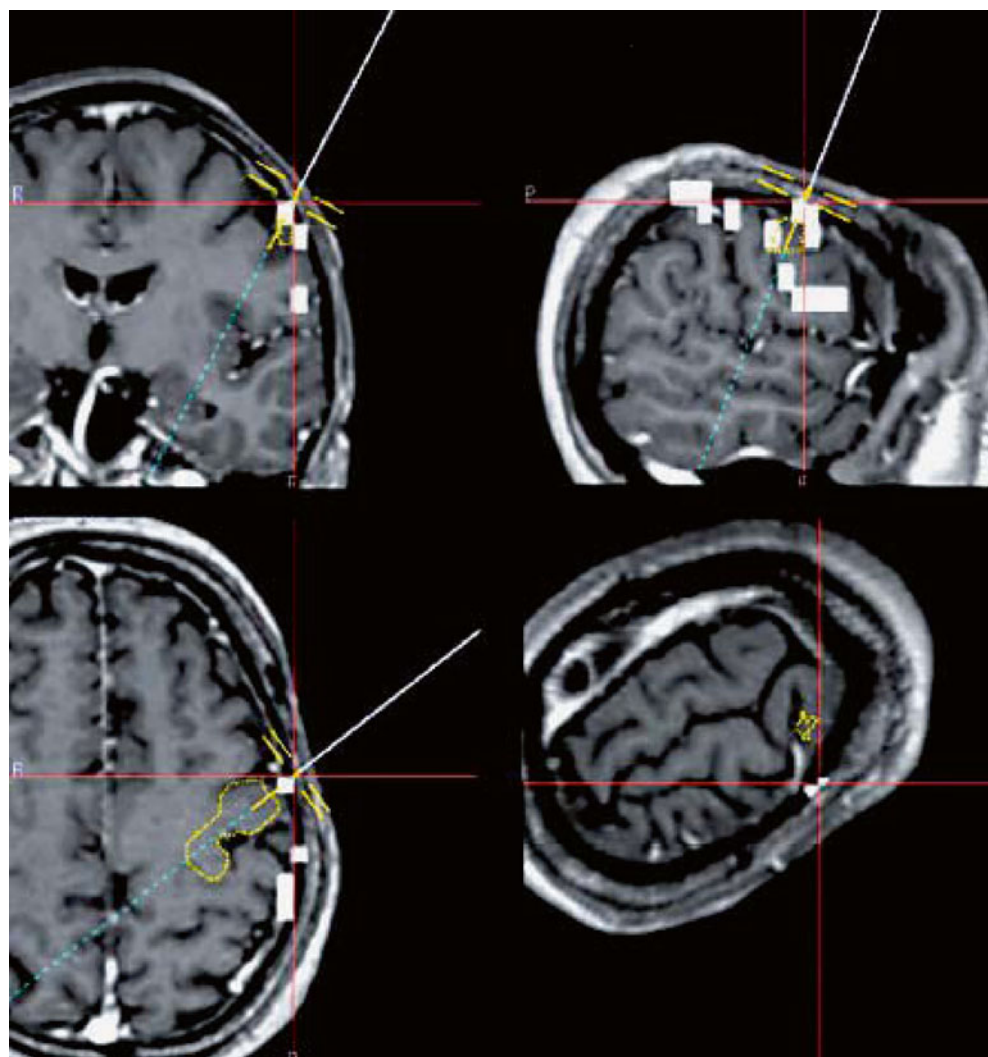
There are numerous studies dealing with the activation of different cortical and subcortical brain areas evoked by mechanical or thermal noxious stimuli. Also therapeutic effects of surgical and nonsurgical measures have been studied. fMRI is used for neuronavigation in cases with central or peripheral neuropathic pain and therapeutic motor cortex stimulation (Pirotte et al. 2005; Roux et al. 2001b; Sol et al. 2001). Depending on the localization of the painful area and the patients' ability to perform the required tasks, a mapping of the motor cortex is performed. The fMRI data are integrated into a neuronavigation system and displayed in the operating room together with the morphological MRI images. In cases of missing limbs or in plegic patients, virtual

movements can be trained or the opposite healthy motor cortex is projected onto the affected site, although in these latter cases, neuroplastic distortions have to be taken into consideration. Via a burrhole approach, an epidural lead electrode can then be placed over the somatotopic representation corresponding to the painful body area (Figs. 6 and 7). Challenging is the fact that due to neuroplastic changes, the functional areas might differ from the morphological data, which is known from several studies on neuroplasticity in pain (Flor 2003; Karl et al. 2004). However, a valid correlation between direct cortical stimulation and fMRI with a mean distance of 3.8 mm has been found in the majority of cases (Pirotte et al. 2005). DTI is used for the detection of the integrity of corticothalamic tracts as presurgical assessment for motor cortex stimulation in central post-stroke pain (Goto et al. 2008). Furthermore, DTI is meanwhile integrated in functional surgery as well. Besides for indications in neuropsychiatric diseases (Bathia et al. 2012; Coenen et al. 2011a, b), it is also used for the stimulation of fiber tracts in chronic pain (Hunsche et al. 2013).

4.6 Psychological Function, Memory

Functional imaging has revolutionized our understanding in different neuropsychiatric diseases. Task-related and resting-state fMRI has revealed the neural circuits and functional connectivity in untreated and treated patients as compared to controls (Cheng et al. 2013; Jung et al. 2013). Additionally morphometric and MR spectroscopy is used to highlight treatment effects (Athmaca 2013; Zurowski et al. 2012). Morphological, functional metabolic, and volumetric data

Fig. 6 Functional neuronavigation used for computer-assisted placement of an epidural motor cortex stimulation leads in the treatment of chronic pain. The fused images display anatomical and functional information as well as the site planned for electrode placement (yellow circular lines) along with the navigation device (pointer instrument, blue line). Coronal (top left), sagittal (top right), and transverse views (bottom left, “navigation view” (bottom right). White clusters indicate primary sensorimotor BOLD activation after DICOM export (Color figures online)



point to several brain regions that are important to the etiology and maintenance of obsessive – compulsive disorder (OCD). However, these imaging techniques have not been used for individual deep brain stimulation targeting, although first attempts are well on the way (Gutman et al. 2009). Another interesting topic is the possibility to predict memory changes or deficits after surgical procedures (Henke et al. 2003). This is most important in patients undergoing epilepsy surgery, especially temporal lobectomy (Powell et al. 2004; Rabin et al. 2004). The implementation of activation patterns in the medial temporal lobe (for episodic-like or “event” memory) or temporal cortex (for semantic-like or “fact” memory) into a neuronavigation system will decrease the probability of postoperative memory deficits. This also holds true for frontal lesions, where the patients, different from temporal amnesia, exhibit impairments in memory of temporal events (order, source, or context). The (pre-) frontal cortex is responsible for the active retrieval of memory and

encoding, while the temporal cortex is mainly responsible for memory storage and automatic retrieval (Miyashita 2004). Therefore, in the future specifically designed event-related fMRI paradigms will help to predict the risk of certain types of postoperative memory deficits. Also the use of preoperative noninvasive neurostimulation techniques in combination with fMRI (so-called concurrent TMS-fMRI) and the integration of these data in a neuronavigation system will be a territory of future research (Bestmann and Feredoes 2013; Blankenburg et al. 2010; Zaehle et al. 2010)

4.7 Resting-State fMRI

There have been an increasing number of studies using resting-state fMRI to characterize abnormal brain connectivity in patients with different neurological and psychiatric disorders (Horwitz et al. 2013). However, it has not been proven



Fig. 7 Lateral x-ray plain film showing the localization of a paddle electrode implanted via a burrhole

that these functional (neuroplastic) changes can be correlated with anatomical structural changes relevant for the planning of surgical approaches. Although measuring spontaneous activity and generating resting-state correlation maps similar to functional maps from activation tasks, imaging of these networks is technically very labor intensive and underlies several conditions as the selection of the “seed regions” in order to identify the “optimal” networks. In a recent study, the implementation of resting-state data into surgical decision making in a restricted number of patients with epilepsy has been tried. The authors described an advantage in identifying areas responsible for speech arrest, but they did not look for paraphasic errors, which are also important for the functional outcome (Mitchell et al. 2013). For more details on resting-state fMRI, we refer to chapter “[Presurgical resting-state fMRI](#)”.

4.8 Diffusion Tensor Imaging (DTI)

While fMRI may be used to highlight cortical structures, DTI is used to map white matter structures and specific fiber connections. It is based on the preferential diffusion of water along white matter tracts within the CNS and allows the neurosurgeon to delineate a lesion with respect to subcortical projection fibers. DTI data can be incorporated into navigational data sets to facilitate the surgeon a radically postoperative resection and to reduce the risks of complications (Elhawary et al. 2011; Wu et al. 2007). Because also the

whiter matter undergoes anatomical changes due to brain shift, the intraoperative update of neuronavigational data with high-field MRI is a promising tool for image-guided surgery. The gold standard for the detection of subcortical fibers remains intraoperative subcortical stimulation. Correlational studies estimate that the via DTI-determined white matter tracts are in a vicinity of 8 mm of the stimulated areas, at which a range between 0 and 15 mm has been described (Maesawa et al. 2010; Prabhu et al. 2011; Zolal et al. 2012). Therefore, a combination of DTI integrated neuronavigation with subcortical stimulation is considered the most effective way for a safe resection within subcortical areas.

Another new approach for intraoperative decision making or preoperative planning is the use of navigated transcranial stimulation (nTMS) for neuronavigation. nTMS is currently examined for its applicability and reliability for the delineation of cortical and subcortical projection areas which have to be spared during surgical resection of brain lesions (Krieg et al. 2012, 2013). The information obtained with nTMS has been compared with direct cortical stimulation, preoperative fMRI, and fiber tracking (Frey et al. 2012). Although nTMS has advantages over fMRI because it does not rely on patients’ compliance, it depends on several parameters (resting motor threshold, intraoperative brain shift), and the value of its use in the daily clinical routine has to be determined yet.

4.9 Implementation of Functional Imaging Data into Intraoperative Imaging

The benefits of integrating functional imaging data into a neuronavigation system have been described so far. In contrast to MEG, fMRI is more widely distributed and therefore nowadays used on a clinical routine basis. fMRI however, depending on the technique and the special requirements, still needs an intense and time-consuming processing phase before the data can be merged into a neuronavigational system. Real-time fMRI packages provided by MR scanner manufacturers now enable the radiologist to get immediate post-imaging results for more “simple” activation tasks. In an earlier study (Moeller et al. 2004), two different routine clinical 1.5 T scanners were used (Magnetom Vision, Siemens and Intera, Philips) for a motor paradigm (finger tapping). The integrated software performed an automatic motion correction and cluster filtering displaying the activated brain area during each scan. An overlay with the 3D T1-weighted data set could be performed semiautomatically. Integrating these software packages into high-field MR scanners situated in the operating room allows direct intraoperative functional imaging (Nimsky et al. 2004). The extent of resection of brain tumors or lesions in epilepsy surgery can nowadays be further tailored according to the functional information obtained from intraoperative fMRI.

4.10 Implementation of Functional Imaging Data into Intraoperative Mapping

The delineation of cortical structures can be performed intraoperatively either via direct visualization, anatomical correlation to a navigational device, or neurophysiological methods. In case of a large craniotomy, the surgeon is able to identify anatomical landmarks on the exposed cortex and to determine various gyri. The localization of eloquent areas by direct inspection of the brain's surface is very limited as there are no reliable landmarks except for the motor hand area of the precentral gyrus. Especially in cognitive functions, localization of the recruited brain areas is highly variable precluding any reliable prediction in individual patients. In patients with distorted anatomy or limited surgical exposure, neuronavigational devices or neurophysiological techniques help the surgeon to reliably determine the boundaries of eloquent brain regions. Especially in perirolandic tumors, neurophysiological methods facilitate the delineation of the motor or sensory cortex. Direct electrical stimulation elicits movements in muscle groups corresponding to the homunculus. However, intraoperatively, electrical cortical stimulation can be hampered by agents as relaxants causing a neuromuscular blockade or by the degree of depth of anesthesia. On the other hand, motor responses are also elicited by stimulation of premotor and even sensory areas. Sensory responses by electrical stimulation of the median or the tibial nerve are able to delineate the sensory cortex. The combination of somatosensory evoked potentials (SEPs) and cortical stimulation has already been described in the late 1970s (Woolsey et al. 1979) and later been refined by the use of the phase reversal to differentiate between the motor and sensory cortices (Cedzich et al. 1996; Romstöck et al. 2002) in brain tumor surgery. Nowadays these techniques are used for the validation of functional imaging data by displaying the distance between cortical activation and neurophysiological response and finally by correlating the data with the clinical outcome or neurological function (Cosgrove et al. 1996; Kober et al. 2001; Krishnan et al. 2004; Puce et al. 1995; Schiffbauer et al. 2003) (Fig. 8). Functional imaging has the advantage of being able to depict activation deep in a sulcus, which is not easily accessible for direct stimulation. For further data regarding the validity of functional imaging data, see chapter “[Presurgical functional localization possibilities, limitations, and validity](#)”. A combination of both techniques is also used in functional surgery, e.g., in motor cortex stimulation for chronic pain states or tinnitus (Sol et al. 2001; Tronnier et al. 1996).

Interesting new developments are to operate using a real-time atlas-based neuronavigation adapting intraoperative changes as brain shift to all morphological and functional images (Vabulas et al. 2014)



Fig. 8 Operative site showing the correlation of intraoperative cortical stimulation and fMRI localization

4.11 Cost-Effectiveness

There are no direct cost analyses of functional imaging in presurgical evaluation. However, it is well demonstrated that neuronavigation is able to lower the duration of hospital stay (Paleologos et al. 2000), hereby significantly reducing the incoming expenses. A study reported the costs of the Wada test to be 3.7 times higher as compared to fMRI (Medina et al. 2004). Increasing the amount of preoperative (functional) imaging will certainly increase the costs produced by manpower and hardware. However, the improved postoperative quality of life is difficult to balance by money. At least in benign lesions or epilepsy surgery, it seems obvious that less invasive procedures will reduce postoperative morbidity and therefore lower the financial burden.

5 Perspectives

5.1 Single-Rack Solution

The creation of a single-rack information system for the surgeon consisting of a collection of data for functional imaging (MEG, fMRI, DTI, and perfusion MRI), navigation and electrophysiological monitoring with online information to support the surgeon's intraoperative decisions is an important goal. A special focus should be put on the imaging and electrophysiological localization of subcortical pathways. This integrated “functional” neuronavigational approach should be beneficial in surgical planning and pre- and intraoperative decision making, providing online information to facilitate surgical resection and decrease postoperative morbidity by protecting eloquent cortical and subcortical areas. Up to now, the surgeon has to work with different information systems and thus has to integrate all this information during surgery separately when appropriate. An integrated multimodal navigation system taking over all these tasks would reduce

the time of surgery, allow a safer resection of brain tumors, and presumably ultimately improve the patients' outcome.

Several topics have to be addressed to create such a system:

- The integration of more complex resting-state fMRI data to allow to predict neuropsychological changes in brain tumor surgery
- The correlation of fusion inaccuracies based on the fact that up to now only a few anatomical landmarks are used for the merging of data
- The correction of distortions of the different techniques (reduction of distortion by new imaging techniques, correction of remaining distortion by data processing) and their fusion
- Automated export of electrophysiological data into a navigation system
- The automatic recognition of electrode or grid configurations by the navigational system and their display on the monitor or microscope (see below) for the operating surgeon

5.2 Overlay of Functional Imaging Data in the Operation Microscope

It would be desirable to overlay the operation site with the operation microscope with all available imaging data in order not only to delineate the tumor volume but also functional cortical and subcortical sites. Interruptions or distractions caused by switching the focus between the monitor and the microscope repeatedly are disturbing and time consuming. Using the methods of augmented reality can realize a more efficient use of the different planning data. This could be achieved by superimposing heads-up displays upon the microscopic view or by a respective planning of the data in the microscopic view (Tronnier et al. 2000). Dedicated micro-optical overlay modules are already designed to provide the insertion and overlay of three-dimensional data within the operating microscope (Aschke et al. 2003; Makela et al. 2001). Further refinements to enhance the surgeon's three-dimensional perception and a fast integration of these data are required to make intraoperative imaging data implementable.

Special tracking methods or computational models to compensate intraoperative brain shift have to be developed. Tracking points could be vessel branches, other anatomical landmarks, or implanted markers (e.g., LEDs). Additional information provided by intraoperative imaging such as ultrasound should be integrated into the surgical workflow by automated actualization and integration of these imaging data into the microscopic view. This will require different import filters and a matching of different data formats.

5.3 Imaging the Basal Ganglia

First trials examining the basal ganglia with functional somatotopic mapping (Maillard et al. 2000) have been performed. If it were possible to demonstrate the somatotopy of the hand, foot, or face areas in distinct basal ganglia nuclei as the internal pallidum or the subthalamic nucleus, these data could be used for surgical planning of the target and trajectories in stereotactic functional procedures such as pallidotomies or deep brain stimulation (DBS). Due to the increased use of DBS for neuropsychiatric disorders, functional imaging as DTI or tractography is more often required as a preoperative imaging method (Coenen et al. 2011a, b; Gutman et al. 2009; Owen et al. 2007) as well as to study the postoperative effect of DBS on neuronal circuits (Albaugh and Shih 2014; Rozansky et al. 2014).

5.4 Neuroplasticity

Although it is known that over- or under use of specific function will create cortical neuroplasticity, either by enhanced afferent normal or pathological activity (musicians, writer's cramp), decreased afferent activity (blind individuals, patients with amputation), or disproportion of agonist/antagonist function (focal dystonia), pathological changes of the cortex (stroke, brain tumor, brain surgery) also demonstrate the brain's capacity for plastic changes (Fujii and Nakada 2003). This has serious implications for the different forms of therapy (Lotze et al. 1999; Wu and Kaas 1999; You et al. 2005). To the best of our knowledge, no longitudinal study has been performed looking for immediate postoperative changes in fMRI and long-term changes after surgical resection and neurological recovery. This will be one of the most interesting applications of resting-state and activation task fMRI pre- and postoperatively in the future.

5.5 Imaging the Spinal Cord

Functional imaging of the spinal cord is still in development. Movement artifacts of the cord itself, CSF flow, its small cross diameter, and inhomogeneities caused by the surrounding bone and cartilage make the interpretation of the images difficult. The detection of changes of function by pathological lesions is far from being technically solved (Giove et al. 2004; Stroman 2005).

5.6 Molecular Imaging

A variety of imaging technologies are being investigated as tools for studying gene expression in living subjects, especially after gene therapy. The application of such tools for

presurgical planning in humans is desired, though it still seems like a far way to implement them and overcome technical difficulties. SPECT and PET are the most mature of the current imaging technologies with high sensitivity and good access to scanners. MRI is also currently used for molecular imaging of different pathologies including brain tumors in rodents in order to evaluate gene therapy protocols (Moffat et al. 2003; Rehemtulla et al. 2002; Varma et al. 2013). However, if applicable to humans in the future, these images could also be used for surgical targeting and neuronavigation.

6 Summary

Functional imaging can provide information on the localization of essential functional cortex and subcortical pathways preoperatively. It enables the surgeon to assess the surgical risk, to take therapeutic decisions, and to advise the patient carefully about the estimated risks and benefits of the procedure. Functional imaging facilitates the surgeon to make his resection plan estimating the position and relationship of the abnormal and the important functional tissue that should be preserved. In addition, it permits to guide the resection according to function and not only morphology as with neuronavigation alone. Limiting factors are the interference with tumor mass and/or surrounding edema compromising local blood flow and the possible presence of preoperative neurological deficits preventing the performance of functional tasks during imaging. To date, the resection borders cannot be determined reliably based on fMRI data. However, first reports in a very limited number of patients have suggested that resection of tumor in a distance of at least 10 mm may be safe and may cause no decline in neurological function. On the other hand, resection in an area less than 5 mm apart from functional cortex will most likely result in – at least temporarily – neurological deficits. To overcome the problem of intraoperative brain shift, a correlation with direct electrical stimulation for motor cortex as well as SEPs for visual, auditory, and sensory cortex can be applied. Finally the use of intraoperative high-field MR scanners will provide insight into the evaluation of some functions intraoperatively. Eventually, intraoperative mapping of speech and other higher cognitive functions still requires awake craniotomy.

References

- Albaugh DL, Shih Y-YI (2014) Neural circuit modulation during deep brain stimulation at the subthalamic nucleus for Parkinson's disease: what have we learned from neuroimaging studies. *Brain Connect* 4:1–14
- Aschke M, Wirtz CR, Raczkowsky J et al (2003) Augmented reality in operating microscopes for neurosurgical interventions. In: Wolf LJ, Strock JL (eds.) 1st International IEEE EMBS Conference on Neural Engineering 652–655
- Athmaca M (2013) The effect of psychopharmacologic and therapeutic approaches on neuro-imaging in obsessive compulsive disorder. *Curr Neuropharmacol* 11:109–113
- Bathia KD, Henderson L, Ramsey-Stewart G et al (2012) Diffusion tensor imaging to aid subgenual cingulum target selection for deep brain stimulation in depression. *Stereotact Funct Neurosurg* 90: 225–232
- Belliveau JW, Kennedy DN, McKinstry RC et al (1991) Functional mapping of the human visual cortex by magnetic resonance imaging. *Science* 254:716–719
- Belliveau JW, Kwong KK, Kennedy DN et al (1992) Magnetic resonance imaging mapping for brain function. Human visual cortex. *Invest Radiol* 27:S59–S65
- Benson RR, Fitzgerald DB, LeSueur LL et al (1999) Language dominance determined by whole brain functional MRI in patients with brain lesions. *Neurology* 52:798–809
- Bestmann S, Feredoes E (2013) Combined neurostimulation and neuroimaging in cognitive neuroscience: past present and future. *Ann N Y Acad Sci* 1296:11–30
- Binder JR, Rao SM, Hammeke TA et al (1994) Functional magnetic resonance imaging of human auditory cortex. *Ann Neurol* 35: 662–672
- Binder JR, Swanson SJ, Hammeke TA et al (1996) Determination of language dominance using functional MRI: a comparison with the Wada test. *Neurology* 46:978–984
- Bittar RG, Olivier A, Sadikot AF et al (2000) Cortical and somatosensory representation: effect of cerebral lesions. *J Neurosurg* 92: 242–248
- Black PM, Moriarty TM, Alexander EA III et al (1997) The development and implementation of intraoperative magnetic resonance imaging and its neurosurgical applications. *Neurosurgery* 41: 831–845
- Blankenburg F, Ruff CC, Bestmann S et al (2010) Studying the role of the parietal cortex in visuospatial attention with concurrent TMS-fMRI. *Cereb Cortex* 20:2711
- Carpentier A, Constable RT, Schlosser MJ et al (2001) Patterns of functional magnetic resonance imaging activation in association with structural lesions in the rolandic region: a classification system. *J Neurosurg* 94:946–954
- Cedzich C, Taniguchi M, Schaefer S et al (1996) Somatosensory evoked potential phase reversal and direct motor cortex stimulation during surgery in and around the central region. *Neurosurgery* 38: 962–970
- Chen W, Ugurbil K (1999) High spatial resolution functional magnetic resonance imaging at very high magnetic field. *Top Magn Reson Imaging* 10:63–78
- Cheng Y, Xu J, Nie B (2013) Abnormal resting-state activities and functional connectivities of the anterior and posterior cortices in medication-naïve patients with obsessive-compulsive disorders. *PLoS One* 8:e67478
- Cheng Y, Morshed RA, Auffinger B, Tobias AL, Lesniak MS (2014) Multifunctional nanoparticle for brain tumor imaging and therapy. *Adv Drug Deliv Res* 66:42–57
- Coenen VA, Krings T, Axer H et al (2003) Intraoperative three-dimensional visualization of the pyramidal tract in a neuronavigation system (PTV) reliably predicts true position of principal pathways. *Surg Neurol* 60:381–390
- Coenen VA, Allert N, Mädler B (2011a) A role for diffusion tensor imaging fiber tracking for deep brain stimulation surgery: DBS of the dentate-rubro-thalamic tract (drt) for the treatment of therapy refractory tremor. *Acta Neurochir* 153:1579–1585
- Coenen VA, Mädler B, Schiffbauer H et al (2011b) Individual fiber anatomy of the subthalamic region revealed with diffusion tensor imaging: a concept to identify the deep brain stimulation target for tremor suppression. *Neurosurgery* 68:1069–1075

- Cosgrove GR, Buchbinder BR, Jiang H (1996) Functional magnetic resonance imaging for intracranial neuronavigation. *Neurosurg Clin N Am* 7:313–322
- DeRidder D, De Mulder G, Walsh V et al (2004) Magnetic and electrical stimulation of the auditory cortex for intractable tinnitus. Case report. *J Neurosurg* 100:560–564
- Duffau H, Capelle L, Sicchez N et al (2002) Intraoperative mapping of the subcortical language pathways using direct stimulations. An anatomo-functional study. *Brain* 125:199–214
- Duffau H, Capelle L, Denvil D et al (2003) Usefulness of intraoperative electrical subcortical mapping during surgery for low-grade gliomas located within eloquent brain regions: functional results in a series of 103 patients. *J Neurosurg* 98:764–768
- Elhawary H, Liu H, Patel P et al (2011) Intraoperative real-time querying of white matter tracts during frameless stereotactic neuronavigation. *Neurosurgery* 68:506–516
- Fandino J, Kolllias S, Wieser HG et al (1999) Intraoperative validation of functional magnetic resonance imaging and cortical reorganization patterns in patients with brain tumors involving the motor cortex. *J Neurosurg* 91:238–250
- Fitzgerald DB, Cosgrove GR, Ronner S et al (1997) Location of language in the cortex: a comparison between functional MR imaging and electrocortical stimulation. *AJNR* 18:1529–1539
- Flor H (2003) Remapping somatosensory cortex after injury. *Adv Neurol* 93:195–204
- Fox PT, Raichle ME (1984) Stimulus rate dependence of regional cerebral blood flow in human striate cortex, demonstrated by positron emission tomography. *J Neurophysiol* 51:1109–1120
- Fox PT, Mintum MA, Raichle ME et al (1986) Mapping human visual cortex with positron emission tomography. *Nature* 323:806–809
- Fox PT, Miezin FM, Allman JM et al (1987) Retinotopic organization of human visual cortex mapped with positron emission tomography. *J Neurosci* 7:913–922
- Frey D, Strack V, Wiener E et al (2012) A new approach for corticospinal tract reconstruction based on navigated transcranial stimulation and standardized fractional anisotropy values. *Neuroimage* 62:1600–1609
- Fried I, Nenov V, Ojemann SG et al (1995) Functional MR and PET imaging of rolandic and visual cortices for neurosurgical planning. *J Neurosurg* 83:854–861
- Fujii Y, Nakada T (2003) Cortical reorganization in patient with subcortical hemiparesis: neural mechanisms of functional recovery and prognostic implication. *J Neurosurg* 98:64–73
- Gallen CC, Bucholz RD, Sobel DF (1994) Intracranial neurosurgery guided by functional imaging. *Surg Neurol* 42:523–530
- Giove F, Gareffa G, Giuletti G et al (2004) Issues about the fMRI of the human spinal cord. *Magn Reson Imaging* 22:1505–1516
- Goto T, Saitoh Y, Hashimoto N et al (2008) Diffusion tensor fiber tracking in patients with central post-stroke pain; correlation with efficacy of repetitive transcranial magnetic stimulation. *Pain* 140:509–518
- Gras-Combe G, Moritz-Gasser S, Herbet G et al (2012) Intraoperative subcortical electrical mapping of optic radiation in awake surgery for gliomas in visual pathways. *J Neurosurg* 117:466–473
- Gutman DA, Holtzheimer PE, Behrens TE (2009) A tractography analysis of deep brain stimulation white matter targets for depression. *Biol Psychiatry* 65:276–282
- Hemm S, Vaissiere N, Zanca M et al (2004) Thallium SPECT-based stereotactic targeting brain tumor biopsies. A technical note. *Stereotact Funct Neurosurg* 82:70–76
- Henke K, Treyer V, Weber B et al (2003) Functional neuroimaging studies predicts individual memory outcome after amygdalohippocampectomy. *Neuroreport* 14:1197–1202
- Hirsch J, Ruge MI, Kim KHS et al (2000) An integrated functional magnetic resonance imaging procedure for preoperative mapping of cortical areas associated with tactile, motor, language and visual functions. *Neurosurgery* 47:711–722
- Horwitz B, Hwang C, Alstott J (2013) Interpreting the effects of altered brain anatomical connectivity on fMRI functional connectivity: a role for computational neural modeling. *Front Hum Neurosci* 7:Article 649; 1–11
- Hunsche S, Sauner D, Runge MJR et al (2013) Tractography-guided stimulation of somatosensory fibers for thalamic pain relief. *Stereotact Funct Neurosurg* 91:328–334
- Jannin P, Morandi X, Fleig OJ et al (2002) Integration of sulcal and functional information for multimodal neuronavigation. *J Neurosurg* 96:713–723
- Jung WH, Kang DH, Kim E et al (2013) Abnormal corticostriatal-limbic functional connectivity in obsessive compulsive disorder during reward processing and resting-state. *Neuroimage Clin* 3: 27–38
- Kamada K, Houkin K, Takeuchi F et al (2003) Visualization of the eloquent motor system by integration of MEG, functional, and anisotropic diffusion-weighted MRI in functional neuronavigation. *Surg Neurol* 59:353–362
- Karl A, Mühlnickel W, Kurth R et al (2004) Neuroelectric source imaging of steady-state movement-related cortical potentials in human upper extremity amputees with and without phantom limb pain. *Pain* 110:90–102
- Keles GE, Berger MS (2004) Advances in neurosurgical technique in the current management of brain tumors. *Semin Oncol* 31:659–665
- Kikinis R, Gleason PL, Moriarty TM et al (1996) Computer-assisted interactive three-dimensional planning for neurosurgical procedures. *Neurosurgery* 38:640–651
- Kober H, Nimsky C, Moeller M et al (2001) Correlation of sensorimotor activation with functional magnetic resonance imaging and magnetoencephalography in presurgical functional imaging: a spatial analysis. *Neuroimage* 14:1214–1228
- Koivukangas J, Louhisalmi Y, Alakuijala J et al (1993) Ultrasound-controlled neuronavigator-guided brain surgery. *J Neurosurg* 79: 36–42
- Kracht LW, Miletic H, Busch S et al (2004) Delineation of brain tumor extent with (11C)L-methionine positron emission tomography: local comparison with stereotactic histopathology. *Clin Cancer Res* 10:7163–7170
- Krieg S, Shiban E, Buchmann N et al (2012) Utility of presurgical navigated transcranial magnetic brain stimulation for the resection of tumors in eloquent motor areas. *J Neurosurg* 116:994–1001
- Krieg SM, Shiban E, Buchmann N et al (2013) Presurgical navigated transcranial magnetic brain stimulation for recurrent gliomas in motor eloquent areas. *Clin Neurophysiol* 124:522–527
- Krings T, Reinges MH, Thiex R et al (2001) Function and diffusion-weighted magnetic resonance images of space-occupying lesions affecting the motor system: imaging the motor cortex and pyramidal tracts. *J Neurosurg* 95:816–824
- Krishnan R, Raabe A, Hattingen E et al (2004) Functional magnetic resonance imaging-integrated neuronavigation: correlation between lesion-to-motor cortex distance and outcome. *Neurosurgery* 55: 904–915
- Kwong KK, Belliveau JW, Chesler DA et al (1992) Dynamic magnetic resonance imaging of human brain activity during primary sensory stimulation. *Proc Natl Acad Sci U S A* 89:5675–5679
- Langguth B, Eichhammer P, Wiegand R et al (2003) Neuro-navigated rTMS in a patient with chronic tinnitus. Effects of 4 weeks treatment. *Neuroreport* 23:977–980
- Lauter JL, Herscovitch P, Formby C et al (1985) Tonotopic organization in human auditory cortex revealed by positron emission tomography. *Hear Res* 20:199–205
- Le Bihan D (2003) Looking into the functional architecture of the brain with diffusion MRI. *Nat Rev Neurosci* 4:469–480
- Leherici S, Duffau H, Cornu P et al (2000) Correspondence between functional magnetic resonance imaging somatotopy and individual

- brain anatomy of the central region,: comparison with intraoperative stimulation in patients with brain tumors. *J Neurosurg* 92:589–598
- Li W, Wait SD, Oqq RJ et al (2013) Functional magnetic resonance imaging of the visual cortex performed in children under sedation to assist in presurgical planning. *J Neurosurg Pediatr* 11:543–546
- Lotze M, Grodd W, Birbaumer N et al (1999) Does use of a myoelectric prosthesis prevent cortical reorganization and phantom limb pain. *Nat Neurosci* 2:501–502
- Maciunas RJ (1993) Interactive image-guided surgery. In: Barrow D (ed) *Neurosurgical topics*. American Association of Neurological Surgeons Park Ridge IL, USA
- Maesawa S, Fuji M, Nakahara N et al (2010) Intraoperative tractography and motor evoked potential (MEP) monitoring in surgery for gliomas around the corticospinal tract. *World Neurosurg* 74:153–161
- Mahlke C, Wallhauser-Franke E (2004) Evidence for tinnitus-related plasticity in the auditory and limbic system, demonstrated by arg3.1 and c-fos immunocytochemistry. *Hear Res* 195:17–34
- Maia AC, Malheiros SM, da Rocha AJ et al (2004) Stereotactic biopsy guidance in adults with supratentorial nonenhancing gliomas: role of perfusion-weighted magnetic resonance imaging. *J Neurosurg* 101:970–976
- Maillard L, Ishii K, Bushara K et al (2000) Mapping the basal ganglia. FMRI evidence for somatotopic representation of face, hand and foot. *Neurology* 55:377–383
- Makela JP, Kirveskari E, Seppa M et al (2001) Three-dimensional integration of brain anatomy and functions to facilitate intraoperative navigation around the sensorimotor strip. *Hum Brain Mapp* 12: 180–192
- Medina LS, Aguirre E, Bernal B et al (2004) Functional MR imaging versus Wada test for evaluation of language lateralization: cost analysis. *Radiology* 230:49–54
- Meier MP, Ilmberger J, Fesl G et al (2013) Validation of functional motor and language MRI with direct cortical stimulation. *Acta Neurochir* 155:675–683
- Miga MI, Roberts DW, Kennedy FE et al (2001) Modeling of retraction and resection for intraoperative updating of images. *Neurosurgery* 49:75–85
- Mikuni N, Okada T, Enatsu R et al (2007) Clinical impact of integrated functional neuronavigation and subcortical stimulation to preserve motor function during resection of brain tumors. *J Neurosurg* 106: 593–598
- Mitchell TJ, Hacker CD, Breshears JD (2013) A novel data-driven approach to preoperative mapping of functional cortex using resting-state functional magnetic resonance imaging. *Neurosurgery* 73:969–983
- Miyashita Y (2004) Cognitive memory: cellular and network machineries and their top-down control. *Science* 306:435–440
- Moche M, Busse H, Dannenberg C et al (2001) Fusion von MRT-, fMRI- und intraoperativen MRT-Daten. *Radiologe* 41:993–1000
- Moeller M, Freund M, Greiner C et al (2004) Real-time fMRI. A tool for the routine presurgical localisation of the motor cortex. *Eur Radiol* 15:292–295
- Moffat BA, Reddy GR, McKonville P et al (2003) A novel polyacrylamide magnetic nanoparticle contrast agent for molecular imaging using MRI. *Mol Imaging* 2:324–332
- Mühlnickel W, Elbert T, Taub E et al (1998) Reorganization of auditory cortex in tinnitus. *Proc Natl Acad Sci U S A* 95:10340–10343
- Nabavi A, Black PM, Gering DT et al (2001) Serial intraoperative magnetic resonance imaging of brain shift. *Neurosurgery* 48:787–798
- Nakasato N, Yoshimoto T (2000) Somatosensory, auditory and visual evoked magnetic fields in patients with brain diseases. *J Clin Neurophysiol* 17:20–22
- Neuner I, Kaffanke JB, Langen K-J et al (2012) Multimodal imaging utilising integrated MR-PET for human brain tumor assessment. *Eur Radiol* 22:2568–2580
- Nimsky C, Ganslandt O, Cerny S et al (2000) Quantification of, visualization of, and compensation for brain shift using intraoperative magnetic resonance imaging. *Neurosurgery* 47: 1070–1079
- Nimsky C, Ganslandt O, Kober H et al (2001) Intraoperative magnetic resonance imaging combined with neuronavigation: a new concept. *Neurosurgery* 48:1082–1091
- Nimsky C, Ganslandt O, Fahlbusch R (2004) Functional neuronavigation and intraoperative MRI. *Adv Tech Stand Neurosurg* 29:229–263
- Okudera H, Takemae T, Kobayashi K (1993) Intraoperative computer tomographic scanning during transsphenoidal surgery. *Neurosurgery* 32:1041–1043
- Owen SL, Heath J, Kringsbach ML et al (2007) Preoperative DTI and probabilistic tractography in an amputee with deep brain stimulation for lower limb stump pain. *Br J Neurosurg* 21:485–490
- Paleologos TS, Wadley JP, Kitchen ND et al (2000) Clinical utility and cost-effectiveness of interactive image-guided craniotomy: clinical comparison between conventional and image-guided meningioma surgery. *Neurosurgery* 47:40–47
- Partovi S, Jacobi B, Rapps N et al (2012) Clinical standardized fMRI reveals altered language lateralization in patients with brain tumor. *AJNR* 33:2151–2157
- Pirotte B, Goldman S, Massager N et al (2004) Combined use of 18 F-fluorodeoxyglucose and 11C-methionine in 45 positron emission tomography guided stereotactic brain biopsies. *J Neurosurg* 101:476–483
- Pirotte B, Voordecker P, Neugroschl C et al (2005) Combination of functional magnetic resonance imaging-guided neuronavigation and intraoperative cortical brain mapping improves targeting of motor cortex stimulation in neuropathic pain. *Neurosurgery* 56(ONS Suppl):344–359
- Powell HWR, Koepp MJ, Richardson MP et al (2004) The application of functional MRI of memory in temporal lobe epilepsy. A clinical review. *Epilepsia* 45:855–863
- Prabhu SS, Gasco J, Tummala S et al (2011) Intraoperative magnetic resonance imaging-guided tractography with integrated monopolar subcortical functional mapping for resection of brain tumors. *J Neurosurg* 114:719–726
- Puce A, Constable RT, Luby ML et al (1995) Functional magnetic resonance imaging of sensory and motor cortex: comparison with electrophysiological localization. *J Neurosurg* 83:262–270
- Rabin ML, Narayan VM, Kimberg DY et al (2004) Functional MRI predicts post surgical memory following temporal lobectomy. *Brain* 127:2286–2298
- Rapp M, Foeth FW, Felberg J et al (2013) Clinical value of O-(2-[¹⁸F]-fluoroethyl)-L-tyrosine positron emission tomography in patients with low grade glioma. *Neurosurg Focus* 34(2):E13
- Rasmussen IA, Lindseth F, Rygh OM et al (2007) Functional neuronavigation combined with intraoperative 3D ultrasound: initial experiences during surgical resections close to eloquent brain areas and future directions in automatic brain shift compensation of pre-operative data. *Acta Neurochir* 149:365–378
- Rehemtulla A, Hall DE, Stegman LD et al (2002) Molecular imaging of gene expression and efficacy following adenoviral-mediated brain tumour gene therapy. *Mol Imaging* 1:43–55
- Risholm P, Golby AJ, Wells W 3rd et al (2011) Multimodal image registration for preoperative planning and image-guided neurosurgical procedures. *Neurosurg Clin N Am* 22:197–206
- Roberts DW, Miga MI, Hartov A et al (1999) Intraoperatively updated neuroimaging using brain modeling sparse data. *Neurosurgery* 45:1199–1206
- Romstöck J, Fahlbusch R, Ganslandt O et al (2002) Localisation of the sensorimotor cortex during surgery for brain tumours: feasibility and waveform patterns of somatosensory evoked potentials. *J Neurol Neurosurg Psychiatry* 72:221–229

- Roux FE, Ibarrola D, Lotterie JA et al (2001a) Perimetric visual field and functional MRI correlation: implications for image-guided surgery in occipital brain tumors. *J Neurol Neurosurg Psychiatry* 71:505–514
- Roux FE, Ibarrola D, Tremoulet M et al (2001b) Methodological and technical issues for integrating functional magnetic resonance imaging data in a neuronavigational system. *Neurosurgery* 49: 1145–1157
- Rozanski VE, Vollmar C, Cunha JP et al (2014) Connectivity patterns of pallidal DBS electrodes in focal dystonia: a diffusion tensor tractography study. *Neuroimage* 84:435–442
- Rutten GJ, Ramsey NF, van Rijen PC et al (2002) fMRI-determined language lateralization in patients with unilateral or mixed language dominance according to the Wada test. *Neuroimage* 17:447–460
- Schiffbauer H, Berger MS, Ferrari P et al. (2003) Preoperative magnetic source imaging for brain tumor surgery: a quantitative comparison with intraoperative sensory and motor mapping. *Neurosurg Focus* 15:E7
- Schulder M, Holodny A, Liu WC et al (1999) Functional magnetic resonance image-guided surgery of tumors in or near the primary visual cortex. *Stereotact Funct Neurosurg* 73:31–36
- Signorelli F, Guyotat J, Schneider F et al (2003) Technical refinements for validating functional MRI-based neuronavigation data by electrical stimulation during cortical language mapping. *Minim Invasive Neurosurg* 46:265–268
- Sol JC, Casaux J, Roux FE et al (2001) Chronic motor cortex stimulation for phantom limb pain: correlations between pain relief and functional imaging. *Stereotact Funct Neurosurg* 77:172–176
- Son BC, Kim MC, Choi BG et al (2001) Proton magnetic resonance chemical shift imaging (1H CSI)-directed stereotactic biopsy. *Acta Neurochir* 143:45–49
- Stadlbauer A, Moser E, Gruber S et al (2004) Integration of biochemical images of a tumor into frameless stereotaxy achieved using a magnetic resonance imaging/magnetic resonance spectroscopy hybrid data set. *J Neurosurg* 101:287–294
- Stippich C, Hofmann R, Kapfer D et al (1999) Somatotopic mapping of the human primary somatosensory cortex by fully automated tactile stimulation using functional MRI. *Neurosci Lett* 277:25–28
- Stippich C, Kapfer D, Hempel E et al (2000) Robust localization of the contralateral precentral gyrus in hemiparetic patients using the unimpaired ipsilateral hand. *Neurosci Lett* 285:155–159
- Stippich C, Kress B, Ochmann H et al (2003) Preoperative functional magnetic resonance imaging (fMRI) in patients with rolandic brain tumors: indication, investigation strategy, possibilities and limitations of clinical application. *Fortschr Roentgenstr* 175:1042–1050
- Stippich C, Rapps N, Dreyhaupt J et al (2007) Localizing and lateralizing language in patients with brain tumors: feasibility of routine preoperative functional MR imaging in 81 consecutive patients. *Radiology* 243:828–836
- Stoeckel MC, Binkofski F (2010) The role of ipsilateral primary motor cortex in movement control and recovery from brain damage. *Exp Neurol* 221:13–17
- Stroman PW, Kornelsen J, Lawrence J (2005) An improved method for spinal functional MRI with large volume coverage of the spinal cord. *J Magn Reson Imaging* 21:520–526
- Taoka T, Sakamoto M, Nagakawa H et al (2008) Diffusion tensor tractography of the Meyer loop in cases of temporal lobe resection for temporal lobe epilepsy. Correlation between postoperative visual field defect and anterior limit of Meyer loop on tractography. *AJR* 29:1329–1334
- Taylor RH, Lavallée S, Burdea GC et al (eds) (1995) Computer integrated surgery. Technology and clinical applications. MIT Press, Boston
- Thulborn KR (1999) Clinical rationale for very-high-field (3.0 Tesla). Functional magnetic resonance imaging. *Top Magn Reson Imaging* 10:37–50
- Tie Y, Rigolo L, Norton IH et al (2014) Defining language networks from resting-state fMRI for surgical planning – a feasibility study. *Hum Brain Mapp* 35(3):1018–30
- Tozakidou M, Wenz H, Reinhardt J et al (2013) Primary motor cortex activation and lateralization in patients with tumors of the central region. *Neuroimage Clin* 2:221–228
- Tronnier VM, Wirtz CR, Knauth M et al (1996) Intraoperative computer-assisted neuronavigation in functional neurosurgery. *Stereotact Funct Neurosurg* 66:65–68
- Tronnier VM, Wirtz CR, Knauth M et al (1997) Intraoperative diagnostic and interventional magnetic resonance imaging in neurosurgery. *Neurosurgery* 40:891–902
- Tronnier V, Staubert A, Bonsanto MM et al (2000) Virtuelle Realität in der Neurochirurgie. *Radiologe* 40:211–217
- Tsuyuguchi N, Takami T, Sunada I et al (2004) Methionine positron emission tomography for differentiation of recurrent brain tumor and radiation necrosis after stereotactic radiosurgery in malignant glioma. *Ann Nucl Med* 18:291–296
- Unsgaard G, Gronningsaeter A, Ommedahl S et al (2002) Brain operations guided by real-time two-dimensional ultrasound: new possibilities as a result of improved image quality. *Neurosurgery* 51:402–412
- Vabulas M, Kumar VA, Hailton JD et al (2014) Real-time atlas-based neuronavigation. *Neurosurgery* 74:128–34
- Varma NR, Barton KN, Janic B, Shankar A, Iskander A, Ali MM, Arbab AS (2013) Monitoring adenoviral based gene delivery in rat glioma by molecular imaging. *World J Clin Oncol* 4(4):91–101
- Weber WA, Wester HJ, Al G et al (2000) O-(2-[18F]fluoroethyl)-L-tyrosine and L-[methyl-11C]methionine uptake in brain tumors: initial results of a comparative study. *Eur J Nucl Med* 27: 542–549
- Wegscheid ML, Moshed RA, Cheng Y, Lesniak MS (2014) The art of attraction: application of multifunctional magnetic nanomaterials for malignant glioma. *Exp Opin Drug Deliv* 11:957–975
- Wengenroth M, Blatow M, Guenther J et al (2011) Diagnostic benefits of presurgical fMRI in patients with brain tumours in the primary sensorimotor cortex. *Eur Radiol* 21:1517–1525
- Winkler D, Strauss G, Lindner D et al (2005) The importance of functional magnetic resonance imaging in neurosurgical treatment of tumors in the central region. *Clin Neuroradiol* 15:182–189
- Winston GP, Yogarajah M, Symms MR (2011) Diffusion tensor imaging tractography to visualize the relationship of the optic radiation to epileptogenic lesion prior to neurosurgery. *Epilepsia* 52: 1430–1438
- Wirtz CR, Knauth M, Hassfeld S et al (1998) Neuronavigation – first experience with three commercially available systems. *Zentralbl Neurochir* 59:14–22
- Wirtz CR, Albert FK, Schwaderer M et al (2000) The benefit of neuronavigation for neurosurgery analyzed by its input on glioblastoma surgery. *Neurol Res* 22:354–360
- Woermann FG, Jokeit H, Luerding R et al (2003) Language lateralization by Wada test and fMRI in 100 patients with epilepsy. *I. Neurology* 61:699–701
- Woolsey CN, Erickson TC, Gilson WE (1979) Localization in somatic sensory and motor areas of human cerebral cortex as determined by direct recording of evoked responses and electrical stimulation. *J Neurosurg* 51:476–506
- Wu CWH, Kaass JH (1999) Reorganization in primary motor cortex of primates with long-standing therapeutic amputations. *J Neurosci* 19:7679–7697
- Wu JS, Zhou LF, Tang WJ et al (2007) Clinical evaluation and follow-up outcome of diffusion tensor imaging-based neuronavigation: a prospective, controlled study in patients with gliomas involving pyramidal tracts. *Neurosurgery* 61:935–948

- You SH, Jang SH, Kim YH et al (2005) Virtual-reality-induced cortical reorganization and associated locomotor recovery in chronic stroke: an experimenter-blinded study. *Stroke* 36:1166–1171
- Yousry TA, Schmid U, Jassoy AG et al (1995) Topography of the cortical motor hand area: prospective study with functional MR imaging and direct motor mapping at surgery. *Radiology* 195:23–29
- Zacà D, Nickerson JP, Deib G et al (2012) Effectiveness of four different clinical fMRI paradigms for preoperative regional determination of language lateralization in patients with brain tumors. *Neuroradiology* 54:1015–1025
- Zaehle T, Rach S, Herrmann CS (2010) Transcranial alternating current stimulation enhances individual alpha activity in human EEG. *PLoS One* 5:e13766
- Zhu FP, Wu JS, Song YY et al (2012) Clinical application of motor pathway mapping using diffusion tensor imaging tractography and intraoperative direct subcortical stimulation in cerebral glioma surgery: a prospective cohort study. *Neurosurgery* 71: 1170–1184
- Zolal A, Hejcl A, Vachata P et al (2012) The use of diffusion tensor images of the corticospinal tract in intrinsic brain tumor surgery: a comparison with direct subcortical stimulation. *Neurosurgery* 71:331–340
- Zurowski B, Kordon A, Weber-Fahr W (2012) Relevance of orbitofrontal neurochemistry for the outcome of cognitive-behavioural therapy in patients with obsessive compulsive disorder. *Eur Arch Psychiatry Clin Neurosci* 262:617–624

Presurgical Functional Localization Possibilities, Limitations, and Validity

Stéphane Lehéricy, Delphine Leclercq, Hugues Duffau,
Pierre-François Van de Moortele, and Christine Delmaire

Contents

| | |
|---|-----|
| 1 Possibilities and Limitations of Functional Brain Mapping | 248 |
| 1.1 Spatial Localization of BOLD Signal | 248 |
| 1.2 fMRI Artifacts and Limitations..... | 249 |
| 2 Validation of Presurgical Mapping Using Established Reference Procedures..... | 252 |
| 2.1 Direct Electrical Stimulations | 252 |
| 2.2 Intracarotid Amobarbital Procedure (IAP) or Wada Test..... | 255 |
| 3 Important Results of Validation Studies in Brain Tumors and Epilepsies, Overview, and Current State..... | 256 |
| 3.1 Motor Function | 256 |
| 3.2 Language Function..... | 258 |
| 3.3 Memory Functions | 260 |
| Conclusion | 261 |
| References..... | 262 |

S. Lehéricy, MD, PhD (✉)

Centre de NeuroImagerie de Recherche – CENIR, Institut du Cerveau et de la Moelle – ICM, Sorbonne Universités, UPMC Univ Paris 06, UMR S 1127, CNRS UMR 7225, Paris, France

Department of Neuroradiology, Groupe Hospitalier Pitié-Salpêtrière, Université Pierre et Marie Curie – Paris 6, 47-83, boulevard de l'hôpital, Paris 75651, France
e-mail: stephane.lehericy@psl.aphp.fr

D. Leclercq, MD
Department of Neuroradiology, Groupe Hospitalier Pitié-Salpêtrière, Université Pierre et Marie Curie – Paris 6, 47-83, boulevard de l'hôpital, Paris 75651, France
e-mail: del.leclercq@gmail.com

H. Duffau, MD, PhD
Department of Neurosurgery, Hôpital Gui de Chauliac and INSERM U1051, Montpellier University Medical Center, Montpellier, France
e-mail: h-duffau@chu-montpellier.fr

P.-F. Van de Moortele, MD, PhD
Center for Magnetic Resonance Research, University of Minnesota, 2021 Sixth Street SE, Minneapolis, MN 55455, USA

C. Delmaire, MD
Department of Neuroradiology, CHRU Lille, Hopital Roger Salengro, boulevard du Pr Leclerc, Lille cedex 59800, France
e-mail: c-delmaire@chru-lille.fr

Abstract

Over the last two decades, presurgical mapping using functional neuroimaging techniques – and particularly fMRI – has made considerable progress. FMRI is now commonly used in the clinical practice and not just for research applications. Presurgical functional neuroimaging with its contributions to *surgical planning and to the prediction of postoperative outcome is now well established.*

Validation studies of functional imaging techniques have shown the potential of fMRI to *localize motor areas* and also to *lateralize and localize language* and, more recently, *memory functions*. However, particularly for cognitive brain functions, the imaging results strongly depend on the methodology requiring optimal clinical standard procedures. Currently, functional neuroimaging is considered as *complementary to direct electrical stimulations (DES)* providing *additional information*, such as information on the entire functional network and on the contralateral hemisphere, which is not accessible to DES. Until now, fMRI cannot replace DES. In contrast, for language functions, fMRI has largely replaced the *intracarotid amobarbital procedure (IAP)*, which could be the case also for memory functions in the near future. *Diffusion tensor imaging (DTI) fiber tracking* is a more recent, but already in some centers, well-established technique, and its value in presurgical mapping requires further work.

1 Possibilities and Limitations of Functional Brain Mapping

In presurgical functional mapping, determination of the accuracy of functional maps is essential, if images are to contribute to the presurgical localization of eloquent areas at risk in order to avoid postoperative deficits. Among the available and established functional imaging methods, functional MRI (fMRI) is the most widely used. fMRI can be easily performed on clinical magnets. Within the same session, high-resolution three-dimensional (3D) images of the brain and functional images with or without contrast injection are acquired (depending on the brain tumor entity), providing accurate anatomic detail about the respective lesion. The following paragraphs will focus on the possibilities and limitations of blood-oxygen-level-dependent (BOLD) contrast fMRI.

1.1 Spatial Localization of BOLD Signal

Because fMRI maps are based on secondary metabolic and hemodynamic events that follow neuronal activity and not on the electrical activity itself, it remains unclear what the exact spatial specificity of fMRI is, despite proven congruence of fMRI localization and neuronal activation (Logothetis and Wandell 2004). Moreover, the physiological phenomenon underlying BOLD contrast is not yet fully understood.

For details, see chapter “[Revealing brain activity and the white matter structure using functional and diffusion-weighted magnetic resonance imaging](#)”.

1.1.1 Spatial Specificity of Deoxyhemoglobin-Based (BOLD fMRI) Methods

Multiple-site single-unit recordings and fMRI studies on the same animal have suggested that the limit of spatial specificity of T_2^* BOLD contrast might be in the range of 4–5 mm for single-condition maps, i.e., the task compared with the rest condition (Ugurbil et al. 2003). This may be adequate for presurgical brain mapping currently performed in the human brain with an image resolution of 3–5 mm, but a much better resolution can be achieved under certain circumstances (Harel et al. 2006).

The explanation for this is that deoxyhemoglobin changes which are initiated at the point of increased neuronal activity do not remain stationary and propagate into large *draining* vessels. Thus, deoxyhemoglobin changes incorrectly appear as *activation* away from the actual site of neuronal activity. Therefore, increased contribution of small vessels (capillaries) versus large *draining* vessels is a critical issue for improving the spatial resolution of BOLD contrast images. The respective contribution of small versus large vessels will depend on several factors, including the field strength and the type of sequence.

1.1.2 The Type of Sequence: Spin Echo (T_2) Versus Gradient Echo (T_2^*) BOLD fMRI

1.1.2.1 The Intra- and Extravascular Components of BOLD Signal

The most commonly used fMRI approach was introduced in 1992 and is based on T_2^* (i.e., gradient echo) BOLD contrast, which visualizes regional alterations in deoxyhemoglobin accompanying changes in neuronal activity (Heeger et al. 2002; Logothetis and Wandell 2004).

BOLD contrast originates from the intravoxel magnetic field inhomogeneity induced by paramagnetic deoxyhemoglobin inside the red blood cells, which in turn are compartmentalized within the blood vessels. Magnetic susceptibility differences between the deoxyhemoglobin-containing compartments and the surrounding space generate magnetic field gradients across and near the boundaries of these compartments. Consequently, BOLD contrast has thus an intravascular and extravascular contribution (Fig. 1).

The intravascular T_2 -BOLD effect is associated with the magnetic field gradient generated outside the red blood cells and inside the vessels. The field gradients around the red blood cells are very small compared to diffusion distances around and across the membranes of these cells (Fig. 1). Therefore, the effect is dynamically averaged and is detectable as a T_2 effect. When regional deoxyhemoglobin content increases, the T_2 of blood decreases (Thulborn et al. 1982). This intravascular effect is present in large as well as in small vessels.

The extravascular BOLD effect is associated with the magnetic field gradient generated outside the boundaries of the blood vessels. This gradient is due to the difference in magnetic susceptibility induced by deoxyhemoglobin between the vessels and the surrounding diamagnetic tissue. For small vessels such as capillaries, water diffusion during image acquisition (typically 50–100 ms for echo planar images (EPI)) dynamically averages the magnetic field gradient and results in a T_2 effect, similarly to the intravascular BOLD effect. For large vessels, dynamic averaging is not possible anymore. In contrast, static averaging will result in a signal loss within the voxel. A water molecule located in the vicinity of the blood vessel will see a static magnetic field, which will vary with the proximity to the vessel (Fig. 1). As this magnetic field varies across the voxel, the signal of the entire voxel will be dephased, resulting in a T_2^* effect.

1.1.2.2 Specificity of Spin Echo (T_2) Versus Gradient Echo (T_2^*) BOLD

As detailed above, the T_2 -BOLD response arises from intra- and extravascular effects originating from small and large vessels. The intravascular contribution originates from both large and small vessels, whereas the extravascular part is dominated by small vessel contributions (Boxerman et al. 1995). Thus, the spin echo (SE) BOLD fMRI response is

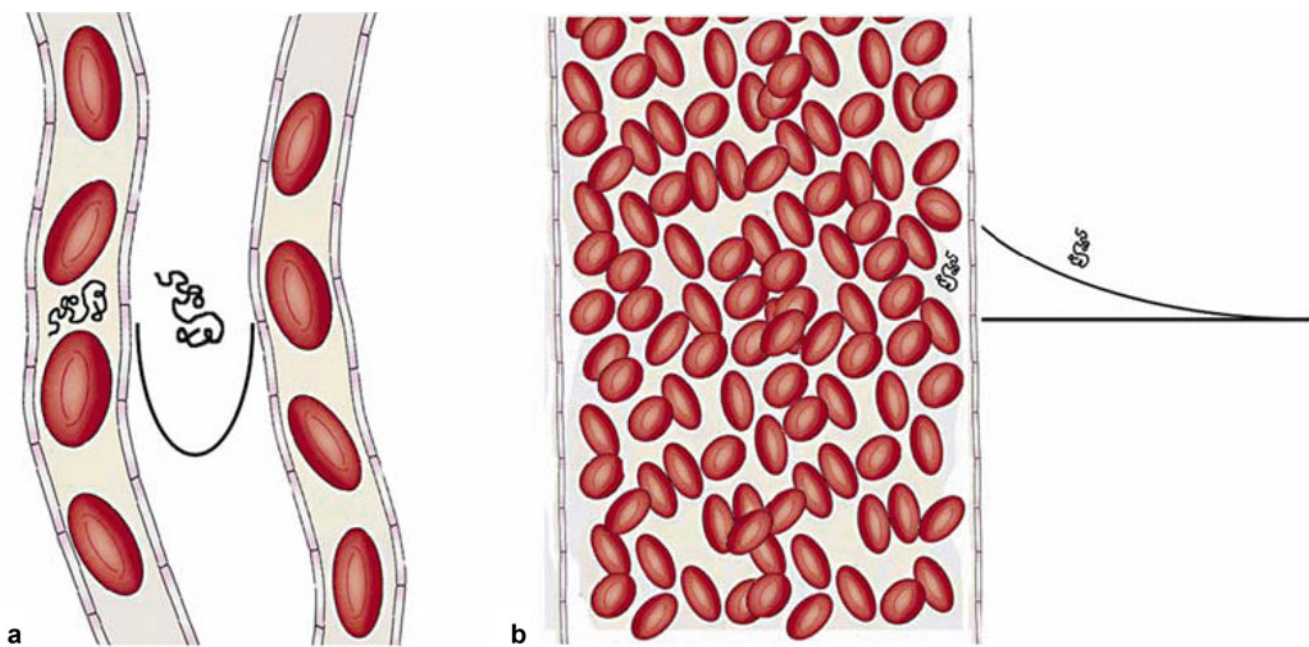


Fig. 1 In (a, b), the extravascular BOLD effect is associated with the magnetic field gradient generated outside the boundaries of the blood vessels, which is due to the difference in magnetic susceptibility induced by deoxyhemoglobin between the vessel and the surrounding diamagnetic tissue (after Hoppel et al. 93). The black curves outside the vessels represent the field gradient produced by the blood, which is inside the vessels. (a) For small vessels such as capillaries, the field gradients around the vessels are large compared to diffusion distances;

due to apparent changes in T_2 originating from the diffusion of water in the presence of magnetic field gradients generated in the extravascular space around the microvasculature (Ogawa et al. 1993; Boxerman et al. 1995), as well as from the exchange of water into and out of red blood cells within the blood itself (Pawlak et al. 1981; van Zijl et al. 1998; Ugurbil et al. 1999). At high magnetic fields, blood has a short T_2 , shorter than the echo times that are used in fMRI experiments. Therefore, the blood is not expected to contribute significantly to the measured BOLD signal changes. Consequently, at high field strength, the SE BOLD mainly originates from the extravascular space around the microvasculature and hence provides greater specificity to changes in neuronal activity (Lee et al. 1999; Duong et al. 2003; Ugurbil et al. 2003; Yacoub et al. 2003).

1.1.2.3 Field Dependence of BOLD Signal

Both the signal-to-noise ratio (SNR) and spatial resolution of BOLD fMRI increase with the main magnetic field strength. Higher magnetic fields will also *preferentially attenuate the macrovascular contribution* (Ugurbil et al. 2003).

The BOLD response is expected to behave differently with increasing magnetic fields in small versus large blood vessels (Ogawa et al. 1993). The dependence on the external

therefore, the extravascular BOLD is a T_2 effect as water diffusion dynamically averages in the magnetic field gradient. (b) For large vessels, the field gradients around the vessels are small compared to diffusion distances. The signal loss in the voxel is the result of a static averaging; therefore, the extravascular BOLD is a T_2^* effect. In (a, b), the intravascular BOLD effect is associated with the magnetic field gradient generated outside the red blood cells inside the vessels. Similarly to the extravascular BOLD effect around capillaries, the intravascular BOLD is detectable as a T_2 effect

magnetic field strength varies quadratically for capillaries. In contrast, the dependence on the static magnetic field (B_0) is linear for the contribution of large vessels (Ogawa et al. 1993). Therefore, in addition to increasing the fMRI signal, higher magnetic fields will specifically enhance the signal components originating from parenchymal capillary tissue. In contrast, BOLD signal originating from large vessels will be overrepresented at lower magnetic field strengths.

1.2 fMRI Artifacts and Limitations

Different types of artifacts and methodological limitations need to be considered in clinical fMRI. They may also interfere with the results of validation studies using established reference procedures – the most important are discussed below.

For details, see chapter “Clinical BOLD fMRI and DTI: artifacts, tips and tricks”.

1.2.1 Movement Artifacts

Head motion is a critical issue in BOLD fMRI. Head motion is mostly reflected in rigid body global deformations and translations. When voxels have side lengths smaller than a millimeter, motion control becomes a crucial issue.

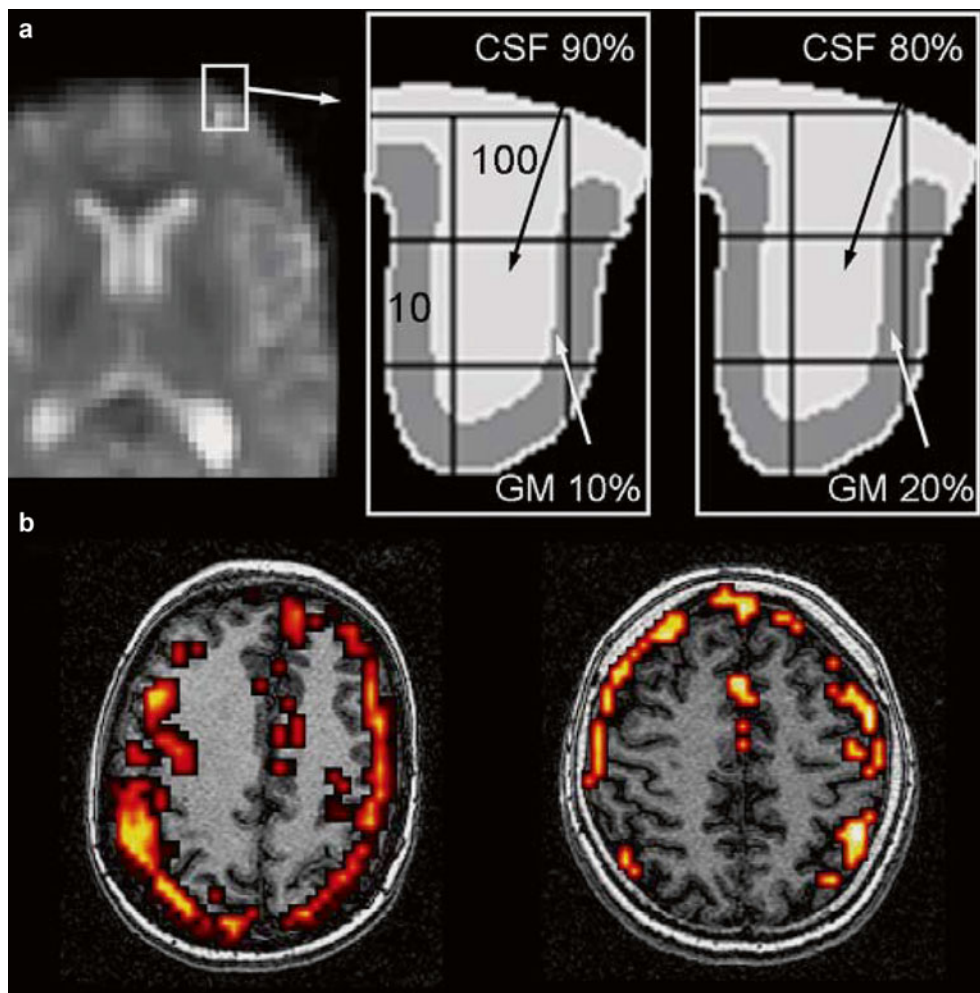


Fig. 2 Head motion artifact. When temporally correlated with task performance, a movement of one tenth of a voxel ($300\text{--}400\text{ }\mu\text{m}$) may result in signal changes similar or even larger than the actual signal increase due to task performance which are virtually impossible to distinguish from each other by the motion correction software. Artifacts predominate in regions of tissue interface where changes in signal intensity are high. An example is provided in (a). The diagrams represent an enlarge-

ment of a frontal sulcus from the left image. In condition 1, the 4 mm voxel of interest in the middle of the image contains 90 % cerebrospinal fluid (CSF, signal = 100 arbitrary units) and 10 % gray matter (GM, signal = 10) resulting in an average signal of 91 (left diagram). In condition 2, a 0.4 mm motion (one tenth of the voxel size) will result in an average signal intensity of 82 (80 % CSF and 20 % GM, right diagram). (b) Typical head motion artifacts in two different subjects

Head motion does not depend on which part of the brain is imaged. Using single-shot EPI, each image is virtually devoid of motion artifacts, given the very short acquisition time (<100 ms). However, head motion may occur between successive images of one fMRI series. Most fMRI studies are currently performed with a spatial resolution of 3–4 mm (in-plane voxel size) and a slice thickness of 4–5 mm (e.g., matrix: 64×64 , FOV = 24 cm). Head motion artifacts predominate in regions of tissue interface where changes in signal intensity are high (Fig. 2). When temporally correlated with task performance, a movement of one tenth of a voxel ($300\text{--}400\text{ }\mu\text{m}$) may result in signal changes similar or even larger than the actual signal increase due to the task performance and which are virtually impossible to distinguish from each other by motion correction software (Fig. 2). A careful setup of the subject in the magnet (padding foams) allows for a reduction of these artifacts. External devices, such as a bite

bar setup, can be used to further minimize head motion but are rarely used in clinical practice. A careful explanation of the task to the subject may also help to reduce head motion. Head motion should be corrected using currently available methods. Furthermore, nowadays real-time motion correction software is also available.

Cardiac and respiratory motion results in physiological fluctuations of the BOLD signal. Brain motion due to cardiac pulsation is negligible in the motor cortex but becomes significant in the upper brain stem and diencephalon (Enzmann and Pelc 1992). Brain motion is of small amplitude (0.16 mm) but can represent as much as 30 % of the voxel size at ultrahigh spatial resolution (0.5 mm in plane). EPI images are particularly sensitive to changes in resonance frequency which can arise from respiration and are more significant at high magnetic field strengths (Van de Moortele et al. 2002). Noise generated from respiration-induced phase and frequency fluctuations as

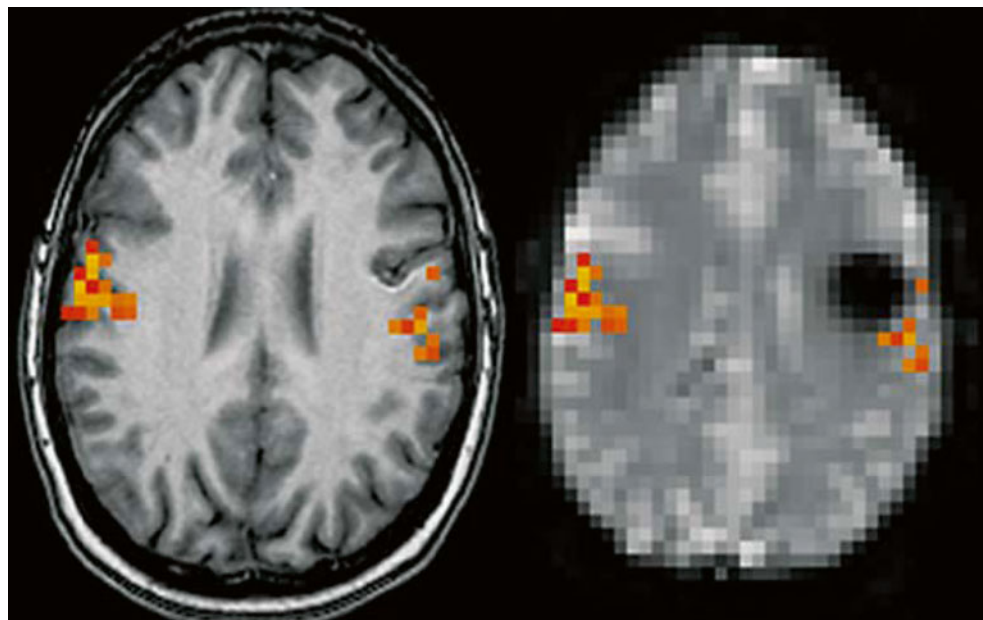


Fig. 3 Magnetic susceptibility artifact. Patient presenting a cavernous angioma of the left central area. *Left:* Activation map during lip movements superimposed on transverse T1-weighted images suggesting that the lesion is located at a distance from the activation in the primary motor area. *Right:* Same activation map superimposed on a transverse

EPI T2* image showing the lesion surrounded by a large area of signal drop due to T2* shortening susceptibility artifact. Although no activation is visible inside the area of signal drop, it is not possible to conclude that the functional area does not extend inside this area

well as from cardiac-induced fluctuations can be corrected using different algorithms (Pfeuffer et al. 2002), some of them based on physiological recordings (Hu et al. 1995).

1.2.2 Magnetic Susceptibility Artifacts

These artifacts are due to differences in magnetic susceptibility between bone, air, and brain structures. These susceptibility differences generate field gradients which result in an inhomogeneous static magnetic field. The consequence is a signal loss, as well as distortion in EPI images and a blurring in spiral images. These artifacts are particularly predominant in regions containing air and bone, such as sinuses and inner ear structures. They are observed in calcified structures and after brain hemorrhage because of metallic particle deposition, such as in vascular malformations (Fig. 3). They are also frequently observed following brain surgery because of the presence of metallic particles deposited during surgery.

Magnetic susceptibility artifacts increase with field strength. Their impact can be reduced using higher bandwidth, shorter TE, thinner slices, and better shimming procedures.

1.2.3 BOLD Response Alterations Induced by the Lesion

Neurovascular coupling that underlies BOLD contrast can be altered in normal aging as well as in vascular diseases (Pineiro et al. 2002; D'Esposito et al. 2003; Hamzei et al. 2003). Pathologies that affect neurovascular coupling can affect the characteristics of the BOLD signal. This is particularly important in BOLD fMRI studies in patients with brain tumors because the abnormal vasculature is an essential

feature of tumor growth (Folkman et al. 1989). Decreased activation has been reported on the side of the tumor predominantly in high-grade glioma (Holodny et al. 1999, 2000). It has been suggested that negative BOLD responses correlate with decreased neuronal activity (Shmuel et al. 2006) or neuronal inhibition in epilepsy (Kobayashi et al. 2005), but the different factors contributing to decreased BOLD activation in patients with brain tumors are not fully understood. They may also include a loss of autoregulation in the tumor vasculature and venous or pressure effects (Holodny et al. 1999, 2000). Several studies have suggested that regional cerebral blood volume (rCBV) using perfusion MRI is altered in gliomas (Ludemann et al. 2001; Cha et al. 2003; Law et al. 2004) and that fMRI activations are decreased in the vicinity of brain tumors (Holodny et al. 2000; Fujiwara et al. 2004; Hou et al. 2006; Jiang et al. 2010).

In patients with brain arteriovenous malformations (AVMs), flow abnormalities may interfere with fMRI detection of language-related areas (Lehericy et al. 2002). In patients with severe flow abnormalities, results of Wada examination and/or postembolization fMRI have shown that abnormal language lateralization is at least partly due to severe flow abnormalities that impair the detection of the BOLD signal (Lehericy et al. 2002). Neurovascular coupling can be altered in several ways in patients with brain AVM. Hypotension or the presence of a so-called steal phenomenon may negatively influence the normal functions in areas adjacent to the lesion (Barnett et al. 1987; Fogarty-Mack et al. 1996). Changes in cerebral blood flow (Barnett et al. 1987; Young et al. 1990), perfusion pressure (Hassler

and Steinmetz 1987; Fogarty-Mack et al. 1996), oxygen metabolism (Fink 1992), autoregulation processes, and vaso-reactivity (Barnett et al. 1987; Hassler and Steinmetz 1987; Young et al. 1994; Fogarty-Mack et al. 1996), all of which have been reported in areas adjacent to AVMs, may alter the BOLD signal intensity and detection.

1.2.4 Alternatives to Task-Related fMRI

Preoperative task-related fMRI depends on subject cooperation. In patients with deficits, fMRI may be negative. The choice of tasks is also an important factor to reliably activate eloquent brain areas. These difficulties can be overcome by using various approaches, e.g., by passive movements for motor mapping (Ogg et al. 2009). More recently, new approaches relying on functional connectivity techniques have been proposed. Functional connectivity refers to the temporal correlation between various fMRI signals in spatially remote regions. Functional connectivity can be studied by measuring coherent signal fluctuations in BOLD fMRI time series in the resting brain (Biswal et al. 1995). For instance, resting-state functional imaging studies have thus revealed covariation of these fluctuations in distributed brain networks.

Previous studies have shown that brain tumors induce a loss of functional connectivity (Bartolomei et al. 2006; Guggisberg et al. 2008). Decreased resting-state functional connectivity in the tumor area has been shown to be strongly associated with the absence of eloquent cortex using DES (Martino et al. 2011). In addition, resection of areas with reduced connectivity has been reported to be associated with a low risk of postoperative deficits (Guggisberg et al. 2008). Resting-state fMRI was also efficient to detect the motor and language network when compared with DES (Mitchell et al. 2013). Functional connectivity techniques have therefore a potential to analyze patients with brain lesions noninvasively.

2 Validation of Presurgical Mapping Using Established Reference Procedures

2.1 Direct Electrical Stimulations

Currently, invasive electrophysiological investigations remain the reference procedure (*gold standard*) for brain surgery, in particular for tumors located near or within eloquent cortical and/or subcortical structures (Keles and Berger 2004; Duffau et al. 2005). Direct electrical stimulations (DES) allow mapping of a large number of motor, somatosensory, and cognitive functions. DES also permits the study of anatomo-functional connectivity by directly stimulating white matter tracts (Duffau et al. 2002, 2003b; Keles et al. 2004). Therefore, DES represent an accurate and reliable technique to localize cortical and subcortical regions at risk regarding

brain function. Consequently, a reproducible functional disturbance induced by DES will indicate where to stop with the resection, both for cortical and subcortical structures. Tumor removal is hence performed according to functional boundaries in order to optimize the accuracy of tumor removal in terms of minimizing the risk of postoperative functional deficits.

DES have some limitations, however. They only allow loco-regional and not whole brain mapping. Further, they are time-consuming, and the number of tasks that can be performed during surgery is limited. *Therefore, DES should still be combined with other metabolic and functional methods.*

2.1.1 Basic Principles

Electrical stimulations increase membrane excitability, via an initial phase of passive modification of the local membrane potential (MP) at the level of the cathode (the negative electrode). The inner side of the membrane becomes progressively less negative than the outer side (the membrane becomes inversely hyperpolarized with regard to the anode). The intensity of this phenomenon depends on the parameters of electrical stimulation and the characteristics of the membrane (Jayakar 1993). Stimulation of the membrane is easier at the level of the initial segment of the axon in myelinated fibers and in fibers of greater diameter (Ranck 1975). If the MP reaches the depolarization threshold, voltage-dependent ion channels will open and allow the entry of Na^+ ions inside the neuron. This Na^+ entry will invert the MP between +20 mV and +30 mV. A secondary output of K^+ ions, associated with an inhibition of the inward flux of Na^+ ions, brings the MP back to its resting state. Once generated, this rapid sequence of MP fluctuations – the action potential – is always the same, regardless of the stimulation parameters (law of *all or nothing*).

2.1.2 Risks Associated with DES

Direct electrical stimulations can damage the brain. Tissue damage can result from numerous causes. Accumulation of a negative charge at the level of the cathode or through the production of metal ions at the level of the anode can damage the brain (Agnew and McCreery 1987). This can be prevented by biphasic impulses because the second stimulus inverts the effects of the first one. Excessive heat produced by hydrolysis induces vacuolization and chromatolysis (Doty and Barlett 1981). A *leaking* of the intracellular current, which goes from the anode to the cathode through the cytoplasm, can damage the mitochondria and the endoplasmic reticulum (Pudenz et al. 1977). Repetitive and synchronous stimulations of neurons can alter neuronal homeostasis (Fertziger and Ranck 1970; Agnew and McCreery 1987). These risks are directly linked to the density of the charge. Animal studies have shown that, when the charge does not exceed 55 $\mu\text{C}/\text{cm}^2/\text{phase}$, lesions do not occur (Gordon et al. 1990).

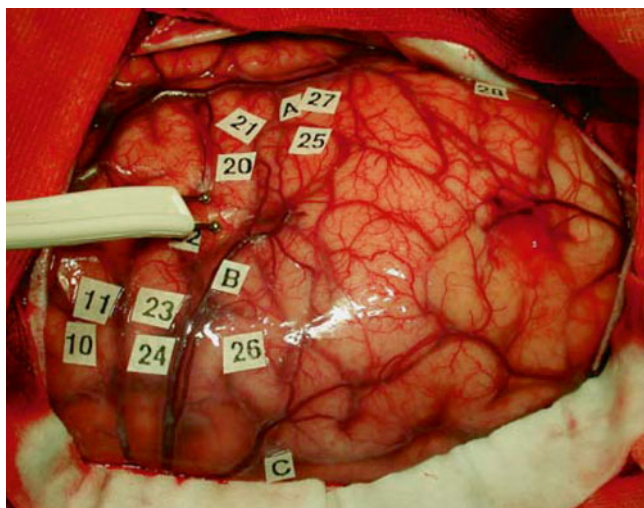


Fig. 4 Intraoperative view of a patient showing bipolar stimulation using a probe with two tips separated by 5 mm. During surgery, the probe is placed on the cortical surface of the patient. Stimulation sites are labeled using small tags

Stimulations can also generate seizures. The frequency of seizures is estimated at 5–20 % (Sartorius and Berger 1998). The monitoring of the stimulation using intra-stimulation electrocorticographic recording avoids the occurrence of *afterdischarge* (Lesser et al. 1984), except in children who have nonmyelinated fibers (Jayakar et al. 1992). Recording electrodes should ideally be located in the immediate proximity of each stimulation and therefore should *follow* the stimulation electrode. They should also have a small diameter to allow stimulation of the cortex.

Finally, the accumulation of any conductive substance such as cerebrospinal fluid or blood can favor the distribution of current beyond the target tissue, thus increasing the risk of false negatives: Any stimulated structure must therefore be kept dry.

2.1.3 Practical Stimulation Methods

The optimal stimulation parameters (best benefit/risk ratio) have been extensively studied (Nathan et al. 1993; Duffau 2004). They can be significantly modified by the degree of cerebral maturation and fiber myelination (Jayakar et al. 1992), as well as by anesthetic drugs and pathological processes (tumor, epilepsy, postictal status) (Jayakar 1993).

Bipolar stimulation is usually performed using a probe with two tips separated by 5 mm (Fig. 4) and the following parameters: rectangular impulses, biphasic current at 50 Hz (Lesser et al. 1987) or 60 Hz (Ojemann et al. 1989; Berger 1995), and intensities of 1–18 mA. Under local anesthesia, current intensities of less than 6–8 mA with an impulse duration of 0.3 ms (Lesser et al. 1987) to 1 ms (Ojemann et al. 1989; Berger 1995) are standard parameters. Typically, the stimulation intensity is progressively increased from 4 mA

(under general anesthesia) or 1 mA (under local anesthesia), by increments of 1 mA in order to find the optimal threshold generating responses without causing seizures.

In children, the rates of response are lower than in adults (less than 20 % <5 years or even no response <1 year) because of the immaturity of fibers (higher chronaxie in non-myelinated fibers). Therefore, a progressively and alternately sequential increase of impulse intensity and duration has been proposed (Jayakar et al. 1992).

2.1.4 Neuropsychological Evaluation

Defining the *eloquent* nature of cortical areas using DES requires appropriate tasks and an accurate recording of the clinical responses to determine whether there is any interference with function during stimulation of the site. For this purpose, speech therapists or psychologists are present in the operative room in order to interpret the disorders induced by DES (Duffau et al. 2002).

Mapping of motor functions can be performed in awake patients or under general anesthesia, by inducing involuntary motor responses. Awake patients are generally passive during stimulation. Rarely, when looking for *negative motor areas* in the premotor cortex (Luders et al. 1995), the patient is asked to make regular movements during the stimulation. Changes in movement parameters are recorded (slowdown, decrease in precision or amplitude, interruption). Under general anesthesia, small movements can be overlooked. This is a frequent problem for neck movements because the intubation cannula often prevents muscular contractions from being perceived. Concomitant intraoperative electromyographic recording and motor evoked potentials improve the detection of positive responses (Yingling et al. 1999). These methods are constraining, however. They require additional equipment, the presence of an electrophysiologist in the operating room, and the positioning of electrodes on the entire hemibody contralateral to the stimulation side if the lesion is in the vicinity of the corona radiata and/or the internal capsule (Duffau et al. 2003a). Sensory functions are mapped by eliciting dysesthesia described by the patient himself intraoperatively (responses are therefore subjective).

For cognitive function, the study of language (spontaneous speech, naming, comprehension, etc.), calculation, memory, reading, or writing evaluation is performed in awake patients by generating transient disturbances (Ojemann et al. 1989; Duffau et al. 2002). The choice of the most appropriate tests is critical. Eloquent sites can be detected only if the *proper* function has been tested. This is why sensitive tasks are used rather than specific ones.

Language mapping usually includes a counting test followed by an object-naming task. The counting test is likely to alter articulatory production, while the following automatic series are being carried out (slowing down, dysarthria, anarthria, complete speech arrest, more

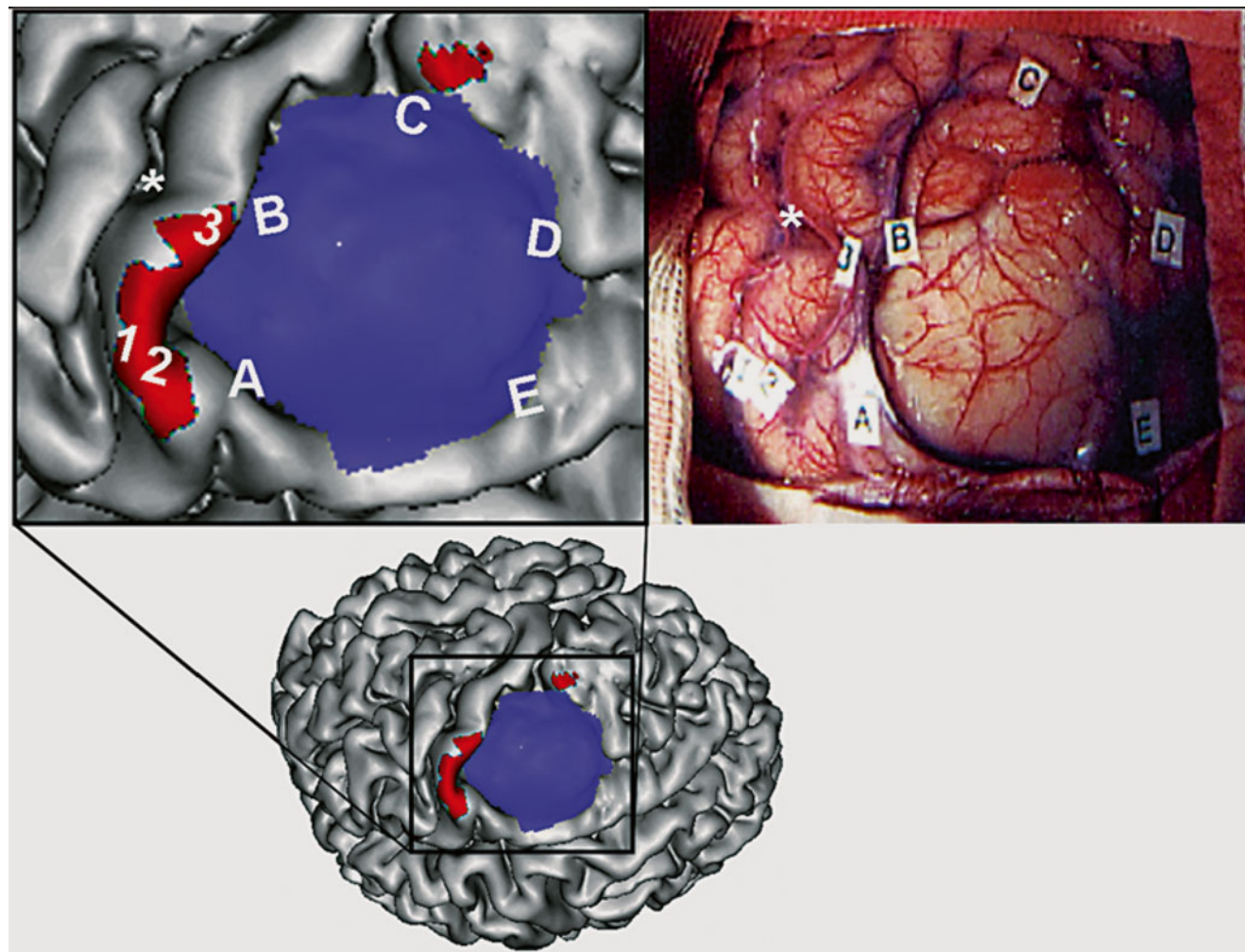


Fig. 5 Correspondence between fMRI and intraoperative cortical stimulation. *Upper left:* Surface rendered of the cortex in a patient with a left premotor low-grade glioma (enlarged view of the figure in the *lower row*). The tumor is represented in blue. Activation obtained during performance of right-hand movement is shown in red. *Upper right:*

Intraoperative view of the same patient (same orientation). The letters outline the tumor margins. The numbers indicate the stimulation sites that elicited hand movements. Note the good correspondence between the fMRI activation map and direct electrical stimulations (Color figure online)

or less associated with facial movements and/or hoarseness and/or automatic swallowing). The object-naming task induces various symptoms such as articulatory disorders, pure anomia, phonemic or semantic paraphasias, or even perseverations. These tasks are short (less than 4 s duration) and therefore compatible with surgical requirements under local anesthesia). Depending on the localization of the lesion, a third more specific task is also performed. This task is chosen in each patient based on the individual cortical language organization, as evaluated preoperatively by a neuropsychological assessment and functional neuroimaging. Tasks include verb generation, tasks in foreign languages in bilingual individuals, memory, calculation, repetition, reading, or even comprehension tasks for posterior temporoparietal lesions (Gatignol et al. 2004).

2.1.5 Coregistration with Functional Imaging Data

Comparison between DES and functional imaging data has been performed using several methods. Initially, simple visual comparisons were obtained between intraoperative views and fMRI data (Jack et al. 1994; Yousry et al. 1995). Coregistration has also been performed by comparing pictures of DES positive sites with the preoperative 3D rendering of the brain (Pujol et al. 1996; Lehericy et al. 2000b) (Fig. 5). These methods have limitations, however, as they are not quantitative. 3D rendering displays brain activation as viewed transparently from the surface of the brain: Therefore, the display includes activation that is located in the depth of the sulci and gyri. More recently, coregistration has been obtained using stereotactic neuronavigation procedures (Lehericy et al. 2000b; Krings et al. 2001b; Krishnan

et al. 2004). This technique allows a 3D multiplanar comparison of the DES positive sites with functional data, as well as measurements of distances and overlap.

2.1.6 Limitations of Functional and DES Comparison

DES and functional imaging methods provide fundamentally different types of data. DES interfere directly by blocking the ability of the patient to perform a task. Therefore, it is assumed that DES depict critical language areas only. In contrast, functional imaging methods provide activation maps obtained during performance of motor, language, or cognitive tasks. Consequently, imaging techniques do usually not only include critical areas but also activity in nonessential areas that are only associated with task performance but could be resected. Functional maps are displayed using a statistical threshold. Therefore, a low threshold may increase both the number of nonessential areas and the size of the critical areas, whereas a stringent threshold may not allow critical areas to reach statistical significance. Craniotomy and debulking may induce deformation, which impairs image registration (Hill et al. 2000; Krings et al. 2001b). Finally, tasks performed during neurofunctional imaging and intraoperative procedures are not identical because of the different setups (Lurito et al. 2000). These issues need to be kept in mind when comparisons between the different techniques are performed.

2.2 Intracarotid Amobarbital Procedure (IAP) or Wada Test

The intracarotid amobarbital procedure (IAP), or Wada test, was first reported as a means to identify the hemisphere of language dominance in patients with epilepsy (Wada and Rasmussen 1960). IAP was then modified to measure memory function in patients undergoing surgery for epilepsy (Milner et al. 1962). The role of IAP is to assess language and amnesic risks by ensuring that the hemisphere contralateral to the operated one is able to subserve language and memory functions. Thus, IAP helps to predict and prevent postoperative language and memory deficits and in the end to give an estimate of linguistic and neuropsychological outcome (Sperling et al. 1994; Loring et al. 1995).

2.2.1 Methods

IAP is performed in the angiography suite in the presence of a neurological and neuroscience team (Rausch et al. 1993; Akanuma et al. 2003). The patient is positioned on the angiography table. EEG monitoring is performed. After local skin anesthesia and femoral artery access, a diagnostic catheter is placed selectively in the internal carotid arteries (ICA) under fluoroscopic guidance. Then amobarbital is injected in

the ICA for either side separately. Therefore, the IAP induces a temporary inactivation of the cortex supplied by the anterior and middle cerebral arteries in the hemisphere ipsilateral to the injection. Rarely, the two hemispheres are tested on two consecutive days. During the 10–15 min of the procedure, patients receive a battery of language and memory tasks following amobarbital injection (Jones-Gotman 1987). Language tasks usually include speech production (serial speech, naming), speech reception (simple motor commands, token test), and other speech tasks, such as reading aloud and spelling. Tasks are scored so that a lateralization index (LI) can be calculated for each task. The LI can be expressed as the difference between the scores during left injection minus the scores during right injection of amobarbital, divided by the maximum possible score.

2.2.2 Risks and Limitations of the Wada Test

The IAP has several disadvantages, however (Simkins-Bullock 2000). Risks include those of intracarotid catheterization. Following cerebral angiography, the ischemic event rate has been estimated between 0.3 and 1.8 % (0.07–0.3 % permanent) (Dion et al. 1987; Cloft et al. 1999). Test-retest reliability and external validation cannot be performed. IAP evaluation is performed within a short period of time (approximately 3–10 min). Anesthesia can induce behavioral effects (e.g., aphasia, attention deficits, neglect, and somnolence). Amobarbital injected via the ICA will inactivate the amygdala and the anterior hippocampus but never or rarely the posterior two thirds of the hippocampus (Jack et al. 1989; Hong et al. 2000b). This represents a critical concern for the validity of memory assessment. Moreover, in some patients, mesial temporal perfusion can be unaffected during IAP (de Silva et al. 1999). In addition, IAP also inactivates the rest of the hemisphere ipsilateral to the injection and in some patients also the contralateral hemisphere (Hong et al. 2000b). To overcome these limitations, selective IAP via an injection in the posterior cerebral artery has therefore been proposed to test for memory function (Jack et al. 1989). The risk of morbidity of this procedure is much greater than via direct ICA injection, and thus it is not widely used (Jack et al. 1989). For language functions, the IAP provides information on the hemispheric language dominance but not on the anatomical location of language areas and their relation to the lesion. Lastly, the total direct costs of the Wada test has been estimated 3.7 times higher than that of fMRI (Medina et al. 2004).

2.2.3 Validation of the Wada Test

Validation of IAP has been performed in several ways. Recording of intrahippocampal activity using depth electrodes has shown that the EEG background activity can be significantly suppressed in the posterior hippocampal regions even in the absence of amobarbital perfusion in these areas (Urbach et al. 1999). Using HMPAO-SPECT, hypoperfusion in the territories of the anterior and middle cerebral arteries

was observed during IAP (de Silva et al. 1999). Hypoperfusion in medial temporal structures was noticed in the great majority of these patients (de Silva et al. 1999). Further, in the epileptogenic hemisphere, the degree of hippocampal damage correlated with the impairment in Wada memory performance (Sass et al. 1991; O'Rourke et al. 1993; Davies et al. 1996).

In a few patients with unilateral temporal lobe epilepsy, IAP may also paradoxically lateralize memory function. In these patients, IAP showed poorer memory performance in the non-epileptogenic hemisphere (Davies et al. 1996; Rouleau et al. 1997; Detre et al. 1998; Spencer et al. 2000). Paradoxical IAP memory lateralization (i.e., ipsilateral to the seizure focus) was still concordant with fMRI lateralization scores in two patients with temporal lobe epilepsy (Detre et al. 1998). Spencer et al. (2000) suggested that in patients with medial temporal lobe epilepsy not well lateralized by noninvasive evaluation and in patients with neocortical or mesial frontal epilepsy, IAP may provide incorrect localization which ultimately alters surgical management (Spencer et al. 2000). This paradoxical lateralization has rarely been reported using FDG-PET (Sperling et al. 1995; Nagarajan et al. 1996). In such cases, combined FDG-PET with IAP studies did not report memory impairment contralateral to the hypometabolic zone (Salanova et al. 1992).

3 Important Results of Validation Studies in Brain Tumors and Epilepsies, Overview, and Current State

3.1 Motor Function

3.1.1 Functional Mapping

Validation of more recent functional noninvasive methods, such as fMRI, magnetoencephalography (MEG), and transcranial magnetic stimulation (TMS), can be performed by comparison with earlier techniques such as PET. Nevertheless, DES remain the current reference procedure, and therefore comparison of functional noninvasive methods with DES is the best method of validation.

Functional mapping of motor areas can be performed either to localize the central area or to locate motor areas at risk of functional deficits. Therefore, there are two different levels of validation.

The first level is to determine whether functional imaging methods can accurately *localize the central sulcus*. In the normal brain, the hand area and therefore the central sulcus can be accurately localized using anatomical landmarks only (Yousry et al. 1997) (Fig. 6). In patients with brain tumors, however, mass effect frequently distorts normal cortical anatomy and can make localization of the central area difficult by using anatomical landmarks alone (Lehericy et al. 2000b). In such

cases, preoperative functional localization is of special interest. See also chapter “[Task-based presurgical functional MRI in patients with brain tumors](#)”.

fMRI vs. PET Compared with PET, 96 % of the fMRI activation peaks were located on either the same or adjacent sulci and gyri (Bittar et al. 1999a).

fMRI vs. DES Compared with DES, fMRI was very reliable in localizing the motor cortex, with complete or almost complete agreement using visual comparison with 3D MRI (Jack et al. 1994; Yousry et al. 1995; Pujol et al. 1996, 1998; Roux et al. 1999) (Fig. 5) or preoperative ultrasonography (Fandino et al. 1999), coregistration of preoperative pictures with 3D rendering of the brain (Puce et al. 1995; Lehericy et al. 2000b), or neuronavigation procedures (Hirsch et al. 2000; Lehericy et al. 2000b). Discordant results were mostly observed when no correlation was possible (no activation or movement artifacts on fMRI, no response using DES). $^{15}\text{H}_2\text{O}$ PET was also reliable in showing the central area compared to DES (Reinges et al. 2004).

fMRI vs. TMS Compared with TMS, fMRI peaks produced no motor evoked potential (MEP) when located more than 2 cm away from TMS sites (Krings et al. 1997b).

The second level is to determine whether functional imaging data can accurately *localize motor areas* and to assess how reliable this information is to assess where to stop with the surgical resection in order to prevent functional deficits.

fMRI vs. PET Compared to PET, fMRI yielded very similar results (Bittar et al. 1999a). The average distance between fMRI and PET activation peaks was 7.9 ± 4.8 mm, with 96 % of the peaks being located on either the same or adjacent sulci or gyri. Overlapping of voxels activated by each modality occurred in 92 % of the studies.

Agreement between PET and fMRI functional localization was 95.6 % for intra-axial lesions and spatially concordant as determined by intracranial stimulation (Bittar et al. 1999b). PET results were overlapping with DES in 60–92 % (<1 cm) and neighboring in 29–75 % (<2 cm) (Krings et al. 2001b; Reinges et al. 2004). The mean localization difference between fMRI and PET was 8.1 ± 4.6 mm (range, 2–18 mm) (Reinges et al. 2004). Another study reported that the evaluation of PET findings by cortical stimulation yielded a 94 % sensitivity and a 95 % specificity for the identification of motor-associated brain areas (Schreckenberger et al. 2001). PET results for extra-axial lesions were even superior to those obtained with fMRI with 75 % overlapping and 25 % neighboring activation, showing no contradictory results (Reinges et al. 2004).

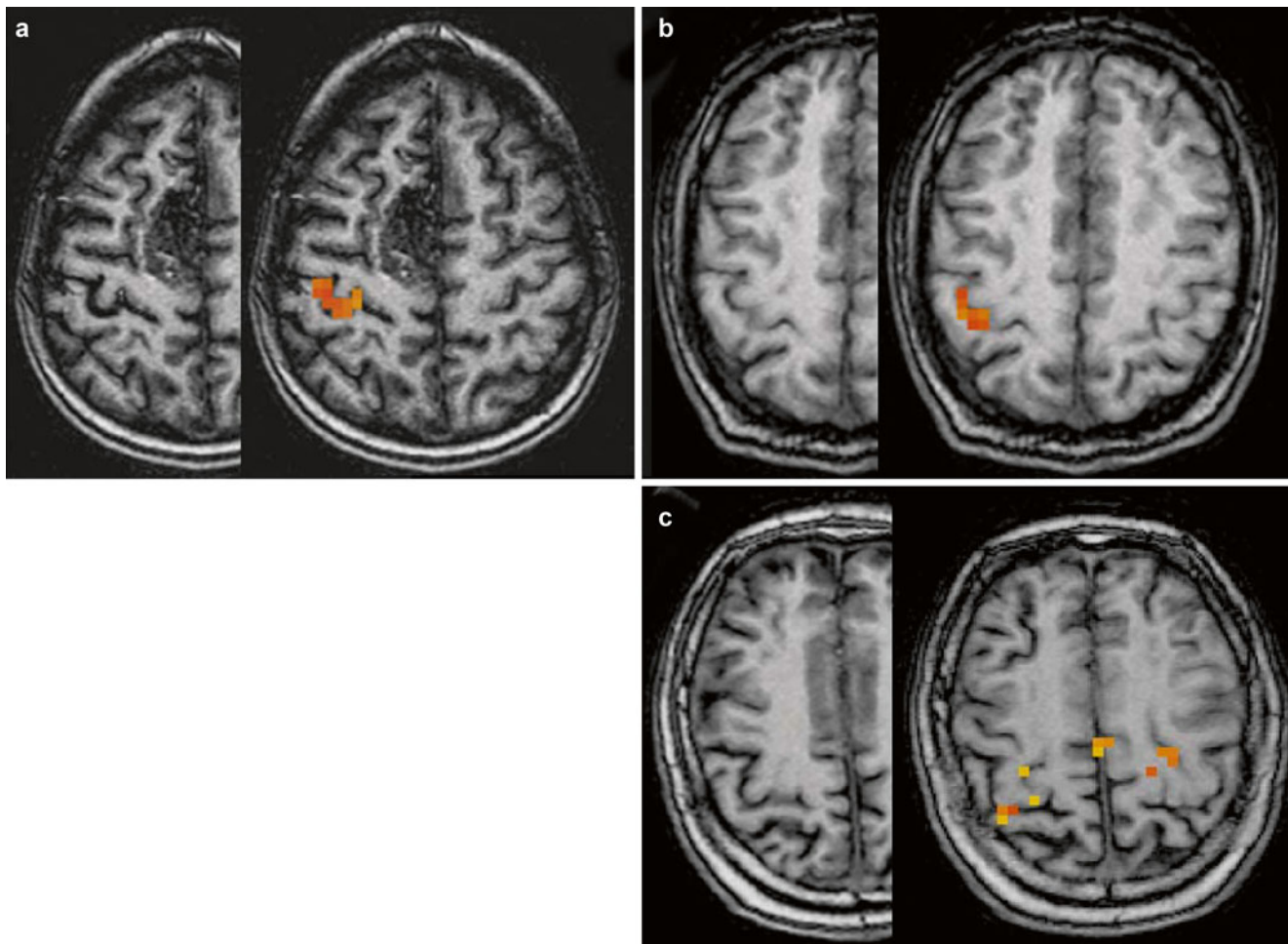


Fig. 6 Typical variations of anatomy of the hand area. Movements of the left hand in three different subjects. Activated pixels are overlaid onto anatomical T1-weighted images in the right hemisphere. (a)

Typical omega-shaped hand area (patient with a right medial frontal arteriovenous malformation). (b) Epsilon-shaped hand knob. (c) More complex aspect of the hand area (three-digit aspect)

fMRI vs. DES Several studies have compared the accuracy of fMRI localization according to DES. Early studies in 28 patients with surgical brain lesions reported that 100 % of positive MR activation sites were within 20 mm of DES positive sites and that 87 % of correlations were within 10 mm of DES (Yetkin et al. 1997). Another study in 8 patients with brain tumors reported a good correlation between fMRI activation and DES sites, with all fMRI activations related to positive DES responses (Roux et al. 1999). In patients with intra-axial lesions, overlapping results were obtained in 25–63 % (<1 cm) and neighboring in 29–75 % (<2 cm), while contradictory results were observed (Krings et al. 2001b; Reinges et al. 2004). Results are less good in patients with extra-axial lesions, with contradictory results in 42 % (activation in a different gyrus or >2 cm from DES site) (Reinges et al. 2004). In another study, quantitative comparison of noninvasive methods with DES did not reveal a significant difference in accuracy (Towle et al. 2003). Other more studies reported an agreement between fMRI and DES

regarding localization in 92 % (Lehericy et al. 2000b), 92.3 % (Spina et al. 2010), 83.7 % (Gonzalez-Darder et al. 2010), and 77 % of subjects (Bartos et al. 2009). The choice of statistical thresholds to display activation maps is also an important factor to take into account as the optimal threshold varies between subjects (Chang et al. 2010).

TMS vs. DES/fMRI TMS combined with neuronavigation has also been used for presurgical motor mapping (Picht et al. 2011; Coburger et al. 2013; Krieg et al. 2013) evaluated by comparison to fMRI and DES. TMS sites were close (within 5 mm) to DES positive sites (Picht et al. 2011). Compared to DES, TMS responses fell within 1 cm of the electrical cortical stimulation sites (Krings et al. 1997a; Forster et al. 2011).

TMS sites further than 2 cm away from fMRI peaks produced no motor evoked potentials (MEPs) (Krings et al. 1997b, 2001b), while the mean distance between the fMRI and TMS activation peaks was below 1.5 cm (Krings et al.

2001a; Forster et al. 2011). Further, TMS was able to locate the motor cortex when fMRI failed (Coburger et al. 2013).

fMRI vs. MSI Magnetic source imaging (MSI) using somatosensory stimulation has also been evaluated in patients with brain tumors (Schiffbauer et al. 2002). In one study, the distance between two corresponding points determined using MSI and DES was 12.5 ± 1.3 mm for somatosensory–somatosensory and 19 ± 1.3 mm for somatosensory–motor comparisons. Intraoperative sites at which DES evoked the same patient response exhibited a spatial variation of 10.7 ± 0.7 mm (Schiffbauer et al. 2002).

Overall, these studies suggest that the localization accuracy among the different functional methods is similar. Earlier studies have suggested that in patients with a minimum distance of 2 cm between tumor and activation site, no deficits in motor function are expected after surgery (Mueller et al. 1996; Yetkin et al. 1997). Other studies have suggested that even a shorter distance of <1 cm (lesion to function site) can be achieved (Krishnan et al. 2004; Bartos et al. 2009). Therefore, fMRI methods are considered a useful adjunct to DES.

The value of functional imaging techniques for the accurate localization of functionally important areas at risk for postoperative deficits can also be assessed empirically by a comparison to the postoperative outcome. In this regard, fMRI has proven to be very accurate for the prediction of occurrence of motor and language deficits after medial frontal lobe surgery (Krainik et al. 2001, 2003; Wood et al. 2011).

It should be kept in mind that fMRI results should be interpreted cautiously as they highly depend on several factors, such as the quality of the examination (movement artifacts), data processing (smoothing), statistical thresholds, and ultimately the experience of the reader. Lastly, functional brain mapping techniques alone cannot assess subcortical white matter tracts. Therefore, combined fMRI and DTI fiber tracking methods have the potential to provide a more complete presurgical mapping than any other functional technique by its own.

3.1.2 DTI Fiber Tracking of the Corticospinal Tract

Compared to the already described functional imaging techniques, fewer validation studies have been published for DTI fiber tracking. Previous studies have shown the reconstruction of well-known fiber tracts, including the corticospinal, long association (Roux et al. 1999; Mori et al. 2002), and brain stem fiber tracts (Stieltjes et al. 2001). Results of fiber tracking have also been correlated with postmortem animal studies in formalin-fixed hearts in rabbits (Holmes et al. 2000) and in the skeletal muscle of rats in vivo (Damon et al. 2002). In vivo DTI has been compared to ex vivo DTI and also to the uptake transport of wheat germ agglutinin–horseradish peroxidase (WGA-HRP)-stained histological

sections in the macaque monkey (Dauguet et al. 2007). A good correspondence has been reported between DTI fiber tracts originating in the left somatosensory cortex and the histological reference. In humans, tractography results have been compared with the expected known anatomy, dissections, or DES (Lawes and Clark 2010).

Validation studies of DTI fiber tracking have been performed using subcortical DES in patients with brain lesions. Two studies from the same group used cortical positive DES as seeding points for fiber tracking (Berman et al. 2004; Henry et al. 2004). Tracts originating from the mouth motor positive DES matched the known connections of the primary motor area of the face. For the corticospinal tract, a good agreement was reported in 92–95 % between DTI reconstructed tracts and positive functional subcortical DES sites (Coenen et al. 2003; Kamada et al. 2005; Bello et al. 2008; Ohue et al. 2012; Zhu et al. 2012). The mean distance range between the stimulated sites and the corticospinal tract was 6–14 mm (Bozzao et al. 2010; Gonzalez-Darder et al. 2010; Prabhu et al. 2011; Zhu et al. 2012; Vassal et al. 2013). These distances depended on the intensity used for stimulation (Kamada et al. 2009). DTI tractography may underestimate the presence of functional fibers in the border of the lesions (Spina et al. 2010). Finally, the topography of the tract, i.e., inside or at the boundary of the tumor, has been confirmed by DES (Bello et al. 2008, 2010).

Conventional diffusion tensor imaging models and tractography techniques are often suboptimal in areas of fiber crossing or fanning. For the corticospinal tract, these techniques are often unable to show the superior medial and lateral portions of the tract. Improved diffusion modeling using high angular resolution diffusion imaging (HARDI) allows a better reconstruction of these parts showing a good agreement with cortical and subcortical DES (Berman et al. 2008; Berman 2009; Bucci et al. 2013).

Therefore, even if the current data are encouraging, further improvement in tractography techniques and more comparisons between DTI and DES in larger series of patients are required.

3.2 Language Function

For language function, functional imaging can determine language dominance and localize the various language areas. For the validation of functional imaging techniques for the hemispheric language dominance, the IAP is used as a reference. In contrast, DES serve as a reference for the validation of the localization of different language areas (corticography).

3.2.1 Hemispheric Dominance for Language

fMRI has shown a high concordance (>90 %) for the degree of asymmetry of activation between brain hemispheres during appropriately selected language tasks indicating language

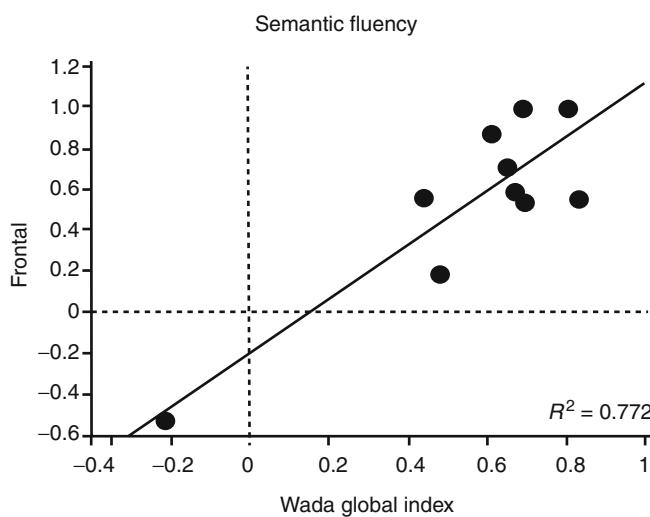


Fig. 7 Correlation between fMRI and Wada results. Pearson linear regression between the Wada and fMRI laterality indices in the frontal lobes in a semantic fluency task obtained in ten patients with temporal lobe epilepsy (From Lehericy et al. (2000a) with permission)

dominance when compared with IAP (Desmond et al. 1995; Binder et al. 1996; Bahn et al. 1997; Hertz-Pannier et al. 1997; Benson et al. 1999; Lehericy et al. 2000a; Carpentier et al. 2001; Gaillard et al. 2002; Rutten et al. 2002b; Sabbah et al. 2003; Woermann et al. 2003). A good correlation has been observed using productive tasks, such as word or verb generation, and semantic decision tasks, whereas no correlation has been observed for receptive tasks (Lehericy et al. 2000a) (Fig. 7).

Overall, language fMRI studies largely agree on a 10 % failure rate to lateralize language as compared to the IAP (Desmond et al. 1995; Binder et al. 1996; Bahn et al. 1997; Hertz-Pannier et al. 1997; Benson et al. 1999; Lehericy et al. 2000a; Carpentier et al. 2001; Gaillard et al. 2002; Rutten et al. 2002b; Sabbah et al. 2003; Woermann et al. 2003). A false categorization using fMRI was more frequent in patients with left temporal lobe epilepsy (Woermann et al. 2003).

The use of well-controlled paradigms with the recording of a patient's performance (such as semantic decision making or picture naming) apparently does not provide better results than more simple paradigms without the control of the patient's performance (such as a silent generation task with a low-level reference condition). The same may also apply to quantitative post-processing (counting the number of activated voxels to calculate the laterality indices) versus visual examination of fMRI maps (Woermann et al. 2003).

3.2.2 Localization of Language Areas

Fewer studies have been performed for quantitative comparison between language functional imaging data and DES. DES were consistent with the MEG-based localization in 13 patients during a visual and auditory word-recognition task

(Simos et al. 1999). Using a verb generation task in eight patients with glioma, via PET-activated areas, showed a 73 % sensitivity and 81 % specificity to predict aphasic disturbance during intraoperative stimulation (Herholz et al. 1997). In seven patients with intractable epilepsy, cortical regions that showed increased rCBF (PET) during both visual and auditory naming tasks were located in the same regions as subdural electrodes disrupting language during electrical stimulation (Bookheimer et al. 1997). In contrast, cortical regions underlying electrodes that did not disrupt language did also not show any consistent rCBF changes during PET activation (Bookheimer et al. 1997).

In three patients with primary tumors, regions involved in receptive language function identified by fMRI and DES were similar but nonidentical (Lurito et al. 2000). In 11 patients with surgical brain lesions, the sensitivity/specificity of a set of five different language tasks ranged from 81 %/53 % for areas that touched DES positive sites to 92 %/0 % for areas separated by 2 cm (FitzGerald et al. 1997). Using a combination of three different fMRI tasks, the sensitivity of fMRI was 100 % in seven of eight patients with temporal lobe epilepsy (<6.4 mm of the DES site). In the remaining patient, the sensitivity was only 38 % (Rutten et al. 2002a). Overall, these data yielded a specificity of 61 % (Rutten et al. 2002a). Compared to DES, the sensitivity and specificity of language tasks were 22 and 97 % for a naming task and 36 and 98 % for a verb generation task, respectively (Roux et al. 2003). A better correlation (sensitivity, 59 %; specificity, 97 %) was achieved by combining the two fMRI tasks (Roux et al. 2003). A more recent study reported a correlation between fMRI and DES in only 42.8 % (Spina et al. 2010). In a meta-analysis of nine studies which compared preoperative fMRI and DES for language mapping, the sensitivity and specificity of fMRI in comparison with DES as a gold standard ranged from 59 to 100 % and from 0 to 97 %, respectively (Giussani et al. 2011). The variety of methods used in these studies contributed to this large range of values. The correspondence between fMRI and DES mapping depended heavily on the statistical threshold used for fMRI data evaluation and varied between patients, tasks, and studies (FitzGerald et al. 1997; Rutten et al. 2002a; Roux et al. 2003; Giussani et al. 2011). Individual language tasks were not as sensitive as a set of language tasks (Fig. 8). Therefore, fMRI results for language mapping largely depend on the quality of the equipment, the type of tasks, as well as the expertise of the analysis and its interpretation (Giussani et al. 2011; Garrett et al. 2012).

3.2.3 DTI Fiber Tracking of Language Tracts

Only few comparisons between DTI fiber tracking of language tracts and DES have been performed in patients with brain lesions (Fig. 9). DTI fiber tracking has been used to delineate the pathways between functional regions

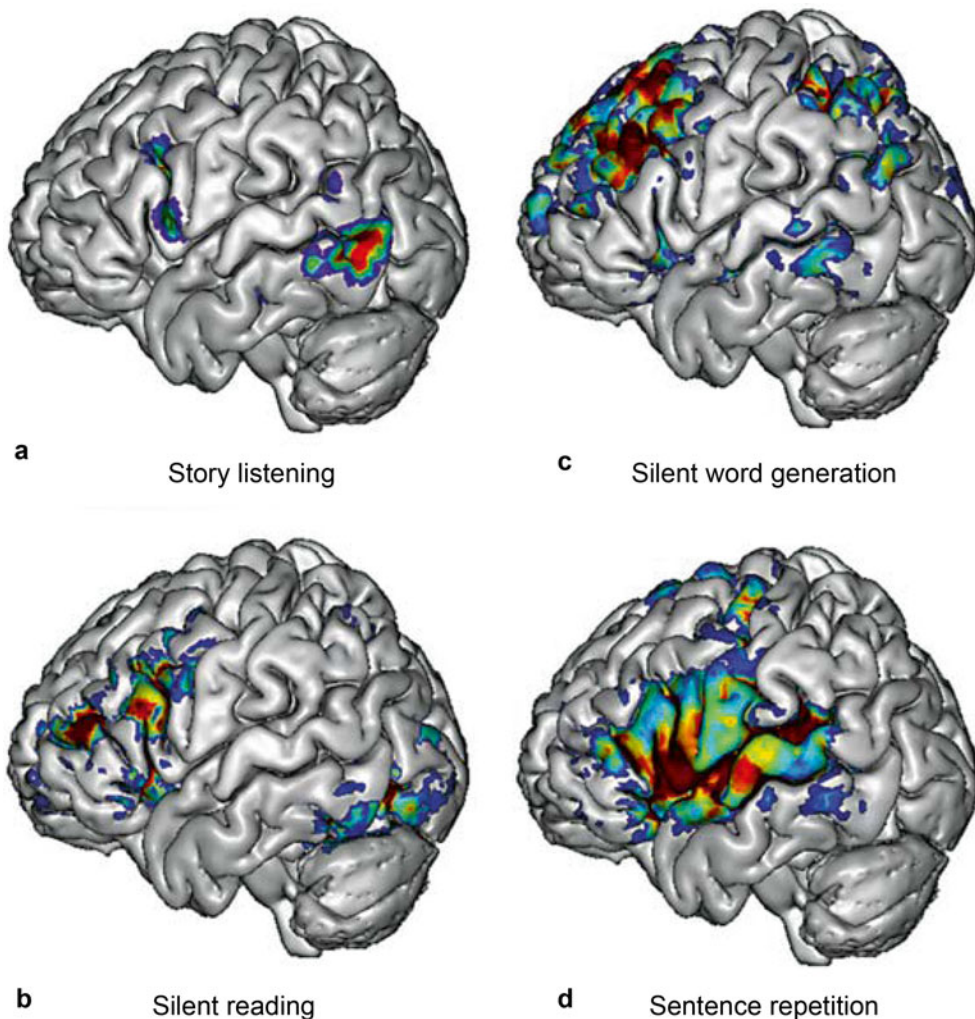


Fig. 8 Activation pattern of four language tasks. *Left:* Receptive tasks. (a) Story listening task compared to the listening to the same story played backward. Activation is mainly located in posterior temporal areas. (b) Silent reading compared to fixation. Activation is located in the inferotemporal cortical areas and Broca's area. *Right:* Productive tasks. (c) Silent word generation task compared to rest. Activation

predominates in the dorsolateral frontal areas and inferior parietal areas, including the angular gyrus. (d) Sentence repetition aloud compared to rest. Activation includes frontal (Broca's area and the lower part of the primary sensorimotor area in the face region) and temporal areas (including the primary auditory cortex)

(Henry et al. 2004). Tracts from stimulated sites in the inferior frontal cortex resulting in mouth motor, speech arrest, and anomia have been generated from the DTI data. Connections were found between speech arrest, mouth motor, and anomia sites and the SMA proper and cerebral peduncle (Henry et al. 2004). Fiber tracking has been performed in brain tumor patients and normal controls to study the connection between the frontal and parieto-temporal lobes through the arcuate fascicle (Henry et al. 2004). Tracts connecting the inferior frontal gyrus to the supramarginal gyrus, the posterior superior temporal gyrus, and the middle temporal gyrus were closely located to the intraoperative cortical stimulation speech arrest sites (Henry et al. 2004). More recent studies combining DES

and tractography for language tracts have shown that DES positive subcortical sites correspond with DTI fiber tracts in 81–97 % (Bello et al. 2008; Leclercq et al. 2010).

3.3 Memory Functions

There is a good correlation between PET and IAP results. Patients with mesial temporal lobe epilepsy showed an ¹⁸F-fluorodeoxyglucose (FDG) PET hypometabolism in the hemisphere ipsilateral to the lesion, functional deficits on the IAP, or both, as well as verbal memory and word fluency impairment (Rausch et al. 1994; Arnold et al. 1996) (Salanova et al. 2001). IAP hemispheric memory performance and

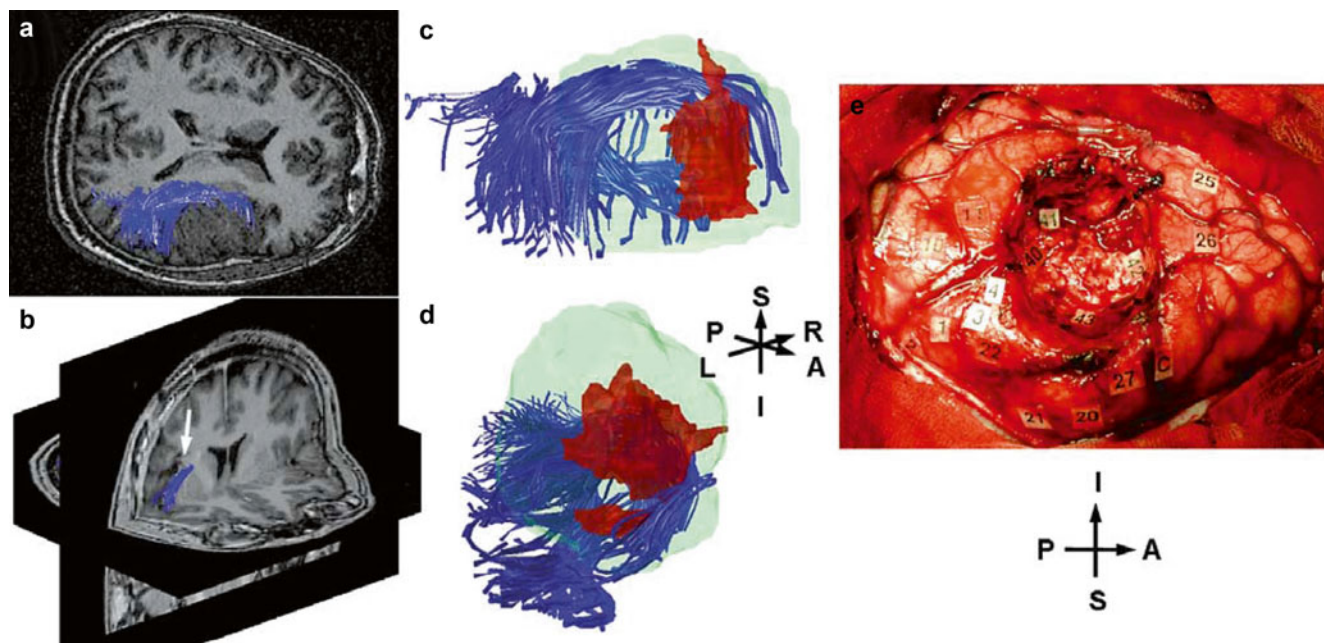


Fig. 9 Relationship between DTI fiber tracking and preoperative electrical stimulations in a patient with a low-grade glioma of the left insula. Electrical stimulations performed during surgery in the depth of the resection cavity resulted in speech arrest. (a) DTI fiber tract reconstruction of the arcuate fasciculus (transverse section; the fiber tract is represented in blue as if viewed from above). (b) Oblique 3D reconstruction of the arcuate fasciculus in blue showing the close proximity between the deep part of the resection cavity and the fiber tract (arrow). (c, d) 3D reconstructions of the fiber tract (blue), the tumor (light green), and the

surgical resection site (red) showing the close proximity between the deep part of the surgical resection and the fiber tract (c superior view as in a; d oblique 3D reconstruction, same view as in b). Note that the resection cavity touches the fiber tract in agreement with DES findings. (e) Surgical view showing positive DES sites for motor responses (1–4 and 40), somatosensory responses (10–11), and speech responses (paraphrasias: 25–26 and 41–43). Sites positive for language were obtained in the depth of the resection cavity (41–43). Abbreviations: A anterior, I inferior, L left, P posterior, R right, S superior (Color figure online)

hippocampal glucose metabolism showed a positive correlation with the frequency of seizures and a negative correlation with the duration of epilepsy (Jokeit et al. 1999). The results of FDG-PET were predictive for an impaired IAP memory performance (Salanova et al. 2001). Memory impairment contralateral to PET hypometabolism in the temporal lobe has never been seen (Salanova et al. 2001). Finally, in patients with temporal lobe epilepsy, the FDG-PET asymmetry index in the mesial temporal lobe correlated with the IAP asymmetry index for memory performance (Hong et al. 2000a).

Functional MRI studies have demonstrated consistent activation of medial temporal structures during memory tasks in normal subjects (Small et al. 1999; Dupont et al. 2000, 2010; Zeineh et al. 2003). In patients with epilepsy, several studies have evaluated the lateralization value of fMRI activation for memory functions (Detre et al. 1998; Dupont et al. 2001, 2010; Jokeit et al. 2001; Golby et al. 2002; Rabin et al. 2004; Janszky et al. 2005; Richardson et al. 2006; Binder et al. 2010). The preoperative fMRI asymmetry index of memory function correlated with the changes between pre- and postsurgical measures for memory retention (Rabin et al. 2004; Janszky et al. 2005). Asymmetry ratios in the medial temporal lobe also significantly

correlated with memory lateralization by IAP testing (Detre et al. 1998; Golby et al. 2002; Rabin et al. 2004). In ten right-handed patients with hippocampal sclerosis, fMRI provided the strongest independent predictor of memory outcome after surgery (Richardson et al. 2004). At the individual subject level, fMRI data had a high positive predictive value for memory decline (Richardson et al. 2004). Overall, preoperative fMRI can predict postoperative verbal memory alterations and improve the accuracy of the prediction of these deficits in patients with temporal lobe epilepsy (Binder 2011). Thus, fMRI has proven to be efficient for the preoperative evaluation and prediction of memory functions following surgery.

Conclusion

In spite of the limitations as detailed above, fMRI is now increasingly used as a clinical noninvasive tool to locate eloquent brain areas, lateralize language and memory functions, and predict postoperative outcome. Care should be taken to control for and reduce the sources of artifacts, including motion, magnetic susceptibility, and alterations in BOLD contrast. DTI tractography is used in addition to

fMRI to evaluate white matter fiber tracts in surgical candidates with brain lesions. Motor mapping has been largely validated against DES. Language lateralization using fMRI has replaced the Wada test in most centers. Localization of language areas using fMRI mainly depends on the choice of tasks, activation thresholds, and subject's performance and is less well validated when compared to DES. Memory mapping, as a more recent application, has been used for a shorter period of time, but results are promising. Overall, preoperative mapping with fMRI can be considered a useful adjunct to DES.

References

- Agnew WF, McCreery DB (1987) Considerations for safety in the use of extracranial stimulation for motor evoked potentials. *Neurosurgery* 20:143–147
- Akanuma N, Koutroumanidis M, Adachi N, Alarcon G, Binnie CD (2003) Presurgical assessment of memory-related brain structures: the Wada test and functional neuroimaging. *Seizure* 12:346–358
- Arnold S, Schlaug G, Niemann H, Ebner A, Luders H, Witte OW, Seitz RJ (1996) Topography of interictal glucose hypometabolism in unilateral mesiotemporal epilepsy. *Neurology* 46:1422–1430
- Bahn MM, Lin W, Silbergeld DL, Miller JW, Kuppusamy K, Cook RJ, Hammer G, Wetzel R, Cross D 3rd (1997) Localization of language cortices by functional MR imaging compared with intracarotid amobarbital hemispheric sedation. *AJR Am J Roentgenol* 169:575–579
- Barnett GH, Little JR, Ebrahim ZY, Jones SC, Friel HT (1987) Cerebral circulation during arteriovenous malformation operation. *Neurosurgery* 20:836–842
- Bartolomei F, Bosma I, Klein M, Baayen JC, Reijneveld JC, Postma TJ, Heimans JJ, van Dijk BW, de Munck JC, de Jongh A, Cover KS, Stam CJ (2006) How do brain tumors alter functional connectivity? A magnetoencephalography study. *Ann Neurol* 59:128–138
- Bartos R, Jech R, Vymazal J, Petrovicky P, Vachata P, Hejcl A, Zolal A, Sames M (2009) Validity of primary motor area localization with fMRI versus electric cortical stimulation: a comparative study. *Acta Neurochir (Wien)* 151:1071–1080
- Bello L, Gambini A, Castellano A, Carrabba G, Acerbi F, Fava E, Giussani C, Cadioli M, Blasi V, Casarotti A, Papagno C, Gupta AK, Gaini S, Scotti G, Falini A (2008) Motor and language DTI fiber tracking combined with intraoperative subcortical mapping for surgical removal of gliomas. *Neuroimage* 39:369–382
- Bello L, Castellano A, Fava E, Casaceli G, Riva M, Scotti G, Gaini SM, Falini A (2010) Intraoperative use of diffusion tensor imaging fiber tractography and subcortical mapping for resection of gliomas: technical considerations. *Neurosurg Focus* 28:E6
- Benson RR, FitzGerald DB, LeSueur LL, Kennedy DN, Kwong KK, Buchbinder BR, Davis TL, Weisskoff RM, Talavage TM, Logan WJ, Cosgrove GR, Belliveau JW, Rosen BR (1999) Language dominance determined by whole brain functional MRI in patients with brain lesions. *Neurology* 52:798–809
- Berger MS (1995) Functional mapping-guided resection of low-grade gliomas. *Clin Neurosurg* 42:437–452
- Berman J (2009) Diffusion MR tractography as a tool for surgical planning. *Magn Reson Imaging Clin N Am* 17:205–214
- Berman JI, Berger MS, Mukherjee P, Henry RG (2004) Diffusion-tensor imaging-guided tracking of fibers of the pyramidal tract combined with intraoperative cortical stimulation mapping in patients with gliomas. *J Neurosurg* 101:66–72
- Berman JI, Chung S, Mukherjee P, Hess CP, Han ET, Henry RG (2008) Probabilistic streamline q-ball tractography using the residual bootstrap. *Neuroimage* 39:215–222
- Binder JR (2011) Functional MRI is a valid noninvasive alternative to Wada testing. *Epilepsy Behav* 20:214–222
- Binder JR, Swanson SJ, Hammeke TA, Morris GL, Mueller WM, Fischer M, Benbadis S, Frost JA, Rao SM, Haughton VM (1996) Determination of language dominance using functional MRI: a comparison with the Wada test. *Neurology* 46:978–984
- Binder JR, Swanson SJ, Sabsevitz DS, Hammeke TA, Raghavan M, Mueller WM (2010) A comparison of two fMRI methods for predicting verbal memory decline after left temporal lobectomy: language lateralization versus hippocampal activation asymmetry. *Epilepsia* 51:618–626
- Biswal B, Yetkin FZ, Haughton VM, Hyde JS (1995) Functional connectivity in the motor cortex of resting human brain using echo-planar MRI. *Magn Reson Med* 34:537–541
- Bittar RG, Olivier A, Sadikot AF, Andermann F, Pike GB, Reutens DC (1999a) Presurgical motor and somatosensory cortex mapping with functional magnetic resonance imaging and positron emission tomography. *J Neurosurg* 91:915–921
- Bittar RG, Olivier A, Sadikot AF, Andermann F, Comeau RM, Cyr M, Peters TM, Reutens DC (1999b) Localization of somatosensory function by using positron emission tomography scanning: a comparison with intraoperative cortical stimulation. *J Neurosurg* 90:478–483
- Bookheimer SY, Zeffiro TA, Blaxton T, Malow BA, Gaillard WD, Sato S, Kufta C, Fedio P, Theodore WH (1997) A direct comparison of PET activation and electrocortical stimulation mapping for language localization. *Neurology* 48:1056–1065
- Boxerman JL, Hamberg LM, Rosen BR, Weisskoff RM (1995) MR contrast due to intravascular magnetic susceptibility perturbations. *Magn Reson Med* 34:555–566
- Bozzao A, Romano A, Angelini A, D'Andrea G, Calabria LF, Coppola V, Mastronardi L, Fantozi LM, Ferrante L (2010) Identification of the pyramidal tract by neuronavigation based on intraoperative magnetic resonance tractography: correlation with subcortical stimulation. *Eur Radiol* 20:2475–2481
- Bucci M, Mandelli ML, Berman JI, Amirbekian B, Nguyen C, Berger MS, Henry RG (2013) Quantifying diffusion MRI tractography of the corticospinal tract in brain tumors with deterministic and probabilistic methods. *Neuroimage Clin* 3:361–368
- Carpentier A, Pugh KR, Westerveld M, Studholme C, Skrinjar O, Thompson JL, Spencer DD, Constable RT (2001) Functional MRI of language processing: dependence on input modality and temporal lobe epilepsy. *Epilepsia* 42:1241–1254
- Cha S, Johnson G, Wadghiri YZ, Jin O, Babb J, Zagzag D, Turnbull DH (2003) Dynamic, contrast-enhanced perfusion MRI in mouse gliomas: correlation with histopathology. *Magn Reson Med* 49:848–855
- Chang CY, Peck KK, Brennan NM, Hou BL, Gutin PH, Holodny AI (2010) Functional MRI in the presurgical evaluation of patients with brain tumors: characterization of the statistical threshold. *Stereotact Funct Neurosurg* 88:35–41
- Cloft HJ, Joseph GJ, Dion JE (1999) Risk of cerebral angiography in patients with subarachnoid hemorrhage, cerebral aneurysm, and arteriovenous malformation: a meta-analysis. *Stroke* 30:317–320
- Coburger J, Musahl C, Henkes H, Horvath-Rizea D, Bittl M, Weissbach C, Hopf N (2013) Comparison of navigated transcranial magnetic stimulation and functional magnetic resonance imaging for preoperative mapping in rolandic tumor surgery. *Neurosurg Rev* 36:65–75; discussion 75–66
- Coenen VA, Krings T, Axer H, Weidemann J, Kranzlein H, Hans FJ, Thron A, Gilsbach JM, Rohde V (2003) Intraoperative three-dimensional visualization of the pyramidal tract in a neuronavigation system (PTV) reliably predicts true position of principal motor pathways. *Surg Neurol* 60:381–390; discussion 390

- D'Esposito M, Deouell LY, Gazzaley A (2003) Alterations in the BOLD fMRI signal with ageing and disease: a challenge for neuroimaging. *Nat Rev Neurosci* 4:863–872
- Damon BM, Ding Z, Anderson AW, Freyer AS, Gore JC (2002) Validation of diffusion tensor MRI-based muscle fiber tracking. *Magn Reson Med* 48:97–104
- Dauguet J, Peled S, Berezovskii V, Delzescaux T, Warfield SK, Born R, Westin CF (2007) Comparison of fiber tracts derived from in-vivo DTI tractography with 3D histological neural tract tracer reconstruction on a macaque brain. *Neuroimage* 37:530–8
- Davies KG, Hermann BP, Foley KT (1996) Relation between intracarotid amobarbital memory asymmetry scores and hippocampal sclerosis in patients undergoing anterior temporal lobe resections. *Epilepsia* 37:522–525
- de Silva R, Duncan R, Patterson J, Gillham R, Hadley D (1999) Regional cerebral perfusion and amygdala distribution during the Wada test. *J Nucl Med* 40:747–752
- Desmond JE, Sum JM, Wagner AD, Demb JB, Shear PK, Glover GH, Gabrieli JD, Morrell MJ (1995) Functional MRI measurement of language lateralization in Wada-tested patients. *Brain* 118(Pt 6):1411–1419
- Detre JA, Maccotta L, King D, Alsop DC, Glosser G, D'Esposito M, Zarahn E, Aguirre GK, French JA (1998) Functional MRI lateralization of memory in temporal lobe epilepsy. *Neurology* 50:926–932
- Dion JE, Gates PC, Fox AJ, Barnett HJ, Blom RJ (1987) Clinical events following neuroangiography: a prospective study. *Stroke* 18:997–1004
- Doty RW, Barlett JR (1981) Stimulation of the brain via metallic electrodes. In: Paterson MM, Kesner RP (eds) *Electrical stimulation research methods*. Academic, New York, pp 71–103
- Duffau H (2004) Intraoperative functional mapping using direct electrical stimulations. Methodological considerations. *Neurochirurgie* 50:474–483
- Duffau H, Capelle L, Sicchez N, Denvil D, Lopes M, Sicchez JP, Bitar A, Fohanno D (2002) Intraoperative mapping of the subcortical language pathways using direct stimulations. An anatomico-functional study. *Brain* 125:199–214
- Duffau H, Capelle L, Denvil D, Gatignol P, Sicchez N, Lopes M, Sicchez JP, Van Effenterre R (2003a) The role of dominant premotor cortex in language: a study using intraoperative functional mapping in awake patients. *Neuroimage* 20:1903–1914
- Duffau H, Capelle L, Denvil D, Sicchez N, Gatignol P, Taillandier L, Lopes M, Mitchell MC, Roche S, Muller JC, Bitar A, Sicchez JP, van Effenterre R (2003b) Usefulness of intraoperative electrical subcortical mapping during surgery for low-grade gliomas located within eloquent brain regions: functional results in a consecutive series of 103 patients. *J Neurosurg* 98:764–778
- Duffau H, Lopes M, Arthuis F, Bitar A, Sicchez JP, Van Effenterre R, Capelle L (2005) Contribution of intraoperative electrical stimulations in surgery of low grade gliomas: a comparative study between two series without (1985–96) and with (1996–2003) functional mapping in the same institution. *J Neurol Neurosurg Psychiatry* 76:845–851
- Duong TQ, Yacoub E, Adriany G, Hu X, Ugurbil K, Kim SG (2003) Microvascular BOLD contribution at 4 and 7 T in the human brain: gradient-echo and spin-echo fMRI with suppression of blood effects. *Magn Reson Med* 49:1019–1027
- Dupont S, Van de Moortele PF, Samson S, Hasboun D, Poline JB, Adam C, Lehericy S, Le Bihan D, Samson Y, Baulac M (2000) Episodic memory in left temporal lobe epilepsy: a functional MRI study. *Brain* 123(Pt 8):1722–1732
- Dupont S, Samson Y, Van de Moortele PF, Samson S, Poline JB, Adam C, Lehericy S, Le Bihan D, Baulac M (2001) Delayed verbal memory retrieval: a functional MRI study in epileptic patients with structural lesions of the left medial temporal lobe. *Neuroimage* 14:995–1003
- Dupont S, Duron E, Samson S, Denos M, Volle E, Delmaire C, Navarro V, Chiras J, Lehericy S, Samson Y, Baulac M (2010) Functional MR imaging or Wada test: which is the better predictor of individual postoperative memory outcome? *Radiology* 255:128–134
- Enzmann DR, Pelc NJ (1992) Brain motion: measurement with phase-contrast MR imaging. *Radiology* 185:653–660
- Fandino J, Kollias SS, Wieser HG, Valavanis A, Yonekawa Y (1999) Intraoperative validation of functional magnetic resonance imaging and cortical reorganization patterns in patients with brain tumors involving the primary motor cortex. *J Neurosurg* 91:238–250
- Fertziger AP, Ranck JB Jr (1970) Potassium accumulation in interstitial space during epileptiform seizures. *Exp Neurol* 26:571–585
- Fink GR (1992) Effects of cerebral angiomas on perifocal and remote tissue: a multivariate positron emission tomography study. *Stroke* 23:1099–1105
- FitzGerald DB, Cosgrove GR, Ronner S, Jiang H, Buchbinder BR, Belliveau JW, Rosen BR, Benson RR (1997) Location of language in the cortex: a comparison between functional MR imaging and electrocortical stimulation. *AJNR Am J Neuroradiol* 18:1529–1539
- Fogarty-Mack P, Pile-Spellman J, Hacein-Bey L, Ostapkovich N, Joshi S, Vulliemoz Y, Young WL (1996) Superselective intraarterial papaverine administration: effect on regional cerebral blood flow in patients with arteriovenous malformations. *J Neurosurg* 85:395–402
- Folkman J, Watson K, Ingber D, Hanahan D (1989) Induction of angiogenesis during the transition from hyperplasia to neoplasia. *Nature* 339:58–61
- Forster MT, Hattingen E, Senft C, Gasser T, Seifert V, Szelenyi A (2011) Navigated transcranial magnetic stimulation and functional magnetic resonance imaging: advanced adjuncts in preoperative planning for central region tumors. *Neurosurgery* 68:1317–1324; discussion 1324–1315
- Fujiwara N, Sakatani K, Katayama Y, Murata Y, Hoshino T, Fukaya C, Yamamoto T (2004) Evoked-cerebral blood oxygenation changes in false-negative activations in BOLD contrast functional MRI of patients with brain tumors. *Neuroimage* 21:1464–1471
- Gaillard WD, Balsamo L, Xu B, Grandin CB, Braniecki SH, Papero PH, Weinstein S, Conry J, Pearl PL, Sachs B, Sato S, Jabbari B, Vezina LG, Frattali C, Theodore WH (2002) Language dominance in partial epilepsy patients identified with an fMRI reading task. *Neurology* 59:256–265
- Garrett MC, Pouratian N, Liau LM (2012) Use of language mapping to aid in resection of gliomas in eloquent brain regions. *Neurosurg Clin N Am* 23:497–506
- Gatignol P, Capelle L, Le Bihan R, Duffau H (2004) Double dissociation between picture naming and comprehension: an electrostimulation study. *Neuroreport* 15:191–195
- Giussani C, Roux FE, Ojemann J, Sganzerla EP, Pirillo D, Papagno C (2011) Is preoperative functional magnetic resonance imaging reliable for language areas mapping in brain tumor surgery? Review of language functional magnetic resonance imaging and direct cortical stimulation correlation studies. *Neurosurgery* 66:113–120
- Golby AJ, Poldrack RA, Illes J, Chen D, Desmond JE, Gabrieli JD (2002) Memory lateralization in medial temporal lobe epilepsy assessed by functional MRI. *Epilepsia* 43:855–863
- Gonzalez-Darder JM, Gonzalez-Lopez P, Talamantes F, Quilis V, Cortes V, Garcia-March G, Roldan P (2010) Multimodal navigation in the functional microsurgical resection of intrinsic brain tumors located in eloquent motor areas: role of tractography. *Neurosurg Focus* 28:E5
- Gordon B, Lesser RP, Rance NE, Hart J Jr, Webber R, Uematsu S, Fisher RS (1990) Parameters for direct cortical electrical stimulation in the human: histopathologic confirmation. *Electroencephalogr Clin Neurophysiol* 75:371–377
- Guggisberg AG, Honma SM, Findlay AM, Dalal SS, Kirsch HE, Berger MS, Nagarajan SS (2008) Mapping functional connectivity in patients with brain lesions. *Ann Neurol* 63:193–203

- Hamzei F, Knab R, Weiller C, Rother J (2003) The influence of extra- and intracranial artery disease on the BOLD signal in fMRI. *Neuroimage* 20:1393–1399
- Harel N, Lin J, Moeller S, Ugurbil K, Yacoub E (2006) Combined imaging-histological study of cortical laminar specificity of fMRI signals. *Neuroimage* 29:879–887
- Hassler W, Steinmetz H (1987) Cerebral hemodynamics in angioma patients: an intraoperative study. *J Neurosurg* 67:822–831
- Heeger DJ, Huk AC, Geisler WS, Albrecht DG (2002) What does fMRI tell us about neuronal activity? *Nat Rev Neurosci* 3:142–151
- Henry RG, Berman JI, Nagarajan SS, Mukherjee P, Berger MS (2004) Subcortical pathways serving cortical language sites: initial experience with diffusion tensor imaging fiber tracking combined with intraoperative language mapping. *Neuroimage* 21:616–622
- Herholz K, Reulen HJ, von Stockhausen HM, Thiel A, Ilmberger J, Kessler J, Eisner W, Yousry TA, Heiss WD (1997) Preoperative activation and intraoperative stimulation of language-related areas in patients with glioma. *Neurosurgery* 41:1253–1260; discussion 1260–1252
- Hertz-Pannier L, Gaillard WD, Mott SH, Cuenod CA, Bookheimer SY, Weinstein S, Conry J, Papero PH, Schiff SJ, Le Bihan D, Theodore WH (1997) Noninvasive assessment of language dominance in children and adolescents with functional MRI: a preliminary study. *Neurology* 48:1003–1012
- Hill DL, Smith AD, Simmons A, Maurer CR Jr, Cox TC, Elwes R, Brammer M, Hawkes DJ, Polkey CE (2000) Sources of error in comparing functional magnetic resonance imaging and invasive electrophysiological recordings. *J Neurosurg* 93:214–223
- Hirsch J, Ruge MI, Kim KH, Correa DD, Victor JD, Relkin NR, Labar DR, Krol G, Bilsky MH, Souweidane MM, DeAngelis LM, Gutin PH (2000) An integrated functional magnetic resonance imaging procedure for preoperative mapping of cortical areas associated with tactile, motor, language, and visual functions. *Neurosurgery* 47:711–721; discussion 721–712
- Holmes AA, Scollan DF, Winslow RL (2000) Direct histological validation of diffusion tensor MRI in formaldehyde-fixed myocardium. *Magn Reson Med* 44:157–161
- Holodny AI, Schulder M, Liu WC, Maldjian JA, Kalnin AJ (1999) Decreased BOLD functional MR activation of the motor and sensory cortices adjacent to a glioblastoma multiforme: implications for image-guided neurosurgery. *AJNR Am J Neuroradiol* 20:609–612
- Holodny AI, Schulder M, Liu WC, Wolko J, Maldjian JA, Kalnin AJ (2000) The effect of brain tumors on BOLD functional MR imaging activation in the adjacent motor cortex: implications for image-guided neurosurgery. *AJNR Am J Neuroradiol* 21:1415–1422
- Hong SB, Roh SY, Kim SE, Seo DW (2000a) Correlation of temporal lobe glucose metabolism with the Wada memory test. *Epilepsia* 41:1554–1559
- Hong SB, Kim KW, Seo DW, Kim SE, Na DG, Byun HS (2000b) Contralateral EEG slowing and amobarbital distribution in Wada test: an intracarotid SPECT study. *Epilepsia* 41:207–212
- Hoppel BE, Weisskoff RM, Thulborn KR, Moore JB, Kwong KK, Rosen BR (1993) Measurement of regional blood oxygenation and cerebral hemodynamics. *Magn Reson Med* 30:715–23
- Hou BL, Bradbury M, Peck KK, Petrovich NM, Gutin PH, Holodny AI (2006) Effect of brain tumor neovasculature defined by rCBV on BOLD fMRI activation volume in the primary motor cortex. *Neuroimage* 32:489–497
- Hu X, Le TH, Parrish T, Erhard P (1995) Retrospective estimation and correction of physiological fluctuation in functional MRI. *Magn Reson Med* 34:201–212
- Jack CR Jr, Nichols DA, Sharbrough FW, Marsh WR, Petersen RC, Hinkeldey NS, Ivnik RJ, Cascino GD, Ilstrup DM (1989) Selective posterior cerebral artery injection of amytal: new method of preoperative memory testing. *Mayo Clin Proc* 64:965–975
- Jack CR Jr, Thompson RM, Butts RK, Sharbrough FW, Kelly PJ, Hanson DP, Riederer SJ, Ehman RL, Hangiandreou NJ, Cascino GD (1994) Sensory motor cortex: correlation of presurgical mapping with functional MR imaging and invasive cortical mapping. *Radiology* 190:85–92
- Janszky J, Jokeit H, Kontopoulou K, Mertens M, Ebner A, Pohlmann-Eden B, Woermann FG (2005) Functional MRI predicts memory performance after right mesiotemporal epilepsy surgery. *Epilepsia* 46:244–250
- Jayakar P (1993) Physiological principles of electrical stimulation. *Adv Neurol* 63:17–27
- Jayakar P, Alvarez LA, Duchowny MS, Resnick TJ (1992) A safe and effective paradigm to functionally map the cortex in childhood. *J Clin Neurophysiol* 9:288–293
- Jiang Z, Krainik A, David O, Salon C, Tropres I, Hoffmann D, Pannetier N, Barbier EL, Bombin ER, Warnking J, Pasteris C, Chabardes S, Berger F, Grand S, Segebarth C, Gay E, Le Bas JF (2010) Impaired fMRI activation in patients with primary brain tumors. *Neuroimage* 52:538–548
- Jokeit H, Ebner A, Arnold S, Schuller M, Antke C, Huang Y, Steinmetz H, Seitz RJ, Witte OW (1999) Bilateral reductions of hippocampal volume, glucose metabolism, and wada hemispheric memory performance are related to the duration of mesial temporal lobe epilepsy. *J Neurol* 246:926–933
- Jokeit H, Okujava M, Woermann FG (2001) Memory fMRI lateralizes temporal lobe epilepsy. *Neurology* 57:1786–1793
- Jones-Gotman M (1987) Psychological evaluation-testing of hippocampal function. In: Engel J (ed) *Surgical treatment of the epilepsies*. Raven, New York, pp 203–211
- Kamada K, Todo T, Masutani Y, Aoki S, Ino K, Takano T, Kirino T, Kawahara N, Morita A (2005) Combined use of tractography-integrated functional neuronavigation and direct fiber stimulation. *J Neurosurg* 102:664–672
- Kamada K, Todo T, Ota T, Ino K, Masutani Y, Aoki S, Takeuchi F, Kawai K, Saito N (2009) The motor-evoked potential threshold evaluated by tractography and electrical stimulation. *J Neurosurg* 111:785–795
- Keles GE, Berger MS (2004) Advances in neurosurgical technique in the current management of brain tumors. *Semin Oncol* 31:659–665
- Keles GE, Lundin DA, Lamborn KR, Chang EF, Ojemann G, Berger MS (2004) Intraoperative subcortical stimulation mapping for hemispherical perioriental gliomas located within or adjacent to the descending motor pathways: evaluation of morbidity and assessment of functional outcome in 294 patients. *J Neurosurg* 100:369–375
- Kobayashi E, Bagshaw AP, Jansen A, Andermann F, Andermann E, Gotman J, Dubeau F (2005) Intrinsic epileptogenicity in polymicrogyric cortex suggested by EEG-fMRI BOLD responses. *Neurology* 64:1263–1266
- Krainik A, Lehéricy S, Duffau H, Vlaicu M, Poupon F, Capelle L, Cornu P, Clemenceau S, Sahel M, Valery CA, Boch AL, Mangin JF, Bihan DL, Marsault C (2001) Role of the supplementary motor area in motor deficit following medial frontal lobe surgery. *Neurology* 57:871–878
- Krainik A, Lehéricy S, Duffau H, Capelle L, Chainay H, Cornu P, Cohen L, Boch AL, Mangin JF, Le Bihan D, Marsault C (2003) Postoperative speech disorder after medial frontal surgery: role of the supplementary motor area. *Neurology* 60:587–594
- Krieg SM, Shiban E, Buchmann N, Meyer B, Ringel F (2013) Presurgical navigated transcranial magnetic brain stimulation for recurrent gliomas in motor eloquent areas. *Clin Neurophysiol* 124:522–527
- Krings T, Buchbinder BR, Butler WE, Chiappa KH, Jiang HJ, Rosen BR, Cosgrove GR (1997a) Stereotactic transcranial magnetic stimulation: correlation with direct electrical cortical stimulation. *Neurosurgery* 41:1319–1325; discussion 1325–1316

- Krings T, Buchbinder BR, Butler WE, Chiappa KH, Jiang HJ, Cosgrove GR, Rosen BR (1997b) Functional magnetic resonance imaging and transcranial magnetic stimulation: complementary approaches in the evaluation of cortical motor function. *Neurology* 48: 1406–1416
- Krings T, Foltys H, Reinges MH, Kemeny S, Rohde V, Spetzger U, Gilsbach JM, Thron A (2001a) Navigated transcranial magnetic stimulation for presurgical planning—correlation with functional MRI. *Minim Invasive Neurosurg* 44:234–239
- Krings T, Schreckenberger M, Rohde V, Foltys H, Spetzger U, Sabri O, Reinges MH, Kemeny S, Meyer PT, Moller-Hartmann W, Korinth M, Gilsbach JM, Buell U, Thron A (2001b) Metabolic and electrophysiological validation of functional MRI. *J Neurol Neurosurg Psychiatry* 71:762–771
- Krishnan R, Raabe A, Hattingen E, Szelenyi A, Yahya H, Hermann E, Zimmermann M, Seifert V (2004) Functional magnetic resonance imaging-integrated neuronavigation: correlation between lesion-to-motor cortex distance and outcome. *Neurosurgery* 55:904–914; discussion 914–905
- Law M, Kazmi K, Wetzel S, Wang E, Iacob C, Zagzag D, Golfinos JG, Johnson G (2004) Dynamic susceptibility contrast-enhanced perfusion and conventional MR imaging findings for adult patients with cerebral primitive neuroectodermal tumors. *AJR Am J Neuroradiol* 25:997–1005
- Lawes INC, Clark CA (2010) Anatomical validation of DTI and tractography. In: Jones DK (ed) *Diffusion MRI. Theory, methods and applications*. Oxford University Press, New York, pp 439–447
- Leclercq D, Duffau H, Delmaire C, Capelle L, Gatignol P, Ducros M, Chiras J, Lehericy S (2010) Comparison of diffusion tensor imaging tractography of language tracts and intraoperative subcortical stimulations. *J Neurosurg* 112:503–511
- Lee SP, Silva AC, Ugurbil K, Kim SG (1999) Diffusion-weighted spin-echo fMRI at 9.4 T: microvascular/tissue contribution to BOLD signal changes. *Magn Reson Med* 42:919–928
- Lehericy S, Cohen L, Bazin B, Samson S, Giacomini E, Rougetet R, Hertz-Pannier L, Le Bihan D, Marsault C, Baulac M (2000a) Functional MR evaluation of temporal and frontal language dominance compared with the Wada test. *Neurology* 54: 1625–1633
- Lehericy S, Duffau H, Cornu P, Capelle L, Pidoux B, Carpentier A, Auliac S, Clemenceau S, Sichez JP, Bitar A, Valery CA, Van Effenterre R, Faillot T, Srour A, Fohanno D, Philippon J, Le Bihan D, Marsault C (2000b) Correspondence between functional magnetic resonance imaging somatotopy and individual brain anatomy of the central region: comparison with intraoperative stimulation in patients with brain tumors. *J Neurosurg* 92:589–598
- Lehericy S, Biondi A, Sourour N, Vlaicu M, du Montcel ST, Cohen L, Vivas E, Capelle L, Faillot T, Casasco A, Le Bihan D, Marsault C (2002) Arteriovenous brain malformations: is functional MR imaging reliable for studying language reorganization in patients? Initial observations. *Radiology* 223:672–682
- Lesser RP, Luders H, Klem G, Dinner DS, Morris HH, Hahn J (1984) Cortical afterdischarge and functional response thresholds: results of extraoperative testing. *Epilepsia* 25:615–621
- Lesser RP, Luders H, Klem G, Dinner DS, Morris HH, Hahn JF, Wyllie E (1987) Extraoperative cortical functional localization in patients with epilepsy. *J Clin Neurophysiol* 4:27–53
- Logothetis NK, Wandell BA (2004) Interpreting the BOLD signal. *Ann Rev Physiol* 66:735–769
- Loring DW, Meador KJ, Lee GP, King DW, Nichols ME, Park YD, Murro AM, Gallagher BB, Smith JR (1995) Wada memory asymmetries predict verbal memory decline after anterior temporal lobectomy. *Neurology* 45:1329–1333
- Ludemann L, Grieger W, Wurm R, Budzisch M, Hamm B, Zimmer C (2001) Comparison of dynamic contrast-enhanced MRI with WHO tumor grading for gliomas. *Eur Radiol* 11:1231–1241
- Luders HO, Dinner DS, Morris HH, Wyllie E, Comair YG (1995) Cortical electrical stimulation in humans. The negative motor areas. *Adv Neurol* 67:115–129
- Lurito JT, Lowe MJ, Sartorius C, Mathews VP (2000) Comparison of fMRI and intraoperative direct cortical stimulation in localization of receptive language areas. *J Comput Assist Tomogr* 24:99–105
- Martino J, Honma SM, Findlay AM, Guggisberg AG, Owen JP, Kirsch HE, Berger MS, Nagarajan SS (2011) Resting functional connectivity in patients with brain tumors in eloquent areas. *Ann Neurol* 69:521–532
- Medina LS, Aguirre E, Bernal B, Altman NR (2004) Functional MR imaging versus Wada test for evaluation of language lateralization: cost analysis. *Radiology* 230:49–54
- Milner B, Branch C, Rasmussen T (1962) Study of short-term memory after intracarotid injection of sodium amytal. *Trans Am Neurol Assoc* 87:224–226
- Mitchell TJ, Hacker CD, Breshears JD, Szrama NP, Sharma M, Bundy DT, Pahwa M, Corbett M, Snyder AZ, Shimony JS, Leuthardt EC (2013) A novel data-driven approach to preoperative mapping of functional cortex using resting-state functional magnetic resonance imaging. *Neurosurgery* 73:969–983
- Mori S, Kaufmann WE, Davatzikos C, Stieltjes B, Amodei L, Fredericksen K, Pearlson GD, Melhem ER, Solaiyappan M, Raymond GV, Moser HW, van Zijl PC (2002) Imaging cortical association tracts in the human brain using diffusion-tensor-based axonal tracking. *Magn Reson Med* 47:215–223
- Mueller WM, Yetkin FZ, Hammeke TA, Morris GL 3rd, Swanson SJ, Reichert K, Cox R, Haughton VM (1996) Functional magnetic resonance imaging mapping of the motor cortex in patients with cerebral tumors. *Neurosurgery* 39:515–520; discussion 520–511
- Nagarajan L, Schaul N, Eidelberg D, Dhawan V, Fraser R, Labar DR (1996) Contralateral temporal hypometabolism on positron emission tomography in temporal lobe epilepsy. *Acta Neurol Scand* 93:81–84
- Nathan SS, Lesser RP, Gordon B, Thakor NV (1993) Electrical stimulation of the human cerebral cortex. Theoretical approach. In: Devinsky O, Beric A, Dogali M (eds) *Electrical and magnetic stimulation of the brain and spinal cord*. Raven, New York
- O'Rourke DM, Saykin AJ, Gilhool JJ, Harley R, O'Connor MJ, Sperling MR (1993) Unilateral hemispheric memory and hippocampal neuronal density in temporal lobe epilepsy. *Neurosurgery* 32:574–580; discussion 580–571
- Ohaga S, Menon RS, Tank DW, Kim SG, Merkle H, Ellermann JM, Ugurbil K (1993) Functional brain mapping by blood oxygenation level-dependent contrast magnetic resonance imaging. A comparison of signal characteristics with a biophysical model. *Biophys J* 64:803–812
- Ogg RJ, Laningham FH, Clarke D, Einhaus S, Zou P, Tobias ME, Boop FA (2009) Passive range of motion functional magnetic resonance imaging localizing sensorimotor cortex in sedated children. *J Neurosurg* 4:317–322
- Ohue S, Kohno S, Inoue A, Yamashita D, Harada H, Kumon Y, Kikuchi K, Miki H, Ohnishi T (2012) Accuracy of diffusion tensor magnetic resonance imaging-based tractography for surgery of gliomas near the pyramidal tract: a significant correlation between subcortical electrical stimulation and postoperative tractography. *Neurosurgery* 70:283–293; discussion 294
- Ojemann G, Ojemann J, Lettich E, Berger M (1989) Cortical language localization in left, dominant hemisphere. An electrical stimulation mapping investigation in 117 patients. *J Neurosurg* 71:316–326
- Pawlak G, Rackl A, Bing RJ (1981) Quantitative capillary topography and blood flow in the cerebral cortex of cats: an in vivo microscopic study. *Brain Res* 208:35–58
- Pfeuffer J, Van de Moortele PF, Ugurbil K, Hu X, Glover GH (2002) Correction of physiologically induced global off-resonance effects in dynamic echo-planar and spiral functional imaging. *Magn Reson Med* 47:344–353

- Picht T, Schmidt S, Brandt S, Frey D, Hannula H, Neuvonen T, Karhu J, Vajkoczy P, Suess O (2011) Preoperative functional mapping for rolandic brain tumor surgery: comparison of navigated transcranial magnetic stimulation to direct cortical stimulation. *Neurosurgery* 69:581–588; discussion 588
- Pineiro R, Pendlebury S, Johansen-Berg H, Matthews PM (2002) Altered hemodynamic responses in patients after subcortical stroke measured by functional MRI. *Stroke* 33:103–109
- Prabhu SS, Gasco J, Tummala S, Weinberg JS, Rao G (2011) Intraoperative magnetic resonance imaging-guided tractography with integrated monopolar subcortical functional mapping for resection of brain tumors. Clinical article. *J Neurosurg* 114:719–726
- Puce A, Constable RT, Luby ML, McCarthy G, Nobre AC, Spencer DD, Gore JC, Allison T (1995) Functional magnetic resonance imaging of sensory and motor cortex: comparison with electrophysiological localization. *J Neurosurg* 83:262–270
- Pudenz RH, Agnew WF, Yuen TG, Bullara LA, Jacques S, Shelden CH (1977) Adverse effects of electrical energy applied to the nervous system. *Appl Neurophysiol* 40:72–87
- Pujol J, Conesa G, Deus J, Vendrell P, Isamat F, Zannoli G, Martí-Vilalta JL, Capdevila A (1996) Presurgical identification of the primary sensorimotor cortex by functional magnetic resonance imaging. *J Neurosurg* 84:7–13
- Pujol J, Conesa G, Deus J, Lopez-Obarrio L, Isamat F, Capdevila A (1998) Clinical application of functional magnetic resonance imaging in presurgical identification of the central sulcus. *J Neurosurg* 88:863–869
- Rabin ML, Narayan VM, Kimberg DY, Casasanto DJ, Glosser G, Tracy JI, French JA, Sperling MR, Detre JA (2004) Functional MRI predicts post-surgical memory following temporal lobectomy. *Brain* 127:2286–2298
- Ranck JB Jr (1975) Which elements are excited in electrical stimulation of mammalian central nervous system: a review. *Brain Res* 98:417–440
- Rausch R, Silfvenius H, Wieser HG, Dodrill CB, Meader KJ, Jones-Gotman M (1993) Interarterial amobarbital procedures. In: Engel JJ (ed) *Surgical treatment of the epilepsies*. Raven, New York, pp 341–357
- Rausch R, Henry TR, Ary CM, Engel J Jr, Mazziotta J (1994) Asymmetric interictal glucose hypometabolism and cognitive performance in epileptic patients. *Arch Neurol* 51:139–144
- Reinges MH, Krings T, Meyer PT, Schreckenberger M, Rohde V, Weidemann J, Sabri O, Mulders EJ, Buell U, Thron A, Gilsbach JM (2004) Preoperative mapping of cortical motor function: prospective comparison of functional magnetic resonance imaging and [¹⁵O]-H₂O-positron emission tomography in the same co-ordinate system. *Nucl Med Commun* 25:987–997
- Richardson MP, Strange BA, Thompson PJ, Baxendale SA, Duncan JS, Dolan RJ (2004) Pre-operative verbal memory fMRI predicts post-operative memory decline after left temporal lobe resection. *Brain* 127:2419–2426
- Richardson MP, Strange BA, Duncan JS, Dolan RJ (2006) Memory fMRI in left hippocampal sclerosis: optimizing the approach to predicting postsurgical memory. *Neurology* 66:699–705
- Rouleau I, Robidoux J, Labrecque R, Denault C (1997) Effect of focus lateralization on memory assessment during the intracarotid amobarbital procedure. *Brain Cogn* 33:224–241
- Roux FE, Boulanouar K, Ranjeva JP, Tremoulet M, Henry P, Manelfe C, Sabatier J, Berry I (1999) Usefulness of motor functional MRI correlated to cortical mapping in Rolandic low-grade astrocytomas. *Acta Neurochir (Wien)* 141:71–79
- Roux FE, Boulanouar K, Lotterie JA, Mejdoubi M, LeSage JP, Berry I (2003) Language functional magnetic resonance imaging in preoperative assessment of language areas: correlation with direct cortical stimulation. *Neurosurgery* 52:1335–1345; discussion 1345–1337
- Rutten GJ, Ramsey NF, van Rijen PC, Noordmans HJ, van Veelen CW (2002a) Development of a functional magnetic resonance imaging protocol for intraoperative localization of critical temporoparietal language areas. *Ann Neurol* 51:350–360
- Rutten GJ, Ramsey NF, van Rijen PC, Alpherts WC, van Veelen CW (2002b) FMRI-determined language lateralization in patients with unilateral or mixed language dominance according to the wada test. *Neuroimage* 17:447–460
- Sabbah P, Chassoux F, Leveque C, Landre E, Baudoin-Chial S, Devaux B, Mann M, Godon-Hardy S, Nioche C, Ait-Ameur A, Sarrazin JL, Chodkiewicz JP, Cordoliani YS (2003) Functional MR imaging in assessment of language dominance in epileptic patients. *Neuroimage* 18:460–467
- Salanova V, Morris HH 3rd, Rehm P, Wyllie E, Dinner DS, Luders H, Gilmore-Pollak W (1992) Comparison of the intracarotid amobarbital procedure and interictal cerebral 18-fluorodeoxyglucose positron emission tomography scans in refractory temporal lobe epilepsy. *Epilepsia* 33:635–638
- Salanova V, Markand O, Worth R (2001) Focal functional deficits in temporal lobe epilepsy on PET scans and the intracarotid amobarbital procedure: comparison of patients with unitemporal epilepsy with those requiring intracranial recordings. *Epilepsia* 42:198–203
- Sartorius CJ, Berger MS (1998) Rapid termination of intraoperative stimulation-evoked seizures with application of cold Ringer's lactate to the cortex. Technical note. *J Neurosurg* 88:349–351
- Sass KJ, Lencz T, Westerveld M, Novelty RA, Spencer DD, Kim JH (1991) The neural substrate of memory impairment demonstrated by the intracarotid amobarbital procedure. *Arch Neurol* 48:48–52
- Schiffbauer H, Berger MS, Ferrari P, Freudenstein D, Rowley HA, Roberts TP (2002) Preoperative magnetic source imaging for brain tumor surgery: a quantitative comparison with intraoperative sensory and motor mapping. *J Neurosurg* 97:1333–1342
- Schreckenberger M, Spetzger U, Sabri O, Meyer PT, Zeggel T, Zimny M, Gilsbach J, Buell U (2001) Localisation of motor areas in brain tumour patients: a comparison of preoperative [¹⁸F]FDG-PET and intraoperative cortical electrostimulation. *Eur J Nucl Med* 28:1394–1403
- Shmuel A, Augath M, Oeltermann A, Logothetis NK (2006) Negative functional MRI response correlates with decreases in neuronal activity in monkey visual area V1. *Nat Neurosci* 9:569–577
- Simkins-Bullock J (2000) Beyond speech lateralization: a review of the variability, reliability, and validity of the intracarotid amobarbital procedure and its nonlanguage uses in epilepsy surgery candidates. *Neuropsychol Rev* 10:41–74
- Simos PG, Papanicolaou AC, Breier JI, Wheless JW, Constantinou JE, Gormley WB, Maggio WW (1999) Localization of language-specific cortex by using magnetic source imaging and electrical stimulation mapping. *J Neurosurg* 91:787–796
- Small SA, Perera GM, DeLaPaz R, Mayeux R, Stern Y (1999) Differential regional dysfunction of the hippocampal formation among elderly with memory decline and Alzheimer's disease. *Ann Neurol* 45:466–472
- Spina G, Nava A, Cassini F, Pepoli A, Bruno M, D'Agata F, Cauda F, Sacco K, Duca S, Barletta L, Versari P (2010) Preoperative and intraoperative brain mapping for the resection of eloquent-area tumors. A prospective analysis of methodology, correlation, and usefulness based on clinical outcomes. *Acta Neurochir (Wien)* 152:1835–1846
- Spencer DC, Morrell MJ, Risinger MW (2000) The role of the intracarotid amobarbital procedure in evaluation of patients for epilepsy surgery. *Epilepsia* 41:320–325
- Sperling MR, Saykin AJ, Glosser G, Moran M, French JA, Brooks M, O'Connor MJ (1994) Predictors of outcome after anterior temporal lobectomy: the intracarotid amobarbital test. *Neurology* 44:2325–2330
- Sperling MR, Alavi A, Reivich M, French JA, O'Connor MJ (1995) False lateralization of temporal lobe epilepsy with FDG positron emission tomography. *Epilepsia* 36:722–727

- Stieltjes B, Kaufmann WE, van Zijl PC, Fredericksen K, Pearlson GD, Solaiyappan M, Mori S (2001) Diffusion tensor imaging and axonal tracking in the human brainstem. *Neuroimage* 14:723–735
- Thulborn KR, Waterton JC, Matthews PM, Radda GK (1982) Oxygenation dependence of the transverse relaxation time of water protons in whole blood at high field. *Biochim Biophys Acta* 714:265–270
- Towle VL, Khorasani L, Uftring S, Pelizzari C, Erickson RK, Spire JP, Hoffman K, Chu D, Scherg M (2003) Noninvasive identification of human central sulcus: a comparison of gyral morphology, functional MRI, dipole localization, and direct cortical mapping. *Neuroimage* 19:684–697
- Ugurbil K, Hu X, Chen W, Zhu XH, Kim SG, Georgopoulos A (1999) Functional mapping in the human brain using high magnetic fields. *Philos Trans R Soc Lond B Biol Sci* 354:1195–1213
- Ugurbil K, Toth L, Kim DS (2003) How accurate is magnetic resonance imaging of brain function? *Trends Neurosci* 26:108–114
- Urbach H, Kurthen M, Klemm E, Grunwald T, Van Roost D, Linke DB, Biersack HJ, Schramm J, Elger CE (1999) Amobarbital effects on the posterior hippocampus during the intracarotid amobarbital test. *Neurology* 52:1596–1602
- Van de Moortele PF, Pfeuffer J, Glover GH, Ugurbil K, Hu X (2002) Respiration-induced B0 fluctuations and their spatial distribution in the human brain at 7 Tesla. *Magn Reson Med* 47:888–895
- van Zijl PC, Eleff SM, Ulatowski JA, Oja JM, Ulug AM, Traystman RJ, Kauppinen RA (1998) Quantitative assessment of blood flow, blood volume and blood oxygenation effects in functional magnetic resonance imaging. *Nat Med* 4:159–167
- Vassal F, Schneider F, Nuti C (2013) Intraoperative use of diffusion tensor imaging-based tractography for resection of gliomas located near the pyramidal tract: comparison with subcortical stimulation mapping and contribution to surgical outcomes. *Br J Neurosurg* 27:668–675
- Wada J, Rasmussen T (1960) Intracarotid injection of sodium amytal for the lateralization of cerebral speech dominance: experimental and clinical observations. *J Neurosurg* 17:266–282
- Woermann FG, Jokeit H, Luerding R, Freitag H, Schulz R, Guertler S, Okujava M, Wolf P, Tuxhorn I, Ebner A (2003) Language lateralization by Wada test and fMRI in 100 patients with epilepsy. *Neurology* 61:699–701
- Wood JM, Kundu B, Utter A, Gallagher TA, Voss J, Nair VA, Kuo JS, Field AS, Moritz CH, Meyerand ME, Prabhakaran V (2011) Impact of brain tumor location on morbidity and mortality: a retrospective functional MR imaging study. *AJNR Am J Neuroradiol* 32:1420–1425
- Yacoub E, Duong TQ, Van De Moortele PF, Lindquist M, Adriany G, Kim SG, Ugurbil K, Hu X (2003) Spin-echo fMRI in humans using high spatial resolutions and high magnetic fields. *Magn Reson Med* 49:655–664
- Yetkin FZ, Mueller WM, Morris GL, McAuliffe TL, Ulmer JL, Cox RW, Daniels DL, Haughton VM (1997) Functional MR activation correlated with intraoperative cortical mapping. *AJNR Am J Neuroradiol* 18:1311–1315
- Yingling CD, Ojemann S, Dodson B, Harrington MJ, Berger MS (1999) Identification of motor pathways during tumor surgery facilitated by multichannel electromyographic recording. *J Neurosurg* 91:922–927
- Young WL, Prohovnik I, Ornstein E, Ostapkovich N, Sisti MB, Solomon RA, Stein BM (1990) The effect of arteriovenous malformation resection on cerebrovascular reactivity to carbon dioxide. *Neurosurgery* 27:257–266; discussion 266–257
- Young WL, Pile-Spellman J, Prohovnik I, Kader A, Stein BM (1994) Evidence for adaptive autoregulatory displacement in hypotensive cortical territories adjacent to arteriovenous malformations. Columbia University AVM Study Project. *Neurosurgery* 34:601–610; discussion 610–611
- Yousry TA, Schmid UD, Jassoy AG, Schmidt D, Eisner WE, Reulen HJ, Reiser MF, Lissner J (1995) Topography of the cortical motor hand area: prospective study with functional MR imaging and direct motor mapping at surgery. *Radiology* 195:23–29
- Yousry TA, Schmid UD, Alkadhi H, Schmidt D, Peraud A, Buettner A, Winkler P (1997) Localization of the motor hand area to a knob on the precentral gyrus. A new landmark. *Brain* 120(Pt 1):141–157
- Zeineh MM, Engel SA, Thompson PM, Bookheimer SY (2003) Dynamics of the hippocampus during encoding and retrieval of face-name pairs. *Science* 299:577–580
- Zhu FP, Wu JS, Song YY, Yao CJ, Zhuang DX, Xu G, Tang WJ, Qin ZY, Mao Y, Zhou LF (2012) Clinical application of motor pathway mapping using diffusion tensor imaging tractography and intraoperative direct subcortical stimulation in cerebral glioma surgery: a prospective cohort study. *Neurosurgery* 71:1170–1183; discussion 1183–1174

Multimodality in Functional Neuroimaging

Jan Kassubek, Hans-Peter Müller,
and Freimut D. Juengling

Contents

| | | |
|-----|---|-----|
| 1 | The Concept of Multimodal Presurgical Imaging | 269 |
| 2 | Combination of Neuroimaging Modalities and Their Applications | 270 |
| 2.1 | Multiparametric MRI Techniques..... | 270 |
| 2.2 | Combination of MRI and Nuclear Medicine | 277 |
| 2.3 | Combination of MRI and MEG (MSI)/ EEG | 281 |
| 3 | Advantages and Limitations of Multimodal Functional Neuroimaging..... | 283 |
| | References | 284 |

Abstract

The multimodal approach which is conceptually based on the combination of different noninvasive functional neuroimaging tools and their registration and co-integration into neuronavigational systems is widely used in presurgical diagnostics. In particular, the combination of imaging techniques that independently map different functional systems is a useful application, such as functional MRI (in its traditional task-related approach as well as in the increasingly used task-free intrinsic functional connectivity approach) as a technique for the localization of eloquent cortex and diffusion-tensor imaging as a method for the mapping of white matter fiber bundles/tracts. Magnetic source imaging as an additional imaging technique for cortical function mapping is of particular advantage in epilepsy surgery. Advanced functional pathoanatomy-based techniques such as nuclear medicine imaging (multi-ligand imaging) or MR spectroscopy might additionally be useful for the delineation of cerebral lesions (e.g., neoplasms). Although “multimodal imaging” may be complex in data acquisition and postprocessing, it is a valuable instrument to improve surgical planning and performance.

1 The Concept of Multimodal Presurgical Imaging

The integration of previously identified functional areas into the neurosurgical setup is most important since follow-up nowadays focuses more on performance than on survival, and preservation of function during and after operation is crucial. First, imaging techniques are increasingly used for the characterization of lesions and perilesional tissue. Second, in order to identify and map those areas near a lesion that contain critical function such as language, vision, motor control, etc., different neuroimaging techniques are used. The MR-based imaging methods sensu stricto which are mainly

J. Kassubek, MD (✉) • H.-P. Müller, PhD
Department of Neurology, University of Ulm,
Oberer Eselsberg 45, Ulm 89081, Germany
e-mail: jan.kassubek@uni-ulm.de

F.D. Juengling, MD
PET/CT Center NW-Switzerland, Claraspital Basel,
Kleinriehenstr. 30, Basel 4010, Switzerland

used for preoperative functional mapping are functional MRI (fMRI) (e.g., Pillai 2010), intrinsic functional connectivity MRI (ifcMRI) (e.g., Weaver et al. 2013), and diffusion-tensor imaging (DTI) (Lazar et al. 2006). Further techniques are positron emission tomography (PET) (Nooraine et al. 2013), single-photon emission computerized tomography (SPECT) (Elwan et al. 2014), evoked response mapping by magnetoencephalography (MEG) (Mohamed et al. 2013), and multi-channel electroencephalography (EEG) (Leijten et al. 2004). As the basic principle, the task-based techniques compare an activated state during which a specific task is performed with a resting state, and the difference between the two conditions implies the involvement of the corresponding area for this specific function, amid the whole connectivity and complexity in the nervous system (Sporns et al. 2000). However, the spatial resolution of the results depends on the kind of signal measured and the technical properties, which markedly differs between the named imaging tools. Furthermore, the relationship between the results of the computer-based analysis and the underlying neurophysiology is often more complex. Independent of these considerations, the functional maps of all techniques have to be co-registered to an anatomical individual image of the patient's brain, i.e., a volume-rendering high-resolution MRI image set serving as a structural brain framework requiring computerized postprocessing. For this purpose, the data have to be integrated into the same stereotactic coordinate system as the 3-D MRI data to be correctly superimposed. The functional maps acquired preoperatively are then registered to the predefined coordinate system in the same way as the preoperative 3-D anatomy data set.

Spatial normalization processing aims at providing the spatial relationship between "functional localization" and "structure" (Brett et al. 2002) at a multiple-subject level, classically using proportional scaling systems to reference the individual brain to an atlas-based brain, such as the template of the Montreal Neurological Institute (MNI template) which has been created from the brain MRI data of 152 healthy subjects (Brett et al. 2002). Another frequently used atlas reference system is the probabilistic whole-brain atlas provided by the Laboratory of Neuroimaging (LONI) at the University of California, Los Angeles, USA (LPBA40) (<http://www.loni.ucla.edu/Atlases/>) (Shattuck et al. 2008). Spatial normalization, i.e., the registration of data within standardized stereotactic space, is a prerequisite for the co-registration of imaging results from different individuals to each other. However, individual features of data (which are important in surgical planning as a per se individual-based action) may get lost in such a process.

Image postprocessing has the advantage of enabling the image fusion of additional functional information (Winkler et al. 2004). It is possible to combine all these different imaging data into one composite image to be visualized during the course of the surgical procedure (Toga et al. 2000; Nimsky et al. 2005a; Shang et al. 2012; Dimou et al. 2013). The multitude of technical approaches to achieve the information of

the localization of the data collected before surgery relative to the anatomy and to its changes during surgery (which are caused by many factors such as the so-called brain shift phenomenon) is beyond the scope of this chapter. The co-registration procedure generally enables multiple-modality comparisons with the same subject. This aspect is all the more important with respect to additional applications of pre-surgical multimodality imaging: the characterization of the lesion considered for resection can also be performed by non-invasive techniques in a wide range of disorders, particularly in cerebral neoplasms and epilepsy surgery. Composite pre-surgical brain mapping techniques with respect to the pharmacological characterization are primarily found in the domain of PET and SPECT which give important information on the metabolic state and molecular events within the tumor (Jacobs et al. 2005) and can be combined with various MRI techniques beyond the structural 3-D data set. In detail, examples for multiparametric/multimodal combinations are fMRI and DTI (Kleiser et al. 2010); PET and DTI (Stadlbauer et al. 2009); PET and MEG (Rheims et al. 2013); MEG, SPECT, and PET (Mohamed et al. 2013); EEG and fMRI (Sierra-Marcos et al. 2013); and PET and fMRI (Pillai 2010). By this composite use of preoperative brain mapping for "lesion identification" and for the "delineation of functionally relevant cortical areas adjacent to the operation area," multimodal presurgical imaging is an important element of modern neurosurgical planning. The concept of the individual visualization of functional landmarks (fMRI) and even networks, i.e., DTI for structural networks (Schonberg et al. 2006) and ifcMRI for functional networks (Mitchell et al. 2013), has evolved to a broader spectrum of MRI applications beyond a simple depiction of activation maps with fMRI (which describes cortical areas) for the preoperative assessment of infiltration zones around (neoplastic) brain lesions and of eloquent systems which will be described in the following.

2 Combination of Neuroimaging Modalities and Their Applications

2.1 Multiparametric MRI Techniques

Conventional MRI with and without contrast media is the method of choice to image brain structures and depict the anatomy of structural lesions at a good soft-tissue contrast and at high (<1 mm) spatial resolution. In addition, for any brain mapping technique in which postprocessing results in activation clusters for visualization purposes it is useful to acquire an individual 3-D MRI data set (including e.g. any lesions) for co-registration. However, additional MRI applications offer various tools to visualize both the extent of brain lesions and the damage associated with them and possible alterations to the function of cortical and subcortical areas localized in the immediate vicinity of lesions.

In addition to these more structure-oriented MRI applications in the course of primary diagnostics and prognosis assessment, MRI-based techniques with computerized post hoc processing can be combined in the presurgical setting as a composite instrument for tissue characterization and function localization. This complex information gained from computer-based postprocessing of one single imaging modality, also called “intramodal multimodality” (Müller and Kassubek 2008), is usually referred to as multiparametric MRI.

As outlined above, the classical functional presurgical MRI approach comprises preoperative activation paradigms by the use of fMRI. However, there are advanced techniques such as ifcMRI (Mitchell et al. 2013), analysis of 3-D MRI (Wehner and Lüders 2008), diffusion-tensor imaging (Kleiser et al. 2010; Schonberg et al. 2006), and MR spectroscopy (Shang et al. 2012) which are increasingly integrated into presurgical brain mapping protocols and hence broaden the spectrum of the noninvasively assessable functional and structural neuroanatomy in patients with brain lesions.

2.1.1 Functional MRI (fMRI)

In a recent review, Stippich emphasized the potential of fMRI as an important neuroimaging modality for patients with brain tumors (Stippich 2010). By noninvasive localization of brain activation, fMRI facilitates the selection of the most appropriate and function-preserving surgery. Prerequisites for the diagnostic use of fMRI are the application of dedicated clinical imaging protocols and the standardization of the respective imaging procedures. The combination with DTI also enables the tracking and visualization of important fiber bundles such as the corticospinal tract and the arcuate fascicle. The practicability, accuracy, and reliability of presurgical fMRI have been validated by large numbers of published data, but to date fMRI cannot be considered as a fully established modality of diagnostic neuroimaging due to the lack of guidelines of the responsible medical associations as well as the lack of medical certification for important hardware and software components (Stippich 2010).

fMRI allows to the indirect measurement of neuronal activity via differential local oxygen extraction and therefore regional blood flow changes and is nowadays an established procedure for presurgical cortical mapping in cases of lesions within or adjacent to eloquent brain areas. Patients with such lesions undergo fMRI with paradigms that activate the appropriate topographic region, and the relative distance between the lesion and the activation sites provides a measure of surgical risk. These paradigms are chosen to identify the regions associated with motor or somatosensory functions in patients with lesions near sensorimotor cortices as well as the regions responsible for language or memory function in patients with lesions in the medial/mesial temporal lobe. The complex setup of the fMRI investigation conception, data acquisition, and postprocessing together with its underlying neurophysiological basics is detailed in chap-

ters “[Revealing brain activity and the white matter structure using functional and diffusion-weighted magnetic resonance imaging](#)” and “[Task-based presurgical functional MRI in patients with brain tumors](#)”. A recent study in a multicenter setup questioned the value of fMRI-based analysis in the presurgical planning (Due-Tonnessen et al. 2014) in comparison with computer-aided topographic MRI analysis with BrainVoyager QX (Brain Innovation, Maastricht, the Netherlands). The authors reported that the central sulcus in the affected hemisphere was readily identified in a significantly higher percentage of patients by 2-D MRI and topographical analysis (77/77 patients) compared to BOLD-fMRI (57 patients). The topographical analysis again identified a significantly larger portion of the total central sulcus than 2-D MRI. They concluded that the identification of the central sulcus in patients with brain lesions is best performed using conventional 2-D readings or topographical analysis and that the robustness of BOLD-fMRI has still to be determined in the clinical setting. An improvement of fMRI performance might be reached by a multiparametric combination of different MRI techniques as will be addressed in the following.

The activation maps resulting from the fMRI data post-processing have to be overlaid onto the individual 3-D MRI data set. These voxel clusters are considered to delineate critical areas for the respective function in particular, but do not image the complete neural network. Therefore, it is useful to combine fMRI cortical mapping with techniques such as DTI (see below) to additionally visualize the subcortical white matter structures, i.e., fiber tracts, that might also be crucial for the maintenance of the respective function (Kleiser et al. 2010; Schonberg et al. 2006; Pillai 2010) also in presurgical planning in a stereoscopic virtual-reality environment (Qiu et al. 2010). Furthermore, the extent of a lesion might only be incompletely assessable by T1-weighted 3-D MRI, so that a combination of different techniques imaging the perilesional tissue, e.g., with MR spectroscopy, metabolic imaging with fluorodeoxyglucose PET (FDG-PET) or other ligand imaging methods might be useful to improve the estimation of the distance between the lesion and critical cortex. It could be demonstrated that ¹¹C-methionine (MET)-PET seems to be more sensitive than MRI for the differentiation between tumor and edema or gliosis and that the simultaneous integration of MRI and MET-PET data into the neuronavigation system can facilitate total tumor resection (Braun et al. 2002). Also, additional combination with functional landmarks gained from fMRI might further improve surgical results. Finally, the co-integration of fMRI data using different paradigms and MET-PET data into one neuronavigation system in cases of brain tumor surgery has proven good postoperative outcome (Braun et al. 2000).

With respect to methodological considerations, the maximum of fMRI activation will in general be found close to vessels (draining veins) and not within neurons. Thus, a combination with alternative functional mapping techniques

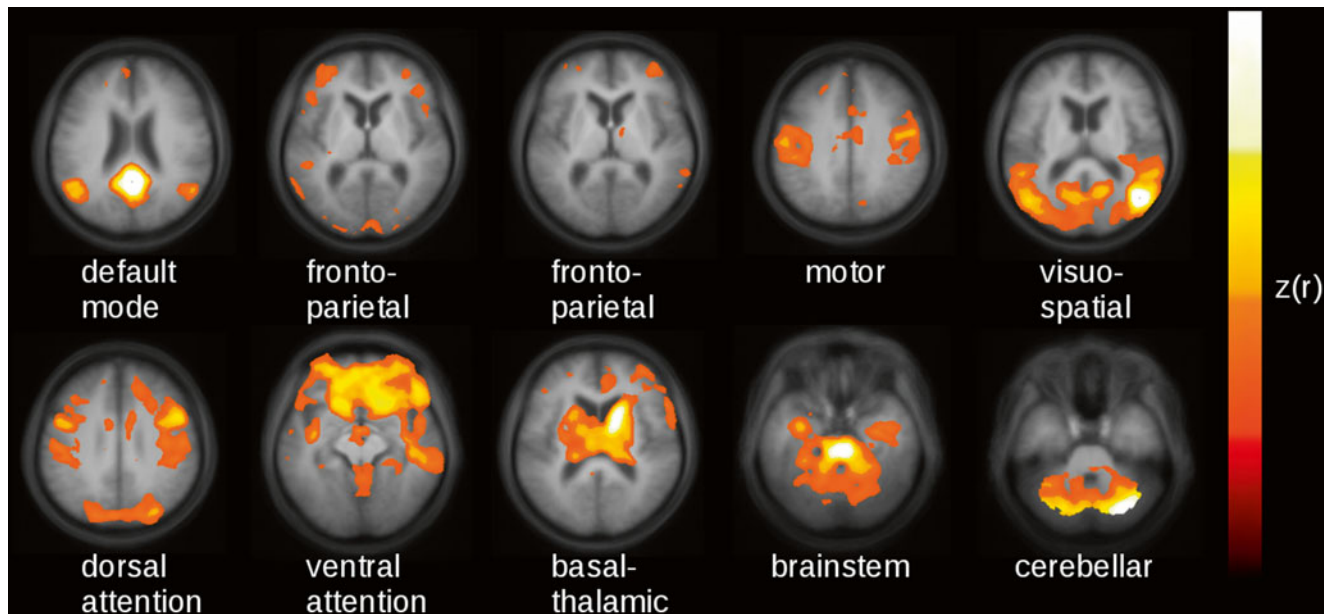


Fig. 1 Representative slices of ifc-MRI networks averaged from 22 healthy controls

might be useful but is of course restricted to few specialized centers. Here, MEG/magnetic source imaging (MSI) is a useful composite technique to map eloquent cortical areas (see below). In particular with respect to the presurgical localization of epileptic activity, MEG might be additive to the results of fMRI with simultaneously recorded epileptiform discharges on EEG (spike-triggered fMRI and continuous EEG/fMRI recordings) (cf. chapter “[Presurgical EEG-fMRI in epilepsy](#)” – which in turn might be combined with DTI and MRS for the improvement of presurgically gained information (Krakow et al. 1999). A combination of fMRI with functional PET (fPET) using $^{15}\text{O}-\text{H}_2\text{O}$ as a further perfusion-based technique is less promising although fPET has been shown to be similarly sensitive and reliable to map the central region in a comparative study using the same frame of reference (Reinges et al. 2004). The mean localization difference in this study ranged between 2 and 18 mm, and the authors commented that fMRI is more prone to artifacts, whereas fPET depicts capillary perfusion changes and therefore shows activation closer to the parenchyma. However, the application of fPET and the tracer $^{15}\text{O}-\text{H}_2\text{O}$ – with its half-time of about 2 min – is restricted to dedicated PET centers including a cyclotron unit. In addition, it requires repetitive injection of radiopharmaceuticals in contrast to fMRI which is easy to be acquired on each clinical scanner with magnetic field strength ≥ 1.5 T and has no known side effects.

2.1.2 Intrinsic Functional Connectivity MRI (ifcMRI)

Intrinsic functional connectivity MRI (ifcMRI), traditionally named resting-state fMRI, constitutes a growing proportion of functional brain imaging studies and is used in research of

brain networks that exhibit correlated fluctuations. IfcMRI does not provide a direct measurement of anatomic connectivity such as DTI but is particularly useful for the characterization of large-scale systems that span distributed areas and has complementary strengths to other tools available for connectivity assessment in humans, i.e., DTI (Greicius et al. 2009; Van Dijk et al. 2010).

This approach detects temporal correlations in spontaneous BOLD signal oscillations while the subjects rest quietly in the scanner. To explore the relationship between ifcMRI (Fig. 1) and structural connectivity in detail, several studies have been performed in the last decade: Koch and coworkers (Koch et al. 2002) found that DTI structural connectivity measures between adjacent gyri correlated with task-free functional connectivity measures. The limited temporal resolution of fMRI does not allow to assess whether the functional connectivity between two nodes reflects a direct (potentially monosynaptic) connection or is conducted across multiple synapses via many intervening nodes. The general hypothesis that (resting-state) functional connectivity reflects structural connectivity has been investigated by combined DTI tractography and resting-state fMRI (Greicius et al. 2010).

In patients with brain tumors, ifcMRI has been used to investigate the connections and strength of the connections between cortical areas (Manglore et al. 2013). In a study of the capacity of ifcMRI to identify the seizure focus in a group of patients with non-lesional epilepsy, the authors concluded that ifc-MRI may serve as an adjunct presurgical tool facilitating the identification of the seizure focus in patients with focal epilepsy (Weaver et al. 2013).

2.1.3 Computer-Based Analysis of Structural MRI

The so-called computational neuroanatomy is an established methodology to characterize the neuroanatomical configuration of different brains, encompassing mainly the following techniques: (1) voxel-based morphometry (VBM) which compares neuroanatomical differences on a voxel by voxel basis; (2) deformation-based morphometry (DBM) which provides information about global differences in brain shape; (3) and tensor-based morphometry (TBM) which provides information about local shape differences (cf. Ashburner et al. 2003 for review). These 3-D MRI analysis techniques which make use of local registration algorithms, however, are only validated for analyses at group level: it could be demonstrated that VBM could not satisfactorily delineate the spatial extent of focal lesions in individuals, even in simulations that avoided preprocessing artifacts (Mehta et al. 2003). To be applicable in the clinical practice and, in particular, in the presurgical setting, the techniques have to be sensitive to quantitative or qualitative alterations of normal brain structures in a given individual patient. In this respect, it is not useful to apply this computerized approach in lesions which are clearly assessable by conventional high-resolution MRI such as in neoplasms. Nevertheless, there are applications of computerized analysis of structural 3-D MRI for presurgical diagnostics, e.g., in the field of epilepsy surgery and here, e.g., in malformations of cortical development (MCD). First, there have been voxel-based 3-D MRI analysis tools developed for an automated observer-independent MCD lesion detection (Huppertz et al. 2005). These algorithms serve mainly as image screening tools in comparison to a healthy control sample in order to facilitate MCD detection and localization. Second, as a consequent continuation of the multimodality approach in the sense of a combined voxel-based mapping (Kassubek et al. 2000), a combination of ligand imaging using PET (which is able to provide relevant information on MCD; Cross 2003) and SPM-based MRI analysis has been proposed for the investigation of MCD (Richardson et al. 1997). Although at the expense of the measurement of absolute quantitative values (the voxel-based comparison of MRI and PET enables an automated objective whole-brain analysis), issues concerning partial volume effects and mixed tissue sampling in ligand images have to be resolved, and disproportionate changes in function and structure to be identified. In a study using the approach of voxel-based MRI analysis and subtraction of ictal SPECT co-registered to MRI (SISCOM), it could be demonstrated that multimodal assessment of MCD may contribute to an advanced observer-independent preoperative assessment of the seizure origin and might thus improve presurgical diagnostics in symptomatic epilepsy (Wiest et al. 2005). Wehner and Lüders (2008) summarized the role of neuroimaging in presurgical mapping focusing on structural MRI, PET, and SPECT.

2.1.4 Diffusion Tensor Imaging (DTI)

Diffusion is a physical process involving the translational movement of molecules via thermally driven random motions, the so-called Brownian motion. The underlying microstructure of the cellular tissue influences the overall mobility of the diffusing molecules by providing numerous barriers and by creating various individual compartments within the tissue (e.g., intra-/extracellular space, neurons, glial cells, axons). Signal intensity of diffusion measured via diffusion-weighted imaging shows a greater signal enhancement and more rapid diffusion of water molecules along the direction parallel to the axis of the fiber bundles (so-called anisotropy) than in the perpendicular direction where signal intensity and diffusion velocity is lowest (so-called isotropy). As diffusion is characterized by hindrances of equal molecular movement caused by oriented barriers, it requires a general tensor which fully describes the mobility of molecules along each direction and the correlation between these directions. A common way to summarize diffusion measurements with DTI is the calculation of a parameter that reflects the overall anisotropy, such as the fractional anisotropy (FA) as a measure of the proportion of the diffusion tensor due to anisotropy. The FA can either be presented as a gray-scale image or the principal diffusion direction of the brain structure to be examined can be encoded in color resulting in color-coded parameter maps (Basser and Jones 2002; Le Bihan and van Zijl 2002).

Concretely, DTI measures the mean longitudinal direction of axons in white matter tracts. For this purpose, the application of fiber-tracking algorithms allows a delineation of the major white matter pathways (Mori and van Zijl 2002). With respect to presurgical mapping, the DTI technique provides information about the deformation, the displacement, or even the interruption of the white matter tracts around a lesion (Sinha et al. (2002)). For instance, DTI is used to differentiate normal white matter from edematous brain and contrast-enhancing tumor margins in patients with high-grade gliomas. Witwer et al. (2002) reported that the visualization of white matter tracts by DTI was beneficial in the surgical planning for patients with intrinsic brain tumors showing that anatomically intact fibers may be present in abnormal-appearing areas of the brain. The knowledge of the course of major white matter tracts in relationship to the exact location of the lesion is of utmost importance to the neurosurgeon for the planning of the most appropriate surgical approach and may thus help to prevent the risk of new postoperative neurological deficits (Clark et al. 2003). For topographical identification, DTI atlas systems have been developed (Oishi et al. 2011). Figure 2 shows an example of a patient with a glioma showing DTI-based structural connectivity changes adjacent to the left cortex.

The role of DTI for the assessment of important pathways in the vicinity of tumor borders has already been described in 2004 by Ulmer and coworkers (2004) who concluded that DTI can significantly enhance the estimation of the

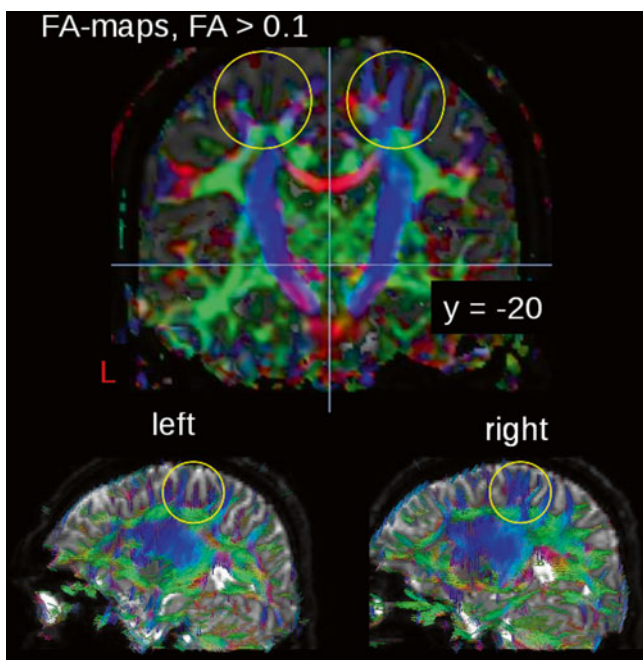


Fig. 2 FA-mapping of a patient with a glioma showing FA reductions in the cortex of the left hemisphere, with locally altered fiber tracts

proximity of functional brain structures/areas to brain tumor borders suggesting DTI to be a valuable tool for presurgical planning. This work was followed by a pre- and postoperative DTI-based analysis (white matter tractography) of brain tumors (Lazar et al. 2006) showing the preservation of white matter tracts during surgery. Ferda and coworkers (2010) reported that DTI offered significant additional information in 24 patients with glial tumors which might help for the differentiation of tumors with infiltrative growth character from more circumscribed tumors, and it has been possible to advance the accuracy of estimation of tumor grading prior to final determination of the morphological diagnosis. The finding of a reduced FA in the white matter around a tumor increases the probability of peritumorous white matter infiltration by tumor invasion. Figure 3 shows an example of the application of a DTI analysis in a patient with a biopsy-proven anaplastic oligoastrocytoma WHO III° by comparing the FA maps acquired before combined radio-/chemotherapy with those obtained 2, 5, and 9 months after radio-/chemotherapy (for the methodological approach, please cf. Müller and Kassubek 2013). After surgery, the patient received combined radio-/chemotherapy and 6 cycles of adjuvant chemotherapy.

Consecutively, DTI measurements are increasingly used in advanced neuronavigation protocols (Rohde et al. 2005). That way, the course of the pyramidal tract can be displayed with DTI for the intraoperative visualization in functional neuronavigation systems (Nimsky et al. 2005b). Moreover, DTI is helpful for the visualization of the optic radiation to preserve the patients' visual field during the surgery of lesions adjacent to the course of the optic radiation. For instance,

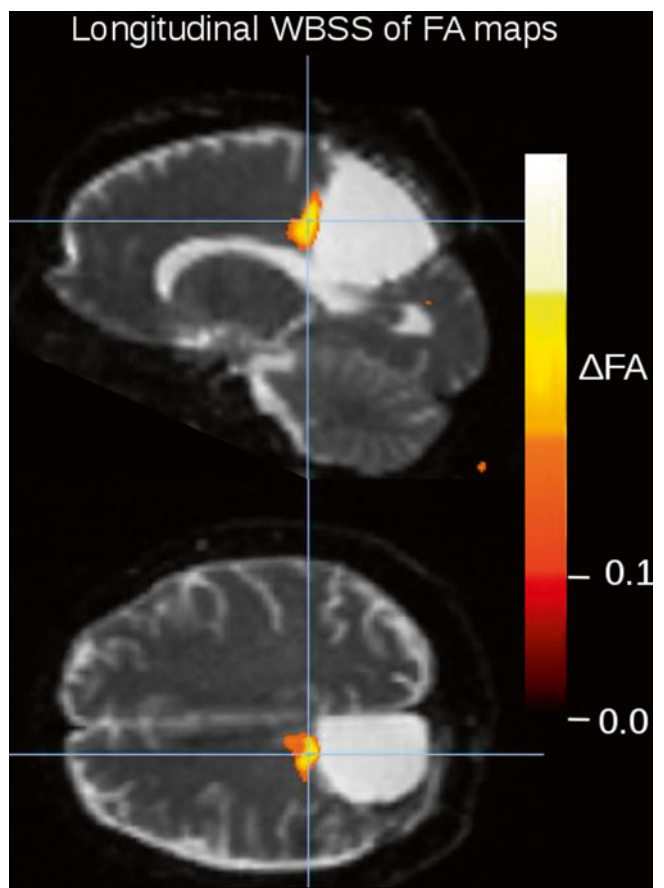


Fig. 3 FA-map differences between the DTI scan after radio-/chemotherapy and the DTI scan 7 months later, i.e., scans of time points 2 and 4. Longitudinal single-subject whole-brain-based spatial statistics (WBSS) was performed with a FDR corrected FA threshold of 0.15

Coenen et al. (2005) could reproduce the course of the optic radiation by using neuronavigation with optic radiation DTI and preoperative and postoperative neuro-ophthalmological testing including perimetry. Also in epilepsy surgery, visual field defects are a well-recognized complication of anterior temporal lobe resection and may occur secondary to disruption of the Meyer loop. The use of DTI tractography for the visualization of the optic radiation before and after surgery has been concluded to be useful for the prediction and perhaps prevention of visual field defects following temporal lobe resection (Powell et al. 2005).

However, there are also limitations for DTI which is not able to correctly identify fiber crossings due to its inability to resolve more than one single axon direction within each voxel. Advanced approaches, such as the so-called q-ball imaging technique, can resolve intra-voxel white matter fiber crossings as well as white matter insertions into the cortex and might hence be able to uncover the complex intra-voxel fiber architecture and thus eliminate a key obstacle for the noninvasively mapping of neural connectivity in the human brain (Tuch et al. 2003). An approach which addresses the limits of diffusion resolution of "crossing" or "kissing" fibers and in the vicinity of tumor or edema is tractography

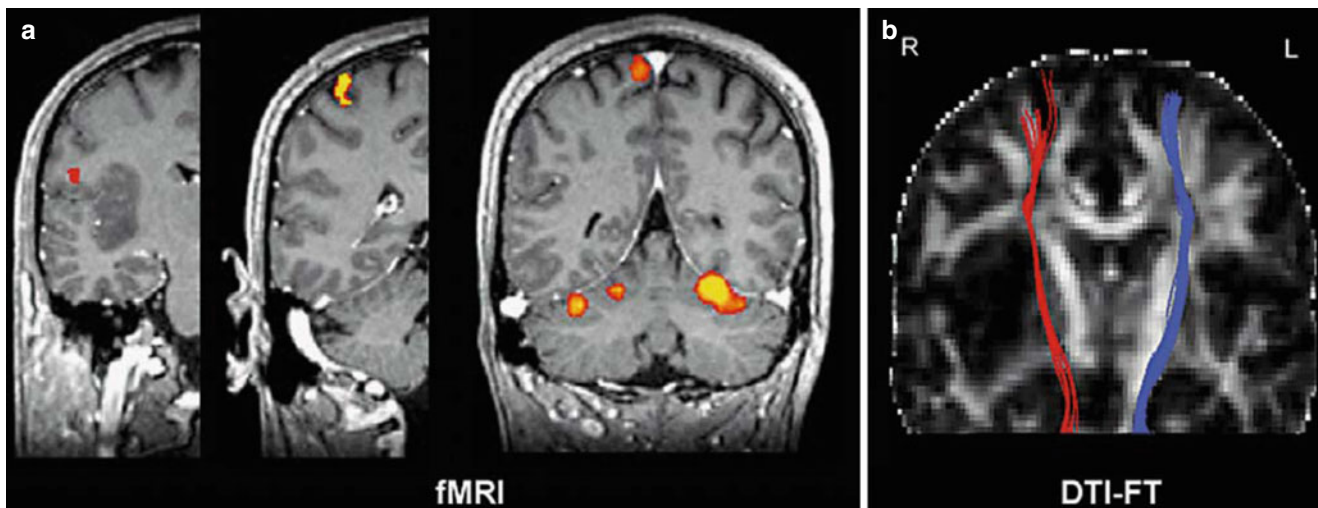


Fig. 4 (a, b) DTI-based fiber tracking of the pyramidal tract for the presurgical delineation of eloquent white matter areas. (a) Somatotopic mapping of primary motor cortex shows a normal activation patterns.

From *left to right*: tongue, hand, and foot movements. (b) DTI fiber tracking visualizing the spatial relationship of the pyramidal tract to an astrocytoma in the right insula (Images courtesy of C. Stippich, MD)

method based on high-angular-resolution diffusion imaging (HARDI). With compressed sensing techniques, HARDI acquisitions with a smaller number of directional measurements can be used, thus enabling the use of HARDI-based fiber tractography in the clinical practice (Kuhnt et al. 2013; Bucci et al. 2013). More recent investigations applied Q-ball imaging as high-definition fiber tractography (HDFT) to patients with intracerebral lesions (Fernandez-Miranda et al. 2012) in order to understand the lesional patterns of structural injury and facilitate neurosurgical interventions. A further application of HFTD was reported in a patient with traumatic brain injury (Shin et al. 2012). An additional technical challenge, especially in presurgical mapping, i.e., the intraoperative displacement of major white matter tracts during mass resection due to brain shift, has been addressed by a comparison of preoperative with intraoperative DTI-based fiber tracking (Nimsky et al. 2005c). The authors described a marked shift and deformation of major white matter tracts due to tumor removal, herewith emphasizing the need for an intraoperative update – in navigation systems – during the resection of deep-seated tumor portions near eloquent brain areas. Consequently fiber tracking is not only useful for pre-operative neurosurgical visualization but also for intraoperative planning and updating. Another emerging challenge for the clinical routine use is the lack of standardization which affects DTI as well as fMRI. There are many different software packages available for tractography, including traditional DTI-based methods (such as the fiber assignment by a continuous tracking algorithm), as well as more advanced methods that take into account each eigenvector within an individual voxel (Pillai 2010).

The integration of DTI into presurgical mapping protocols is also useful with respect to MRI multimodality, since the bi-parametric combination of DTI with fMRI provides valuable information that cannot be obtained by the use of

either technique alone. The use of fMRI and DTI in a multimodality approach enables the connection of the advantages of both techniques. While fMRI is able to highlight the localization of function within the cortex, DTI visualizes white matter structures *in vivo* (Dimou et al. 2013; Kleiser et al. 2010; Wu et al. 2007). The validity and sensitivity of noninvasive functional mapping for surgical guidance can be improved by considering the results obtained with both methods, and the use of 3-D visualization seems crucial and unique for the representation and understanding of the complicated spatial relationship among the lesion, gray matter activation, and white matter fiber bundles (Hendler et al. 2003). In neoplastic brain lesions, the combined use of fMRI with DTI can provide a better estimation of the proximity of the tumor borders to eloquent brain systems, such as language, speech, vision, motor, and premotor functions (Ulmer et al. 2004). DTI and fMRI can thus be used as complementary techniques for the delineation of eloquent subcortical and cortical areas (Fig. 4).

The use of fMRI together with or without DTI currently seems to be a promising application of the available neuroimaging techniques in the clinical context. These multiparametric MRI data can be implemented in computer systems for functional neuronavigation or radiation treatment (Stippich 2010). There has been significant interest in using this bi-parametric MRI approach for the localization of potential brain regions which may be at risk during neurosurgical procedures. There is an increasing number of groups worldwide that have integrated both modalities in stereotaxic guidance systems, providing clinical insight in the mapping of eloquent gray matter and white matter regions to the neurosurgeon (Dimou et al. 2013). It has been reported that as the distance between tumor and eloquent cortex ("lesion to eloquent area distance" or "LEAD") decreases, so does the likelihood of a complete surgical resection. Consequently, DTI was pro-

posed as a tool for the identification of those patients who would benefit most from total surgical resection and, thus, having longer survival time (Castellano et al. 2011). Used in conjunction, both techniques provide important information both prior to surgery for a thorough preoperative planning, as well as during surgery for the intraoperative update of the information via integration into frameless stereotactic neuro-navigational systems.

The use of fMRI landmarks for ROI selection has been shown to enhance the fiber-tracking performance compared to a strictly anatomically based ROI selection and is usually considered reliable in controls. Nevertheless, this approach may be inaccurate in patients with brain lesions (Schonberg et al. 2006). Kleiser and coworkers (2010) found that DTI-related results were more accurate than results using anatomical landmarks alone. Four patterns of regional anisotropy have been observed in relation to WM tracts in the vicinity of tumors (Jellison et al. 2004), i.e., (1) normal signal with altered position or direction, observed in cases of tract displacement; (2) decreased but present signal with normal direction and location, supposedly corresponding to vasogenic edema; (3) decreased signal with disrupted maps, believed to be related to tumor infiltration; and (4) loss of anisotropic signal corresponding to fiber tract destruction. In two trials addressing a potential modification of the surgical approach to corticotomy, the presurgical use of combined DTI/fMRI led to a change in the surgical approach in 16–21 % of cases (Dimou et al. 2013). Together, these techniques show great promise for improved neurosurgical outcomes. Clinical reports have suggested that the additional information provided by the combination of the two imaging modalities, via a co-registered map delivered to the neurosurgeon on a heads-up display, is valuable and facilitates a safe resection (Berntsen et al. 2010). While further research is required for a more widespread clinical validity and acceptance, results from the literature (e.g., Schonberg et al. 2006; Bello et al. 2008; Kleiser et al. 2010; Kuhnt et al. 2012, 2013) are very promising to cement these techniques into the clinical setup in the very new future. For instance, more recent works have applied DTI-based fiber tracking in intraoperative glioma surgery (Kuhnt et al. 2012).

2.1.5 MR Spectroscopy

In vivo proton (¹H)-MR spectroscopy (MRS) visualizes signals from carbon-bound, non-exchangeable protons, showing the highest information density in the spectral region from 1 to 5 ppm (Trabesinger et al. 2003). Principal metabolites detected by MRS include the neuronal marker *N*-acetylaspartate as an indirect expression of the integrity of neurons, choline-containing compounds (such as metabolites involved in phospholipid membrane synthesis) as markers for glial activity, creatine (including phosphocreatine) as a marker for energy metabolism, and lactate as

an indicator for anaerobic glycolysis detected under pathologic conditions. For data acquisition, there are single-voxel and multiple-voxel techniques, depending on the information required. If applied in a larger area of expected signal alteration, the latter would be preferable as a screening for abnormalities in different locations within a bigger region (Barker 2005).

In the presurgical diagnostics of epilepsy surgery, MRS has shown to have additional potential to be used in imaging protocols for the presurgical evaluation of non-lesional frontal lobe epilepsy (Guye et al. 2005) and for the assessment of the surgical outcome in patients with temporal lobe epilepsy (Antel et al. 2002). In this context, the combination of different approaches such as MRS and 3-D MRI-based measurements of regions of interests (ROIs) such as the amygdala-hippocampal volume has been found to provide complementary results in presurgical neuroimaging protocols (Cendes et al. 1997). MRS has been established as part of presurgical multimodality neuroimaging studies using various MRI-based techniques and PET in patients with non-lesional unilateral temporal lobe epilepsy (Knowlton et al. 1997) and also in the in vivo analysis of metabolic disturbances associated with partial epilepsy (Knowlton 2004).

MRS may be used in the diagnostics of brain tumors for the identification of regions of viable tumor, investigation of the tumor extent, and monitoring of the effectiveness of the applied therapy (Vigneron et al. 2001). Consecutively, MRS has now been integrated into presurgical mapping protocols for glioma surgery to indicate the degree of tumor invasion by the co-registration of the metabolic maps derived from MRS postprocessing onto the anatomical 3-D MRI data set for its use in neuronavigation/frameless stereotaxy systems (Ganslandt et al. 2005). In this study, the stereotactic biopsies were acquired by the use of the spectral data, and the tumor areas as defined by the metabolic maps and as histopathologically confirmed by biopsy exceeded the T2-weighted signal change on conventional MRI in all seven cases investigated. The authors concluded that MRS may be useful for a more accurate definition of the tumor infiltration zone in glioma surgery than conventional anatomical MRI alone. Furthermore, a combination of MRS with functional landmarks obtained from fMRI is possible to increase the sensitivity for the assessment of tumor borders and the localization of functionally eloquent areas. Furthermore, intraoperative high-field MRI with integrated microscope-based neuronavigation enables the acquisition of MRS also during the surgical procedure for immediate intraoperative update and control (Nimsky et al. 2005a).

Recently, the application of MRS in a multimodal setup with MRI volumetry, EEG, PET, and SPECT has been reported in epilepsy (Cendes 2013) as well as in glioma surgery (Shang et al. 2012).

2.2 Combination of MRI and Nuclear Medicine

2.2.1 Principles of PET/CT, PET/MRI, and SPECT/CT

The integration of PET/CT, PET/MRI, and SPECT/CT in combination into presurgical multimodal functional neuroimaging allows the augmentation of a quantitative information of regionally disturbed brain function or regional tumor metabolism into the common framework of image analysis and display, depending on the radiopharmaceutical used for the imaging study. In general, PET and SPECT generate images of the regional and temporal distribution of a radiolabeled pharmaceutical after IV injection. Integrated scanner designs allow for sequential or simultaneous acquisition of PET and SPECT data, respectively, with CT scanning and, more recently, with simultaneous MRI as well. For SPECT, pharmaceuticals are usually labeled with the photon emitters ^{99m}Tc or ^{123}I , which, due to their radiochemical properties and half-life of 6 and 13 h, respectively, require either a daily on-site preparation of the radiopharmaceuticals or a delivery from a regional provider. The positron emitters needed for PET, however, have half-lives ranging from 2 h (^{18}F) to 2 min (^{15}O) which implies that for all preparations of radiopharmaceuticals apart from the ^{18}F -labeled compounds, a local cyclotron facility is mandatory. Image resolution depends on the technique and instrumentation used, ranging from a physical resolution of 10–15 mm full width at half maximum (FWHM) for SPECT to 3 mm FWHM for PET/CT in high-resolution techniques. For SPECT, image resolution directly correlates with the distance between the detector and the patient's head. Further, the number of detectors used (single-headed cameras versus triple-headed cameras) markedly improves image quality as well. From a technical point of view, there is no doubt that, whenever possible, PET should be preferred to SPECT and that when not available, SPECT using triple-headed cameras should be preferred to SPECT using a double-headed camera.

Recent publications allude to a promising wide range of SPECT application in the research of epilepsy (Kumar and Chugani 2013; Hagiwara et al. 2013; Elwan et al. 2014).

2.2.2 Radiopharmaceuticals, Their Applications, and Clinical Indications for Combined MRI and Nuclear Medicine Imaging

^{99m}Tc -d,l-Hexamethylene-propylenamin-oxime (^{99m}Tc -HMPAO) and ^{99m}Tc -ethyl-cysteinate-dimer (^{99m}Tc -ECD) are lipophilic molecules with a high first-pass extraction and near-total intracranial retention, used for the depiction of regional blood flow. As these tracers are trapped within the perfused cortex within seconds, the time of injection and not the time of brain scanning determines the measured perfusion state which makes these two tracers ideal for ictal stud-

ies in epilepsy, where the imaging itself can be postponed to a time after seizure cessation. The sensitivity and specificity of the detection of the ictally hyperperfused epileptogenic zones is increased when using the SISCOM procedure, where an interictal SPECT perfusion scan using HMPAO-SPECT or ECD-SPECT is subtracted from a strictly ictally injected perfusion scan and consequently co-registered to a 3-D MRI image set (O'Brien et al. 2004). The combination of SISCOM with voxel-based analysis from MRI has been shown to further improve the detection of temporal and extratemporal epileptogenic lesions (Wiest et al. 2005; Matsuda et al. 2009; Kimura et al. 2012) (Fig. 5).

In addition, ^{123}I -iomazenil, a selective antagonist for the central GABA-A-benzodiazepine-receptor complex is used for presurgical epilepsy diagnostics (Kaneko et al. 2006) and ^{123}I -tyrosine, an amino acid tracer, is used for the depiction of the amino acid metabolism of tumors (cf. Juengling and Kassubek 2002; Kassubek and Juengling 2002 for reviews).

^{18}F -Fluorodeoxyglucose (FDG), the most commonly used PET radiopharmaceutical, is a glucose analog actively transported into the cell compartment by the glucose transporter GT-1 and then metabolically trapped within the cell. Tumor cells express more glucose transporters on their cell membrane than normal cells and are usually characterized by an increased demand in glucose. Furthermore, brain tumors show an increased uptake of FDG in contrast to normal tissue. As normal cortical FDG uptake is already high, co-registration with a 3-D MRI data set is mandatory to differentiate tumor uptake from cortical uptake, whenever integrated PET/MRI scanning is not available. An increased FDG uptake may also occur due to locally increased cell density or increased neuronal activity during the uptake period (usually 60–90 min). Decreased FDG uptake is associated with regional neuronal dysfunction. Consequently, FDG-PET may also delineate peritumoral neuronal dysfunction as the interictal area of regional functional deficit in epilepsy. FDG-PET has been demonstrated to indicate the metabolically most demanding tumor part and thus the most informative location for taking a biopsy which therefore may increase the probability of a proper biopsy sample (Levivier et al. 1995; Goldman et al. 1997; Pirotte et al. 2003). In epilepsy surgery, changes in focal FDG-PET uptake (regional decreases) allude to the localization of cortical abnormalities (Muzik et al. 2005).

^{18}F -Ethyl-tyrosine and ^{18}F -tyrosine (FET/F-TYR) are radio-labeled amino acids with the same physical half-life as FDG, developed as substitutes for ^{11}C -methionine (MET), the most commonly used amino acid tracer with a physical half-life of 20 min. FET, F-TYR, and MET show a very low uptake in the normal brain, while they are avidly taken up by gliomas of any grade. Their uptake is mainly mediated by the L-type amino acid transporter system at the blood-brain barrier (BBB). Therefore, increased uptake is typical even in low-grade gliomas in the absence of a BBB disruption, which is a substantial

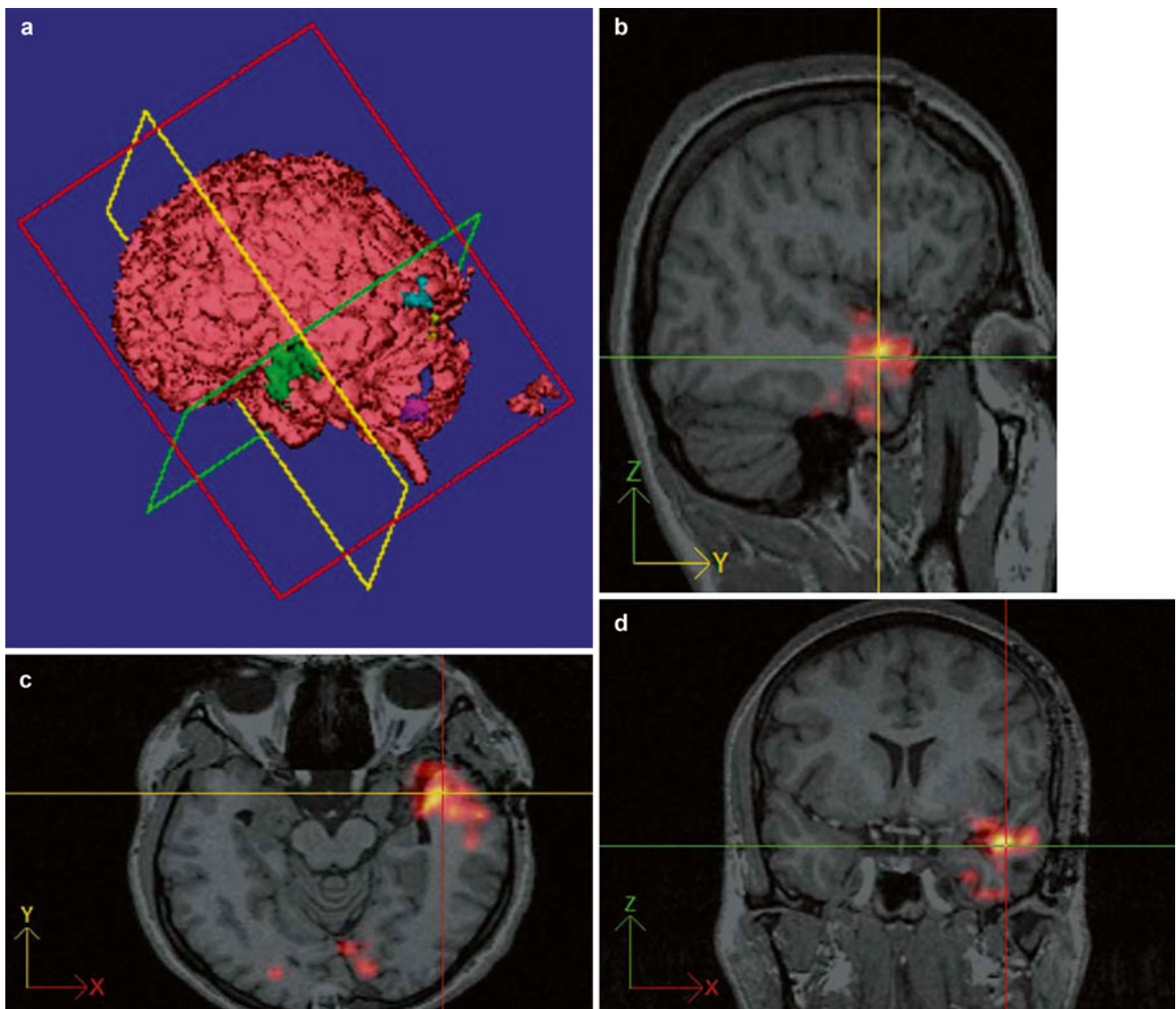


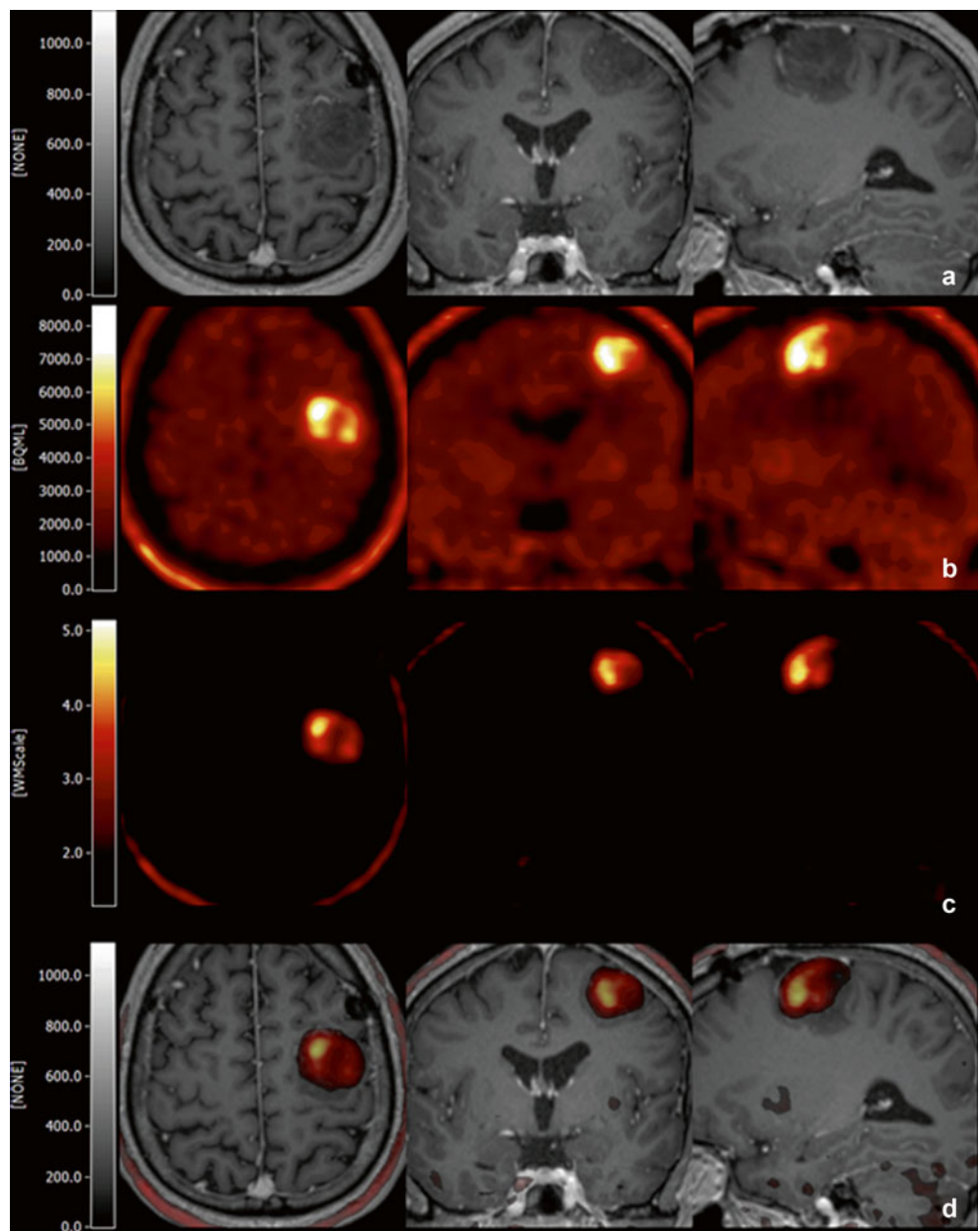
Fig. 5 (a–d) Presurgical activation map of ictally hyperperfused brain areas (using the SISCOM procedure and ^{99m}Tc ECD for the SPECT scan) in a patient with left temporal seizures scheduled for epilepsy surgery. Activated brain areas (a) (i.e., perfusion differs more than two

standard deviations from the mean difference) are projected onto the co-registered 3-D MRI data set in the sagittal (c), coronal (d), and transverse (b) planes as well as on a surface reconstruction (Images by F.D. Juengling, MD)

advantage over contrast-enhanced CT or MRI. In contrast-enhancing gliomas, the spatial extent of the increased MET uptake is larger than that of the contrast enhancement (Ericson et al. 1985; Ogawa et al. 1993) and may include not only solid tumor portions but also their surrounding, probably reflecting tumor infiltration. There is also a close correlation with tumor vessel density (Kracht et al. 2003) and prognosis (Ribom et al. 2001). In a series of 89 low-grade gliomas, MET uptake was a significant survival factor among patients with astrocytomas and oligodendroglomas (Ribom et al. 2001). These results suggest that MET uptake (or FET/F-TYR-Uptake) should be evaluated with respect to therapeutic response as tumor resection seems to be a favorable prognostic factor in patients with a high MET uptake but not in patients with a low uptake.

Herholz et al. showed the sensitivity and specificity of MET-PET in the differentiation between non-tumoral tissue and low-grade gliomas to be 76 and 87 %, respectively (Herholz et al. 1998). Comparative analyses between CT, MRI, MET-PET, and stereotactic biopsies have suggested that MET-PET has a greater accuracy in defining the extent of gliomas than CT or MRI alone (Bergstrom et al. 1983; Braun et al. 2002; Mosskin et al. 1989; Ogawa et al. 1993). To improve intraoperative tumor delineation, fused images of FET/FMT/MET-PET and contrast-enhanced MRI have been integrated into neuronavigation systems such as the Zeiss MKM system (Braun et al. 2002) or the BrainLab Vector Vision system (Grosu et al. 2003; Cizek et al. 2004; Vollmar 2006). In a matched comparison of presurgical MET-PET

Fig. 6 (a–d) Example of presurgical multimodality imaging in a patient with a glioblastoma multiforme. T1-weighted MRI (a), fused with the tumor-normalized MET-PET/CT (d) within VINCI (Vollmar et al. 2004). The full range MET-PET is shown in b, and the MET-PET normalized to white matter in (c) (Images by F.D. Juengling, MD)



with stereotactic histopathology, it has been shown that MET-PET can delineate solid parts of brain tumors as well as the surrounding infiltration area with a high sensitivity and specificity, if global maxima are normalized to contralateral normal brain tissue and thresholded at a value of 1.3-fold uptake of contralateral normal brain tissue (Kracht et al. 2004). Suitable tumor normalization and thresholding methods have been implemented since then, e.g. via a dedicated visualization tool called “VINCI” (Vollmar et al. 2004) (Fig. 6).

In Cushing disease, where determination of the exact localization of an ACTH-secreting macro- or microadenoma of the pituitary gland is essential for the cure of this otherwise potentially fatal disease, MR imaging is often unsatisfactory missing up to 60 % of surgically removed microadenomas. Even in combination with superselective

cavernous sinus sampling, localization of a microadenoma may fail. Presumably due to a higher cellularity and secretory activity, corticotroph adenoma presents with a higher MET uptake than the normal pituitary tissue, resulting in higher sensitivity for the localization and delineation of a Cushing adenoma as compared to high-resolution 3 T-MRI (including dynamic techniques) or CT scanning alone (Ikeda et al. 2010). This has induced to use MET-PET for surgical planning in specialized centers (Fig. 7).

^{18}F -DOPA is a fluorinated form of L-DOPA and primarily used to measure the aromatic amino acid decarboxylase activity in monoaminergic neurons of the presynaptic pathways in movement disorders. It has gained attention for imaging newly diagnosed or recurrent brain tumors with similar physical properties as ^{11}C -methionine (Becherer et al.

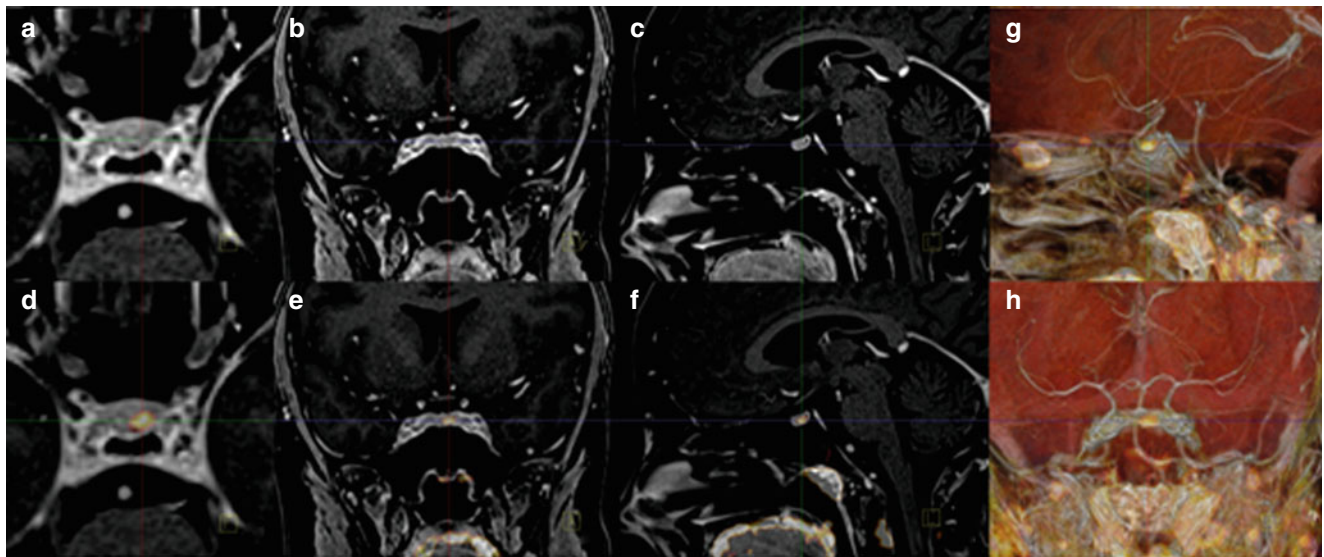


Fig. 7 (a–h) T1-weighted MRI of a patient with a Cushing microadenoma (a–c) fused with MET-PET/CT (d–h). Please note the excellent localization of the microadenoma as visualized by MET-PET/CT,

co-registered to MRI, and confirmed by clinical remission after surgery (Images by F.D. Juengling)

2003). It could be shown that the ¹⁸F-DOPA uptake in human astrocytomas is mediated by the L-type amino acid transporters 1 and 2 (LAT1/LAT2) (Youland et al. 2013) and can thus be used as an alternative radiotracer for FET, F-TYR, and MET. In a direct comparison, ¹⁸F-DOPA has demonstrated higher contrast ratios over FET for lesions outside the striatum (Kratochwil et al. 2014), which was most pronounced in low-grade gliomas, and thus might be superior to FET for the preoperative delineation of tumor borders. Additionally, ¹⁸F-DOPA has proven capabilities for the differentiation between progressive brain metastases from late or delayed radiation injury (Lizarraga et al. 2014).

¹⁵O-H₂O (physical half-life 2 min) is the most frequently used CBF tracer for PET, applied for functional activation (fPET) and allowing up to 12 quantitative measurements of CBF. Compared to fMRI, fPET provides a more physiologically specific and robust signal (Herholz et al. 1997; Kaplan et al. 1999; Krings et al. 2001; Vinas et al. 1997). An essential advantage of fPET over fMRI may be the clinical application in language activation studies, where active speaking during language production tasks does not induce technical artifacts (as is common with fMRI), and therefore a direct monitoring of task performance is possible even in functionally impaired subjects (Thiel et al. 1998). However, more recent advanced fMRI language mapping protocols might in the meantime overcome this problem, thus equalizing the described advantage of fPET.

¹⁸F-Flumazenil and ¹¹C-flumazenil (FMZ) are selective antagonists for the GABA-A-benzodiazepine-receptor complex and are mainly used for the detection of epileptogenic areas. It has been demonstrated that FMZ binding is reduced in epileptogenic foci which is probably rather due to a

decrease in the affinity of the tracer to the receptor than to a reduction in receptor density alone. Foci of reduced FMZ binding may be found with a high sensitivity of up to 94 % in patients with temporal lobe epilepsy (Ryvlin et al. 1998). As the area of focally decreased FMZ binding may probably indicate the epileptogenic zone that has to be resected to become seizure-free (Muzik et al. 2000; Juhasz et al. 2001), the need for the integration of FMZ into a multimodal approach for the facilitation of the resection of the epileptic zone becomes obvious. The co-registration of PET/CT and SPECT/CT findings to a volumetric MR image or the simultaneous acquisition of PET and MRI (PET/MRI) and their incorporation into an image-guided system has allowed surgeons to offer surgery to patients who may previously not have been considered eligible, with outcomes comparable to those obtained from patients with more straightforward epileptic lesions (Murphy et al. 2004).

¹¹C-Alpha-methyl-tryptophane (AMT) is a marker of the serotonin synthesis capacity, and its uptake is elevated in tuberous sclerosis (Chugani et al. 1998). In the latter, the multiplicity of tubers precludes the resection of the whole potentially epileptogenic tissue, and no MRI technique has proven to be able to differentiate epileptogenic from non-epileptogenic tubers, yet. Recent work has shown that AMT-PET may specifically detect epileptogenic tubers in tuberous sclerosis (Asano et al. 2000), in particular within a multimodality imaging approach (including video-EEG monitoring, FDG-PET, and different MRI techniques), and may even be helpful in the detection of cortical dysplasia (Juhasz et al. 2003). AMT-PET may contribute to the pre-surgical planning with invasive electroencephalography by determining the localization and extent of the implanta-

tion of the grid electrodes and consecutively by defining the resection volume. There are data suggesting that AMT-PET is able to detect non-resected epileptic foci in patients with previously failed neocortical resection and to improve outcome after reoperation of AMT positive tissue (Juhasz et al. 2004). Based on surgical outcome data, resection of tubera with increased AMT uptake yielded an optimal accuracy of 83 % for the detection of tubers that needed to be resected to achieve a seizure-free outcome. These findings suggest that presurgical multimodal imaging for the resection of tubers with increased AMT uptake is highly desirable to achieve a seizure-free surgical outcome in children with tuberous sclerosis and intractable epilepsy (Kagawa et al. 2005). One major drawback, however, is that the radiosynthesis of AMT is complicated, so that its use is still restricted to specialized PET centers.

In summary, the application of PET/CT in the presurgical planning in epilepsy is well documented (Nooraine et al. 2013; Vivash et al. 2013; Kumar and Chugani 2013). Up-to-date data suggest that PET and MEG might be complementary and in combination yield increased sensitivity and specificity as compared to each technique applied on its own. For a review of the current knowledge concerning the usefulness of PET/CT and MEG for the presurgical assessment of MRI-negative epilepsy and the discussion of the impact of the combination of the results on the local seizure onset zone, see Rheims et al. (2013).

In presurgical planning of tumor resection, multimodal approaches using ¹⁸F-fluoroethyl-L-tyrosine PET/CT in combination with DTI for the detection of tumor invasion into the pyramidal tract in glioma patients with sensorimotor deficits (Stadlbauer et al. 2009) have been suggested.

Analyses from PET-guided resection of supratentorial high-grade gliomas have suggested a significantly better survival in patients with PET-guided volumetric resection and no postoperative residual tracer uptake as compared to MRI-guided volumetric resection with no residual postoperative contrast enhancement (Pirotte et al. 2009).

Additionally, in patients with central Cushing disease, ¹¹C-methionine or ¹⁸F-tyrosine PET/CT co-registered to MRI has shown to significantly increase the accuracy of the presurgical localization and delineation of pituitary microadenomas.

2.3 Combination of MRI and MEG (MSI)/ EEG

Magnetoencephalography (MEG) is an analysis technique which uses electromagnetic signals to localize the source of biomagnetic fields derived from intracellular electric current flows in the brain, thus providing direct information about neural activity (Hamalainen et al. 1993). One of the most important advantages of MEG is that its temporal resolution is very high (i.e., in the order of 1 ms) and is mainly

restricted only by the sampling frequency of the recording system (Lounasmaa et al. 1996). Since magnetic fields are not distorted by conduction inhomogeneities in the head, MEG is a potentially powerful tool for the localization of brain function, providing a spatial discrimination below 5 mm. As a major limitation, MEG has a fundamental source identification problem (inverse problem), by determining the active site within the brain from the magnetic field pattern recorded outside the skull. Thus, some a priori assumptions must be made about the source. Usually, signal generators in the brain are described as current dipoles which are physiologically reasonable models for relatively small active cortical areas. MEG results can be directly co-registered to 3-D MRI. The merging of the data obtained from MEG with anatomical MRI images, i.e., magnetic source imaging (MSI), allows the integration of the functional information as obtained from MEG into the structural information of MR (Orrison 1999).

MEG is still a rarely used technique due to its complex and cost-intensive technology. However, the potential of MSI for the presurgical mapping of functionally important cortex has been extensively demonstrated. MSI can be used for decision-making and surgical treatment planning in brain lesions (in particular tumors) in order to minimize the risk of postoperative deficits (Ganslandt et al. 2002). Its most frequently used application is in motor evoked and somatosensory evoked fields for the mapping of sensorimotor cortex in patients with lesions around the motor cortex (Hund et al. 1997; Ganslandt et al. 1997, 1999) (Fig. 8). Furthermore, the determination of the primary visual cortex by the investigation of visual evoked fields has also been reported (Ganslandt et al. 2004). For these purposes, the single equivalent dipole model is usually sufficient for MEG data analysis. In more complex tasks such as those intended for language lateralization and localization, more differentiated models have to be applied for source localization to simultaneously separate the multiple sources of activity from each other. Nevertheless, MSI has been successfully used for the identification of the speech-dominant hemisphere and the functional mapping of speech-related brain areas (primary language areas) in individuals (Kober et al. 2001a).

MEG has the additional advantage of providing supplementary information to epilepsy surgery: beyond the presurgical identification of eloquent cortex (Ossenblok et al. 2003), MEG has the potential to directly detect and localize epilepsy-associated activity (epileptic discharges), like EEG. That way, MSI can be applied for the presurgical evaluation in epilepsy surgery to identify the brain tissue generating epileptic activity (Fischer et al. 2005). Here, it has been described to be an appropriate technique for temporal lobe epilepsy and even for extratemporal epilepsies (Stefan et al. 2003). Furthermore, interictal spike localization on MEG/MSI has been found to be consistent with ictal and, where relevant, functional localization of somatosensory mapping (Tang et al. 2003). The application of clinical MEG/MSI is mainly focused on the

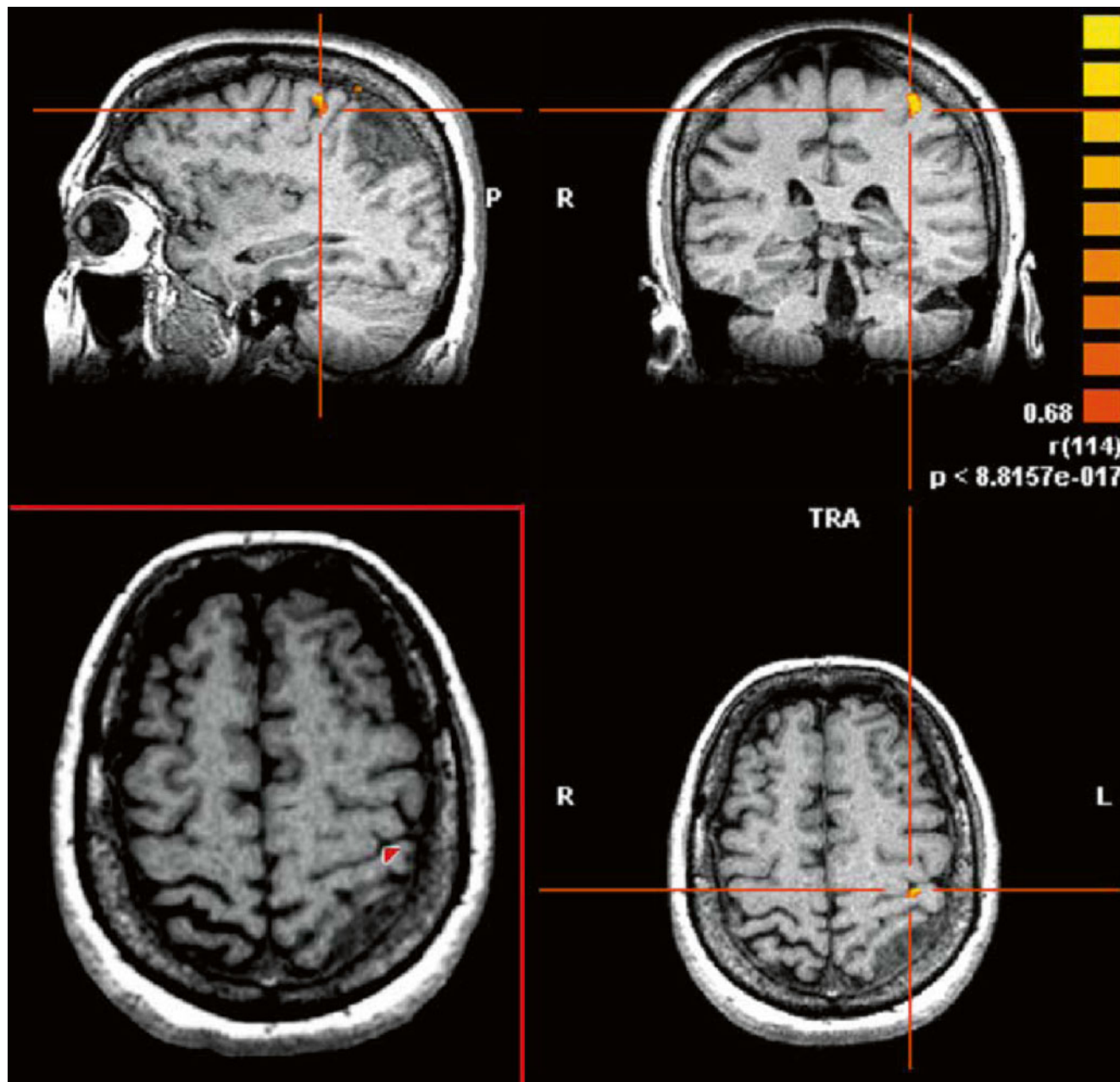


Fig. 8 Presurgical fMRI (central sulcus) (*upper row and lower row, right*: sagittal, coronal, and axial view of the center of activation) and MSI (somatosensory evoked fields) in a patient with a glioma (Images

courtesy of Prof. Dr. Oliver Ganslandt, Dept. of Neurosurgery, University of Erlangen, Germany, with kind permission)

presurgical localization of the epileptogenic zone and eloquent cortex in candidates for epilepsy surgery, including in patients with Landau-Kleffner syndrome. However, MEG/MSI co-registered with fMRI is also an excellent noninvasive tool for the examination of the epileptic source distribution in childhood epilepsy syndromes and epileptic encephalopathies (Paetau and Mohamed 2013). The use of MEG in the presurgical evaluation of refractory insular epilepsy has recently been reported by Mohamed and coworkers (2013).

With respect to the multimodality approach, combined MEG and EEG acquisition and postprocessing can identify subcompartments of the temporal lobe involved in epileptic activity and may be helpful to differentiate between different subtypes of mesial temporal lobe epilepsy noninvasively (Patarraia et al. 2005). In a further study, MEG and video-EEG results were equivalent in one-third of cases, and additional localization information was obtained using MEG in 40 % of the patients. The authors found MEG to be most

useful for presurgical planning in patients who have either partially or nonlocalizing video-EEG results (Pataraia et al. 2004). Although aspects of this study have been criticized, it has to be admitted that MSI is a further noninvasive tool that, when used in conjunction with other techniques applied for presurgical evaluation, can increase the clinician's confidence for the determination of the accurate localization in epilepsy surgery and may reduce the need of invasive intracranial monitoring (Marks 2004).

In general, a combination of techniques with basically different underlying neurophysiological correlates such as MEG/MSI and fMRI is very promising. Spatial comparisons between MSI and fMRI for the local identification particularly of the sensorimotor cortex have been performed by comparing the activation sites between MEG and fMRI after co-registration and by overlaying the data onto the same anatomical 3-D MRI set, both in healthy subjects (Stippich et al. 1998) and in patients (Kober et al. 2001b). In both studies, the MSI and fMRI localization results were in agreement with respect to the localized gyrus. However, they showed different activation sites for the motor and sensory tasks with a distance mismatch of 10 and 15 mm, probably reflecting the correlation between electrophysiological and hemodynamic responses. In a validation study on the same group of patients, the MSI results were compared with the intraoperative cortical recording of somatosensory evoked potentials (so-called phase reversal), and the localizations (incorporating the distance mismatch) in the pre- and postcentral gyrus were verified in each case (Ganslandt et al. 1997).

Thus, although both modalities, MSI and fMRI, are useful for the estimation of the sensorimotor cortex, a single modality may not be accurate enough of the exact topographical identification, and if possible, a combination of both methods should be used in order to avoid neurological deficits in certain unclear cases (Kober et al. 2001b). Consecutively, the value of the integration of these two imaging modalities for the spatiotemporal mapping of brain activity has been strengthened in several studies (Dale and Halgren 2001) and has led to the co-integration of both techniques into presurgical protocols in specialized centers (Ganslandt et al. 2002), especially in candidates of epilepsy surgery (Assaf et al. 2004; Duffner et al. 2003; Knake et al. 2004).

It is useful to perform the postprocessing of MEG and fMRI data with the same software to avoid potential methodologically based problems, as previously suggested (Dale et al. 2000). The integration of fMRI, 3-D MRI, and MSI in one unique coordinate frame allows the activation achieved by fMRI analysis to be used as possible sites of current sources for MEG source reconstruction (MSI) as an elegant approach for multimodality integration (Müller et al. 2005) (Fig. 9).

Finally, with respect to the multimodal presurgical concept, the combination of MEG/MSI with functional MRS

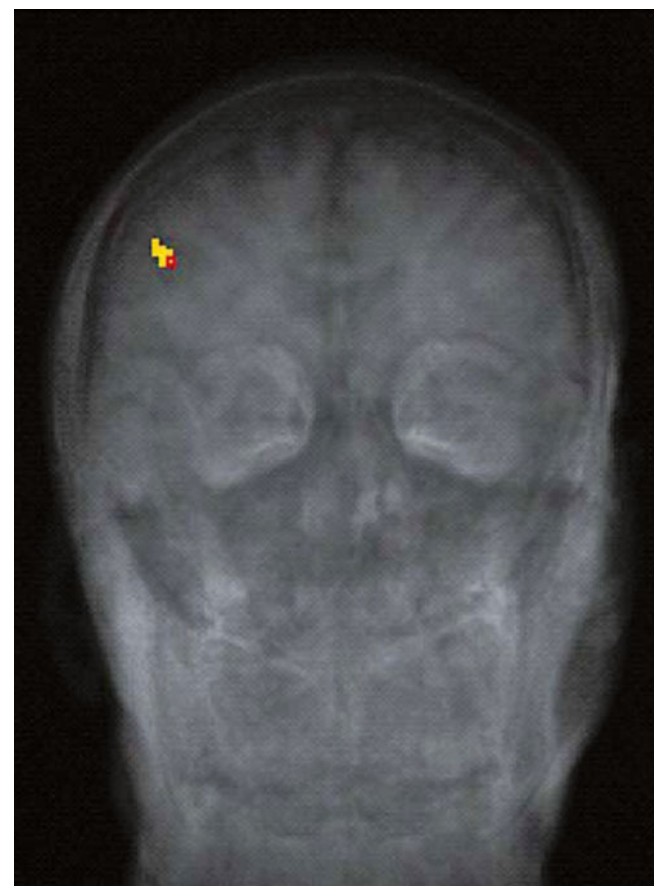


Fig. 9 FMRI and MSI colocalization (*motor paradigm*) within one unique coordinate frame in a coronal projectional view (Müller et al. 2005). Yellow clusters of fMRI activation are used as possible sites of current sources for MEG source reconstruction (red dipole)

may provide information about the metabolic, hemodynamic, and electrical activity of the brain and also be useful for the verification of one imaging modality by the other ones (Ramon et al. 2004).

3 Advantages and Limitations of Multimodal Functional Neuroimaging

The combination of different noninvasive neuroimaging tools and their co-integration into frameless stereotaxy/neuronavigational systems after registration is an important and valuable element for presurgical diagnostics. Here, various technical approaches such as task-based fMRI and MSI techniques, DTI, ifc-MRI, MRS, as well as PET/CT, PET/MRI, and SPECT/CT, have been reviewed, and options of useful combinations have been described. It has to be kept in mind that additional techniques exist such as (multichannel) EEG which is a major presurgical diagnostic element for epilepsy surgery. However, the latter is rarely used for direct source

co-registration with MRI and neuronavigation and has therefore not been discussed in this chapter, although in particular the spatiotemporal relationship between MSI and EEG for the epileptic focus localization (Leijten et al. 2003) and the combination of EEG with fMRI (Lantz et al. 2001) have been subject to several studies. Furthermore, also functional transcranial magnetic stimulation might provide additional presurgical information as well (Najib et al. 2011).

The use of functional neuronavigation has been shown to be a safe and reliable instrument (Winkler et al. 2004), in particular in lesions which are difficult to delineate or which are located adjacent to functionally important areas. Of course, the presurgically acquired data reflect only the situation before initiation of the intervention and may change intraoperatively, causing differences between preoperatively acquired neuroimaging results and on-site findings during surgery. The surgeon has to be aware of this – alternatively, there are solutions for real-time imaging, e.g., by the advanced but expensive implementation of intraoperative open MRI systems (Nimsky et al. 2004, 2005a, d), either as low-field or as high-field (1.5 Tesla) systems. Furthermore, inherent sources of error require continuous critical reevaluation, i.e., for the accurateness of the localization process itself and postprocessing algorithms.

With respect to cost-effectiveness and the burden of often time-consuming data acquisition procedures in critically ill patients, multimodality presurgical imaging does not necessarily mean “the more, the better.” Some options are complementary, such as the techniques for the localization of eloquent cortex (fMRI or MSI) and DTI for the imaging of white matter fiber bundles. Among the available imaging methods for the assessment of cortical areas, fMRI can be performed on most regular clinical MRI scanners, whereas MSI, although appearing a promising technique, is still limited due to the low distribution of MEG devices. Nuclear medicine techniques in terms of (multi-)ligand function-targeted imaging are valuable tools for the delineation of cerebral neoplasms and may be complemented by MRS. Therefore, depending on the information which is imperatively needed preoperatively for each individual patient, the clinician may choose from the available techniques. If different neuroimaging modalities are used, it has to be kept in mind that the fusion of the results of these techniques is only possible after co-registration but that equivalent co-localizations in respect to the “ideal neuroanatomy” are very difficult to achieve and sometimes impossible due to the different neurophysiological substrates, acquisition methods, and spatial resolution.

In summary, the variety of different neuroimaging options for presurgical imaging offers wide opportunities for the combination of MRI-based techniques (functional techniques, fMRI; functional connectivity techniques, ifcMRI; structural diffusion-mapping techniques, DTI) with radionuclide techniques (PET or SPECT), in order to obtain detailed information of anatomic structures and function in the

lesioned brain both preoperatively (e.g., Dimou et al. 2013) and intraoperatively (e.g., Kuhnt et al. 2012).

References

- Antel SB, Li LM, Cendes F, Collins DL, Kearney RE, Shinghal R, Arnold DL (2002) Predicting surgical outcome in temporal lobe epilepsy patients using MRI and MRSI. *Neurology* 58:1505–1512
- Asano E, Chugani DC, Muzik O, Shen C, Juhasz C, Janisse J, Ager J, Canady A, Shah JR, Shah AK, Watson C, Chugani HT (2000) Multimodality imaging for improved detection of epileptogenic foci in tuberous sclerosis complex. *Neurology* 54:1976–1984
- Ashburner J, Csernansky JG, Davatzikos C, Fox NC, Frisoni GB, Thompson PM (2003) Computer-assisted imaging to assess brain structure in healthy and diseased brains. *Lancet Neurol* 2:79–88
- Assaf BA, Karkar KM, Laxer KD, Garcia PA, Austin EJ, Barbaro NM, Aminoff MJ (2004) Magnetoencephalography source localization and surgical outcome in temporal lobe epilepsy. *Clin Neurophysiol* 115:2066–2076
- Barker PB (2005) Fundamentals of MR spectroscopy. In: Gillard J, Waldman A, Barker P (eds) *Clinical MR neuroimaging*, vol 7. Cambridge University Press, Cambridge, p 26
- Basser PJ, Jones DK (2002) Diffusion-tensor MRI: theory, experimental design and data analysis – a technical review. *NMR Biomed* 15: 456–467
- Becherer A, Karanikas G, Szabó M, Zettinig G, Asenbaum S, Marosi C, Henk C, Wunderbaldinger P, Czech T, Wadsak W, Kletter K (2003) Brain tumour imaging with PET: a comparison between [¹⁸F]fluorodopa and [¹¹C]methionine. *Eur J Nucl Med Mol Imaging* 30:1561–1567
- Bello L, Gambini A, Castellano A, Carrabba G, Acerbi F, Fava E, Giussani C, Cadioli M, Blasi V, Casarotti A, Papagno C, Gupta AK, Gaini S, Scotti G, Falini A (2008) Motor and language DTI fiber tracking combined with intraoperative subcortical mapping for surgical removal of gliomas. *Neuroimage* 39:369–382
- Bergstrom M, Collins VP, Ehrin E, Ericson K, Eriksson L, Greitz T, Halldin C, von Holst H, Langstrom B, Lilja A (1983) Discrepancies in brain tumor extent as shown by computed tomography and positron emission tomography using [⁶⁸Ga]EDTA, [¹¹C]glucose, and [¹¹C]methionine. *J Comput Assist Tomogr* 7:1062–1066
- Berntsen EM, Gulati S, Solheim O, Kvistad KA, Torp SH, Selbekk T, Unsgard G, Haberg AK (2010) Functional magnetic resonance imaging and diffusion tensor tractography incorporated into an intraoperative 3-dimensional ultrasound-based neuronavigation system: impact on therapeutic strategies, extent of resection, and clinical outcome. *Neurosurgery* 67:251–264
- Braun V, Dempf S, Tomczak R, Wunderlich A, Weller R, Richter HP (2000) Functional cranial neuronavigation. Direct integration of fMRI and PET data. *J Neuroradiol* 27:157–163
- Braun V, Dempf S, Weller R, Reske SN, Schachenmayr W, Richter HP (2002) Cranial neuronavigation with direct integration of (¹¹C) methionine positron emission tomography (PET) data – results of a pilot study in 32 surgical cases. *Acta Neurochir (Wien)* 144:777–782
- Brett M, Johnsrude IS, Owen AM (2002) The problem of functional localization in the human brain. *Nat Rev Neurosci* 3:243–249
- Bucci M, Mandelli ML, Berman JI, Amirbekian B, Nguyen C, Berger MS, Henry RG (2013) Quantifying diffusion MRI tractography of the corticospinal tract in brain tumors with deterministic and probabilistic methods. *Neuroimage Clin* 3:361–368
- Castellano A, Bello L, Michelozzi C, Gallucci M, Fava E, Iadanza A, Riva M, Casaceli G, Falini A (2011) Role of diffusion tensor magnetic resonance tractography in predicting the extent of resection in glioma surgery. *Neuro Oncol* 14:192–202

- Cendes F (2013) Neuroimaging in investigation of patients with epilepsy. *Continuum (Minneapolis)* 19(3 Epilepsy):623–642
- Cendes F, Caramanos Z, Andermann F, Dubeau F, Arnold DL (1997) Proton magnetic resonance spectroscopic imaging and magnetic resonance imaging volumetry in the lateralization of temporal lobe epilepsy: a series of 100 patients. *Ann Neurol* 42:737–746
- Chugani DC, Chugani HT, Muzik O, Shah JR, Shah AK, Canady A, Mangner TJ, Chakraborty PK (1998) Imaging epileptogenic tubers in children with tuberous sclerosis complex using alpha-[11C]methyl-L-tryptophan positron emission tomography. *Ann Neurol* 44:858–866
- Cizek J, Herholz K, Vollmar S, Klein J, Schrader R, Heiss WD (2004) Fast and robust registration of PET and MR images. *Neuroimage* 22:434–442
- Clark CA, Barrick TR, Murphy MM, Bell BA (2003) White matter fiber tracking in patients with space-occupying lesions of the brain: a new technique for neurosurgical planning? *Neuroimage* 20:1601–1608
- Coenen VA, Huber KK, Krings T, Weidemann J, Gilsbach JM, Rohde V (2005) Diffusion-weighted imaging-guided resection of intracerebral lesions involving the optic radiation. *Neurosurg Rev* 28:188–195
- Cross JH (2003) Functional neuroimaging of malformations of cortical development. *Epileptic Disord* 5(2):S73–S80
- Dale AM, Halgren E (2001) Spatiotemporal mapping of brain activity by integration of multiple imaging modalities. *Curr Opin Neurobiol* 11:202–208
- Dale AM, Liu AK, Fischl BR, Buckner RL, Belliveau JW, Lewine JD, Halgren E (2000) Dynamic statistical parametric mapping: combining fMRI and MEG for high resolution imaging of cortical activity. *Neuron* 26:55–67
- Dimou S, Battisti RA, Hermens DF, Lagopoulos J (2013) A systematic review of functional magnetic resonance imaging and diffusion tensor imaging modalities used in presurgical planning of brain tumour resection. *Neurosurg Rev* 36:205–214
- Due-Tonnessen P, Rasmussen I, Berntsen EM, Bjørnerud A, Emblem KE (2014) Identifying the central sulcus in patients with intra-axial lesions: a multicenter study comparing conventional presurgical MRI to topographical analysis and BOLD-fMRI. *J Comput Assist Tomogr* 38:1–8
- Duffner F, Freudentstein D, Schiffbauer H, Preissl H, Siekmann R, Birbaumer N, Grote EH (2003) Combining MEG and MRI with neuronavigation for treatment of an epileptiform spike focus in the precentral region: a technical case report. *Surg Neurol* 59:40–45
- Elwan SA, Wu G, Huang SS, Najm IM, So NK (2014) Ictal single photon emission computed tomography in epileptic auras. *Epilepsia* 55:133–136
- Ericson K, Lilja A, Bergstrom M, Collins VP, Eriksson L, Ehrin E, von Holst H, Lundqvist H, Langstrom BB, Mosskin M (1985) Positron emission tomography with ([11C]methyl)-L-methionine, [11C]d-GLUCOSE, and [68Ga]EDTA in supratentorial tumors. *J Comput Assist Tomogr* 9:683–689
- Ferda J, Kastner J, Mukensnabl P, Choc M, Horemuzová J, Ferdová E, Kreuzberg B (2010) Diffusion tensor magnetic resonance imaging of glial brain tumors. *Eur J Radiol* 74:428–436
- Fernandez-Miranda JC, Pathak S, Engh J, Jarbo K, Verstynen T, Yeh FC, Wang Y, Mintz A, Boada F, Schneider W, Friedlander R (2012) High-definition fiber tractography of the human brain: neuroanatomical validation and neurosurgical applications. *Neurosurgery* 71:430–453
- Fischer MJ, Scheler G, Stefan H (2005) Utilization of magnetoencephalography results to obtain favourable outcomes in epilepsy surgery. *Brain* 128:153–157
- Ganslandt O, Steinmeier R, Kober H, Vieth J, Kassubek J, Romstock J, Strauss C, Fahlbusch R (1997) Magnetic source imaging combined with image-guided frameless stereotaxy: a new method in surgery around the motor strip. *Neurosurgery* 41:621–627
- Ganslandt O, Fahlbusch R, Nimsky C, Kober H, Moller M, Steinmeier R, Romstock J, Vieth J (1999) Functional neuronavigation with magnetoencephalography: outcome in 50 patients with lesions around the motor cortex. *J Neurosurg* 91:73–79
- Ganslandt O, Fahlbusch R, Kober H, Gralla J, Nimsky C (2002) Use of magnetoencephalography and functional neuronavigation in planning and surgery of brain tumors. *Nervenarzt* 73:155–161
- Ganslandt O, Buchfelder M, Hastreiter P, Grummich P, Fahlbusch R, Nimsky C (2004) Magnetic source imaging supports clinical decision making in glioma patients. *Clin Neurol Neurosurg* 107:20–26
- Ganslandt O, Stadlbauer A, Fahlbusch R, Kamada K, Buslei R, Blumcke I, Moser E, Nimsky C (2005) Proton magnetic resonance spectroscopic imaging integrated into image-guided surgery: correlation to standard magnetic resonance imaging and tumor cell density. *Neurosurgery* 56(Suppl):291–298
- Goldman S, Levivier M, Pirotte B, Brucher JM, Wikler D, Damhaut P, Dethy S, Brotchi J, Hildebrand J (1997) Regional methionine and glucose uptake in high-grade gliomas: a comparative study on PET-guided stereotactic biopsy. *J Nucl Med* 38:1459–1462
- Greicius MD, Supekard K, Menon V, Dougherty RF (2009) Resting-state functional connectivity reflects structural connectivity in the default mode network. *Cereb Cortex* 19:72–78
- Grosu AL, Lachner R, Wiedenmann N, Stark S, Thamm R, Kneschaurek P, Schwaiger M, Molls M, Weber WA (2003) Validation of a method for automatic image fusion (brain-LAB system) of CT data and 11C-methionine-PET data for stereotactic radiotherapy using a LINAC: first clinical experience. *Int J Radiat Oncol Biol Phys* 56:1450–1463
- Guye M, Ranjeva JP, Le Fur Y, Bartolomei F, Confort-Gouny S, Regis J, Chauvel P, Cozzone PJ (2005) 1H-MRS imaging in intractable frontal lobe epilepsies characterized by depth electrode recording. *Neuroimage* 26:1174–1183
- Haginoya K, Uematsu M, Munakata M, Kakisaka Y, Kikuchi A, Nakayama T, Hino-Fukuyo N, Tsuburaya R, Kitamura T, Sato-Shirai I, Abe Y, Matsumoto Y, Wakusawa K, Kobayashi T, Ishitobi M, Togashi N, Iwasaki M, Nakasato N, Inuma K (2013) The usefulness of subtraction ictal SPECT and ictal near-infrared spectroscopic topography in patients with west syndrome. *Brain Dev* 35:887–893
- Hamalainen M, Hari R, Ilmoniemi RJ, Knuutila J, Lounasmaa OV (1993) Magnetoencephalography – theory, instrumentation, and applications to noninvasive studies of the working human brain. *Rev Mod Phys* 65:413–497
- Hendler T, Pianka P, Sigal M, Kafri M, Ben-Bashat D, Constantini S, Graif M, Fried I, Assaf Y (2003) Delineating gray and white matter involvement in brain lesions: three-dimensional alignment of functional magnetic resonance and diffusion-tensor imaging. *J Neurosurg* 99:1018–1027
- Herholz K, Reulen HJ, von Stockhausen HM, Thiel A, Ilmberger J, Kessler J, Eisner W, Yousry TA, Heiss WD (1997) Preoperative activation and intraoperative stimulation of language-related areas in patients with glioma. *Neurosurgery* 41:1253–1260
- Herholz K, Holzer T, Bauer B, Schroder R, Voges J, Ernestus RI, Mendoza G, Weber-Luxenburger G, Lottgen J, Thiel A, Wienhard K, Heiss WD (1998) 11C-methionine PET for differential diagnosis of low-grade gliomas. *Neurology* 50:1316–1322
- Hund M, Rezai AR, Kronberg E, Cappell J, Zonenshayn M, Ribary U, Kelly PJ, Llinas R (1997) Magnetoencephalographic mapping: basic of a new functional risk profile in the selection of patients with cortical brain lesions. *Neurosurgery* 40:936–942
- Huppertz HJ, Grimm C, Fauser S, Kassubek J, Mader I, Hochmuth A, Spreer J, Schulze-Bonhage A (2005) Enhanced visualization of blurred gray-white matter junctions in focal cortical dysplasia by voxel-based 3D MRI analysis. *Epilepsy Res* 67:35–50
- Ikeda H, Abe T, Watanabe K (2010) Usefulness of composite methionine-positron emission tomography/3.0-tesla magnetic

- resonance imaging to detect the localization and extent of early-stage Cushing adenoma. *J Neurosurg* 112:750–755
- Jacobs AH, Kracht LW, Gossman A, Ruger MA, Thomas AV, Thiel A, Herholz K (2005) Imaging in neurooncology. *NeuroRx* 2:333–347
- Jellison B, Field A, Medow J, Lazar M, Salamat M, Alexander A (2004) Diffusion tensor imaging of cerebral white matter: a pictorial review of physics, fiber tract anatomy and tumor imaging patterns. *Am J Neuroradiol* 25:356–369
- Juengling FD, Kassubek J (2002) Nuclear medicine imaging in epilepsy diagnostics – I: perfusion and metabolism. *Nervenheilkunde* 21:420–425
- Juhasz C, Chugani DC, Muzik O, Shah A, Shah J, Watson C, Canady A, Chugani HT (2001) Relationship of flumazenil and glucose PET abnormalities to neocortical epilepsy surgery outcome. *Neurology* 56:1650–1658
- Juhasz C, Chugani DC, Muzik O, Shah A, Asano E, Mangner TJ, Chakraborty PK, Sood S, Chugani HT (2003) Alpha-methyl-L-TRYPTOPHAN PET detects epileptogenic cortex in children with intractable epilepsy. *Neurology* 60:960–968
- Juhasz C, Chugani DC, Padhye UN, Muzik O, Shah A, Asano E, Mangner TJ, Chakraborty PK, Sood S, Chugani HT (2004) Evaluation with alpha-[11C]methyl-L-tryptophan positron emission tomography for reoperation after failed epilepsy surgery. *Epilepsia* 45:124–130
- Kagawa K, Chugani DC, Asano E, Juhasz C, Muzik O, Shah A, Shah J, Sood S, Kupsky WJ, Mangner TJ, Chakraborty PK, Chugani HT (2005) Epilepsy surgery outcome in children with tuberous sclerosis complex evaluated with alpha-[11C]methyl-L-tryptophan positron emission tomography (PET). *J Child Neurol* 20:429–438
- Kaneko K, Sasaki M, Morioka T, Koga H, Abe K, Sawamoto H, Ohya N, Yoshiura T, Miura F, Honda H (2006) Pre-surgical identification of epileptogenic areas in temporal lobe epilepsy by 123I-iomazenil SPECT: a comparison with IMP SPECT and FDG PET. *Nucl Med Commun.* 27:893–899
- Kaplan AM, Bandy DJ, Manwaring KH, Chen K, Lawson MA, Moss SD, Duncan JD, Wodrich DL, Schnur JA, Reiman EM (1999) Functional brain mapping using positron emission tomography scanning in preoperative neurosurgical planning for pediatric brain tumors. *J Neurosurg* 91:797–803
- Kassubek J, Juengling FD (2002) Nuclear medicine imaging in epilepsy diagnostics – II: receptor diagnostics and functional imaging. *Nervenheilkunde* 21:475–481
- Kassubek J, Juengling FD, Otte A (2000) Improved interpretation of cerebral PET with respect to structural MRI changes using combined voxel-based statistical mapping. *Eur J Nucl Med* 27:880
- Kimura Y, Sato N, Ito K, Kamiya K, Nakata Y, Saito Y, Matsuda H, Sugai K, Sasaki M, Sugimoto H (2012) SISCOM technique with a variable Z score improves detectability of focal cortical dysplasia: a comparative study with MRI. *Ann Nucl Med* 26: 397–404
- Kleiser R, Staempfli P, Valvanis A, Boesiger P, Kollias S (2010) Impact of fMRI-guided advanced DTI fiber tracking techniques on their clinical applications in patients with brain tumours. *Neuroradiology* 52:37–46
- Knake S, Grant PE, Stufflebeam SM, Wald LL, Shiraishi H, Rosenow F, Schomer DL, Fischl B, Dale AM, Halgren E (2004) Aids to telemetry in the presurgical evaluation of epilepsy patients: MRI, MEG and other non-invasive imaging techniques. *Suppl Clin Neurophysiol* 57:494–502
- Knowlton RC (2004) Multimodality imaging in partial epilepsies. *Curr Opin Neurol* 17:165–172
- Knowlton RC, Laxer KD, Ende G, Hawkins RA, Wong ST, Matson GB, Rowley HA, Fein G, Weiner MW (1997) Presurgical multimodality neuroimaging in electroencephalographic lateralized temporal lobe epilepsy. *Ann Neurol* 42:829–837
- Kober H, Moller M, Nimsky C, Vieth J, Fahlbusch R, Ganslandt O (2001a) New approach to localize speech relevant brain areas and hemispheric dominance using spatially filtered magnetoencephalography. *Hum Brain Mapp* 14:236–250
- Kober H, Nimsky C, Moller M, Hastreiter P, Fahlbusch R, Ganslandt O (2001b) Correlation of sensorimotor activation with functional magnetic resonance imaging and magnetoencephalography in presurgical functional imaging: a spatial analysis. *Neuroimage* 14:1214–1228
- Koch MA, Glauke V, Finsterbusch J, Nolte UG, Frahm J, Weiller C, Büchel C (2002) Distortion-free diffusion tensor imaging of cranial nerves and of inferior temporal and orbitofrontal white matter. *Neuroimage* 17:497–506
- Kracht LW, Friese M, Herholz K, Schroeder R, Bauer B, Jacobs A, Heiss WD (2003) Methyl-[11C]-L-methionine uptake as measured by positron emission tomography correlates to microvessel density in patients with glioma. *Eur J Nucl Med Mol Imaging* 30:868–873
- Kracht LW, Miletic H, Busch S, Jacobs AH, Voges J, Hoevels M, Klein JC, Herholz K, Heiss WD (2004) Delineation of brain tumor extent with [11C]-L-methionine positron emission tomography: local comparison with stereotactic histopathology. *Clin Cancer Res* 10:7163–7170
- Krakow K, Wiesemann UC, Woermann FG, Symms MR, McLean MA, Lemieux L, Allen PJ, Barker GJ, Fish DR, Duncan JS (1999) Multimodal MR imaging: functional, diffusion tensor, and chemical shift imaging in a patient with localization-related epilepsy. *Epilepsia* 40:1459–1462
- Kratochwil C, Combs SE, Leotta K, Afshar-Oromieh A, Rieken S, Debus J et al (2014) Intra-individual comparison of 18F-FET and 18F-DOPA in PET imaging of recurrent brain tumors. *Neuro Oncol* 16:434–440
- Krings T, Schreckenberger M, Rohde V, Foltys H, Spetzger U, Sabri O, Reinges MH, Kemeny S, Meyer PT, Moller-Hartmann W, Korinth M, Gilsbach JM, Buell U, Thron A (2001) Metabolic and electrophysiological validation of functional MRI. *J Neurol Neurosurg Psychiatry* 71:762–771
- Kuhnt D, Bauer MH, Becker A, Merhof D, Zolal A, Richter M, Grummich P, Ganslandt O, Buchfelder M, Nimsky C (2012) Intraoperative visualization of fiber tracking based reconstruction of language pathways in glioma surgery. *Neurosurgery* 70:911–919
- Kuhnt D, Bauer MH, Egger J, Richter M, Kapur T, Sommer J, Merhof D, Nimsky C (2013) Fiber tractography based on diffusion tensor imaging compared with high-angular-resolution diffusion imaging with compressed sensing: initial experience. *Neurosurgery* 72 (Suppl1):165–175
- Kumar A, Chugani HT (2013) The role of radionuclide imaging in epilepsy, part 1: sporadic temporal and extratemporal lobe epilepsy. *J Nucl Med* 54:1775–1781
- Lantz G, Spinelli L, Menendez RG, Seeck M, Michel CM. Localization of distributed sources and comparison with functional MRI. *Epileptic Disord.* 2001;Special Issue:45–58
- Lazar M, Alexander AL, Thottakara PJ, Badie B, Field AS (2006) White matter reorganization after surgical resection of brain tumors and vascular malformations. *AJR Am J Neuroradiol* 27: 1258–1271
- Le Bihan D, van Zijl P (2002) From the diffusion coefficient to the diffusion tensor. *NMR Biomed* 15:431–434
- Leijten FS, Huiskamp GJ, Hilgersom I, Van Huffelen AC (2003) High-resolution source imaging in mesiotemporal lobe epilepsy: a comparison between MEG and simultaneous EEG. *J Clin Neurophysiol* 20:227–238
- Leijten FS, Ramsey NF, Van Rijen PC (2004) Function localisation in neurosurgery: new tools, new practices? *Clin Neurol Neurosurg* 107:17–19
- Levivier M, Goldman S, Pirotte B, Brucher JM, Baleriaux D, Luxen A, Hildebrand J, Brotchi J (1995) Diagnostic yield of stereotactic brain biopsy guided by positron emission tomography with [18F]fluorodeoxyglucose. *J Neurosurg* 82:445–452
- Lizarraga KJ, Allen-Auerbach M, Czernin J, Desalles AAF, Yong WH, Phelps ME et al (2014) 18F-FDOPA PET for differentiating recurrent or progressive brain metastatic tumors from late or delayed radiation injury after radiation treatment. *J Nucl Med* 55:30–36

- Lounasmaa OV, Hamalainen M, Hari R, Salmelin R (1996) Information processing in the human brain: magneto-encephalographic approach. *Proc Natl Acad Sci U S A* 93:8809–8815
- Manglore S, Bharath RD, Panda R, George L, Thamodharan A, Gupta AK (2013) Utility of resting fMRI and connectivity in patients with brain tumor. *Neurol India* 61:144–151
- Marks WJ Jr (2004) Utility of MEG in presurgical localization. *Epilepsy Curr* 4:208–209
- Matsuda H, Matsuda K, Nakamura F, Kameyama S, Masuda H, Otsuki T, Nakama H, Shamoto H, Nakazato N, Mizobuchi M, Nakagawara J, Morioka T, Kuwabara Y, Aiba H, Yano M, Kim YJ, Nakase H, Kuji I, Hirata Y, Mizumura S, Imabayashi E, Sato N (2009) Contribution of subtraction ictal SPECT coregistered to MRI to epilepsy surgery: a multicenter study. *Ann Nucl Med* 23:283–291
- Mehta S, Grabowski TJ, Trivedi Y, Damasio H (2003) Evaluation of voxel-based morphometry for focal lesion detection in individuals. *Neuroimage* 20:1438–1454
- Mitchell TJ, Hacker CD, Breshears JD, Szrama NP, Sharma M, Bundy DT, Pahwa M, Corbetta M, Snyder AZ, Shimony JS, Leuthardt EC (2013) A novel data-driven approach to preoperative mapping of functional cortex using resting-state functional magnetic resonance imaging. *Neurosurgery* 73:969–982
- Mohamed IS, Gibbs SA, Robert M, Bouthillier A, Leroux JM, Khoa Nguyen D (2013) The utility of magnetoencephalography in the presurgical evaluation of refractory insular epilepsy. *Epilepsia* 54:1950–1959
- Mori S, van Zijl PC (2002) Fiber tracking: principles and strategies – a technical review. *NMR Biomed* 15:468–480
- Mosskin M, Ericson K, Hindmarsh T, von Holst H, Collins VP, Bergstrom M, Eriksson L, Johnstrom P (1989) Positron emission tomography compared with magnetic resonance imaging and computed tomography in supratentorial gliomas using multiple stereotactic biopsies as reference. *Acta Radiol* 30:225–232
- Müller HP, Kassubek J (2008) Multimodal imaging in neurology – special focus on MRI applications and MEG. In: Enderle JD *Synthesis lectures in biomedical engineering*, #16 edn. Morgan & Claypool Publishers, San Rafael, CA, USA; (ISBN paperback: 1-59829-550-0, ebook: 1-59829-551-9)
- Müller HP, Kassubek J (2013) Diffusion tensor magnetic resonance imaging in the analysis of neurodegenerative diseases. *J Vis Exp* 77. doi: [10.3791/50427](https://doi.org/10.3791/50427)
- Müller HP, DeCesaris I, DeMelis M, Marzetti L, Pasquarelli A, Erne SN, Ludolph AC, Kassubek J (2005) Open magnetic and electric graphic analysis. *IEEE Eng Med Biol Mag* 24:109–116
- Murphy MA, O'Brien TJ, Morris K, Cook MJ (2004) Multimodality image-guided surgery for the treatment of medically refractory epilepsy. *J Neurosurg* 100:452–462
- Muzik O, da Silva EA, Juhasz C, Chugani DC, Shah J, Nagy F, Canady A, von Stockhausen HM, Herholz K, Gates J, Frost M, Ritter F, Watson C, Chugani HT (2000) Intracranial EEG versus flumazenil and glucose PET in children with extratemporal lobe epilepsy. *Neurology* 54:171–179
- Muzik O, Pourabdollah S, Juhasz C, Chugani DC, Janisse J, Draghici S (2005) Application of an objective method for localizing bilateral cortical FDG PET abnormalities to guide the resection of epileptic foci. *IEEE Trans Biomed Eng* 52:1574–1581
- Najib U, Bashir S, Edwards D, Rotenberg A, Pascual-Leone A (2011) Transcranial brain stimulation: clinical applications and future directions. *Neurosurg Clin N Am* 22:233–251
- Nimsky C, Ganslandt O, Von Keller B, Romstock J, Fahlbusch R (2004) Intraoperative high-field-strength MR imaging: implementation and experience in 200 patients. *Radiology* 233:67–78
- Nimsky C, Ganslandt O, Fahlbusch R (2005a) 1.5 T: intraoperative imaging beyond standard anatomic imaging. *Neurosurg Clin N Am* 16:185–200, vii
- Nimsky C, Grummich P, Sorensen AG, Fahlbusch R, Ganslandt O (2005b) Visualization of the pyramidal tract in glioma surgery by integrating diffusion tensor imaging in functional neuronavigation. *Zentralbl Neurochir* 66:133–141
- Nimsky C, Ganslandt O, Hastreiter P, Wang R, Benner T, Sorensen AG, Fahlbusch R (2005c) Preoperative and intraoperative diffusion tensor imaging-based fiber tracking in glioma surgery. *Neurosurgery* 56:130–137
- Nimsky C, Ganslandt O, Hastreiter P, Wang R, Benner T, Sorensen AG, Fahlbusch R (2005d) Intraoperative diffusion-tensor MR imaging: shifting of white matter tracts during neurosurgical procedures – initial experience. *Radiology* 234:218–225
- Nooraine J, Iyer RB, Raghavendra S (2013) Ictal PET in presurgical workup of refractory extratemporal epilepsy. *Ann Indian Acad Neurol* 16:676–677
- O'Brien TJ, So EL, Cascino GD, Hauser MF, Marsh WR, Meyer FB, Sharbrough FW, Mullan BP (2004) Subtraction SPECT coregistered to MRI in focal malformations of cortical development: localization of the epileptogenic zone in epilepsy surgery candidates. *Epilepsia* 45:367–376
- Ogawa T, Shishido F, Kanno I, Inugami A, Fujita H, Murakami M, Shimosegawa E, Ito H, Hatazawa J, Okudera T (1993) Cerebral glioma: evaluation with methionine PET. *Radiology* 186:45–53
- Oishi K, Faria A, van Zijl PCM, Mori S (2011) MRI atlas of human white matter, 2nd edn. Elsevier, Amsterdam
- Orrison WW Jr (1999) Magnetic source imaging in stereotactic and functional neurosurgery. *Stereotact Funct Neurosurg* 72:89–94
- Ossenblok P, Leijten FS, de Munck JC, Huiskamp GJ, Barkhof F, Boon P (2003) Magnetic source imaging contributes to the presurgical identification of sensorimotor cortex in patients with frontal lobe epilepsy. *Clin Neurophysiol* 114:221–232
- Paetau R, Mohamed IS (2013) Magnetoencephalography (MEG) and other neurophysiological investigations. *Handb Clin Neurol* 111:461–465
- Patarraja E, Simos PG, Castillo EM, Billingsley RL, Sarkari S, Wheless JW, Maggio V, Maggio W, Baumgartner JE, Swank PR, Breier JJ, Papanicolaou AC (2004) Does magnetoencephalography add to scalp video-EEG as a diagnostic tool in epilepsy surgery? *Neurology* 62:943–948
- Patarraja E, Lindinger G, Deecke L, Mayer D, Baumgartner C (2005) Combined MEG/EEG analysis of the interictal spike complex in mesial temporal lobe epilepsy. *Neuroimage* 24:607–614
- Pillai JJ (2010) The evolution of clinical functional imaging during the past 2 decades and its current impact on neurosurgical planning. *AJNR Am J Neuroradiol* 31:219–225
- Pirotte B, Goldman S, Salzberg S, Wikler D, David P, Vandesteene A, Van Bogaert P, Salmon I, Brotchi J, Levivier M (2003) Combined positron emission tomography and magnetic resonance imaging for the planning of stereotactic brain biopsies in children: experience in 9 cases. *Pediatr Neurosurg* 38:146–155
- Pirotte BJM, Levivier M, Goldman S, Massager N, Wikler D, Dewitte O et al (2009) Positron emission tomography-guided volumetric resection of supratentorial high-grade gliomas: a survival analysis in 66 consecutive patients. *Neurosurgery* 64(3):471–481
- Powell HW, Parker GJ, Alexander DC, Symms MR, Boulby PA, Wheeler-Kingshott CA, Barker GJ, Koepf MJ, Duncan JS (2005) MR tractography predicts visual field defects following temporal lobe resection. *Neurology* 65:596–599
- Qiu TM, Zhang Y, Wu JS, Tang WJ, Zhao Y, Pan ZG, Mao Y, Zhou LF (2010) Virtual reality presurgical planning for cerebral gliomas adjacent to motor pathways in an integrated 3-D stereoscopic visualization of structural MRI and DTI tractography. *Acta Neurochir (Wien)* 152:1847–1857
- Ramon C, Haueisen J, Richards T, Maravilla K (2004) Multimodal imaging of somatosensory evoked cortical activity. *Neurol Clin Neurophysiol* 2004:96
- Reinges MH, Krings T, Meyer PT, Schreckenberger M, Rohde V, Weidemann J, Sabri O, Mulders EJ, Buell U, Thron A, Gilsbach JM (2004) Preoperative mapping of cortical motor function: prospec-

- tive comparison of functional magnetic resonance imaging and [15O]-H₂O-positron emission tomography in the same co-ordinate system. *Nucl Med Commun* 25:987–997
- Rheims S, Jung J, Ryvlin P (2013) Combination of PET and magnetoencephalography in the presurgical assessment of MRI-negative epilepsy. *Front Neurol* 4:188
- Ribom D, Eriksson A, Hartman M, Engler H, Nilsson A, Langstrom B, Bolander H, Bergstrom M, Smits A (2001) Positron emission tomography 11C-methionine and survival in patients with low-grade gliomas. *Cancer* 92:1541–1549
- Richardson MP, Friston KJ, Sisodiya SM, Koepp MJ, Ashburner J, Free SL, Brooks DJ, Duncan JS (1997) Cortical grey matter and benzodiazepine receptors in malformations of cortical development. A voxel-based comparison of structural and functional imaging data. *Brain* 120:1961–1973
- Rohde V, Spangenberg P, Mayfrank L, Reinges M, Giltsbach JM, Coenen VA (2005) Advanced neuronavigation in skull base tumors and vascular lesions. *Minim Invasive Neurosurg* 48:13–18
- Ryvlin P, Bouvard S, Le Bars D, De Lamerie G, Gregoire MC, Kahane P, Froment JC, Mauguire F (1998) Clinical utility of flumazenil-PET versus [18F]fluorodeoxyglucose-PET and MRI in refractory partial epilepsy. A prospective study in 100 patients. *Brain* 121:2067–2081
- Schonberg T, Pianka P, Hendler T, Pasternak O, Assaf Y (2006) Characterization of displaced white matter by brain tumours using combined DTI and fMRI. *Neuroimage* 30:1100–1111
- Shang HB, Zhao WG, Zhang WF (2012) Preoperative assessment using multimodal functional magnetic resonance imaging techniques in patients with brain gliomas. *Turk Neurosurg* 22:558–565
- Shattuck DW, Mirza M, Adisetiyo V, Hojatkashani C, Salamon G, Narr KL, Poldrack RA, Bilder RM, Toga AW (2008) Construction of a 3D probabilistic atlas of human cortical structures. *Neuroimage* 39:1064–1080
- Shin SS, Verstynen T, Pathak S, Jarbo K, Hricik AJ, Maserati M, Beers SR, Puccio AM, Boada FE, Okonkwo DO, Schneider W (2012) High-definition fiber tracking for assessment of neurological deficit in a case of traumatic brain injury: finding, visualizing, and interpreting small sites of damage. *J Neurosurg* 116:1062–1069
- Sierra-Marcos A, Maestro I, Falcón C, Donaire A, Setoain J, Aparicio J, Rumià J, Pintor L, Boget T, Carreño M, Bargalló N (2013) Ictal EEG-fMRI in localization of epileptogenic area in patients with refractory neocortical focal epilepsy. *Epilepsia* 54:1688–1698
- Sinha S, Bastin ME, Whittle IR, Wardlaw JM (2002) Diffusion tensor MR imaging of high-grade cerebral gliomas. *AJNR Am J Neuroradiol* 23:520–527
- Sporns O, Tononi G, Edelman GM (2000) Connectivity and complexity: the relationship between neuroanatomy and brain dynamics. *Neural Netw* 13:909–922
- Stadlbauer A, Pölking E, Prante O, Nimsky C, Buchfelder M, Kuwert T, Linke R, Doelken M, Ganslandt O (2009) Detection of tumour invasion into the pyramidal tract in glioma patients with sensorimotor deficits by correlation of (18)F-fluoroethyl-L-tyrosine PET and magnetic resonance diffusion tensor imaging. *Acta Neurochir (Wien)* 151:1061–1069
- Stefan H, Hummel C, Scheler G, Genow A, Druschky K, Tilz C, Kaltenhauser M, Hopfengartner R, Buchfelder M, Romstock J (2003) Magnetic brain source imaging of focal epileptic activity: a synopsis of 455 cases. *Brain* 126:2396–2405
- Stippich C (2010) Presurgical functional magnetic resonance imaging. *Radiologe* 50:110–122
- Stippich C, Freitag P, Kassubek J, Soros P, Kamada K, Kober H, Scheffler K, Hopfengartner R, Bilecen D, Radu EW, Vieth JB (1998) Motor, somatosensory and auditory cortex localization by fMRI and MEG. *Neuroreport* 9:1953–1957
- Tang L, Mantle M, Ferrari P, Schiffbauer H, Rowley HA, Barbaro NM, Berger MS, Roberts TP (2003) Consistency of interictal and ictal onset localization using magnetoencephalography in patients with partial epilepsy. *J Neurosurg* 98:837–845
- Thiel A, Herholz K, von Stockhausen HM, van Leyen-Pilgram K, Pietrzyk U, Kessler J, Wienhard K, Klug N, Heiss WD (1998) Localization of language-related cortex with 15O-labeled water PET in patients with gliomas. *Neuroimage* 7:284–295
- Toga AW, Ojemann GA, Ojemann JG, Cannestra AF (2000) Intraoperative brain mapping. In: Mazziotta JC, Toga AW, Frackowiak RSJ (eds) *Brain mapping: the disorders*. Academic, San Diego, pp 77–105
- Trabesinger AH, Meier D, Boesiger P (2003) In vivo 1H NMR spectroscopy of individual human brain metabolites at moderate field strengths. *Magn Reson Imaging* 21:1295–1302
- Tuch DS, Reese TG, Wiegell MR, Wedeen VJ (2003) Diffusion MRI of complex neural architecture. *Neuron* 40:885–895
- Ulmer JL, Salvant CV, Mueller WM, Krouwer HG, Stroe GO, Aralasmak A, Prost RW (2004) The role of diffusion tensor imaging in establishing the proximity of tumor borders to functional brain systems: implications for preoperative risk assessments and postoperative outcomes. *Technol Cancer Res Treat* 3:567–576
- Van Dijk KR, Hedden T, Venkataraman A, Evans KC, Lazar SW, Buckner RL (2010) Intrinsic functional connectivity as a tool for human connectomics: theory, properties, and optimization. *J Neurophysiol* 103:297–321
- Vignerón D, Bollen A, McDermott M, Wald L, Day M, MoyherNoworolski S, Henry R, Chang S, Berger M, Dillon W, Nelson S (2001) Three-dimensional magnetic resonance spectroscopic imaging of histologically confirmed brain tumors. *Magn Reson Imaging* 19:89–101
- Vinas FC, Zamorano L, Mueller RA, Jiang Z, Chugani H, Fuerst D, Muzik O, Mangner TJ, Diaz FG (1997) [15O]-water PET and intraoperative brain mapping: a comparison in the localization of eloquent cortex. *Neurology* 49:601–608
- Vivash L, Gregoire MC, Lau EW, Ware RE, Binns D, Roselt P, Bouilleret V, Myers DE, Cook MJ, Hicks RJ, O'Brien TJ, Elwan SA, Wu G, Huang SS, Najm IM, So NK (2013) Ictal single photon emission computed tomography in epileptic auras. *J Nucl Med* 54:1270–1277
- Vollmar S (2006) Integration of functional imaging (PET) to surgery planning in brain tumors. PhD thesis, University of Cologne
- Vollmar S, Cizek J, Sue M, Klein J, Jacobs A, Herholz K (2004) VINCI – Volume Imaging in Neurological Research, Co-Registration and ROIs included. In: Kremer K, Macho V (eds) *Forschung und wissenschaftliches Rechnen 2003*. Gesellschaft für wissenschaftliche Datenverarbeitung, Göttingen, pp 115–131
- Weaver KE, Chaovatitwongse WA, Novotny EJ, Poliakov A, Grabowski TG, Ojemann JG (2013) Local functional connectivity as a pre-surgical tool for seizure focus identification in non-lesion, focal epilepsy. *Front Neurol* 4:43
- Wehner T, Lüders H (2008) Role of neuroimaging in the presurgical evaluation of epilepsy. *J Clin Neurol* 4:1–16
- Wiest R, Kassubek J, Schindler K, Loher TJ, Kiefer C, Mariani L, Wissmeyer M, Schroth G, Mathis J, Weder B, Juengling FD (2005) Comparison of voxel-based 3-D MRI analysis and subtraction ictal SPECT coregistered to MRI in focal epilepsy. *Epilepsy Res* 65:125–133
- Winkler D, Strauss G, Hesse S, Goldammer A, Hund-Georgiadis M, Richter A, Sabri O, Kahn T, Meixensberger J (2004) Preoperative imaging as the basis for image-guided neurosurgery. *Radiologe* 44:723–732
- Witwer BP, Moftakhar R, Hasan KM, Deshmukh P, Haughton V, Field A, Arfanakis K, Noyes J, Moritz CH, Meyerand ME, Rowley HA, Alexander AL, Badie B (2002) Diffusion-tensor imaging of white matter tracts in patients with cerebral neoplasm. *J Neurosurg* 97:568–575
- Wu JS, Zhou LF, Tang WJ, Mao Y, Hu J, Song YY, Hong XN, Du GH (2007) Clinical evaluation and follow-up outcome of diffusion tensor imaging-based functional neuronavigation: a prospective, controlled study in patients with gliomas involving pyramidal tracts. *Neurosurgery* 61:935–948
- Youland RS, Kitange GJ, Peterson TE, Pafundi DH, Ramiscal JA, Pokorny JL, Giannini C, Laack NN, Parney IF, Lowe VJ, Brinkmann DH, Sarkaria JN (2013) The role of LAT1 in (18)F-DOPA uptake in malignant gliomas. *J Neurooncol* 111:11–18

Brain Plasticity in fMRI and DTI

R. Beisteiner and E. Matt

Contents

| | | |
|-----|--|-----|
| 1 | Introduction..... | 289 |
| 2 | What Are the Clinical Benefits of Neuroplasticity Investigations? | 290 |
| 2.1 | Better Evaluation of the Patients' Functional State | 291 |
| 2.2 | Better Individual Prognosis..... | 291 |
| 2.3 | Improvement of Treatment Strategies..... | 291 |
| 2.4 | Progress in Understanding How the Nervous System Acts in Response to Disease | 292 |
| 3 | Mechanisms of Neuroplasticity..... | 292 |
| 3.1 | Molecular Changes | 292 |
| 3.2 | Cellular Changes..... | 292 |
| 3.3 | Neuronal Population Changes..... | 292 |
| 4 | Review of the Literature..... | 293 |
| 4.1 | Stroke | 293 |
| 4.2 | Epilepsy..... | 296 |
| 4.3 | Tumor | 297 |
| 4.4 | Multiple Sclerosis | 297 |
| 4.5 | Peripheral Nervous System Disorders | 298 |
| 5 | Methodological Considerations | 299 |
| 5.1 | Technical Interpretation of Findings | 299 |
| 5.2 | Neurophysiological Interpretation of Findings..... | 299 |
| 5.3 | Consequences for Neuroplasticity Investigations | 299 |
| 6 | Clinical Examples..... | 300 |
| 6.1 | Longitudinal Neuroplasticity Associated with Peripheral Nerve Regeneration | 300 |
| 6.2 | Neuroplasticity After Nerve Repair in Brachial Plexus Lesions..... | 300 |
| 6.3 | Neuroplastic Changes of Effective Connectivity in Patients with Heterotopic Hand Replantation..... | 301 |
| 6.4 | Neuroplastic Reorganization of Hand Functions After Hemispherectomy | 303 |
| 6.5 | Structural Neuroplasticity in Patients with Chronic Stroke | 303 |
| 6.6 | Neuroplastic Network Changes in Traumatic Brain Injury | 305 |
| | References..... | 307 |

Abstract

This chapter describes what kind of neuroplastic information may be generated by functional magnetic resonance imaging (fMRI) and diffusion tensor imaging (DTI) after brain damage. Clinical neuroplasticity may be defined as an active reorganization contrary to loss of activation or connectivity simply due to brain damage. After giving an overview about general aspects of clinical neuroplasticity, this chapter introduces specific benefits of neuroplasticity investigations for patient care. These include better definition of the patients' functional state, better individual prognosis, improvement of treatment strategies, and progress in understanding how the nervous system acts in response to disease. Since fMRI and DTI are restricted to detecting neuroplastic changes on the level of neuronal populations and their connections, some important molecular and cellular mechanisms driving these effects are also discussed. Further, a review is given about previously described neuroplastic responses of the diseased brain. This focuses on neuroplasticity evoked by pathomorphological changes of a previously healthy nervous system. It allows an illustration of the complexity and limitations of neuroplasticity research. To ease a critical evaluation of published data, this chapter also includes methodological considerations, which deal with the limitations of the technical or neurophysiological interpretation of neuroplasticity investigations. Finally, some clinical examples illustrating the potential of fMRI and DTI are given.

1 Introduction

Clinical neuroplasticity may be defined as functional or structural alterations of the nervous system in the sense of active reorganization after damage. This functional and structural reorganization is possible throughout the entire life span and also occurs as nonclinical neuroplasticity. The latter is a physiological response within the healthy brain to adapt to changing individual demands or changing physiological states.

R. Beisteiner (✉) • E. Matt
Department of Neurology, Highfield MR Center, Medical University of Vienna, Vienna 1090, Austria
e-mail: roland.beisteiner@meduniwien.ac.at

Defining nervous system alterations as neuroplastic is not always a trivial task. For example, changes in functional connectivity after a major traumatic brain injury leading to coma may be an immediate consequence of the brain damage itself but not of reorganization. For instance, changes in structural connectivity like reductions in fiber tract integrities may be a result of tract damage but not of structural reorganization (where weakening of non-damaged tracts may also occur (Simões et al. 2012)). Correspondingly, reduced local brain activity may also be a consequence of damage to connecting tracts but not of functional reorganization (e.g., Hamzei et al. 2008). Moreover, clinical improvements after brain damage may occur independently of functional reorganization. Within the first days after a functionally relevant brain damage, secondary effects regress spontaneously, and accordingly, their disturbing influence on brain function disappears (Seitz and Donnan 2010; Buma et al. 2010). Such secondary (non-neuroplastic) effects include inflammation, edema, compromised perfusion close to pathology, and diaschisis (malfunctioning of disconnected brain areas distant from the pathology).

Another important issue with regard to the clinical neuroplasticity literature concerns the functional outcome. The ultimate goal of clinical neuroplasticity is the *regeneration of function* in terms of a reestablishment of the compromised function. However, *physiologic compensation* of the lost function may also occur, and this may induce a (non-neuroplastic) brain activation change, simply due to altered functioning. Examples include compensation of a distal paresis by recruitment of more proximal muscles or increased activity associated with mirror movements of the non-affected limb. A differentiation is possible via repeated functional magnetic resonance imaging (fMRI) measurements and simultaneous documentation of motor performance. Importantly, worsening of function (maladaptation) is also a possible outcome.

All these interrelationships need to be considered when functional or structural alterations are described with fMRI or diffusion tensor imaging (DTI). However, the current literature is not always consistent. This is partly due to the methodological constraints of the individual study. Therefore, a critical question is, what can be measured with clinical fMRI or DTI? Generally, these techniques enable *in vivo* assessment of spatial and temporal patterns of functional and structural changes. In recent years, an impressive extension of the MR armamentarium suited for neuroplasticity investigations has been established. Detailed descriptions of these methodologies can be found in the methodological chapters of this book. In brief, classical fMRI allows the detection of local increases and local decreases of brain activity. It is possible to monitor brain activation changes occurring spontaneously (resting-state or task-free fMRI), occurring in response to a task (task-based fMRI), or occurring in response to medication (pharmacological fMRI). A correct reflection of neuronal activity by the fMRI blood oxygen level-dependent (BOLD) signal requires an

undisturbed vascular situation. Disturbed situations may be found in early stages after ischemic stroke, where vessels are maximally dilated. It should also be kept in mind that an increase in BOLD signal can reflect excitatory as well as inhibitory neuronal activity. Concerning spatial reorganization, increase in BOLD signal may occur within a typical task active area or in a nontypical but functionally related area due to activation of additional resources. This may be seen as increased activity in spared brain areas close to the pathology or as increased activity in secondary brain areas remote from the pathology. For example, in the motor network the secondary premotor cortex is extensively connected to the primary motor cortex (M1) and can partly substitute M1 via projections to the spinal cord. Increase of local neuronal activity (overactivation) may be locally driven or be a consequence of disinhibition mediated by remote connected areas. Decrease of local neuronal activity (underactivation) may also be mediated by remote areas (inhibition). However, underactivation may also be a consequence of damage to local or distant (diaschisis) tissue. The monitoring of such changes in brain activation can also be used to investigate how brain areas are functionally connected to each other, that is, which brain areas form networks and how these networks do neuroplastically change. The most published measures are functional connectivity, effective connectivity, and graph theory networks. Functional connectivity defines networks of brain areas by integrating all areas which show similar signal behaviors. Effective connectivity determines which brain areas may change the activity of other brain areas. Graph theoretical approaches classify brain areas according to the hierarchy they represent within the global brain connections. All these methods may be applied to describe functional alterations of the nervous system.

For description of structural alterations, DTI techniques are used (for review see Huston and Field 2013). They allow the estimation of the structural integrity and connectivity of white matter tracts at a level that cannot be achieved with anatomical imaging or volumetric white matter analysis. To some extent it is also possible to characterize tissue architecture (e.g., cellular density, vasculature, necrosis, extent, or margins of a neoplasm). The DTI results indicate local increases or decreases of tract integrity and tract volume, dislocation of white matter tracts or alterations of structural connectivity between brain areas.

2 What Are the Clinical Benefits of Neuroplasticity Investigations?

Information about neuroplastic alterations generated by fMRI and DTI is important to improve patient care. By extending standard clinical findings, fMRI/DTI information allow a better definition of the patients' functional state, better individual prognosis, improvement of treatment strategies, and

progress in understanding how the nervous system acts in response to disease (for recent reviews, see Grefkes and Ward 2014; Wahl and Schwab 2014; Gillebert and Mantini 2013; Havsteen et al. 2013; Jiang et al. 2013; Rehme and Grefkes 2013; Shah et al. 2013; Stinear and Ward 2013; Dijkhuizen et al. 2012; Gale and Pearson 2012; Saur and Hartwigsen 2012; Smits et al. 2012; Hamberger and Cole 2011; Westlake and Nagarajan 2011; Buma et al. 2010; Chen et al. 2010; Rowe 2010; Seghier et al. 2010; Seitz and Donnan 2010). Importantly, the information generated by different fMRI/DTI techniques – brain activation, functional or effective connectivity, and structural connectivity – often complement one another or complement other diagnostic techniques. For instance, connectivity analyses may detect disease or treatment effects even when brain activation techniques are insensitive (Rowe 2010). Tractography may allow assessment of Wallerian degeneration better than conventional MR imaging (Huston and Field 2013). Tractography may be even more sensitive than recording of motor evoked potentials – as described in a study of clinically critical disruptions of the posterior limb of the internal capsule (Stinear et al. 2007).

2.1 Better Evaluation of the Patients' Functional State

fMRI/DTI benefits for evaluating the patients' functional state are evident from the motor system plasticity literature. A change of motor lateralization to the contralesional hemisphere often indicates a reduced functional competence in the lesioned hemisphere (which does not need to correlate with the extent of morphological destruction!). As also evidenced by brain stimulation data (O'Shea et al. 2014), patients with functionally compromising ipsilateral lesions depend more on their contralesional hemisphere than those with good residual ipsilateral function. Compensatory lateralization changes are informative about the stage of rehabilitation and may be transient (Grefkes and Ward 2014).

2.2 Better Individual Prognosis

fMRI/DTI neuroplasticity investigations help to improve the individual prognosis. In pediatric epilepsy, for example, the chronic nature of epileptic activity can result in a shift of language from the left to the right hemisphere or rerouting of language pathways from traditional to nontraditional areas within the dominant left hemisphere. The capability to reorganize may correlate with a better prognosis (evidence for stroke patients exists (Ovadia-Caro et al. 2013)). However, clinical variables have not been reliable predictors of altered language networks in individual patients (Hamberger and Cole 2011), whereas fMRI/DTI data are promising with this respect

(see Sect. 4.2). For stroke patients, Puig et al. (2011) showed that DTI data about corticospinal tract damage correlate better with clinical recovery than baseline clinical scores or even lesion volume. Improved prognosis generates further clinical benefits by enabling adequate setting of rehabilitation goals and more efficient allocation of resources. For example, Appel-Cresswell et al. (2010) showed that clinical performance of patients with Parkinson's disease could be maintained when intact cerebellar circuits were detected which were able to compensate for basal ganglia deficits. In contrast, despite adequate therapy the goal of maintaining performance may be unrealistic when neuroplastic compensation cannot be evidenced. Recently, some prognostic indices have been suggested which combine MR data with clinical data: the PLORAS system (Predicting language outcome and recovery after stroke, Price et al. 2010) combines anatomical images of a lesion with clinical data. The PREP system (Predicting recovery potential, Stinear et al. 2012) combines DTI results about structural integrity with clinical data. Both try to help clinicians to estimate the prognosis of an individual patient. Help for prognostic judgments can also be provided by fMRI data (Marshall et al. 2009) or combinations of fMRI data with clinical data (Zarahn et al. 2011; Saur et al. 2010). In these studies, the fMRI results were classified with various data analysis methods, including multivariate machine learning techniques. Such analyses try to extract fMRI patterns typical for good or bad later recovery.

2.3 Improvement of Treatment Strategies

Improvement of treatment strategies concerns any type of intervention, be it behavioral, pharmacological, surgical, or brain stimulation therapies. For example, the definition of typical reorganizational profiles with fMRI/DTI may guide the development of brain stimulation protocols that focus on brain regions most relevant for functional recovery. Such protocols can then be applied across the respective group of patients. Improvement of treatment strategies may also be possible for surgical interventions. Robles et al. (2008) suggested the monitoring of brain reorganization after a first incomplete tumor resection in essential eloquent brain areas, where complete initial tumor removal is mostly not possible due to the danger of generating a nonreversible functional deficit (e.g., aphasia, paresis). The expectation of this approach is that after postsurgical functional reorganization a reoperation allows an optimization of the residual tumor resection. This concept is supported by other data which indicate that tumors within essential brain areas like Broca's area can indeed be removed without generation of clinical deficits, when previous neuroplastic reorganization has been occurred, and there is no clinical aphasia despite Broca's lesion (Benzagmout et al. 2007; Ius et al. 2011). For optimizing

treatment strategies fMRI/DTI neuroplasticity investigations allow the evaluation of the interaction of therapies with learning-dependent and non-learning-dependent mechanisms of recovery. For example, in a brain stimulation study in patients with Parkinson's disease, González-García et al. (2011) found that clinical improvement after repetitive transcranial magnetic stimulation was associated with caudate nucleus activity increases and functional connectivity changes. This kind of studies will allow clinicians to learn which type of neuroplastic changes need to be evoked by therapeutic interventions when they shall be effective.

2.4 Progress in Understanding How the Nervous System Acts in Response to Disease

A very important benefit of neuroplasticity investigations concerns the progress in understanding how the nervous system acts in response to disease. For this, the most valuable clinical data are provided by longitudinal measurements. In contrast to cross-sectional data representing the neuroplastic state of the nervous system at a single time point, longitudinal data allow the clarification of nonlinear, time-dependent dynamics and recognition of adaptive compensation strategies. The latter is important to distinguish the restitution of original function from the establishment of a new compensatory function to accomplish the requested task. Longitudinal measurements are also important for understanding which neuroplastic changes are physiological (e.g., compatible with normal aging) as opposed to a pathological response (Heitger et al. 2013; Marchand et al. 2011). Further, descriptions of longitudinal changes allow the recognition of typical reorganizational profiles of neural networks post damage (Turkeltaub et al. 2011). Knowledge about typical reorganization profiles allows the identification of the critical degenerative and restorative processes and the definition of the brain regions most relevant for functional recovery. This may generate new possibilities for a better subclassification of diseases (Richiardi et al. 2012). Also, knowledge about typical reorganization profiles is the basis for the determination of individual anomalies. On the other hand, even if neuroplastic changes are absent, important clinical information may be generated by the fMRI/DTI techniques. They allow the documentation of which networks are still functional and may serve as a therapeutic target (Enzinger et al. 2008).

3 Mechanisms of Neuroplasticity

Neuroplasticity as detectable with fMRI/DTI may be driven by molecular changes, cellular changes, or changes concerning the action and interaction of neuronal populations

(for reviews see references in Sect. 2). The latter may also be a consequence of the molecular and cellular changes following brain lesions.

3.1 Molecular Changes

On the molecular level, changes for the expression of growth-associated genes resulting in increased growth-promoting factors, decreased growth-inhibiting factors and expression of maturation regulating proteins have been described (e.g., Anderson et al. 2013; Carmichael et al. 2005). These gene expressions are associated with axonal sprouting in peri-infarct cortex and with synapse formation. In addition, the level of glutamate and gamma amino butyric acid (GABA) may change as may the expression and responsiveness of cholinergic and GABA receptors with the latter resulting in a loss of inhibitory interneurons (Clarkson et al. 2010; Zepeda et al. 2004).

3.2 Cellular Changes

On the cellular level, a major neuroplastic mechanism concerns the changes in the function or number of synapses. This includes reinforcement of existing but functionally silent synapses (particularly at the periphery of lesions) and formation of new synapses. Further neuroplastic changes concern the dendritic arborization and axonal sprouting which may happen over considerable distances. These mechanisms may be influenced by changed inhibitory and excitatory inputs on local neurons. It is important to realize that the cellular changes may occur not only perilesionally but also in functionally/structurally connected brain areas remote from a lesion. Cellular neuroplasticity may also be modulated by glial cells which have been shown to affect excitability and synaptic transmission and to coordinate activity across networks (Araque and Navarrete 2010; Fields and Stevens-Graham 2002). Furthermore, recent research indicates that brain lesions may also stimulate neurogenesis and migration of neuroblasts (Kernie and Parent 2010). Neurogenesis in the adult brain persists in the subventricular zone, the olfactory bulb region, and the subgranular zone of the dentate gyrus of the hippocampus. These neurogenetic areas may be stimulated by brain injury with the consequence of a proliferation of neural progenitor cells which then migrate to the injured region (Kernie and Parent 2010; Ohab et al. 2006).

3.3 Neuronal Population Changes

Concerning neuronal populations, their action and interaction is influenced by the neuroplastic mechanisms described above. The molecular and cellular alterations change inhibitory

and excitatory influences on the neuronal populations and lead to altered anatomical connections. The consequences are functional and structural network changes on a local (changed activity of a network node) or global (changed network configuration) level. These comprise local overactivations or deactivations, increase or decrease of functional connectivity, and increase or decrease of modulatory influences between neuronal populations. Concerning structural network changes, the most important mechanisms are the reduction or increase of preexisting fiber tracts and the generation of new axonal connections. Detailed examples for resulting patterns of functional and structural network changes are described in context with specific diseases below.

4 Review of the Literature

Previous literature about clinical neuroplasticity detectable by fMRI and DTI may be divided in general patterns of neuroplastic changes – irrespective of the functional outcome and therefore including maladaptation – and neuroplastic changes leading to recovery. The latter relate clinical outcome with specific neuroplastic effects. Neuroplastic changes detectable with fMRI or DTI concern either local brain activation measures or functional/structural network measures. A problem for the classification of neuroplastic findings is the large number of factors which may affect neuroplasticity. These include type and stage of the disease, location and size of the lesions, type and intensity of clinical interventions (standard treatment, special training techniques, pharmacological interventions, brain stimulation techniques, surgery), age, biological characteristics of the individual, type of the investigated function, and particularly the method used for the detection of neuroplasticity. Knowledge how these factors influence fMRI/DTI findings is still rather limited.

For the investigated diseases, most of the clinical neuroplastic literature relates to neuroplasticity evoked by pathomorphological changes of a previously healthy nervous system. This review will therefore focus on this type of disease. However, descriptions of clinical neuroplastic effects also exist for other diseases like genetic diseases, or psychiatric disorders, or inborn morphological defects. For illustration of the large variety of diseases already studied, interesting recent publications include neuroplastic changes in schizophrenia (e.g., Palaniyappan et al. 2012), dementia (e.g., Jacobs et al. 2012), Parkinson's disease (e.g., van Nuenen et al. 2012), Huntington's disease (e.g., Scheller et al. 2013), focal dystonia (e.g., Altenmüller and Müller 2013), amyotrophic lateral sclerosis (e.g., Mohammadi et al. 2011), traumatic brain injury (e.g., Caeyenberghs et al. 2012a, b), spinal cord injury and spinal cord plasticity (e.g., Cadotte et al. 2012), agenesis of the corpus callosum (e.g., Wolf et al. 2011), congenital blindness (e.g., Collignon et al. 2011),

effects of therapeutic immobilization (e.g., Langer et al. 2012), systemic lupus erythematosus (e.g., Hou et al. 2013), fibromyalgia (e.g., Craggs et al. 2012), small vessel disease (e.g., List et al. 2013), hepatic encephalopathy (e.g., Qi et al. 2013), tinnitus and hearing loss (e.g., Schmidt et al. 2013), and Mal de Debarquement syndrome (e.g., Cha et al. 2012).

To give an overview of previously described neuroplastic responses of the diseased brain, we here discuss exemplary findings based on important neurological diseases which are represented in a relatively large body of published data. This allows an illustration of the complexity and limitations of clinical neuroplasticity research but cannot be comprehensive. We will start with neuroplasticity after stroke. Most data about clinical neuroplasticity have been published for this disease, and several of the neuroplastic effects described here can also be found in other diseases. To present other findings related to differing disease conditions, we will then review studies on epilepsy, tumor, multiple sclerosis, and peripheral nervous system disorders. All these illnesses include largely different pathophysiologies which affect neuroplasticity. Typical stroke consists of a single event which generates neuronal destructions followed by a regeneration period without the influence of additional pathologies. Typical epilepsy is characterized by the perseveration of pathological neuronal activity which may function as a continuous neuroplastic driving factor – and this may happen within a brain without morphological abnormalities (based on routine clinical imaging). Classical brain tumors continuously increase the area of brain destruction at a single specific site at different speeds. Multiple sclerosis is typically caused by the accumulation of new brain lesions over many years but not at a single specific site but in a multitopic fashion. With peripheral nervous system disorders, brain neuroplasticity is not induced by brain lesions. Instead, the changed information flow between the somatic periphery and the brain constitutes the driving factor.

4.1 Stroke

4.1.1 General Patterns of Neuroplastic Changes

4.1.1.1 Local Brain Activation Changes

The literature about neuroplastic changes following stroke is very heterogeneous. Early spontaneous reorganization and repair is largely variable within the first months and the speed of spontaneous (non-neuroplastic, see Introduction) neurological recovery correlates with the final outcome. Therefore, the majority of studies investigated neuroplastic changes in a chronic stage of stroke starting after about 6 months post tissue damage. After a stroke neuroplastic changes typically lead to improvement of the disturbed function. However, in some cases neuroplasticity may also result

in functional disturbance – called maladaptation. Besides preventing optimal motor performance (Bütfisch et al. 2008; Grefkes et al. 2008), maladaptation may also be found for other senses. Dilks et al. (2007) reported a case study of a patient whose fiber tracts providing input for the primary visual cortex were partly disconnected due to a stroke. The patient was blind in the deafferented part of the visual cortex (upper left visual field) and suffered from distorted perception in the unaffected lower left visual field. For example, he perceived a square presented in the lower left visual field as a rectangle extending upward (toward and into the blind part of the visual field). FMRI data revealed activation of the deafferented area when stimulating the lower left visual field and thus confirmed maladaptive reorganization of the primary visual cortex leading to perceptual distortion. Beauchamp and Ro (2008) described maladaptive neuroplasticity after a thalamic lesion which resulted in sound-touch synesthesia. They found abnormal brain activity to sounds in the parietal operculum, an area belonging to secondary somatosensory cortex. Only with sounds activating this somatosensory area, a sound-touch synesthesia occurred.

Criteria determining regeneration or maladaptation are not well understood. This is due to the large number of factors which may affect neuroplasticity. One such factor is the level of destruction of a primary brain area. Primary brain areas consist of functionally essential eloquent cortex. In contrast to lesions affecting nonessential cortex, neuroplastic reorganization cannot completely recover the disturbed function of a lesioned *primary* brain area. It is important to note that classical definitions of what constitutes a primary brain area have recently been challenged by results from voxelwise lesion-behavior mapping (Bates et al. 2003) or resections guided by intraoperative direct electrical stimulation (Ius et al. 2011). The latter data also emphasize that besides essential cortex there also are essential white matter tracts. An illustrative example how neuroplasticity may depend on the level of essential cortex destruction has been given by Vitali et al. (2007) in two aphasic patients with Broca's area lesions. After speech training, the patient with the smaller lesion showed left perilesional reactivation; however, the patient with complete destruction of Broca's area showed activation in the right Broca's homologue and therefore a lateralization change. Saur and Hartwigsen (2012) summarized factors which might influence right hemisphere language involvement in the chronic phase after stroke: (1) the amount of individual premorbid language lateralization (i.e., patients with a more bilateral premorbid language representation could better use homologue right areas), (2) the lateralization of the language function of interest (more bilaterally organized functions like language comprehension might involve right hemisphere areas to a greater extent compared with left-lateralized functions, like language production or syntax), and (3) the site and size of the left hemisphere lesion (i.e., small

strategic or large cortical damage of left hemisphere language zones more likely result in a permanent involvement of right homologue areas). In general, the literature indicates that the chronically reorganized language system post stroke comprises undamaged areas and perilesional tissue in the left hemisphere as well as homologue areas in the right hemisphere and that these reorganization networks are largely consistent across studies (Turkeltaub et al. 2011). However, the concrete distribution of activity depends on the elapsed time after stroke. A plausible model suggests that language recovery proceeds in three phases: first, a strongly reduced activation of remaining left language areas in the acute phase; second, an upregulation with recruitment of homologue contralateral language zones – which correlates with language improvement – and third, a normalization of activation (Saur et al. 2006). A similar interhemispheric time course has been found for the motor network in rodent stroke models (Dijkhuizen et al. 2012) and patients (Binkofski and Seitz 2004). The description of these temporal and localizational factors affecting neuroplasticity is extended by findings concerning effects of biological age and white matter lesions. Age at brain damage influences the extent of poststroke reorganization and the clinical outcome with extraordinary reorganizational capabilities early in life (e.g., Guzzetta et al. 2008; Rath et al. 2008). The amount of corticospinal tract lesions also affects reorganization, with more damage resulting in less neuronal activation (e.g., Hamzei et al. 2008). Altogether, the neuroplastic patterns described above argue for reorganization in preexisting redundant systems in which preserved ipsilesional and homotopic contralesional areas compensate for the damage. There is little evidence for takeover of areas previously completely unrelated to the specific brain function (e.g., takeover of motor functions by the visual system). An exception exists for cases where a functionally unrelated brain area is intact but deafferented. This has been described for early blind subjects where somatosensory or auditory processing has been found in the “visual” occipital cortex (e.g., Collignon et al. 2011).

4.1.1.2 Network Changes

Several studies investigated neuroplastic changes of functional and structural network connections after stroke. Concerning the principles of neuroplastic reorganization, an interesting dissociation between interhemispheric decoupling but increased local (intrahemispheric) coupling was described in animal studies by van Meer et al. (2010a, b). They found that strong interhemispheric correlations between resting-state fMRI signals of primary sensorimotor regions disappear in the first days after unilateral stroke in rats. In the subsequent weeks and coinciding with recovery of sensorimotor function, interhemispheric functional connectivity partially recovered. On the other hand, intrahemispheric functional connectivity did not deteriorate: connections

between primary somatosensory and motor cortices were preserved in the lesion's border zone and moderately enhanced within the contralesional hemisphere. In humans, persistence of intrahemispheric functional connectivity post stroke has also been described. Within the affected hemisphere excitatory interactions between frontoparietal areas and primary motor cortex exist (Rehme and Grefkes 2013). Concerning the interhemispheric interactions in humans, it is well known that primary motor cortex generally inhibits its contralateral homologue. If lesioned, this inhibitory influence is reduced resulting in a disinhibition of the contralesional motor cortex. In contrast, contralesional primary motor cortex still inhibits the lesioned area what may be maladaptive (Bütfisch et al. 2008; Grefkes et al. 2008). Interestingly, some studies indicate that connectivity changes persist even long time after stroke. For example, Mintzopoulos et al. (2009) investigated patients more than 6 months post stroke and found decreased effective connectivity between the primary motor cortex (M1) and the cerebellum. However, connectivity between the supplementary motor area (SMA) and the cerebellum was increased – as was the SMA-M1 connectivity. The authors conclude that this kind of neuroplasticity compensates for a dysfunctional M1. Using motor imagery tasks Sharma et al. (2009) reported that connectivity changes persisted even despite good recovery and normal local brain activity. Complementing the investigations about functional and effective connectivity, a few studies investigated network reorganization using Graph theory. For example, Wang et al. (2010) found that the motor execution network gradually shifted toward a random mode during the stroke recovery process. The authors conclude that a less optimized reorganization is involved in regaining function in the affected limbs. Although methodological limitations have to be considered (see Sect. 5), it is possible that some of the described connectivity changes do have structural correlates. For example, Jang et al. (2010) described a new motor pathway posterior to a lesion in the midbrain and upper pons.

4.1.2 Neuroplastic Changes Driving Recovery

4.1.2.1 Evidence with Standard Therapy

Several studies extend pure descriptions of poststroke neuroplasticity by correlating neuroplastic effects with clinical outcome. The results however are not unequivocal and the neuroplastic findings critically depend on disease duration. For the motor system, there is evidence that – after initial compensatory overactivations – the reconstitution of physiological brain activation patterns is a consistent predictor of a favorable recovery. Initial compensatory overactivations may be found in ipsilesional motor areas but also in contralateral areas from which uncrossed fibers may activate paretic muscles. Activation changes go along with functional and structural connectivity changes which also contribute to recovery. For example in chronic stroke patients, Schaechter

et al. (2009) found an association between the integrity of ipsilesional corticospinal tracts (as a result of degeneration and remodeling) and improved motor function. Further, brain stimulation findings indicate that enhanced excitability of disinhibited contralesional motor cortex typically normalizes within 90 days in patients with good recovery. Persistent recruitment of contralesional primary and bilateral secondary motor areas is often found in poorly recovered patients. In these patients, enhanced contralesional motor cortex excitability also persists (Buma et al. 2010; Bütfisch et al. 2008), and maladaptive inhibitory coupling from the contralateral upon the ipsilesional M1 may be found (Rehme et al. 2011). The importance of a physiological interhemispheric connectivity has been demonstrated by Carter et al. (2010, 2012): disruption of resting-state functional connectivity between left and right sensorimotor areas correlated with motor impairment (compare van Meer et al. 2010a, b, above). Within this context contradictory results of some studies can be understood. For example, two investigations of chronic paretic stroke patients found larger brain activations either with poor (Enzinger et al. 2008) or good (Laible et al. 2012) recovery. Enzinger et al. (2008) reported that particularly in the contralesional hemisphere, the extent of activation was increased, being compatible with an earlier “overactivation stage” of individual recovery. Laible et al. (2012) reported larger brain activation for the ipsilesional hemisphere, indicating that these patients were investigated at a later stage of individual recovery with a more typical (recovered) brain activation pattern. Consistent with this interpretation, Laible et al. described their patients as only moderately paretic at the time of the fMRI investigation. Besides primary and secondary sensorimotor cortices, also cerebellar activation changes contribute to successful recovery. In a longitudinal study over the first 6 months of stroke recovery, Small et al. (2002) found that increased activation in the contralesional cerebellum during rehabilitation supports a good recovery. From the data of Mintzopoulos et al. (2009, see above), it can be inferred that this goes along with an increased connectivity between the cerebellum and SMA and between the SMA and M1. Indeed, evidence for a positive correlation between SMA-M1 coupling and clinical outcome exists (Rehme et al. 2011; Grefkes et al. 2008).

As for the motor system, data for the language system are not unequivocal but several studies indicate that – again, after initial compensatory overactivations – reconstitution of physiological brain activation correlates with favorable recovery. This goes along with functional and structural connectivity changes. An instructive example is given by Papoutsi et al. (2011) who found that good recovery of syntactic function after left hemisphere damage was associated with an enhanced left frontotemporal effective connectivity and tract integrity. Correspondingly, in the patient population described by Warren et al. (2009), a reconstituted (or

preserved) physiological connectivity between the left and right temporal cortex correlated with receptive language performance, and Marcotte et al. (2012) found a better language recovery with reduced compensatory overactivations. For the early phase of recovery, it seems particularly positive if the brain is flexible enough to generate neuroplastic changes: Ovadia-Caro et al. (2013) described a correlation between lesion-induced connectivity changes and clinical outcome (the more, the better). Despite the general notion that normalization of brain activity drives recovery, there are indications that persistence of some residual neuroplastic deviations may be supportive to restore or maintain function. In a longitudinal study, Elkana et al. (2013) performed language fMRI scans years apart. They found that right hemisphere activation was associated with a better recovery in this extended chronic stage. In a typical left-dominant patient, a successful neuroplastic response of the language system might therefore consist of two factors: reconstitution of the typical left hemispheric activation pattern and ongoing right hemispheric activity supporting further recovery in the later chronic stage. These and other data generally challenge the classical view of recovery as ending within the first year after onset.

4.1.2.2 Evidence with Specific Interventions

The abovementioned correlations between neuroplastic changes and clinical outcome result from clinical standard interventions like physiotherapy, ergotherapy, logopedics, and standard medications. Various publications indicate that functional recovery can be enhanced or modified by specific interventions. Sawaki et al. (2008) showed that constraint-induced movement therapy may considerably improve reconstitution of physiological brain activation patterns and thereby clinical recovery. Ertelt et al. (2007) reported that observation of action generated widespread cerebral overactivations despite the patients being in a chronic (stable) phase. These neuroplastic overactivations correlated with improved motor function. Increased functional connectivity in motor and visuospatial networks of stroke patients has been reported by Várkuti et al. (2013) using very sophisticated behavioral interventions (robot-assisted upper-extremity training and brain computer interface with motor imagery). The individual gain in motor scores over 12 weeks could be predicted from functional connectivity changes. Very recent data render it likely that these correlations between functional neuroplastic findings and recovery are accompanied by structural brain changes. For example, in a longitudinal study describing the application of a novel MR-compatible hand-induced robotic device in chronic stroke patients (Lazaridou et al. 2013a, b), structural neuroplasticity after 8 weeks of hand training was found with the appearance of new corticospinal tract fibers, increased fiber number and tract length, and cortical thickness gain in the postcentral gyrus. Corresponding to Mintzopoulos et al. (2009) (see above), the authors also found that effective

connectivity between the SMA and M1 as well as between the SMA and cerebellum were increased by robotic training. The importance of an increased SMA-M1 coupling during motor rehabilitation is further underlined by an exemplary fMRI study of Wang et al. (2011) using a pharmacological intervention. With a placebo-controlled, double-blind crossover design, they showed that noradrenaline specifically improved the ipsilesional SMA-M1 coupling and the motor performance by the application of an oral noradrenaline reuptake inhibitor. Examples for nonstandard interventions with neuroplastic consequences exist also within the brain stimulation literature (Stagg and Johansen-Berg 2013). Inhibition of the contralateral motor cortex by repetitive transcranial magnetic stimulation (TMS) with 1-Hz for 10 min improved motor performance of the affected hand but also generated a contralateral overactivation (Nowak et al. 2008). Grefkes et al. (2010) reported that motor improvement after inhibitory TMS of the contralateral primary motor cortex correlated with a reduction of the negative influences originating from the contralateral M1 during paretic hand movements.

Concerning the language domain, Marcotte et al. (2013) reported that a special aphasia therapy (semantic feature analysis) improved integration in the posterior areas of the default-mode network and this correlated with language recovery. Zipse et al. (2012) described an interesting case of an adolescent aphasia lacking further language improvement despite intense and long-term standard speech-language therapy. After changing to a therapy which specifically involves right hemispheric functions (Melodic Intonation Therapy), language performance improved. This was associated with fMRI activation changes in the right frontal lobe and increased volume of white matter pathways in the right hemisphere. Similarly, associations between TMS evoked white matter changes and improvements in cortical function have also been postulated by Allendorfer et al. (2012). They found increased white matter integrity in the left frontal lobe as a result of excitatory TMS stimulation over the ipsilateral left hemisphere in aphasics.

4.2 Epilepsy

In general, MR signal changes related to the neuroplastic principles described for stroke – for example, compensatory overactivations or functional connectivity changes – are also found in epilepsy. For example, in temporal lobe epilepsy patients with normal structural MRI, Schwarze et al. (2009) described that hippocampal overactivation was necessary for a successful encoding of face-name associations. Intra- and interhemispheric functional connectivity for language tasks was found to be reduced in patients with both left- and right-sided epileptogenic foci (Pravatà et al. 2011). Since a characteristic feature of epilepsy is the perseveration of pathological neuronal activity,

in some patients this may hinder the reconstitution of a physiological brain state as described for recovery from stroke. In other patients, successful control of epilepsy may eliminate the neuroplastic driving factor, and reconstitution of physiological activation and connection patterns may follow (Helmstaedter et al. 2006). Several specific patterns of functional reorganization in patients with epilepsy have previously been described. In a multicenter study of pediatric localization-related epilepsy, You et al. (2011) identified three language activation patterns: first, a typical left hemispheric language network with left inferior frontal gyrus (Broca's area) and left superior temporal gyrus (Wernicke's area) activity; second, a variant left-dominant pattern with greater activation in Broca's area, mesial left frontal lobe, and right cerebellum; and third, activation in the right counterparts of the first pattern particularly in Broca's area. In a study on localization-related epilepsy with adults, Mbwana et al. (2009) found similar types of reorganization. In addition, they provided evidence for intra-hemispheric reorganization of language limited to the margins of typical left temporal activation.

Structural reorganization with epilepsy has also been investigated. In a study with patients with temporal lobe epilepsy (TLE), Powell et al. (2007) found that patients with more lateralized functional activation had also more lateralized connecting pathways within the functionally dominant hemisphere, compatible with a compensatory structural process. On the other hand, the epileptic seizure focus may disturb white matter tracts as shown by interhemispheric comparisons in children with focal cortical dysplasia (Kim et al. 2013) and patients with TLE (Liaci et al. 2012). They demonstrated increased DTI abnormalities ipsilateral to the seizure focus.

Due to the therapeutic option of epilepsy surgery, various studies investigated neuroplastic changes in this context. Weaver et al. (2013) investigated the potential of functional connectivity techniques for presurgical seizure focus identification in non-lesional focal epilepsy and concluded that it is possible to reliably predict its location. Results from studies which compare pre- and postsurgical neuroplastic changes are rather complex. Some studies indicate that neuroplastic reorganization patterns depend on the lateralization of the seizure focus. Wong et al. (2009) describe preoperatively increased right frontal activation with language tasks in both patients with right- and left-sided TLE. After anterior temporal lobectomy, however, only the left lobectomy patients showed a reduction of the right frontal overactivation. Similarly, Bonelli et al. (2012) found a postoperative fMRI activation change and stronger functional connectivity between frontal lobes only in the left lobectomy patients (and not in right TLE). Structural changes related to surgery have been described in the sense of loss of fiber tract integrity ipsilateral to the side of surgery (Faber et al. 2013) and in the sense of simultaneous decreases and increases of fiber tract integrity in different parts of the brain (Yogarajah et al. 2010).

4.3 Tumor

Again, the typical MR indices for neuroplastic changes described above can also be detected with different tumor types. The majority of data concerns compensatory overactivations and changed functional/structural connectivity. Both may be influenced by a large variety of factors. In a study with 68 patients with diffuse glioma, Harris et al. (2014) investigated changes of the default-mode network (DMN). In an evaluation of the influence of tumor grade, tumor volume, postsurgical clinical status, and tumor location, they found tumor grade to be the most significant predictor of DMN integrity with lower integrity in high-grade tumors. Effects on the DMN were also found for prior surgery. Although – as in other studies (e.g., Briganti et al. 2012) – tumor location influenced connectivity, the fact whether a tumor resided within or outside the DMN nodes did not influence the results.

A special feature of the various types of brain tumors is the fact that they continuously increase the area of brain destruction but do this with differing speed. Slow-growing lesions may generate less clinical symptoms and less neuroplastic changes. The infiltrative character of low-grade gliomas makes it even possible that function persists within the tumor (Duffau 2006). These facts may account for some of the discrepancies previously reported for the neuroplastic reorganization in tumoral lesions. An example is provided by a comparison of two patient groups with similar surgical lesions to the right medial temporal lobe (Braun et al. 2008). The groups differed clinically with respect to the preoperative course of disease. One group suffered from benign brain tumors with a slow but continuous increase of brain destruction; the other group suffered from hippocampal sclerosis, a stable pathology. The authors found a significant memory deficit for the tumor group only. They concluded that a stable pathology (hippocampal sclerosis) can yield significant functional reorganization which is not possible with a progressive pathology (tumors).

4.4 Multiple Sclerosis

Whereas earlier imaging studies with patients with multiple sclerosis (MS) predominantly described brain activation changes, recent literature focused on connectivity changes. Again the findings for this disease are not unequivocal and there is a large number of factors which may affect neuroplasticity in MS. These include age (effective connectivity increases with age, Rocca et al. 2010) and MS subtype (increased cerebellar-frontal effective connectivity with benign MS course, Rocca et al. 2012a). Given that the disease is characterized by a process which typically adds new lesions continuously over many years, and this in a multi-topic fashion, neuroplastic changes specifically depend on

the stage of the disease (Rocca and Filippi 2007). Therefore, brain activation changes which represent compensatory overactivations are common but variable. Concerning functional connectivity and disease stage, Cruz-Gómez et al. (2014) found that connectivity was reduced in four resting-state networks in cognitively impaired patients but only in one resting-state network in cognitively preserved patients. Rocca et al. (2012b) described a correlation between reduced resting-state connectivity and clinical disability and lesion volumes on T2-weighted MR images. In contrast, in a study investigating effective connectivity, Forn et al. (2012) described stronger connectivity for more cognitively impaired patients (relapsing-remitting MS). This is compatible with an increased demand on some brain areas to modulate others, which theoretically could even happen when general connectivity is reduced. Richiardi et al. (2012) suggested using functional connectivity analysis as a biomarker for the prognosis of the disease. Comparing a whole-brain connectivity matrix between minimally disabled MS patients and healthy controls, they found decreased connectivity for patients which correlated with white matter lesion load. Concerning structural neuroplasticity an interesting DTI study of Calabrese et al. (2011) described increased fractional anisotropy of normal-appearing gray matter in 168 patients with relapsing-remitting MS. This possibly reflects activation of microglia which then changes morphology in the sense of a more bipolar-oriented structure which would give rise to fractional anisotropy increase in gray matter. This finding was correlated with disease stage (i.e., clinical disability). Another study about structural connectivity of relapsing-remitting MS patients used graph theoretical methods (Shu et al. 2011). The authors found decreased white matter network efficiencies which correlated with the expanded disability status scale scores, disease duration, and total white matter lesion load. Correlations between altered structural and altered functional connectivity have also been described. In the study of Rocca et al. (2009), altered effective connectivity (increased and decreased) was correlated with structural damage of task specific fiber bundles, that is, fiber bundles involved in the tested cognitive performance. In contrast, no correlation between altered effective connectivity and fiber damage was found for bundles not directly related with the task.

4.5 Peripheral Nervous System Disorders

The special feature of peripheral nervous system lesions concerns the fact that brain neuroplasticity is not induced by brain lesions. Instead, the changed information flow between the somatic periphery and brain constitutes the driving factor. As with central nervous system lesions, a typical initial response to peripheral damage constitutes compensatory

overactivations. Fornander et al. (2010) and Rath et al. (2011, see Sect. 6.1 below) described an initial increase in the volume of the cortical activation in secondary brain areas after surgical restoration of complete median nerve injury. This overactivation subsequently declined during the following course of rehabilitation. For later recovery phases, Taylor et al. (2009) reported a correlation of decreased fMRI amplitude with gray matter loss 1.5 years after peripheral nerve transection and surgical repair. Initial overactivation is not only required to reestablish previous function but also to learn new functions. This has been shown by Chen et al. (2006) after transplanting a toe for replacement of a lost finger and by Eickhoff et al. (2008) for heterotopic hand replantation. In the latter study, effective connectivity between the healthy and affected (contralateral to the replanted hand) primary motor cortices was also determined. The results showed a maladaptive inhibition of the healthy on the affected motor cortex (see Sect. 6.3 below). Further examples for neuroplastic maladaptation can be found in amputees, where intact somatotopic representations extend into the representation area of the amputated limb and generate phantom limb pain. For instance, in a study of upper limb amputees, MacIver et al. (2008) found that cortical activation with lip movements extended to the area of the denervated hand and correlated with phantom limb pain. After special mental imagery training, overactivation was reduced and this correlated with a reduction of pain intensity, demonstrating that maladaptive neuroplasticity is reversible. This type of functional reorganization may also be accompanied by the structural reorganization of callosal fiber tracts (Simões et al. 2012).

Another feature consistently described is the fact that somatotopic brain activation typically corresponds to the peripheral nervous system output, but not to the effector activated by the output. Bitter et al. (2011) compared three types of peripheral surgical reorganization after facial nerve damage: classical hypoglossal-facial nerve anastomosis, hypoglossal-facial nerve jump anastomosis, and facial nerve interpositional graft. With all operations the effector (mimic musculature) is the same; however, the peripheral nervous system output required for identical movements changes. Lip movements after facial nerve interposition led to selective brain activation in the original facial motor cortex. Lip movements after hypoglossal-facial anastomosis were associated with activation in the hypoglossal motor cortex. For the jump anastomosis, however, overlapping activation encompassing both the original facial and the hypoglossal motor cortex was found. Another impressive example of brain activation corresponding to peripheral nervous system output (and not the changed effector) is presented in patients with brachial plexus lesions. In case of a complete avulsion of a brachial plexus, it is possible to connect the denervated biceps with fibers of the contralateral C7 root. The brain is then required to control flexion of the diseased arm with the

ipsilesional motor cortex. Functional imaging data have shown that this is achieved via activation of the typical ipsilesional C7 arm area (controlling the contralateral C7 root), though initially a bilateral activation pattern may occur (Hua et al. 2013; Beaulieu et al. 2006). More complex neuroplastic effects can be found when biceps reinnervation is done via a connection to the side of the phrenic nerve (Beisteiner et al. 2011, see Sect. 6.2 below).

An instructive example that evocation of cortical neuroplasticity is not restricted to macroscopic nerve changes but may also be induced by affections of terminal nerve endings and mechanoreceptors was provided by Kapreli et al. (2009). In patients with complete right unilateral anterior cruciate ligament rupture, afferent information flow from mechanoreceptors to the brain is disturbed. Despite the central and peripheral nervous system being undamaged otherwise, the authors found cortical reorganization in sensorimotor and other brain areas (as determined relative to healthy controls).

5 Methodological Considerations

As with every neurophysiological technique, there are also limitations and pitfalls for fMRI and DTI (compare book chapter, Clinical BOLD fMRI and DTI: Artifacts, Tips, and Tricks). Some limitations are of special importance for neuroplasticity investigations. These relate to the technical and neurophysiological interpretation of findings.

5.1 Technical Interpretation of Findings

Technically, it is important to realize that sensitivity and specificity of fMRI and DTI are limited, so that false-negative and false-positive findings can be encountered. With standard fMRI methods major risk factors for false findings include limited signal to noise and contrast to noise ratios, image artifacts (e.g., ghosting, signal voids, motion artifacts, registration errors), effects of data analysis thresholds (e.g., statistical thresholds set for “true” activation), altered hemodynamic responses due to changed neurovascular coupling in pathological tissue, and inadequate patient compliance. With standard DTI methods major risk factors for false findings are similar: limited signal to noise ratio, image artifacts, and effects of data analysis thresholds (e.g., anisotropy thresholds set to define tract endings). Specific DTI problems concern the variability and limitations of current DTI techniques: deterministic vs. probabilistic tractography, Gaussian vs. non-Gaussian model of diffusion, number of diffusion-weighted gradient directions, and specific effects of spatial resolution.

5.2 Neurophysiological Interpretation of Findings

Even when the fMRI/DTI data are technically perfect according to the state of the art, the neurophysiological interpretation is not always unequivocal. Particularly with fMRI data one has to bear in mind that results are correlative in nature and causal conclusions are limited. If there is information provided with fMRI only, it is also difficult to differentiate activations of essential primary cortical areas from modulatory secondary activity within neuroplastically changed activation patterns. Further, the results may be specific for the given MR methodology and incongruent to findings with other techniques. For example, in patients with temporal lobe epilepsy, Bettus et al. (2011) found lower functional connectivity in regions with epileptiform abnormalities based on intracerebral electroencephalography (EEG). However, an opposite pattern resulted from fMRI data of the same patients. As already discussed in the chapters above, possible reasons for fMRI activation changes are manifold. FMRI overactivations may indicate both beneficial functional compensation and maladaptation. Lateralization changes may be due to contralateral overactivation or ipsilateral underactivation. The dependence of lateralization on experimental (e.g., task difficulty) and patient factors (e.g., cognitive efforts, epileptic activity) also needs to be considered. Further, altered fMRI signals may result from a changed vascular situation (e.g., preexisting vasodilation or stenosis) instead of a changed functional organization.

For the neurophysiological interpretation of DTI data, it is important to realize that DTI “tracts” are an imperfect model-based construct which typically does not directly correspond to a physical fiber. Due to the methodological difficulties named above, current DTI techniques are limited with regard to a complete identification of the true fiber situation. Particularly in areas with many intersecting pathways like the centrum semiovale, fractional anisotropy values may be artificially low. Also, for pathological tissue like edema or infiltrating tumor, involved tracts may show reduced anisotropy despite not being destroyed. They may also show complex directional tensor changes. Clinicians should therefore be careful with qualitative and quantitative conclusions. It is also mandatory to include the known intraindividual (homologue tracts may differ between hemispheres, Smits et al. 2012) and interindividual tract variability from healthy subject studies in the interpretation.

5.3 Consequences for Neuroplasticity Investigations

The foremost consequence for achieving significant neuroplasticity data is to consider all known pitfalls with performance of fMRI/DTI patient investigations. This includes optimization of patient cooperation, patient performance, and adequate task

selection including patient training. Exploring tasks of different complexity may help to clarify the role of overactivated brain areas. For sound associations of clinical outcome with neuroplastic findings, meaningful outcome measures are required – for example, specific testing of the disturbed function (maximum rate, range, force, and accuracy of a recovered movement) instead of a constriction to gross clinical scales. Outcome measures should capture all relevant functions (e.g., determination of dexterity in a paretic limb, detection of possible mirror movements) to separate behavioral compensation from recovery of the original function. To allow a valid interpretation, the neuroplastic findings need to be reported with an intrascan behavioral documentation and in relation to the location and extent of the lesion. Further, it is important to capture possible confounding factors for neuroplasticity like medication and co-interventions. Concerning the setup of new investigations, it should be regarded that the comprehensive detection of neuroplastic transformations requires longitudinal studies in homogeneous patient populations starting at an early stage of the disease. Currently, such data are sparse (e.g., most stroke studies investigated patients in a chronic stage).

From the technical viewpoint it is beneficial to apply the latest methodological developments like ultrahigh-field MR for functional imaging (Beisteiner 2013) and new diffusion imaging methods for DTI (compare Huston and Field 2013). This is also true for new data-driven analysis strategies which reduce the amount of model assumptions (e.g., Robinson et al. 2013). Validation and an improved interpretation of fMRI/DTI findings can be achieved by multimethodological approaches. For example, arterial spin labeling may be used to detect abnormal brain perfusion and alternative neurophysiological techniques (EEG, magnetoencephalography, positron emission tomography, intraoperative electrical stimulation) can provide independent functional data. Brain stimulation techniques (transcranial magnetic stimulation, transcranial direct current stimulation) allow controlled variation of the brain's functional state.

6 Clinical Examples

6.1 Longitudinal Neuroplasticity Associated with Peripheral Nerve Regeneration

Surgical repair of a transected peripheral nerve is usually followed by a regeneration process involving neuroplastic changes. Rath et al. (2011) provided the first longitudinal fMRI study of cortical somatosensory reorganization following peripheral nerve repair. They presented a case report of a 43-year-old man with isolated complete transection of the right median nerve at the volar side of the wrist who underwent an immediate end-to-end coaptation of the affected nerve.

Clinical assessment revealed initial sensory and motor deficits typical for this nerve lesion with distal loss of sensation of digits II and III, loss of thumb opposition, and weakening of thumb abduction. The patient received an intensive sensory relearning treatment, and his sensory and motor functions were regularly clinically evaluated. Functional imaging was performed at 1, 7, and 15 weeks as well as 1 year after surgery by using a somatosensory stimulation paradigm that consisted of vibrotactile stimulation of digits II and III on the affected and healthy hand, respectively. Functional regions of interest (ROIs) were defined according to previous literature and comprised bilateral primary somatosensory cortices and bilateral frontoparietal areas. Peak *t*-values within these ROIs were used to calculate ratios comparing the injured with the healthy hand. While the patient exhibited no functional activation in the primary somatosensory cortex in the first week after surgery, this activity recovered steadily within a year (compare Fig. 1a). Further, initial frontoparietal overactivation of the affected hemisphere diminished within the same time period (Fig. 1b). This recovery of physiological fMRI patterns corresponded with the clinical recovery of the operated hand. One year after surgery, the diseased hand had recovered 66 % of the sensory and motor function level compared to the healthy hand. Rath et al. proposed to embrace the neuroplastic changes in the primary somatosensory cortex and frontoparietal areas in a regeneration index for the restoration of somatosensory functions (Fig. 1c).

6.2 Neuroplasticity After Nerve Repair in Brachial Plexus Lesions

Complete brachial plexus lesions lead to a total paresis of the affected arm resulting in a significant impairment in everyday life. Reinnervation of the affected musculocutaneous nerve via an intact C7 root or via the ipsilateral phrenic nerve can be performed to regain elbow flexion. In an fMRI study, Beisteiner et al. (2011) analyzed functional activation in three patients with complete brachial plexus lesions and in three healthy controls. Two patients underwent an end-to-side nerve reconstruction of the musculocutaneous nerve with the ipsilateral phrenic nerve and one patient received an end-to-end coaptation of the healthy contralateral C7 root with the musculocutaneous nerve. The advantage of the end-to-side technique is the preservation of the donor nerve function – that is, the control of the diaphragm persists via the modified phrenic nerve. However, after establishing an end-to-side connection, the phrenic nerve and its cortical projection area are required to perform a new double function: independent control of breathing and elbow flexion. In contrast, in the control patient (C7 – musculocutaneous connection) the phrenic nerve remained unchanged. FMRI tasks comprised elbow flexion of the healthy arm, elbow flexion of the diseased arm, forced abdominal inspiration, and foot flexion

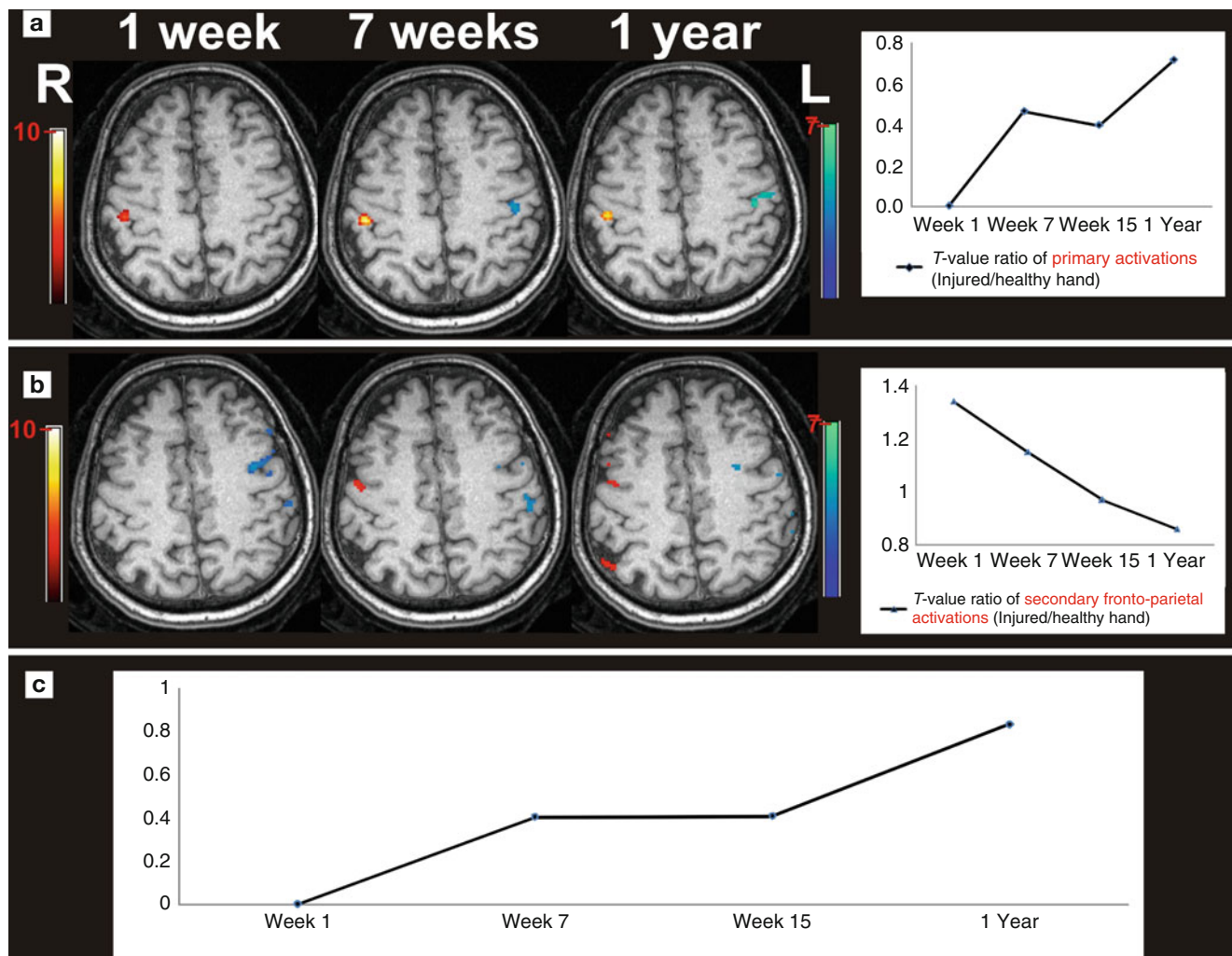


Fig. 1 Functional magnetic resonance imaging brain activations with vibrotactile hand stimulation shown on anatomical images. The patient was investigated after complete median nerve transection of the right hand and immediate epineural end-to-end coaptation. Vibrotactile stimulation was separately applied to the left and right hands. **(a)** Representative anatomical slice illustrating the time course of maximum *t*-values in the primary somatosensory cortex (injured hand: blue

voxels; healthy hand: red voxels). The graph illustrates the peak *t* value ratios of the injured/healthy hand ($p < .01$ uncorrected). Only top 150 *t* value voxels per brain volume are shown for display purposes and color bars indicate *t*-values. **(b)** Same illustration for frontoparietal cortex. **(c)** Proposed regeneration index calculated from graphs A and B (ratio primary cortex)/(ratio frontoparietal cortex) (Reproduced with permission from Rath et al. (2011)) (Color figure online)

on the affected side. Clinical documentations such as electromyographic recording, chest radiography, and fluoroscopy of the thorax confirmed that end-to-side patients were able to control the diaphragm and the arm independently. In Fig. 2, functional imaging findings in patients and controls are summarized. Forced inspiration activated the diaphragm (phrenic nerve) area of the primary motor cortex bilaterally in all participants. In patients with end-to-side anastomoses, elbow flexion of the diseased arm resulted in unilateral activation of the arm area in the primary motor cortex and in an additional activation of the diaphragm area. This recruitment of the diaphragm area was absent when these patients performed movements of the healthy arm or the foot. As expected, neither the control patient nor the healthy control subjects showed activations in the

phrenic nerve area during arm movement. These findings suggest that neuroplasticity may even transform a healthy mono-functional cortical area into a bifunctional area – here shown for the diaphragm area.

6.3 Neuroplastic Changes of Effective Connectivity in Patients with Heterotopic Hand Replantation

Eickhoff et al. (2008) investigated cortical plasticity in two patients that underwent a resection of parts of the forearm including the elbow joint due to a malignant soft tissue tumor and a subsequent reimplantation of the amputated distal

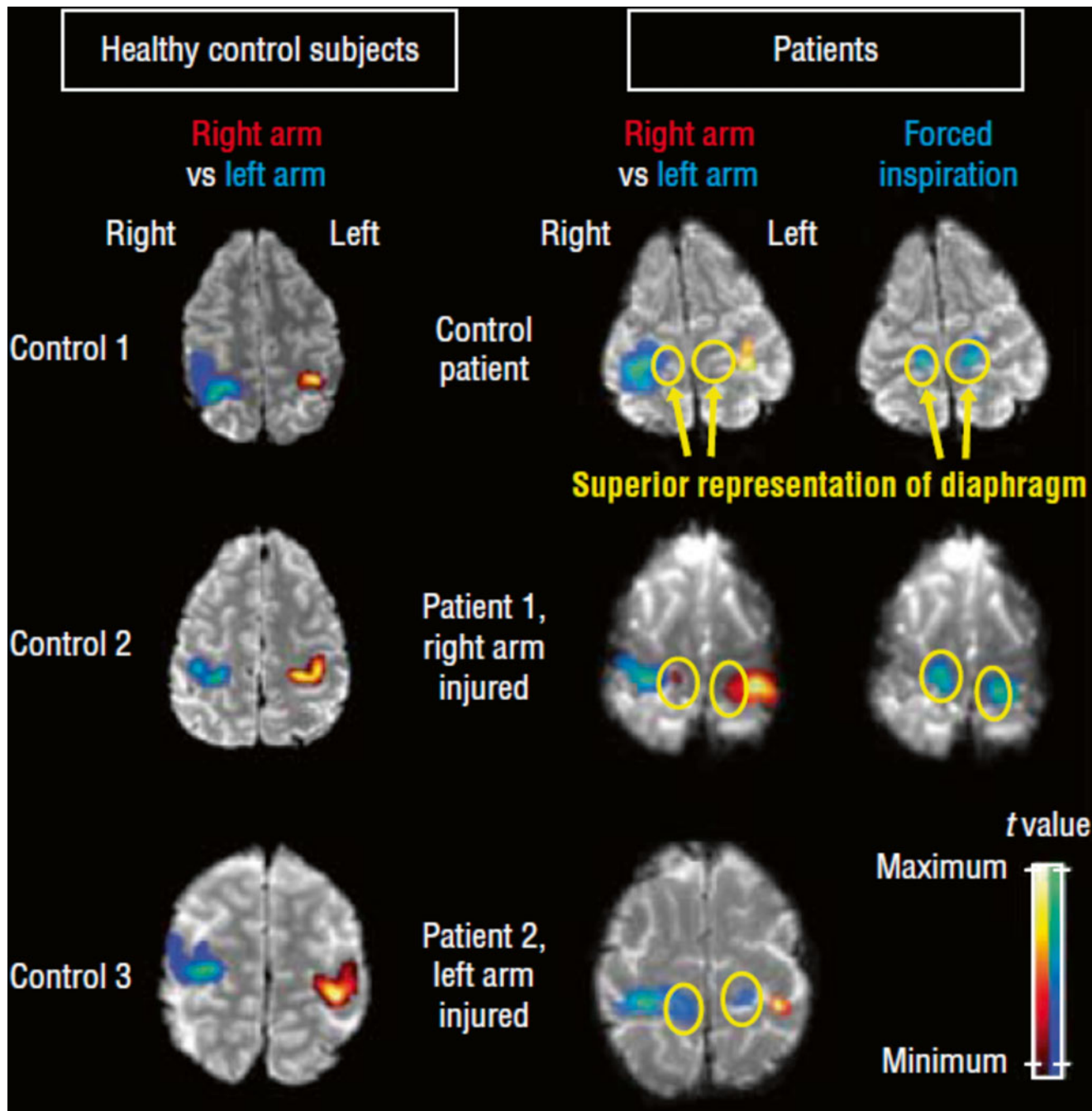


Fig. 2 Original functional magnetic resonance images showing brain activation in the diaphragm area (*circles*) in the superior primary motor cortex and in the adjacent arm areas. The right hemisphere is shown on the left side. Only primary motor cortex activations are depicted, and colors indicate *t* value distributions within depicted activation clusters (relative scaling according to local maxima and minima). All images are thresholded at $p < .001$ uncorrected. Representative slices are shown for the three healthy control subjects, the control patient with C7 end-to-end coaptation, and the two patients with phrenic nerve end-to-side

coaptation. The columns labeled “right arm vs left arm” show significant activation differences of right > left arm (red) and left > right arm (blue). In the patients with phrenic nerve end-to-side coaptation, the diaphragm area is activated only with flexion of the injured arm, not with flexion of the healthy arm. In all controls, arm flexion did not activate the diaphragm area. Forced abdominal inspiration selectively activated the diaphragm area in all subjects (rightmost column, blue activation clusters) (Reproduced with permission from Beisteiner et al. (2011)) (Color figure online)

forearm including the hand. Thereby, tendons of the finger flexors and extensors were attached to upper arm muscles, and distal forearm nerves were coapted with the nerve trunks of the upper arm.

The 2 patients and 14 healthy control subjects performed a motor fMRI task comprising fist-closing movements with the right, left, or both hands simultaneously. Dynamic causal modeling (DCM) was applied to explore effective

connectivity within an anatomically and functionally defined bilateral motor network consisting of the primary motor cortex (M1), the supplementary motor area (SMA), the ventral premotor cortex (PMC), and extrastriatal visual cortex (V5). The latter region was defined as the input region for the bilateral SMA and PMC as movements were visually paced in the fMRI task. All regions were defined for the affected hemisphere (hemisphere contralateral to the side of peripheral surgery) and the healthy hemisphere (hemisphere ipsilateral to the side of peripheral surgery). Effects of interest analysis revealed a significantly increased activation during tasks compared to the baseline in the motor ROIs. Intrinsic connectivity, that is, task-independent connectivity, was symmetrically organized in controls (Fig. 3, top panel) with a positive influence (green arrows) of the SMA and PMC on M1 and an inhibition (red arrows) between bilateral M1 and SMA. In contrast, both patients showed altered influence of the PMC of the affected hemisphere. However, the actual patterns of intrinsic connectivity differed between both patients as depicted in Fig. 3 (bottom panel). When moving the healthy hand, the PMC of the affected hemisphere was inhibited by the PMC and M1 of the healthy hemisphere in both patients. Eickhoff and colleagues interpreted this result as an enhanced suppression of the influence of the affected hemisphere on the control of the healthy hand. In both patients, movements of the replanted hand resulted in increased activation of the affected PMC that might reflect an increased effort required to perform the task. In addition, a pathological inhibition of the healthy M1 on the affected M1 was present in both patients when moving the replanted hand. The most prominent difference between the two patients was present in the affected PMC (Fig. 3, bottom panel). In patient J.H., the affected PMC had an increased positive influence (compared to controls) on the M1 of the same hemisphere at rest (intrinsic connectivity) as well as during movements of the replanted hand, while in patient G.M., the M1 was inhibited by the PMC. Correspondingly, motor performance of G.M. was worse than that of J.H. Eickhoff et al. concluded that different neuroplastic connectivity changes were related to clinical progress and behavioral performance stressing the importance of an early and intense rehabilitative exercise as it was the case for patient J.H.

6.4 Neuroplastic Reorganization of Hand Functions After Hemispherectomy

Rath et al. (2008) reported a single-case fMRI study of a 27-year-old man who underwent a functional hemispherectomy at the age of 11. The patient suffered from an infarction of the right middle cerebral artery at 2 years of age. After the stroke he showed considerable improvements of motor functions of the left paretic hand; however, he developed intrac-

table generalized epilepsy that required a resection of the affected right hemisphere. Although his hemiparesis worsened after hemispherectomy, hand function recovered again after physiotherapy and orthopedic surgeries. At the time of the MR investigation, the patient had spastic hemiparesis but voluntary control and sustained weak motor functions in the hemiparetic arm. Anatomical MRI revealed no pathological findings in the remaining left hemisphere. Functional imaging showed that movements of both hands induced significant activation in the remaining primary motor cortex. Movements of the healthy hand corresponded to activation in the typical hand motor area, whereas movements of the paretic hand produced two activation clusters in the periphery of the hand motor area (Fig. 4). This reorganization is likely to be induced by the hemispherectomy rather than by the initial stroke since hemiparesis showed an initial worsening after hemispherectomy and a secondary improvement after rehabilitation. This single case demonstrates that functional transition zones (i.e., the periphery of a functional cortical area) in the ipsilateral hemisphere can be used to restore functions when no contralateral functional tissue anymore exists.

6.5 Structural Neuroplasticity in Patients with Chronic Stroke

Acute stroke often leads to impaired motor and cognitive functions that are sought to be improved by rehabilitation. Patients with only partial recovery suffering from residual impairments after rehabilitation are referred as chronic stroke patients.

Lazaridou et al. (2013b) investigated structural neuroplastic changes corresponding to a rehabilitative motor training by assessing cortical thickness with voxel-based morphometry (VBM) and white matter integrity with DTI in four patients with chronic stroke. The time interval between the onset of left-sided ischemic subcortical middle cerebral artery stroke and the participation in the study was more than 6 months. The patients underwent an 8-week-lasting motor training consisting of 1 h squeezing an exercise ball with the paretic hand for 3 days per week. MR scans were performed at baseline (before the training), after 4 weeks of training, at the end of the training period (after 8 weeks), and finally another 4 weeks later. For DTI fiber reconstruction, deterministic tractography was performed and visually inspected for directionality and location. The pons, the posterior limb of the internal capsule, and the motor cortex were selected as seed regions to reconstruct the corticospinal tract (CST).

Statistical analysis of CST fibers of the affected hemisphere revealed a significant increase in the number of fibers and average tract length as illustrated in Fig. 5 depicting CST fibers of a representative patient before, during, and after motor training. CST fibers (in blue) projected

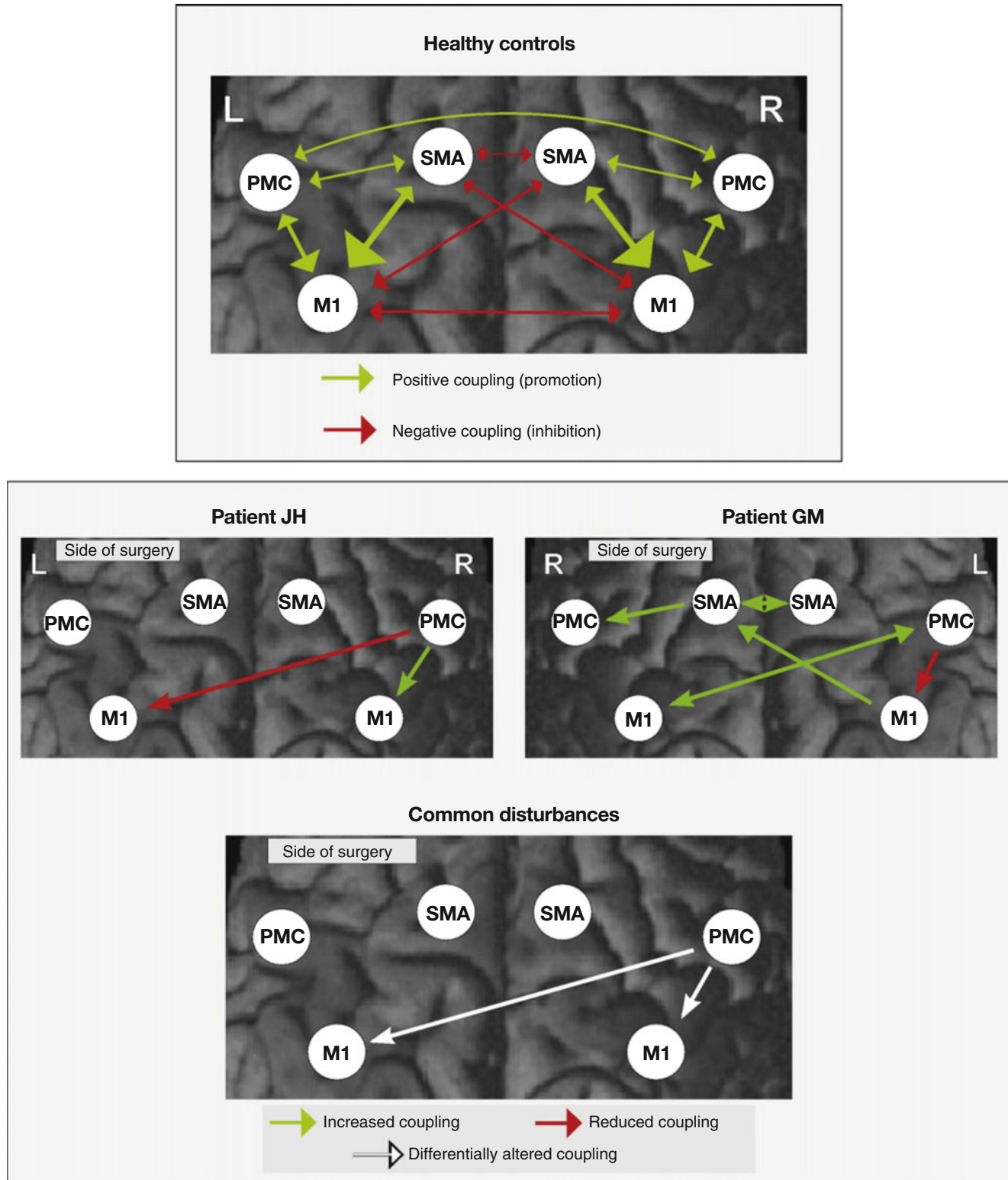


Fig. 3 Top panel: regions of interest selected for estimating cortical connectivity shown on a surface rendering of the MNI single-subject template. Displayed regions were significant at $p < 0.05$ (corrected) in an F-contrast testing for the effects of interest, that is, regions where hand task-related variance was significantly greater than noise. The intrinsic connectivity in healthy controls ($N=14$) as estimated by means of dynamic causal modeling is displayed. Reciprocal connectivity is assumed for the six motor regions, while visual input is provided via left and right V5 into all four premotor regions. Coupling parameters indicate connection strength, which are coded for size and color. Positive coupling (green arrows) suggests facilitation, whereas negative coupling (red arrows) can be interpreted

as neural inhibition. Bottom panel: differences in intrinsic connectivity between the two patients and the control group. Only those connections whose strength was significantly different ($p < 0.05$ corrected) from those of the controls in a two sample T -test are displayed. Green arrows denote coupling parameters which were significantly higher (more positive) as compared to normal subjects, red arrows those significantly lower, that is, more negative. In the synaptical panel in the bottom row, white arrows indicated those connections which were significantly altered in both patients but effect changes in opposite directions (Reproduced with permission from Eickhoff et al. (2008)) (Color figure online)

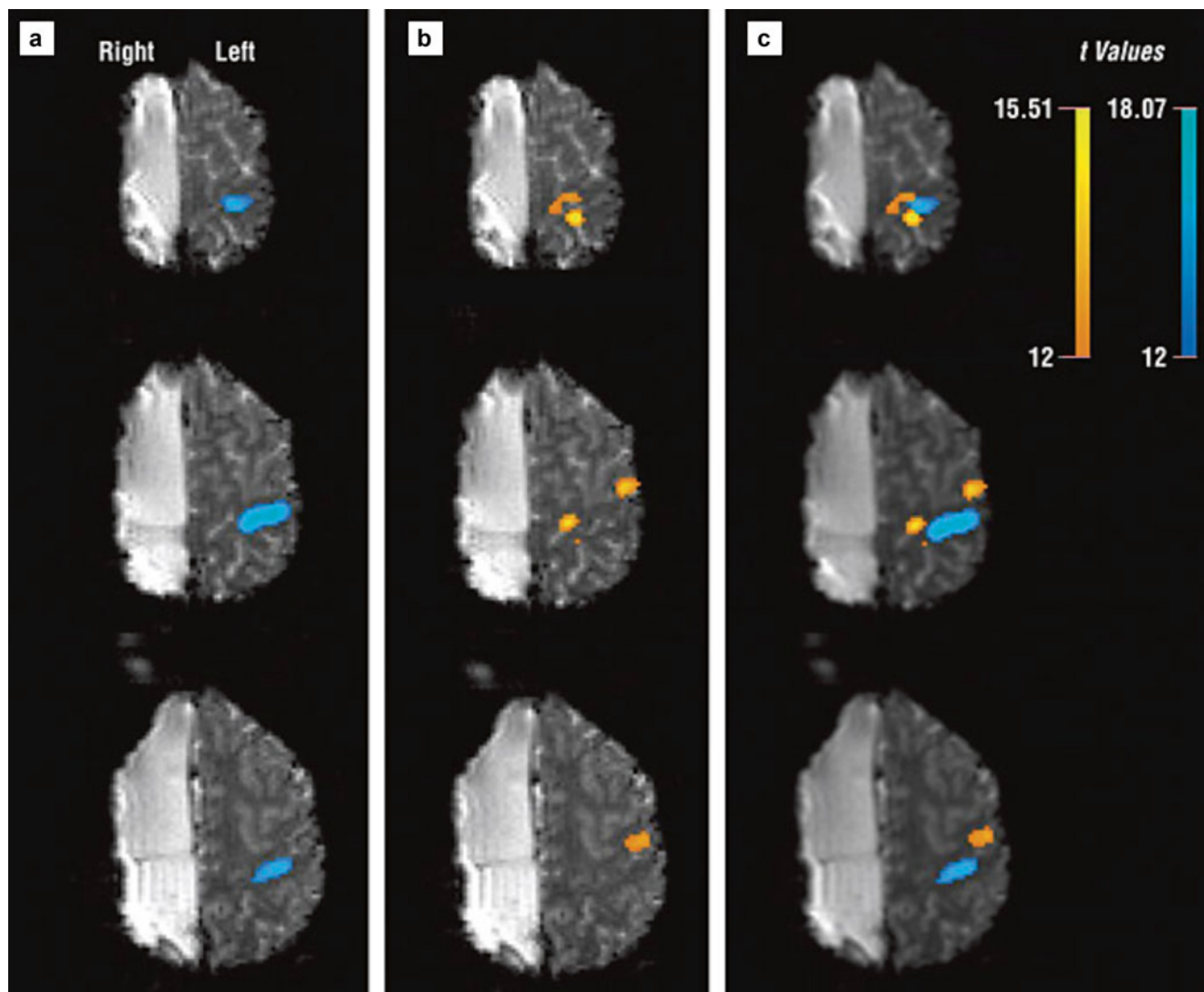


Fig. 4 Functional echoplanar imaging originals ($t > 12$) showing activation in three slices covering the hand motor area (top row is most superior slice). (a) Contralateral healthy hand activation shown in blue.

(b) Ipsilateral paretic hand activation shown in orange. (c) Activation in both hands (Reproduced with permission from Rath et al. (2008)) (Color figure online)

progressively closer to the motor cortex and showed increased density with ongoing training progress. In addition, VBM analysis showed a significantly increased cortical thickness of the ventral postcentral gyrus after training compared to the baseline. With this study, Lazaridou et al. could demonstrate that intensive motor training resulted in structural neuroplasticity in the sensorimotor system in chronic stroke patients and provided a new approach for the evaluation of the rehabilitation progress.

6.6 Neuroplastic Network Changes in Traumatic Brain Injury

Traumatic brain injury (TBI) is often followed by persistent cognitive deficits affecting several cognitive domains like attention, working memory, speech, and executive functions such as planning, inhibition, and cognitive control.

Caeyenberghs et al. (2012b) addressed the latter issue using a functional imaging approach combined with a graph theoretical analysis. They examined 23 patients with mild to moderate TBI and 26 healthy control subjects applying an event-related fMRI paradigm previously used to investigate cognitive control in young and elderly adults (Coxon et al. 2010) and in TBI patients (Leunissen et al. 2013). Participants performed temporally coupled circular hand movements (either clockwise or counterclockwise) with each hand using a joystick. Visual cues indicated whether to switch the movement patterns from asymmetric to symmetric or vice versa or to continue the prior movement. The authors constructed a switching motor network consisting of 22 regions of interest that were defined as 10 mm spheres centered on peak activation coordinates reported by Coxon et al. (2010) and Leunissen et al. (2013). The network comprised regions of the medial frontal cortex, anterior cingulate cortex, bilateral dorsolateral prefrontal cortex, bilateral inferior frontal cortex

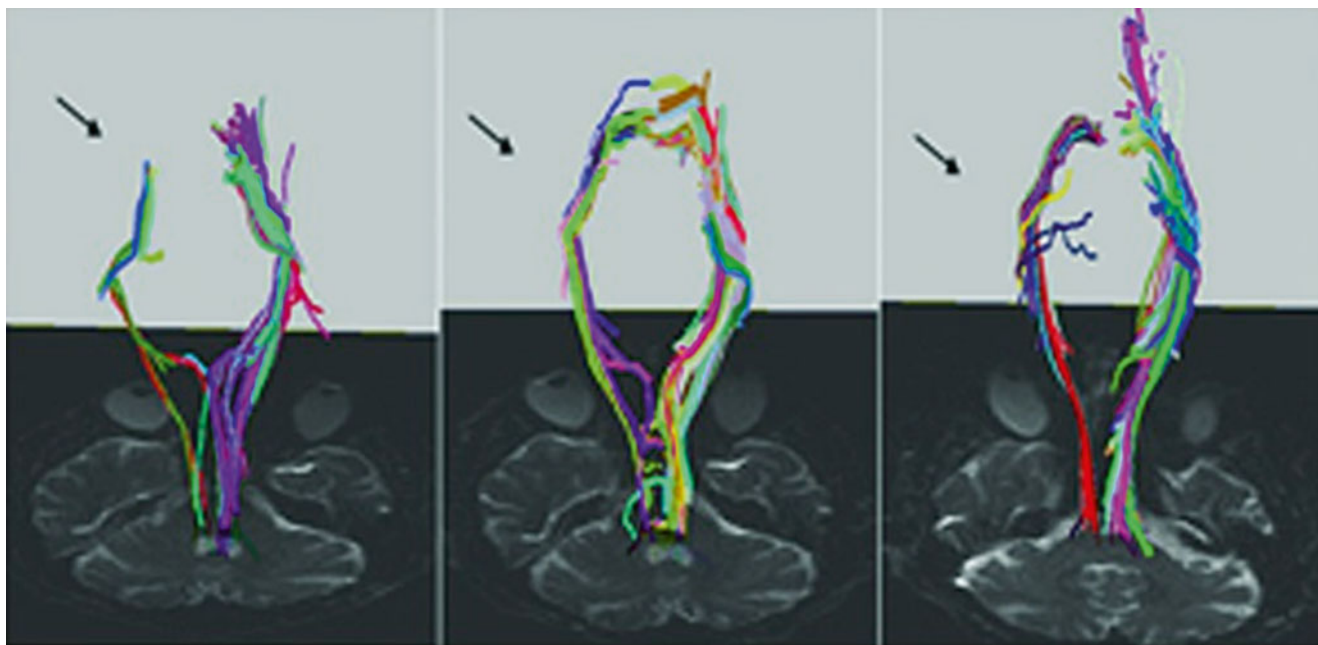


Fig. 5 Reconstructed corticospinal tracts (CSTs) from the same stroke patient before training (left panel), after 4 weeks of training (middle panel) and after 8 weeks of training (right panel). Note that

reconstructed CST fibers increased dramatically on the right side with training (arrows) (Reproduced with permission from Lazaridou et al. (2013b))

(BA 44), basal ganglia, cerebellum, right precuneus, left pre-motor cortex, bilateral insula, and right superior and inferior parietal cortex. First, a contrast Switch > Continue was conducted to compute the average time series for each ROI of each subject which was then subjected to a partial correlation analysis. This method allowed a quantification of the unique correlation between two ROIs and the content filtering of the effects of all the other ROIs giving an appropriate measure for functional connections. For graph theoretical analysis, matrices with significant connections weighted by the correlation values between nodes (i.e., ROIs) were constructed. Weighted matrices were used to calculate the mean connection strength of the single nodes as well as of the overall network connection strength. The Brain Connectivity Toolbox (Rubinov and Sporns 2010) was employed to assess global network architecture and nodal properties.

TBI patients exhibited slower response times and more disruptions during the switching task than the controls that could not be explained by motor difficulties. Graph theoretical analysis revealed a significantly altered functional network in patients with higher connectivity degree and strength than in controls. Specifically, the patients exhibited a higher connectivity in the left ventral portion of M1 (compare yellow sphere in Fig. 6) possibly reflecting functional

compensation as this area is involved in coordination and is strongly interconnected within the primary motor cortex. In addition, local efficiency was enhanced in patients with TBI which might indicate a compensatory increase of short-range connections between adjacent nodes. Besides, graph theoretical analysis provided information about hubs, that is, regions with a central role in a functional network. In both the patients and controls, the right insula with its critical role in the differentiation between internal and external stimuli presented as a hub, putatively due to the strong directive of a visual input to trigger movement switching. Interestingly, two regions mainly involved in movement planning (right dorsolateral prefrontal cortex and left dorsal premotor cortex) acted as hubs in the TBI group only. Caeyenberghs and colleagues (2012b) concluded that TBI patients might rely more on cognitive control and performance monitoring during the switching task. However, the higher mean connectivity degree in patients was related with poorer switching performance implying that increased connectivity not necessarily improves function. Moreover, higher connectivity degree was positively correlated with injury severity and might therefore be a result of a more severe brain damage reflecting a higher effort to manage cognitive control tasks.

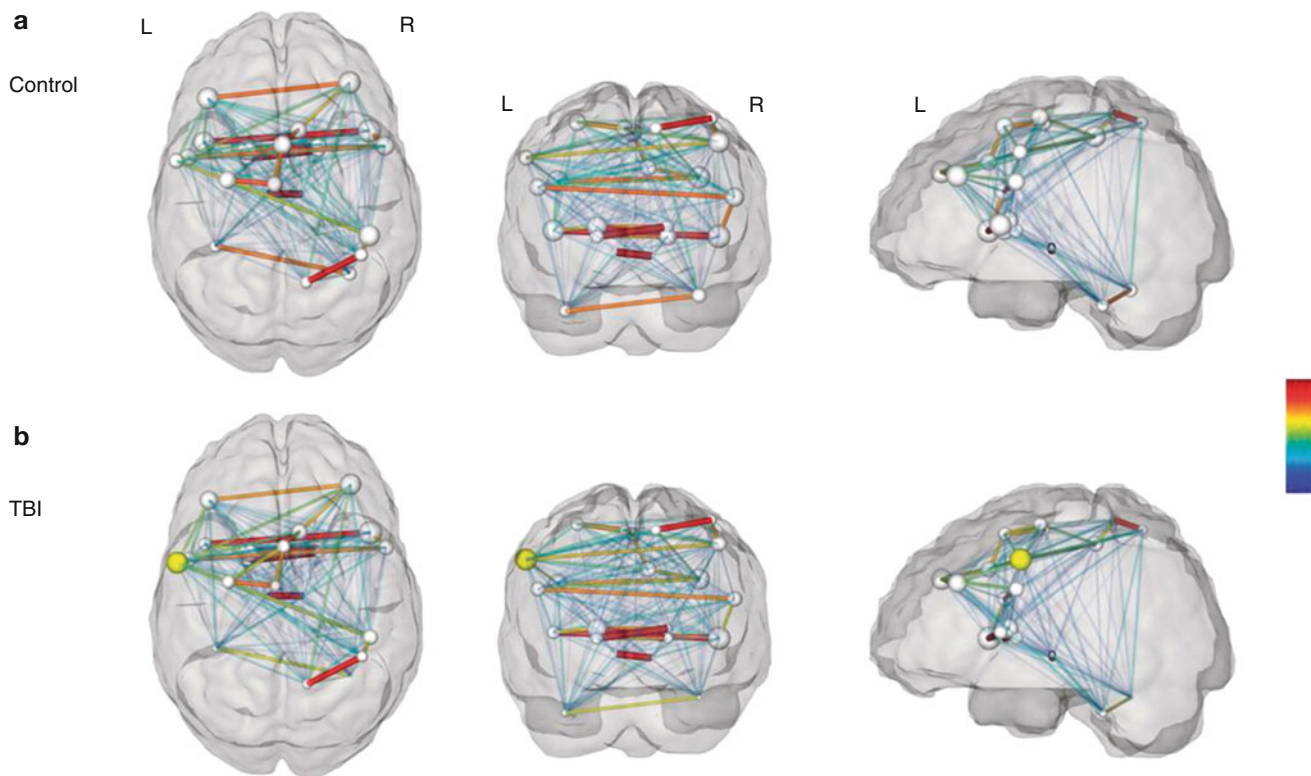


Fig. 6 Group differences in connectivity degree. (a) Controls and (b) patients with TBI. The size of the regions of interest (spheres) represents connectivity degree. The edge widths represent the strength of the partial correlations between nodes. Notably, the networks shown here were constructed by summing the partial correlation matrices of all subjects in each

group (as shown by the color bar). Yellow sphere indicates higher connectivity in left ventral premotor cortex ($p < 0.002$ corrected) in patients with TBI (Reproduced with permission from Caeyenberghs et al. (2012b)) (Color figure online)

References

- Allendorfer JB, Storrs JM, Szaflarski JP (2012) Changes in white matter integrity follow excitatory rTMS treatment of post-stroke aphasia. *Restor Neurol Neurosci* 30:103–113. doi: [10.3233/RNN-2011-0627](https://doi.org/10.3233/RNN-2011-0627)
- Altenmüller E, Müller D (2013) A model of task-specific focal dystonia. *Neural Netw* 48:25–31. doi: [10.1016/j.neunet.2013.06.012](https://doi.org/10.1016/j.neunet.2013.06.012)
- Andersson D, Wilhelmsson U, Nilsson M, Kubista M, Ståhlberg A, Pekna M, Pekny M (2013) Plasticity response in the contralesional hemisphere after subtle neurotrauma: gene expression profiling after partial deafferentation of the hippocampus. *PLoS One* 8:e70699
- Appel-Cresswell S, de la Fuente-Fernandez R, Galley S, McKeown MJ (2010) Imaging of compensatory mechanisms in Parkinson's disease. *Curr Opin Neurol* 23:407–412. doi: [10.1097/WCO.0b013e32833b6019](https://doi.org/10.1097/WCO.0b013e32833b6019)
- Araque A, Navarrete M (2010) Glial cells in neuronal network function. *Philos Trans R Soc Lond B Biol Sci* 365:2375–2381. doi: [10.1098/rstb.2009.0313](https://doi.org/10.1098/rstb.2009.0313)
- Bates E, Wilson SM, Saygin AP, Dick F, Sereno MI, Knight RT, Dronkers NF (2003) Voxel-based lesion-symptom mapping. *Nat Neurosci* 6:448–450
- Beauchamp MS, Ro T (2008) Neural substrates of sound-touch synesthesia after a thalamic lesion. *J Neurosci* 28:13696–13702. doi: [10.1523/JNEUROSCI.3872-08.2008](https://doi.org/10.1523/JNEUROSCI.3872-08.2008)
- Beaulieu JY, Blustajn J, Teboul F, Baud P, De Schonen S, Thiebaud JB, Oberlin C (2006) Cerebral plasticity in crossed C7 grafts of the brachial plexus: an fMRI study. *Microsurgery* 26:303–310
- Beisteiner R (2013) Clinical fMRI – improving paradigms or field strengths? *AJNR Am J Neuroradiol* 34:1972–1973. doi: [10.3174/ajnr.A3722](https://doi.org/10.3174/ajnr.A3722)
- Beisteiner R, Höllinger I, Rath J, Wurnig M, Hilbert M, Klinger N, Geißler A, Fischmeister F, Wöber C, Klösch G, Millesi H, Grishold W, Auff E, Schmidhamer R (2011) New type of cortical neuroplasticity after nerve repair in brachial plexus lesions. *Arch Neurol* 68:1147–1150. doi: [10.1001/archneurol.2011.596](https://doi.org/10.1001/archneurol.2011.596)
- Benzagmout M, Gatignol P, Duffau H (2007) Resection of World Health Organization Grade II gliomas involving Broca's area: methodological and functional considerations. *Neurosurgery* 61:741–752
- Bettus G, Ranjeva JP, Wendling F, Bénar CG, Confort-Gouny S, Régis J, Chauvel P, Cozzzone PJ, Lemieux L, Bartolomei F, Guye M (2011) Interictal functional connectivity of human epileptic networks assessed by intracerebral EEG and BOLD signal fluctuations. *PLoS One* 6:e20071. doi: [10.1371/journal.pone.0020071](https://doi.org/10.1371/journal.pone.0020071)
- Binkofski F, Seitz RJ (2004) Modulation of the BOLD-response in early recovery from sensorimotor stroke. *Neurology* 63:1223–1229
- Bitter T, Sorger B, Hesselmann V, Krug B, Lackner K, Guntinas-Lichius O (2011) Cortical representation sites of mimic movements after facial nerve reconstruction: a functional magnetic resonance imaging study. *Laryngoscope* 121:699–706. doi: [10.1002/lary.21399](https://doi.org/10.1002/lary.21399)
- Bonelli SB, Thompson PJ, Yogarajah M, Vollmar C, Powell RH, Symms MR, McEvoy AW, Micallef C, Koepf MJ, Duncan JS (2012) Imaging language networks before and after anterior temporal lobe resection: results of a longitudinal fMRI study. *Epilepsia* 53:639–650. doi: [10.1111/j.1528-1167.2012.03433.x](https://doi.org/10.1111/j.1528-1167.2012.03433.x)

- Braun M, Finke C, Ostendorf F, Lehmann TN, Hoffmann KT, Ploner CJ (2008) Reorganization of associative memory in humans with long-standing hippocampal damage. *Brain* 131:2742–2750. doi:[10.1093/brain/awm191](https://doi.org/10.1093/brain/awm191)
- Briganti C, Sestieri C, Mattei PA, Esposito R, Galzio RJ, Tartaro A, Romani GL, Caulo M (2012) Reorganization of functional connectivity of the language network in patients with brain gliomas. *AJNR Am J Neuroradiol* 33:1983–1990. doi:[10.3174/ajnr.A3064](https://doi.org/10.3174/ajnr.A3064)
- Buma FE, Lindeman E, Ramsey NF, Kwakkel G (2010) Functional neuroimaging studies of early upper limb recovery after stroke: a systematic review of the literature. *Neurorehabil Neural Repair* 24:589–608. doi:[10.1177/1545968310364058](https://doi.org/10.1177/1545968310364058)
- Bütfisch CM, Wessling M, Netz J, Seitz RJ, Hömberg V (2008) Relationship between interhemispheric inhibition and motor cortex excitability in subacute stroke patients. *Neurorehabil Neural Repair* 22:4–21
- Cadotte DW, Bosma R, Mikulis D, Nugaeva N, Smith K, Pokrupa R, Islam O, Stroman PW, Fehlings MG (2012) Plasticity of the injured human spinal cord: insights revealed by spinal cord functional MRI. *PLoS One* 7:e45560. doi:[10.1371/journal.pone.0045560](https://doi.org/10.1371/journal.pone.0045560)
- Caeyenberghs K, Leemans A, De Decker C, Heitger M, Drijkoningen D, Linden CV, Sunaert S, Swinnen SP (2012a) Brain connectivity and postural control in young traumatic brain injury patients: a diffusion MRI based network analysis. *Neuroimage Clin* 1:106–115. doi:[10.1016/j.jncl.2012.09.011](https://doi.org/10.1016/j.jncl.2012.09.011)
- Caeyenberghs K, Leemans A, Heitger MH, Leunissen I, Dhollander T, Sunaert S, Dupont P, Swinnen SP (2012b) Graph analysis of functional brain networks for cognitive control of action in traumatic brain injury. *Brain* 135:1293–1307. doi:[10.1093/brain/aws048](https://doi.org/10.1093/brain/aws048)
- Calabrese M, Rinaldi F, Seppi D, Favaretto A, Squarcina L, Mattisi I, Perini P, Bertoldo A, Gallo P (2011) Cortical diffusion-tensor imaging abnormalities in multiple sclerosis: a 3-year longitudinal study. *Radiology* 261:891–898. doi:[10.1148/radiol.11110195](https://doi.org/10.1148/radiol.11110195)
- Carmichael ST, Archibeque I, Luke L, Nolan T, Momiy J, Li S (2005) Growth-associated gene expression after stroke: evidence for a growth-promoting region in peri-infarct cortex. *Exp Neurol* 193:291–311
- Carter AR, Astafiev SV, Lang CE, Connor LT, Rengachary J, Strube MJ, Pope DL, Shulman GL, Corbetta M (2010) Resting interhemispheric functional magnetic resonance imaging connectivity predicts performance after stroke. *Ann Neurol* 67:365–375. doi:[10.1002/ana.21905](https://doi.org/10.1002/ana.21905)
- Carter AR, Patel KR, Astafiev SV, Snyder AZ, Rengachary J, Strube MJ, Pope A, Shimony JS, Lang CE, Shulman GL, Corbetta M (2012) Upstream dysfunction of somatomotor functional connectivity after corticospinal damage in stroke. *Neurorehabil Neural Repair* 26:7–19. doi:[10.1177/1545968311411054](https://doi.org/10.1177/1545968311411054)
- Cha YH, Chakrapani S, Craig A, Baloh RW (2012) Metabolic and functional connectivity changes in mal de débarquement syndrome. *PLoS One* 7:e49560. doi:[10.1371/journal.pone.0049560](https://doi.org/10.1371/journal.pone.0049560)
- Chen CJ, Liu HL, Wei FC, Chu NS (2006) Functional MR imaging of the human sensorimotor cortex after toe-to-finger transplantation. *AJNR Am J Neuroradiol* 27:1617–1621
- Chen H, Epstein J, Stern E (2010) Neural plasticity after acquired brain injury: evidence from functional neuroimaging. *PM R* 2:306–312. doi:[10.1016/j.pmrj.2010.10.006](https://doi.org/10.1016/j.pmrj.2010.10.006)
- Clarkson AN, Huang BS, Macisaac SE, Mody I, Carmichael ST (2010) Reducing excessive GABA-mediated tonic inhibition promotes functional recovery after stroke. *Nature* 468:305–309. doi:[10.1038/nature09511](https://doi.org/10.1038/nature09511)
- Collignon O, Vandewalle G, Voss P, Albouy G, Charbonneau G, Lassonde M, Lepore F (2011) Functional specialization for auditory-spatial processing in the occipital cortex of congenitally blind humans. *Proc Natl Acad Sci U S A* 108:4435–4440. doi:[10.1073/pnas.1013928108](https://doi.org/10.1073/pnas.1013928108)
- Coxon JP, Goble DJ, Van IA, De VJ, Wenderoth N, Swinnen SP (2010) Reduced basal ganglia function when elderly switch between coordinated movement patterns. *Cereb Cortex* 20:2368–2379. doi:[10.1093/cercor/bhp306](https://doi.org/10.1093/cercor/bhp306)
- Craggs JG, Staud R, Robinson ME, Perlstein WM, Price DD (2012) Effective connectivity among brain regions associated with slow temporal summation of C-fiber-evoked pain in fibromyalgia patients and healthy controls. *J Pain* 13:390–400. doi:[10.1016/j.jpain.2012.01.002](https://doi.org/10.1016/j.jpain.2012.01.002)
- Cruz-Gómez AJ, Ventura-Campos N, Belenguer A, Avila C, Forn C (2014) The link between resting-state functional connectivity and cognition in MS patients. *Mult Scler* 20:338–348. doi:[10.1177/1352458513495584](https://doi.org/10.1177/1352458513495584)
- Dijkhuizen RM, van der Marel K, Otte WM, Hoff EI, van der Zijden JP, van der Toorn A, van Meer MP (2012) Functional MRI and diffusion tensor imaging of brain reorganization after experimental stroke. *Transl Stroke Res* 3:36–43. doi:[10.1007/s12975-011-0143-8](https://doi.org/10.1007/s12975-011-0143-8)
- Dilks DD, Serences JT, Rosenau BJ, Yantis S, McCloskey M (2007) Human adult cortical reorganization and consequent visual distortion. *J Neurosci* 27:9585–9594
- Duffau H (2006) New concepts in surgery of WHO grade II gliomas: functional brain mapping, connectionism and plasticity – a review. *J Neurooncol* 79:77–115
- Eickhoff SB, Dafotakis M, Grefkes C, Shah NJ, Zilles K, Piza-Katzer H (2008) Central adaptation following heterotopic hand replantation probed by fMRI and effective connectivity analysis. *Exp Neurol* 212:132–144. doi:[10.1016/j.expneurol.2008.03.025](https://doi.org/10.1016/j.expneurol.2008.03.025)
- Elkana O, Frost R, Kramer U, Ben-Bashat D, Schweiger A (2013) Cerebral language reorganization in the chronic stage of recovery: a longitudinal fMRI study. *Cortex* 49:71–81. doi:[10.1016/j.cortex.2011.09.001](https://doi.org/10.1016/j.cortex.2011.09.001)
- Enzinger C, Johansen-Berg H, Dawes H, Bogdanovic M, Collett J, Guy C, Ropele S, Kischka U, Wade D, Fazekas F, Matthews PM (2008) Functional MRI correlates of lower limb function in stroke victims with gait impairment. *Stroke* 39:1507–1513. doi:[10.1161/STROKEAHA.107.501999](https://doi.org/10.1161/STROKEAHA.107.501999)
- Ertelt D, Small S, Solodkin A, Dettmers C, McNamara A, Binkofski F, Buccino G (2007) Action observation has a positive impact on rehabilitation of motor deficits after stroke. *Neuroimage* 36:164–173
- Faber J, Schoene-Bake JC, Trautner P, von Lehe M, Elger CE, Weber B (2013) Progressive fiber tract affection after temporal lobe surgery. *Epilepsia* 54:53–57. doi:[10.1111/epi.12077](https://doi.org/10.1111/epi.12077)
- Fields RD, Stevens-Graham B (2002) New insights into neuron-glia communication. *Science* 298:556–562
- Forn C, Rocca MA, Valsasina P, Boscá I, Casanova B, Sanjuan A, Ávila C, Filippi M (2012) Functional magnetic resonance imaging correlates of cognitive performance in patients with a clinically isolated syndrome suggestive of multiple sclerosis at presentation: an activation and connectivity study. *Mult Scler* 18:153–163. doi:[10.1177/1352458511417744](https://doi.org/10.1177/1352458511417744)
- Fornander L, Nyman T, Hansson T, Ragnedhed M, Brismar T (2010) Age- and time-dependent effects on functional outcome and cortical activation pattern in patients with median nerve injury: a functional magnetic resonance imaging study. *J Neurosurg* 113:122–128. doi:[10.3171/2009.10.JNS09698](https://doi.org/10.3171/2009.10.JNS09698)
- Gale SD, Pearson CM (2012) Neuroimaging predictors of stroke outcome: implications for neurorehabilitation. *NeuroRehabilitation* 31:331–344
- Gillebert CR, Mantini D (2013) Functional connectivity in the normal and injured brain. *Neuroscientist* 19:509–522. doi:[10.1177/1073858412463168](https://doi.org/10.1177/1073858412463168)
- González-García N, Armony JL, Soto J, Trejo D, Alegría MA, Drucker-Colín R (2011) Effects of rTMS on Parkinson's disease: a longitudinal fMRI study. *J Neurol* 258:1268–1280. doi:[10.1007/s00415-011-5923-2](https://doi.org/10.1007/s00415-011-5923-2)
- Grefkes C, Ward NS (2014) Cortical reorganization after stroke: how much and how functional? *Neuroscientist* 20:56–70. doi:[10.1177/1073858413491147](https://doi.org/10.1177/1073858413491147)
- Grefkes C, Nowak DA, Eickhoff SB, Dafotakis M, Küst J, Karbe H, Fink GR (2008) Cortical connectivity after subcortical stroke assessed with functional magnetic resonance imaging. *Ann Neurol* 63:236–246

- Grefkes C, Nowak DA, Wang LE, Dafotakis M, Eickhoff SB, Fink GR (2010) Modulating cortical connectivity in stroke patients by fTMS assessed with fMRI and dynamic causal modeling. *Neuroimage* 50:233–242. doi:[10.1016/j.neuroimage.2009.12.029](https://doi.org/10.1016/j.neuroimage.2009.12.029)
- Guzzetta A, Pecini C, Biagi L, Tosetti M, Brizzolara D, Chilosì A, Cipriani P, Petacchi E, Cioni G (2008) Language organisation in left perinatal stroke. *Neuropediatrics* 39:157–163. doi:[10.1055/s-0028-1085465](https://doi.org/10.1055/s-0028-1085465)
- Hamberger MJ, Cole J (2011) Language organization and reorganization in epilepsy. *Neuropsychol Rev* 21:240–251. doi:[10.1007/s11065-011-9180-z](https://doi.org/10.1007/s11065-011-9180-z)
- Hamzei F, Dettmers C, Rijntjes M, Weiller C (2008) The effect of cortico-spinal tract damage on primary sensorimotor cortex activation after rehabilitation therapy. *Exp Brain Res* 190:329–336. doi:[10.1007/s00221-008-1474-x](https://doi.org/10.1007/s00221-008-1474-x)
- Harris RJ, Bookheimer SY, Cloughesy TF, Kim HJ, Pope WB, Lai A, Nghiemphu PL, Liau LM, Ellingson BM (2014) Altered functional connectivity of the default mode network in diffuse gliomas measured with pseudo-resting state fMRI. *J Neurooncol* 116:373–379
- Havsteen I, Madsen KH, Christensen H, Christensen A, Siebner HR (2013) Diagnostic approach to functional recovery: functional magnetic resonance imaging after stroke. *Front Neurol Neurosci* 32:9–25. doi:[10.1159/000346408](https://doi.org/10.1159/000346408)
- Heitger MH, Goble DJ, Dhollander T, Dupont P, Caeyenberghs K, Leemans A, Sunaert S, Swinnen SP (2013) Bimanual motor coordination in older adults is associated with increased functional brain connectivity—a graph-theoretical analysis. *PLoS One* 8:e62133. doi:[10.1371/journal.pone.0062133](https://doi.org/10.1371/journal.pone.0062133)
- Helmstaedter C, Fritz NE, González Pérez PA, Elger CE, Weber B (2006) Shift-back of right into left hemisphere language dominance after control of epileptic seizures: evidence for epilepsy driven functional cerebral organization. *Epilepsy Res* 70:257–262
- Hou J, Lin Y, Zhang W, Song L, Wu W, Wang J, Zhou D, Zou Q, Fang Y, He M, Li H (2013) Abnormalities of frontal-parietal resting-state functional connectivity are related to disease activity in patients with systemic lupus erythematosus. *PLoS One* 8:e74530. doi:[10.1371/journal.pone.0074530](https://doi.org/10.1371/journal.pone.0074530)
- Hua XY, Liu B, Qiu YQ, Tang WJ, Xu WD, Liu HQ, Xu JG, Gu YD (2013) Long-term ongoing cortical remodeling after contralateral C-7 nerve transfer. *J Neurosurg* 118:725–729. doi:[10.3171/2012.12.JNS12207](https://doi.org/10.3171/2012.12.JNS12207)
- Huston JM, Field AS (2013) Clinical applications of diffusion tensor imaging. *Magn Reson Imaging Clin N Am* 21:279–298. doi:[10.1016/j.mric.2012.12.003](https://doi.org/10.1016/j.mric.2012.12.003)
- Ius T, Angelini E, Thiebaut de Schotten M, Mandonnet E, Duffau H (2011) Evidence for potentials and limitations of brain plasticity using an atlas of functional resectability of WHO grade II gliomas: towards a “minimal common brain”. *Neuroimage* 56:992–1000. doi:[10.1016/j.neuroimage.2011.03.022](https://doi.org/10.1016/j.neuroimage.2011.03.022)
- Jacobs HI, Van Boxtel MP, Heinecke A, Gronenschild EH, Backes WH, Ramakers IH, Jolles J, Verhey FR (2012) Functional integration of parietal lobe activity in early Alzheimer disease. *Neurology* 78:352–360. doi:[10.1212/WNL.0b013e318245287d](https://doi.org/10.1212/WNL.0b013e318245287d)
- Jang SH, Hong JH, Ahn SH, Son SM, Cho YW (2010) Motor function reorganization in a patient with a brainstem lesion: DTT, fMRI and TMS study. *NeuroRehabilitation* 26:167–171. doi:[10.3233/NRE-2010-0550](https://doi.org/10.3233/NRE-2010-0550)
- Jiang L, Xu H, Yu C (2013) Brain connectivity plasticity in the motor network after ischemic stroke. *Neural Plast* 2013:924192. doi:[10.1155/2013/924192](https://doi.org/10.1155/2013/924192)
- Kapreli E, Athanasopoulos S, Gliatis J, Papathanasiou M, Peeters R, Strimpakos N, Van Hecke P, Gouliamis A, Sunaert S (2009) Anterior cruciate ligament deficiency causes brain plasticity: a functional MRI study. *Am J Sports Med* 37:2419–2426. doi:[10.1177/0363546509343201](https://doi.org/10.1177/0363546509343201)
- Kernie S, Parent J (2010) Forebrain neurogenesis after focal ischemic and traumatic brain injury. *Neurobiol Dis* 37:267–274. doi:[10.1016/j.nbd.2009.11.002](https://doi.org/10.1016/j.nbd.2009.11.002)
- Kim H, Harrison A, Kankirawatana P, Rozelle C, Blount J, Torgerson C, Knowlton R (2013) Major white matter fiber changes in medically intractable neocortical epilepsy in children: a diffusion tensor imaging study. *Epilepsy Res* 103:211–220. doi:[10.1016/j.eplepsres.2012.07.017](https://doi.org/10.1016/j.eplepsres.2012.07.017)
- Laible M, Grieshammer S, Seidel G, Rijntjes M, Weiller C, Hamzei F (2012) Association of activity changes in the primary sensory cortex with successful motor rehabilitation of the hand following stroke. *Neurorehabil Neural Repair* 26:881–888. doi:[10.1177/1545968312437939](https://doi.org/10.1177/1545968312437939)
- Langer N, Hägggi J, Müller NA, Simmen HP, Jäncke L (2012) Effects of limb immobilization on brain plasticity. *Neurology* 78:182–188. doi:[10.1212/WNL.0b013e31823fcdf9c](https://doi.org/10.1212/WNL.0b013e31823fcdf9c)
- Lazaridou A, Astrakas L, Mintzopoulos D, Khanicheh A, Singhal A, Moskowitz M, Rosen B, Tzika A (2013a) fMRI as a molecular imaging procedure for the functional reorganization of motor systems in chronic stroke. *Mol Med Rep* 8:775–779. doi:[10.3892/mmr.2013.1603](https://doi.org/10.3892/mmr.2013.1603)
- Lazaridou A, Astrakas L, Mintzopoulos D, Khanicheh A, Singhal AB, Moskowitz MA, Rosen B, Tzika AA (2013b) Diffusion tensor and volumetric magnetic resonance imaging using an MR-compatible hand-induced robotic device suggests training-induced neuroplasticity in patients with chronic stroke. *Int J Mol Med* 32:995–1000. doi:[10.3892/ijmm.2013.1476](https://doi.org/10.3892/ijmm.2013.1476)
- Leunissen I, Coxon JP, Geurts M, Caeyenberghs K, Michiels K, Sunaert S, Swinnen SP (2013) Disturbed cortico-subcortical interactions during motor task switching in traumatic brain injury. *Hum Brain Mapp* 34:1254–1271. doi:[10.1002/hbm.21508](https://doi.org/10.1002/hbm.21508)
- Liacu D, Idy-Peretti I, Ducreux D, Bouilleret V, de Marco G (2012) Diffusion tensor imaging tractography parameters of limbic system bundles in temporal lobe epilepsy patients. *J Magn Reson Imaging* 36:561–568. doi:[10.1002/jmri.23678](https://doi.org/10.1002/jmri.23678)
- List J, Duning T, Kürten J, Deppe M, Wilbers E, Flöel A (2013) Cortical plasticity is preserved in nondemented older individuals with severe ischemic small vessel disease. *Hum Brain Mapp* 34:1464–1476. doi:[10.1002/hbm.22003](https://doi.org/10.1002/hbm.22003)
- MacIver K, Lloyd DM, Kelly S, Roberts N, Nurmiikko T (2008) Phantom limb pain, cortical reorganization and the therapeutic effect of mental imagery. *Brain* 131:2181–2191. doi:[10.1093/brain/awn124](https://doi.org/10.1093/brain/awn124)
- Marchand WR, Lee JN, Suchy Y, Garn C, Johnson S, Wood N, Chelune G (2011) Age-related changes of the functional architecture of the cortico-basal ganglia circuitry during motor task execution. *Neuroimage* 55:194–203. doi:[10.1016/j.neuroimage.2010.12.030](https://doi.org/10.1016/j.neuroimage.2010.12.030)
- Marcotte K, Adrover-Roig D, Damien B, de Práumont M, Généreux S, Hubert M, Ansaldi AI (2012) Therapy-induced neuroplasticity in chronic aphasia. *Neuropsychologia* 50:1776–1786. doi:[10.1016/j.neuropsychologia.2012.04.001](https://doi.org/10.1016/j.neuropsychologia.2012.04.001)
- Marcotte K, Perlberg V, Marrelec G, Benali H, Ansaldi AI (2013) Default-mode network functional connectivity in aphasia: therapy-induced neuroplasticity. *Brain Lang* 124:45–55. doi:[10.1016/j.bandl.2012.11.004](https://doi.org/10.1016/j.bandl.2012.11.004)
- Marshall RS, Zarahn E, Alon L, Minzer B, Lazar RM, Krakauer JW (2009) Early imaging correlates of subsequent motor recovery after stroke. *Ann Neurol* 65:596–602. doi:[10.1002/ana.21636](https://doi.org/10.1002/ana.21636)
- Mbwana J, Berl MM, Ritzl EK, Rosenberger L, Mayo J, Weinstein S, Conry JA, Pearl PL, Shamim S, Moore EN, Sato S, Vezina LG, Theodore WH, Gaillard WD (2009) Limitations to plasticity of language network reorganization in localization related epilepsy. *Brain* 132:347–356. doi:[10.1093/brain/awn329](https://doi.org/10.1093/brain/awn329)
- Mintzopoulos D, Astrakas LG, Khanicheh A, Konstas AA, Singhal A, Moskowitz MA, Rosen BR, Tzika AA (2009) Connectivity alterations assessed by combining fMRI and MR-compatible hand robots in chronic stroke. *Neuroimage* 47:90–97. doi:[10.1016/j.neuroimage.2009.03.007](https://doi.org/10.1016/j.neuroimage.2009.03.007)
- Mohammadi B, Kollewe K, Samii A, Dengler R, Münte TF (2011) Functional neuroimaging at different disease stages reveals distinct

- phases of neuroplastic changes in amyotrophic lateral sclerosis. *Hum Brain Mapp* 32:750–758. doi:[10.1002/hbm.21064](https://doi.org/10.1002/hbm.21064)
- Nowak DA, Grefkes C, Dafotakis M, Eickhoff S, Küst J, Karbe H, Fink GR (2008) Effects of low-frequency repetitive transcranial magnetic stimulation of the contralateral primary motor cortex on movement kinematics and neural activity in subcortical stroke. *Arch Neurol* 65:741–747. doi:[10.1001/archneur.65.6.741](https://doi.org/10.1001/archneur.65.6.741)
- O’Shea J, Boudrias MH, Stagg CJ, Bachtar V, Kischka U, Blicher JU, Johansen-Berg H (2014) Predicting behavioural response to TDCS in chronic motor stroke. *Neuroimage* 85:924–933. doi:[10.1016/j.neuroimage.2013.05.096](https://doi.org/10.1016/j.neuroimage.2013.05.096)
- Ohab JJ, Fleming S, Blesch A, Carmichael ST (2006) A neurovascular niche for neurogenesis after stroke. *J Neurosci* 26:13007–13016
- Ovadia-Caro S, Villringer K, Fiebach J, Junghuhnsen GJ, van der Meer E, Margulies DS, Villringer A (2013) Longitudinal effects of lesions on functional networks after stroke. *J Cereb Blood Flow Metab* 33:1279–1285. doi:[10.1038/jcbfm.2013.80](https://doi.org/10.1038/jcbfm.2013.80)
- Palaniyappan L, White TP, Liddle PF (2012) The concept of salience network dysfunction in schizophrenia: from neuroimaging observations to therapeutic opportunities. *Curr Top Med Chem* 12:2324–2338
- Papoutsi M, Stamatakis EA, Griffiths J, Marslen-Wilson WD, Tyler LK (2011) Is left fronto-temporal connectivity essential for syntax? Effective connectivity, tractography and performance in left-hemisphere damaged patients. *Neuroimage* 58:656–664. doi:[10.1016/j.neuroimage.2011.06.036](https://doi.org/10.1016/j.neuroimage.2011.06.036)
- Powell HW, Parker GJ, Alexander DC, Symms MR, Boulby PA, Wheeler-Kingshott CA, Barker GJ, Koepp MJ, Duncan JS (2007) Abnormalities of language networks in temporal lobe epilepsy. *Neuroimage* 36:209–221
- Pravatà E, Sestieri C, Mantini D, Briganti C, Colicchio G, Marra C, Colosimo C, Tartaro A, Romani GL, Caulo M (2011) Functional connectivity MR imaging of the language network in patients with drug-resistant epilepsy. *AJNR Am J Neuroradiol* 32:532–540. doi:[10.3174/ajnr.A2311](https://doi.org/10.3174/ajnr.A2311)
- Price CJ, Seghers ML, Leff AP (2010) Predicting language outcome and recovery after stroke: the PLORAS system. *Nat Rev Neurol* 6:202–210. doi:[10.1038/nrneuro.2010.15](https://doi.org/10.1038/nrneuro.2010.15)
- Puig J, Pedraza S, Blasco G, Daunis-I-Estadella J, Prados F, Remollo S, Prats-Galino A, Soria G, Boada I, Castellanos M, Serena J (2011) Acute damage to the posterior limb of the internal capsule on diffusion tensor tractography as an early imaging predictor of motor outcome after stroke. *AJNR Am J Neuro-radiol* 32:857–863. doi:[10.3174/ajnr.A2400](https://doi.org/10.3174/ajnr.A2400)
- Qi R, Zhang LJ, Zhong J, Zhang Z, Ni L, Jiao Q, Liao W, Zheng G, Lu G (2013) Altered effective connectivity network of the basal ganglia in low-grade hepatic encephalopathy: a resting-state fMRI study with Granger causality analysis. *PLoS One* 8:e53677. doi:[10.1371/journal.pone.0053677](https://doi.org/10.1371/journal.pone.0053677)
- Rath J, Schmidhammer R, Steinkellner T, Klinger N, Geißler A, Beisteiner R (2008) Evaluation of functional cortex for the diseased hand in a patient after hemispherectomy. *Arch Neurol* 65:1664–1665. doi:[10.1001/archneur.65.12.1664](https://doi.org/10.1001/archneur.65.12.1664)
- Rath J, Klinger N, Geißler A, Höllinger I, Gruber S, Wurnig M, Hausner T, Auff E, Schmidhammer R, Beisteiner R (2011) An fMRI marker for peripheral nerve regeneration. *Neurorehabil Neural Repair* 25:577–579. doi:[10.1177/1545968310397552](https://doi.org/10.1177/1545968310397552)
- Rehme AK, Grefkes C (2013) Cerebral network disorders after stroke: evidence from imaging-based connectivity analyses of active and resting brain states in humans. *J Physiol* 591:17–31. doi:[10.1113/jphysiol.2012.243469](https://doi.org/10.1113/jphysiol.2012.243469)
- Rehme AK, Eickhoff SB, Wang LE, Fink GR, Grefkes C (2011) Dynamic causal modelling of cortical activity from the acute to the chronic stage after stroke. *Neuroimage* 55:1147–1158. doi:[10.1016/j.neuroimage.2011.01.014](https://doi.org/10.1016/j.neuroimage.2011.01.014)
- Richiardi J, Gschwind M, Simioni S, Annoni JM, Greco B, Hagmann P, Schluep M, Vuilleumier P, Van De Ville D (2012) Classifying minimally disabled multiple sclerosis patients from resting state functional connectivity. *Neuroimage* 62:2021–2033. doi:[10.1016/j.neuroimage.2012.05.078](https://doi.org/10.1016/j.neuroimage.2012.05.078)
- Robinson SD, Schöpf V, Cardoso P, Geissler A, Fischmeister FP, Wurnig M, Trattning S, Beisteiner R (2013) Applying independent component analysis to clinical fMRI at 7T. *Front Hum Neurosci* 2:496. doi:[10.3389/fnhum.2013.00496](https://doi.org/10.3389/fnhum.2013.00496)
- Robles SG, Gatignol P, Lehéricy S, Duffau H (2008) Long-term brain plasticity allowing a multistage surgical approach to World Health Organization Grade II gliomas in eloquent areas. *J Neurosurg* 109:615–624. doi:[10.3171/JNS/2008/109/10/0615](https://doi.org/10.3171/JNS/2008/109/10/0615)
- Rocca MA, Filippi M (2007) Functional MRI in multiple sclerosis. *J Neuroimaging* 17:36–41
- Rocca MA, Valsasina P, Ceccarelli A, Absinta M, Ghezzi A, Riccitelli G, Pagani E, Falini A, Comi G, Scotti G, Filippi M (2009) Structural and functional MRI correlates of stroop control in benign MS. *Hum Brain Mapp* 30:276–290
- Rocca MA, Absinta M, Moiola L, Ghezzi A, Colombo B, Martinelli V, Comi G, Filippi M (2010) Functional and structural connectivity of the motor network in pediatric and adult-onset relapsing-remitting multiple sclerosis. *Radiology* 254:541–550. doi:[10.1148/radiol.09090463](https://doi.org/10.1148/radiol.09090463)
- Rocca MA, Bonnet MC, Meani A, Valsasina P, Colombo B, Comi G, Filippi M (2012a) Differential cerebellar functional interactions during an interference task across multiple sclerosis phenotypes. *Radiology* 265:864–873. doi:[10.1148/radiol.12120216](https://doi.org/10.1148/radiol.12120216)
- Rocca MA, Valsasina P, Martinelli V, Misci P, Falini A, Comi G, Filippi M (2012b) Large-scale neuronal network dysfunction in relapsing-remitting multiple sclerosis. *Neurology* 79:1449–1457. doi:[10.1212/WNL.0b013e31826d5f10](https://doi.org/10.1212/WNL.0b013e31826d5f10)
- Rowe JB (2010) Connectivity analysis is essential to understand neurological disorders. *Front Syst Neurosci* 17:144. doi:[10.3389/fnsys.2010.00144](https://doi.org/10.3389/fnsys.2010.00144)
- Rubinov M, Sporns O (2010) Complex network measures of brain connectivity: uses and interpretations. *Neuroimage* 52:1059–1069. doi:[10.1016/j.neuroimage.2009.10.003](https://doi.org/10.1016/j.neuroimage.2009.10.003)
- Saur D, Hartwigsen G (2012) Neurobiology of language recovery after stroke: lessons from neuroimaging studies. *Arch Phys Med Rehabil* 93:15–25. doi:[10.1016/j.apmr.2011.03.036](https://doi.org/10.1016/j.apmr.2011.03.036)
- Saur D, Lange R, Baumgaertner A, Schräknepper V, Willmes K, Rijntjes M, Weiller C (2006) Dynamics of language reorganization after stroke. *Brain* 129:1371–1384
- Saur D, Ronneberger O, Kummerer D, Mader I, Weiller C, Kloppel S (2010) Early functional magnetic resonance imaging activations predict language outcome after stroke. *Brain* 133:1252–1264. doi:[10.1093/brain/awq021](https://doi.org/10.1093/brain/awq021)
- Sawaki L, Butler AJ, Leng X, Wassenaar PA, Mohammad YM, Blanton S, Sathian K, Nichols-Larsen DS, Wolf SL, Good DC, Wittenberg GF (2008) Constraint-induced movement therapy results in increased motor map area in subjects 3 to 9 months after stroke. *Neurorehabil Neural Repair* 22:505–513. doi:[10.1177/1545968308317531](https://doi.org/10.1177/1545968308317531)
- Schaechter JD, Fricker ZP, Perdue KL, Helmer KG, Vangel MG, Greve DN, Makris N (2009) Microstructural status of ipsilesional and contralateral corticospinal tract correlates with motor skill in chronic stroke patients. *Hum Brain Mapp* 30:3461–3474. doi:[10.1002/hbm.20770](https://doi.org/10.1002/hbm.20770)
- Scheller E, Abdulkadir A, Peter J, Tabrizi SJ, Frackowiak RS, Klöppel S (2013) Interregional compensatory mechanisms of motor functioning in progressing preclinical neurodegeneration. *Neuroimage* 75:146–154. doi:[10.1016/j.neuroimage.2013.02.058](https://doi.org/10.1016/j.neuroimage.2013.02.058)
- Schmidt SA, Akrofi K, Carpenter-Thompson JR, Husain FT (2013) Default mode, dorsal attention and auditory resting state networks exhibit differential functional connectivity in tinnitus and hearing loss. *PLoS One* 8:e76488. doi:[10.1371/journal.pone.0076488](https://doi.org/10.1371/journal.pone.0076488)
- Schwarze U, Hahn C, Bengner T, Stodieck S, Büchel C, Sommer T (2009) Enhanced activity during associative encoding in the affected

- hippocampus in right temporal lobe epilepsy patients. *Brain Res* 1297:112–117. doi:[10.1016/j.brainres.2009.08.036](https://doi.org/10.1016/j.brainres.2009.08.036)
- Seghier ML, Zeidman P, Neufeld NH, Leff AP, Price CJ (2010) Identifying abnormal connectivity in patients using dynamic causal modeling of fMRI responses. *Front Syst Neurosci* 4:142. doi:[10.3389/fnsys.2010.00142](https://doi.org/10.3389/fnsys.2010.00142)
- Seitz RJ, Donnan GA (2010) Role of neuroimaging in promoting long-term recovery from ischemic stroke. *J Magn Reson Imaging* 32:756–772. doi:[10.1002/jmri.22315](https://doi.org/10.1002/jmri.22315)
- Shah PP, Szaflarski JP, Allendorfer J, Hamilton RH (2013) Induction of neuroplasticity and recovery in post-stroke aphasia by non-invasive brain stimulation. *Front Hum Neurosci* 7:888
- Sharma N, Baron JC, Rowe JB (2009) Motor imagery after stroke: relating outcome to motor network connectivity. *Ann Neurol* 66:604–616. doi:[10.1002/ana.21810](https://doi.org/10.1002/ana.21810)
- Shu N, Liu Y, Li K, Duan Y, Wang J, Yu C, Dong H, Ye J, He Y (2011) Diffusion tensor tractography reveals disrupted topological efficiency in white matter structural networks in multiple sclerosis. *Cereb Cortex* 21:2565–2577. doi:[10.1093/cercor/bhr039](https://doi.org/10.1093/cercor/bhr039)
- Simões EL, Bramati I, Rodrigues E, Franzoi A, Moll J, Lent R, Tovar-Moll F (2012) Functional expansion of sensorimotor representation and structural reorganization of callosal connections in lower limb amputees. *J Neurosci* 32:3211–3220. doi:[10.1523/JNEUROSCI.4592-11.2012](https://doi.org/10.1523/JNEUROSCI.4592-11.2012)
- Small SL, Hlustik P, Noll DC, Genovese C, Solodkin A (2002) Cerebellar hemispheric activation ipsilateral to the paretic hand correlates with functional recovery after stroke. *Brain* 125:1544–1557
- Smits M, Visch-Brink EG, van de Sandt-Koenderman ME, van der Lugt A (2012) Advanced magnetic resonance neuroimaging of language function recovery after aphasic stroke: a technical review. *Arch Phys Med Rehabil* 93:4–14. doi:[10.1016/j.apmr.2011.02.023](https://doi.org/10.1016/j.apmr.2011.02.023)
- Stagg CJ, Johansen-Berg H (2013) Studying the effects of transcranial direct-current stimulation in stroke recovery using magnetic resonance imaging. *Front Hum Neurosci* 7:857
- Stinear CM, Ward NS (2013) How useful is imaging in predicting outcomes in stroke rehabilitation? *Int J Stroke* 8:33–37. doi:[10.1111/j.1747-4949.2012.00970.x](https://doi.org/10.1111/j.1747-4949.2012.00970.x)
- Stinear CM, Barber PA, Smale PR, Coxon JP, Fleming MK, Byblow WD (2007) Functional potential in chronic stroke patients depends on corticospinal tract integrity. *Brain* 130:170–180
- Stinear CM, Barber PA, Petoe M, Anwar S, Byblow WD (2012) The PREP algorithm predicts potential for upper limb recovery after stroke. *Brain* 135:2527–2535. doi:[10.1093/brain/aws146](https://doi.org/10.1093/brain/aws146)
- Taylor KS, Anastakis DJ, Davis KD (2009) Cutting your nerve changes your brain. *Brain* 132:3122–3133. doi:[10.1093/brain/awp231](https://doi.org/10.1093/brain/awp231)
- Turkeltaub PE, Messing S, Norise C, Hamilton RH (2011) Are networks for residual language function and recovery consistent across aphasic patients? *Neurology* 76:1726–1734. doi:[10.1212/WNL.0b013e31821a44c1](https://doi.org/10.1212/WNL.0b013e31821a44c1)
- van Meer MP, van der Marel K, Otte WM, Berkelbach van der Sprenkel JW, Dijkhuizen RM (2010a) Correspondence between altered functional and structural connectivity in the contralateral sensorimotor cortex after unilateral stroke in rats: a combined resting state functional MRI and manganese-enhanced MRI study. *J Cereb Blood Flow Metab* 30:1707–1711. doi:[10.1038/jcbfm.2010.124](https://doi.org/10.1038/jcbfm.2010.124)
- van Meer MP, van der Marel K, Wang K, Otte WM, El Bouazati S, Roeling TA, Viergever MA, Berkelbach van der Sprenkel JW, Dijkhuizen RM (2010b) Recovery of sensorimotor function after experimental stroke correlates with restoration of resting-state interhemispheric functional connectivity. *J Neurosci* 30:3964–3972. doi:[10.1523/JNEUROSCI.5709-09.2010](https://doi.org/10.1523/JNEUROSCI.5709-09.2010)
- van Nuenen BF, Helmich RC, Ferraye M, Thaler A, Hendl T, Orr-Urtreger A, Mirelman A, Bressman S, Marder KS, Giladi N, van de Warrenburg BP, Bloem BR, Toni I, LRRK2 Ashkenazi Jewish Consortium (2012) Cerebral pathological and compensatory mechanisms in the premotor phase of leucine-rich repeat kinase 2 parkinsonism. *Brain* 135:3687–3698. doi:[10.1093/brain/aws288](https://doi.org/10.1093/brain/aws288)
- Várkuti B, Guan C, Pan Y, Phua KS, Ang KK, Kuah CW, Chua K, Ang BT, Birbaumer N, Sitaram R (2013) Resting state changes in functional connectivity correlate with movement recovery for BCI and robot-assisted upper-extremity training after stroke. *Neurorehabil Neural Repair* 27:53–62. doi:[10.1177/1545968312445910](https://doi.org/10.1177/1545968312445910)
- Vitali P, Abutalebi J, Tettamanti M, Danna M, Ansaldi AI, Perani D, Joanette Y, Cappa SF (2007) Training-induced brain remapping in chronic aphasia: a pilot study. *Neurorehabil Neural Repair* 21:152–160
- Wahl AS, Schwab ME (2014) Finding an optimal rehabilitation paradigm after stroke: enhancing fiber growth and training of the brain at the right moment. *Front Hum Neurosci* 7:911
- Wang L, Yu C, Chen H, Qin W, He Y, Fan F, Zhang Y, Wang M, Li K, Zang Y, Woodward TS, Zhu C (2010) Dynamic functional reorganization of the motor execution network after stroke. *Brain* 133:1224–1238. doi:[10.1093/brain/awq043](https://doi.org/10.1093/brain/awq043)
- Wang LE, Fink GR, Diekhoff S, Rehme AK, Eickhoff SB, Grefkes C (2011) Noradrenergic enhancement improves motor network connectivity in stroke patients. *Ann Neurol* 69:375–388. doi:[10.1002/ana.22237](https://doi.org/10.1002/ana.22237)
- Warren JE, Crinion JT, Lambon Ralph MA, Wise RJ (2009) Anterior temporal lobe connectivity correlates with functional outcome after aphasic stroke. *Brain* 132:3428–3442. doi:[10.1093/brain/awp270](https://doi.org/10.1093/brain/awp270)
- Weaver KE, Chaovalltwongse WA, Novotny EJ, Poliakov A, Grabowski TG, Ojemann JG (2013) Local functional connectivity as a pre-surgical tool for seizure focus identification in non-lesion, focal epilepsy. *Front Neurol* 4:43. doi:[10.3389/fneur.2013.00043](https://doi.org/10.3389/fneur.2013.00043)
- Westlake KP, Nagarajan SS (2011) Functional connectivity in relation to motor performance and recovery after stroke. *Front Syst Neurosci* 5:8. doi:[10.3389/fnsys.2011.00008](https://doi.org/10.3389/fnsys.2011.00008)
- Wolf CC, Ball A, Ocklenburg S, Otto T, Heed T, Röder B, Güntürkün O (2011) Visuotactile interactions in the congenitally acallosal brain: evidence for early cerebral plasticity. *Neuropsychologia* 49:3908–3916. doi:[10.1016/j.neuropsychologia.2011.10.008](https://doi.org/10.1016/j.neuropsychologia.2011.10.008)
- Wong SW, Jong L, Bandur D, Bhari F, Yen YF, Takahashi AM, Lee DH, Steven DA, Parrent AG, Pigott SE, Mirsattari SM (2009) Cortical reorganization following anterior temporal lobectomy in patients with temporal lobe epilepsy. *Neurology* 73:518–525. doi:[10.1212/WNL.0b013e3181b2a48e](https://doi.org/10.1212/WNL.0b013e3181b2a48e)
- Yogarajah M, Focke NK, Bonelli SB, Thompson P, Vollmar C, McEvoy AW, Alexander DC, Symms MR, Koepp MJ, Duncan JS (2010) The structural plasticity of white matter networks following anterior temporal lobe resection. *Brain* 133:2348–2364. doi:[10.1093/brain/awq175](https://doi.org/10.1093/brain/awq175)
- You X, Adjouadi M, Guillen MR, Ayala M, Barreto A, Rishe N, Sullivan J, Dlugos D, Vanmeter J, Morris D, Donner E, Bjornson B, Smith ML, Bernal B, Berl M, Gaillard WD (2011) Sub-patterns of language network reorganization in pediatric localization related epilepsy: a multisite study. *Hum Brain Mapp* 32:784–799. doi:[10.1002/hbm.21066](https://doi.org/10.1002/hbm.21066)
- Zarahn E, Alon L, Ryan SL, Lazar RM, Vry MS, Weiller C, Marshall RS, Krakauer JW (2011) Prediction of motor recovery using initial impairment and fMRI 48 h poststroke. *Cereb Cortex* 21:2712–2721. doi:[10.1093/cercor/bhr047](https://doi.org/10.1093/cercor/bhr047)
- Zepeda A, Sengpiel F, Guagnelli MA, Vaca L, Arias C (2004) Functional reorganization of visual cortex maps after ischemic lesions is accompanied by changes in expression of cytoskeletal proteins and NMDA and GABA(A) receptor subunits. *J Neurosci* 24:1812–1821
- Zipse L, Norton A, Marchina S, Schlaug G (2012) When right is all that is left: plasticity of right-hemisphere tracts in a young aphasic patient. *Ann NY Acad Sci* 1252:237–245. doi:[10.1111/j.1749-6632.2012.06454.x](https://doi.org/10.1111/j.1749-6632.2012.06454.x)

Clinical BOLD fMRI and DTI: Artifacts, Tips, and Tricks

Ronald Peeters and Stefan Sunaert

Contents

| | |
|---|-----|
| 1 Introduction..... | 313 |
| 1.1 Artifacts Related to BOLD fMRI Signal in Both Active and Resting State fMRI | 314 |
| 1.2 The Influence of Brain Lesions on DTI Results | 320 |
| 1.3 Patient-Related Artifacts and Physiological Noise | 320 |
| 1.4 Technical-Related Artifacts..... | 328 |
| 1.5 Statistical Post-processing “Artifacts” | 332 |
| References | 332 |

Abstract

DTI and BOLD functional MRI techniques suffer from many different types of *artifacts*. These *artifacts* can have a technical origin like *susceptibility artifacts* in specific brain regions or vibration and eddy-current artifacts, but they can also be related to physiology. The *draining vein* activation observed in the neighborhood of functionally active regions or *flow artifacts* are such physiologically induced artifacts. In clinical fMRI, there are also several specific effects. These can be pathology-induced *reduction or absence of brain activation* in the vicinity of lesions, which can lead to false interpretation of the resulting fMRI maps. As patients are most of the time ill, the *pharmaceuticals* they are taking can influence the BOLD signal, and the same applies to a lack of *cooperation* during the scan and *head motion which is also detrimental for DTI acquisition*. The success rate in clinical fMRI/DTI protocols is clearly related to the clinician’s/technician’s ability to recognize and cope with these technical, physiological, and patient-induced artifacts.

1 Introduction

FMRI and DTI techniques suffer from many different types of *artifacts* (Zeffiro 1996; Le Bihan et al. 2006; Haller and Bartsch 2009; Jones and Cercignani 2010; Murphy et al. 2013; Davis and Poldrack 2013). Some of these artifacts are of purely technical origin (e.g., spikes in EPI images), others may be related to physiology (e.g., cardiac-related physiological brain motion), and, finally, there are also pathology-induced artifacts, which can lead to a false interpretation of the results. Clinical fMRI, which is nowadays mostly performed at a field strength of 3 T, is a rather insensitive technique since signal intensity changes induced by neuronal activity are typically in the order of a few percent, i.e., in the range of the magnitude of noise (Boxerman et al. 1995; Aguirre et al. 1998). Many artifacts will therefore be related to the weak signal-to-noise ratio of fMRI. DTI acquisition techniques are

R. Peeters, PhD (✉) • S. Sunaert, MD, PhD
Department of Radiology, University Hospitals of the Catholic University of Leuven, Herestraat 49, Leuven 3000, Belgium

also very sensitive to hardware-related instabilities and eddy currents and also suffer from a very low signal-to-noise ratio (Koch and Norris 2000; Le Bihan et al. 2006).

The low signal-to-noise ratio and various possible artifacts limit the *success rate* of clinical fMRI and DTI. *Claustrophobia and patient cooperation*, especially in more difficult tasks such as cognitive or language tasks, hamper the use of active fMRI in severely ill patients. Nonetheless, the reported success rate of presurgical fMRI in the literature is about 80–85 % (Lee et al. 1999; Krings 2001a; Håberg et al. 2004). This reported rate is probably overestimated since most patients undergoing fMRI have already undergone a selection by the referring clinician and not all patients with brain pathologies are referred for presurgical fMRI. When a failure occurs, head movement artifacts are the most frequent cause, followed by a low contrast-to-noise ratio. In the case of the DTI scans and also in resting state fMRI where patient cooperation is less stringent (no task has to be performed), the overall success rate may be higher, and also noncooperative patients, pediatric patients and neonates (Heemskerk et al. 2013), and even comatose patients may still be scanned (Vanhaudenhuyse et al. 2010).

The success rate of advanced clinical neuroimaging is clearly related to the clinician's/technician's ability to recognize and cope with the technical, physiological, and patient-induced artifacts and limitations. But there are some tips and tricks of how to detect and minimize these artifacts and to distinguish real from false brain activation in fMRI, as well as real pathologic white matter structure changes from artifacts.

1.1 Artifacts Related to BOLD fMRI Signal in Both Active and Resting State fMRI

As discussed in chapter “[Revealing brain activity and white matter structure using functional and diffusion-weighted magnetic resonance imaging](#)” by Goebel, neurovascular coupling between brain activation and cerebrovascular physiology leads to three effects that can contribute to the fMRI signal: an increase in the regional blood flow velocity (rCBF), regional blood volume (rCBV), and local blood oxygenation level. According to the latter, the most widely used fMRI technique has been called “blood oxygenation level-dependent (BOLD) fMRI” (Ogawa and Lee 1990; Rao et al. 1993; Turner et al. 1993; Yang et al. 1997).

All imaging modalities that extrapolate task-driven or resting state alterations from hemodynamic changes in neuronal activity produce functional maps that have passed through “a vascular filter.” This means that the regional sensitivity of the imaging modality for detecting functional changes following neuronal activation depends on the vascular baseline state and the vascular density in and around the activated neuronal cluster. Due to the contrast mechanism of the BOLD technique

exploiting changes in deoxyhemoglobin concentration, this also applies to fMRI experiments (Menon and Kim 1999; Mandeville et al. 2001; Logothetis 2002; Goense et al. 2012). Thus, the observed area of signal change in BOLD images is larger than and can be displaced relative to the actual activated zone. These intrinsic effects of the BOLD mechanism limit the temporal and spatial resolution of fMRI, independently of the acquisition protocol used (Engel et al. 1997; Menon et al. 1998; Kriegeskorte et al. 2010).

1.1.1 Artifacts in Localization of Brain Activity (Brain or Vein)

The spatial specificity of activated patches obtained from fMRI and the accuracy of the activation location in relation to the sites of neuronal (electrical) activity have been shown to depend on the acquisition technique (Kim et al. 2000; Logothetis 2000; Duong et al. 2004; Siero et al. 2013). Several authors have raised the concern that BOLD fMRI exams performed at lower field strengths may predominantly detect large draining veins, not necessarily in the direct neighborhood of the activated brain region (Frahm et al. 1994).

In order to recognize BOLD signals arising from veins draining the excess of blood from activated areas (Kansaku et al. 1998; Menon 2002; Nencka and Rowe 2007), the principles described in the following can be used:

The activated spots observed from a draining vein are mostly small, contiguous on several adjacent slices, and of tubular configuration following the (often intrasulcal) path of the vein through different slices, whereas the activated functional area tends to appear more area-measured inside the brain parenchyma (Gati et al. 1997; Krings 2001a).

By co-registering (overlay) fMRI activation maps or rsfMRI network maps with anatomical T1-weighted contrast-enhanced images – which visualize the larger contrast-filled draining veins – it is possible to check for the position and possible overlap of BOLD clusters with the draining vessels. The additional co-registration of a venous MR angiogram is also helpful to distinguish intra-venous BOLD signal from parenchymal brain activation (Baudendistel et al. 1998).

In addition, when analyzing the signal time course, differences between signal from activated parenchyma and that from draining veins can be observed. Because the draining veins are fed by venules and arterioles of the activated brain area, the signal change can be expected to have a later onset as compared to that of the parenchyma (Kansaku et al. 1998; Hall et al. 2002), reflected by a later onset of contrast change in the time course of the MR signal of the draining vein. However, this difference in temporal offset between the microvasculature in the activated parenchyma and the microvasculature of the draining veins is not very large, i.e., in the order of 1–2 s which is the time necessary for the blood to pass the smaller veins and reach the larger vessels (Lee et al.

1995). Consequently, this effect is almost never observed in a standard clinical fMRI acquisition protocol with a typical temporal resolution of around 3 s. On the other hand, the relative signal change observed in the draining vein is considerably larger as compared to that of the parenchyma (typically twice as large at a 1.5 T scanner) in a gradient echo pulse sequence. This is the result of several different effects. The magnetic susceptibility effects and the resulting percentage of signal change are increased around large draining veins. As the microvessels occupy a considerable smaller volume in a voxel as compared to the large draining veins, the partial volume effect will also increase the percent signal change in the voxels containing the draining veins as compared to those containing the parenchymal venules/arterioles. Inflow effects are also less pronounced in the randomly oriented microvasculature as compared to the large tubular draining veins (Krings 2001a).

In general, the activated areas observed in functional BOLD imaging studies can be divided in two different types of appearance based on the high-resolution T_2^* -weighted and T_1 -weighted images. The “venous” type is highly spatially confined, tends to be located along the sulcus, is of tubular configuration, and accounts for a higher percentage of BOLD contrast changes upon stimulation. High-resolution anatomical images demonstrate that areas with the most intense stimulation-related signal intensity changes correlate with dark spots or lines on T_2^* -weighted images and contrast-filled superficial tubuli in contrast-enhanced T_1 -weighted images arising from macroscopic venous blood vessels. The latter observation is also consistent with the fact that the relatively large blood vessels are located on the sulcal cortical surface rather than within the brain tissue itself (Yamada et al. 1997). Besides these “venous hot spots” of activation, however, the parenchymal stimulation-/activation-related BOLD contrast changes spread more diffusely and are not at all associated with any visible large venous vessel on anatomical images. This “parenchymal” type accounts for most of the spatial extension of the BOLD activation.

1.1.1.1 How to Minimize the Contribution of Draining Veins?

The contribution to fMRI signals from large draining veins is especially present when single slices, large flip angles, and short TR gradient echo sequences are used (Duyn et al. 1994; Haacke et al. 1994), since these enhance the contribution of the increase in blood flow and blood volume (inflow effect). Gao et al. (1996) have demonstrated that fMRI images more sensitive to the microcirculation in the brain parenchyma may be obtained when the pulse sequence is designed toward minimizing inflow effects and maximizing the BOLD contribution. This can be achieved with multislice, heavily T_2^* -weighted single-shot echo-planar images with a long TR (Gao et al. 1996). Therefore, when performing clinical fMRI,

the implementation of these imaging parameters should be a prerequisite for maximizing the fMRI signal toward the site of neuronal activity. In doing so, several studies have shown a good correlation between the BOLD fMRI signal and intraoperative mapping, suggesting that the functional-anatomical specificity is adequate for presurgical mapping, provided an optimal acquisition technique is used (Nitschke et al. 1998; Tomczak et al. 2000; Krings 2001b; Stippich et al. 2003; Meier et al. 2013).

The use of higher magnetic field strengths will also decrease the effect of the draining veins (Gati et al. 1997; Moon et al. 2007). The decrease in draining vein influence by increasing field strengths is a result of the field dependence on the alteration in T_2^* values due to susceptibility-induced gradients around blood vessels which in turn depend on diffusional averaging. Thus, the change in T_2^* is a function of the motion of protons in the brain tissue as well as of the magnitude of the field gradients encountered by the tissue protons. The latter depends on the size of the blood vessels and orientation of these vessels relative to the main magnetic field direction (Ogawa et al. 1993). In this study by Ogawa et al. (1993), it was predicted that the overall effect in susceptibility difference on a T_2^* -sensitive imaging technique would be somewhere between linear and quadratic depending on the main magnetic field. In addition, it was reported that at high magnetic fields, the contribution of small vessels is more pronounced than at low magnetic fields (Ogawa et al. 1993; Menon et al. 1995). Thus, with respect to signal intensity changes induced by susceptibility alterations of the blood vessels secondary to neuronal activity, this effect will increase more than linearly with the magnetic field strength, with a larger contribution of the more desired small vessel effect and therefore resulting in advantages toward higher fields (Ugurbil et al. 1999) for distinguishing parenchymal from venous activation. However, higher fields are also more sensitive to other artifacts such as susceptibility-induced image deformations in EPI sequences (see Sect. 4.1), a larger influence of scanner instability (Cohen and DuBois 1999), and physiological effects (Weisskoff 1996) which will be discussed below.

BOLD functional activation maps can also be obtained by using the spin echo (SE)-based T_2 -weighted contrast rather than the gradient echo (GRE)-based T_2^* -weighted contrast (Duong et al. 2004; Moon et al. 2007). However the observed BOLD effect is much smaller on the T_2 -relaxation parameter (SE technique) resulting in a much lower contrast-to-noise ratio (CNR) making this technique less sensitive. On the other hand, the use of the T_2 effect can be preferable if one wants to avoid spurious activation in large veins (Lowe et al. 2000; Uludağ et al. 2009) since SE sequences have a high specificity for microvessels and are therefore less sensitive to susceptibility effects around larger blood vessels in optimized settings (Oja et al. 1999; Uludağ et al. 2009).

Another technique to maximize parenchymal activation compared to venous activation has been demonstrated by Cohen et al. (2004) where hypercapnic normalization of the BOLD activation maps with the aid of CO₂ inhalation has been used to normalize the BOLD-activated areas making them independent of the resting state CBV in the voxels (Cohen et al. 2004). Maximizing the fMRI signal toward the site of neuronal activity can also be achieved by optimizing the mode of stimulation. A study by Rumeur et al. (2000) has shown that different types of sensory stimulation are capable of differentiating primary sensory cortex from the venous draining network (Rumeur et al. 2000). Discontinuous stimulation of a limited skin area elicited activity in the microvasculature of the sensory cortex only, whereas robust continuous stimulation of a larger skin area led to activation not only in functional sites but also in the venous network. The authors claimed that the discontinuous stimulation paradigm induced less effective summation of the hemodynamic response and thus less migration of BOLD contrast to the venous network. As a result resting state fMRI will also be less sensitive to the venous draining network due to the lower mode of activation in the resting state. Also, if the activated region has a rather small surface area (<100 mm²), the oxygenation state in the vein draining the respective area will spread within this vein without dilution only up to 4–5 mm beyond the edge of the activated region (Turner 2002), minimizing the influence of the draining vein signal on presurgical BOLD maps.

Practical tip: In preoperative fMRI, the impact of spurious venous signals is important in order to know which distance to keep between the lesion to be removed and the adjacent functionally active area clear of when removing a lesion. Despite the fact that functionally “safe” resection borders cannot be determined from fMRI studies due to the statistical nature of the activation maps, there are several studies that recommend distances of 1 cm or higher between resection border and functional area as reasonably safe regarding the risk for surgically induced postoperative neurological deficits (see chapters “Task-based presurgical functional MRI in patients with brain tumors” and “Presurgical functional localization possibilities, limitations and validity” for details). This does not apply to the draining venous vessels as they do not represent “real” activated regions, so that here it is merely required to keep clear of the vessels. Practically, it is advised to always acquire anatomical high-resolution images of the patient, preferably contrast enhanced, to depict large blood vessels and to co-register the fMRI activation images with these anatomical images in order to distinguish “activation” in anatomically visible vessels from “activation” within the brain parenchyma. When small very intensely activated patches are observed, it is also recommended to compare these time courses with those of the more diffusely activated parenchymal regions to distinguish both types of activation

(see chapter “Task-based presurgical functional MRI in patients with brain tumors”).

1.1.2 The Influence of Brain Lesions on BOLD fMRI Signal

An important aspect of the validity of functional MRI for clinical purposes is the significance of absent, reduced, or artificial BOLD activation. Here, it is important to know whether absent or reduced BOLD signal also reflects absent or reduced neuronal activation and whether BOLD signals in hyperperfused tissue (e.g., nearby or in the boundaries of highly vascularized tumors and metastases) or in areas with altered hemodynamic properties (e.g., in AVMs) represent truly functional neuronal activation. Until now the knowledge on these issues and also on their prevalence is very limited. The different phenomena have been described anecdotally, but investigators using fMRI preoperatively should be aware of their existence (Lüdemann et al. 2006; Chen et al. 2008; Jiang et al. 2010). As pointed out in an editorial by (Bryant and Jackson 1998), these “negative results” still deserve further study (Bryant and Jackson 1998).

1.1.2.1 Absent or Reduced BOLD Signal

Different pathological conditions can attenuate the hemodynamic response which is the source of any fMRI signal. Brain tumor vessels typically lack cerebral autoregulation. Their vasculature is less responsive than that of the surrounding normal tissue. Intracranial space-occupying lesions can alter physiologic conditions; they may induce proliferation of pathologic vessels in the tissue adjacent to the lesion, thus altering the density, size, and topography of the vessels and consequently increase blood volume. The blood-brain barrier may break down within the tumor mass and partially extend into the tissue adjacent to the tumor. The mass effect of the lesion itself and the peritumoral vasogenic edema may change the apparent diffusion coefficient and therefore also cause mechanical vascular compression. If, however, the brain’s ability to autoregulate the flow of blood is completely lost in the brain tissue in the immediate vicinity to the tumor, which may still be functioning, this area may not respond to an increase in neural activity with corresponding increase in blood flow and subsequent BOLD signal (Lüdemann et al. 2006; Chen et al. 2008). The biochemical environment (adenosine 5'-triphosphate, pH, glucose, lactate, etc.) and the cortical levels of neurotransmitters in and around gliomas might be altered. Specifically, the release of nitric oxide by reactive astrocytes and macrophages at the normal brain tissue-glioma interface may increase the “resting state” regional cerebral blood flow and thus alter the physiological hemodynamic response (Schreiber et al. 2000; Hund-Georgiadis et al. 2003; Fujiwara et al. 2004; Maravita and Iriki 2004). Similarly, therapeutic drugs administered to the

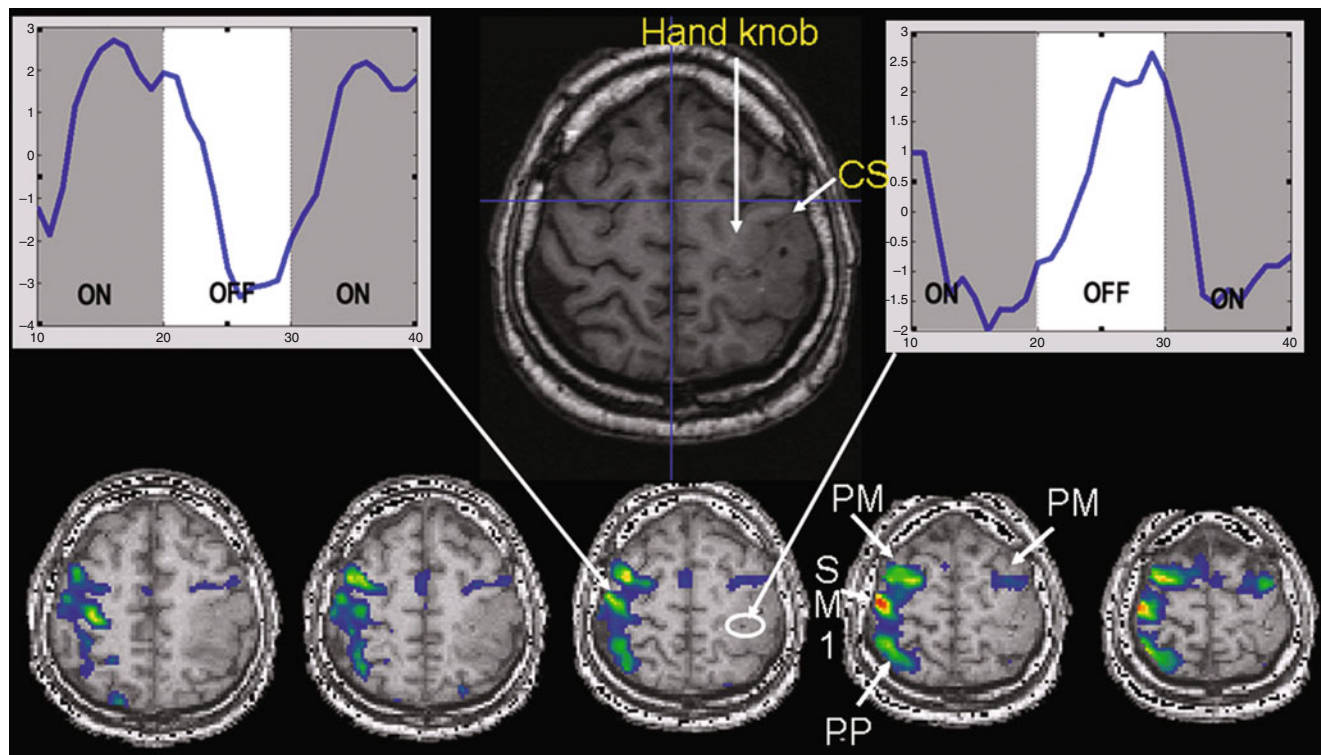


Fig. 1 Case study of a patient showing an inverted BOLD signal in the neighborhood of a lesion

patients may also interact with hemodynamic autoregulation (Seifritz et al. 2000; Braus and Brassen 2005). In regions more distant from the gliomas, where tumor vasculature is not encountered, the release of nitric oxide by reactive astrocytes and macrophages at the normal brain tissue-glioma interface may result in a luxury perfusion and reduced oxygen extraction fraction, resulting and leading to a reduced BOLD contrast enhancement (Schreiber et al. 2000).

1.1.2.2 Case of a Patient Showing an Inverted BOLD Signal Change

It is of utmost importance to realize that the absence of fMRI activity in a particular brain region *does not mean* that electrical activity within this area does not exist and it is thus safe to surgically remove this brain tissue. We will demonstrate this important point using the following case report: Fig. 1 illustrates fMRI activity during bilateral finger-tapping versus rest in a patient with a left Rolandic tumor (glioma WHO grade II in the postcentral gyrus extending through the central sulcus into the “hand knob” of the precentral gyrus). In the non-lesioned right hemisphere, fMRI activity is observed within the right sensorimotor cortex (SM1; pre- and postcentral gyri), the right premotor cortex (PM), and the right parietal cortex (PP). In contrast, in the lesioned left hemisphere, fMRI activation is only observed anteriorly to the tumor in

the left premotor cortex (PM). While this fMRI activation map might be interpreted as an absence of electrical neuronal activity within the left SM1 and PP areas (e.g., due to plastic changes and a takeover of motor function by the ipsilateral non-lesioned hemisphere), the signal time courses clearly show that this is a false conclusion. In the left-sided, tumor-infiltrated SM1 hand representation, the BOLD signals decrease during performance of the motor task and increase during baseline condition (rest), i.e., an *inverse* BOLD MR signal change as compared to physiological activation. This finding may result from lesion-induced neurovascular uncoupling, where oxygen extraction (cause of the initial dip of the BOLD signal) occurs without an increase in regional cerebral blood flow and volume (rCBF and rCBV), resulting in a steady decrease of fMRI signal despite an increased electrical neuronal activity driving the actual movements. As pointed out in an editorial by Bryan and Kraut (1998), these “negative results” deserve further study (Bryan and Kraut 1998; Sunaert et al. 1998). One may speculate that – depending on the lesion-induced hemodynamic changes in different patients – there could be continuous alterations of BOLD signals from “normal” via “absent” to “inverse.” Possible BOLD alterations should be taken into account when functional lateralization is determined using fMRI as they may lead to an incorrect interpretation of clinical fMRI data.

1.1.2.3 BOLD Signal in Contrast-Enhancing Parts of Brain Malignancies

In some patients with low- or high-grade gliomas, BOLD signal changes can be observed in those gliomas, which in principle should not contain functional tissue. This issue has been investigated in several studies (Skirboll et al. 1996; Schiffbauer et al. 2001; Ganslandt et al. 2004). From these studies using magnetic source imaging methods (which is a combination of EEG and anatomical MRI), it can be concluded that real functional activity might be located within or at the margins of the tumor in a considerable percentage of patients (e.g., 25 % in the study of Schiffbauer et al. (2001), so that only partial resection is possible. The interpretation of this activity at the tumor margin remains ambiguous, either the cortex has been “displaced” by the growing tumor or is near the mark of being invaded by infiltrative tumor. Therefore, activated areas in tumor tissue are not always related to artifacts but could also be “real” functionally active tissue infiltrated by a tumor. If in doubt of the real or artificial nature of the activations, it is advised to combine different techniques (like MEG) to pinpoint the real nature of the BOLD signal change. More information about the combination of these different techniques can be found in chapter “[Multimodality in functional neuroimaging](#)”).

1.1.2.4 BOLD Signal in Patients with Brain AVMs

Arteriovenous malformations (AVMs) can produce widespread vascular steal effects beyond their nidus that preclude a normal hemodynamic response (for details see chapter “[Presurgical functional localization possibilities, limitations and validity](#)”). However, cerebral blood flow reductions do not necessarily cause cerebral dysfunction, as suggested in previous reports. Alterations of the microvascular architecture are prone to exist in the neighborhood of vascular malformations, and neovascularization is characteristic for malignant brain tumors and brain metastases of different pathologies, resulting in a change in the observed BOLD signal in the near neighborhood of the AVM. Also several studies have been published in different patient populations with AVMs reporting a shift of the functionally active regions in the neighborhood of the AVMs (Caramia et al. 2009). Vascular malformations are believed to form during gestation, and the development of these lesions and the associated brain damage due to hemorrhage or ischemia can lead to reorganization not only of the local anatomy but also of the functional cortex (Lehéricy et al. 2002). This can result in a cortical reorganization where the real functionally active region has been shifted into other previously defined functional regions (Maldjian et al. 1996; Fandino et al. 1999). More about brain plasticity has been explained in chapter “[Brain plasticity in fMRI & DTI](#)”.

1.1.3 The Effect of Different Pharmaceuticals on BOLD fMRI Signal

Chemicals and pharmaceuticals can have an effect on different aspects of brain physiology and/or hemodynamic cou-

pling (Seifritz et al. 2000; Braus and Brassen 2005). The next paragraph introduces some known effects of substances on BOLD signal.

1.1.3.1 Caffeine

The effect of caffeine – a vasoconstrictor – on BOLD signals has been studied by several researchers (Parrish et al. 2001; Laurienti et al. 2002; Chen and Parrish 2009; Rack-Gomer et al. 2009) with different results. In an experiment determining the hemodynamic response function, volunteers were presented a short visual flash to activate primary visual areas and triggering a finger to thumb opposition. They were scanned in two consecutive sessions: before and after drinking three cups of coffee (~250 mg caffeine). The observed hemodynamic response function before and after administration of caffeine demonstrated a large increase (up to 50 %) in BOLD signal after caffeine intake as compared to the control session (Fig. 2a). The explanation for this effect may rely on the different properties of caffeine, i.e., its property to modulate neural activity and neurovascular tone. The influence on neurovascular tone decreases the resting state CBF (Rack-Gomer et al. 2009). As a result the increase in rCBF and respective BOLD signal change during stimulation is higher after intake of caffeine. Caffeine also has an excitatory action on neurons through the blockade of A1 adenosine receptors increasing neural activity following stimulation (Parrish et al. 2001; Laurienti et al. 2002). On the other hand, caffeine can have an influence on the observed resting state connectivity in the brain, which can be a real effect on brain activity or a result of the influence of caffeine on the baseline and reactive cerebral blood flow; therefore, one should be very careful while interpreting resting state fMRI data of patients (Rack-Gomer et al. 2009).

1.1.3.2 Alcohol

The effect of alcohol on BOLD signals is shown in Fig. 2b. A similar experiment as the one described above has been performed in volunteers before and after the consumption of three glasses of beer (~34 ml of alcohol). The graph demonstrates that alcohol has an adverse effect as compared to caffeine on the hemodynamic response. The effect of alcohol is twofold: First, alcohol is a vasodilator which increases the baseline CBF resulting in a smaller increase in rCBF and hence relative BOLD signal after stimulation (Levin et al. 1998; Seifritz et al. 2000). Second, alcohol also decreases the attention to the task the subjects have to perform and consequently neuronal activation of the stimulated brain areas (Luchtmann et al. 2010).

1.1.3.3 Other Chemicals

It is also important to note that various pharmacological agents may potentially alter the BOLD signal. Cocaine, e.g.,

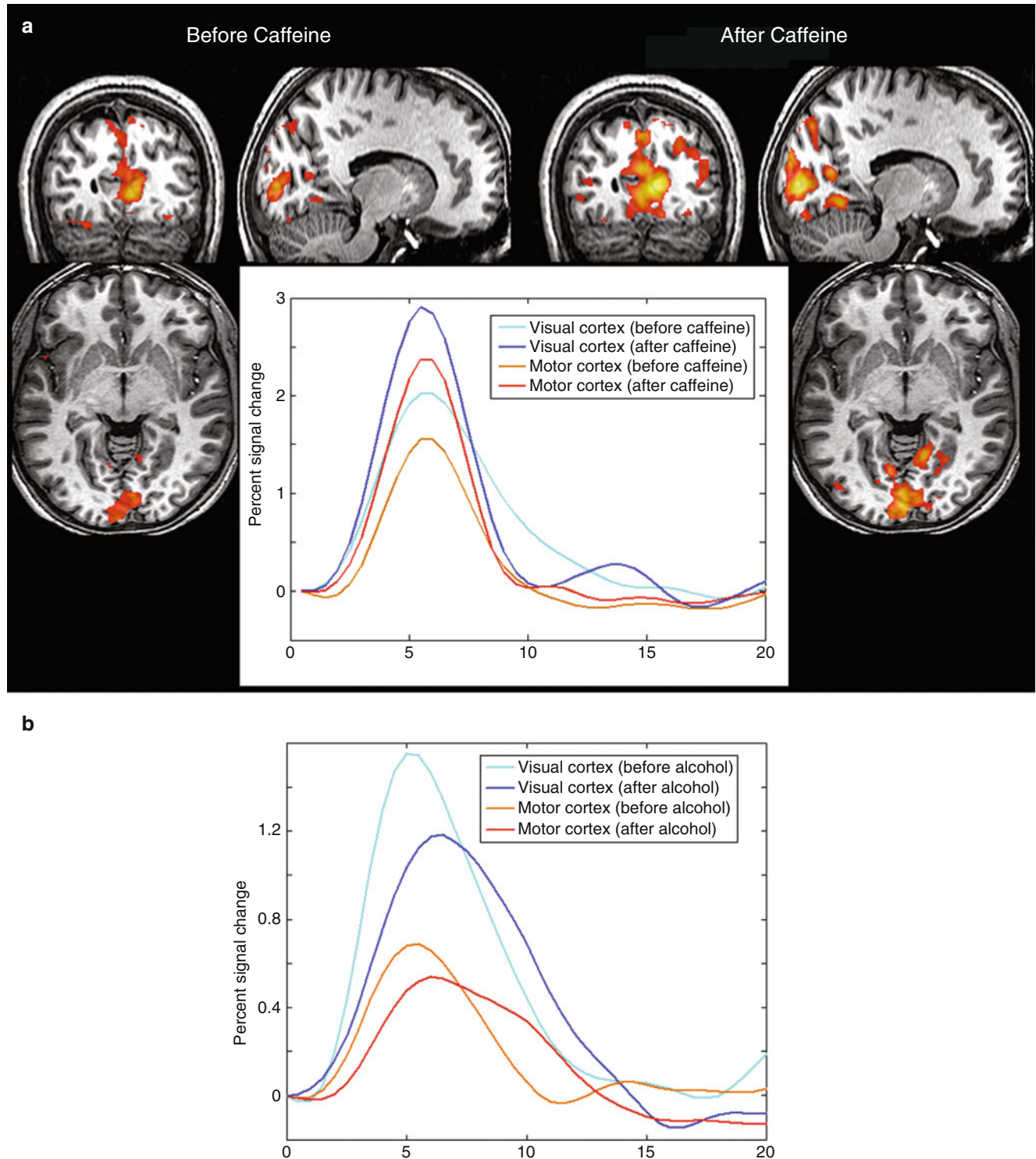


Fig. 2 (a) Activation maps and mean percent signal change of the hemodynamic response function (HRF) after caffeine intake. (b) Mean signal change in the visual and motor cortex before and after drinking three glasses of beer as a result of the visual flash stimulation with a single finger-tap, demonstrating a decrease in BOLD signal change following alcohol intake

function (HRF) after caffeine intake. (b) Mean signal change in the visual and motor cortex before and after drinking three glasses of beer as a result of the visual flash stimulation with a single finger-tap, demonstrating a decrease in BOLD signal change following alcohol intake

influences neuronal connectivity (Li et al. 2000; Tomasi et al. 2010), neuronal activation, and cerebral blood flow in the resting state (Breiter et al. 1997; Lee et al. 2003; Lowen

et al. 2009). However, the BOLD signal has been reported to remain unaffected after cocaine administration (Gollub et al. 1998). Theophylline has been shown to increase the BOLD

signal in the rat primary motor cortex (Morton et al. 2002), a finding which has also been observed in patients with hyposmia where theophylline has been shown to increase odor-induced BOLD responses (Levy et al. 1998). The decrease in cerebral blood flow in the resting condition, due to a vasoconstrictor response, might possibly account for the increased BOLD response after theophylline administration. Furthermore, theophylline has also known neuroexcitatory effects, e.g., as an antagonist of the inhibitory neurotransmitter adenosine. This neuroexcitatory effect of theophylline could increase the number of neurons that are activated in response to a given stimulus, hereby increasing the observed BOLD response (Morton et al. 2002).

On the other hand, nicotine – a drug without effects on local brain hemodynamics as demonstrated in a simple visual task (Jacobsen et al. 2002) – has been demonstrated to increase attention to cognitive tasks both in patients with schizophrenia and in smokers (Kumari et al. 2003; Jacobsen et al. 2004) but also changing the resting state connectivity and possible subsequent stimulus-driven responses (Hahn et al. 2007). It is important to keep in mind that many other pharmacological agents, which have not yet been tested in this respect, may influence the BOLD response and that patients with brain tumors may receive such pharmaceutical products (D'Esposito et al. 2003).

1.1.3.4 CO₂

Several studies report on the effect of CO₂ on the resting state BOLD signal and on the BOLD response during activation while inhaling this mixture of gas. CO₂ is a potent vasodilator increasing the BOLD signal. Breathing a mixture of air with 5 % CO₂ increases the measured BOLD signal by 10 % (Kastrup et al. 1998). This effect can have consequences on patient studies as well. A change in the breathing rate during task performance, as a result of excitement and stress at the beginning of the experiment, can occur in some patients. This change in breathing rate alters the oxygen supply to the brain and the CO₂ content in the blood affecting vasodilatation and thus the global BOLD signal in the brain. This can interfere with the task-related BOLD response. When a volunteer is asked to change his breathing rate from normal breathing to hyperventilation and vice versa, the time course of the BOLD signals clearly displays the large effect of hyperventilation on the resting state fMRI signal (Fig. 3). Therefore, in order to minimize effects of anxiousness and the change in breathing rate in clinical fMRI studies, it is very important to instruct and comfort the patients comprehensively and allow them to accommodate themselves to the scanner environment before initiation of the experiment. RsfMRI exams which are not driven by external stimuli (chapter “Presurgical resting state fMRI”) are even more susceptible to changes in breathing rate and cardiac cycle. Thus, careful instruction of the patients, and possibly also the monitoring of functions of the autonomic nervous system

(ANS), could improve rsfMRI results (Murphy et al. 2011; Iacobella and Hasson 2011).

1.2 The Influence of Brain Lesions on DTI Results

The lesion of the patient can also influence DTI images as well as the resulting FA maps and finally the fiber tracts. Degenerative diseases and demyelination disorders will reduce the measured FA values focally as observed, e.g., in amyotrophic lateral sclerosis (Sage et al. 2009), multiple sclerosis (Reich et al. 2008), and Alzheimer's disease (Kantarci et al. 2010). More confined brain lesions can also influence the measured FA and diffusivity. Vasogenic edema reduces the local fiber density hereby lowering the measured FA, which in turn will influence the number of reconstructed fibers in the fiber-tracking algorithm around the respective lesion (Buzzi et al. 2012). Tumoral tissue can also destroy white matter fibers by reducing the number of intact axons (Sinha et al. 2002). On the other hand, in an abscess cavity the FA values are higher, which possibly reflects organized and oriented inflammatory cells (Toh et al. 2011).

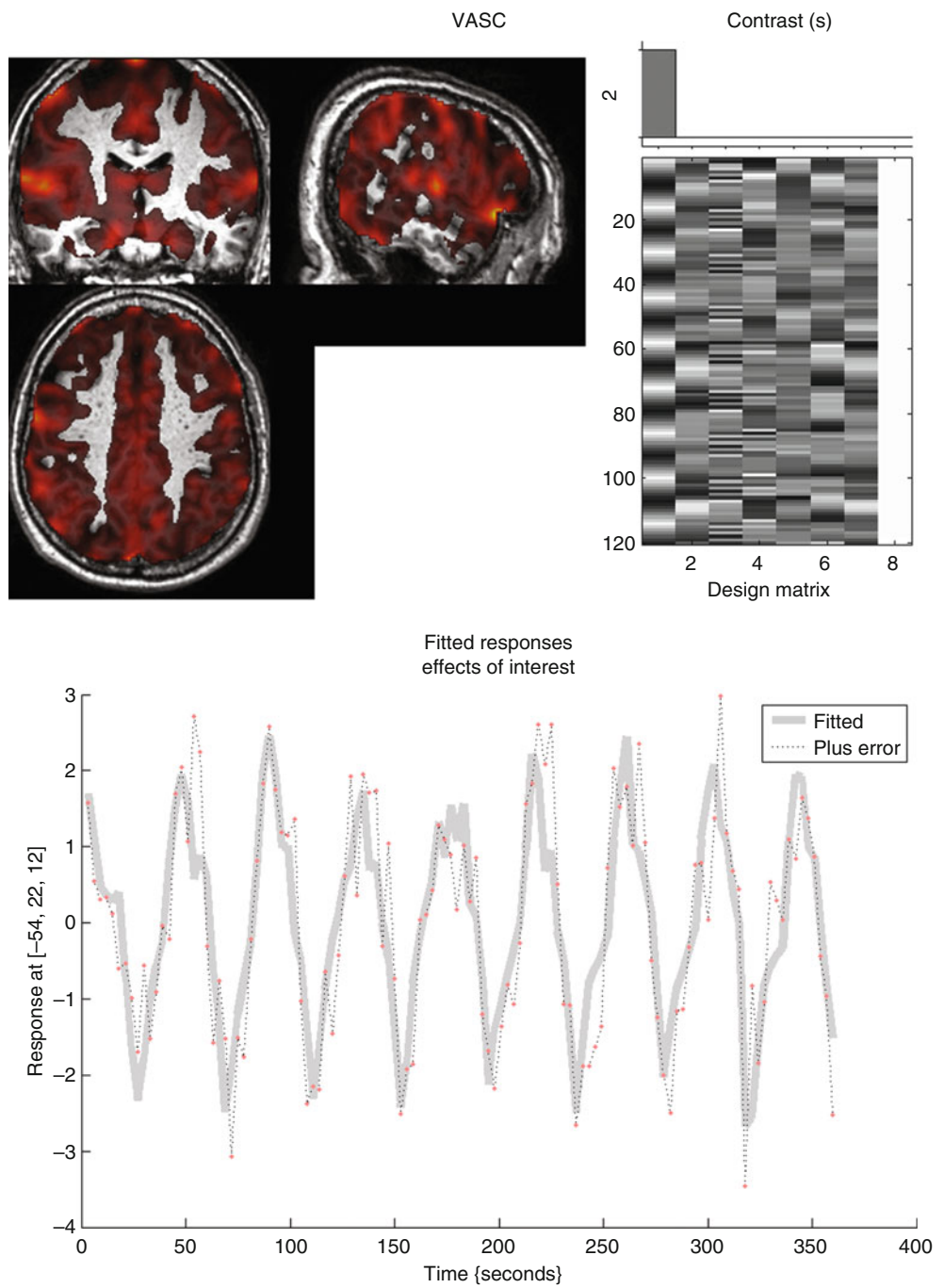
The distorted anatomy resulting from the mass effect of a lesion hampers the positioning of the tracking ROIs at the correct position needed for a reliable and reproducible fiber tracking. One solution for this problem might be the use of fMRI activation regions as seed ROIs for fiber tractography, herewith using functional information for a better understanding of the structural status and its alterations (Kleiser et al. 2010).

1.3 Patient-Related Artifacts and Physiological Noise

1.3.1 Flow and Pulsation Artifacts

Flow artifacts result from the pulsating in- and outflow of the blood perpendicular to the imaging slices, hereby producing signal changes in different slices. At 1.5 T, these artifacts are especially observed in pathological flow conditions such as in AVMs. However, with the trend toward using higher magnetic field strengths (3 T and above), flow and pulsation artifacts become more prominent (Biswal et al. 1996; Srivastava et al. 2005). These artifacts manifest themselves as a slowly varying signal change with a sinusoidal rhythm, which is the result of an undersampling of the real underlying blood pulsation. In Fig. 4a, a pulsation artifact is demonstrated in an fMRI experiment acquired at 3 T without any specific brain activation, demonstrating several tubular-shaped regions with a signal intensity of sinusoidal shape. If the stimulation paradigm shows a period similar to the period of this sine wave (in this case a period of 100 s), these areas will highlight as false positives (Dagli et al. 1999). RsfMRI data are

Fig. 3 Effect of hyperventilation on the BOLD resting state signal. During the scanning session the volunteer switched from hyperventilation periods to breath-hold periods of 24 s. The activation map shows MR signal change following the breath-hold/hyperventilation paradigm in the entire cortex of the volunteer. The MR signal time trace in the bottom of the figure clearly demonstrates the signal fluctuation for a random voxel in the cortex



also very sensitive to such artifacts as these sinusoidal signal time traces do temporally very closely resemble real synchronized brain activation in different areas constituting the respective functional network.

1.3.2 Artifacts from Bulk Head Motion

The small intensity changes typically observed in fMRI images (ranging from a fraction of 1 % signal change to a few percentages) can easily be contaminated by a variety of sources. In clinical fMRI, the major contribution to signal artifacts arises from bulk head motion during acquisition of

the functional data series (Seto et al. 2001). A further minor contribution originates from physiological brain motion (pulsation of the brain, overlying vessels, and cerebrospinal fluid) driven by cardiac pulsations (Dagli et al. 1999; Windischberger et al. 2002). Nevertheless, the primary reason for failed clinical fMRI examinations is head motion. In the study of Krings et al. (2001a), the most frequent cause for the failure of 15 % of their clinical exams was due to head movement artifacts (Krings 2001a).

The motion and its effect occurring during an fMRI time series acquisition can be divided into two separate categories:

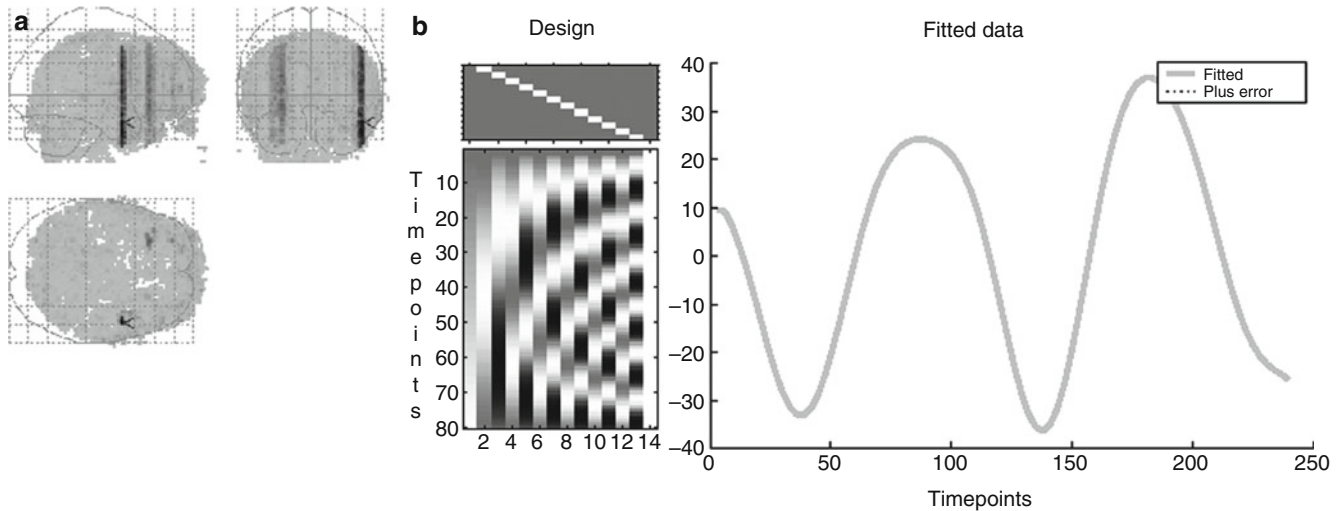


Fig. 4 Example of a pulsation artifact: 80 dynamic resting state BOLD scans were acquired with a TR of 3 s during 4 min in a volunteer. (a) Pulsation artifacts are observed behaving as tubuli-like BOLD fMRI

activation regions. (b) The time course of the signal in this structure demonstrating a sinusoidal shape with a period of 100 s

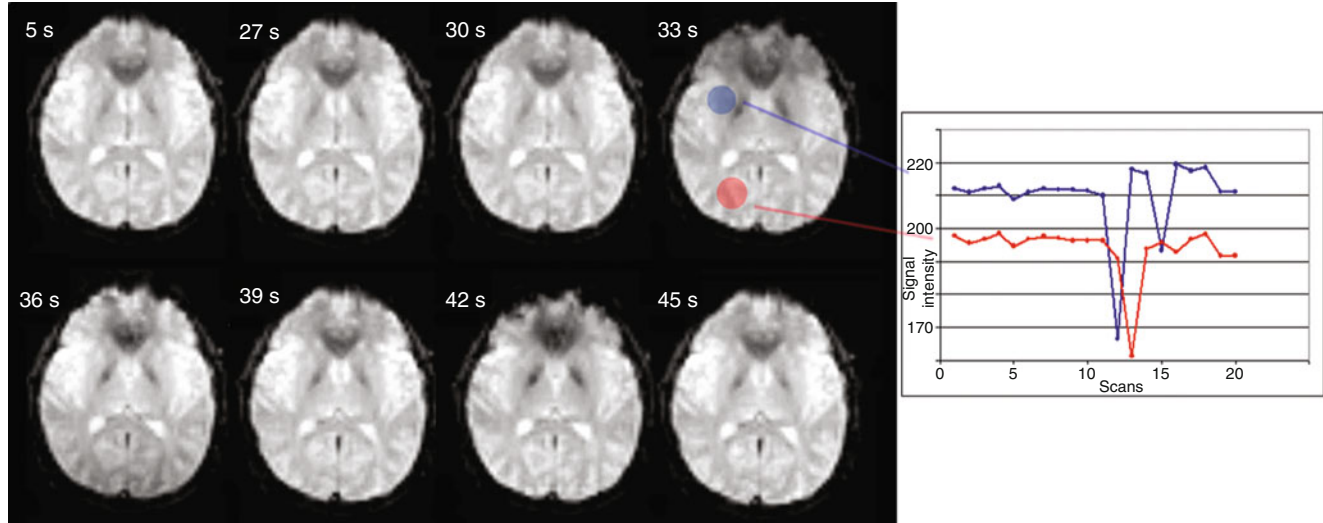


Fig. 5 Different time points in an fMRI series (TR=3 s) of a volunteer. During the scan he moved his head through the plane of acquisition. The time trace shown on the right displays the signal intensity change

of the voxels in the filled regions; a large motion-induced signal drop is apparent resulting from this through-plane motion at around 30 s

intra-image motion which is generally a very fast and sudden motion (i.e., at a time scale smaller than the image acquisition time) and inter-image motion on a time scale between a couple of seconds to minutes reflected in a slow movement of the subject (i.e., at a time scale larger than the time necessary to acquire a single image volume). These two subcategories of motion have different effects on the acquired images and functional map properties. The intra-image motion, typically induced by sudden head movement, results in “blurring” and “ghosting” in older GE-based acquisition sequences and is less present in single-shot echo-planar

imaging, where all data for an image are collected in less than 100 ms (Duerk and Simonetti 1991). But if present, this sudden motion can have the following effects on EPI images: If the motion is very fast (<100 ms), it can still cause ghosting artifacts in several slices of the acquired volume. Slower, longer-lasting motion can also change image contrast; this especially applies to motion perpendicular to the acquisition plane. The latter will result in a change of the apparent repetition time for the acquisition of the same slice in the different volume (Fig. 5) which changes the T1 weighting of the tissue for the different slices and thus the signal intensity of

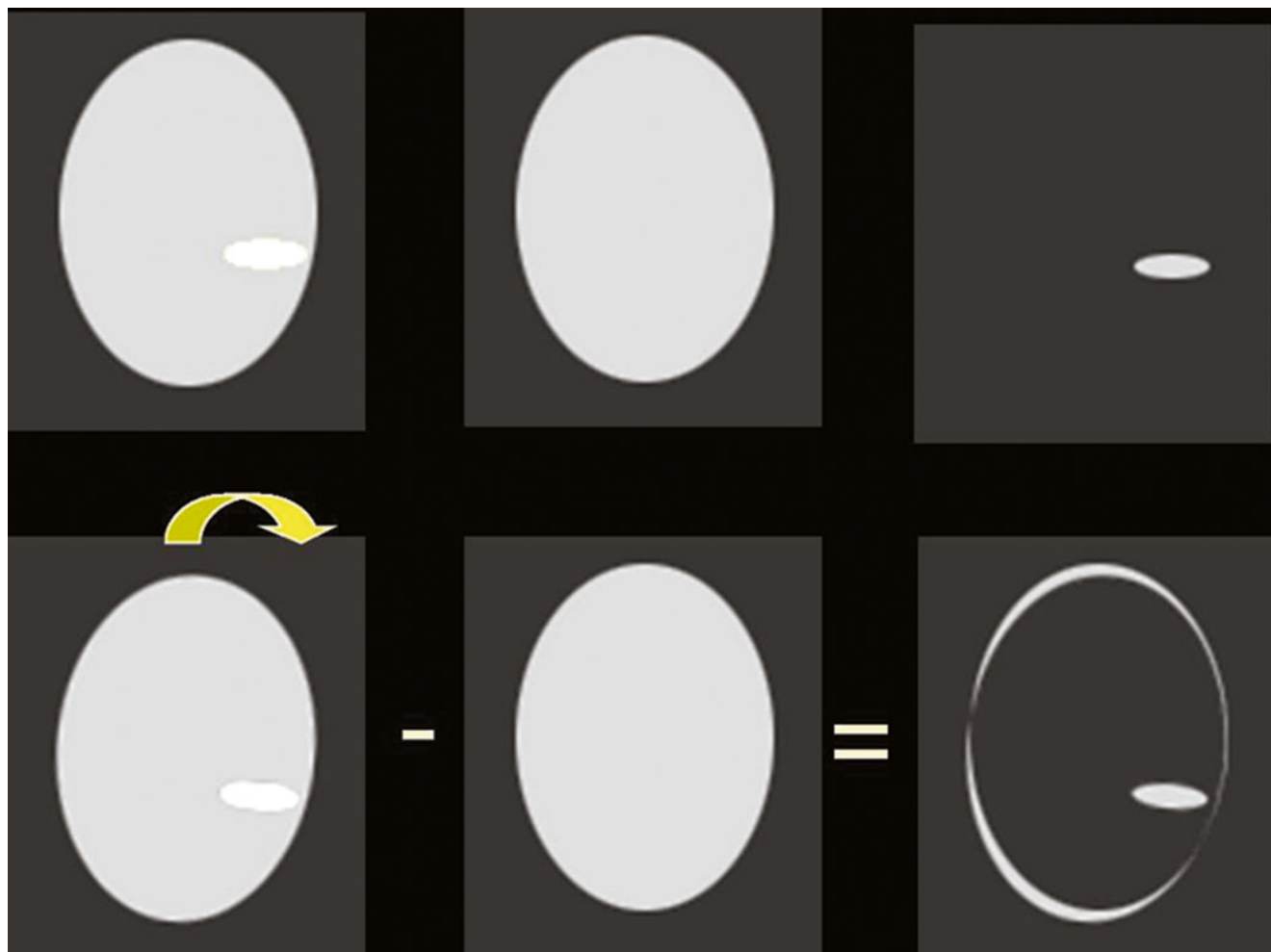


Fig. 6 Simulation of the effect of head motion between different states of activation on the observed activation in a subtraction map. In the *top row* without motion only the real activated region is discerned; in the

bottom row on the other hand motion between both images is introduced, and a rim of false activation appears in the subtraction map

the tissue. In other words, the tissue has experienced a different “spin history” (Friston et al. 1996b; Muresan et al. 2005).

In resting state fMRI, motion-related confounds can be even more troublesome. Due to a differential effect on resting BOLD signal of motion artifacts, connectivity measures can be largely influenced. Even subtle motion artifacts <0.5 mm can provoke a specific bias increasing short-range connections while decreasing long-range connections which can result in group differences between certain patient groups which will generally suffer from more motion than healthy controls (Power et al. 2013).

Motion on a time scale larger than the image acquisition time causes a misregistration of the images within the time series and makes activation foci undetectable or, even worse, induces artificial activation when the motion is temporally correlated to the stimulus (Hajnal et al. 1994) (Fig. 6). This will especially have an effect in those brain regions that show steep image intensity gradients (e.g., at the edges of the brain

or in patients at the border of a T2-weighted hyperintense lesion), which are particularly prone to these artifacts. The effect of this inter-image motion has been shown to be particularly problematic in clinical examinations. Results from Hill et al. (2000) indicate that head motion occurs with a greater magnitude in patients with epilepsy than in healthy volunteers.

1.3.2.1 Minimizing and Correcting for Motion

Several solutions exist to correct for or to minimize inter-image motion which have been proposed by several researchers. Head movement during the acquisition phase can be restricted by fixation of the head with molds and straps (Fitzsimmons et al. 1997; Edward et al. 2000; Debus et al. 2008), which represents an intermediate level of head fixation. The use of a “bite-bar” (Fig. 7) – a custom-molded dental fixation, regularly used in our institution to restrain head motion while imaging volunteers – provides a highly rigid

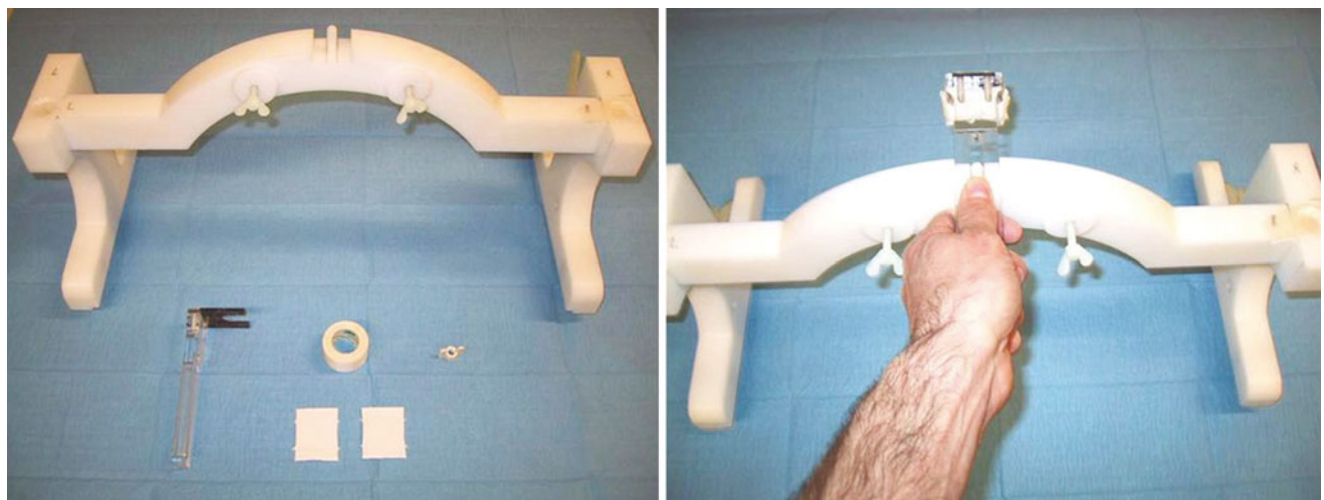


Fig. 7 Pictures of a custom-built bite-bar system used to minimize patient motion during the fMRI experiment, consisting of a plastic bridge which is positioned over the subject's shoulder and a small detachable piece which the subject puts in his mouth

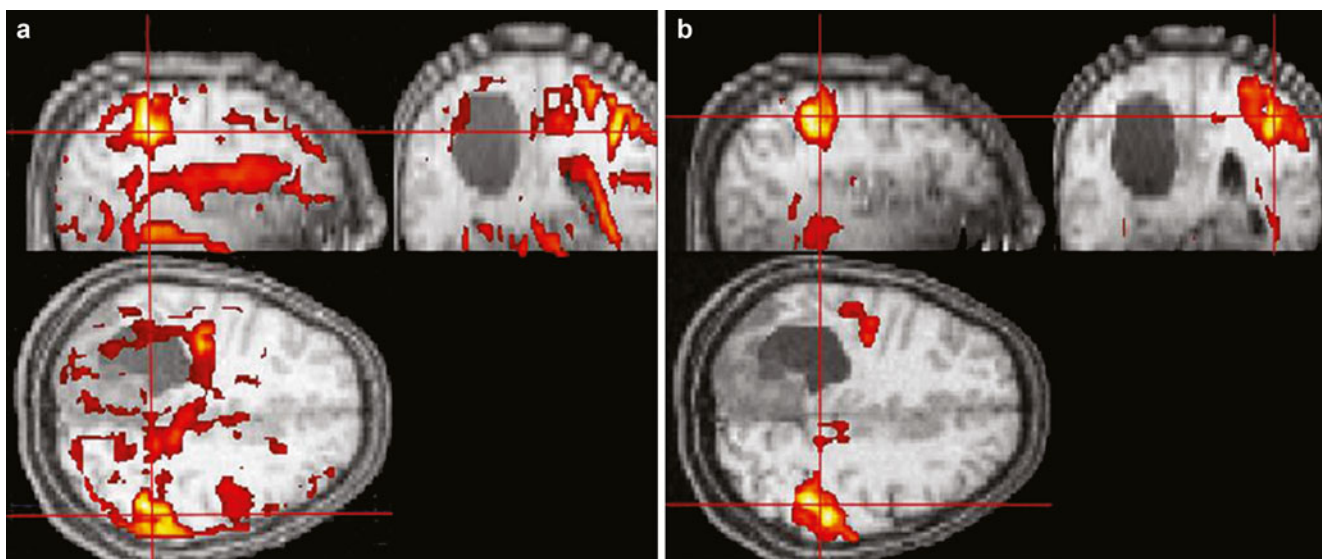


Fig. 8 Effect of subject motion on the resulting fMRI activation map of a patient (a) and the effect of the correction of this motion (b) on the observed real and false motion-induced activation in the calculated fMRI map

fixation, but can only be used in a limited number of patients (Dymarkowski et al. 1998). The presence of dental prosthesis interferes, and not all patients tolerate this kind of fixation. Furthermore, safety precautions preclude its use in these patients who are at risk of having epileptic seizures during imaging (Jiang et al. 1995; Freire and Mangin 2001).

Another solution is the use of motion correction algorithms during data post-processing, which are nowadays integrated in most different fMRI analysis software. Motion correction is typically achieved by the rigid realignment of the consecutively acquired images in the data series with the first image (or an arbitrary other image) (Friston et al. 1995, 1996b). If the patient moves with a frequency unrelated to

the frequency of the applied stimulation paradigm, this realignment post-processing can successfully separate this motion caused by the patient himself from true activation (Fig. 8). As most motion correction algorithms are intensity based, it is also possible that false motion is observed in the time series which may actually be the result of a large activation at a specific brain region shifting the center of intensity to a certain direction following the activation paradigm (Biswal and Hyde 1997).

However, most of the patient motion is attributed to the applied stimulus (Hill et al. 2000), which is certainly the case if the patient is performing different motor paradigms (e.g., the patient is moving his head at the start of the task for looking

at his fingers performing the task). This effect cannot be easily separated from the real functional activation due to their temporal synchrony (Hajnal et al. 1994).

The problem of patient motion could be further reduced in a number of different ways. First, stimulation paradigms can be optimized to minimize head motion, an issue that is currently under investigation. Much attention is given to differences in anatomic-functional information that can be obtained from active versus passive tasks which will inherently reduce motion (Gasser et al. 2004). Also, resting state fMRI does not suffer from task-based patient motion as there is no active task performed.

As described earlier the effect of through-plane motion is a combination of a misregistration of different subsequent BOLD images with the T1-weighted slice effect varying the signal intensity resulting from changes in TR. Therefore, it is recommended to adapt the scanning planes in such a way that the maximal observed motion is in parallel to the acquisition plane, e.g., if head nodding is expected from left to right, axial slices should be acquired. However, if head motion is expected from front to back, sagittal slices should be obtained. There are also techniques to correct for spin history effects due to through-plane motion (Muresan et al. 2005).

Adapted acquisition sequences have been presented that change the position of the acquired EPI volume in order to come up for the motion of the subject. For this, subject motion has to be calculated online between two consecutive acquired volumes which can be done on the images itself or by calculation of the position of external markers using laser guidance or separate video cameras (Qin et al. 2009). This information can then be used to predict the position of the head for the following (third) acquisition. This technique thus uses a prospective motion correction algorithm in contrast to the retrospective motion correction techniques used in fMRI post-processing software tools. As the scan planes are adapted to motion, the T1-weighted slice effect is also diminished (Ward et al. 2000; Thesen et al. 2000; Maclarens et al. 2013).

If motion artifacts still persist in the resulting BOLD activation maps, there is an option in most software packages to incorporate the motion parameters calculated in the preprocessing step in the statistical calculation of the functional activation (e.g., using the general linear model (GLM)). In doing so the signal variability within the voxels, correlating with these motion parameters, will be reflected in this contrast hereby decreasing the influence of the motion-induced signal changes in the other conditions (contrasts) of interest of the stimulation paradigm. Although this will effectively remove motion-induced “false” activations, it can also remove or decrease “real activation” ascribed to motion (Johnstone et al. 2006).

For further information on fMRI data processing, see also chapter “[Revealing brain activity and white matter structure using functional and diffusion-weighted magnetic resonance imaging](#)”.

1.3.2.2 How to Distinguish Real Activation from Motion-Induced False Activation

If it is not possible to completely eliminate motion during image acquisition and data processing (e.g., in the case of paradigm-related motion), motion artifacts need to be identified in the activation maps. This paragraph provides some practical tips to distinguish motion-induced “false activations” from the “real activation” of the BOLD signal. Most of the motion-induced “false activations” are localized at the border of different structures which show large signal intensity gradients (Weisskoff 1995; Orchard and Atkins 2003). These motion-induced signal changes at the tumor borders typically have a ringlike spatial appearance; in other words they are observed as a thin rim of hyperactivation in the neighborhood of large image intensity gradients (Figs. 6 (simulation), 8, and 9). The BOLD hemodynamic response curve typically rises 4 s after onset of the stimulation and reaches its maximum after 6–8 s. If the movement follows the paradigm, the onset of the movement will be at the same time as the onset of the paradigm. Movement-related signal changes will follow the movements instantaneously. Therefore the temporal profile of the movement-related “false activations” will temporally coincide with the different conditions of the block design and will occur prior to the physiologically delayed hemodynamic response, which is reflecting the “real activation” temporal profile (which typically has a delay of approximately 2–4 s compared to the stimulation onset). The signal intensity variation will also be more abrupt compared to the more gradual activation-induced BOLD signal intensity change. Movement-related signal changes tend to display much higher signal intensity changes as compared to physiological BOLD signal changes (Fig. 9).

1.3.3 Motion Artifacts in DTI

Typically DTI scans last between 5 and 20 min for the acquisition of an entire brain volume data set. Subject movement during this scan time can result in motion artifacts on the different diffusion-encoded images. These artifacts can manifest themselves differently according to the amplitude and speed of the patient movement. Slight movement occurring during the 5–20 min of scanning will result in a misalignment of the different diffusion-weighted images. In the post-processing steps of DTI data, the different data volumes should then be realigned by registration to, e.g., the b_0 image, but attention should be paid that the orientation information of the applied diffusion gradients should also be rotated according to the images (Leemans and Jones 2009). Large and fast movements will result in large signal dropouts and interleave artifacts (Fig. 10). These large artifacts will disturb the resulting DTI maps if they are not identified. Different software solutions exist which can trace these signal dropouts and exclude them from further data analysis (Tournier et al. 2011).

Another problem related to patient motion but induced by the diffusion gradients themselves is the so-called vibration

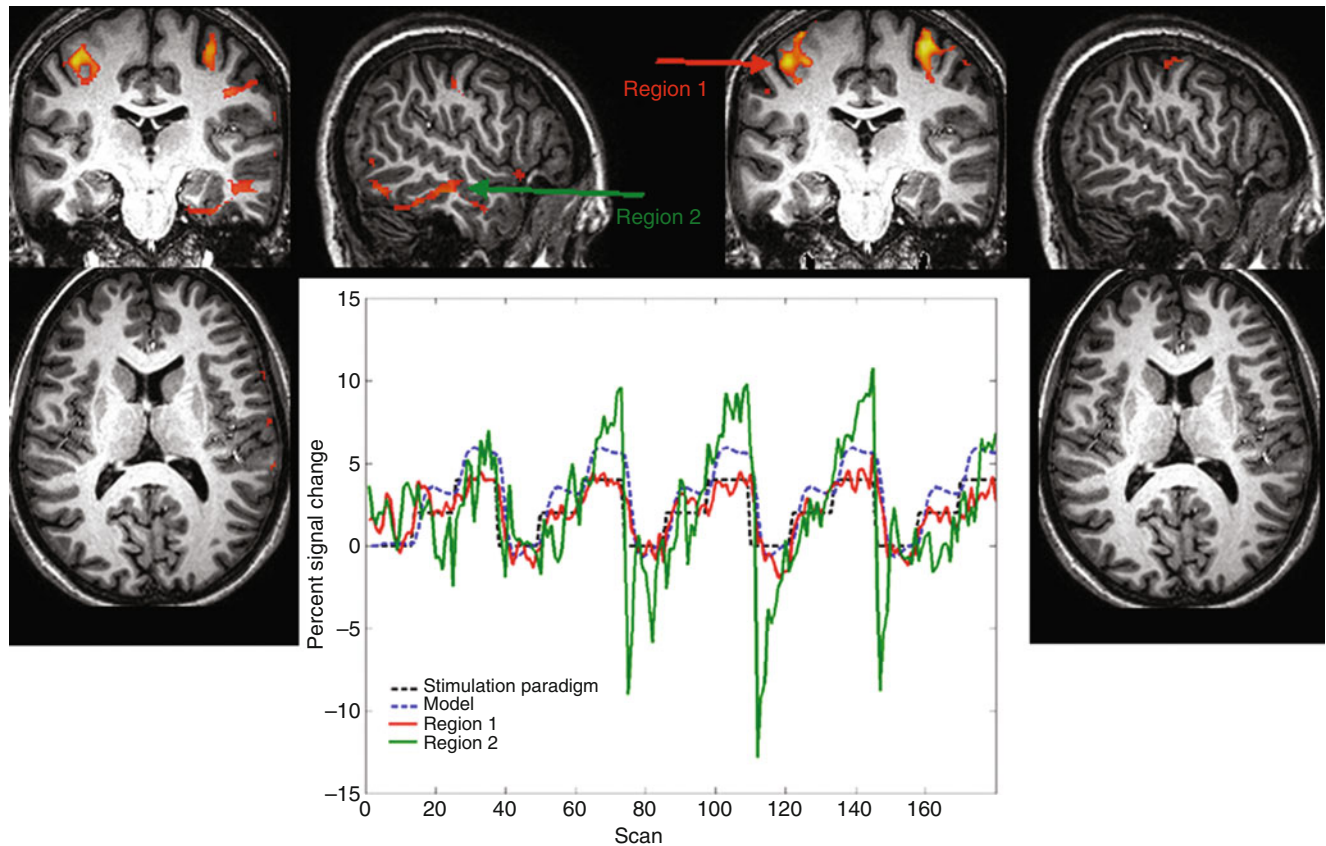


Fig. 9 fMRI activation map of a volunteer who moved (*left*) and did not move (*right*). Signal time traces in a motion-related region (*green*) and a real activation region (*red*) demonstrate the temporal mismatch

between both signal traces and between the motion-related signal change and the model of activation (Color figure online)

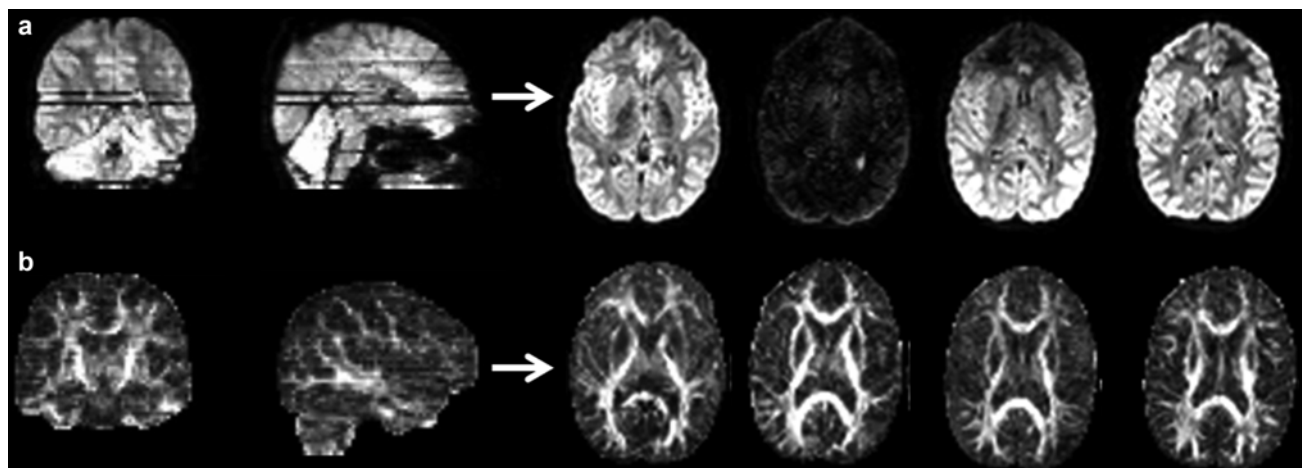


Fig. 10 An example of motion-corrupted diffusion-weighted images. **(a)** The native diffusion-weighted axial images show a loss of signal at those slices where large motion was apparent. **(b)** The calculated FA

maps from these images also suffer intensity changes due to this motion although being less apparent

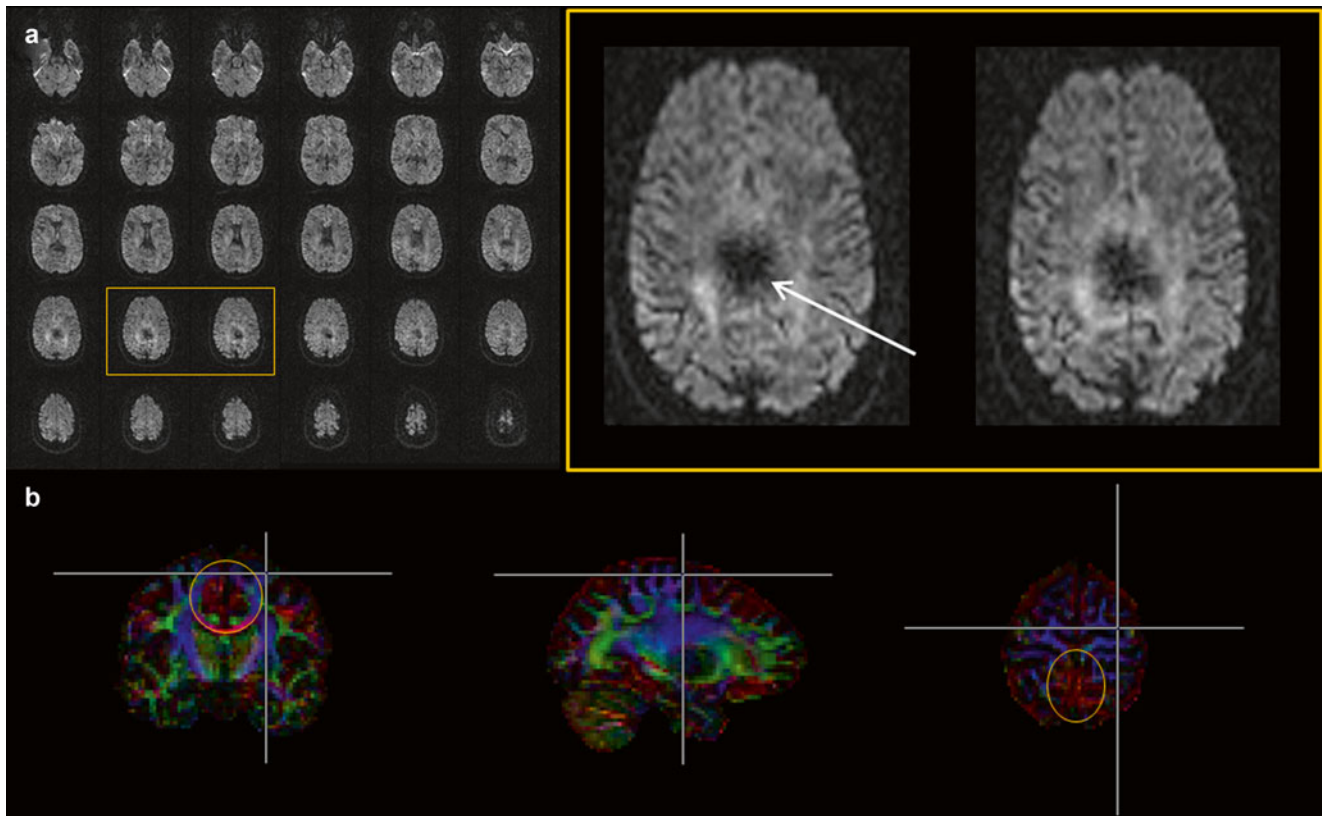


Fig. 11 (a) Cross sections of diffusion-weighted images demonstrating the vibration artifact located mainly in the mesial parietal lobe with a large diffusion gradient being switched on in the left-right direction.

(b) Colored fractional anisotropy maps displaying artifactual left-right dominance in the mesial parietal lobe

artifacts (Gallichan et al. 2010; Mohammadi et al. 2012) which typically manifest as a signal loss in a large region of the mesial parietal lobe (Fig. 11). Strong diffusion gradients cause low-frequency vibrations of the MR system, which results in vibration of the patient table. When the patient is well fixated to the table with pads, this table vibration will be translated into head motion of the patient which is synchronized with the applied diffusion gradient. It has been observed that this artifact is largest when the left-right component (x -gradient) of the diffusion gradient is large. Different solutions have been proposed to avoid this artifact. The uncoupling of the table from the MR system could result in less synchronized motion of the subject resulting in lower artifacts. A longer TR between consecutive scans can also reduce this artifact (Gallichan et al. 2010). Finally, recently combined acquisition and post-processing methods have been proposed to eliminate such artifacts (Mohammadi et al. 2012).

1.3.4 Patient Cooperation

Patient cooperation during the fMRI exam is very important; therefore, control of task performance during the scanning is a prerequisite for clinical functional MRI. In an active motor task, cameras are very handy to observe whether the patient

understands and performs the task correctly. In patients with limited ability to cooperate, direct instruction plus direct supervision of proper task performance by the investigator standing next to the scanner is strongly recommended. In visual experiments, it is important to monitor eye movements using an eye-tracking camera. Figure 12 displays the difference in activation maps between a fixating and a non-fixating subject in a visual retinotopy experiment. In cognitive and language tasks, an indirect control can be implemented in the paradigm. Cognitive paradigms can be devised in such a way that the patient has to respond by pressing a button. These responses can be recorded during the scanning and controlled afterward for correctness. Also in resting state fMRI cooperation of the patient is necessary, e.g., there already are large differences in brain activation synchrony patterns between “eyes open” and “eyes closed” scans (Zou et al. 2009).

To precisely inform the patients before scanning about what is expected from them to do during the exam is very important. Real-time fMRI analysis allows a direct control of the experimental success so that a failed functional session can be repeated immediately afterward, which is much less time demanding than asking the patient to come back after a couple of days for an additional scanning session.

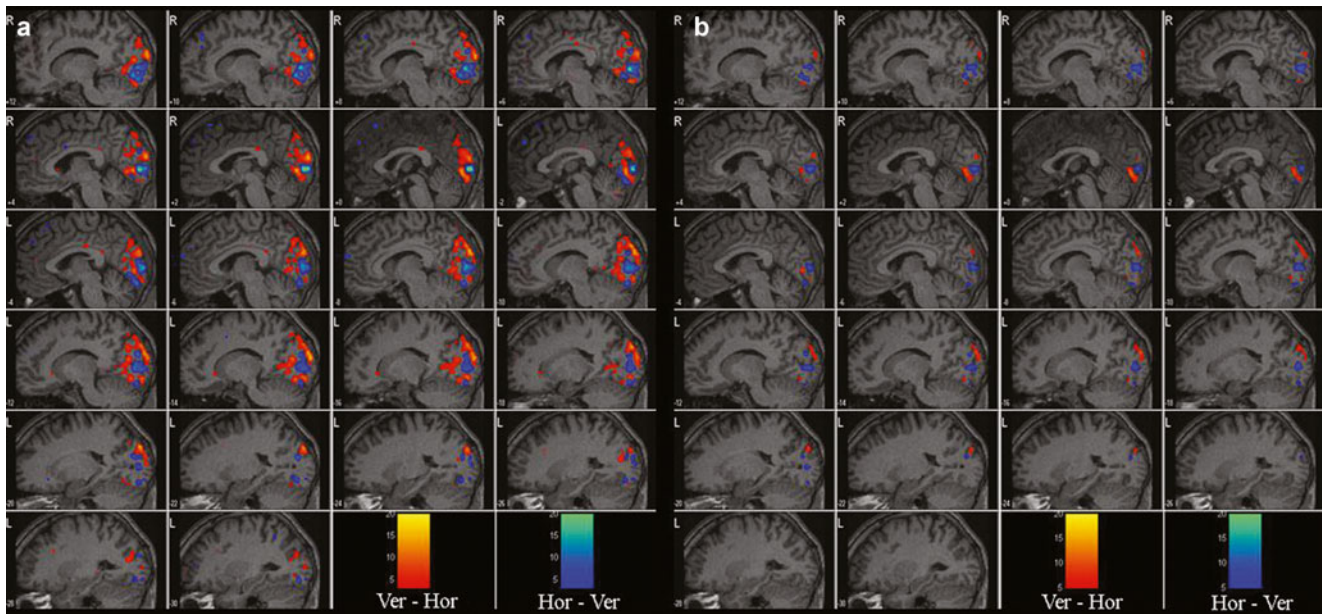


Fig. 12 Effect when the subject is not cooperating during the fMRI exam: (a) a retinotopic map of a subject fixating to the middle of the visual stimulus (alternating *horizontal* and *vertical* wedges).

(b) Retinotopic map of the same subject looking around (i.e., not fixating) during the fMRI exam

1.4 Technical-Related Artifacts

1.4.1 Susceptibility Artifacts

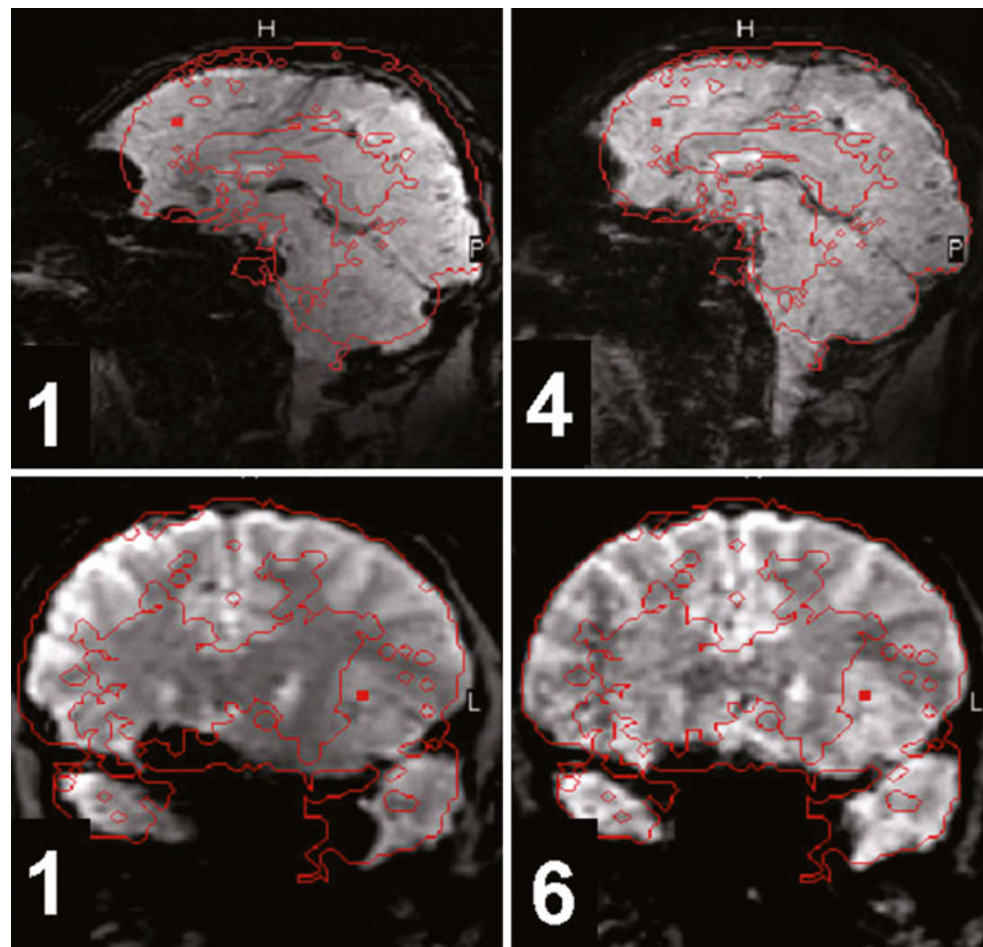
Almost all BOLD fMRI acquisitions and DTI acquisitions are performed with multislice single-shot EPI acquisition sequences. These techniques have a very high temporal resolution and are very sensitive to the BOLD effect which manifests itself as a change in susceptibility in the activated regions. But these single-shot EPI sequences also suffer from distortion and susceptibility artifacts as a result of their high sensitivity to susceptibility and the resulting high T2* weighting (Devlin et al. 2000). In most fMRI studies, these drawbacks are of less importance and do not come up to the vast advantages of the EPI technique to both detect and localize brain activation. But the susceptibility-related signal drop in those brain areas which are located in the skull base and in the neighborhood of large air cavities like the orbitofrontal cortex and the anterior and medial temporal cortex pose a problem for fMRI studies expecting brain activation in these areas (Friston et al. 1996a; Devlin et al. 2000; O'doherty et al. 2000; Small et al. 2004). In patients this effect can also be observed adjacent to metal implants or certain types of lesions (e.g., lesions containing deoxyhemoglobin or hemosiderin), where the susceptibility difference between the lesion and the surrounding brain tissue is large (Håberg et al. 2004). With the trend of using higher static magnetic field strengths, this effect of local signal loss and image distortion is even more pronounced (Abduljalil and Robitaille 1999). For clinical fMRI this poses a problem

both for studies searching for activated regions in the orbitofrontal cortex (like taste and smell-related regions, emotional processing) (Deichmann et al. 2003; Smits et al. 2007) and anterior temporal cortex (regions responsible for object recognition) (Devlin et al. 2000).

1.4.1.1 Methods to Decrease Susceptibility-Related Artifacts

Different strategies for experiments in susceptibility-prone regions have been proposed including the use of other less susceptibility-sensitive acquisition sequences like multi-shot EPI sequences, spin echo EPI sequences, or flash sequences (Menon et al. 1997), but these techniques are also less sensitive to the BOLD contrast (Song et al. 2000). On the other hand, various ingenious image processing methods have also been developed to recover the local signal and reduce image distortions from EPI images, albeit the gain in signal with other sequences and methods suffers from reduced temporal resolution, temporal stability, spatial resolution, and/or contrast-/signal-to-noise ratio. Other methods proposed to reduce local signal loss in EPI sequences are (1) a decrease in slice thickness of the acquired images, (2) minimization of slice-induced susceptibility artifacts (Hoogenraad et al. 2000), (3) local shimming to decrease local magnetic field inhomogeneity (Deichmann et al. 2003), and (4) maximization of the readout bandwidth in order to minimize the EPI echo train length, which in turn decreases the T2* decay and thus susceptibility effects but increases noise in the images. Another solution is the use of parallel imaging techniques (Sodickson and

Fig. 13 Comparison of the geometrical distortion of both NO-SENSE (without parallel imaging) and SENSE (with parallel imaging) images acquired in the sagittal (top row) and coronal plane (bottom row). The red border lines delineate the boundaries of the anatomical 3D T1 image, demonstrating the large improvement of geometric compliance using parallel imaging. The number on the images represents the SENSE acceleration factor (Color figure online)



Manning 1997; Pruessmann et al. 1999) which have the potential to decrease the problems inherent to single-shot EPI imaging sequences, making it possible to perform fMRI studies in those brain areas which suffer from large susceptibility artifacts in standard single-shot BOLD fMRI experiments (Preibisch et al. 2003). In these methods, receiver coil arrays consisting of a combination of a number of receiver coils (ranging from 2 to 64 elements) (De Zwart et al. 2002; Keil et al. 2013) are used. The spatial inhomogeneity and sensitivity of the separate elements are employed to decrease the number of acquired phase-encoding steps for every separate coil element by combining the different resulting images or raw data into one new reconstructed image (Sodickson and Manning 1997; Pruessmann et al. 1999). As a result, this reduces the number of acquired phase-encoding steps and thus EPI readout train length. In BOLD fMRI experiments, this decrease in phase-encoding steps during a single readout step entails a decline of susceptibility-related artifacts. The potential of parallel imaging techniques has been demonstrated in several studies at all field strengths (Schmidt et al. 2002; Preibisch et al. 2003; Moeller et al. 2010). The advantage of

parallel imaging techniques is shown in Fig. 13 demonstrating the gain of geometric correctness by using higher parallel imaging factors. In Fig. 14, the loss of signal intensity is calculated and represented for images acquired with different parallel imaging factors. The drawback of the use of high SENSE factors is the increase of noise in the images especially in central regions, which is clearly visible when using very high parallel imaging factors (Fig. 13). Therefore, it is recommended to only use very high SENSE factors when it is really necessary and when enough separate coil elements are available, e.g., when looking for activations in the orbitofrontal or anterior temporal regions of the respective lobes.

Acquisition-related susceptibility effects can also give rise to the following question: If an expected activation in a certain region cannot be found, is this a true non-activation or a susceptibility effect? On the other hand, activated regions can be encountered in areas not expected. Possible ways to overcome this problem are first to look at the original (not post-processed) images, where it can be checked whether in this region raw BOLD signal is present or not, and second to acquire a B0 field map, which can be automatically generated on most

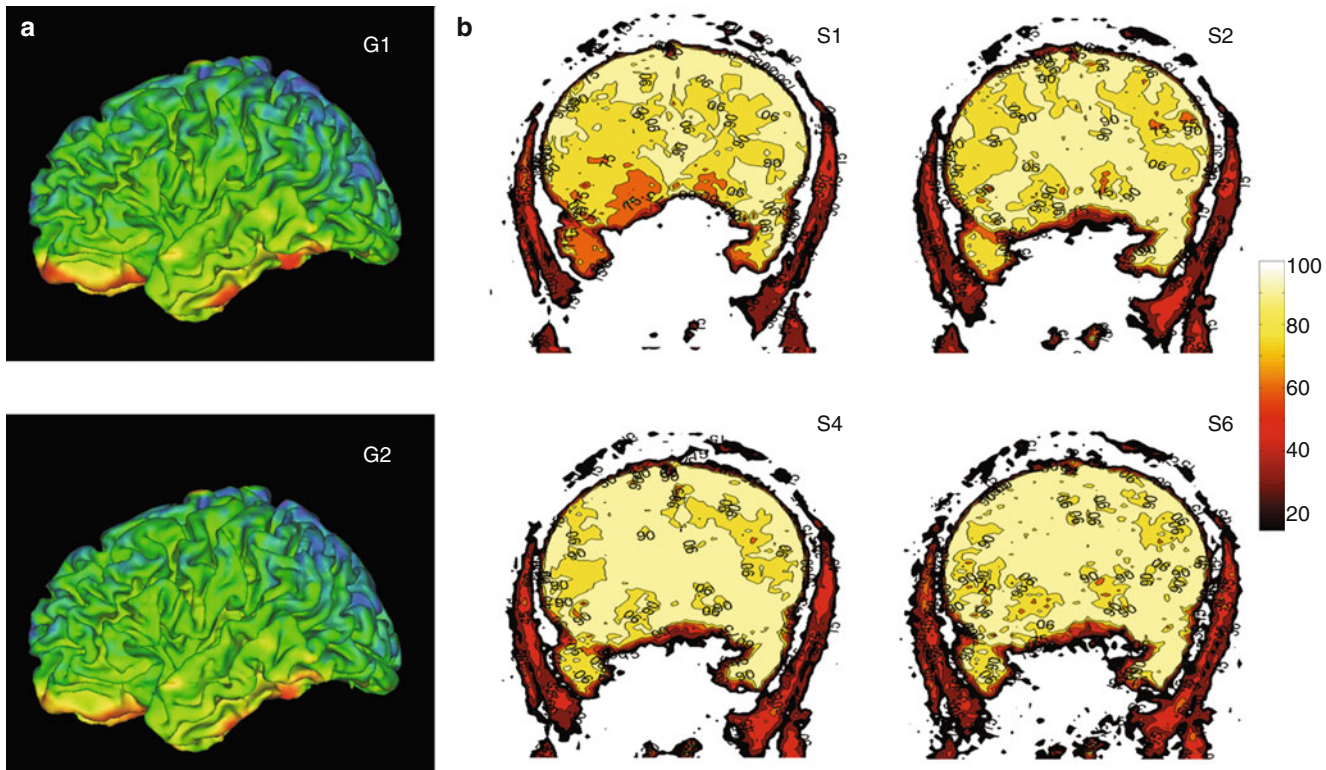


Fig. 14 (a) Signal loss maps on a rendered brain of an EPI acquisition without (above) and with GRAPPA acquisition (below). The regions in red are those which suffer the largest signal intensity loss; note the difference between the GRAPPA factor 2 (smaller, less intense red areas) and non-grappa images (large red regions). (b) Percentage signal intensity in two different coronal EPI slices acquired with different SENSE factors compared to the mean brain signal intensity of the same

slice. The dark (orange/red) areas in the slices suffer a signal loss higher than 40 %. The maps demonstrate that images acquired without SENSE (S1) display a larger and a more inhomogeneous signal loss as compared to the scans with a high parallel imaging factor in the susceptibility-sensitive areas. The number next to the images represents the SENSE factor used (Color figure online)

modern scanners. In such a B0 field map two different scans with a different echo time (TE) are combined for local T2* decay calculation, hereby highlighting regions suffering from large susceptibility effects. This field map can then be used to mask the fMRI maps to visualize only these areas where artifacts are indiscernible (Hutton et al. 2002).

1.4.2 Sensitivity of EPI Sequences to Spikes

Spikes in MR images arise from external interferences and can generate large signal changes in the affected images (Zhang et al. 2001). If there is a suspicion of spikes in an fMRI time series, the signal time course of the activated regions has to be carefully analyzed, since spikes will typically change the signal in the order of tens of percent and are also easily observed in the original images. In DTI images, spikes can also be a major source of artifacts. If spikes are supposed to be present, all separate b-vector images should be checked, and the image volumes containing spikes should be removed from DTI analyses by the post-processing software (Tournier et al. 2011). To eliminate spikes in images, it should be inspected if the faraday cage had been closed and

intact during image acquisition; scanning with an open door is troublesome (Fig. 15, the effect of opening the door of the faraday cage during an fMRI scan). Sometimes spikes can arise from an external device in the scanner room. Therefore, it is recommended to switch off unnecessary electrical devices or, even better, to remove them from the scanner room. Alternatively, spikes can be scanner related and, in this case, the scanner service team should be contacted.

1.4.3 Eddy Current-Induced Distortions in DTI

When an MR gradient pulse is switched on, this will result in a current induction in conductive parts of the MRI scanner (gradient coils, RF coils, shim irons, etc.) called eddy currents. These eddy currents in turn will generate magnetic field gradients, which can last longer than the applied primary gradients. When using fast sequences or strong gradients, these eddy currents induce extra gradient fields which will distort the images being acquired. Although BOLD fMRI scans will also suffer from eddy currents, the effect on the quality of the resulting DTI maps will be much higher. In DTI, for every direction of the b-vector, different gradients and strengths are

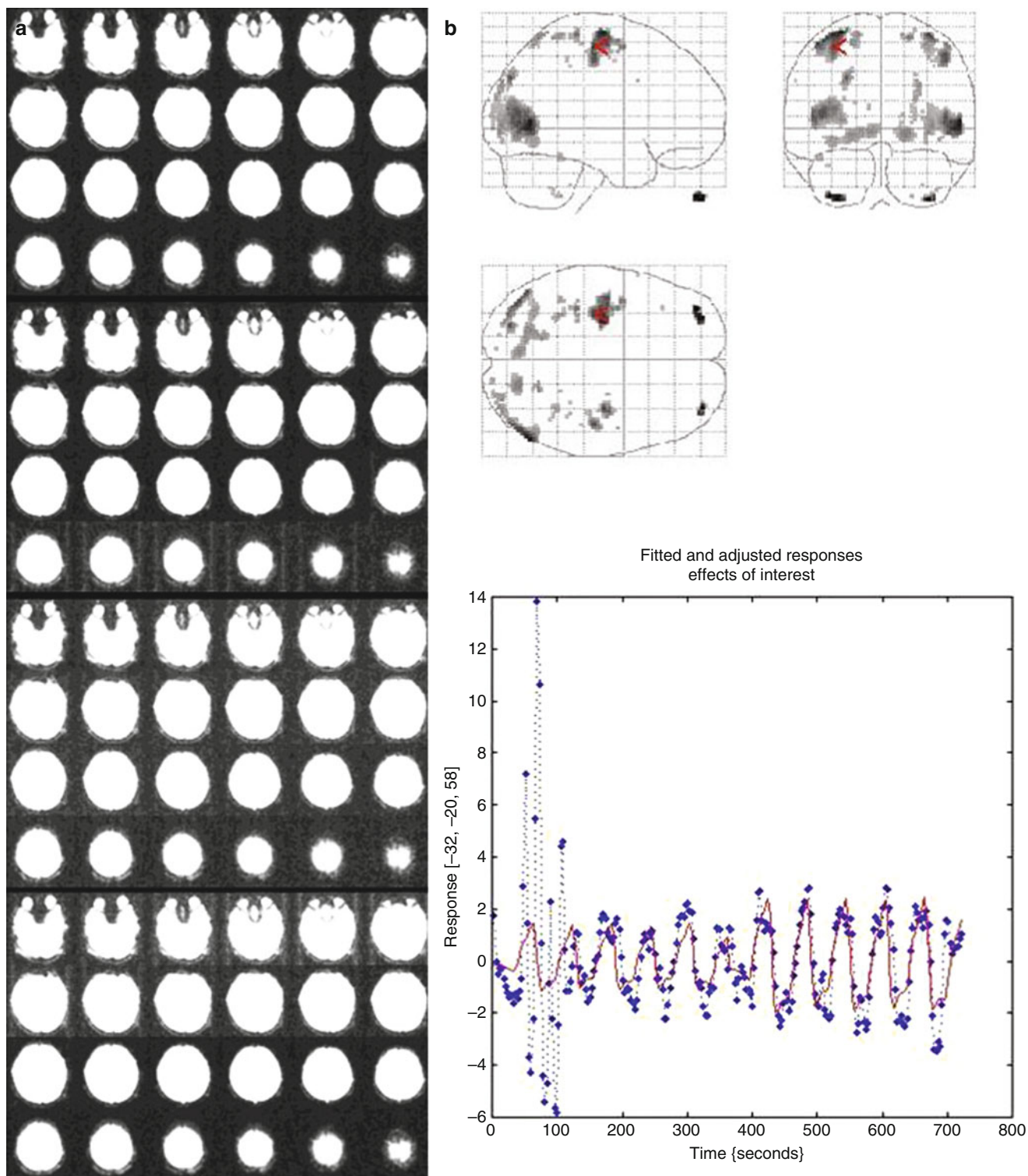


Fig. 15 (a) Spikes apparent in the fMRI time trace induced by opening the door of the faraday cage during the acquisition of an fMRI exam. (b) The signal changes induced by the spikes are around 20 % and

much higher compared to the motor task-induced signal change (red circle) (Color figure online)

switched on and off resulting in possibly different eddy current-induced artifacts for every direction of the b-vector. The eddy-current artifacts manifest themselves mainly as image distortions like contractions of the images in a single direction, as well as shifts and shears of the images (Le Bihan et al. 2006). Eddy currents can be reduced by optimally adjusting and calibrating the gradient settings to counteract and minimize induced currents and by using specifically designed self-shielded gradients (which is standard in modern MRI scanners nowadays). Although these hardware adaptations will minimize eddy currents, there will still be other negative effects which may possibly be corrected for by the post-processing software (Jones and Cercignani 2010).

1.5 Statistical Post-processing “Artifacts”

Generation of functional activation maps in an fMRI experiment requires independent statistical analysis of each of the many voxels in the brain. The hypothesis in testing each voxel is based on the assumption that there is no effect of the task compared to the baseline condition, as statistical analysis implies making a decision as to whether or not this null hypothesis is true or false. A type I error constitutes a false positive, i.e., a decision stating that the voxel is showing a difference in activation during the condition of interest when in reality it does not. A type II error represents a false negative, i.e., an assumption claiming that there is no activation at this voxel when in reality there is one (Desmond and Annabel Chen 2002).

In basic neuroscience studies, statistical analysis is essentially designed to prevent false positives: The colored activation maps show where an activation different from zero can be expected. Since fMRI measurements are intrinsically noisy, this always leads to a relative high number of false negatives: Areas with real neuronal activation but large physiological and/or technique-dependent noise will not be visible on activation maps. For clinical fMRI applications, it has to be considered whether false positives or false negatives may have more deleterious consequences for the patient. For example, in the presurgical planning for the resection of pathologic brain regions, false positives (type I errors) may bias the surgeon to avoid the resection of areas that may not be so important to be removed. This could result in an incomplete removal of the brain lesion. In contrast, false negatives (type II errors) may bias the surgeon to remove too much tissue, possibly leading to an irreversible deficit in function. Therefore, clinical fMRI data should be analyzed differently than basic neuroscience data. More research is required for discovering a new method for clinical fMRI analysis, which may allow the assessment of both type I and type II errors (Voyvodic et al. 2009; Gross and Binder 2014). For instance, each voxel that has not reached significance could be tested to find out whether an fMRI response of a certain magnitude

(such as 0.5 % MR signal change) would have reached significance if the signal-to-noise ratio in that voxel had been higher. This would lead to a separate color map showing voxels with low signal change and noisy voxels, as well as areas where artifacts or signal dropouts would otherwise not allow potential activation to be detected.

References

- Abduljalil AM, Robitaille PM (1999) Macroscopic susceptibility in ultra high field MRI. *J Comput Assist Tomogr* 23:832–841
- Aguirre GK, Zarahn E, D'esposito M (1998) The variability of human, BOLD hemodynamic responses. *Neuroimage* 8:360–369. doi:[10.1006/nimg.1998.0369](https://doi.org/10.1006/nimg.1998.0369)
- Baudendistel KT, Reichenbach JR, Metzner R, Schroeder J, Schad LR (1998) Comparison of functional MR-venography and EPI-BOLD fMRI at 1.5 T. *Magn Reson Imaging* 16:989–991
- Biswal BB, Hyde JS (1997) Contour-based registration technique to differentiate between task-activated and head motion-induced signal variations in fMRI. *Magn Reson Med* 38:470–476
- Biswal B, DeYoe AE, Hyde JS (1996) Reduction of physiological fluctuations in fMRI using digital filters. *Magn Reson Med* 35:107–113
- Bizzi A, Nava S, Ferrè F, Castelli G, Aquino D, Ciaraffa F, Broggi G, DiMeco F, Piacentini S (2012) Aphasia induced by gliomas growing in the ventrolateral frontal region: assessment with diffusion MR tractography, functional MR imaging and neuropsychology. *Cortex* 48:255–272. doi:[10.1016/j.cortex.2011.11.015](https://doi.org/10.1016/j.cortex.2011.11.015)
- Boxerman JL, Bandettini PA, Kwong KK, Baker JR, Davis TL, Rosen BR, Weisskoff RM (1995) The intravascular contribution to fmri signal change: Monte Carlo modeling and diffusion-weighted studies in vivo. *Magn Reson Med* 34:4–10
- Braus DF, Brassen S (2005) Functional magnetic resonance imaging and antipsychotics. Overview and own data. *Radiologe* 45:178–185. doi:[10.1007/s00117-004-1156-z](https://doi.org/10.1007/s00117-004-1156-z)
- Breiter HC, Gollub RL, Weisskoff RM, Kennedy DN, Makris N, Berke JD, Goodman JM, Kantor HL, Gastfriend DR, Riorden JP, Mathew RT, Rosen BR, Hyman SE (1997) Acute effects of cocaine on human brain activity and emotion. *Neuron* 19:591–611
- Bryan R, Kraut M (1998) Functional magnetic resonance imaging: you get what you (barely) see. *Am J Neuroradiol* 19:991–992
- Bryant CA, Jackson SH (1998) Functional imaging of the brain in the evaluation of drug response and its application to the study of aging. *Drugs Aging* 13:211–222
- Caramia F, Francia A, Mainiero C, Tinelli E, Giuseppina M, Colonnese C, Bozzao L, Donatella M (2009) Neurophysiological and functional MRI evidence of reorganization of cortical motor areas in cerebral arteriovenous malformation. *Magn Reson Imaging* 27:1360–1369. doi:[10.1016/j.mri.2009.05.029](https://doi.org/10.1016/j.mri.2009.05.029)
- Chen Y, Parrish T (2009) Caffeine dose effect on activation-induced BOLD and CBF responses. *Neuroimage* 46:577–583
- Chen CM, Hou BL, Holodny AI (2008) Effect of age and tumor grade on BOLD functional MR imaging in preoperative assessment of patients with glioma. *Radiology* 248:971–978. doi: [10.1148/radiol.2483071280](https://doi.org/10.1148/radiol.2483071280)
- Cohen MS, DuBois RM (1999) Stability, repeatability, and the expression of signal magnitude in functional magnetic resonance imaging. *J Magn Reson Imaging* 10:33–40
- Cohen ER, Rostrup E, Sidaros K, Lund TE, Paulson OB, Ugurbil K, Kim S-G (2004) Hypercapnic normalization of BOLD fMRI: comparison across field strengths and pulse sequences. *Neuroimage* 23:613–624. doi:[10.1016/j.neuroimage.2004.06.021](https://doi.org/10.1016/j.neuroimage.2004.06.021)
- D'Esposito M, Deouell LY, Gazzaley A (2003) Alterations in the BOLD fMRI signal with ageing and disease: a challenge for neuroimaging. *Nat Rev Neurosci* 4:863–872. doi:[10.1038/nrn1246](https://doi.org/10.1038/nrn1246)

- Dagli MS, Ingeholm JE, Haxby JV (1999) Localization of cardiac-induced signal change in fMRI. *Neuroimage* 9:407–415. doi:[10.1006/nimg.1998.0424](https://doi.org/10.1006/nimg.1998.0424)
- Davis T, Poldrack R a (2013) Measuring neural representations with fMRI: practices and pitfalls. *Ann N Y Acad Sci* 1296:108–134. doi:[10.1111/nyas.12156](https://doi.org/10.1111/nyas.12156)
- De Zwart JA, Van Gelderen P, Kellman P, Duyn JH (2002) Application of sensitivity-encoded echo-planar imaging for blood oxygen level-dependent functional brain imaging. *Magn Reson Med* 48:1011–1020
- Debus J, Essig M, Schad LR, Wenz F, Baudendistel K, Knopp MV, Engenhart R, Lorenz WJ (2008) Functional magnetic resonance imaging in a stereotactic setup. *Magn Reson Imaging* 26:1007–1012
- Deichmann R, Gottfried J, Hutton C, Turner R (2003) Optimized EPI for fMRI studies of the orbitofrontal cortex. *Neuroimage* 19: 430–441
- Desmond JE, Annabel Chen SH (2002) Ethical issues in the clinical application of fMRI: factors affecting the validity and interpretation of activations. *Brain Cogn* 50:482–497
- Devlin JT, Russell RP, Davis MH, Price CJ, Wilson J, Moss HE, Matthews PM, Tyler LK (2000) Susceptibility-induced loss of signal: comparing PET and fMRI on a semantic task. *Neuroimage* 11:589–600. doi:[10.1006/nimg.2000.0595](https://doi.org/10.1006/nimg.2000.0595)
- Duerk JL, Simonetti OP (1991) Theoretical aspects of motion sensitivity and compensation in echo-planar imaging. *J Magn Reson Imaging* 1:643–650
- Duong TQ, Yacoub E, Adriany G, Hu X, Andersen P, Vaughan JT, Uğurbil K, Kim S-G (2004) Spatial specificity of high-resolution, spin-echo BOLD, and CBF fMRI at 7 T. *Magn Reson Med* 51:646–647
- Duyn JH, Moonen CT, Van Yperen GH, De Boer RW, Luyten PR (1994) Inflow versus deoxyhemoglobin effects in BOLD functional MRI using gradient echoes at 1.5 T. *NMR Biomed* 7:83–88
- Dymarkowski S, Sunaert S, Van Oostende S, Van Hecke P, Wilms G, Demaerel P, Nuttin B, Plets C, Marchal G (1998) Functional MRI of the brain: localisation of eloquent cortex in focal brain lesion therapy. *Eur Radiol* 8:1573–1580
- Edward V, Windischberger C, Cunningham R, Erdler M, Lanzenberger R, Mayer D, Endl W, Beisteiner R (2000) Quantification of fMRI artifact reduction by a novel plaster cast head holder. *Hum Brain Mapp* 11:207–213
- Engel SA, Glover GH, Wandell BA (1997) Retinotopic organization in human visual cortex and the spatial precision of functional MRI. *Cereb Cortex* 7:181–192. doi:[10.1093/cercor/7.2.181](https://doi.org/10.1093/cercor/7.2.181)
- Fandino J, Kollias SS, Wieser HG, Valavanis A, Yonekawa Y (1999) Intraoperative validation of functional magnetic resonance imaging and cortical reorganization patterns in patients with brain tumors involving the primary motor cortex. *J Neurosurg* 91:238–250
- Fitzsimmons JR, Scott JD, Peterson DM, Wolverton BL, Webster CS, Lang PJ (1997) Integrated RF coil with stabilization for fMRI human cortex. *Magn Reson Med* 38:15–18
- Frahm J, Merboldt KD, Hänicke W, Kleinschmidt A, Boecker H (1994) Brain or vein–oxygenation or flow? On signal physiology in functional MRI of human brain activation. *NMR Biomed* 7:45–53
- Freire L, Mangin JF (2001) Motion correction algorithms may create spurious brain activations in the absence of subject motion. *Neuroimage* 14:709–722
- Friston KJ, Holmes AP, Poline JB, Grasby PJ, Williams SC, Frackowiak RS, Turner R (1995) Analysis of fMRI time-series revisited [see comments]. *Neuroimage* 2:45–53. doi:[10.1006/nimg.1995.1007](https://doi.org/10.1006/nimg.1995.1007)
- Friston KJ, Holmes A, Poline JB, Price CJ, Frith CD (1996a) Detecting activations in PET and fMRI: levels of inference and power. *Neuroimage* 4:223–235. doi:[10.1006/nimg.1996.0074](https://doi.org/10.1006/nimg.1996.0074)
- Friston KJ, Williams S, Howard R, Frackowiak RS, Turner R (1996b) Movement-related effects in fMRI time-series. *Magn Reson Med* 35:346–355
- Fujiwara N, Sakatani K, Katayama Y, Murata Y, Hoshino T, Fukaya C, Yamamoto T (2004) Evoked-cerebral blood oxygenation changes in false-negative activations in BOLD contrast functional MRI of patients with brain tumors. *Neuroimage* 21:1464–1471
- Gallichan D, Scholz J, Bartsch A, Behrens TE, Robson MD, Miller KL (2010) Addressing a systematic vibration artifact in diffusion-weighted MRI. *Hum Brain Mapp* 31:193–202. doi:[10.1002/hbm.20856](https://doi.org/10.1002/hbm.20856)
- Ganslandt O, Buchfelder M, Hastreiter P, Grummich P, Fahlbusch R, Nimsky C (2004) Magnetic source imaging supports clinical decision making in glioma patients. *Clin Neurol Neurosurg* 107:20–26
- Gao JH, Miller I, Lai S, Xiong J, Fox PT (1996) Quantitative assessment of blood inflow effects in functional MRI signals. *Magn Reson Med* 36:314–319
- Gasser TG, Sandacioglu EI, Wiedemayer H, Hans V, Gizewski E, Forsting M, Stolke D (2004) A novel passive functional MRI paradigm for preoperative identification of the somatosensory cortex. *Neurosurg Rev* 27:106–112
- Gati JS, Menon RS, Ugurbil K, Rutt BK (1997) Experimental determination of the BOLD field strength dependence in vessels and tissue. *Magn Reson Med* 38:296–302
- Goense J, Merkle H, Logothetis N (2012) High-resolution fMRI reveals laminar differences in neurovascular coupling between positive and negative BOLD responses. *Neuron* 76:629–639
- Gollub RL, Breiter HC, Kantor H, Kennedy D, Gastfriend D, Mathew RT, Makris N, Guimaraes A, Riorden J, Campbell T, Foley M, Hyman SE, Rosen B, Weisskoff R (1998) Cocaine decreases cortical cerebral blood flow but does not obscure regional activation in functional magnetic resonance imaging in human subjects. *J Cereb Blood Flow Metab* 18:724–734
- Gross WL, Binder JR (2014) Alternative thresholding methods for fMRI data optimized for surgical planning. *Neuroimage* 84:554–561. doi:[10.1016/j.neuroimage.2013.08.066](https://doi.org/10.1016/j.neuroimage.2013.08.066)
- Haacke EM, Hopkins A, Lai S, Buckley P, Friedman L, Meltzer H, Hedera P, Friedland R, Klein S, Thompson L (1994) 2D and 3D high resolution gradient echo functional imaging of the brain: venous contributions to signal in motor cortex studies. *NMR Biomed* 7:54–62
- Håberg A, Kvistad KA, Unsgård G, Haraldseth O (2004) Preoperative blood oxygen level-dependent functional magnetic resonance imaging in patients with primary brain tumors: clinical application and outcome. *Neurosurgery* 54:902–914; discussion 914–915
- Hahn B, Ross TJ, Yang Y, Kim I, Huestis M a (2007) Nicotine enhances visuospatial attention by deactivating areas of the resting brain default network. *J Neurosci* 27:3477–3489. doi:[10.1523/JNEUROSCI.5129-06.2007](https://doi.org/10.1523/JNEUROSCI.5129-06.2007)
- Hajnal JV, Myers R, Oatridge A, Schwieso JE, Young IR, Bydder GM (1994) Artifacts due to stimulus correlated motion in functional imaging of the brain. *Magn Reson Med* 31:283–291
- Hall D a, Gonçalves MS, Smith S, Jezzard P, Haggard MP, Kornak J (2002) A method for determining venous contribution to BOLD contrast sensory activation. *Magn Reson Imaging* 20:695–706
- Haller S, Bartsch AJ (2009) Pitfalls in fMRI. *Eur Radiol* 19:2689–2706. doi:[10.1007/s00330-009-1456-9](https://doi.org/10.1007/s00330-009-1456-9)
- Heemskerk a M, Leemans A, Plaisier A, Pieterman K, Lequin MH, Dudink J (2013) Acquisition guidelines and quality assessment tools for analyzing neonatal diffusion tensor MRI data. *AJNR Am J Neuroradiol* 34:1496–1505. doi:[10.3174/ajnr.A3465](https://doi.org/10.3174/ajnr.A3465)
- Hill D, Smith A, Simmons A, Maurer C Jr, Cox TC, Elwes R, Brammer M, Hawkes DJ, Polkey CE (2000) Sources of error in comparing functional magnetic resonance imaging and invasive electrophysiological recordings. *J Neurosurg* 93:214–223
- Hoogenraad FGC, Pouwels PJW, Hofman MBM, Rombouts SAR, Lavini C, Leach MO, Haacke EM (2000) High-resolution segmented EPI in a motor task fMRI study. *Magn Reson Imaging* 18:405–409. doi:[10.1016/S0730-725X\(00\)00127-2](https://doi.org/10.1016/S0730-725X(00)00127-2)
- Hund-Georgiadis M, Mildner T, Georgiadis D, Weih K, Von Cramon DY (2003) Impaired hemodynamics and neural activation? A fMRI study of major cerebral artery stenosis. *Neurology* 62:1276–1279

- Hutton C, Bork A, Josephs O, Deichmann R, Ashburner J, Turner R (2002) Image distortion correction in fMRI: a quantitative evaluation. *Neuroimage* 16:217–240. doi:[10.1006/nimg.2001.1054](https://doi.org/10.1006/nimg.2001.1054)
- Iacobella V, Hasson U (2011) The relationship between BOLD signal and autonomic nervous system functions: implications for processing of “physiological noise”. *Magn Reson Imaging* 29:1338–1345. doi:[10.1016/j.mri.2011.03.006](https://doi.org/10.1016/j.mri.2011.03.006)
- Jacobsen LK, Gore JC, Skudlarski P, Lacadie CM, Jatlow P, Krystal JH (2002) Impact of intravenous nicotine on BOLD signal response to photic stimulation. *Magn Reson Imaging* 20:141–145
- Jacobsen LK, D’Souza DC, Mencl WE, Pugh KR, Skudlarski P, Krystal JH (2004) Nicotine effects on brain function and functional connectivity in schizophrenia. *Biol Psychiatry* 55:850–858
- Jiang A, Kennedy DN, Baker JR, Weisskoff RM, Tootell RBH, Woods RP, Benson RR, Kwong KK, Brady TJ, Rosen BR, Belliveau JW (1995) Motion detection and correction in functional MR imaging. *Hum Brain Mapp* 3:224–235. doi:[10.1002/hbm.460030306](https://doi.org/10.1002/hbm.460030306)
- Jiang Z, Krainik A, David O, Salom C, Tropriès I, Hoffmann D, Pannetier N, Barbier EL, Bombin ER, Warnking J, Pasteris C, Chabardes S, Berger F, Grand S, Segebarth C, Gay E, Le Bas J-F (2010) Impaired fMRI activation in patients with primary brain tumors. *Neuroimage* 52:538–548. doi:[10.1016/j.neuroimage.2010.04.194](https://doi.org/10.1016/j.neuroimage.2010.04.194)
- Johnstone T, Ores Walsh KS, Greischar LL, Alexander AL, Fox AS, Davidson RJ, Oakes TR (2006) Motion correction and the use of motion covariates in multiple-subject fMRI analysis. *Hum Brain Mapp* 27:779–788. doi:[10.1002/hbm.20219](https://doi.org/10.1002/hbm.20219)
- Jones DK, Cercignani M (2010) Twenty-five pitfalls in the analysis of diffusion MRI data. *NMR Biomed* 23:803–820. doi:[10.1002/nbm.1543](https://doi.org/10.1002/nbm.1543)
- Kansaku K, Kitazawa S, Kawano K (1998) Sequential hemodynamic activation of motor areas and the draining veins during finger movements revealed by cross-correlation between signals from fMRI. *Neuroreport* 9:1969–1974
- Kantarci K, Avula R, Senjem M, Samikoglu A, Zhang B, Weigand S, Przybelski S, Edmonson H, Vemuri P, Knopman D, Ferman T, Boeve B, Petersen R, Jack C Jr (2010) Dementia with Lewy bodies and Alzheimer disease Neurodegenerative patterns characterized by DTI. *Neurology* 74:1814–1821
- Kastrup A, Li TQ, Takahashi A, Glover GH, Moseley ME (1998) Functional magnetic resonance imaging of regional cerebral blood oxygenation changes during breath holding. *Stroke A J Cereb Circ* 29:2641–2645
- Keil B, Blau JN, Biber S, Hoecht P, Tountcheva V, Setsompop K, Triantafyllou C, Wald LL (2013) A 64-channel 3T array coil for accelerated brain MRI. *Magn Reson Med* 70:248–258. doi:[10.1002/mrm.24427](https://doi.org/10.1002/mrm.24427)
- Kim DS, Duong TQ, Kim SG (2000) High-resolution mapping of iso-orientation columns by fMRI. *Nat Neurosci* 3:164–169
- Kleiser R, Staempfli P, Valavanis A, Boesiger P, Kollias S (2010) Impact of fMRI-guided advanced DTI fiber tracking techniques on their clinical applications in patients with brain tumors. *Neuroradiology* 52:37–46. doi:[10.1007/s00234-009-0539-2](https://doi.org/10.1007/s00234-009-0539-2)
- Koch M, Norris D (2000) An assessment of eddy current sensitivity and correction in single-shot diffusion-weighted imaging. *Phys Med Biol* 45:3821–3832
- Kriegeskorte N, Cusack R, Bandettini P (2010) How does an fMRI voxel sample the neuronal activity pattern: compact-kernel or complex spatiotemporal filter? *Neuroimage* 49:1965–1976. doi:[10.1016/j.neuroimage.2009.09.059](https://doi.org/10.1016/j.neuroimage.2009.09.059)
- Krings T (2001a) Functional MRI for presurgical planning: problems, artefacts, and solution strategies. *J Neurol Neurosurg Psychiatry* 70:749–760. doi:[10.1136/jnnp.70.6.749](https://doi.org/10.1136/jnnp.70.6.749)
- Krings T (2001b) Metabolic and electrophysiological validation of functional MRI. *J Neurol Neurosurg Psychiatry* 71:762–771. doi:[10.1136/jnnp.71.6.762](https://doi.org/10.1136/jnnp.71.6.762)
- Kumari V, Gray JA, Ffytche DH, Mitterschiffthaler MT, Das M, Zachariah E, Vythelingum GN, Williams SCR, Simmons A, Sharma T (2003) Cognitive effects of nicotine in humans: an fMRI study. *Neuroimage* 19:1002–1013
- Laurienti PJ, Field AS, Burdette JH, Maldjian JA, Yen Y-F, Moody DM (2002) Dietary caffeine consumption modulates fMRI measures. *Neuroimage* 17:751–757
- Le Bihan D, Poupon C, Amadon A, Lethimonnier F (2006) Artifacts and pitfalls in diffusion MRI. *J Magn Reson Imaging* 24:478–488. doi:[10.1002/jmri.20683](https://doi.org/10.1002/jmri.20683)
- Le Rumeur E, Allard M, Poiseau E, Jannin P (2000) Role of the mode of sensory stimulation in presurgical brain mapping in which functional magnetic resonance imaging is used. *J Neurosurg* 93: 427–431
- Lee A, Glover G, Meyer C (1995) Discrimination of large venous vessels in time-course spiral blood-oxygen-level-dependent magnetic-resonance functional neuroimaging. *Magn Reson Med* 33:745–754
- Lee C, Ward H, Sharbrough F, Meyer F, Marsh W, Elson C, So L, Cascino G, Shin C, Xu Y, Riederer S, Jack C Jr (1999) Assessment of functional MR imaging in neurosurgical planning. *Am J Neuroradiol* 20:1511–1519
- Lee J-H, Telang FW, Springer CS, Volkow ND (2003) Abnormal brain activation to visual stimulation in cocaine abusers. *Life Sci* 73:1953–1961
- Leemans A, Jones DK (2009) The B-matrix must be rotated when correcting for subject motion in DTI data. *Magn Reson Med* 61:1336–1349. doi:[10.1002/mrm.21890](https://doi.org/10.1002/mrm.21890)
- Lehéricy S, Biondi A, Sourour N (2002) Arteriovenous brain malformations: is functional MR imaging reliable for studying language reorganization in patients? Initial observations. *Radiology* 223: 672–682
- Levin JM, Ross MH, Mendelson JH, Kaufman MJ, Lange N, Maas LC, Mello NK, Cohen BM, Renshaw PF (1998) Reduction in BOLD fMRI response to primary visual stimulation following alcohol ingestion. *Psychiatry Res* 82:135–146
- Levy L, Henkin R, Lin C, Hutter A, Schelling D (1998) Increased brain activation in response to odors in patients with hyposmia after theophylline treatment demonstrated by fMRI. *J Comput Assist Tomogr* 22:760–770
- Li SJ, Biswal B, Li Z, Risinger R, Rainey C, Cho JK, Salmeron BJ, Stein EA (2000) Cocaine administration decreases functional connectivity in human primary visual and motor cortex as detected by functional MRI. *Magn Reson Med* 43:45–51
- Logothetis N (2000) Can current fMRI techniques reveal the micro-architecture of cortex? *Nat Neurosci* 3:413
- Logothetis N (2002) The neural basis of the blood-oxygen-level-dependent functional magnetic resonance imaging signal. *Philos Trans R Soc London Ser B Biol Sci* 357:1003–1037
- Lowe M, Lurito J, Mathews V, Phillips MD, Hutchins GD (2000) Quantitative comparison of functional contrast from BOLD-weighted spin-echo and gradient-echo echoplanar imaging at 1.5 Tesla and H21O PET in the whole brain. *J Cereb Blood Flow Metab* 20:1331–1340
- Lowen S, Nickerson L, Levin J (2009) Differential effects of acute cocaine and placebo administration on visual cortical activation in healthy subjects measured using BOLD fMRI. *Pharmacol Biochem Behav* 92:277–282
- Luchtman M, Jachau K, Tempelmann C, Bernarding J (2010) Alcohol induced region-dependent alterations of hemodynamic response: implications for the statistical interpretation of pharmacological fMRI studies. *Exp Brain Res* 204:1–10. doi:[10.1007/s00221-010-2277-4](https://doi.org/10.1007/s00221-010-2277-4)
- Lüdemann L, Förtschler A, Grieger W, Zimmer C (2006) BOLD signal in the motor cortex shows a correlation with the blood volume of brain tumors. *J Magn Reson Imaging* 23:435–443. doi:[10.1002/jmri.20530](https://doi.org/10.1002/jmri.20530)
- Maclarens J, Herbst M, Speck O, Zaitsev M (2013) Prospective motion correction in brain imaging: a review. *Magn Reson Med* 69: 621–636. doi:[10.1002/mrm.24314](https://doi.org/10.1002/mrm.24314)

- Maldjian J, Atlas S, Howard R, Greenstein E, Alsop D, Detre J, Listerud J, D'Esposito M, Flamm E (1996) Functional magnetic resonance imaging of regional brain activity in patients with intracerebral arteriovenous malformations before surgical or endovascular therapy. *J Neurosurg* 84:477–483
- Mandeville J, Jenkins B, Kosofsky BE, Moskowitz MA, Rosen BR, Marota JJ (2001) Regional sensitivity and coupling of BOLD and CBV changes during stimulation of rat brain. *Magn Reson Med* 45:443–447
- Maravita A, Iriki A (2004) Tools for the body (schema). *Trends Cogn Sci* 8:79–86. doi:[10.1016/j.tics.2003.12.008](https://doi.org/10.1016/j.tics.2003.12.008)
- Meier MP, Ilmberger J, Fesl G, Ruge MI (2013) Validation of functional motor and language MRI with direct cortical stimulation. *Acta Neurochir (Wien)* 155:675–683. doi:[10.1007/s00701-013-1624-1](https://doi.org/10.1007/s00701-013-1624-1)
- Menon R (2002) Postacquisition suppression of large-vessel BOLD signals in high-resolution fMRI. *Magn Reson Med* 47:1–9
- Menon R, Kim S-G (1999) Spatial and temporal limits in cognitive neuroimaging with fMRI. *Trends Cogn Sci* 3:207–216
- Menon R, Ogawa S, Uğurbil K (1995) High-temporal-resolution studies of the human primary visual cortex at 4 T: teasing out the oxygenation contribution in fMRI. *Int J Imaging Syst Technol* 6:209–215
- Menon R, Thomas C, Gati J (1997) Investigation of BOLD contrast in fMRI using multi-shot EPI. *NMR Biomed* 10:179–182
- Menon R, Gati J, Goodyear B, Luknowsky D, Thomas CG (1998) Spatial and temporal resolution of functional magnetic resonance imaging. *Biochem Cell Biol* 76:560–571
- Moeller S, Yacoub E, Olman CA, Auerbach E, Strupp J, Harel N, Uğurbil K (2010) Multiband multislice GE-EPI at 7 tesla, with 16-fold acceleration using partial parallel imaging with application to high spatial and temporal whole-brain fMRI. *Magn Reson Med* 63:1144–1153. doi:[10.1002/mrm.22361](https://doi.org/10.1002/mrm.22361)
- Mohammadi S, Nagy Z, Hutton C, Josephs O, Weiskopf N (2012) Correction of vibration artifacts in DTI using phase-encoding reversal (COVIPER). *Magn Reson Med* 68:882–889. doi:[10.1002/mrm.23308](https://doi.org/10.1002/mrm.23308)
- Moon C, Fukuda M, Park S, Kim S-G (2007) Neural interpretation of blood oxygenation level-dependent fMRI maps at submillimeter columnar resolution. *J Neurosci* 27:6892–6902
- Morton D, Maravilla K, Meno J, Winn HR (2002) Systemic theophylline augments the blood oxygen level—dependent response to fore-paw stimulation in rats. *Am J Neuroradiol* 23:588–593
- Muresan L, Renken R, Roerdink J, Duifhuis H (2005) Automated correction of spin-history related motion artefacts in fMRI: simulated and phantom data. *Biomed Eng IEEE Trans* 52:1450–1460
- Murphy K, Harris AD, Wise RG (2011) Robustly measuring vascular reactivity differences with breath-hold: normalising stimulus-evoked and resting state BOLD fMRI data. *Neuroimage* 54:369–379. doi:[10.1016/j.neuroimage.2010.07.059](https://doi.org/10.1016/j.neuroimage.2010.07.059)
- Murphy K, Birn RM, Bandettini PA (2013) Resting-state fMRI confounds and cleanup. *Neuroimage* 80:349–359
- Nencka AS, Rowe DB (2007) Reducing the unwanted draining vein BOLD contribution in fMRI with statistical post-processing methods. *Neuroimage* 37:177–188. doi:[10.1016/j.neuroimage.2007.03.075](https://doi.org/10.1016/j.neuroimage.2007.03.075)
- Nitschke M, Melchert U, Hahn C, Otto V, Arnold H, Herrmann H-D, Nowak G, Westphal M, Wessel K (1998) Preoperative functional magnetic resonance imaging (fMRI) of the motor system in patients with tumours in the parietal lobe. *Acta Neurochir* 140:1223–1229
- O'doherty J, Rolls E, Francis S, Bowtell R, McGlone F, Kobal G, Renner B, Ahne G (2000) Sensory-specific satiety-related olfactory activation of the human orbitofrontal cortex. *Neuroreport* 11:893–897
- Ogawa S, Lee T (1990) Magnetic resonance imaging of blood vessels at high fields: in vivo and in vitro measurements and image simulation. *Magn Reson Med* 16:9–18
- Ogawa S, Menon R, Tank D, Kim S, Merkle H, Ellermann J, Ugurbil K (1993) Functional brain mapping by blood oxygenation level-dependent contrast magnetic resonance imaging. A comparison of signal characteristics with a biophysical model. *Biophys J* 64: 803–812
- Oja J, Gillen J, Kauppinen R, Kraut M, van Zijl P (1999) Venous blood effects in spin-echo fMRI of human brain. *Magn Reson Med* 42:617–626
- Orchard J, Atkins M (2003) Iterating registration and activation detection to overcome activation bias in fMRI motion estimates. *Med Image Comput Comput Interv* 2879:886–893
- Parrish T, Mulderink T, Gitelman D, Mesulam M (2001) Caffeine as a BOLD contrast booster. *Neuroimage* 13:1001
- Power JD, Mitra A, Laumann TO, Snyder AZ, Schlaggar BL, Petersen SE (2013) Methods to detect, characterize, and remove motion artifact in resting state fMRI. *Neuroimage* 84:320–341. doi:[10.1016/j.neuroimage.2013.08.048](https://doi.org/10.1016/j.neuroimage.2013.08.048)
- Preibisch C, Pilatus U, Bunke J, Hoogenraad F, Zanella F, Lanfermann H (2003) Functional MRI using sensitivity-encoded echo planar imaging (SENSE-EPI). *Neuroimage* 19:412–421
- Pruessmann K, Weiger M, Scheidegger M, Boesiger P (1999) SENSE: sensitivity encoding for fast MRI. *Magn Reson Med* 42:952–962
- Qin L, van Gelderen P, Derbyshire JA, Jin F, Lee J, de Zwart JA, Tao Y, Duyn JH (2009) Prospective head-movement correction for high-resolution MRI using an in-bore optical tracking system. *Magn Reson Med* 62:924–934. doi:[10.1002/mrm.22076](https://doi.org/10.1002/mrm.22076)
- Rack-Gomei A, Liau J, Liu T (2009) Caffeine reduces resting-state BOLD functional connectivity in the motor cortex. *Neuroimage* 46:56–63
- Rao S, Binder J, Bandettini P, Hammeke T, Yetkin F, Jesmanowicz A, Lisk L, Morris G, Mueller W, Estkowski L, Wong E, Haughton V, Hyde J (1993) Functional magnetic resonance imaging of complex human movements. *Neurology* 43:2311–2318
- Reich D, Zackowski K, Gordon-Lipkin E, Smith S, Chodkowski B, Cutter G, Calabresi PA (2008) Corticospinal tract abnormalities are associated with weakness in multiple sclerosis. *Am J Neuroradiol* 29:333–339
- Sage CA, Van Hecke W, Peeters R, Sijbers J, Robberecht W, Parizel P, Marchal G, Leemans A, Sunaert S (2009) Quantitative diffusion tensor imaging in amyotrophic lateral sclerosis: revisited. *Hum Brain Mapp* 30:3657–3675. doi:[10.1002/hbm.20794](https://doi.org/10.1002/hbm.20794)
- Schiffbauer H, Ferrari P, Rowley H, Berger M, Roberts T (2001) Functional activity within brain tumors: a magnetic source imaging study. *Neurosurgery* 49:1313–1321
- Schmidt C, Pruessmann K, Jaermann T, Lamerichs R, Boesiger P (2002) High-resolution fMRI using SENSE at 3 Tesla. *Proc Int Soc Magn Reson Med* 10:125
- Schreiber A, Hubbe U, Ziyeh S, Hennig J (2000) The influence of gliomas and non-glial space-occupying lesions on blood-oxygen-level-dependent contrast enhancement. *AJNR Am J Neuroradiol* 21: 1055–1063
- Seifritz E, Bilecen D, Hänggi D, Haselhorst R, Radü E, Wetzel S, Seelig J, Scheffler K (2000) Effect of ethanol on BOLD response to acoustic stimulation: implications for neuropharmacological fMRI. *Psychiatry Res Neuroimaging* 99:1–13
- Seto E, Sela G, McIlroy W, Black S, Staines W, Bronskill M, McIntosh A, Graham A (2001) Quantifying head motion associated with motor tasks used in fMRI. *Neuroimage* 14:284–297
- Siero J, Hermes D, Hoogduin H, Luijten P, Petridou N, Ramsey N (2013) BOLD consistently matches electrophysiology in human sensorimotor cortex at increasing movement rates: a combined 7T fMRI and ECoG study on neurovascular coupling. *J Cereb Blood Flow Metab* 33:1448–1456
- Sinha S, Bastin M, Whittle I, Wardlaw J (2002) Diffusion tensor MR imaging of high-grade cerebral gliomas. *Am J Neuroradiol* 23: 520–527
- Skirboll S, Ojemann G, Berger M, Lettich E, Winn H (1996) Functional cortex and subcortical white matter located within gliomas. *Neurosurgery* 38:678–685

- Small D, Voss J, Mak Y, Simmons K, Parrish T, Gitelman D (2004) Experience-dependent neural integration of taste and smell in the human brain. *J Neurophysiol* 92:1892–1903
- Smits M, Peeters RR, Van Hecke P, Sunaert S (2007) A 3 T event-related functional magnetic resonance imaging (fMRI) study of primary and secondary gustatory cortex localization using natural tastants. *Neuroradiology* 49:61–71. doi:[10.1007/s00234-006-0160-6](https://doi.org/10.1007/s00234-006-0160-6)
- Sodickson D, Manning W (1997) Simultaneous acquisition of spatial harmonics (SMASH): fast imaging with radiofrequency coil arrays. *Magn Reson Med* 38:591–603
- Song A, Popp C, Mao J, Dixon W (2000) fMRI: methodology—acquisition and processing. *Adv Neurol* 83:177–185
- Srivastava G, Crottaz-Herbette S, Lau K, Glover G, Menon V (2005) ICA-based procedures for removing ballistocardiogram artifacts from EEG data acquired in the MRI scanner. *Neuroimage* 24:50–60
- Stippich C, Kress B, Ochmann H, Tronnier V, Sartor K (2003) Preoperative functional magnetic resonance tomography (fMRI) in patients with rolandic brain tumors: indication, investigation strategy, possibilities and limitations of clinical application. *Röfo* 175:1042–1050
- Sunaert S, Dymarkowski S, Van Oostende S, Van Hecke P, Wilms GMG (1998) Functional magnetic resonance imaging (fMRI) visualises the brain at work. *Acta Neurol Belg* 98:8–16
- Thesen S, Heid O, Mueller E, Schad LR (2000) Prospective acquisition correction for head motion with image-based tracking for real-time fMRI. *Magn Reson Med* 44:457–465
- Toh CH, Wei K-C, Ng S-H, Wan Y-L, Lin C-P, Castillo M (2011) Differentiation of brain abscesses from necrotic glioblastomas and cystic metastatic brain tumors with diffusion tensor imaging. *AJNR Am J Neuroradiol* 32:1646–1651. doi:[10.3174/ajnr.A2581](https://doi.org/10.3174/ajnr.A2581)
- Tomasi D, Volkow ND, Wang R, Carrillo JH, Maloney T, Alia-Klein N, Woicik PA, Telang F, Goldstein RZ (2010) Disrupted functional connectivity with dopaminergic midbrain in cocaine abusers. *PLoS One* 5:10815
- Tomeczak RJ, Wunderlich AP, Wang Y, Braun V, Antoniadis G, Görich J, Richter H-P, Brambs H-J (2000) fMRI for preoperative neurosurgical mapping of motor cortex and language in a clinical setting. *J Comput Assist Tomogr* 24:927–934
- Tournier J-D, Mori S, Leemans A (2011) Diffusion tensor imaging and beyond. *Magn Reson Med* 65:1532–1556. doi:[10.1002/mrm.22924](https://doi.org/10.1002/mrm.22924)
- Turner R (2002) How much cortex can a vein drain? Downstream dilution of activation-related cerebral blood oxygenation changes. *Neuroimage* 16:1062–1067. doi:[10.1006/nimg.2002.1082](https://doi.org/10.1006/nimg.2002.1082)
- Turner R, Jezzard P, Wen H (1993) Functional mapping of the human visual cortex at 4 and 1.5 tesla using deoxygenation contrast EPI. *Magn Reson Med* 29:277–279
- Ugurbil K, Xiaoping H, Wei C, Zhu X-H, Kim S-G, Georgopoulos A (1999) Functional mapping in the human brain using high magnetic fields. *Philos Trans R Soc Lond B Biol Sci* 354:1195–1213
- Uludağ K, Müller-Bierl B, Uğurbil K (2009) An integrative model for neuronal activity-induced signal changes for gradient and spin echo functional imaging. *Neuroimage* 48:150–165. doi:[10.1016/j.neuroimage.2009.05.051](https://doi.org/10.1016/j.neuroimage.2009.05.051)
- Vanhadenhuyse A, Noirhomme Q, Tshibanda LJ-F, Bruno M-A, Boveroux P, Schnakers C, Soddu A, Perlberg V, Ledoux D, Brichant J-F, Moonen G, Maquet P, Greicius MD, Laureys S, Boly M (2010) Default network connectivity reflects the level of consciousness in non-communicative brain-damaged patients. *Brain* 133:161–171. doi:[10.1093/brain/awp313](https://doi.org/10.1093/brain/awp313)
- Voyvodic JT, Petrella JR, Friedman AH (2009) fMRI activation mapping as a percentage of local excitation: consistent presurgical motor maps without threshold adjustment. *J Magn Reson Imaging* 29:751–759. doi:[10.1002/jmri.21716](https://doi.org/10.1002/jmri.21716)
- Ward HA, Riederer SJ, Grimm RC, Ehman RL, Felmlee JP, Jack CR (2000) Prospective multiaxial motion correction for fMRI. *Magn Reson Med* 43:459–469
- Weisskoff R (1995) Functional MRI: are we all moving towards artifactual conclusions?—or fMRI fact or fancy? *NMR Biomed* 8:101–103
- Weisskoff R (1996) Simple measurement of scanner stability for functional NMR imaging of activation in the brain. *Magn Reson Med* 36:643–645
- Windischberger C, Langenberger H, Sycha T, Tscherkno EM, Fuchsjäger-Mayerl G, Schmetterer L, Moser E (2002) On the origin of respiratory artifacts in BOLD-EPI of the human brain. *Magn Reson Imaging* 20:575–582
- Yamada K, Naruse S, Nakajima K, Furuya S, Morishita H, Kizu O, Maeda T, Takeo K, Shimizu K (1997) Flow velocity of the cortical vein and its effect on functional brain MRI at 1.5 t: preliminary results by Cine-MR venography. *J Magn Reson Imaging* 7: 347–352
- Yang X, Hyder F, Shulman R (1997) Functional MRI BOLD signal coincides with electrical activity in the rat whisker barrels. *Magn Reson Med* 38:874–877
- Zeffiro T (1996) Clinical functional image analysis: artifact detection and reduction. *Neuroimage* 4:S95–S100
- Zhang X, De Moortele V, Pfeuffer J, Hu X (2001) Elimination of k-space spikes in fMRI data. *Magn Reson Imaging* 19:1037–1041
- Zou Q, Long X, Zuo X, Yan C, Zhu C, Yang Y, Liu D, He Y, Zang Y (2009) Functional connectivity between the thalamus and visual cortex under eyes closed and eyes open conditions: a resting-state fMRI study. *Hum Brain Mapp* 30:3066–3078. doi:[10.1002/hbm.20728](https://doi.org/10.1002/hbm.20728)

Index

A

Abela, E., 159–173

Absence epilepsy (AE), 165, 168

Absence seizures (AS), 168, 169

Accessory gyrus, 65

Acoustic stimulation, 95, 124, 126

AC-PC line, 71

Activated

map, 255, 257

peak, 256, 257

Adenosine receptor, 316

Afferent fiber, 75

Agranular

cortex, 76

isocortex, 76

Air cavity, 326

Alcohol, 316

Allendorfer, J.B., 294

Allen, M.G., 143–155

Allocortex, 82

¹¹C-Alpha-methyl-tryptophane (AMT), 278, 279

Ametropia, 126

Amnesia, 237

Amobarbital injection, 255

Amygdala, 255

Anarthria, 253

Anatomical

landmark, 8, 230, 239, 240

structure, 72, 79

Anesthesia, 239, 253, 255

Angiography, 91, 130, 255

Angular

gyrus, 62–65

sulcus, 63, 64

Anisotropy, 271

Anomia, 254, 260

Anterior

calcarine sulcus, 64, 67, 70, 73, 76

commisure, 71, 80

horizontal ramus, 61, 62

horn cell, 79

insula, 65, 83, 84

lobule, 65, 66, 84

subcentral sulcus, 61–63

temporal cortex, 326

Antiseizure drugs (ASD), 170

Apex of the insula, 65

Aphasia, 83–85

Appel-Cresswell, S., 289

Apraxia, 83, 84

Archer, J.S., 166, 168

Arcuate fasciculus (AF)

AG and STG, 207

fasciculus, 85, 261

intraparietal sulcus, 63, 65

language system, 207

“out-ROI” filters, 207

and SLF, 208

two-ROI approach, 207

Area Tpt, 68, 84

Arteriovenous malformations (AVMs), 91–92, 104, 106, 316

BOLD signal, 316

cerebral blood flow, 251–252

glial tumors, 105

language-related areas, 251

neuroplastic changes, 94

neurovascular coupling, 251

steal phenomenon, 104

Articulation, 83

Artifact, 9, 249–251

Assaf, Y., 188

Astrocyte, 314–315

Astrocytoma, 276

Asymmetry ratio, 261

Attention-intention network, 81

Auditory

cortex, 70, 120–121, 126

acoustic stimulation, 126

neurosurgical procedures/neuronavigation, 235

somatotopy, 77

sound stimulation, 236

superior temporal gyri, 121

hallucination, 83

system, 292

Automatic motion correction, 238

Averaging

dynamic, 248

static, 248

Awake craniotomy, 91, 128, 235

Axon, 252

B

Bagshaw, A.P., 171

Bai, X., 168–169

Ballistocardiogram (BCG)

gradient artifacts, 162

pulse artifact, 162

Bandettini, P.A., 14

Barbiturate, 91, 123

Basal ganglia, 240

Basser, P.J., 184, 186

- Baxendale, S., 123
 Beauchamp, M.S., 292
 Beer, 316
 Beisteiner, R., 287–305
 Benar, C.G., 171
 Benson, R.R., 121
 Benuzzi, F., 169
 Berman, R., 168
 Berntsen, E.M., 105
 Bettus, G., 149, 297
 Betz's cell, 76–79
 Biomagnetic field, 279
 Biopsy, 274
 Bite bar, 250, 321
 Bitter, T., 296
 Bizzì, A., 179–223
 Blatow, M., 89–132
Block
 design, 103, 109, 125
 duration, 109
Blood
 vessel, 313
 volume, 105
Blood-brain barrier (BBB), 275
Blood-oxygenation-level-dependent functional MRI (BOLD fMRI)
 complications and diagnostic errors, 9
 EPI sequences, 4
 high spatial accuracy, 2–3
 local hemodynamic changes, 2–3
 oxy-Hb and deoxy-Hb, 3
 presurgical task-based, 8
 SNR and spatial resolution, 4
 synaptic activity, 2
Blood oxygen level-dependent (BOLD) signal, 3, 94, 288, 297
 brain parenchyma, 4
 contrast, 248, 249, 251, 261
 extravascular effects 169, 248
 field dependence, 249
 frequency bands, 169
 hemodynamic response, 22–24
 intensity, 252
 inverse MR signal, 315
 neuronal activity, 93, 145, 161
 neurovascular coupling, 24
 peri-synaptic activity, 163
 seizure onset zones, 160
 spatial and temporal resolution, 24
 stimulus-related motion artifacts, 131
 task-related response, 318
 temporal lobe epilepsy, 121
 vascularized cerebral metastases, 132
Blurring, 251, 320
BOLD fMRI and DTI
 acquisition techniques, 311–312
 active and resting state fMRI
 alcohol, 316
 brain activity (*see* Brain activity)
 brain lesions, 314–316
 caffeine, 316
 chemicals, 316, 318
 CO₂, 318
 clinical neuroimaging, 312
 low signal-to-noise ratio, 312
 neuronal activity, 311
 statistical post-processing artifacts, 330
 technical-related (*see* Technical-related artifacts)
Bolus-tracking, 3
Bonelli, S.B., 295
Boynton, G.M., 23
Brain
 activity (*see* Brain activity)
 area, mesiotemporal, 93
 damage, 252
 function, 2, 90, 92, 247, 252
 lateralizing, 5
 localization, 5
 injury, 273, 290
 lesion, 257–259
 metastasis, 316
 motion, 250
 parenchyma, 312–314
 plasticity (*see* Brain plasticity)
 shift, 9, 130, 132, 231, 238–241, 268
 spatula, 231
 surface, 130, 239
 surgery, 122
Brain activity
 draining veins, 312–314
 magnetic susceptibility effects, 313
 temporal offset, 312
 “venous” type, 313
Brain lesions
 absent/reduced BOLD signal, 314–315
 contrast-enhancing parts, 315–316
 signal change, 315
Brain plasticity
 anatomical imaging, 288
 BOLD signal, 288
 fMRI/DTI, 288
 graph theoretical approaches, 288
 neuroplasticity (*see* Neuroplasticity)
 physiologic compensation, 288
 traumatic brain injury, 288
Brain tumor, 234, 235, 240, 256, 291, 295
 central, 90
 diagnostic work-up, 181
 fMRI and DTI, 181
 “functional margins”, 181
 histology, 90
 malignant, 90
 morbidity, 90
 neuro-oncology of gliomas
 ALA cohort study, 183
 anatomic structures, 184
 CST network, 183
 functional boundaries, 183
 GBM patients, 183
 growth and velocity, 182
 histology and molecular markers, 181–182
 LGG and HGG, 182
 preoperative symptoms, 183
 residual tumor volume, 183
 neuroradiological intervention, 90
 neurosurgery, 180
 radiotherapy, 90
 rolandic, 8, 90, 104, 106
 surgery, 239, 240
 vascular malformation, 90
Broca
 aphasia, 83
 area, 83, 85, 94, 103, 122, 126, 127, 234, 289, 292, 295
Brodman area, 73, 76, 77, 117
Brodmann, K., 73, 76
Brownian motion, 271

- Brown, M.A., 14
Bryan, R., 315
Bulk head motion, 319
adapted acquisition sequences, 323
categories, 319–320
fMRI activation map, 322
inter-image motion, 321
motion-induced false activation, 323
motor paradigms, 322
physiological brain motion, 319
through-plane motion, 323
Burholt approach, 236
Buxton, R.B., 21–22, 163
- C**
Caeyenberghs, K., 303, 304
Caffeine, 316
Calabrese, M., 296
Calcarine
fissure, 235
sulcus, 64, 65, 67
Camera system, 230
Capillary, 248, 249
Cardiac
motion, 250
pulsation, 250, 319
Carter, A.R., 293
Catani, M., 56, 206–208
Cathode, 252
Cell density, 74, 79
Center of gravity, 98
Central
lobe, 71
sulcus, 65, 68, 104, 114, 256
Cerebral
blood flow (CBF), 251
cortex, 90, 235
maturation, 253
neoplasm, 268
workload, 100, 131
Cerebrospinal fluid (CSF), 90, 240, 253
Chemotherapy, 90
Chen, C.J., 296
Chromatolysis, 252
Chronic pain, 236, 239
Cingulate
gyrus, 64, 68, 69
motor area (CMA), 78
motor cortex, 78–79
sulcus, 69–71
Cingulate motor area (CMA), 81–82
Clinical environment, 5
Cluster
filtering, 238
size, 98, 101
Cocaine, 316
Coenen, V.A., 272
Coffee, 316
Cognitive
brain function, 92, 122
deficit, 5
Cohen, E.R., 314
Collateral sulcus, 64–67
Color-coded parameter map, 273
Computational neuroanatomy, 272
Computer-assisted surgery (CAS), 231
Conduction aphasia, 85
Consumption, 3
Continuous performance task (CPT), 166
Convexity surface
frontal lobe, 62–63
insula, 65, 66
occipital lobe, 65, 73
parietal lobe, 64–65
sylvian fissure, 61–62
temporal lobe, 63–64
Corbetta, M., 196
Corona radiata, 234
Corpus callosum, 68, 80
Correction algorithm, 232
Cortical architecture
dysplasia, 278
entry, 232
neuroplasticity, 240
somatotopy, 77–78
stimulation, 232, 234
Corticospinal tract (CST), 258, 291, 294, 303
Coxon, J.P., 305
Cox, R.W., 14
Craniotomy, 127, 255
Creatine, 271
Crura cerebri, 234
Cruz-Gómez, A.J., 298
Cunningham, C.J., 158
Current
dipole, 281
intensity, 253
Cyclotron, 272
Cytoarchitectonics
afferents and efferents, 75
granule and pyramidal cells, 76
motor cortex, human, 76–77
regions, 76
six cell layers, 74–75
thickness, 76
variations, 76
Cytoarchitectonic zone, 68
Cytoplasm, 252
- D**
Data acquisition
data-processing algorithms, 161
double gamma hemodynamic, 164
electrodes and wires, 160–161
evaluation, 98
gradient fields, 161
hemodynamic response, 163–164
magnetic field strength, 160
matlab toolbox, 161
Maxwell equations, 160
metal transmission wires, 161
nuisance parameters, 165
optimal resistor, 161
radio-frequency electromagnetic, 161
recording procedure, 162–163
rigid-body movement, 162
scanners, 161
signal-to-noise ratio, 161
spike/IED-triggered, 161
topographic voltage map, 164
veto analysis, 162
voxelwise correlations, 165

- Data analysis methods, fMRI
 Bayesian statistics, 49
 brain normalization, 49–50
 data-driven analysis methods, 50
 nonparametric statistical approaches, 49
 real-time analysis, 50–51
- Daunizeau, J., 160
- Debulking, 255
- Decision making, 95, 104
- Deep brain stimulation, 240
- Default-mode network (DMN), 295
 bilateral frontoparietal networks, 169
 neurological disorders, 167
- Deformation-based morphometry (DBM), 270
- Dejerine, J., 193, 200, 220
- Dejerine-Klumpke, A., 193, 200, 220
- Delmaire, C., 247–262
- Dental prosthesis, 324
- Deoxyhemoglobin, 3, 248, 312, 326
- Depth electrode, 255
- Desmond, J.E., 121, 123
- De Tisi, J., 170
- Dexamethasone, 234
- Diamagnetic tissue, 248
- Diffusion tensor imaging (DTI), 9, 105, 129, 130, 233–234, 238
 anaplastic oligoastrocytoma, 272
 anatomical landmarks, 274
 anisotropy, 184
 applications, 55–56
 bi-parametric, 273
 Brownian motion, 271
 in clinical practice, 222–223
 color-coded parameter map, 271
 corona radiata, 234
 corticospinal tract, 258
 and DEC maps, 185
 ellipsoid tensor formalism, 184
 fiber tracking, 247, 258–260
 functional neuronavigation/radiation treatment, 273
 human connectome, 57
 imaging parameters, 184
 intra-voxel, 272
 language tracts, 259–260
 left hemisphere, 273, 274
 metrics and brain tumor microstructure, 185–186
 meyer loop, 272
 nTMS, 238
 presurgical fMRI
 cortical activations, 6
 CPT codes, 5
 diagnosis, brain tumor, 5
 electrophysiological techniques, 6
 function-preserving therapies, 6
 high reliability, 5
 morbidity and mortality, 7
 neuronavigation systems, 5–6
 neuroscience research, 5
 neurosurgical interventions, 6–7
 primary motor and somatosensory cortices, human, 5, 6
 RS-MRI, 5
 stimulation and data processing, 5
 tumor-induced hemodynamic changes, 6
 and presurgical fMRI (*see* Presurgical fMRI)
- q-ball imaging, 274
- radio-/chemotherapy, 274
- scalar metric, FA, 185
- structural connectivity, 2
 subcortical and cortical, 275
 tractography, 53–55, 273, 291, 297
 WM tracts, 276
- Dilks, D.D., 294
- Direct electrical stimulations (DES)
 coregistration, 254–255
 functional imaging methods, 255
 homunculus, 237
 language tracts, 259
 neurons, 252
 neuropsychological evaluation, 253–254
 practical stimulation methods, 253
 principles, 252
 recording electrodes, 253
 subcortical, 258
 tissue damage, 252
- Directionally encoded color (DEC) maps
 CST trajectories, 197
 face/mouth area, CST fibers, 199–201
 focal lesions, 202
 GBM WHO IV, 199
 histopathological examination, 202
 IFOF, temporal stem, 201
 intraoperative DTI, 199
 right-handed female, 197, 198
 WM tract, 202–204
- Display parameter, 98
- Dorsal pathway. *See* Arcuate fasciculus (AF)
- Draining
 vein signal, 316
 vessel, 248
- Draper, N.R., 34
- Dronker's area, 84
- Duffau, H., 210, 218, 219, 222, 247–262
- Duvernoy, H., 64, 71
- Dynamic causal modeling (DCM), 300–301
- Dysarthria, 253
- Dysesthesia, 253
- E**
- Echo-planar imaging (EPI), 4
 time, 330
 volume, 325
- Edema, 233, 234, 290, 299
- Eickhoff, J.H., 303
- Eickhoff, S.B., 298, 301, 303
- Electrical
 cortical stimulation, 235, 239
 stimulation, 239
- Electrocortical stimulation, 122
- Electrocorticogram (ECoG) recording, 90, 130, 164, 171, 253
- Electroencephalography (EEG), 4, 9, 91, 229
 Alzheimer's disease, 167
 BECTS/Rolando epilepsy, 165
 bilateral paroxysmal, 165
 communication, 173
 cortical and subcortical networks, 160
 data acquisition and analysis, 160–165
 electric activity, 160
 “genetic epilepsies”, 165
 mild oral automatisms/bilateral eye, 165
 motor imagery, 160
 multimodal data integration, 160
 neuronal current imaging, 173

- nodes and edges, 173
“permissive/gate-keeper”, 169
postoperative anatomical, 172
prototypical dynamic disease, 173
seizure-onset zone, 165
spike-wave discharges, 167, 168
suboptimal pharmacological control, 160
“supporting hardwire”, 173
synaptic and suprathreshold, 173
- Electrogoniometer, 230
- Elkana, O., 296
- Eloquent brain area, 229–230
- Empty map, 101
- Endoplasmic reticulum, 252
- Energy metabolism, 276
- Enzinger, C., 295
- Epidural paddle electrode, 236
- Epilepsy, 5, 121–123, 256
activity, 281
Broca’s area, 297
in children, 297
intra and interhemispheric functional connectivity, 296
language activation patterns, 297
lobectomy patients, 297
pre and postsurgical neuroplastic changes, 297
surgery, 234, 237–239, 281
Wernicke’s area, 297
- Epileptogenic zone (EZ), 91, 119
epileptiform activity, 170
epileptogenic network, 171
- Ertelet, D., 296
- Examination protocol, 8
- Experimental setup, 5
- Extra-axial lesion, 256, 257
- Eye tracking camera, 327
- F**
- False
activation, 325
discovery rate (FDR), 103
- Faraday cage, 330
- Fascicles, 216–219
- Feasibility test, 108, 125
- Ferda, J., 273
- ¹⁸F-ethyl-tyrosine, 277
- ¹⁸F-flumazenil, 280
- ¹⁸F-fluorodeoxyglucose (FDG)
ligand imaging, 271
and MET, 277
PET radiopharmaceutical, 277
- Fiber
bundle, 273
crossing, 274
tract, 258
- Field dependence, 249
- Flash sequence, 326
- Flow
abnormality, 251
artifact, 313, 320
- ¹¹C-flumazenil, 280
- Fluorodesoxyglucose PET (FDG-PET), 260
- Focal hand dystonia, 293
- Fornander, L., 298
- Forn, C., 298
- Fox, P.T., 21
- Fractional anisotropy (FA), 298, 299
grayscale image, 273
left hemisphere, 274
white matter, 273
- Friederici, A.D., 194, 195
- Fried, I., 81
- Friston, K.J., 34, 42
- Frontal aslant tract (FAT), 216
cortex, 76, 77, 260
lobe, 62–63
operculum, 63
parietal operculum, 61, 66
- Full-width at half maximum (FWHM), 162
- Functional brain mapping. *See also* Functional magnetic resonance imaging (fMRI)
area, 2
BOLD signal, 248–249
cortex, 126
diagnosis, 5, 93, 98, 128
fMRI artifacts and limitations
AVMs, 251–252
magnetic susceptibility, 251
movement artifacts, 249–251
neurovascular coupling, 251
rCBV, 251
task-related, 252
landmark, 6, 100, 130
neuroimaging, 2, 229
neuronavigation (*see* Neuronavigation)
somatotopic mapping, 240
- Functional magnetic resonance imaging (fMRI), 2, 229, 237–238
anatomical and functional data
coregistration, 44
reconstructed cortex representations, 45
statistical maps, 44
arcuate fascicle, 271
auditory, 236
BrainVoyager QX, 271
central sulcus, 271
cooperation of the patient, 327
cortical mapping, 271
cyclotron unit, 272
vs. DES, 256
diagnostics, 2
distortion correction, 31
3D motion correction, 27
drifts and temporal smoothing, 28
DTI (*see* Diffusion tensor imaging (DTI))
edema or gliosis, 271
epilepsy, 8
event-related designs, 26
fiber bundles, 271
group analysis
brain normalization, 46
cortex-based normalization, 47
functional localizer experiments, 48
integration, fMRI, 45
statistical analysis, 48–49
Talairach transformation, 46–47
- hardware and software, 271
left temporal lobe, 221
localization accuracy, 258
medial/mesial, 271
motion correction, 30
vs. MSI, 258
neuroanatomy, 8

- Functional magnetic resonance imaging (*cont.*)
 neuronavigation, 8
 neuroplasticity, 9
 neurovascular coupling, 21–22
 noninvasive imaging technique, 2
 oxygen extraction, 271
 vs. PET and TMS, 256
 and presurgical (*see* Presurgical fMRI)
 resting-state networks, 51–52
 ROI-based analysis, 24
 slice scan time correction, 28
 somatosensory functions, 271
 spatial relationship and smoothing, 8–9, 28–29
 statistical data analysis
 deconvolution analysis, 43
 event-related averaging, 42
 linear model (*see* Linear model)
 maps, 40
 multiple comparison, 40–42
 subtraction to statistical comparison, 30–31
 t-test and correlation analysis, 32–34
 structural connectivity and presurgical tractography, 7–8
 topographical analysis, 271
 topological representations, 25
 T1-weighted 3D post-contrast data, 2
 ultrafast MR sequences, 2
- Functional MR imaging (fMRI). *See* Functional magnetic resonance imaging (fMRI)
- Functional neuroanatomy
 cortical (*see* Cortical architecture)
 Heschl's gyrus, 73, 75
 interrelationship, 61
 lobar
 borders (*see* Lobar borders)
 morphing, 71
 Talairach-Tournoux coordinate system
 and space, 71–72
 occipital lobe, 73, 76
 pericentral cortex (*see* Pericentral cortex)
 superior temporal plane, 73
- Functional neuroimaging
 anatomic structures, 284
 DTI, 273–276
 eloquent cortex, 282
 epileptic focus, 284
 fMRI, 271–272
 MR spectroscopy, 276
 nuclear medicine
 PET/CT, PET/MRI, and SPECT/CT, 276–277
 radiopharmaceuticals, 277–281
 postprocessing algorithms, 284
 presurgical imaging, 269–270
 radiopharmaceuticals (*see* Radiopharmaceuticals)
 real-time imaging, 284
 safe and reliable instrument, 284
 stereotaxy/neuronavigational systems, 283
 transcranial magnetic stimulation, 284
- Fusiform gyrus, 64, 67, 71
- Fusion inaccuracy, 240
- Gasser, T., 106
- Generalized spike-wave (GSW)
 IGE syndromes, 169
 spatial patterns and temporal dynamics, 169
 thalamocortical network, 169
- General linear model (GLM), 101, 323
 nuisance parameters, 165
 voxel timeseries, 163
- Genovese, C.R., 42
- Geometric correctness, 329
- Geschwind, N., 124, 131
- Ghosting, 322
- Glial activity, 276
- Glioblastoma, 105
- Glioma, 90, 230–232, 316, 317
 high grade, 231, 235, 251
 low grade, 105
 radicality of resection, 232
 surgery, 232, 276
- Glosser, G., 123
- Glucose transporter, 277
- Goebel, R., 13–57
- González-García, N., 292
- Gotman, J., 161
- Gradient echo (GE) pulse sequence, 4, 315
- Grafton, S.T., 78
- Granule cell, 74, 76, 78
- Graziano, M., 79
- Grefkes, C., 296
- Greicius, M.D., 144
- Grey
 matter, 275
 scale image, 273
- Grid
 configuration, 240
 electrode, 280
- Grouiller, F., 164
- Guidance, 5
 auditory, 83
 somatosensory, 70, 83
 visual, 83
- Gulati, S., 105
- Gyrus
 accessory, 65
 angular, 62, 63, 65
 cingulate, 64, 68
 configuration, 70
 fusiform, 64, 67, 71
 inferior frontal (IFG), 62, 63, 71
 medial occipitotemporal, 64–66, 68
 middle frontal, 62, 63, 66
 orbital, 63, 65, 67
 parahippocampal, 64–67
 postcentral, 62–65, 68
 precentral, 62, 63, 65, 69
 subcentral, 61–63, 65
 superior frontal (SFG), 62, 68
 supramarginal, 62, 63, 65
 transverse temporal, 62, 63, 67
 triangular, 63

G

- GABA-A-benzodiazepine–receptor complex, 277, 280
- Gaillard, W.D., 122
- Gao, J.H., 315
- Garcia, M., 89–133

H

- Hacker, C.D., 143–155
- Hallucination auditory, 83
- Hall, W.A., 105

- Hammeket, T.A., 123
- H**
- Hand
area, 256
knob, 91, 106, 315
motor area, 91
- Harris, R.J., 295
- Hartwigsen, G., 292
- Hasegawa, R.P., 83
- Hauf, M., 165
- Head
fixation, 96, 130–131
holder, 230
motion, 249–250
movement artifact, 312, 319
- Heads-up display, 240
- Hemiparesis, 131, 234
- Hemisphere dominance, 121, 258–259
- Hemodynamic response function (HRF), 2, 92, 105
coupling, 316
non-neural signals, 163
physiological waveforms, 171
reference function (HRF), 101–103
- Hemosiderin, 328
- Herholz, K., 278
- Heschl's gyrus, 62, 63, 66–68
- Heterotypical agranular isocortex, 76, 78, 81–83
- High-angular-resolution diffusion
imaging (HARDI)
directional measurements, 274
fiber tractography, 274
- Hill, D., 323
- Hippocampal sclerosis, 297
- Homunculus, 110, 239
- Horizontal plane, 71
- Huettel, S.A., 14
- Hydrocephalus, 90
- Hypercapnic normalization, 316
- Hyperperfused tissue, 316
- Hypoperfusion, 255–256
- Hyposmia, 320
- Hypotension, 251
- Hypothalamus, 82
- I**
- Idiopathic generalized epilepsies (IGE)
heterogeneous syndromes, 165
thalamic BOLD signal, 166
- ¹²³I-iomazenil, 275
- Image-guided surgery (IGS), 231
alignment, 97, 101
fusion, 270
postprocessing, 270
protocol, 95, 98
resolution, 248
- Impulse intensity, 253
- Independent component analysis (ICA)
data-driven techniques, 164
spectral amplitude, 164–165
- Inferior
frontal gyrus (IFG), 260
frontal lobe, 65
superior surface, temporal lobe, 67–68
temporo-occipital lobes, 64–67
- Infiltrative tumor, 318
- Inhibitory neuron, 76
- Inner
ear, 251
speech, 83
- Integration, operating room, 222
- Inter-image motion, 322, 323
- Intermediate sulcus, 62, 63, 65
- Internal
capsule, 253
carotid artery (ICA), 255
- Interposed multimodal lobe, 70
- Intra-axial
lesion, 256, 257
tumor, 90
- Intracarotid amobarbital procedure (IAP) asymmetry index, 261
- Intracellular recording, 80, 82
- Intracortical stimulation (ICS), 104
- Intracranial EEG (iEEG), 160
- Intracranial monitoring, 283
- Intra-image motion, 321–322
- Intraoccipital sulcus, 62, 65
- Intraoperative stimulation, 259
- Intra-voxel fiber architecture, 274
- Intrinsic functional connectivity MRI (ifcMRI)
DTI, 272
large-scale systems, 272
resting-state, 272
tractography and resting-state, 272
- Irritative zone (IZ), 170
- Ischemic event, 255
- Island of Reil, 65
- Isocortex, 76, 78, 81, 82
- J**
- Jack, C.R. Jr., 104
- Jacobs, A.H., 106
- Jang, S.H., 293
- Juengling, F.D., 267–282
- Juvenile myoclonic epilepsy (JME), 165
- K**
- Kapreli, E., 299
- Kassubek, J., 269–284
- Kawashima, R., 83
- Killgore, W.D., 123
- Kilner, J.M., 169
- Kim, T.S., 163
- Kleinschmidt, A., 78
- Kleiser, R., 273
- Kobayashi, E., 169
- Koch, M.A., 272
- Kokkonen, S.M., 149
- Korogi, Y., 73
- Koskinas, G.N., 76, 84
- Krakow, K., 171
- Kraut, M., 315
- Krings, T., 319
- Krishnan, R., 105
- Kutner, M.H., 34
- L**
- Laboratory of neuroimaging (LONI), 270
- Lactate, 276
- Laible, M., 295

- Landmark, 70, 72, 74, 75, 92
 anatomical, 8
 functional, 5
- Language function
 brain function, 116
 cortex, 121
 deficit, 123–124
 dominance, 68, 119, 121, 255, 258
 function, 116, 122, 125, 258
 hemiparetic patient, 115, 116
 left hemisphere, 115, 119
 and logistical requirements, 119
 mapping, 234, 253, 258
 neuropsychological symptoms, 119
 personnel and logistical requirements, 119
 preoperative neuroimaging, 119
 representation, 121, 122
 in rolandic brain tumors, 118
 shift, 291
 Wada test, 119
 Wernicke's speech areas, 119
- Language system
 aphasias, 193
 clinical-anatomical postmortem studies, 193
 cortical and subcortical regions, 193
 dorsal and ventral WM pathways, 195
 human ability and lesion method, 193
 human species, 192
 morphology, 192–193
 network redundancy, 194
 semantic/syntactic process, 195
 structural connections, 194
 syntactic and semantic information, 194
 WM tracts, brain surgery, 207
- Large blood vessel, 249
- Lateralization index, 102, 130, 255
 parietotemporal line, 70, 71
 sagittal plane, 73
- Laufs, H., 171
- Lazaridou, A., 303
- Leclercq, D., 247–262
- Lee, C.C., 104–105
- Left hemisphere, 63, 81, 85
- Lehéricy, S., 247–262
- Lemieux, L., 160, 161
- Le Rumeur, E., 316
- Lesion test, 123
- Leunissen, I., 305
- Leuthardt, E.C., 143–155
- Limbic lobe, 70, 71
- Linear model
 conjunction analysis, 37
 denominator, 37
 error values, 35
 GLM assumptions, 38
 matrix-matrix multiplication, 36
 matrix-vector multiplication, 35
 multicollinear design matrices, 37–38
 quantitative independent variables, 34
 serial correlations, 38–40
 significance tests, 36–37
- Lingual gyrus, 64, 65, 67, 123, 126
- Liu, H., 149
- Lobar borders
 arbitrary and uncertain, 71
 definitions, 68
- gyral configuration, 70
 identification, 68
 temporo-occipital line, 70
 TPO confluence, 68, 70
- Localization error, 132
 magnetic field inhomogeneity, 2, 328
 skin anesthesia, 255
- Locke, S., 216
- Longitudinal sulcus of Beck, 68
- Lymphoma, 90
- M**
- Macaque monkey, 258
- MacIver, K., 298
- Macrophage, 316–317
- Magistretti, P.J., 22
- Magnetencephalography (MEG), 229, 238
- Magnetic resonance imaging (MRI)
 anatomical and functional images, 15
 computer-based analysis, 272–273
 cortical and subcortical, 270
 crossing fibers, 188–189
 diffusion tensor imaging, 184–185
 and DTI limitations, 187–188
 feasible brain mapping, 189
 field
 gradient, 248–249
 strength, 2, 315, 320, 328
 hoc processing, 270
 ifcMRI, 272
 image reconstruction
 Echo-Planar imaging, 20–21
 frequency encoding, 19
 parallel imaging and excitation, 21
 phase encoding, 19–20
 slice excitation, 18
 two-dimensional k space, 20
 intramodal multimodality, 270
 mapping strategies, 202–204
- motor system
 CST, 204–206
 SMA connectivity, 206–207
- MR tractography, 184
- nuclear medicine, 276–277
- physical principles, 15
- registration algorithms, 272
- RF coil, 15
- seizure origin, 273
- soft-tissue contrast, 270
- source imaging (MSI), 258
- spin excitation (*see* Spin excitation
 and signal reception)
- structural connectivity
 body sensory receptors, 190
 corpus callosum, 190
 information processing, 190
 language system, 192–195
 macro/micro components, 190
 motor system, 191–192
 WM pathways, 190
- susceptibility, 248, 251
- T2-and T1-weighted MR images, 184
- T2/FLAIR images, 184
- voxel-based mapping, 273
- whole-body scanner, 14

- Magnetic resonance spectroscopy (MRS).
See also Magnetic resonance imaging (MRI)
- amygdala-hippocampal, 276
 - carbon-bound, 276
 - neuronavigation/frameless stereotaxy, 276
 - non-exchangeable protons, 276
 - single and multiple-voxel, 274
 - temporal lobe epilepsy, 276
- Magnetic source imaging (MSI)
- functional information, 281
 - intraoperative cortical records, 283
 - sensorimotor cortex, 283
 - speech-dominant hemisphere, 281
- Magnetoencephalography (MEG), 4, 9, 72, 91, 256
- complex and cost-intensive, 281
 - electromagnetic signals, 281
 - eloquent cortex, 281
 - fMRI and MSI colocalization, 283
 - Landau–Kleffner syndrome, 282
 - magnetic field pattern, 281
 - sensorimotor cortex, 281
- Malformations of cortical development (MCD)
- detection and localization, 273
 - seizure origin, 273
- Mandonnet, E., 183
- Marcotte, K., 296
- Martino, J., 210
- Massa intermedia, 73, 75
- Matt, E., 289–307
- Mbwana, J., 297
- Measurement time, 95, 125
- Medial, 68, 69
- occipitotemporal gyrus, 64, 65
 - parietal region, 70
- Memory
- assessment, 255
 - function, 247, 260
 - impairment, 261
 - lateralization, 261, 262
 - performance, 256, 260, 261
- Meningioma, 232
- Meningioma intraventricular, 235
- Mesial temporal lobe epilepsy (MTLE), 166, 170, 171
- Mesiotemporal brain area, 93
- Metal
- implant, 328
 - ion, 252
- Metallic particle deposition, 251
- Metastases, 90, 132, 232
- Metastatic disease, 90
- ¹¹C-Methionine (MET)
- and PET data, 277, 278
 - uptake, 277–278
- Meyer loop, 274
- Meynert, T.H., 216
- Microvessel, 315
- Middle frontal gyrus (MFG), 63, 66, 67
- Middle sagittal plane, 73
- Mintzopoulos, D., 295, 296
- Mirror
- movement, 290, 300
 - neuron, 83
- Mitchell, T.J., 143–155
- Mitochondria, 252
- Moeller, F., 171
- Mohamed, I.S., 273
- Molds, 323
- Molecular imaging, 240–241
- Möller, M., 106
- Montreal neurological institute (MNI)
- template, 270
- Morphological imaging, 116, 130
- Morphometry, 270
- Motion
- artifact, 96, 107, 125, 131, 323, 325
 - correction, 96, 250
 - algorithm, 324, 325
 - real time, 250
- Motoneuron, 76, 79, 82
- Motor
- aphasia, 83
 - behaviour, 81
 - cortex, 72, 76, 77, 79, 250, 256, 279
 - deficit, 105
 - evoked potential (MEP), 256, 257
 - function, 131, 253, 256
 - hand area, 72, 74, 78, 106, 116
 - map, 79
 - response, 239
 - and sensory systems, 233–234
 - speech area, 77, 83
 - and speech function
 - Broca's area, 83
 - CMA, 81–82
 - Dronkers' area, 84
 - prefrontal cortex (pre-FC), 83
 - premotor area (pre-MA), 82–83
 - pre-SMA, 81
 - primary, 78–79
 - sensory appreciation, 84
 - supplementary motor area (SMA)
- Movement artifact, 249–251
- ^{99m}Tc-ethyl cysteinat-dimer (^{99m}Tc-ECD), 277
- Müller, H.-P., 269–284
- Multilinguality, 92, 124
- Multimodal association cortex, 70
- Multiple-modality comparison, 270
- Multiple sclerosis (MS), 293, 297–298
- Multi-voxel pattern analysis (MVPA), 50
- Muscle, 78, 79, 84
- Myelinated fiber, 252
- N**
- Naidich, T.P., 61–85, 92
- Navigated transcranial stimulation (nTMS), 238
- Neocortex, 74
- Neoplasm, 273
- Neovascularization, 132, 318
- Nervous system, 269
- NessAiver, M., 14
- Neural activity, 281
- Neuroanatomy, 8
- Neurofunctional system, 2
- Neuroimaging, 90
- Neurological dysfunction, 130
- Neuromuscular blockade, 239
- Neuronal
- activity, 2, 248, 249
 - homeostasis, 252
 - network, 105, 106, 271

- Neuronavigation, 5, 132, 256, 257
 auditory, 235–236
 basal ganglia, 240
 cortical entry, 232
 frameless intraoperative 152
 functional activation maps, 232
 glioma surgery, 232
 imaging technologies, 240–241
 language, 234–235
 micro-optical overlay modules, 240
 motor and sensory systems, 233–234
 neuroplasticity, 240
 neurosurgeons, 231
 optimized preoperative protocols, 232
 psychological function
 cost-effectiveness, 239
 DTI, 238
 intraoperative imaging, 238
 intraoperative mapping, 239
 memory, 236–237
 resting-state fMRI, 237–238
 single-rack solution, 239–240
 spinal cord, 240
 station, 230
 stereotaxy, 230–231
 visual cortex, 235
- Neurooncology, 98, 106
- Neurophysiology, 269
- Neuroplasticity
 brachial plexus lesions, 300–301
 cellular changes, 292
 chronic stroke, 303–305
 complexity and limitations, 293
 cortical, 240
 epilepsy (*see* Epilepsy)
 fMRI/DTI techniques, 291, 292
 functional/structural network measures, 293
 heterotopic hand replantation
 bilateral motor network, 302–303
 cortical connectivity, 303, 304
 DCM, 302–303
 malignant soft tissue tumor, 301–302
 individual prognosis, 291
 longitudinal and peripheral
 nerve regeneration, 300
 maladaptation, 293
 medication and co-interventions, 300
 molecular changes, 292
 motor system, 9
 MS, 297–298
 multimethodological approaches, 300
 multiple sclerosis, 293
 nervous system, 289
 neuronal population changes, 292–293
 neurophysiological interpretation, 299
 patients' functional state and cooperation, 291
 peripheral nerve regeneration, 300
 peripheral nervous system disorders, 298–299
 reorganization, hand, 303
 sensorimotor areas, 105
 stroke (*see* Stroke)
 technical interpretation, 299
 tractography, 291
 traumatic brain injury, 305–307
 treatment strategies, 291–292
 ultrahigh-field MR, 300
- Neuropsychological testing, 123
- Neuroradiology, 90
- Neuroscience, 5, 93
- Neurovascular
 coupling, 2, 251, 297
 uncoupling, 317
- Nichols, T.E., 37
- Nicotine, 320
- Nitric oxide, 316
- Noisy voxel, 332
- Nomenclature, 68, 70, 82
- Non-paretic hand, 110, 116
- Non-primary sensorimotor area, 105
- Noun generation, 121
- Number needed to treat (NNT), 170, 171
- Nunez, P.L., 161
- O**
- Obsessive-compulsive disorder (OCD), 237
- Occipital
 lobe, 65
 pole, 66, 68, 76
- Ogawa, S., 315
- Olfactory sulcus, 65
- Oligodendrogioma, 278
- Optic radiation, 274
- Oral apraxia, 84
- Orbital
 gyrus, 62, 63, 65
 sulcus, 62, 65
- Orbitofrontal cortex, 328
- Ovadia-Caro, S., 296
- Oxygen
 consumption, 2
 extraction fraction, 317
 metabolism, 252
 supply, 320
- P**
- Pain, 230, 236, 239, 298
- Pallidotomy, 240
- Papoutsi, M., 295
- Paracentral
 gyrus, 68, 69
 lobule, 65, 68, 69
 sulcus, 68, 69, 80
- Parahippocampal gyrus, 64–67, 71
- Parallel
 imaging, 328, 329
 sulcus, 63, 64
- Paraphrasia, 84, 254
- Parenchyma, 314–316
- Parietal
 cortex, 76, 317
 lobe, 62–65
- Parieto-occipital sulcus, 62, 68, 69, 70, 71
- Pars
 bracket sign, 72, 73
 marginalis, 68, 69, 73
 opercularis, 62, 63, 83
 orbitalis, 62, 63, 67
- Patient-related artifacts
 bulk head motion (*see* Bulk head motion)
 flow and pulsation artifacts, 320–321

- motion artifacts, DTI, 325–327
patient cooperation, 327, 328
- Patient-to-image registration, 231
- Paus, T., 82
- Peeters, R., 313–332
- Performance test, 96
- Perfusion
MRI, 239
pressure, 251–252
- Pericentral cortex
axial plane
pars bracket sign, 72–73
precentral knob, 72
thickness, pre-and postcentral gyri, 73
- cerebral margin, 72
- functional MRI (fMRI), 72
- lateral medial sagittal plane, 73, 74
- preCG and postCG fuse, 72
- sensitivity and specificity, 72
- Talairach space, 72
- Peri-insular sulcus, 65, 66
- Perirolandic tumor, 233, 239
- Phalanges, 230
- Pharmacoresistant focal epilepsies
intracranial electrodes, 172
ischemic stroke, 170
non-lesional/multifocal epilepsies, 172
overlapping zones, 171
pharmacoresistant disease, 169
post-operative imaging, 172
temporal lobe, 171
- Phase reversal, 283
- Phonemic deficit, 83
- Photon emitter, 277
- Picture naming, 122
- Pitfall, 9
- Planum
polare, 67, 68
temporale, 67, 68, 84
- Plegic patient, 236
- Plexus papilloma, 235
- Polar cortex, 76, 77
- Positron emission tomography (PET), 4, 72, 229, 235, 241, 256, 259, 260
cyclotron unit, 272
fluorodeoxyglucose, 280
- Postcentral gyrus, 62, 64, 65, 69, 91, 106, 115
- Posterior
ascending ramus, 61–63, 65
descending ramus, 61, 62, 70
horizontal ramus, 70
subcentral sulcus, 61–63
- Post-processing, 96, 120
- Post-scan interview, 96
- Powell, H.W., 297
- Practical issues
clinical fMRI protocols, 94
custom-tailored developments, 94
electrical equipment, 96
equipment, visual stimulation, 96, 97
evaluation and interpretation, 98
methodological variability, 98
post-scan interviews, 96
pre-measurement training, 96
“real-time fMRI” software packages, 98
tactile stimulation, 96, 97
- Prefrontal cortex, 83, 85
- Premotor
activation, 110, 116
area, 79, 82
cortex, 79, 81, 253, 290, 303, 306–307, 317
- Preoperative mapping of functional cortex
analysis, rsfMRI, 151
ECS positive sites were, 154–155
electrodes, 151
epilepsy, 151
generation, ROC curves, 152
motor and language networks, 153–154
preoperative rsfMRI analysis, 151
probability, MLP false negative, 154
seizure-monitoring, 151
trained MLP, 151–153
- Pressure effect, 251
- Pre-supplementary motor area, 81
- Presurgical fMRI. *See also* Presurgical imaging,
functional neuroimaging
activation pattern, 120
anatomical landmarks, 91
artifact, 9
atypical language dominance, 126
BOLD signal, 119
brain tumors and surgery, 90
Broca’s area, 125, 126
categorical analyses, 123
clinical and neuropsychological examination, 127
consensus, 7
data processing, 93
diagnostic capabilities and limitations
brain tumor and functional cortex, 130
Broca’s/Wernicke’s areas, 131
language lateralization, 131
patient-specific and methodological factors, 130
somatotopic fMRI, 133
tumor-related hemipareses, 131
T1-weighted image sequences, 132
- hemispheric dominance, 91
- hemodynamic changes, 93
- indications and limitations, 94
- in individual patients
BOLD signal characteristics, 100
2D fMRI activation maps, 101
dynamic thresholding, 101, 102
“steal phenomenon”, 104
- intrahemispheric localization, 120
- intraoperative electrocortical stimulation, 123
- language lateralization assessment, 123
- legal aspects, 98
- “lesion test”, 123
- localization, right-handed male patient, 126, 127
- memory-related brain activation, 93
- multimodality imaging, 279
- prelinguistic auditory processing, 120
- preoperative diagnostic workup, 122
- sensorimotor/language areas, 121
- Wada test, 121
- word-generation tasks, 121
- Presurgical imaging, functional neuroimaging
brain shift phenomenon, 270
eloquent systems, 270
fMRI, 269
functional brain mapping, 248–252
functional localization and structure, 270

- Presurgical imaging, functional neuroimaging (*cont.*)
- ifcMRI, 269
 - imaging tools, 269
 - language
 - DTI fiber tracking, 259–260
 - hemispheric dominance, 258–259
 - localization, 259
 - lesion identification, 270
 - memory, 260–261
 - metabolic state and molecular, 270
 - multiparametric/multimodal, 270
 - PET and SPECT, 269
 - proportional scaling, 270
 - sensu stricto, 269
 - surgical procedure, 270
 - Wada test, 255–256
- Price, S.J., 186
- P**
- Primary motor cortex
- fMRI motor cortex somatotopy, 110
 - hemiparetic patient, 115, 116
 - left postcentral high-grade glioma, 112
 - left rolandic cavernoma, 113, 115
 - morphological images, 111, 112
 - precentral gyrus, 115, 116
 - rolandic metastasis, 111, 114
 - somatosensory
 - fMRI protocols, 114, 115
 - presurgical fMRI somatotopic mapping, 113, 115
- Proportional scaling system, 270
- Prosody, 84
- Proton (1H)-MR spectroscopy, 276
- Puig, J., 291
- Pulsation artifact, 320, 322
- Pyramidal cell, 74, 76, 77
- Q**
- Q-ball imaging, 274
- R**
- Radionecrosis, 231
- Radio pharmaceuticals
- aromatic amino acid decarboxylase, 279
 - astrocytomas and oligodendrogiomas, 280
 - brainlab vector vision, 278
 - FDG, 277
 - ¹⁸F-ethyl-tyrosine and ¹⁸F-tyrosine, 279
 - ¹⁸F-flumazenil and ¹¹C-flumazenil, 280
 - glioblastoma multiforme, 279
 - MET-PET, 279, 280
 - ^{99m}Tc-ECD, 277
 - ^{99m}Tc-HMPAO, 277
 - ¹⁵O-H₂O, 280
 - PET/CT, 281
 - sensorimotor deficits, 281
 - SISCOM, 277
 - temporal and extratemporal, 277, 278
 - VINCI, 279
- Raichle, M.E., 52
- Ramus
- anterior horizontal, 63
 - posterior ascending, 61–64
 - posterior descending, 62, 70, 71
- Rapid image transformation, 230
- Rath, J., 230, 298, 303
- Read-out bandwidth, 328
- Real-time
- fMRI, 93, 98, 122, 232, 238
 - imaging, 284
- Receiver coil array, 329
- Red blood cell, 248, 249
- Regional blood volume (rCBV), 251
- Registration error, 232
- Resection
- border, 6
 - margin, 98, 107, 130
- Resonance frequency, 250
- Respiratory motion, 250
- Resting-state fMR (RS-fMRI), 5, 8, 269, 314, 316
- clustering algorithms, 148
 - detection, BOLD signal, 143–144
 - localization, 143
 - preprocessing, 146
 - presurgical planning
 - epilepsy, 149–150
 - higher spatial resolution, 149
 - ICA data evaluation, 150
 - localization, motor and language system, 149
 - MLP-based RSN mapping, 151–155
 - morbidity, 149
 - resection, brain, 149
 - sensorimotor mapping (*see* Sensorimotor mapping)
 - processing methods, 145–146
 - resting-state networks, 144–145
 - RSN mapping, MLP, 148–149
 - seed-based correlation mapping, 146–147
 - SICA approach, 147–148
- Rheims, S., 281
- Rhyming, 121
- Richiardi, J., 298
- Right hemisphere, 64, 69, 72
- Rigid body
- global deformation, 249
 - transformation, 230
 - translation, 249
- Risk assessment, 104, 132
- Ritter, P., 161
- Robles, S.G., 291
- Rocca, M.A., 298
- Rolandic
- brain tumor, 102, 234
 - landmark, 106
- Root mean square error (RMS), 231
- Ro, T., 294
- Roux, F.E., 105
- Rummel, C., 159–173
- Rutten, G.J., 122, 124
- S**
- Sagittal plane, 73, 80
- Sanai, N., 210
- Satellite navigation, 230
- Saur, D., 294
- Sawaki, L., 296
- Saxe, R., 42
- Scan
- plane, 325
 - time, 95, 115
- Scanner room, 330
- Schaechter, J.D., 295

- Schiffbauer, H., 318
Schild, H.H., 14
Schizophrenic
 hand area, 78
 speech area, 77, 84
Schonberg, T., 221
Schwarze, U., 296
Seeck M, 171
Seeding point, 258
Seizure onset zone (SOZ)
 cortical epileptogenic lesions, 170
 multifocal lesions, 170
Semantic
 language task, 119
 processing, 119
Semelka, R.C., 14
Sensorimotor mapping
 cortex, 260, 281
 diagnosis, glioblastoma multiforme, 150
 focal motor seizures, 150–151
 seed-based approach, 52, 150
 task-based fMRI, 150
Sensory
 cortex, 239
 deficit, 104
 response, 239
Sentence
 generation task, 124
 processing, 122
Sharma, N., 295
Shima, K., 81
Shimming, 251, 328
Shimony, J.S., 143–155
Shulman, G.L., 195
Signal
 artifact, 321
 drop-out, 325
 generator, 281
 intensity, 250, 273, 315, 325
 loss, 248, 251
 time course, 314, 317, 330
Signal-to-noise ratio (SNR), 2, 232, 249, 313–314, 328
Silberstein, R.B., 161
Single-photon emission computerized
 tomography (SPECT), 4, 229
 anatomic structures, 284
 axon direction, 274
 ⁹⁹mTc/¹²³I, 277
 rack information system, 239
 shot EPI, 250
 triple-headed cameras, 277
 unit discharge, 81
Single-rack solution, 239–240
Sinus, 251
Sinusoidal rhythm, 320
Skull base, 230, 328
Small, S.L., 295
Smith, H., 34
Snyder, A.Z., 143–155
Software, 4, 238
Solution, 2
Somatosensory function
 activation patterns, 108
 arbitrary movements, 107
 brain tumor patients, 107
 contrast-enhancing tumor areas, 107
 cortex, 258
 evoked potential (SEP), 239
 fMRI sensitivity, 108
 intra-and extra-axial tumors, 105
 magnetic field scanners, 106
 morphological imaging, 106
 non-paretic hand, 110
 pretherapeutic decision-making, 105
 self-paced movements, 108
 sensorimotor areas, 105
 somatotopy, 104
 stimulation, 109
 tumor-related pareses, 107
 unilateral movements, 107
Spatial
 coordinate, 98
 data smoothing, 96
 extent, 98
 normalization, 270
 resolution, 232, 248–250
 specificity, 248
Spencer, D.C., 256
Spike, 330
Spin
 echo (SE), 4, 248
 history, 323, 325
Spinal cord, 76, 79, 82, 240
Spin excitation and signal reception
 axis of rotation, 15
 electromagnetic pulse, 16
 inhomogeneities, 17, 18
 Larmor equation, 16
 longitudinal relaxation, 17
 protons, 15
 spin dephasing, 17
 transversal relaxation, 16
Spin-tagging, 3
Splenium, 64, 66, 69, 70
Springer, J.A., 121
Standardization, 94
Statistical
 correlation, 4
 parametric mapping (SPM), 273
 threshold, 6, 255, 258, 259
Steal phenomenon, 104, 105
Steep image intensity gradient, 323
Stejskal, E.O., 53
Stereotactics
 coordinate system, 270
 frame, 231
 neuronavigation, 254
Stereotaxy, 229, 231
 brain shift, 231
 frame-based, 231
 neuronavigation
 camera system, 230
 deep/subcortical regions, 229
 optical/acoustic devices, 230
 three-dimensional digitizing device, 230
 noninvasive neuroimaging tools, 283
Stimulation
 electrode, 253
 frequency, 99–100, 125
 protocol, 4
Stippich, C., 1–9, 89–133, 232
Striate cortex, 73

- Stroke**
 aphasia therapy, 296
 cerebellum and SMA, 295, 296
 chronic (stable) phase, 296
 contralesional motor cortex, 295
 ipsilesional corticospinal tracts, 295
 local brain activation changes, 293–294
 network changes, 294–295
 temporal cortex, 295–296
- Stufflebeam, S.M., 149
- Subcallosal area**, 70
- Subcortical**, fiber tract, 233
- Subdural grid**, 231
- Sulcus**, 239
 anterior subcentral, 61–63
 branching, 70
 callosal, 68, 80
 central, 62, 63, 65, 69
 cingulate, 68–71
 collateral, 64, 66, 70
 inferior occipital, 64, 71
 intermediate, 62, 75
 olfactory, 65
 orbital, 62, 65
 paracentral, 68, 69, 80
 parallel, 63, 64
 parieto-occipital, 68–70
 peri-insular, 65, 66
 perisylvian, 65
 posterior subcentral, 61–63, 72
 subparietal, 68–70
- Sum, J.M., 121, 123
- Sunaert, S., 313–332
- Superior parietal lobule**, 62, 63, 65
- Supplementary motor area (SMA)**, 107, 295, 303
 action, 79–80
 attention-intention network, 81
 connections to cervical motor neurons, 79
 coordination and cooperation, 81
 crude somatotopy, 79
 heterotypical agranular isocortex
 characteristics, 79
 laterality, 80
 primary motor cortex, 79
 proper, caudal and posterior, 79
 sequences of action, 81
 synonyms, 79
- Supramarginal gyrus**, 62, 63, 65, 260
- Surface anatomy**, brain
 convexity (*see* Convexity surface)
 inferior (*see* Inferior)
- Surgery**
 decision making, 229, 238
 planning, 104
- Susceptibility difference**, 315, 328
- Synaptic activity**, 2
- Synchronicity**, 327
- Syntax**, 120
- T**
 Tactile stimulation, 95, 131
- Talairach-Tournoux baseline, 71–72
- Talairach transformation, 46–47, 71–72
- Tanji, J., 79–81
- Tanner, J.E., 53
- Taylor, K.S., 298
- Technical-related artifacts**
 Eddy current-induced distortions, 330–332
 EPI sequences to spikes, 330
 susceptibility-related artifacts, 328–330
- Temporal**
 data smoothing, 96
 lobe epilepsy (TLE), 119, 121
 resolution, 4
- Temporal lobe epilepsy (TLE)**, 297
- Temporo-occipital lobe**, 65–67
- Temporoparietal fiber intersection area**
 axial and coronal DEC, 211
 IPL and posterior temporal lobes, 210
 medial and lateral views, 211
 MR tractography, 212
 postmortem dissections, 210
 temporo-occipital WM, 211–213
 tractography, 214–215
 transcortical approach, 211
- Tensor-based morphometry (TBM)**, 272
- Ternovoi, S.K., 105
- Test-retest reliability**, 255
- Thallium SPECT**, 231
- Theophylline**, 318
- Thiebaut de Schotten, M., 56, 196
- Thompson, P.M., 104
- Tie, Y., 150
- Tinnitus**, 236, 239, 291
- Tissue**
 contrast, 231
 damage, 252
- Tone discrimination task**, 121
- Tracer** 15O-H₂O, 272
- Tracking point**, 240
- Tractography**, 106
- Transcranial magnetic stimulation (TMS)**, 79, 256, 257, 296
- Transverse**
 temporal gyrus of Heschl, 62, 63, 73
 temporal sulcus, 64, 65
- Triangular gyrus**, 63, 230
- Tronnier, V.M., 229–241
- Trunk muscle**, 79
- T test**, 101
- Tuberous sclerosis**, 278, 279
- Tuch, D.S., 188
- Tumor**, 251
 borders, 276
 of the brain, 89
 extent, 276
 growth, 231, 232, 233
 infiltration, 276, 277
 intraaxial, 90
 invasion, 281
 metabolism, 277
 removal, 252
 resection, 230, 231, 234
 tissue, 105
 vasculature, 316
 vessel density, 277
- Tumor-related paresis**, 105, 108, 116, 232, 233, 290, 300
- U**
 Ulmer, J.L., 273
- Ultrasonography**, 256
- Ultrasound**, 231, 240
- Uncinate fasciculus**, 85

- V**
Vacuolization, 252
Van de Moortele, P.-F., 247–262
Van Meer, M.P., 294
Van Westen, D., 121
Várkuti, B., 296
Vascular
 autoregulation, 132
 compression, 314
 malformation, 316
 steal effect, 316
Vasogenic edema, 320
Vaudano A.E., 169
Vein, 132
Venous
 drainage, 234
 effect, 251
 hot spot, 315
Ventral pathway
 macaque monkey, 208
 posterior-anterior progression, 210
 semantic processing, 209
 temporal stem, 208
Verb generation task, 121
 fluency, 121–123
 memory, 123, 260
Vergani, F., 206
Vessel branch, 240
Video EEG, 282
Villringer, A., 161
Visual cortex
 cerebral, 235
 field defect, 274
 left and right visual field, 23
 left parietooccipital meningioma, 235, 236
 localizer approach, 48
 neuron, 190
 orientation columns, 24
 retinotopy experiment, 327
 stimulation, 95
 stroke, 292
Visuospatial attention system
 external and internal stimuli, 195
 fMRI studies, 195
 frontoparietal network, 196
 hemisphere lesions, 196
 monkey brain, 195
 parietofrontal network, 196
 saccadic eye movements, 195
 SLF-II damage, 196–197
 superior longitudinal fasciculus, 220
Vitali, P., 292
Volume imaging in neurological research (VINCI), 277
Volume map, 101
Von Economo, C., 76, 84
Voxel-based morphometry (VBM), 272, 274, 315, 316, 325, 332
 size, 250
W
Wada test, 91, 101, 119–122, 130, 234, 235, 239
 angiography, 255
 BOLD signal, 121
 brain surgery, 122
 ECOG, 100
 hemispheric dominance, 91
 reference procedure, 130
 risks and limitations, 255
 validation, 255–256
Wang, L., 295
Wang, L.E., 296
Ward, H.A., 104
Warren, J.E., 295–296
Weaver, K.E., 149, 150, 297
Wehner, T., 271
Wernicke area, 99, 121, 124, 125, 129, 234, 235, 297
Wheat germ agglutinin-horse radish peroxidase (WGA-HRP), 258
White matter, 77, 107, 132, 238, 252, 258, 273, 275
Wiebe, S., 170
Wiest, R., 159–173
Williams, P.L., 67
Witwer, B.P., 273
Wong, S.W., 297
Word
 fluency, 260
 generation task, 121, 122, 124
Word-finding difficulty, 84
Worsley, K.J., 41
Y
Yakovlev, P.I., 216
Yasargil, M.G., 71
Yeatman, J.D., 56
Yousry, T.A., 61–85
You, X., 297
Z
Zeiss MKM, 278
Zhang, D., 150
Zhang, Z., 149
Zijlmans, M., 171
Zilles, K., 79, 81
Zipse, L., 296